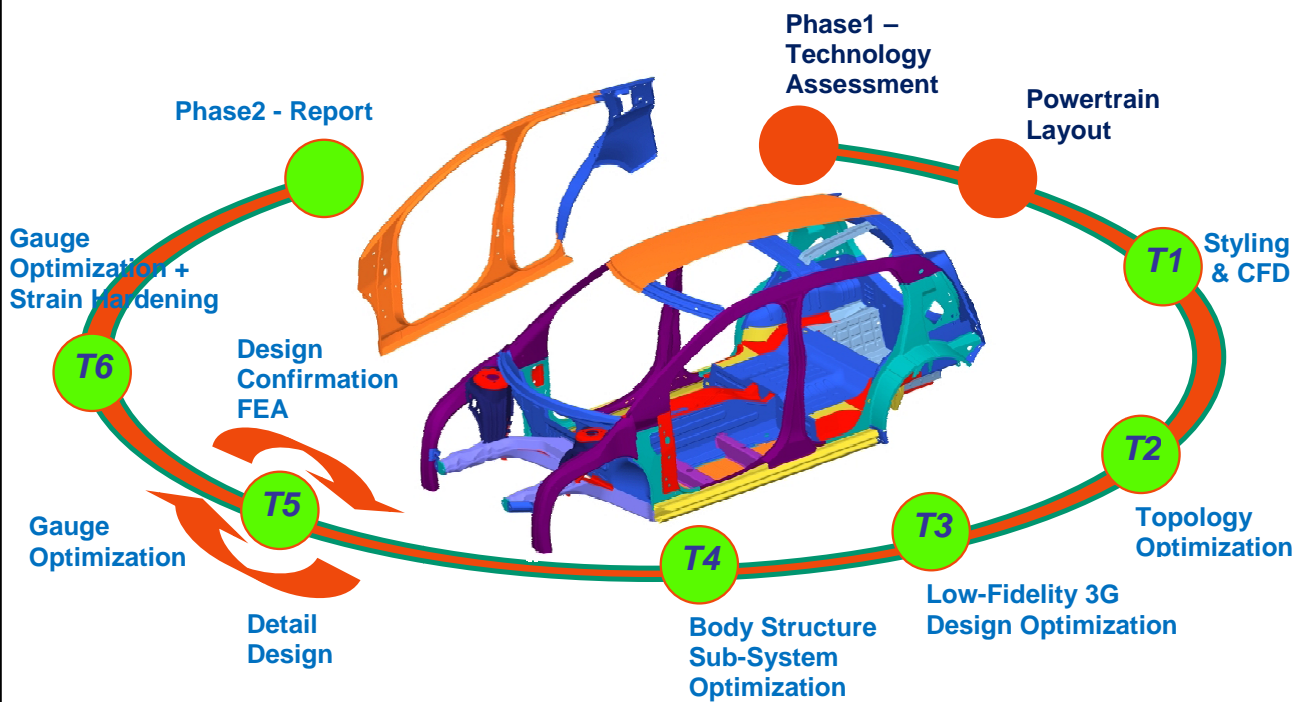
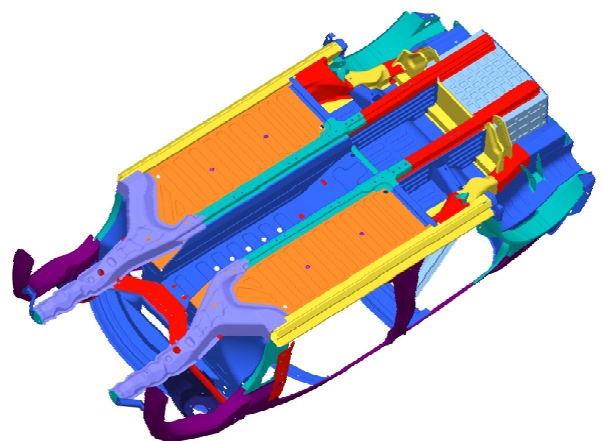


FutureSteelVehicle

Phase 2 – Report
April 20, 2011



Detailed Design, Engineering and Cost Analysis of Advanced High Strength Steel Body Structures for Advanced Powertrain Vehicles



© 2011 WorldAutoSteel. All rights reserved.

The content of this document may be downloaded, transmitted, and/or reproduced; however, under no circumstances may the content be altered, modified, or edited in any way, without the expressed permission of WorldAutoSteel.

WorldAutoSteelTM and FutureSteelVehicleTM are trademarks of WorldAutoSteel

Contents

1	Preface	1
1.1	WorldAutoSteel Member Companies	2
1.2	FSV Technology Partners (Phase 2)	2
1.3	FutureSteelVehicle Steering Team Members	3
2	Executive summary	4
2.1	Project Objectives	4
2.2	FSV Project Phases Overview	5
2.3	FSV Program Achievements	6
2.3.1	FSV Program Achievement #1 - 35% Mass Savings	6
2.3.2	FSV Program Achievement #2 - Optimal Utilization of Advanced High Strength Steel Grades	14
2.3.3	FSV Program Achievement #3 - Life Cycle Assessment	16
2.3.4	FSV Program Achievement #4 - Continued Evolution of Ultra High Strength Steel	18
2.3.5	FSV Program Achievement #5 - Continued Evolution of Advancements in Steel Technology	19
2.3.6	FSV Program Achievement #6 - Continued Innovation of Advancements in Steel Technology	23
2.3.7	FSV Program Achievement #7 - Design Innovation that Exploit the Versatility of Steel	25
2.3.8	FSV Program Achievement #8 - Design Innovation that Exploit the Strength of Steel	28
2.3.9	FSV Program Achievement #9 - Design Innovation that Exploit the Versatility of Steel	29
2.3.10	FSV Program Achievement #10 - Innovative Optimization Methodology	30
2.4	FSV Advanced Powertrain Options & Performances	33
2.5	FSV Body Structure Mass targets	33
2.6	Phase 2 Summary	34
2.6.1	Overview	34
2.6.2	T1 - Styling and CFD	34
2.6.3	T2 - Topology Optimization	36
2.6.4	T3 - Low Fidelity 3G (Geometry, Grade & Gauge) Optimization	38
2.6.5	T4-Body Structure Sub-System Optimization	40
2.6.6	T5-Detailed Body Structure Design	44

2.6.7	T5-Body Structure Performance CAE Analysis	51
2.6.8	Stamping Simulation	53
2.6.9	Body Structure Cost Assessment	54
2.6.10	Life Cycle Assessment	58
2.7	FSV Design and Engineering Process	63
2.8	FSV Mass Evolution	65
3	Steel Technology	66
3.1	FutureSteelVehicle Materials Portfolio	66
3.1.1	Steel Grade Descriptions	69
3.2	Manufacturing Processes	73
3.2.1	Laser welded blank	73
3.2.2	Laser welded coil	74
3.2.3	Tailor rolled coil	75
3.2.4	Conventional Electric-Resistance-Welded (ERW) Tube	76
3.2.5	Tubular Blanks (laser-welded)	76
3.2.6	Multiple walled tubes	76
3.2.7	Manufacturing Processes Considered for FSV	77
4	FSV-1 BEV Package	86
4.1	Background	86
4.2	Packaging Approach	87
4.3	Powertrain Package	88
4.3.1	Battery	88
4.3.2	'I - Shape' Battery Pack	90
4.3.3	Electric Drive Motor	92
4.3.4	Front and Rear Suspension	93
4.4	Occupant Positions	93
4.5	Bumper Positions and Front Crush Zones	94
4.6	Vision Requirements	95
4.7	Luggage Volume	96
4.8	Vehicle Styling Theme	97
5	Structural Targets	98
5.1	Vehicle Crash Targets	98
5.1.1	Frontal Impact	99
5.1.2	Side Impact	103
5.1.3	Rear Impact	106
5.1.4	Side Pole Impact	108
5.1.5	Roof Crush	110
5.1.6	Low Speed Regulations	111
5.2	Stiffness Targets	112
5.2.1	Body Structure - Dynamic (NVH) Targets	112
5.2.2	Body Structure Targets - Static Torsion and Bending	113
5.3	Body Structure Mass Targets	114

5.3.1	Target Setting Approach	114
5.3.2	Updates to Baseline Reference	115
5.3.3	FSV-1 Body-Structure Final Mass Target	116
5.4	Body Structure - Lightweight Index	119
6	Styling and CFD	121
6.1	Styling and Aerodynamic Performance	121
6.1.1	Introduction	121
6.1.2	Coefficient of Drag and Lift	122
6.1.3	Targets and Assumptions	123
6.2	FSV-1 Aerodynamics Development	125
6.2.1	Baseline FSV Model	125
6.2.2	FSV model - with New Spoiler and Air-dam	127
6.2.3	FSV Model - with New Roof Skin, New Spoiler, New Air-dam	130
6.2.4	FSV Model - with Rounded Front Shape and Smooth Exterior Sides	132
6.2.5	FSV Full Vehicle CFD Model - Detailed Motor Compartment Geometry	135
6.2.6	FSV Full Vehicle CFD Model - Cooling Flow Optimization	137
6.2.7	FSV Full Vehicle CFD Model - Effect of Add-on Parts/Features	139
6.3	Modified Original FSV Model - Multiple Changes Based on Lessons Learnt	140
6.3.1	C_d and C_L Values with Add-on Parts	141
6.4	New FSV Styling CFD Analysis	143
6.4.1	Final C_d and C_L Values for FSV-1	145
6.5	Summary of Aerodynamic Performance Results	146
7	T2 Topology Optimization	148
7.1	Introduction	148
7.2	Objective	149
7.3	Background	150
7.4	Optimization Methodology	150
7.5	Design Space	151
7.6	Finite Element Model	152
7.7	Boundary Conditions and Analysis Assumptions	153
7.7.1	Mass Assumptions	153
7.7.2	Loads and Boundary Conditions	154
7.7.3	Loads and Weighting Factors	159
7.8	Topology Results	160
7.8.1	Battery Floor Optimization	160
7.8.2	Battery Bulkhead Optimization	162
7.8.3	Full Vehicle Optimization	163
7.9	Conclusion	176
8	T3 - Low Fidelity 3G (Geometry, Grade & Gauge) Optimization	177
8.1	Introduction	177
8.2	Objective	178
8.3	LF3G: An integrated Optimization Process	178

8.4	LF3G Optimization Model	179
8.5	LF3G Parameterization	179
8.5.1	B-Pillar	180
8.5.2	Front Bumper Beam	180
8.5.3	Radiator Support to Shock Tower Beam	181
8.5.4	Shotgun	182
8.5.5	Instrument Panel Beam	183
8.5.6	Front Longitudinal above Tunnel	183
8.5.7	Front Cross-Bar	184
8.5.8	Side Roof Rail	184
8.5.9	Roof Bow and Headers	185
8.5.10	Rear Cargo Area Cross Bar	187
8.5.11	Front Seat Crossmember	187
8.5.12	Rocker	188
8.5.13	C-Pillar	188
8.5.14	Rear Longitudinal Rail	189
8.5.15	Bulkheads	190
8.6	Material and Gauge Choices	191
8.7	LF3G Targets	195
8.8	LF3G Optimization Results	195
8.8.1	NCAP Frontal Impact	197
8.8.2	IIHS Front Crash 40% ODB	198
8.8.3	FMVSS 301 Rear 70% ODB	199
8.8.4	IIHS Side Impact	200
8.8.5	FMVSS 216 Roof Crush with IIHS 4*strength to weight ratio	201
8.8.6	Static Torsion	202
8.8.7	Performance Results Summary	202
8.9	LF3G Battery Optimization	203
8.9.1	Model	203
8.9.2	Optimization	204
8.9.3	Battery Shape Conclusion	208
8.10	Conclusion	209
9	FSV LF3G Results Interpretation to Baseline Body Structure Design	225
9.1	LF3G Geometry Interpretation	225
9.1.1	Background	225
9.1.2	Body Structure - Sheet Steel First Iteration Baseline Design	226
9.1.3	Body Structure - Sub Systems for T4 - HF3G Optimization	227
10	Structural Sub-System Design Optimization - Methodology	235
10.1	Introduction	235
10.2	Objective	235
10.3	Background	236
10.4	Optimization Methodology Overview	236
10.5	Loadpath Mapping: Sub-System Selection and Loadcases	237

10.6	Rocker Sub-System	238
10.6.1	Development of Sub-System from the Full Model	239
10.6.2	Generating Boundary Conditions	239
10.6.3	Stamped Rocker Concept	241
10.6.4	Hydroformed Rocker Concept	250
10.6.5	Roll formed Rocker Concept	257
10.6.6	Extruded Aluminum Rocker Concept	264
10.7	B-Pillar Sub-System	272
10.7.1	Development of Sub-System from the Full Model	272
10.7.2	Generating Boundary Conditions	273
10.7.3	Stamped B-pillar Concept	274
10.7.4	Hydroformed B-Pillar Concept	279
10.7.5	Stamped Aluminum B-Pillar Concept	284
10.8	Side Roof Rail Sub-System	289
10.8.1	Development of Sub-system from Full Model	289
10.8.2	Generating Boundary Conditions	290
10.8.3	Stamped Side Roof Rail Concept	291
10.8.4	Hydroformed Side Roof Rail Concept	298
10.8.5	Aluminum Side Roof Rail Concept	303
10.9	Rear Rail Sub-System	308
10.9.1	Development of Sub-System from Full Model	308
10.9.2	Generating Boundary Conditions	308
10.9.3	Stamped Rear Rail Concept	309
10.9.4	Hydroformed Rear Rail Concept	314
10.9.5	Stamped Aluminum Rear Rail Concept	318
10.10	Battery Tunnel Rail Sub-System	323
10.10.1	Development of sub-system From Full model	323
10.10.2	Generating Boundary Conditions	324
10.10.3	Stamped Tunnel Rail Concept	325
10.10.4	Open Roll Formed Tunnel Rail Concept	331
10.10.5	Extruded Aluminum Tunnel Rail Concept	337
10.11	Shotgun Sub-System	341
10.11.1	Development of Sub-System from Full Model	341
10.11.2	Generating Boundary Conditions	342
10.11.3	Stamped Shotgun Concept	343
10.11.4	Aluminum Shotgun Concept	348
10.12	Front Rail Sub-System	351
10.12.1	Development of Sub-System from the Full Model	351
10.12.2	Generating Boundary Conditions	352
10.12.3	Stamped Front Rail Sub-System	353
10.12.4	Hydroformed Front Rail Sub-System	358
10.12.5	Stamped Aluminum Front Rail Sub-System	363
10.13	Front End Optimization	366
10.14	Front End : Discussion of the Design Strategy for the FSV Design	369

11 Structural Sub-System Design and Manufacturing Interpretation	375
11.1 Introduction	375
11.2 Rocker 3G Optimized Solution	376
11.3 Rocker Manufacturing Interpretation (Design for Manufacturing)	376
11.4 Verification of Interpreted Results	379
11.5 Rocker Tubular Solutions	383
11.6 B-Pillar 3G Optimized solution	387
11.7 B-Pillar Interpreted Results	387
11.8 Rear Rail 3G Optimized Solution	392
11.9 Rear Rail Interpreted Results	393
11.10 Roof Rail 3G Optimized solution	397
11.11 Roof Rail Interpreted Results	398
11.12 Shotgun 3G Optimized Solution	401
11.13 Shotgun Interpreted Results	401
11.14 Tunnel 3G Optimized Solution	405
11.15 Tunnel Interpreted Results	406
11.16 Front Rail Stamped Solution (Concept 1)	410
11.17 Front Rail Stamped Solution (Concept-2)	412
11.18 Front Rail Stamped Aluminum Solution	414
11.19 Front Rail Hydroformed Solution	415
12 Sub-Systems Selection Methods	416
12.1 Introduction	416
12.2 Sub-System Cost Assessment	417
12.2.1 Approach	417
12.2.2 General Assumptions	420
12.2.3 Plant Parameters	420
12.2.4 Process Parameters	421
12.2.5 Sub-System Components Fabrication Input	423
12.2.6 Material Prices	425
12.2.7 Cost Assessment Results	428
12.3 Total Life Cycle Assessment	436
12.3.1 Life Cycle Emissions Studies for FutureSteelVehicle Variants	439
12.3.2 BEV Emissions Technology Assessment - Using the UCSB Model	440
13 Design of Body Structure	445
13.1 Sub-Systems Selection for BEV	445
13.1.1 FSV Selection Criteria	446
13.1.2 Sub-Systems Selection for BEV	447
13.2 Sub-System Integration into Body Design	463
13.2.1 Rocker Sub-System	463
13.2.2 B-Pillar Sub-System	464
13.2.3 Roof Rail Sub-System	465
13.2.4 Shotgun Sub-System	466
13.2.5 Tunnel Sub-System	466

13.2.6	Rear Rail Sub-System	468
13.2.7	Front Rail Sub-System	469
13.2.8	Final BEV Body Structure Design	470
13.3	Body Structure Assembly and Joining Methods	475
13.3.1	Joining Methods	475
13.3.2	Body Structure Assembly	490
14	Body Structure Performance CAE Analysis Results	523
14.1	Crash Worthiness	523
14.1.1	FSV-1 BEV Body Structure Load Paths	523
14.1.2	Frontal Impact	528
14.1.3	Side Impact	543
14.1.4	Rear Impact	555
14.1.5	Side Pole Impact	561
14.1.6	Roof Crush	571
14.1.7	Low Speed Regulations	574
14.2	Static Stiffness Study	578
14.2.1	Loading and Boundary Conditions	579
14.2.2	Static Stiffness Results	580
14.3	Dynamic Stiffness Study	581
14.3.1	Global Modes Results	582
14.4	Full Vehicle Dynamic Analysis	583
14.4.1	Vehicle Information	583
14.4.2	Fishhook Test	584
14.4.3	Industry Standard Maneuvers	586
14.4.4	Results	588
14.4.5	Conclusions	592
14.5	Durability Study	593
14.5.1	Process and Tools used for Durability Study	593
14.5.2	Results	594
14.6	FSV NVH Assessment Conducted by LMS	598
15	Manufacturing Process Simulation Results	599
15.1	Single Step Metal Stamping Simulation	599
15.2	Single Step Hot Stamping Simulation	601
15.3	Incremental Metal Stamping Simulation	602
15.3.1	Front Shock Tower (Material TWIP 980 - 1.0mm)	603
15.3.2	Rear Header Reinforcement Panel (Material BH 340 - 1.0mm)	605
15.3.3	Rear Floor Panel (Material BH 340 - 0.5mm)	606
15.3.4	Rear Rail Reinforcement (LWB, Stamping and Indirect Hot Stamping)	607
15.3.5	Rear Rail Outer	608
15.3.6	Rear Rail Inner	610
15.3.7	Front Rail Upper & Lower	611
15.3.8	Body Side	615

16 Other FSV Body Structure and Powertrain Variants	618
16.1 FSV-1 PHEV ₂₀	618
16.1.1 PHEV ₂₀ Body Structure	619
16.1.2 PHEV ₂₀ Front End	624
16.1.3 PHEV ₂₀ Powertrain Package	624
16.2 FSV-2	629
16.2.1 FSV-2 Body Structure	634
16.2.2 FSV-2 PHEV ₄₀	634
16.2.3 FSV-2 FCEV	638
17 Body Structure Cost Assessment	642
17.1 Part Manufacturing Cost	642
17.2 Body Assembly Cost	643
17.2.1 General Assumptions	643
17.2.2 Plant Parameters	644
17.2.3 Process Parameters	645
17.2.4 Assembly Inputs	646
17.2.5 Assembly Cost Assessment Results	647
17.3 Sensitivity Analysis	649
18 Life Cycle Assessment and Fuel Cycle Analysis	650
18.1 Body Structure Life Cycle Analysis (LCA)	650
18.2 Full Vehicle Body Structure LCA Results	653
18.3 Well-to-Pump Assessment	656
18.4 Pump-to-Wheel Assessment-FSV	657
18.5 FSV-1 Well-to-Wheel CO ₂ e Emissions	658
19 2G Full System Design Optimization and Bead Optimization	659
19.1 2G (Grade and Gauge) Full System Design Optimization	659
19.1.1 Objective	659
19.1.2 T5 Optimization Methodology Overview	660
19.1.3 T5 Base and Optimization Model Evaluations	661
19.1.4 T5 Base Model Coarsening and Baseline Performance Evaluation	663
19.1.5 Correlation of Baseline Model and Coarse Model (Optimization Model)	669
19.1.6 T5 2G (Grade and Gauge) Optimization Process	670
19.1.7 Intermediate Designs Observations	673
19.2 Bead Optimization	692
19.2.1 Objective	692
19.2.2 Background	692
19.2.3 Beading Optimization Strategy	693
19.2.4 Panels Considered in the FSV Body Structure	695
19.2.5 Bead Optimization Process	696
19.2.6 Comparison of Design and Optimization Beads	701
20 Appendix	703

20.1	Process Planning Sheets for FSV-1 BEV	704
20.2	Assembly Trees Body Structure	774
20.3	Energy Target Value Calculations	818
20.4	Energy Target Value Calculation for Aluminum Concepts	823
20.5	Body Structure - Baseline Design List of Parts (Tables 1 - 3)	826

1.0 Preface

This report documents the results of Phase 2 of the FutureSteelVehicle program.

The FutureSteelVehicle program is the most recent addition to the global steel industry's series of initiatives offering steel solutions to the challenges facing automakers around the world to increase the fuel efficiency of automobiles, reducing Green-House Gas emissions (GHG), while improving safety, performance and maintaining affordability.

This program follows the Ultra-Light Steel Auto Body (ULSAB) 1998, the Ultra-light Steel Auto Closures (ULSAC) 2000, Ultra-light Steel Auto Suspension (ULSAS) 2000, and ULSAB-AVC (Advanced Vehicle Concepts) 2001.

WorldAutoSteel has commissioned EDAG, Inc., Auburn Hills, Michigan, USA, to conduct an advanced powertrain technology assessment, and to provide vehicle design and program engineering management for the FutureSteelVehicle program. For the FutureSteelVehicle program, EDAG, along with its engineering partners ETA and LMS, applied a holistic approach to vehicle layout design using advanced future powertrains and creating a new vehicle architecture that offers mass efficient, all steel solutions. The future advanced powertrains that have major influence on vehicle layout and body structure architecture are: Plug-In Hybrid Electric Vehicle (PHEV), Battery Electric Vehicles, (BEV) and Fuel Cell Electric Vehicles (FCEV).

1.1 WorldAutoSteel Member Companies

- Anshan Iron & Steel Group Corporation
- ArcelorMittal
- Baoshan Iron & Steel Co. Ltd.
- China Steel Corporation
- Hyundai-Steel Company
- JFE Steel Corporation
- Kobe Steel, Ltd.
- Nippon Steel Corporation
- Nucor Corporation
- POSCO
- Severstal
- Sumitomo Metal Industries, Ltd.
- Tata Steel
- ThyssenKrupp Steel
- United States Steel Corporation
- Usinas Siderurgicas de Minas Gerais S.A.
- voestalpine Stahl GmbH

1.2 FSV Technology Partners (Phase 2)

- Engineering Technologies Associates Inc., USA
- LMS Engineering Services, Belgium

1.3 FutureSteelVehicle Steering Team Members

Program Chair: Jody Shaw, United States Steel Corporation

Program Manager: Harry Singh, EDAG Inc.

Steering Team Members:

T. Chen	China Steel Corporation
K. Fukui	Sumitomo Metal Industries, Ltd.
A. Gauriat	ArcelorMittal
O. Hoffmann	ThyssenKrupp Steel Europe
S. Hong	Hyundai Steel Company
T. Inazumi	JFE Steel Corporation
D. Kanelos	Nucor Corporation
J. Kim	POSCO
R. Krupitzer	American Iron and Steel Institute
Y. Kuriyama	Nippon Steel Corporation
M. Lambriks	Tata Steel Europe
J. Meng	Anshan Iron & Steel Group Corporation
E. Opbroek	WorldAutoSteel
M. Peruzzi	voestalpine Stahl GmbH
J. Powers	Severstal
E. Taiss	Usinas Siderúrgicas de Minas Gerais S.A.
C. ten Broek	WorldAutoSteel
K. Watanabe	Kobe Steel, Ltd.
W. Xu	Baoshan Iron & Steel Co. Ltd.

2.0 Executive summary

2.1 Project Objectives

The future direction of the transportation industry is being influenced by an increasing demand for better fuel economy, and to reduce emissions that result in greenhouse gas induced global warming. Increasing vehicle efficiency through advanced powertrains and the use of alternate low-carbon content fuels will not only reduce petroleum consumption, but also decrease the carbon footprint associated with the burning of fossil fuels. The use of advanced powertrains will lead to an increased focus on vehicle weight reduction and hence, material selection.

The FutureSteelVehicle (FSV) program will address the global environmental and regulatory concerns through the application of lightweight multi-grade advanced high strength all steel body-structures in vehicle designs using advanced powertrain technologies.

EDAG's focus is on a holistic approach to the concept development of innovative vehicle layout and optimized vehicle body structure, using the latest advanced steels and manufacturing technologies. The adopted 'clean-sheet' design methodology for the FSV body structure pushes the limits of computer aided optimization techniques, to achieve an optimal mass efficient design.

The objective of the FutureSteelVehicle Project is to meet year 2015-2020 performance criteria while achieving a 35% mass reduction target in addition to a detailed project cost analysis and life cycle impact assessment.

2.2 FSV Project Phases Overview

Two phases of the FutureSteelVehicle program have been completed:

- Phase 1: Engineering study (2008 - July, 2009)
- Phase 2: Concept design (August, 2009 - 2010)

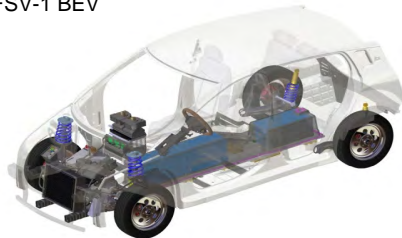
The content of Phase 1 was a comprehensive assessment and identification of advanced power-trains and future automotive technology applicable to year 2020 high volume vehicle production. The results of Phase 1 were documented in a separate report. This report documents the activities of Phase 2.

FSV Phase 2 produced detailed design concepts for a Battery Electric Vehicle (BEV), and these detailed design concepts were then extended to illustrate how they can be applied to Plug-In Hybrid Electric Vehicles (PHEV) and Fuel Cell Electric Vehicles (FCEV).

The vehicle specifications of the different FSV variants are shown in Table 2.1.

Vehicle	BIW Mass (kg)	Length (mm)	Width (mm)	Height (mm)	Wheelbase (mm)	Track Frt/Rr (mm)	Powertrain Mass (kg)	Curb Mass (kg)	GVW (kg)
BEV	187.5	3820	1705	1495	2524	1470	328.7	958	1433
PHEV-20	176.4	3820	1705	1495	2524	1470	335.4	988	1463
PHEV-40	200.8	4350	1805	1495	2800	1570	460.7	1195	1670
FCEV	200.8	4350	1805	1495	2800	1570	293.2	1029	1504

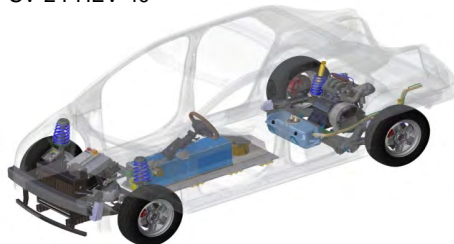
FSV-1 BEV



FSV-1 PHEV-20



FSV-2 PHEV-40



FSV-2 FCEV



Table 2.1: *Future Steel Vehicle specifications*

2.3 FSV Program Achievements

2.3.1 FSV Program Achievement #1 - 35% Mass Savings

The Battery Electric Vehicle (BEV) body structure achieved a mass savings of 102 kg (-35%) compared to the baseline body structure mass as shown in Table 2.2. The baseline body structure is the same benchmark as used for the ULSAB-AVC, adjusted for a BEV powertrain and year 2020 regulatory requirements (see Section 5.3: “Body Structure Mass Targets”). The mass reduction has been realized through the use of advanced high strength steel grades and an optimized design. Any cost increase that may be associated with the use of higher grades of steel, including overall manufacturing and assembly costs of the FSV body structure, is balanced by the consequently achieved weight savings. Additionally, the FSV body structure also meets all the structural targets for crashworthiness, NVH and durability; no compromise has been made in the performance of the body structure. The BEV body structure is shown in Figure 2.1, Figure 2.2 and Figure 2.3.

Body Structure	FSV-1 BEV
Benchmark Mass (kg)	290
Target Mass (kg)	190
Achieved Mass (kg)	187.7

Table 2.2: FSV program achievement

2.3 FSV Program Achievements

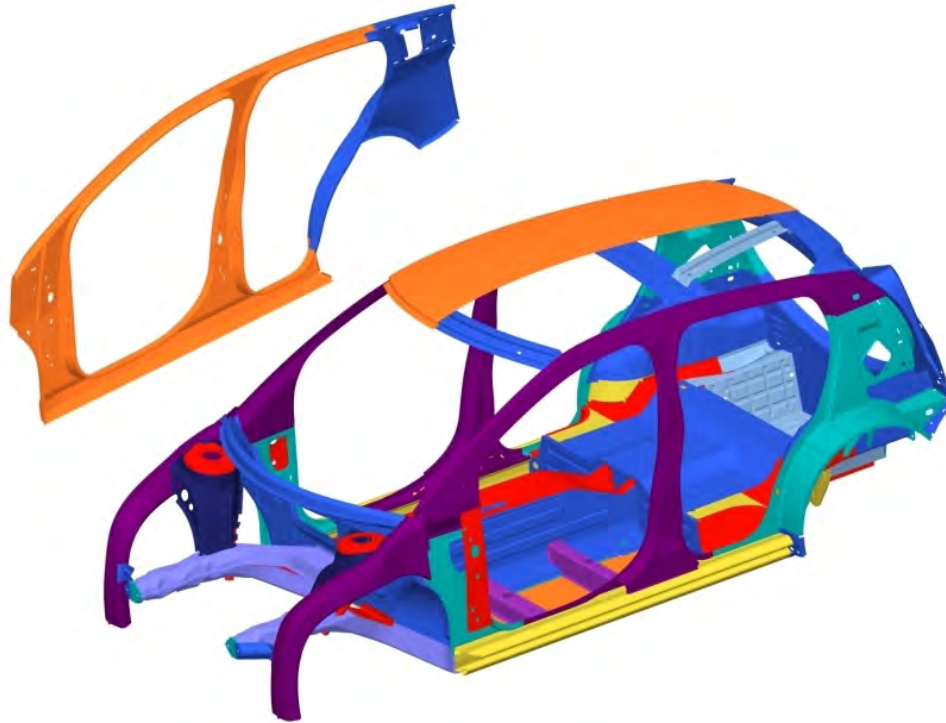


Figure 2.1: FSV-1 BEV body structure

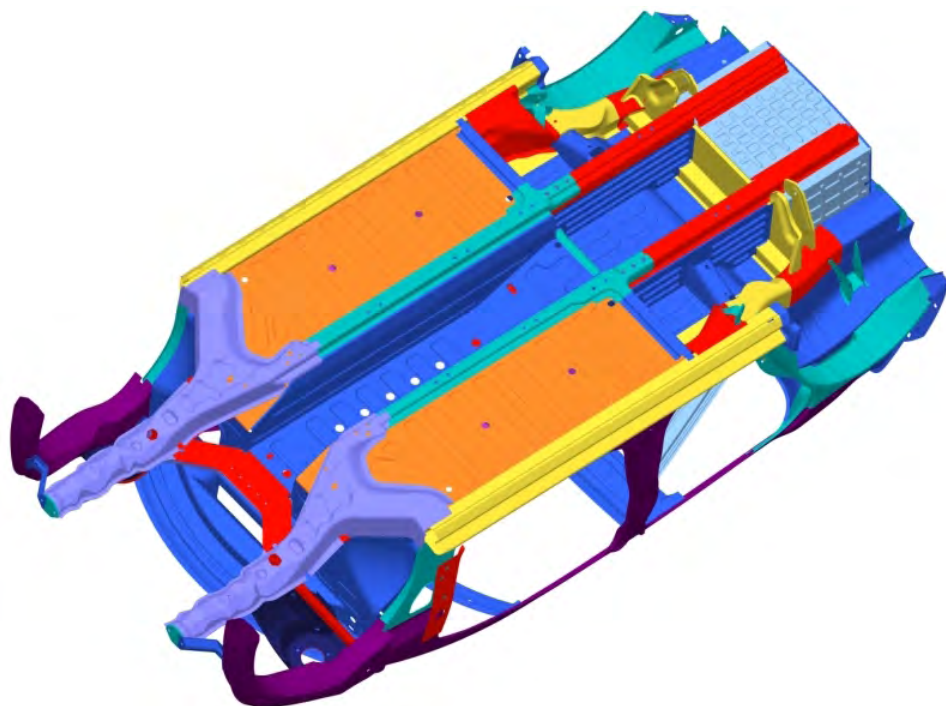


Figure 2.2: FSV-1 BEV body structure underside

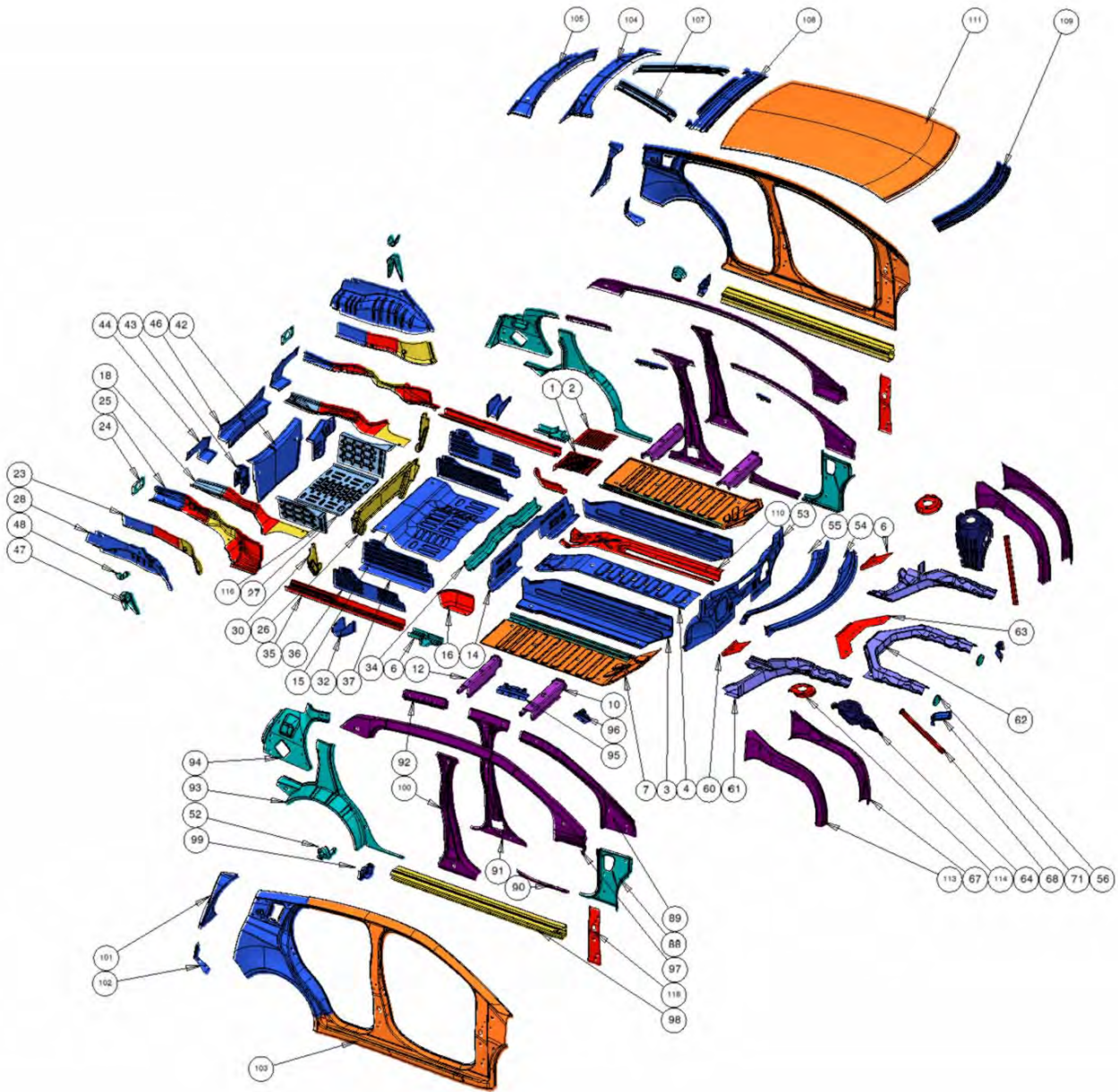


Figure 2.3: BEV exploded view

The FSV BEV parts lists showing material grades, thickness and mass are shown in Table 2.3 Table 2.4.

Part No	Part Description	Forming	Grade	Yeild (MPa)	Tensile (MPa)	Thickness (mm)	Mass (kg)	Total Mass (kg)
1	50.1 0401 Bulkhead Lower - Tunnel	S	DP	700	1000	0.80	0.679	0.679
2	50.1 0400 Bulkhead Upper - Tunnel	S	DP	700	1000	0.80	0.543	0.543
3	50.1 0402 Panel - Tunnel Side RH	S	BH	280	400	0.50	2.342	2.342
4	50.1 0404 Reinf - Tunnel Top	S	BH	280	400	0.50	1.713	1.713
5	50.1 0403 Panel - Tunnel Side LH	S	BH	280	400	0.50	2.342	2.342
6	50.1 0321 Tunnel Rail Bulkhead RH	S	DP	500	800	1.00	0.381	0.381
7	50.1 0011 Floor - Front RH	S	DP	300	500	0.50	2.84	4.61
			DP	500	800	1.50	1.77	
8	50.1 0322 Tunnel Rail Bulkhead LH	S	DP	500	800	1.00	0.381	0.381
9	50.1 0025 Floor - Front LH	S	DP	300	500	0.50	2.84	4.61
			DP	500	800	1.50	1.77	
10	50.1 0093 Crossmember - Front Seat RH Front	RF	MS	950	1200	0.50	0.542	0.542
11	50.1 0094 Crossmember - Front Seat LH Front	RF	MS	950	1200	0.50	0.542	0.542
12	50.1 0095 Crossmember - Front Seat RH Rear	RF	MS	950	1200	0.60	0.688	0.688
13	50.1 0096 Crossmember - Front Seat LH Rear	RF	MS	950	1200	0.60	0.688	0.688
14	50.1 0100 Heel Board	S	BH	210	340	0.60	1.603	1.603
15	50.1 0016 Seat Pan - Rear	S	BH	210	340	0.50	2.919	2.919
16	50.1 0099 Panel - Seat Side RH	S	DP	700	1000	0.70	0.359	0.359
17	50.1 0101 Panel - Seat Side LH	S	DP	700	1000	0.70	0.359	0.359
18	50.1 0109 Reinf - Frame Rail Rear RH	S	CP	1000	1200	1.10	0.361	1.555
			DP	700	1000	0.65	0.528	
			Mild	140	270	1.55	0.666	
19	50.1 0110 Reinf - Frame Rail Rear LH	S	CP	1000	1200	1.10	0.361	1.555
			DP	700	1000	0.65	0.528	
			Mild	140	270	1.55	0.666	
20	50.1 0015 Frame Rail - Outer Rear LH	S	CP	1000	1200	0.60	0.304	1.037
			DP	700	1000	1.40	0.469	
			HSLA	350	450	0.80	0.264	
21	50.1 0334 Mounting Plate - Crush Can Rear LH	S	DP	500	1200	1.20	0.132	0.132
22	50.1 0336 Frame Rail - Inr Rear LH	S	CP	1000	1200	0.60	0.247	2.635
			DP	700	1000	1.40	1.963	
			HSLA	350	450	0.80	0.425	
23	50.1 0014 Frame Rail - Outer Rear RH	S	CP	1000	1200	0.60	0.304	1.037
			DP	700	1000	1.40	0.469	
			HSLA	350	450	0.80	0.264	
24	50.1 0333 Mounting Plate - Crush Can Rear RH	S	DP	500	800	1.20	0.132	0.132
25	50.1 0335 Frame Rail - Inr Rear RH	S	CP	1000	1200	0.60	0.247	2.635
			DP	700	1000	1.40	1.963	
			HSLA	350	450	0.80	0.425	
26	50.1 0032 Crossmember - Battery and Suspension	S	CP	800	1000	1.00	2.944	2.944
27	50.1 0330 Panel - Cargo Box Floor	S	Mild	140	270	0.50	1.326	1.326
28	50.1 0017 Wheelhouse Inner - Rear RH	S	BH	210	340	0.70	0.835	2.58
			BH	210	340	1.20	1.745	
29	50.1 0018 Wheelhouse Inner - Rear LH	S	BH	210	340	0.70	0.835	2.58
			BH	210	340	1.20	1.745	
30	50.1 0079 Brkt - Rear Suspension RH	S	CP	800	1000	1.00	0.342	0.342
31	50.1 0080 Brkt - Rear Suspension LH	S	CP	800	1000	1.00	0.342	0.342
32	50.1 0077 Gusset - Rear RH	S	BH	210	340	1.00	0.465	0.465
33	50.1 0078 Gusset - Rear LH	S	BH	210	340	1.00	0.465	0.465
34	50.1 0320 Rail - Side to Side	S	DP	500	800	0.80	1.074	1.074
35	50.1 0108 Rail - Longitudinal RR RH	S	DP	700	1000	1.20	2.201	2.201
36	50.1 0075 Close Off - Battery Otr RH	S	BH	210	340	0.60	0.805	0.805
37	50.1 0073 Close Off - Battery Inr RH	S	BH	210	340	0.60	1.195	1.195
38	50.1 0107 Rail - Longitudinal RR LH	S	DP	700	1000	1.20	2.201	2.201
39	50.1 0076 Close Off - Battery Otr LH	S	BH	210	340	0.60	0.805	0.805
40	50.1 0074 Close Off - Battery Inr LH	S	BH	210	340	0.60	1.195	1.195
41	50.1 0329 Pnl - Rear Liftgate Lower Inr LH	S	BH	210	340	1.00	0.585	0.585
42	50.1 0013 Pnl - Rear Liftgate Lower Inr	S	BH	210	340	0.70	1.866	1.866
43	50.1 0328 Pnl - Rear Liftgate Lower Inr RH	S	BH	210	340	1.00	0.585	0.585
44	50.1 0019 Panel - Back Outboard RH	S	BH	210	340	1.00	0.577	0.577
45	50.1 0025 Panel - Back Outboard LH	S	BH	210	340	1.00	0.577	0.577
46	50.1 0020 Panel - Back Lower	S	BH	210	340	1.00	1.405	1.405
47	50.1 2601 Mount - Rear Shock RH	S	DP	500	800	2.50	0.566	0.566
48	50.1 2602 Reinf - Rear Shock RH	S	DP	500	800	2.00	0.176	0.176
49	50.1 2701 Reinf - Rear Shock LH	S	DP	500	800	2.00	0.176	0.176
50	50.1 2702 Mount - Rear Shock LH	S	DP	500	800	2.50	0.566	0.566
51	50.1 2001 Mount - Trailing Arm LH	S	DP	500	800	2.00	0.37	0.37
52	50.1 2002 Mount - Trailing Arm RH	S	DP	500	800	2.00	0.37	0.37
53	50.1 0001 Dash - Toe Pan	S	BH	280	400	0.50	2.839	2.839
54	50.1 0002 Cowl Upper	S	BH	210	340	1.00	0.866	2.268
			BH	210	340	0.60	1.402	
55	50.1 0070 Cowl Lower	S	BH	210	340	1.20	0.709	1.494
			BH	210	340	0.60	0.785	
56	60.2 0007 Mounting Plate - Crush Can Front RH	S	DP	500	800	1.75	0.121	0.121
57	60.2 0008 Mounting Plate - Crush Can Front LH	S	DP	500	800	1.75	0.121	0.121
58	50.1 0306 Closeout - Lower Rail LH	S	DP	700	1000	0.80	0.309	0.309
59	50.1 0302 Front Rail - Lower LH	S	TRIP	600	980	1.90	0.359	5.998
			TRIP	600	980	2.00	0.419	
			TRIP	600	980	1.90	0.535	
			TRIP	600	980	1.80	4.685	

Table 2.3: FSV BEV Bill of Materials (BOM)

Part No	Part Description	Forming	Grade	Yield (MPa)	Tensile (MPa)	Thickness (mm)	Mass (kg)	Total Mass (kg)
60	50.1 0305 Closeout - Lower Rail RH	S	DP 700	1000	0.80	0.309	0.309	
61	50.1 0301 Front Rail - Lower RH	S	TRIP 600	980	1.90	0.359	5.998	
			TRIP 600	980	2.00	0.419		
			TRIP 600	980	1.90	0.535		
			TRIP 600	980	1.80	4.685		
62	50.1 0303 Front Rail - Upper	S	TRIP 600	980	1.80	0.667	5.743	
			TRIP 600	980	2.00	0.811		
			TRIP 600	980	1.80	4.265		
63	50.1 0304 Closeout - Upper Rail	S	DP 700	1000	1.00	0.616	0.616	
64	50.1 0044 Shock Tower - Frt RH	S	TWIP 500	980	1.00	1.457	1.457	
65	50.1 0063 Shock Tower - Frt LH	S	TWIP 500	980	1.00	1.457	1.457	
66	50.1 0022 Shotgun Inner LH	HS	HF 1050	1500	1.20	0.476	2.15	
			HF 1050	1500	0.80	0.759		
			HF 1050	1500	1.50	0.915		
67	50.1 0021 Shotgun Inner RH	HS	HF 1050	1500	1.20	0.476	2.15	
			HF 1050	1500	0.80	0.759		
			HF 1050	1500	1.50	0.915		
68	50.1 0326 A-Pillar Brace	RF	DP 700	1000	1.20	0.695	0.695	
69	50.1 0326 A-Pillar Brace LH	RF	DP 700	1000	1.20	0.695	0.695	
70	50.1 0318 Shotgun Brace LH	S	BH 210	340	1.20	0.206	0.206	
71	50.1 0308 Shotgun Brace RH	S	BH 210	340	1.20	0.206	0.206	
72	50.6 0023 Roof Rail Inner Front LH	HS	HF 1050	1500	0.70	0.84	1.171	
			HF 1050	1500	0.95	0.331		
73	50.6 0064 FBHP Inner LH	S	DP 500	800	1.20	1.667	1.667	
74	50.6 0056 Rocker Filler Front LH	S	BH 210	340	0.60	0.199	0.199	
75	50.6 0017 B-Pillar Inner LH	HS	HF 1050	1500	0.80	0.547	1.491	
			HF 1050	1500	0.60	0.944		
76	50.6 0053 Roof Rail Inner Rear LH	S	BH 210	340	1.10	0.372	0.372	
77	50.1 0067 Panel - Wheel House Outer LH	S	DP 500	800	0.65	1.732	1.732	
78	50.6 0004 C-Pillar Inner LH	S	DP 500	800	0.70	1.428	1.428	
79	50.2 0034 Bracket - Roof Rail to Header LH	S	BH 210	340	1.00	0.103	0.103	
80	50.2 0035 Bracket - Roof Rail to Roof Bow LH	S	BH 210	340	1.00	0.254	0.254	
81	50.6 0018 Reinf - Roof Rail LH	HS	HF 1050	1500	0.70	2.049	2.049	
82	50.6 0066 Rocker RH	RF	CP 1050	1470	1.00	6.032	6.032	
83	50.6 0072 Rocker Cap LH	S	BH 210	340	0.85	0.244	0.244	
84	50.6 0028 Reinf - B-Pillar LH	HS	HF 1050	1500	0.60	0.547	1.491	
			HF 1050	1500	1.00	0.944		
85	50.6 0006 Body Side Outer LH	S	DP 350	600	0.80	8.189	10.928	
			BH 210	340	0.60	2.739		
86	50.6 0069 Panel Rear Quarter Lwr LH	S	BH 210	340	1.20	0.198	0.198	
87	50.6 0051 Panel - Gutter Rear LH	S	BH 210	340	1.00	0.795	0.795	
88	50.6 0046 FBHP Inner RH	S	DP 500	800	1.20	1.667	1.667	
89	50.6 0022 Roof Rail Inner Front RH	HS	HF 1050	1500	0.70	0.84	1.171	
			HF 1050	1500	0.95	0.331		
90	50.6 0055 Rocker Filler Front RH	S	BH 210	340	0.60	0.199	0.199	
91	50.6 0009 B-Pillar Inner RH	HS	HF 1050	1500	0.80	0.547	1.491	
			HF 1050	1500	0.60	0.944		
92	50.6 0052 Roof Rail Inner Rear RH	S	BH 210	340	1.10	0.372	0.372	
93	50.1 0049 Panel - Wheel House Outer RH	S	DP 500	800	0.65	1.732	1.732	
94	50.6 0005 C-Pillar Inner RH	S	DP 500	800	0.70	1.428	1.428	
95	50.2 0033 Bracket - Roof Rail to Roof Bow RH	S	BH 210	340	1.00	0.254	0.254	
96	50.2 0032 Bracket - Roof Rail to Header RH	S	BH 210	340	1.00	0.103	0.103	
97	50.6 0012 Reinf - Roof Rail RH	S	HF 1050	1500	0.70	2.049	2.049	
98	50.6 0048 Rocker RH	RF	CP 1050	1470	1.00	6.032	6.032	
99	50.6 0071 Rocker Cap RH	S	BH 210	340	0.85	0.244	0.244	
100	50.6 0026 Reinf - B-Pillar RH	HS	HF 1050	1500	0.60	0.547	1.491	
			HF 1050	1500	1.00	0.944		
101	50.6 0050 Panel - Gutter Rear RH	S	BH 210	340	1.00	0.795	0.795	
102	50.6 0068 Panel Rear Quarter Lwr RH	S	BH 210	340	1.20	0.198	0.198	
103	50.6 0002 Body Side Outer RH	S	DP 350	600	0.80	8.189	10.928	
			BH 210	340	0.60	2.739		
104	50.2 0007 Rear Header Reinf	S	BH 210	340	2.00	2.759	3.775	
			BH 210	340	0.70	1.016		
105	50.2 0006 Rear Header	S	BH 210	340	0.70	1.662	1.662	
106	50.2 0009 Support - Roof LH	S	Mild 140	270	0.50	0.463	0.463	
107	50.2 0008 Support - Roof RH	S	Mild 140	270	0.50	0.463	0.463	
108	50.2 0013 Roof Bow	RF	BH 210	340	0.50	0.941	0.941	
109	50.2 0011 Header - Roof Front	RF	BH 210	340	0.80	1.131	1.131	
110	50.1 0405 Top Panel - Tunnel	S	DP 1150	1270	1.00	3.067	3.067	
111	50.2 0010 Pnl - Roof Outer	S	BH 210	340	0.50	9.011	9.011	
112	50.1 0069 Shotgun Outer LH	HS	HF 1050	1500	1.00	0.431	2.088	
			HF 1050	1500	0.80	0.689		
			HF 1050	1500	1.50	0.968		
113	50.1 0051 Shotgun Outer RH	HS	HF 1050	1500	1.00	0.431	2.088	
			HF 1050	1500	0.80	0.689		
			HF 1050	1500	1.50	0.968		
114	50.1 3002 Reinf - Shock Tower Frt	S	DP 500	980	2.00	0.69	0.69	
115	50.1 3003 Reinf - Shock Tower Frt	S	DP 500	980	2.00	0.69	0.69	
116	50.1 2112 Panel - Cargo Box Side RH	S	Mild 140	270	0.50	0.611	0.611	
117	50.1 2113 Panel - Cargo Box Side LH	S	Mild 140	270	0.50	0.611	0.611	
118	50.6 6354 Reinf - FBHP RH	S	DP 700	1000	0.80	0.453	0.453	
119	50.6 1354 Reinf - FBHP LH	S	DP 700	1000	0.80	0.453	0.453	
Total							187.7	187.7

Table 2.4: FSV BEV Bill of Materials (BOM) (contd.)

2.3 FSV Program Achievements

The weight of the other FSV variants body structures are also significantly low: the Plug-in-Hybrid Electric Vehicle (PHEV₂₀) is 176.4 kg and the Fuel Cell Electric Vehicle (FCEV), PHEV₄₀ is 200.8 kg. The PHEV₂₀ body structure is shown in Figure 2.4, and the FSV-2 body structure is shown in Figure 2.5.

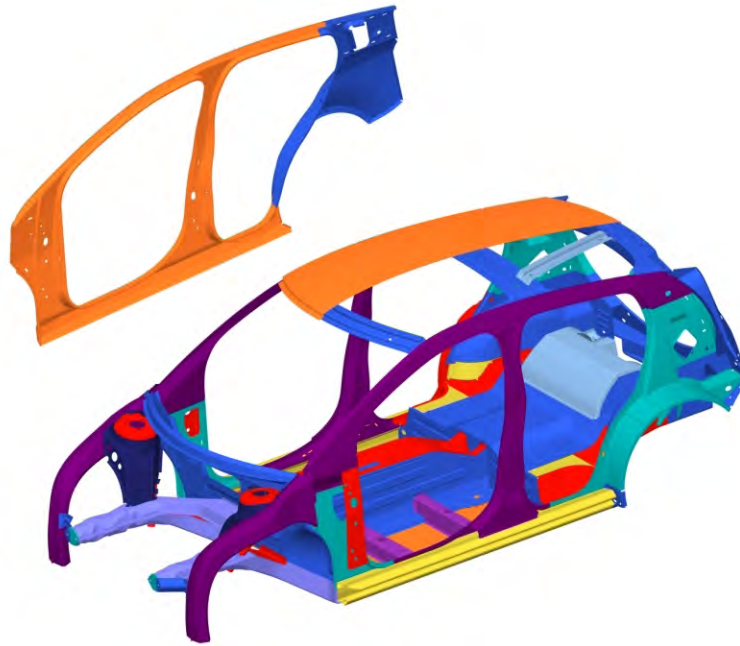


Figure 2.4: FSV-1 PHEV₂₀ body structure

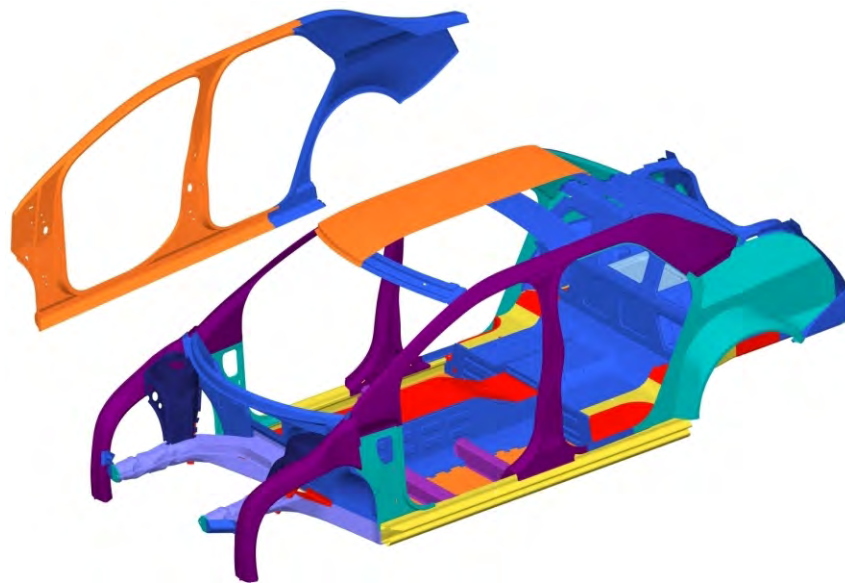


Figure 2.5: FSV-2 (FCEV and PHEV₄₀) body structure

The BEV Body-In-Prime (BIP) mass is lower than the ULSAB-AVC benchmark vehicles with the exception of the 2003 Peugeot 206. However the 2003 Peugeot is not designed to meet year 2020 crash standards as the BEV does. Furthermore, the BEV has the additional mass of a battery tray. When all regulatory standards are considered, the BEV BIP mass is remarkable. See Table 2.5 and Table 2.6 for the FSV BIP component mass and the FSV-BEV comparison, respectively.

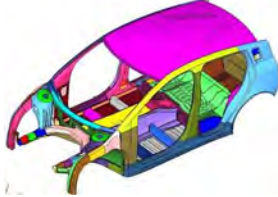

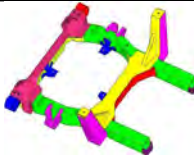




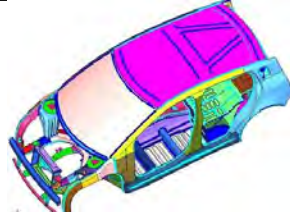
S.No.	Assemblies	Total mass of the assembly (kg)	Illustration
1	Body Structure	187.7	
2	Battery Tray	12.0	
3	Engine Cradle	13.9	
4	Rear Bumper	3.2	
5	Front Bumper	5.9	
6	Radiator Support	1.8	
7	Windshield	15.0	
	BIP	239.5	

Table 2.5: *Body-In-Prime (BIP) description*

2.3 FSV Program Achievements

	FSV-BEV (kg)	VW Polo (kg)	ULSAB-AVC				
			C-Class	PNGV	Ford Focus	Peugeot 206	Audi A6
Model Year	2020	2010	2004	2004	2005	2003	
Body Structure w/Paint		242.5			294.5	220	347.5
Body Structure minus Paint	187.7	231.0	201.8	218.1	282.5	208.0	335.5
Engine Cradle	13.9	10.5	44.2	44.2	19.3	12.4	14.1
Bumper Beam Front	5.9	7.5	4.58	4.58	9.6	1.45	4.3
Bumper Beam Rear	3.2	4.7	3.4	3.9	4.6	n/a	4.5
Windshield	15.0	11.1	9.7	9.7	13.2	15.4	13.0
Battery Tray	12.02						
Radiator Support	1.83						
Total	239.5	264.9	263.7	280.5	329.2	237.2	371.3

* Assuming paint & Sealer is 12kg

ULSAB-AVC C-Class benchmark vehicles were the Ford Focus & Peugeot 206
 ULSAB-AVC PNGV benchmark vehicles were the Audi A6 & DaimlerChrysler E-Class
 Ford Focus and Peugeot data from A2Mac1
 ULSAB-AVC data from WorldAutoSteel (<http://www.worldautosteel.org/projects/ulsab-avc>)

Table 2.6: Body In Prime (BIP), FSV-BEV comparison

2.3.2 FSV Program Achievement #2 - Optimal Utilization of Advanced High Strength Steel Grades

The FSV body structure materials selected were chosen to meet the mass and performance targets. The FSV body structure demonstrated the best attributes of steel by an optimal utilization of advanced high and ultra strength steel grades. The materials included some grades of steel currently available but not commonly used in auto bodies. The BEV steel grade distribution is shown in Figure 2.6 (the color scheme of the parts shown represent the color coding of the material classification chart as shown in Table 2.7). The FSV uses high strength and ultra high strength steel for more than 97 percent of the body structure to improve structural performance and reduce mass.

Steels: corresponding metallurgical classes	Color Code	BEV Mix (%)
Low Strength Steels: Mild Steels		2.6
High Strength Steels (HSS): HSLA, BH		32.7
DP 500, 600		11.8
DP 800		9.5
DP 1000		10.0
TRIP		9.5
TWIP		2.3
Complex Phase (CP)		9.3
Martensitic (MS)		1.3
Hot forming (HF)		11.1

Table 2.7: BEV body structure material mix

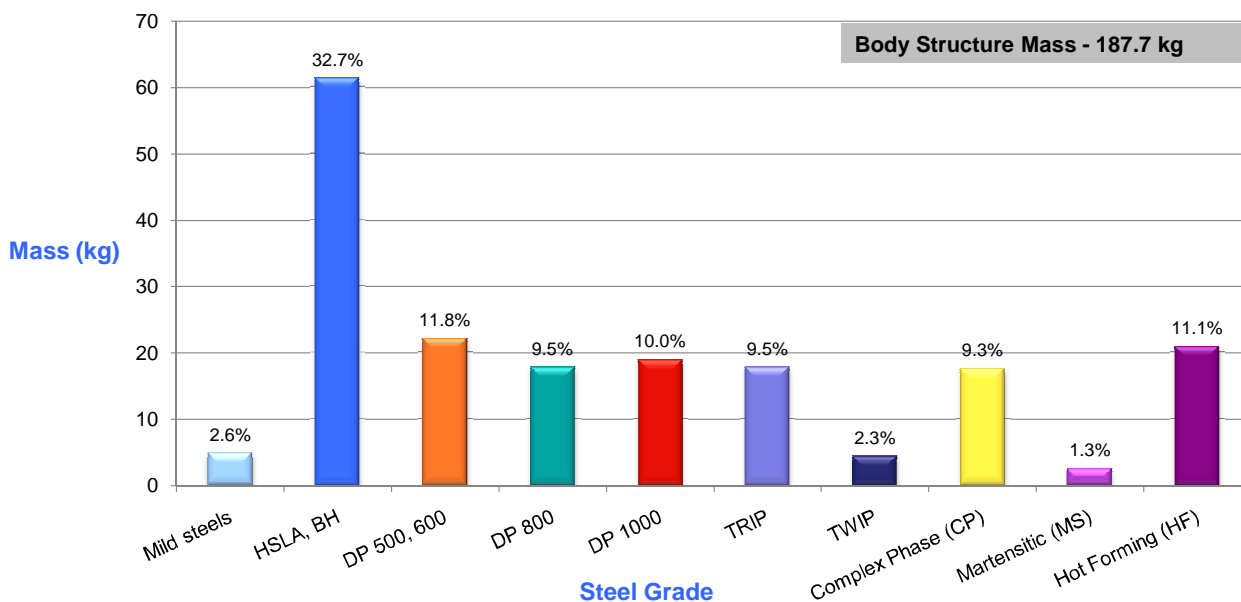


Figure 2.6: FSV-1 BEV body structure steel grade distribution

The PHEV₂₀ steel grade distribution is shown in Figure 2.7 and the FSV-2 distribution is shown in Figure 2.8.

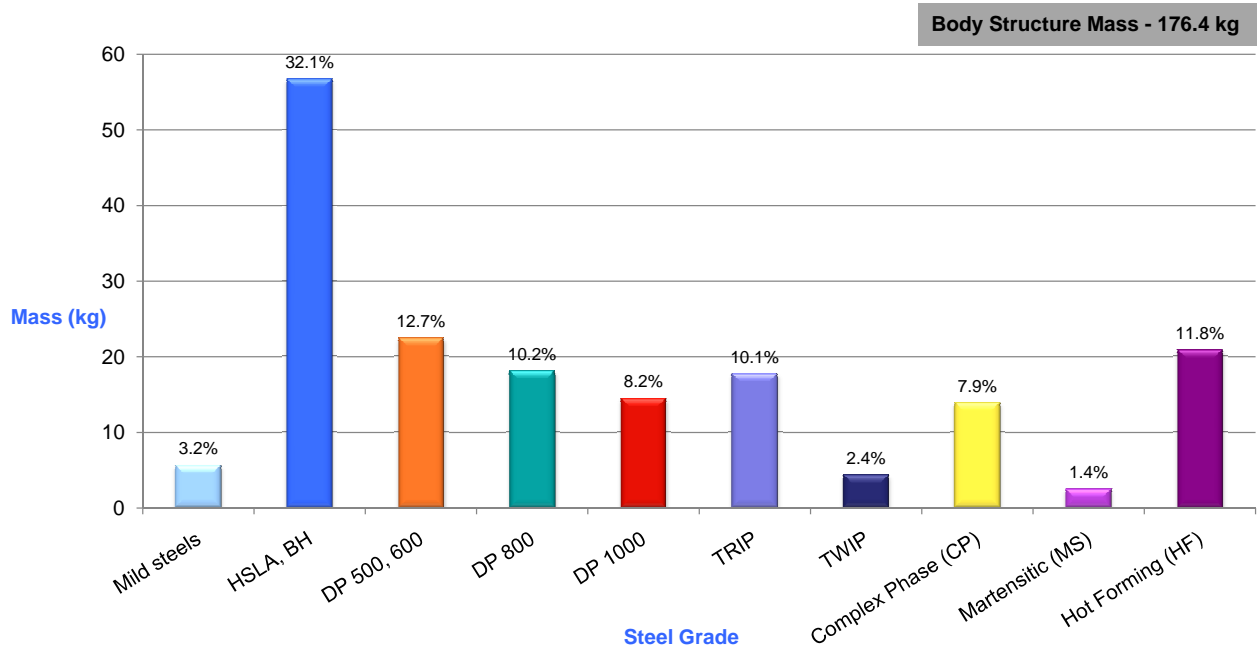


Figure 2.7: PHEV₂₀ bodystructure material mix

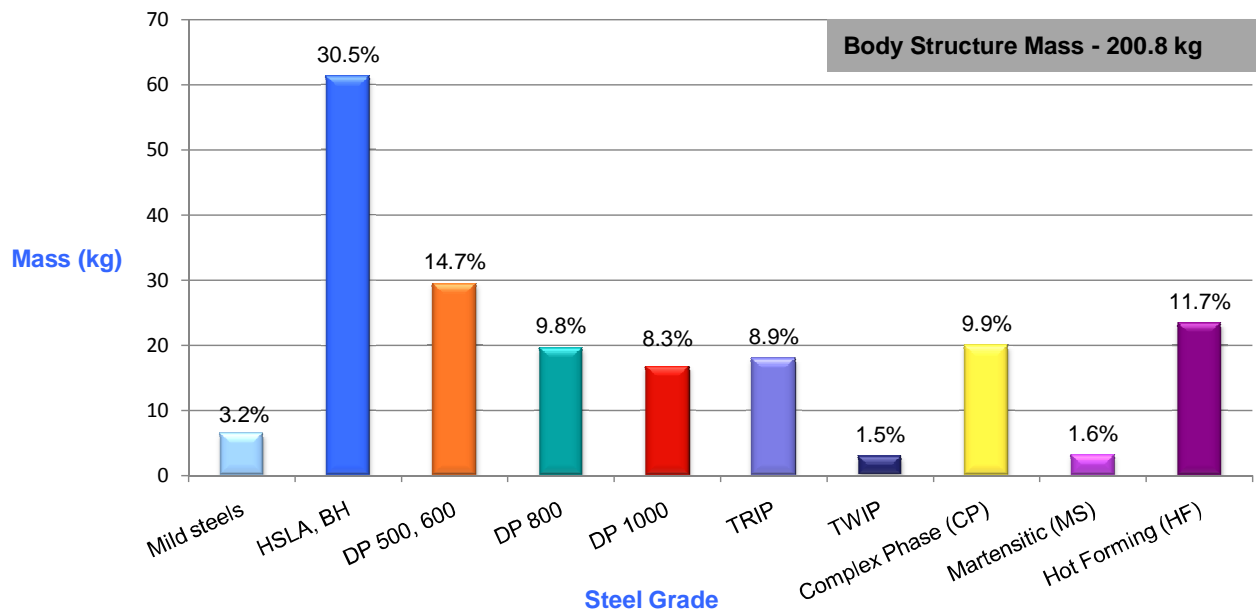


Figure 2.8: FSV-2 (FCEV and PHEV₄₀) body structure material mix

2.3.3 FSV Program Achievement #3 - Life Cycle Assessment

The significant mass reduction that can be realized by the use of AHSS has a further added advantage, when one considers the application of Life Cycle Assessment (LCA) to Green House Gas (GHG) emissions for the total vehicle life cycle. The manufacturing process of steel produces the least amount of carbon dioxide equivalent (CO₂e)^[1] GHG emissions when compared with other materials that are considered suitable for automotive structures.

Life Cycle Assessment (LCA) is a technique used to determine the environmental impacts of products, processes or services, through production, usage, and disposal. LCA is the only appropriate way to account for and reduce GHG emissions attributable to the automotive sector, because it assesses the entire vehicle life including the fuels that power it and the materials from which it is made.

Studies show that LCA of a vehicle's environmental footprint is critical for material selection decisions. Adopting a lifecycle perspective is important because the use of alternative material choices in a vehicle body structure may result in significant increases in material production emissions, thus offsetting the reduction in the vehicle use phase emissions that comes with mass reduction.

Material production for alternative material vehicles will load the environment with significantly more GHG emissions than that of a steel vehicle, as shown in Figure 2.9. Mass Reduction is therefore only one component of a comprehensive and effective greenhouse gas reduction strategy for the automotive industry.

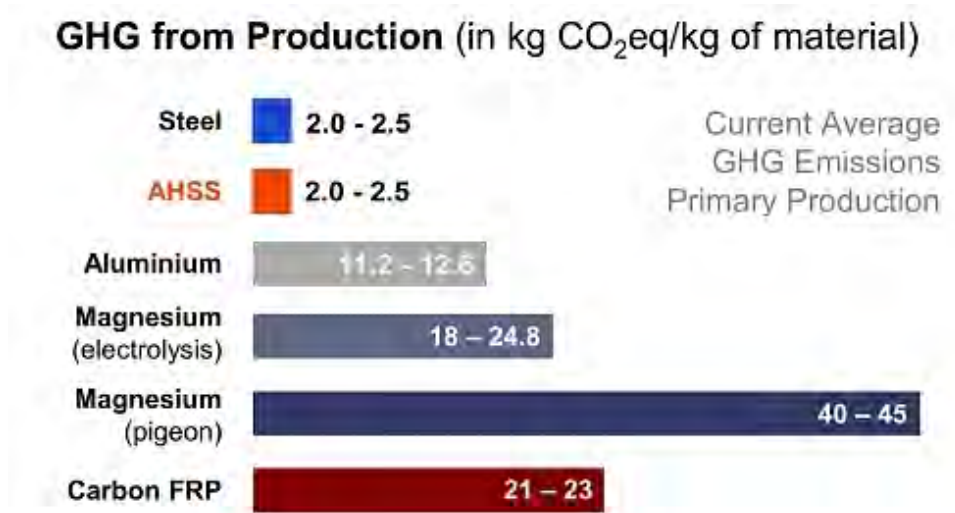


Figure 2.9: Material production Green House Gas (GHG) emissions

¹Carbon dioxide equivalents (CO₂e) is a measure of all greenhouse gases attributable to a product that affect global warming potential. Thus, CO₂e includes gases other than CO₂.

As the automotive industry's efforts to reduce CO₂e emissions are increasingly moving towards more advanced powertrains and fuel sources, material production will account for a much larger percentage of total CO₂e. This is due to the fact that these powertrains will greatly reduce the vehicle use phase CO₂e emissions, which means that material production phase emissions will make up a greater percentage of total vehicle emissions. Therefore, use of low GHG-intensive material such as steel becomes even more important.

As we consider future vehicle programs, the application of LCA allows us to explore the impact of design, material and powertrain choices on life cycle vehicle emissions. This knowledge will help derive optimized solutions for both vehicle performance, safety, and our environment.

The results as shown in Table 2.8 and Figure 2.10 vividly demonstrate that the coupling of a lightweight advanced high strength steel body structure with a battery electric powertrain results in a 40% to 50% reduction in life cycle emissions, compared to comparably sized vehicles with conventional ICE-gasoline engines.

Vehicle	Material Production (kg CO ₂ e)	Use (kg CO ₂ e)	Recycling (kg CO ₂ e)	Parts Fabrication (kg CO ₂ e)	Total CO ₂ e (kg)
FSV-BEV	2,337	13,844	(1009)	199	15,371

Table 2.8: Full Vehicle body structure LCA results

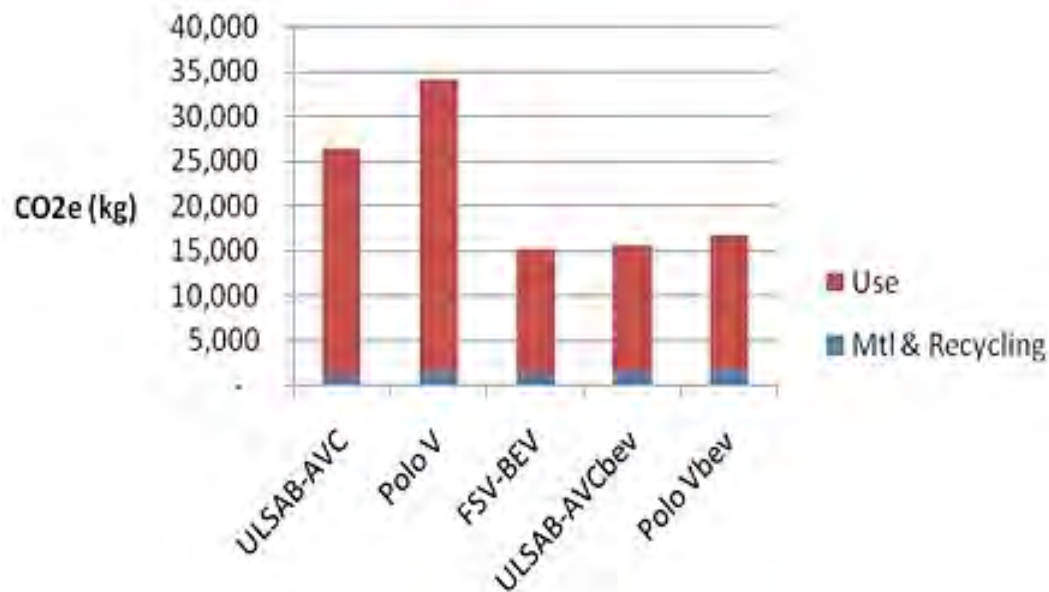


Figure 2.10: FSV BEV Life Cycle Emissions (U.S. Grid)

2.3.4 FSV Program Achievement #4 - Continued Evolution of Ultra High Strength Steel

Steel producers have always been in the forefront of efforts to answer the challenges of car makers around the world: reduce the weight of auto body structures while maintaining their performance and costs. The advantages of steel to counter this challenge have already been demonstrated in Ultra-Light Steel Auto Body (ULSAB) 1998, and ULSAB-AVC (Advanced Vehicle Concepts) 2001. However, weight reduction targets are becoming more difficult to meet while maintaining vehicle performance characteristics with ever increasing safety regulations. The FSV demonstrated the continued evolution of Ultra High Strength Steel (UHSS) to meet increasing performance requirements and higher mass reduction targets, as illustrated in Figure 2.11. The FSV uses an average 0.98 mm, 789 MPa tensile strength steel as compared to 1.16 mm, 413 MPa average tensile strength steel in the ULSAB and 1.00 mm, 758 MPa average tensile strength steel in the ULSAB-AVC, as shown in Table 2.9.

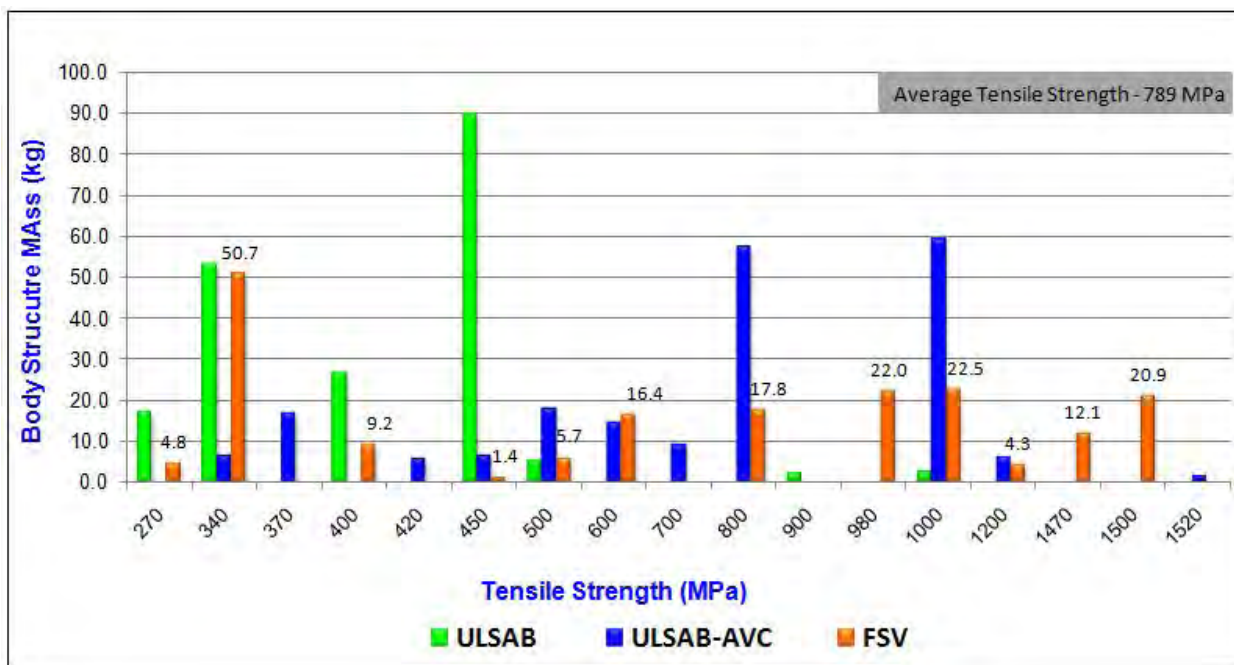


Figure 2.11: FSV materials tensile strengths compared to ULSAB and ULSAB-AVC

Vehicle	Tensile Strength (MPa)	Average Material Thickness (mm)
ULSAB	413	1.16
ULSAB-AVC	758	1.00
FSV BEV	789	0.98

Table 2.9: FSV material mix tensile strength average compared to ULSAB and ULSAB-AVC

2.3.5 FSV Program Achievement #5 - Continued Evolution of Advancements in Steel Technology

To achieve very aggressive mass reduction targets required by the automotive industry, the WorldAutoSteel companies have developed a very comprehensive portfolio of Advanced and Ultra High Strength Steels (AHSS & UHSS), for future vehicles as shown in Table 2.10 and Table 2.11. These grades are commercially available now, or are expected to be in production between 2015 and 2020. The AHSS family of products in the portfolio reflects the demand for improved materials that are required for using existing and future production methods.

Advanced and Ultra High Strength Steels (AHSS & UHSS) contribute dramatically to the lightweight FSV design. AHSS & UHSS grade development has been driven by the need to achieve better performance in crash energy management, which allows gauge reduction and lower mass. In addition, engineered AHSS & UHSS address the automotive industry's need for steels with both higher strength and enhanced formability. As an example, the DP (Dual phase) and TRIP (Transformation induced plasticity) steels may provide additional formability within the same strength range, compared to conventional steels such as High Strength Low Alloy (HSLA), steels.

Item #	Steel Grade	Thickness (mm)		Gage Length	YS (MPa)	YS (MPa)	UTS (MPa)	UTS (MPa)	Tot EL (%)	N-value Typical	Modulus of Elasticity (MPa)	Fatigue Strength Coeff (MPa) *	K Value (MPa)
		Min t	Max t		Min	Typical	Min	Typical					
1	Mild 140/270	0.35	4.60	A50	140	150	270	300	42-48	0.24	21.0 x 10 ⁴	645	541
2	BH 210/340	0.45	3.40	A50	210	230	340	350	35-41	0.21	21.0 x 10 ⁴	695	582
3	BH 260/370	0.45	2.80	A50	260	275	370	390	32-36	0.18	21.0 x 10 ⁴	735	550
4	BH 280/400	0.45	2.80	A50	280	325	400	420	30-34	0.16	21.0 x 10 ⁴	765	690
5	IF 260/410	0.40	2.30	A50	260	280	410	420	34-48	0.20	21.0 x 10 ⁴	765	690
6	IF 300/420	0.50	2.50	A50	300	320	420	430	29-36	0.19	21.0 x 10 ⁴	775	759
7	FB 330/450	1.60	5.00	A80	330	380	450	490	29-33	0.17	21.0 x 10 ⁴	835	778
8	HSLA 350/450	0.50	5.00	A80	350	360	450	470	23-27	0.16	21.0 x 10 ⁴	815	807
9	DP 300/500	0.50	2.50	A80	300	345	500	520	30-34	0.18	21.0 x 10 ⁴	865	762
10	HSLA 420/500	0.60	5.00	A50	420	430	500	530	22-26	0.14	21.0 x 10 ⁴	875	827
11	FB 450/600	1.40	6.00	A80	450	530	560	605	18-26	0.15	21.0 x 10 ⁴	950	921
12	HSLA 490/600	0.60	5.00	A50	490	510	600	630	20-25	0.13	21.0 x 10 ⁴	975	952
13	DP 350/600	0.60	5.00	A80	350	385	600	640	24-30	0.17	21.0 x 10 ⁴	985	976
14	TRIP 350/600	0.60	4.00	A50	350	400	600	630	29-33	0.25	21.0 x 10 ⁴	975	952
15	SF 570/640	2.90	5.00	A50M	570	600	640	660	20-24	0.08	21.0 x 10 ⁴	1005	989
16	HSLA 550/650	0.60	5.00	A50	550	585	650	675	19-23	0.12	21.0 x 10 ⁴	1020	1009
17	TRIP 400/700	0.60	4.00	A80	400	420	700	730	24-28	0.24	21.0 x 10 ⁴	1075	1077
18	SF 600/780	2.00	5.00	A50	600	650	780	830	16-20	0.07	21.0 x 10 ⁴	1175	1201
19	HSLA 700/780	2.00	5.00	A50	700	750	780	830	15-20	0.07	21.0 x 10 ⁴	1175	1200
20	CP 500/800	0.80	4.00	A80	500	520	800	815	10-14	0.13	21.0 x 10 ⁴	1160	1183
21	DP 500/800	0.60	4.00	A50	500	520	800	835	14-20	0.14	21.0 x 10 ⁴	1180	1303
22	TRIP 450/800	0.60	2.20	A80	450	550	800	825	26-32	0.24	21.0 x 10 ⁴	1170	1690
23	CP 600/900	1.00	4.00	A80	600	615	900	910	14-16	0.14	21.0 x 10 ⁴	1255	1301
24	CP 750/900	1.60	4.00	A80	750	760	900	910	14-16	0.13	21.0 x 10 ⁴	1255	1401
25	TRIP 600/980	0.90	2.00	A50	550	650	980	990	15-17	0.13	21.0 x 10 ⁴	1335	1301
26	TWIP 500/980	0.80	2.00	A50M	500	550	980	990	50-60	0.40	21.0 x 10 ⁴	1335	1401
27	DP 700/1000	0.60	2.30	A50	700	720	1000	1030	12-17	0.12	21.0 x 10 ⁴	1375	1521
28	CP 800/1000	0.80	3.00	A80	800	845	1000	1005	8-13	0.11	21.0 x 10 ⁴	1350	1678
29	DP 800/1180	1.00	2.00	A50	800	880	1180	1235	10-14	0.11	21.0 x 10 ⁴	1555	1700
30	MS 950/1200	0.50	3.20	A50M	950	960	1200	1250	5-7	0.07	21.0 x 10 ⁴	1595	1678
31	CP 1000/1200	0.80	2.30	A80	1000	1020	1200	1230	8-10	0.10	21.0 x 10 ⁴	1575	1700
32	DP1150/1270	0.60	2.00	A50M	1150	1160	1270	1275	8-10	0.10	21.0 x 10 ⁴	1620	1751
33	MS 1150/1400	0.50	2.00	A50	1150	1200	1400	1420	4-7	0.06	21.0 x 10 ⁴	1765	1937
34	CP 1050/1470	1.00	2.00	A50M	1050	1060	1470	1495	7-9	0.06	21.0 x 10 ⁴	1840	2030
35	HF 1050/1500												
	<i>Conventional Forming</i>	0.60	4.50	A80	340	380	480	500	23-27	0.16	21.0 x 10 ⁴	845	790
	<i>Heat Treated after forming</i>	0.60	4.50	A80	1050	1220	1500	1600	5-7	0.06	21.0 x 10 ⁴	1945	2161
36	MS 1250/1500	0.50	2.00	A50M	1250	1265	1500	1520	3-6	0.05	21.0 x 10 ⁴	1865	2021

* Un-notched specimens, FSc = UTS + 345 (Mpa)
Alternate approximation = 3.45*HB

Table 2.10: FSV materials portfolio

Item #	Steel Grade	Availability						
		HR	CR		HDG/GA/GI		EG	
		U	U	E	U	E	U	E
1	Mild 140/270	1.6 - 4.6	.35 - 3.0	.35-3.0	.35-3.0	.35-3.0	0.35 - 2.5	0.35 - 1.5
2	BH 210/340	N.A.	0.45 - 3.4	0.45 - 3.4	0.45 - 3.4	0.45 - 3.4	0.45 - 2.5	0.45 - 1.5
3	BH 260/370	N.A.	0.45 - 2.8	0.45 - 2.8	0.45 - 2.8	0.45 - 2.8	0.45 - 2.5	0.45 - 1.5
4	BH 280/400	N.A.	0.45 - 2.8	0.45 - 2.8	0.45 - 2.8	0.45 - 2.8	0.45 - 2.5	0.45 - 1.5
5	IF 260/410	N.A.	0.4 - 2.3	0.4 - 2.3	0.4 - 2.3	0.4 - 2.3	0.4 - 2.3	0.4 - 1.5
6	IF 300/420	N.A.	0.5 - 2.5	0.5 - 2.5	0.5 - 2.5	0.5 - 2.5	0.5 - 2.5	0.5 - 1.5
7	FB 330/450	1.6 - 5.0	N.A.	N.A.	N.A.	N.A.	N.A.	N.A.
8	HSLA 350/450	1.6 - 5.0	0.5 - 2.5	N.A.	0.5 - 2.5	N.A.	0.5 - 2.5	N.A.
9	DP 300/500	N.A.	0.5 - 2.5	0.5 - 2.5	0.5 - 2.5	0.5 - 2.5	0.5 - 2.5	0.5 - 2.5
10	HSLA 420/500	1.6 - 5.0	0.6 - 2.5	N.A.	0.6 - 2.5	N.A.	0.6 - 2.5	N.A.
11	FB 450/600	1.4 - 6.0	N.A.	N.A.	N.A.	N.A.	N.A.	N.A.
12	HSLA 490/600	1.8 - 5.0	0.6 - 2.5	N.A.	0.6 - 2.5	N.A.	0.6 - 2.5	N.A.
13	DP 350/600	1.6 - 5.0	0.6 - 2.5	0.6 - 2.5	0.6 - 2.5	0.6 - 2.5	0.6 - 2.5	0.6 - 2.5
14	TRIP 350/600	1.6 - 4.0	0.6 - 2.3	N.A.	N.A.	N.A.	0.6 - 2.3	N.A.
15	SF 570/640	2.9 - 5.0	N.A.	N.A.	N.A.	N.A.	N.A.	N.A.
16	HSLA 550/650	1.8 - 5.0	0.6 - 2.5	N.A.	0.6 - 2.5	N.A.	0.6 - 2.5	N.A.
17	TRIP 400/700	1.6 - 4.0	0.6 - 2.3	N.A.	0.6 - 2.3	N.A.	N.A.	N.A.
18	SF 600/780	2.0 - 5.0	N.A.	N.A.	N.A.	N.A.	N.A.	N.A.
19	HSLA 700/780	2.0 - 5.0	N.A.	N.A.	N.A.	N.A.	N.A.	N.A.
20	CP 500/800	2.2 - 4.0	0.8 - 1.8	N.A.	0.8 - 1.8	N.A.	0.8 - 1.8	N.A.
21	DP 500/800	2.5 - 4.0	0.6 - 2.0	N.A.	0.75 - 2.0	N.A.	0.6 - 1.5	N.A.
22	TRIP 450/800	N.A.	0.6 - 2.2	N.A.	0.6 - 2.2	N.A.	N.A.	N.A.
23	CP 600/900	1.6 - 4.0	1.0 - 1.8	N.A.	1.0 - 1.8	N.A.	1.0 - 1.8	N.A.
24	CP 750/900	1.6 - 4.0	N.A.	N.A.	<2.4	N.A.	N.A.	N.A.
25	TRIP 600/980	N.A.	0.9 - 2.0	N.A.	0.9 - 2.0	N.A.	0.9 - 2.0	N.A.
26	TWIP 500/980	N.A.	N.A.	N.A.	.8 - 2.0	N.A.	N.A.	N.A.
27	DP 700/1000	N.A.	0.6 - 2.3	N.A.	0.75 - 2.0	N.A.	0.6 - 2.3	N.A.
28	CP 800/1000	1.6 - 3.0	0.8 - 2.0	N.A.	0.8 - 2.0	N.A.	N.A.	N.A.
29	DP 800/1180	N.A.	1.0 - 2.0	N.A.	1.0 - 2.0	N.A.	N.A.	N.A.
30	MS 950/1200	N.A.	0.5 - 3.2	N.A.	N.A.	N.A.	0.5 - 2.5	N.A.
31	CP 1000/1200	N.A.	0.8 - 2.3	N.A.	N.A.	N.A.	0.8 - 2.3	N.A.
32	DP1150/1270	N.A.	0.6 - 2.0	N.A.	0.75 - 2.0	N.A.	0.6 - 1.5	N.A.
33	MS 1150/1400	N.A.	0.5 - 2.0	N.A.	N.A.	N.A.	0.5 - 2.0	N.A.
34	CP 1050/1470	N.A.	1.0 - 2.0	N.A.	1.0 - 2.0	N.A.	N.A.	N.A.
35	HF 1050/1500							
	<i>Conventional Forming</i>	1.8 - 4.5	0.6 - 2.3	N.A.	N.A.	N.A.	N.A.	N.A.
	<i>Heat Treated after forming</i>	1.8 - 4.5	0.6 - 2.3	N.A.	N.A.	N.A.	N.A.	N.A.
36	MS 1250/1500	N.A.	0.5 - 2.0	N.A.	N.A.	N.A.	0.5 - 2.0	N.A.

* Un-notched specimens, FSc = UTS + 345 (Mpa)
Alternate approximation = 3.45*HB

Table 2.11: FSV materials portfolio (contd.)

The different grades of steel in the FSV material portfolio are shown in Table 2.12. It can be seen that the FSV utilizes several new grades of steel that were not considered in the earlier studies. Hence, the FSV demonstrated the advancements in steel technology since the completion of ULSAB and ULSAB-AVC as illustrated in Figure 2.12.

Mild 140/270	DP 350/600	TRIP 600/980	
BH 210/340	TRIP 350/600	TWIP 500/980	
BH 260/370	SF 570/640	DP 700/1000	
BH 280/400	HSLA 550/650	CP 800/1000	
IF 260/410	TRIP 400/700	MS 950/1200	denotes steel included in ULSAB-AVC
IF 300/420	SF 600/780	CP 1000/1200	denotes steel grades added for FSV
DP300/500	CP 500/800	DP 1150/1270	
FB 330/450	DP 500/800	MS 1150/1400	
HSLA 350/450	TRIP 450/800	CP 1050/1470	
HSLA 420/500	CP 600/900	HF 1050/1500	
FB 450/600	CP 750/900	MS 1250/1500	
HSLA 490/600			

Table 2.12: FSV material portfolio compared to ULSAB-AVC

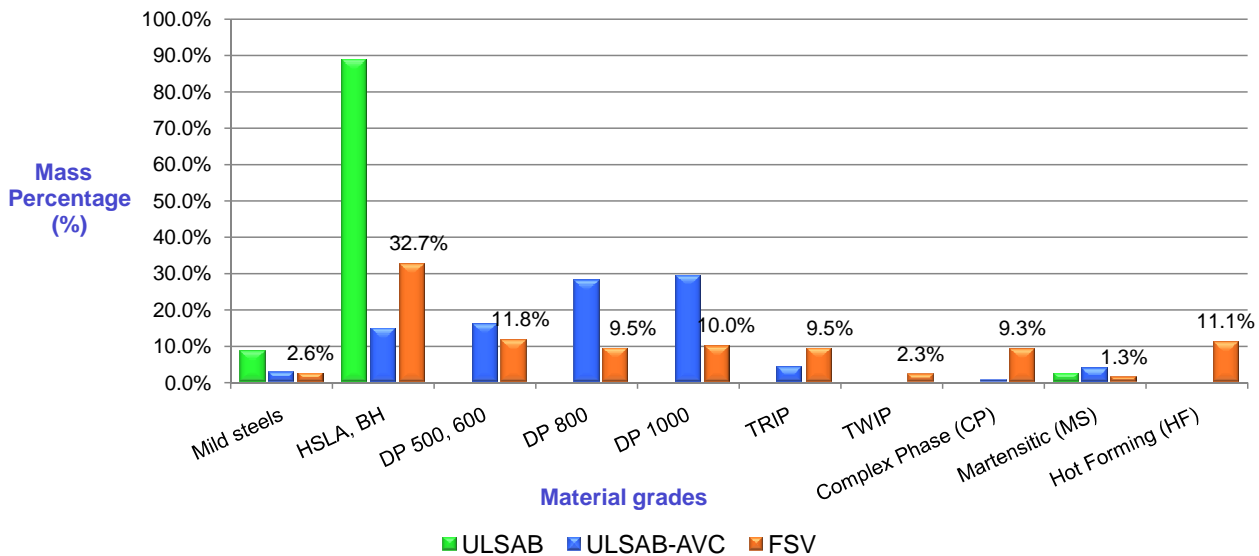


Figure 2.12: FSV material mix compared to ULSAB and ULSAB-AVC

2.3 FSV Program Achievements

2.3.6 FSV Program Achievement #6 - Continued Innovation of Advancements in Steel Technology

Further mass reduction potential of AHSS is realized by use of advances in steel availability in the forms of:

1. Hot Stamping
2. Laser Welded Blanks (LWB)
3. Laser Welded Coils (LWC)
4. Tailor Rolled Coils (TRC)
5. Tubes:
 - Conventional tubes (single thickness and grade)
 - Tubular blanks (i.e. laser welded tubes), these can be either from conventional blanks, tailor rolled blanks or laser welded blanks

The FSV body structure consists of parts that require laser welded blanks, which enable the design engineer to allocate the specific steel grade/gauge attributes as needed within a part, thereby removing mass that does not contribute to performance. The FSV body structure also consists of several hot stamped parts. Through the use of hot stamping, complex shapes can be manufactured with very high tensile strengths (1500 to 1600 MPa). Rollforming technology was also considered for some of the unique section profiles and steel grades derived using the optimization methodology.

The FSV manufacturing processes breakdown is shown in Figure 2.13.

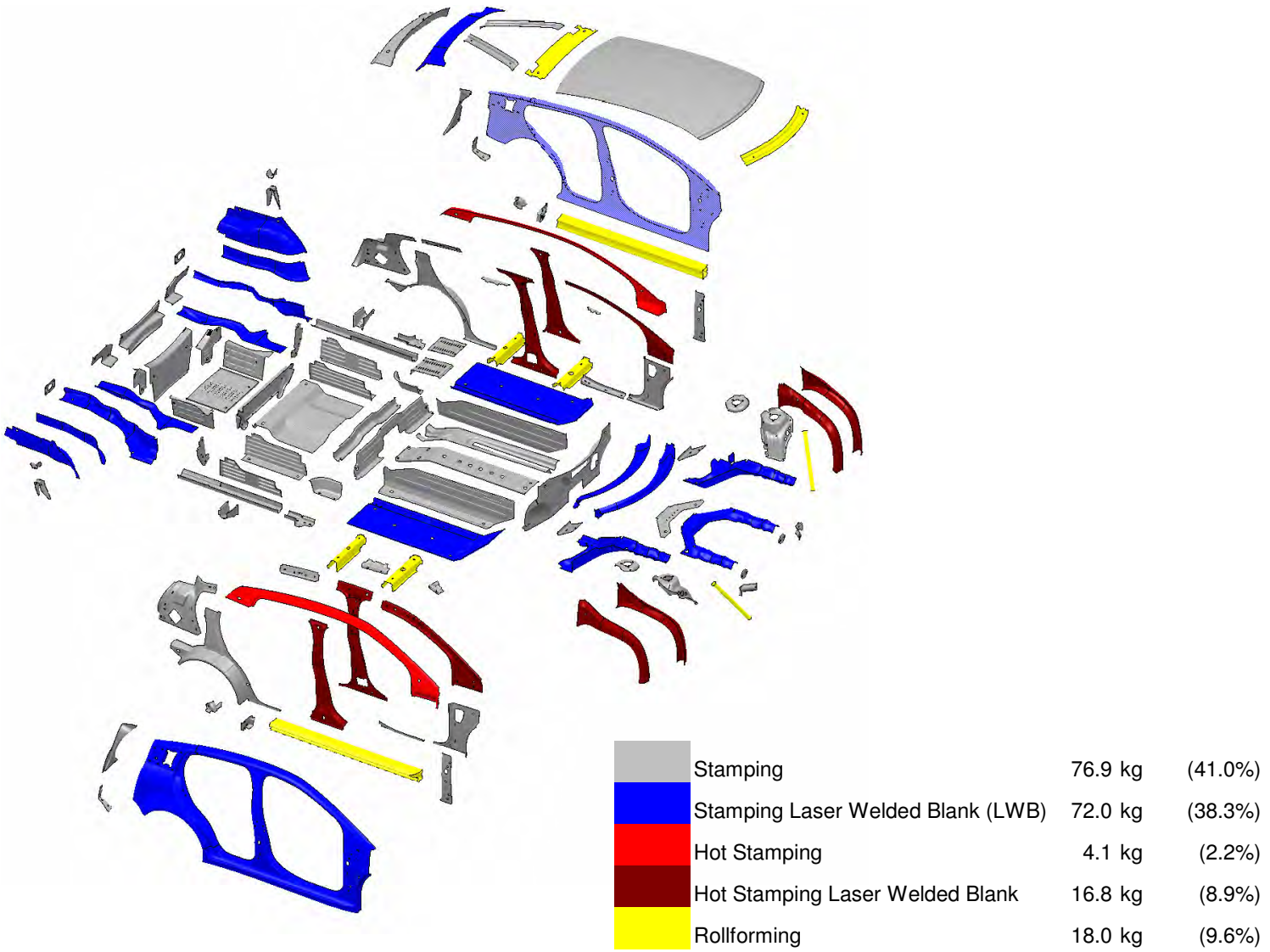


Figure 2.13: FSV manufacturing processes breakdown

2.3.7 FSV Program Achievement #7 - Design Innovation that Exploit the Versatility of Steel

The body structure of the FSV BEV is designed with very efficient load paths that were identified through the application of a unique design and optimization methodology. The front end of the BEV takes full advantage of the smaller package space required for the electric drive motor as compared with a typical Internal Combustion Engine (ICE) and transmission package. The additional packaging space allows for straighter, fully optimized front rails with larger sections as shown in Figure 2.14 and Figure 2.15. The front rails load path 1, curved shotguns load path 2 and the motor cradle load path 3, work together to manage frontal crash events with minimal intrusions into the passenger compartment.

With the availability of several high strength grades of steel with higher elongation, the complex geometric sections determined through computer geometry optimization, can be manufactured using laser welded blanks with the following three manufacturing options and materials:

1. Hot Stamping with tailor quenching - HF 1050/1500 grade of steel
2. TWIP 500/980 grade of steel
3. TRIP 600/980 grade of steel

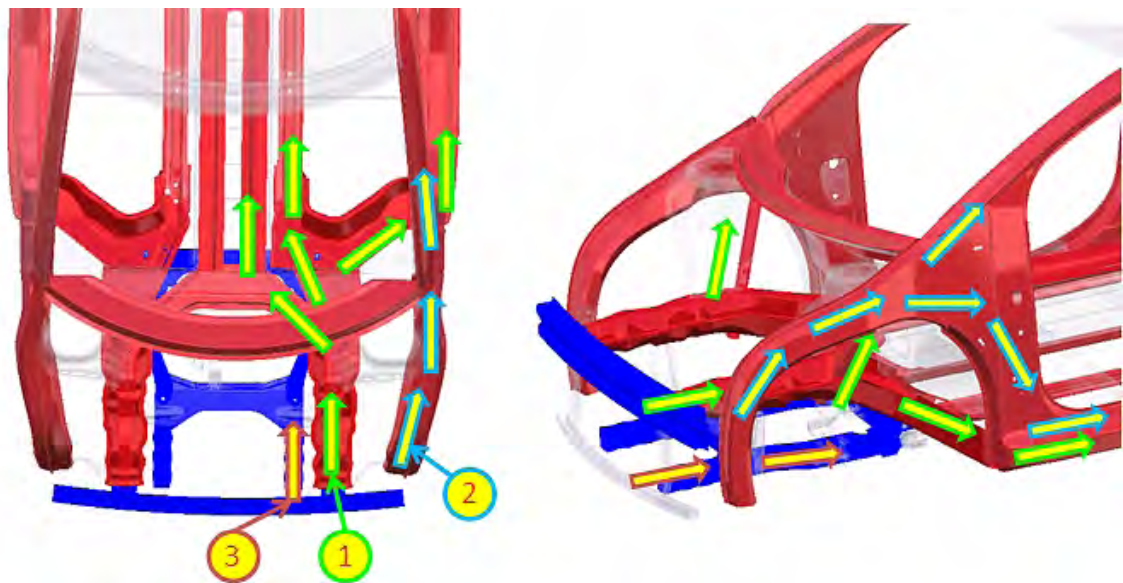


Figure 2.14: BEV front end rails, curved shotguns and motor cradle

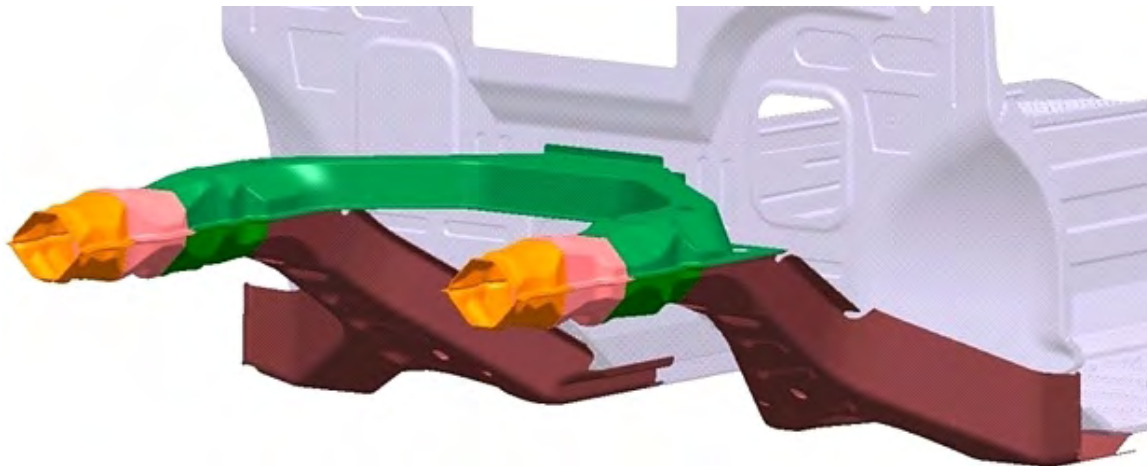


Figure 2.15: BEV front end optimized rails

The loads from the front rails illustrated in Figure 2.14 (load path 1), are reacted by a tripod construction through the rocker section, base and top of the tunnel. To stabilize the rear of the rails, an additional load path is introduced behind the shock tower to direct the loads into the base of the 'A-Pillar'. The BEV requires a deep tunnel to house the 30 kWh (end of life) battery pack. The top and bottom of the tunnel structure, when combined with the bolt-on 207 kg, battery pack, acts as a structural "backbone" of the vehicle structure.

The energy absorption of the front end is further enhanced with the addition of distinctively curved upper shotgun members as shown in Figure 2.14, load path number 2. These members absorb a significant amount of energy during frontal impact (USNCAP). The shotguns inner and outer panels also take advantage of high strength grades of steel for manufacturing options similar to the front rails. The motor mounting cradle shown in blue in Figure 2.14, load path number 3, is also designed to absorb energy during frontal crash load cases as well as support the motor assembly and front suspension.

With the combination of the three active load paths, the deceleration pulse of the structure can be tailored to achieve a more aggressive front end structure during the 0 to 30 millisecond crash time frame and then is reduced to a normal level during the 30 to 60 millisecond time frame when the occupant is interacting with the airbag. This approach has been shown to be beneficial for the occupants of smaller vehicles when involved in frontal crashes with larger vehicles [2]. The deceleration pulse for the BEV (US NCAP 35 mph Rigid Barrier Impact), is shown in Figure 2.16.

²ref: Jeremy J. Blum et al: Vehicle Related Factors that Influence Injury Outcome in Head-On Collisions. 52nd AAAM Annual Conference, Annals of Advances in Automotive Medicine, October 2008

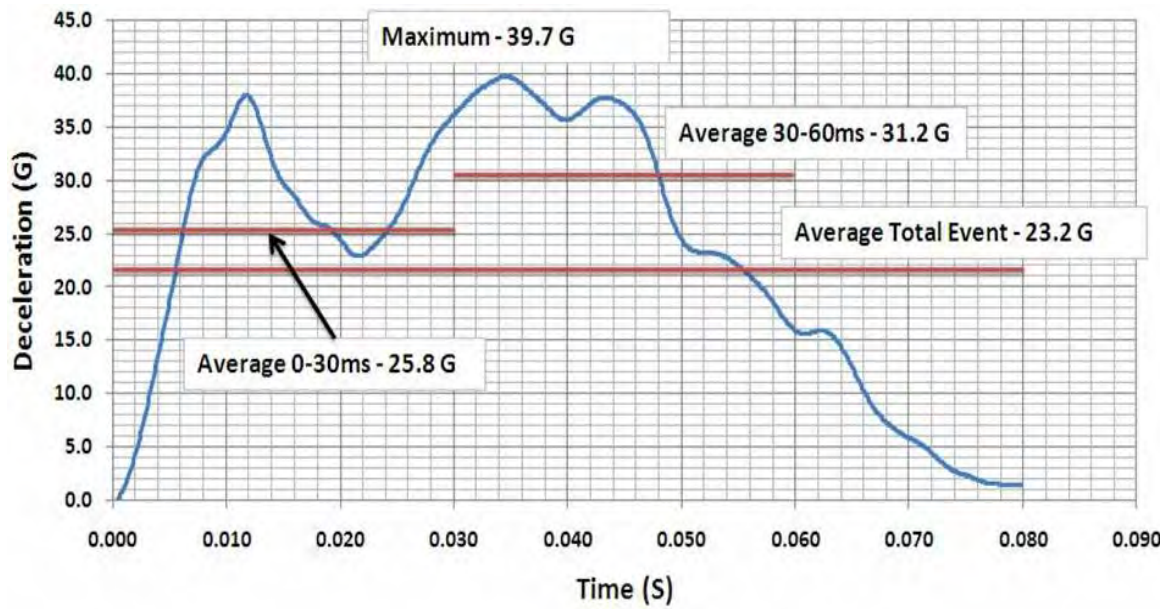


Figure 2.16: US NCAP 35 mph front rigid barrier pulse at B-Pillar

2.3.8 FSV Program Achievement #8 - Design Innovation that Exploit the Strength of Steel

The design and construction of the FSV side structure incorporates several load paths that take advantage of very high strength levels afforded by Ultra High Strength Steels (UHSS). The B-pillar Inner & Outer shown in Figure 2.17 as load path 1, are constructed from hot stamped (HF1050/1500), steel. Load path 2, of the Roof Rail Inner & Outer is also hot stamped. Through the use of hot stamping, complex shapes can be manufactured with very high tensile strengths (1500 to 1600 MPa). This level of strength is highly effective in achieving lower intrusions into the occupant compartment and strengthens the upper body structure for roll-over protection (roof test). The rocker section, (load path 3 Figure 2.17), plays a major role in side impact protection; in particular for the pole impact. The rocker is constructed from an optimized closed roll-formed section using a Complex Phase (CP) steel grade (CP1050/1470). The unique section profile was derived using the optimization methodology developed for the FSV project.

Additional side impact load paths through the body structure, make use of the front seat mounting cross members, shown as load path 4 in Figure 2.17. The two seat mounting cross members are roll formed from a very high strength martensitic grade of steel (MS950/1200). The fore-aft position of these members is aligned with bolt on cross-members that form the base of the battery structure, forming continuous load paths across the floor structure. Another unique load path for side impact is created through strengthened seat back cross tubes, shown as load path 5 in Figure 2.17. This cross car load path is at a higher vertical height and is very effective in transferring the loads through the side structure (body and door), the driver seat and top of the tunnel. This load path is further explained in Section 14.1.3.1 (CAE Analysis Results - Side Impact) of this report.

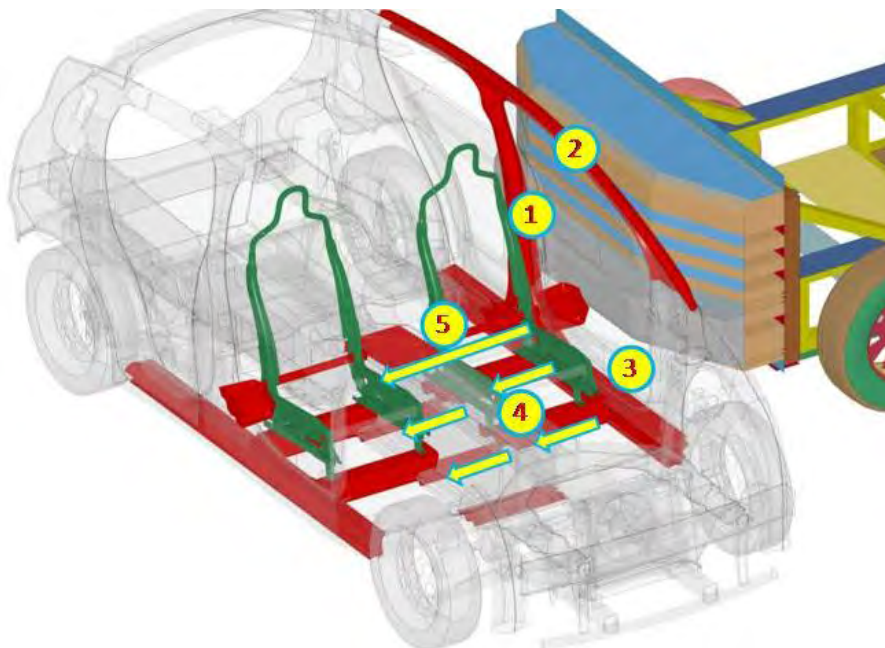


Figure 2.17: *FSV side impact structural load paths*

2.3.9 FSV Program Achievement #9 - Design Innovation that Exploit the Versatility of Steel

The design and construction of the FSV rear structure, incorporates two major load paths as shown in Figure 2.18. Load path number 1 is the rear rail section that is constructed from three LWB stampings as shown in Figure 2.19. The shape of the rear rail section was determined through optimization methodology applied to this project. To protect the battery pack during rear impact, roll formed sections were included from the bottom of the tunnel towards the rear of the vehicle under the rear floor as shown by load path number 2 in Figure 2.18. These two load paths, in combination with the rear cross-member, form a very rigid cage around the battery pack.

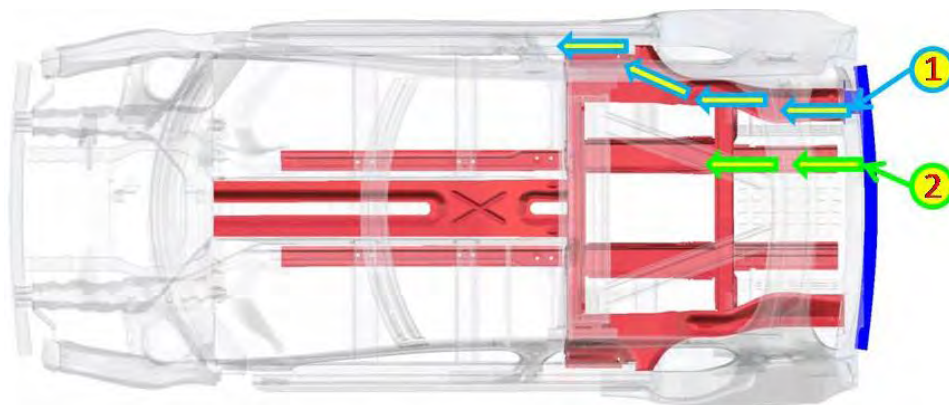


Figure 2.18: FSV rear impact structural load paths

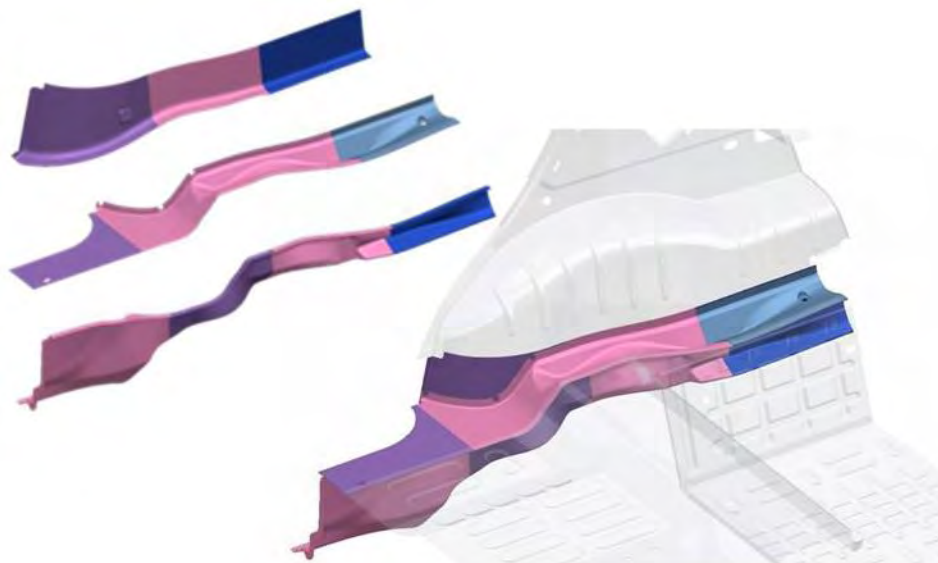


Figure 2.19: FSV rear rail - optimized sections

2.3.10 FSV Program Achievement #10 - Innovative Optimization Methodology

Structures in nature are subjected to many different load conditions, through the process of evolution structures are optimized for mass and performance. In the FSV body structure design, this innovative methodology was utilized as a basic design tool to identify the material requirement and to imitate the natural bionic structure within the vehicle packaging space. The topology optimization provided an initial structure for the FSV, subject to the different load cases: IIHS front 40% ODB, NCAP front impact, FMVSS 301 rear 70% ODB, IIHS side impact, FMVSS 214 pole impact, FMVSS 216 roof crush, bending and torsional static stiffnesses, as shown in Figure 2.20. Considering all loadcases simultaneously, the optimization determined the initial vehicle structure from the design space.

The initial topology optimization was based on a linear static analysis. The limitations of the topology optimization is later addressed by the the Low Fidelity 3G (LF3G) optimization which is a non-linear dynamic model. The geometry of the LF3G model was based on the skeleton structure developed from the initial topology optimization. The initial goal of the LF3G optimization was to define the optimal position of the structure's major loadpaths. Once located, the optimization then sought to define the approximate size and general cross-section, grade and gauge of the structure along the loadpath. The final goal of the LF3G optimization was to create a robust set of boundary conditions for the next task of the project, the sub-system loadpath optimization.

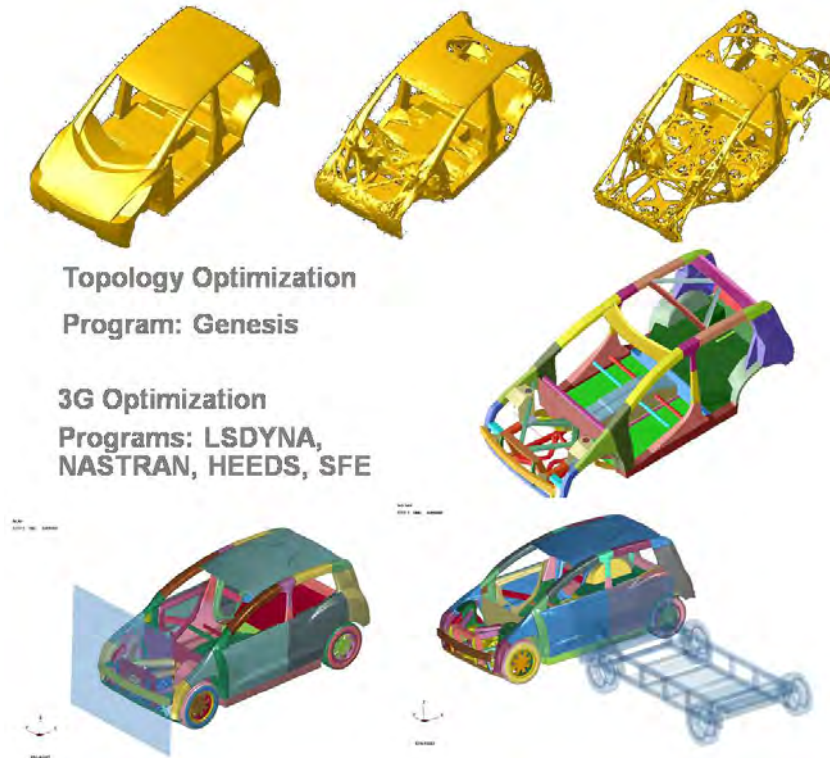


Figure 2.20: *FSV Topology and LF3G optimization*

An overview of the LF3G optimization process is shown in Figure 2.21. Once the parameterized model is created, the multi-disciplinary software, HEEDS^[3], is used to conduct the optimization. HEEDS directs the SFE software to output a model with parameters of its choice. HEEDS then directs the dynamic solver LS/DYNA^[4] to analyze the finite element model for the load cases being considered. Once the analyses are complete, HEEDS analyzes the finite element output and compares it to optimization targets. Using this information, the HEEDS software directs SFE to output an updated finite element model with another set of parameters, and the cycle begins again.

As the optimization software gains more information about the design space, it uses various algorithms to develop better and better designs that meet the performance targets while maximizing design objectives.

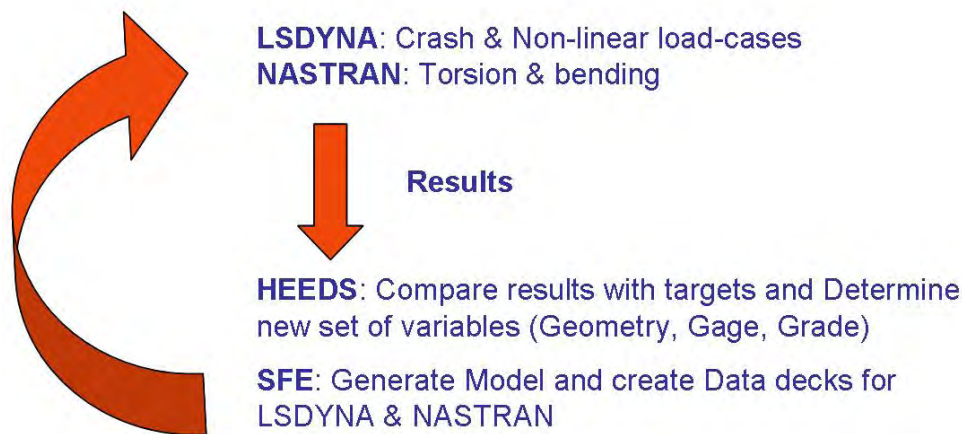


Figure 2.21: LF3G optimization process overview

For the FSV final body structure design, the sub-system optimization methodology was applied to the FSV LF3G (Low Fidelity 3G) vehicle structural sub-systems. The best combination of material grade, gauge, geometry and manufacturing process for the particular sub-system were established using the sub-system optimization methodology. The LF3G design from the T3 LF3G Optimization was used as the basis for sub-system optimization, as it was the source of boundary conditions. However, the geometry of each component used were from the interpretation of LF3G results. Performing loadpath mapping on this model, the most critical load carrying components and their controlling loadcases for the sub-system optimization were identified. The critical FSV sub-systems are shown in Figure 2.22.

³HEEDS interfaces with CAE applications to automate the design optimization process. For more information visit <http://www.redcedartech.com/>

⁴LS/Dyna is an advanced general-purpose multiphysics simulation software package. For more information visit <http://www.lstc.com/lstdyna.htm>

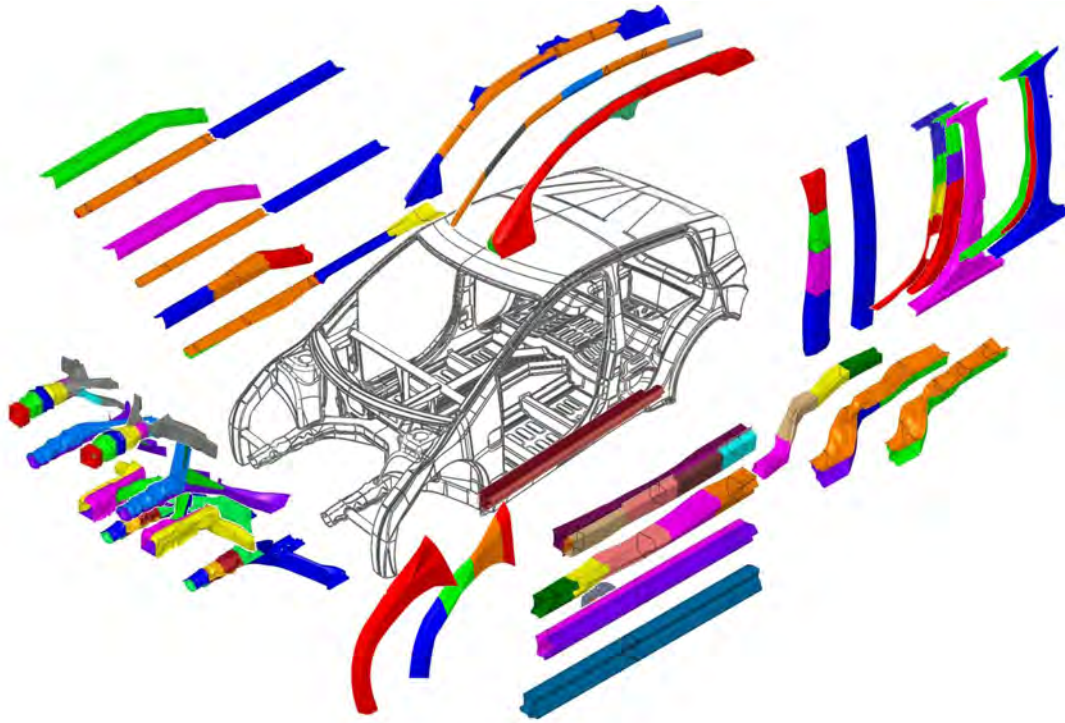


Figure 2.22: FSV Sub-Systems

2.4 FSV Advanced Powertrain Options & Performances

Assessment of year 2015 to 2020 powertrain component mass, cost and sizes were taken into account when determining the suitability of each powertrain for each vehicle size. The chosen powertrain options and performance parameters, from Phase 1, are shown in Table 2.13.

	Plug-in Hybrid (PHEV)	Fuel Cell (FCEV)	Battery Electric (BEV)
FSV 1 A-B class	PHEV 20 Electric Range - 32km (20mi) Total Range - 500km Max Speed -150km/h 0-100km/h 11-13s		BEV Total Range - 250km Max Speed -150km/h 0-100km/h 11-13s
FSV 2 C-D class	PHEV 40 Electric Range - 64km (40mi) Total Range - 500km Max Speed - 161km/h 0-100km/h 10-12s	FCEV Total Range - 500km Max Speed - 161km/h 0-100km/h 10-12s	

Table 2.13: Powertrain options & performance

Detailed design and development of the Battery Electric Vehicle (BEV) with a range of 250 km was the primary focus of FSV Phase 2. Plug-in Hybrid Electric Vehicles (PHEVs) are already being introduced by many automotive manufacturers. Considering the time frame of the FSV program, the BEV was the preferred powertrain, as concluded from the Phase 1 technology assessment. The BEV was also considered to be a more challenging design for steel because it was the heaviest powertrain option; hence a solution that works for the BEV would also work for the other powertrain options.

2.5 FSV Body Structure Mass targets

The FSV BEV body structure mass target of 190 kg meets the projected year 2020 safety regulations, and is 35% lower than a conventional baseline vehicle which is the 1990's reference vehicle used in the previous WorldAutoSteel vehicle program, ULSAB-AVC. ULSAB-AVC achieved a 25% mass reduction. Hence, the FSV program extends mass reduction beyond what has yet been achieved with steel.

Compared with a modern 2010 vehicle (e.g. VW Polo), with a powertrain mass of 233.1 kg and FSV with a powertrain mass of 328.9 kg, the targeted FSV year 2020 body structure is 41 kg lighter. The FSV reference vehicle is a VW Polo, because it is of comparable size and is a best-in-class vehicle which won the European Car Of The Year award for 2010.

2.6 Phase 2 Summary

2.6.1 Overview

An overview of the FSV design process is shown in Figure 2.23. The Phase 2 activities are covered by the tasks, T1 through T6, as illustrated in the figure.

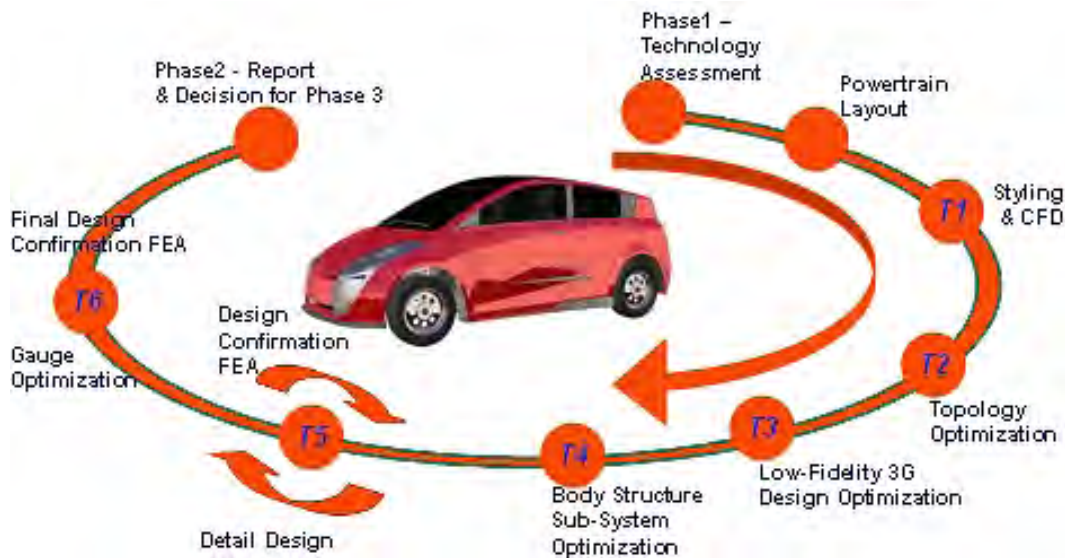


Figure 2.23: Phase 2 design process

2.6.2 T1 - Styling and CFD

After the Phase 1 technology assessment, a powertrain packaging study combined with a study of the interior occupant space was used to establish a styling theme on which the original FSV-13D surfaces were based. The styling of a vehicle combined with other external features and airflow through the motor compartment has a significant influence on its aerodynamic drag, which in turn determines the fuel consumption and CO₂e emissions of the vehicle.

The initial styling of the FSV project is shown in Figure 2.24.


Figure 2.24: FSV-1 baseline CFD Model

The initial styling shown above was subjected to detailed Computational Fluid Dynamic (CFD) simulation to predict and minimize the aerodynamic drag. The CFD process simulates the wind tunnel testing. Aerodynamic drag and vehicle stability at high speed is normally assessed initially using scale models. Full size models, in a wind tunnel, are used for a detailed assessment. The results were used to enhance the vehicle styling and other external features that reduce the aerodynamic drag and improve the vehicle stability.

Aerodynamic studies on the FSV focused on three major areas:

1. Coefficient of drag (C_D)
2. Coefficient of lift (C_L)
3. Optimum flow rate through the motor compartment

Table 2.14 shows the final results of the aerodynamic studies on the FSV-1 model.

The C_D value of 0.354 for the original FSV styling model is 42% higher than the required C_D target of 0.25. Through various incremental design changes, the C_D value was reduced to 0.237 for the final proposed style, including rear tire covers. The new FSV styling model reduces both drag and lift coefficients to 0.237 and 0.073, respectively. The C_D value of 0.237 for the FSV compares to a typical value of 0.31 for an A/B class vehicle. Final styling image for the latest FSV vehicle is shown in Figure 2.25, without rear fender skirts, which increases the C_D to 0.252 but could possibly be more appealing to buyers in this vehicle segment.

Model	Drag Force (N)	Lift Force (N)	Drag Coefficient	Lift Coefficient
FSV baseline CFD Model	485	-113	0.354	-0.082
Latest FSV styling model	325	101	0.237	0.073

Table 2.14: FSV-1 aerodynamic final results summary



Figure 2.25: Latest FSV-1 BEV styling

2.6.3 T2 - Topology Optimization

The objective of the topology optimization is to provide an initial structure for the FSV, subject to the following load cases: three longitudinal load cases (IIHS front 40% ODB, NCAP front impact, FMVSS 301 rear 70% ODB), two lateral load cases (IIHS side impact, FMVSS 214 pole impact), one vertical load case (FMVSS 216 roof crush using the IIHS 4*strength-to-weight ratio), bending and torsional static stiffnesses. Considering all loadcases simultaneously, the optimization will determine the initial vehicle structure from the design space.

From a finite element mesh that represents the blocked out structural design space, the volume within which structure can exist, the topology optimization eliminates elements thus revealing the optimal structure. The decision to remove an element is made based on its strain energy for the given loading condition, thus effectively eliminating structure that is carrying the least amount of load, while retaining structure that is most effective. The target reduction or mass fraction is defined as a goal for the optimization. For this analysis the topology optimization was run at 30%, 20% and 10% mass fractions. That is 70%, 80% and 90% of the mass was eliminated from the original design space.

The 30% and 10% mass fraction from the initial vehicle structure design space is shown in Figure 2.26.

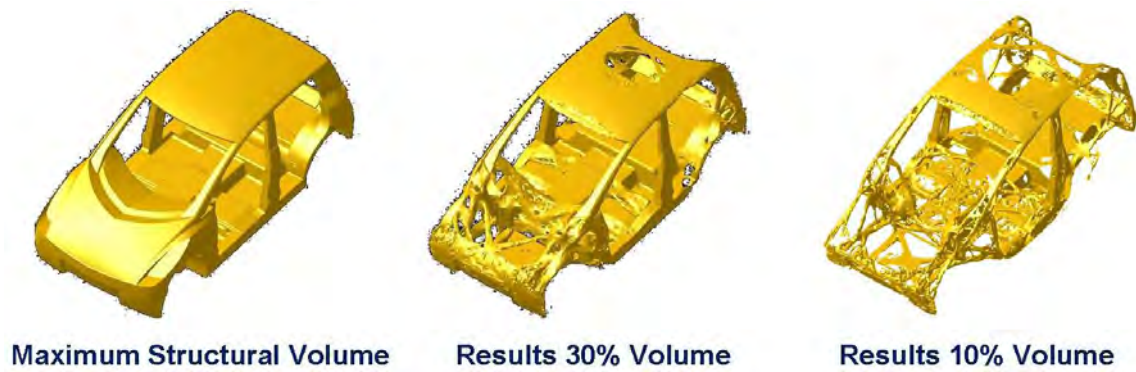


Figure 2.26: *Topology Optimization Overview*

With the results obtained from the topology optimization, the geometry was manually interpreted into a CAD model using engineering judgment. This model represents the initial skeleton geometry of the FSV shown in Figure 2.27 and will form the basis of the next step in the optimization process.

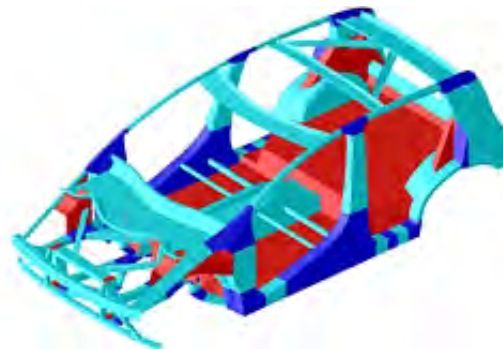


Figure 2.27: *Topology Optimization Result - Interpreted CAD Model*

2.6.4 T3 - Low Fidelity 3G (Geometry, Grade & Gauge) Optimization

Though the topology optimization was able to provide an initial starting point for the FSV's geometry, it is limited by the static approximation of dynamic crash loads and it is unable to consider grade and gauge variations of the sheet metal within the structure. Thus the initial selections of grade and gauge were based on engineering judgment and experience. Further refinement of these choices were addressed by the Low Fidelity 3G (Geometry, Grade & Gauge) (LF3G) optimization.

LF3G design addresses topology and a rough estimate of grade, gauge and geometry (section) in the dynamic domain and is intended to provide a starting place for detailed design which will address manufacturing, joint design, and local section geometries. For example most sections are modeled as rectangular hollow tubes. Such sections are not necessarily efficient structures and as a result the LF3G design is very heavy at 287 kg. However, the load paths established by the LF3G results are very efficient and will enable an overall efficient structure in the remainder of the design development.

The final FSV body structure attained from the LF3G optimization is shown in Figure 2.28. The baseline model is also shown in the background for a comparison.

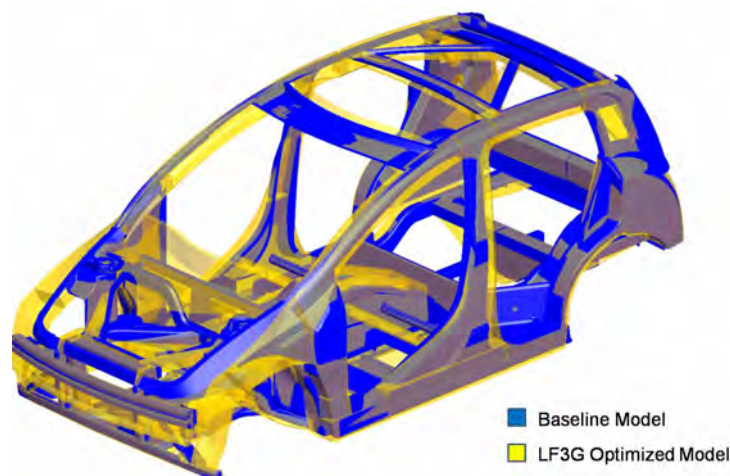


Figure 2.28: LF3G final result

2.6.4.1 LF3G Results Interpretation to Baseline Body Structure Design

The structural load paths, section sizes and section positions, represented by the LF3G optimized geometry (Figure 2.28) are optimized for topology, and a rough estimate for topography to meet global stiffness and crash performance targets. This model does not, however, represent section shapes that can necessarily be manufactured and assembled from sheet steel, nor are they structurally efficient from a topography perspective. To assist with the interpretation of the design optimization results, the program requires a reference body structure representative of a typical state of the art body structure applied to the LF3G architecture.

The LF3G topology, grade, gauge, and geometry combined with engineering judgment of current benchmarked body structure designs are used to create the required reference body structure. This reference assumes typical manufacturable section and joint designs combined with extensive use of advanced high strength steels. This provides the FSV program with state of the art reference of body structure mass, sub-system mass, part count, and manufacturing costs for the comparison in the rest of the design process.

The LF3G optimized geometry was interpreted to represent a sheet steel design, which can be further used to assess and optimize various body structure sub-systems and related manufacturing processes. Side by side comparison of the first iteration of the sheet steel body structure design and LF3G geometry is shown in Figure 2.29. The interpreted design encompasses comparable sectional load paths and the necessary allowances for spot welding flanges. In this design, all the parts were assigned material grades and thicknesses based on the results from the LF3G optimization analysis and engineering judgment. This baseline sheet steel body structure is equivalent to what can be achieved using current manufacturing and assembly technologies. The mass of the baseline structure is estimated to be 218 kg.



Figure 2.29: FSV body structure comparison - Sheet Steel Design Vs. LF3G Geometry

2.6.5 T4-Body Structure Sub-System Optimization

2.6.5.1 Optimization Methodology Overview

The basic steps for the sub-system optimization are the following:

- Sub-system development and validation
- Initial design representing manufacturing approach
- Establish design space
- Parameterize geometry
- Time history, constraints and targets from LF3G
- Detailed 3G optimization; geometry (shape), grade (material) and gauge

The final design attained from the LF3G optimization was used as the basis for the sub-system optimization. The LF3G results were also the source of the boundary conditions.

Loadpath mapping was conducted on this final LF3G model to select the candidate components and their controlling loadcases for the sub-system optimization. Table 2.15 summarizes the critical components and the loadcases that will be considered as part of the sub-system optimization.

Sub-System	Loadcase				
	1	2	3	4	5
Rocker	Front NCAP	Front ODB	Rear ODB	IIHS Side	Pole
B-Pillar	IIHS Side	Roof Crush			
Side Roof Rail	Front ODB	Rear ODB	IIHS Side	Pole	Roof Crush
Rear Rails	Rear ODB	Torsional Stiffness			
Tunnel Rails	Front ODB	Rear ODB	IIHS Side	3G Jounce	
Shotgun	Front NCAP	Front ODB			
Front Rail	Front ODB				

Table 2.15: Sub-System optimization: critical components and loadcases

2.6.5.2 Optimization Objective

The optimization objective is to minimize the mass of the sub-system and simultaneously maintain the performance, so that the total strain energy in the sub-system remains the same as the sub-system in the full model LF3G for the respective loadcases.

2.6.5.3 Initial Geometry and Boundary Conditions

As shown in Figure 2.30, the initial geometry of the sub-system is obtained from the baseline sheet steel body structure (Figure 2.29), and the nodal displacement time history is used as the boundary conditions for the sub-system so that it sees the same loading as the sub-system in the full LF3G optimized model (also shown in Figure 2.29). For both models a series of common

boundaries were defined so that the appropriate time histories could be extracted from the LF3G model and applied to the sub-system model.

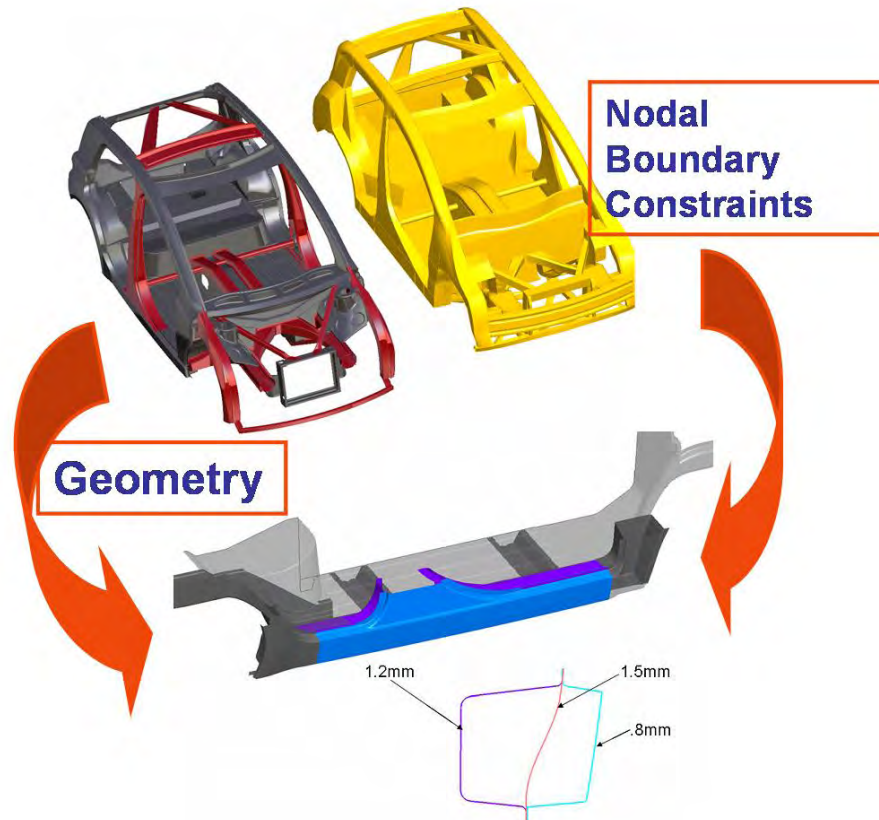


Figure 2.30: Sub-System Optimization Overview

2.6.5.4 Optimization Constraint

The energy absorbed by the sub-system in the LF3G model (full model), was used as a constraint for the optimization. For load cases that experience plastic deformation, the energy absorbed was maintained at $\pm 15\%$ of the LF3G's performance. For load cases that resulted in elastic deformation, the energy absorbed was maintained at a level less than that of LF3G's performance.

This approach is shown to ensure that the optimized sub-system designed outside of the full LF3G can be integrated back into the full structure and perform equivalent to the LF3G baseline.

The optimized stamped rocker solution from the sub-system optimization is shown in Figure 2.31, as an example. The steel grades shown in Figure 2.31 are commercially available gauges for each steel grade. The "MAT" number refers to the tensile strength of the steel expressed in MPa. The grades represent the intended strength levels only. See Table 8.1 for a listing of minimum and maximum gauge sizes for each steel material type.

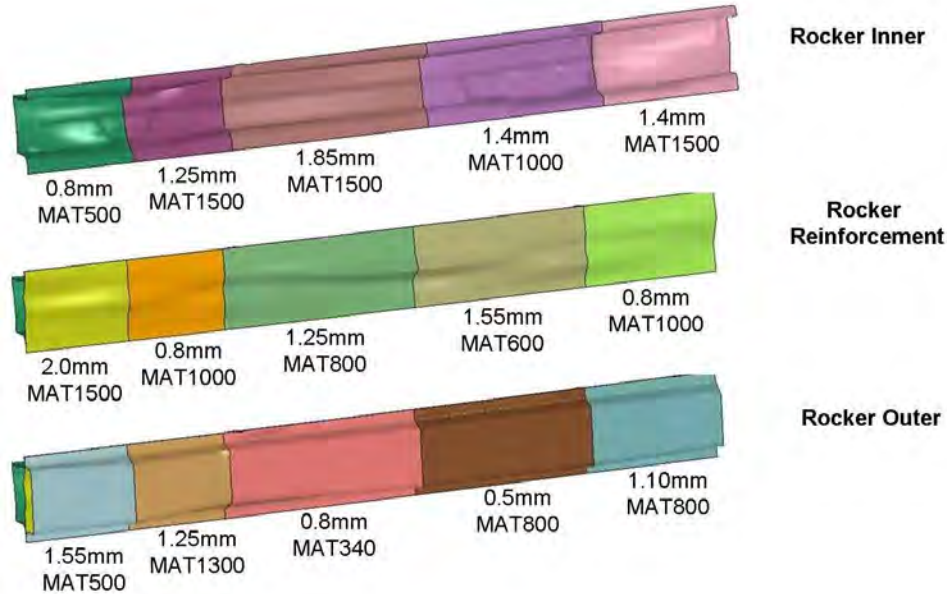


Figure 2.31: Rocker solution from 3G optimization runs

2.6.5.5 Optimization Validation

The performance of the sub-system models are validated under the loadcases considered, front NCAP, front ODB, rear ODB, IIHS side and pole impacts, to confirm that it behaved similar to the full model.

2.6.5.6 Manufacturing Interpretation

The solutions obtained from the structural sub-system multidiscipline 3G optimization runs had appropriate material strengths and gauges, optimized to give a low mass solution, that met the structural performance targets. These solutions were assessed considering the respective manufacturing technology guidelines, to ensure manufacturability of the sub-system.

For example, the rocker sub-system model was optimized for four different manufacturing methods which included stamping, roll forming, hydroforming, and aluminum extrusion, as shown in Figure 2.32.

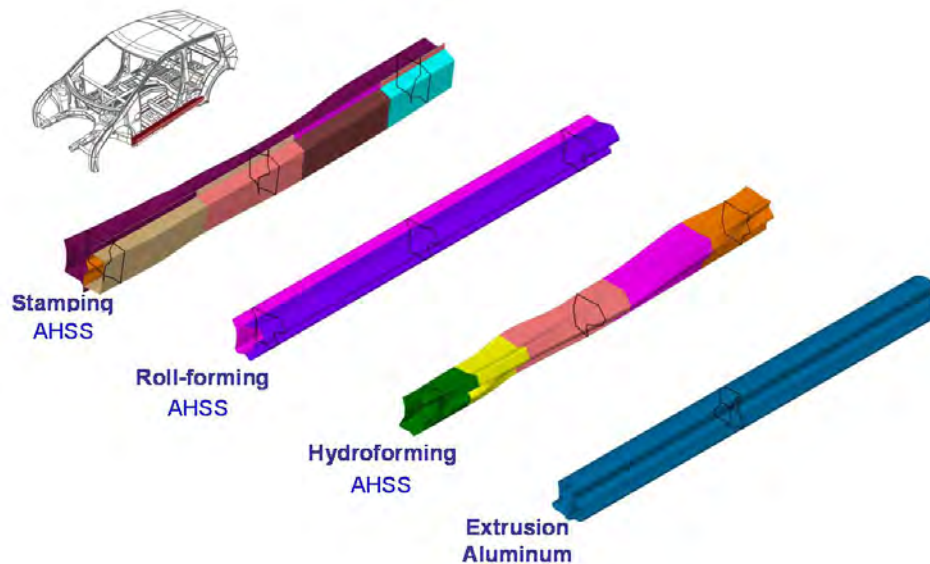


Figure 2.32: *Rocker Solutions using AHSS*

The stamping solution was further developed to consider several alternative manufacturing scenarios, such as:

1. Regular Stamping (ST)
2. Stamping Laser Welded Blank (ST LWB)
3. Stamping Tailor Rolled Blank (ST TRB)
4. Hot Stamping (HST)
5. Hot Stamping Laser Welded Blank (HST LWB)
6. Hot Stamping Tailor Rolled Blank (HST TRB)

The roll forming solution was further developed to consider:

1. Roll forming (RF)
2. Roll forming Tailor Welded Coil (RF TWC)
3. Roll forming Tailor Rolled Blank (RF TRB)

The hydroforming solution was further developed to consider:

1. Hydroforming (HF)
2. Hydroforming Laser Welded Tube (HF LWT)
3. Hydroforming Tailor Rolled Tube (HF TRT)

The manufacturing interpretations of the different sub-systems formed the basis for determining the blank size, blank mass, part mass and the other related manufacturing parameters. These parameters were used as the input for the cost model developed by EDAG, to determine the manufacturing costs of the sub-systems. The assembly costs were not assessed at this stage of the program.

2.6.6 T5-Detailed Body Structure Design

2.6.6.1 Sub-Systems Selection for BEV

The FSV sub-systems were selected giving higher priority to mass savings, while taking into consideration the high volume production feasibility. Hence, the FSV sub-systems recommendations were divided into three categories based on the level of difficulty of the manufacturing technology, and the time period during when these technologies would be more practical leading to feasible high volume production. The three categories were the following:

- 2010-2015 - Conservative approach (C)
- 2015-2020 - Mid-term approach (M)
- 2020- Beyond - Aggressive approach (A)

All of the structural sub-system solutions are considered to be viable solutions. The preferred solution depends on the criteria of the OEM and the market a vehicle is intended to fill. Possible criteria are the low cost solution, the light weight solution, the low CO₂e solution, the manufacturing capability of the OEM etc. In most cases it will be a combination of these factors plus other considerations.

A comparison of mass, cost and LCA CO₂e provide a useful tool for evaluating the relative attributes of each solution and applying a selection criteria that meets a vehicle manufacturer's and a vehicle's particular requirements.

2.6.6.2 Selection Criteria

The selection of the most appropriate sub-system was made by giving weight to these factors:

- Mass
- Cost: "technical cost modeling" approach was applied to all the parts to estimate the sub-system manufacturing costs
- Life Cycle Assessment (LCA) for CO₂e: an extended Greenhouse Gases (GHG) emissions comparison model was used to conduct a LCA assessment for the FSV using input data from Forschungsgesellschaft Kraftfahrwesen mbH Aachen (fka), University of California, Santa Barbara (UCSB) and EDAG

The masses and LCA CO₂e values are shown for the rocker sub-system in Figure 2.33.. The mass premium and CO₂e premium isolines are also shown on the graph, to account for the impact of the respective savings on cost.

There is a new aspect of vehicle design associated with advanced powertrains, such as BEVs, called the "mass/cost paradigm shift."

Contrary to conventional vehicle design where the low cost solution is often the preferred solution, the high cost of batteries increases the value of mass reduction. As an example, the FSV

2.6 Phase 2 Summary

Phase 1 Study indicated that, for the 2015-2020 timeframe, a lightweight solution saving 1 kg can subsequently reduce the battery size and cost by approximately US\$9.39. Therefore, vehicle manufacturers could employ lightweight solutions that are more costly (up to US\$9.39 per kg mass saving in this case), than those used with conventional powertrains, with the net result being break-even on the total manufacturing costs. Consequently, higher cost lightweighting solutions become attractive for more vehicle applications since their cost is offset by the reduction in battery powertrain cost.

However, when the solution is evaluated on an LCA basis, choosing the higher cost solution, though lighter, could lead to an increase in total life cycle GHG. Each graph is shown with a set of isovalue lines, enabling evaluation of solutions relative to each other on a total vehicle manufacturing cost basis. Any solutions that fall on the same isoline result are the same value due to the off-setting reduction in powertrain costs.

In a similar manner to the mass/cost paradigm shift, the cost effect of carbon (GHG emissions), reduction can be assessed. Isovalue lines can be constructed to compare the LCA GHG saved by a lightweighting solution compared to the 'carbon cost' (US\$100 per tonne used for this example ^[5]).

By conducting this comparison, a better decision can be made based on the vehicle design targets. In FutureSteelVehicle's case, a critical target is the reduction of total life cycle emissions while maintaining affordability. The preferred solution depends on the selection criteria: low cost solution, lightweight solution, or low GHG solution.

This selection criteria was applied to all of the FSV sub-systems to evaluate solutions in terms of mass, cost and life cycle emissions for the BEV.

Another aspect of this project is the inclusion of an aluminum solution as a means for the steel industry to judge the competitiveness of steel solutions in these applications. The aluminum solution was developed by EDAG, who has expertise in aluminum automotive structures, using the same aggressive design optimization and technology approach as the competing steel designs. In the case of the rocker panel, the aluminum design is not as competitive as many of the steel designs.

⁵Heritage Foundation review of Lieberman-Warner climate change legislation sites cost of CO₂e emission ranging from \$50 to \$100 per tonne (<http://www.heritage.org/Research/Reports/2008/05/The-Economic-Costs-of-the-Lieberman-Warner-Climate-Change-Legislation>)

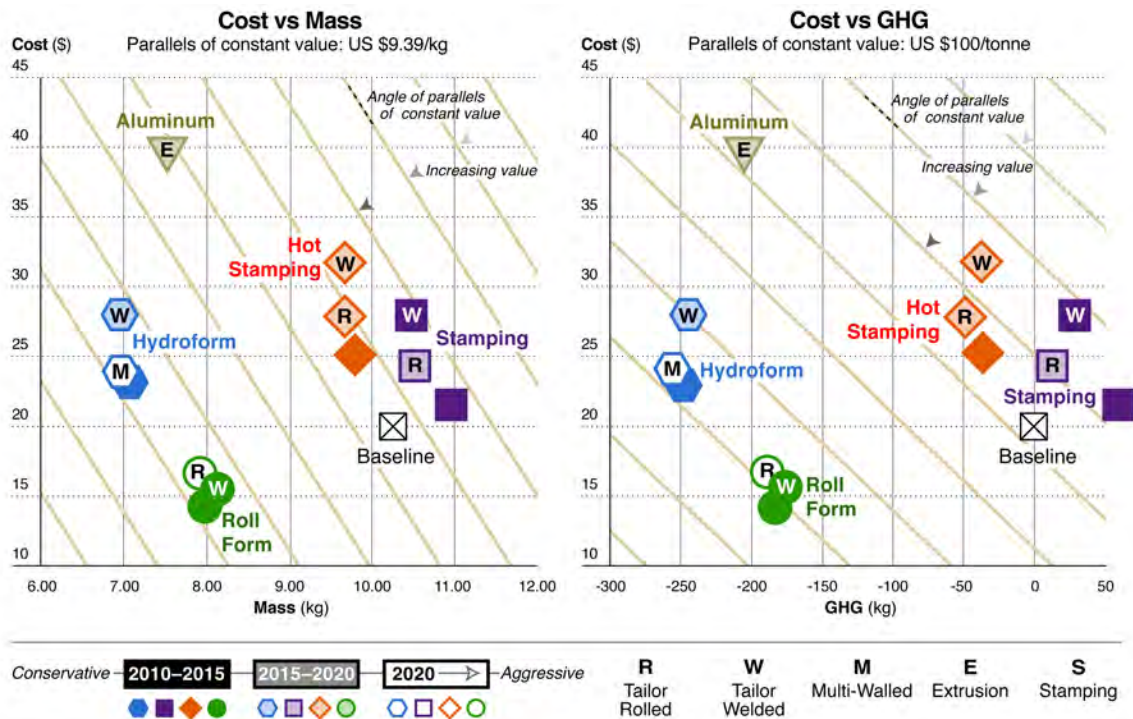


Figure 2.33: T4 comparison FSV subsystems: Rocker

The preferred solution depends on the selection criteria: low cost solution, light weight solution, or low CO₂e solution. For the BEV, the selection was made on the basis of achieving maximum mass savings, with the most viable high volume production steel technology for the years 2015 to 2020. The chosen solutions were the basis for the further tasks in Phase 2, starting with T5-detailed body structure design .

The sub-systems selected for the FSV BEV are summarized in Table 2.16. As shown in the table, all the FSV sub-systems, except the shotgun sub-system, show significant mass savings. The shotgun sub-system design required to meet the performance requirements resulted in a higher mass solution.


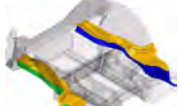




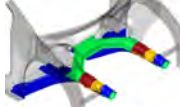
FSV Sub-system	FSV Selection (Mid-Term)	Baseline		FSV Selected Sub-system			
		Weight (kg)	Manufacturing Cost (\$ USD)	Weight (kg)	Manufacturing Cost (\$ USD)	LCA CO ₂ e Savings (kg)	Illustration
Rocker	Rollformed single thickness or rollformed TWC (with conventional outer)	10.26	\$19.99	7.98 / 8.07	\$14.27 / \$15.7	-183 / -177	
Rear Rail	Stamping LWB/TRB	6.28	\$12.73	4.98 / 5.19	\$16.86 / \$12.95	-92 / -86	
B-Pillar	Hot stamping LWB with conventional B-pillar outer	8.79	\$30.84	5.48	\$30.44	-247	
Roof Rail	Hot stamping LWB	12.73	\$27.71	9.31	\$31.71	-256	
Shotgun	Hot stamping LWB (with tailor quench)	4.2	\$14.24	4.98	\$22.11	73	
Tunnel	Open rollform	7.72	\$20.20	4.29	\$11.56	-277	
Front Rail	Stamped LWB	6.24	\$28.91	5.72	\$20.91	-65	

Table 2.16: FSV BEV sub-system selection summary

2.6.6.3 Sub-System Integration into Body Design

The selected sub-systems, as summarized in Table 2.16, formed the basis for the detailed body structure design. Even though the overall designs of the sub-systems were maintained, the designs were further adapted to integrate with the other sub-systems in the complete vehicle. There were also design changes driven by the manufacturability analysis and design for assembly con-

siderations. For example, the solution chosen from the tunnel sub-system 3G optimization was the open roll formed design, as shown in Figure 2.34. However, the formability analysis results showed that the one piece tunnel was not a feasible design. Moreover, strengthening of the side walls required additional stiffening beads, which necessitated the side walls to be designed as individually stamped parts as illustrated in Figure 2.35. Further, to reduce the assembly costs and to maintain a less complex sub-assembly/assembly structure, it was necessary to integrate the recommended tunnel design with the floor panel and the tunnel side panel. The integration was done such that the section geometry of the tunnel, attained from the 3G optimization, was maintained. Further, the side impact CAE simulations showed that it was necessary to add an additional stiffening feature along the critical loadpath within the tunnel sub-system. As shown in Figure 2.36, the tunnel bulkhead was added as an additional part to improve the side impact performance of the vehicle.

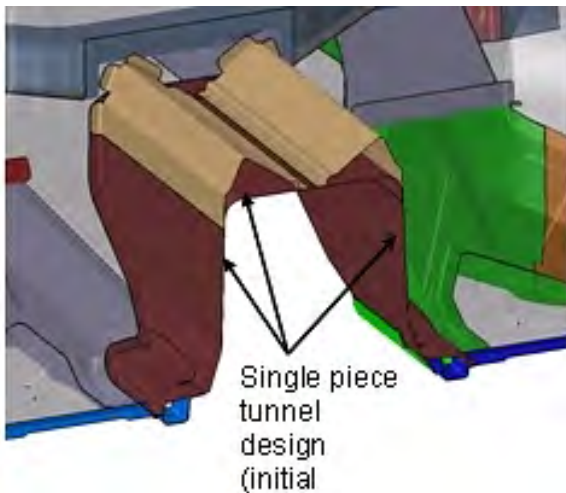


Figure 2.34: *Tunnel sub-system initial design*

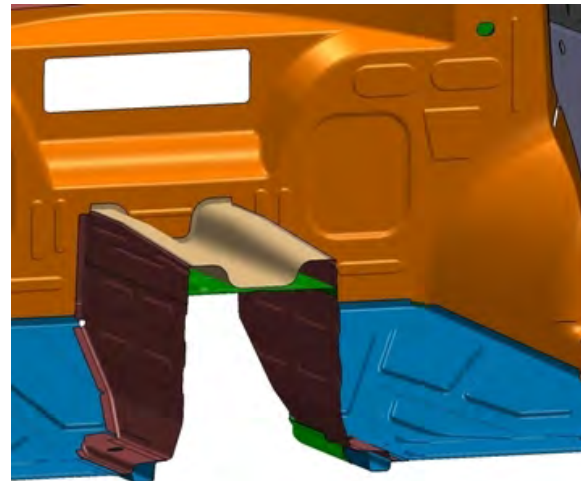


Figure 2.35: *Tunnel sub-system current design*



Figure 2.36: *Tunnel sub-system shown with the tunnel bulkhead*

2.6.6.4 Body Structure Assembly

Some of the most common assembly joining techniques were considered for the FSV program, as shown in Figure 2.37. The joining processes selected for the FSV body structure assembly are the following:

- Resistance Spot Welding
- Laser Welding
- Laser Brazing
- Roller Hemming
- Adhesive Bonding

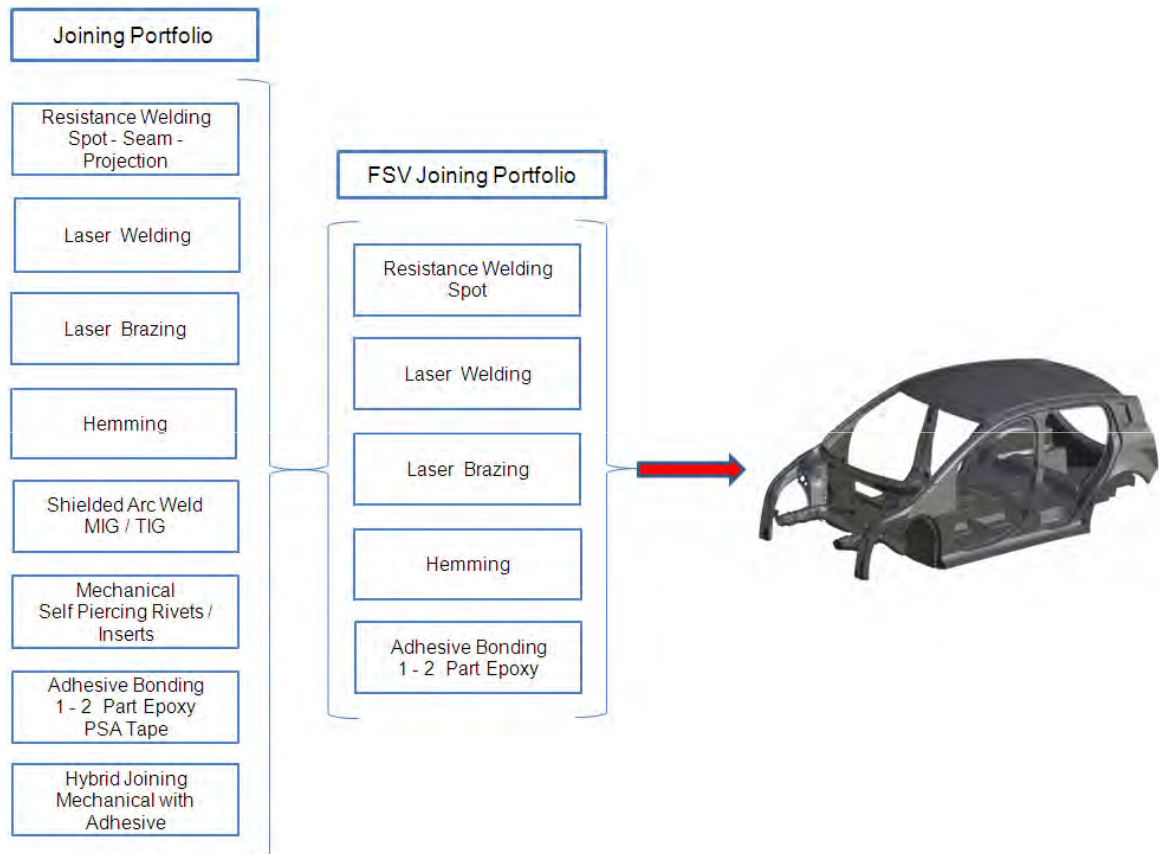


Figure 2.37: FSV assembly joining process portfolio

During the design process, various part joining methods, spot welding, laser welding and adhesive bonding were evaluated for the different combination of parts. This considered the assembly method, part material and material stack-up (2T or 3T). Refer to Section 20.2 (Appendix) for more

detailed information.

For the purpose of this program, the FSV body structure is considered without the closures/hang on parts (the hood, front/rear doors, lift gate and front fenders). To ensure the desired level of quality, both at the individual part level and assembly level, a number of quality checks need to be made. Each part and assembly will have its own dedicated checking.

The FSV program body structure assembly has been sub-divided into a number of major assemblies, as illustrated in Figure 2.38. The major assemblies in the FSV body structure are the following:

- Front Structure
- Front Floor
- Rear Floor
- Under-Body
- Body Side LH/RH
- Upper Structure and Shotgun

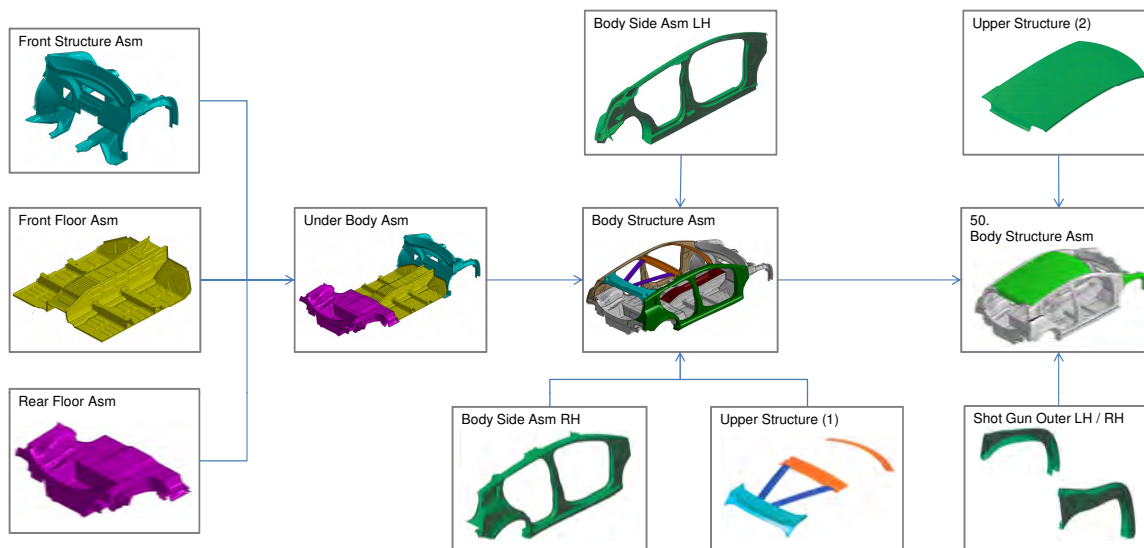


Figure 2.38: FSV body structure assembly flowchart

The completed body structure assembly would then transfer to a line where the closures, front and rear doors, hood, liftgate and the front fenders would be added. This makes the complete body structure which would then transfer to the vehicle paint shop.

2.6.7 T5-Body Structure Performance CAE Analysis

The detailed design of the FSV body structure was supported by CAE analysis, to verify the structural performance. The CAE analysis results were compared to the FSV targets to quantify the performance of the FSV body structure in terms of static stiffness, crashworthiness and durability. The FSV crash event is evaluated by structural criteria and targets that satisfy actual structural criteria or that will enable passenger safety. These structural targets are based on previous WorldAutoSteel programs (ULSAB, ULSAB-AVC, FGPC, etc.), accepted by vehicle makers and have been shared and accepted by vehicle makers in Phase 1 of the FSV program.

Additionally, the ride and handling conditions of the BEV were evaluated with a dynamic simulation analysis of the following tests:

- Fish-Hook test - Based on NHTSA statistics, the probability of rollover for the BEV is less than 10%, which corresponds to a 5 star rating
- Double Lane Change Maneuver (ISO 3888-1) - The BEV remains within the boundary lines defined in the test, which is a “Pass”

As illustrated in Table 2.17, Table 2.18 and Table 2.19, the FSV body structure meets or surpasses all the performance targets with the additional considerations of the US NCAP Full Frontal Crash as described here. This, coupled with the conservative deceleration pulse target and the 39.7 g maximum deceleration pulse achieved, led the engineering team to conclude that performance is sufficient to support achievement of a five-star safety rating in conjunction with passive safety equipment.

Analysis Type	Target	FSV Model Results
Torsion stiffness (KN-m/deg)	20.0	19.604
Bending stiffness (N/mm)	12.0	15.552
Global Modes	Target	Frequency (Hz)
Torsion	>40 Hz (both modes), separated by 3 Hz	54.8
Vertical bending		60.6

Table 2.17: FSV CAE analysis results - Static Stiffness

Analysis Type	Target	FSV Model Results
US NCAP frontal	Peak pulse range < 35 to 38 g, footwell intrusion < 100 mm	Peak pulse - 39.7 g, footwell intrusion 90.0 mm (average)
Euro NCAP/IIHS	Peak pulse (driver side) < 42 g, footwell intrusion < 150 mm	Peak pulse 41.2 g, footwell intrusion 101.0 mm (average)
IIHS Side Impact	B-pillar intrusion with respect to driver seat centerline \geq 125 mm	134 mm
US SINCAP Side Impact	B-pillar intrusion with respect to driver seat centerline \geq 125 mm	215 mm
FMVSS 301 Rear Impact	Battery remains protected and should not contact other parts after the crash	Battery is protected and there is no contact with other parts after crash
ECE R32 Rear Impact	Battery remains protected and should not contact other parts after the crash	Battery is protected and there is no contact with other parts after crash
FMVSS 214 Pole Impact	Door inner intrusion with respect to driver seat centerline \geq 125 mm	159 mm
Euro NCAP Pole Impact	Door inner intrusion with respect to driver seat centerline \geq 125 mm	169 mm
FMVSS 216a and IIHS Roof Crush	Driver and passenger side roof structure should sustain load > 28.2 kN within the plate movement of 127 mm (FMVSS 216a), > 37.5 kN (IIHS)	Sustains load = 55 kN for driver side, = 53 kN for passenger side
RCAR/IIHS Low Speed Impact	Damage is limited to the bumper and crashbox	No damage to components other than the bumper and crashbox

Table 2.18: FSV CAE analysis results - Crashworthiness

Analysis Type	Target life cycles	Predicted life cycles (FSV Model)
3 g pot hole	200,000	927,100
0.7 g cornering	100,000	1,676,000
0.8 g forward braking	100,000	274,700 (engine cradle life), 17,340,000 (body life)

Table 2.19: FSV CAE analysis results - Durability

2.6.7.1 FSV NVH Assessment Conducted by LMS

The FutureSteelVehicle (FSV) - Battery Electric Vehicle (BEV) was fully assessed for noise and vibration at concept design stage of this program. As very little data is available on Noise Vibration and Harshness (NVH) performance of BEV, this project was supported by first measuring the performance of a Mitsubishi BEV and an internal combustion engine based vehicles.

Measurements were conducted on two small Mitsubishi vehicles that both share the same body, yet one is equipped with an internal combustion engine and the other with an electric motor. The outcome was used as a starting point to identify advantages and disadvantages of electric motor noise and draw a set of NVH targets for FSV. Compared to a combustion engine, the electric motor shows significantly lower sound pressure levels, except for an isolated high frequency peak heard at high speeds (3500 Hz when the vehicle drives at top speed). The prominence of this peak is lowered by increased use of acoustic absorbent materials in the motor compartment. For low and mid frequencies, moderate electric motor forces imply less stringent noise and vibration design constraints and a possibility to reduce the body mass. To take full advantage of this opportunity, NVH is integrated early into the FSV design cycle and optimized in parallel with crash performances.

Finite element simulations at low and mid frequencies lead to reshaping the suspension mounts, the rear roof, the front header and the cowl top connection area, each change driving large reductions of noise levels while adding little to no mass. Damping sheets prove unnecessary. Lighter damping solutions such as vibration damping steels were examined and proved to be successful in the mid frequency range. Overall, the change from combustion engine to electric motor is compatible with mass reductions and similar or better noise and vibration performances. The body structure of FSV is designed with several panels that are made from 0.5mm AHSS. The results of this NVH study show that the implementation of these low gauges does not lead to deterioration of the NVH performance.

(The NHV assessment of BEV is fully documented in a separate WorldAutoSteel report)

2.6.8 Stamping Simulation

For the FSV BEV vehicle, single step simulation was done on all the parts of the body structure using Hyperform Radioss One Step. Single step stamping simulation is a quick process for getting an approximate idea that for a given blank shape and size whether a component can be stamped or not. The single step simulation method is very helpful in the product development stage.

Most of the parts of the body structure can be made through cold forming. Parts which play an important role in crashworthiness like B-pillars, Shotguns and Roof rails are made using a hot forming process. The hot stamping process is also simulated using Single Step process by assuming IF Steel forming properties. The more complex stamping parts were analyzed using 'incremental' forming simulations.

2.6.9 Body Structure Cost Assessment

The manufacturing costs of the FSV body structure components were assessed; only the technical cost modeling approach was used for the assessment, no supplier cost estimates were used. The technical cost modeling approach used in the cost model is similar to the one used by MIT in the ULSAB AVC and Future Generation Passenger Compartment (FGPC)^[6]. The manufacturing costs were estimated for all the body structure components, using the different manufacturing processes.

The cost breakdown for the fabrication of the steel components/systems are shown in Table 2.20 and Table 2.21 shows the comparison to ULSAB-AVC parts costs. The parts costs for the FSV are shown for two different production volume scenarios: 100,000 vehicles per year (FSV assumption) and 225,000 vehicles per year (ULSAB-AVC assumption).

Manufacturing Technology	Parts Weight (kg)	Unit Cost Per Vehicle (\$ USD)
Stamping	76.1	\$306.1
Stamping -Laser Welded Blanks	72.0	\$270.4
Hot Stamping	4.8	\$48.7
Hot Stamping - Laser Welded Blanks	16.8	\$118.5
Open Rollforming	4.5	\$7.7
Closed Rollforming	13.5	\$23.6
Total Body Structure (Manufacturing)	187.7	\$775.0

Table 2.20: *FSV body structure parts manufacturing costs breakdown*

⁶References:

1. Auto/Steel Partnership Future Generation Passenger Compartment (FGPC), VERSION 1.0 JUL, 2009
2. ULSAB AVC:VERSION 2.1C FEB, 2002
3. TM27C (EDAG Internal Cost Model)

Parameter	FSV		ULSAB AVC
Body Structure Weight (kg)	187.7 kg		202 kg
Production Volume Scenario	100000/yr	225000/yr	225000/yr
Total Body Structure Parts Costs	\$775	\$684	\$620
Base material Price	\$0.73		\$0.73
Material	50%	57%	66%
Labor	7%	7%	7%
Equipment	14%	15%	10.5%
Tooling	17%	9%	8%
Energy	3%	3%	2%
Overhead	5%	5%	4%
Building	1%	1%	0.5%
Maintenance	3%	3%	2%
Number Stamped Parts	75		64
Number of Hot Stamped parts	16		0
Number of Tubular parts	10 (Rollformed)		4 (Hydroformed)
Number of LWB Parts	18		11
Total Number of Parts	119		79

Table 2.21: FSV body structure parts costs v/s. ULSAB AVC parts costs

Each sub-assembly in the overall body structure assembly was reviewed to determine the following parameters that are related to the specific sub-assembly/assembly:

- Sub-assembly/Assembly Structure
- Joining Process
- Assembly Process Parameters
- Length of Weld (Laser Welding, Laser Brazing)
- Number of Welds (Resistance Spot Welding)
- Length of Bond (Adhesive Bonding)
- Length of Hem Flange (Hemming)

Based on the assembly sequence and joining specifications determined from the overall sub-assembly/assembly assessment, the assembly costs were estimated for each of the sub-assembly and assembly concepts, using the following different assembly processes:

- Laser Welding
- Laser Braze
- Adhesive Bonding

- Resistance Spot Welding
- Hemming

Table 2.22 shows the costs for the FSV body structure sub-assemblies and the total assembly. Table 2.23 shows the comparison to ULSAB-AVC assembly costs. The assembly costs for both the FSV and the ULSAB-AVC are shown for two different production volume scenarios: 100,000 vehicles per year (FSV assumption) and 225,000 vehicles per year (ULSAB-AVC assumption).

Assembly Name	Assembly (\$ USD) Cost
Body Side Inner Sub Assembly RH	\$17.59
Body Side Inner Sub Assembly LH	\$17.59
Body Side Outer Sub Assembly RH	\$5.29
Body Side Outer Sub Assembly LH	\$5.29
Body Side Assembly RH	\$24.95
Body Side Assembly LH	\$24.95
Front Structure Assembly	\$46.53
Front Floor Sub-Assembly	\$39.91
Rear Floor Assembly	\$89.63
Underbody Assembly	\$22.20
Body Structure Assembly	\$45.79
Total Cost of Body Structure Assembly	\$339.73

Table 2.22: *Body structure assembly costs*

Parameter	FSV		ULSAB AVC	
	100000/yr	225000/yr	225000/yr	100000/yr
Body Structure Assembly Cost	\$339.73	\$294.60	\$283.81	\$310.01
Number of parts	119		79	
Number of sub-assemblies	54		28	
Production Volume	100000/yr	225000/yr	225000/yr	100000/yr
Number of spot welds:	1023		723	
Length of laser welds	77 m		114 m	
Length of adhesive	18 m		2 m	
Length of hem	2 m		-	

Table 2.23: *FSV body structure assembly costs v/s. ULSAB AVC assembly costs*

2.6 Phase 2 Summary

Since the FSV cost model had certain assumptions specific to the program, sensitivity analyses were performed to demonstrate the effect on the overall vehicle cost as a result of changing certain key parameters including: production volume, product life, and steel prices.

Figure 2.39 shows the results of the sensitivity analyses and the range within which the key parameters were varied.

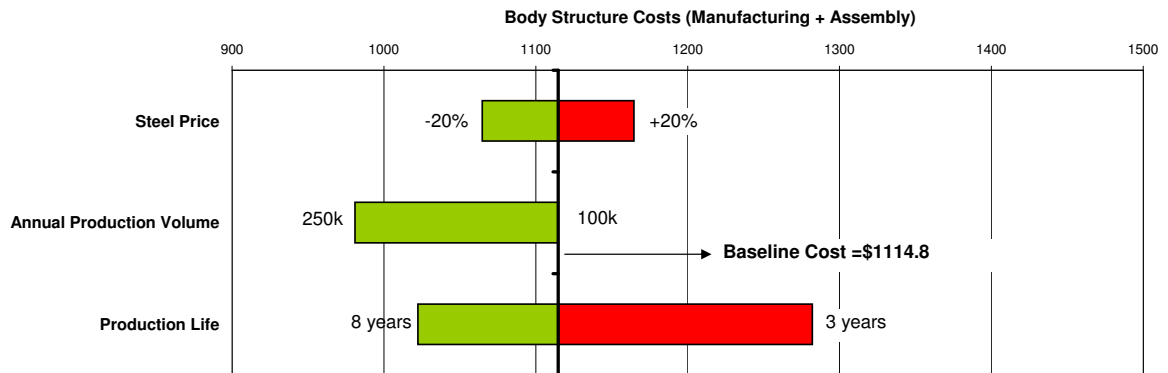


Figure 2.39: FSV body structure costs sensitivity analysis results

2.6.10 Life Cycle Assessment

With a fast growing automotive sector and global concern over climate change from anthropogenic GHG's (attributable to human activities), the key priorities are improving fuel economy, reducing emissions and shifting to a sustainable automotive industry. In Europe, strict tailpipe carbon dioxide (CO₂) emissions legislation has been passed with a view towards further reductions by 2020 and beyond. This trend is observed globally, as shown in Table 2.40.

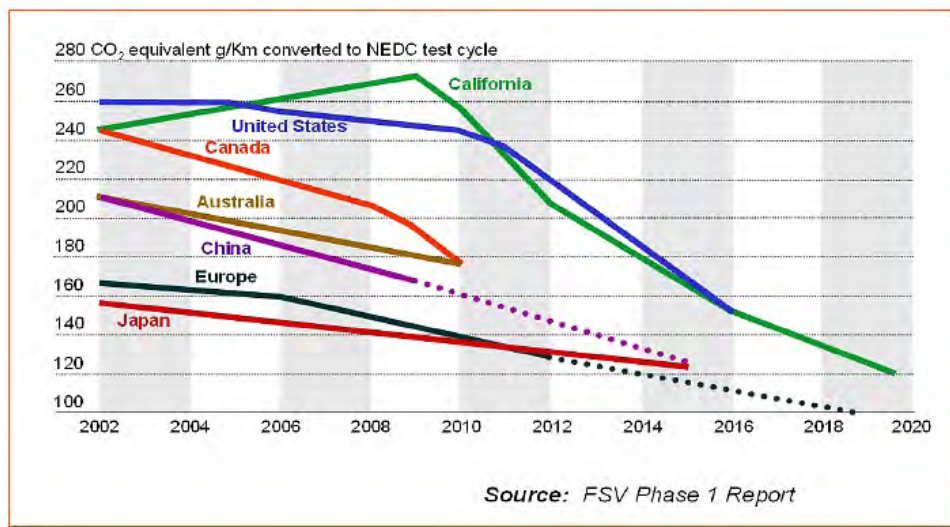


Figure 2.40: Trends in Global Fuel Economy/Vehicle Emissions Regulations

One of the challenges concerning automotive emissions regulations is to achieve the intended control without creating unintended consequences or unexpected results. Climate change and energy concerns prompt increased fuel efficiency standards or tailpipe emission regulations. And improving fuel economy and reducing tailpipe emissions during the “use” phase of a vehicle is very important.

However, the “use” phase represents only part of the total emissions associated with a vehicle throughout its life. A more comprehensive evaluation can be achieved if emissions from all phases of a vehicle's life are considered - from materials production through the end-of-life disposal. Decisions based on total life cycle data prevent the possibility of unintended consequences.

Life Cycle Assessment (LCA) is a technique to determine the environmental impacts of products, processes or services, through production, usage, and disposal. LCA is the only appropriate way to account for and reduce greenhouse gas emissions attributable to the automotive sector, because it assesses the entire vehicle life including the fuels that power it and the materials from which it is made.

Studies show that Life Cycle Assessment of a vehicle's environmental footprint is critical for material selection decisions. Adopting a lifecycle perspective is important because the use of alternative material choices in a vehicle body structure may result in significant increases in material production emissions, thus offsetting the reduction in use phase emissions that comes with mass reduction.

Material production for alternative material vehicles will load the environment with significantly more GHG emissions than that of a steel vehicle, as shown in Figure 2.41. Mass Reduction is therefore only one component of a comprehensive and effective greenhouse gas reduction strategy for the automotive industry.

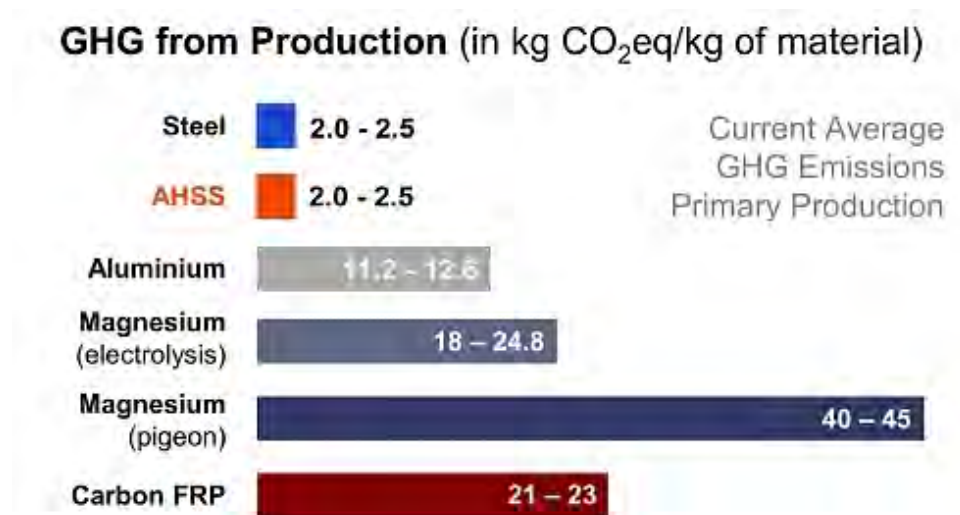


Figure 2.41: Material production GHG emissions

As the automotive industry's efforts to reduce CO₂e emissions are increasingly moving towards more advanced powertrains and fuel sources, material production will account for a much larger percentage of total CO₂e. This is due to the fact that these powertrains will greatly reduce the use phase CO₂e emissions, which means that the material production phase emissions will make up a greater percentage of total vehicle emissions. Therefore, use of low GHG-intensive material such as steel becomes even more important.

As we consider future vehicle programs, the application of LCA allows us to explore the impact of design, material and powertrain choices on life cycle vehicle emissions. This knowledge will help derive optimized solutions for both vehicle performance, safety, and our environment.

There are a variety of LCA models in use today. Dr. Roland Geyer at the University of California, Santa Barbara (UCSB) Bren School of Environmental Science, has developed a fully parameterized model which calculates life cycle GHG emissions attributable to vehicles as a function of their

material composition and power train characteristics. This model enables comparisons of various body structure and component materials across all phases of the vehicle life cycle, and has been used extensively by WorldAutoSteel in their application programs.

The UCSB GHG Automotive Materials Comparison model has been constructed with data from independent engineering studies. In the FutureSteelVehicle program, the UCSB model has been used to assess the impact of subsystems shown in Figure 2.42 and body structure design, steel fabrication choices, and advanced powertrains on vehicle life emissions. The UCSB model develops distinct CO₂e values for material production, vehicle use and vehicle recycling. Fabrication emissions, converted from fabrication energies, are then added to the UCSB results to achieve total vehicle life cycle emissions associated with the FSV BEV body structure. The results as shown in Table 2.24, Figure 2.43 and Figure 2.44 vividly demonstrate that the coupling of a lightweight advanced high strength steel body structure with a battery electric powertrain results in a 40% to 50% reduction in life cycle emissions compared to comparably-sized vehicles with conventional ICE-gasoline engines.

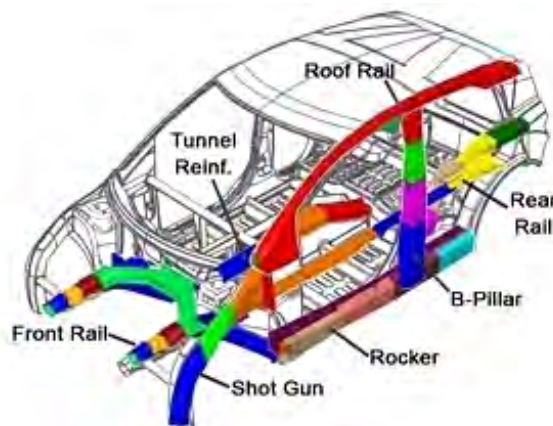


Figure 2.42: BEV body sub-structures

Vehicle	Material Production (kg CO ₂ e)	Use (kg CO ₂ e)	Recycling (kg CO ₂ e)	Parts Fabrication (kg CO ₂ e)	Total CO ₂ e (kg)
FSV-BEV	2,337	13,844	(1009)	199	15,371

Table 2.24: Full Vehicle body structure LCA results

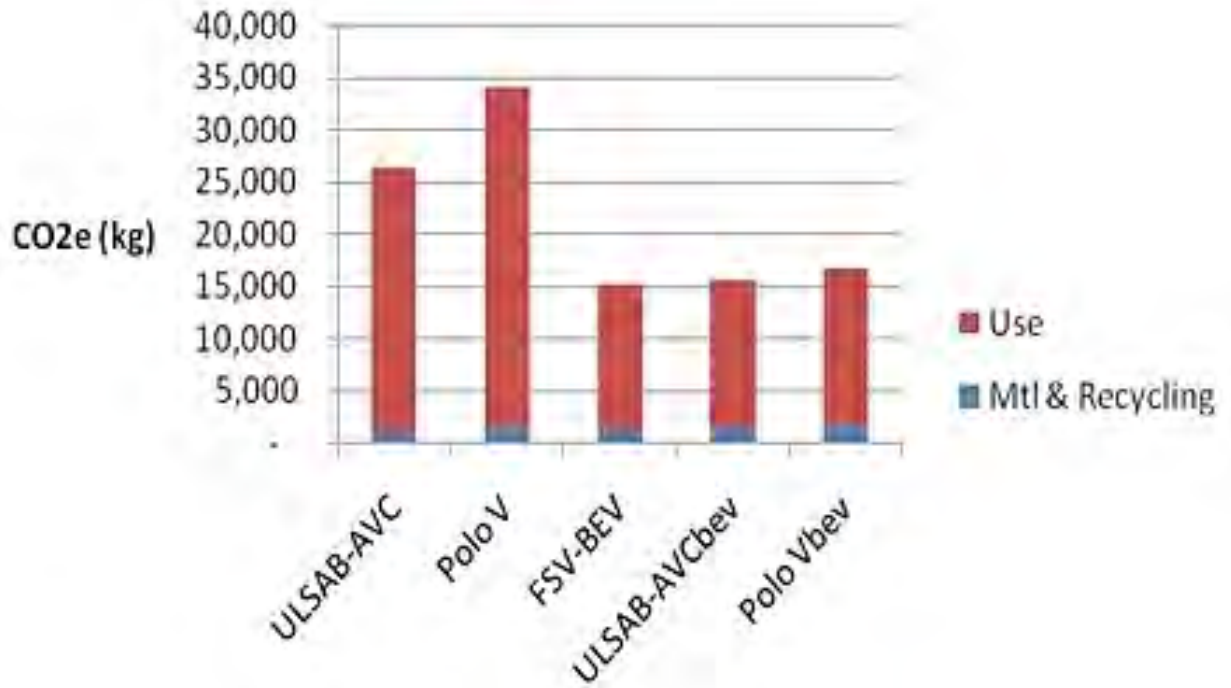


Figure 2.43: FSV BEV Life Cycle Emissions (U.S. Grid)

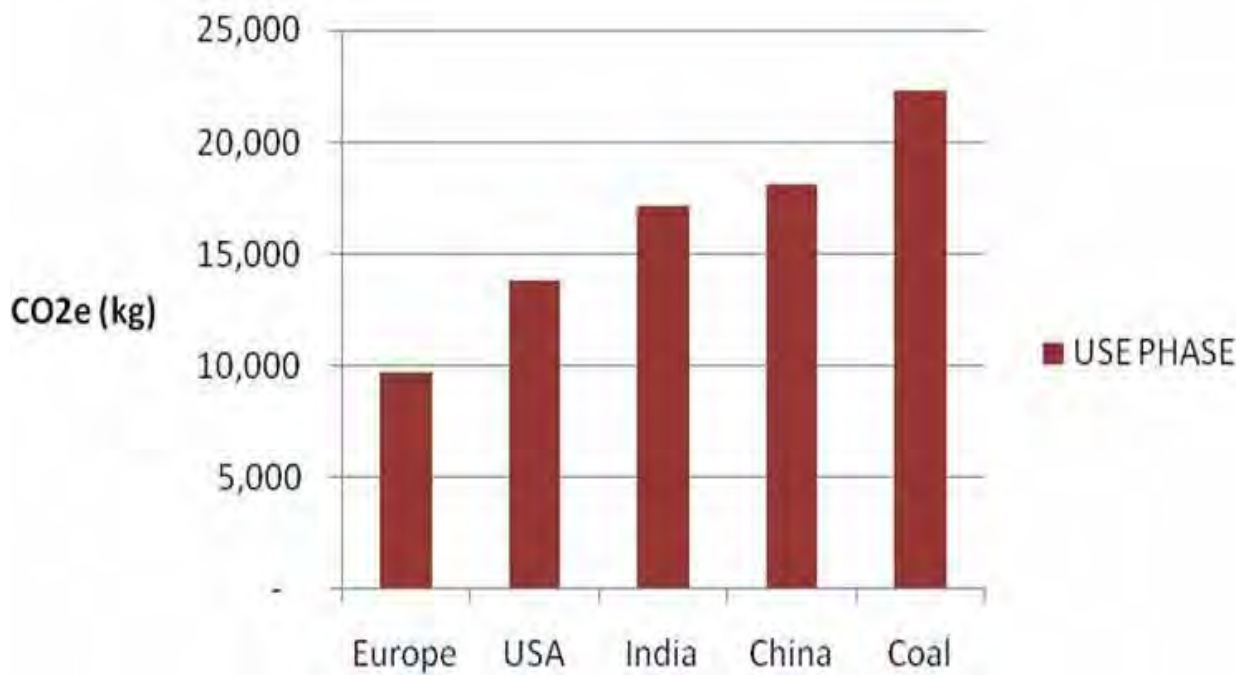


Figure 2.44: FSV BEV Use Phase Emissions - Various Electric Grids

2.6.10.1 Future LCA Work

The FutureSteelVehicle Life Cycle Assessment was conducted with the UCSB GHG Automotive Materials Comparison model, and is limited in its capability to assess all material and design contributions. An extension of this study would include a full vehicle analysis, where emissions contributions from all vehicle components, alternative body designs and materials could be evaluated and measured. Such a study would allow a comprehensive comparison of cost, mass and vehicle greenhouse gas emissions, and is recommended for automotive OEM's seeking low carbon footprint solutions. It is recommended that alternative body structure design options and material selections be compared on cost versus mass reduction and cost versus GHG emissions charts. A full vehicle life cycle assessment will insure that the automotive industry develops a broader strategy to vehicle emissions reductions, beyond the present focus on light weighting only. As demonstrated in the FutureSteelVehicle UCSB modeling, only a strategy that evaluates emissions from all phases of a vehicle life will prevent unintended consequences.

2.7 FSV Design and Engineering Process

The FSV design and engineering process steps are summarized in Figure 2.45 and Figure 2.46.

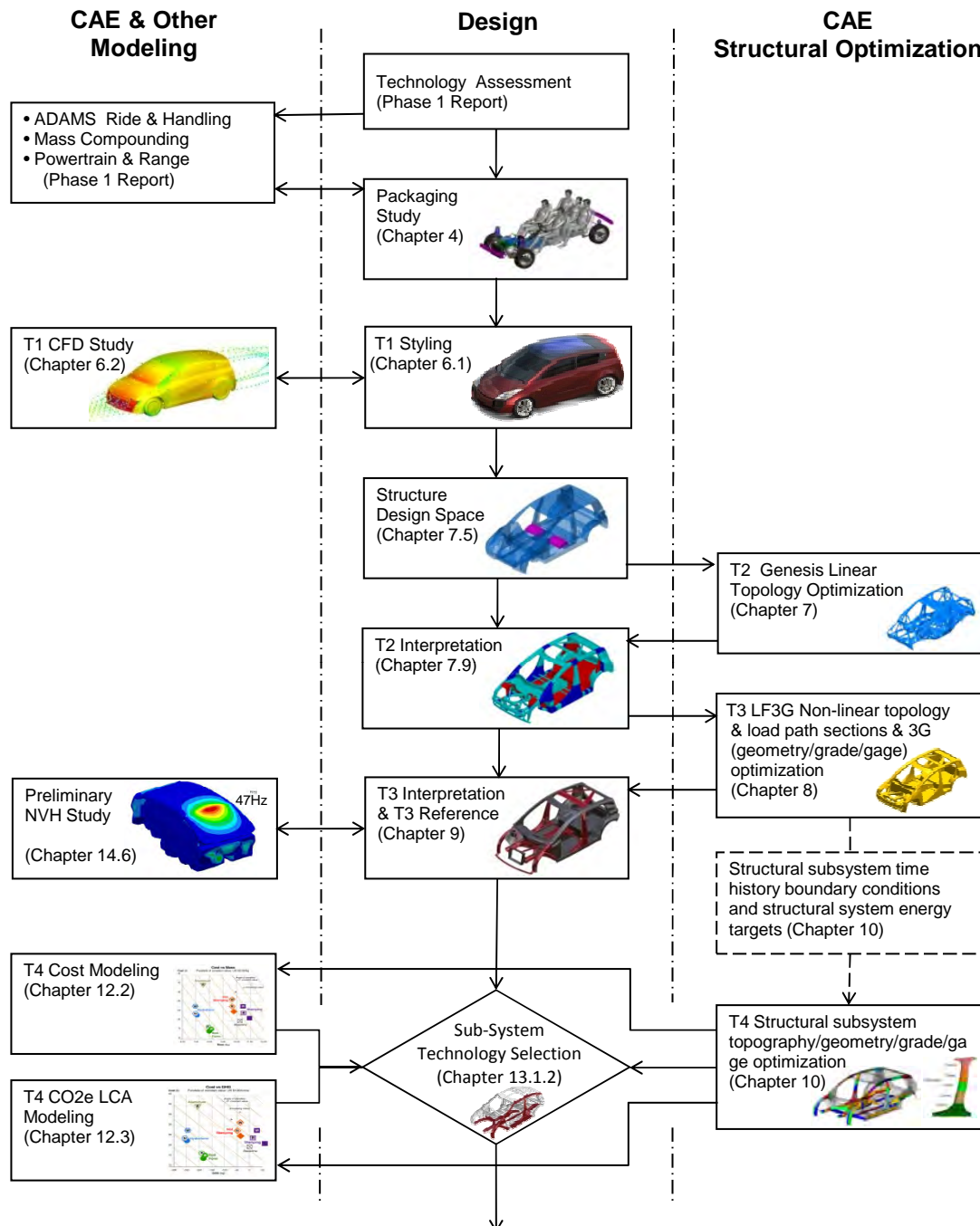


Figure 2.45: FSV design and engineering process steps

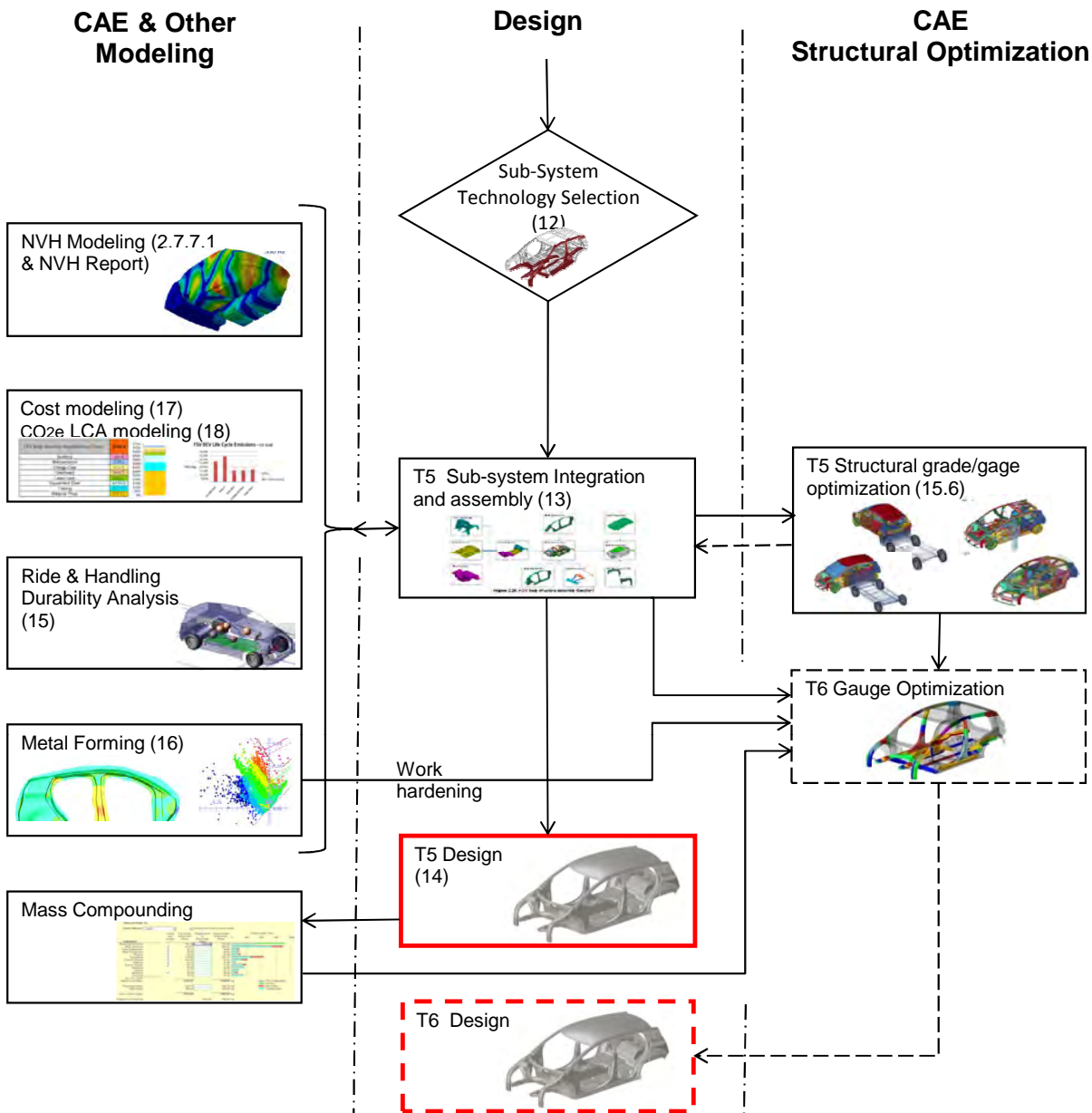


Figure 2.46: FSV design and engineering process steps (contd.)

2.8 FSV Mass Evolution

2.8 FSV Mass Evolution

The evolution of the FSV body structure mass through the different stages of the program are shown in Figure 2.47.

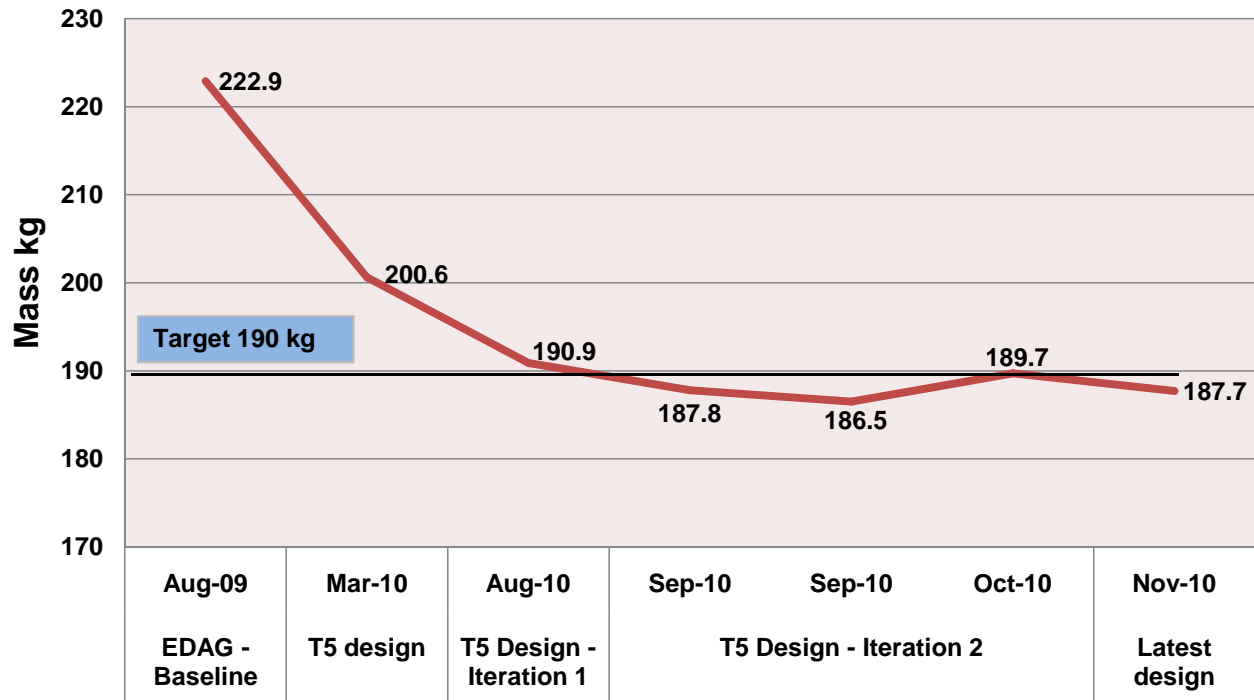


Figure 2.47: FSV body structure mass evolution

3.0 Steel Technology

3.1 FutureSteelVehicle Materials Portfolio

The FutureSteelVehicle (FSV) materials portfolio summarizes steel grades considered in the design of FSV; all are commercially available now or in the near future. The AHSS family of products in the portfolio provide a key role to the FSV program: the combination of new design technologies, emerging steel grades and advanced steel processing technologies enable optimal vehicle lightweighting and significant reductions in Green house Gas (GHG) emissions over the entire vehicle life cycle.

Advanced High Strength Steels (AHSS) contribute dramatically to the lightweight FSV design. AHSS grade development has been driven by the need to achieve better performance in crash energy management, which allows thickness reduction and lower mass. In addition, engineered AHSS address the automotive industry's need for steels with both higher strength and enhanced formability. As an example, the DP (Dual phase) and TRIP (Transformation induced plasticity) steels may provide additional formability within the same strength range, compared to conventional steels such as HSLA steels.

Detailed information about AHSS grades is available in the WorldAutoSteel AHSS Application Guidelines document online, at <http://www.worldautosteel.org>.

Table 3.1 and Table 3.2 shows the steel grades available for the FutureSteelVehicle (FSV) design. This FSV Materials Portfolio illustrates generalized properties used for the FSV program. There are sufficient worldwide steel products available globally from steel producers, based on each of their capabilities. To determine grade availability and steel properties, we suggest direct communication with individual steel companies. The following list of information is important when determining the suitability of a steel type and grade for any given design requirement:

- Hot-rolled, cold-rolled, and coating availability.
- Thickness and width capabilities.
- Chemical composition specifications.
- Mechanical properties and ranges.
- Joining requirements



FSV Materials Portfolio Updated March 4, 2011

Item #	Steel Grade	Thickness (mm)		Gage Length	YS (MPa) Min	YS (MPa) Typical	UTS (MPa) Min	UTS (MPa) Typical	Tot EL (%) Typical	N-value Typical	Modulus of Elasticity (MPa)	Fatigue Strength Coeff (MPa) *	K Value (MPa)
		Min t	Max t										
1	Mild 140/270	0.35	4.60	A50	140	150	270	300	42-48	0.24	21.0 x 10 ⁴	645	541
2	BH 210/340	0.45	3.40	A50	210	230	340	350	35-41	0.21	21.0 x 10 ⁴	695	582
3	BH 260/370	0.45	2.80	A50	260	275	370	390	32-36	0.18	21.0 x 10 ⁴	735	550
4	BH 280/400	0.45	2.80	A50	280	325	400	420	30-34	0.16	21.0 x 10 ⁴	765	690
5	IF 260/410	0.40	2.30	A50	260	280	410	420	34-48	0.20	21.0 x 10 ⁴	765	690
6	IF 300/420	0.50	2.50	A50	300	320	420	430	29-36	0.19	21.0 x 10 ⁴	775	759
7	FB 330/450	1.60	5.00	A80	330	380	450	490	29-33	0.17	21.0 x 10 ⁴	835	778
8	HSLA 350/450	0.50	5.00	A80	350	360	450	470	23-27	0.16	21.0 x 10 ⁴	815	807
9	DP 300/500	0.50	2.50	A80	300	345	500	520	30-34	0.18	21.0 x 10 ⁴	865	762
10	HSLA 420/500	0.60	5.00	A50	420	430	500	530	22-26	0.14	21.0 x 10 ⁴	875	827
11	FB 450/600	1.40	6.00	A80	450	530	560	605	18-26	0.15	21.0 x 10 ⁴	950	921
12	HSLA 490/600	0.60	5.00	A50	490	510	600	630	20-25	0.13	21.0 x 10 ⁴	975	952
13	DP 350/600	0.60	5.00	A80	350	385	600	640	24-30	0.17	21.0 x 10 ⁴	985	976
14	TRIP 350/600	0.60	4.00	A50	350	400	600	630	29-33	0.25	21.0 x 10 ⁴	975	952
15	SF 570/640	2.90	5.00	A50M	570	600	640	660	20-24	0.08	21.0 x 10 ⁴	1005	989
16	HSLA 550/650	0.60	5.00	A50	550	585	650	675	19-23	0.12	21.0 x 10 ⁴	1020	1009
17	TRIP 400/700	0.60	4.00	A80	400	420	700	730	24-28	0.24	21.0 x 10 ⁴	1075	1077
18	SF 600/780	2.00	5.00	A50	600	650	780	830	16-20	0.07	21.0 x 10 ⁴	1175	1201
19	HSLA 700/780	2.00	5.00	A50	700	750	780	830	15-20	0.07	21.0 x 10 ⁴	1175	1200
20	CP 500/800	0.80	4.00	A80	500	520	800	815	10-14	0.13	21.0 x 10 ⁴	1160	1183
21	DP 500/800	0.60	4.00	A50	500	520	800	835	14-20	0.14	21.0 x 10 ⁴	1180	1303
22	TRIP 450/800	0.60	2.20	A80	450	550	800	825	26-32	0.24	21.0 x 10 ⁴	1170	1690
23	CP 600/900	1.00	4.00	A80	600	615	900	910	14-16	0.14	21.0 x 10 ⁴	1255	1301
24	CP 750/900	1.60	4.00	A80	750	760	900	910	14-16	0.13	21.0 x 10 ⁴	1255	1401
25	TRIP 600/980	0.90	2.00	A50	550	650	980	990	15-17	0.13	21.0 x 10 ⁴	1335	1301
26	TWIP 500/980	0.80	2.00	A50M	500	550	980	990	50-60	0.40	21.0 x 10 ⁴	1335	1401
27	DP 700/1000	0.60	2.30	A50	700	720	1000	1030	12-17	0.12	21.0 x 10 ⁴	1375	1521
28	CP 800/1000	0.80	3.00	A80	800	845	1000	1005	8-13	0.11	21.0 x 10 ⁴	1350	1678
29	DP 800/1180	1.00	2.00	A50	800	880	1180	1235	10-14	0.11	21.0 x 10 ⁴	1555	1700
30	MS 950/1200	0.50	3.20	A50M	950	960	1200	1250	5-7	0.07	21.0 x 10 ⁴	1595	1678
31	CP 1000/1200	0.80	2.30	A80	1000	1020	1200	1230	8-10	0.10	21.0 x 10 ⁴	1575	1700
32	DP1150/1270	0.60	2.00	A50M	1150	1160	1270	1275	8-10	0.10	21.0 x 10 ⁴	1620	1751
33	MS 1150/1400	0.50	2.00	A50	1150	1200	1400	1420	4-7	0.06	21.0 x 10 ⁴	1765	1937
34	CP 1050/1470	1.00	2.00	A50M	1050	1060	1470	1495	7-9	0.06	21.0 x 10 ⁴	1840	2030
35	HF 1050/1500												
	Conventional Forming	0.60	4.50	A80	340	380	480	500	23-27	0.16	21.0 x 10 ⁴	845	790
	Heat Treated after forming	0.60	4.50	A80	1050	1220	1500	1600	5-7	0.06	21.0 x 10 ⁴	1945	2161
36	MS 1250/1500	0.50	2.00	A50M	1250	1265	1500	1520	3-6	0.05	21.0 x 10 ⁴	1865	2021

* Un-notched specimens, FSc = UTS + 345 (Mpa)
Alternate approximation = 3.45*HB

Table 3.1: FSV materials portfolio

Item #	Steel Grade	Availability						
		HR	CR		HDG/GA/GI		EG	
		U	U	E	U	E	U	E
1	Mild 140/270	1.6 - 4.6	.35 - 3.0	.35-3.0	.35-3.0	.35-3.0	0.35 - 2.5	0.35 - 1.5
2	BH 210/340	N.A.	0.45 - 3.4	0.45 - 3.4	0.45 - 3.4	0.45 - 3.4	0.45 - 2.5	0.45 - 1.5
3	BH 260/370	N.A.	0.45 -2.8	0.45 -2.8	0.45 -2.8	0.45 -2.8	0.45 - 2.5	0.45 - 1.5
4	BH 280/400	N.A.	0.45 -2.8	0.45 -2.8	0.45 -2.8	0.45 -2.8	0.45 - 2.5	0.45 - 1.5
5	IF 260/410	N.A.	0.4 - 2.3	0.4 - 2.3	0.4 - 2.3	0.4 - 2.3	0.4 - 2.3	0.4 - 1.5
6	IF 300/420	N.A.	0.5 - 2.5	0.5 - 2.5	0.5 - 2.5	0.5 - 2.5	0.5 - 2.5	0.5 - 1.5
7	FB 330/450	1.6 - 5.0	N.A.	N.A.	N.A.	N.A.	N.A.	N.A.
8	HSLA 350/450	1.6 - 5.0	0.5 - 2.5	N.A.	0.5 - 2.5	N.A.	0.5 - 2.5	N.A.
9	DP 300/500	N.A.	0.5 - 2.5	0.5 - 2.5	0.5 - 2.5	0.5 - 2.5	0.5 - 2.5	0.5 - 2.5
10	HSLA 420/500	1.6 - 5.0	0.6 - 2.5	N.A.	0.6 - 2.5	N.A.	0.6 - 2.5	N.A.
11	FB 450/600	1.4 - 6.0	N.A.	N.A.	N.A.	N.A.	N.A.	N.A.
12	HSLA 490/600	1.8 - 5.0	0.6 - 2.5	N.A.	0.6 - 2.5	N.A.	0.6 - 2.5	N.A.
13	DP 350/600	1.6 - 5.0	0.6 - 2.5	0.6 - 2.5	0.6 - 2.5	0.6 - 2.5	0.6 - 2.5	0.6 - 2.5
14	TRIP 350/600	1.6 - 4.0	0.6 - 2.3	N.A.	N.A.	N.A.	0.6 - 2.3	N.A.
15	SF 570/640	2.9 - 5.0	N.A.	N.A.	N.A.	N.A.	N.A.	N.A.
16	HSLA 550/650	1.8 - 5.0	0.6 - 2.5	N.A.	0.6 - 2.5	N.A.	0.6 - 2.5	N.A.
17	TRIP 400/700	1.6 - 4.0	0.6 - 2.3	N.A.	0.6 - 2.3	N.A.	N.A.	N.A.
18	SF 600/780	2.0 - 5.0	N.A.	N.A.	N.A.	N.A.	N.A.	N.A.
19	HSLA 700/780	2.0 - 5.0	N.A.	N.A.	N.A.	N.A.	N.A.	N.A.
20	CP 500/800	2.2 - 4.0	0.8 - 1.8	N.A.	0.8 - 1.8	N.A.	0.8 - 1.8	N.A.
21	DP 500/800	2.5 - 4.0	0.6 - 2.0	N.A.	0.75 - 2.0	N.A.	0.6 - 1.5	N.A.
22	TRIP 450/800	N.A.	0.6 - 2.2	N.A.	0.6 - 2.2	N.A.	N.A.	N.A.
23	CP 600/900	1.6 - 4.0	1.0 - 1.8	N.A.	1.0 - 1.8	N.A.	1.0 - 1.8	N.A.
24	CP 750/900	1.6 - 4.0	N.A.	N.A.	<2.4	N.A.	N.A.	N.A.
25	TRIP 600/980	N.A.	0.9 - 2.0	N.A.	0.9 - 2.0	N.A.	0.9 - 2.0	N.A.
26	TWIP 500/980	N.A.	N.A.	N.A.	.8 - 2.0	N.A.	N.A.	N.A.
27	DP 700/1000	N.A.	0.6 - 2.3	N.A.	0.75 - 2.0	N.A.	0.6 - 2.3	N.A.
28	CP 800/1000	1.6 - 3.0	0.8 - 2.0	N.A.	0.8 - 2.0	N.A.	N.A.	N.A.
29	DP 800/1180	N.A.	1.0 - 2.0	N.A.	1.0 - 2.0	N.A.	N.A.	N.A.
30	MS 950/1200	N.A.	0.5 - 3.2	N.A.	N.A.	N.A.	0.5 - 2.5	N.A.
31	CP 1000/1200	N.A.	0.8 - 2.3	N.A.	N.A.	N.A.	0.8 - 2.3	N.A.
32	DP1150/1270	N.A.	0.6 - 2.0	N.A.	0.75 - 2.0	N.A.	0.6 - 1.5	N.A.
33	MS 1150/1400	N.A.	0.5 - 2.0	N.A.	N.A.	N.A.	0.5 - 2.0	N.A.
34	CP 1050/1470	N.A.	1.0 - 2.0	N.A.	1.0 - 2.0	N.A.	N.A.	N.A.
35	HF 1050/1500							
	<i>Conventional Forming</i>	1.8 - 4.5	0.6 - 2.3	N.A.	N.A.	N.A.	N.A.	N.A.
	<i>Heat Treated after forming</i>	1.8 - 4.5	0.6 - 2.3	N.A.	N.A.	N.A.	N.A.	N.A.
36	MS 1250/1500	N.A.	0.5 - 2.0	N.A.	N.A.	N.A.	0.5 - 2.0	N.A.

* Un-notched specimens, FSc = UTS + 345 (Mpa)
Alternate approximation = 3.45*HB

Table 3.2: FSV materials portfolio (cont.)

3.1.1 Steel Grade Descriptions

Automotive steels are commonly classified by a metallurgical designation and strength level. In this document, we use the general terms HSS and AHSS to designate all higher strength steels. Common designations include low-strength steels (interstitial-free and mild steels); conventional HSS (carbon-manganese, bake hardenable, high-strength interstitial-free, and high-strength, low-alloy steels); and the newer types of AHSS (dual phase, transformation-induced plasticity, complex phase, and martensitic steels). Additional higher strength steels for the automotive market include ferritic-bainitic, twinning-induced plasticity, hot-formed, and post-forming heat-treated steels.

The different grades have distinctly different microstructures and deformation characteristics; the results are different performance levels in part formability, crash, and energy management. For example, Figure 3.1 compares strength and total elongation (a steel property related to formability) for different types of steel.

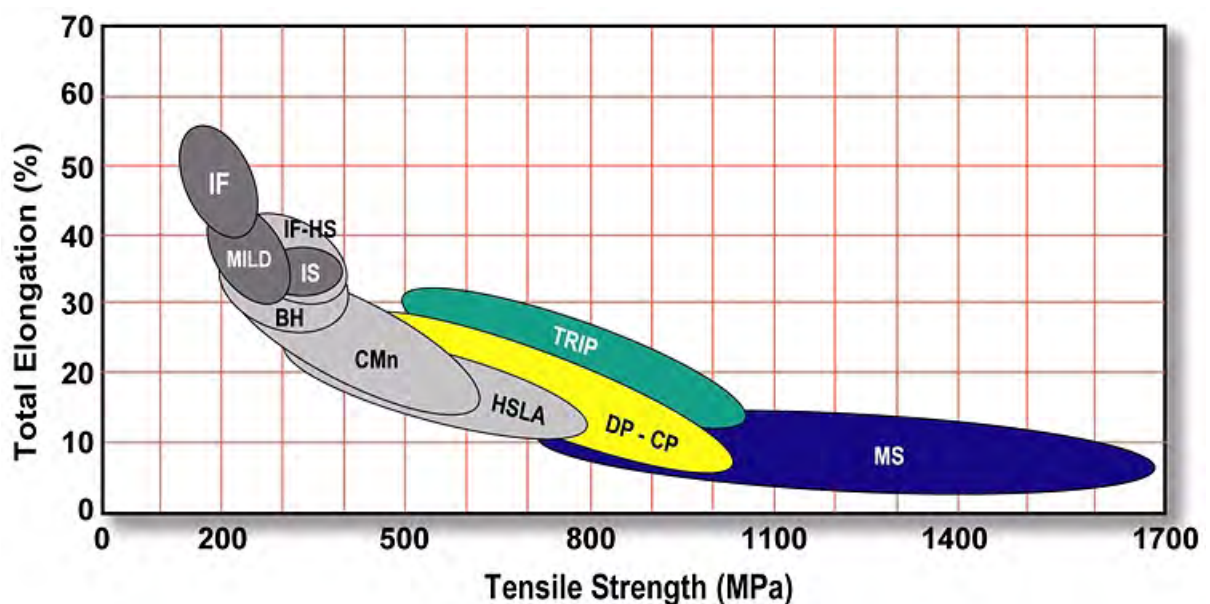


Figure 3.1: Schematic of AHSS steels (shown in colour) compared to low strength steels (dark grey) and traditional HSS (light grey)

Figure 3.2 shows the schematic of newer higher strength steels utilizing unique chemistries, processing, and microstructure to gain specific properties and forming characteristics. For hot formed steels (HF, shown in red), the part is heated to a very high temperature to prior to forming, and then cooled rapidly to achieve desired part strength. For post forming, heat-treatable steels (PFHT, shown in orange) the stamping is formed cold at a lower strength (ellipse 1) and then raised to a much higher strength by heat treatment (ellipse 2).

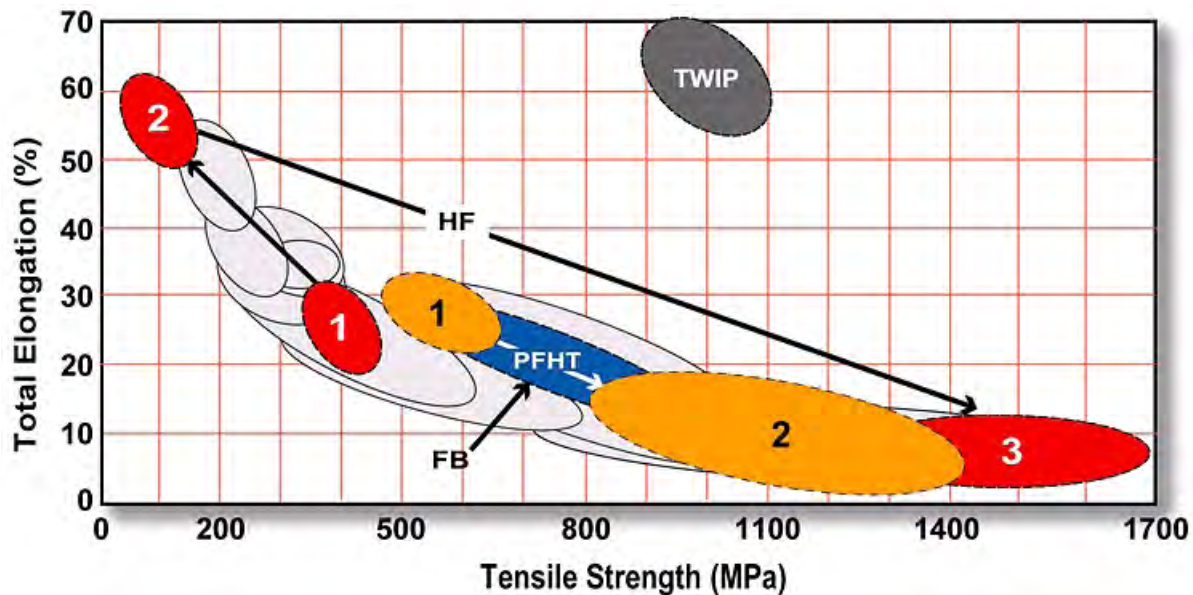


Figure 3.2: Schematic of newer higher strength steels utilizing unique chemistries, processing, and microstructure to gain specific properties and forming characteristics

Since the terminology used to classify steel products varies considerably throughout the world, the FSV materials portfolio uses a combination of methods to define the steels. Each steel grade is identified by metallurgical type, yield strength and sequenced by minimum ultimate tensile strength (in MPa). As an example, DP 500/800 means a dual phase steel type with 500 MPa minimum yield strength and 800 MPa minimum ultimate tensile strength.

3.1.1.1 Conventional Low and High Strength Automotive Sheet Steels

A. Mild (conventional) Steels

Mild steels are the conventional steels historically used in automotive applications, and are characterized by low strength and good formability. Drawing Quality (DQ) and Aluminum Killed (AKDQ) steels are examples and often serve as a reference base because of their widespread application and production volume.

B. Interstitial-Free (IF) Steels (Low strength and high strength)

IF steels have ultra-low carbon levels which reduce their yield strengths, while achieving high work hardening rates. This results in steels with excellent formability as compared to mild steels. The higher strength grades of IF steel are widely used for both structural and closure applications.

C. Bake Hardenable (BH) Steels

BH steels have more complex chemistries and production processing requirements, compared to mild and IF steels. BH steels have excellent formability, but strengthen considerably during the

paint bake operation in an automotive plant, netting increased part dent resistance.

D. High-Strength Low-Alloy (HSLA) Steels

This group of steels achieve increased strength primarily through the addition of micro-alloying elements.

3.1.1.2 Advanced High Strength Automotive Sheet Steels

A. Dual Phase (DP) Steels

DP steels consist of a multiple micro-structural phases (one a soft phase “Ferrite”, the other a hard phase “Martensite”). The result is a family of steels that combine high strength and excellent formability. They also work harden rapidly - the forming process actually increases the strength level of the part, compared to the initial strength level of the steel. This work hardening characteristic, plus excellent elongation creates DP steels with much higher ultimate tensile strengths than conventional steels of similar yield strength.

B. Transformation-Induced Plasticity (TRIP) Steels

Another multi-phase steel with complex metallurgy and production processing, TRIP steels use higher quantities of carbon and other alloying elements than DP steels to achieve uncommon micro-structural phases at or below ambient temperature. TRIP steels contain metastable Austenite, that transforms to the hard phase Martensite during plastic strain of metal forming or crash. During deformation, the TRIP steel micro structure results in higher work hardening rates at higher strain levels, beyond that of DP steels, providing a slight advantage over DP in the most severe stretch forming applications. TRIP steels therefore can be engineered or tailored to provide excellent formability for the manufacturing of complex part shapes, and exhibit high work hardening during crash deformation for excellent crash energy absorption. The additional alloying requirements of TRIP steels degrade their resistance spot-welding behavior.

C. Complex Phase (CP) Steels

CP steels typify the transition to advanced metallurgical complexity to achieve very high ultimate tensile strengths. Additional alloying and processing result in steels that show significantly higher yield strengths at equal tensile strengths of 800 MPa and greater, compared to DP steels. CP steels are characterized by high energy absorption and high residual deformation capacity, excellent features for crash structures.

D. Martensitic (MS) Steel

To create MS steels, the steel is quenched rapidly from very high temperatures, resulting in a microstructure of very high martensite (high strength) levels. Within the group of multiphase steels, MS steels show the highest tensile strength level - up to 1700 MPa. This martensite structure can also be developed with post-forming heat treatment. MS steels are often subjected to post-quench tempering (re-heating) to improve ductility, and can provide adequate formability even at extremely high strengths.

E. Ferritic-Bainitic (FB) Steels (including Stretch Flangeable (SF))

FB steels have a very fine dual-phase microstructure, achieved from additional alloying and steel processing requirements. These steels are sometimes utilized to meet specific customer application requirements defining Stretch Flangeable (SF) or High Hole Expansion (HHE) capabilities for improved edge stretch capability. They are very formable and are available as hot-rolled products.

The primary advantage of FB steels over HSLA and DP steels is the improved stretchability of sheared edges as measured by the hole expansion test (λ). Compared to HSLA steels with the same level of strength, FB steels also have a higher strain hardening exponent (n) and increased total elongation. Because of their good weldability, FB steels are good candidates for tailored blank applications. These steels also are characterized by both good crash performances and good fatigue properties.

F. Twinning-Induced Plasticity (TWIP) Steel

TWIP steels (C-4), have a high manganese content (17-24%) that causes the steel to be fully austenitic at room temperatures. A large amount of deformation is driven by the formation of deformation twins. This deformation mode leads to the naming of this steel class. The twinning causes a high value of the instantaneous hardening rate (n value) as the microstructure becomes finer and finer. The resultant twin boundaries act like grain boundaries and strengthen the steel. TWIP steels combine extremely high strength with extremely high stretchability. The n value increases to a value of 0.4 at an approximate engineering strain of 30% and then remains constant until both uniform and total elongation reach 50%. The tensile strength is higher than 1000 MPa.

G. Hot Formed (HF) Steel

As automotive designs evolve to more complex, aerodynamic shapes, formability and springback are common problems encountered with conventional stamping processes. Hot-formed or hot-stamped steels (characterized by boron levels between 0.002% and 0.005%) have been in use since the 1990s in to solve these issues. In these processes, a part is either heated to very high temperatures prior to forming, or formed partially and then heated, to achieve the final part shape. Rapid cooling then results in parts that have retained critical dimensional characteristics, while achieving extremely high strength levels.

There are two types of press-hardening or hot forming applications:

1. Direct Hot-Forming: the part is formed at very high temperatures (above 850 degrees celsius), followed by quenching (rapid cooling) to ambient temperature.
2. Indirect Hot-Forming: pre-forms the part at room temperature to a high percentage of the final part shape followed by additional high temperature forming and quenching.

3.2 Manufacturing Processes

In the automotive industry conventional stamping process is the most commonly used to produce parts that make up the vehicle body structure. But with the increasing use of higher strength steels other stamping techniques and forming processes are being used. These include hot stamping, roll forming and hydroforming. Various grades of sheet steel material for these processes is available in the form of coils.

These coils can be either:

- Single material sheet (thickness and grade)
- Laser welded coils
- Tailor rolled coils

These coils or sheet steel can be further processed into blanks and the following tubes or tubular products:

- Blanks:
 - Conventional blanks
 - Tailor rolled blanks
 - Laser welded blanks
- Tubes:
 - Conventional tubes (single thickness and grade)
 - Tubular blanks (i.e. laser welded tubes), these can be either from conventional blanks, tailor rolled blanks or laser welded blanks
 - Multiple walled tubes

Below is a brief description of each base material processes.

3.2.1 Laser welded blank

A laser welded blank is two or more sheets of steel seam-welded together into a single blank which is then stamped into a part. As a result of laser welding technology, a single blank can contain different material grades and thickness of steel. See Figure 3.3 Laser welded blank technology allows for the placement of various steel grades and thicknesses within a specific part, placing steel's attributes where they are most needed and removing weight that does not contribute to part performance.



Figure 3.3: Example of a laser weld blank used for a body side panel (FSV body side outer shown)

3.2.2 Laser welded coil

Laser welded coil is a process of producing a continuous coil of steel from individual separate coils of varying thickness and grades. The basic process takes separate coils prepares the edges, and laser welds these together and re-coils the strip ready for other blanking or to be used as a continuous feed in a transfer press line. See Figure 3.4

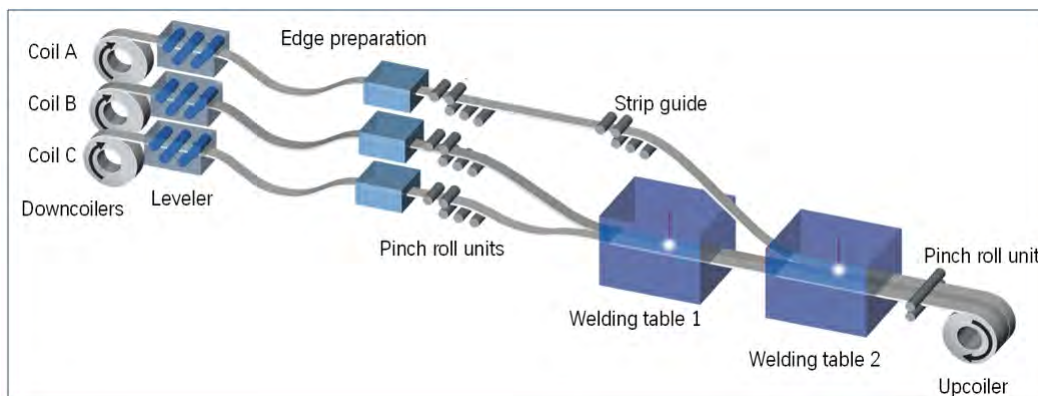


Figure 3.4: Laser welded coils production process

3.2.3 Tailor rolled coil

This is a manufacturing process of flexible cold strip rolling by varying the gap between two rolls which allows for different strip thicknesses in the direction of rolling. See Figure 3.5. The accurate measuring and controlling technology guarantees the strip thickness tolerances.

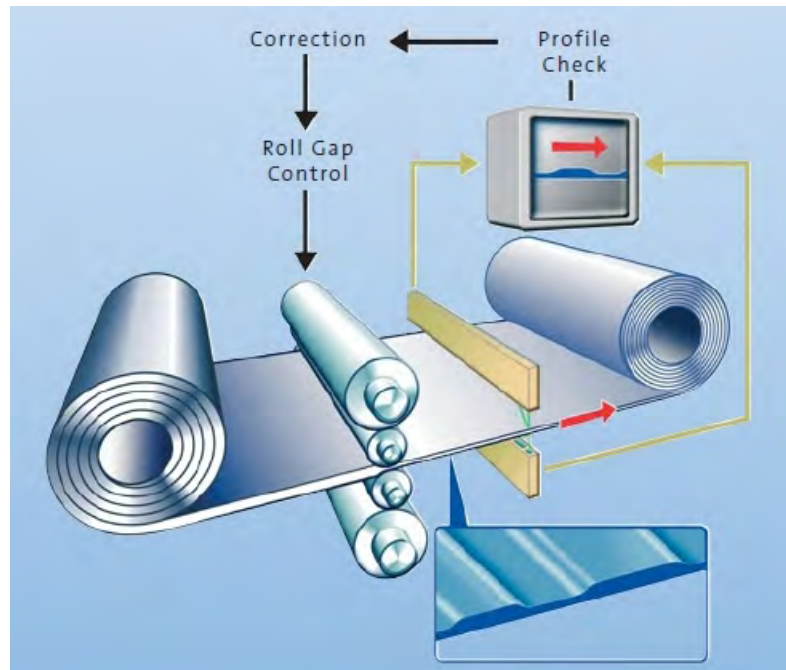


Figure 3.5: *The principle of producing a Tailor Rolled Coil*

A tailor rolled coil can be either used for blanking operations (for stamping or tubular blanks), or can be directly fed into a rollforming line.

3.2.4 Conventional Electric-Resistance-Welded (ERW) Tube

ERW tubes are produced specifically for hydroforming. The process can utilize either a standard single thickness and grade coil, a laser welded coil or a tailor rolled coil. See Figure 3.6.

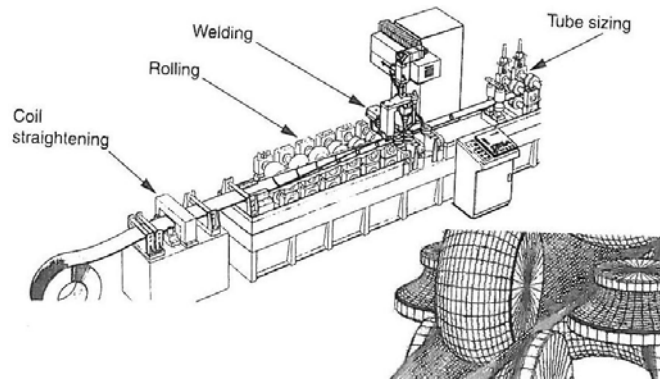


Figure 3.6: Typical roll form layout for making ERW tubes

3.2.5 Tubular Blanks (laser-welded)

Laser welded tubes used in the hydroforming process are made from individual blanks. This blank is then formed into a tube of constant diameter or a tapered tube.

3.2.6 Multiple walled tubes

Multiple Walled Tubes (MWT), which is a proprietary process, are tubes that vary in wall thickness, which for the FSV are used for hydroforming. The MWT process produces a tube in which the wall thickness is varied along the length in discrete steps in a single formed tube. See Figure 3.7. The wall thickness can vary on either the inside or outside of the tube.

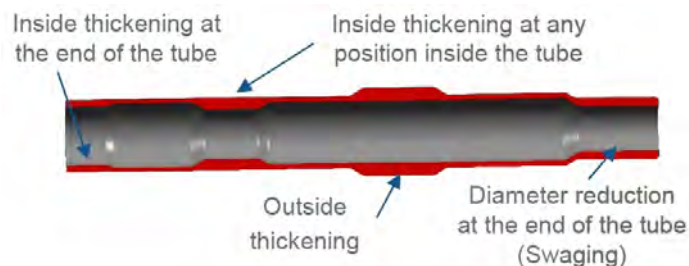


Figure 3.7: Multiple walled tube showing varying wall thickness

However, other approaches to a MWT that have been applied to production vehicles are, laser welding of a tailor welded blank, (also known as a tailor laser welded tube) and a tailor rolled blank laser welded into a tube with the laser welded tube process.

3.2.7 Manufacturing Processes Considered for FSV

For the FSV cost model a number of manufacturing processes have been considered, these are:

Conventional cold stamping

- Single material blank, thickness and grade.
- Laser welded blanks (LWB), can be both different material thickness and grade
- Laser welded blanks (LWB), produced from a laser welded coil
- Tailor rolled blank (TRB), made from a tailor rolled coil of single material grade but with varying thickness

Hot stamping (Direct)

- Single material blank, thickness and grade
- Laser welded blanks (LWB), of different material thickness but of a single material grade
- Tailor rolled blank (TRB), single material grade but with varying thickness

One additional process was considered as a possibility to produce parts 'hot stamping with tailor quenching' this was evaluated for feasibility only.

Roll forming (Closed and open roll form)

- Single material coil, thickness and grade
- Laser welded coil (LWC), can be both different material thickness and grade
- Tailor rolled coil (TRC), single material grade but with varying thickness

Hydroforming (Tube)

- Conventional tube; single material tube, thickness and grade
- Tubular blanks (i.e laser welded tubes) these can be either from conventional blanks, tailor rolled blanks (single material grade but with varying thickness), or laser welded blanks (different material grades and varying thickness)

Below is a brief description of each forming process.

3.2.7.1 Stamping (cold)

When producing parts using a conventional cold stamping process there are a number of die set-ups that can possibly be utilized depending on the final part geometry. Types of dies used are, progressive, transfer, compound and combination.

For the FSV only a transfer die configuration was considered. This process is used for high volume production where several dies are mounted of a common base plate. Material is fed into the press mostly in blank form and is generally transferred from die to die automatically. When using a single material thickness and grade a steel coil will be delivered to the stamping plant and blanking operation completed prior to feeding the blank into the transfer press. This can be completed either as part of the transfer press or off-line in a separate operation. When using either a laser welded or tailor rolled blank the blanking operation will normally be completed by the steel service provider and the blank delivered to the stamping plant. The transfer line presses would normally complete the following stamping operations, blank, form, pierce and trim. To keep tooling cost to a minimum the number of stamping dies in a transfer press should be kept to the minimum necessary to produce the part. Traditionally the maximum number of stations in a transfer press was 6 but through part and die design improvements many OEM's have limited the number of stations to 4. For the FSV cost model we considered a 4 die transfer press process.

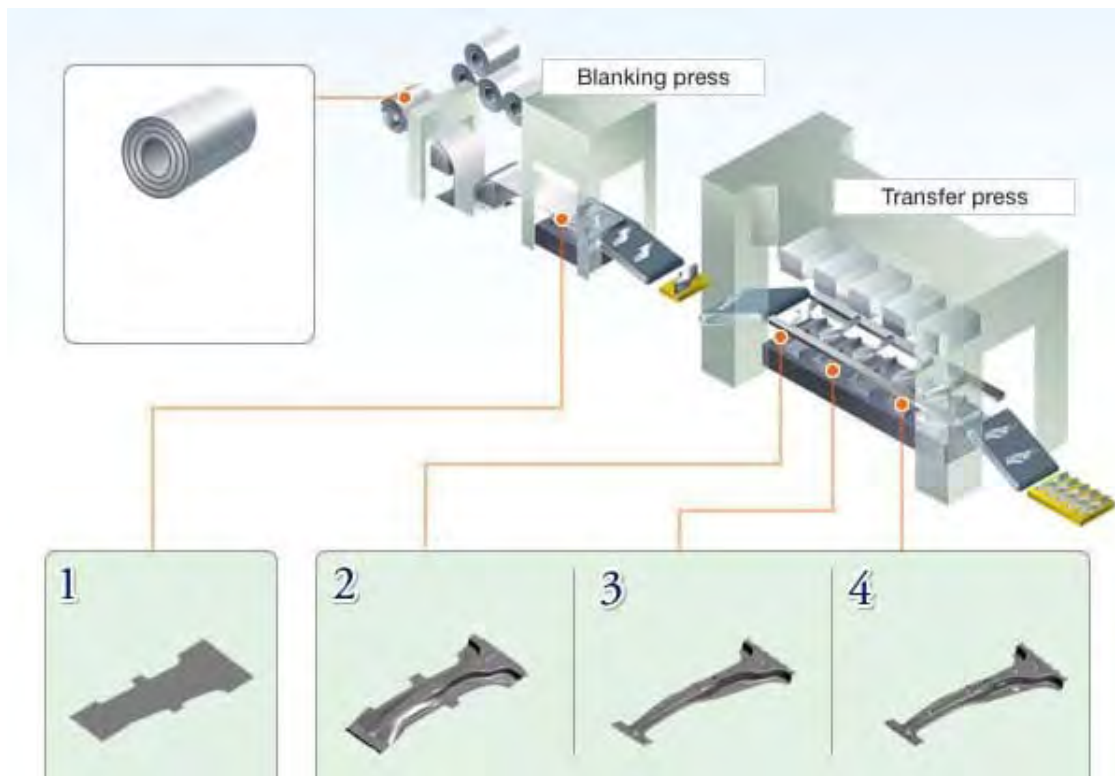


Figure 3.8: Schematic of a typical transfer press layout

3.2.7.2 Hot Stamping

For the FSV cost model only 'Direct' hot stamping was considered. Hot stamping uses a base material, 22MnB5, ferritic-pearlitic structure, with a tensile strength of approximately 600MPa. After the hot stamping process the part now has a martensitic structure and increased strength up to 250% of its original value.

The hot stamping direct process, see Figure 3.10, uses blanks heated in a continuous feed furnace to temperatures between 900 and 950 C°. During this heating process an austenitic structure is formed. Blanks are then transferred to a stamping die to form the correct geometry. The die is then rapidly cooled, this quenching takes place after the forming process has been completed. This rapid cooling transforms the austenitic structure to a martensitic microstructure with a tensile strength of up to 1500 MPa. See Figure 3.9.

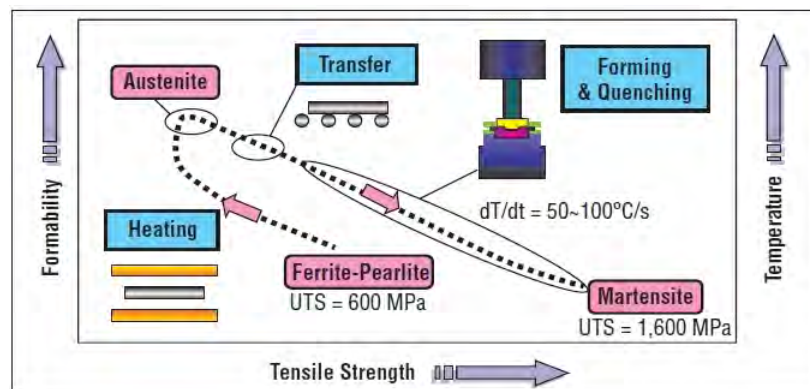


Figure 3.9: Tensile strength and microstructure changes during hot stamping

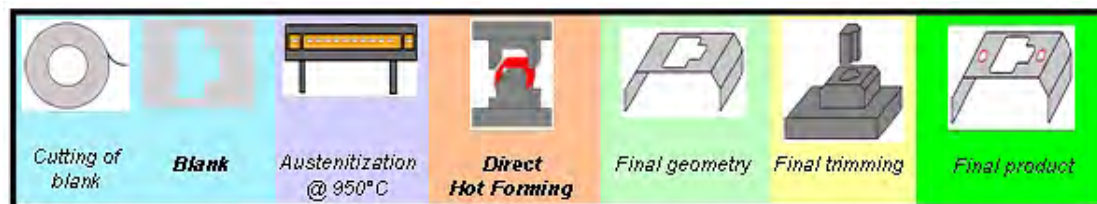


Figure 3.10: Typical direct hot stamping line

The preparation of the blank for hot stamping is similar to that for a cold stamped part, this applies to both direct and in-direct hot stamping. The difference in the stamping operation comes when the decision is made if the part is to be produced using a direct or indirect stamping process. In an indirect process, see Figure 3.11, differs from the direct process in that the part can be formed up to 100% of its required geometry prior the transfer of the part to a continuous feed furnace. This can be achieved in a similar process as used for cold stamping using a transfer press process. The part is placed in a continuous feed furnace then transferred to the hot stamping die. At this stage there is minimal geometry changes to the part in the die. This process gives minimal post

forming trimming operations.

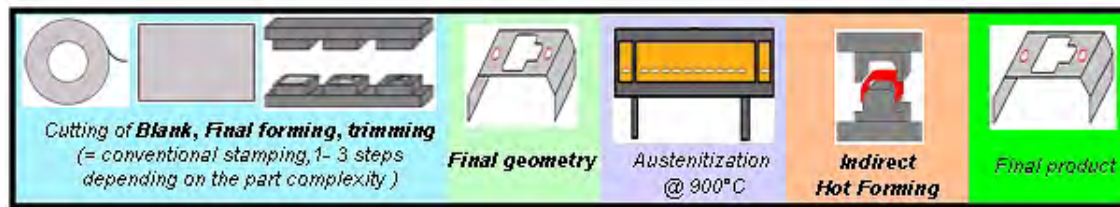


Figure 3.11: In-direct hot stamping process

This is in contrast to a direct process where no pre-forming of the part is done prior to the hot stamping operation. As minimal stamping operations other than forming can be completed in the direct hot stamping die there is a greater use of post stamping laser trimming operations. In both processes, oxidation of the part due to exposure to the ambient atmosphere may occur a de-scaling operation may be necessary. Due to the extreme hardness of the scale and movement of the blank in the die during the stamping operation, high die wear may result. To address the scale formation in hot stamping operations, steel products are provided that include an Aluminized, Galvanized, or other barrier coating that prevents oxidation of the surface and formation to address die wear issues and post-process scale removal. A typical in-direct hot stamping line is shown in Figure 3.12

3.2.7.3 Roll Forming

FSV considered both closed and open roll forming. Rollforming is a continuous forming process. During the rollforming process a flat strip is transported through powered or unpowered metal forming stands, rollers gradually forming the desired profile in a step by step process. The typical process consists of:

- Uncoiler
- Hydraulic hole and notch punch
- Roll forming main machine
- Straightener
- Automatic cutting station
- Control System
- Product unload station

The roll forming process is performed on a roll forming line in which the sheet stock or coil is fed through a series of roll stations. Each station has a roller positioned on both sides of the sheet. The shape and size of the roller die may be unique to that station, or several identical roller dies may be used in different positions. The roller dies may be above and below the sheet, along



Figure 3.12: Typical in-direct hot stamping line

the sides, at an angle, etc. As the sheet is forced through the roller dies in each roll station, it plastically deforms and bends. Each roll station performs one stage in the complete bending of the sheet to form the desired part as shown in Figure 3.13 and the sequence of single-forming is shown in Figure 3.14, as an example .



Figure 3.13: Typical roll forming line

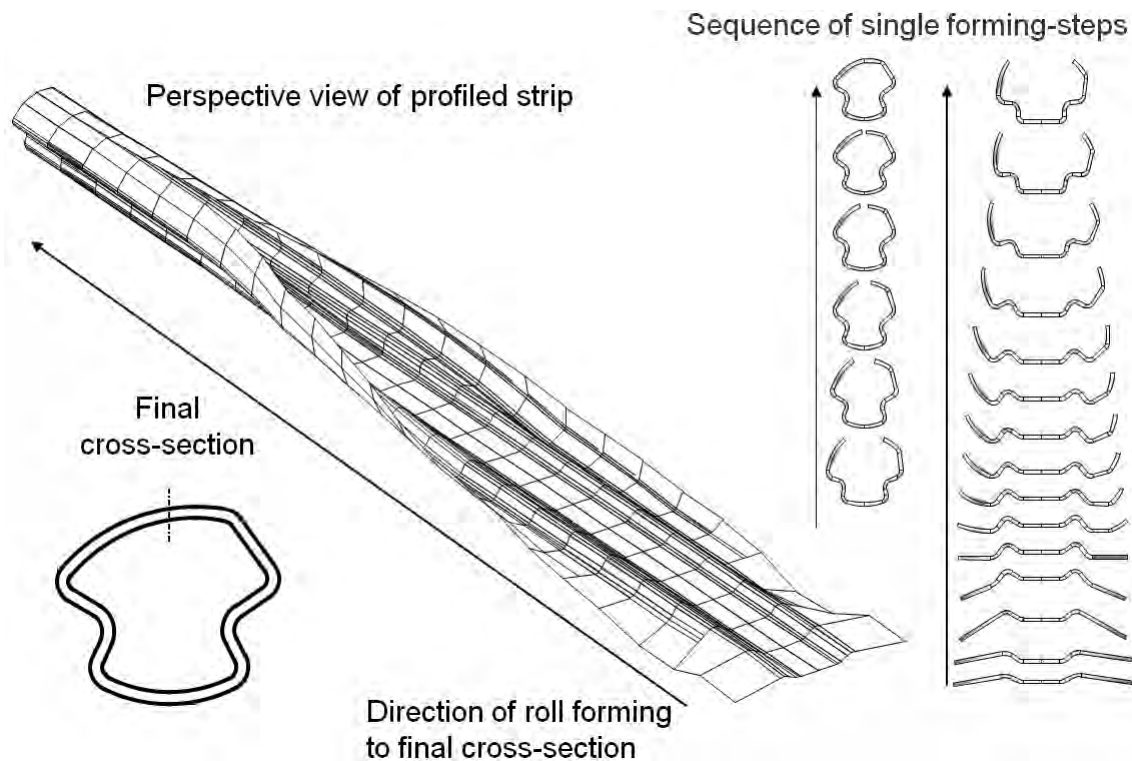


Figure 3.14: Typical roll forming operation showing a step-by-step

The roller dies are lubricated to reduce friction between the die and the sheet, thus reducing the tool wear. Lubricant can also allow for a higher production rate, this will also depend on the material thickness, number of roll stations, and radius of each bend. The roll forming line can also include other sheet metal fabrication operations before or after the roll forming, such as hole punching notching or shearing.

The roll forming process can be used to form a sheet into a wide variety of cross-section profiles. An open profile is most common, but a closed tube-like shape can also be produced with either a laser welding or a high frequency welding operation to close the seam. The roll forming process is capable of producing parts with tolerances as tight as $\pm 0.125\text{mm}$.

3.2.7.4 Hydroforming

For parts being hydroformed FSV cost model considered using a standard tube of single thickness and grade, laser welded and tailor rolled (multiple walled) tubes. Sheet hydroforming was not considered. The hydroforming process includes 4 stages:

- Incoming and in-plant material
- Pre-Hydroforming operations (pre-forming)

- Hydroforming
- Post-Hydroforming operations (trimming)

In tube hydroforming there are two major processes using either high or low pressure. With the high pressure process the tube is fully enclosed in a die prior to pressurization of the tube. In low pressure the tube is slightly pressurized to a fixed volume during the closing of the die. Pressure is applied to the inside of a tube that is held by dies with the desired cross sections and forms. When the dies are closed, the tube ends are sealed by axial punches and the tube is filled with hydraulic fluid. Fluid is injected into the tube through one of the two axial punches. Axial punches are movable and their action is required to provide axial compression and to feed material towards the center of the tube. The plant layout for tube hydroforming is shown in Figure 3.15 ^[1] and the schematic is shown in Figure 3.16.

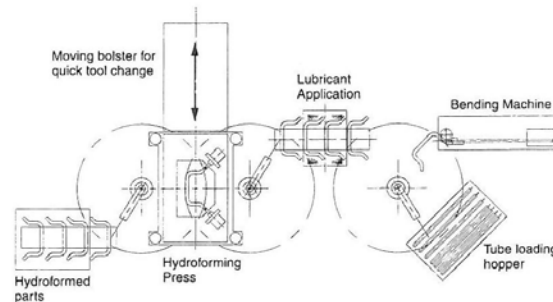


Figure 3.15: Plant layout for tube hydroforming

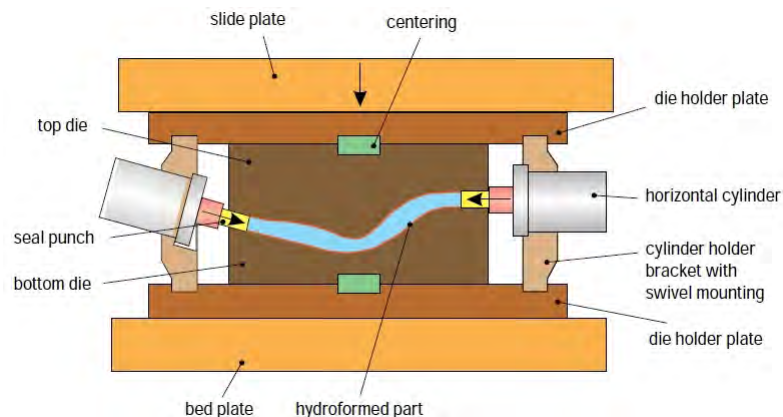


Figure 3.16: Schematic showing tube hydroforming die (Courtesy Schuler (Metal Forming Handbook 1998))

Punches may also be incorporated in the hydroforming die to form protrusions and/or depressions as shown in Figure 3.17. Punches may also be added to the die used to punch holes in the work piece at the end of the forming process.

¹Fundamentals of Hydroforming, Society of Manufacturing Engineers 2003

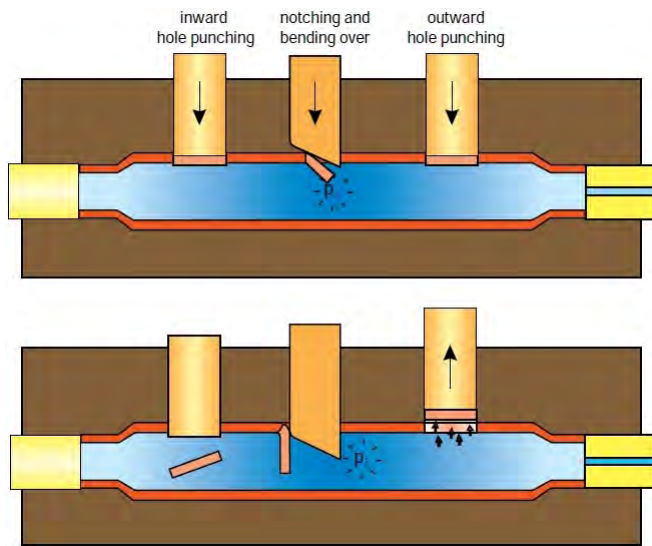


Figure 3.17: Schematic showing hole punching and notching in a hydroforming die (Courtesy Schuler (Metal Forming Handbook 1998))

Each part when necessary requires laser trimming operation to remove unwanted material at each end of the part that is necessary for the hydroforming process. A typical hydroforming press is shown in Figure 3.18.



Figure 3.18: Typical example of a hydroforming press (Courtesy: Schuler)

3.2.7.5 Laser Welded Finalized Tubes

Laser Welded Finalized Tubes is a forming process of producing a tubular component to the required form. The process consists of pre-stamping in a form die to a U-shape then closing the profile using lateral dies. The seam is then laser welded as shown in Figure 3.19. The end component can be straight or curved

Parts can be formed with or without the aid of a mandrel, depressions and changes in profile can also be added.

Figure 3.20 shows the steps to produce a tube with a curve and with a varying profile.

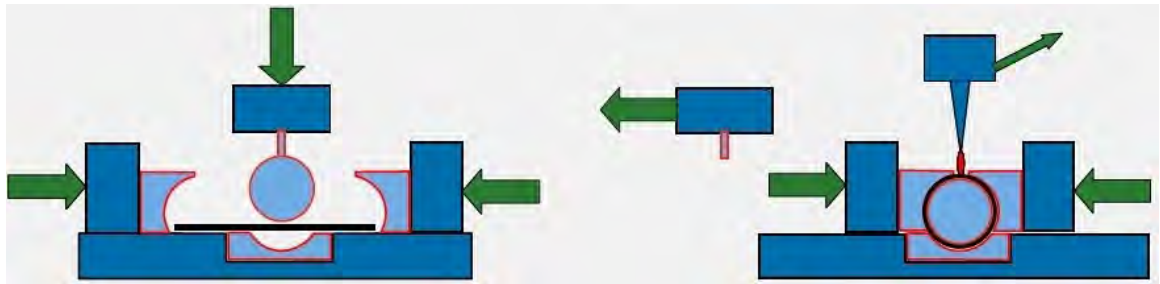


Figure 3.19: Forming process to produce tubular component using a mandrel and lateral dies

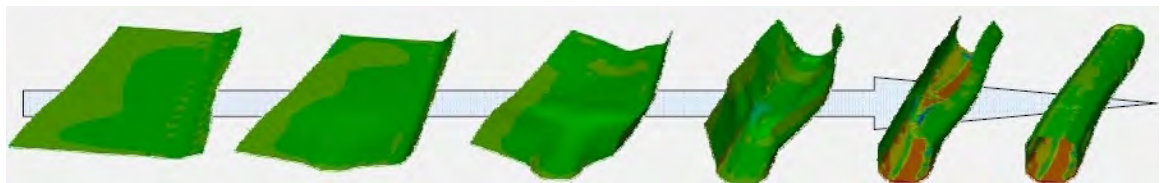
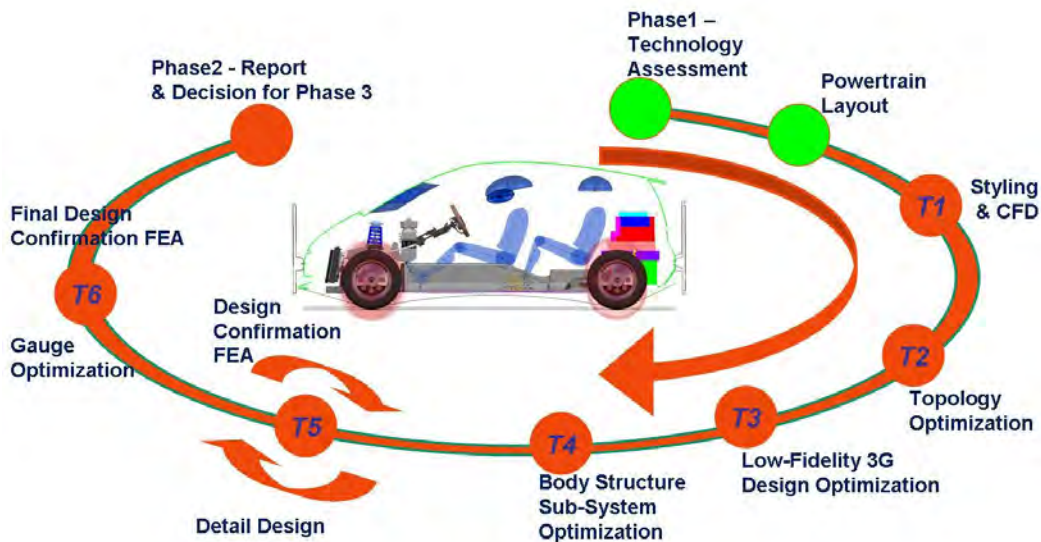


Figure 3.20: Method to produce a finalized tube

4.0 FSV-1 BEV Package



4.1 Background

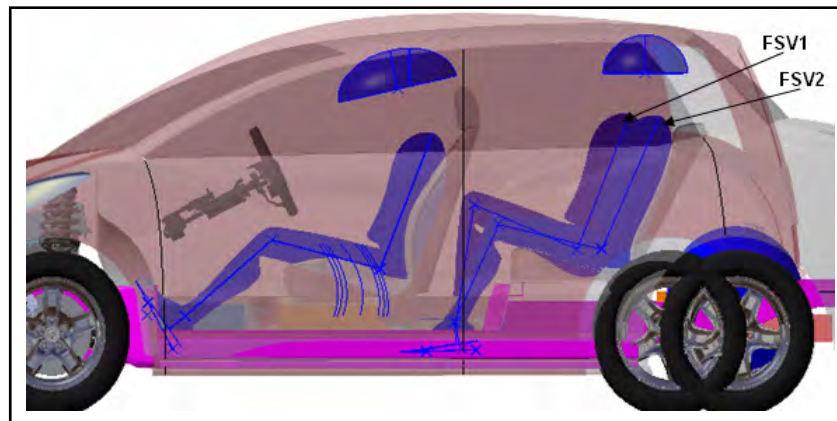
The FutureSteelVehicle (FSV) packaging studies began with the assessment of alternative powertrain technologies that are likely to be in production by year 2020. The objective being to achieve a low mass, low GHG footprint, aerodynamically efficient vehicle layout that structurally and environmentally meets future requirements. Environmental assessment, CO_{2e} - Green House Gas (GHG) emissions are computed on the basis of total Life Cycle Assessment (LCA). Worldwide market analysis conducted during Phase 1 of this project, showed that over 70% of the cars sold in today's marketplace share two vehicle sizes; the small car (A & B Class) up to 4,000 mm long and the mid-class car (C & D class) up to 4,900 mm long. To encompass both segments of the worldwide market, the FutureSteelVehicle program included two vehicle sizes, FSV-1 and FSV-2, and four powertrain options as shown in Table 4.1. Using electric front wheel drive, the result was an efficient common front end between these two vehicles and all four powertrains. The larger FSV-2 vehicle being 100 mm wider than FSV-1. The over-all length of FSV-1 & 2 is shorter than similarly sized vehicles, with comparable amounts of passenger and luggage volumes, that are driven with Internal Combustion Engine (ICE) based powertrains.

4.2 Packaging Approach

	Plug-in Hybrid (PHEV)	Fuel Cell (FCEV)	Battery Electric (BEV)
FSV 1 4 door hatchback 3820mm	PHEV 20 Electric Range - 32km (20mi) Total Range - 500km Max Speed -150km/h 0-100km/h 11-13s		BEV Total Range - 250km Max Speed -150km/h 0-100km/h 11-13s
FSV 2 4 door sedan 4350mm	PHEV 40 Electric Range - 64km (40mi) Total Range - 500km Max Speed - 161km/h 0-100km/h 10-12s	FCEV Total Range - 500km Max Speed - 161km/h 0-100km/h 10-12s	

Table 4.1: Vehicle size and powertrain options

During Phase 1 of this program, for FSV 1 & 2, the front and rear leg-room and luggage carrying capacity was also established as shown in Table 4.2. These capacity numbers are typical for the A&B Class and C&D Class vehicles.



Class	Front Leg Room [mm]	Rear Leg Room [mm]	Luggage [Liters]
FSV-1	1065	850	250
FSV-2	1065	925	370

Table 4.2: FSV leg room and luggage capacity

4.2 Packaging Approach

For this phase of the program, the FSV-1 Battery Electric Vehicle (BEV), was selected because its largest mass was most challenging for developing a lightweight vehicle structure. Relative to other advanced powertrains, the body-structure mass should be conservative. To achieve efficient packaging a holistic design methodology that considers several automotive systems simultaneously has to be implemented. This requires the vehicle integration engineering and design teams

working on the following systems to be in very close proximity and sharing a common design data base.

1. Powertrain sizing (performance assessment)
2. Powertrain layout in vehicle
3. Suspension design, wheel clearance envelopes, ride and handling performance assessment
4. Occupant packaging considerations - ingress/egress, vision, comfort and safety requirements
5. Overall vehicle geometry - ground clearances, front to rear mass split, center of gravity, safety, aerodynamics and styling, and luggage carrying capacity

4.3 Powertrain Package

The major components of the BEV powertrain are:

1. Battery pack
2. Electric drive motor
3. Converter (converts DC current to AC and control motor speed)

4.3.1 Battery

For a BEV several battery layout solutions are possible, as shown in Figure 4.1 and Figure 4.2. Various other options were considered during Phase 1 (details can be found in FSV Phase 1 report). After studying several design iterations of battery layout, the following four options are worthy of further discussion. These options are for Li-ion battery packs with energy densities on the order of $130 \frac{\text{Wh}}{\text{kg}}$ to $180 \frac{\text{Wh}}{\text{kg}}$. The actual size of the battery pack is dependent on the required driving range for the vehicle and the energy density of the battery pack.

Various battery considerations are:

1. Battery under front floor and tunnel (Figure 4.1)
2. Battery pack in the tunnel (Figure 4.2)
3. Battery pack in tunnel & under rear passenger seat-pan (Figure 4.2)
4. Battery pack under rear passenger seat-pan (Figure 4.2)

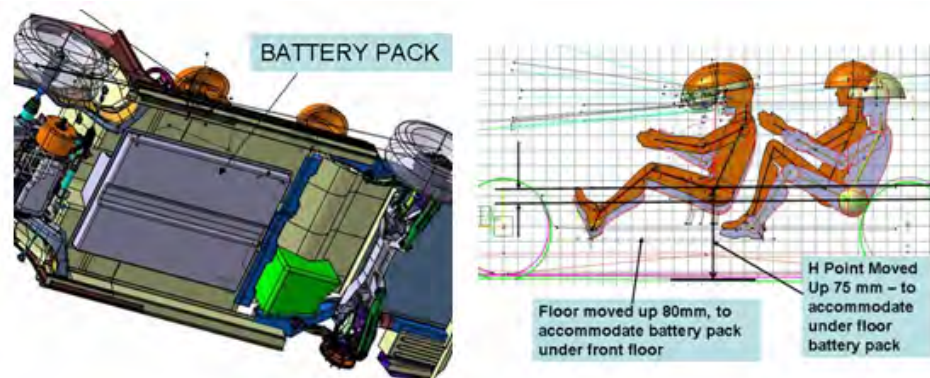


Figure 4.1: Battery pack under-floor

The battery under the front floor as shown in Figure 4.1 can also be extended rearward to under the rear passenger seat pan if additional volume/capacity is required. Accommodation of the battery pack under the floor raises the floor by a minimum of 80mm and the occupant Hip (H)-Point up by a similar amount. This is reflected in the vehicle height, and hence, the vehicle frontal cross-sectional area. This will increase the aerodynamic drag of the vehicle which reduces fuel efficiency.

Battery layout options shown in Figure 4.2 accommodate the battery in the tunnel and/or under rear passenger seat pan without raising height of the front floor. During Phase 1 of this project, our assumed battery pack energy density was $130 \frac{\text{Wh}}{\text{kg}}$. At this energy density, for a driving range of 250 km, the BEV requires a 35 kWh battery-pack with a 275 liter volume. This size battery pack can be packaged under the tunnel and the rear seat floor pan, similar to the 'T-shape' battery pack shown in Figure 4.2.

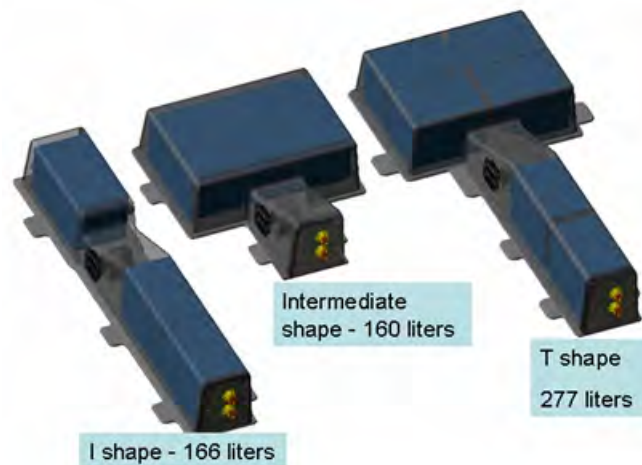


Figure 4.2: Battery pack in tunnel and under rear floor

Worldwide, the progress in battery technology is advancing at a very fast pace. After further

review of battery technology and a meeting with NEDO 'New Energy and Industrial Technology Development Organization' of Japan, the battery pack energy density target for year 2020 was revised to $180 \frac{\text{Wh}}{\text{kg}}$. At this higher energy density level, the battery pack is reduced in size and weight such that the required End-Of-Life (EOL), capacity of 30 kWh (with a volume of 165 liters, including cooling system), is needed for a 250 km range. This volume can be packaged in the 'I-shape' battery pack configuration shown in Figure 4.2. The FSV battery specifications are shown in Table 4.3 ^[1].

Battery Specification (New)	Cell	Sub-Pack	Battery Pack
Quantity	192	6	1
Volume (L)	0.35	17.9	140
Mass (kg)	0.71	26.7	188
Energy (kWh)	0.18	5.8	35
Energy Density ($\frac{\text{Wh}}{\text{kg}}$)	255	215	180

Table 4.3: FSV battery (new) specifications

4.3.2 'I - Shape' Battery Pack

The battery packs are generally constructed from standardized sub-packs and include the Battery Management System (BMS) and battery cooling system. Each sub-pack is constructed from 'prismatic cells' and heat-sink assemblies as shown in Figure 4.3. Each individual cell used in the FSV-1 battery sub-pack is a 50 Ah, 3.7 V nominal voltage prismatic-type cell weighing 0.71 kg. A total of 192 of these cells are packed into 6 sub-packs (32 cells in each) which make up the entire battery pack as shown in Figure 4.4.

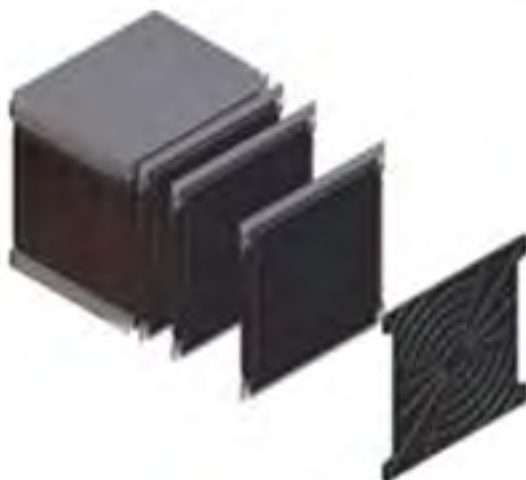


Figure 4.3: Sub-pack with individual prismatic cells

¹The battery specifications shown are for a new battery, the End-of-Life (EOL), energy density specifications are as follows: Cell - $217 \frac{\text{Wh}}{\text{kg}}$, Sub-Pack - $183 \frac{\text{Wh}}{\text{kg}}$, Battery Pack - $160 \frac{\text{Wh}}{\text{kg}}$

4.3 Powertrain Package

This 180 $\frac{\text{Wh}}{\text{kg}}$ 'I-shape' battery pack of the FSV-1 weighs a total of 207 kg, a reduction of 140 kg from the earlier 130 $\frac{\text{Wh}}{\text{kg}}$ 'T-shape' version which weighed 347 kg. This large reduction in battery weight, resulting from the higher energy density, reduced the overall weight of the FSV-1 to 995 kg due to its compounding effect on other components of the vehicle. This reduction in vehicle weight led to significantly lower energy consumption, enabling the reduction in required kWh of stored energy.

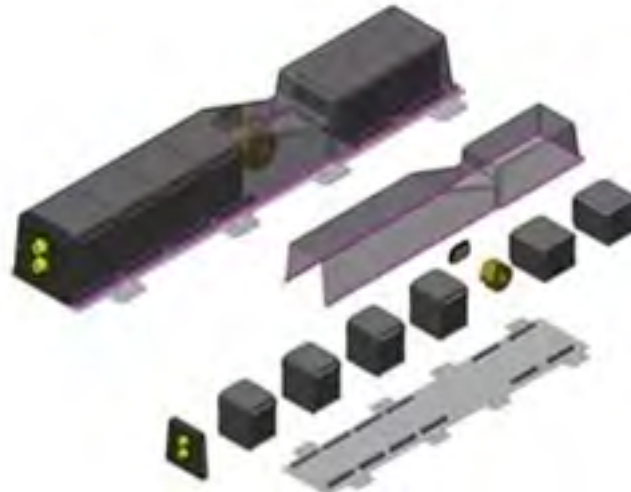


Figure 4.4: FSV-1 "I-shape" battery pack

The 'I-shaped' battery pack in the vehicle is placed underneath the tunnel and under the rear passenger seat pan as shown in Figure 1.7. Use of this space in the tunnel does not lead to any packing conflict with interior packaging space required for the occupants and luggage.

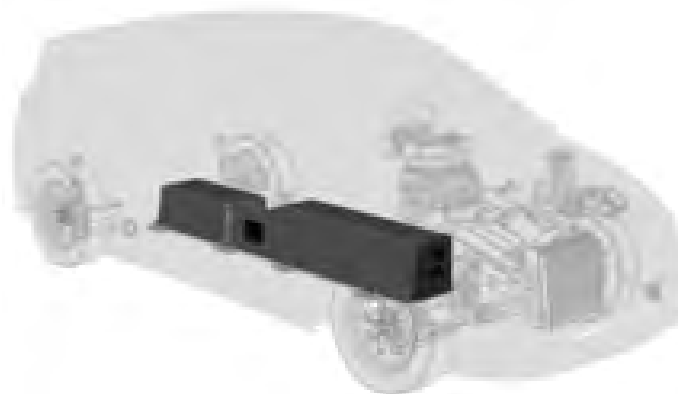


Figure 4.5: FSV-1 'I-shape' battery in vehicle tunnel

4.3.3 Electric Drive Motor

With a lighter battery and consequentially a lower vehicle mass, the size of the electric drive motor can also be reduced. With the higher mass 'T-shape' battery the FSV-1 required a motor with 60 kW of peak power. A 55 kW peak power motor is sufficient to meet all the performance requirements of the FSV-1 when using a lower mass 'I-shape' battery pack. The new smaller drive motor with the inverter is packaged in front of the vehicle as shown in Figure 4.6.

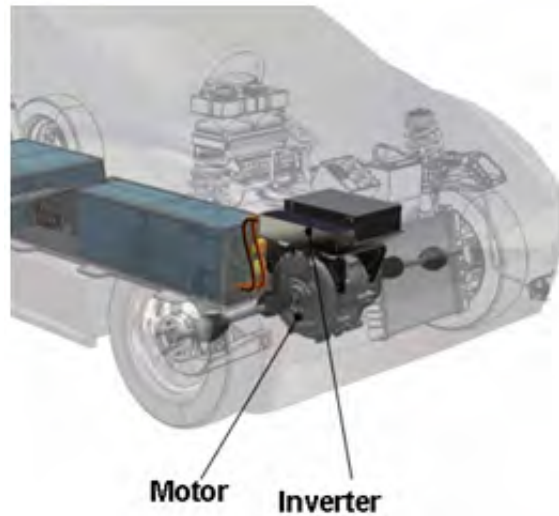


Figure 4.6: FSV-1 front wheel drive motor and inverter

4.3.4 Front and Rear Suspension

The choice of front and rear suspension designs were fully reported in the FSV Phase 1 report. Figure 4.7 shows front MacPherson strut and rear multi-link trailing arm suspension design chosen for the FSV-1 BEV. For vehicle packaging lay-out it is very important to consider the suspension design and performance for ride and handling at an early stage of the program. This was done during Phase 1 by accurate mass tracking and using ADAMS simulation program to predict handling performance. It is also important to establish the required wheel clearance envelopes for all possible wheel travel up/down and front wheel steering positions as shown in Figure 4.7.

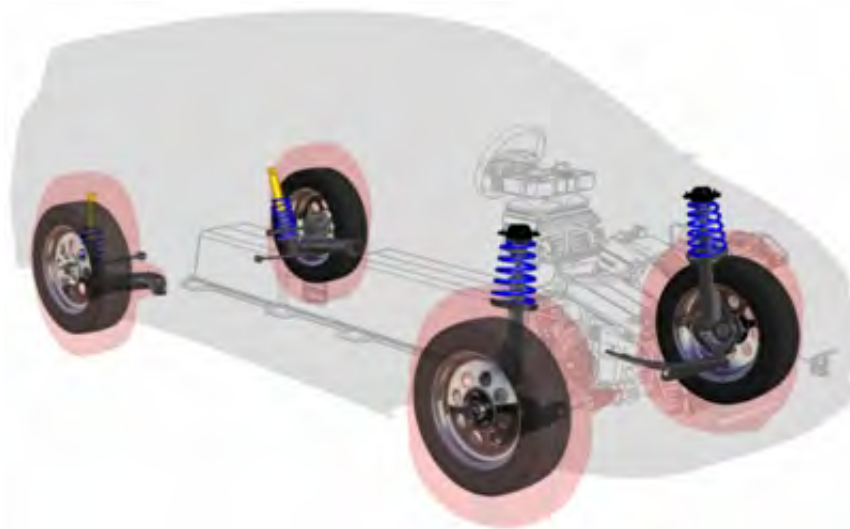


Figure 4.7: *FSV-1 front and rear suspension and wheel clearance envelopes*

4.4 Occupant Positions

To establish the overall vehicle size, the packaging begins with the occupant and luggage space requirements. The driver and occupant seating positions are established with the required leg-room and vertical Hip (H)-point positions. A 95th percentile male dummy with a 99% eye ellipse and head contour placed in the front and rear seat positions are shown in Figure 4.8.

SAE and CAVA guidelines along with FSV-1 tire size estimates, were used to establish the appropriate ground clearances, H-point estimation and distances from center of wheel to driver foot.

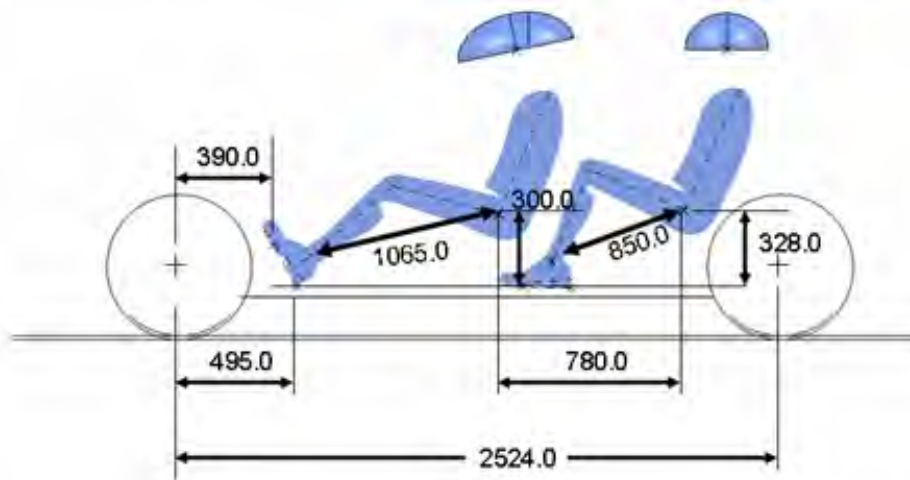


Figure 4.8: FSV-1 occupant positioning

4.5 Bumper Positions and Front Crush Zones

The vehicle exterior boundaries are determined by the position of the front and rear bumpers. Worldwide regulations mandate low speed impact requirements on all passenger cars. This regulation simulates a low speed impact with a pendulum that impacts the vehicle bumper. The height of the pendulum was used as a constraint for determining the height of the front and rear bumper positions on the FSV-1. The front end length is based on the required front end crush distance plus the space taken by the electric drive train. The rear overhang, which is the distance from the center of the rear wheel to the back of the vehicle, is determined by the required luggage volume (250 liters for the BEV). The packaging layout with the interior occupant positions, front and rear bumper positions, and front and rear overhangs on the FSV-1 is shown in Figure 4.9.

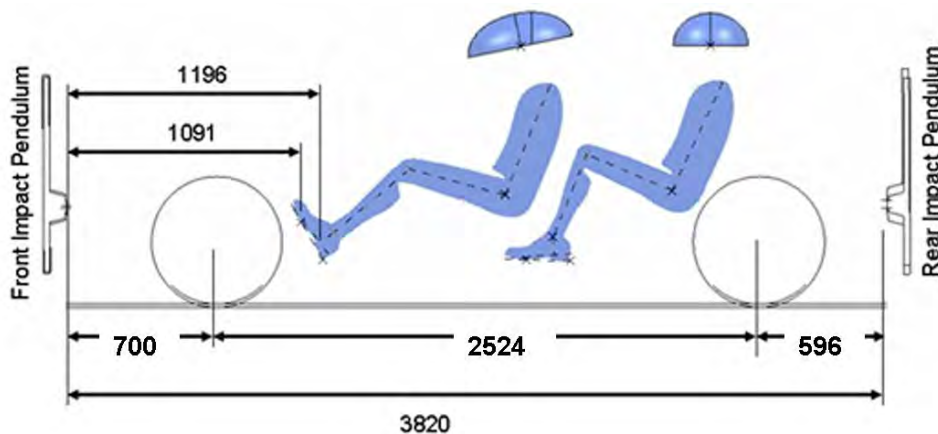


Figure 4.9: FSV-1 bumper heights, front and rear overhangs

4.6 Vision Requirements

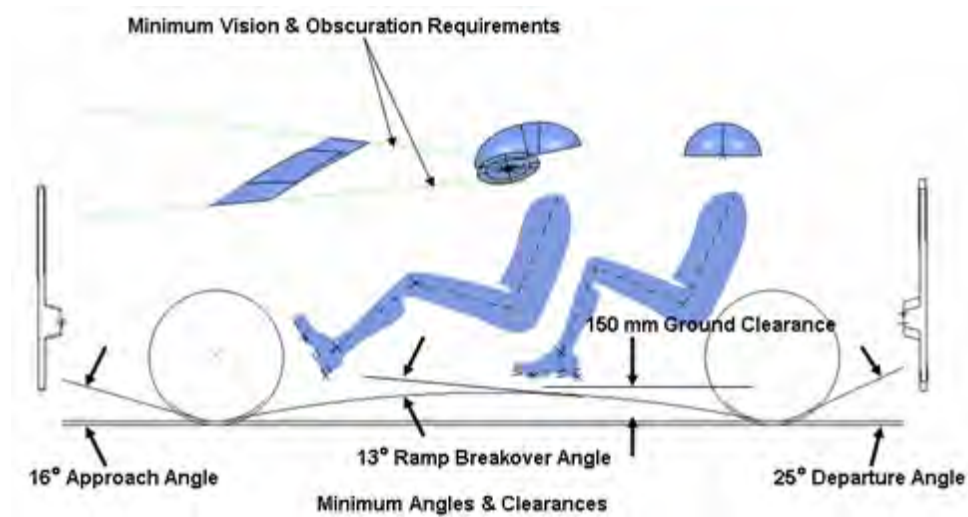


Figure 4.10: FSV-1 - ground clearance and ramp angles

4.6 Vision Requirements

The driver field of view studies conducted in accordance with SAE 1050 and EEC 92/22 requirements determined the optimal position of the front seat occupant (95th male with 99% eye-ellipse) as shown in Figure 4.10 and Figure 4.11. A-pillar obscuration studies conducted in accordance with EEC regulation 77/649 determined the position and width of the A-pillars on the vehicle. The vehicle width was established based on the FSV-1 rear seat passenger seating requirements of 2 adults and a child, typical of B-class vehicles.

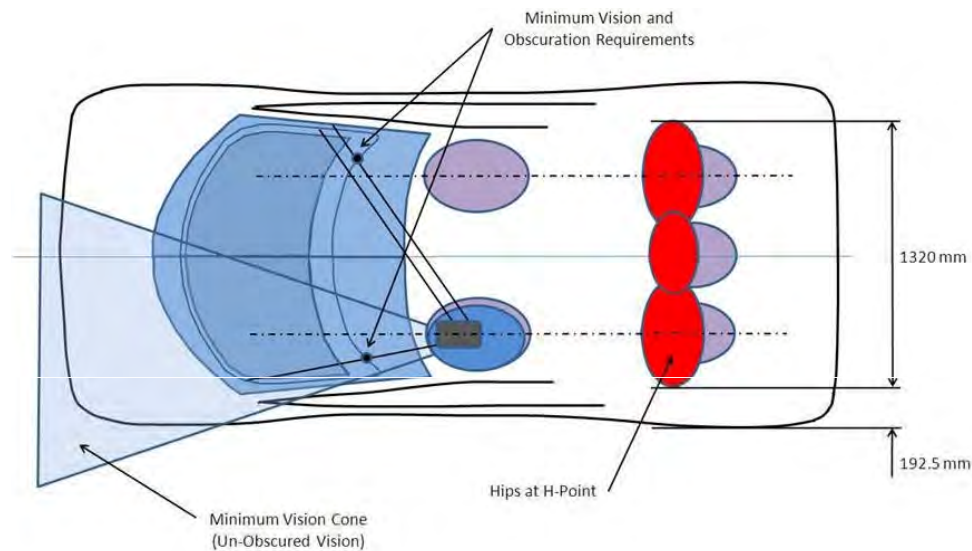


Figure 4.11: FSV-1 A-Pillar obscuration angle and vehicle width

4.7 Luggage Volume

Luggage volume is determined by the rear seat position, which was calculated for both seats unfolded (25 degrees) and in the folded position. Compartment volumes were designed according to the specifications outlined in SAE J1100 and ISO 3832 to meet the 250 liter volume target, for the FSV-1.

Figure 4.12 and Figure 4.13 show the luggage compartment volume representation with the seat back up and seat back folded positions respectively.

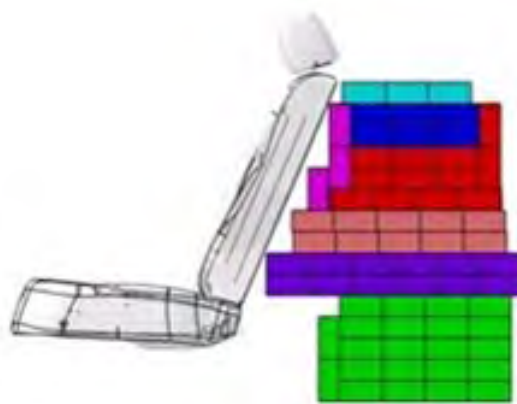


Figure 4.12: *FSV-1 luggage volume with seat unfolded*

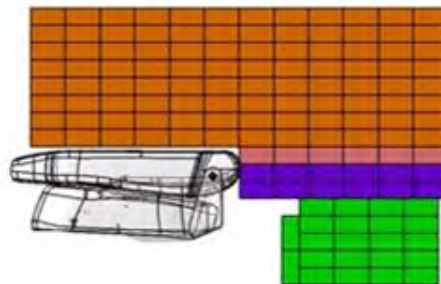


Figure 4.13: *FSV-1 luggage volume with seat folded*

Table 4.4 shows the calculated numbers for luggage volumes in both of these positions.

Index	Seat Position	Luggage Volume (l)
ISO 3832	Unfolded	266
ISO 3832	Folded	700

Table 4.4: *FSV-1 luggage compartment volumes*

4.8 Vehicle Styling Theme

With the power train packaged and driver vision and vehicle luggage volume requirements satisfied, other components like the steering column and wheel were packaged using the results of passenger ergonomics and reach studies. The exterior styling theme was then applied to the packaging as shown in Figure 4.14.

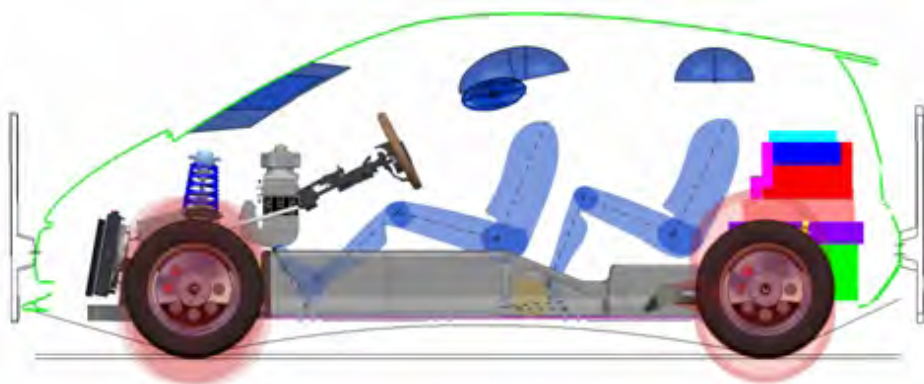


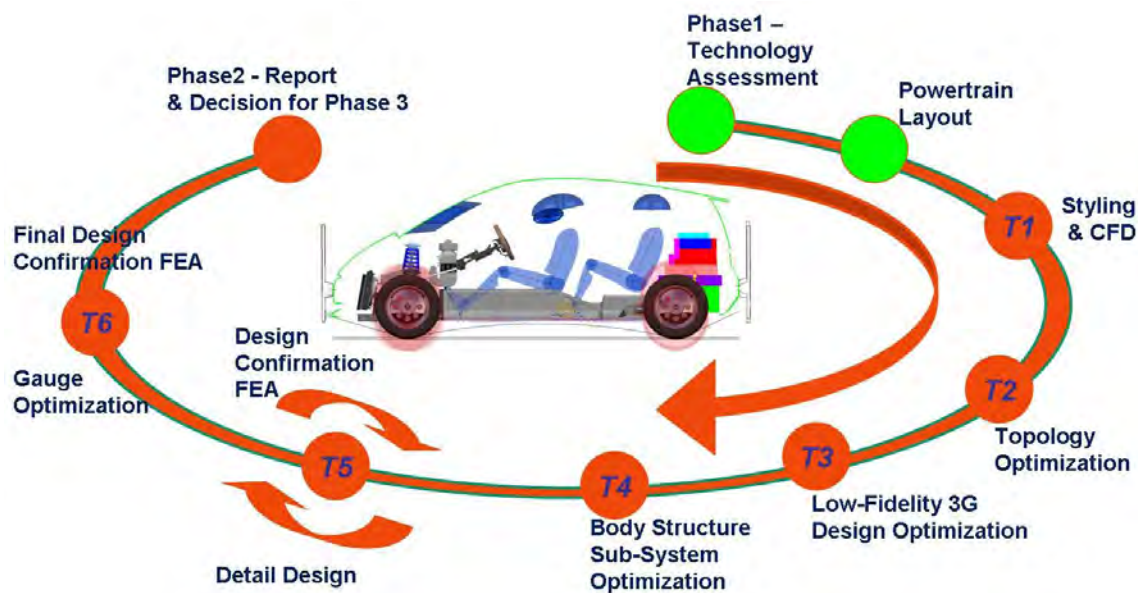
Figure 4.14: *FSV-1 exterior styling theme*

This styling theme provided the necessary data to derive a rough sketch of the exterior body shape of the FSV-1 as shown in Figure 4.15.



Figure 4.15: *FSV-1 vehicle sketch*

5.0 Structural Targets



5.1 Vehicle Crash Targets

Crash worthiness is the one of the most important characteristics of any vehicle design. The FutureSteelVehicle will be designed to meet all the crash worthiness requirements both currently applicable and future safety requirements (2015-2020). Vehicle crash worthiness evaluations are mainly based on occupant injury criteria. The occupant injury values are influenced by seatbelt and airbag deployment strategies, whose optimum performance depends on the efficiency of the body structure design. This makes it imperative that the body structure should be designed to provide the best energy absorption and minimum intrusion characteristics.

Of the database of vehicle crash tests required for compliance to worldwide standards, a few of the crash tests are considered critical to the body structure design due to the mode and speed of impact. The following body structure critical crash tests were chosen to be evaluated using Computer Aided Engineering (CAE) simulation studies to ensure that the body structure of the FSV meets those targets.

5.1 Vehicle Crash Targets

5.1.1 Frontal Impact

5.1.1.1 US NCAP - 56 $\frac{\text{km}}{\text{h}}$ 0° Frontal Impact

This is a frontal impact for the US New Car Assessment Program (NCAP), and due to its high velocity impact into a rigid barrier (100% overlap), is one of the critical regulations to meet for frontal impact. This test needs the vehicle front-end structure to absorb very high kinetic energy while decelerating the car at an optimal rate (as close to a square pulse as possible). The rate of deceleration is critical as it minimizes the effect of impact on the occupant and helps with the seat-belt and air-bag deployment strategy. The vehicle is designed to meet intrusion, dynamic crush and B-pillar pulse targets as shown in Table 5.1. The body structure peak pulse target is 35 g's, however, a range of 35 to 38 g's is generally acceptable because each body structure design is unique and actual restraint system performance is "fine tuned" for that structure through seat belt and airbag dynamic performance parameters. Seatbelts retractors are designed to limit seatbelt webbing payout (release of webbing from the retractor spool), with the use of pyrotechnically activated seatbelt webbing pre-tensioners. The goal is to control forward movement. Seatbelt retractors also control occupant loading through internal force limiting mechanisms. Likewise, airbag cushions incorporate various technologies like dual-stage airbag inflators, active and passive airbag venting, custom cushion volumes, shapes and folds, all in the effort to control "ride down" of the occupant. These are just some of the technologies available that are designed to work in concert with each other to limit the injury criteria numbers in a vehicle under development. The test set-up for the BEV US NCAP Frontal Impact is shown in Figure 5.1.

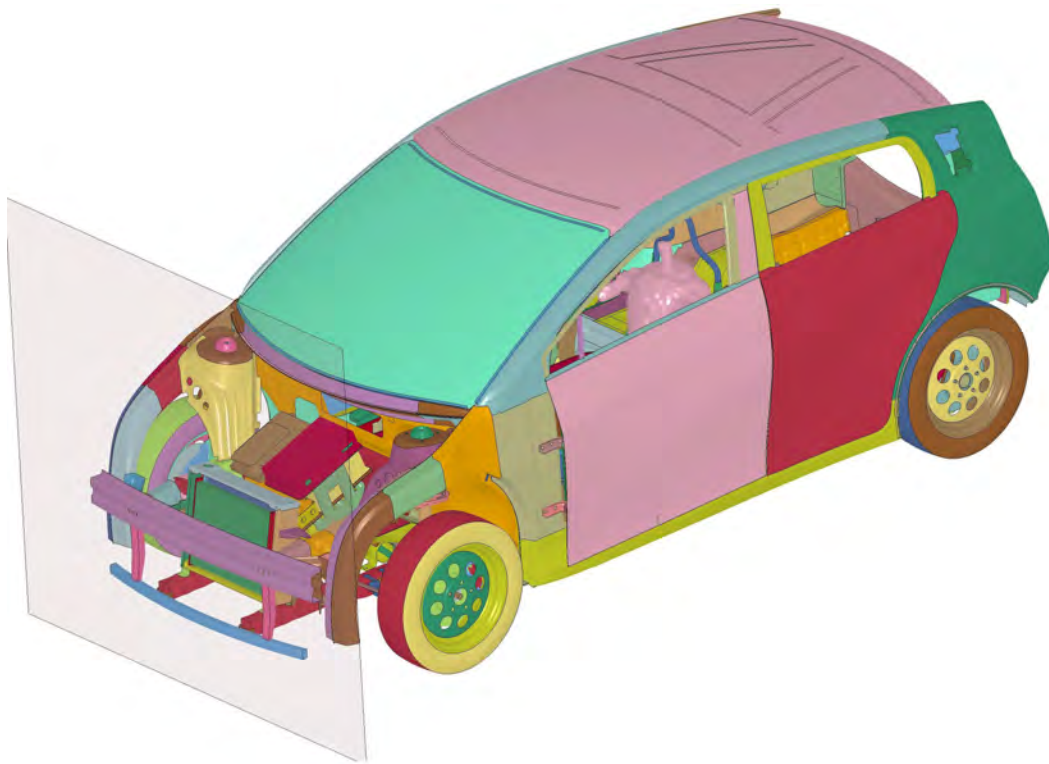


Figure 5.1: *USNCAP - frontal impact*

Body Location	USNCAP Targets
Foot Well Intrusion	< 100 mm
Peak Pulse	< 35 g's after 30 ms

Table 5.1: *USNCAP - target values*

5.1.1.2 EURO NCAP - 64 $\frac{\text{km}}{\text{h}}$ 40% Offset Deformable Barrier

In the European New Car Assessment Program for frontal impact, a vehicle moving at 65 $\frac{\text{km}}{\text{h}}$ (40 $\frac{\text{m}}{\text{h}}$) strikes a deformable barrier that is offset to 40% of vehicle width as shown in Figure 5.2. This test is very severe on the vehicle front-end structure as only one-half of the structure absorbs most of the energy of impact. The peak pulse on the driver side should be less than 42 g's (Peak Pulse < 42 g's), which is a program subjective "due care" target. Comparatively, the VW Super Light Car (SLC), has a 56 g peak deceleration pulse (See Figure 5.3). To ensure that the vehicle meets the occupant based targets, the structure should meet the 'good' targets shown in Figure 5.4, which are based on the intrusion guidelines of the IIHS offset deformable barrier test.

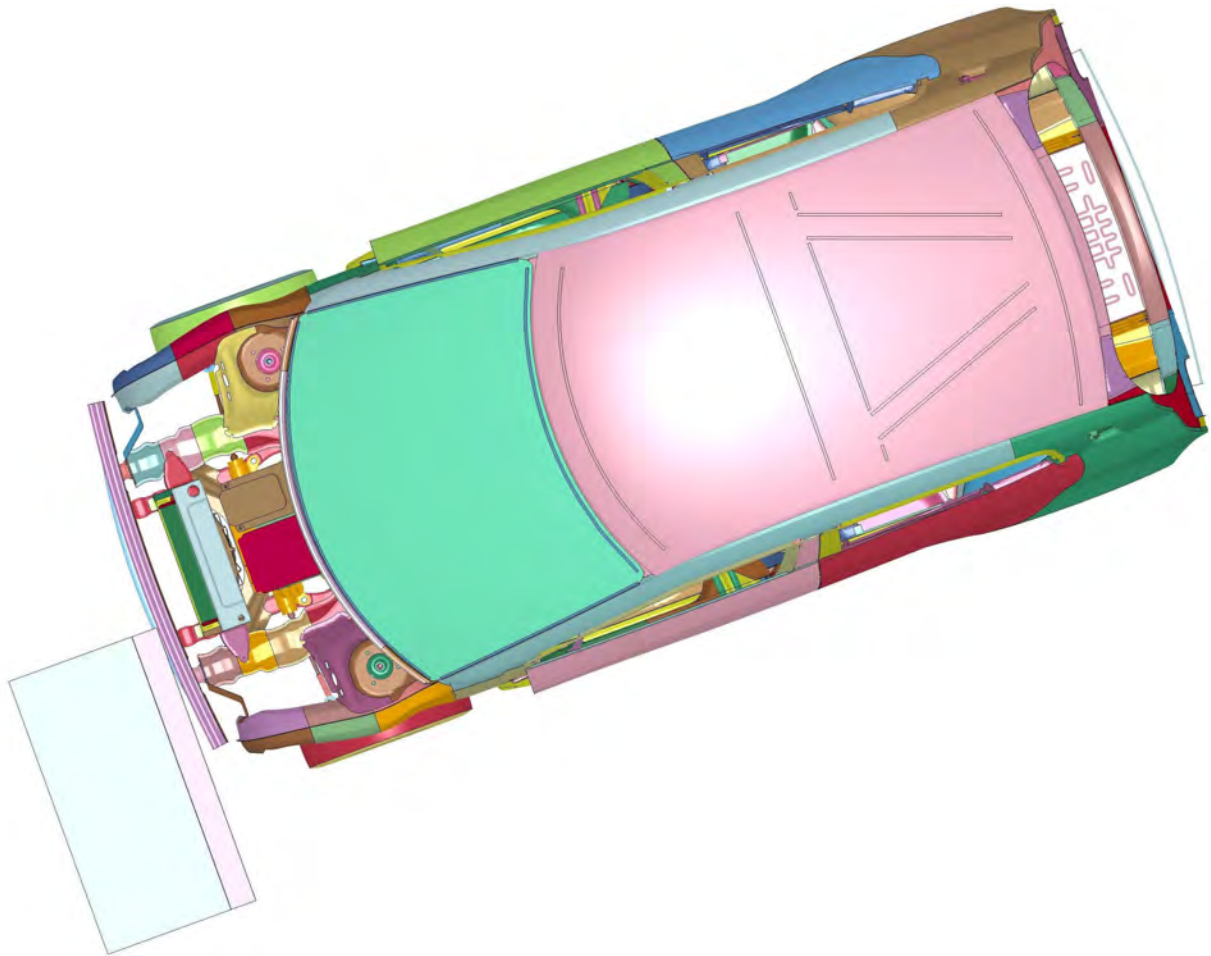


Figure 5.2: *EURO NCAP - 64 $\frac{\text{km}}{\text{h}}$ 40% offset frontal impact*

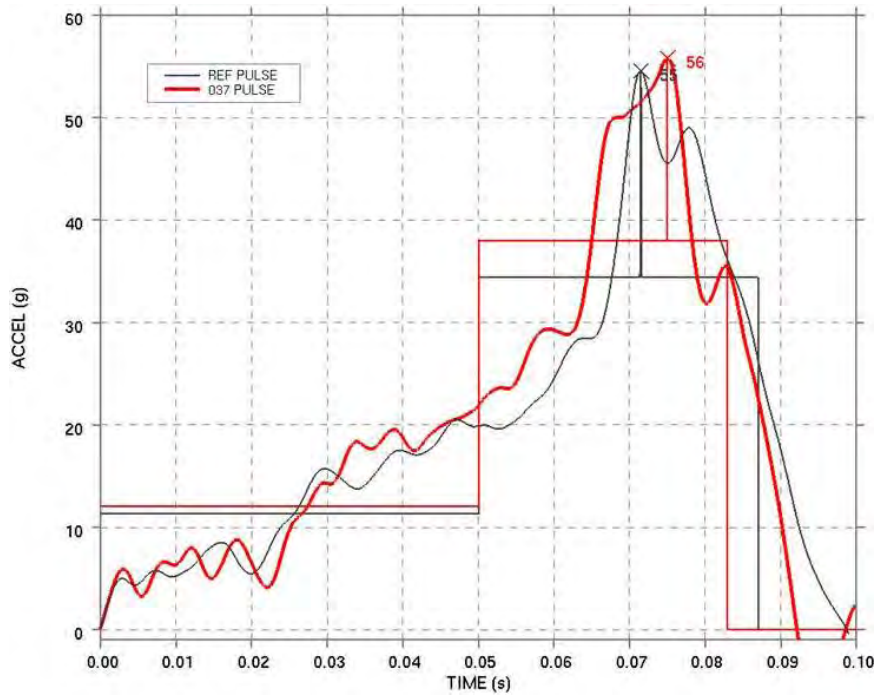


Figure 5.3: VW SLC Euro NCAP peak deceleration pulse

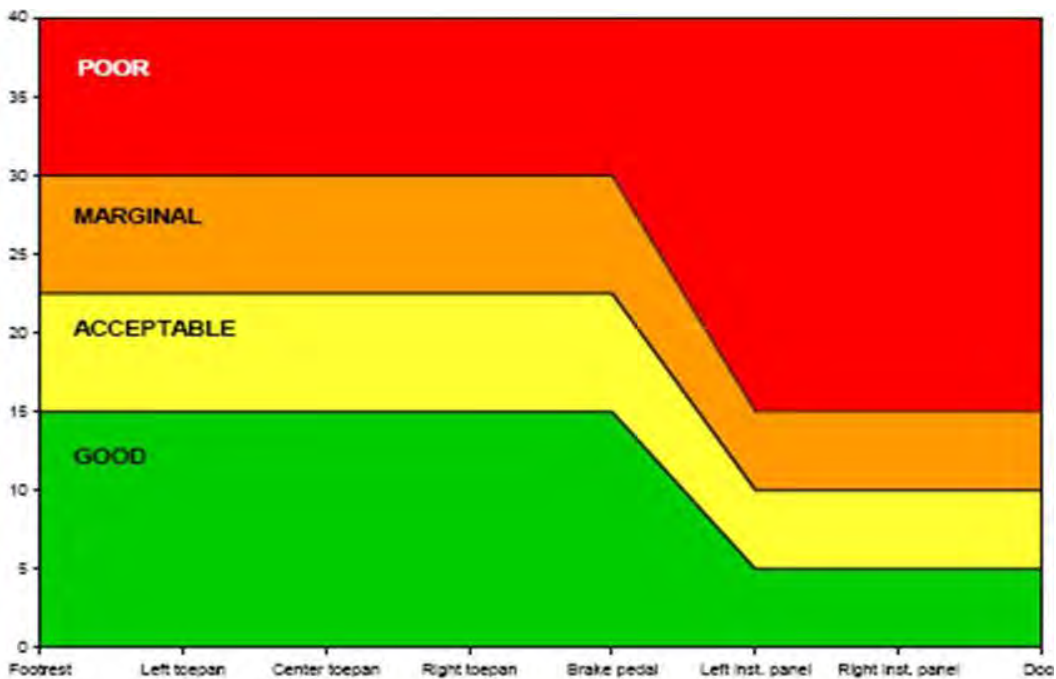


Figure 5.4: IIHS - intrusion guidelines

5.1 Vehicle Crash Targets

5.1.2 Side Impact

5.1.2.1 Insurance Institute for Highway Safety (IIHS) Side - 50 $\frac{\text{km}}{\text{h}}$ 90° Deformable Barrier

This event is carried out by having a 1500 kg Movable Deformable Barrier (MDB) impact the driver's side of the vehicle at 50 $\frac{\text{km}}{\text{h}}$. The injury protection is assessed by placing a side impact test dummy in the driver's seat which is controlled by the amount of B-pillar intrusion into the passenger compartment. Therefore it is critical that the body side structure provide optimal resistance to the impact of the barrier. Figure 5.5 shows the FSV model set-up for this load case. The IIHS side impact targets are shown in Table 5.2 and Figure 5.6.

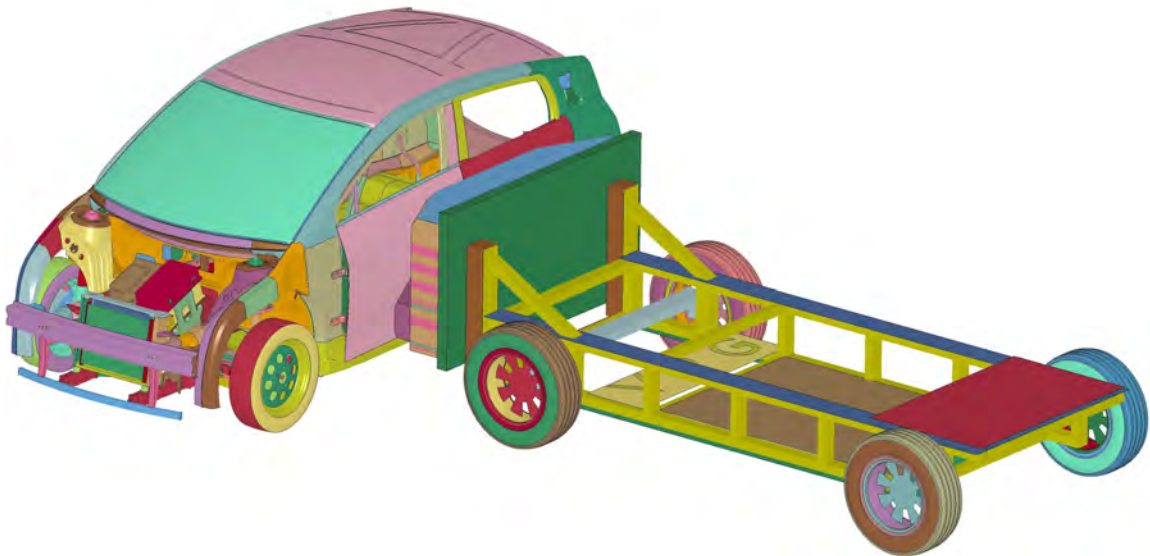


Figure 5.5: IIHS Side 50 $\frac{\text{km}}{\text{h}}$ 90° deformable barrier

IIHS Side Impact Targets	
B Pillar Intrusion	Green in (Figure 5.6)

Table 5.2: IIHS side impact - target values

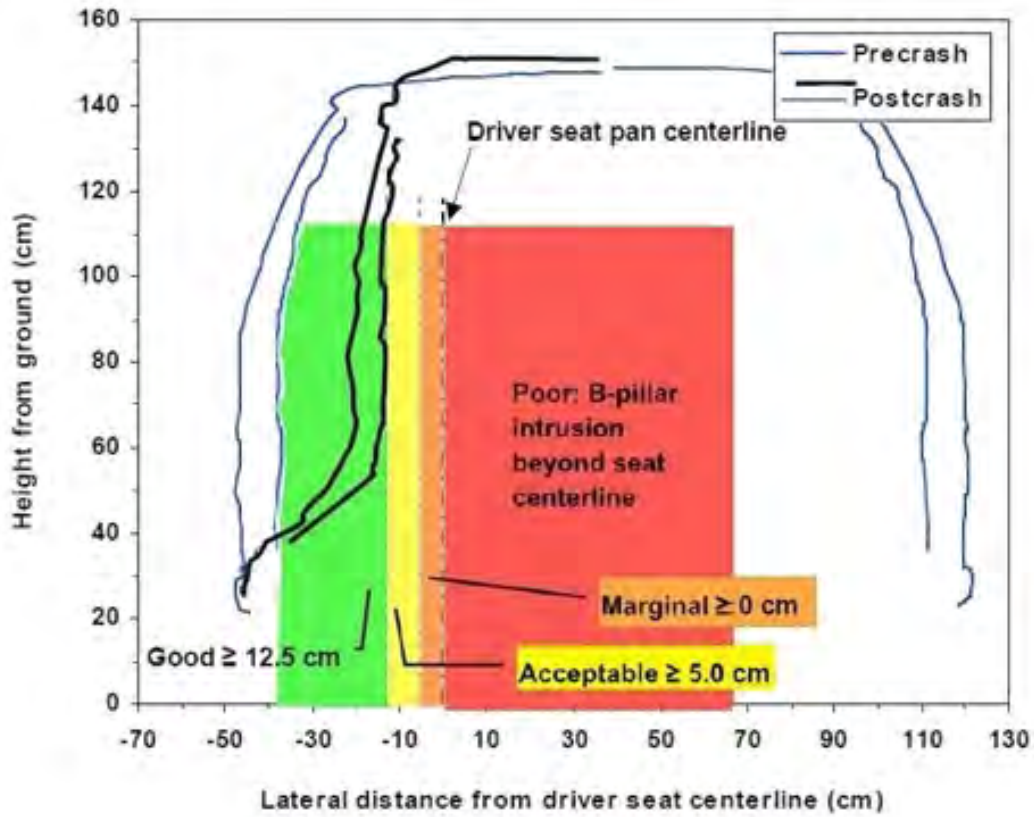


Figure 5.6: IHS side impact target intrusion requirements

5.1 Vehicle Crash Targets

5.1.2.2 US SINCAP - $61 \frac{\text{km}}{\text{h}}$ 27° Crabbed Impact

In this load case for compliance with the US Side Impact New Car Assessment Program, a 1370 kg moving trolley is impacted into the driver's side of a car. This load case represents a typical intersection-type collision and is simulated by impacting the vehicle which is positioned at 63° to the forward line of motion with a moving deformable barrier with 27° crabbed angles at $62 \frac{\text{km}}{\text{h}}$ ($38.5 \frac{\text{m}}{\text{h}}$). The body side structure design (B-pillar, rocker etc.), and the crossmembers (seat cross-member, side impact protection system etc.), in the passenger compartment play critical roles in meeting targets for this load case. Meeting the structural targets shown in Figure 5.7 and Figure 5.6 will ensure that the occupant based targets could be met. Figure 5.7 shows the FSV model for this load case.

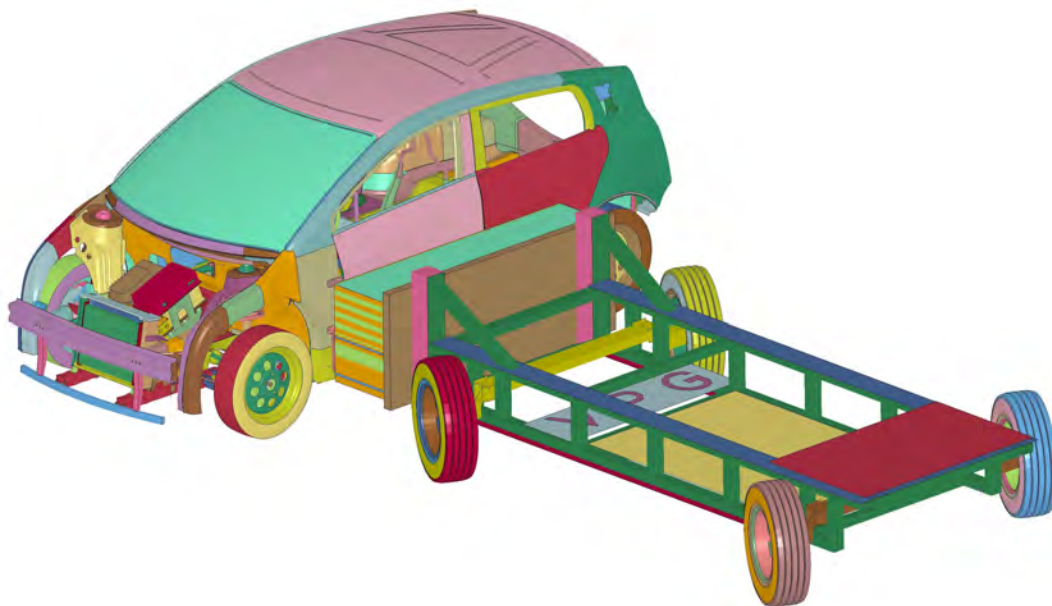


Figure 5.7: *US SINCAP $61 \frac{\text{km}}{\text{h}}$ 27° crabbed impact*

5.1.3 Rear Impact

5.1.3.1 FMVSS 301 - 80 $\frac{\text{km}}{\text{h}}$ 70% Offset Deformable Barrier

The US Federal Motor Vehicle Safety Standards (FMVSS) represents a severe dynamic rear impact load case in which the vehicle is impacted at 80 $\frac{\text{km}}{\text{h}}$ at 70% offset of vehicle width. This is to simulate a rear car to car collision. In the case of typical gasoline vehicles, the fuel system integrity is the criteria and in case of electric vehicles, the battery system integrity is critical. Since the event is run at a high speed, the body structure needs to absorb very high kinetic energy while minimizing the intrusion without impacting the battery module. Table 5.3 shows the structure targets for this rear crash regulation. Figure 5.8 shows the FSV model set-up for this load case.

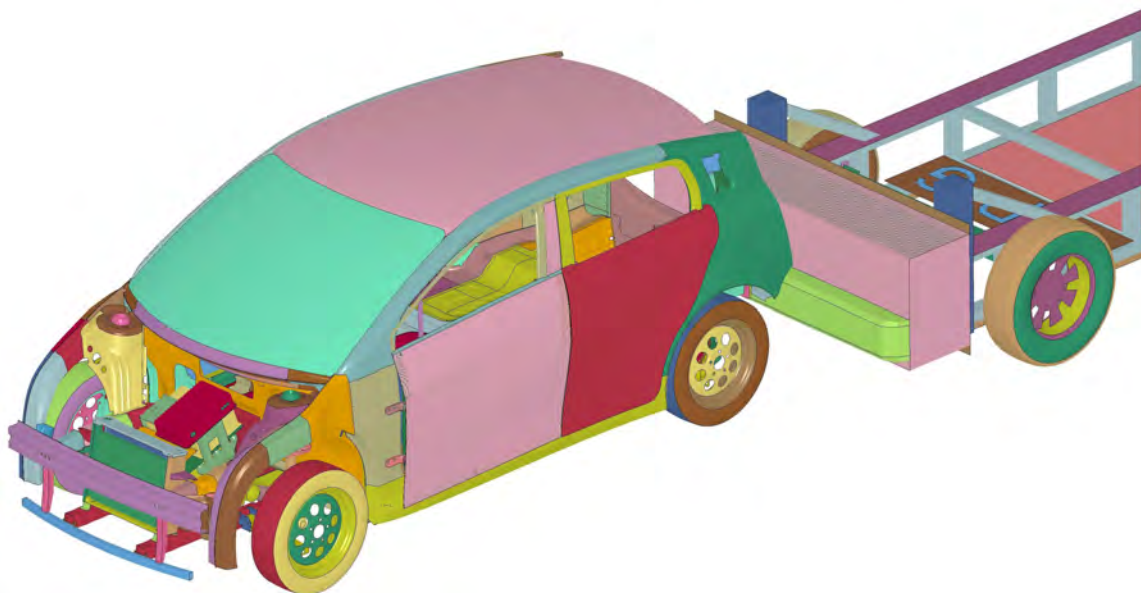


Figure 5.8: FMVSS 301 80 $\frac{\text{km}}{\text{h}}$ 70% offset deformable barrier

FMVSS 301 - Rear Impact Targets	
Maximum Plastic Strain in Battery Structure	< 0% (no contact in CAE)

Table 5.3: FMVSS 301 rear impact target values

5.1 Vehicle Crash Targets

5.1.3.2 ECE R32 - 55 $\frac{\text{km}}{\text{h}}$ 0° Deformable Barrier

In this test, the vehicle is impacted in the rear with a moving deformable barrier at a speed of 55 $\frac{\text{km}}{\text{h}}$ (29.8 $\frac{\text{m}}{\text{s}}$) with 100% overlap. The vehicle structure is evaluated based on its effectiveness in protecting the fuel tank in case of gasoline vehicle and the battery in case of the BEV vehicles. Figure 5.9 shows this load case and the structural targets are same as the previous load case shown in Table 5.3.

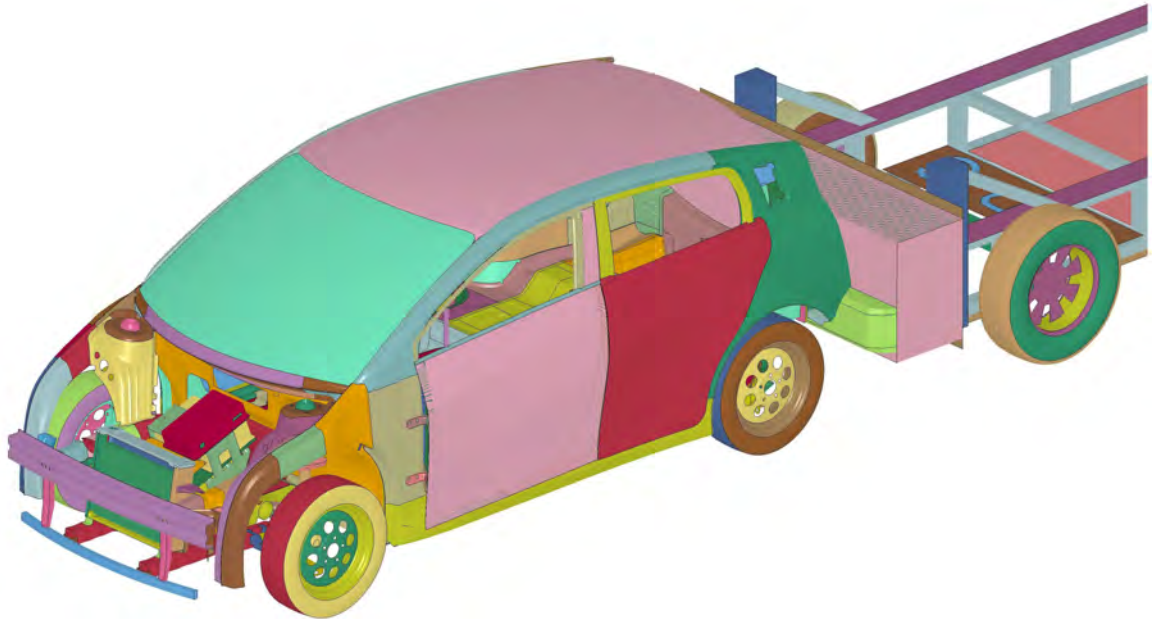


Figure 5.9: ECE R32 - 55 $\frac{\text{km}}{\text{h}}$ 0° deformable barrier

5.1.4 Side Pole Impact

The side pole impact test has difficult structural requirements, because of the narrow contact area of the rigid pole.

5.1.4.1 FMVSS 214 - $32 \frac{\text{km}}{\text{h}}$ 75° Oblique Pole

In this test a rigid steel cylinder (pole) is impacted against the outer door panel of the vehicle at $32 \frac{\text{km}}{\text{h}}$ ($19.9 \frac{\text{m}}{\text{h}}$). The car is positioned in such a way that the point of impact in the fore-aft (length of car) location is at the center-of-gravity of head of the dummy sitting on the front seat.

FMVSS-214 Pole impact protocol does not measure crashworthiness in terms of structural deformation. It takes into account occupant injury data like Head Injury Criteria (HIC), Neck Injury Criteria (NIJ), etc. But the FSV vehicle is not designed in detail with a restraint system, side airbags and accurate interior parts, so occupant injury criteria cannot be used for determining the crashworthiness of the FSV vehicle in a pole impact scenario. Therefore, for passing this test with a good rating, a structural target has been set such that the distance of the most intruding point of the door inner post-test should be ≥ 125 mm from the driver seat centerline. The 125 mm reference target is based on the IIHS Side Impact intrusion criteria. It is assumed that meeting this target provides a good basis for the development of passenger safety systems (seatbelt, airbag and interior trim), to meet passenger injury criteria. Figure 5.10 shows the FSV model set-up for this dynamic impact load case, Table 5.4 shows the target values for this load case and the intrusion requirements are the same as shown in Figure 5.6

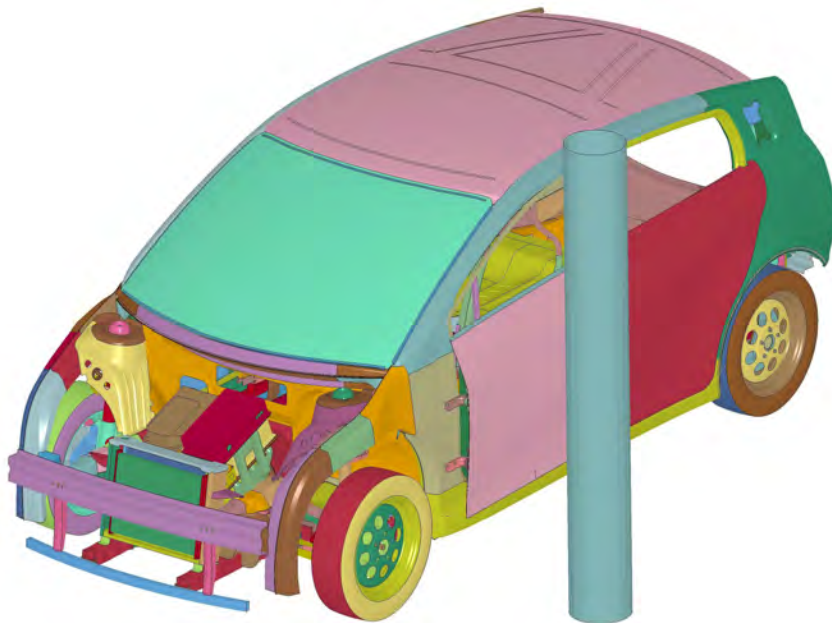


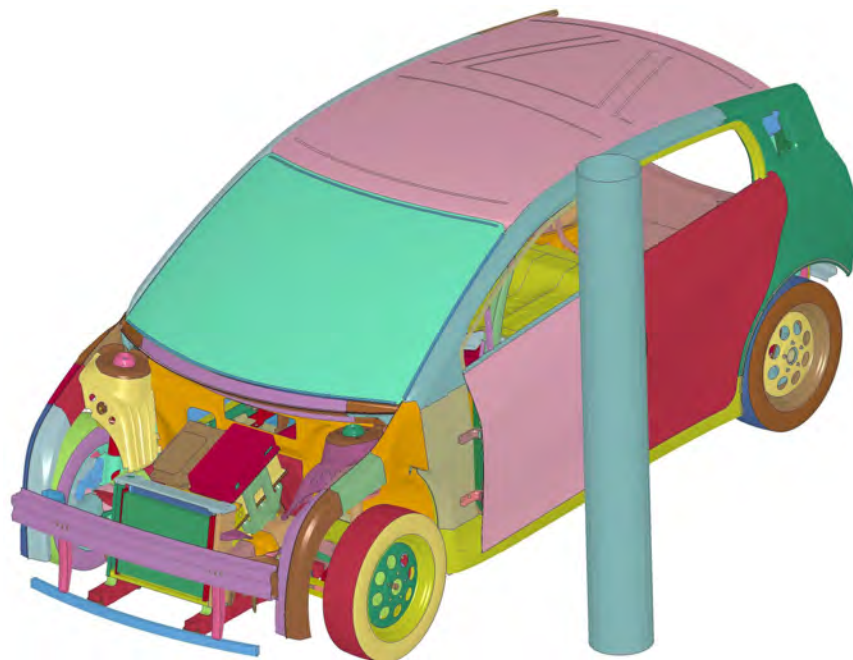
Figure 5.10: FMVSS 214P $32 \frac{\text{km}}{\text{h}}$ 75° pole impact

FMVSS - 214 Side Pole Targets	
Body Intrusion at Pole Centerline	Green in (Figure 5.6)

Table 5.4: FMVSS 214p - Side Pole Target Values

5.1.4.2 EURO NCAP - 29 $\frac{\text{km}}{\text{h}}$ 0° Impact

The EURO NCAP is similar to the US Federal requirement except that the speed of impact is 29 $\frac{\text{km}}{\text{h}}$ and the pole is impacted perpendicular to the direction of the movement of the vehicle. For this test, the BEV uses the same performance target as the FMVSS 214 Pole impact (the most intruding point of the door inner post-test should be ≥ 125 mm from the driver seat centerline, for passing the test with a good rating). There is no structural performance target for the Euro NCAP Side Pole impact test; the 125 mm reference target is based on the IIHS Side Impact intrusion criteria. It is assumed that meeting this target provides a good basis for the development of passenger safety systems (seatbelt, airbag and interior trim), to meet passenger injury criteria. Figure 5.11 shows the FSV model for this load case.


Figure 5.11: EURO NCAP - 29 $\frac{\text{km}}{\text{h}}$ 0° pole impact

5.1.5 Roof Crush

5.1.5.1 FMVSS 216 - 3* Strength to Weight Ratio

The FMVSS 216 roof strength crush test is conducted by pushing a rigid metal plate at constant speed against both sides of a vehicle's roof in successive order. The first side of the vehicle roof is tested to a minimum strength, before the second side is tested. In order to earn a good rating, a vehicle's roof must withstand a force of 3 times the vehicle's unloaded weight before reaching 127 mm of crush, also referred to as the "strength-to-weight ratio". The crush is measured from the first side of the test. Figure 5.12 shows the FSV vehicle model in this load case. The structural targets are shown in Table 5.5.

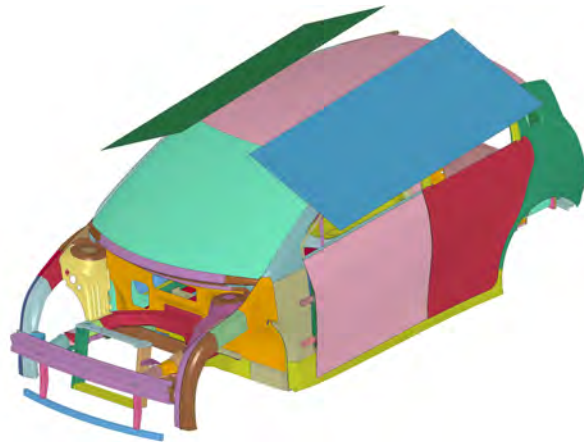


Figure 5.12: Roof crush

FMVSS 216 - Roof Crush Targets	
Peak Force on Roof	> 3*UVW (both sides)
Maximum Displacement of Roof	< 127mm

Table 5.5: FMVSS 216 - Roof Crush Target Values

5.1.5.2 IIHS - 4* Strength to Weight Ratio

The IIHS roof crush test is similar to the FMVSS 216, except the following differences:

- The IIHS roof crush is conducted by pushing a rigid metal plate at constant speed against only one side of the vehicle's roof
- In order to earn a good rating according to IIHS, a vehicle's roof must withstand a force of 4 times the vehicle's unloaded weight before reaching 127 mm of crush

5.1.6 Low Speed Regulations

The Research Committee for Automobile Repairs (RCAR) is a European consumer organization that conducts a series of tests that measure how well the vehicle's bumper system protects the headlights, hood and other vehicle parts and also to reduce the real world property damage costs associated with low speed crashes by promoting stability, compatibility and energy absorption.

5.1.6.1 RCAR/IIHS ($10 \frac{\text{km}}{\text{h}}$ 0° Rigid Barrier)

The vehicle is attached to a cable that pulls it down a test track at $10 \frac{\text{km}}{\text{h}} \pm 0.5 \frac{\text{km}}{\text{h}}$ toward the impact barrier, which is an unyielding rigid block of reinforced concrete positioned 455 mm (± 3 mm) in height for frontal impact and 405 mm or 455 mm (± 3 mm) in height for rear impacts (depending on the local market). Figure 5.13 shows the FSV model for this type of low speed dynamic impact.

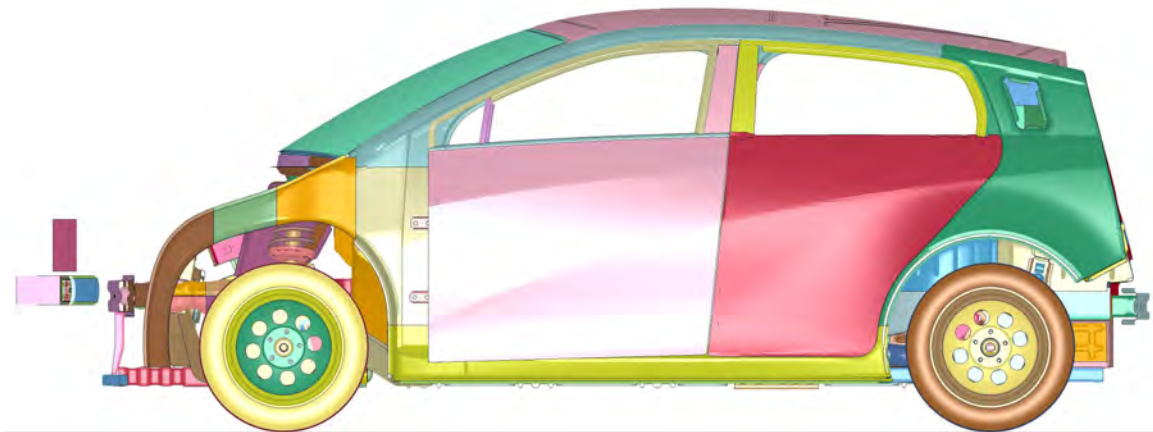


Figure 5.13: RCAR low speed impact - $10 \frac{\text{km}}{\text{h}}$ 0° rigid barrier

The structural requirements for the FSV are such that any type of damage be limited to the bumper system and crash box only. No load transfer into the vehicle's other components is allowed. The damage criteria for non-bumper components is assessed from CAE results as having less than 3% maximum plastic strain, (Table 5.6).

RCAR - 40% Offset Rigid Barrier Targets	
Maximum Plastic Strain in Rail	< 3% (CAE)

Table 5.6: RCAR - Rigid Barrier Target Values

5.2 Stiffness Targets

5.2.1 Body Structure - Dynamic (NVH) Targets

For a vehicle to be dynamically stiff it is important to have high natural frequencies for the global modes. So, for the FSV vehicle the trim-body targets are set for these critical global modes of vehicle bending and torsion that influence the body global stiffness. Since the trim-body development is usually towards the end of the program, these targets are further cascaded down to the body-in-prime level. The BIP model includes the body structure, the windshield, and bolted assemblies like the front and the rear bumpers, the radiator support, the engine cradle and the battery tray assembly. Figure 5.14 and the Table 5.7 show these modes and their targets.

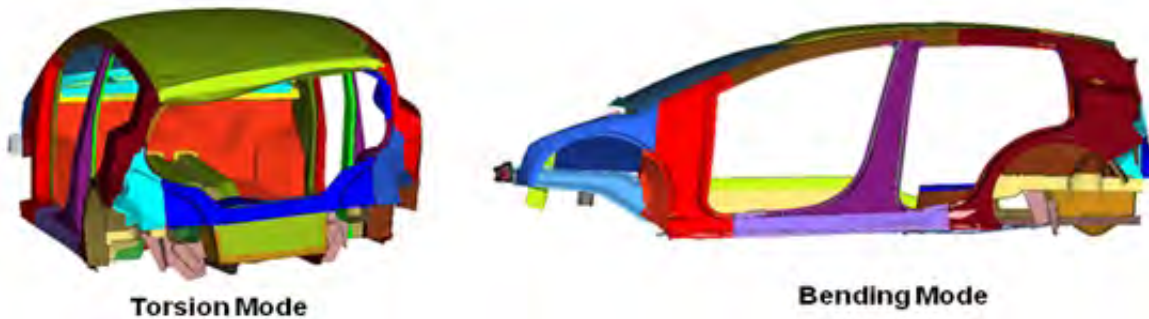


Figure 5.14: *Torsion & bending frequency modes*

Body Structure	Torsion	Bending	Comment
BIP (BIW + Glass)	> 40 Hz	> 40 Hz	The modes also need be separated by 3 Hz, being above 40 ensures that the trim-body level targets are met
Trim-body	> 25 Hz	> 21 Hz	The modes also need be separated by 3 Hz

Table 5.7: *Dynamic stiffness target values*

(The NHV assessment of BEV is fully documented in a separate WorldAutoSteel report)

5.2 Stiffness Targets

5.2.2 Body Structure Targets - Static Torsion and Bending

5.2.2.1 Torsional Stiffness (Applied Torque/Twist (deg))

Body structure with higher torsional stiffness is better for handling and NVH performance. For the FSV, a static stiffness target of 20kN-m/deg or higher was set based on research data on competitive C-class vehicles whose body stiffness values ranged between 15 and 20 kN-m/deg.

5.2.2.2 Bending Stiffness (Vertical Load/Maximum deflection)

For the FSV, a static bending stiffness target of 12kN/mm or higher was set based on research data on competitive C-class vehicles whose body stiffness values ranged between 8 and 15 kN/mm. See Table 5.8 for torsion & bending modes target values.

Body Structure	Torsion Rigidity (kNm/deg)	Bending Stiffness (kN/mm)
BIP (BIW + Glass)	20	12

Table 5.8: *Static stiffness target values*

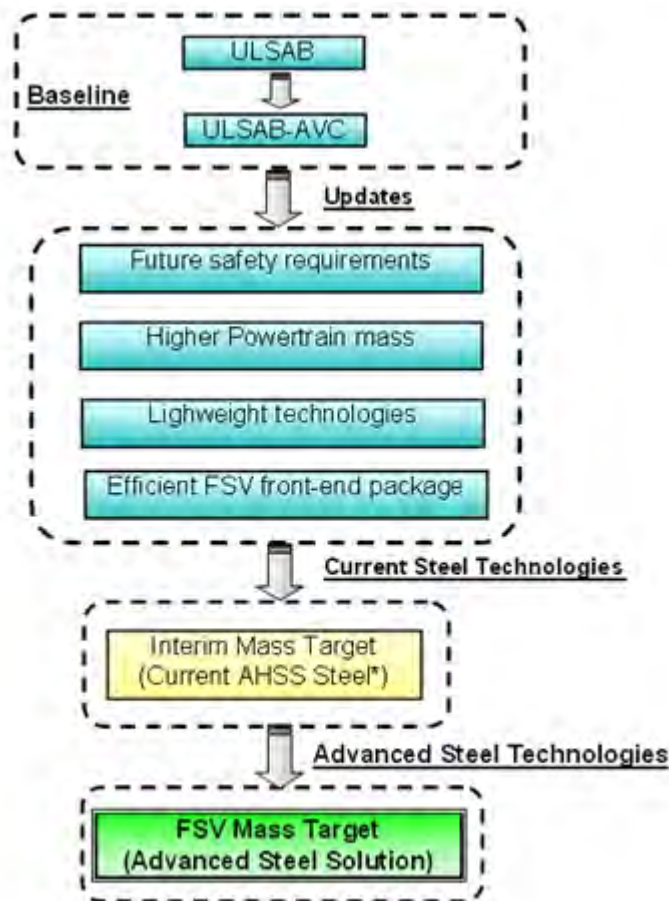
5.3 Body Structure Mass Targets

5.3.1 Target Setting Approach

During Phase 1 of the FSV project, the FSV-1 body structure target of 190 kg for the battery electric version was set based on the already achieved mass of the ULSAB and the ULSAB-AVC while taking into account the following factors.

- Meet expected safety requirements for the year 2020
- Additional vehicle mass due to higher mass of the powertrain
- Anticipated mass reduction due to future lightweight technologies
- Mass reduction due to an efficient FSV front-end package design

The approach used for setting the FSV mass targets is shown in Figure 5.15 below.



*Advanced High Strength Steel

Figure 5.15: FSV mass target setting approach - FSV Phase 1

5.3.2 Updates to Baseline Reference

The safety regulations considered for the FSV-1, took into account the developments beyond the ULSAB-AVC, and anticipated future requirements. Additionally, the following factors were considered:

- Increase in body-structure mass in order to achieve the 2020 crashworthiness targets: 5 kg (as shown in Table 5.9)
- Increase in body-structure mass as a result of higher powertrain mass: 38 kg for BEV and 17 kg for PHEV₂₀ (calculated using the mass compounding program)
- Reduction in body-structure mass as a result of lightweight technologies implementation: 10 kg (details are discussed in the Phase-1 report, "Chapter - Market Analysis")
- Reduction in body-structure mass due to more efficient FSV front-end package: 11 kg

Regulation	Timeline	FSV-1 [kg]	Cost [USD]	Fuel Used	Remarks
Roof Crush/Rollover	2016	2	N/A	N/A	Already included in ULSAB-AVC
Roof Crush/Rollover to 4x mass	2016	2	N/A	N/A	
Electronic Stability Control (ESC)	2011	1	\$92.00	2.6 gal (9.8 l)	Not Included in body-structure
Pole Impact	2011	6	\$208.00	N/A	Already included in ULSAB-AVC
Frontal Impact	TBD	TBD	N/A	N/A	
Bumper Impact	2008	1	N/A	N/A	
Ped-Pro	2011	2	N/A	N/A	
Total Impact		5			

Table 5.9: FSV-1 body-structure mass increase - Future safety regulations

The overall mass impact on the FSV-1 body-structure, after assessment of all the factors, was calculated to be +22 kg for the BEV, and +1 kg for the PHEV₂₀. Therefore, in order to account for the different architecture and objectives of the FSV program, the formula shown in Figure 5.16 was used to update the ULSAB-AVC benchmarked body-structure mass.

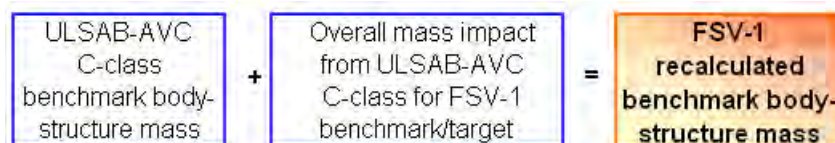


Figure 5.16: FSV-1 body-structure mass target - Updates to ULSAB-AVC benchmark

Using the formula from Figure 5.16, the recalculated benchmark body-structure mass is 290 kg for BEV and 269 kg for the PHEV₂₀ as illustrated in Table 5.10.

	WorldAutoSteel		FSV-1	
	ULSAB	ULSAB AVC C Class	BEV	PHEV ₂₀
	1997	2004	2015-2020	
Vehicle Mass [kg]	1350	966	1232	1055
***Powertrain Mass [kg]		195 20%	449 36%	343 33%
References	1994 Ford Taurus (1450 kg)	243	268	268
*Additional mass - Crash requirements for 2004		*25		
Updates to ULSAB-AVC				
Additional mass for crash requirements 2020			5	5
Additional mass for: Higher Mass Powertrain*** (mass compounding)			38	17
Mass reduction for 2020 Technology Implementation			-10	-10
Mass reduction Efficient Front-end Package			-11	-11
** Total Updates to ULSAB-AVC for 2020			22	1
Reference/Benchmark Body-Structure Mass	271	268 (=243+25*)	290 (268+22**)	269 (268+1**)

Table 5.10: FSV-1 recalculated benchmark body-structure mass

5.3.3 FSV-1 Body-Structure Final Mass Target

The ULSAB-AVC C-class aimed for a 208 kg body-structure based on the ULSAB body-structure mass, while acknowledging the more severe crash requirements for 2004 (25 kg) and the mass reduction from ULSAB to ULSAB-AVC C-class vehicle (20 kg). As shown in Table 5.11, the interim FSV-1 body-structure mass targets were determined to be 224 kg for the BEV, and 203 kg for the PHEV₂₀, also accounting for the overall mass impact from the ULSAB-AVC C-class for the FSV-1 target (+22 kg for BEV and +1 kg for PHEV₂₀). The interim FSV-1 body-structure targets are based on currently available steel materials that require no further investments in technology development, and hence, is considered to be a low cost solution.

The FSV-1 body-structure mass target is 190 kg and 173 kg for the BEV and PHEV₂₀ respectively, achievable with the application of advanced steel materials and advanced manufacturing technologies. The goal is to offset the potential overall vehicle cost savings offered by lighter density materials with the adoption of advanced steels and innovative manufacturing technologies.

The FSV body-structure mass targets are summarized in Table 5.11.

	WorldAutoSteel		FSV-1
	ULSAB	ULSAB AVC C Class	BEV
	1997	2004	2015-2020
Vehicle Mass kg	1350	966	1232
Powertrain Mass kg		195	449
		20%	36%
References	1994 Ford Taurus (1450kg)	243	268
Reference/Benchmark BIW Mass	271	268	290
ULSAB - Achieved BIW Mass	203		
	25%		
***Mass reduction from ULSAB for C-class target		20	
*Additional mass - Crash requirements for 2004		25	
ULSAB AVC - Target BIW Mass		208 (=203- 20***+25*)	
ULSAB AVC - Achieved BIW Mass		202	
		3%	
ULSAB AVC - Achieved BIW Mass relative to Reference Benchmark		25%	
Updates to ULSAB-AVC			
Additional mass - Crash requirements 2020			5
Additional mass for: Higher Mass Powertrain (mass compounding)			38
Mass reduction for 2020 Technology Implementation			-10
Mass reduction Efficient Front-end Package			-11
** Total Updates to ULSAB-AVC for 2020			22
FSV-1 - Interim BIW Mass Target (Current AHSS Steel Solution)			224 (=202+22**)
			-23%
Additional Mass Reduction Advanced Steel Technology	-15%		-33.6
FSV-1 - Final BIW Mass Target (Advanced Steel Solution)			190
			-34%

Table 5.11: FSV-1 BEV body-structure mass target summary

The body structure mass target of the FSV-1 BEV was compared with the 2010 model year VW Polo, the world car of the year. The 2010 VW Polo is a front wheel drive European subcompact car with dimensions of 3970 mm in length, 1682 mm in width and 1462 mm in height with a base curb mass of 1,089 kg. The Polo is about the same size as that of the Battery electric version of the FSV-1. Figure 5.17 shows the 2010 VW Polo.



Figure 5.17: 2010 VW Polo

The 2010 VW Polo has a high static torsional rigidity of 18 kNm/deg. The high static rigidity of the new Polo is attained through the efficient use of high-strength and ultra high-strength steels and optimal structural design for loading and reinforcement of body nodal points.

Profile-intensive lightweight envelope construction can be found throughout the Polo's body structure which weighs 231 kg. This car also has an excellent lightweight construction factor of 3.6. The lower this factor, the more efficient the implementation of body structure in terms of lightness and rigidity. The new Polo is therefore a good example of a 2010 model year lightweight Advanced High Strength Steel (AHSS) construction to compare the FSV with.

In spite of the higher powertrain mass of the BEV, the BEV target body-structure mass of 190 kg is 41 kg lighter than the 2010 VW Polo body-structure.

5.4 Body Structure - Lightweight Index

The body structure Lightweight Index (L), is defined as the ratio of the body structure weight to the torsional rigidity of the body structure multiplied by the contact area of the body structure. Figure 5.18 shows the body structure lightweight index calculation method.

$$\frac{M_{BIW}}{C_T \cdot A} \left[\frac{kg}{N \cdot m / \text{deg} \cdot m^2} \cdot 10^3 \right] = 4.01$$

M_{BIW} [kg]: BIW mass including bolted elements and glued windscreen
C_T [kNm/deg]: Torsion stiffness of BIW including bolted elements and glued windscreen
A [m²]: Projected area (wheel base + tread)

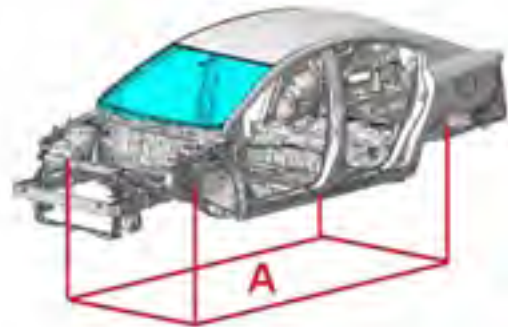


Figure 5.18: Body structure lightweight index calculation

Table 5.12 shows the body lightweight index for the FSV, the Super Light Car (SLC), and the 2010 VW Polo. The SLC has a lower lightweight index number than the FSV, because the SLC is a multi-material vehicle, whereas the FSV is comprised entirely of advanced lightweight steels. As can be seen in Table 5.12, the FSV has a lower lightweight index number than the best-in-class current production all-steel vehicles.

Vehicle	Lightweight Index (L)	Torsional Stiffness (kN-m/deg)	Body Mass (kg)	Contact Area (m ²)
FSV-BEV	2.56	20	190	3.71
SLC	1.8	25.5	180	3.9
VW Polo V (2010)	3.5	18	227	3.6
VW Golf V	2.88	25	281	3.9
Toyota Avensis (2008)	4.01	n/a	n/a	3.99

Table 5.12: Body structure lightweight index comparison

Figure 5.19 shows a graph of the body structure lightweight index versus the contact area for these vehicles.

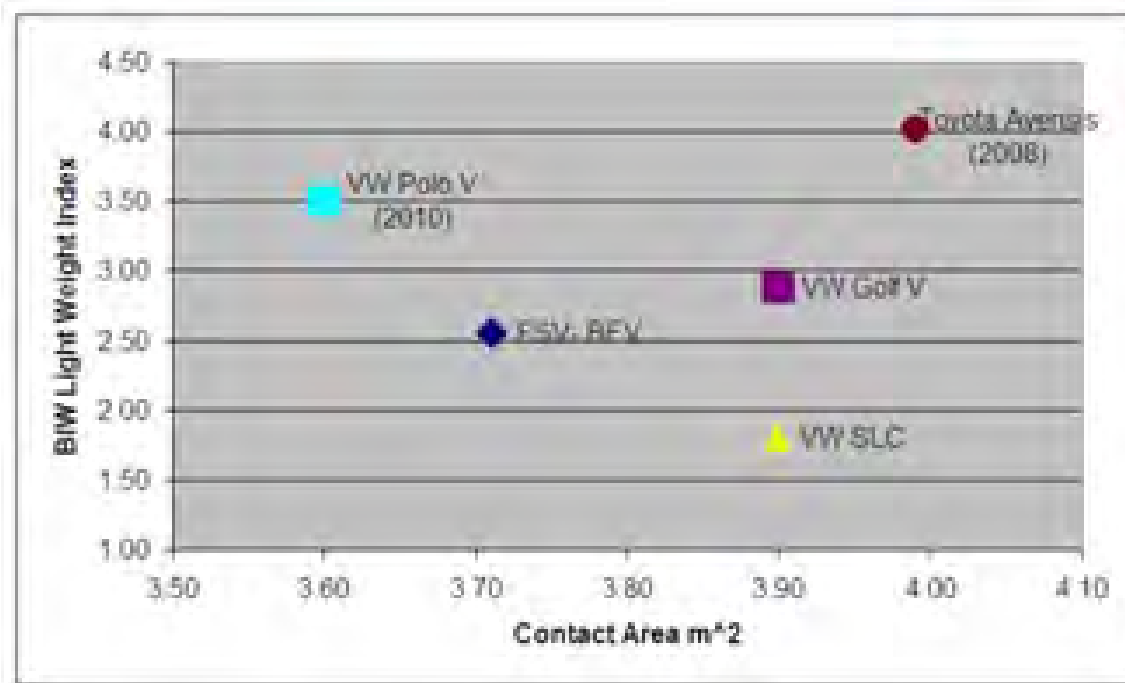
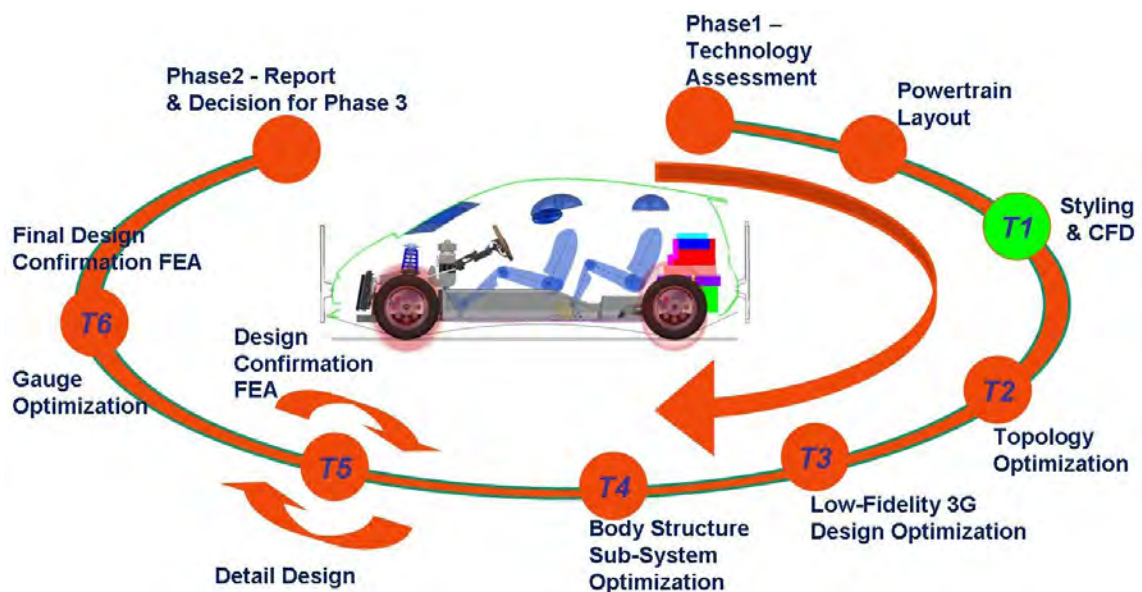


Figure 5.19: Body structure lightweight index comparison

6.0 Styling and CFD

6.1 Styling and Aerodynamic Performance



6.1.1 Introduction

The styling of a vehicle combined with other external features and airflow through the motor compartment has a significant influence on its aerodynamic drag, which in turn determines the fuel consumption and CO_2 emissions of the vehicle. For the FSV project the initial styling shown in Figure 6.1 was subjected to detailed Computational Fluid Dynamic (CFD), simulation to predict and minimize the aerodynamic drag. The CFD process simulates the wind tunnel testing. Aerodynamic drag and vehicle stability at high speed is normally assessed, first using scale models and finally full size models in a wind tunnel.

The FSV styling phase was supported by aerodynamic studies using the ESI Group's CFD-ACE+ simulation program. The results were used to enhance the vehicle styling and other external features that reduce the aerodynamic drag and improve the vehicle stability.

Aerodynamic studies on the FSV focused on three major areas:

1. Coefficient of drag (C_d)
2. Coefficient of lift (C_L)
3. Optimum flow rate through the motor compartment



Figure 6.1: FSV-1 baseline CFD model

6.1.2 Coefficient of Drag and Lift

Coefficient of drag (C_d) and coefficient of lift (C_L) of an automobile are dimensionless quantities that are used to quantify the drag resistance and vertical lift tendency of the vehicle traveling through the air. A lower C_d indicates the vehicle will have less drag and hence it will be more efficient, reducing fuel consumption and CO_2 emissions. The value of C_L is used to calculate the vehicle lift force that influences the vehicle stability at higher travel speed.

The vehicle's C_d and C_L are determined by the following equations:

$$C_d = \frac{\text{DragForce}}{\frac{1}{2} * \text{Density} * \text{Velocity}^2 * \text{FrontalArea}}$$

$$C_L = \frac{\text{LiftForce}}{\frac{1}{2} * \text{Density} * \text{Velocity}^2 * \text{FrontalArea}}$$

The aerodynamic drag is caused by various features of a vehicle as shown in Table 6.1. The

vehicle body shape and the wheel features are major contributors of the drag force.

Vehicle Feature	Drag Force Contribution (%)
Rear view mirrors	3 - 6 %
Engine cooling	5- 9 %
Underbody	14 - 20 %
Wheels, rims and wheel housings	30 - 35 %
Vehicle body (shape and sealing)	39 - 42 %

Table 6.1: Aerodynamic drag force contribution break-down for a modern car

6.1.3 Targets and Assumptions

Aerodynamic data, (C_d and C_L values), for various current vehicles was gathered through publicly available information (e.g. internet, OEM publications). Table 6.2 and Table 6.3 show the drag coefficient (C_d) and lift coefficient (C_L) values for some typical production vehicles. Figure 6.2 and Figure 6.3 show two recent production vehicles, (a 2010 Toyota Prius & a 2009 Mercedes E-class coupe) that show some of the aerodynamic features that are implemented on modern vehicles to achieve low aerodynamic drag. Based on this data, a drag coefficient of 0.25 or less and a lift coefficient value in the range of 0 to 0.3 were set as targets for the FSV-1 vehicle.

Vehicle	Drag Coefficient (C_d)
Formula 1	0.7 - 1.1
Tesla Roadster	0.35
Honda Civic	0.31
Nissan Tiida	0.31
Chevrolet Volt	0.301
Chevrolet Corvette	0.29
Tesla Model S	0.27
FSV-1	≤ 0.25
Toyota Prius	0.25
Honda Insight	0.25
GM EV-1	0.19
Volkswagen 1-liter	0.159

Table 6.2: Vehicle drag coefficient values

Vehicle	Lift Coefficient (C_L)
Typical race car	-3
Typical family sedan	0.1 - 0.3
FSV-1	0 - 0.3
Boeing 747 (during climb)	5.5

Table 6.3: Typical lift coefficient values

Toyota Prius 2010 ($C_d=0.25$)



Figure 6.2: 2010 Toyota Prius

Mercedes E-class 2009 coupe ($C_d=0.24$)



Figure 6.3: 2009 Mercedes E-class

6.2 FSV-1 Aerodynamics Development

The aerodynamic development process on the FSV-1 began with establishing a baseline CFD model for future enhancements. This original FSV model was based on 3D styling surfaces that were a result of the packaging exercise as outlined in chapter 4.

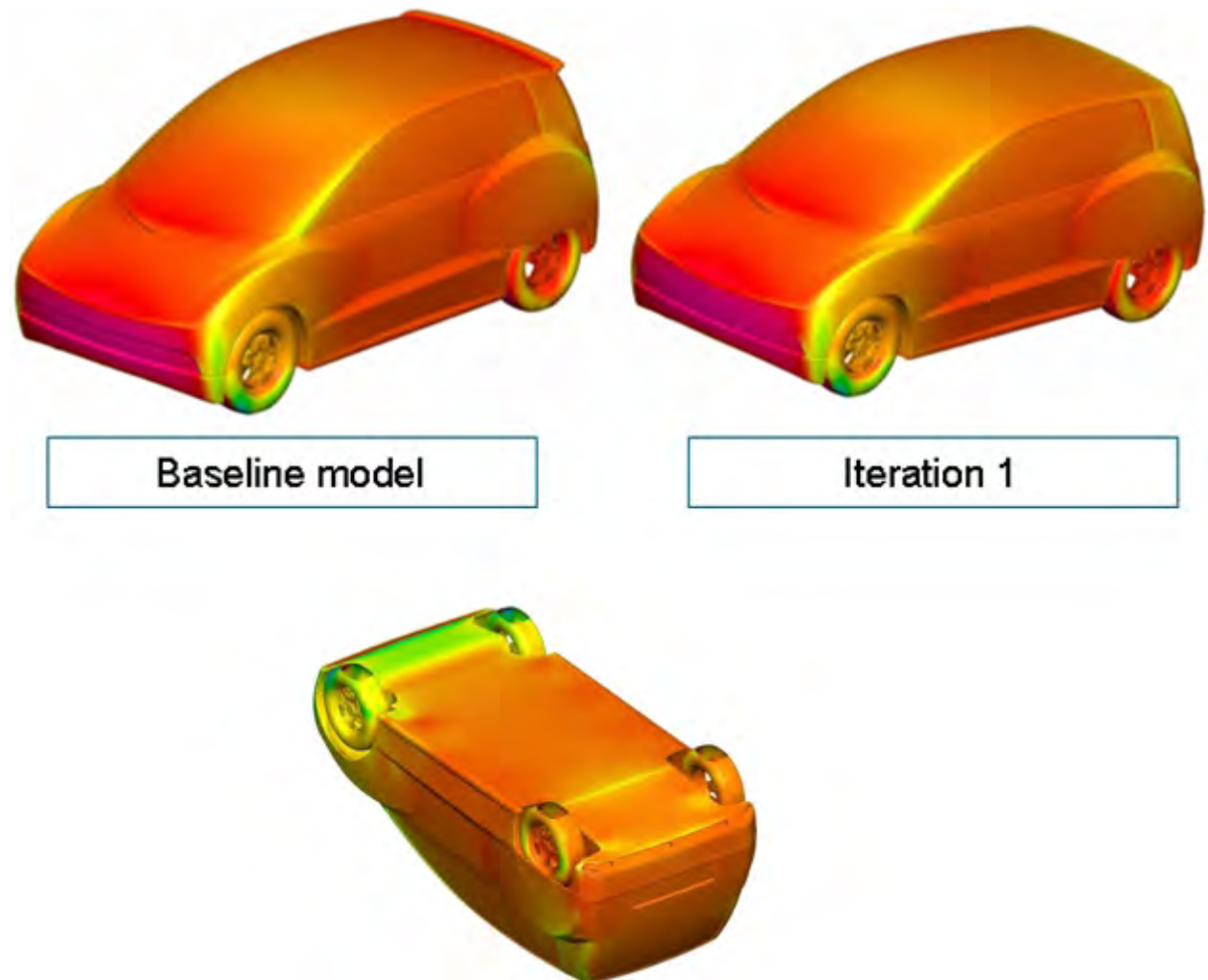


Figure 6.4: FSV-1 baseline vehicle skin with rear spoiler, wheel skirts and smooth Floor

6.2.1 Baseline FSV Model

A rear spoiler, rear wheel skirts and flat under-body were included in the baseline model. The aerodynamic model is shown in Table 6.4. Typically, the values for C_d and C_L are established for higher vehicle speed limits. The CFD analysis for the FSV was established for a speed of 117.4 km/h (73 MPH), with a yaw angle-to-wind of zero degrees. The predicted CFD results for the baseline model are shown in Table 6.4.

Model	Specification	Drag Force (N)	Lift Force (N)	Drag Coefficient	Lift Coefficient
FSV baseline model	with spoiler, wheel skirts	485.0	-113.0	0.354	-0.082
Iteration 1	without spoiler, with wheel skirts	462.2	163.7	0.337	0.119

Table 6.4: *Baseline model - CFD analysis results*

As can be seen from the results shown in Table 6.4, the design of the spoiler used on the base-line model decreases lift force but increases drag force.

Figure 6.5 shows the pressure contour plots for the baseline vehicle with and without the rear spoiler. The results indicate the presence of a high pressure area (circled on the picture) on the roof around the rear spoiler. This validates the fact stated earlier that this spoiler design helps reduce the lift forces. The purpose of the spoiler for the FSV is to control the air flow behind the vehicle, to minimize the low pressure zone on the rear vertical surfaces and decrease the C_d value.

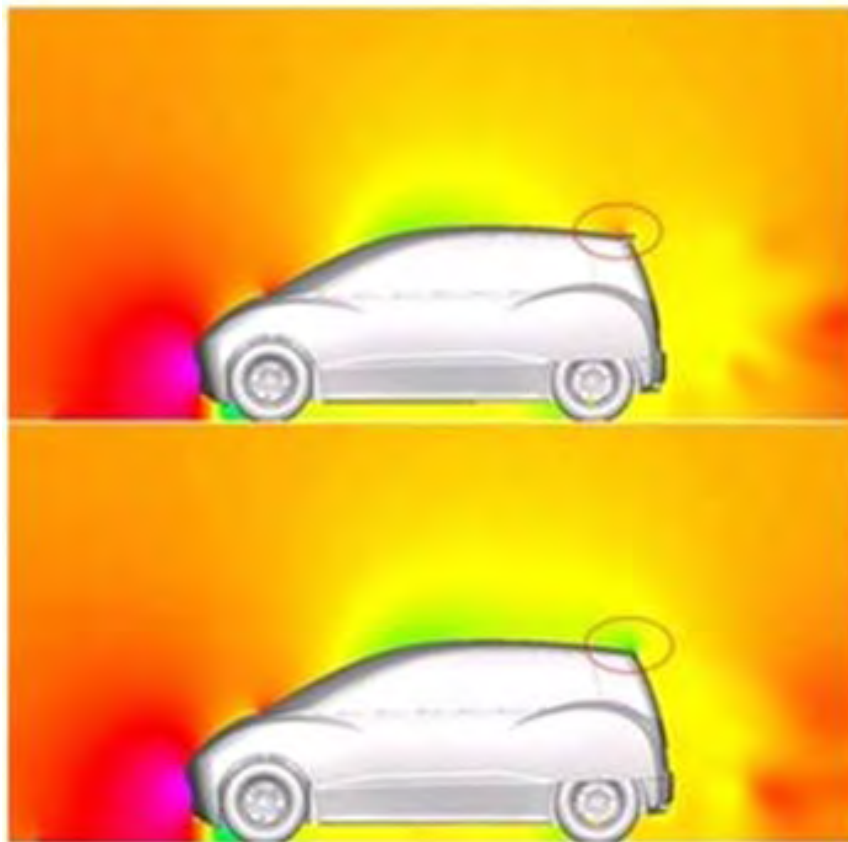


Figure 6.5: *FSV-1 pressure differences with and without rear spoiler*

Based on these results, the following recommendations were provided to the design team.

1. The spoiler was helpful for reducing the lift coefficient, but increased drag coefficient. Spoiler needed to be more flush with the roof-line and extend rearward.
2. Rear wheel skirts reduced the drag coefficient and were recommended.
3. Incorporate front air-dam below the front bumper area

6.2.2 FSV model - with New Spoiler and Air-dam

Based on the recommendations from the previous CFD analysis, the rear spoiler was redesigned to have a smoother top surface. The under-body floor was improved and a new air dam was included into the front as shown in Figure 6.6.

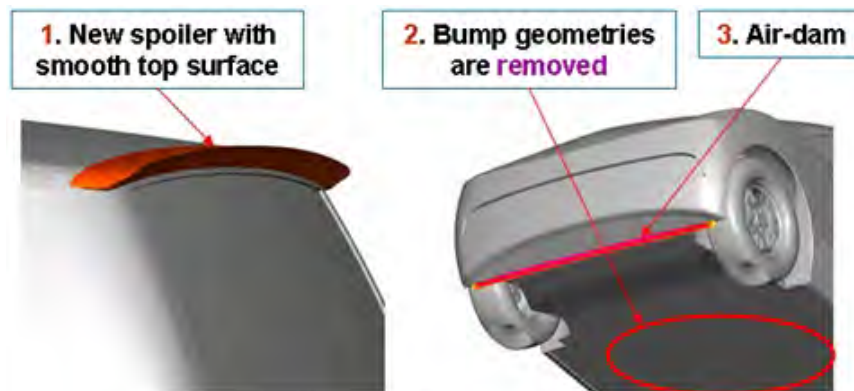


Figure 6.6: Original FSV model - new spoiler and air-dam

Three configurations of this model as shown in Figure 6.7 were analyzed and its impact on vehicle drag and lift coefficient values were computed.

1. Original FSV model without spoiler, with side skirt
2. Original FSV model with new spoiler, with side skirt
3. Original FSV model with new spoiler, side skirt and air-dam

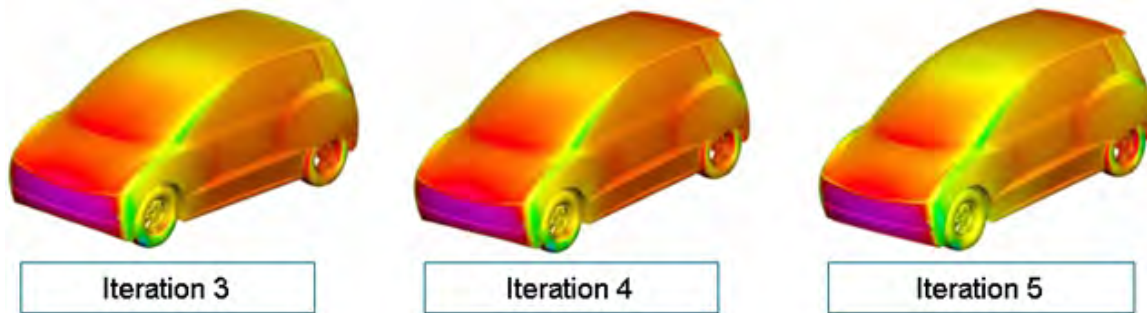


Figure 6.7: Original FSV model - new spoiler and air-dam models

The pressure contour plots show that the spoiler still increases the pressure on the roof and thus reduces the lift coefficient but increases the drag coefficient. The velocity vector plots indicate that the air dam acts as an obstacle in this case and obstructs the airflow due to the bumper bottom edge being already too low. Figure 6.8 shows the velocity vector plots for these three models.

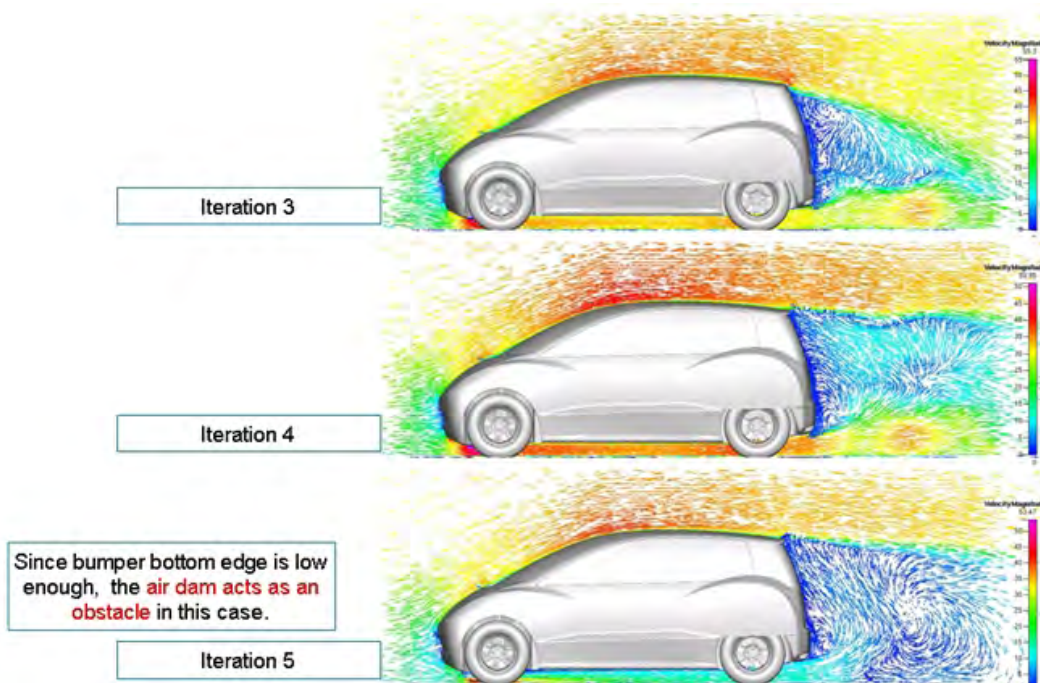


Figure 6.8: Velocity vector with new spoiler and air-dam

6.2.2.1 C_d and C_L Values - with New Spoiler and Air-dam

Table 6.5 shows the C_d and C_L values based on the CFD analysis on the three configurations. The model without the rear spoiler and with rear skirts still has the best C_d value so far. The inclusion of the new spoiler and air-dam increased the C_d value to 0.363.

Model	Specification	Drag Force (N)	Lift Force (N)	Drag Coefficient	Lift Coefficient
Iteration 3	w/o spoiler, with wheel skirts, w/o bump in floor	425.0	191.7	0.311	0.140
Iteration 4	with new spoiler, with wheel skirts, w/o bump in floor	451.5	-52.9	0.330	-0.039
Iteration 5	with new spoiler, with air dam, with wheel skirts, w/o bump in floor	497.3	70.7	0.363	0.052

Table 6.5: Model with new spoiler and air-dam - C_d and C_L results

The best predicted C_d result for the FSV, (iteration 3), of 0.311, is still 24% higher than FSV target of 0.25. The recommendations shown in Figure 6.9 were provided to the design team.

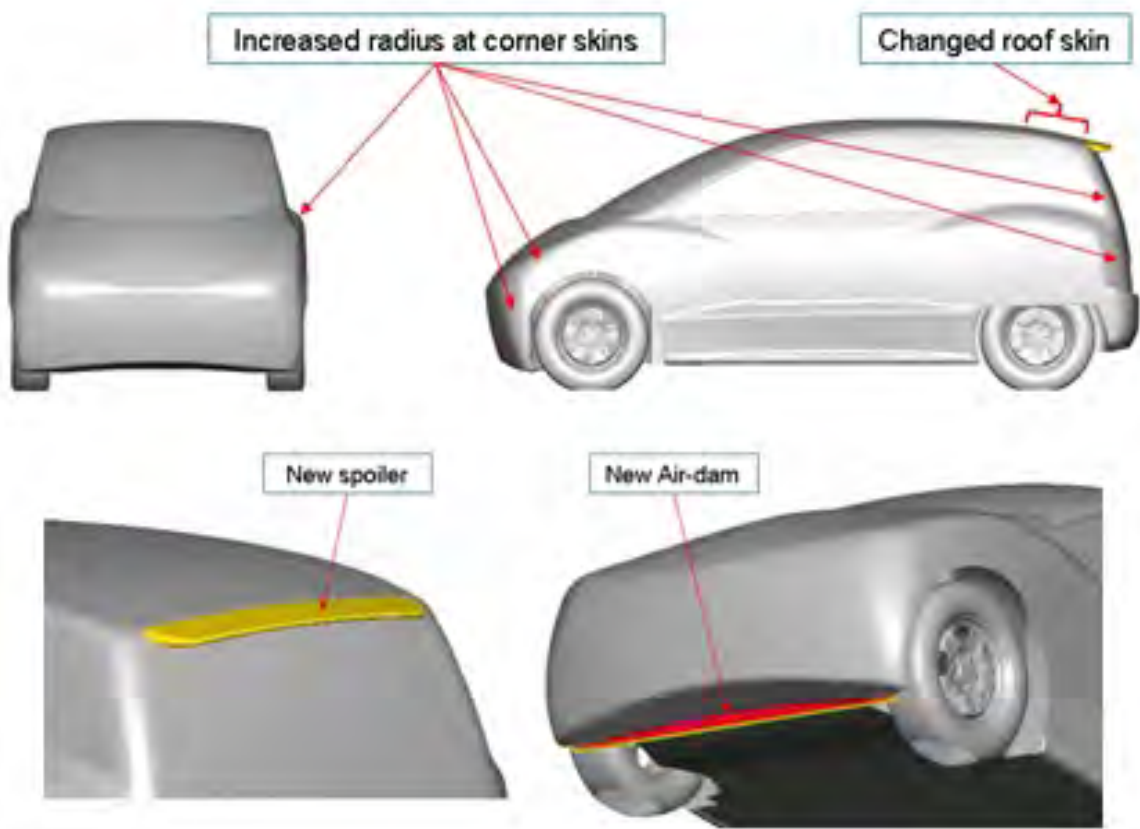


Figure 6.9: Original FSV model - new spoiler and air-dam

6.2.3 FSV Model - with New Roof Skin, New Spoiler, New Air-dam

The baseline vehicle design was updated to include the following new changes as shown in Figure 6.9.

1. Increased radii at the corners and new roof skin
2. New spoiler
3. New air dam

Three configurations in this design as shown in Figure 6.10 were analyzed and its effect on the C_d and C_L values were computed.

1. New roof skin without spoiler and air-dam (iteration 6)
2. New roof skin with spoiler and without air-dam (iteration 7)
3. New roof skin with spoiler and air-dam (iteration 8)

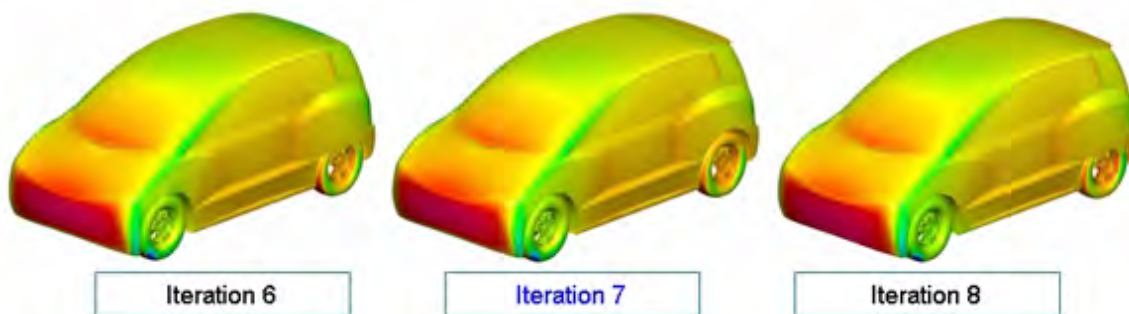


Figure 6.10: FSV model - new spoiler and air-dam

Figure 6.11 shows the airflow pattern for the above mentioned configurations. The airflow on the vehicle with the spoiler but without air-dam, (iteration 7), has a more streamlined pattern behind the vehicle than the others. This helps the aerodynamics of the vehicle.

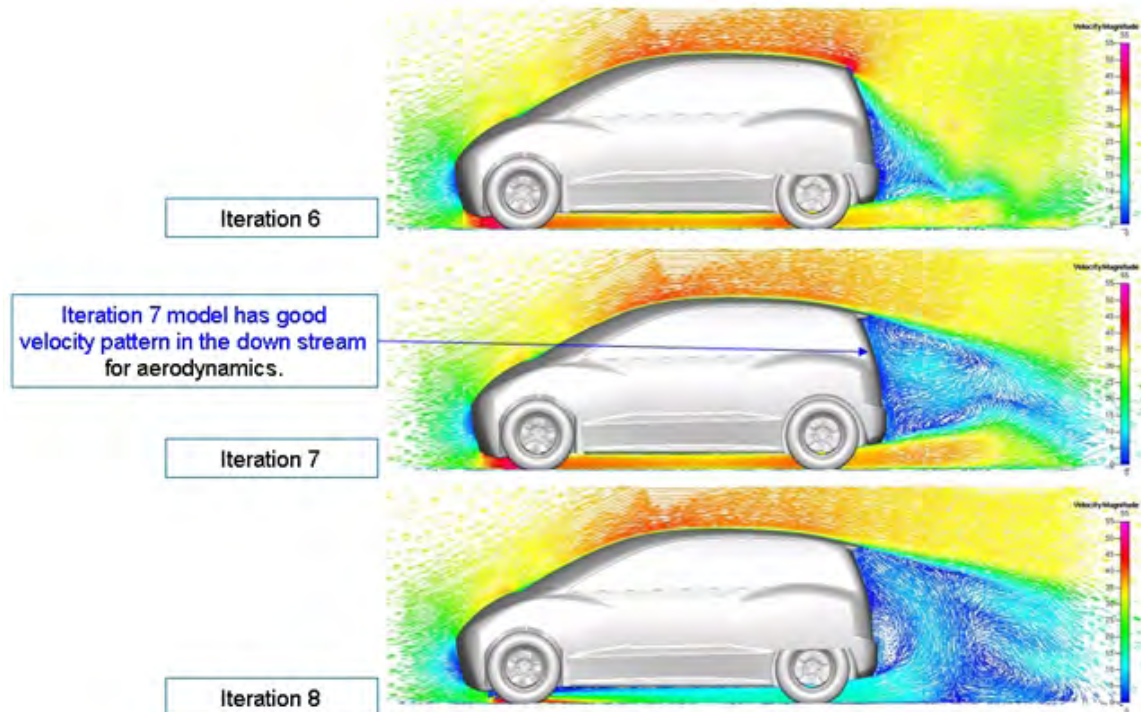


Figure 6.11: FSV model - new spoiler and air-dam - airflow velocity contour plots

6.2.3.1 C_d and C_L Values - with New Roof Skin, New Spoiler and Air-dam

Table 6.6 shows the C_d and C_L values of the three configurations based on CFD analysis results.

Model	Specification	Drag Force (N)	Lift Force (N)	Drag Coefficient	Lift Coefficient
Iteration 6	new skin, w/o spoiler, W/O air dam	482.6	218.9	0.352	0.160
Iteration 7	new skin , with spoiler , w/O air dam	411.9	10.7	0.301	0.008
Iteration 8	new skin , with spoiler , with air dam	453.7	182.8	0.331	0.133

Table 6.6: Model with new roof skin, spoiler and air-dam - C_d and C_L results

The best predicted C_d result for the FSV, (iteration 7), of 0.301 is comparable to typical C_d values for A-B class vehicles which is on the order of 0.31 to 0.33. The roof line along with the rounded edges on the vehicle exterior skin makes a reasonable impact on the vehicle's drag characteristics. From these results it can be concluded that significant changes to the vehicle shape have to be considered in order to meet the C_d target of 0.25.

The recommendations shown in Figure 6.12 were provided to the design team.

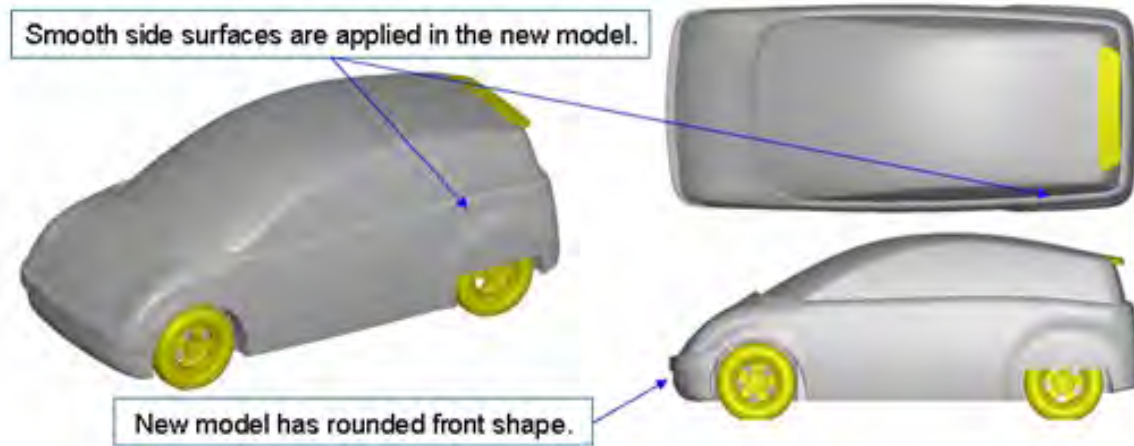


Figure 6.12: *Recommended changes*

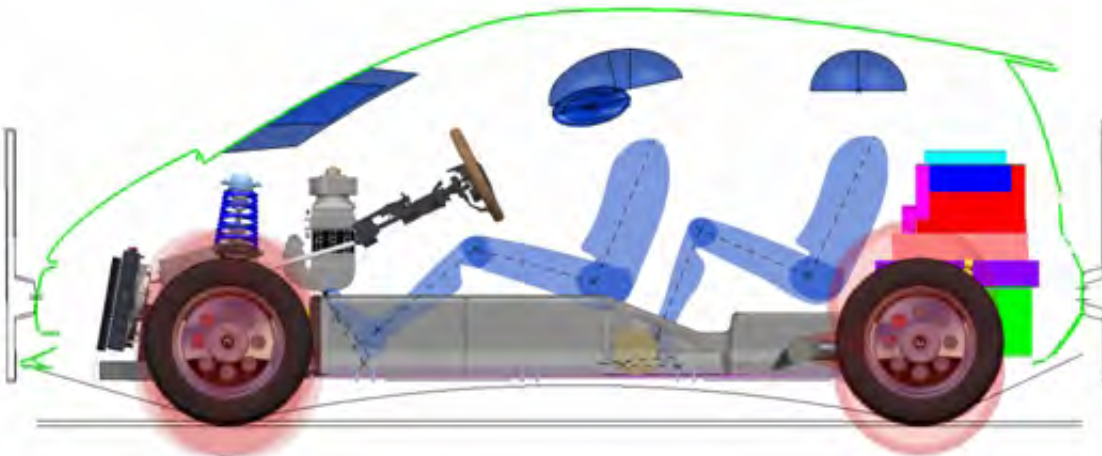


Figure 6.13: *Occupant package*

6.2.4 FSV Model - with Rounded Front Shape and Smooth Exterior Sides

Figure 6.14 shows the CFD model of iteration 7 with a C_d of 0.301 and modified per Figure 6.12. The updates for the 'new model' included significant surface changes to the overall geometry. The rearward sloping roof angle required repositioning of the rear seat occupants in order to maintain sufficient head room clearance. (See Figure 6.13).

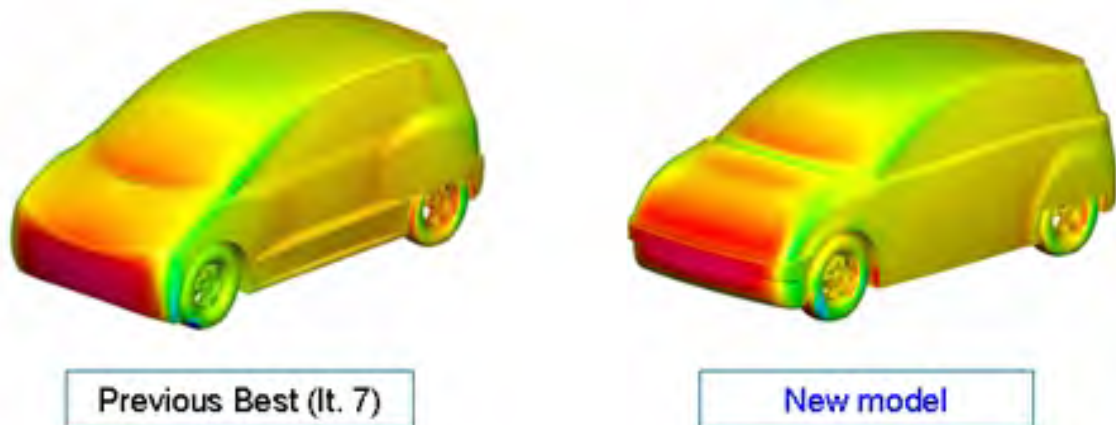


Figure 6.14: FSV model - rounded front and smooth side exterior surfaces

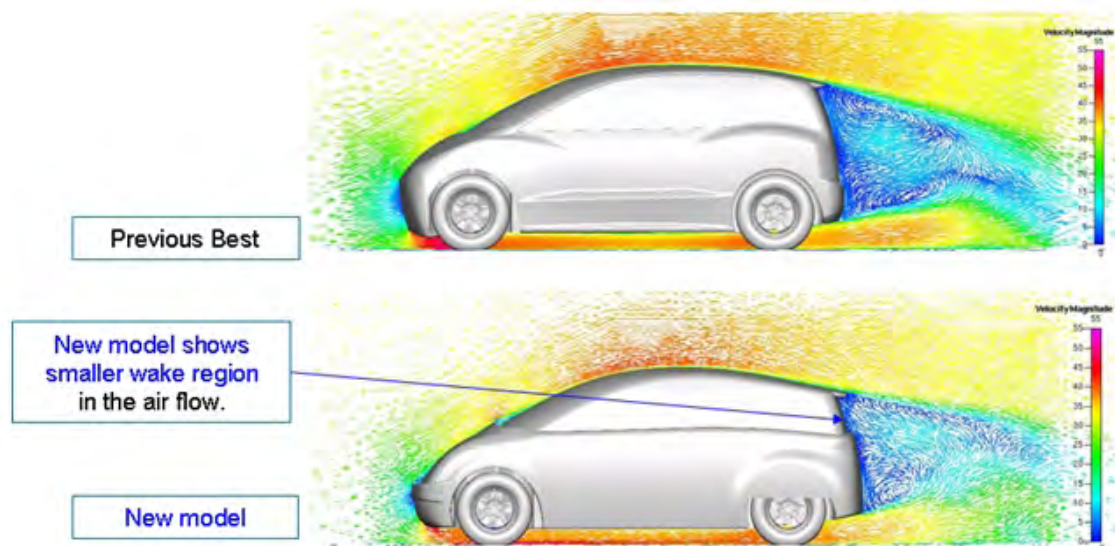


Figure 6.15: Velocity vector plots for both designs

Figure 6.15 compares the velocity vector plots for the previous baseline vehicle, (iteration 7), that had a C_d value of 0.301, to the modified original FSV model with a rounded front end. The modified FSV model, (iteration 8), shows a smaller wake region in the air flow, reducing the drag of this vehicle.

The modified original FSV model also has increased pressure at the rear of the vehicle, as compared to the baseline vehicle as shown by the pressure contour plots in Figure 6.16.

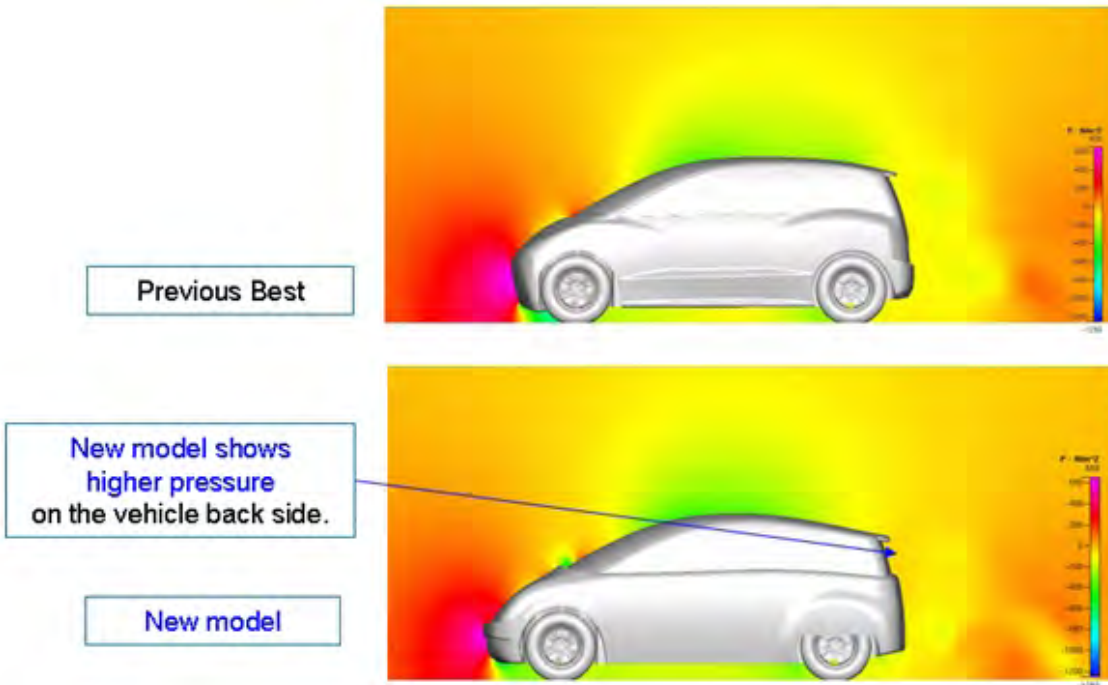


Figure 6.16: Pressure contour plots for both designs

6.2.4.1 C_d and C_L Values with Rounded Front Shape and Smooth Side Surfaces

Table 6.7 shows the difference in C_d and C_L values of iteration 9. The C_d values dropped from the previous best of 0.301 to 0.248 while the C_L values increased from 0.008 to 0.095.

Iteration 9 design changes include:

1. Smooth side surfaces
2. Rounded front shape
3. Sloped roof

Model	Specification	Drag Force (N)	Lift Force (N)	Drag Coefficient	Lift Coefficient
Previous best (iteration 7)	new skin , with spoiler , w/O air dam	411.9	10.7	0.301	0.008
New model (iteration 9)	rounded front shape, smooth side surfaces, sloped roof	339.8	130.0	0.248	0.095

Table 6.7: Model with rounded front shape and smooth side surfaces - C_d and C_L results

6.2.5 FSV Full Vehicle CFD Model - Detailed Motor Compartment Geometry

The air-flow into the motor (engine) compartment required for the cooling system, contributes appreciably to the overall drag coefficient. Since the electric drive system on the FSV BEV, (as compared with an internal combustion engine vehicle), has significantly lower cooling requirements. CFD simulation was used to optimize the radiator opening for the required cooling air flow. The CFD model from a previous analysis, (iteration 9), with a C_d value of 0.248 was further revised and updated to include motor/engine compartment and representative under-body floor geometry. A side-by-side comparison of the two models is shown in Figure 6.17.

The normal methods of determining the cooling system drag is to measure the overall drag of the car in its normal condition, then subtract the drag measured with the front air-intake opening closed off. Including air flow through the engine compartment will increase drag as the air flow interacts with the complex geometry of the components within the compartment, and as that flow exits the engine compartment, initiating turbulent flow along the underbody.

■ Detail comparison of New-skin model and Full-vehicle model

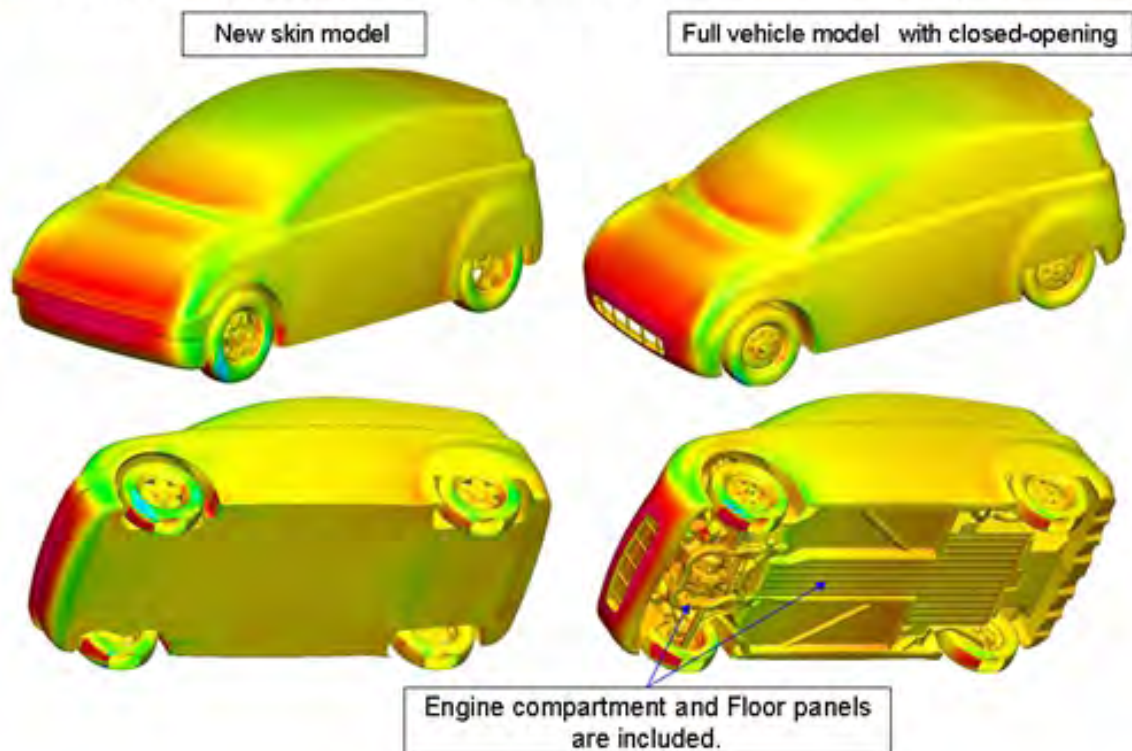


Figure 6.17: Full vehicle CFD model with representative underfloor

The results for the full vehicle with air intake opening 'blocked' fully closed and fully open are shown in Table 6.8.

Model	Drag Force (N)	Lift Force (N)	Drag Coefficient	Lift Coefficient
Iteration 9	339.8	130.0	0.248	0.095
Air Intake: closed	286.8	203.5	0.209	0.149
Air Intake: open	448.6	320.1	0.327	0.234

Table 6.8: C_d and C_l values for full vehicle with closed/open air intake opening

The results in Table 6.8 show a significant improvement of under-floor air flow as it exits the rear of the vehicle as shown in Figure 6.18 & Figure 6.19. The increase in the pressure on the back vertical surface of the vehicle leads to a reduction in the drag force from 339.8 N to 286.8 N. See Table 6.7 for Iteration 9 model specification.

■ Detail comparison of pressure in the rear flow

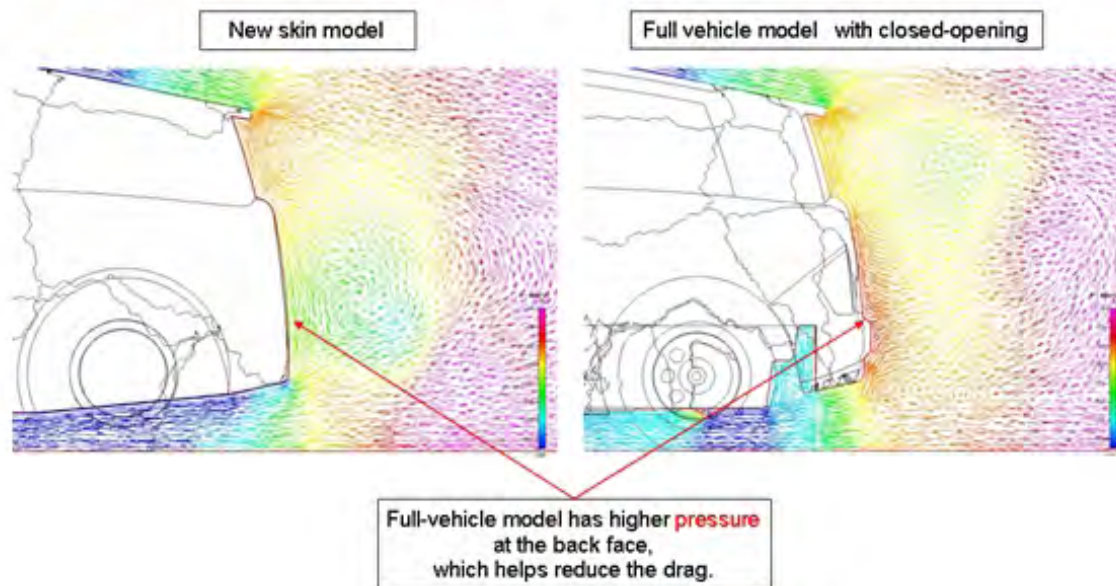


Figure 6.18: Full vehicle CFD model under floor air-flow comparison

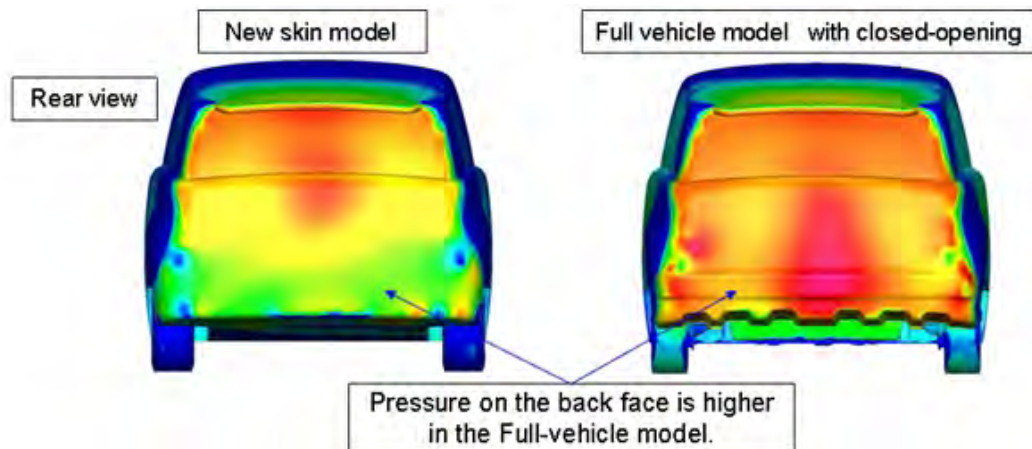


Figure 6.19: Full vehicle CFD model rear surface pressure comparison

The comparison of the C_d values for the full vehicle model with the air-intake fully open and closed is 0.327 and 0.209 respectively. The drag force is increased from a value of 286.8 N to 448.6 N with a fully open air intake, a 56% increase. Air flow velocity is illustrated in Figure 6.20.

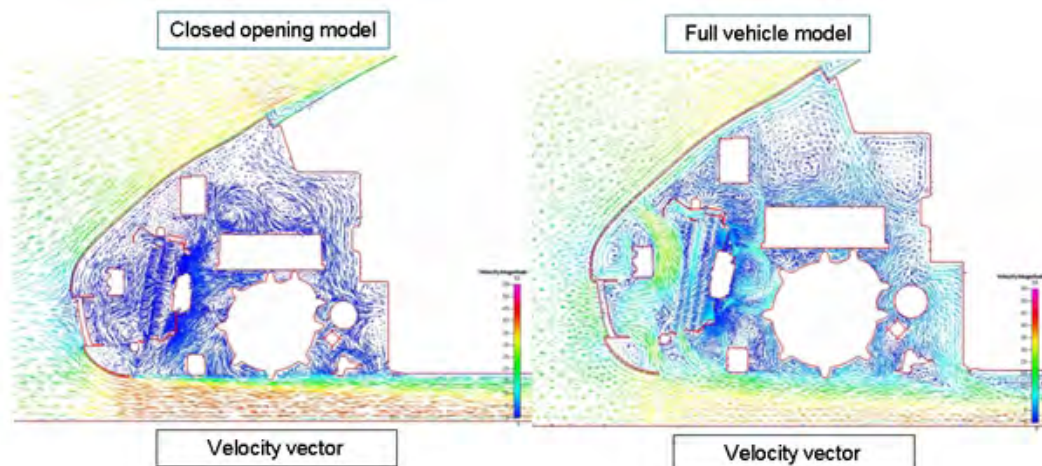


Figure 6.20: Full vehicle CFD air velocity comparison

6.2.6 FSV Full Vehicle CFD Model - Cooling Flow Optimization

Based on the results of iteration 9, (closed vs. open), additional studies were conducted to improve cooling air flow through the engine compartment. The modified original FSV model was now updated to include the (a) air-in duct, (b) air-out duct, (c) front tire spoiler, and (d) underbody cover as illustrated in Figure 6.21. The air intake opening is reduced to the minimum size required for the motor and inverter cooling.

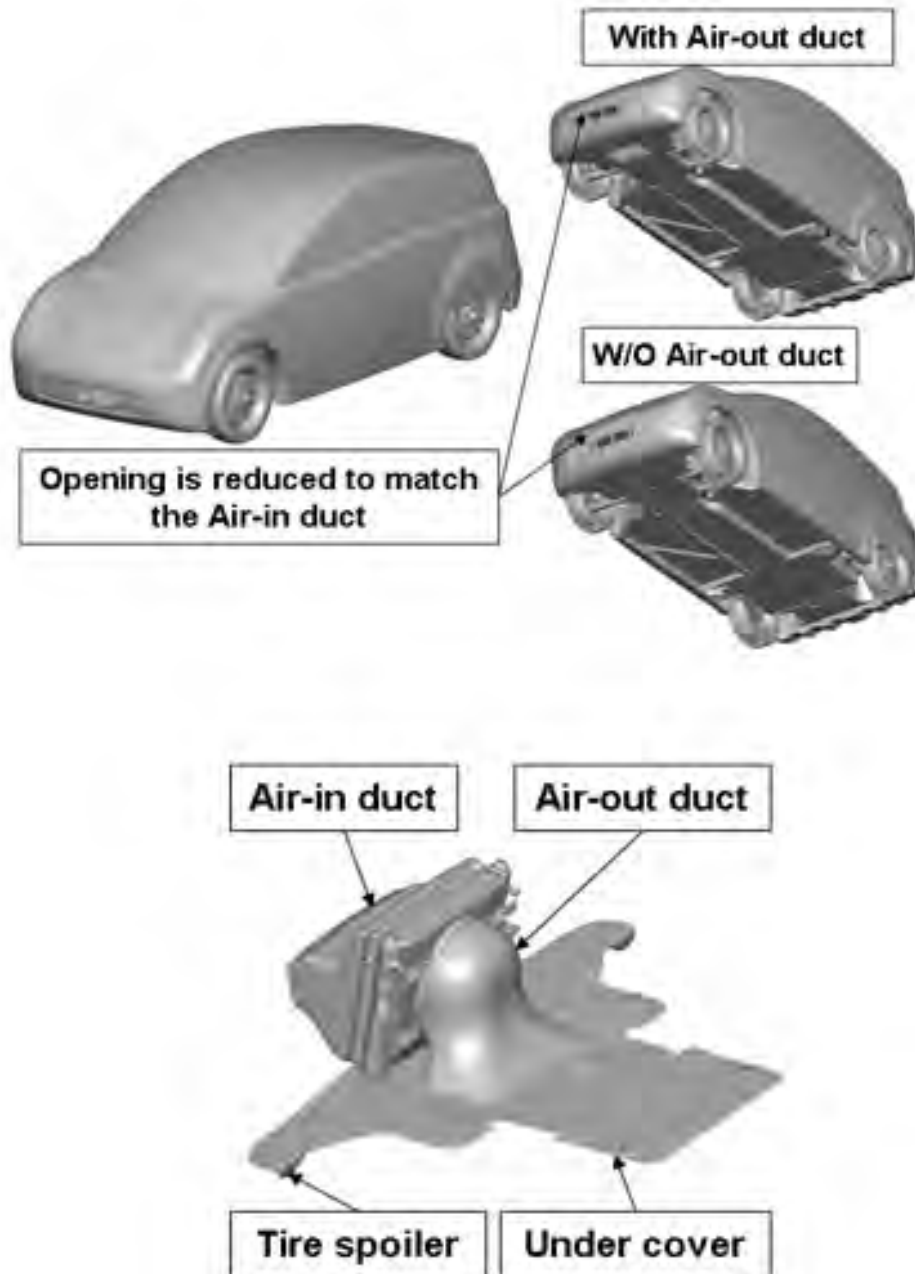


Figure 6.21: Air ducts, tire, spoiler and underbody cover

Three studies were conducted to understand the value of these modifications as shown in Table 6.9. The reduced opening and air-intake duct reduce the C_d from 0.327 in iteration 9, to 0.264 in iteration 10a. A comparison of iteration 10a and 10b conclude the spoiler increased the C_d , and that the air-duct improved the C_d from .267 to .264. However, it is felt that this small gain in C_d justifies the added cost and weight of the air-duct.

Model	Configuration	Drag Force (N)	Lift Force (N)	Drag Coefficient	Lift Coefficient
Full vehicle model iteration-1	with air-out duct and tire-spoiler	361.2	242.0	0.264	0.177
Iteration 2	with air-out duct w/o tire-spoiler	360.3	272.2	0.263	0.199
Iteration 3	w/o air-out duct with tire-spoiler	366.1	351.4	0.267	0.256

Table 6.9: Cooling flow optimization- C_d and C_L results

6.2.7 FSV Full Vehicle CFD Model - Effect of Add-on Parts/Features

This iteration of the CFD analysis involved the addition of some exterior parts to the original vehicle model. The following parts were considered:

1. Rear view mirror
2. Wheel caps
3. Smooth underbody
4. Rear tire spoiler

Figure 6.22 shows the vehicle CFD model of iteration 10c with all the above mentioned add-on parts.

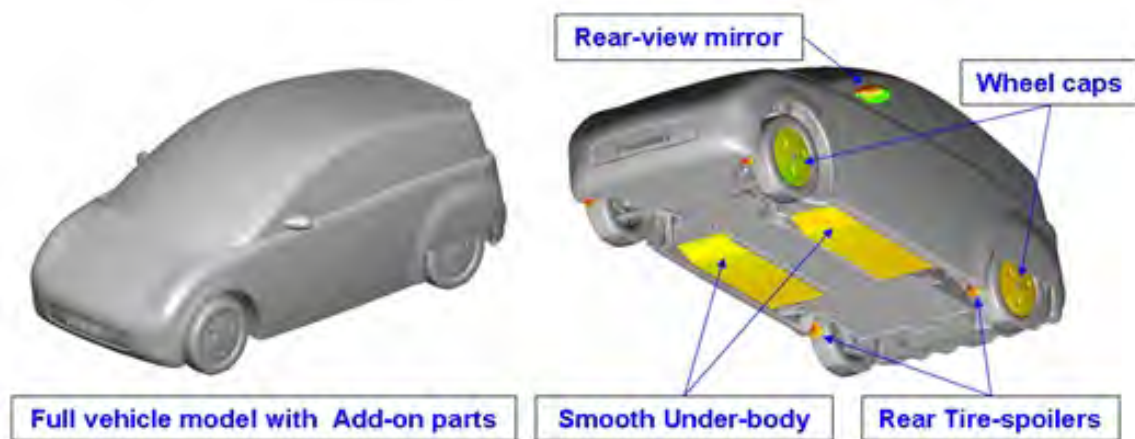


Figure 6.22: Modified original FSV model - with add-on parts

6.2.7.1 C_d and C_L Values with Add-on Parts

Table 6.10 shows the aerodynamic coefficients of the vehicle under these new configurations. Wheel caps improve the C_d value by 5.5% to a value of 0.257. Rear-view mirrors increase the C_d

by 0.004 on this style of vehicle, a smaller than expected increase.

Model	Configuration	Drag Force (N)	Lift Force (N)	Drag Coefficient	Lift Coefficient
Full vehicle model iteration-3	(from previous result) w/o air-out duct with tire-spoiler	366.1	351.4	0.267	0.256
With smooth under-body	smooth under-body	371.9	180.2	0.272	0.132
+ wheel caps	smooth under-body + wheel caps	351.9	218.4	0.257	0.159
+ rear tire-spoiler	smooth under-body + wheel caps + rear tire-spoiler	357.2	211.3	0.261	0.154
+ rear view mirror	smooth under-body + wheel caps + rear tire-spoiler + rear view mirror	362.5	179.7	0.265	0.131

Table 6.10: Add-on parts - aerodynamic CFD results

6.3 Modified Original FSV Model - Multiple Changes Based on Lessons Learnt

The original FSV model was modified to include the features that improved the aerodynamic performance and other exterior changes as shown in Figure 6.23 and outlined below:

1. Modified roof and fender surfaces
2. Rear spoiler with side wings
3. Sharp edges around back face
4. Rear tire spoilers
5. Inclined flange

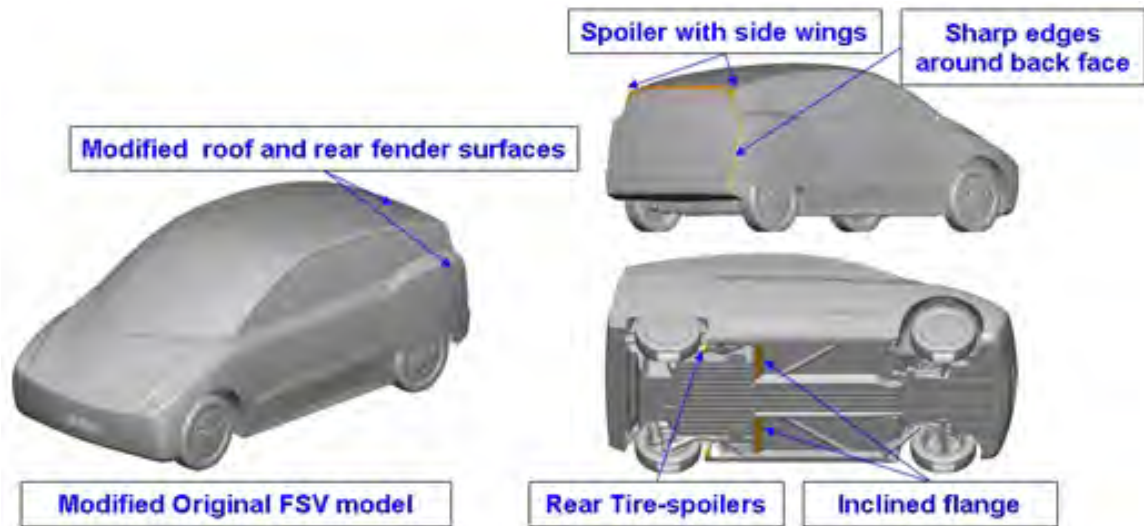


Figure 6.23: Modified original FSV design with recommended design changes

6.3.1 C_D and C_L Values with Add-on Parts

The upper and side spoiler with side wings increases pressure on the back face when compared to the model without the spoiler side wings as shown in the pressure contour plots on the two configurations in Figure 6.24.

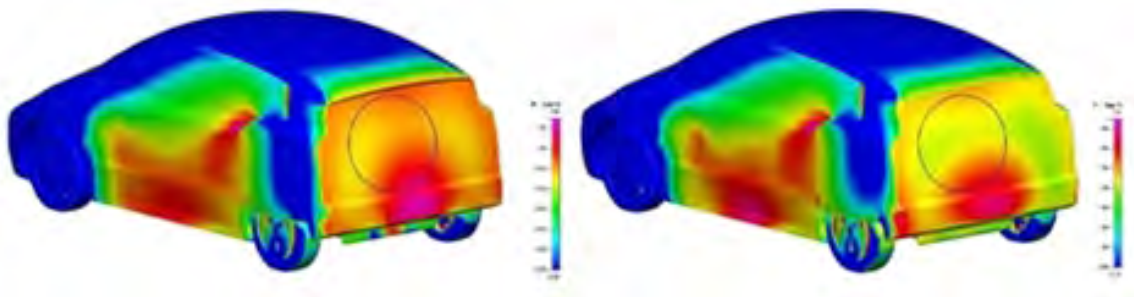


Figure 6.24: Pressure plots - with and without spoiler side wings

Table 6.11 shows the C_d and C_L values calculated based on the CFD results on different configurations. The rear spoiler with wings improves the drag coefficient to 0.259 in the FSV model. The wing-part decreases the drag coefficient by 0.006.

The inclined flange does not show any positive effect in terms of drag coefficient. (Iteration 12b vs. 12d)

The rear tire-spoiler has very little effect on the drag coefficient but has positive effect in the lift coefficient reduction.

Model	Configuration	Drag Force (N)	Lift Force (N)	Drag Coefficient	Lift Coefficient
Full vehicle model (previous best)	smooth under-body, wheel caps	351.9	218.4	0.257	0.159
Modified original FSV model	inclined under-body flange, wheel caps, with spoiler wings	355.0	223.7	0.259	0.163
with no spoiler wings	inclined under-body flange, wheel caps, w/o spoiler wings	362.5	246.0	0.265	0.180
with rear tire-spoiler	inclined under-body flange, wheel caps, w/o spoiler wings, with rear tire-spoiler	360.7	236.6	0.263	0.173
with vertical under-body flange	vertical under-body flange, wheel caps, w/o spoiler wings	263.4	223.7	0.265	0.163

Table 6.11: Modified original FSV model with recommended design changes - C_d and C_L values

6.4 New FSV Styling CFD Analysis

In FSV Phase 1, a styling theme was created. However, based on this CFD study, a new styling theme is required to accommodate the design features which enable a C_d value that meets the 0.25 target. See Figure 6.25 below for the FSV-1 BEV latest styling theme and Figure 6.26 for the FSV-1 BEV latest vehicle package.



Figure 6.25: FSV-1 BEV - latest styling theme

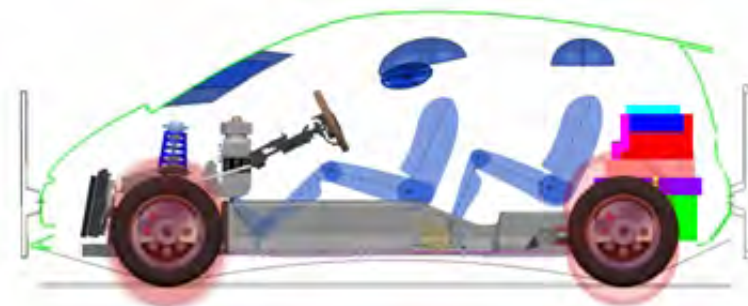


Figure 6.26: FSV-1 BEV - latest vehicle package

The CFD model based on the new styling model incorporated the recommendations provided during the course of the aerodynamic development of the FSV. Some of the distinct aerodynamic features of the new FSV-1 styling shown in Figure 6.27 included:

1. Rounded front shape
2. Smooth side surfaces
3. Spoiler with side wings
4. Sharp edges around the back face

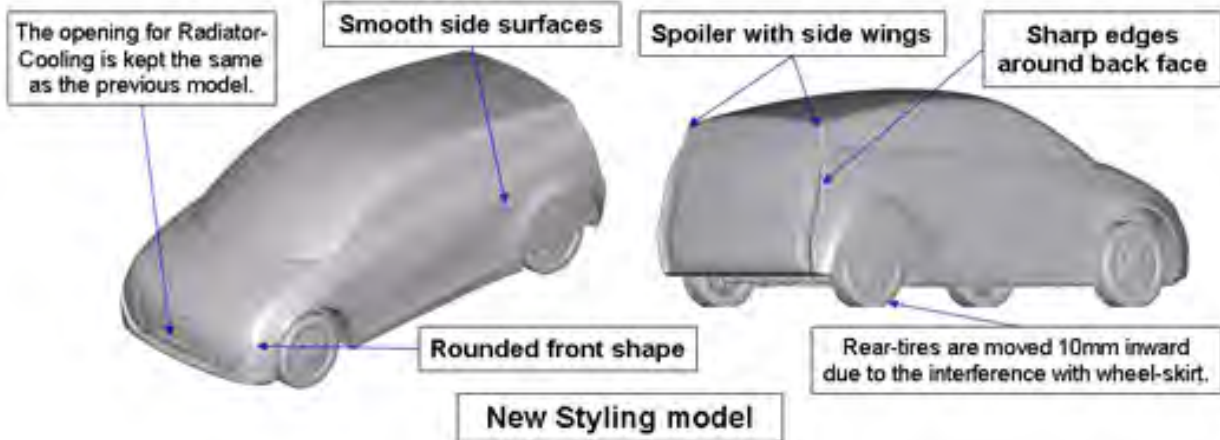


Figure 6.27: FSV-1 BEV - latest CFD model with key aerodynamic features

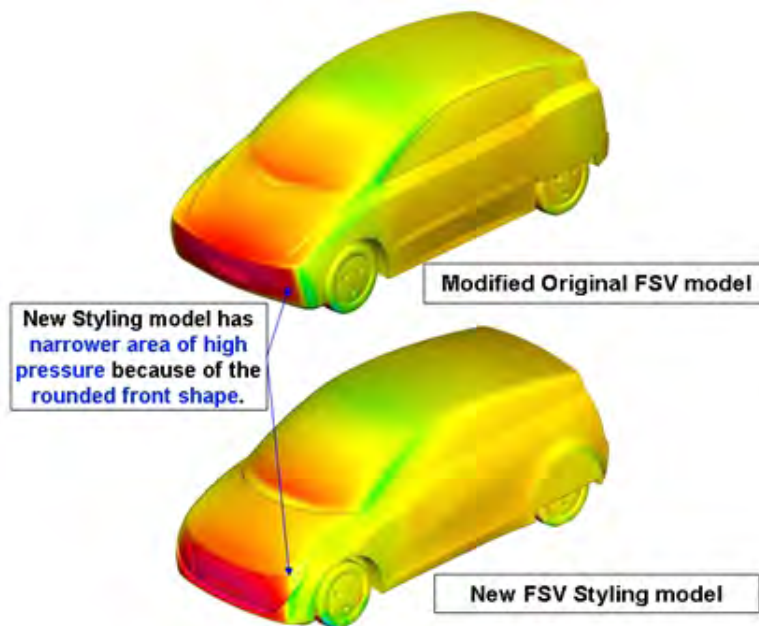


Figure 6.28: Latest FSV styling model pressure contour

The new FSV model has a narrower area of high pressure in the front due to the rounded front face as shown in the pressure contour plot in Figure 6.28. This helps reduce the drag coefficient of the vehicle.

Figure 6.29 shows the pressure plots on the rear surfaces of the modified original FSV model (top) and the new FSV model (bottom).

6.4 New FSV Styling CFD Analysis

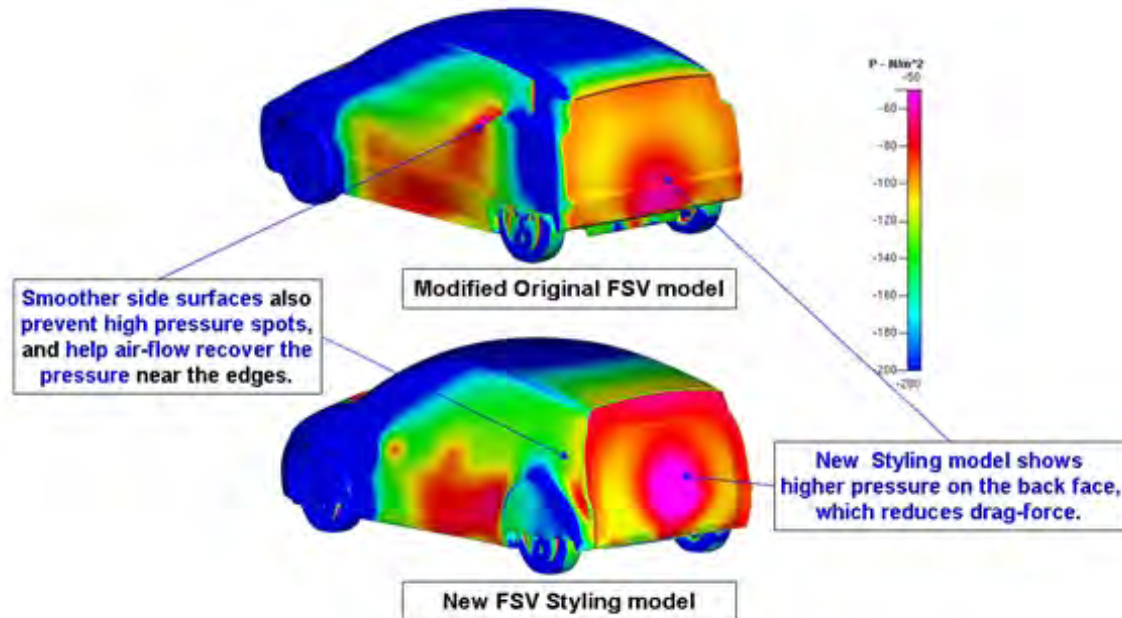


Figure 6.29: Pressure plots - with and without spoiler side wings

Smoother side surfaces on the new FSV model prevent high pressure spots, and helps air-flow recover the pressure near the edges. The styling feature of the new FSV model shows higher pressure on the back face, which also helps reduce drag force and in turn reduce the C_d of the vehicle.

6.4.1 Final C_d and C_L Values for FSV-1

Table 6.12 shows the final results of the aerodynamic studies on the FSV-1 model. The new FSV styling model reduces both drag and lift coefficients to 0.237 and 0.073, respectively. The main features of new FSV-1 styling are the spoiler with wings, sharp edges around back-face, rounded front shape and smooth side-surfaces, and sloping 14° rear roof line.

Model	Drag Force (N)	Lift Force (N)	Drag Coefficient	Lift Coefficient
Modified original FSV model	355	224	0.259	0.163
Latest FSV styling model	325	101	0.237	0.073

Table 6.12: FSV-1 final results for C_d and C_L

6.5 Summary of Aerodynamic Performance Results

For this project immediately after the advanced powertrain technology assessment, an early powertrain packaging study combined with interior occupant space was used to establish a styling theme on which the original FSV-1 3D surfaces were based. The aerodynamic performance results for the original and the new FSV styles are shown in Table 6.13. The C_d value of 0.354 for the original FSV model is 42% higher than the required C_d target of 0.25. Through various incremental design changes discussed in this report, the C_d value was reduced to 0.237 for the final proposed style. The C_d value of 0.237 for the FSV compares to a typical value of 0.31 for an A-B class vehicle. Various styling images for the latest FSV-1 style are shown in Figure 6.30 and Figure 6.31.

Model	Drag Force (N)	Lift Force (N)	Drag Coefficient	Lift Coefficient
FSV baseline CFD Model	485	-113	0.354	-0.082
Modified original FSV model	355	224	0.259	0.163
Latest FSV styling model	325	101	0.237	0.073

Table 6.13: FSV-1 aerodynamic results summary

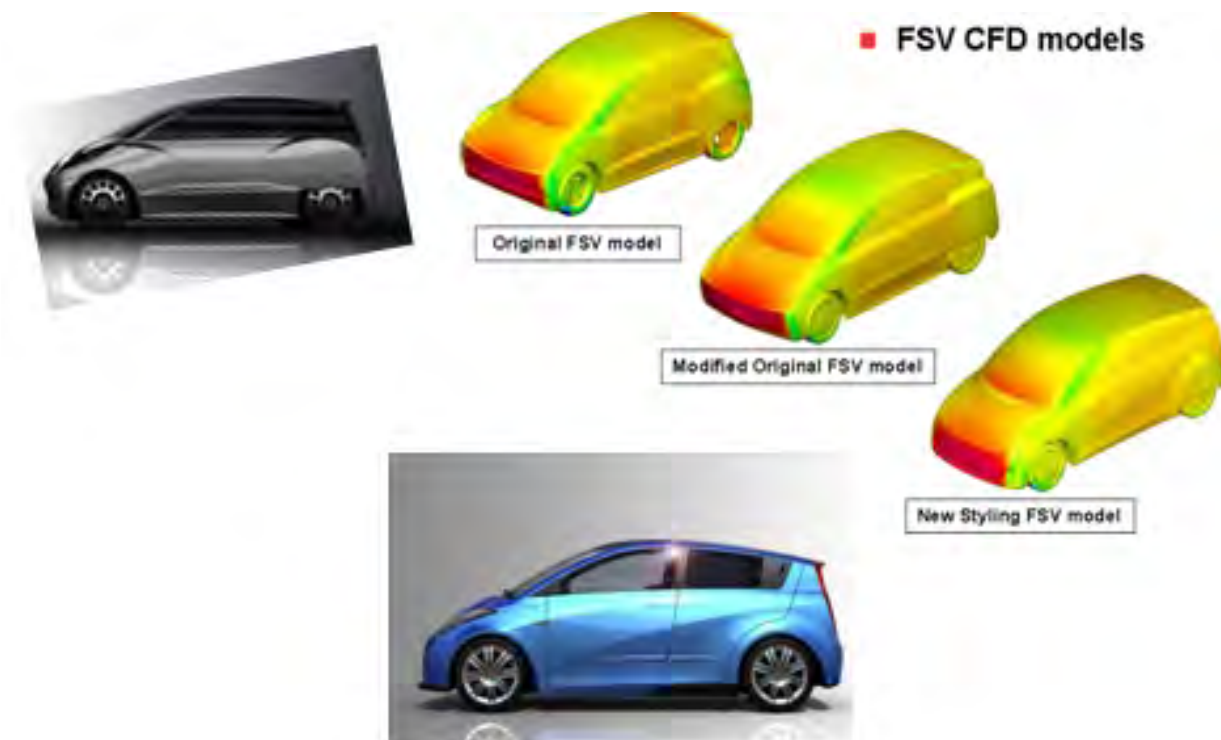
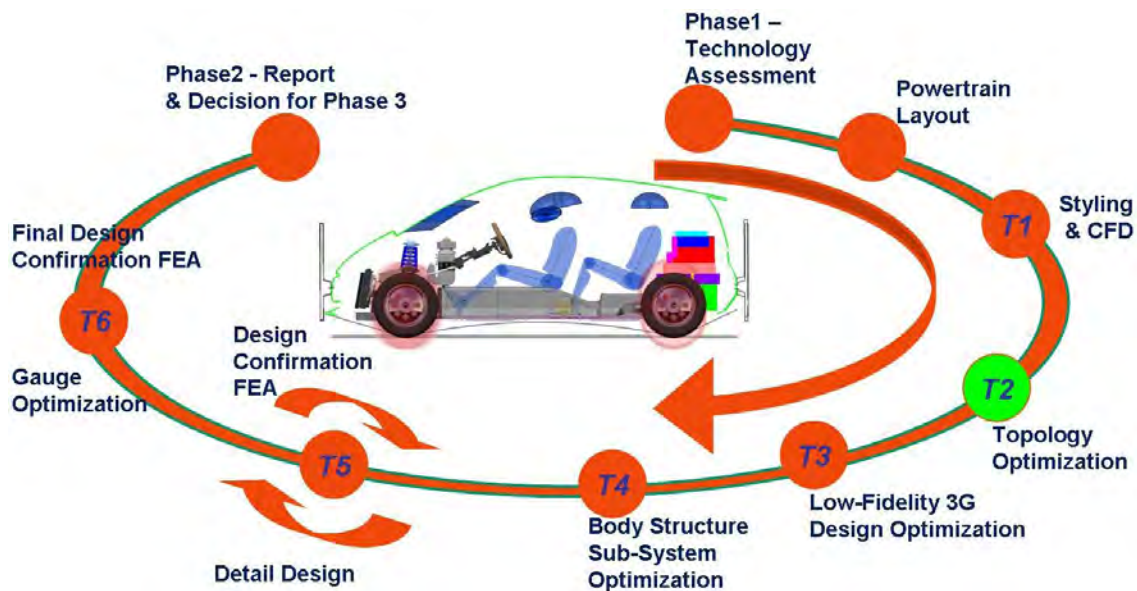


Figure 6.30: Latest FSV styling and CFD models



Figure 6.31: Latest FSV-1 BEV styling images - showing utilities access hatch and charging

7.0 T2 Topology Optimization



7.1 Introduction

Evolutionary Topology Optimization of Continuum Structures treads new ground with a comprehensive study on the techniques and applications of evolutionary structural optimization (ESO) and its later version bionic methods. Since the ESO method was first introduced by Xie and Steven in 1992 and the publication of their well-known book *Evolutionary Structural Optimization* in 1997, there have been significant improvements in the techniques as well as important practical applications.

In vehicle design, such as any other structure in nature that is subjected to many different load conditions, we must design a basic structure that is then optimized for mass and performance. In the FSV body structure design, we utilized this methodology as a basic design tool to identify the material requirement and to imitate the natural bionic structure within the vehicle packaging space. This report completes the Full Vehicle Topology Optimization of the FSV (FutureSteelVehicle). Topology optimization study was completed by ETA.

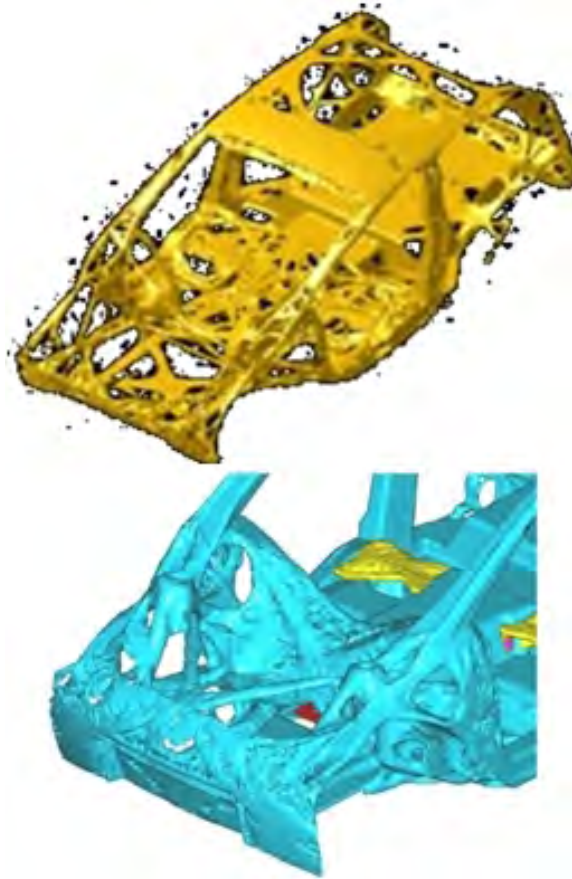


Figure 7.1: Vehicle "skeletal" structure

7.2 Objective

The objective of the topology optimization is to provide an initial structure for the FSV, subject to the following load cases: IIHS front 40% ODB, NCAP front impact, FMVSS 301 rear 70% ODB, IIHS side impact, FMVSS 214 pole impact, FMVSS 216 roof crush, bending and torsional static stiffnesses. Considering all loadcases simultaneously, the optimization will determine the initial vehicle structure from the design space shown in Figure 7.2.

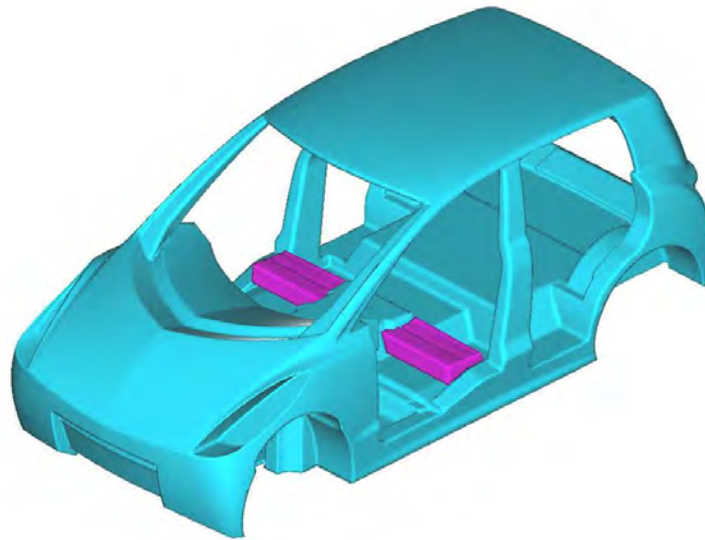


Figure 7.2: FSV-1 design space - initial vehicle structure

7.3 Background

The full vehicle topology optimization uses the FSV design methodology. In this case, the topology optimization will be applied to a design space that represents the entire vehicle and from this, will determine the most efficient distribution of material for the loading conditions considered. There are four main parts of the vehicle that will be considered separately:

1. Battery floor
2. Battery bulkhead
3. Seat crossmember
4. Body structure

7.4 Optimization Methodology

From a finite element mesh that represents the blocked out design space, the volume within which structure can exist, the topology optimization eliminates elements thus revealing the optimal structure as shown in Figure 7.3. The decision to remove an element is made based on its strain energy for the given loading condition, thus effectively eliminating structure that is carrying the least amount of load, while retaining structure that is most effective. The target reduction or mass fraction is defined as a goal for the optimization. For this analysis the topology optimization was run at 30%, 20% and 10% mass fractions. That is 70%, 80% and 90% of the mass was eliminated from the original design space.

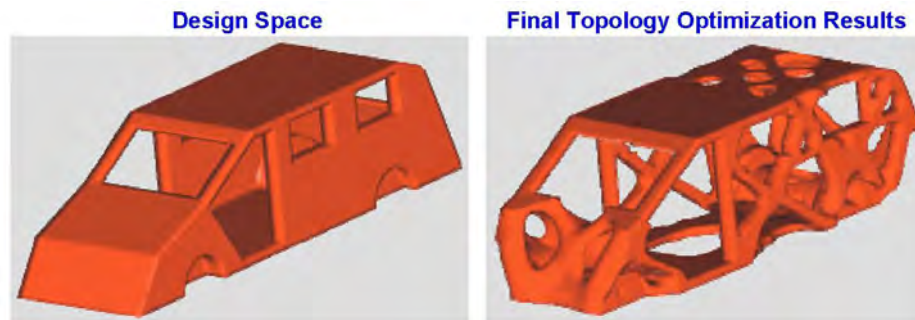


Figure 7.3: *Overview of topology optimization*

The topology optimization was conducted in two phases

1. Optimization of the battery pack structure. This will define the geometry of the battery floor and bulkhead.
2. Definition of the vehicle structure using the results of the battery optimization. This will define the seat cross-member and body structure.

7.5 Design Space

The design space represents the greatest volume within which the topology optimization can create the vehicle's structure, thus allowing the optimization to create structure wherever it did not conflict with the vehicle's styling, packaging or passenger requirements. The outer surface represents the vehicle's external styling surfaces, the volume under the hood for the powertrain and its components and the wheel wells. The internal surfaces define the passenger compartment. The difference between the two surfaces establishes the packaging envelop within which the vehicle structure must exist. See Figure 7.2.

During the course of the optimization, it was decided to provide the opportunity for a load bearing bulkhead through the battery module. This was accomplished by rigidly connecting the battery design space to the vehicle and removing a portion of the "underbody skid plate" from the bottom of the vehicle. The initial design space was setup so that the underbody was completely flat in line with the lowest part of the vehicle. The battery is positioned slightly higher thus creating a sheet of design space that for the purposes of discussion has been called the "underbody skid plate". When the underbody skid plate was complete it created a bridge allowing the external loads, especially from side and pole impacts, to bypass the battery. By removing the hashed portion of the skid plate the external load was forced to transition through the battery thus allowing the optimization to explore potential structural bulkheads within the battery pack itself as shown in Figure 7.4.

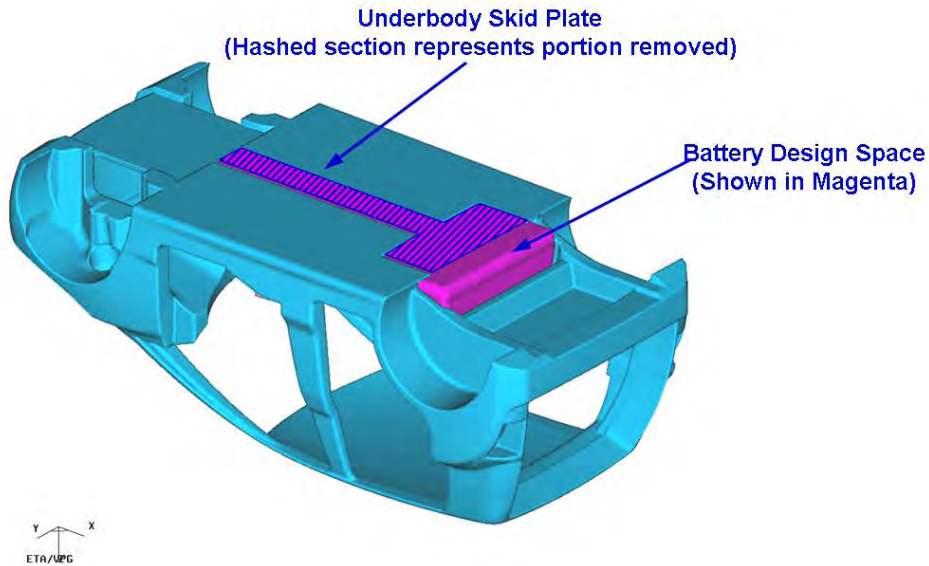


Figure 7.4: FSV-1 battery design space within the vehicle

7.6 Finite Element Model

The full vehicle optimization model contains approximately 2.8 million solid tetrahedral elements. This includes a representation of the battery's design space as shown in Figure 7.4 and the seat cross-members as shown in Figure 7.5.

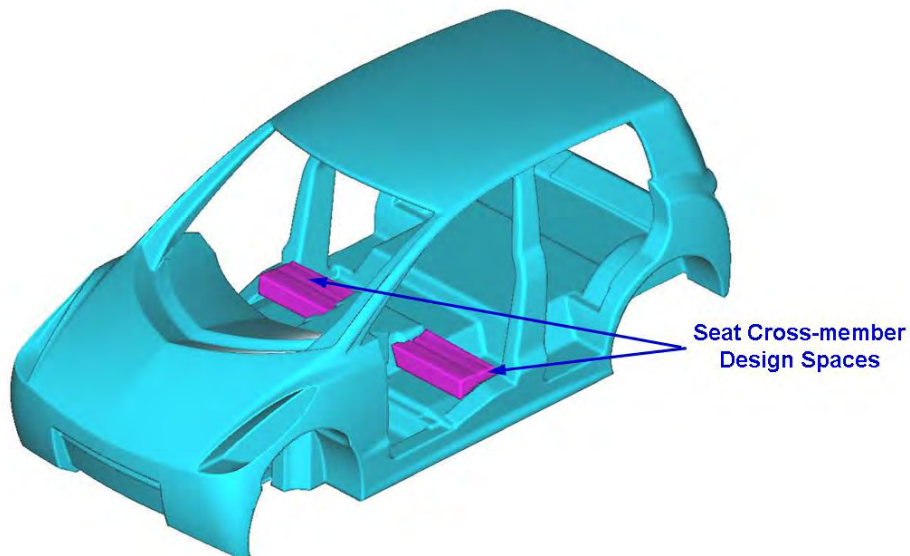


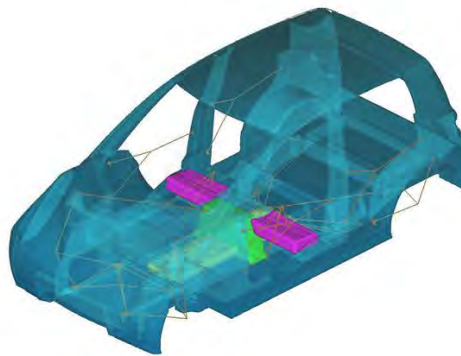
Figure 7.5: FSV-1 finite element model used for topology optimization

7.7 Boundary Conditions and Analysis Assumptions

Genesis, the software package used to perform the topology optimization is based on linear static theory. As many of the loadcases considered are highly dynamic non-linear crash events, an equivalent static load was used as an analogy of these impact loadings. While there are limitations to this approach, it provides a first approximation of the optimized structural load path. These limitations will be addressed in the next step of the project were the optimization will transition from the linear static to the non-linear dynamic domain.

7.7.1 Mass Assumptions

The crash loads considered use an Inertia Relief form of constraint this means that the applied forces are reacted at the vehicle's CG (Center of Gravity) rather than at arbitrarily defined rigid points of constraint using SPCs (Single Points of Constraint). An SPC is a constraint in any or all degrees of freedom, that is translations and rotations about the global X, Y and Z applied to the individual nodes within the Finite Element Mesh. Thus it is important to define the mass of the vehicle accurately. Figure 7.6 below, summarizes the masses of the vehicle's major components. Each component is represented by a concentrated mass connected to the vehicle using Rigid Body Element 3 (RBE3) elements. The concentrated mass representing the "Rest of Vehicle" includes the passengers, seats and other non-structure components of the vehicle, was positioned at the vehicle's center of gravity and was connected via RBE3s to the vehicle's front and rear shock towers.



COMPONENT	MASS (kg)
Front Wheel (Tire, Brake & Wheel)	40.5 each
Rear Wheel (Tire, Brake & Wheel)	31.1 each
Front Door	12.1 each
Rear Door	11.3 each
Front Seat	16 each
Powertrain	40.6
DC Inverter	19.1
Battery	347
Rest of Vehicle	556
GVW	1184.7 kg

Figure 7.6: FSV-1 mass assumptions

7.7.2 Loads and Boundary Conditions

As mentioned, the topology optimization software used is based on linear static theory and so it was necessary to create equivalent static loads for the dynamic non-linear crash events. The impact loadcases, as shown in Figure 7.8, Figure 7.7, Figure 7.9, Figure 7.10 and Figure 7.11, were constrained using inertia relief boundary conditions in order to best represent the actual conditions of the tests. Non-rigid spiders^[1] were used to distribute the applied loads over an area that represented the contact areas of the barriers. For the IIHS side impact loading, the contact area was extended to include the footprints of the combined IIHS and FMVSS barriers as shown in Figure 7.9. In each case, the impact load was represented by a unit load of 1000N applied at a location and direction that best represented the actual loadings. It should be noted that for this analysis, the actual magnitude of the loads does not matter or change the results.

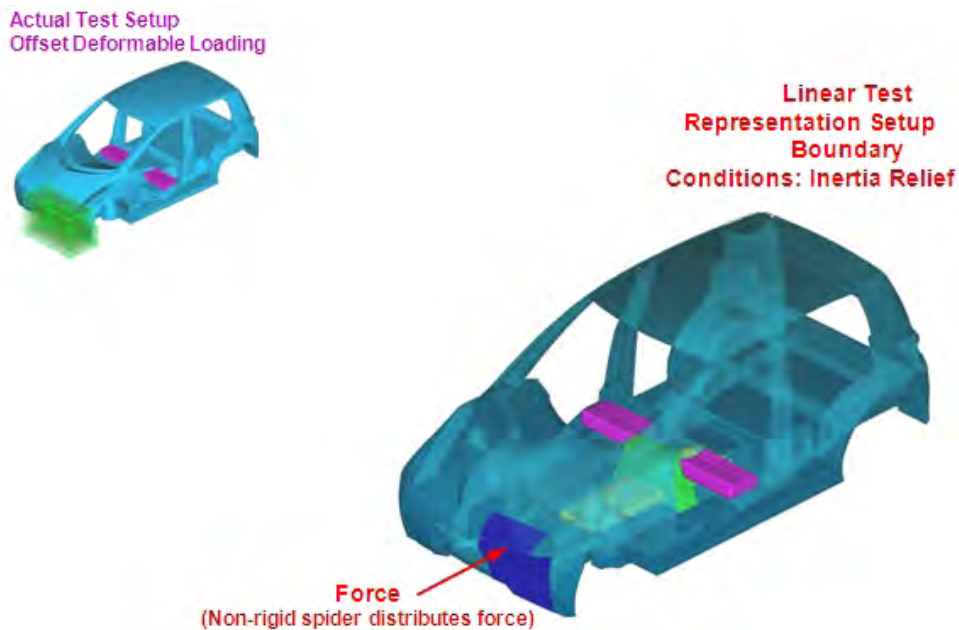


Figure 7.7: FSV-1 IIHS front 40% ODB

¹Non-rigid spiders are used when local stiffness is not desired over the area upon loading

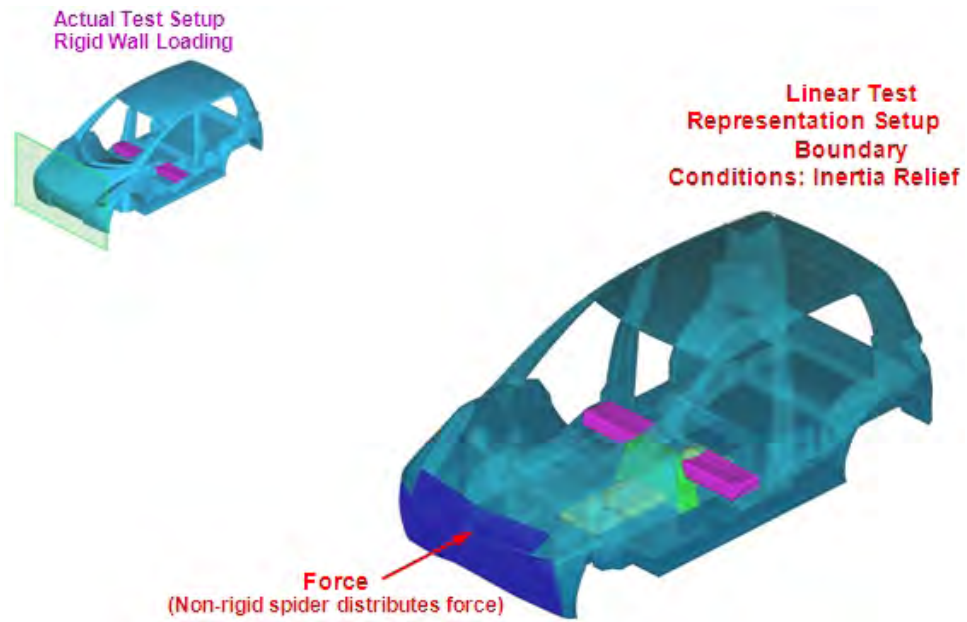


Figure 7.8: FSV-1 NCAP front impact

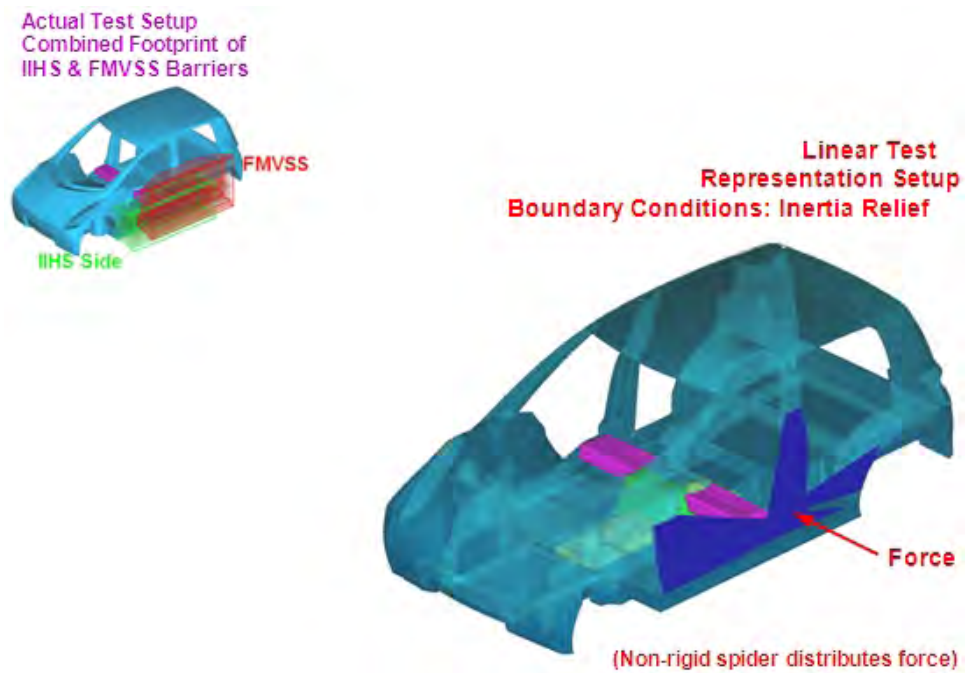


Figure 7.9: FSV-1 IIHS side impact

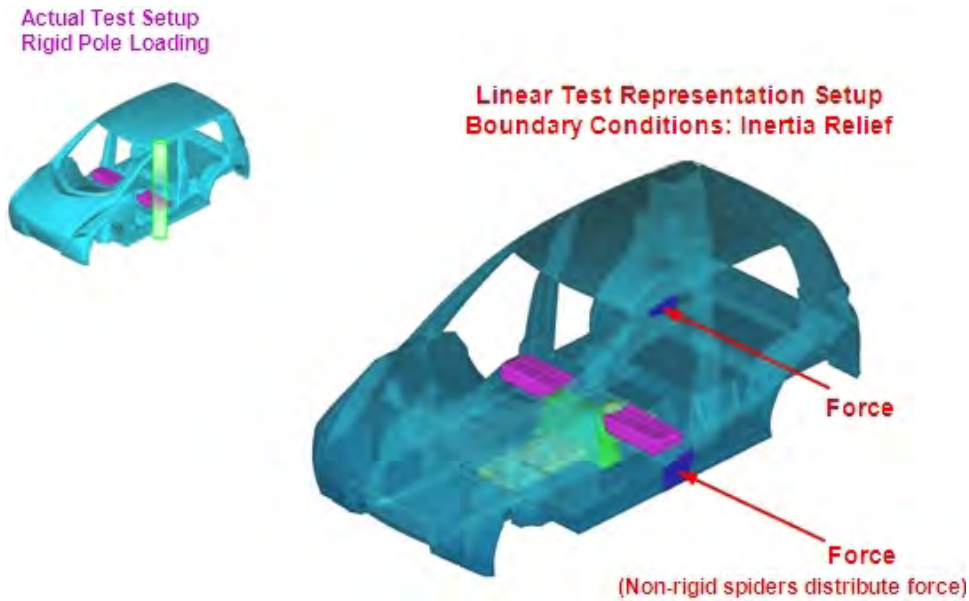


Figure 7.10: FSV-1 FMVSS 214 pole impact

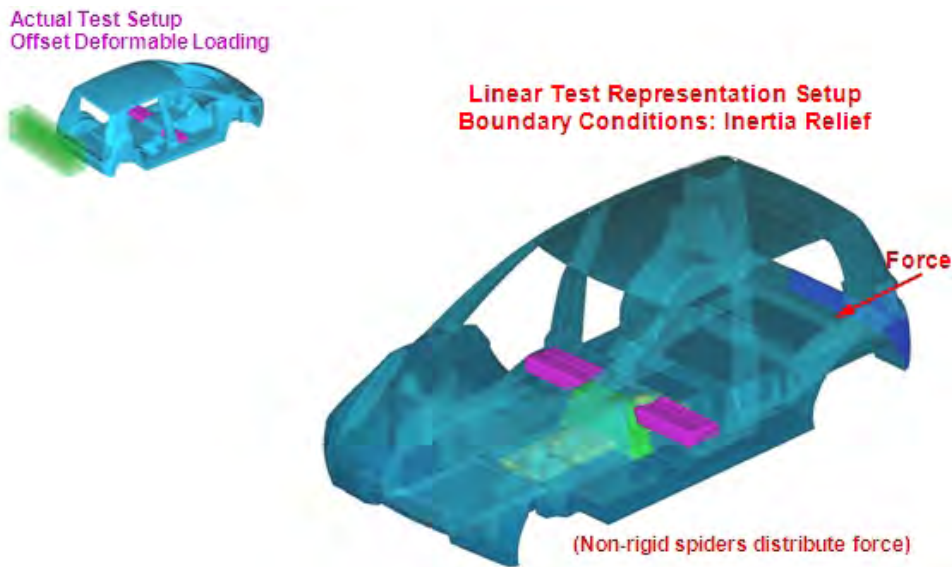


Figure 7.11: FSV-1 FMVSS 301 rear 70% ODB

The FMVSS 216 roof crush is a quasi-static loading and so was optimized using single point boundary constraints applied to the rocker, which were fixed in all translations as shown in Figure 7.12. Bending and torsional static stiffnesses were also defined using single point boundary conditions as shown in Figure 7.13 & Figure 7.14. Since all three loadcases were constrained using the Single Point Constraint (SPC) methodology, it was also necessary to use symmetric loadings. Symmetric design constraints were applied to the model for several reasons. First, it reduced the number of design variables by one half, thus reducing the computational time. Secondly, it assured the final optimized shape would be symmetric when constrained by both single point and Inertia Relief methods. While crash loading is not symmetric, the structure must be capable of addressing crash loading from both sides. This approach enables a more robust structure.

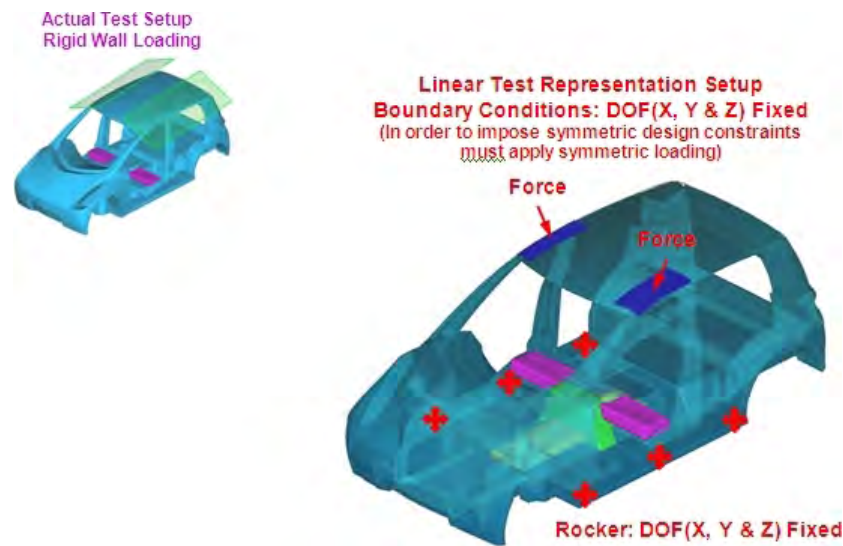


Figure 7.12: FSV-1 FMVSS 216 roof crush

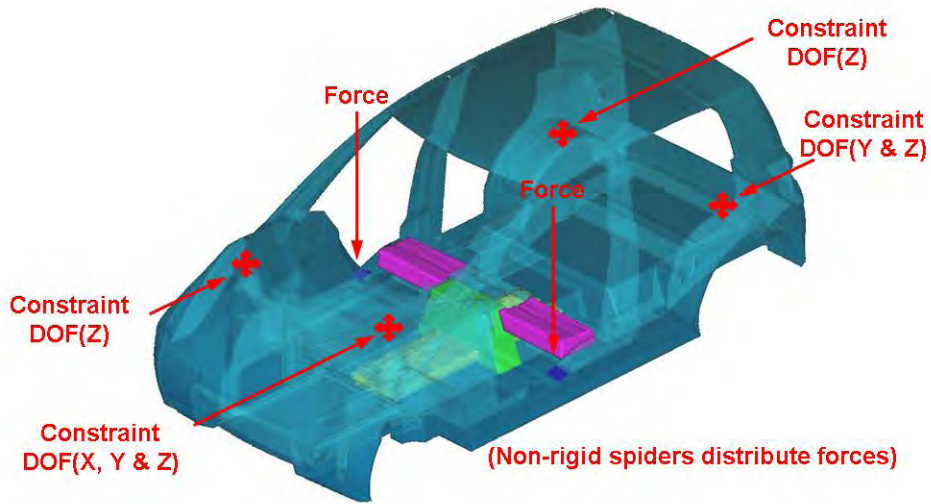


Figure 7.13: FSV-1 bending static stiffness

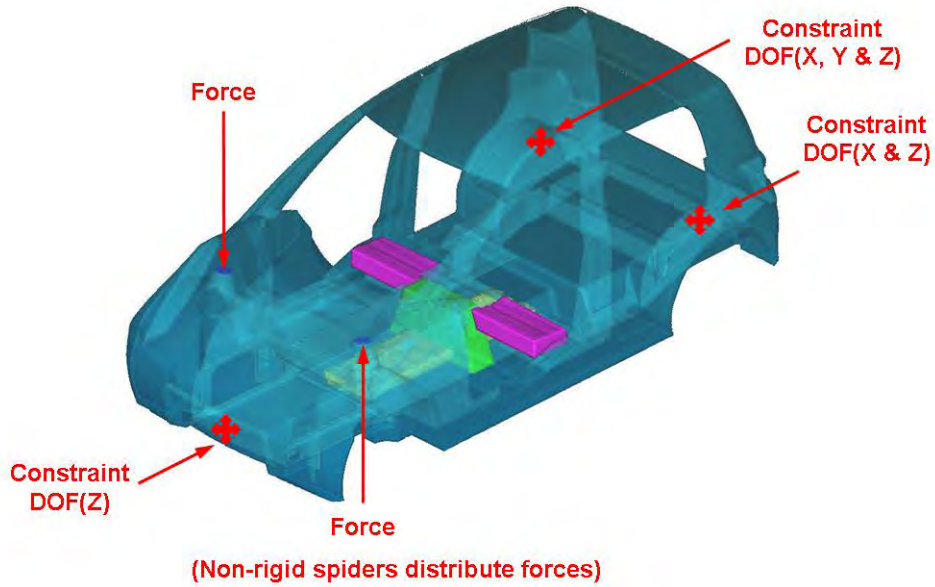


Figure 7.14: FSV-1 Torsional static stiffness

7.7.3 Loads and Weighting Factors

The topology optimization defines a single optimized geometry based on the loading of all eight loadcases, which it considers simultaneously. However, three of the loadcases, IIHS front impact 40% ODB, NCAP front impact and FMVSS 301 rear impact 70% ODB are longitudinal loads, while IIHS side impact and FMVSS 214 pole impact are lateral loads. Therefore if each loadcase was given equal importance, the final optimized shape would be biased toward the longitudinal loading and to a lesser extent the lateral loads at the detriment of FMVSS 216 roof crush and bending and torsional static stiffnesses. For example, if the longitudinal loadings were given equally weighting the resulting solution would represent a structure that considered the three longitudinal loadings happening simultaneously. Based upon previous experience from programs such as the A/SP (Auto/Steel Partnership) Future Generation Passenger Compartment, Roof Crush and Torsional Static Stiffness are controlling loadcases for some of the structure that will play a significant role in determining the most mass efficient BIW. It is thus essential that these loadcases are proportionally represented at this initial stage of the vehicle's structural development.

To reduce a potential bias toward any particular loading direction, vertical, longitudinal or lateral, it was decided to weight them equally as shown in Table 7.1. Thus for the three longitudinal loadcases, IIHS front impact 40% ODB, NCAP front impact and FMVSS 301 rear impact 70% ODB, their combined weighting was set to one (1). Similarly the combined lateral loads and the single vertical load were each set to one (1). Bending static stiffness was considered a localized loading, predominately affecting the Rocker and so was not included with the FMVSS 216 roof crush for the vertical loading. Thus though a total of eight individual loadcases were considered, when the weighting factors are accounted for, there are five combined objectives.

LOADCASES		WEIGHTING FACTOR
Longitudinal	IIHS Front Impact 40% ODB	1
	NCAP Front Impact	
	FMVSS 301 Rear Impact 70% ODB	
Lateral	IIHS Side Impact	1
	FMVSS 214 Pole Impact	
Vertical	FMVSS 216 Roof Crush	1
Static Bending Stiffness		1
Static Torsional Stiffness		1
TOTAL NUMBER OF OBJECTIVES		5

Table 7.1: FSV-1 loadcase weighting factors

7.8 Topology Results

The topology optimization was conducted in two phases

1. Optimization of the battery pack structure. This will define the geometry of the battery floor and bulkhead.
2. Definition of the vehicle structure using the results of the battery optimization. This will define the seat cross-member and BIW.

7.8.1 Battery Floor Optimization

7.8.1.1 Design space

As mentioned, it was decided to use portions of the battery structure as load bearing members. This was accomplished by rigidly connecting the battery design space to the vehicle and removing a portion of the underbody skid plate from the bottom of the vehicle. Thus external loads are forced to transition through the battery as shown in Figure 7.4

7.8.1.2 Boundary Conditions

The battery floor was optimized by using all eight loadcases. Refer to section 7.7.2 for the boundary conditions and loading used for each loadcase.

7.8 Topology Results

7.8.1.3 Results

Figure 7.15 shows where the optimization eliminated material from the battery design space, resulting in a flat plate concentrated toward the front of the battery. For the second phase of the optimization, these results were interpreted as a constant thickness floor, represented by the yellow portion of the new design space.

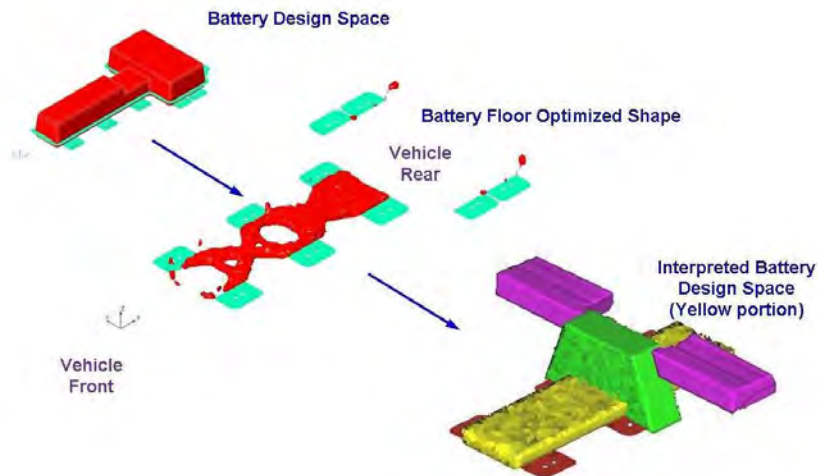


Figure 7.15: FSV-1 battery floor - analysis process & optimization result

7.8.2 Battery Bulkhead Optimization

7.8.2.1 Boundary Conditions

For the Battery bulkhead, the optimization only considered IIHS Side Impact and FMVSS 214 pole impact thus biasing the optimization in favour of the lateral loads. This forced the optimization to consider a bulkhead directly in line with the loadings transferred through the seat crossmembers. These are represented by the purple blocks in Figure 7.16 below and are in direct line with the B-Pillars. Thus lateral loads would be transferred from the B-Pillar, through the seat crossmember and the battery bulkhead to the opposite side of the vehicle. Again refer to 7.7.2 for the boundary conditions and loading used for each loadcase.

7.8.2.2 Results

Figure 7.16 shows where the optimization eliminated material from the battery design space, resulting in a bulkhead in line with the lateral loadings. For the second phase of the optimization, these results were interpreted as a constant thickness bulkhead, represented by the green portion of the new design space.

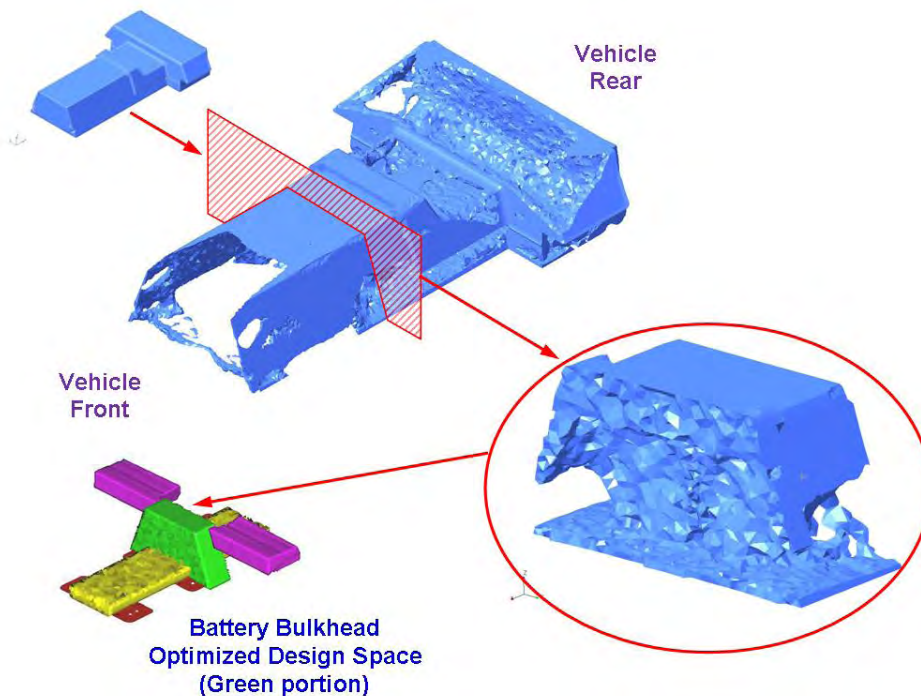


Figure 7.16: FSV-1 battery bulkhead - analysis process & optimization Result

7.8 Topology Results

7.8.3 Full Vehicle Optimization

7.8.3.1 Boundary Conditions

The full vehicle design space was updated with the revised battery geometry as shown in Figure 7.17. This new model was then optimized for all eight loadcases as described in section 7.7.2.

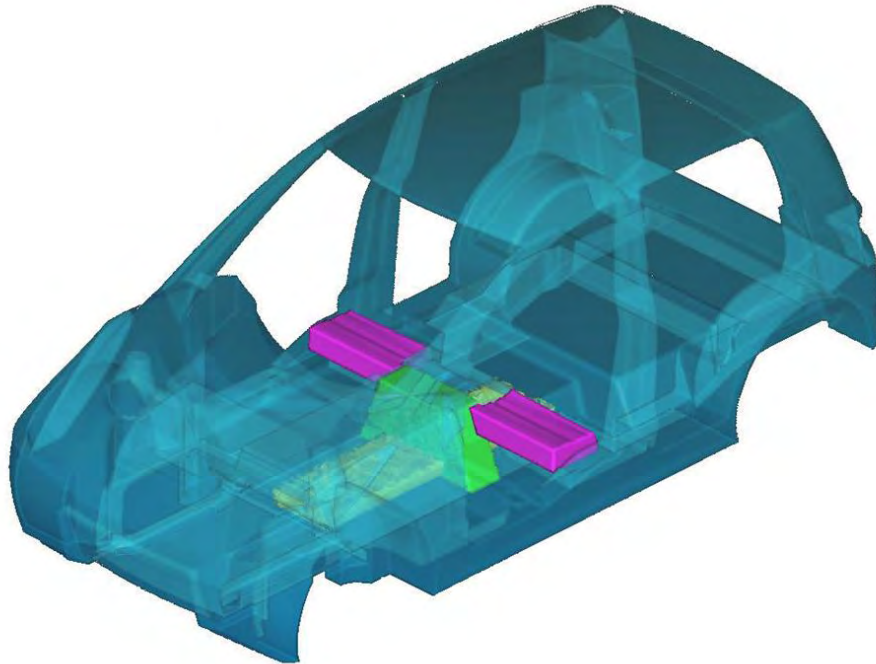


Figure 7.17: FSV-1 Updated full vehicle design space with revised battery from Phase 1

7.8.3.2 Results

The following sections show the final geometry for the 30%, 20% and 10% mass fractions. That is if 70%, 80% and 90% of the original mass were eliminated from the original design space.

Figure 7.18, Figure 7.19 & Figure 7.20 show the details of the final optimized shapes of the battery floor, bulkhead and seat cross-member for each mass fraction of 30%, 20% and 10% respectively.

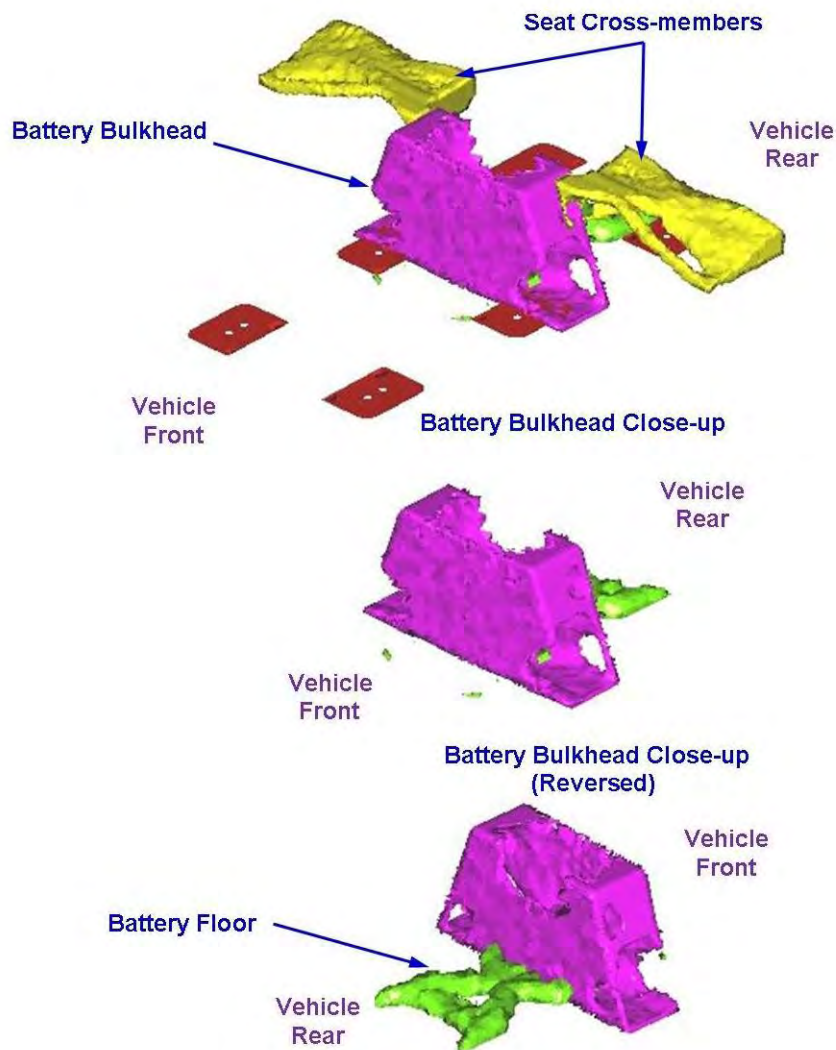


Figure 7.18: *FSV-1 30% mass fraction - battery floor, bulkhead & seat cross-member*

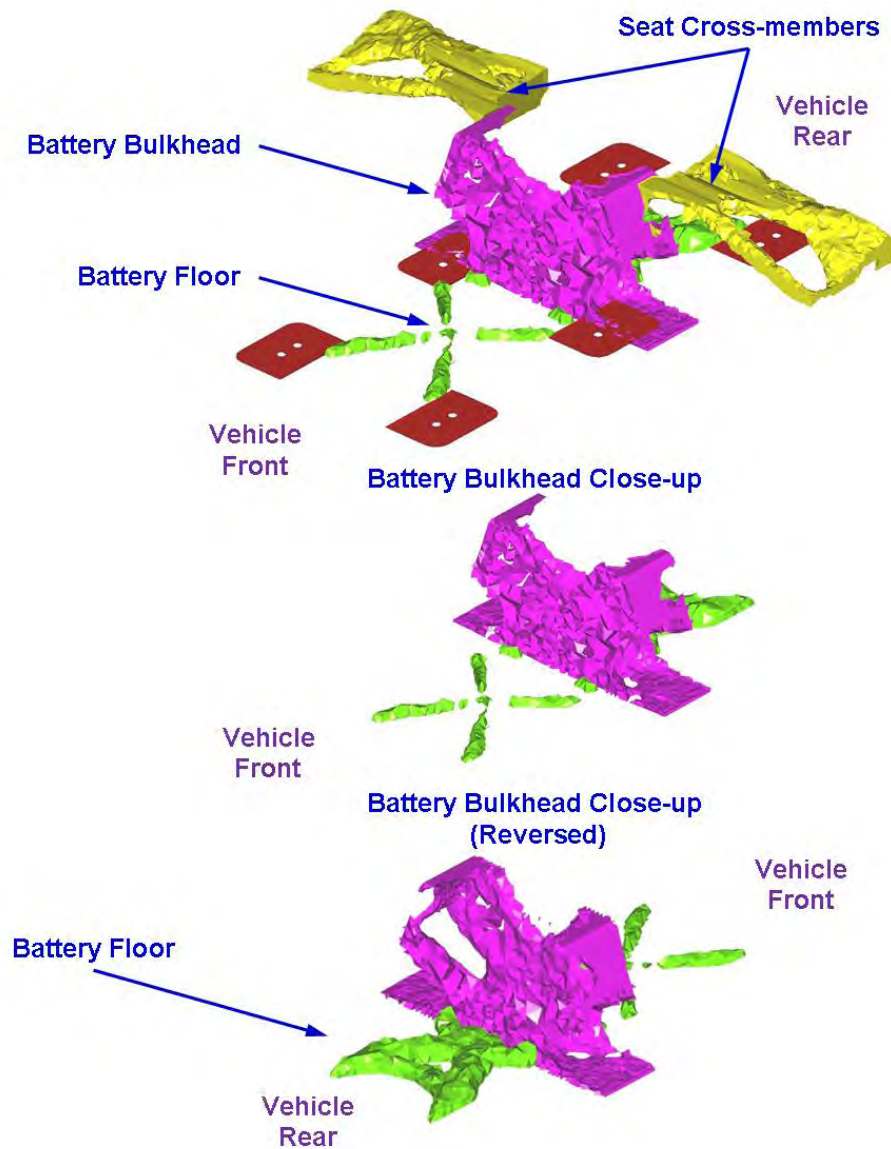


Figure 7.19: FSV-1 20% mass fraction - battery floor, bulkhead & seat cross-member

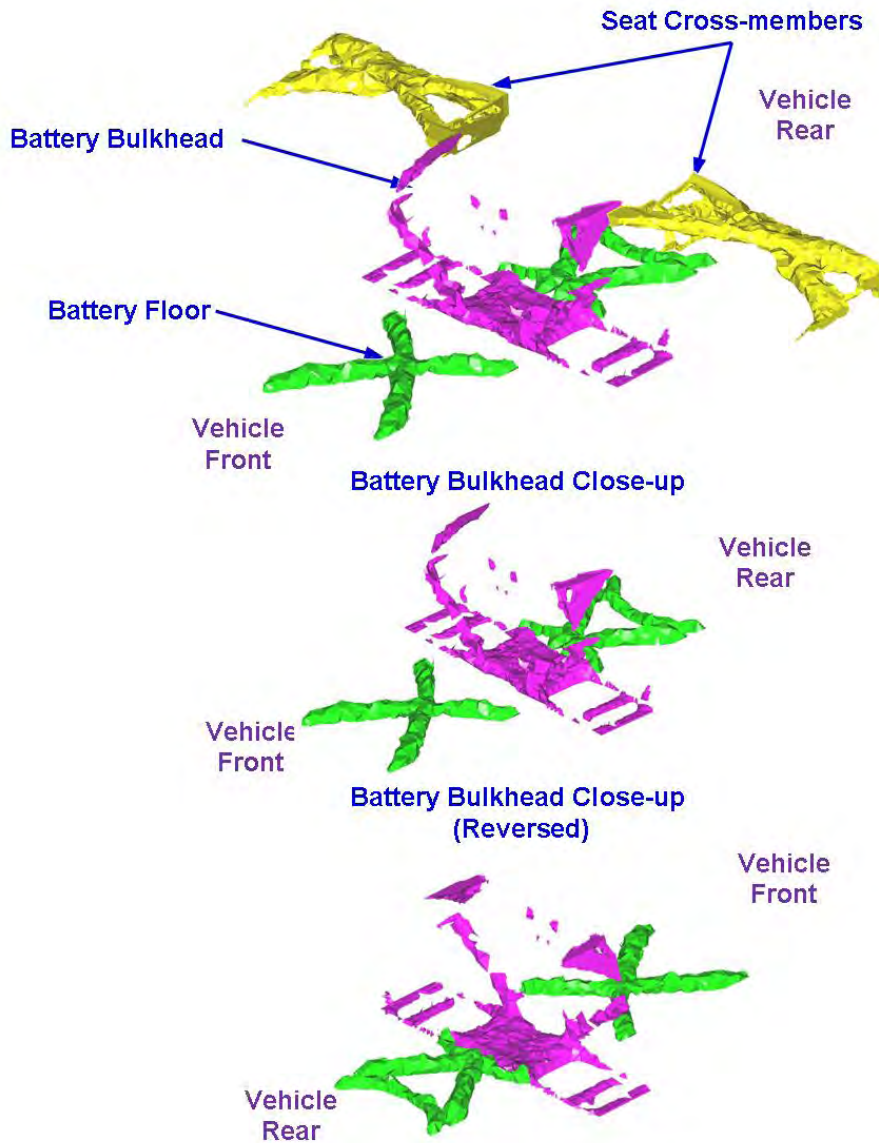


Figure 7.20: FSV-1 10% mass fraction - battery floor, bulkhead & seat cross-member

7.8 Topology Results

7.8.3.3 30% Mass Factor Optimization Results

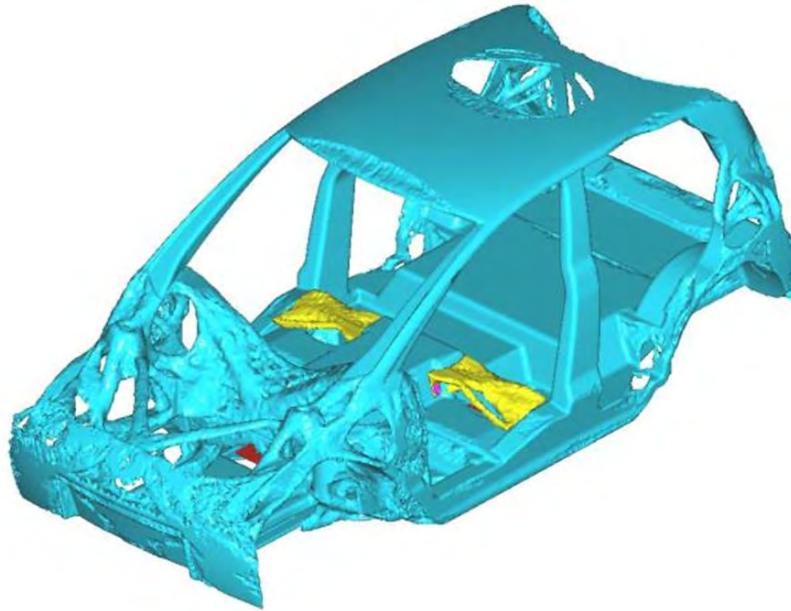


Figure 7.21: FSV-1 30% mass fraction - front isometric view

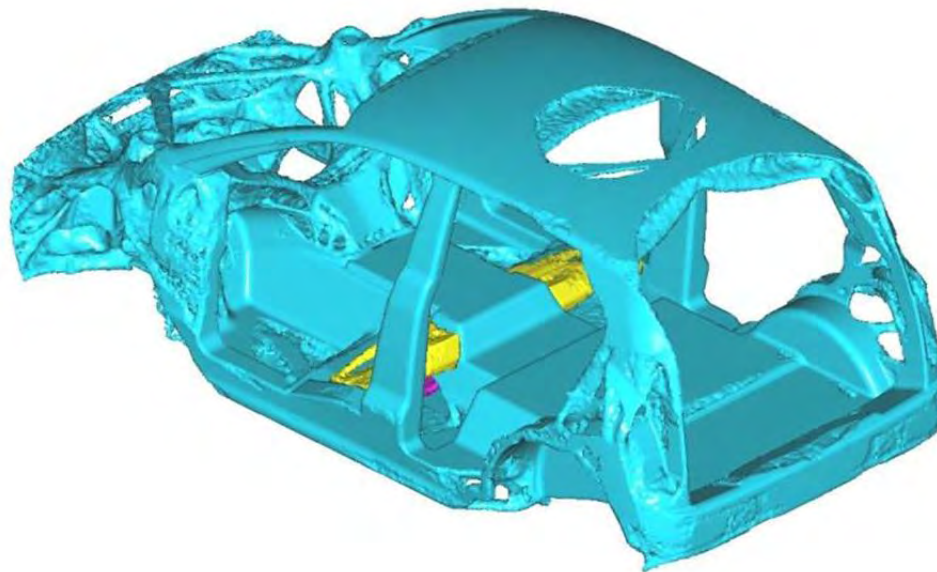


Figure 7.22: FSV-1 30% mass fraction - rear isometric view

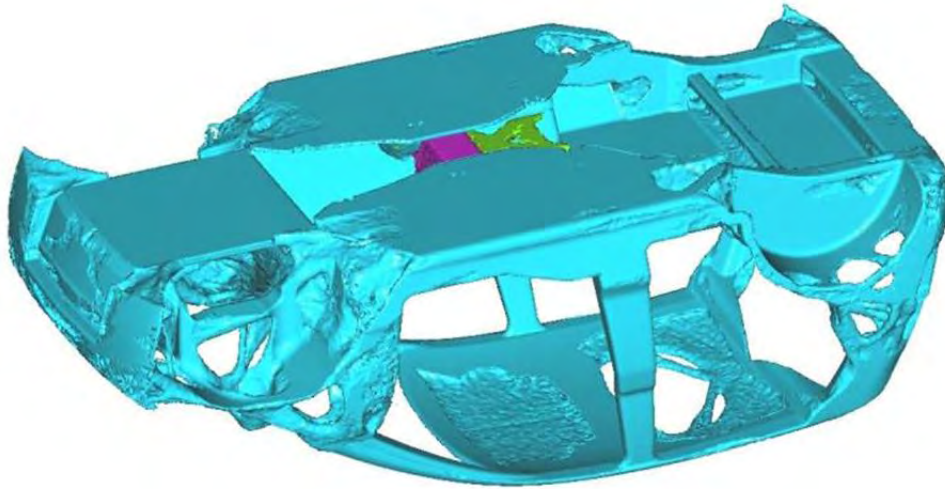


Figure 7.23: FSV-1 30% mass fraction - bottom view

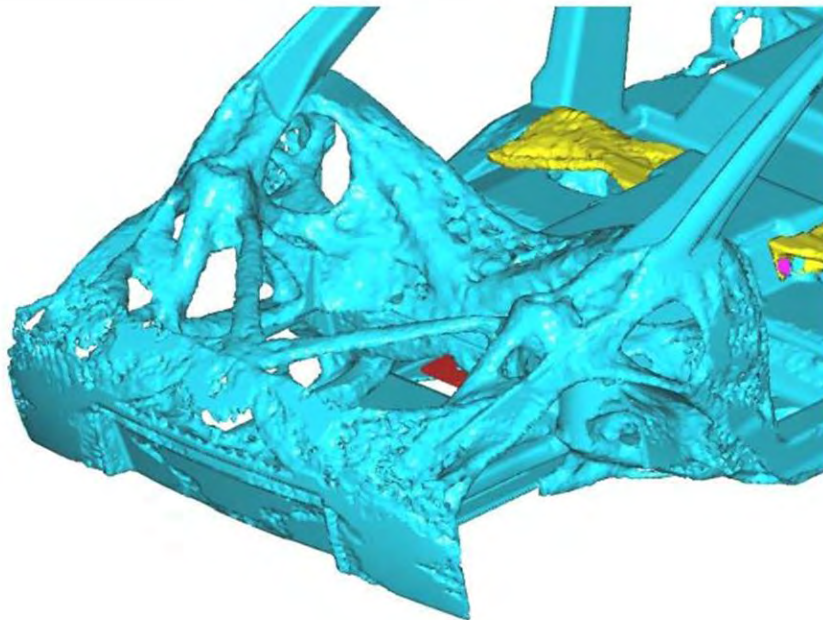


Figure 7.24: FSV-1 30% mass fraction - front end

7.8 Topology Results

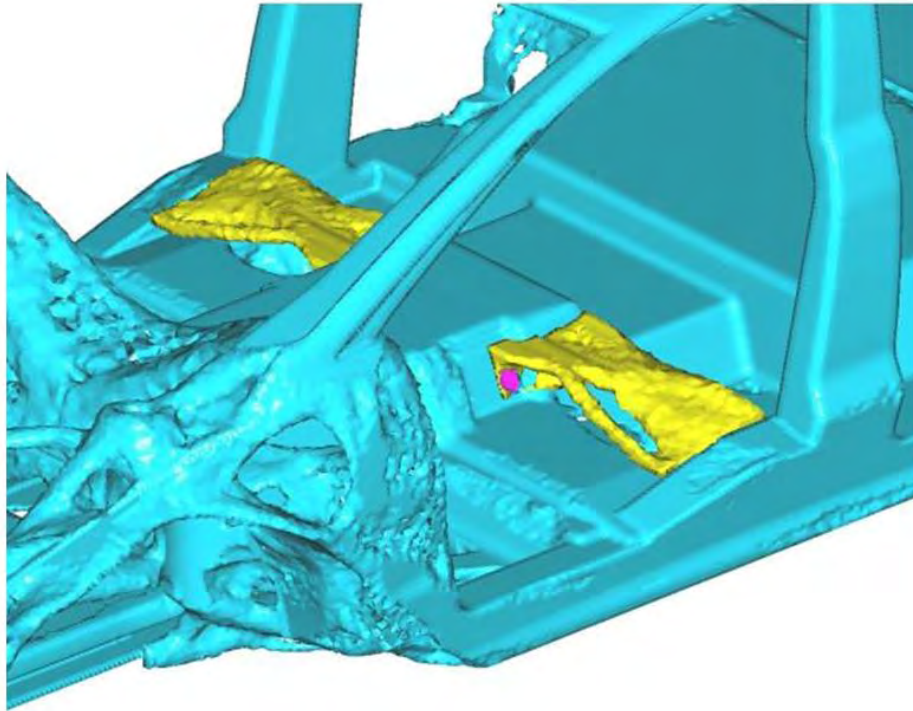


Figure 7.25: FSV-1 30% mass fraction - floor pan and tunnel

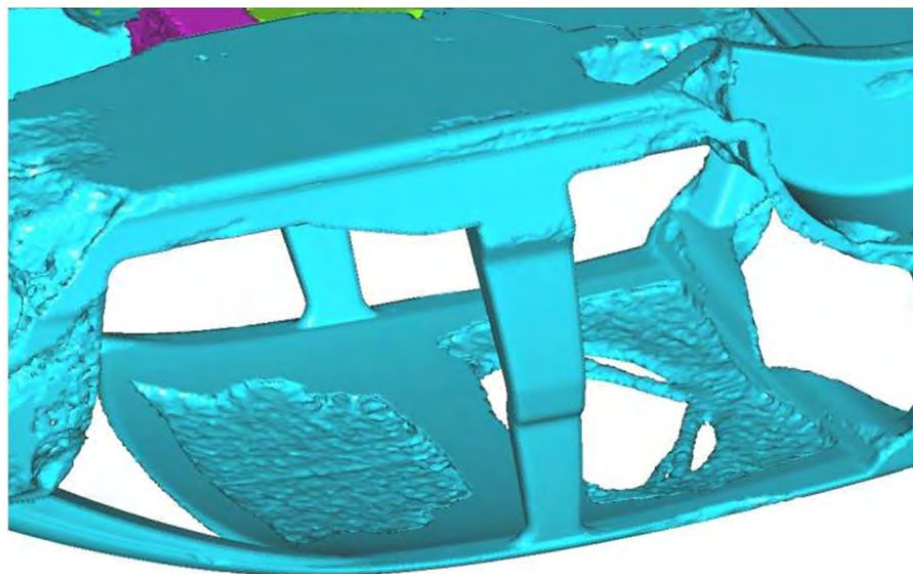


Figure 7.26: FSV-1 30% mass fraction - roof panel

7.8.3.4 20% Mass Factor Optimization Results

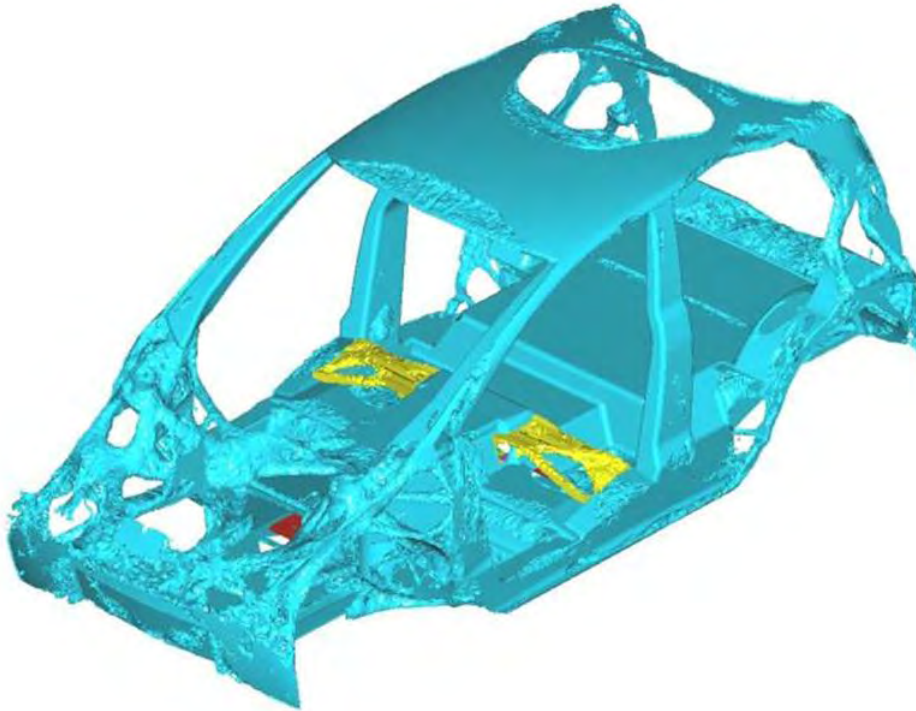


Figure 7.27: FSV-1 20% mass fraction - front isometric view

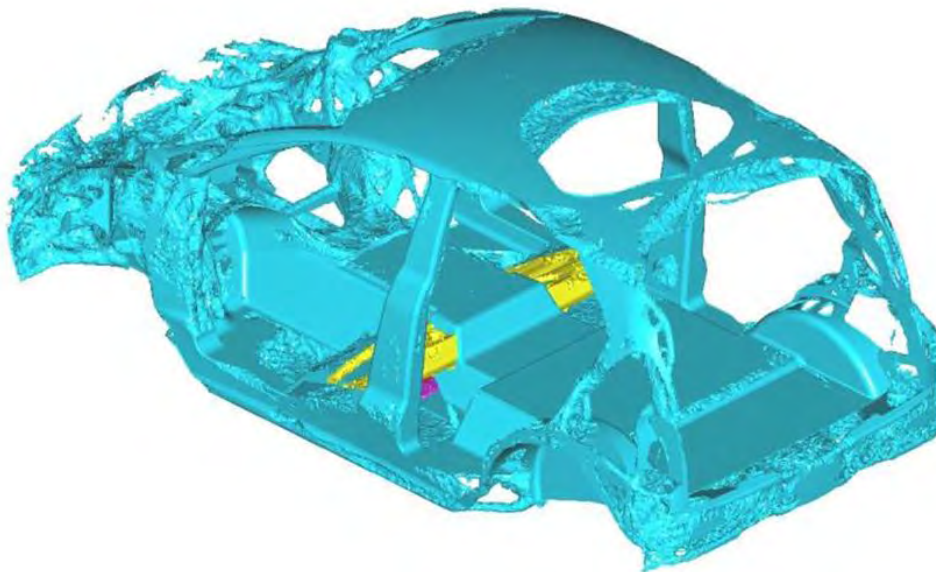


Figure 7.28: FSV-1 20% mass fraction - rear isometric view

7.8 Topology Results

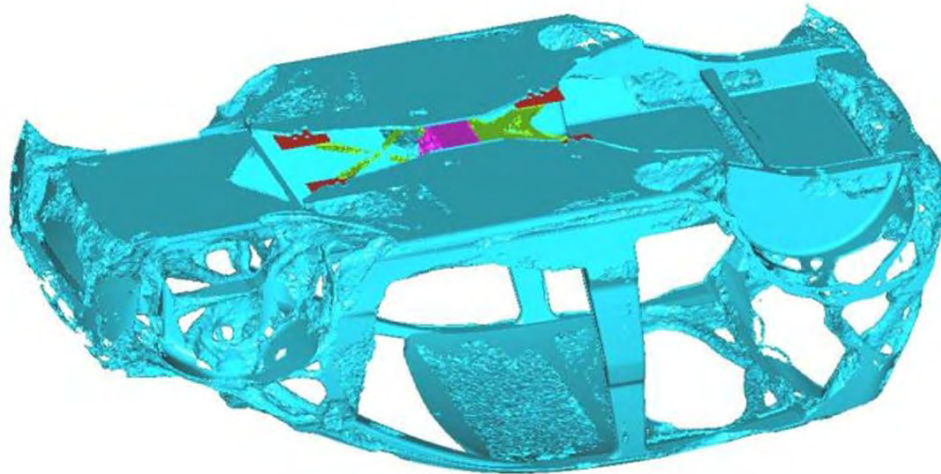


Figure 7.29: FSV-1 20% mass fraction - bottom view

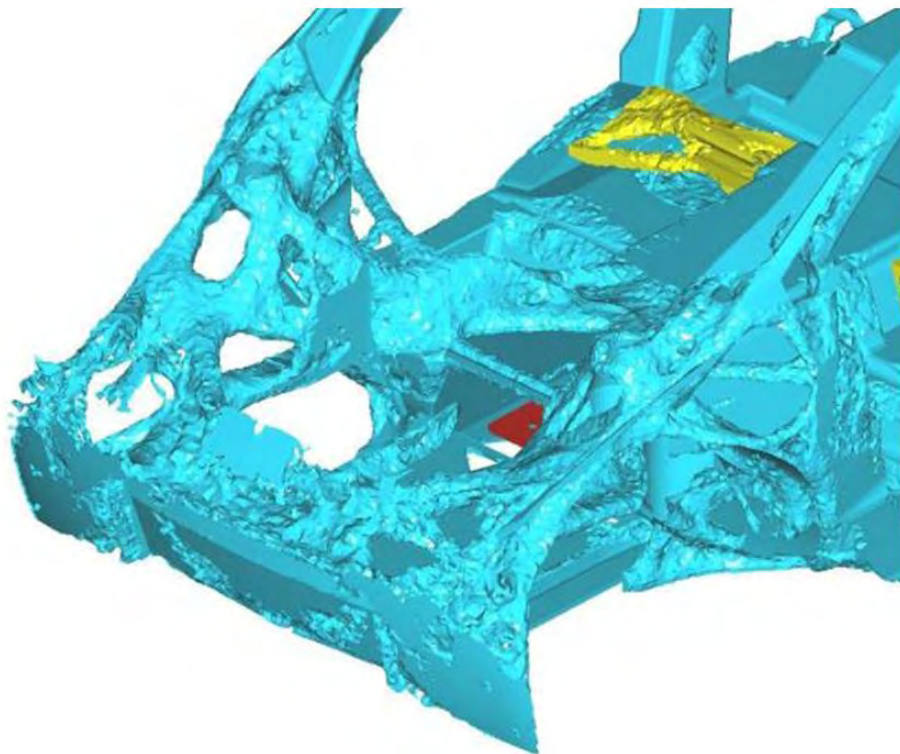


Figure 7.30: FSV-1 20% mass fraction - front end

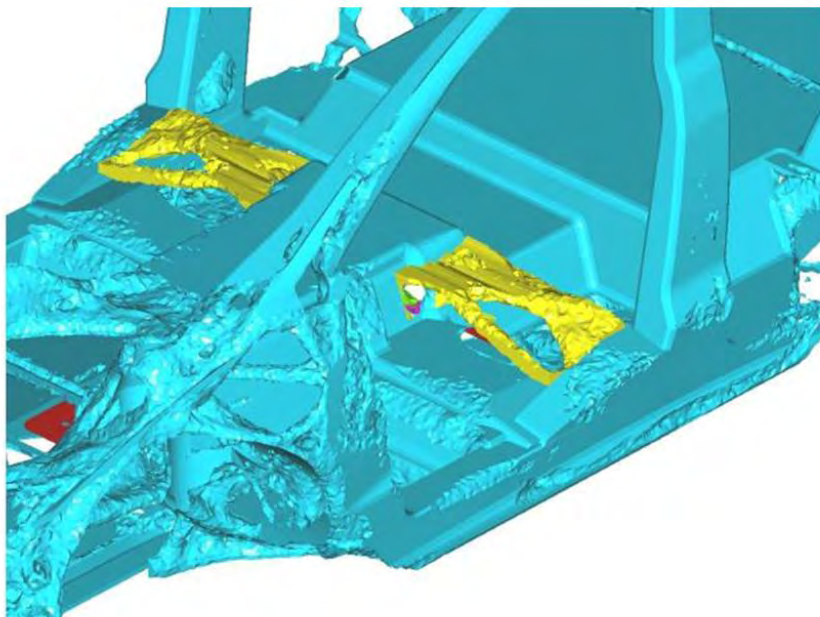


Figure 7.31: FSV-1 20% mass fraction - floor pan and tunnel

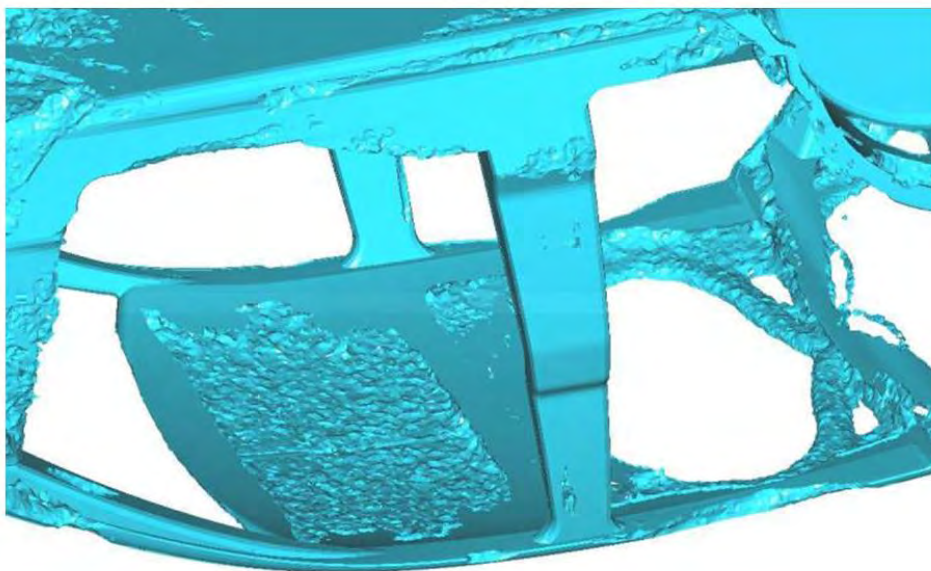


Figure 7.32: FSV-1 20% mass fraction - roof panel

7.8 Topology Results

7.8.3.5 10% Mass Factor Optimization Results

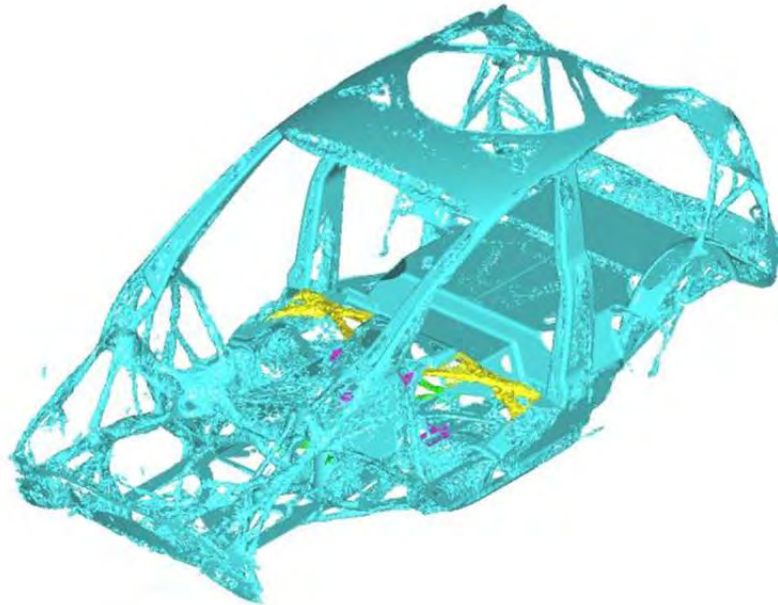


Figure 7.33: FSV-1 10% mass fraction - front isometric view

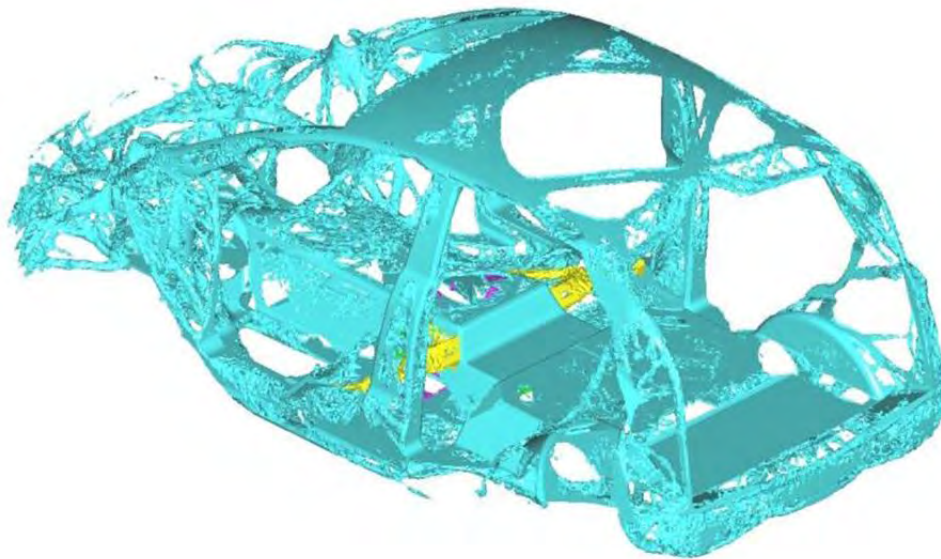


Figure 7.34: FSV-1 10% mass fraction - rear isometric view

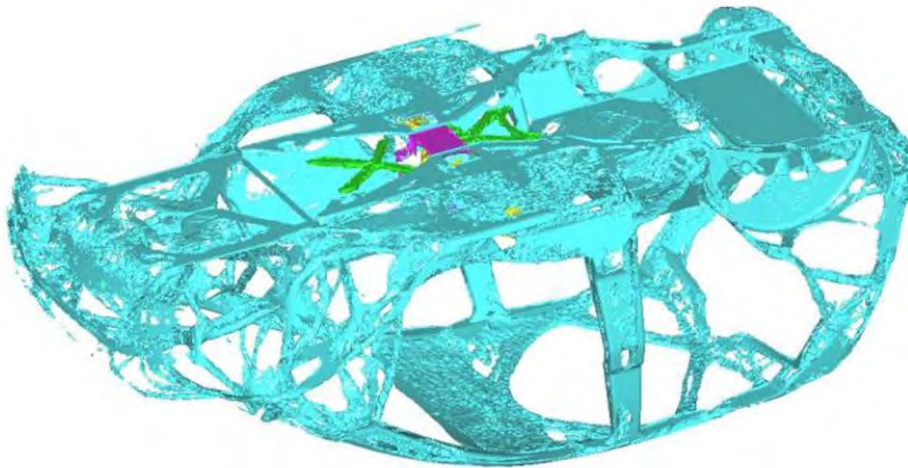


Figure 7.35: FSV-1 10% mass fraction - bottom view

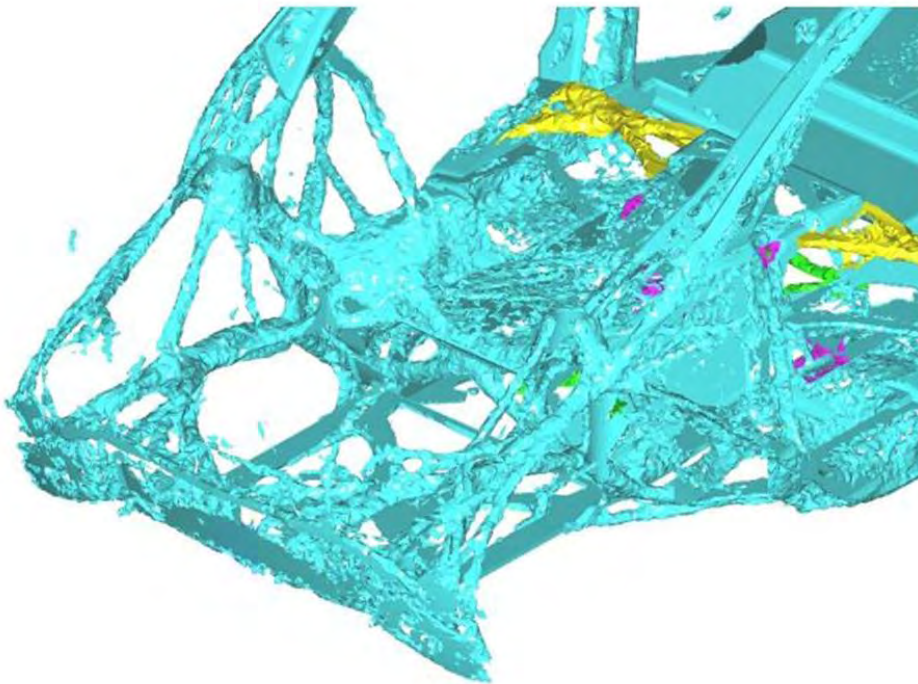


Figure 7.36: FSV-1 10% mass fraction - front end

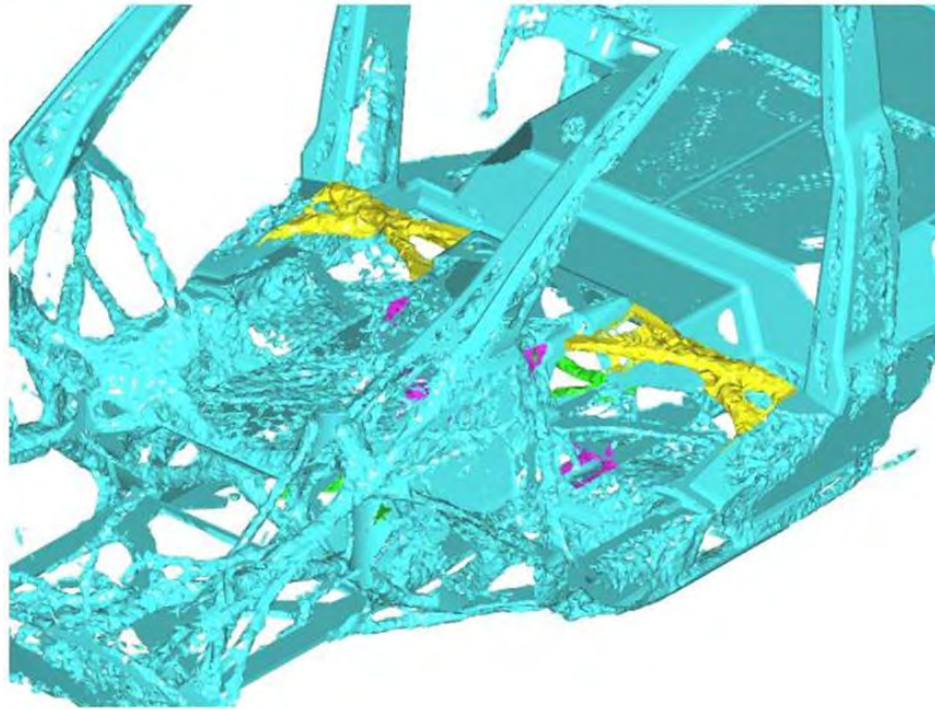


Figure 7.37: FSV-1 10% mass fraction - floor pan and tunnel

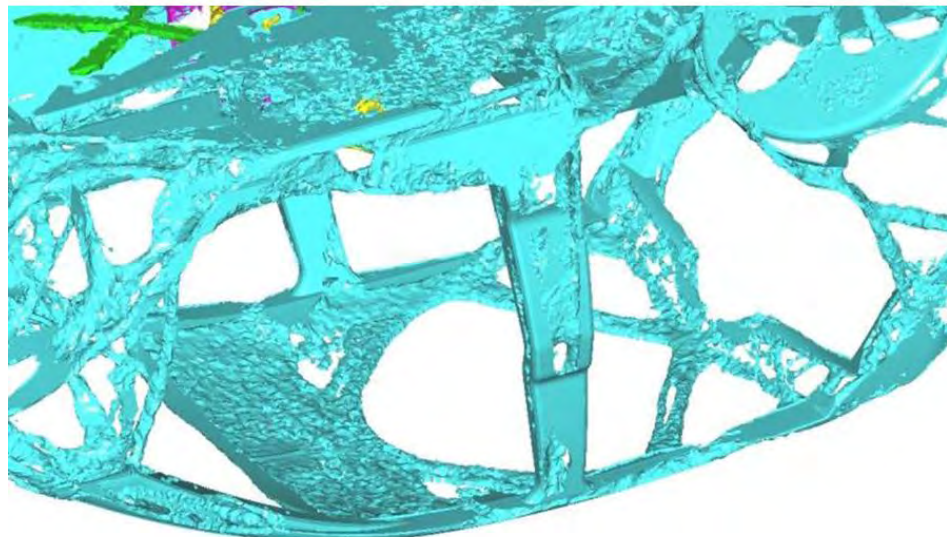


Figure 7.38: FSV-1 10% mass fraction - roof panel

7.9 Conclusion

With reference to all results, the geometry developed by the topology optimization was manually interpreted into a CAD (Computer Aided Design) model using engineering judgment. This model represents the initial skeleton geometry of the FSV shown in Figure 7.39 and will form the basis of the next step in the optimization process. It should be realized that because the development of the CAD model was based on engineering judgment, there are many possible interpretations. In this case the aim was to allow as many load paths as possible, with minimal constraints from manufacturing concerns, recognizing that simplification and manufacturing constraints will be addressed in later stages of the design process.

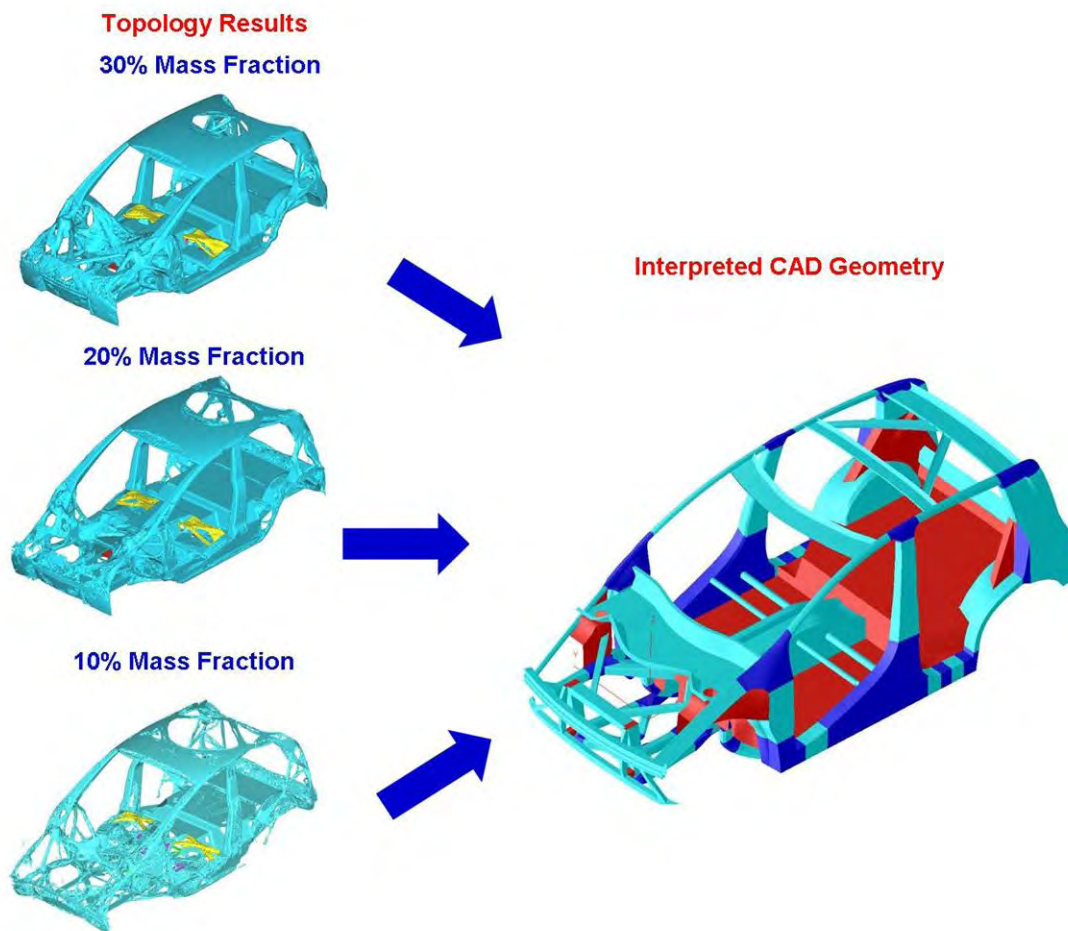
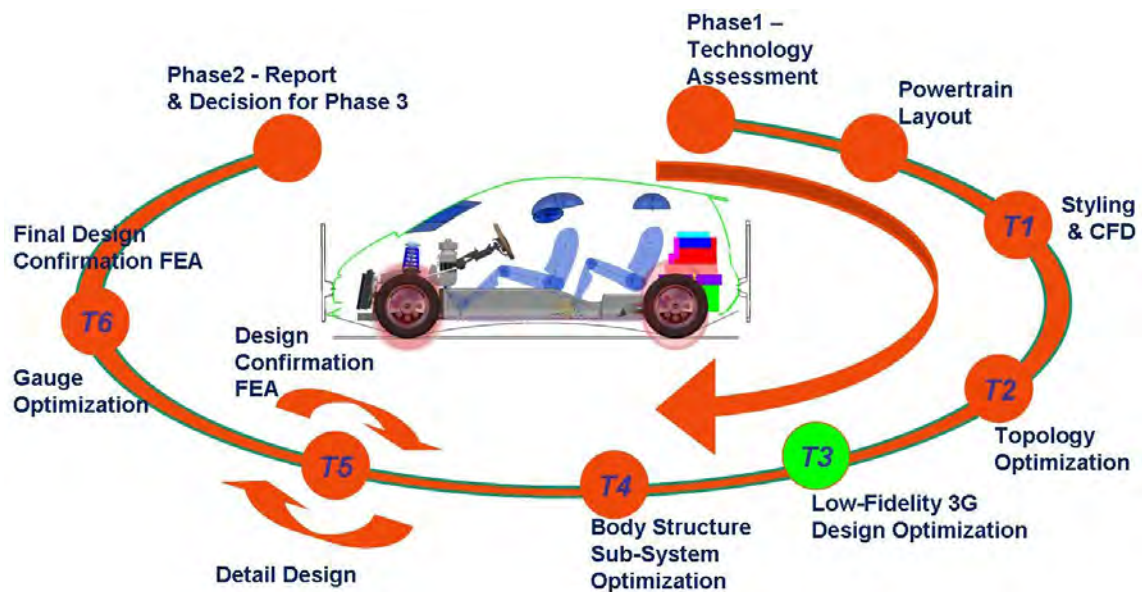


Figure 7.39: Interpreted CAD model developed from topology optimization results

8.0 T3 - Low Fidelity 3G (Geometry, Grade & Gauge) Optimization



8.1 Introduction

This chapter discusses the LF3G (Low Fidelity Geometry, Grade & Gauge) optimization of the FutureSteelVehicle (FSV). The first half of this report documents the development of the first non-linear dynamic analysis of the FSV and the calibration of its performance. The geometry of the LF3G model was based on the skeleton structure developed from the initial topology optimization. The report then discusses the definition of the Low Fidelity 3G (LF3G) optimization, the optimization targets and the results. Both the calibration and optimization consider the following load cases:

1. NCAP frontal impact
2. IIHS front crash 40% ODB (Offset Deformable Barrier)
3. FMVSS 301 rear 70% ODB
4. IIHS side impact

5. FMVSS 214 pole impact
6. FMVSS 216 roof crush (using the IIHS 4* strength to weight ratio)
7. Bending and torsional static stiffness

LF3G optimization was completed by ETA.

8.2 Objective

The objective of this study was a LF3G optimization of the parameterized FSV model. The initial topology optimization was based on a linear static analysis. In this case the LF3G optimization is based on the non-linear dynamic model developed in the first phase of the task and thus addresses the limitations of the topology optimization. The first goal of the LF3G optimization was to define the optimal position of the structure's major loadpaths. Once located, the optimization then sought to define the approximate size and general cross-section, grade and gauge of the structure along the loadpath. The final goal of the LF3G optimization was to create a robust set of boundary conditions for the next phase of the project, the sub-system loadpath optimization.

8.3 LF3G: An integrated Optimization Process

A parameterized CAD model is first constructed using SFE ^[1] software based on various design inputs and a comprehension of the styling and packaging constraints. The parameterization includes the size, shape, and/or position of various parts of the dominant load paths, such as the B-pillar and rocker. The SFE software is capable of outputting finite element models for any combination of parameterized parameters.

An overview of the LF3G optimization process is shown in Figure 8.1. Once the parameterized model is created, the multi-disciplinary software, HEEDS ^[2], is used to conduct the optimization. HEEDS directs the SFE software to output a model with parameters of its choice. HEEDS then directs the dynamic solver LS/DYNA ^[3] to analyze the finite element model for the load cases being considered. Once the analyses are complete, HEEDS analyzes the finite element output and compares it to optimization targets. Using this information, the HEEDS software directs SFE to output an updated finite element model with another set of parameters, and the cycle begins again.

As the optimization software gains more information about the design space, it uses various algorithms to develop better and better designs that meet the performance targets while maximizing

¹SFE applies numerical methods in order to solve complex problems in the field of engineering physics. For more information visit <http://www.sfe-berlin.de/>

²HEEDS interfaces with CAE applications to automate the design optimization process. For more information visit <http://www.redcedartech.com/>

³LS/Dyna is an advanced general-purpose multiphysics simulation software package. For more information visit <http://www.lstc.com/lstdyna.htm>

8.4 LF3G Optimization Model

design objectives.

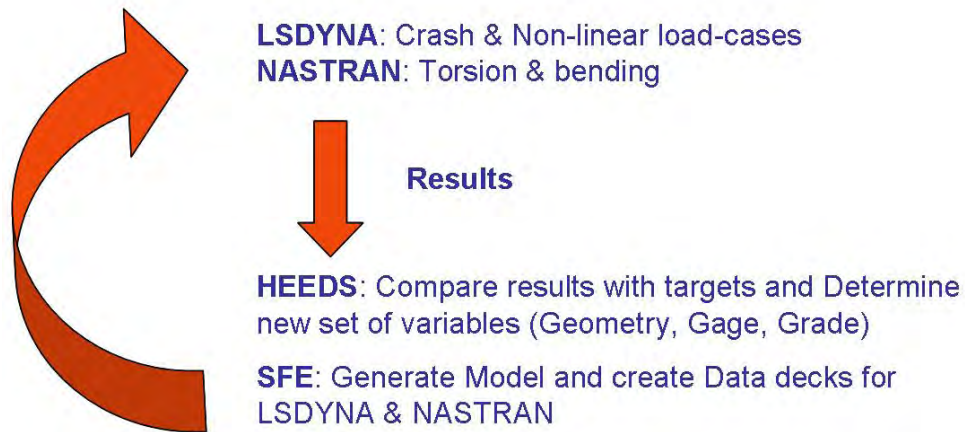


Figure 8.1: LF3G optimization process overview

8.4 LF3G Optimization Model

The parameterized model is shown Figure 8.2. The LF3G model is made up of surfaces from which the finite element model is generated.

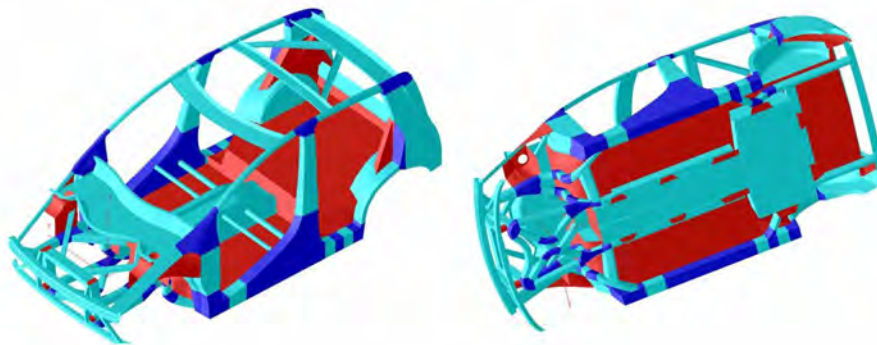


Figure 8.2: Parameterized model

8.5 LF3G Parameterization

Various parts of the FSV vehicle were parameterized, which allowed their position and shape to be modified by the optimization. It should be noted that all ranges of movement in the parameterization conformed to the allowable structural packaging space.

8.5.1 B-Pillar

The design parameters for the B-pillar are shown in Figure 8.3. The upper B-pillar is allowed to move side to side, and all section widths can vary up to 50 mm.

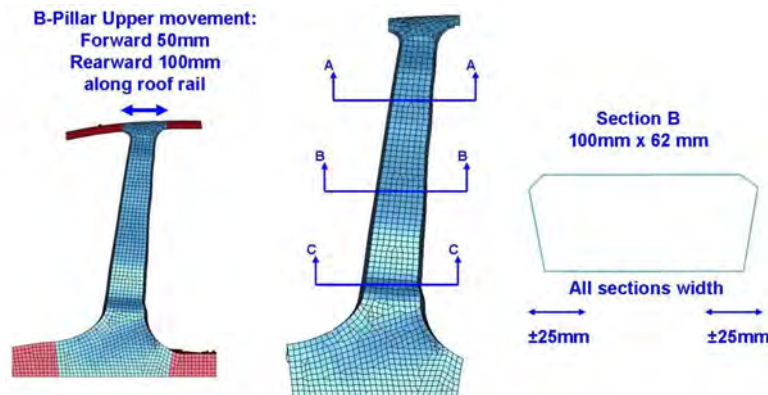


Figure 8.3: B-Pillar parameterization

8.5.2 Front Bumper Beam

The design parameters for the front bumper beam and rails are shown in Figure 8.4 & Figure 8.5. The bumper beam and associated parts was allowed to move 50 mm fore and 100 mm aft. The front rail section was also allowed to grow 50 mm horizontally and vertically. The bumper location was established to allow 550mm of crush space before any stackup. However, the optimization was given the facility to vary the bumper location as needed thus allowing the design to meet the performance requirements while enabling the lightest weight solution.

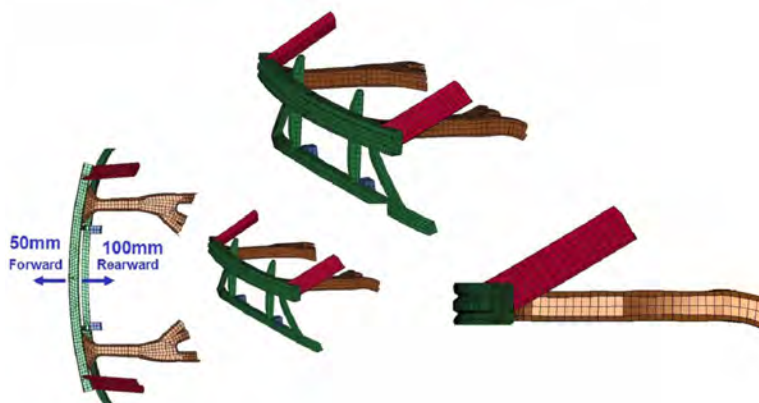


Figure 8.4: Front bumper beam position parameterization

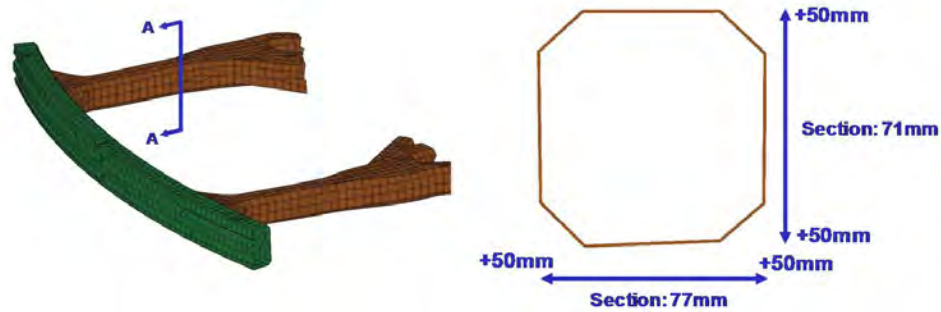


Figure 8.5: Front bumper beam section parameterization

8.5.3 Radiator Support to Shock Tower Beam

The design parameters for the beam connecting the radiator support to the shock tower are shown in Figure 8.6 and Figure 8.7. The beam is allowed to move 100 mm laterally, while the end connected to the radiator support may move 90 mm vertically. The section is allowed to vary by 50 mm vertically and 25 mm horizontally.

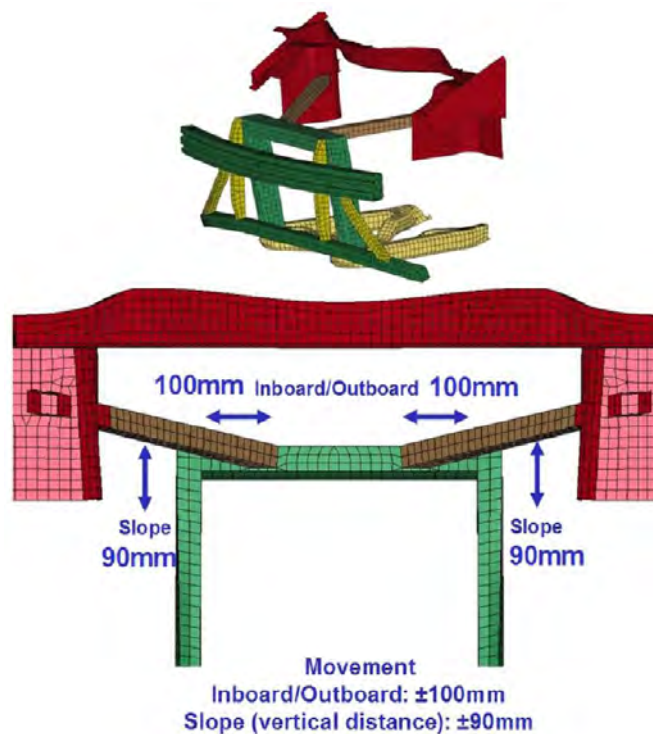


Figure 8.6: Radiator support to shock tower position parameterization

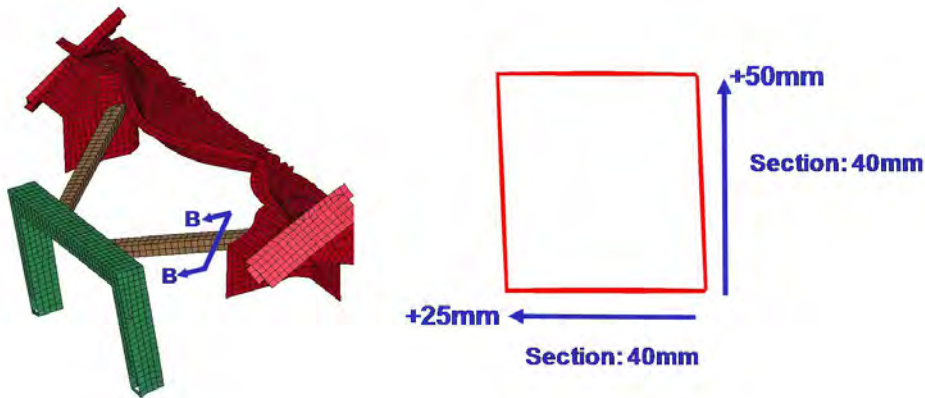


Figure 8.7: Radiator support to shock tower section parameterization

8.5.4 Shotgun

The design parameters for the shotgun are shown in Figure 8.8. The section is allowed to vary as shown. The angle and position also change with the position of the front bumper beam as detailed in section 8.5.2

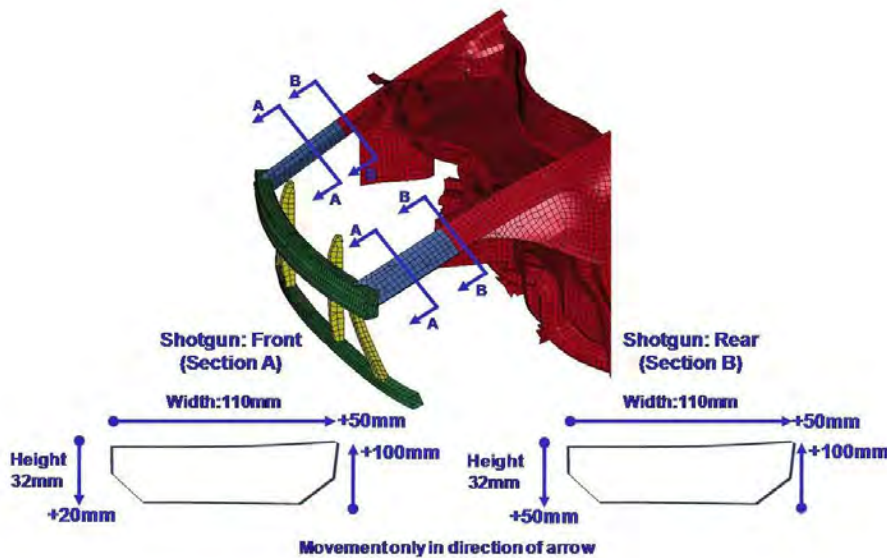


Figure 8.8: Shotgun parameterization

8.5.5 Instrument Panel Beam

The design parameters for the IP beam are shown in Figure 8.9. The beam is allowed to move 180 mm vertically and 160 mm horizontally. The section is also allowed to vary by 50 mm in each direction.

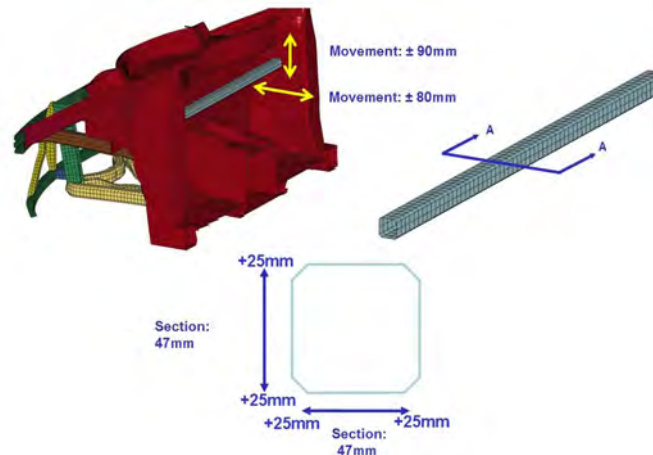


Figure 8.9: Instrument panel beam parameterization

8.5.6 Front Longitudinal above Tunnel

The design parameters shown in Figure 8.10 are for the portion of the front rail that extends into the passenger compartment along the top of the transmission tunnel. The rail is allowed to change height by 50 mm.

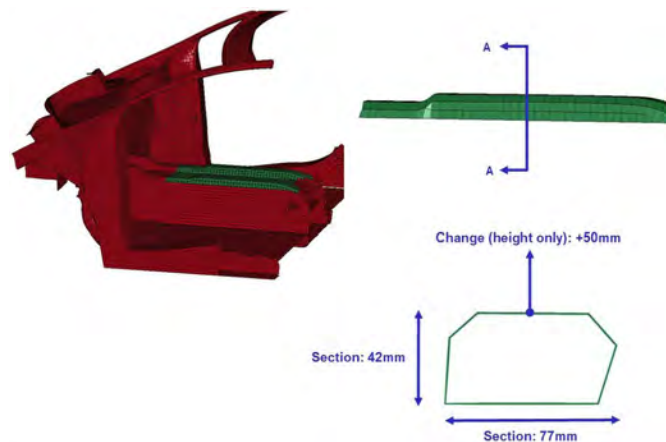


Figure 8.10: Front longitudinal rail above tunnel parameterization

8.5.7 Front Cross-Bar

The front longitudinal rail splits into three sections in front of the dash. One section connects with the rocker and the other extends along the bottom of the tunnel. The third section continues into the passenger compartment on the top of the tunnel. The brace between the rocker and bottom of the tunnel is parameterized as shown in Figure 8.11. The section width varies by 50 mm, and it is allowed to move 200 mm in the fore/aft direction.

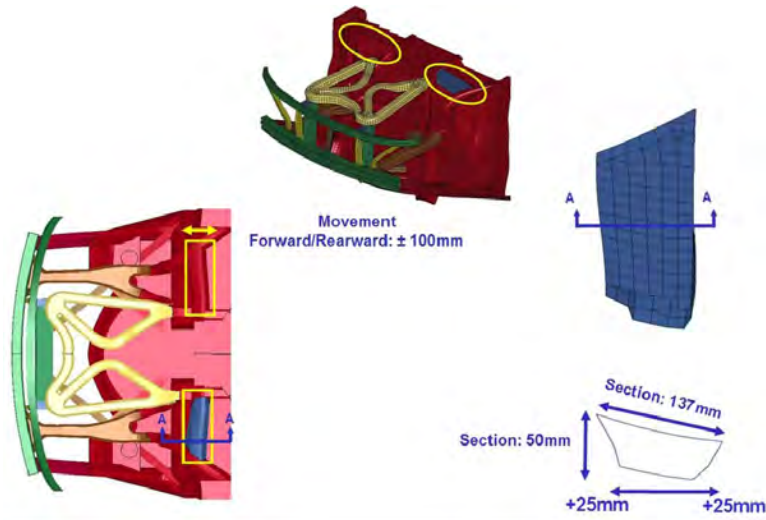


Figure 8.11: Front longitudinal cross bar parameterization

8.5.8 Side Roof Rail

The design parameters for the roof rail are shown in Figure 8.12. The section is allowed to vary by 50 mm on the inboard side only.

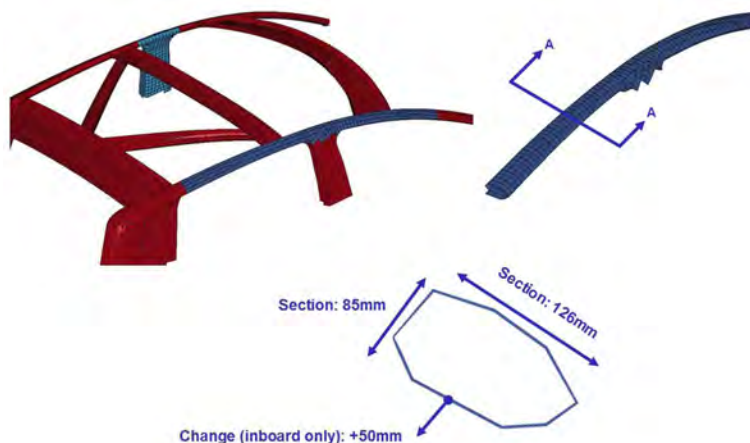


Figure 8.12: Roof rail parameterization

8.5.9 Roof Bow and Headers

The design parameters for the roof bow and roof headers are shown in Figure 8.13 & Figure 8.14. The figures show that the roof bow and headers have a wide range of movement and possible section shapes.

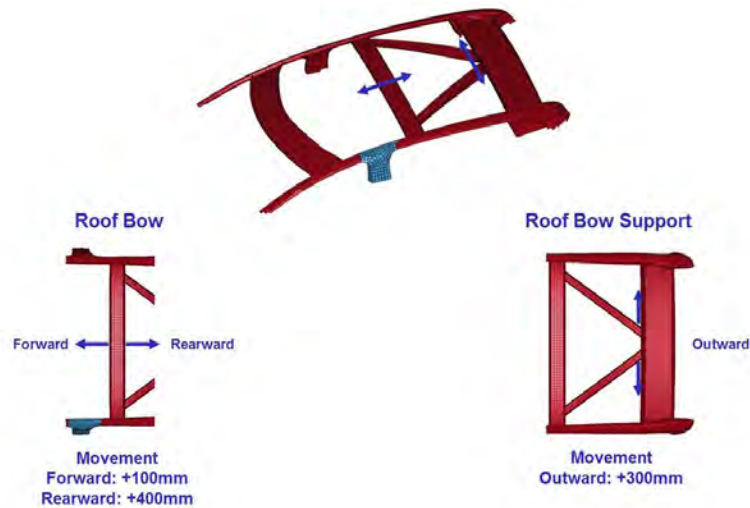


Figure 8.13: *Roof bow parameterization*

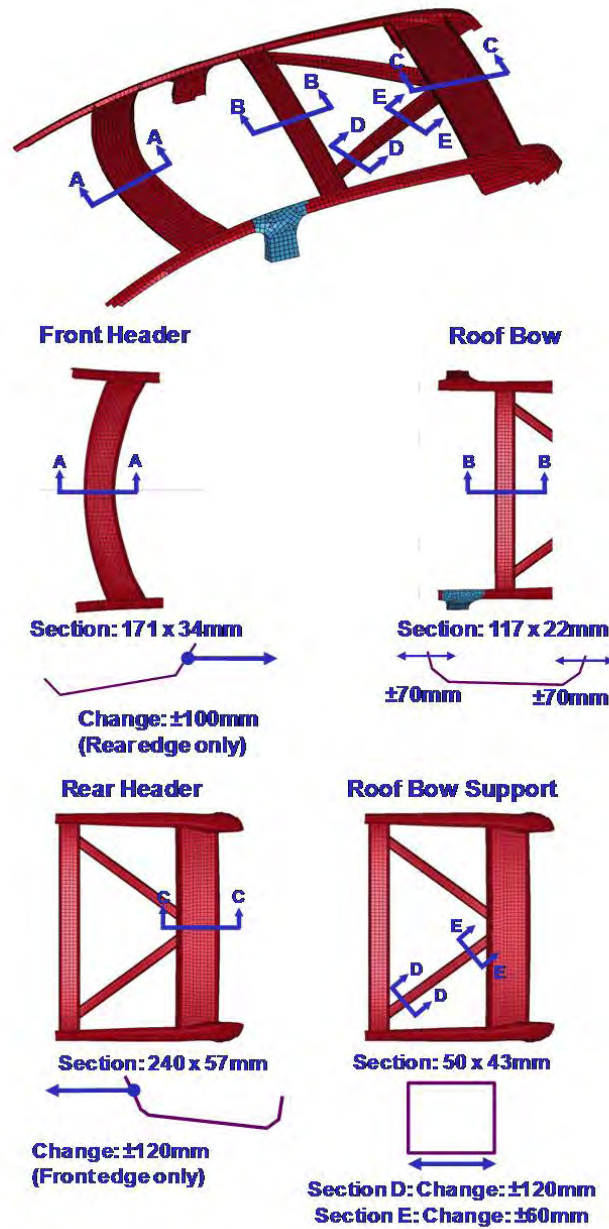


Figure 8.14: Roof bow parameterization

8.5.10 Rear Cargo Area Cross Bar

The design parameters for the rear cargo area cross bar are shown in Figure 8.15. The section position is allowed to vary by 100 mm in the horizontal and vertical directions. Due to packaging restrictions, the section size was not parameterized. Instead the maximum allowable section size was used.

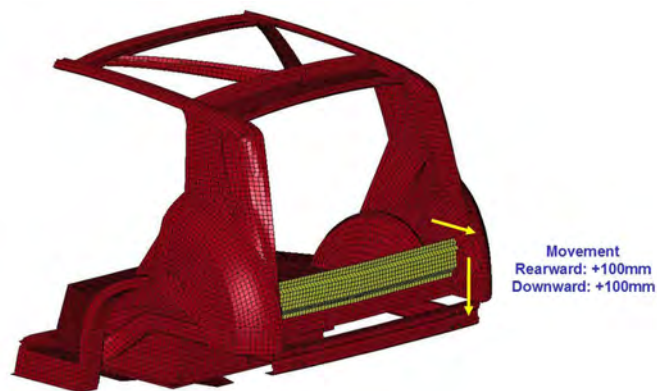


Figure 8.15: Rear cargo area cross bow parameterization

8.5.11 Front Seat Crossmember

The design parameters for the front seat cross member are shown in Figure 8.16. The section is allowed increase by 20 mm in the fore-aft direction.

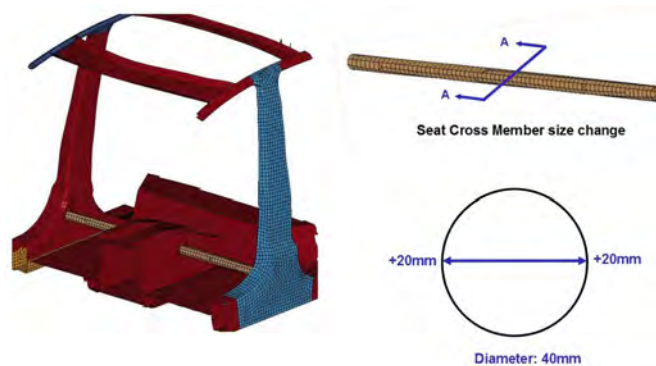


Figure 8.16: Front seat crossmember parameterization

8.5.12 Rocker

The design parameters for the rocker are shown in Figure 8.17. The section is allowed increase by 50 mm in the in-board direction.

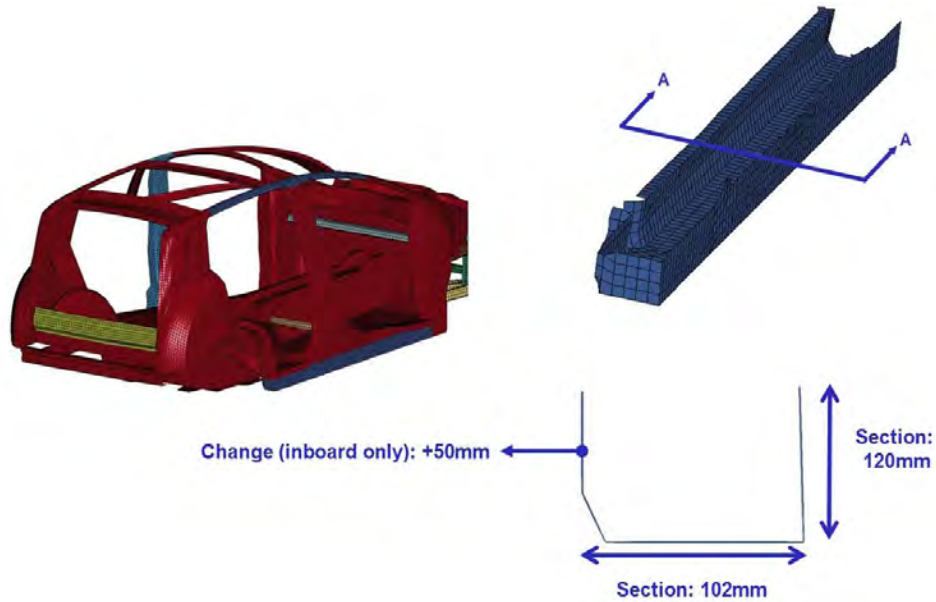


Figure 8.17: *Rocker parameterization*

8.5.13 C-Pillar

The design parameters for the C-pillar are shown in Figure 8.18. The section is allowed increase by 50 mm in the in-board direction.

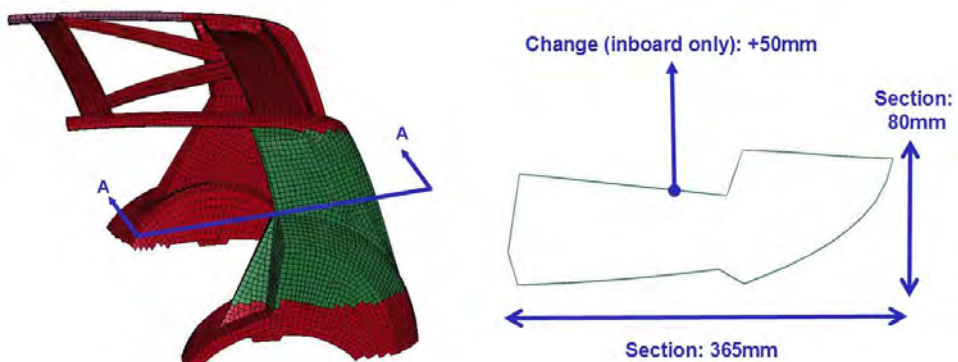


Figure 8.18: *C-Pillar parameterization*

8.5.14 Rear Longitudinal Rail

The design parameters for the rear longitudinal rail are shown in Figure 8.19. The rail is allowed move 140 mm laterally, and the curvature at the kickdown is allowed to vary. Also, the depth and width of the section are allowed to vary by 50 mm.

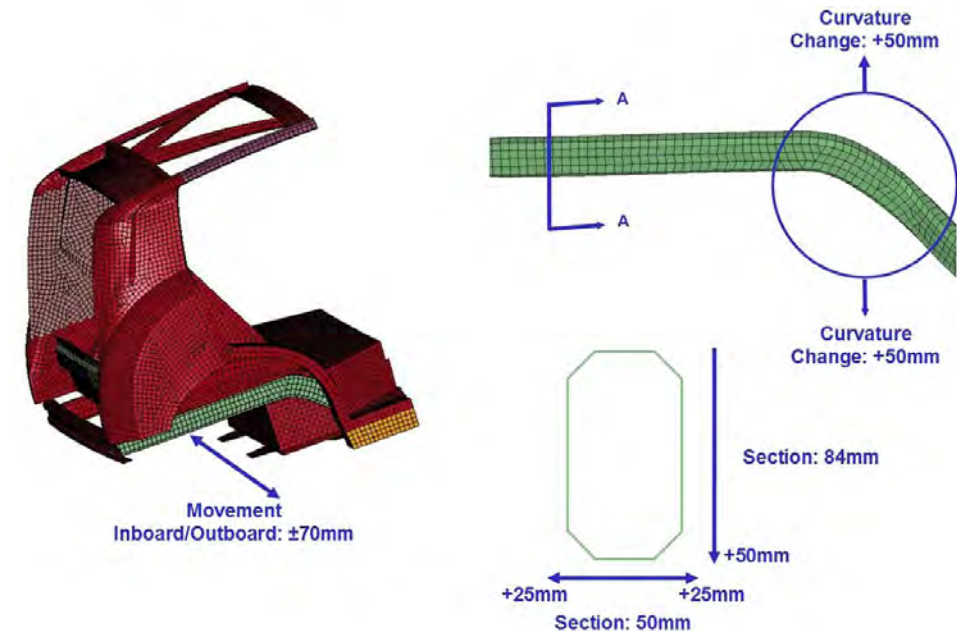


Figure 8.19: Rear longitudinal rail parameterization

8.5.15 Bulkheads

At this stage of the design process, the section joints have not been fully developed. Thus bulkheads and reinforcements were used to represent the expected stiffnesses of the mature joint designs. See Figure 8.21 & Figure 8.20. This allowed the major loadpath sections to be optimized in anticipation properly designed joints.

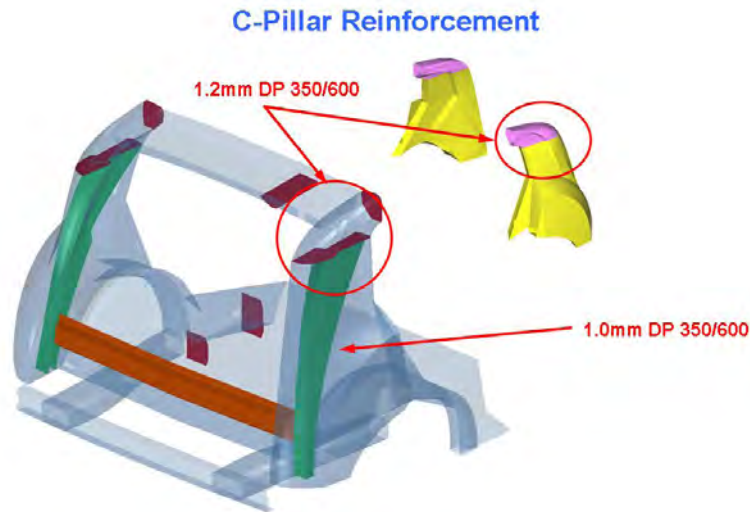


Figure 8.20: Additional C-Pillar reinforcement

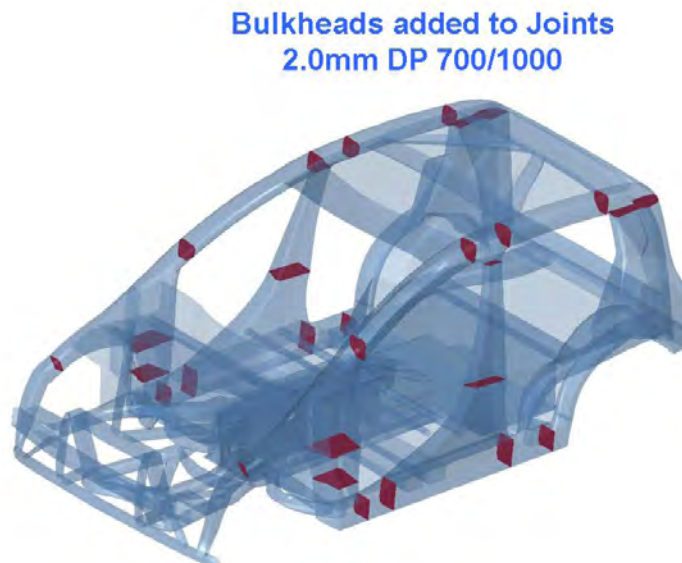


Figure 8.21: Added bulkheads

8.6 Material and Gauge Choices

8.6 Material and Gauge Choices

The materials and gauges for each part in the model were chosen based on the results of the load path study, as well as the initial evaluation of the parameterized model.

The available materials for use in this study are shown in Table 8.1. The minimum and maximum gauges are the range of commercially available thicknesses for each steel grade. At this stage of the study, specific grades are not identified. The grades represent the intended strength levels only. For vehicle performance two or more grades with the same tensile strength are equivalent (at least for this level of design). The differences between the grades are more important for manufacturing capability.

MATERIAL	GAUGE	
	MIN (mm)	MAX (mm)
Mat 270	0.50	4.60
Mat 340	0.50	3.40
Mat 450	0.50	2.30
Mat 500	0.50	5.00
Mat 600	0.60	2.30
Mat 800	0.60	2.30
Mat 1000	0.60	2.30
Mat 1300	0.60	2.00
Mat 1500	0.42	2.92

Table 8.1: *Materials used in optimization*

Based on the Load Path Study, six critical components were identified that should be given the widest range of optimization variables possible. These components are listed in Table 8.2

COMPONENT	POSITION	MATERIAL	GAUGE RANGE
Front Rail	Outboard	Mat 340 or Mat 500	1.5 to 2.5mm
	Mid	Mat 450 or Mat 500	
	Inboard	Mat 450 or Mat 600	
Rear Rail	Outboard	Mat 450 or Mat 600	1.5 to 3.0mm
	Inboard	Mat 1000	
Side Roof Rail	N/A	Mat 600 or Mat 1000	0.8 to 1.2mm
B-Pillar	N/A	Mat 1000 or Mat 1300	0.8 to 1.2mm
Rocker	N/A	Mat 1000 or Mat 1300	0.8 to 1.6mm
Battery	N/A	Mat 1300	2.0 to 3.0mm

Table 8.2: *Components with gauge and grade variation in optimization*

The front and rear rails were modeled with multiple zones for material and gauge variation, as shown in Figure 8.22. The roof rail, B-pillar, rocker, and battery were allowed only one mate-

rial/thickness combination each, as shown in Figure 8.23

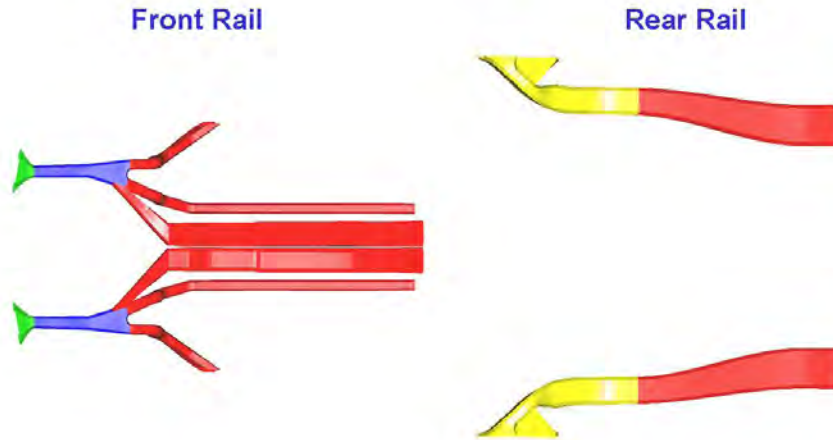


Figure 8.22: Components with gauge and grade variation in optimization

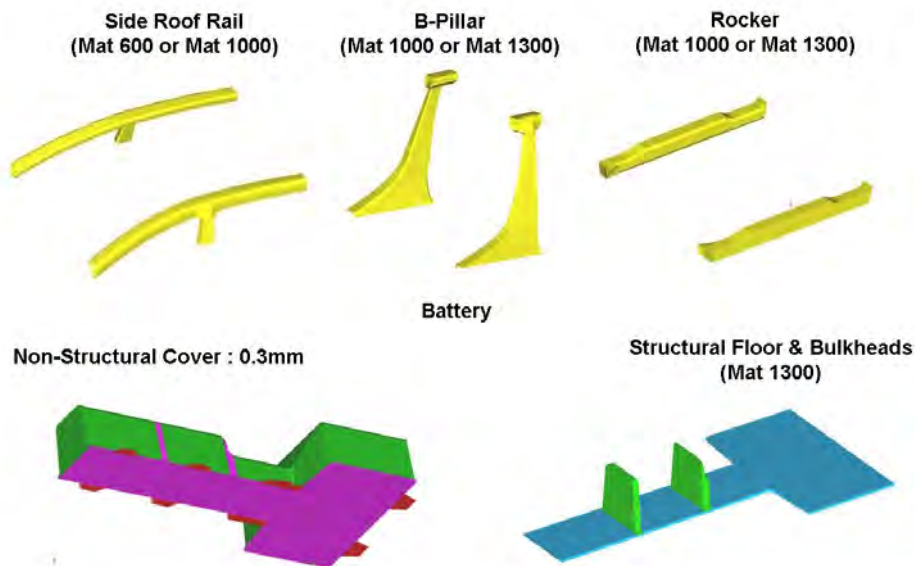


Figure 8.23: Components without zones of independent gauge and grade variation

The remaining parts were assigned materials based on the results of the calibration study and the initial evaluation of the parameterized model. The components and their corresponding materials are shown in Figure 8.24 & Figure 8.25

8.6 Material and Gauge Choices

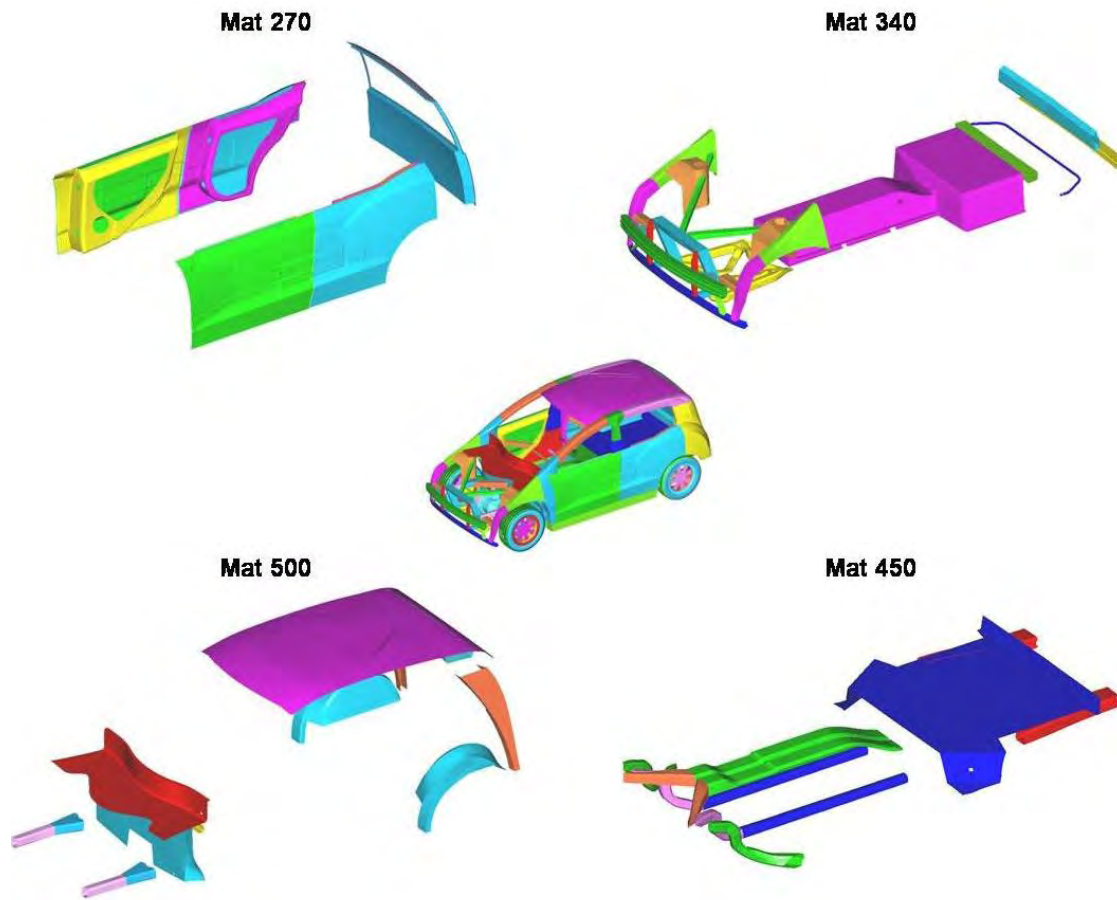


Figure 8.24: Material selection for optimization

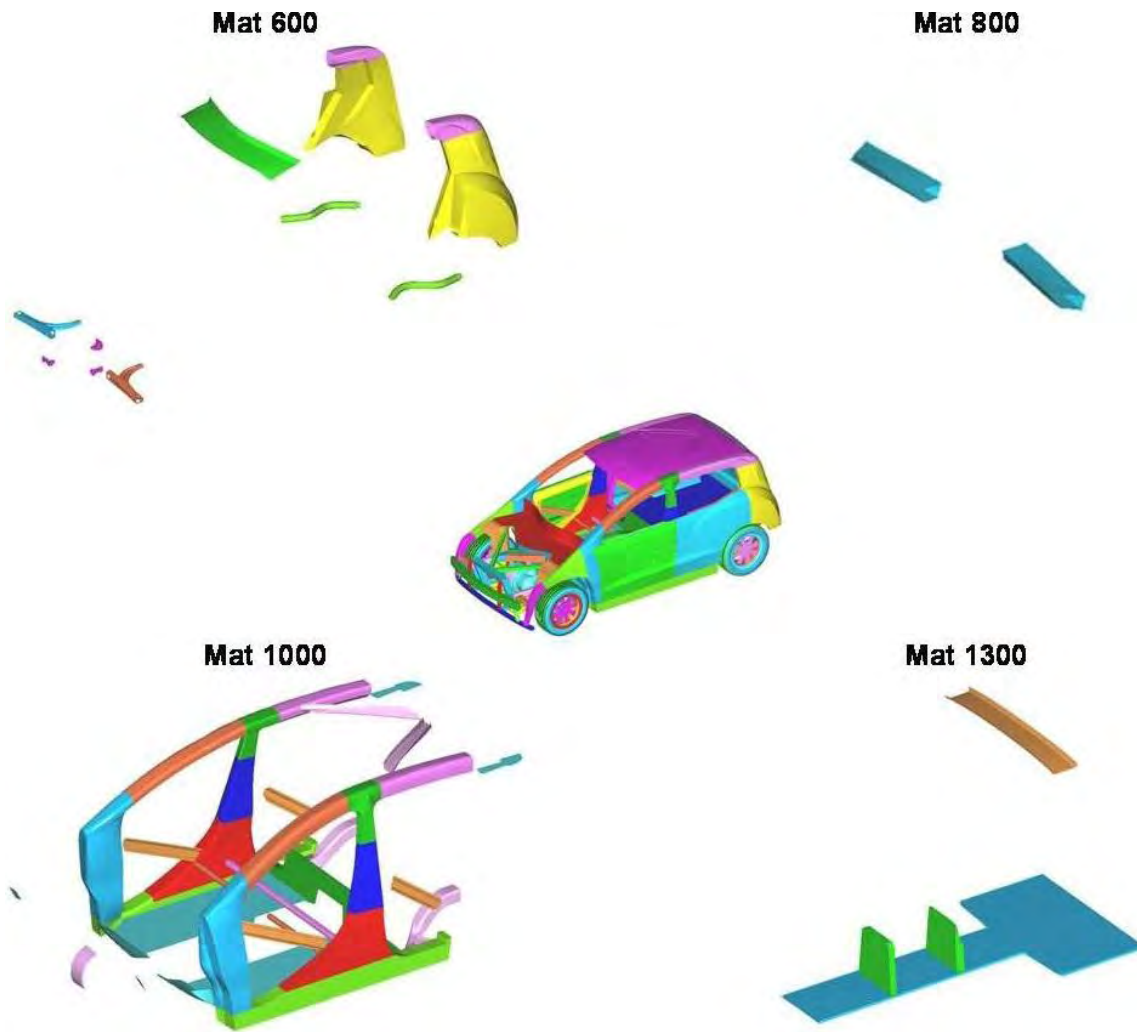


Figure 8.25: Material selection for optimization

8.7 LF3G Targets

8.7 LF3G Targets

The optimization software submitted and analyzed 6 load cases for each set of variables. The results of the 6 load cases were compared to the targets, shown in Table 8.3, to determine the feasibility of each design. Note that these are optimization performance targets which are slightly relaxed from the baseline performance targets in order to identify as many feasible designs are possible. Also note that two load cases of Static Bending and Pole Impact are not included. Due to past experience, pole impact and static bending do not contribute as much as the load cases in Table 8.3. Their performance can be easily achieved by adding local reinforcements without the need of adding much mass. On the other hand once all the following six load cases have been met, 80%-90% of the static bending and pole impact requirements will be satisfied. This will further benefit the optimization running time.

LOADCASE	TARGET
NCAP Frontal Impact	45g Peak Acceleration
IIHS Front Crash 40% ODB	GOOD Rating
FMVSS 301 Rear 70% ODB	40g Peak B-Pillar Acceleration Good Rear Door Openability
IIHS Side Impact	GOOD Rating
FMVSS 216 Roof Crush (with IIHS 4*strength to weight ratio)	55 kN (4.0 × Curb Weight)
Torsional Static Stiffness	18,082 Nm/deg

Table 8.3: Optimization targets

8.8 LF3G Optimization Results

Once the model was parameterized, variable range and performance targets established, the optimization process was initiated.

The optimization analyzed 110 designs, of which 17 were “feasible”, or satisfied the performance targets. The mass of each design is plotted in Figure 8.26. The red line shows the progress of the optimization. Each time a lower mass feasible design is found, the line shows a step down.

Each of the 110 designs considered by the optimization algorithms represents a different combination of loadpaths, loadpath cross sections, grade and gauge. With each successive iteration, the optimization algorithm expands its base of solution to those that meet the performance objectives, to those that do not meet, and the combination of variables. The result is the least mass solution. In simplest terms, it learns about the response of the system to the range of variable inputs. The best design found by the optimization was the 60th case, or “design 60”, which had the lowest mass of the feasible designs. It is very possible that other feasible designs have better

performance (higher/lower than target) than design 60, but certainly higher mass.

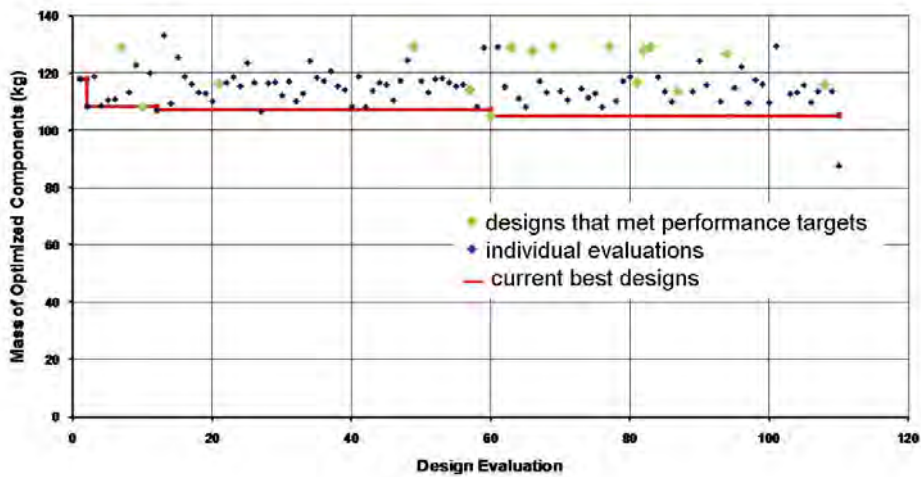


Figure 8.26: Mass of 110 optimization cases

A full description of the optimization process is discussed in Section 13 of the FSV Phase 1 report. Further information is also available from the Red Cedar Technologies website, producers of the HEEDS software.

Figure 8.27 shows a graph, which is produced by the optimization software, of the feasible designs. Each line represents a different design, and maps the response against each of the load cases. Design 60, the lightest design solution, is highlighted.

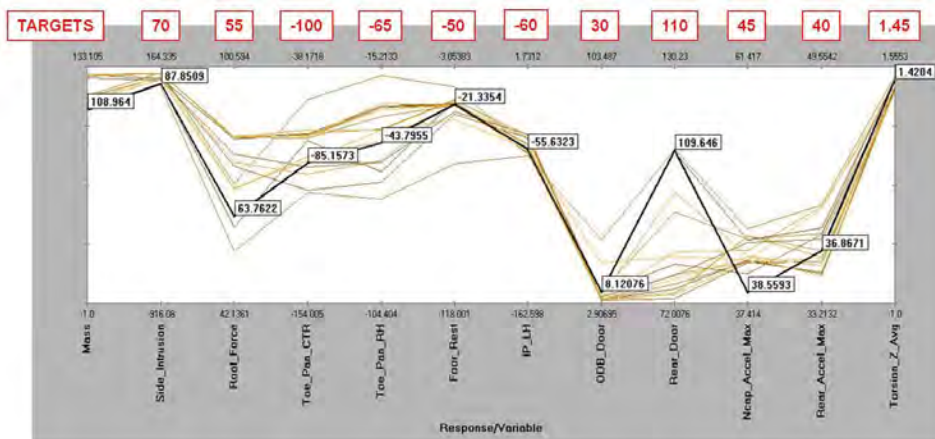


Figure 8.27: Feasible designs found by optimization

8.8 LF3G Optimization Results

8.8.1 NCAP Frontal Impact

Figure 8.28 shows the deformed shape of design 60 at the end of the NCAP 56 $\frac{\text{km}}{\text{h}}$ simulation, while Figure 8.29 shows the resulting pulse.

The results show little deformation of the passenger compartment, and the maximum pulse of 37.9 g is below the target of 45 g.



Figure 8.28: NCAP deformed shape : design 60

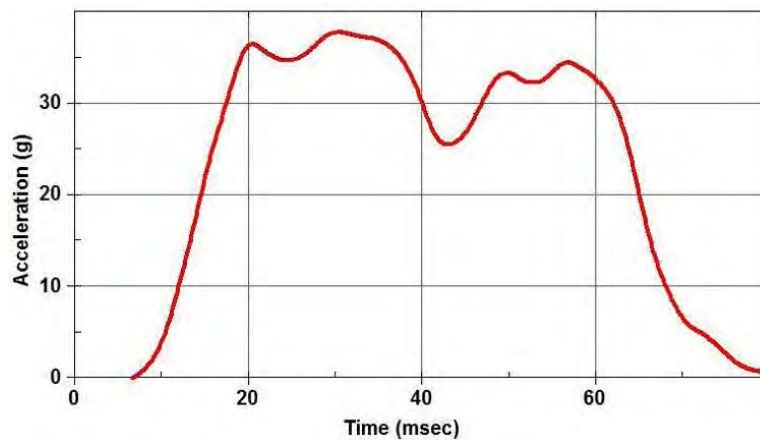


Figure 8.29: NCAP pulse : design 60

8.8.2 IIHS Front Crash 40% ODB

Figure 8.30 shows the deformed shape of design 60 at the end of the $56 \frac{\text{km}}{\text{h}}$ offset deformable barrier simulation.

The deformation looks acceptable, with no bending in the A-pillar or rocker. The passenger compartment shows little damage. Figure 8.31 shows the intrusion performance.

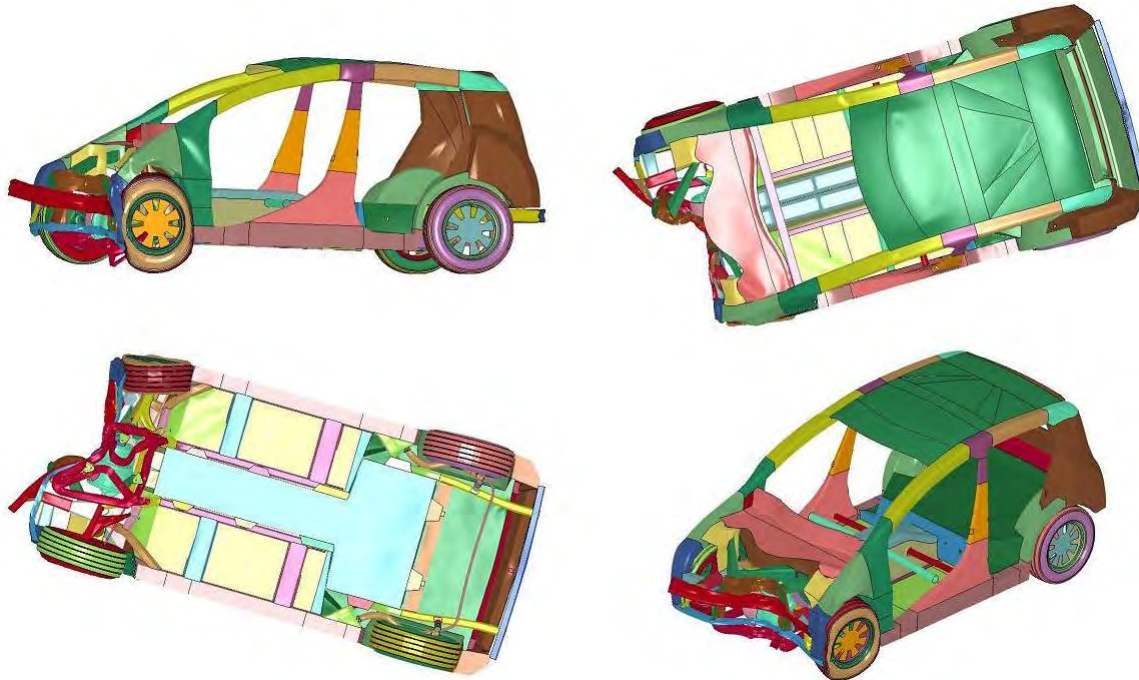


Figure 8.30: IIHS 40% ODB deformed shape : design 60

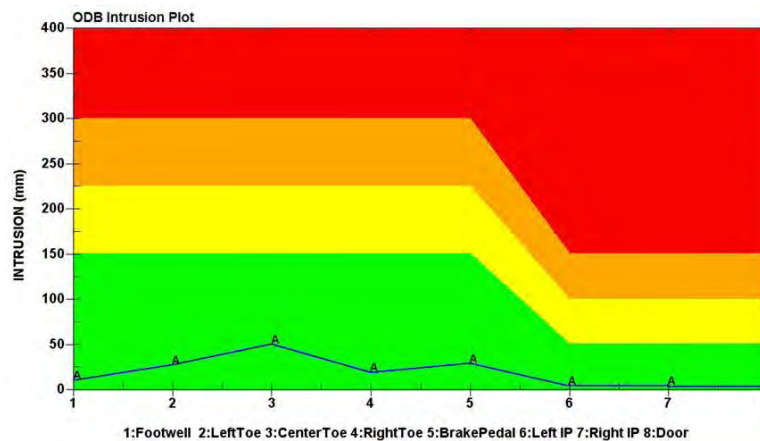


Figure 8.31: IIHS 40% ODB intrusion performance

8.8.3 FMVSS 301 Rear 70% ODB

Figure 8.32 shows the deformed shape of design 60 at the end of the $80 \frac{\text{km}}{\text{h}}$ rear barrier impact simulation.

The figure shows that the deformation of the passenger area is small, which signifies good occupant protection and rear door openability. The peak B-Pillar acceleration of 34.8g is well within the 40g target as shown in Figure 8.33. The battery is also protected with negligible deformation.



Figure 8.32: Rear offset deformable barrier deformed shape : design 60

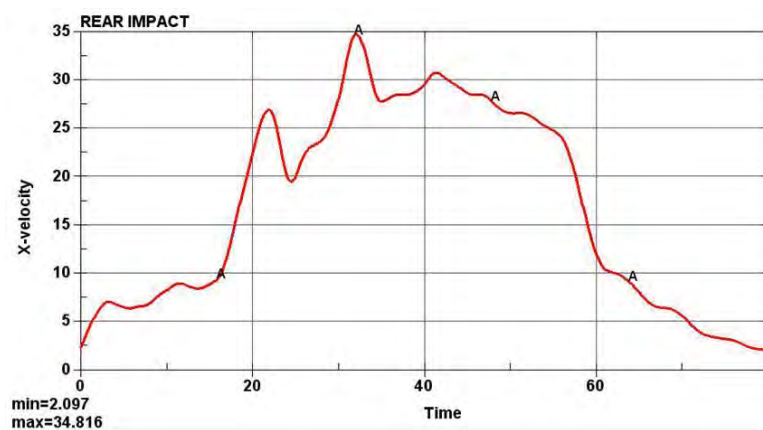


Figure 8.33: Rear offset deformable barrier acceleration pulse

8.8.4 IIHS Side Impact

Figure 8.34 shows the deformed shape of design 60 at the end of the $50 \frac{\text{km}}{\text{h}}$ side barrier impact simulation.

The structure shows little deformation of the floor or roof, with much of the side impact load transferred through the tunnel by the front seat cross-member. The B-pillar intrusion is low enough to meet the target of a “Good” IIHS side impact rating.



Figure 8.34: IIHS side impact deformed shape : design 60

8.8.5 FMVSS 216 Roof Crush with IHS 4*strength to weight ratio

Figure 8.35 shows the deformed shape of design 60 at the end of the roof crush simulation. Figure 8.36 shows the force-deflection curve.

The A-pillar shows no kinking, with the major deformation in the B-pillar, which is a typical result for roof crush. The maximum force is 58.2 kN, which is above the target of 55 kN.



Figure 8.35: Roof crush deformed shape : design 60



Figure 8.36: Roof crush force-deformation curve : design 60

8.8.6 Static Torsion

The static torsion setup and result is shown in Figure 8.37. The value of $18,459 \frac{\text{Nm}}{\text{Deg}}$ is above the target of $18,082 \frac{\text{Nm}}{\text{Deg}}$

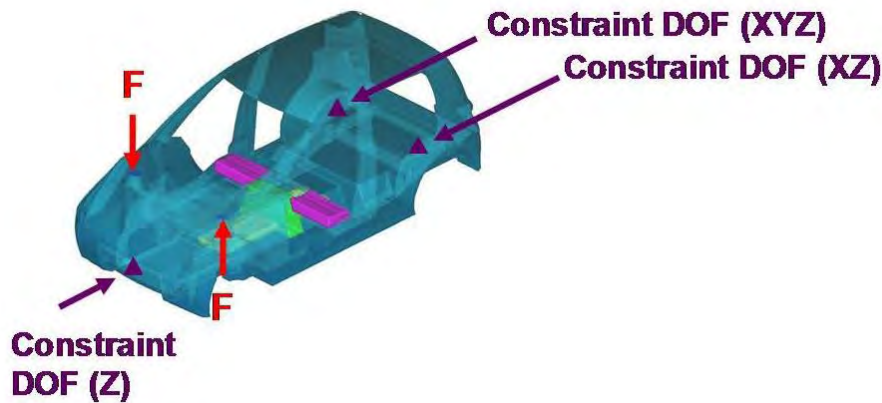


Figure 8.37: Torsional stiffness: design 60

8.8.7 Performance Results Summary

The results of the lowest mass configuration, design 60, are compared to the targets in Table 8.4.

LOADCASE	TARGET	PERFORMANCE
NCAP Frontal Impact	45g Peak Acceleration	38.6g Peak Acceleration
IIHS Front Crash 40% ODB	GOOD Rating	GOOD Rating
FMVSS 301 Rear 70% ODB	40g Peak B-Pillar Good Rear Door Openability	36.9g Peak B-Pillar Acceleration
IIHS Side Impact	GOOD Rating	GOOD Rating
FMVSS 216 Roof Crush (with IIHS 4*strength to weight ratio)	55 kN (4.0x Curb Weight)	58.2 kN
Torsional Static Stiffness	18,082 Nm/deg	18,459 Nm/deg

Table 8.4: Optimization results summary: design 60

Optimization defined an optimal location for the major loadpaths and their approximate shape to meet design targets. It also approximated the gauge and grade of the major loadpaths, which will be refined in later stages of the design process.

Using a holistic approach, a robust, non-intuitive baseline geometry for the vehicle has now been created.

The optimization result of this phase will provide boundary conditions for the subsystem manu-

facturing process selection of the major loadpath components in the next phase.

8.9 LF3G Battery Optimization

All previous optimization was based on use of a T-Shaped battery. Various battery configurations were considered during the Phase-1 (details can be found in FSV Phase 1 report). Based on the availability of a higher energy density battery cells, it was ultimately decided to use the I-shaped battery. The team then asked if the configuration of the battery could be modified to the I-Shape what impact would that have on the vehicle's structure. The objective of this study was to identify the most mass efficient shape for the FSV vehicle battery, as well as the most robust rear load path. The total mass of each design includes the body structure mass and the battery. Two battery configurations are studied; the original T-Shaped and the newly revised I-Shaped, which are shown in Figure 8.38. A gauge only optimization was performed to determine the best structural design for each battery configuration.

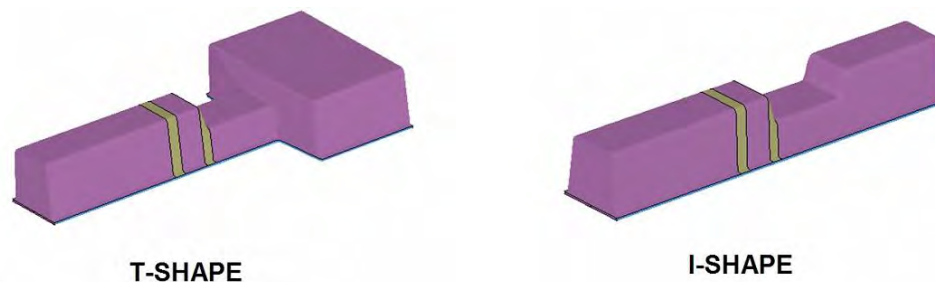


Figure 8.38: *Battery shapes considered*

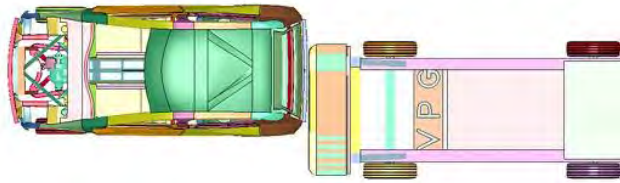
8.9.1 Model

The best design from the LF3G Optimization, design 60, is used as a basis for this study. The model was modified for the I-shaped configuration. Modifications include a new mass for the battery and new structure to accommodate the different packaging requirement.

8.9.2 Optimization

The two battery configurations allow different designs of the rear longitudinals and associated members. The two load cases most affected by rear longitudinal design were considered for this optimization, Rear 70% Offset Deformable Barrier and Static Torsion, as shown in Figure 8.39. A gauge only optimization was performed.

Rear 70% Impact ODB (Offset Deformable Barrier)



Static Torsion

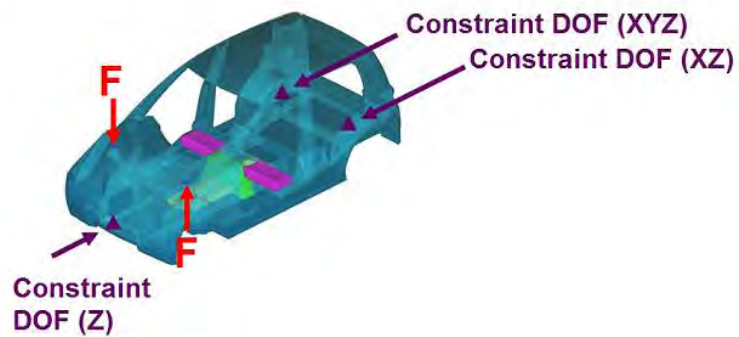


Figure 8.39: Battery shape evaluation load cases

8.9.2.1 T shaped Battery

The rear structure of the T-shape battery configuration was optimized with 3 thickness parameters, shown in Figure 8.40 and tabulated in Table 8.5. The material for each component was carried over from the previous design 60 result.

A total of 76 designs were investigated by the optimizer, of which 32 met the targets and were therefore feasible. The lowest mass configuration was the 37th design tested.

ITEM #	GAUGE			MATERIAL
	MIN	MAX	Design 37	
1	1.2mm	2.5mm	1.7mm	Mat 450
2	1.2mm	2.3mm	1.8mm	Mat 1000
3	1.0mm	1.5mm	1.2mm	Mat 450

Table 8.5: T battery optimization results table

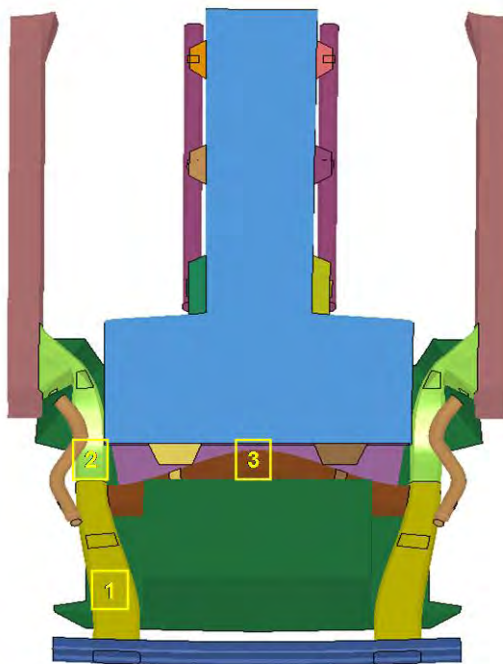


Figure 8.40: T-shaped battery optimization result

8.9.2.2 I shaped Battery

The rear structure of the I-shape battery configuration was optimized with 4 thickness parameters, shown in Figure 8.41 and tabulated in Table 8.6. The material for each component was carried over from the previous design 60 result.

A total of 89 designs were investigated by the optimizer, of which 35 met the targets and were therefore feasible. The lowest mass configuration was the 70th design tested.

ITEM #	GAUGE			MATERIAL
	MIN	MAX	Design 70	
1	1.2mm	2.5mm	2.2mm	Mat 450
2	1.2mm	2.3mm	2.1mm	Mat 1000
3	1.0mm	1.5mm	1.2mm	Mat 450
4	0.3mm	2.3mm	1.1mm	Mat 800

Table 8.6: I battery optimization table

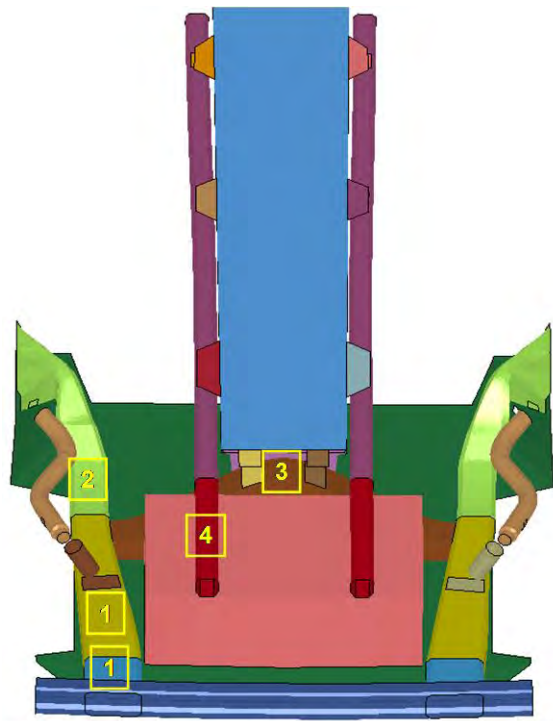


Figure 8.41: I-shaped battery optimization result

8.9.2.3 T versus I shaped Battery Comparison

The rear impact deformed shapes of the T-shape and I-shape configurations are shown in Figure 8.42 & Figure 8.43. The batteries show little damage in either configuration.



Figure 8.42: T-shape versus I-shape rear impact deformation shape : side view



Figure 8.43: T-shape versus I-shape rear impact deformation shape : bottom view

A comparison of the optimization results for the two configurations is shown in Figure 8.45 and tabulated in Table 8.44. Both structures met the optimization targets, with the I-shape doing slightly better in door openability. Static torsion was the controlling load case.

The mass of the optimized parts are 7 kg higher for the I-shape, 96 kg vs. 89 kg. This does not take into account the different masses of the batteries.

ITEM	GAUGES		MATERIAL	MASS OF OPTIMIZED PARTS		REAR IMPACT PEAK ACCELERATION		DOOR OPENABILITY		TORSIONAL STIFFNESS	
	T-SHAPED	I-SHAPED		T	I	T	I	T	I	T	I
	1	1.7mm		2.2mm	Mat 450						
2	1.8mm	2.1mm	Mat 1000	89kg	96kg	34G	34G	108mm	99mm	1.44mm	1.44mm
3	1.2mm	1.2mm	Mat 450								
4		1.1mm	Mat 800								

Figure 8.44: T versus I shaped battery optimization results table



Figure 8.45: T-shape versus I-shape optimization result comparison

Table 8.7 compares the functional mass of the two battery configurations. When the mass of the structural components required for the two batteries is included in the total, the I-shape configuration has a lower mass, 118 kg. This does not include the battery itself, which is also lighter for the I-shape due to its smaller size.

COMPONENT	T-SHAPE	I-SHAPE
Optimized BIW Components	88 kg	98 kg (+8%)
Battery* (Structural Floor Only)	34 kg	22 kg (-35%)
TOTAL FUNCTIONAL MASS	123 kg	118 kg (-4%)

* Does not include mass of battery cells or cover

Table 8.7: T-shape versus I-shape functional mass result comparison

8.9.3 Battery Shape Conclusion

The body structure mass of the I-shape configuration is higher than the T-shape, but the total functional mass, which includes the battery, is lower. It is also expected that the lower total system mass of the battery configuration will drive additional mass reduction in the rest of the structure when designed for other crash and stiffness criteria. Also, the I-shape battery configuration had a slightly better rear impact performance than the T-shape battery.

8.10 Conclusion

The results of the initial LF3G optimization and the battery shape optimization were combined into a single model. This model is called the LF3G and will be used as the basis for the next phase in the FSV's development. This next step is a subsystem optimization of the seven major body structure components. Figure 8.46 thru Figure 8.50 show details of the final grade and gauge selections for the LF3G model.

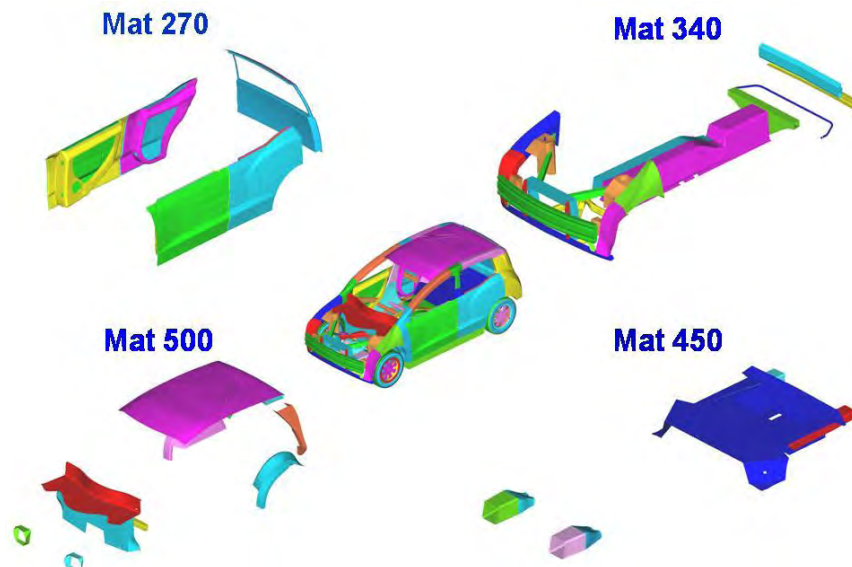


Figure 8.46: *LF3G - final gauge selections*

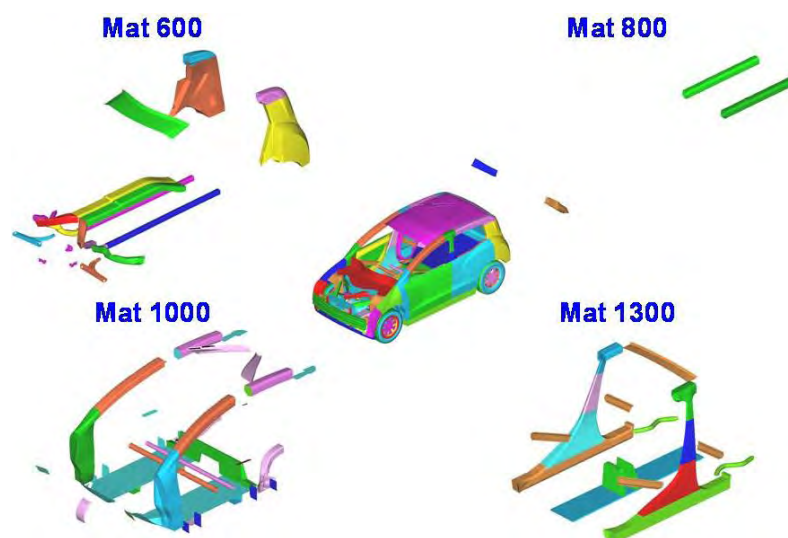


Figure 8.47: *LF3G - final gauge selections (continued)*

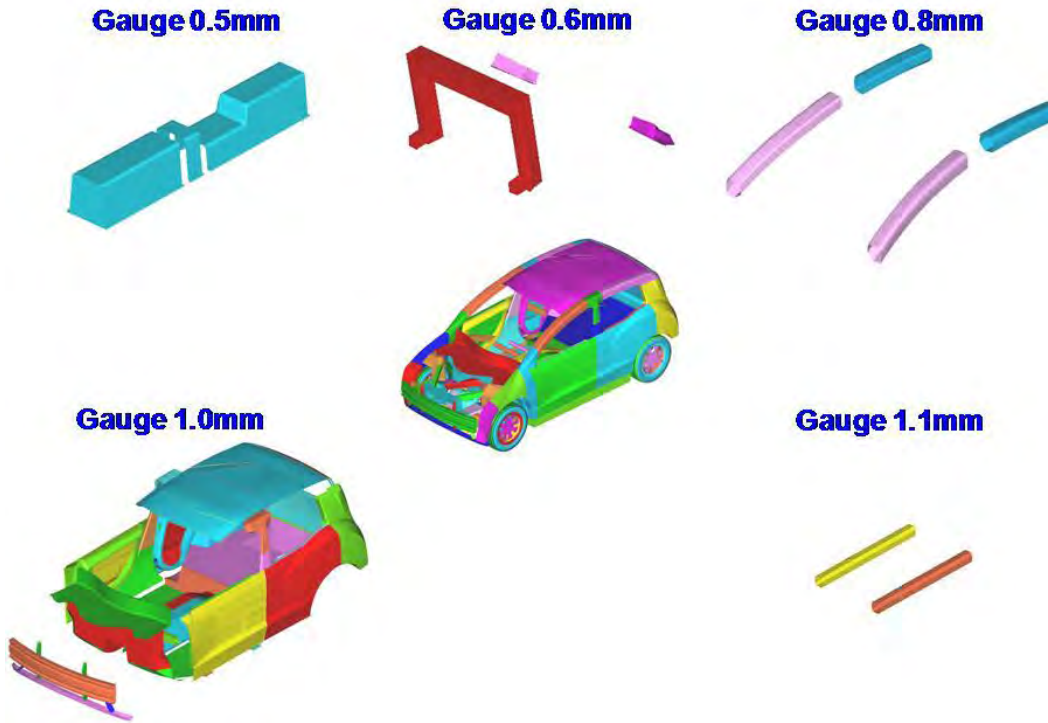


Figure 8.48: LF3G - final gauge selections

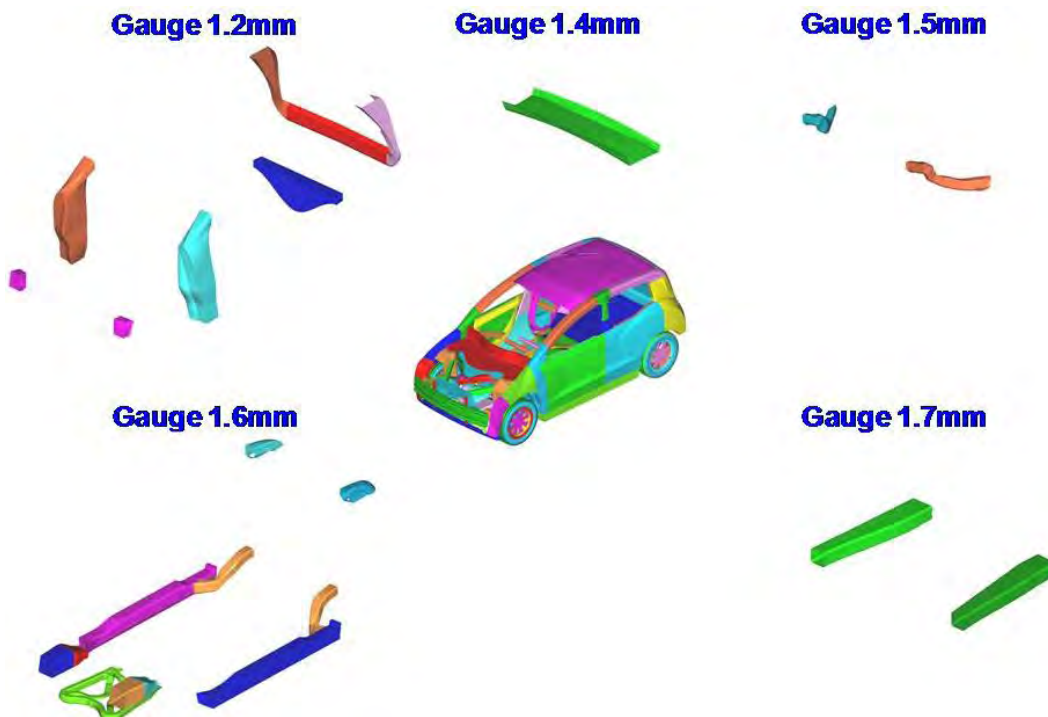


Figure 8.49: LF3G - final gauge selections (continued)

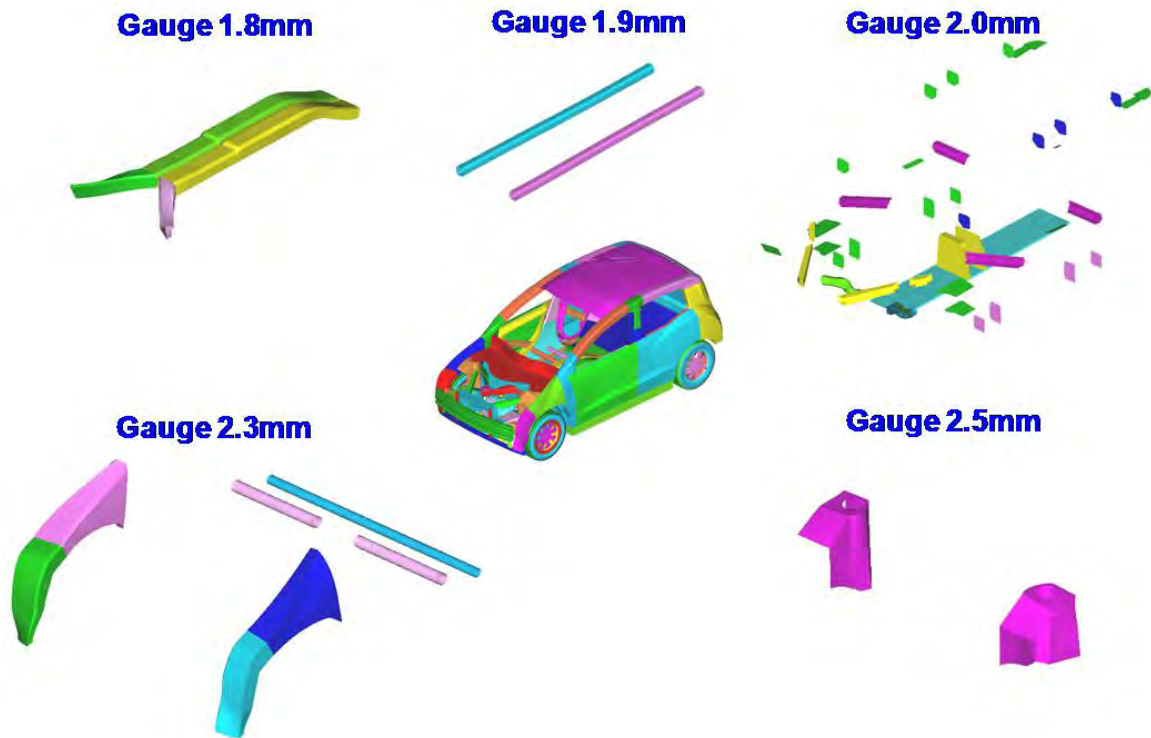


Figure 8.50: LF3G - final gauge selections (continued)

Figure 8.51, Figure 8.52, Figure 8.53 & Figure 8.54 show the shape changes of LF3G model after optimization overlapped with the baseline-starting model. The baseline model is defined as the interpretation of the topology optimization, and setting all geometry changes to minimum. Optimization will use the baseline model as a starting point for its search. The blue color represents the baseline and the red color represents the optimized LF3G model.

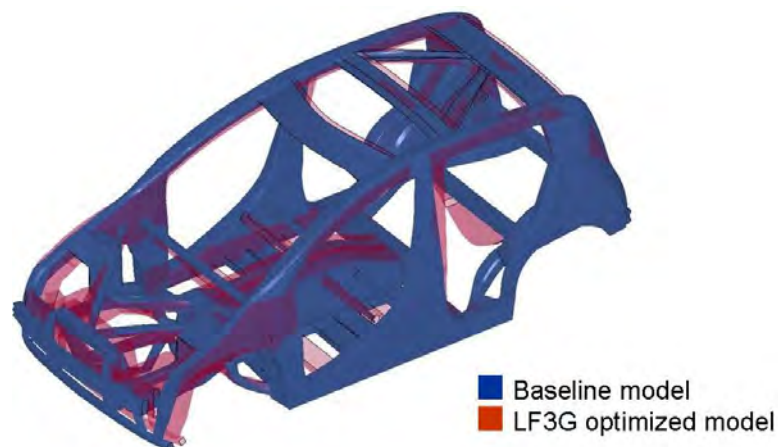


Figure 8.51: LF3G - final shape selection (iso view)

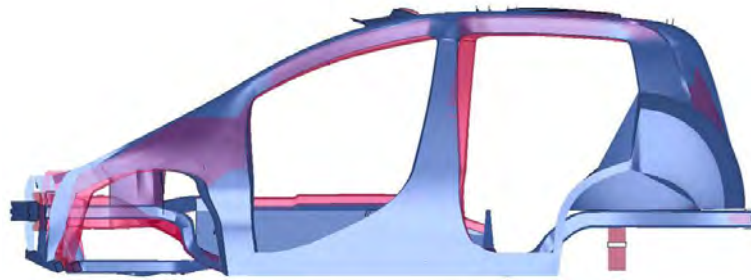


Figure 8.52: LF3G - final shape selection(side view)

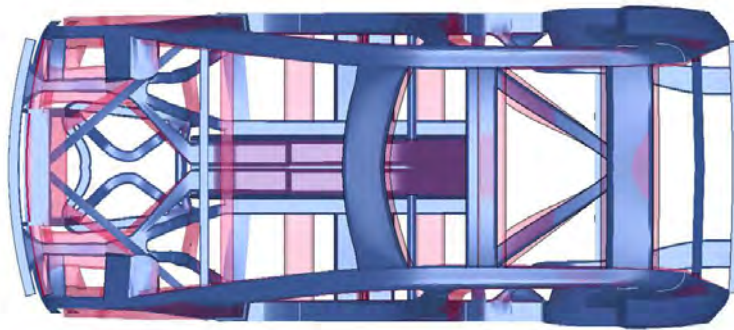


Figure 8.53: LF3G - final shape selection(top view)

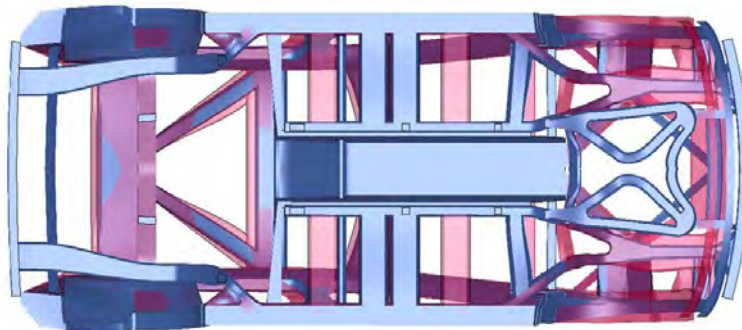


Figure 8.54: LF3G - final shape selection(bottom view)

Figure 8.55 through Figure 8.66 show specific details of the shape changes for various components of LF3G model after its optimization.

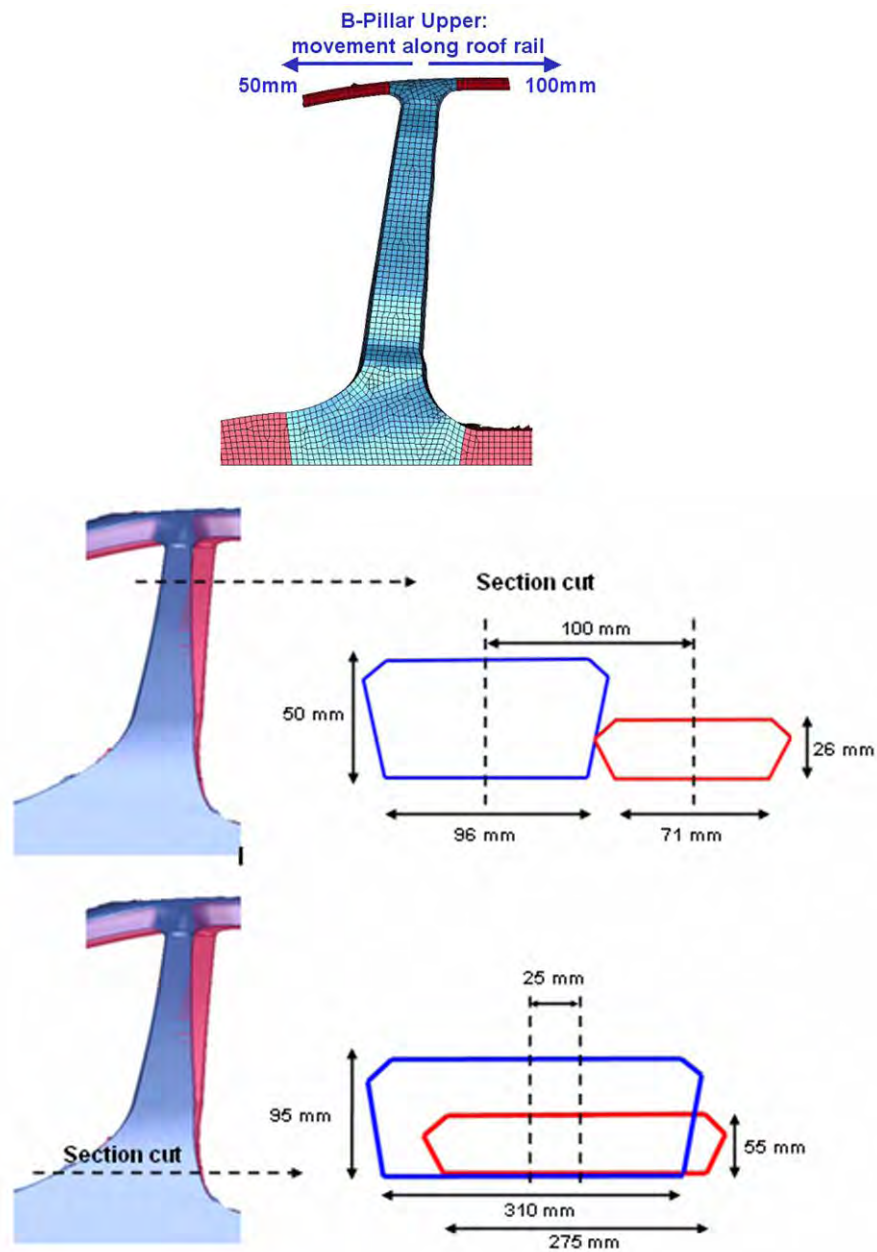


Figure 8.55: B-Pillar final shape (red) overlapped with baseline (blue)-(side view)

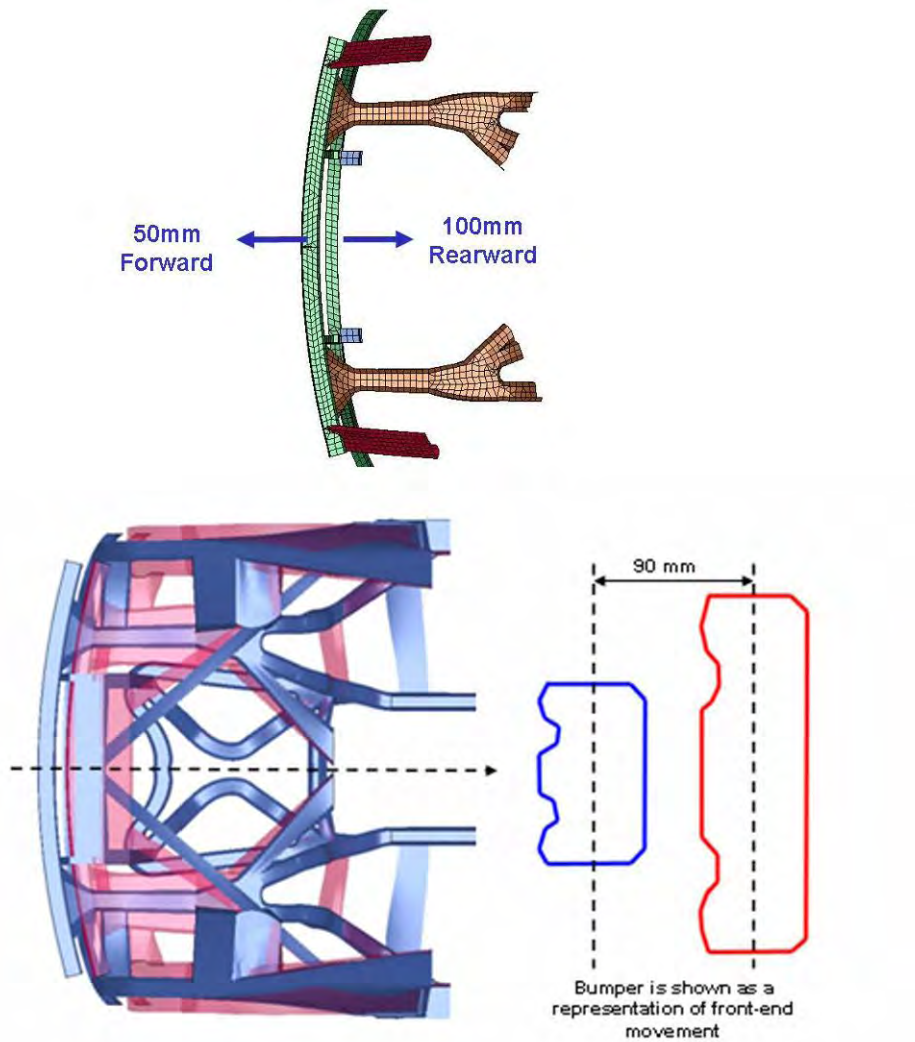


Figure 8.56: Front end final shape (red) overlapped with baseline (blue)-(top view)

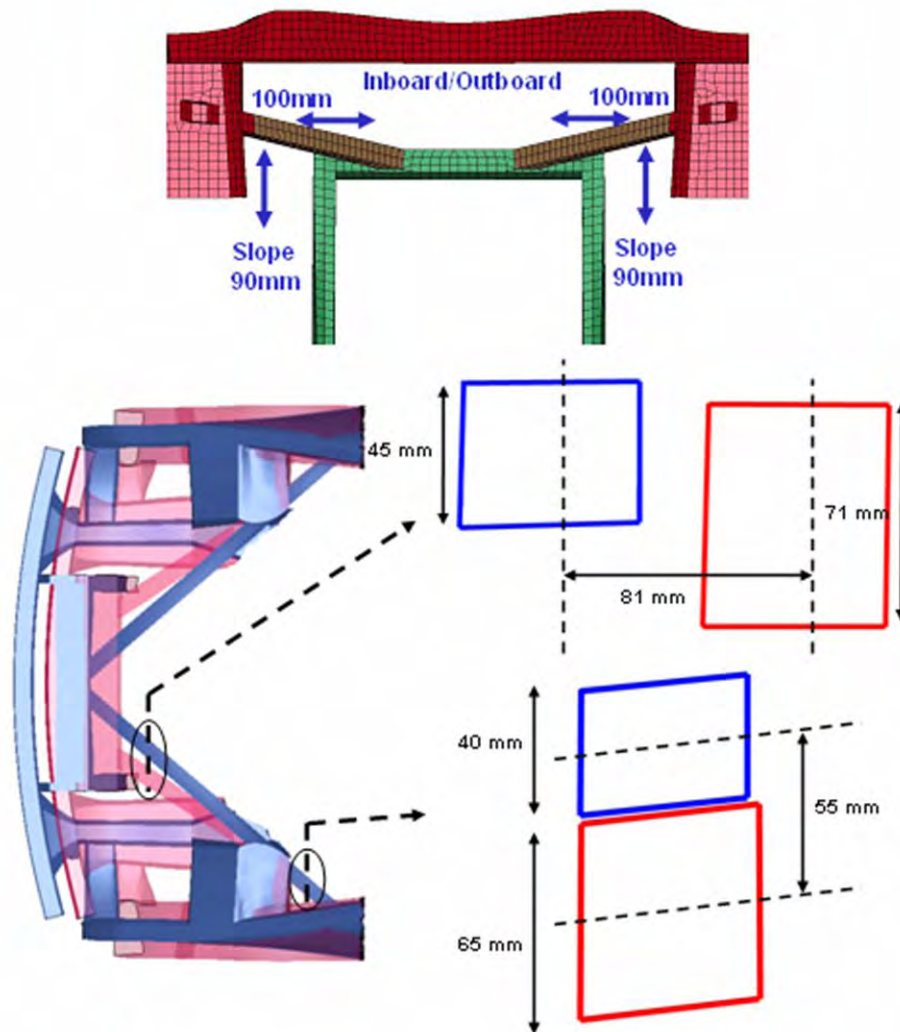


Figure 8.57: Radiator support final shape (red) overlapped with baseline (blue)-(top view)

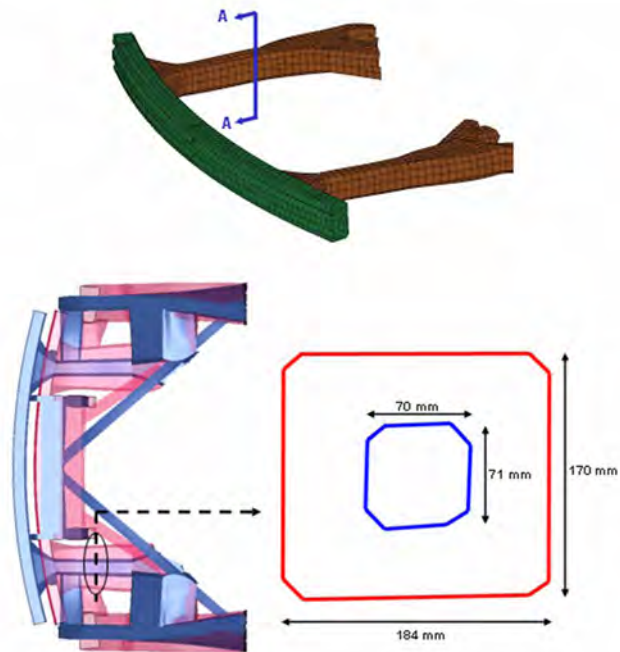


Figure 8.58: Front rail final shape (red) overlapped with baseline (blue)-(top view)

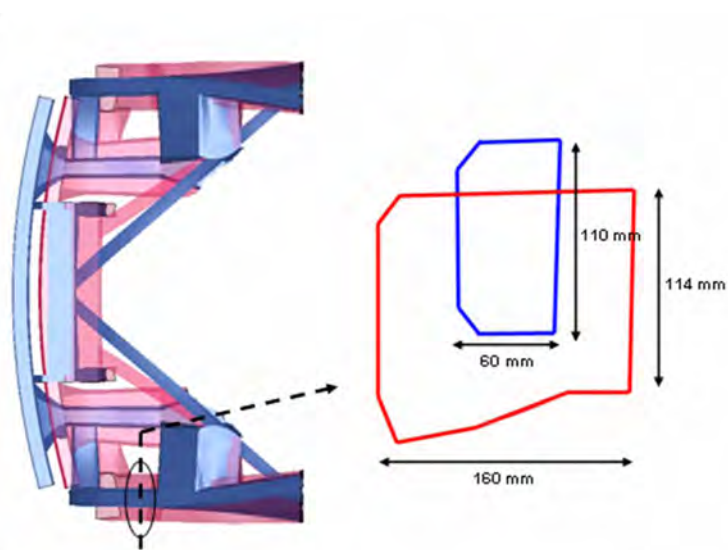


Figure 8.59: Shotgun final shape (red) overlapped with baseline (blue)-(top view)

8.10 Conclusion

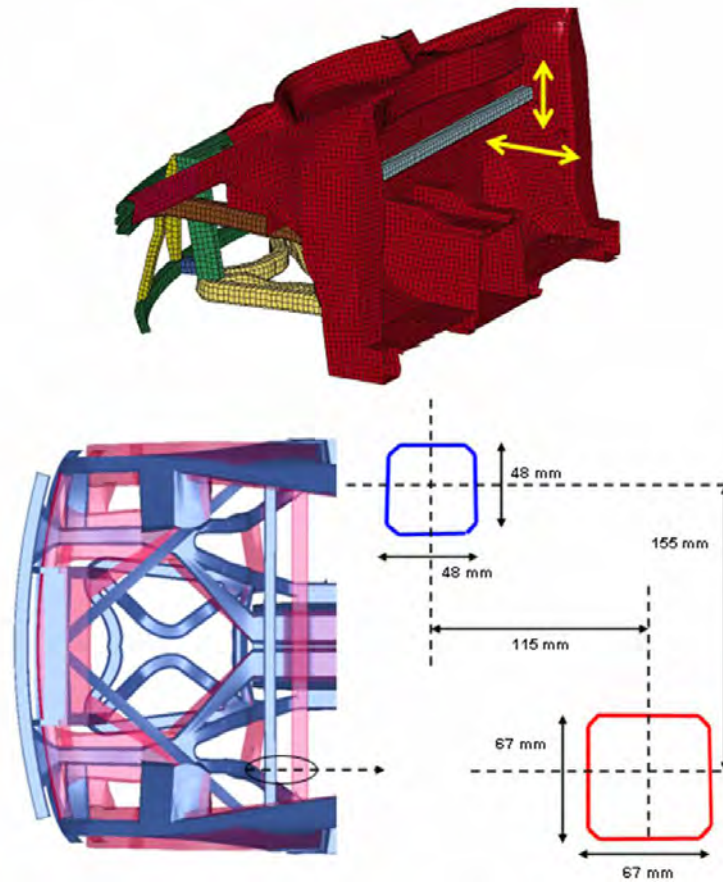


Figure 8.60: Lower IP final shape (red) overlapped with baseline (blue)-(top view)

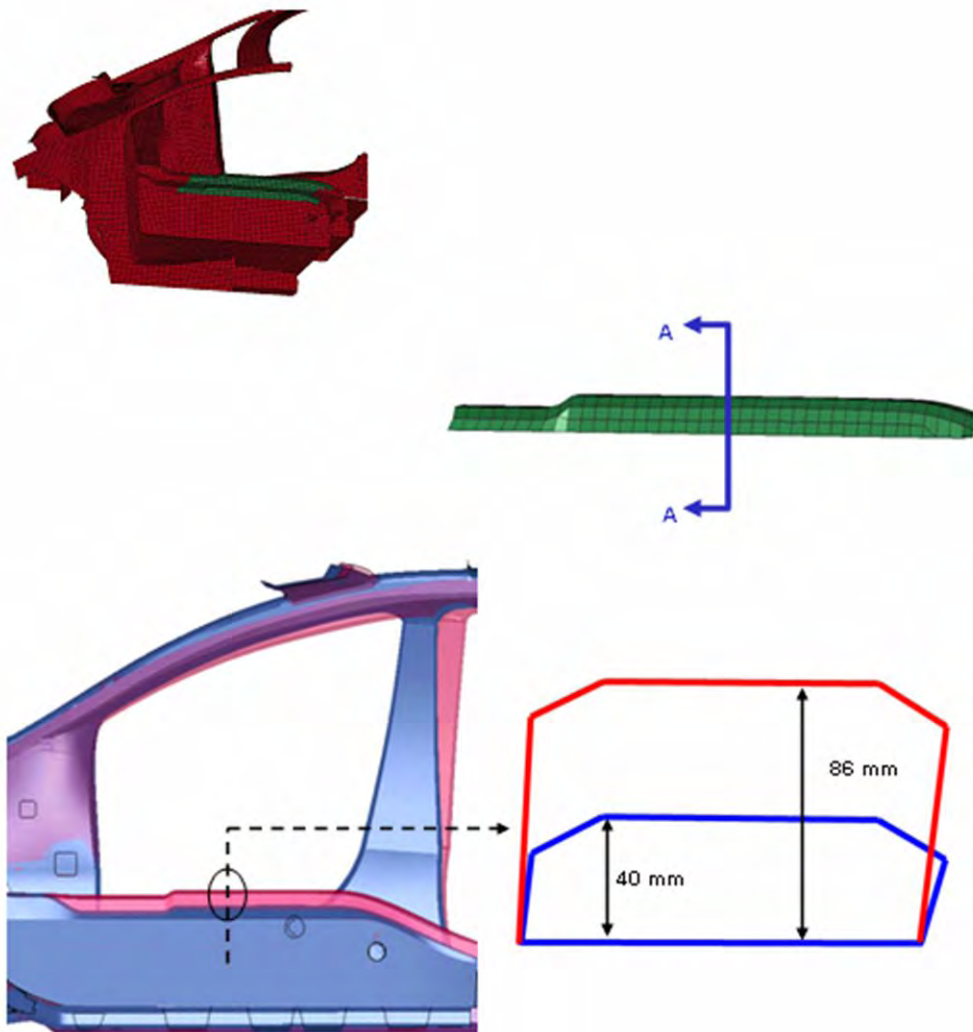


Figure 8.61: Tunnel top member final shape (red) overlapped with baseline (blue)-(top view)

8.10 Conclusion

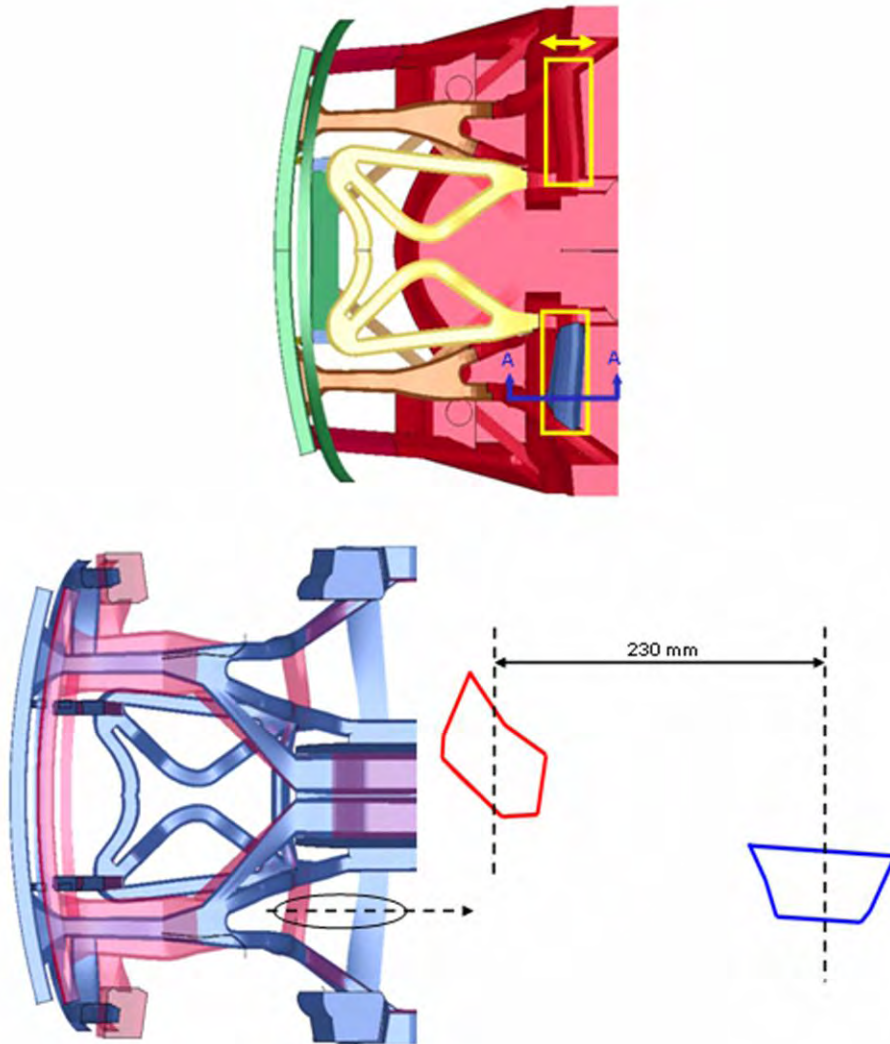


Figure 8.62: Torque box member final shape (red) overlapped with baseline (blue)-(top view)

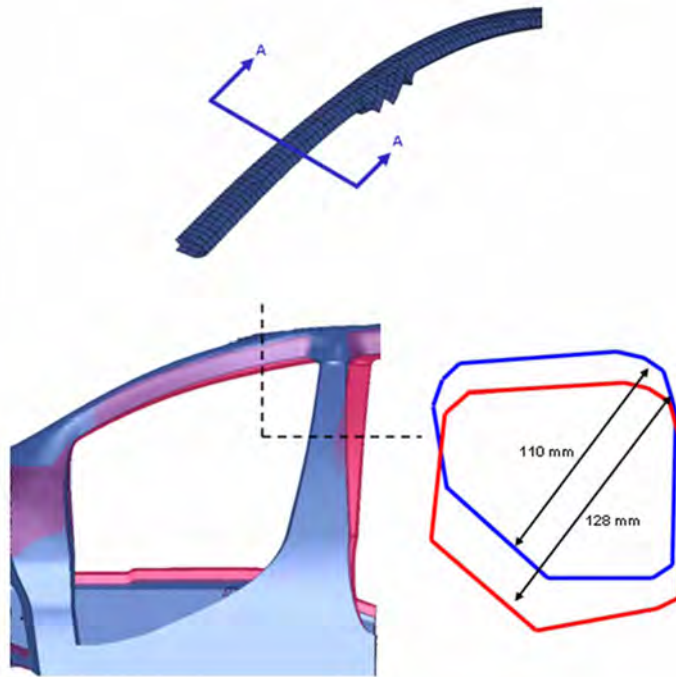


Figure 8.63: Roof rail member final shape (red) overlapped with baseline (blue)-(side view)

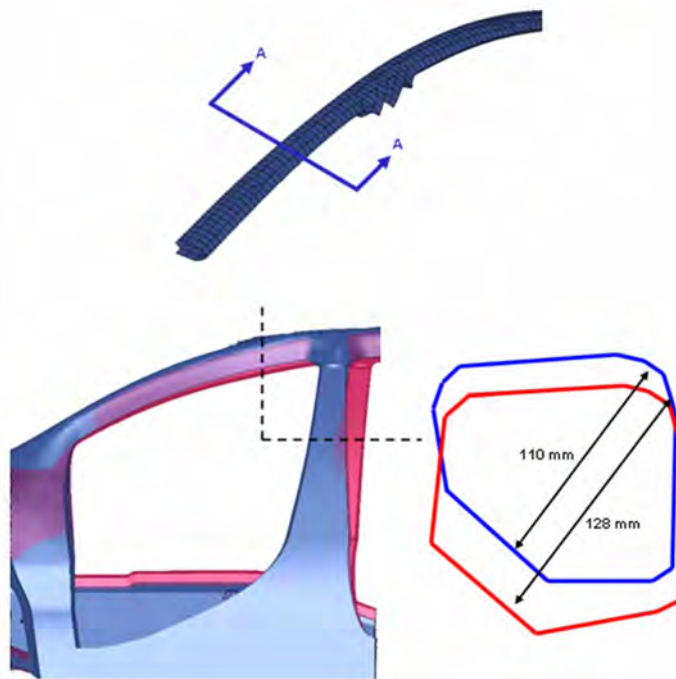


Figure 8.64: Roof bow final shape (red) overlapped with baseline (blue)-(top view)

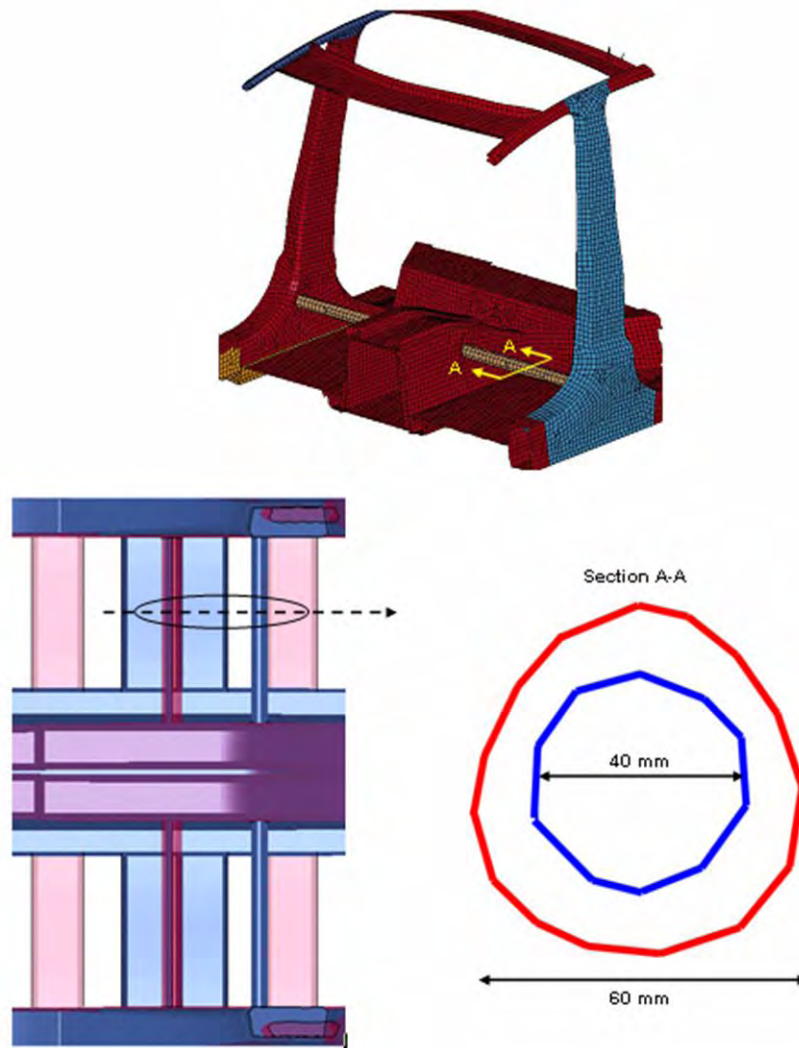


Figure 8.65: Seat crossmember final shape (red) overlapped with baseline (blue)-(top view)

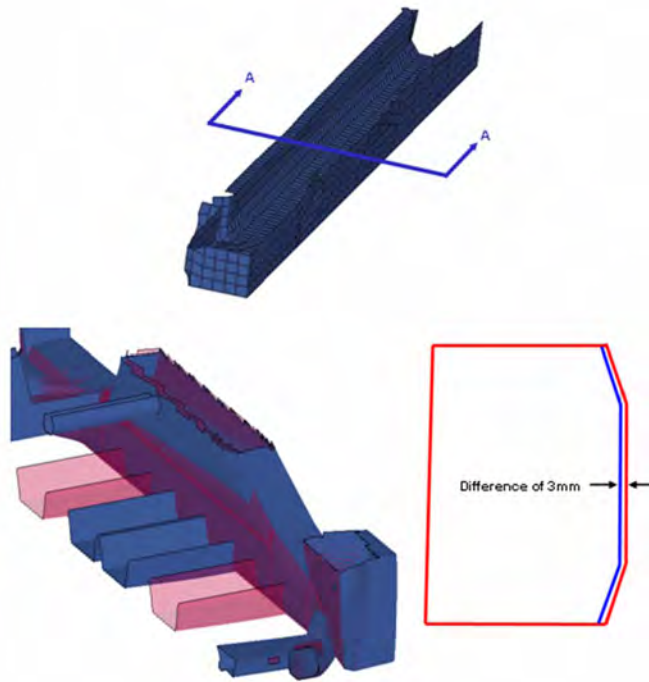


Figure 8.66: *Rocker final shape (red) overlapped with baseline (blue)-(top view)*

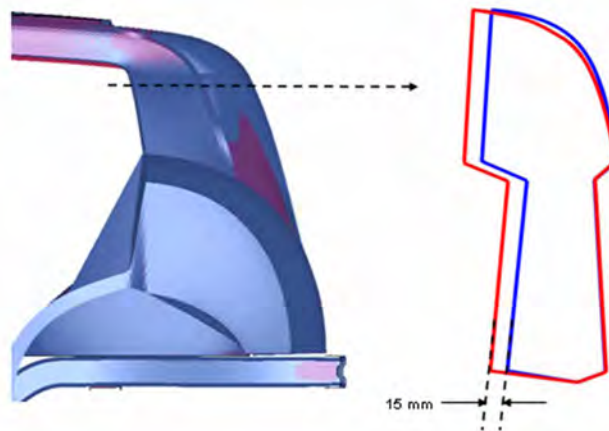


Figure 8.67: *Joint rear upper final shape (red) overlapped with baseline (blue)-(top view)*

8.10 Conclusion

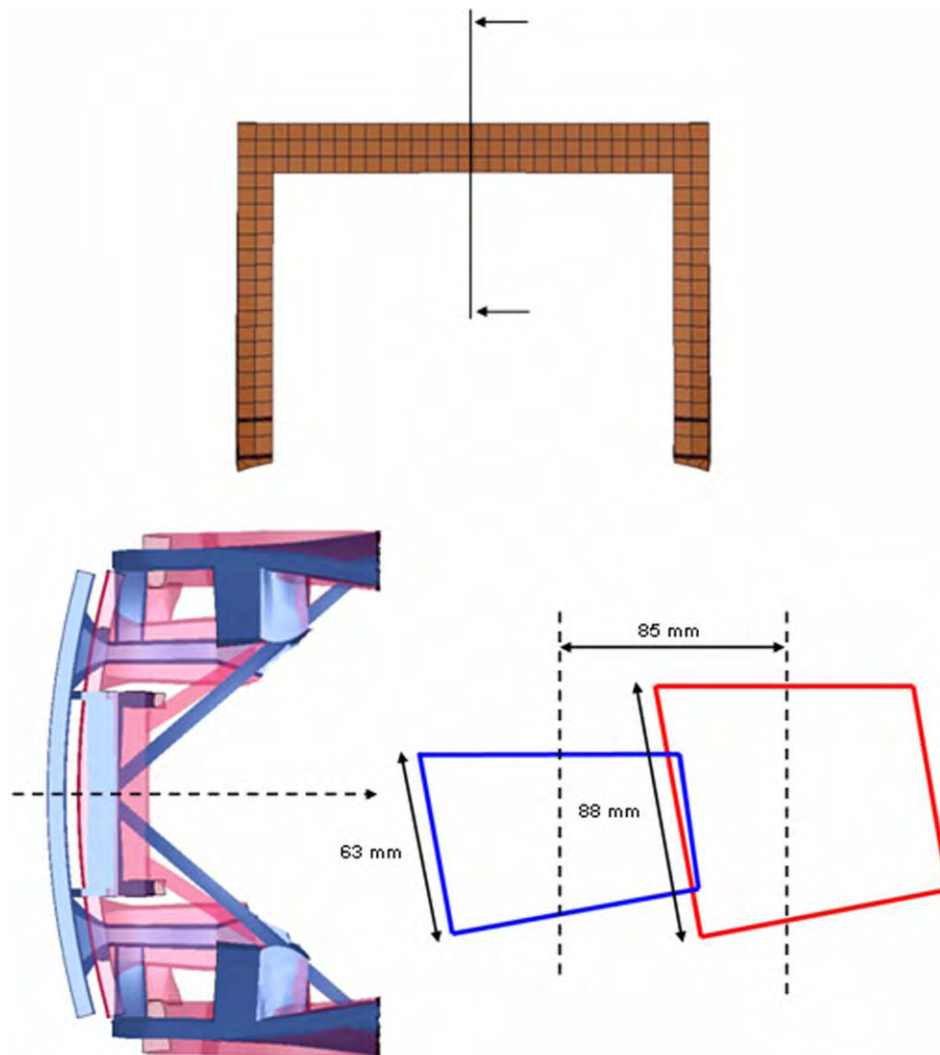


Figure 8.68: Radiator support final shape (red) overlapped with baseline (blue)-(top view)

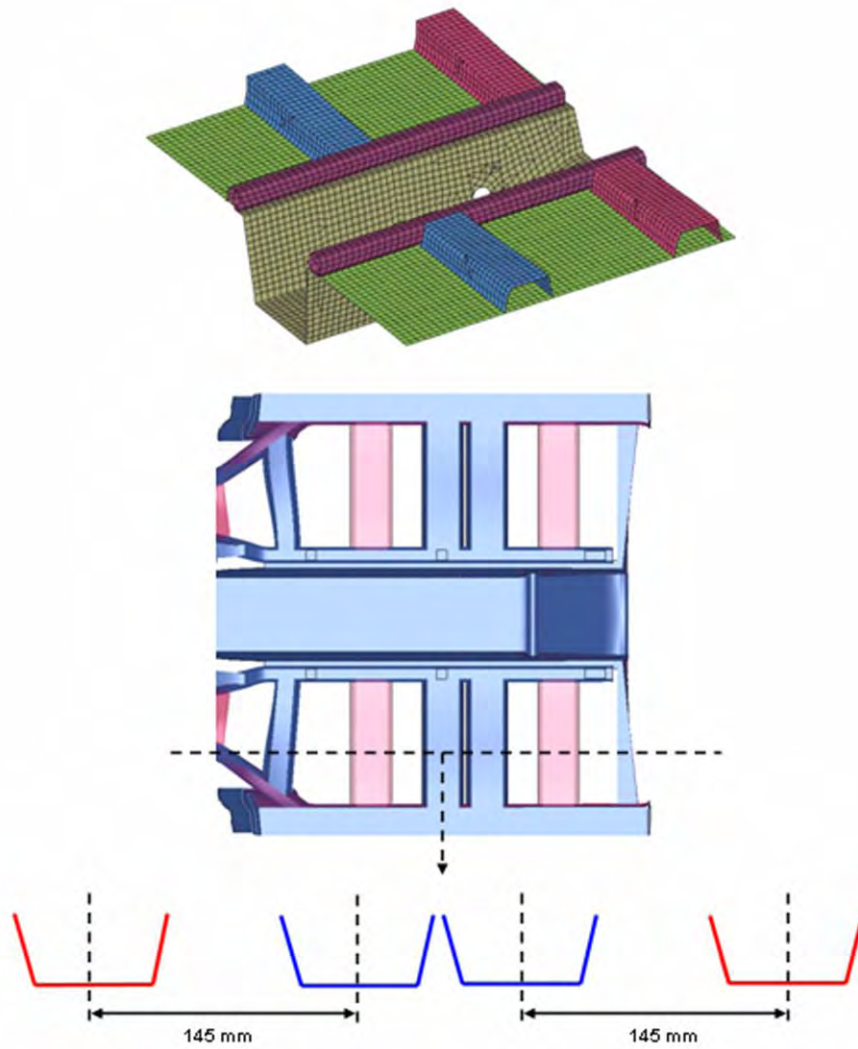
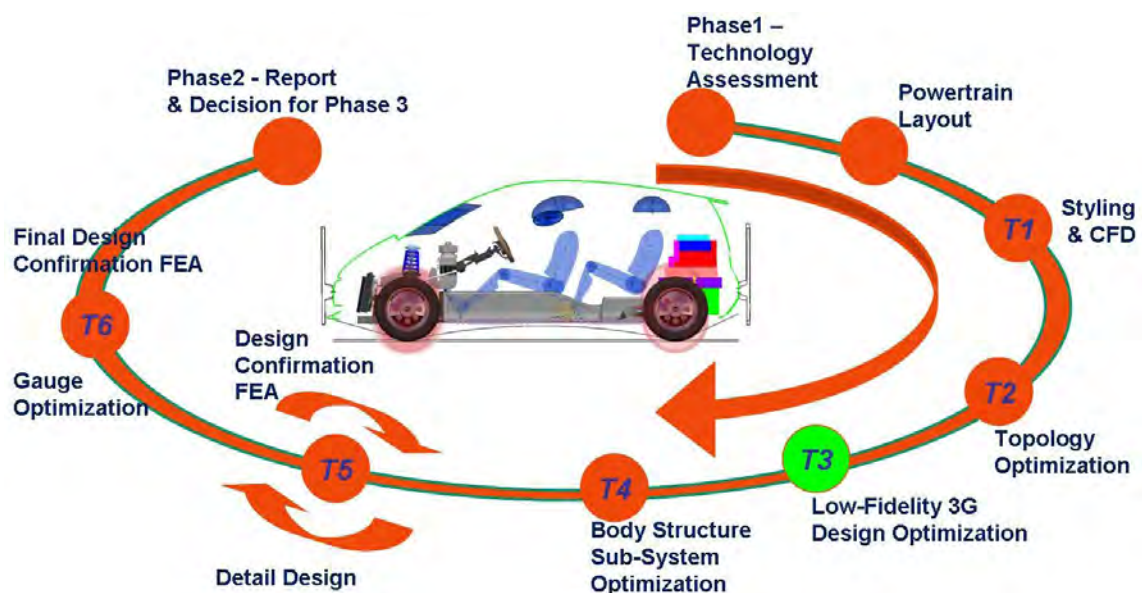


Figure 8.69: Underbody crossmembers final shape (red) overlapped with baseline (blue)-(top view)

9.0 FSV LF3G Results Interpretation to Baseline Body Structure Design



9.1 LF3G Geometry Interpretation

9.1.1 Background

For the BEV body structure the results from the Task 3 - Low Fidelity Gauge, Grade & Geometry (LF3G) Optimization are shown in Figure 9.1. The LF3G analysis approach is fully discussed in chapter 8. The structural load paths, section sizes and section positions, represented by this geometry are optimized for topology and a rough estimate for topography to meet global stiffness and crash performance targets. This model does not, however, represent section shapes that can necessarily be manufactured and assembled from sheet steel. Also, the mass for this model (287 kg), although optimized for the chosen grade and gauge of material, is not the lowest possible that can be achieved by further detailed optimization of a more refined design. The next step in the design process is to interpret the geometry from this model to represent a sheet steel design, which can be further used to assess and optimize various body structure sub-systems and related

manufacturing processes.



Figure 9.1: FSV BEV - optimized LF3G geometry

9.1.2 Body Structure - Sheet Steel First Iteration Baseline Design

Side by side comparison of the first iteration of the sheet steel body structure design and LF3G geometry is shown in Figure 9.2. The interpreted design encompasses comparable sectional load paths and the necessary allowances for spot welding flanges. In this design, all the parts were assigned material grades and thicknesses based on the results from the LF3G optimization analysis and engineering judgment. This baseline sheet steel body structure is equivalent to what can be achieved using current manufacturing and assembly technologies. The mass of the baseline structure is estimated to be 218 kg. A list of all the panels for the body structure, with assigned gauge, grade and calculated mass, is shown in Appendix- See Table 20.1, Table 20.2 and Table 20.3.

9.1 LF3G Geometry Interpretation



Figure 9.2: FSV body structure comparison - sheet steel design Vs. LF3G geometry

9.1.3 Body Structure - Sub Systems for T4 - HF3G Optimization

From this baseline body structure design the following 'sub-system' Finite Element Models were created for further High Fidelity Gauge, Grade and Geometry (HF3G) optimization:

1. Rocker (Figure 9.3)
2. B-pillar (Figure 9.4)
3. Roof side rail (Figure 9.5)
4. Rear rail (Figure 9.6)
5. Front rail (Figure 9.7)
6. Front upper rail (shotgun) (Figure 9.8)
7. Battery upper & lower (Figure 9.9)

9.1.3.1 Rocker

Figure 9.3 shows the body structure rocker sub-system. The redesigned section shows a typical section flange for spot welding and also a reinforcement panel.

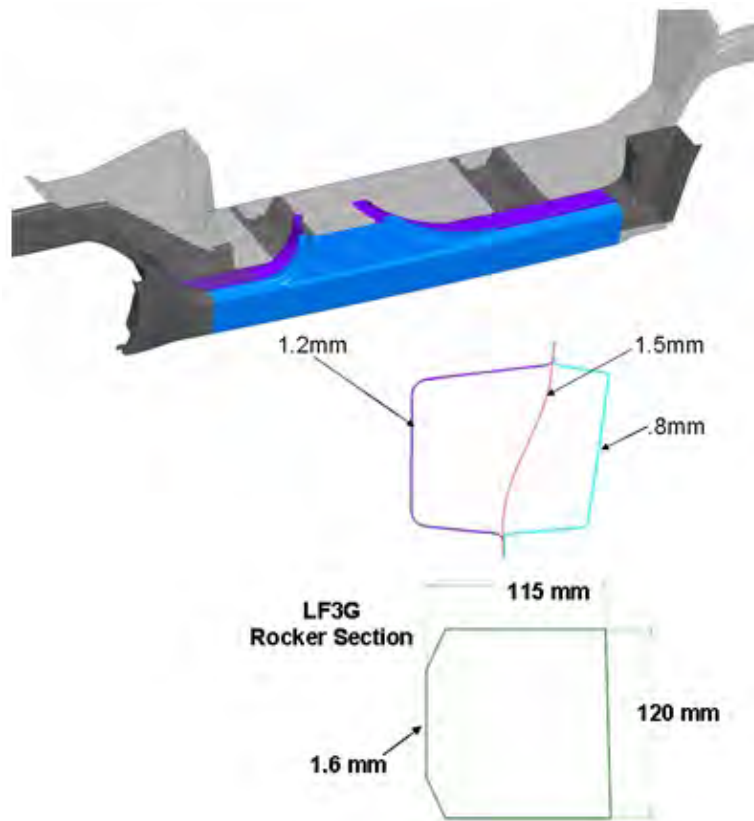


Figure 9.3: *FSV body sub-structure - rocker for LF3G FEA*

9.1.3.2 B-Pillar

Figure 9.4 shows the B-pillar with a typical section including inner, reinforcement and an outer panel. As shown in the figure, a larger section was chosen for the B-pillar as a starting point for the T4-sub-system optimization, compared to LF3G B-pillar section. This gave more flexibility to the sub-system optimization process by taking advantage of the additional space available in the package design space.

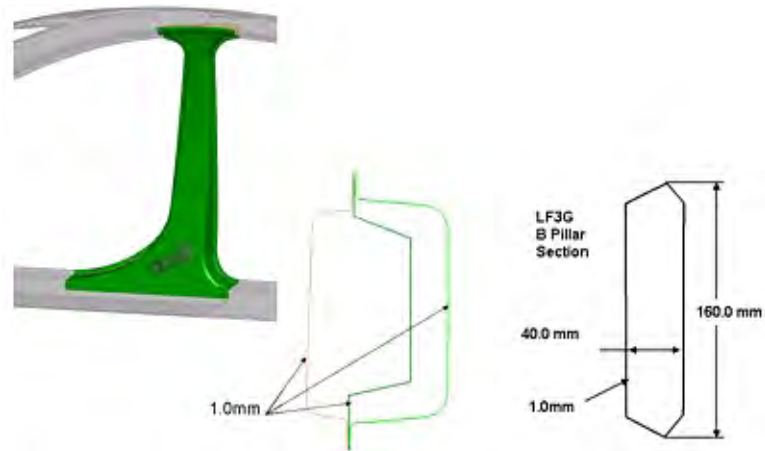


Figure 9.4: FSV body sub-structure - B Pillar for LF3G FEA

9.1.3.3 Roof Side Rail

Figure 9.5 shows the roof side rail with a typical section including inner, reinforcement and an outer panel.

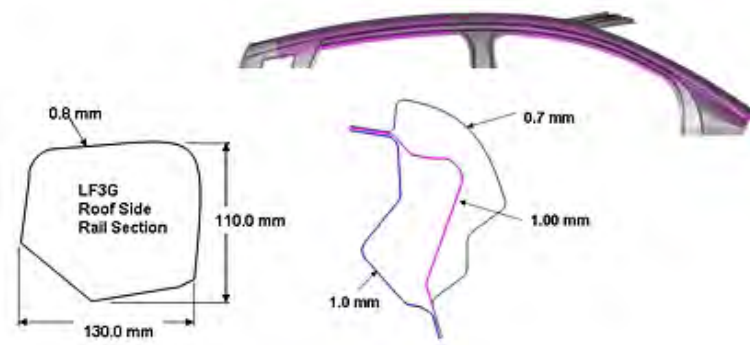


Figure 9.5: FSV body sub-structure - roof side rail for LF3G FEA

9.1 LF3G Geometry Interpretation

9.1.3.4 Rear Rail

Figure 9.6 shows the rear rail with a typical section including top reinforcement and a lower panel.

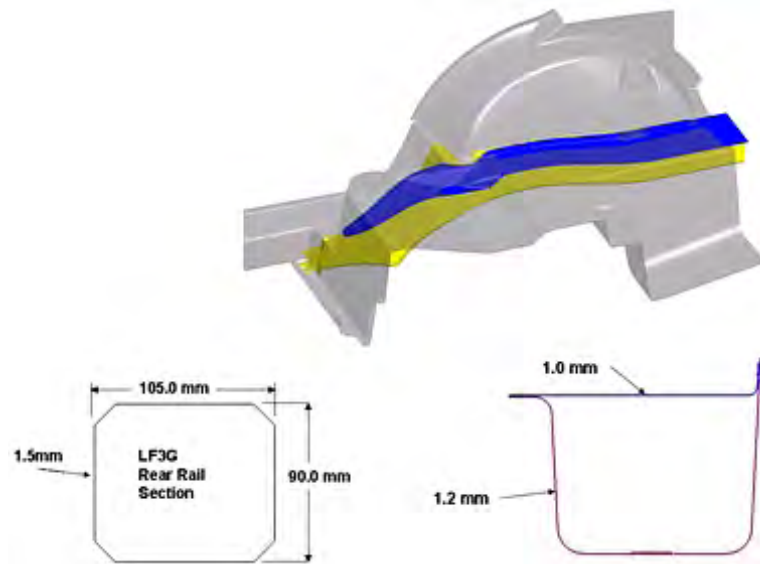


Figure 9.6: FSV body sub-structure - rear rail for LF3G FEA

9.1.3.5 Front Rail

Figure 9.7 shows the front rail with a typical octagonal section made up with upper and lower rail panels.

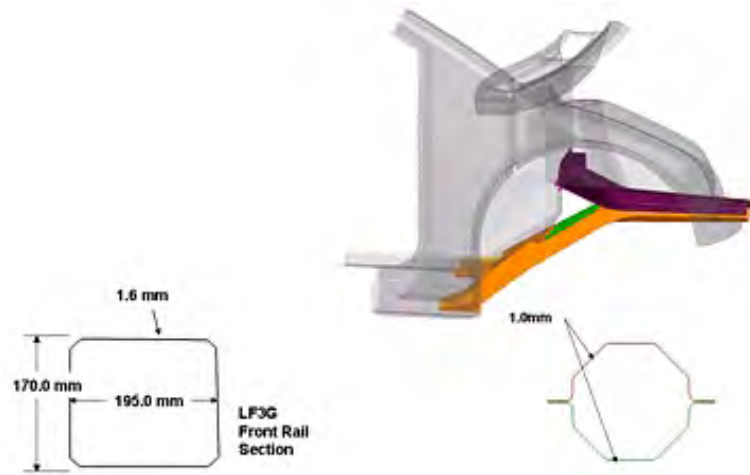


Figure 9.7: FSV body sub-structure - front rail for LF3G FEA

9.1 LF3G Geometry Interpretation

9.1.3.6 Front Rail (Shotgun)

Figure 9.8 shows the front upper rail with typical section inner and outer panels.

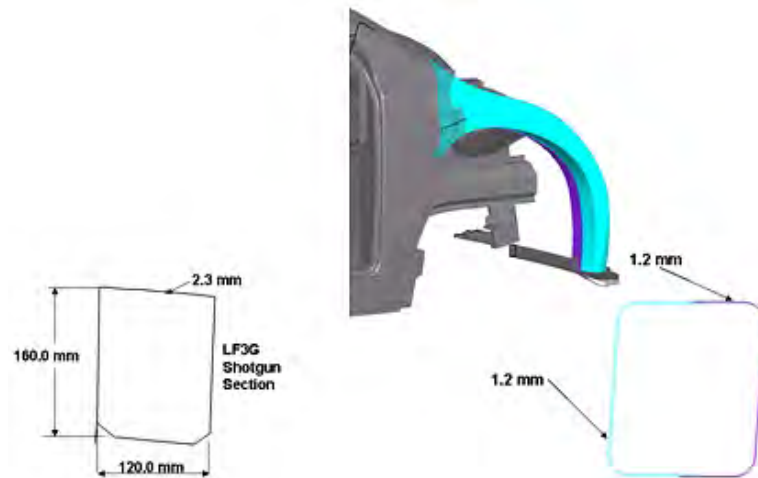


Figure 9.8: FSV body sub-structure - front upper rail for LF3G FEA

9.1.3.7 Tunnel Upper & Lower Rails

Figure 9.9 shows the tunnel upper & lower members. These section are required to support the battery assembly mass and mounting structure.

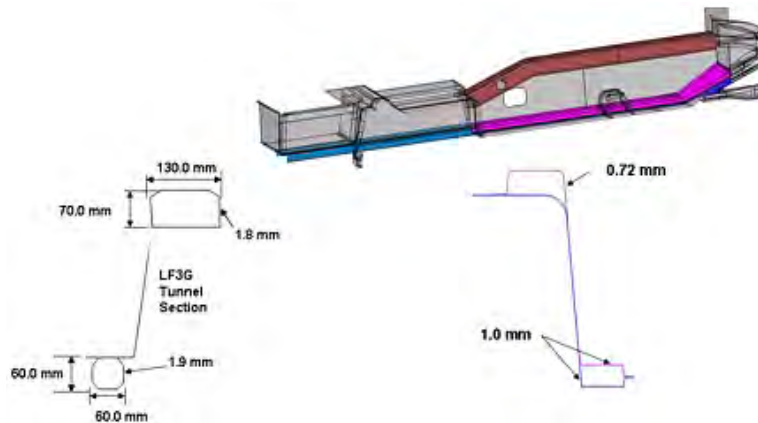
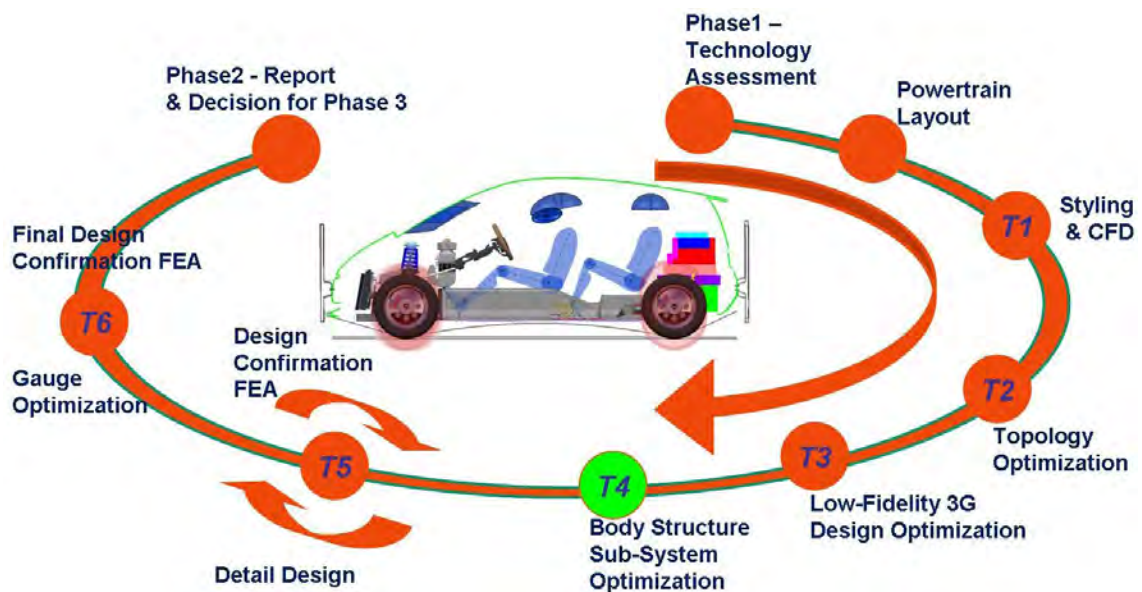


Figure 9.9: *FSV body sub-structure - tunnel rails for LF3G FEA*

10.0 Structural Sub-System Design Optimization - Methodology



10.1 Introduction

This chapter addresses the FSV (FutureSteelVehicle) sub-system optimization. Its purpose is to document the development of the optimization process and the manufacturing process, shape, material and gauge selections of the optimized sub-systems considered. Sub-system 3G optimization was completed by ETA.

10.2 Objective

The objective is to apply the optimization methodology to the FSV LF3G (Low Fidelity 3G) vehicle structural sub-systems and establish the best combination of material grade, gauge, geometry and manufacturing process for particular sub-system. Although the optimization set up comprehends a specific manufacturing approach, the range of material strengths, gauge, and geometry options may allow solutions that are not manufacturable. This was allowed in the optimization in order

to introduce more freedom for the optimizer to achieve lower mass and push the manufacturing processes to incorporate innovative technologies to attain low mass designs. Interpretation of the optimized solution to address manufacturing constraints is accomplished in chapter 11.

10.3 Background

The FSV pilot project (FSV Phase 1 report) previously validated the major portions of this design and development process for an existing structure. This process is referred to as 3G optimization and represents full shape, material and gauge (Geometry, Grade and Gauge) optimization. The FSV program will track the major load path for governing load cases such as front NCAP, front ODB, rear ODB, IIHS side, pole impacts and roof crush. This will provide the ground work for considering controlling load cases for different sub-systems while performing sub-system level optimization.

10.4 Optimization Methodology Overview

The basic steps for the sub-system optimization are as follows:

- Sub-system development and validation
- Initial design representing manufacturing approach
- Establish design space
- Parameterize geometry
- Time history, constraints and targets from LF3G
- Detailed 3G optimization; geometry (shape), grade (material) and gauge

Optimization load cases considered are the following:

- NCAP frontal impact
- IIHS front crash 40% ODB (Offset Deformable Barrier)
- FMVSS 301 rear 70% ODB
- IIHS side impact
- FMVSS 214 pole impact
- FMVSS 216 roof crush (with IIHS 4* strength to weight ratio)
- Bending and torsional static stiffness

Not all load cases are used for each sub-system. Only load cases relevant to particular sub-system are used based on load path mapping. Figure 10.1 summarizes the steps in the sub-system optimization process.

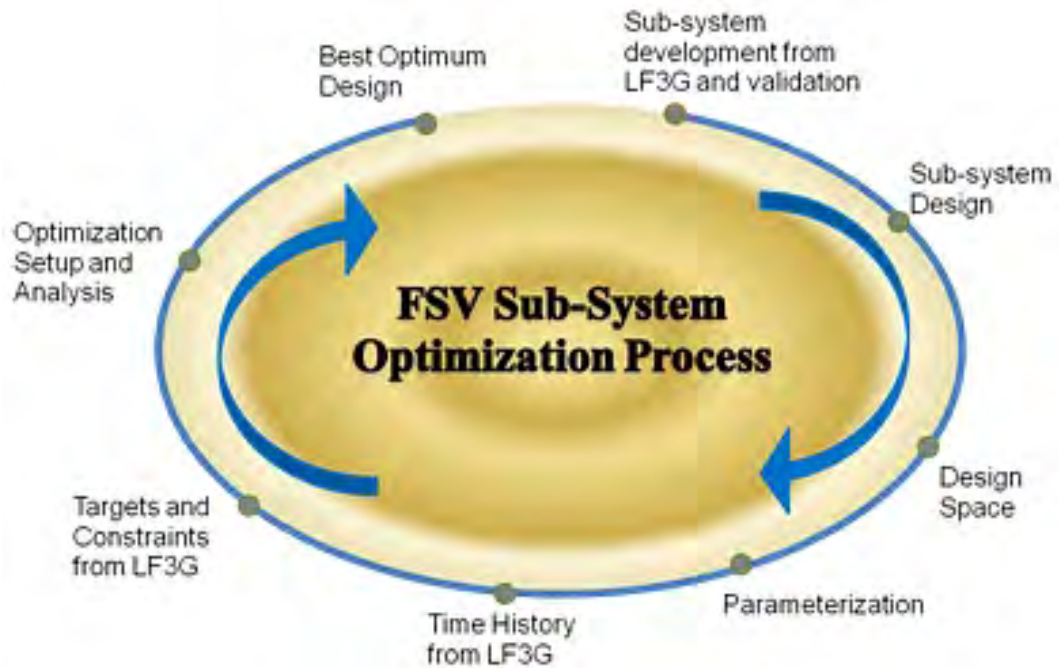
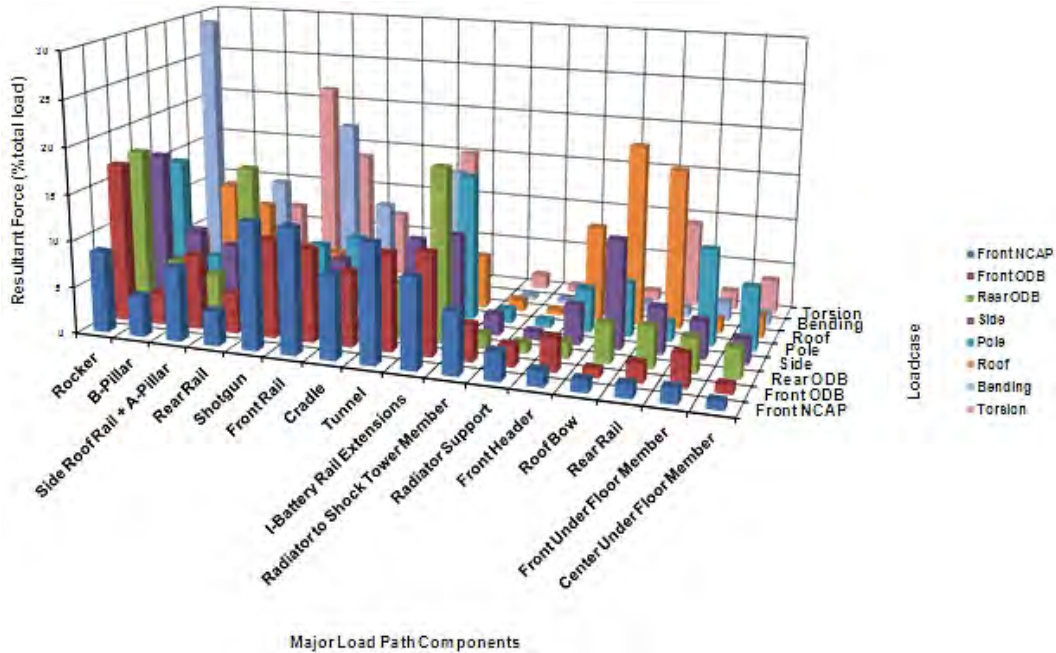


Figure 10.1: Detailed FSV sub-system optimization process

10.5 Loadpath Mapping: Sub-System Selection and Loadcases

The LF3G design from Chapter 8 (T3 LF3G Optimization) was used as the basis for sub-system optimization. It was the source of boundary conditions. However, the geometry of each component used are from the interpretation of LF3G results shown in Chapter 9 (LF3G Results Interpretation), Figure 9.2. Performing loadpath mapping on this model, the most critical load carrying components and their controlling loadcases for the sub-system optimization were identified. The final loadpath mapping results are summarized in Figure 10.2. Table 10.1 summarizes the critical components and the loadcases that will be considered as part of the sub-system optimization.


Figure 10.2: LF3G loadpath mapping results

SUBSYSTEM	LOADCASE				
	1	2	3	4	5
Rocker	Front NCAP	Front ODB	Rear ODB	IIHS Side	Pole
B-Pillar	IIHS Side	Roof Crush			
Side Roof Rail	Front ODB	Rear ODB	IIHS Side	Pole	Roof Crush
Rear Rails	Rear ODB	Torsional Stiffness			
Tunnel Rails	Front ODB	Rear ODB	IIHS Side	3G Jounce	
Shotgun	Front NCAP	Front ODB			
Front Rail	Front ODB				

Table 10.1: Sub-system optimization: candidate components and loadcases

10.6 Rocker Sub-System

The rocker sub-system optimization considered four manufacturing concepts: stamping, hydro-forming, roll forming and aluminum extrusion.

10.6.1 Development of Sub-System from the Full Model

The rocker sub-system was developed from the full model (LF3G) such that when analyzed under the same loading conditions it behaved in the same way as the full model. The sub-system model consists of the rocker and the major attachment components it is attached to such as the B-pillar, hinge pillar, rear rail, floor and underbody crossbeams. See Figure 10.3.

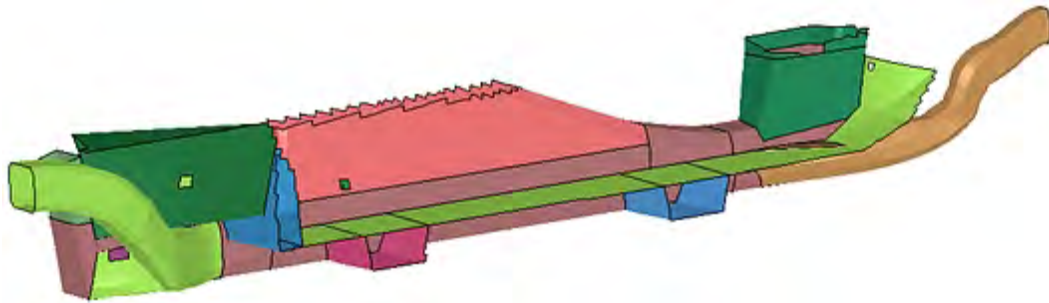


Figure 10.3: *Rocker sub-system from LF3G*

10.6.2 Generating Boundary Conditions

The nodal displacement time history is used as the boundary conditions for the sub-system so that it behaves in a similar manner to the full LF3G model. For both models a series of common boundaries were defined so that the appropriate time histories could be extracted from the LF3G model and applied to the sub-system model. Referring to Figure 10.4, the yellow highlighted areas are the boundaries setup in the sub-system model. Similar boundaries were created in the full model. Where appropriate the time history of the any barriers was also included. For example the figure shows the setup for the pole impact loadcase, which included the barrier. Including the barrier is particularly important when the barrier is deformable because the individual design evaluations may drive different responses in the barrier itself.

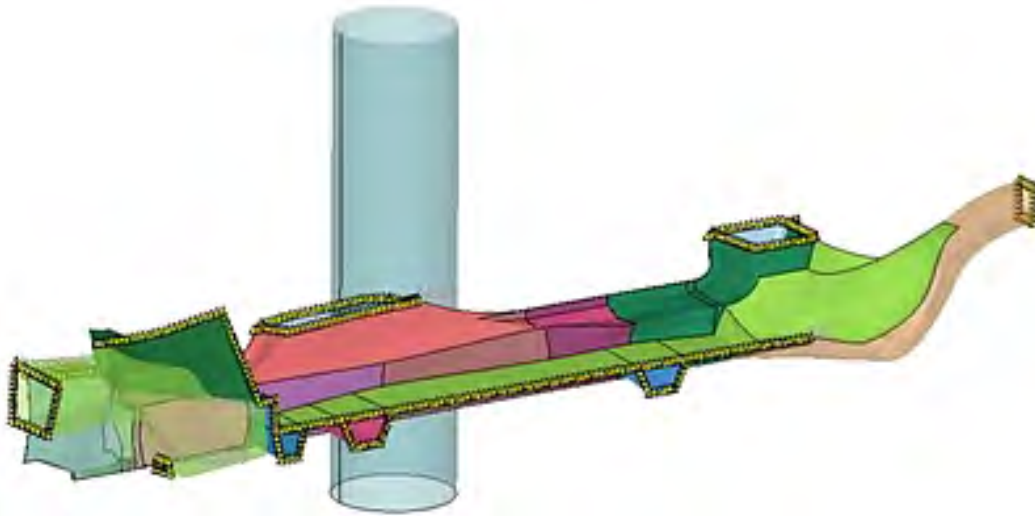
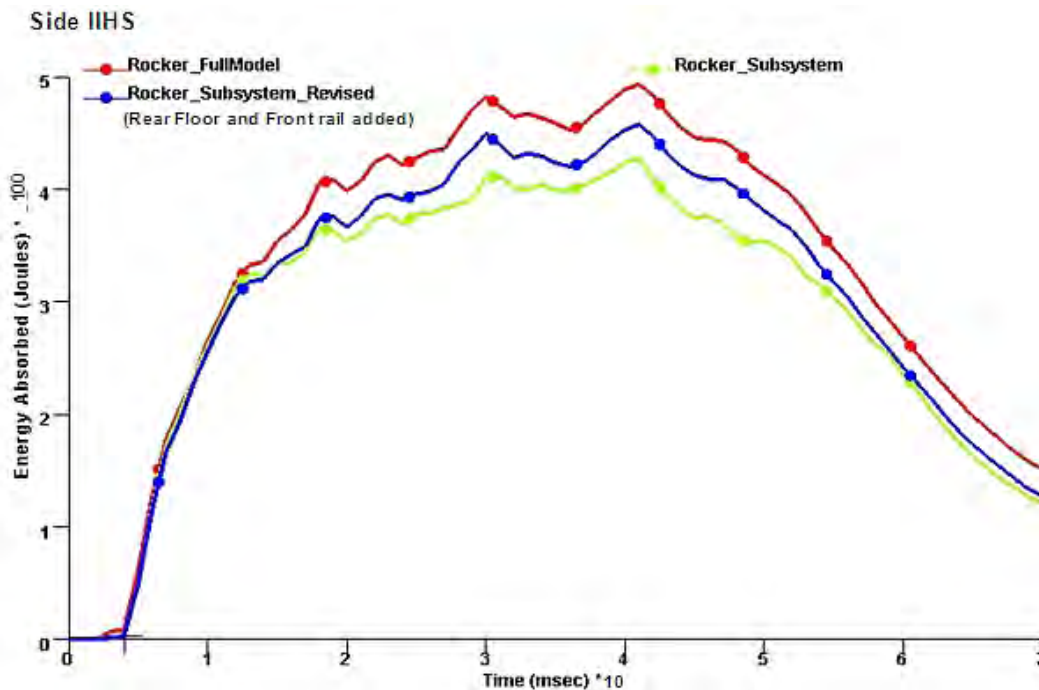


Figure 10.4: Rocker sub-system with highlighted boundaries for time history

The performance of sub-system model was validated under the loadcases considered, front NCAP, front ODB, rear ODB, IIHS side and pole impacts, to confirm that it behaved as the full model did. The energy absorbed by the rocker under the loading conditions considered was used as the performance target. Figure 10.5 shows such validation results for IIHS side and pole impacts.



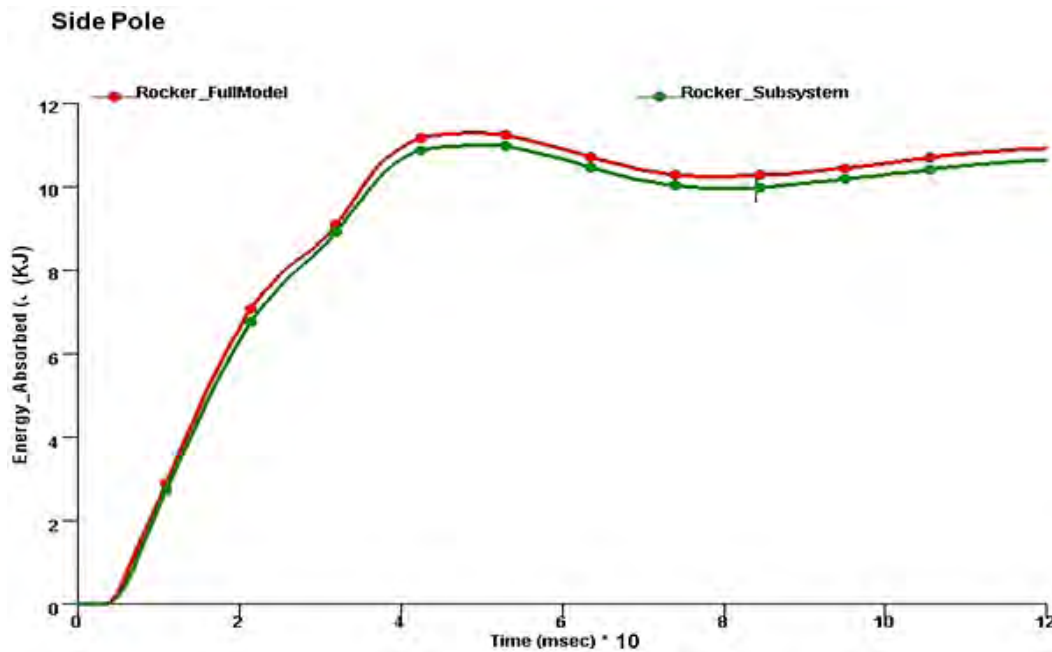


Figure 10.5: Sub-System performance validation

10.6.3 Stamped Rocker Concept

10.6.3.1 Grade and Gauge Geometry Design Space

The stamped rocker concept consists of a rocker outer which is also part of the body side outer, a rocker reinforcement and a rocker inner. Each component was divided into 5 regions. Referring to Figure 10.6; these are shown as regions A through E. The choices of number of regions are based on engineering judgment, difficulty of manufacturing; complexity of joining and assembly and number of design variables (optimization time). The choice of grade and gauge of each region could be varied independently of the others. Details of the available grade and gauge choices are listed in Table 10.2.

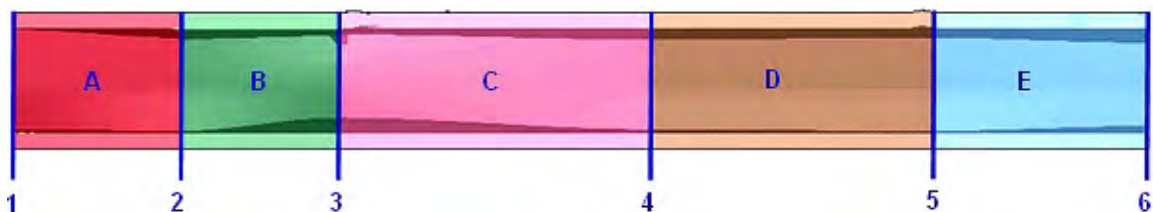


Figure 10.6: Stamped rocker concept - zones of grade and gauge variation

STAMPED ROCKER GAUGE CHOICES			STAMPED ROCKER GRADE CHOICES	
FROM	0.5 mm (INNER & OUTER)	In 0.01 mm increments	ULTIMATE TENSILE (MPa)	MAT 270
	0.2 mm (REINFORCEMENT)			MAT 340
TO	2.0 mm			MAT 450
		MAT 500		
		MAT 600		
		MAT 800		
		MAT 1000		
		MAT 1300		
		MAT 1500		

Table 10.2: Stamped rocker concept available grade and gauge choices

In the above table the gauge of 0.2 was chosen as minimum for the reinforcement in order to allow the optimization to eliminate a part. Therefore any part that was picked by the process to be 0.2 mm, indicates elimination of that part. Numbers smaller than 0.2 mm would cause instability in the analysis.

10.6.3.2 Geometry Parameterization

The geometry design space is limited as an outer boundary package space established in chapter 4. Referring to Figure 10.6, the cross-section at locations 1 through 6 can be varied independently of each other. Thus for each region, A through E, the shape will vary along the length of the region based on the cross sections at each end. The range of the packaging space for each cross section 1 through 6 is shown in Figure 10.7.

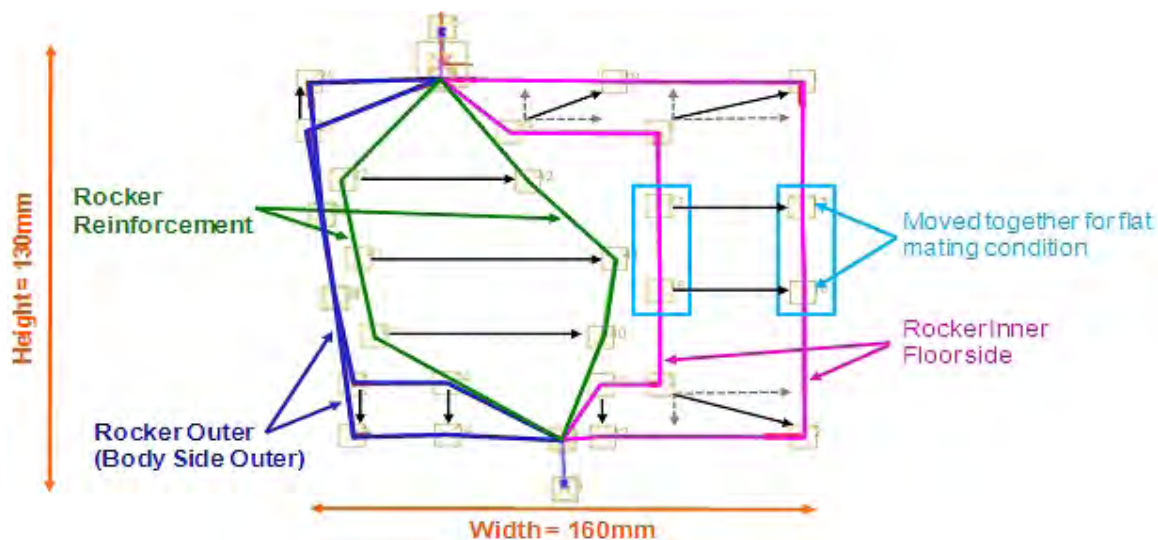


Figure 10.7: Stamped rocker concept cross-sectional parameterization

10.6.3.3 Optimization Setup

- Objective: The optimization objective is to maintain the performance of the rocker so that the total strain energy remains the same as the LF3G for front NCAP, front ODB, rear ODB, IIHS side and pole impacts. The mass of the LF3G rocker is 12.4 kg.
- Target: The optimization target is to minimize the mass of the rocker.
- Constraint: The energy absorbed by the rocker in the LF3G model (full model) was used as a constraint for the optimization. For load cases that experience plastic deformation, the energy absorbed was maintained at $\pm 15\%$ of the LF3G's performance. For load cases that resulted in elastic deformation in the rocker structure, the energy absorbed was maintained at a level less than that of LF3G's performance. Thus for IIHS side and pole impacts, the energy absorption was held at $\pm 15\%$ of energy absorption for the LF3G and for front NCAP, front ODB and rear ODB impacts the energy absorption target was ≤ 650 J. (For further information on target energy value calculations, refer to Appendix 20.3 for details)

10.6.3.4 Stamped Rocker: Design Solution

All results from the optimization are compared to the baseline LF3G rocker. Figure 10.8 and Figure 10.9 show the deformation of the baseline LF3G design and the optimized stamped concept for front NCAP, front ODB, rear ODB, IIHS side and pole impacts. It clearly shows that for the front NCAP, front ODB and rear ODB there is limited deformation of the rocker. In these cases, the rocker is just absorbing the elastic energy. In the case of IIHS side and pole impacts, the rocker has considerable plastic deformation leading to high strain energy absorption by the rocker.

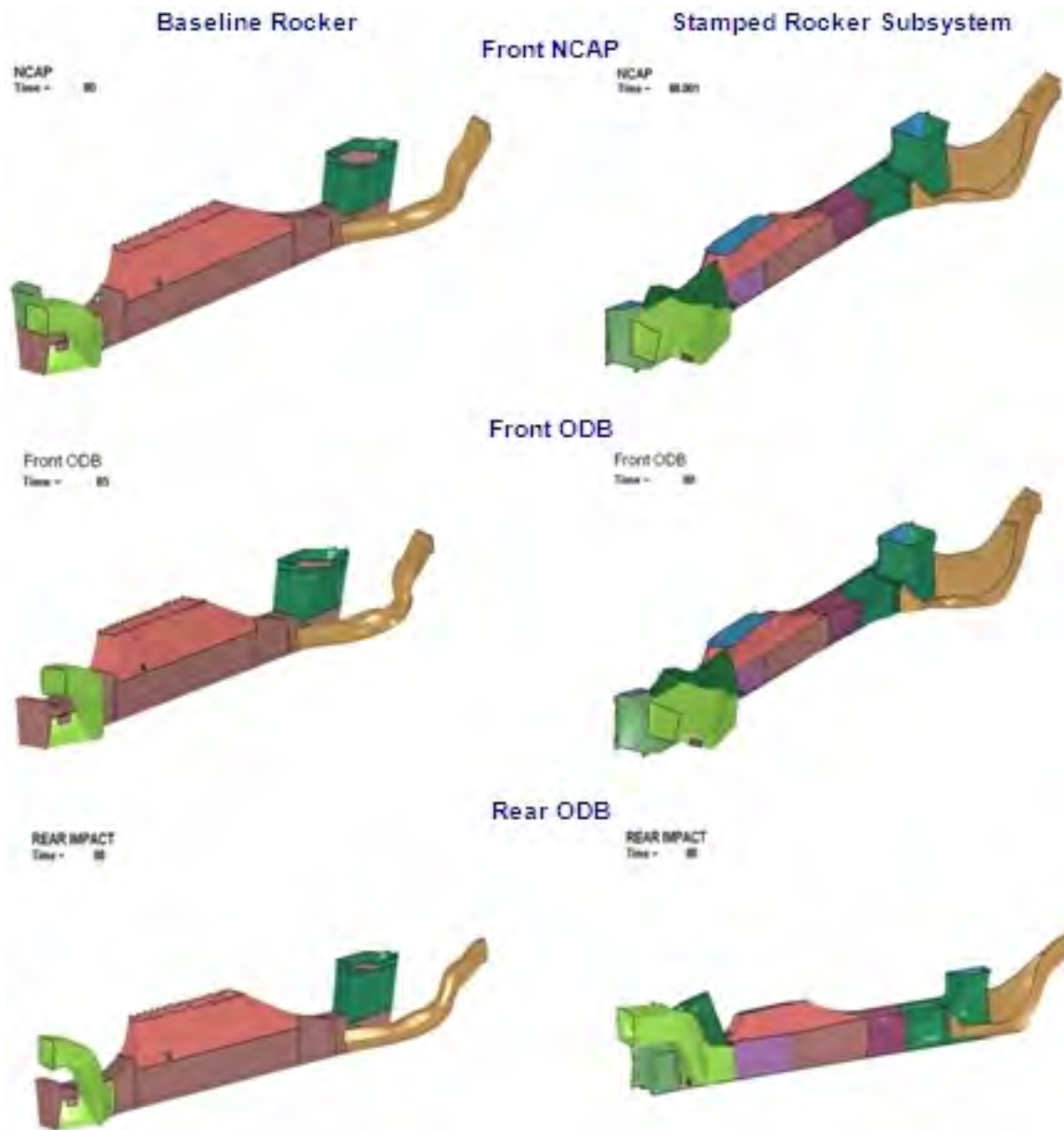


Figure 10.8: Stamped rocker design solution deformation comparison to baseline

10.6 Rocker Sub-System

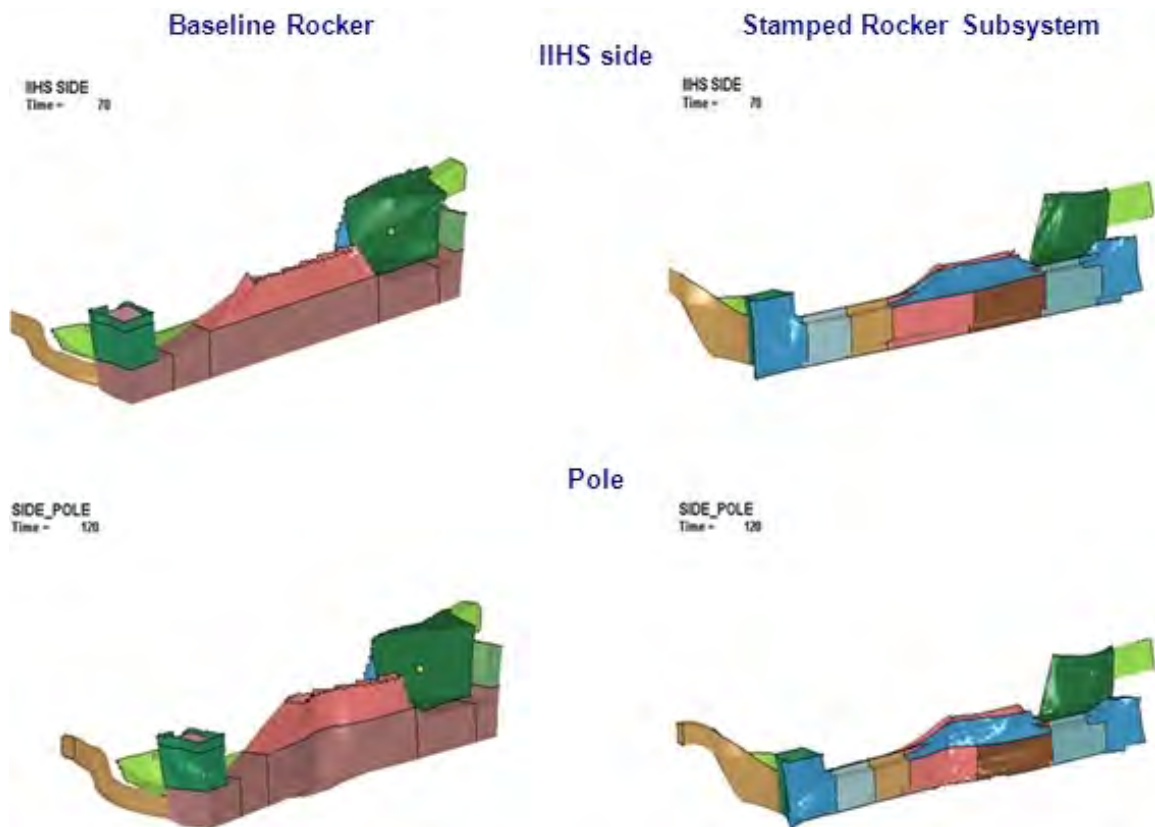


Figure 10.9: Stamped rocker design solution deformation comparison to baseline

Figure 10.10 , Figure 10.11 and Figure 10.12 show the comparison of energy absorption for the baseline LF3G rocker compared to the optimized stamped rocker concept. In the case of the front NCAP, front ODB and rear ODB impacts the energy absorbed by the stamped rocker concept is purely elastic energy as there is limited deformation. The total energy of the system has been maintained and so the kinetic energy has been absorbed in the rocker as elastic energy. In the case of pole impact, the rocker experienced significant deformation resulting in a high amount of strain energy absorption.

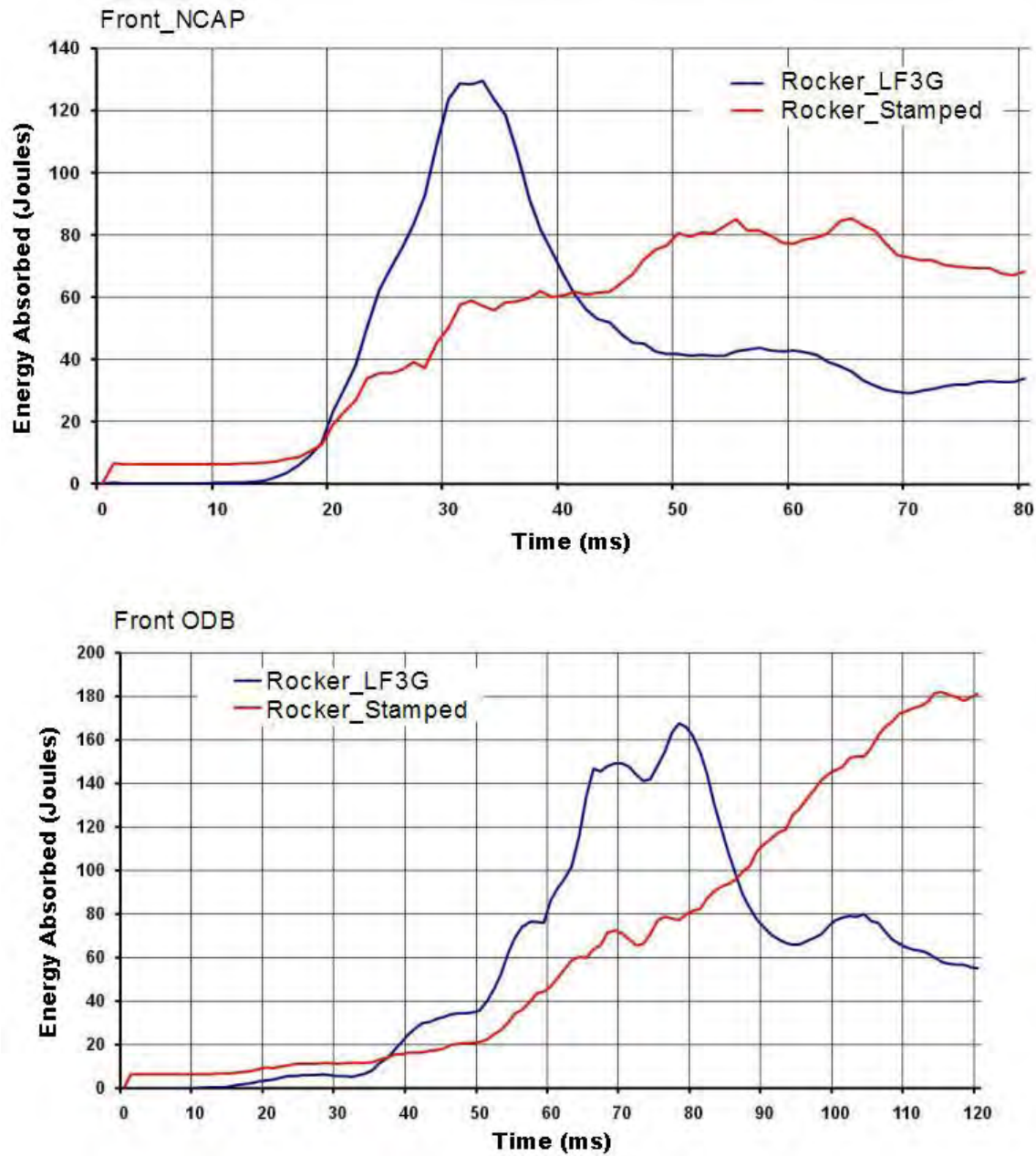


Figure 10.10: Stamped rocker design solution - energy absorption comparison to baseline

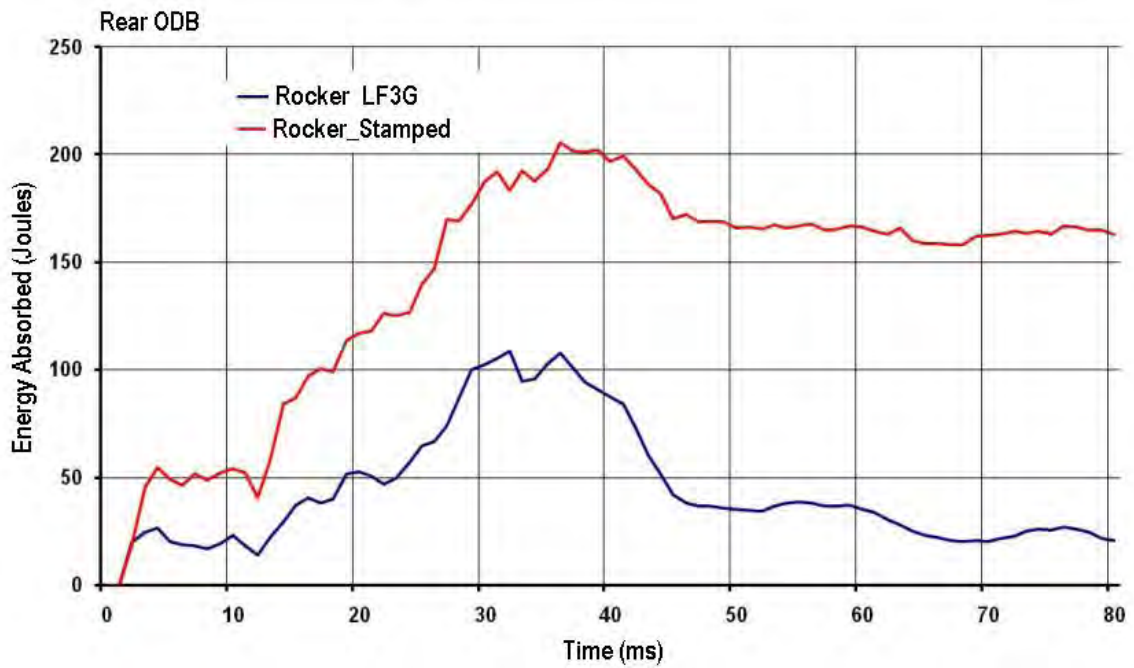


Figure 10.11: Stamped rocker design solution - energy absorption comparison to baseline (contd.)

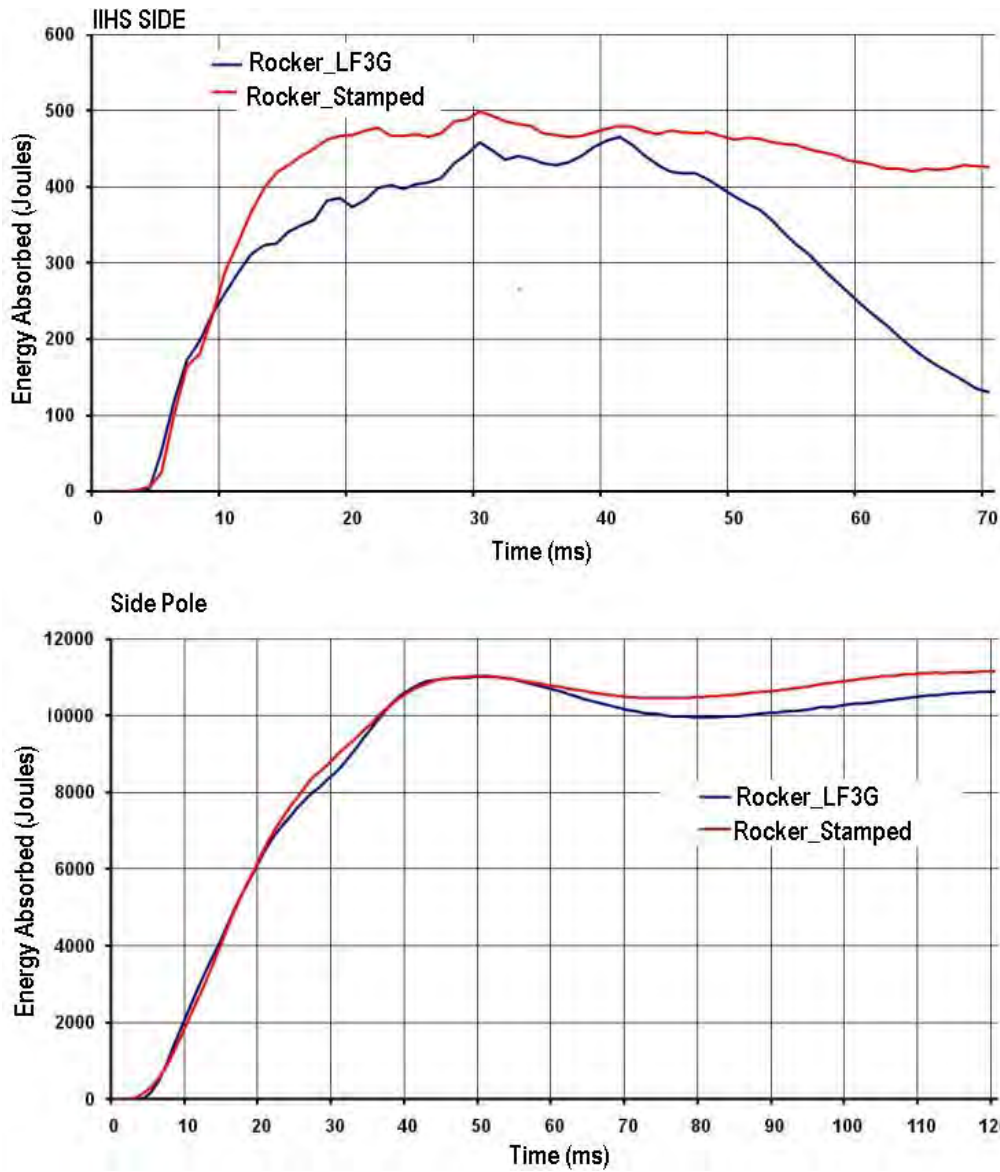


Figure 10.12: Stamped rocker design solution - energy absorption comparison to baseline

Figure 10.13 shows the geometry, grade and gauge selections for the stamped rocker design solution. The final mass for this design solution was 9.5 kg, which is a 24% mass reduction compared to the baseline design (12.4 kg).

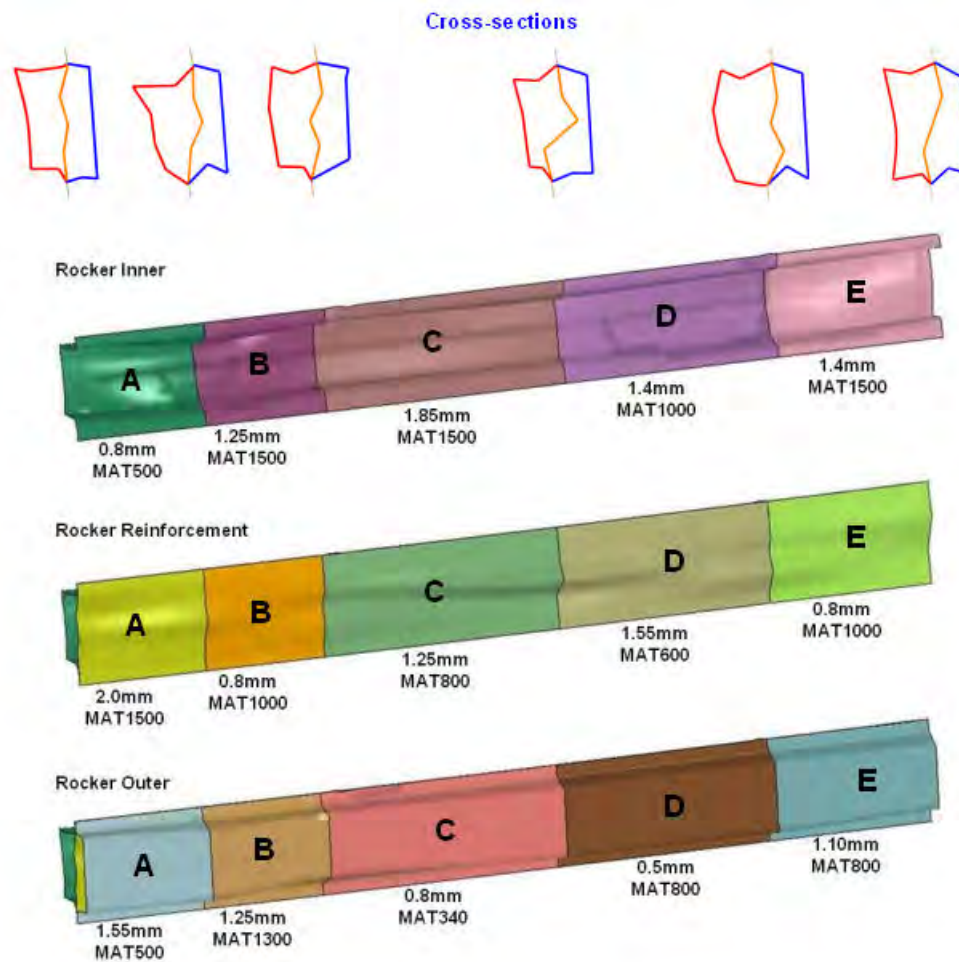


Figure 10.13: Stamped rocker design solution final grade and gauge selections

10.6.4 Hydroformed Rocker Concept

The complete sub-system optimization process for the rocker has already been discussed previously. Here the only differences in the grade and gauge selection and geometry parameterization for this concept are discussed.

10.6.4.1 Grade and Gauge Geometry Design Space

The hydroformed rocker concept consists of a rocker outer, which is also part of the body side outer and a rocker inner. There is no rocker reinforcement. Each component was divided into five regions. Referring to Figure 10.14; these are shown as regions A through E. The choice of grade and gauge of each region could be varied independently of the others. Details of the available grade and gauge choices are listed in Table 10.3. Note that for hydroforming, material variation is limited to an ultimate tensile strength of 1000 MPa.

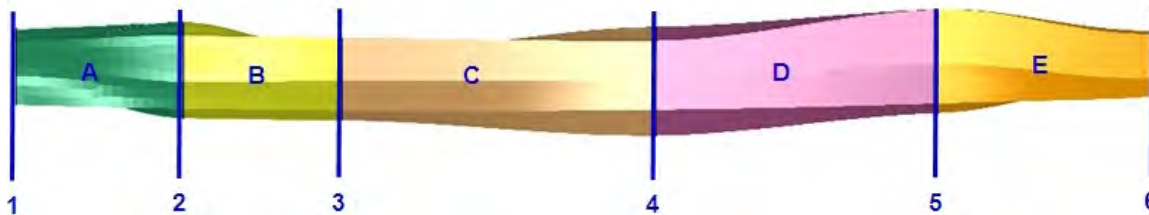


Figure 10.14: Hydroformed rocker concept - zones of grade and gauge variation

HYDROFORMED ROCKER GAUGE CHOICES			HYDROFORMED ROCKER GRADE CHOICES	
FROM	0.5 mm (INNER & OUTER)	In 0.01 mm increments	ULTIMATE TENSILE (MPa)	MAT 270
TO	2.0 mm			MAT 340
		MAT 450		
		MAT 500		
		MAT 600		
		MAT 800		
		MAT 1000		

Table 10.3: Hydroformed rocker concept available grade and gauge choices

10.6.4.2 Geometry Parameterization

Referring to Figure 10.14, the cross-section at locations 1 through 6 can be varied independently of each other and so the shape will vary along the length of each region, A through E, based on the cross sections at each end. The range of the packaging space for each cross section 1 through 6 is shown in Figure 10.15.

10.6 Rocker Sub-System

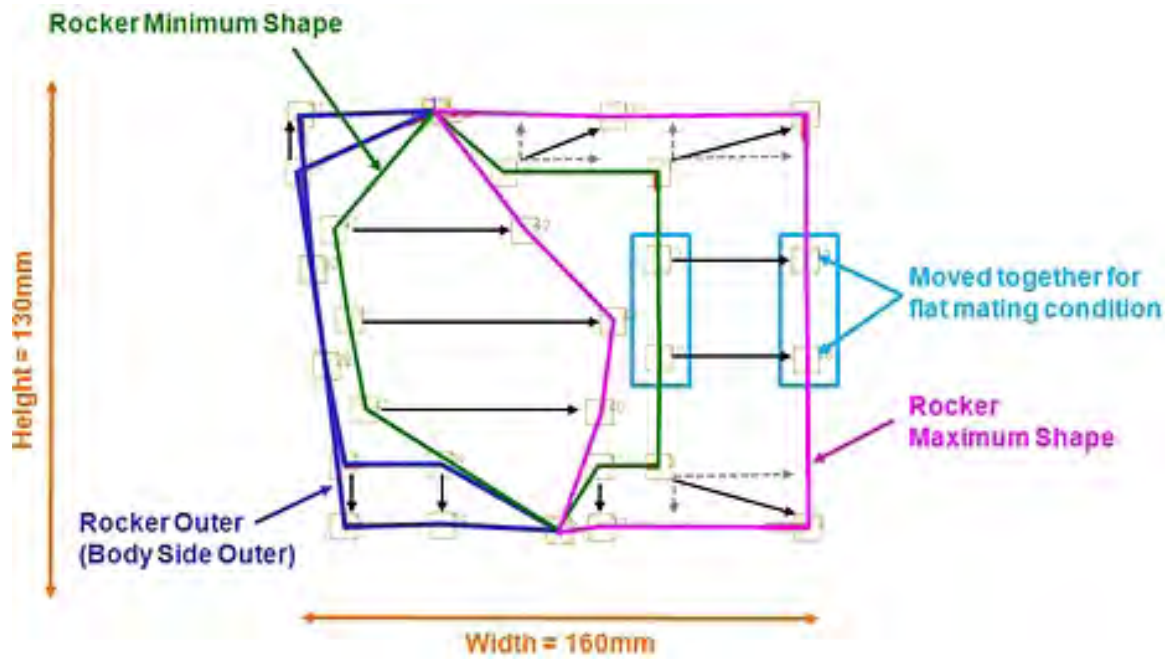


Figure 10.15: Hydroformed rocker concept - cross-sectional parameterization

10.6.4.3 Hydroformed Rocker: Design Solution

All results from the optimization are compared to the baseline LF3G rocker. Figure 10.16 and Figure 10.17 show the deformation of the baseline LF3G design and the optimized hydroformed concept for front NCAP, front ODB, rear ODB, IIHS side and pole impacts. It clearly shows that for the front NCAP, front ODB and rear ODB there is limited deformation of the rocker. In these cases, the rocker is just absorbing the elastic energy. In the case of IIHS side and pole impacts, the rocker has considerable plastic deformation leading to high strain energy absorption by the rocker.

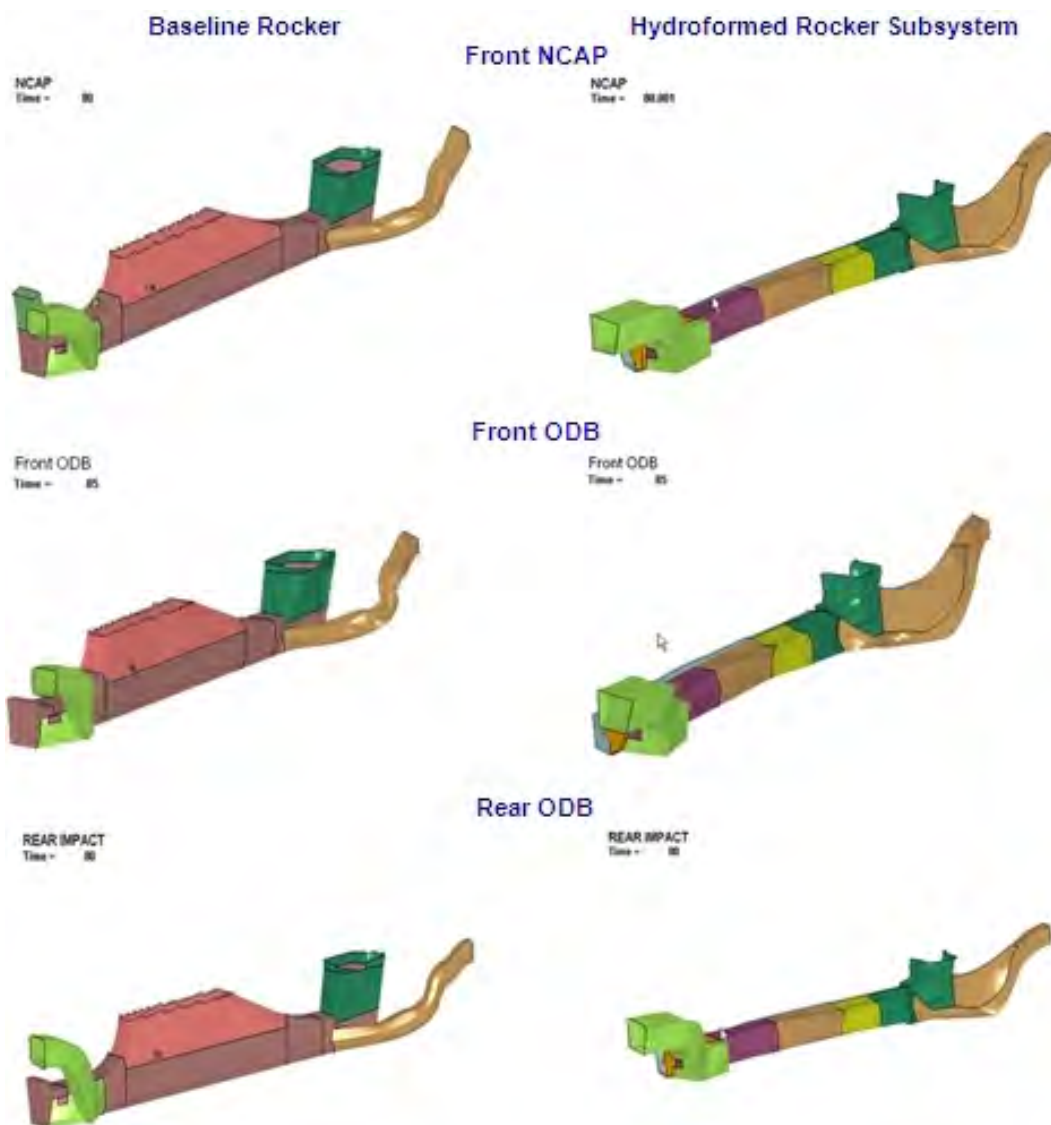


Figure 10.16: Hydroformed rocker design solution deformation comparison to baseline

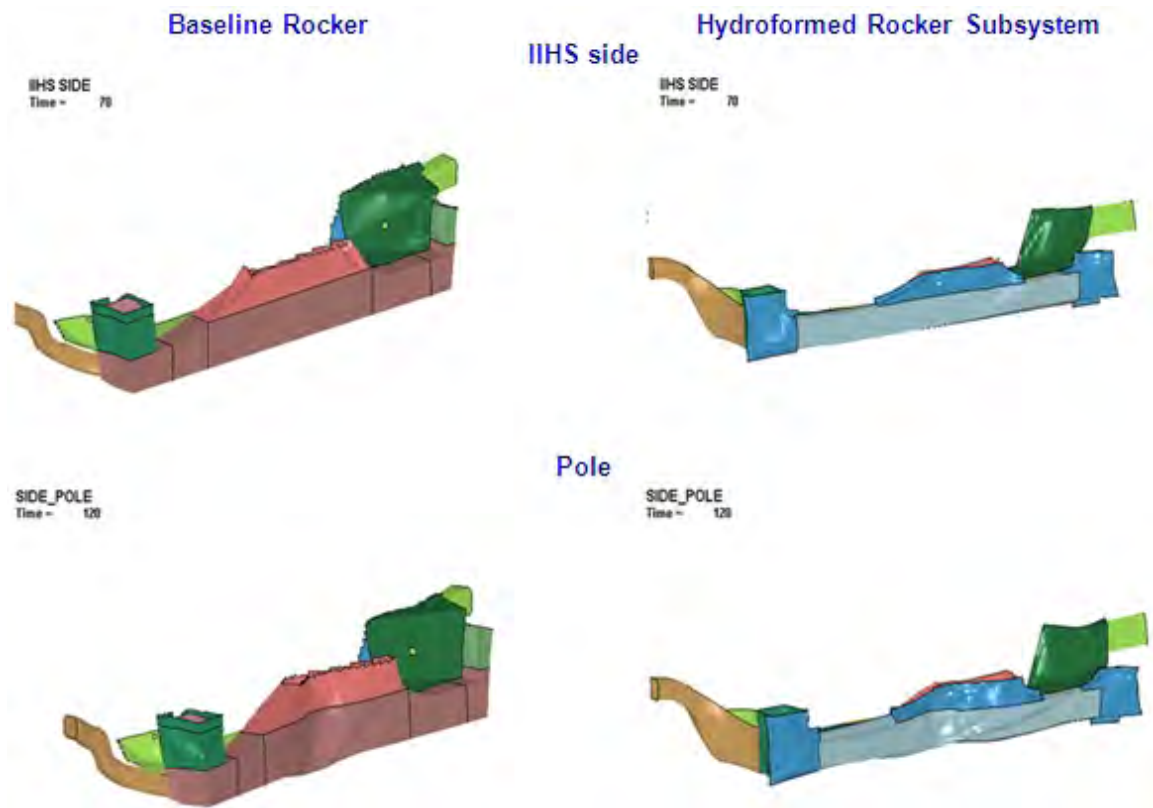


Figure 10.17: Hydroformed rocker design solution - deformation comparison to baseline

Figure 10.18, Figure 10.19 and Figure 10.20 show the comparison of energy absorption for the baseline LF3G rocker compared to the optimized hydroformed rocker concept. In case of the front NCAP, front ODB and rear ODB impacts the energy absorbed by the stamped rocker concept is purely elastic energy as there is limited deformation. The total energy of the system has been maintained and so the kinetic energy has been absorbed in the rocker as elastic energy. In the case of pole impact, the rocker experienced significant deformation resulting in a high amount of strain energy absorption.

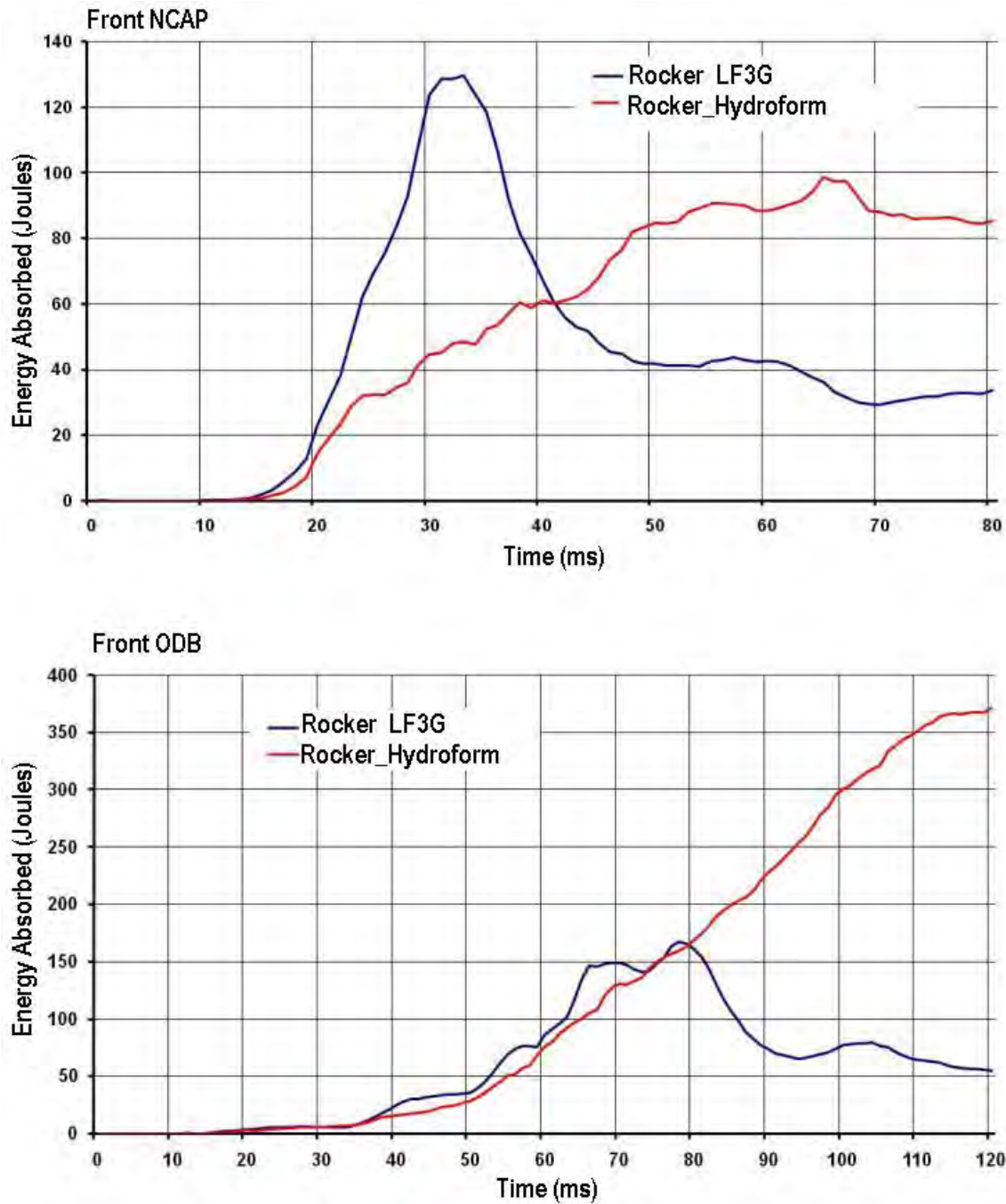


Figure 10.18: Hydroformed rocker design solution - energy absorption comparison to baseline

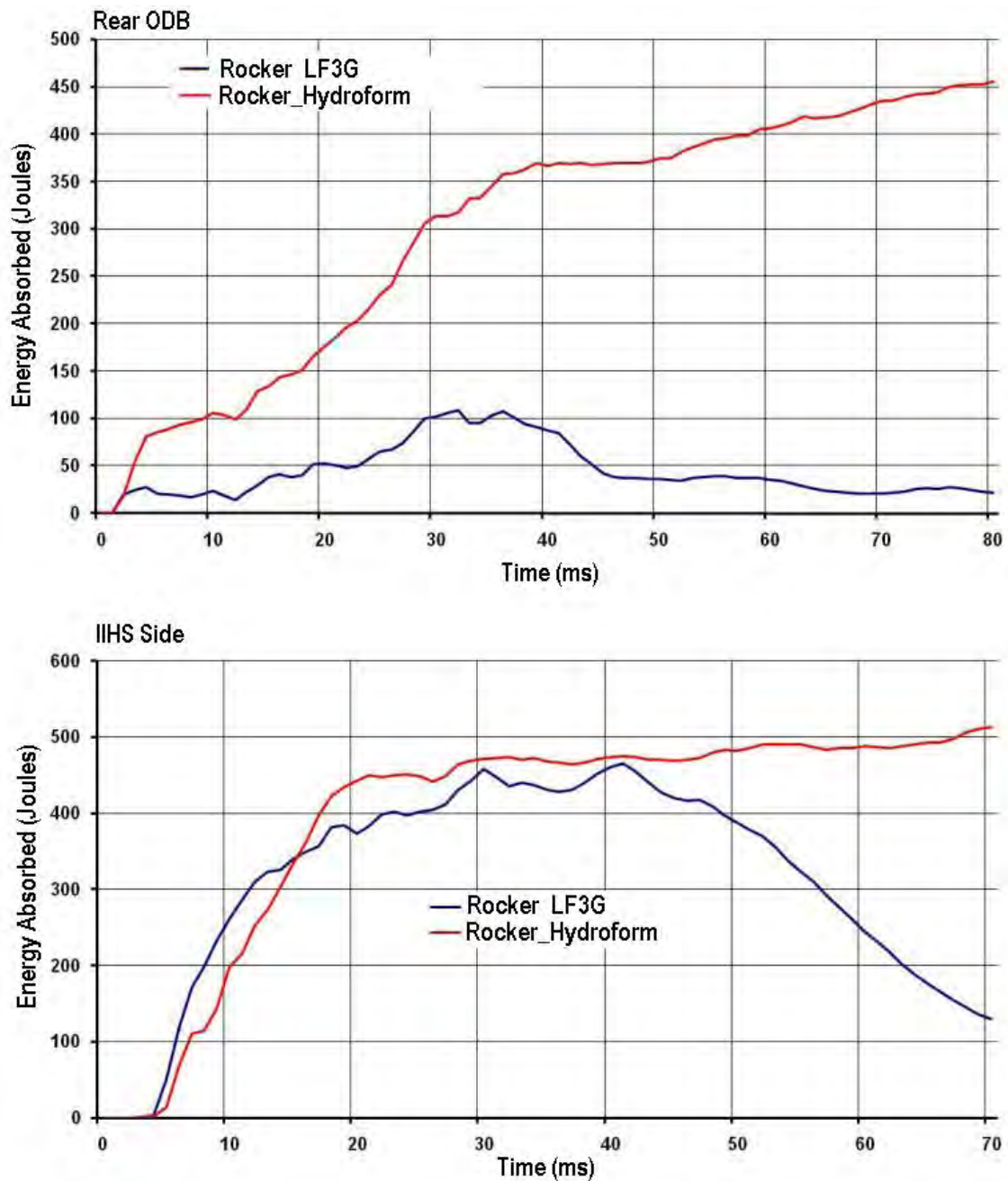


Figure 10.19: Hydroformed rocker design solution - energy absorption comparison to baseline

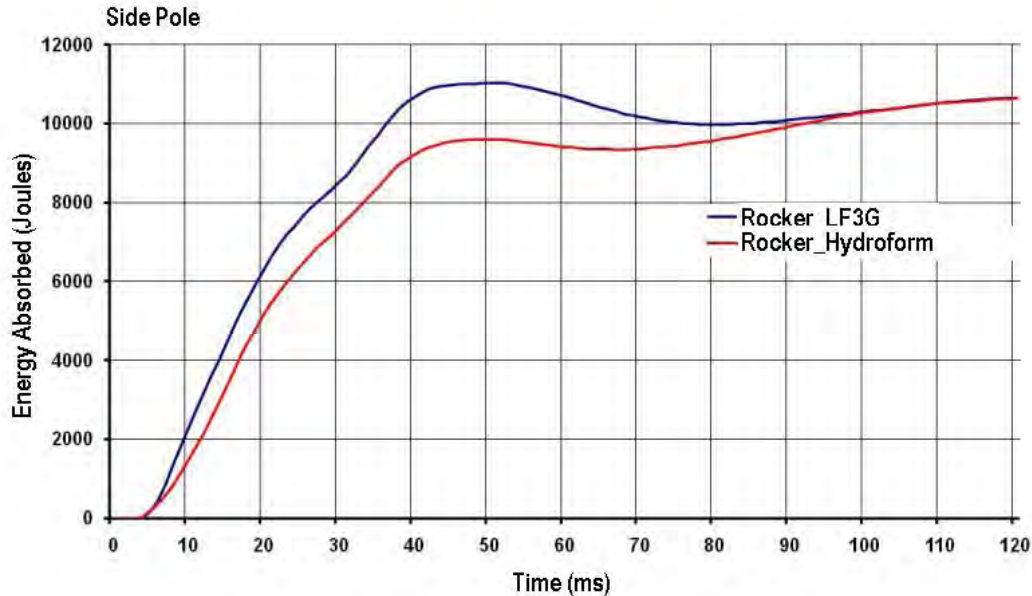


Figure 10.20: Hydroformed rocker design solution - energy absorption comparison to baseline (contd.)

Figure 10.21 shows the geometry, grade and gauge selections for the hydroformed rocker design solution. The final mass for this design solution was 6.8 kg, which is a 46% mass reduction compared to the baseline design (12.4 kg).

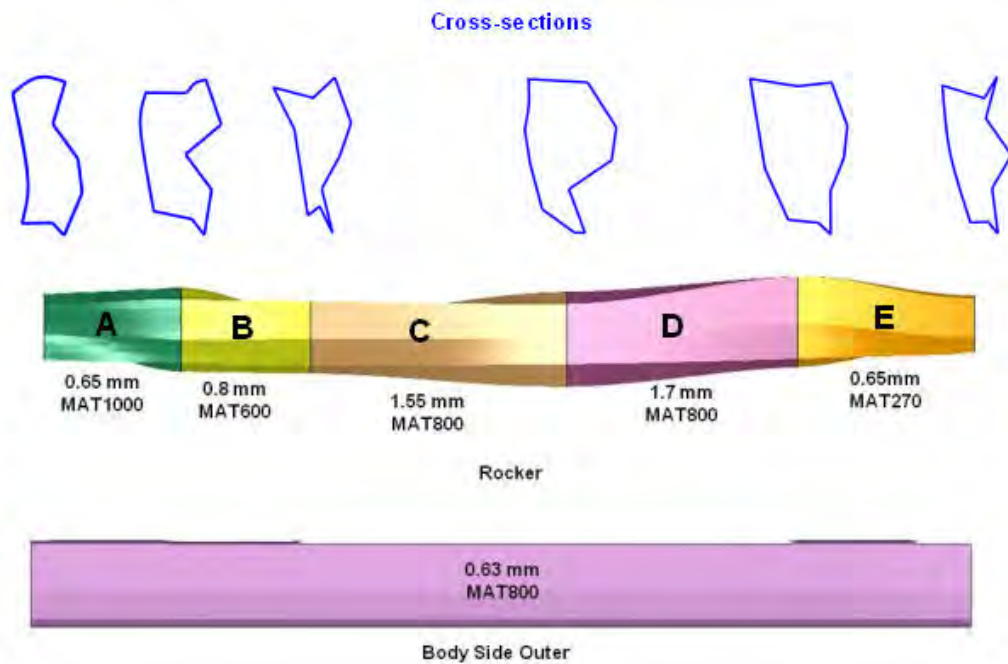


Figure 10.21: Hydroformed rocker design solution - final grade and gauge selections

10.6 Rocker Sub-System

10.6.5 Roll formed Rocker Concept

The complete sub-system optimization process for the rocker has already been discussed previously. Here the only differences in the grade and gauge selection and geometry parameterization for this concept are discussed.

10.6.5.1 Grade and Gauge Geometry Design Space

The roll formed rocker concept consists of a rocker outer, which is also part of the body side outer and a rocker inner, there is no rocker reinforcement. Each component was divided into 5 regions. Referring to Figure 10.22; these are shown as regions A through E. The choice of grade and gauge of each region could be varied independently of the others. Details of the available grade and gauge choices are listed in Table 10.4.



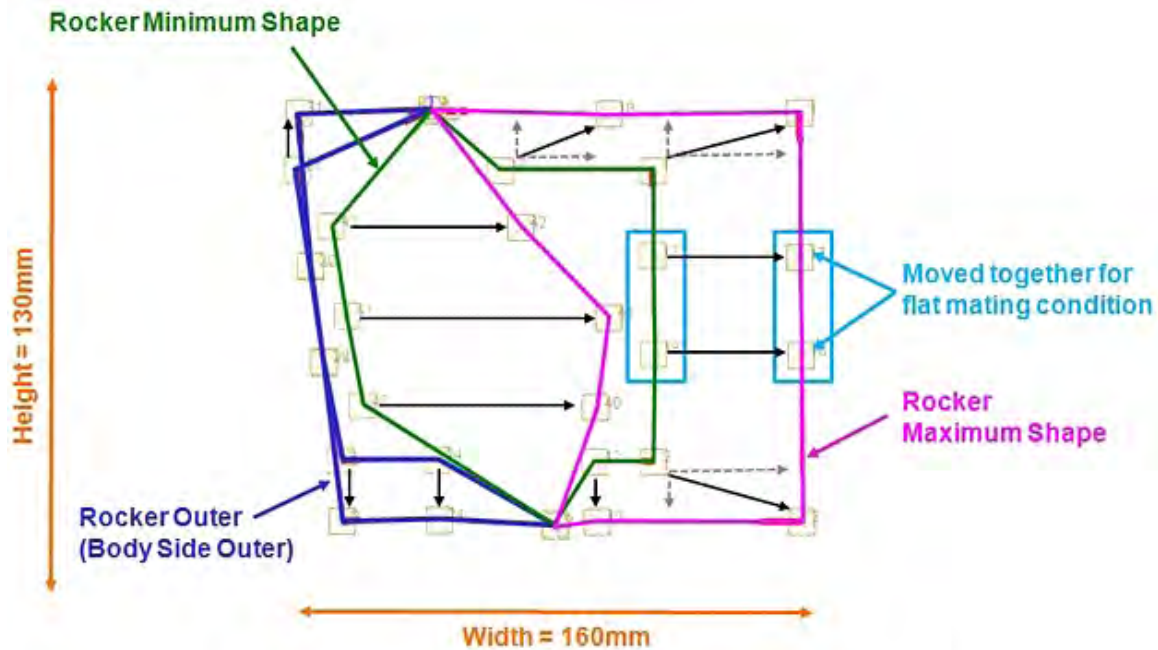
Figure 10.22: : Roll formed rocker concept - zones of grade and gauge variation

ROLL FORMED ROCKER GAUGE CHOICES			ROLL FORMED ROCKER GRADE	
FROM	0.5 mm (INNER & OUTER)	In 0.01 mm increments	ULTIMATE TENSILE (MPa)	MAT 270
TO	2.0 mm			MAT 340
		MAT 450		
		MAT 500		
		MAT 600		
		MAT 800		
		MAT 1000		
		MAT 1300		
		MAT 1500		

Table 10.4: Roll formed rocker concept - available grade and gauge choices

10.6.5.2 Geometry Parameterization

Unlike the previous rocker concepts, in this case though the shape of the cross section can be varied it is held constant along the whole length of the rocker. The range of the packaging space to the cross section is shown in Figure 10.23.



Black Arrows Indicate Independent Point Movement From Min to Max

Figure 10.23: Roll formed rocker concept - cross-sectional parameterization

10.6.5.3 Roll Formed Rocker Design Solution

All results from the optimization are compared to the baseline LF3G rocker. Figure 10.24 and Figure 10.25 show the deformation of the baseline LF3G design and the optimized roll formed concept for front NCAP, front ODB, rear ODB, IIHS side and pole impacts. It clearly shows that for the front NCAP, front ODB and rear ODB there is limited deformation of the rocker. In these cases, the rocker is just absorbing the elastic energy. In the case of IIHS side and pole impacts, the rocker has considerable plastic deformation leading to high strain energy absorption by the rocker.

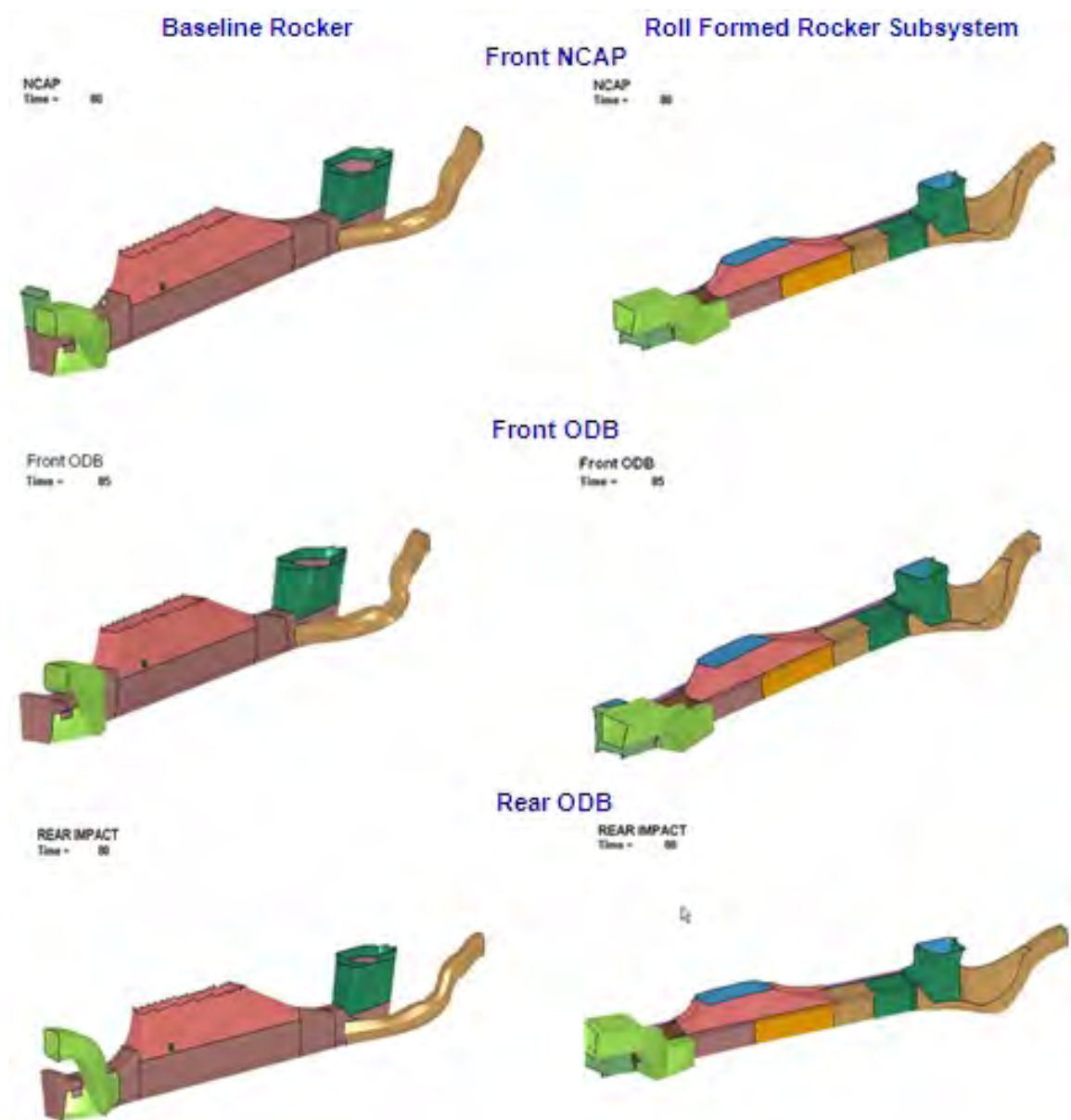


Figure 10.24: Roll formed rocker design solution - deformation comparison to baseline

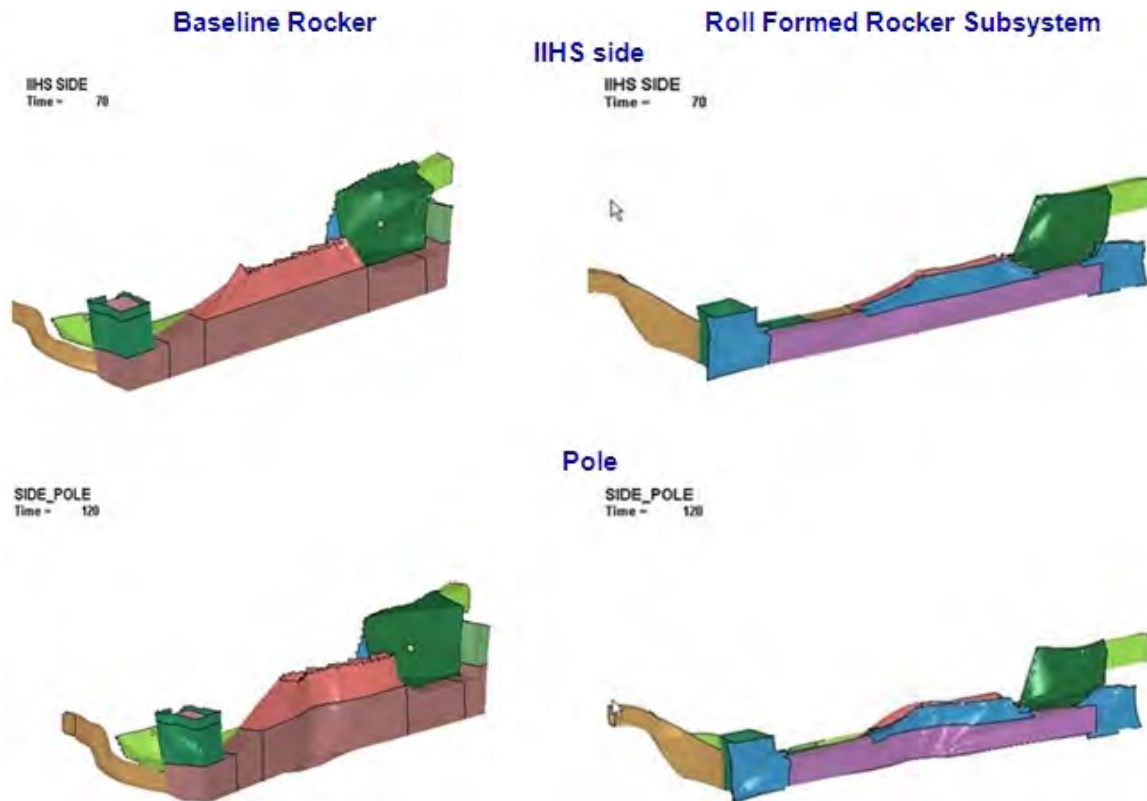


Figure 10.25: Roll formed rocker design solution - deformation comparison to baseline

Figure 10.26, Figure 10.27 and Figure 10.28 show the comparison of energy absorption for the baseline LF3G rocker compared to the optimized roll formed rocker concept. In case of the front NCAP, front ODB and rear ODB impacts the energy absorbed by the stamped rocker concept is purely elastic energy as there is limited deformation. The total energy of the system has been maintained and so the kinetic energy has been absorbed in the rocker as elastic energy. In the case of pole impact, the rocker experienced significant deformation resulting in a high amount of strain energy absorption.

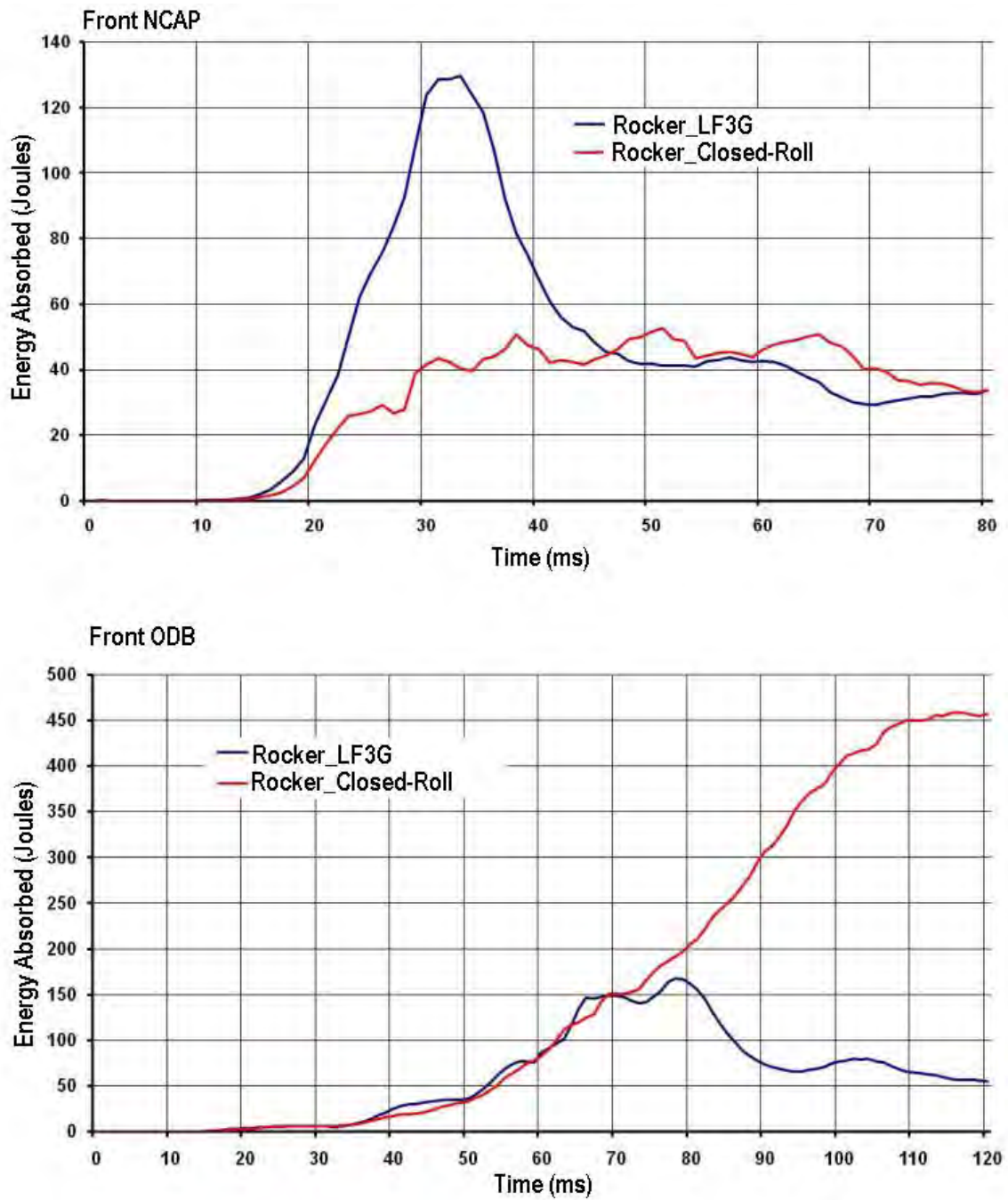


Figure 10.26: Roll formed rocker design solution - energy absorption comparison to baseline

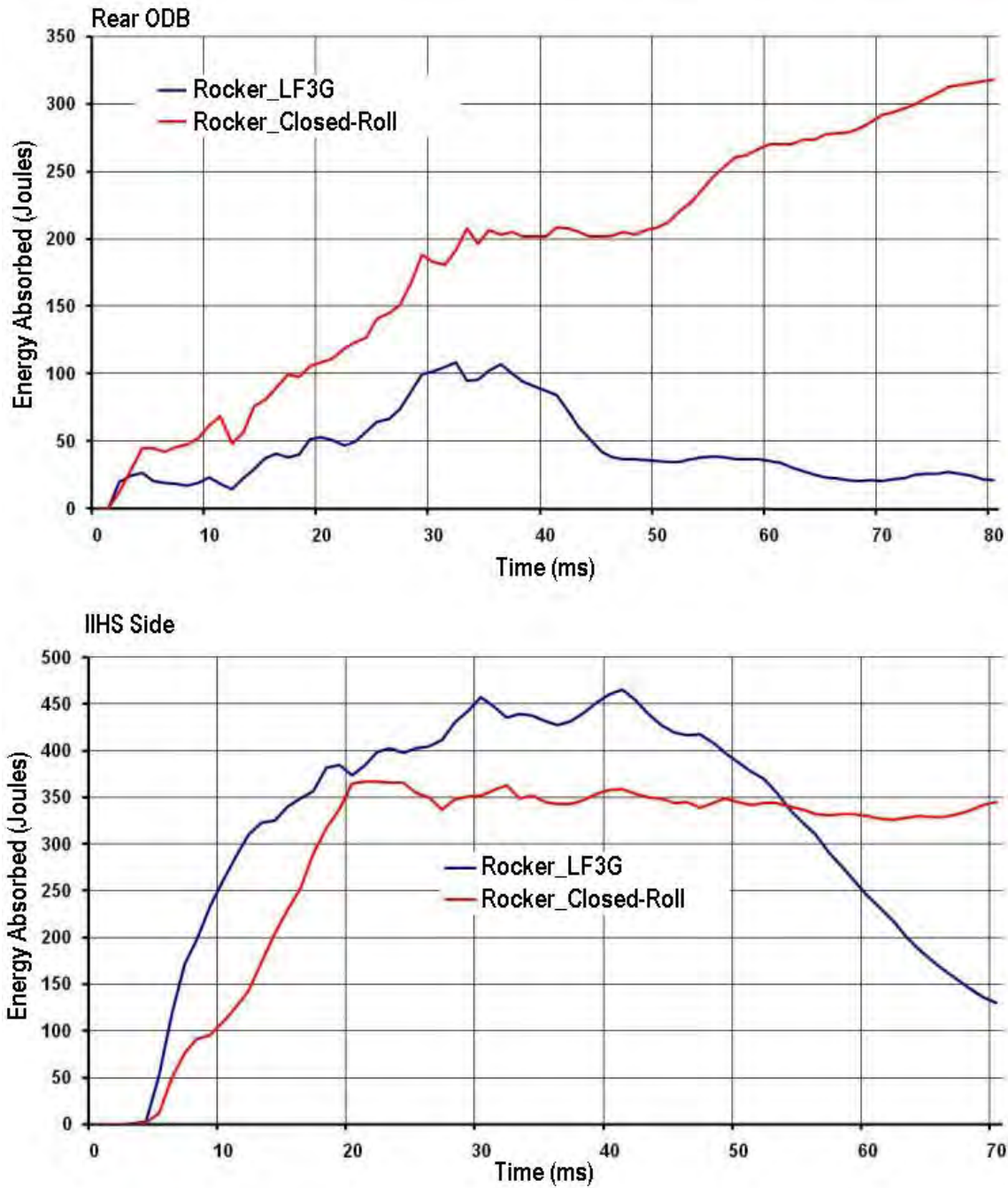


Figure 10.27: Roll formed rocker design solution - energy absorption comparison to baseline

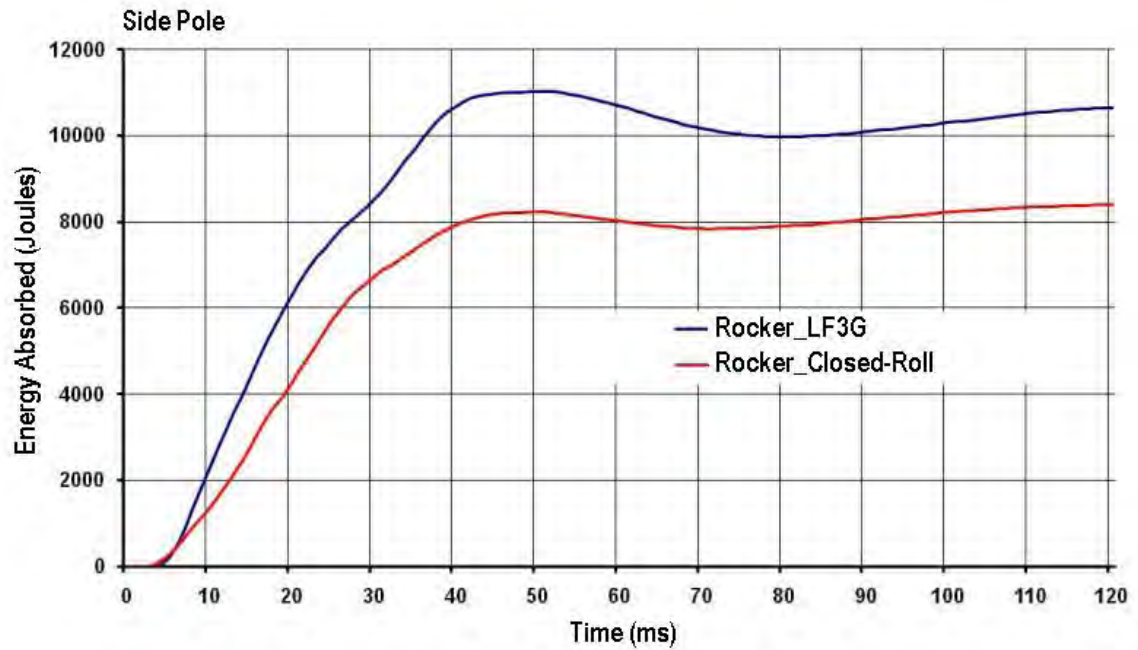


Figure 10.28: Roll formed rocker design solution - energy absorption comparison to baseline (contd.)

Figure 10.29 shows the geometry, grade and gauge selections for the roll formed rocker design solution. The final mass for this design solution was 7.3 kg, which is a 42% mass reduction compared to the baseline design (12.4 kg).

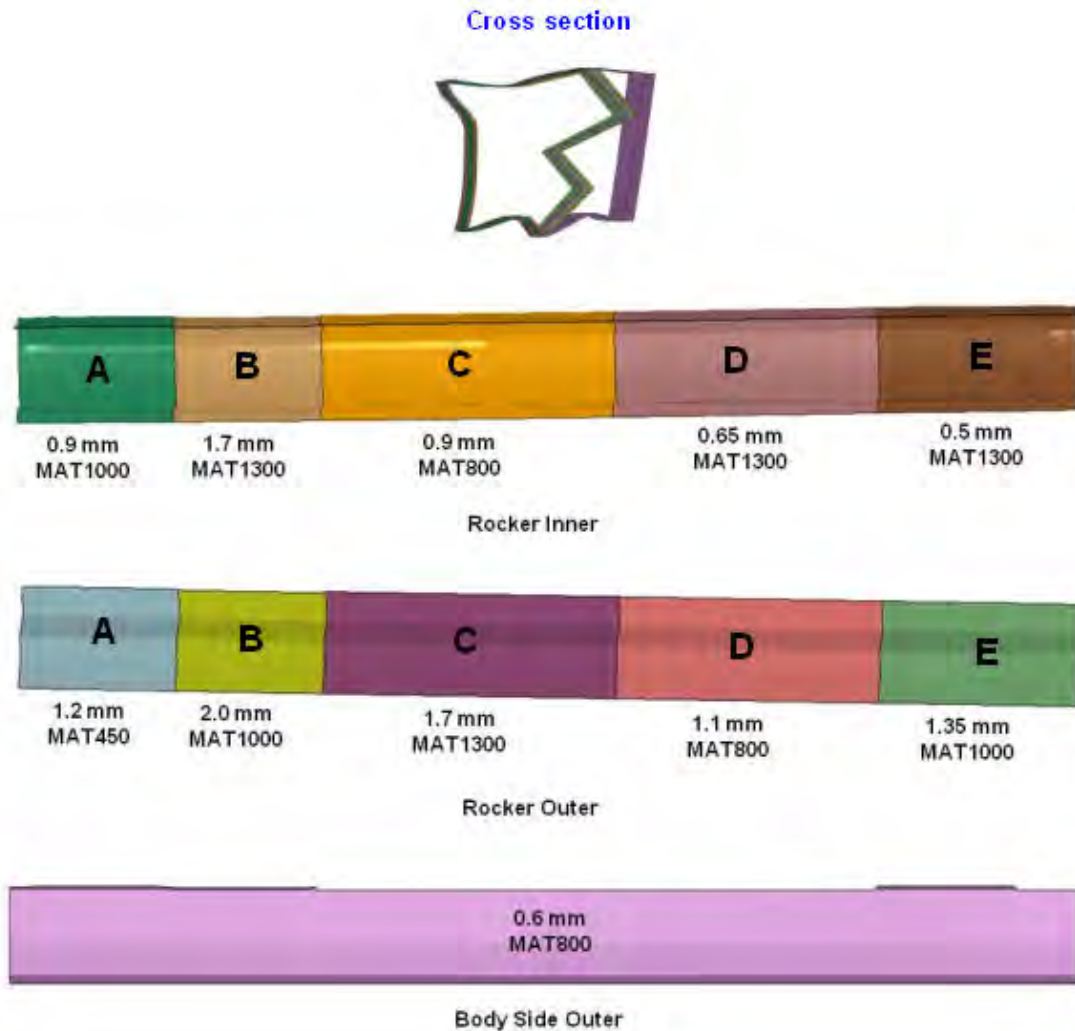


Figure 10.29: Roll formed rocker design solution - final grade and gauge selections

10.6.6 Extruded Aluminum Rocker Concept

10.6.6.1 Grade and Gauge Geometry Design Space

The extruded aluminum rocker concept consists of a rocker outer, which is separate from the steel body side outer, a rocker inner and a rocker reinforcement. See Figure 10.30. This is an extruded concept and so there is no variation in gauge along the length of the component, only differences in cross section are allowed. There is no variation in the grade of aluminum.

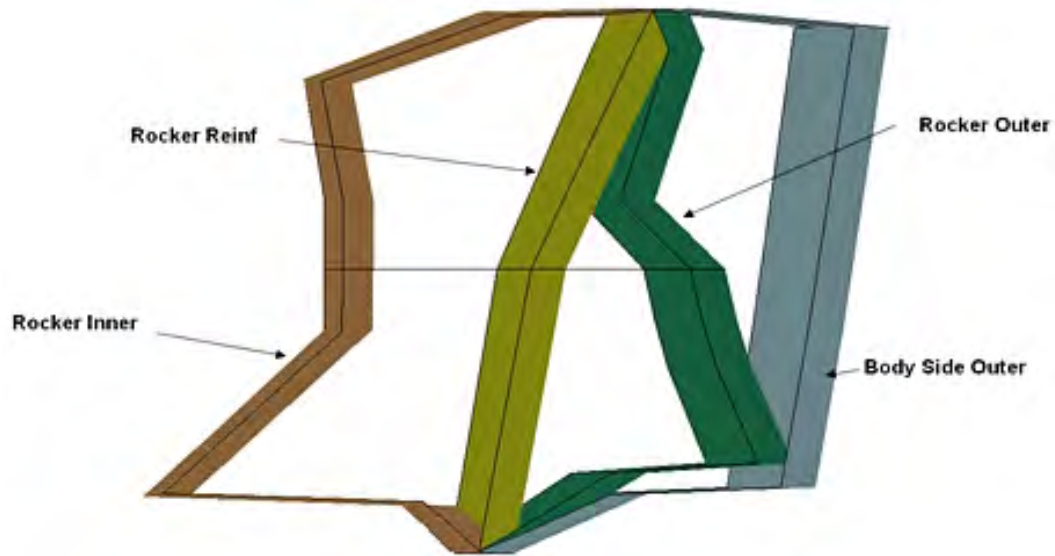


Figure 10.30: Extruded aluminum rocker concept - design space

Details of the available grade and gauge choices for the rocker and body side outer are listed in Table 10.5.

EXTRUDED ALUMINUM ROCKER GAUGE CHOICES			EXTRUDED ALUMINUM ROCKER GRADE CHOICES		EXTRUDED ALUMINUM ROCKER GRADE CHOICES (Steel Bodyside Outer Only)	
FROM	2.0 mm	In 0.01 mm increments	ALUMINUM GRADE	AL 6061	ULTIMATE TENSILE (MPa)	MAT 270
TO	6.0 mm					MAT 340
		MAT 450				
		MAT 500				
		MAT 600				
		MAT 800				
		MAT 1000				
		MAT 1300				
		MAT 1500				

Table 10.5: Extruded aluminum rocker concept available grade and gauge choices

10.6.6.2 Geometry Parameterization

This is an extruded concept and so though the shape of the cross section can be varied it is held constant along the whole length of the rocker. The range of the packaging space to the cross section is shown in Figure 10.31.

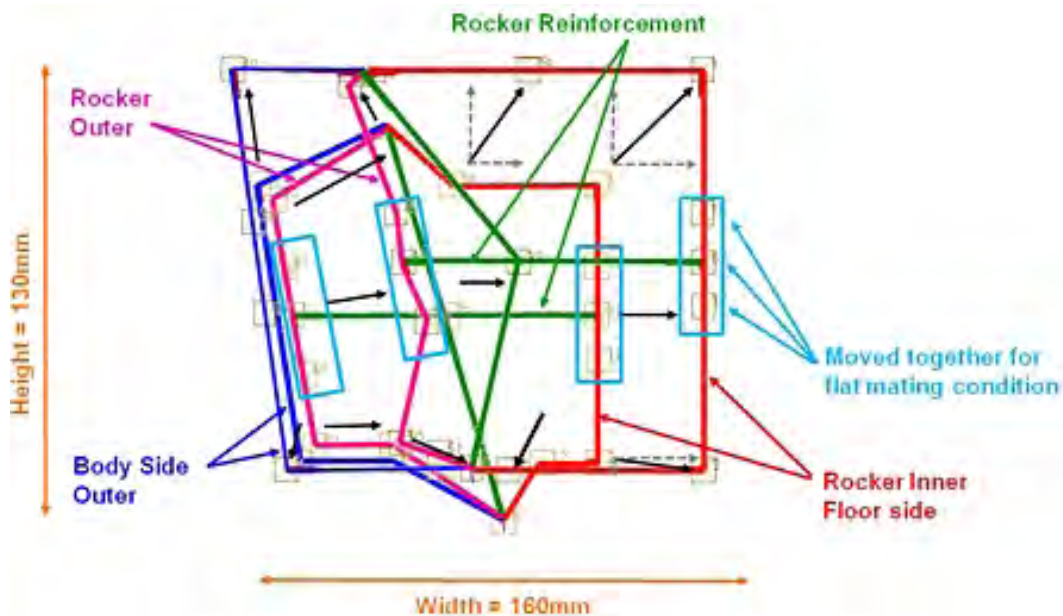


Figure 10.31: Extruded aluminum rocker concept - cross-sectional parameterization

10.6.6.3 Optimization Setup

- Objective: The optimization objective is to maintain the performance of the rocker so that the total strain energy remains the same as the LF3G for front NCAP, front ODB, rear ODB, IIHS side and pole impacts. The mass of the LF3G rocker is 12.4 kg.
- Target: The optimization target is to minimize the mass of the rocker.
- Constraint: The energy absorbed by the rocker in the LF3G model (full model) was used as a constraint for the optimization. However, because this is an aluminum concept, the energy values were recalculated from an updated version of the full LF3G model. In this case, the rocker material was revised from steel to aluminum. For load cases that experience plastic deformation, the energy absorbed was maintained at $\pm 15\%$ of the LF3G's performance. For load cases that result in elastic deformation, the energy absorbed was maintained at a level less than that of the LF3G's performance. Thus for IIHS side and pole impacts, the energy absorption was held at $\pm 15\%$ of energy absorption for the revised LF3G and for front NCAP, front ODB and rear ODB impacts the energy absorption target was ≤ 650 J. (For further information on target energy value calculations for aluminum, refer to Appendix 20.4 for details)

10.6.6.4 Extruded Aluminum Rocker Design Solution

All results from the optimization are compared to the baseline LF3G rocker. Figure 10.32 and Figure 10.33 show the deformation of the baseline LF3G rocker design and the optimized extruded aluminum rocker concept for front NCAP, front ODB, rear ODB, IIHS side and pole impacts. It clearly shows that for the front NCAP, front ODB and rear ODB there is limited deformation of the rocker. In these cases, the rocker is just absorbing the elastic energy. In the case of IIHS side and pole impacts, the rocker has considerable plastic deformation leading to high strain energy absorption by the rocker.

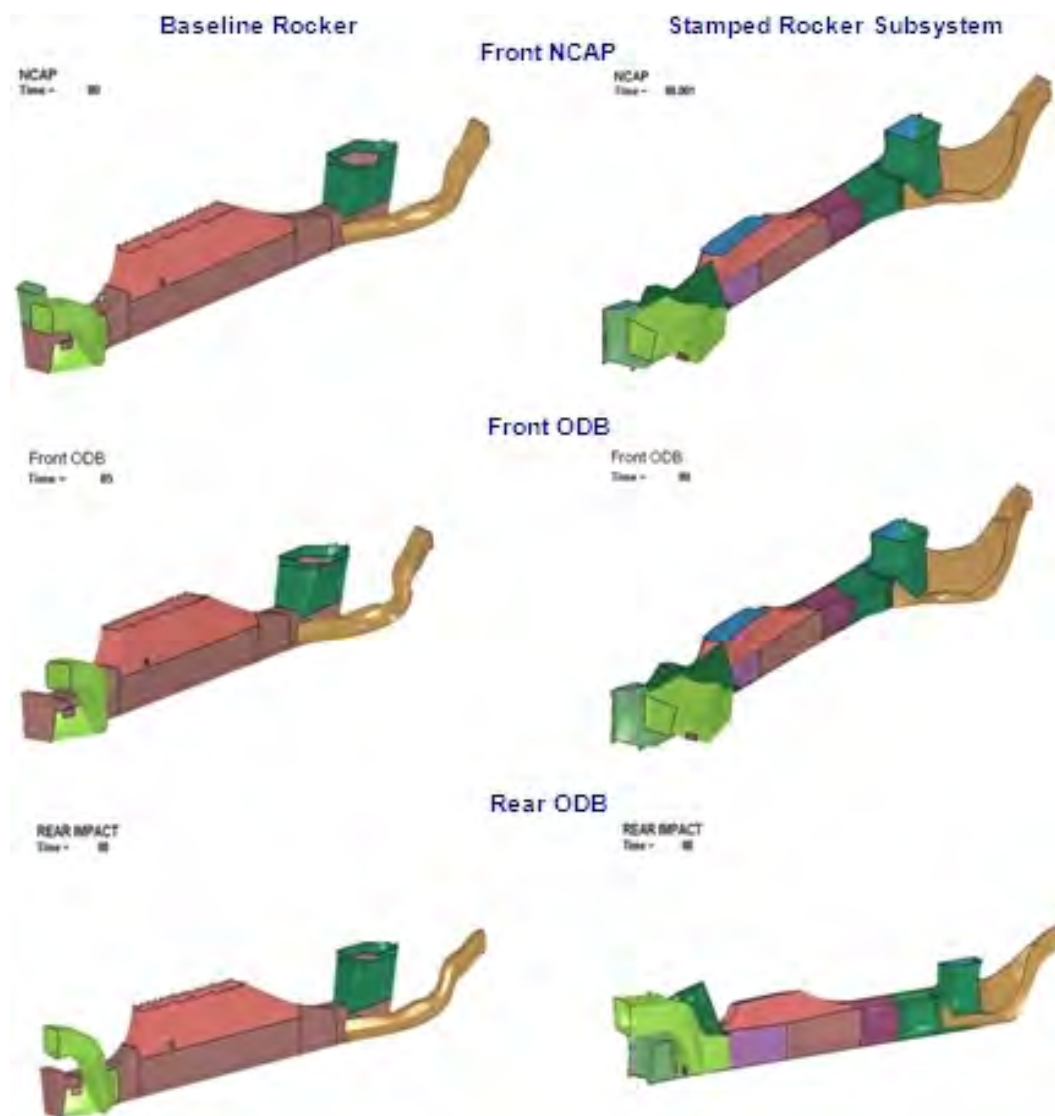


Figure 10.32: Extruded aluminum rocker design solution - deformation comparison to baseline

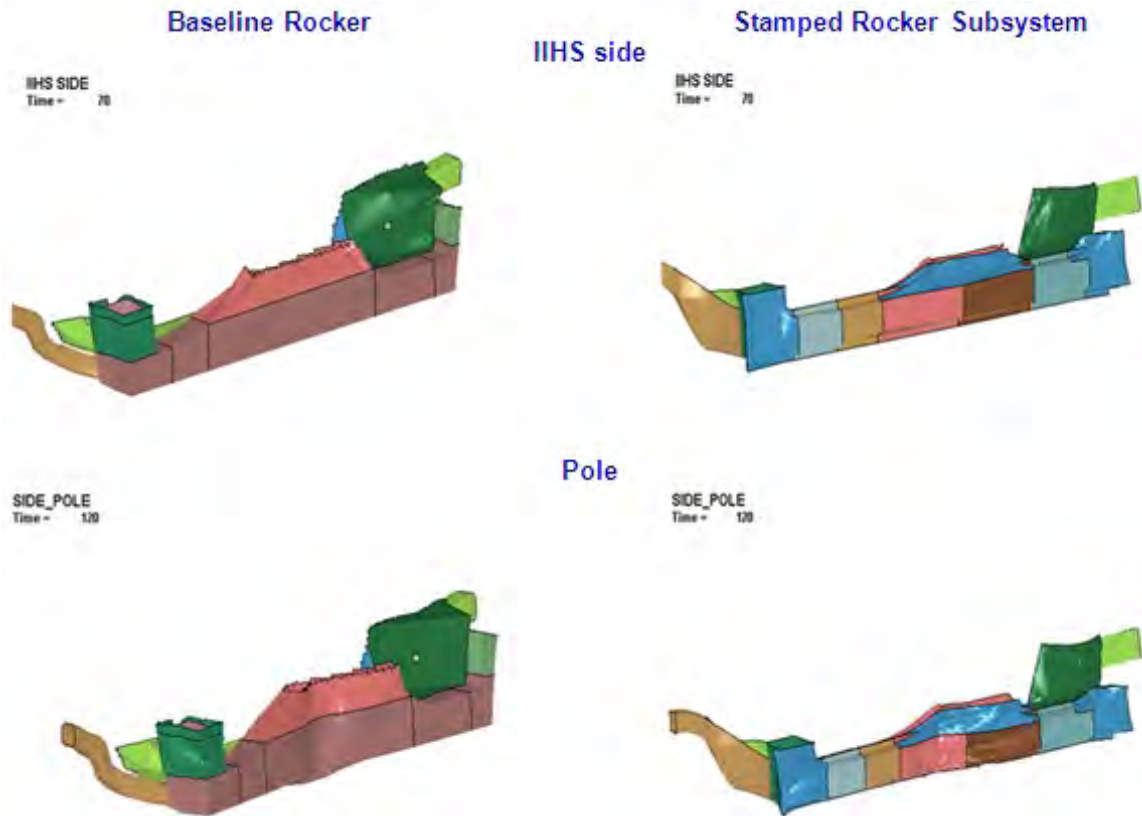


Figure 10.33: Extruded aluminum rocker design solution - deformation comparison to baseline

Figure 10.34, Figure 10.35 and Figure 10.36 show the comparison of energy absorption for the baseline LF3G rocker compared to the optimized extruded aluminum rocker concept. In case of the front NCAP, front ODB and rear ODB impacts the energy absorbed by the stamped rocker concept is purely elastic energy as there is limited deformation. The total energy of the system has been maintained and so the kinetic energy has been absorbed in the rocker as elastic energy. In the case of pole impact, the rocker experienced significant deformation resulting in a high amount of strain energy absorption.

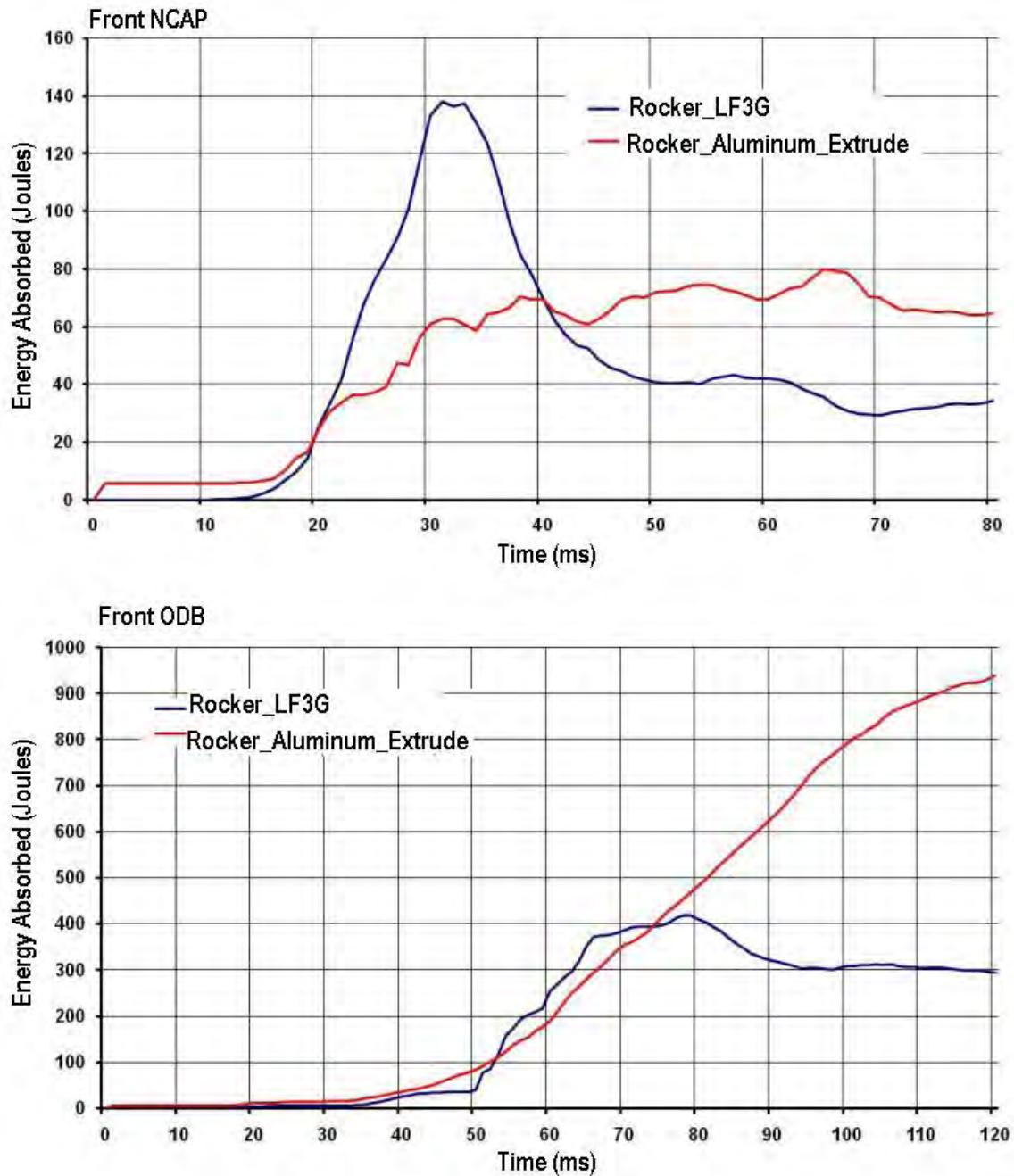


Figure 10.34: Extruded Aluminum Roll Rocker Design Solution - Energy Absorption Comparison to Baseline

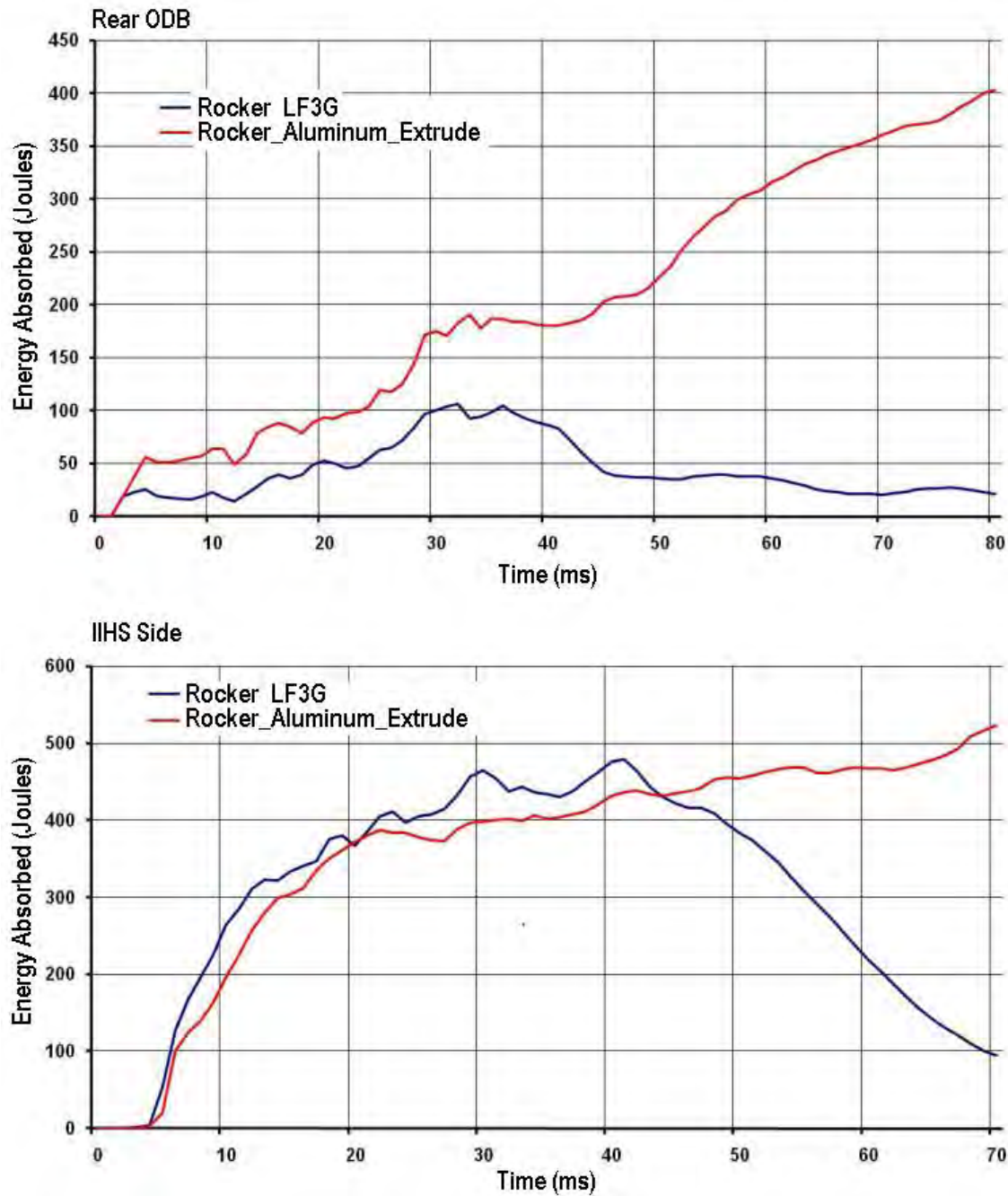


Figure 10.35: Extruded Aluminum Roll Rocker Design Solution - Energy Absorption Comparison to Baseline

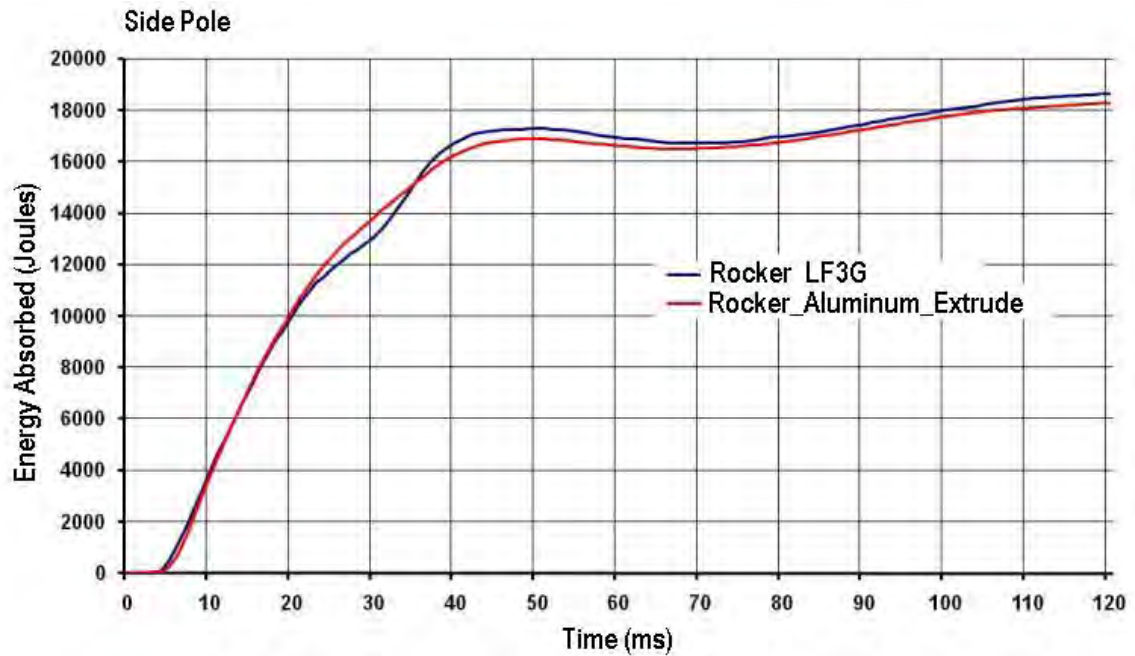


Figure 10.36: Extruded Aluminum Roll Rocker Design Solution - Energy Absorption Comparison to Baseline

Figure 10.37 below shows the geometry, grade and gauge selections for the extruded aluminum rocker design solution. The final mass for this design solution was 7.3 kg, which is a 42% mass reduction compared to the baseline design (12.4 kg).

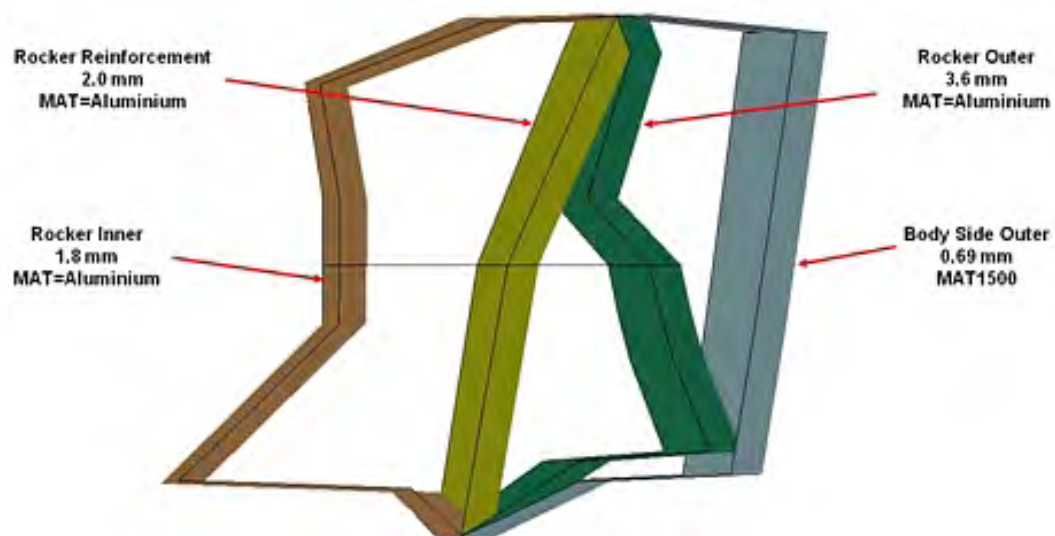


Figure 10.37: Extruded rocker design solution - final grade and gauge selections

10.7 B-Pillar Sub-System

The B-pillar subsystem optimization considered three manufacturing concepts; a steel stamping, a steel hydroform and an aluminum stamping.

10.7.1 Development of Sub-System from the Full Model

The B-pillar sub-system was developed from the full model (LF3G) such that when analyzed under the same loading conditions it behaved in the same way as the full model. The sub-system model consists of the B-pillar and the major attachment components it is attached to such as the rocker, roof rail and the seat cross-member. See Figure 10.38.

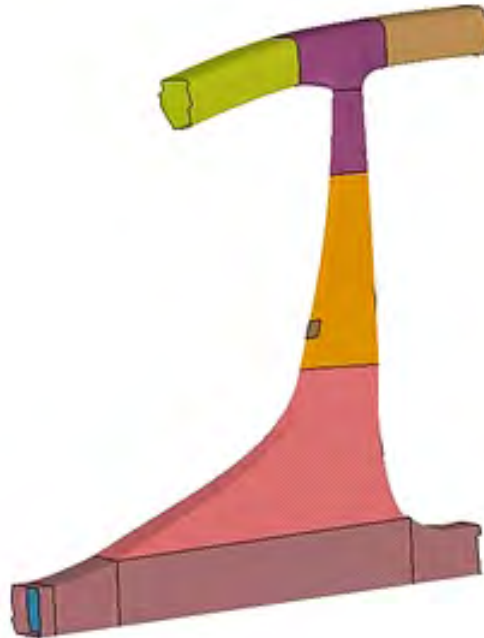


Figure 10.38: B-Pillar sub-system from LF3G

10.7.2 Generating Boundary Conditions

The nodal displacement time history is used as the boundary conditions for the sub-system so that it behaves in a similar manner to the the full LF3G model. The method used was exactly the same as was described for the rocker in 10.6.2. Figure 10.39 shows the specific boundaries and IIHS Side Impact barrier applied to the B-pillar sub-system model.

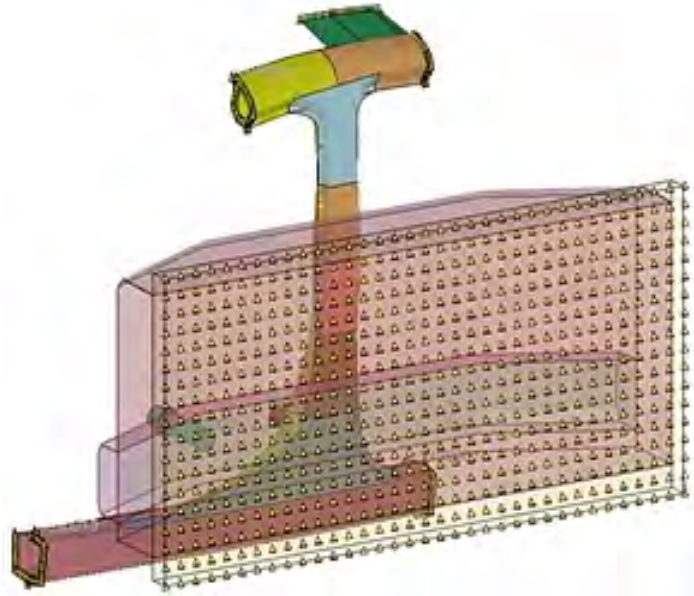


Figure 10.39: *B-Pillar Sub-system with highlighted boundaries for time history*

10.7.3 Stamped B-pillar Concept

10.7.3.1 Grade and Gauge Design Space

The stamped B-pillar concept consists of a B-pillar outer, which is also part of the body side outer, a B-pillar reinforcement and a B-pillar inner. Each component was divided into 5 regions. Referring to Figure 10.40; these are shown as regions A through E. The choice of grade and gauge of each region could be varied independently of the others. Details of the available grade and gauge choices are listed in Table 10.6.

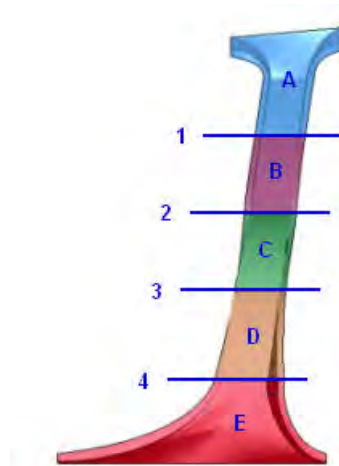


Figure 10.40: Stamped B-Pillar concept - zones of grade and gauge variation

STAMPED B-PILLAR GAUGE CHOICES			STAMPED B-PILLAR GRADE CHOICES	
FROM	0.5 mm (INNER & OUTER)	In 0.01 mm increments	ULTIMATE TENSILE (MPa)	MAT 270
	0.2 mm (REINFORCEMENT)			MAT 340
TO	2.0 mm			MAT 450
		MAT 500		
		MAT 600		
		MAT 800		
		MAT 1000		
		MAT 1300		
		MAT 1500		

Table 10.6: Stamped B-pillar - available grade and gauge choices

10.7.3.2 Geometry Parameterization

The geometry design space is limited as an outer boundary package space established in chapter 4. Referring to Figure 10.40, the cross-section at locations 1 through 4 can varied independently

of each other. Thus for each region A-E the shape will vary along the length of the region based on the cross sections at each end. The range of the packaging space for each cross section 1 through 4 is shown in Figure 10.41.

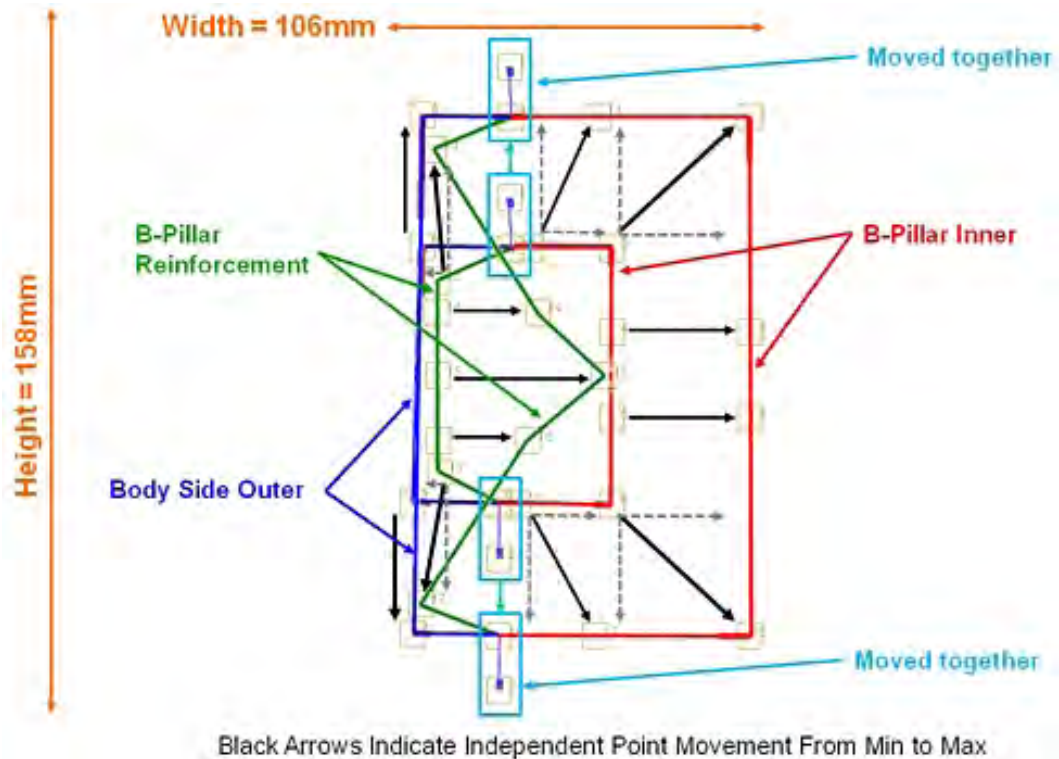


Figure 10.41: Stamped B-Pillar concept - cross-sectional parameterization

10.7.3.3 Optimization Setup

- Objective: The optimization objective is to maintain the performance of the B-pillar so that the total strain energy remains the same as the LF3G for IIHS side impact and roof crush. The mass of the LF3G B-pillar is 6.0 kg.
- Target: The optimization target is to minimize the mass of the B-pillar.
- Constraint: The energy absorbed by the B-pillar in the LF3G model (full model) was used as a constraint for the optimization. IIHS side impact and roof crush experience plastic deformation and so the energy absorbed was maintained at $\pm 15\%$ of the LF3G's performance. (For further information on target energy value calculations, refer to Appendix 20.3 for details)

10.7.3.4 Stamped B-Pillar Design Solution

All results from the optimization are compared to the baseline LF3G B-pillar. Figure 10.42 shows the deformation of the baseline LF3G design and the optimized stamped concept for IIHS side impact and roof crush.

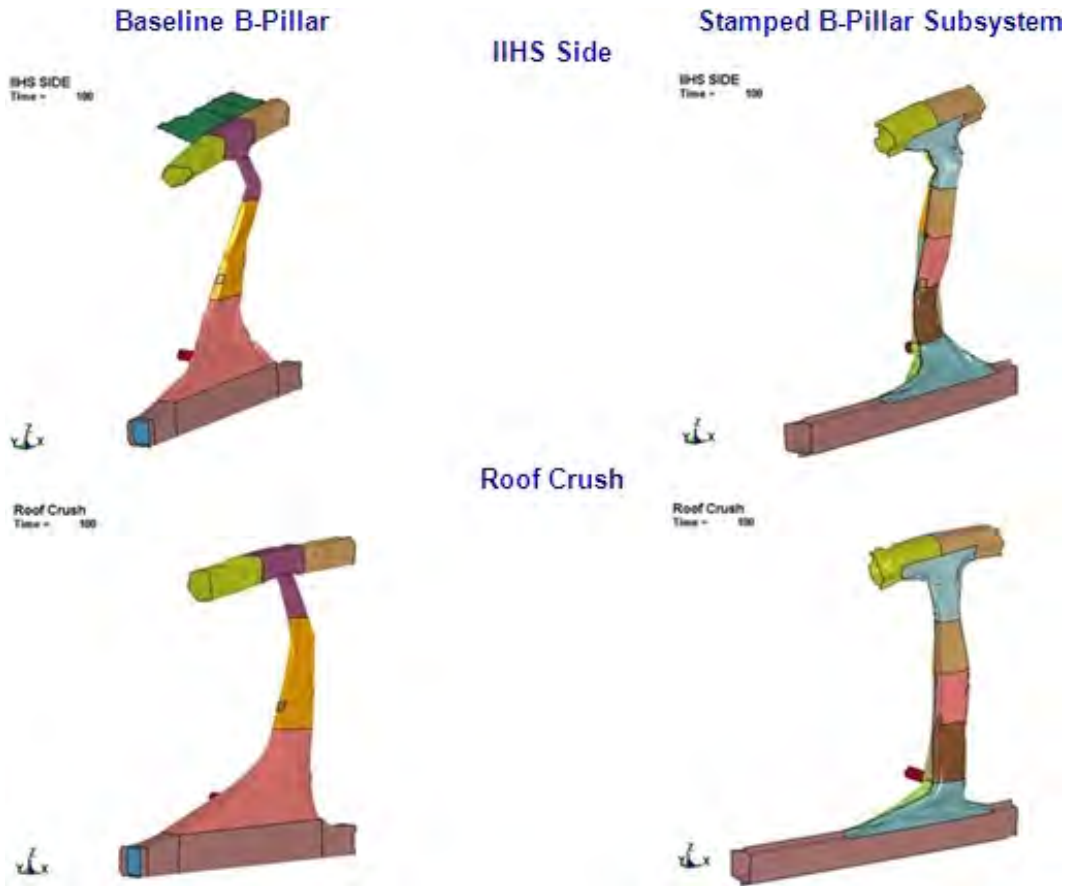


Figure 10.42: Stamped B-Pillar design solution - deformation comparison to baseline

Figure 10.43 shows the comparison of energy absorption for the baseline LF3G B-pillar compared to the optimized stamped B-pillar concept. For both loadcases, IIHS side impact and roof crush, the B-pillar experiences plastic deformation and the optimized stamped concept shows good correlation to the baseline design for both deformation shape and strain energy absorption.

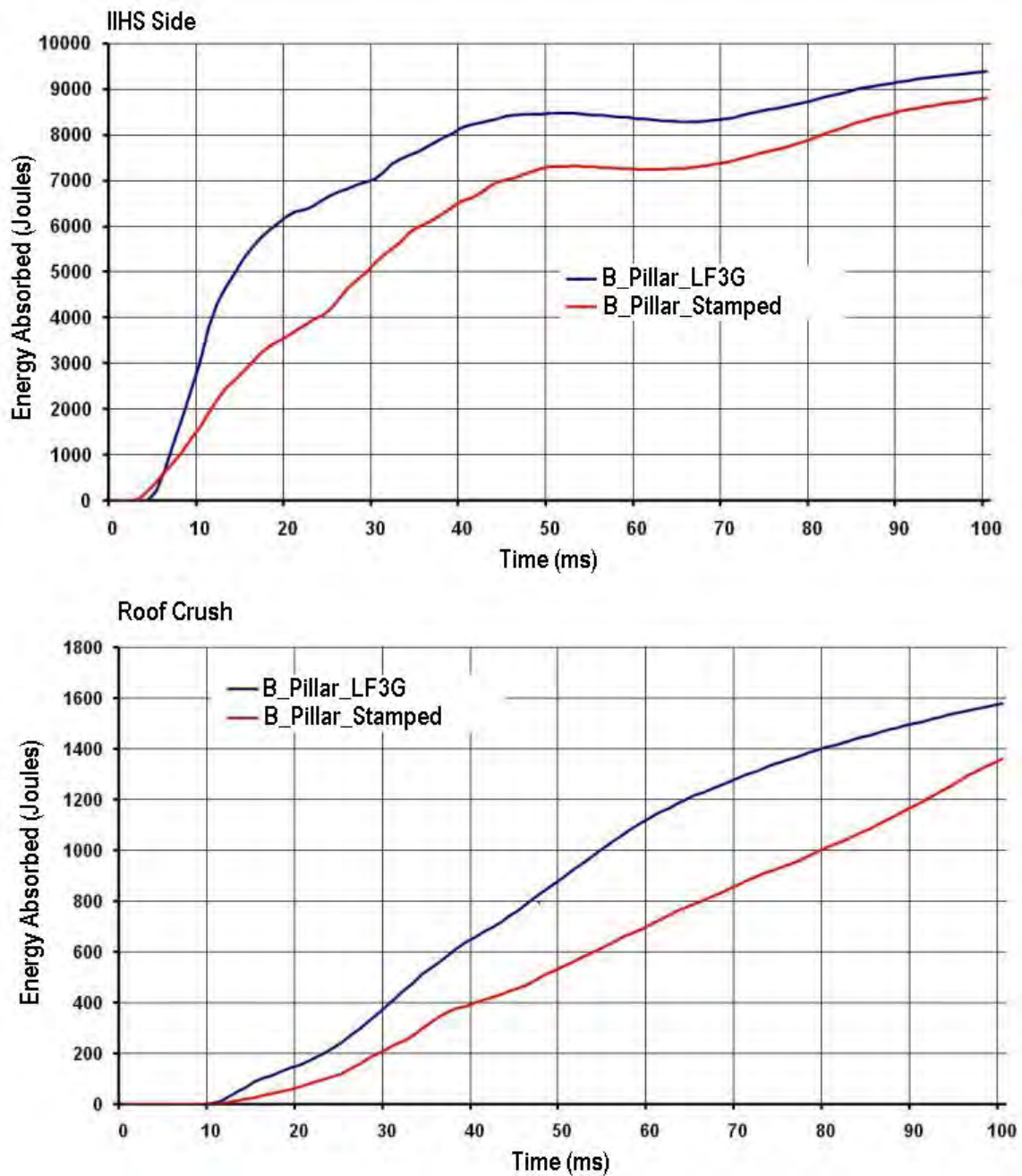


Figure 10.43: Stamped B-Pillar design solution - energy absorption comparison to baseline

Figure 10.44 shows the geometry, grade and gauge selections for the stamped B-pillar concept with reinforcement. The final mass for this design solution was 5.88 kg, which is almost the same mass as the baseline design (6.0 kg).

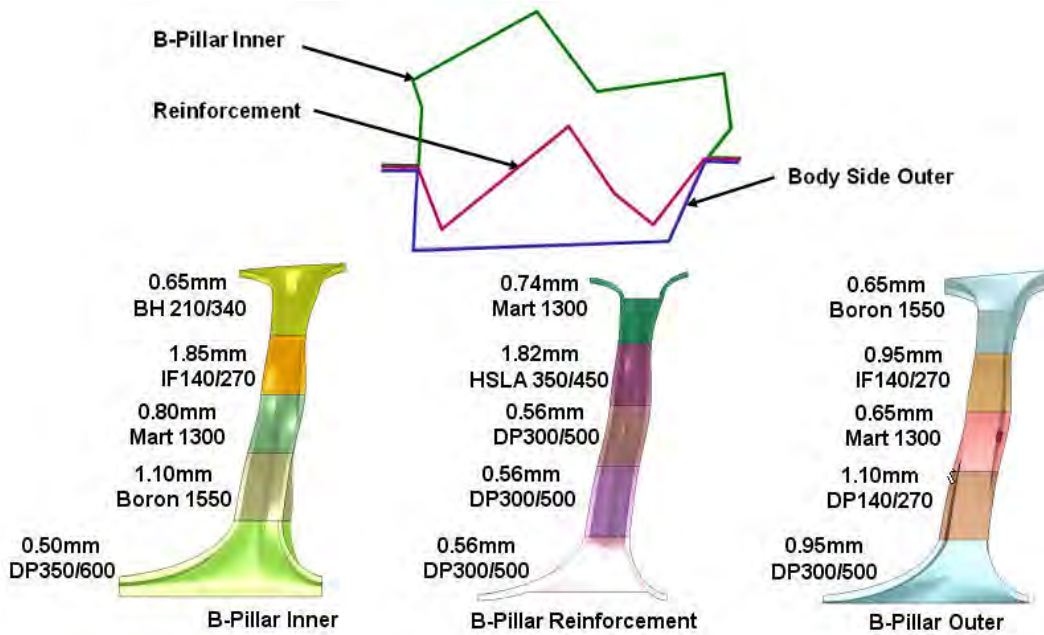


Figure 10.44: Stamped B-Pillar with reinforcement - final grade and gauge selections

The stamped B-pillar optimization was repeated without the reinforcement. This was done to enable the optimization to reduce the B-pillar mass by eliminating a component.

Figure 10.45 shows the geometry, grade and gauge selections for the stamped B-pillar concept without reinforcement. The final mass for this design solution was 5.4 kg, which is a 10% mass reduction compared to the baseline design (6.0 kg).

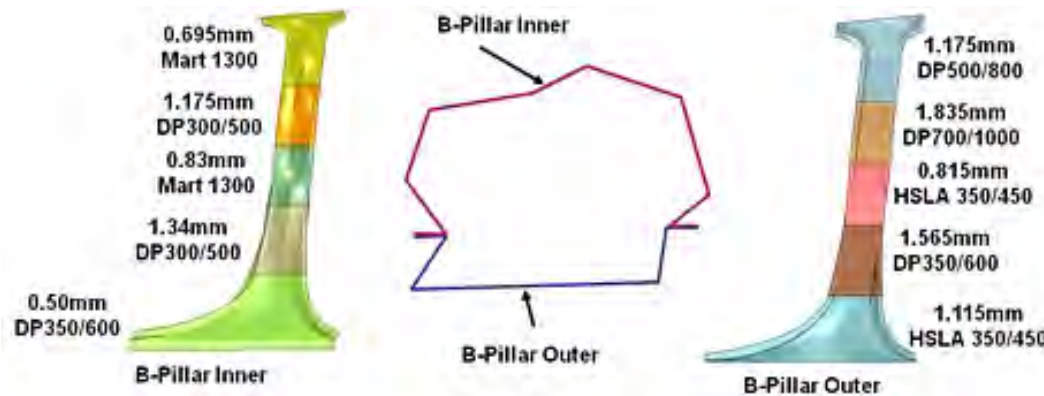


Figure 10.45: Stamped B-Pillar without reinforcement - final grade and gauge selections

10.7.4 Hydroformed B-Pillar Concept

The complete sub-system optimization process for the B-pillar has already been discussed previously. Here the only differences in the grade and gauge selection and geometry parameterization for this concept are discussed.

10.7.4.1 Grade and Gauge Design Space

The hydroformed B-pillar concept consists of a B-pillar outer, which is also part of the body side outer and a B-pillar inner there is no reinforcement. Each component was divided into 4 regions. Referring to Figure 10.46; these are shown as regions A through D. The choice of grade and gauge of each region could be varied independently of the others. Details of the available grade and gauge choices are listed in Table 10.7. Note that for hydroforming, material variation is limited to an ultimate tensile strength of 1000 MPa.

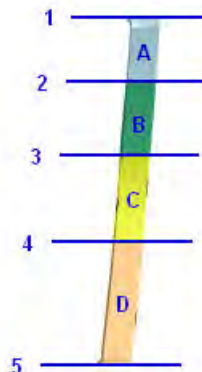


Figure 10.46: Hydroformed B-Pillar concept - zones of grade and gauge variation

HYDROFORMED B-PILLAR GAUGE CHOICES			HYDROFORMED B-PILLAR GRADE CHOICES	
FROM	0.5 mm (INNER & OUTER)	In 0.01 mm increments	ULTIMATE TENSILE (MPa)	MAT 270
TO	2.0 mm			MAT 340
		MAT 450		
		MAT 500		
		MAT 600		
		MAT 800		
		MAT 1000		

Table 10.7: Hydroformed B-Pillar - available grade and gauge choices

10.7.4.2 Geometry Parameterization

Referring to Figure 10.46, the cross-section at locations 1 through 5 can be varied independently of each other and so the shape will vary along the length of each region, A through D, based on the cross sections at each end. The range of the packaging space for each cross section 1 through 6 is shown in Figure 10.47.

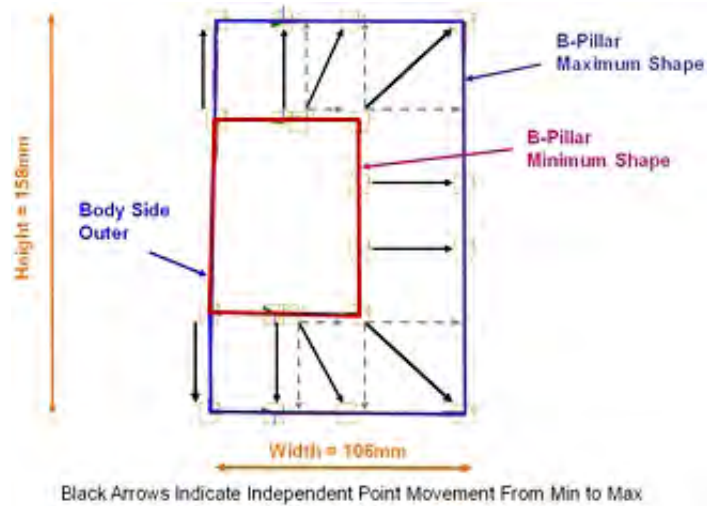


Figure 10.47: Hydroformed B-Pillar concept - cross-sectional parameterization

10.7.4.3 Hydroformed B-Pillar Design Solution

The optimization was setup with two hydroformed concepts. The first concept, hydroformed-1, was a grade and gauge optimization with the geometry of the cross-sections set to the minimum size. The second concept, hydroformed-2 was a full geometry, grade and gauge optimization. All results from the optimization are compared to the baseline LF3G B-pillar. Figure 10.48 shows the deformation of the baseline LF3G B-pillar design and the optimized hydroformed-1 B-pillar concept for IIHS side impact and roof crush.

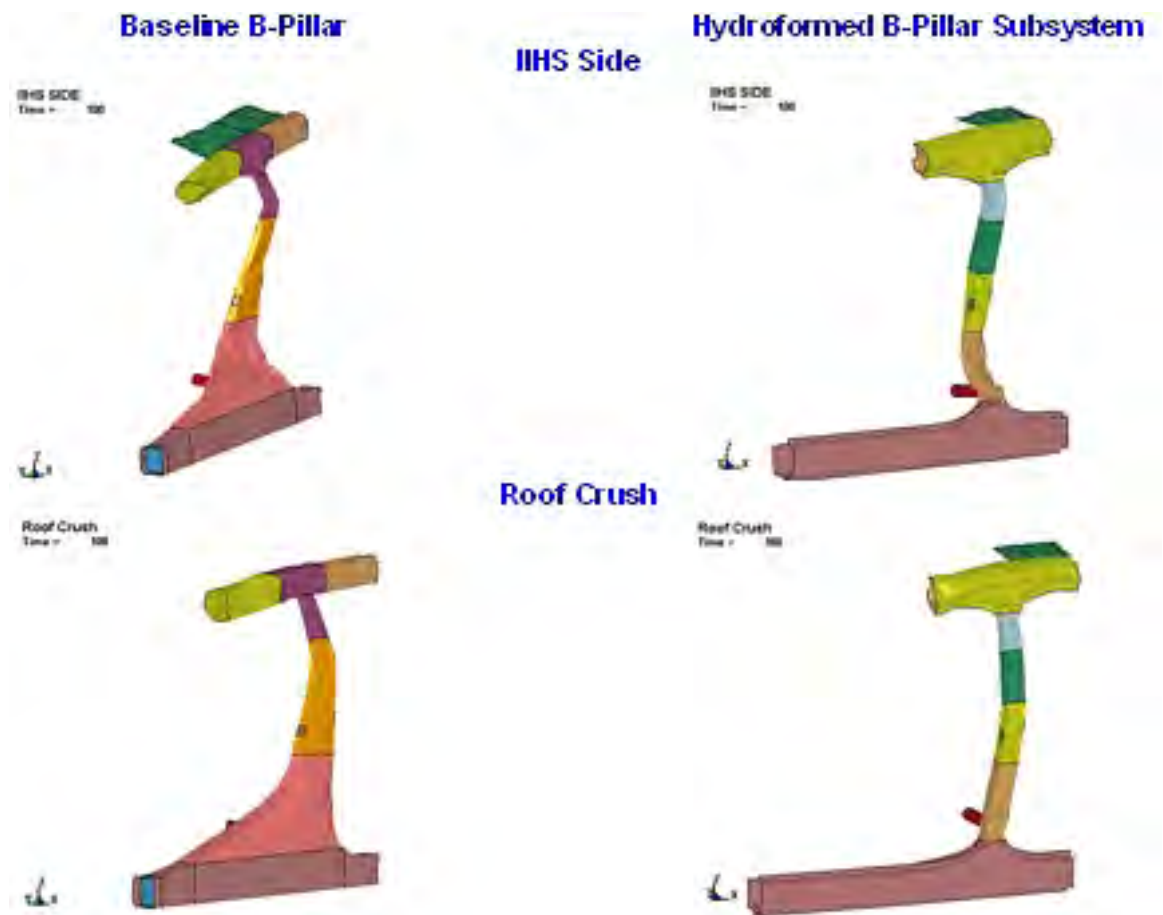


Figure 10.48: Hydroformed-1 B-Pillar design solution deformation comparison to baseline

Figure 10.49 shows the comparison of energy absorption for the baseline LF3G B-pillar compared to the both optimized hydroformed B-pillar concepts. For both loadcases, IIHS side impact and roof crush, the B-pillar experiences plastic deformation and the optimized stamped concept shows good correlation to the baseline design for strain energy absorption.

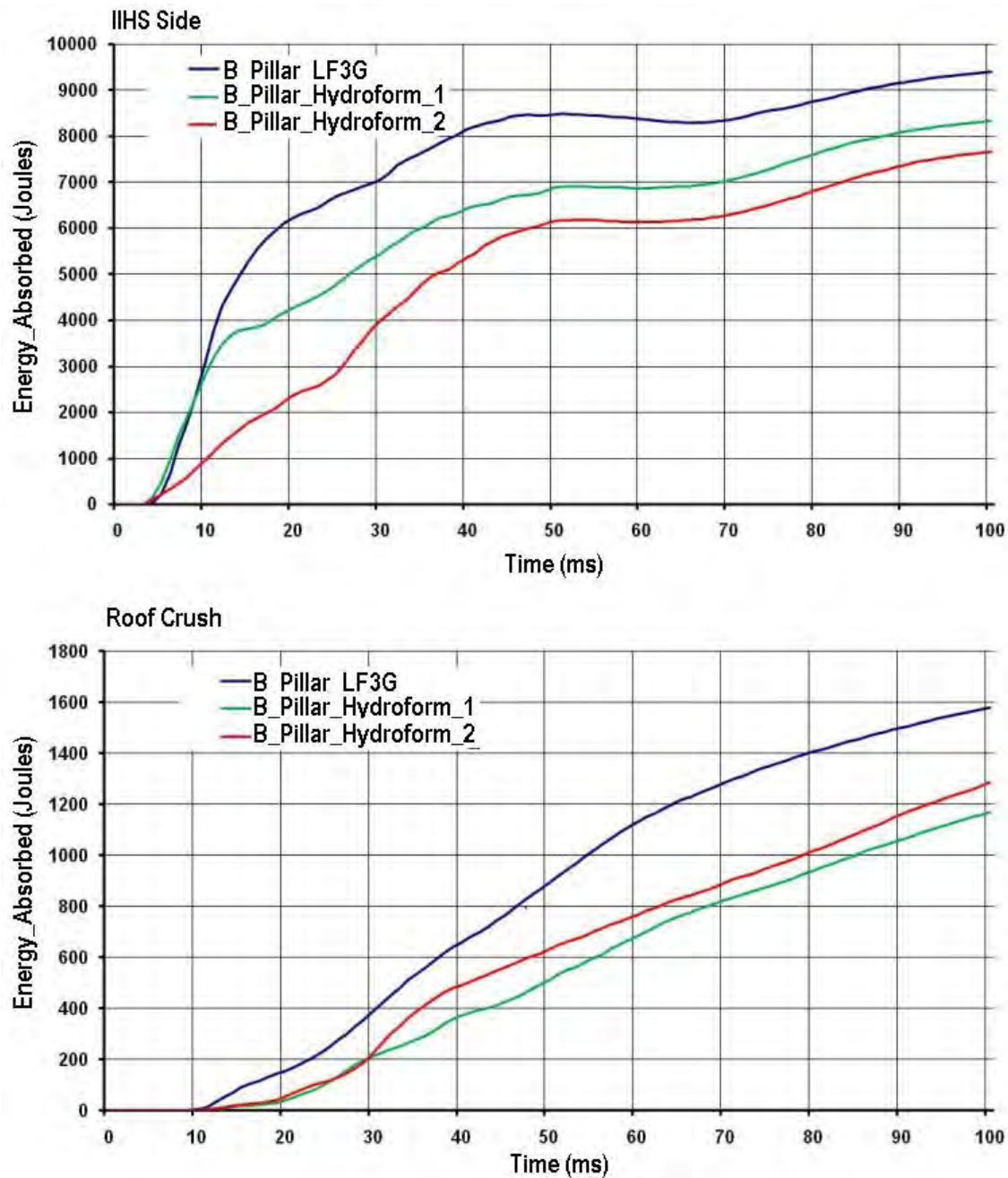


Figure 10.49: Hydroformed-1 B-Pillar design solution - energy absorption comparison to baseline

Figure 10.50 shows the geometry, grade and gauge selections for the two hydroformed B-pillar design solutions. The final mass for these design solutions was 3.0 kg for hydroformed-1 and 3.1 kg for hydroformed-2, which is a 50% mass reduction compared to the baseline design (6.0 kg).

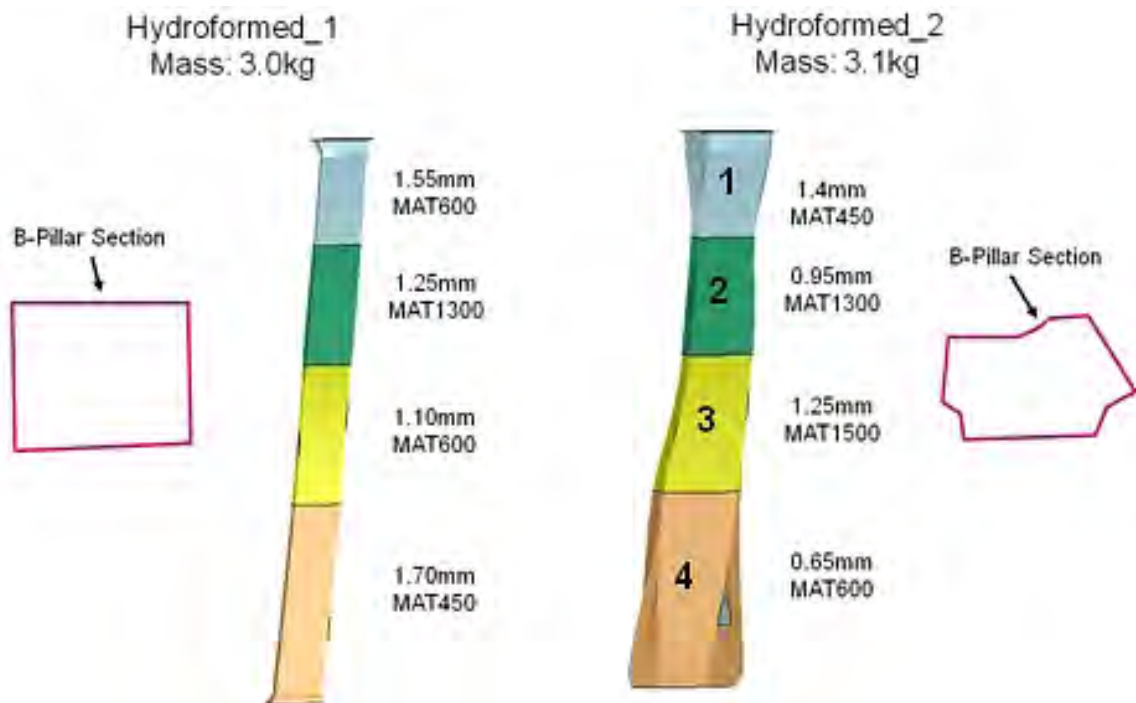


Figure 10.50: Hydroformed-1 B-Pillar final grade and gauge selections

10.7.5 Stamped Aluminum B-Pillar Concept

10.7.5.1 Grade and Gauge Design Space

The stamped aluminum B-pillar concept consists of a B-pillar outer, a B-pillar inner and a B-pillar reinforcement. See Figure 10.51. There is no variation in gauge along the length of the component, only differences in cross section are allowed. See Table 10.8 for the available grade choices. There is no variation in the grade of aluminum.



Figure 10.51: Stamped aluminum B-Pillar concept design space

STAMPED ALUMINUM B-PILLAR GAUGE CHOICES			STAMPED ALUMINUM B-PILLAR GRADE CHOICES	
FROM	0.8 mm (INNER, OUTER & REINFORCEMENT)	In 0.01 mm increments	ALUMINUM GRADE	AL 7075
TO	6.0 mm			

Table 10.8: Stamped aluminum B-Pillar available grade and gauge choices

10.7.5.2 Geometry Parameterization

Figure 10.52 shows the parameterization of the cross section.

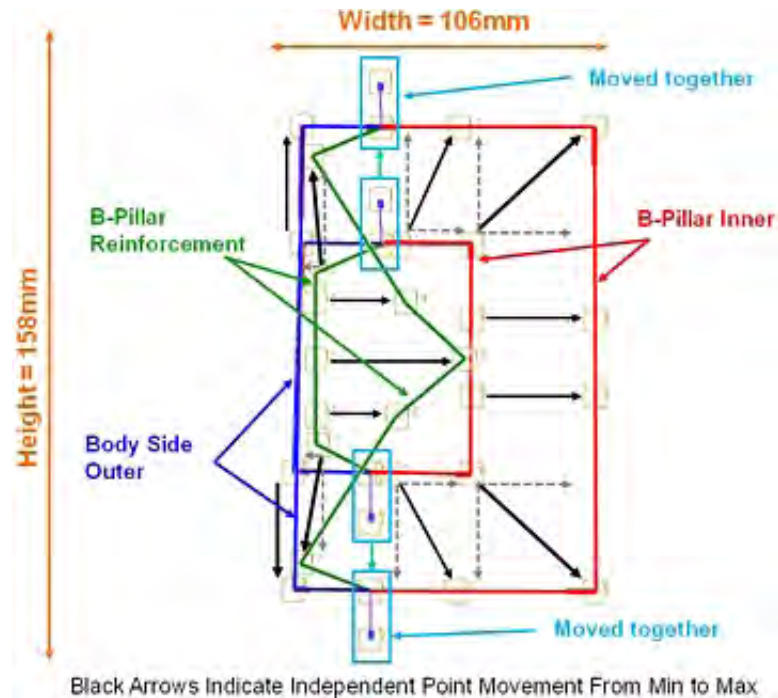


Figure 10.52: Stamped aluminum B-Pillar concept cross-sectional parameterization

10.7.5.3 Optimization Setup

- Objective: The optimization objective is to maintain the performance of the B-pillar so that the total strain energy remains the same as the LF3G for IIHS side impact and roof crush. The mass of the LF3G B-pillar is 6.0 kg.
- Target: The optimization target is to minimize the mass of the B-pillar.
- Constraint: The energy absorbed by the B-pillar in the LF3G model (full model) was used as a constraint for the optimization. However, because this is an aluminum concept, the energy values were recalculated from an updated version of the full LF3G model. In this case, the B-pillar material was revised from steel to aluminum. For load cases that experience plastic deformation, the energy absorbed was maintained at $\pm 15\%$ of the LF3G's performance. Thus for IIHS side impact and roof crush, the energy absorption was held at $\pm 15\%$ of energy absorption for the LF3G. (For further information on target energy value calculations for aluminum, refer to Appendix 20.4 for details)

10.7.5.4 Stamped Aluminum B-Pillar Design Solution

All results from the optimization are compared to the baseline LF3G B-pillar. Figure 10.53 shows the deformation of the baseline LF3G design and the optimized stamped aluminum concept for IIHS side impact and roof crush.

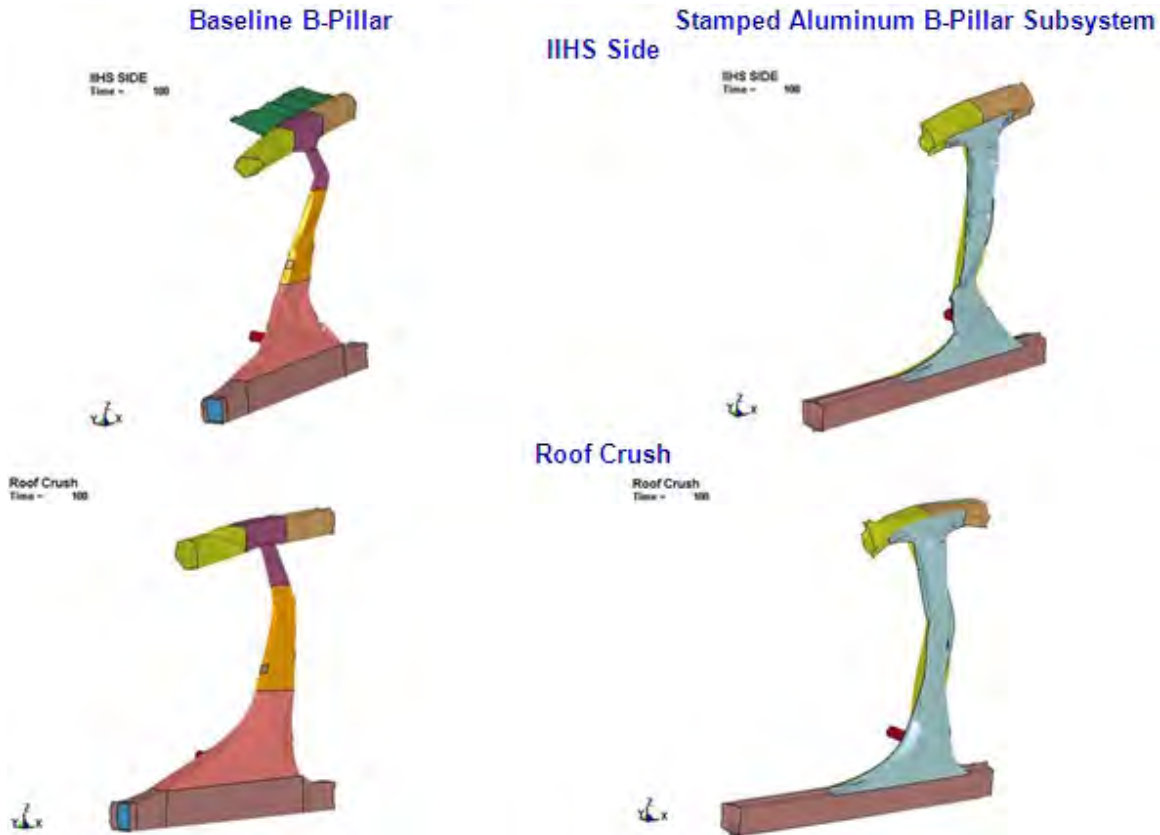


Figure 10.53: *Stamped aluminum B-Pillar design solution deformation comparison to baseline*

Figure 10.54 shows the comparison of energy absorption for the baseline LF3G B-pillar compared to the optimized stamped aluminum B-pillar concept. For both loadcases, IIHS side impact and roof crush, the B-pillar experiences plastic deformation and the optimized stamped concept shows good correlation to the baseline design for both deformation shape and strain energy absorption.

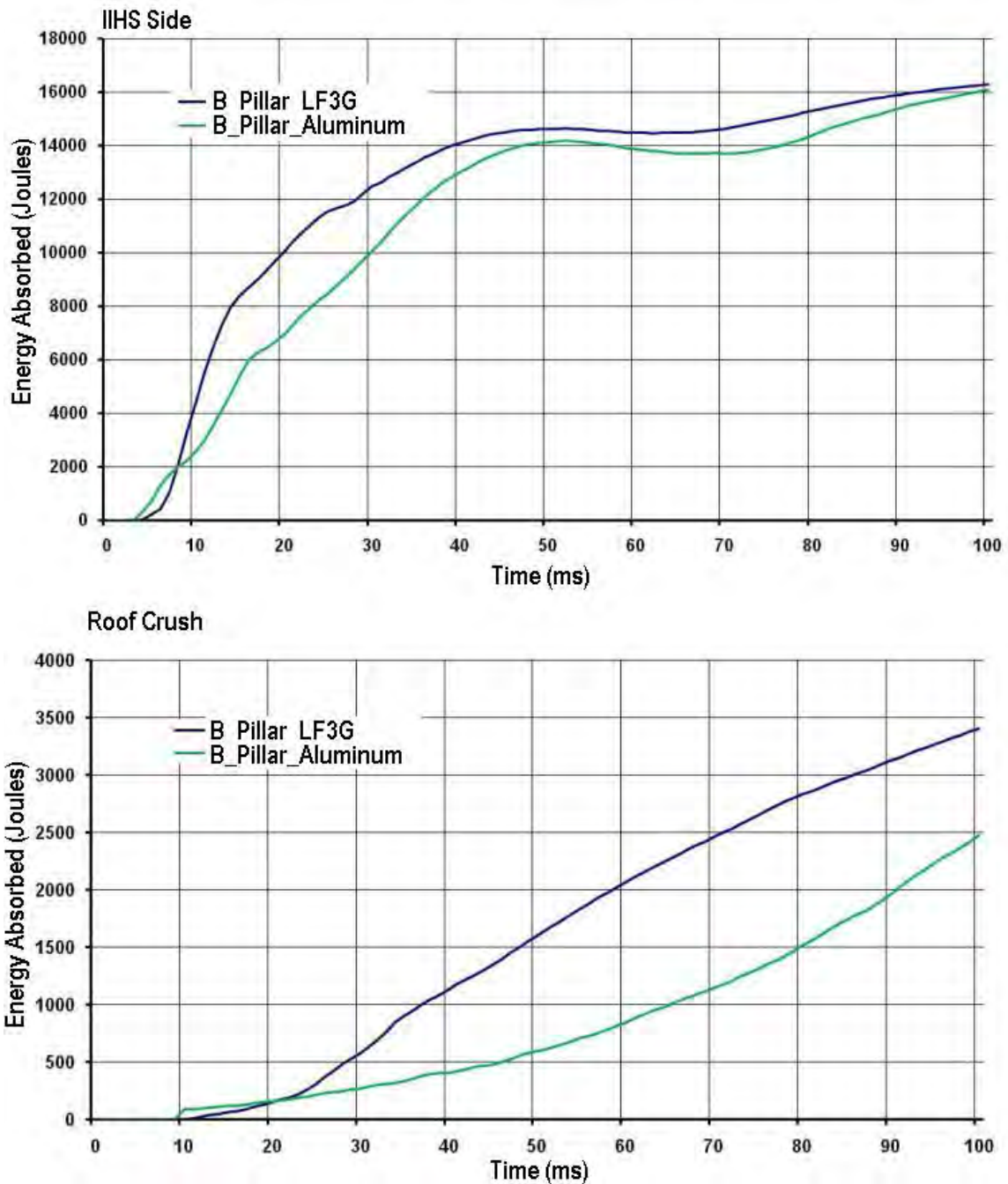


Figure 10.54: Stamped aluminum B-Pillar design solution - energy absorption comparison to baseline

Figure 10.55 shows the geometry, grade and gauge selections for the stamped aluminum B-pillar concept with reinforcement. The final mass for this design solution was 4.9 kg, which is an 18% mass reduction compared to the baseline design (6.0 kg).

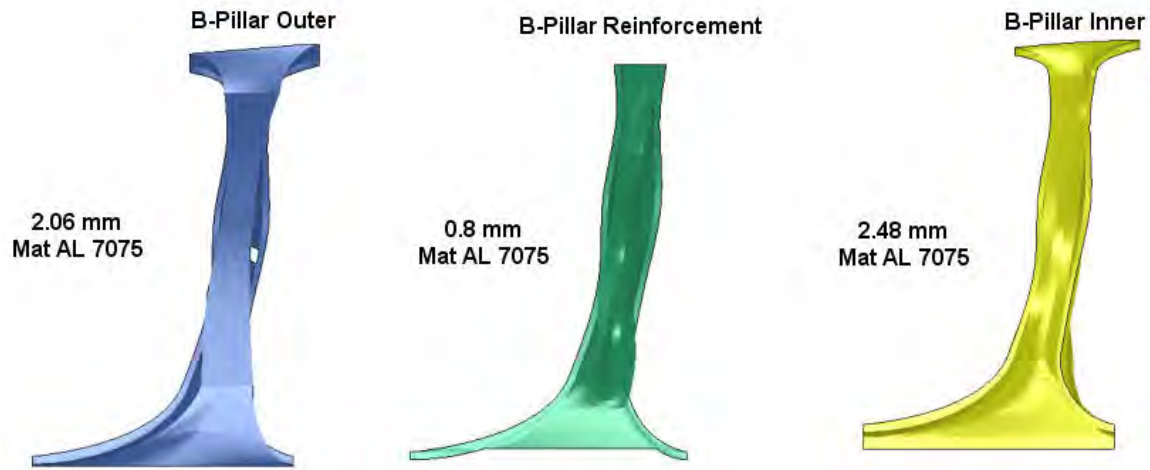


Figure 10.55: Stamped aluminum B-Pillar final grade and gauge selections

10.8 Side Roof Rail Sub-System

The rear rail sub-system optimization considered three manufacturing concepts; a steel stamping, a steel hydroformed extrusion and an aluminum extrusion.

10.8.1 Development of Sub-system from Full Model

The side roof rail sub-system was developed from full model (LF3G) such that when analyzed under the same loading conditions it behaved in the same way as the full model. The sub-system model consists of the A-pillar and roof rail and the major attachment components they are attached to such as the hinge pillar, B-pillar upper, C-pillar, front and rear headers, roof bow and roof. See Figure 10.56

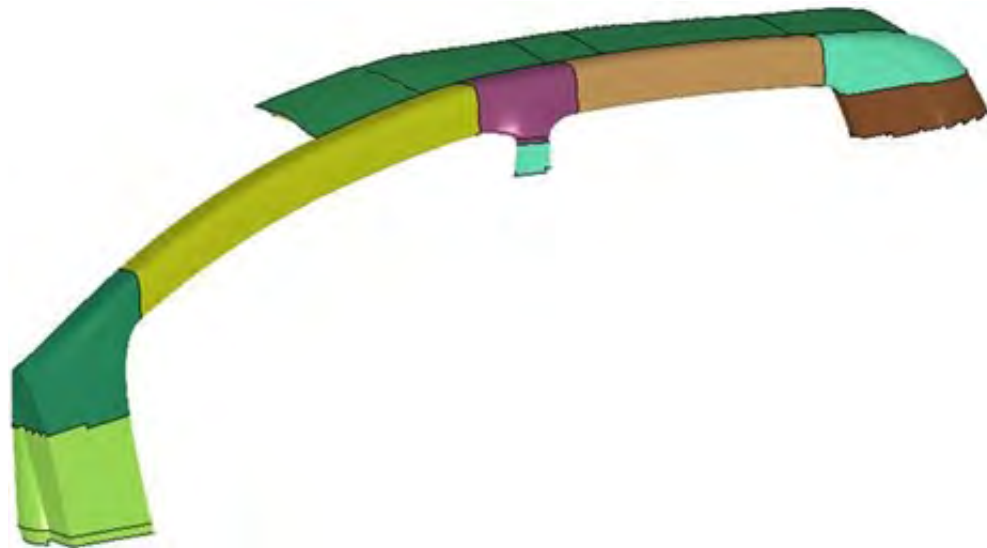


Figure 10.56: *Side roof rail sub-system from LF3G*

10.8.2 Generating Boundary Conditions

The nodal displacement time history is used as the boundary conditions for the sub-system so that it behaves in a similar manner to the full LF3G model. The method used was exactly the same as was described for the rocker in section 10.6.2. Referring to Figure 10.57, shows the specific boundaries and pole impact barrier applied to the side roof rail sub-system model.

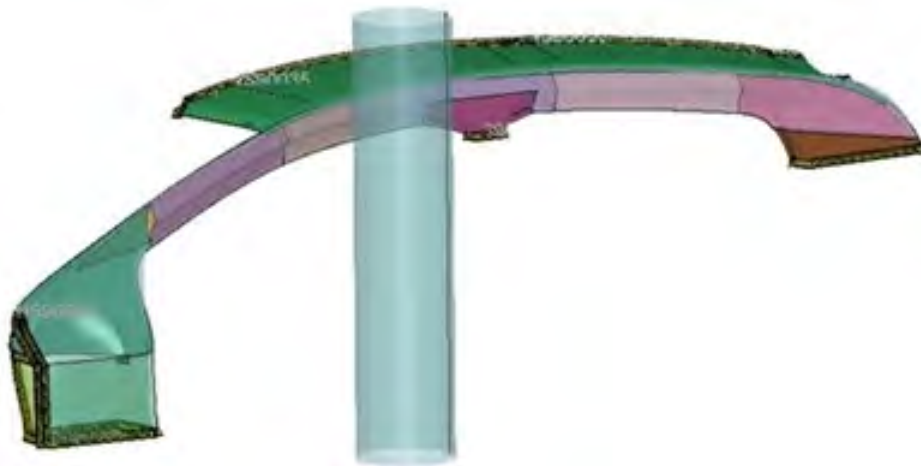


Figure 10.57: Roof rail sub-system with highlighted boundaries for time history

The performance of sub-system model was validated under the load cases considered, front ODB, rear ODB, IIHS side and pole impacts and roof crush, to confirm that it behaved as the full model did. The energy absorbed by the side roof rail under the loading conditions considered was used as the performance target.

10.8 Side Roof Rail Sub-System

10.8.3 Stamped Side Roof Rail Concept

10.8.3.1 Grade & Gauge Design Space

The stamped side roof rail concept consists of the body side outer, a side roof rail outer and a side roof rail inner. Each component was divided into 6 regions. Referring to Figure 10.58; these are shown as regions A through F. The choice of grade and gauge of each region could be varied independently of the others. Details of the available grade and gauge choices are listed in Table 10.9.

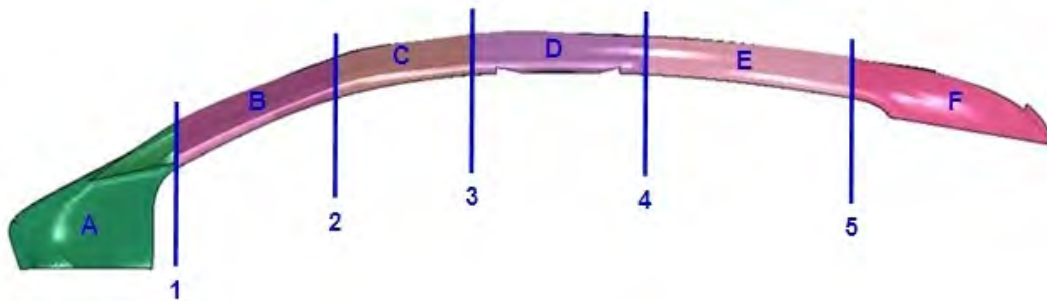


Figure 10.58: Stamped side roof rail concept - zones of grade & gauge variation

STAMPED SIDE ROOF RAIL GAUGE CHOICES			STAMPED SIDE ROOF RAIL GRADE CHOICES	
FROM	0.5 mm (INNER & OUTER)	In 0.01 mm increments	ULTIMATE TENSILE (MPa)	MAT 270
	0.2 mm (REINFORCEMENT)			MAT 340
TO	2.0 mm			MAT 450
		MAT 500		
		MAT 600		
		MAT 800		
		MAT 1000		
		MAT 1300		
		MAT 1500		

Table 10.9: Stamped side roof rail - available grade & gauge choices

10.8.3.2 Geometry Parameterization

The geometry design space is limited as an outer boundary package space established in chapter 4. Referring to Figure 10.58, the cross-section at locations 1 through 5 can be varied independently of each other. Thus for each region, A through F, the shape will vary along the length of the region based on the cross sections at each end. The range of the packaging space for each cross section 1 through 6 is shown in Figure 10.59.

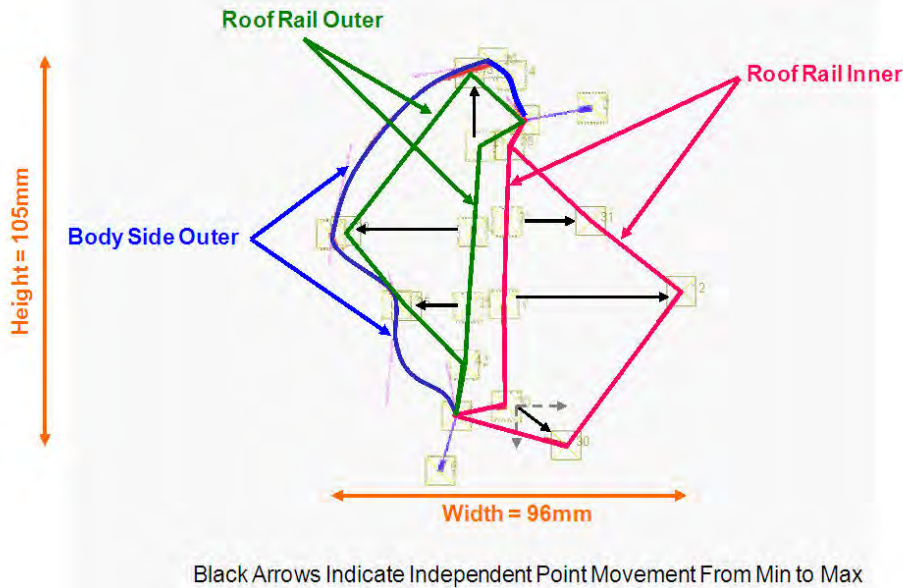


Figure 10.59: Stamped side roof rail concept - cross-sectional parameterization

10.8.3.3 Optimization Setup

- Objective: The optimization objective is to maintain the performance of the side roof rail so that the total strain energy remains the same as the LF3G for front ODB, rear ODB, IIHS side and pole impacts, and roof crush. The mass of the LF3G side roof rail is 11.42 kg.
- Target: The optimization target is to minimize the mass of the side roof rail.
- Constraint: The energy absorbed by the side roof rail in the LF3G model (full model), was used as a constraint for the optimization. For load cases that experience plastic deformation, the energy absorbed was maintained at $\pm 15\%$ of the LF3G's performance. For load cases that result in elastic deformation, the energy absorbed was maintained at a level less than that of LF3G's performance. Thus for rear ODB, IIHS side and pole impacts, the energy absorption was held at $\pm 15\%$ of energy absorption for the LF3G. However, because of the over performance under roof crush loading the energy absorption was held within $\pm 30\%$ of LF3G. For front ODB the energy absorption was held at $\leq 650\text{J}$.

(For further information on target energy value calculations, refer to Appendix 20.3 for details)

10.8.3.4 Stamped Side Roof Rail: Design Solution

All results from the optimization are compared to the baseline LF3G side roof rail. Figure 10.60 & 62 show the deformation of the baseline LF3G design and the optimized stamped concept for front ODB, rear ODB, IIHS side and pole impacts and roof crush. It clearly shows that for the front ODB there is limited deformation of the side roof rail. For the other load cases there is some local deformation of the rail. For example, under IIHS side and pole impacts the deformation is primarily in the center area of the rail, while for rear ODB impact the deformation is in the rear of the rail.

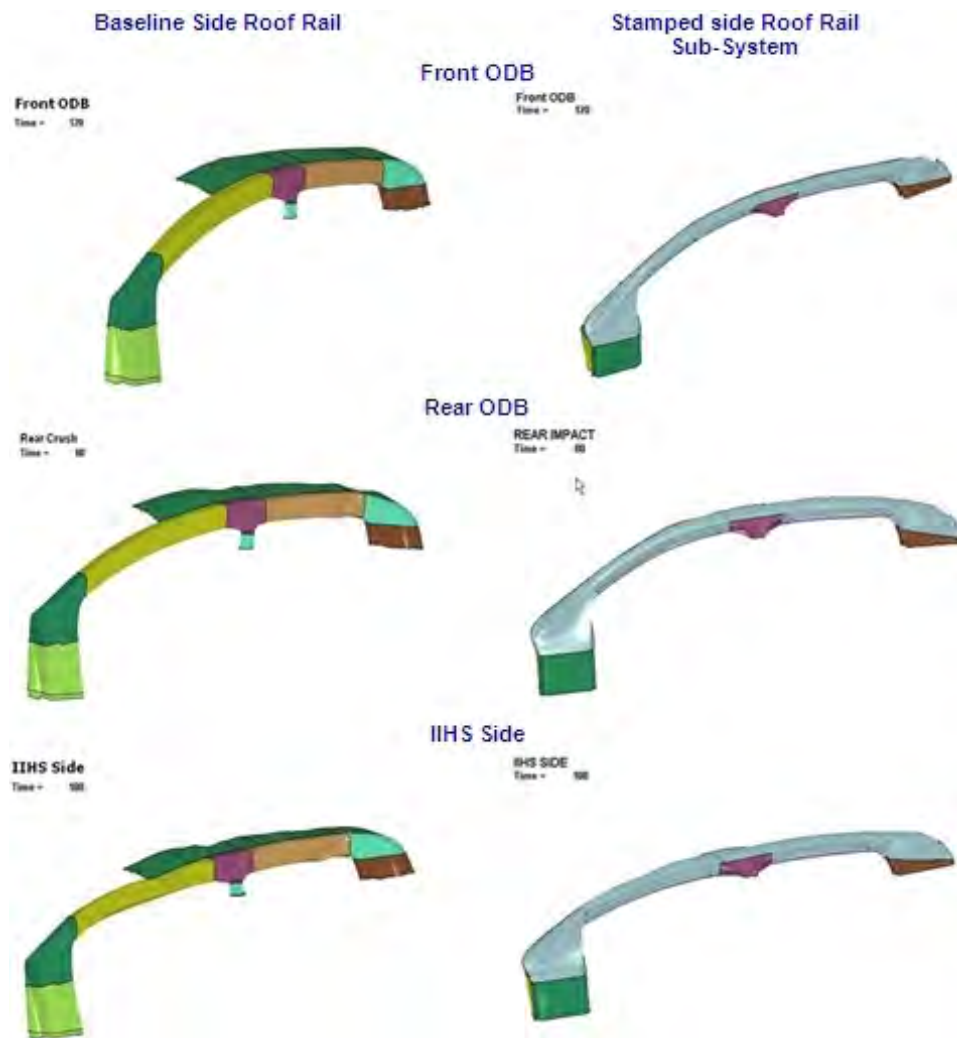


Figure 10.60: Stamped side roof rail design solution - deformation comparison to baseline

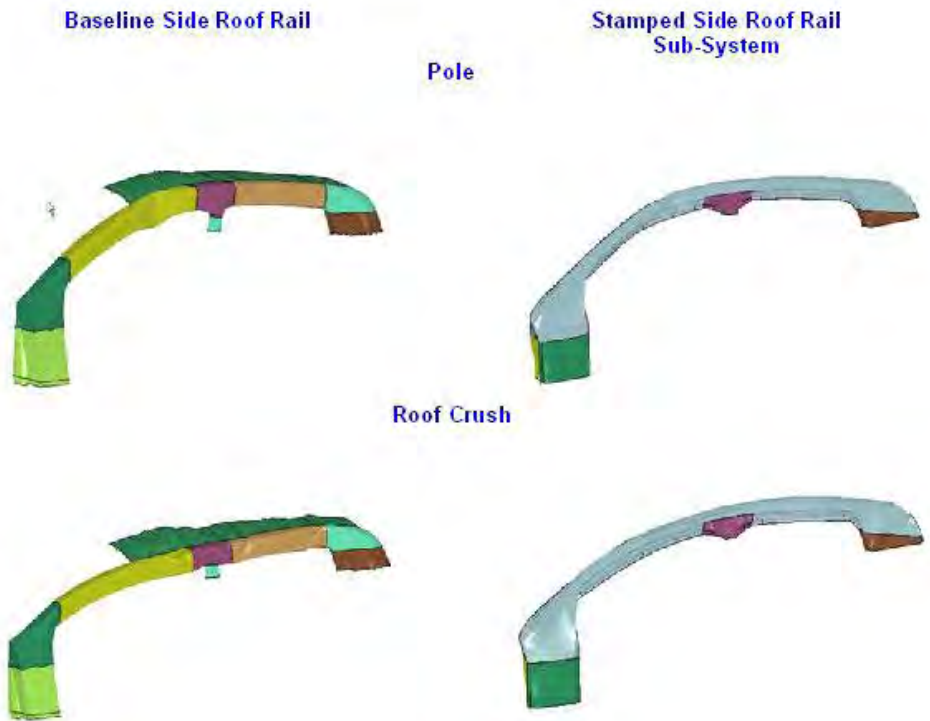


Figure 10.61: Stamped side roof rail design solution - deformation comparison to baseline

Figure 10.62 & Figure 10.63 show the comparison of energy absorption for the baseline LF3G side roof rail compared to the optimized stamped concept. In case of the front ODB impact the energy absorbed by the side roof rail is purely elastic energy as there is limited deformation. The total energy of the system has been maintained and so the kinetic energy has been absorbed in the rail as elastic energy. In the case of rear ODB, IHS side and pole impacts and roof crush, the rail experienced significant deformation resulting in a high amount of strain energy absorption.

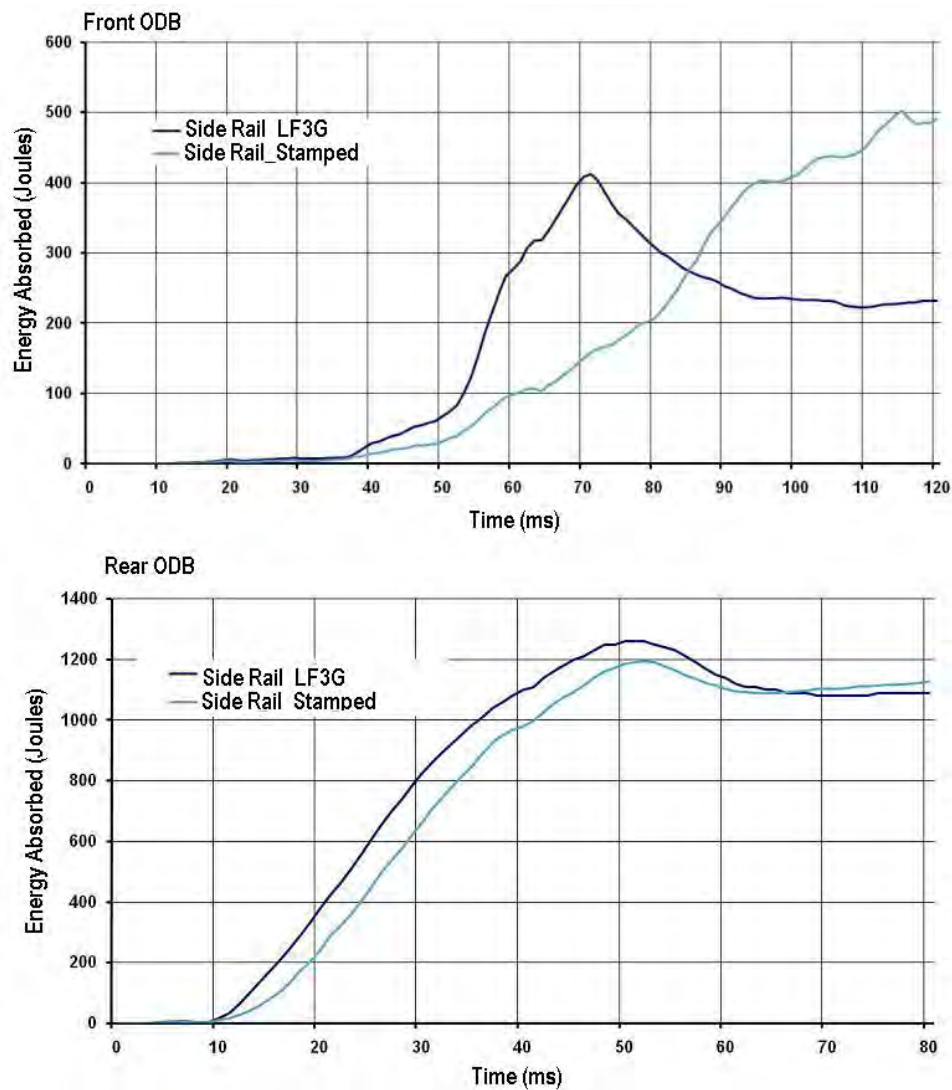


Figure 10.62: Stamped side roof rail design solution - energy absorption comparison to baseline

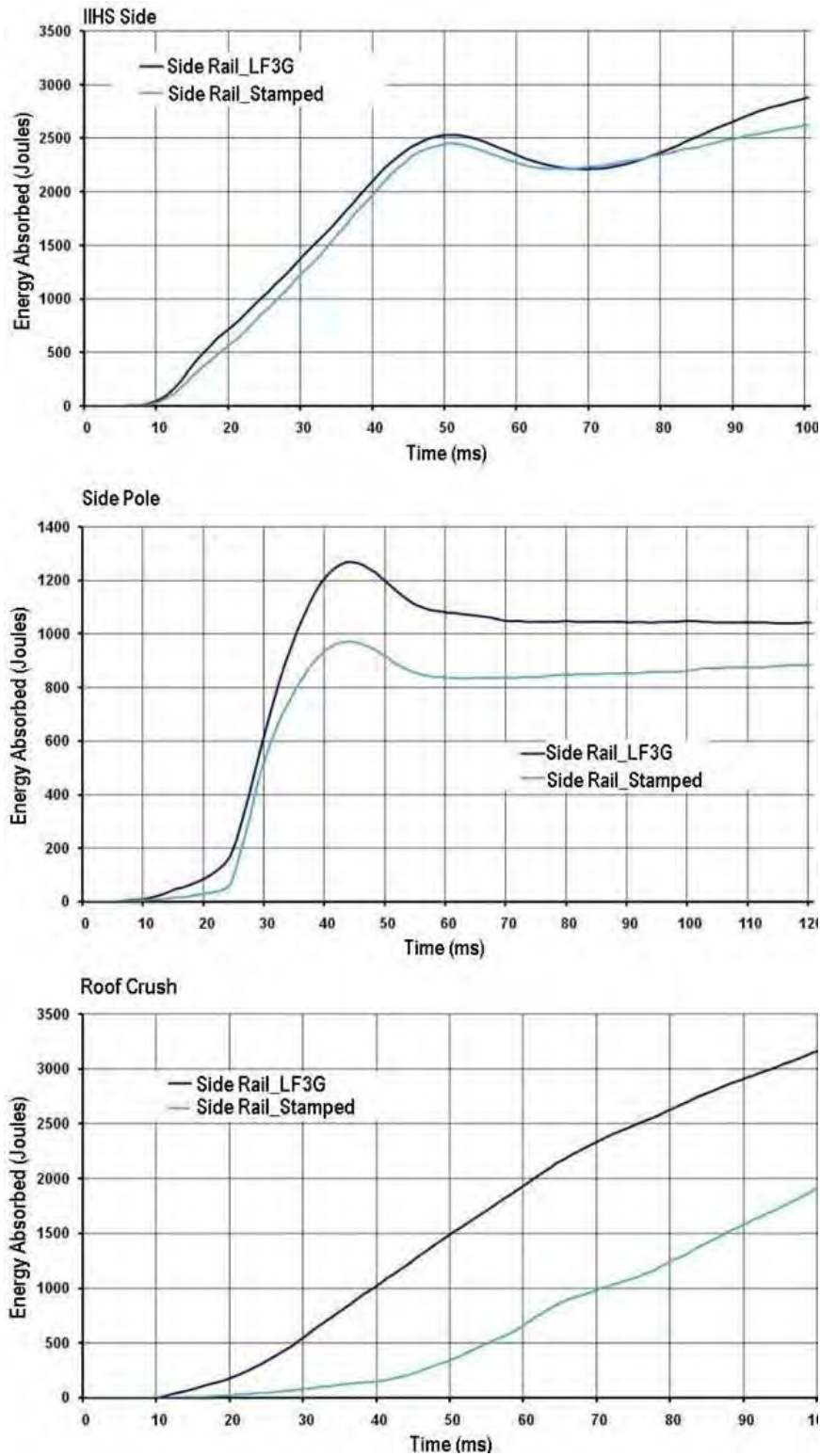


Figure 10.63: Stamped side roof rail design solution - energy absorption comparison to baseline

Figure 10.64 shows the geometry, grade and gauge selections for the stamped side roof rail concept. The final mass for this design solution was 9.98 kg, which is an 13% mass reduction compared to the baseline design (11.42 kg).

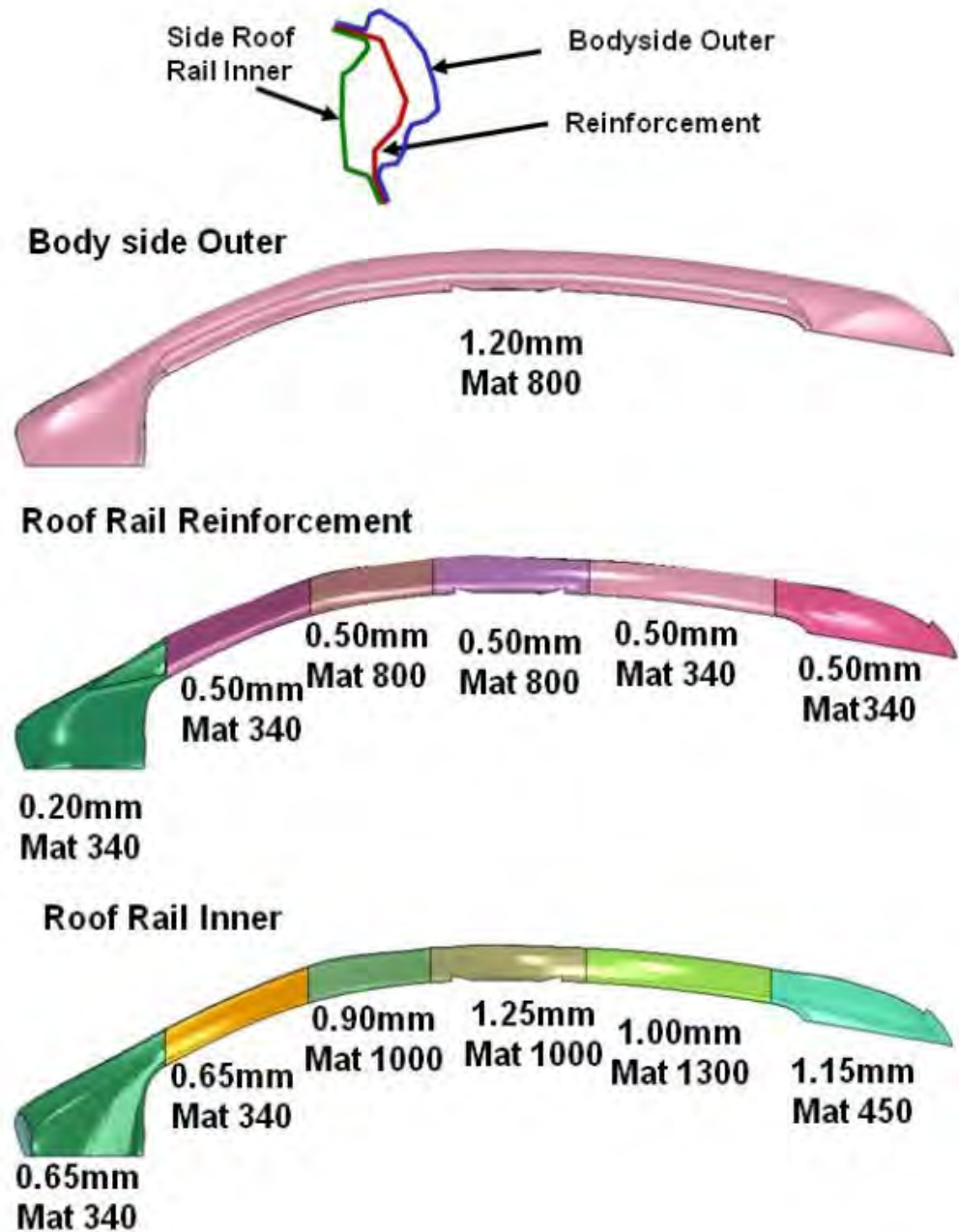


Figure 10.64: Stamped side roof rail - final grade & gauge selections

10.8.4 Hydroformed Side Roof Rail Concept

The complete sub-system optimization process for the side roof rail has already been discussed previously. Here the only differences in the grade and gauge selection and geometry parameterization for this concept are discussed.

10.8.4.1 Grade and Gauge Design Space

The hydroformed side roof rail concept consists of a body side outer and a side roof rail, there is no reinforcement. Each component was divided into 6 regions. Referring to Figure 10.65; these are shown as regions A through F. The choice of grade and gauge of each region can be varied independently of the others. Details of the available grade and gauge choices are listed in Table 10.10. Note that for hydroforming, material variation is limited to an ultimate tensile strength of 1000 MPa.

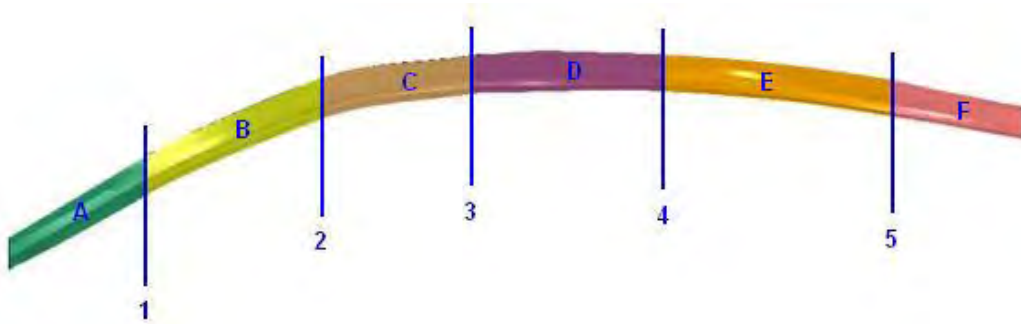


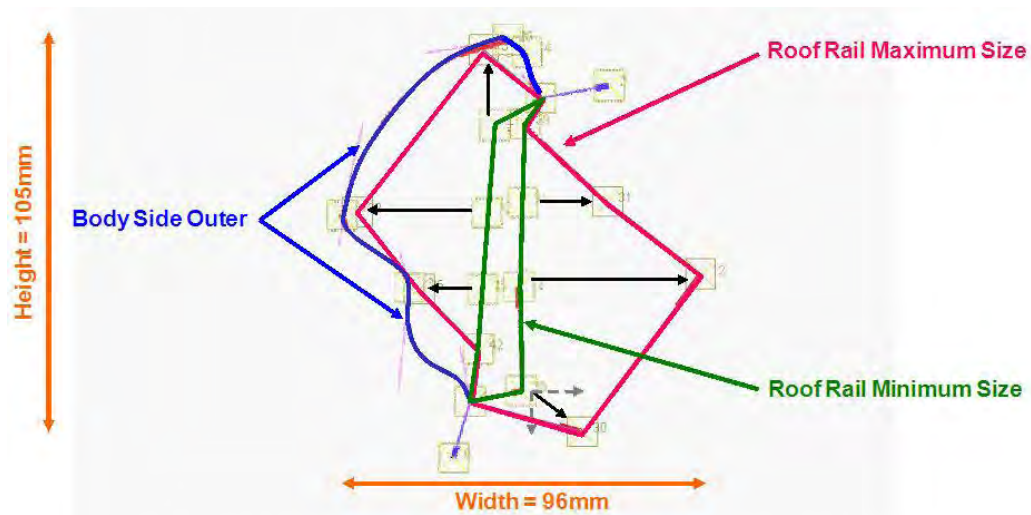
Figure 10.65: Hydroformed side roof rail concept - zones of grade & gauge variation

HYDROFORMED SIDE ROOF RAIL GAUGE CHOICES			HYDROFORMED SIDE ROOF RAIL GRADE CHOICES	
FROM	0.5 mm (INNER & OUTER)	In 0.01 mm increments	ULTIMATE TENSILE (MPa)	MAT 270
TO	2.0 mm			MAT 340
		MAT 450		
		MAT 500		
		MAT 600		
		MAT 800		
		MAT 1000		

Table 10.10: Hydroformed side roof rail - available grade & gauge choices

10.8.4.2 Geometry Parameterization

Referring to Figure 10.65, the cross-section at locations 1 through 6 can be varied independently of each other and so the shape will vary along the length of each region, A through F, based on the cross sections at each end. The range of the packaging space for each cross section 1 through 6 is shown in Figure 10.66.



Black Arrows Indicate Independent Point Movement From Min to Max

Figure 10.66: Side roof rail concept - cross-sectional parameterization

10.8.4.3 Hydroformed Side Roof Rail : Design Solution

Figure 10.67 & Figure 10.68 show the comparison of energy absorption for the baseline LF3G side roof rail compared to the optimized hydroformed concept. In case of the front ODB impact the energy absorbed by the side roof rail is purely elastic energy as there is limited deformation. The total energy of the system has been maintained and so the kinetic energy has been absorbed in the rail as elastic energy. In the case of rear ODB and IIHS side impacts and roof crush, the rail experienced significant deformation resulting in a high amount of strain energy absorption.

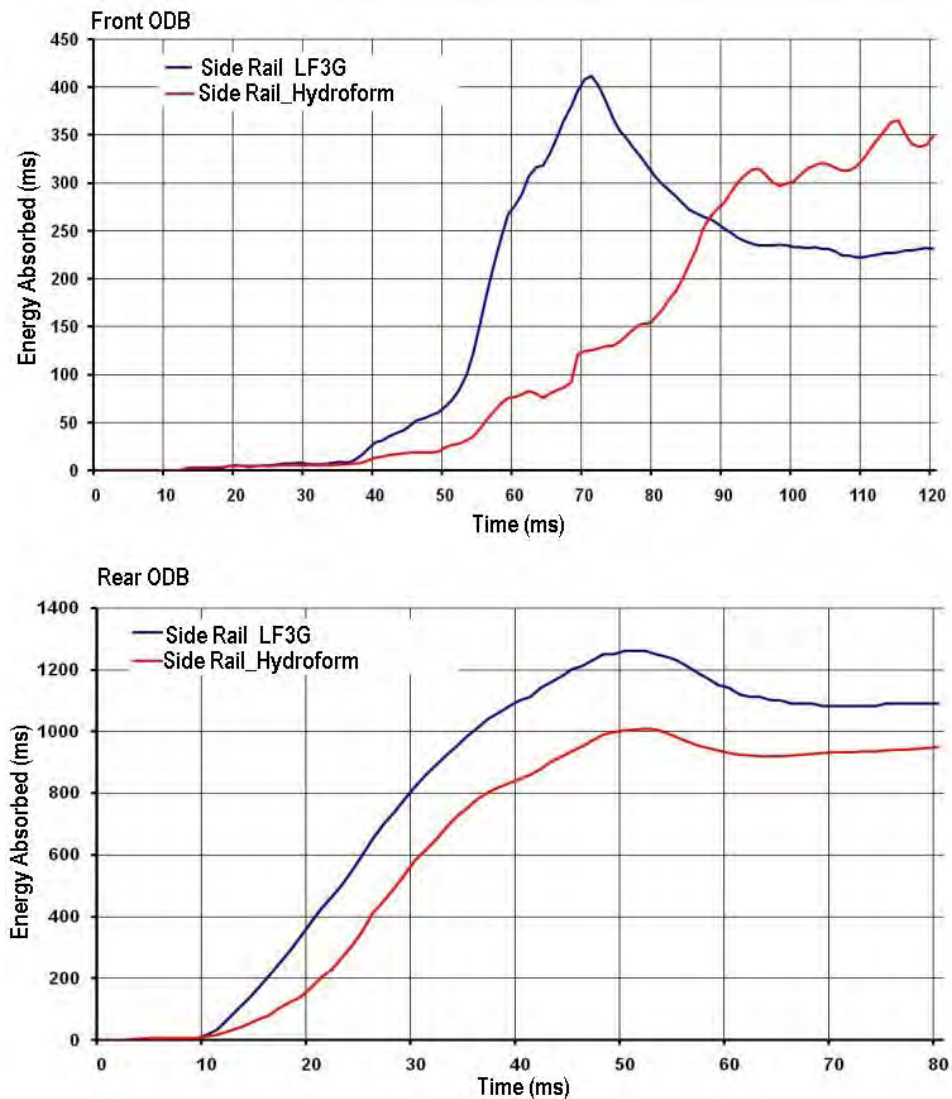


Figure 10.67: Side roof rail concept - cross-sectional parameterization

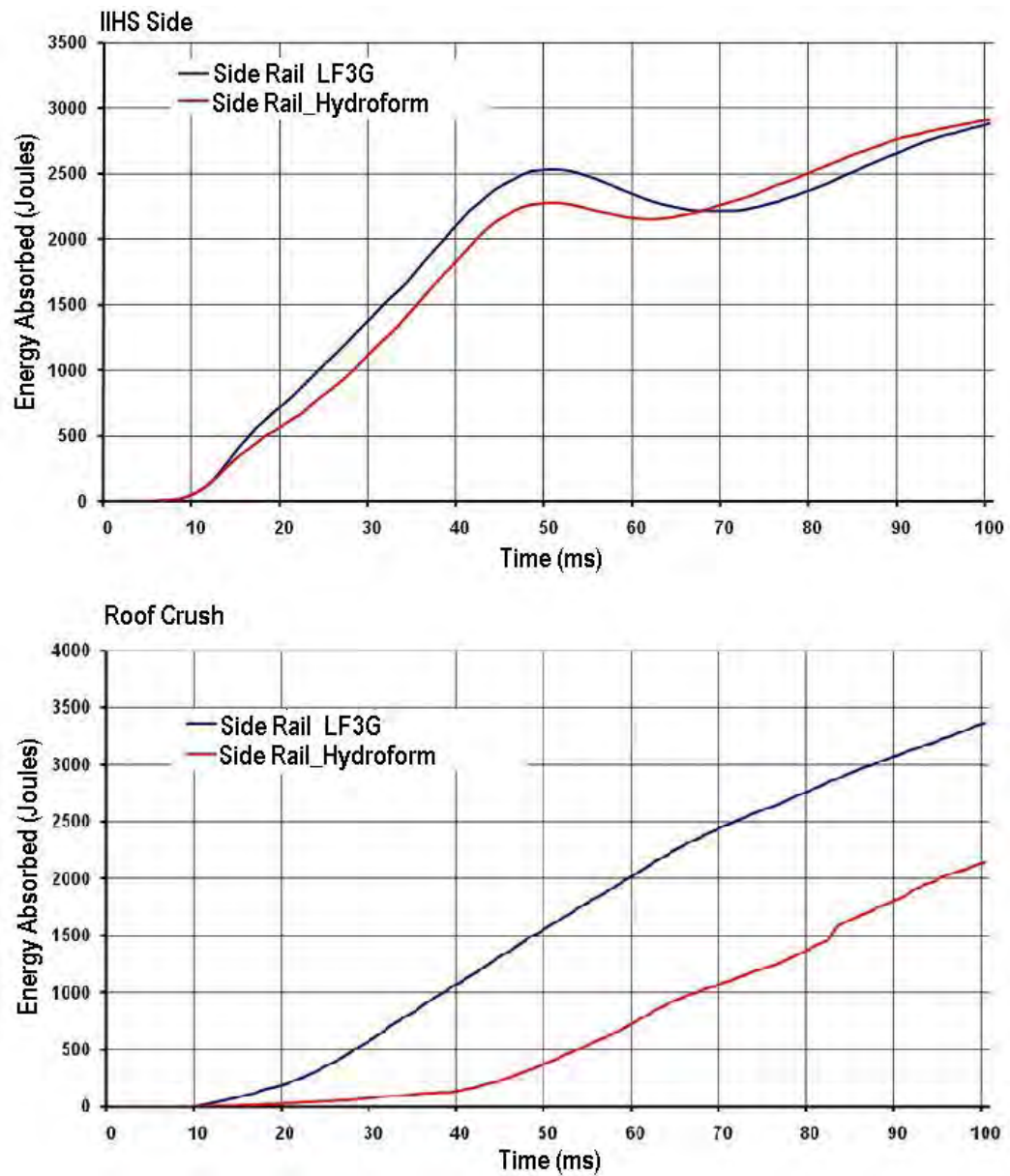


Figure 10.68: Side roof rail concept - cross-sectional parameterization

Figure 10.69 shows the geometry, grade and gauge selections for the hydroformed side roof rail concept. The final mass for this design solution was 9.8 kg, which is an 14% mass reduction compared to the baseline design (11.42 kg).

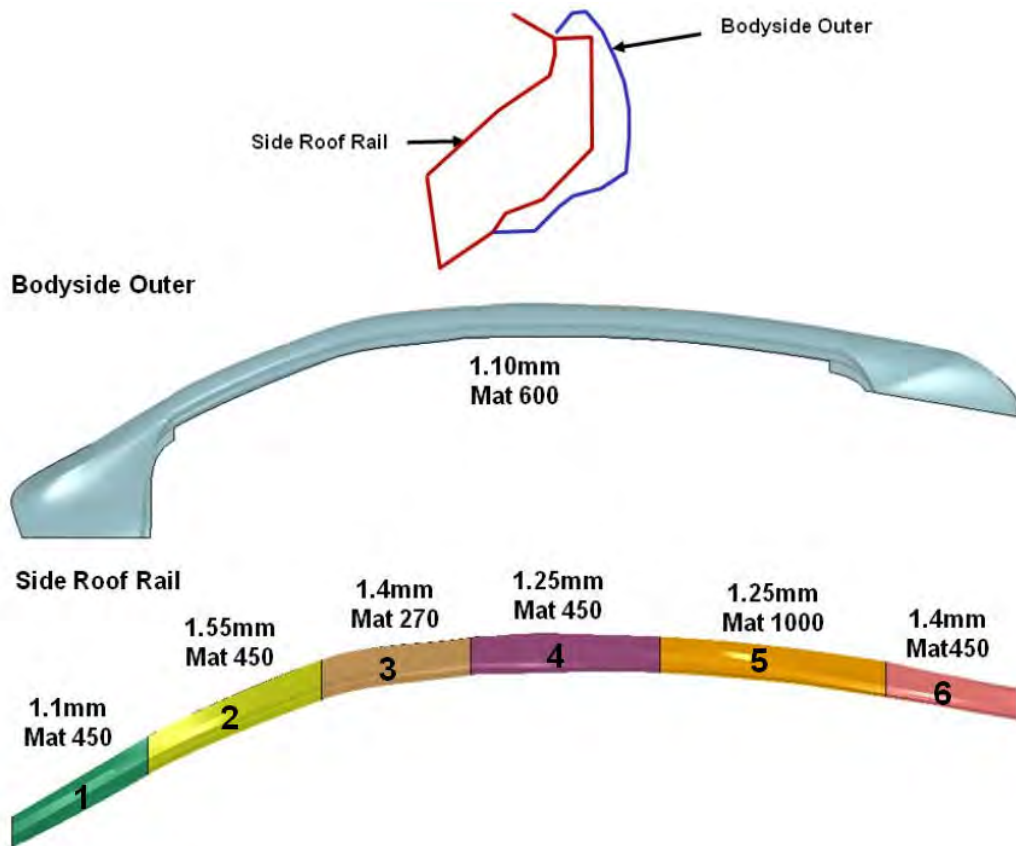


Figure 10.69: *Hydroformed side roof rail - final grade & gauge selections*

10.8 Side Roof Rail Sub-System

10.8.5 Aluminum Side Roof Rail Concept

10.8.5.1 Grade and Gauge Design Space

The aluminum side roof rail concept consists of a body side outer and side roof rail both made from aluminum. See Figure 10.70. There is no variation in gauge along the length of the component, only differences in cross section were allowed. Details of the gauge choices for the side roof rail and body side outer are listed in Table 10.11. For both components the material was set to aluminum.



Figure 10.70: Aluminum side roof rail concept - zones of grade & gauge variation

EXTRUDED ALUMINUM SIDE ROOF RAIL GAUGE CHOICES			EXTRUDED ALUMINUM SIDE ROOF RAIL GRADE CHOICES	
FROM	0.8 mm	In 0.01 mm increments	ALUMINUM GRADE	AL 7075
TO	6.0 mm			

Table 10.11: Extruded aluminum side roof rail - available grade & gauge choices

10.8.5.2 Geometry Parameterization

Figure 10.71 shows the parameterization of the cross section.

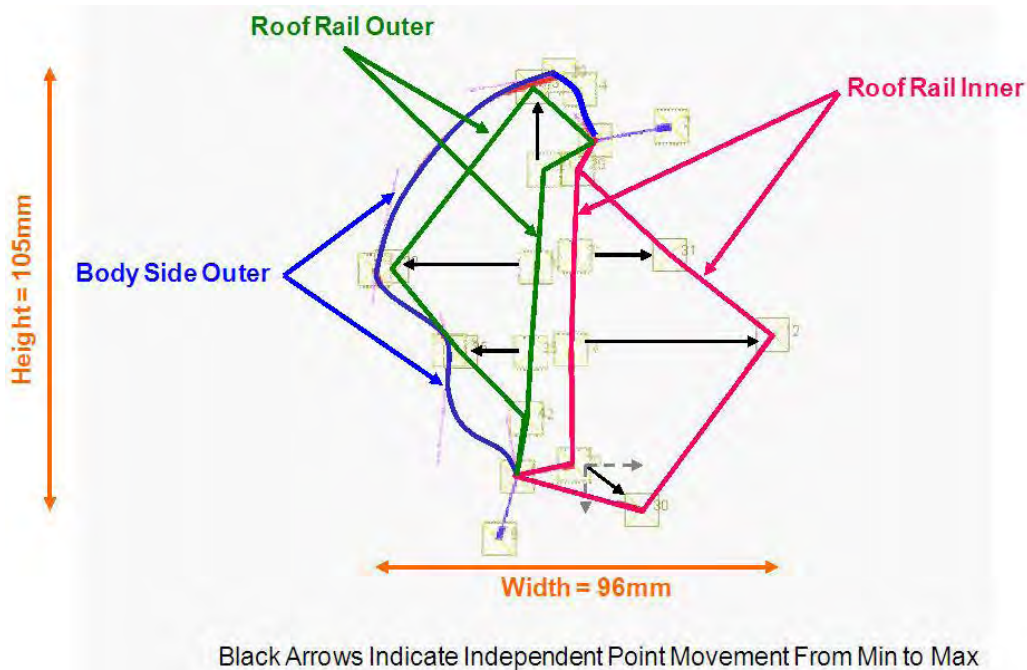


Figure 10.71: Extruded aluminum side roof rail concept - cross-sectional parameterization

10.8.5.3 Optimization Setup

- Objective: The optimization objective is to maintain the performance of the side roof rail so that the total strain energy remains the same as the LF3G for front ODB, rear ODB, IIHS side and pole impacts and roof crush. The mass of the LF3G side roof rail is 11.42 kg
- Target: Optimization target is to minimize the mass of the side roof rail.
- Constraint: The energy absorbed by the side roof rail in the LF3G model (full model) was used as a constraint for the optimization. However, because this is an aluminum concept the energy values were recalculated from an updated version of the full LF3G model. In this case, the side roof rail and body side outer material was revised from steel to aluminum. For load cases that experience plastic deformation, the energy absorbed was maintained at $\pm 15\%$ of the LF3G's performance. For load cases that result in elastic deformation, the energy absorbed was maintained at a level less than that of LF3G's performance. Thus for rear ODB, IIHS side and pole impacts and roof crush, the energy absorption was held at $\pm 15\%$ of energy absorption for the revised LF3G and for front ODB impact the energy absorption target was 650J. (For further information on target energy value calculations for aluminum, refer to Appendix 20.4 for details)

10.8.5.4 Extruded Aluminum Side Roof Rail : Design Solution

Figure 10.72 & Figure 10.73 show the comparison of energy absorption for the baseline LF3G side roof rail compared to the optimized extruded aluminum concept. In case of the front ODB impact the energy absorbed by the side roof rail is purely elastic energy as there is limited deformation. The total energy of the system has been maintained and so the kinetic energy has been absorbed in the rail as elastic energy. In the case of rear ODB, IIHS side and pole impacts and roof crush, the rail experienced significant deformation resulting in a high amount of strain energy absorption.

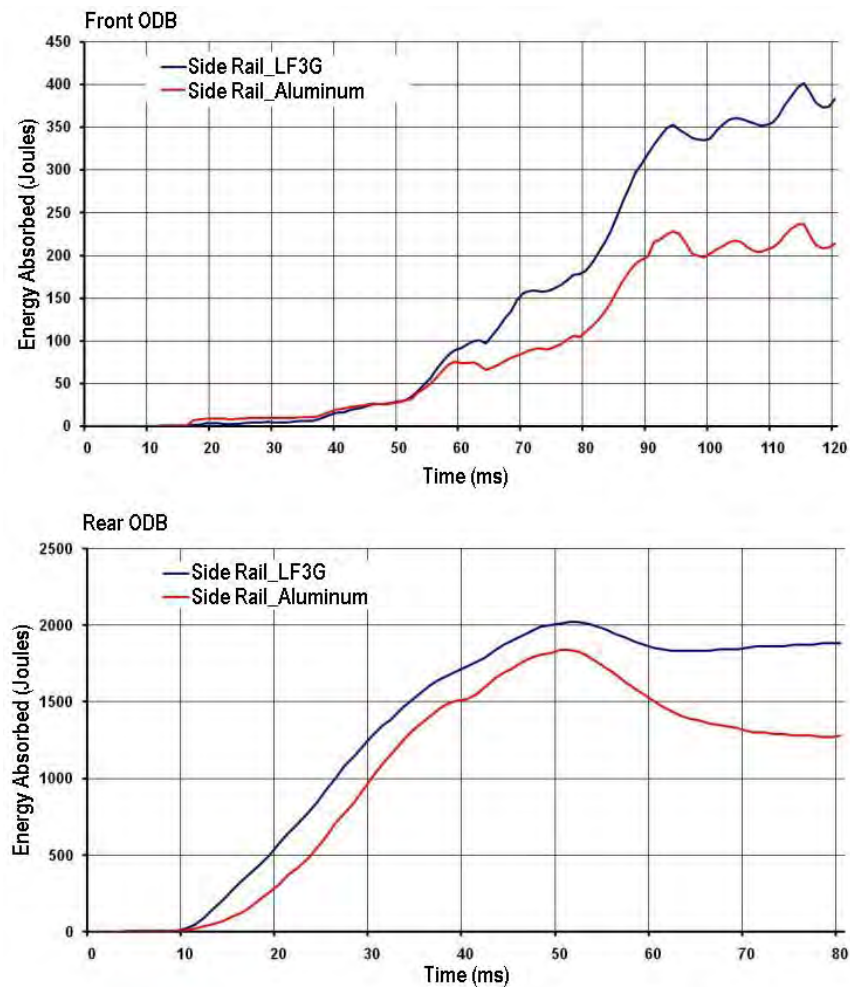


Figure 10.72: Extruded aluminum side roof rail design solution - energy absorption comparison to baseline

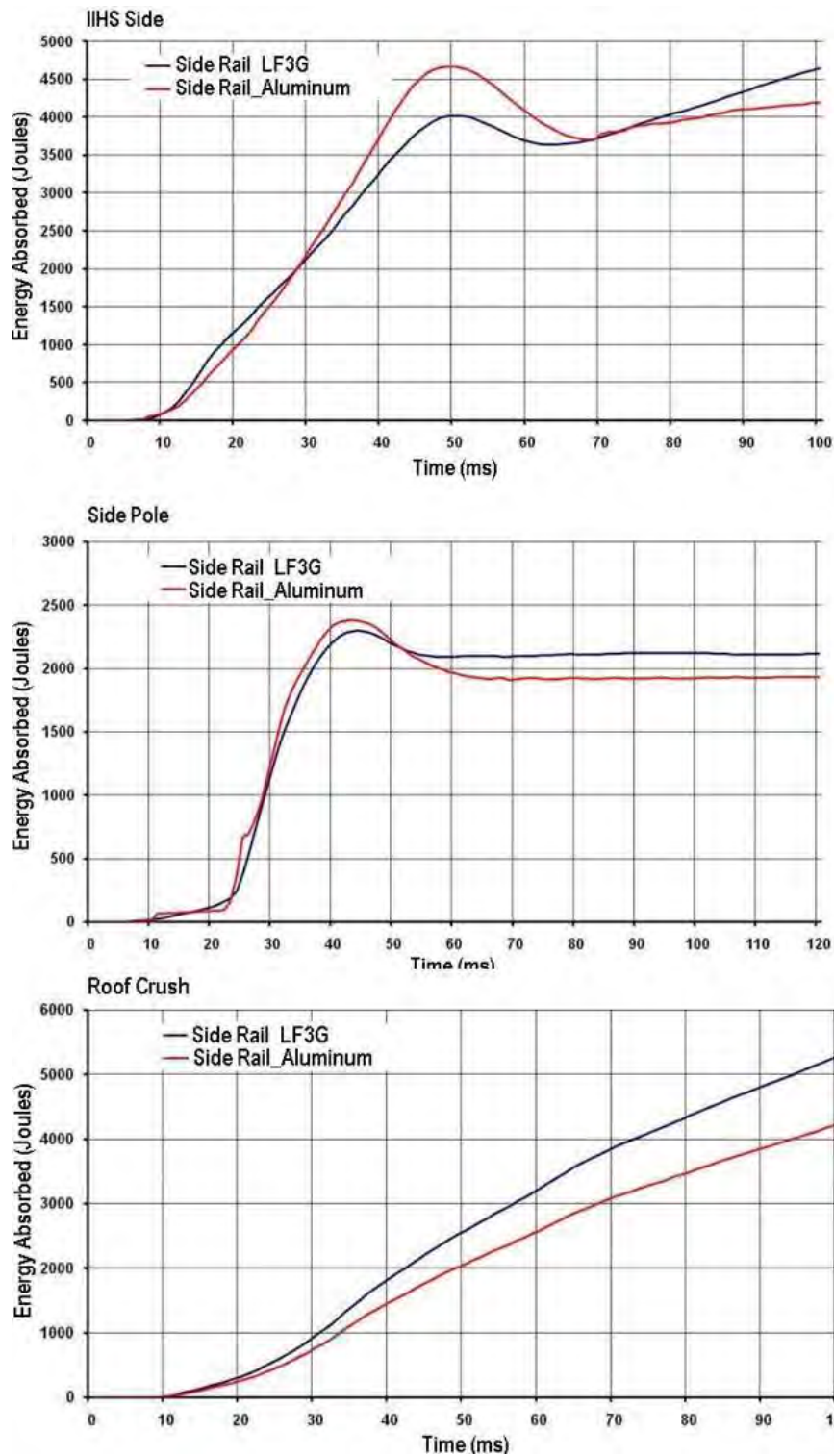


Figure 10.73: Extruded aluminum side roof rail design solution - energy absorption comparison to baseline

Figure 10.74 shows the geometry, grade and gauge selections for the extruded aluminum side roof rail concept. The final mass for this design solution was 10.43 kg, which is an 8.67% mass reduction compared to the baseline design (11.42 kg).

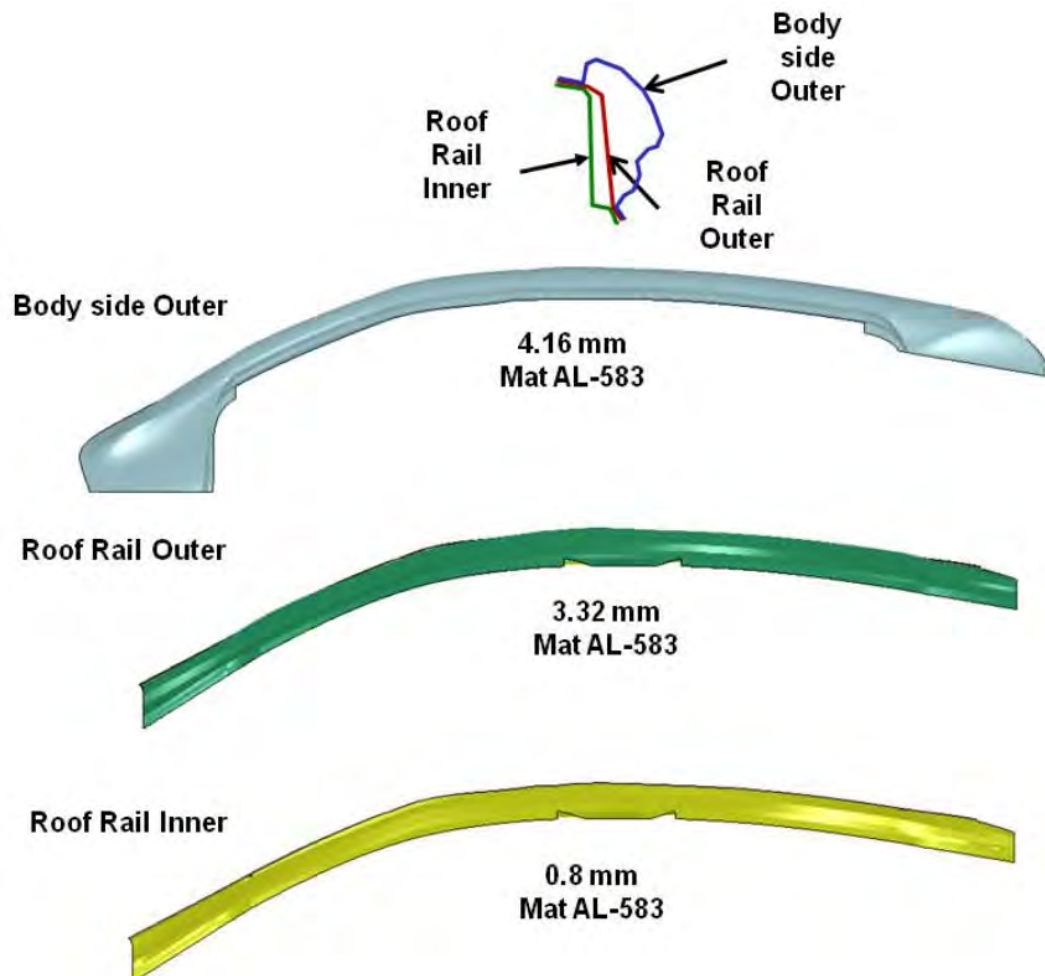


Figure 10.74: Extruded aluminum side roof rail - final grade & gauge selections

10.9 Rear Rail Sub-System

The rear rail sub-system optimization considered three manufacturing concepts; a steel stamping, a steel hydroform and an aluminum stamping

10.9.1 Development of Sub-System from Full Model

The rear rail sub-system was developed from full model (LF3G) such that when analyzed under the same loading conditions it behaved in the same way as the full model. The sub-system model consists of the rear rail and the major attachment components it is attached to such as the rear floor, rocker, rear wheel arch and cross beam. See Figure 10.75.

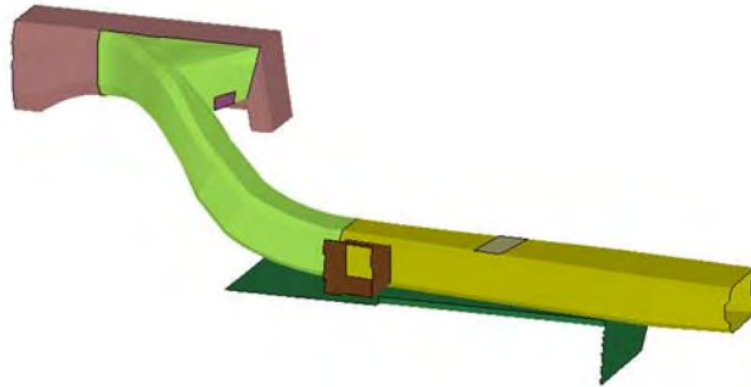


Figure 10.75: *Rear Rail sub-system from LF3G*

10.9.2 Generating Boundary Conditions

The nodal displacement time history is used as the boundary conditions for the sub-system so that it behaves in a similar manner to the full LF3G model. The method used was exactly the same as was described for the rocker in section 10.6.2. Referring to Figure 10.76, shows the specific boundaries applied to the rear rail sub-system model.

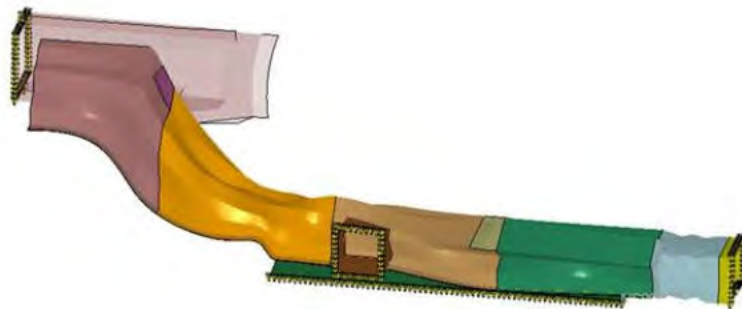


Figure 10.76: *Rear Rail sub-system with highlighted boundaries for time history*

10.9 Rear Rail Sub-System

The performance of sub-system model was validated under the loadcases considered, rear ODB impact and torsional stiffness, to confirm that it behaved as the full model did. The energy absorbed by the rear rail under the loading conditions considered was used as the performance target.

10.9.3 Stamped Rear Rail Concept

10.9.3.1 Grade and Gauge Design Space

The stamped rear rail concept consists of the rear rail outer and rear rail reinforcement. Each component was divided into 4 regions. Referring to Figure 10.77; these are shown as regions A through D. The choice of grade and gauge of each region could be varied independently of the others. Details of the available grade and gauge choices are listed in Table 10.12.

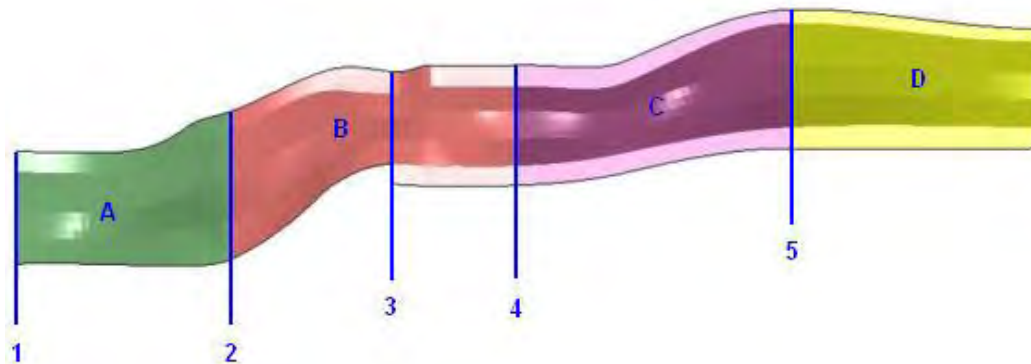


Figure 10.77: *Stamped rear rail concept - zones of grade & gauge variation*

STAMPED REAR RAIL GAUGE CHOICES			STAMPED REAR RAIL GRADE CHOICES	
FROM	0.5 mm (INNER & OUTER)	In 0.01 mm increments	ULTIMATE TENSILE (MPa)	MAT 270
TO	2.0 mm			MAT 340
		MAT 450		
		MAT 500		
		MAT 600		
		MAT 800		
		MAT 1000		
		MAT 1300		
		MAT 1500		

Table 10.12: *Stamped rear rail - available grade & gauge choices*

10.9.3.2 Geometry Optimization

The geometry design space is limited as an outer boundary package space established in chapter 4. Referring to Figure 10.77, the cross-section at locations 1 through 3 can be varied independently of each other. Thus for each region, A through D, the shape will vary along the length of the region based on the cross sections at each end. The range of the packaging space for each cross section 1 through 3 is shown in Figure 10.78.

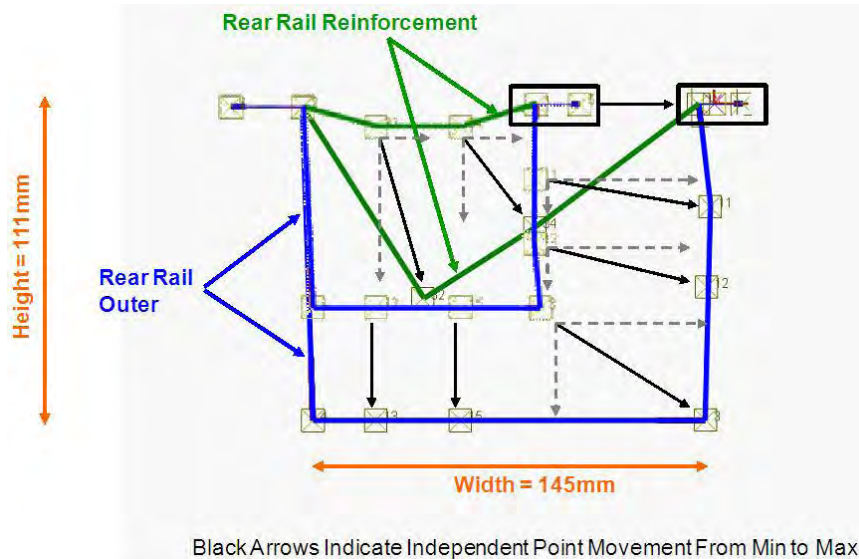


Figure 10.78: Stamped rear rail concept - cross-sectional parameterization

10.9.3.3 Optimization Setup

- Objective: The optimization objective is to maintain the performance of the rear rail so that the total strain energy remains same as the LF3G for rear ODB and torsional stiffness. The mass of the LF3G rear rail is 7.3 kg.
- Target: The optimization target is to minimize the mass of the rear rail.
- Constraint: The energy absorbed by the rear rail in the LF3G model (full model) was used as a constraint for the optimization. For torsional stiffness the energy absorbed was also used as the constraint rather than a displacement due to the lack of a representative measurement point on the rear rail itself. Thus for rear ODB and torsional stiffness the energy absorption was held at $\pm 15\%$ of energy absorption for the LF3G.

10.9.3.4 Stamped Rear Rail : Design Solution

All results from the optimization are compared to the baseline LF3G rear rail. Figure 10.79 shows the deformation of the baseline LF3G design and the optimized stamped concept for rear ODB impact. It clearly shows considerable high plastic deformation leading to high strain energy absorption by the rear rail.

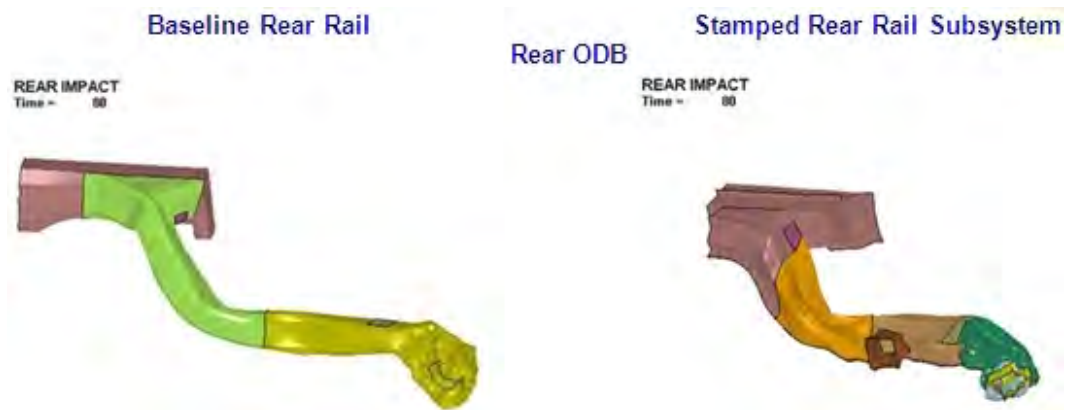


Figure 10.79: Stamped rear rail design solution - deformation comparison to baseline

Figure 10.80 shows the comparison of energy absorption for the baseline LF3G rear rail compared to the optimized stamped concept. In the case of the rear ODB impact, the rear rail experienced significant deformation, leading to high level of strain energy absorption. The torsional stiffness also correlates well.

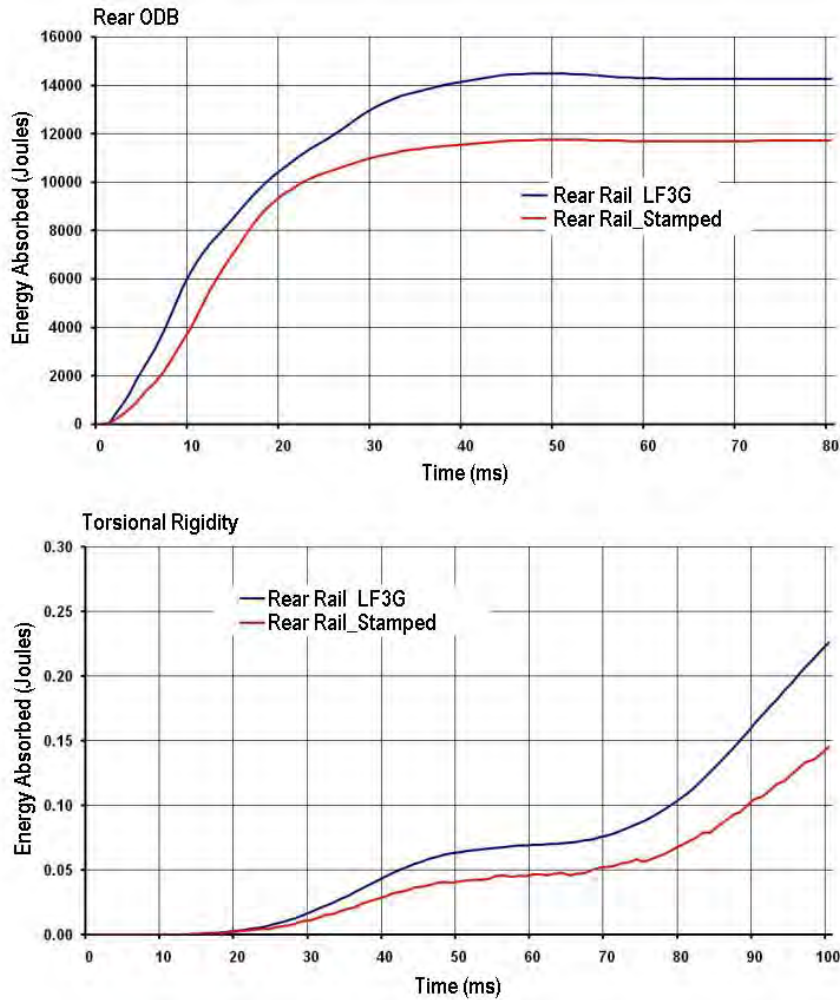


Figure 10.80: Stamped rear rail design solution - energy absorption comparison to baseline

Figure 10.81 shows the geometry, grade and gauge selections for the stamped rear rail concept. The final mass for this design solution was 5.6 kg, which is a 23% mass reduction compared to the baseline design (7.3 kg).

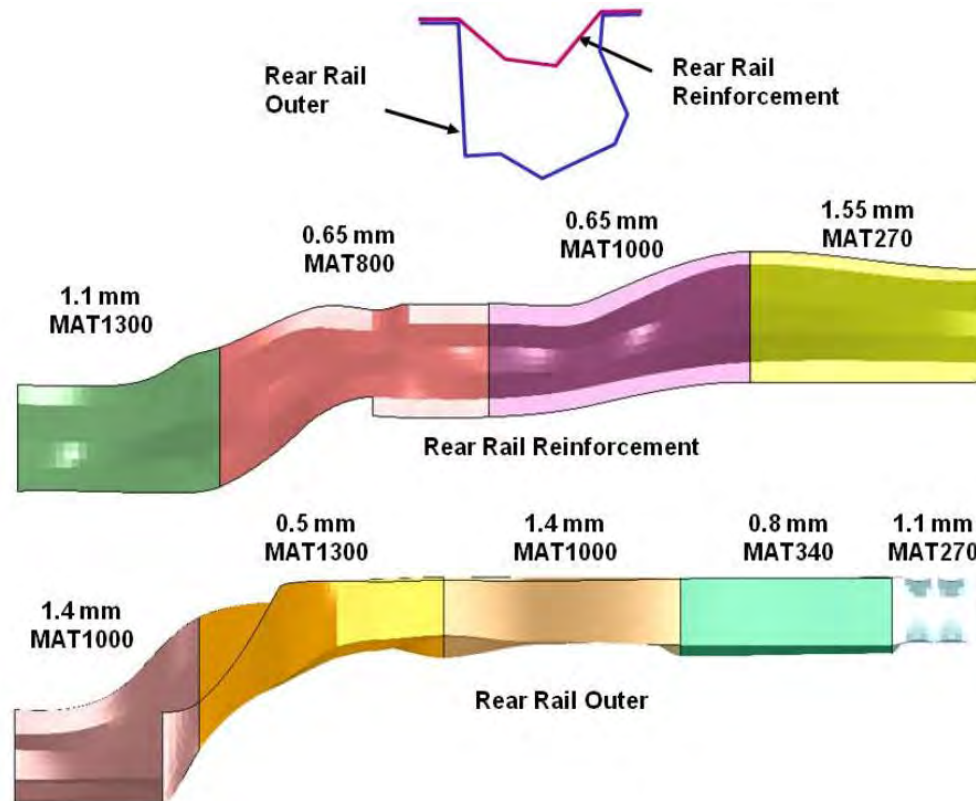


Figure 10.81: Stamped rear rail - final grade & gauge selections

10.9.4 Hydroformed Rear Rail Concept

The complete sub-system optimization process for the rear rail has already been discussed previously. Here the only differences in the grade and gauge selection and geometry parameterization for this concept are discussed.

10.9.4.1 Grade and Gauge Design

The hydroformed rear rail concept consists of a rear rail tube, there is no reinforcement. Each component was divided into 5 regions. Referring to Figure 10.82; these are shown as regions A through E. Region E represents a rear crush can. The choice of grade and gauge of each region can be varied independently of the others. Details of the available grade and gauge choices are listed in Table 10.13. Note that for hydroforming, material variation is limited to an ultimate tensile strength of 1000 MPa.

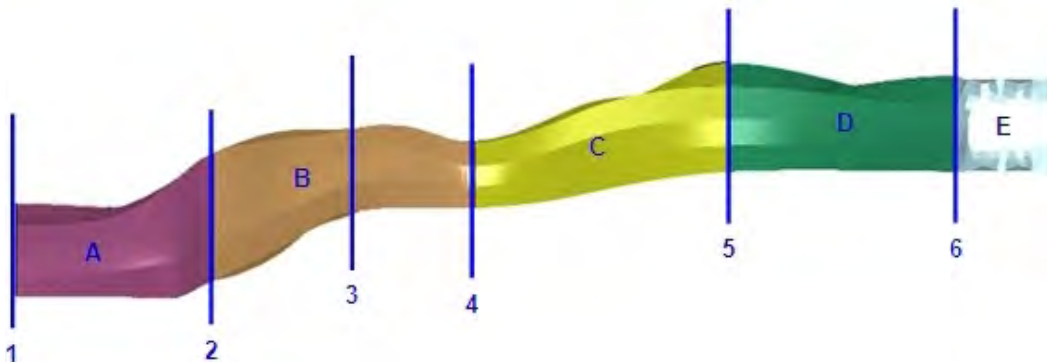


Figure 10.82: Hydroformed rear rail concept - zones of grade & gauge variation

HYDROFORMED REAR RAIL GAUGE CHOICES			HYDROFORMED REAR RAIL GRADE CHOICES	
FROM	0.5 mm	In 0.01 mm increments	ULTIMATE TENSILE (MPa)	MAT 340
TO	2.0 mm			MAT 450
		MAT 500		
		MAT 600		
		MAT 800		
		MAT 1000		

Table 10.13: Hydroformed rear rail - available grade & gauge choices

10.9.4.2 Geometry Parameterization

Referring to Figure 10.82, the cross-section at locations 1 through 4 can be varied independently of each other and so the shape will vary along the length of each region, A through E, based on the

cross sections at each end. The range of the packaging space for each cross section 1 through 4 is shown in Figure 10.83.

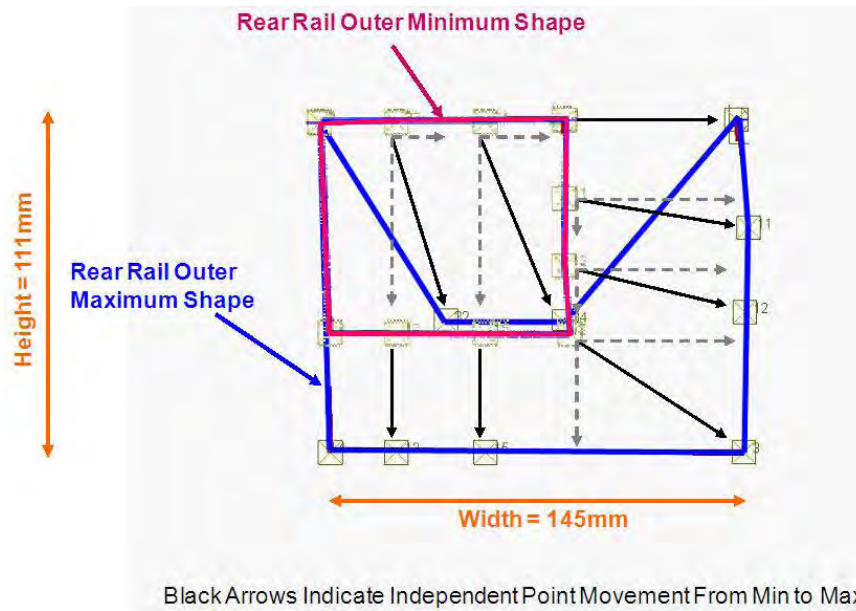


Figure 10.83: Hydroformed rear rail concept - cross-sectional parameterization

10.9.4.3 Hydroformed Rear Rail : Design Solution

All results from the optimization are compared to the baseline LF3G rear rail. Figure 10.84 shows the deformation of the baseline LF3G design and the optimized hydroformed concept for rear ODB impact. It clearly shows considerable high plastic deformation leading to high strain energy absorption by the rear rail.

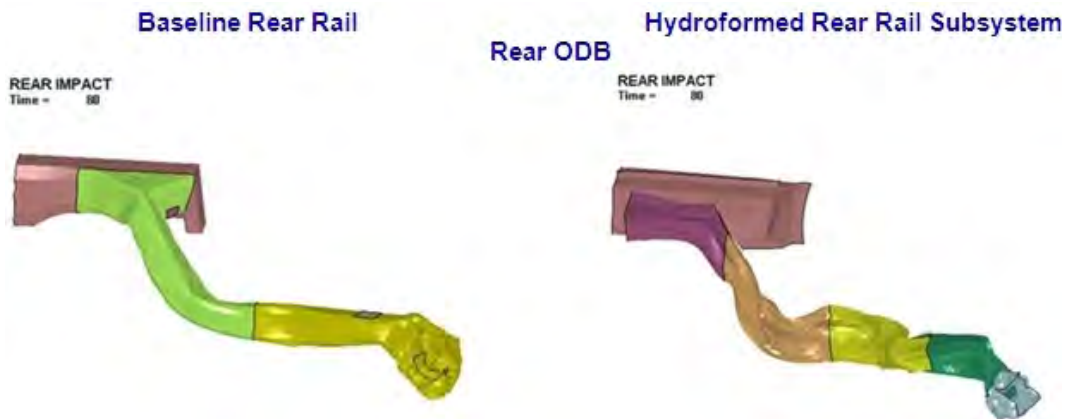


Figure 10.84: Hydroformed rear rail design solution - deformation comparison to baseline

Figure 10.85 shows the comparison of energy absorption for the baseline LF3G rear rail compared to the optimized hydroformed concept. In the case of the rear ODB impact, the rear rail experienced significant deformation, leading to high level of strain energy absorption. The torsional stiffness also correlates well.

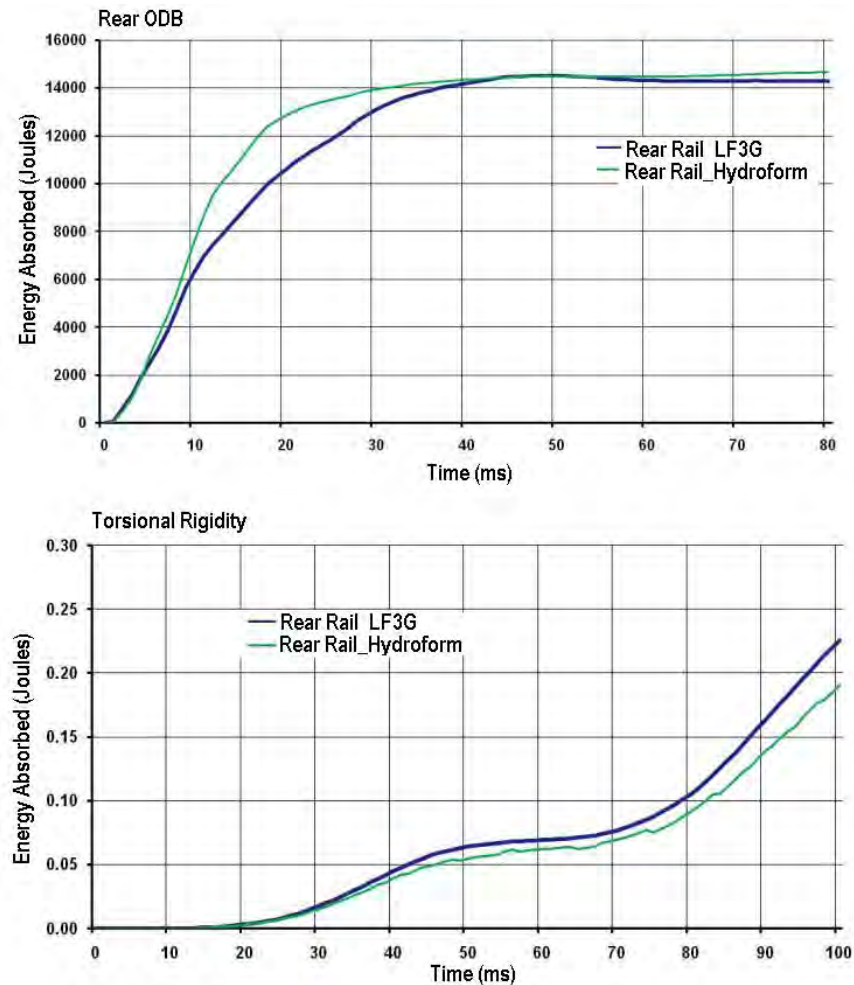


Figure 10.85: Hydroformed rear rail design Solution - energy absorption comparison to baseline

Figure 10.86 shows the geometry, grade and gauge selections for the hydroformed rear rail concept. The final mass for this design solution was 5.1 kg, which is a 30% mass reduction compared to the baseline design (7.3 kg).

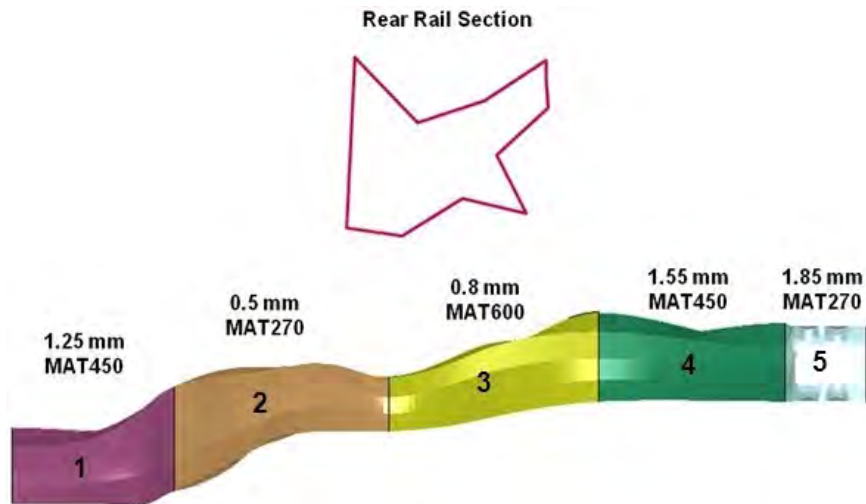


Figure 10.86: Hydroformed rear rail - final grade & gauge selections

10.9.5 Stamped Aluminum Rear Rail Concept

10.9.5.1 Grade and Gauge concept

The stamped aluminum rear rail concept consists of the rear rail outer and rear rail reinforcement. Referring to Figure 10.87 shows the a single gauge was applied along the entire length of the rail. Details of the available grade and gauge choices are listed in Table 10.14

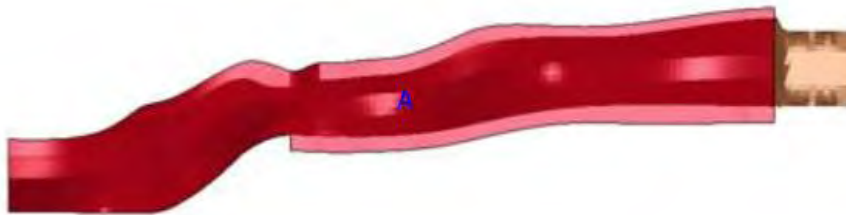


Figure 10.87: Stamped aluminum rear rail concept - zones of grade & gauge variation

STAMPED ALUMINUM REAR RAIL GAUGE CHOICES			STAMPED ALUMINUM REAR RAIL GRADE	
FROM	2.0 mm	In 0.01 mm increments	ALUMINUM GRADE	AL 7075
TO	6.0 mm			

Table 10.14: Stamped aluminum rear rail - available grade & gauge choices

10.9.5.2 Geometry Parameterization

Figure 10.88 shows the parameterization of the cross section.

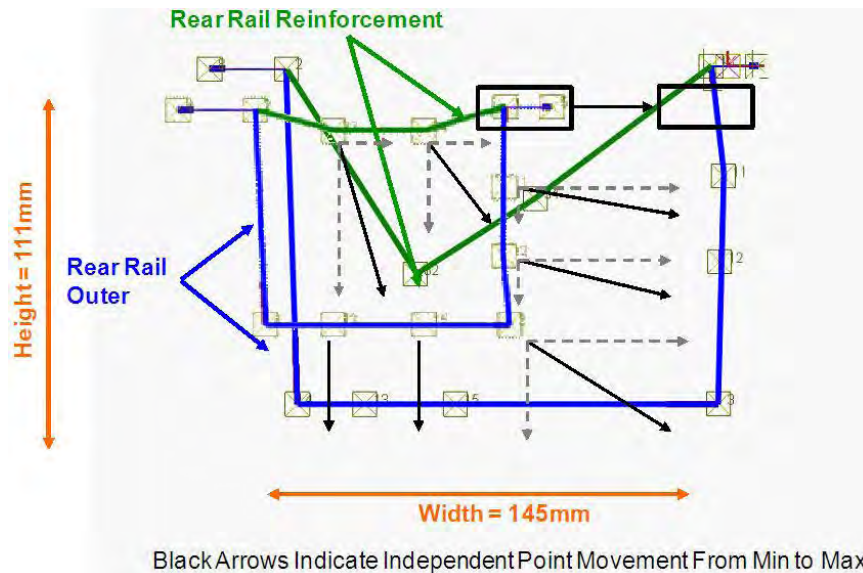


Figure 10.88: Stamped aluminum rear rail concept - cross-sectional parameterization

10.9.5.3 Optimization Setup

- Objective: The optimization objective is to maintain the performance of the rear rail so that the total strain energy remains the same as the LF3G for rear ODB impact and torsional stiffness. The mass of the LF3G rear rail is 7.3 kg
- Target: Optimization target is to minimize the mass of the rear rail.
- Constraint: The energy absorbed by the rear rail in the LF3G model (full model) was used as a constraint for the optimization. For torsional stiffness the energy absorbed was also used as the constraint rather than a displacement due to the lack of a representative measurement point on the rear rail itself. However, because this is an aluminum concept the energy values were recalculated from an updated version of the full LF3G model. In this case, the rear rail material was revised from steel to aluminum. Thus for the rear ODB and torsional stiffness the energy absorption was held at $\pm 15\%$ of energy absorption for the LF3G. (For further information on target energy value calculations for aluminum, refer to Appendix 20.4 for details)

10.9.5.4 Stamped Aluminum Rear Rail : Design Solution

All results from the optimization are compared to the baseline LF3G rear rail. Figure 10.89 shows the deformation of the baseline LF3G design and the optimized stamped aluminum concept for rear ODB impact. It clearly shows considerable high plastic deformation leading to high strain energy absorption by the rear rail.

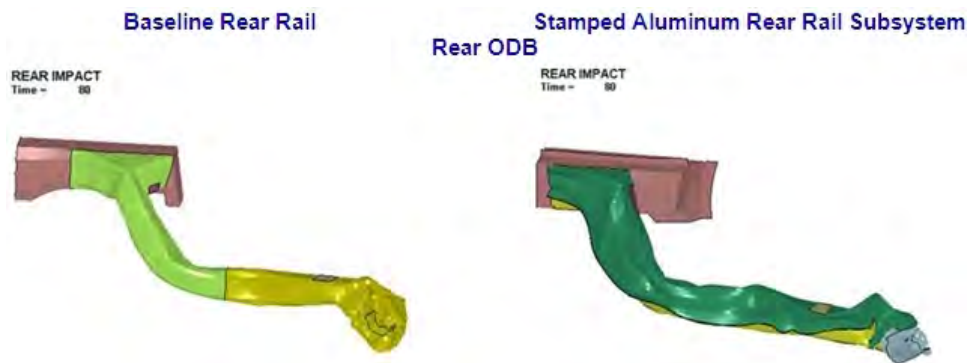


Figure 10.89: Stamped aluminum rear rail design solution - deformation comparison to baseline

Figure 10.90 shows the comparison of energy absorption for the baseline LF3G rear rail compared to the optimized stamped aluminum concept. In the case of the rear ODB impact, the rear rail experienced significant deformation, leading to high level of strain energy absorption. The torsional stiffness also correlates well.

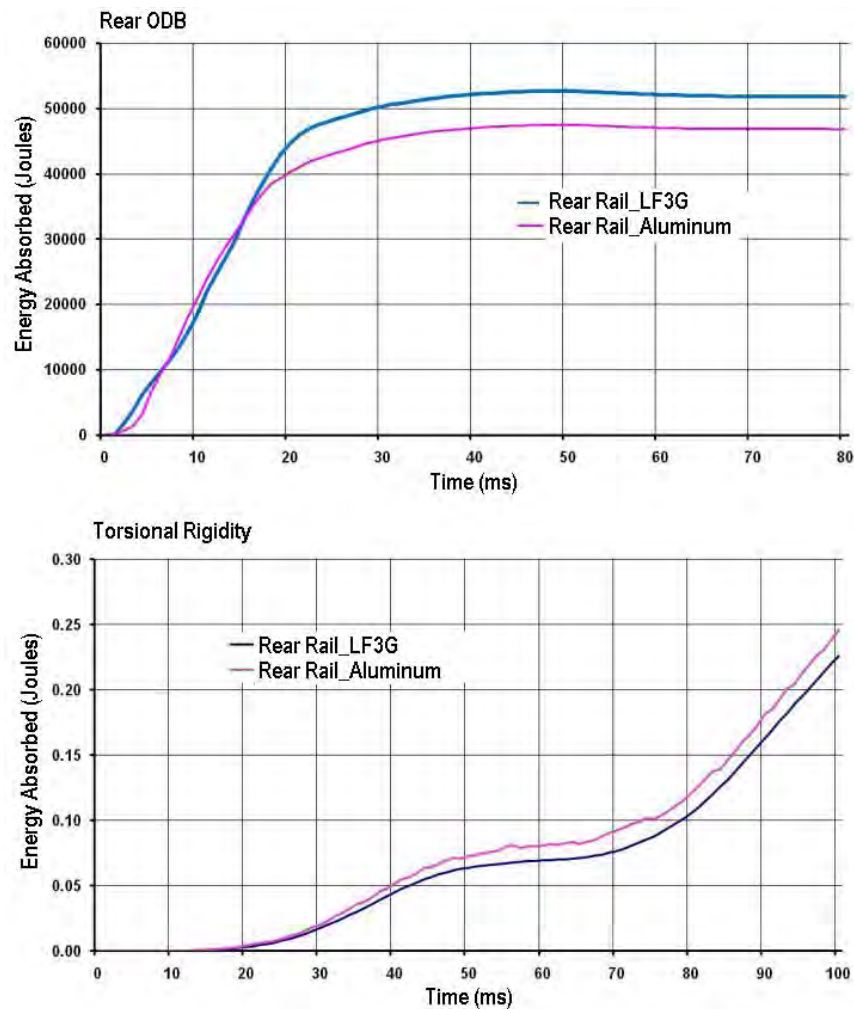


Figure 10.90: Stamped aluminum rear rail design solution - energy absorption comparison to baseline

Figure 10.91 shows the geometry, grade and gauge selections for the stamped aluminum rear rail concept. The final mass for this design solution was 5.8 kg, which is a 21% mass reduction compared to the baseline design (7.3 kg).

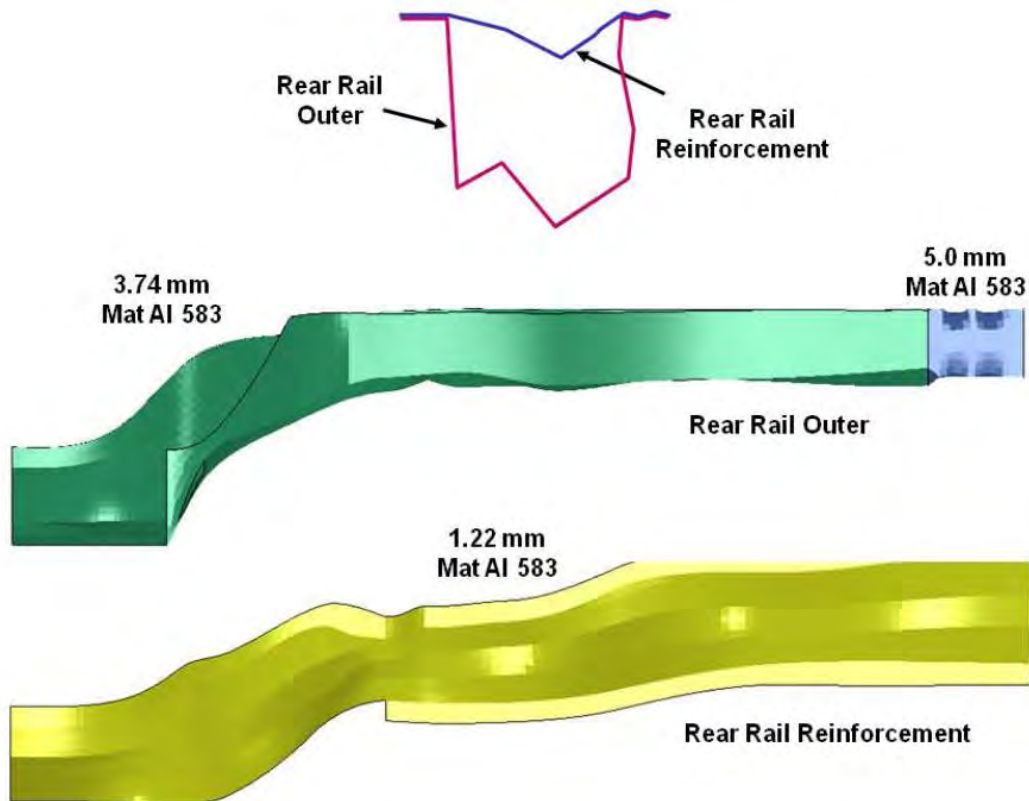


Figure 10.91: Stamped aluminum rear rail design solution - energy absorption comparison to baseline

10.10 Battery Tunnel Rail Sub-System

The tunnel rail sub-system optimization considered three manufacturing concepts; a steel stamping, a steel open roll form and an aluminum extrusion

10.10.1 Development of sub-system From Full model

The tunnel rail sub-system was developed from full model (LF3G) such that when analyzed under the same loading conditions it behaved in the same way as the full model. The sub-system model consists of upper and lower tunnel rails and the major attachment components they are attached to such as the front rail, cradle, firewall, the underbody cross-beams, floor and batter cover. See Figure 10.92.

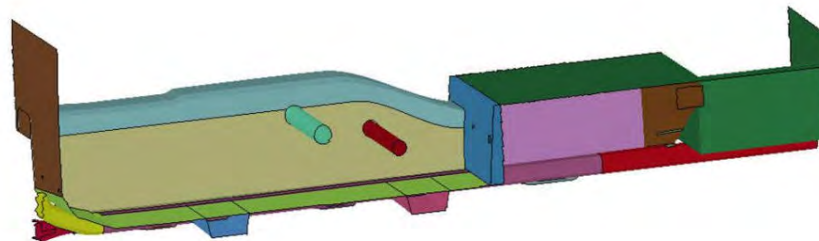


Figure 10.92: Stamped aluminum rear rail design solution - energy absorption comparison to baseline

10.10.2 Generating Boundary Conditions

The nodal displacement time history is used as the boundary conditions for the sub-system so that it behaves in a similar manner to the full LF3G model. The method used was exactly the same as was described for the rocker in section 10.6.2. Referring to Figure 10.93, shows the specific boundaries applied to the tunnel rail sub-system model.

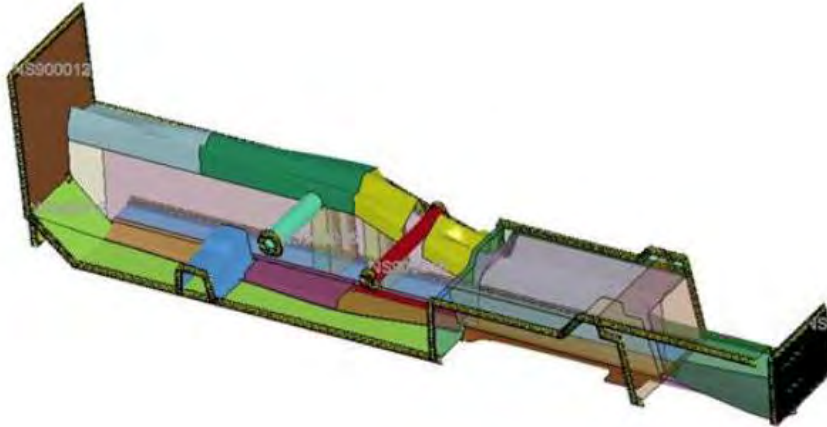


Figure 10.93: Tunnel rails sub-system from LF3G

The performance of sub-system model was validated under the loadcases considered, front ODB, rear ODB and IIHS side impacts and 3G jounce, to confirm that it behaved in the same way as the full model. The energy absorbed by the tunnel rails under the loading conditions considered was used as the performance target.

10.10 Battery Tunnel Rail Sub-System

10.10.3 Stamped Tunnel Rail Concept

10.10.3.1 Grade and Gauge Concept

The stamped tunnel rails concept consists of the upper tunnel rail and the front and rear portions of the lower tunnel rail. Referring to Figure 10.94, the upper tunnel rail was divided into 3 regions, A through C. The Front lower tunnel rail was divided into 6 regions, D through I and the rear lower tunnel rail into 2 regions, J and K. The choice of grade and gauge of each region could be varied independently of the others. Details of the available grade and gauge choices are listed in Table 10.15.

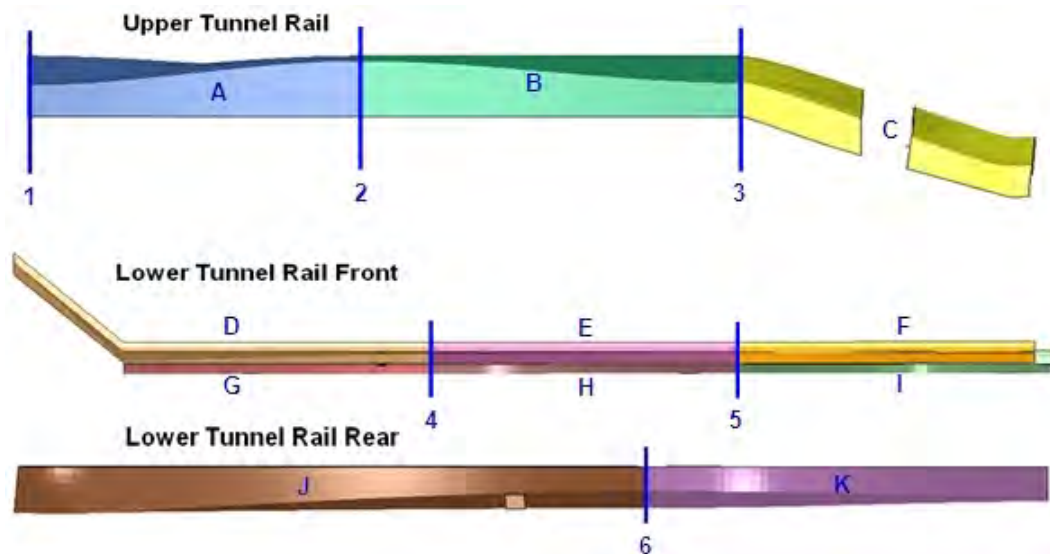


Figure 10.94: Stamped tunnel rail concept - zones of grade & gauge variation

STAMPED TUNNEL RAILS GAUGE CHOICES			STAMPED TUNNEL RAILS GRADE CHOICES	
FROM	0.5 mm	In 0.01 mm increments	ULTIMATE TENSILE (MPa)	MAT 270
TO	2.0 mm			MAT 340
		MAT 450		
		MAT 500		
		MAT 600		
		MAT 800		
		MAT 1000		
		MAT 1300		
		MAT 1500		

Table 10.15: Stamped tunnel rails - available grade & gauge choices

10.10.3.2 Geometry Parameterization

The geometry design space is limited as an outer boundary package space established in chapter 4. Referring to Figure 10.94, the cross-section at locations 1 through 6 can be varied independently of each other. Thus for each region, A through K, the shape will vary along the length of the region based on the cross sections at each end. The range of the packaging space for each cross section 1 through 6 is shown in Figure 10.95.

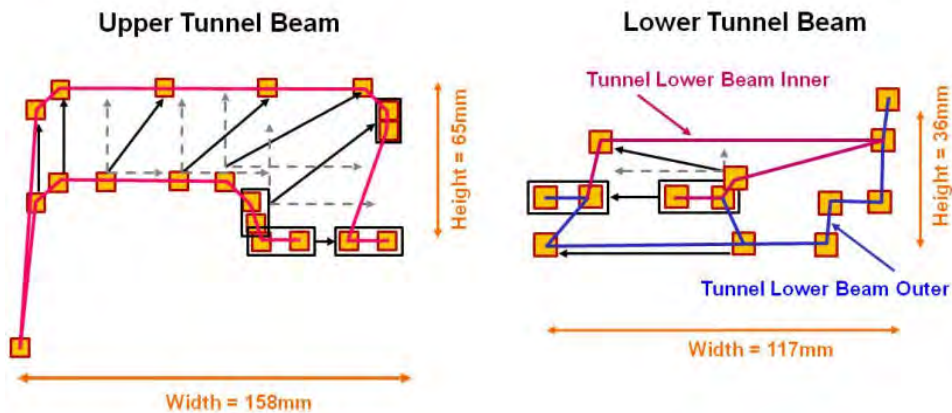


Figure 10.95: Stamped tunnel tail concept - cross-sectional parameterization

10.10.3.3 Optimization Setup

- Objective: The optimization objective is to maintain the performance of the upper and lower tunnel rails so that the total strain energy remains same as the LF3G for front ODB, rear ODB, IIHS side and 3G jounce. The mass of the LF3G tunnel rails is 12.5 kg.
- Target: The optimization target is to minimize the mass of the tunnel rails.
- Constraint: The energy absorbed by the tunnel rails in the LF3G model (full model) was used as a constraint for the optimization. For load cases that experience plastic deformation, the energy absorbed was maintained at $\pm 15\%$ of the LF3G's performance. For load cases that result in elastic deformation, the energy absorbed was maintained at a level less than that of LF3G's performance. Thus for rear ODB the energy absorption was held at $\pm 15\%$ of the energy absorption for the LF3G. For front ODB the energy absorption was 800 J and IIHS side the energy absorption was 600 J. For 3G jounce the Z-displacement of the tunnel lower rail was held within 10% of 2.3 mm. (For further information on target energy value calculations, refer to Appendix 20.3 for details)

10.10.3.4 Stamped Tunnel Rail : Design Solution

All results from the optimization are compared to the baseline LF3G tunnel rails. Figure 10.96 shows the deformation of the baseline LF3G design and the optimized stamped concept for front ODB, rear ODB, IIHS side impacts. It clearly shows that for the front ODB and IIHS side impact there is limited deformation of the rails. In these cases, the rails are just absorbing the elastic energy. In the case of rear ODB impact, the rails have considerable plastic deformation leading to high strain energy absorption.

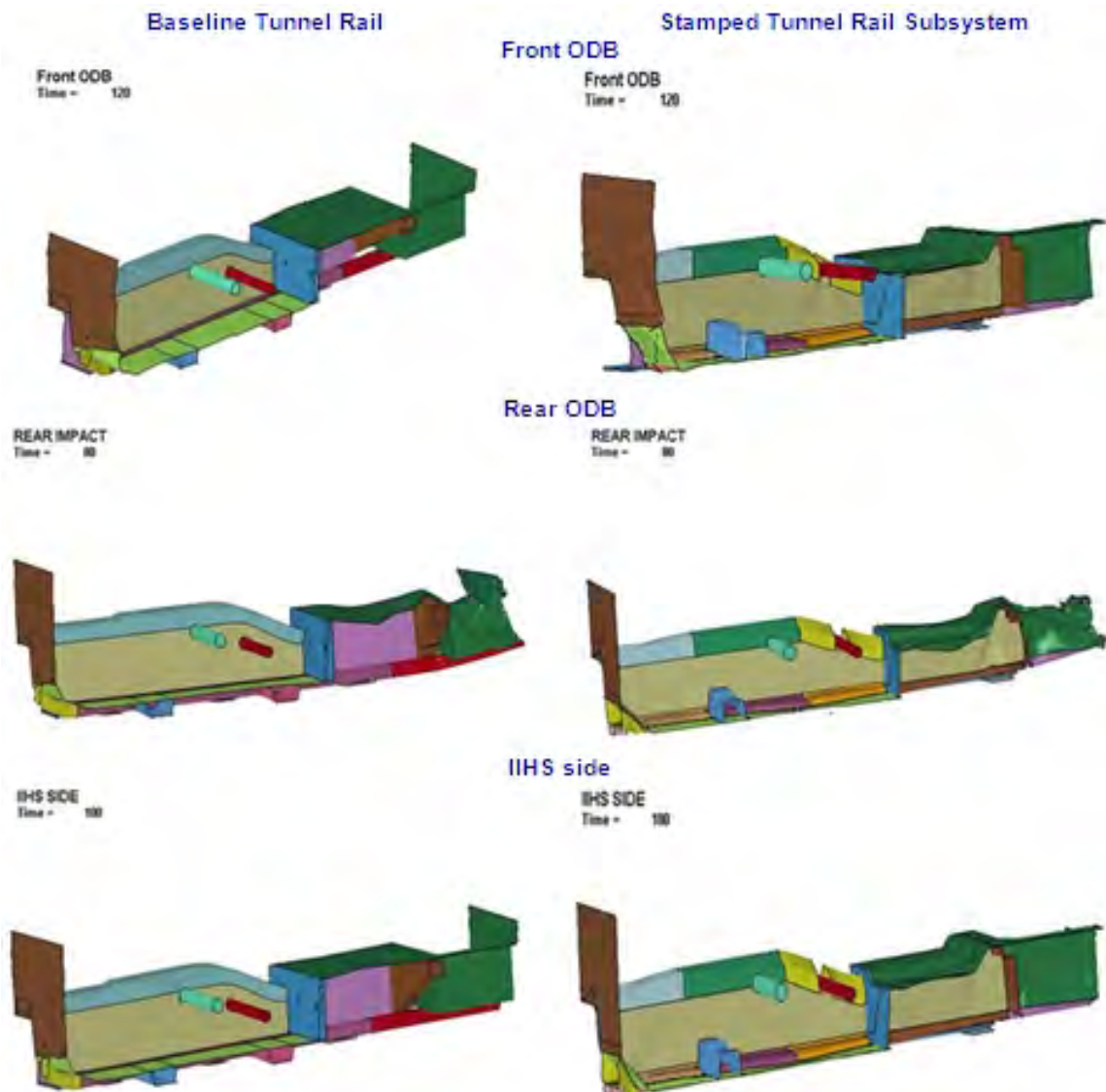


Figure 10.96: Stamped tunnel rail design solution - deformation comparison to baseline

Figure 10.97 & Figure 10.98 show the comparison of energy absorption for the baseline LF3G

tunnel rails compared to the optimized stamped concept. In case of the front ODB and IIHS side impacts the energy absorbed by the tunnel rails is purely elastic energy as there is limited deformation. The total energy of the system has been maintained and so the kinetic energy has been absorbed in the rails as elastic energy. In the case of rear ODB impact the lower rear rail experienced significant deformation resulting in a high amount of strain energy absorption. For the 3G jounce loadcase the rails showed good correlation to the baseline.

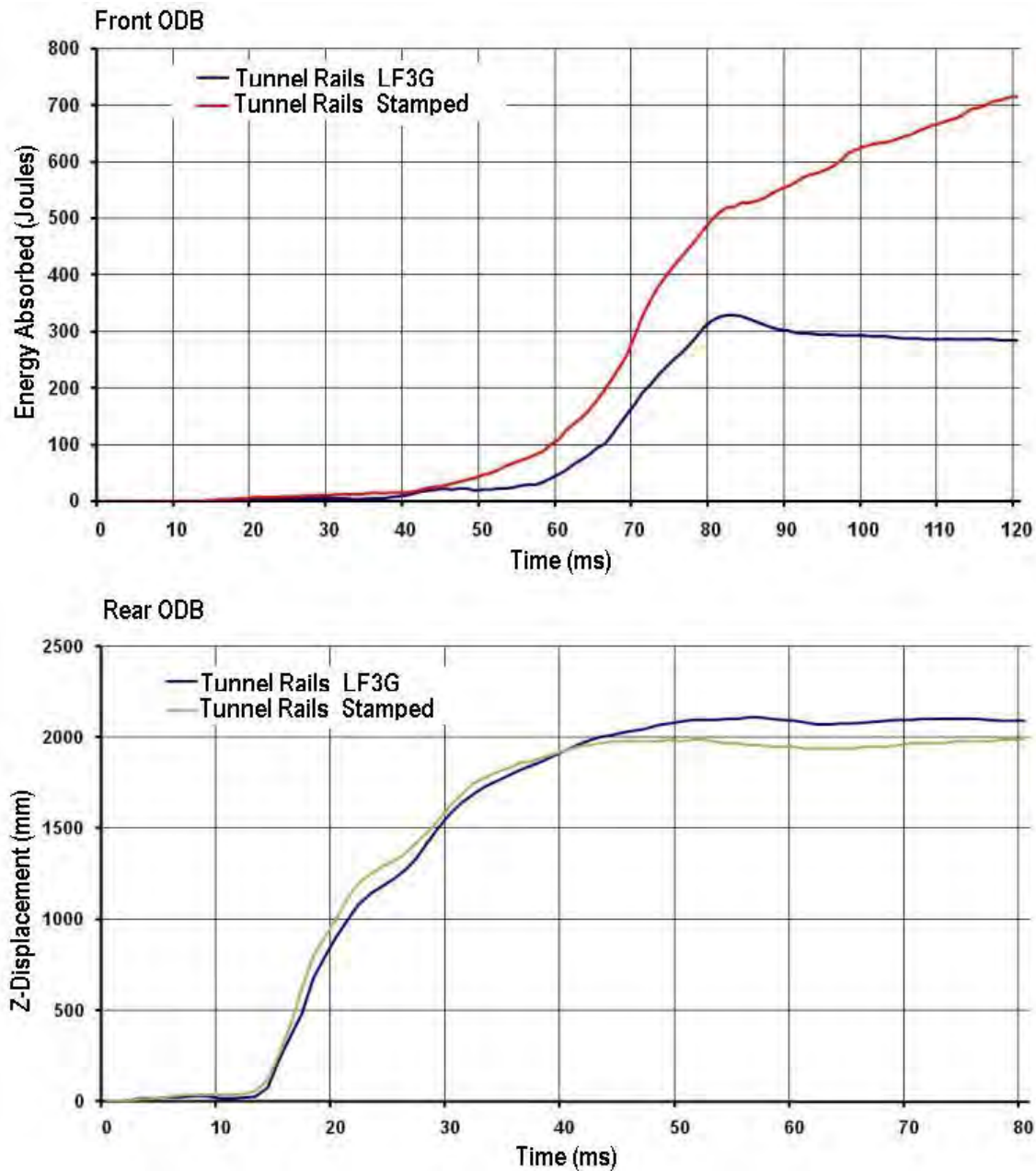


Figure 10.97: Stamped tunnel rail design solution - energy absorption comparison to baseline

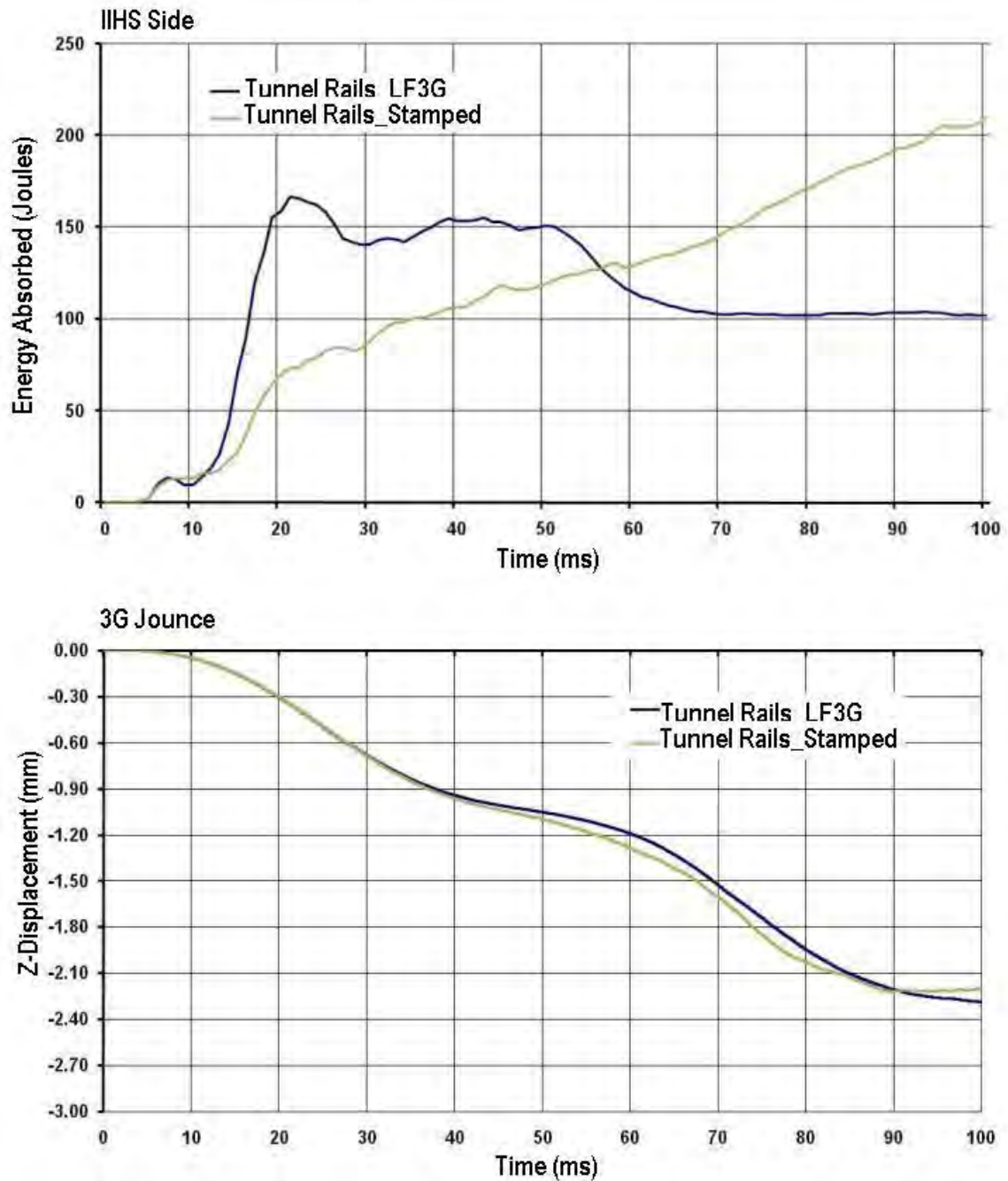


Figure 10.98: Stamped tunnel tail design solution - energy absorption comparison to baseline

Figure 10.99 shows the geometry, grade and gauge selections for the stamped tunnel rail concept. The final mass for this design solution was 5.8 kg, which is a 54% mass reduction compared to the baseline design (12.5 kg).

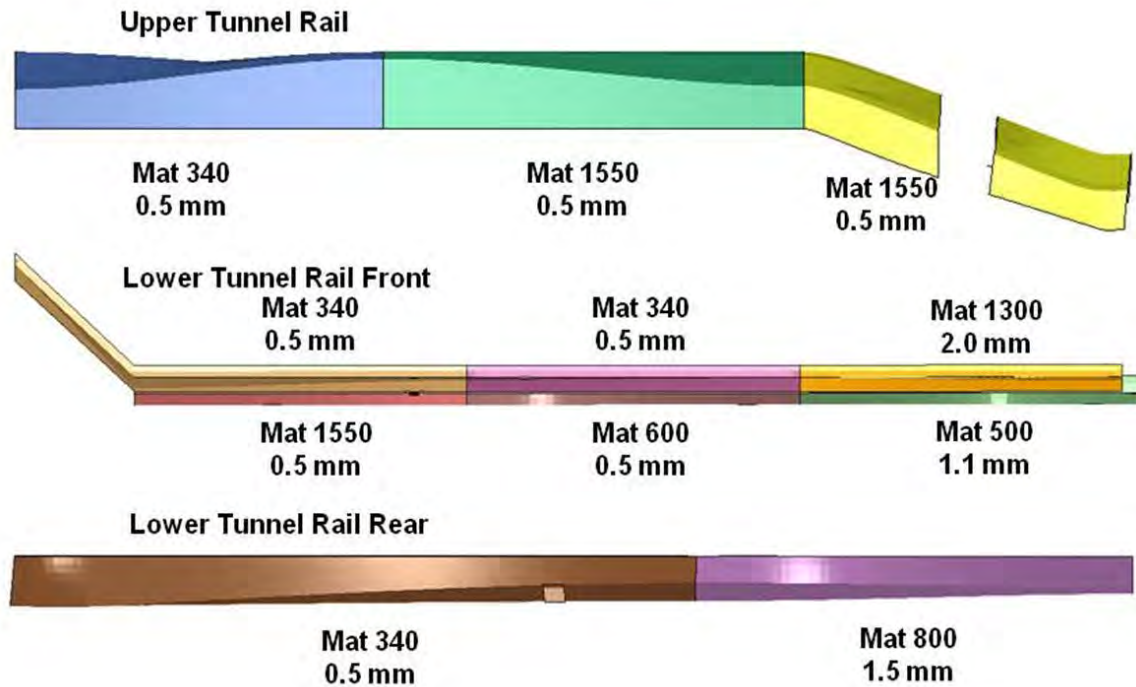


Figure 10.99: Stamped tunnel rails - final grade & gauge selections

10.10.4 Open Roll Formed Tunnel Rail Concept

The complete sub-system optimization process for the tunnel rails has already been discussed previously. Here the only differences in the grade and gauge selection and geometry parameterization for this concept are discussed.

10.10.4.1 Grade and Gauge Optimization

The open roll formed tunnel rail concept consists of the upper tunnel rail and the front and rear portions of the lower tunnel rail. Referring to Figure 10.100, the upper tunnel rail was divided into 3 regions, A through C. The Front lower tunnel rail was divided into 6 regions, D through I and the rear lower tunnel rail into 2 regions, J and K. The choice of grade and gauge of each region could be varied independently of the others. Details of the available grade and gauge choices are listed in Table 10.16.

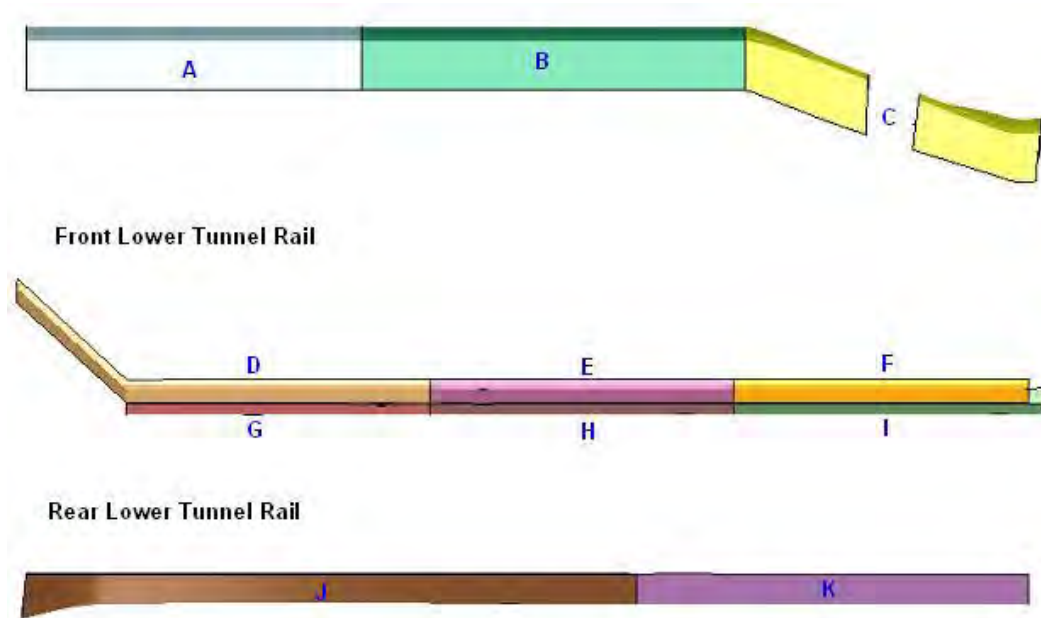


Figure 10.100: Open roll formed tunnel rails - zones of grade & gauge variation

OPEN ROLL FORMED TUNNEL RAILS GAUGE CHOICES			OPEN ROLL FORMED TUNNEL RAILS GRADE CHOICES	
FROM	0.5 mm	In 0.01 mm increments	ULTIMATE TENSILE (MPa)	MAT 270
TO	2.0 mm			MAT 340
		MAT 450		
		MAT 500		
		MAT 600		
		MAT 800		
		MAT 1000		
		MAT 1300		
		MAT 1500		

Table 10.16: Open roll formed tunnel rails - available grade & gauge choices

10.10.4.2 Geometry Parameterization

Unlike the previous stamped tunnel rail concept, in this case though the shape of the cross section can be varied it is held constant along the whole length of the tunnel rails. The range of the packaging space to the cross section is shown in Figure 10.101.

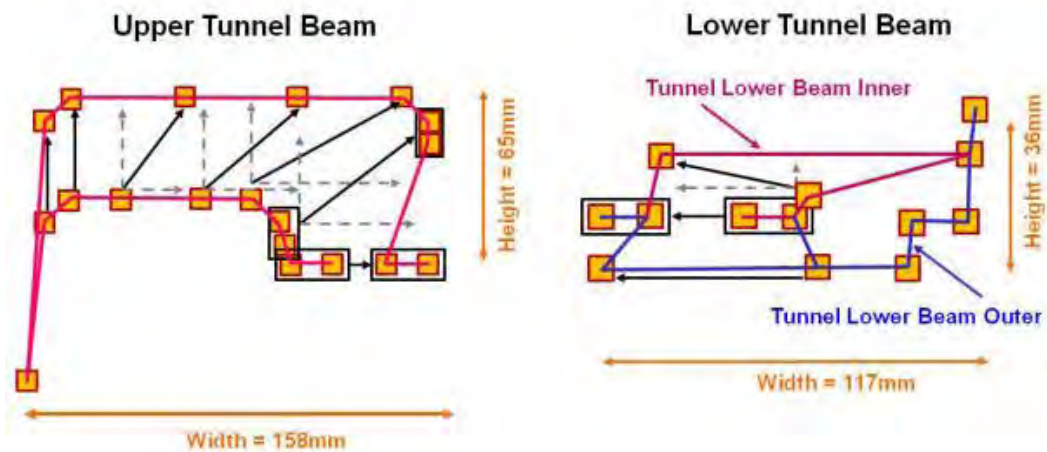


Figure 10.101: Open roll formed tunnel rail concept - cross-sectional parameterization

10.10.4.3 Open Roll Formed Tunnel Rail : Design Solution

All results from the optimization are compared to the baseline LF3G tunnel rails. Figure 10.102 shows the deformation of the baseline LF3G design and the optimized stamped concept for front ODB, rear ODB, IIHS side impacts. It clearly shows that for the front ODB and IIHS side impact there is limited deformation of the rails. In these cases, the rails are just absorbing the elastic energy. In the case of rear ODB impact, the rails have considerable plastic deformation leading to high strain energy absorption.

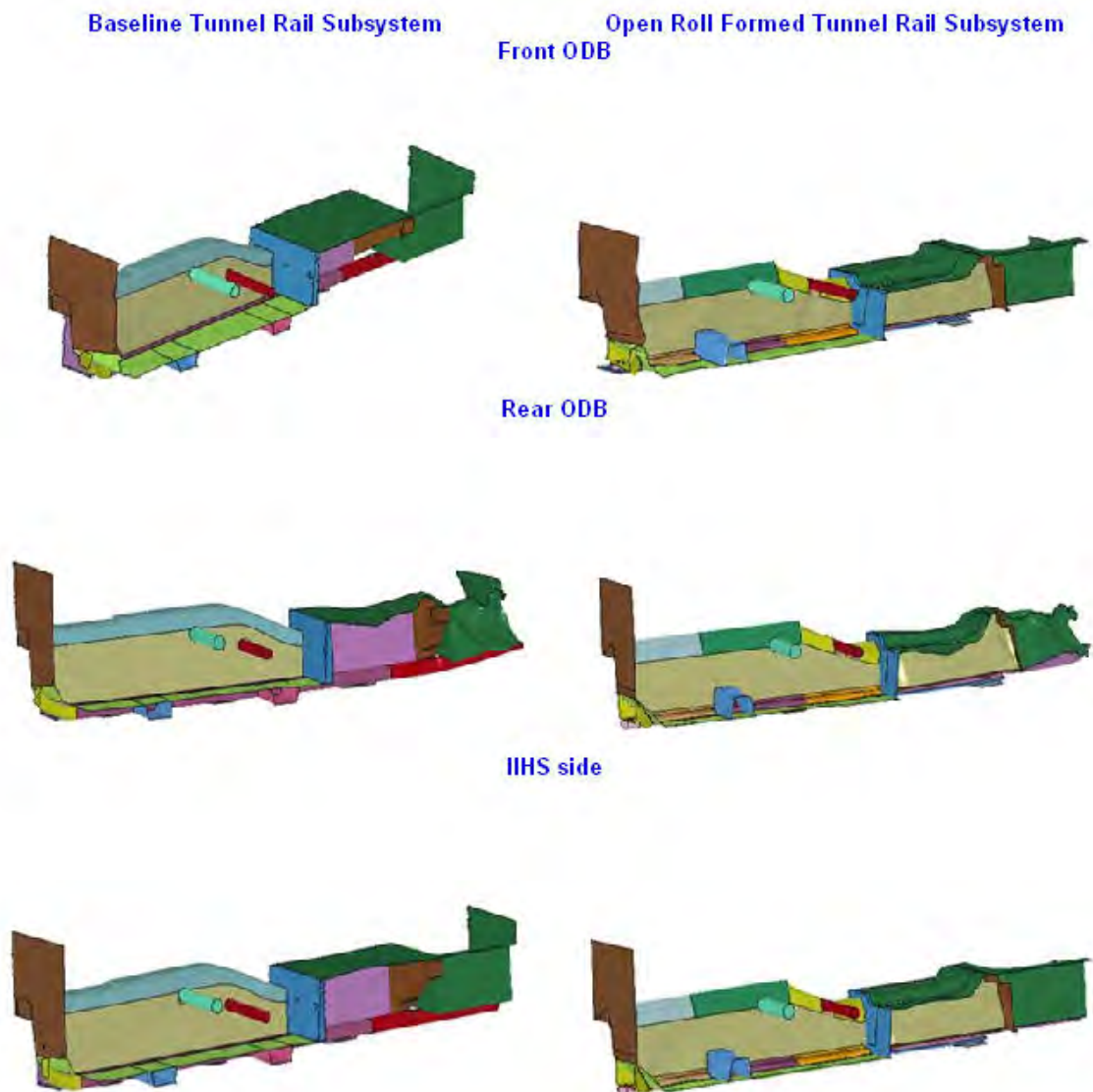


Figure 10.102: Open roll formed tunnel rail design solution - deformation comparison to baseline

Figure 10.103 & Figure 10.104 show the comparison of energy absorption for the baseline LF3G

tunnel rails compared to the optimized roll formed concept. In case of the front ODB and IIHS side impacts the energy absorbed by the tunnel rails is purely elastic energy as there is limited deformation. The total energy of the system has been maintained and so the kinetic energy has been absorbed in the rails as elastic energy. In the case of rear ODB impact the lower rear rail experienced significant deformation resulting in a high amount of strain energy absorption. For the 3G jounce loadcase the rails showed good correlation to the baseline.

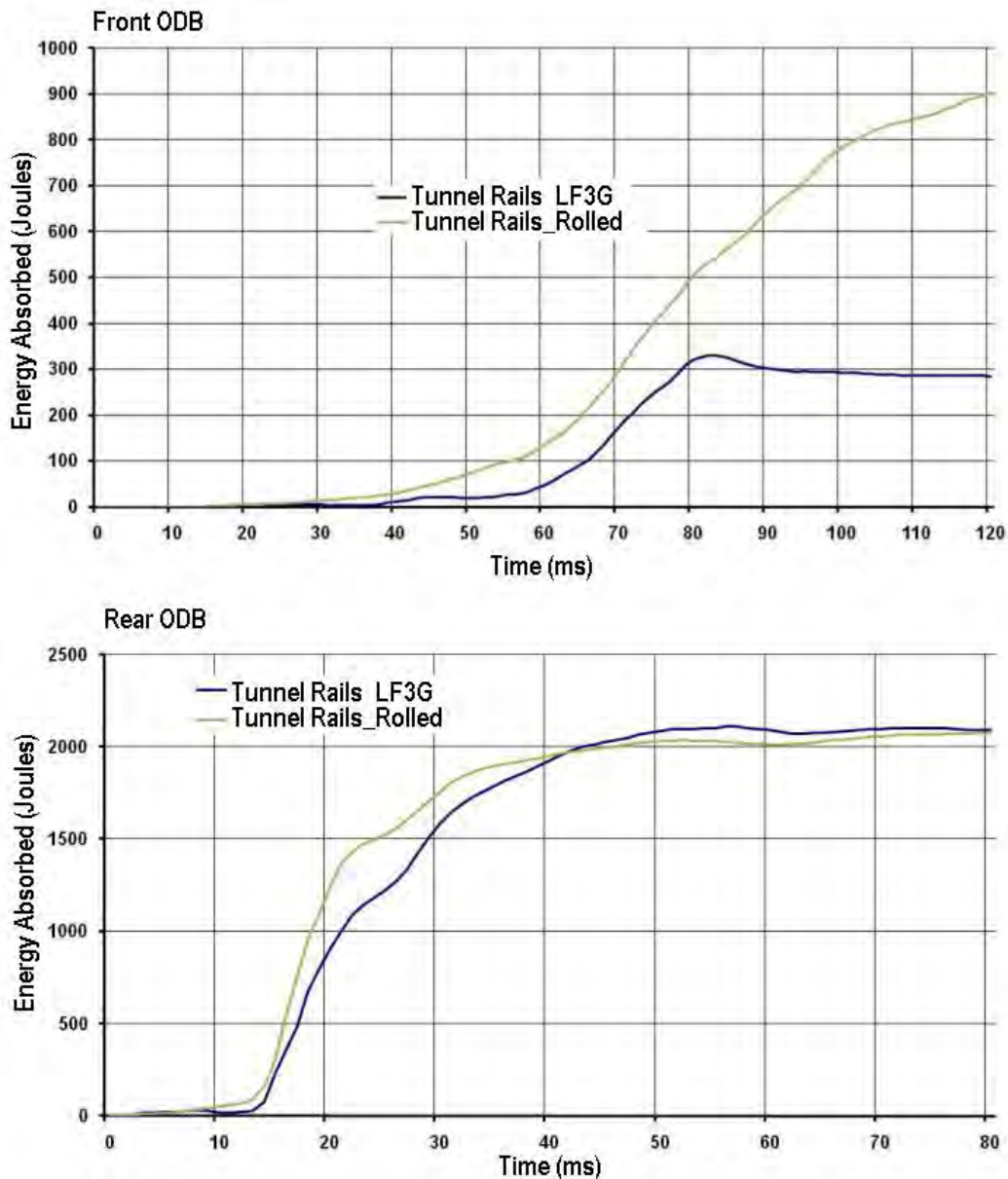


Figure 10.103: *Open roll formed tunnel rail design solution - energy absorption comparison to baseline*

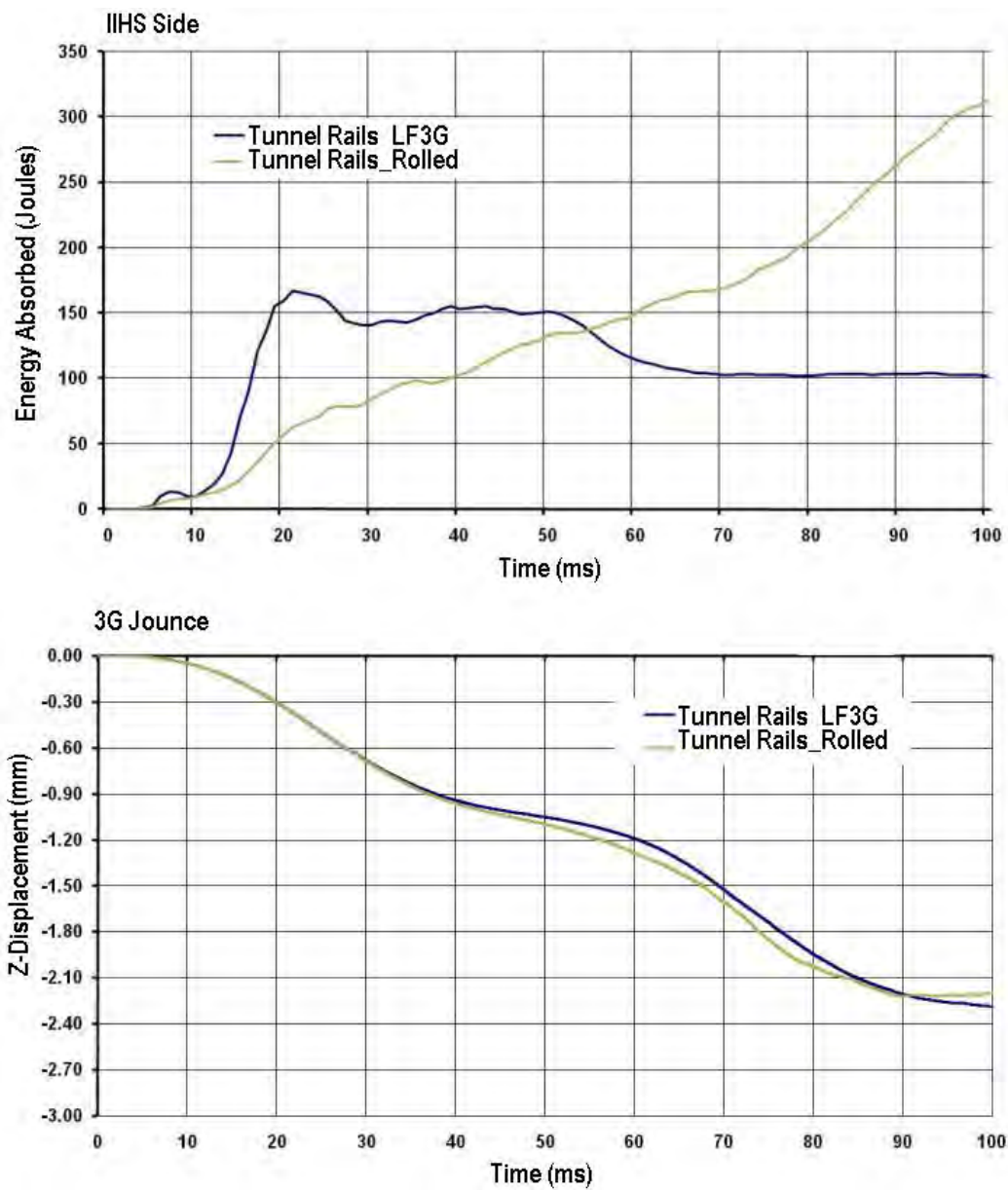


Figure 10.104: Open roll formed tunnel rail design solution - energy absorption comparison to baseline

Figure 10.105 shows the geometry, grade and gauge selections for the roll formed tunnel rail concept. The final mass for this design solution was 4.3 kg, which is a 65% mass reduction compared to the baseline design (12.5 kg).

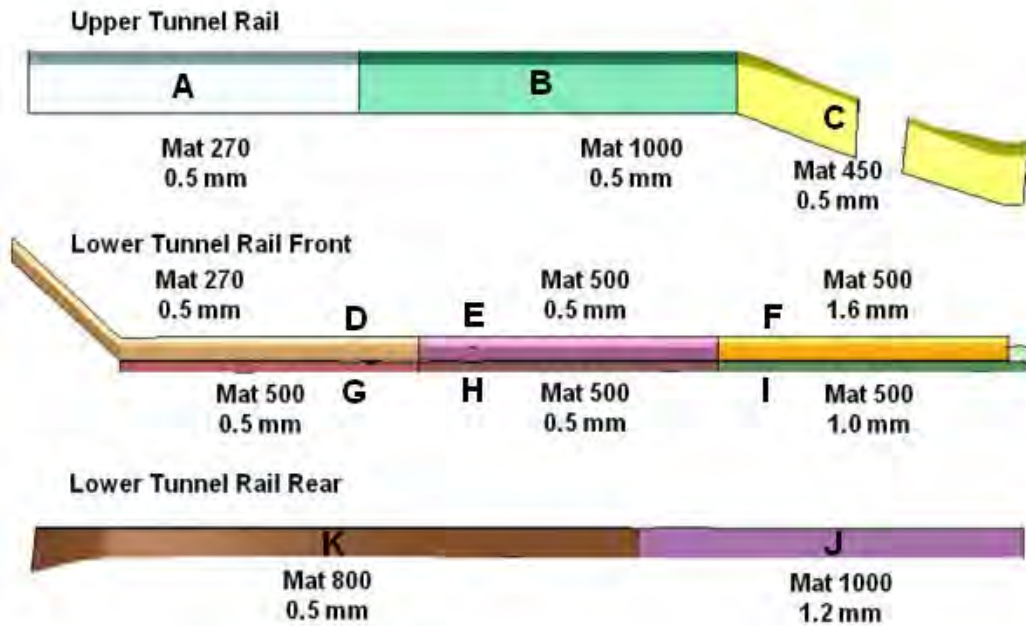


Figure 10.105: Open roll formed tunnel rails - final grade & gauge selections

10.10.5 Extruded Aluminum Tunnel Rail Concept

10.10.5.1 Grade and gauge design space

The extruded aluminum tunnel rail concept used the geometry of the optimized open roll formed concept. The material was updated to aluminum and a gauge optimization was performed on the new geometry. The regions of gauge variation were also simplified. The upper tunnel rail was setup as a single uniform gauge along its entire length. The lower front tunnel rail was setup as two regions and the lower rear rail as a single region. See Figure 10.106. Refer Table 10.17 for details of the available grades and gauges.

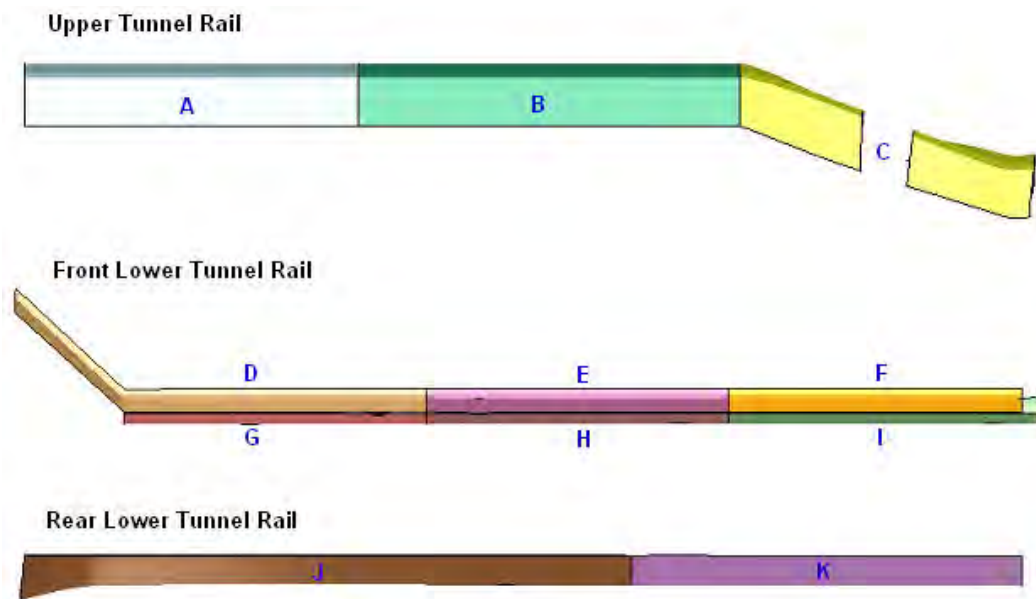


Figure 10.106: Aluminum tunnel rail concept - zones of grade & gauge variation

EXTRUDED ALUMINUM TUNNEL RAILS GAUGE CHOICES		EXTRUDED ALUMINUM TUNNEL RAILS GRADE CHOICES	
FROM	0.8 mm	In 0.01 mm increments	ALUMINUM GRADE
TO	6.0 mm		
			AL 7075

Table 10.17: Extruded aluminum tunnel rails - available grade & gauge choices

10.10.5.2 Optimization setup

- Objective: The optimization objective is to maintain the performance of the tunnel rails so that the total strain energy remains the same as the LF3G for rear ODB impact and 3G jounce. The other loadcases were not considered because they had little effect on the tunnel rails. The mass of the LF3G tunnel rails is 12.5 kg
- Target: The optimization target is to minimize the mass of the tunnel rails.
- Constraint: The energy absorbed by the tunnel rails in the LF3G model (full model) was used as a constraint for the optimization. However, because this is an aluminum concept, the energy values were recalculated from an updated version of the full LF3G model. In this case, the tunnel rail material was revised from steel to aluminum. For rear ODB, the energy absorption was maintained at $\pm 5\%$ of the revised LF3G's performance. For 3G jounce the Z-displacement of the tunnel lower rail was held within 10% of 2.3 mm. (For further information on target energy value calculations for aluminum, refer to Appendix 20.4 for details)

10.10.5.3 Extruded Aluminum Tunnel Rail : Design Solution

Figure 10.107 shows the comparison of energy absorption for the baseline LF3G tunnel rails compared to the optimized extruded aluminum concept. For rear ODB impact the lower rear rail experienced significant deformation resulting in a high amount of strain energy absorption. For the 3G jounce loadcase the rails showed good correlation to the baseline.

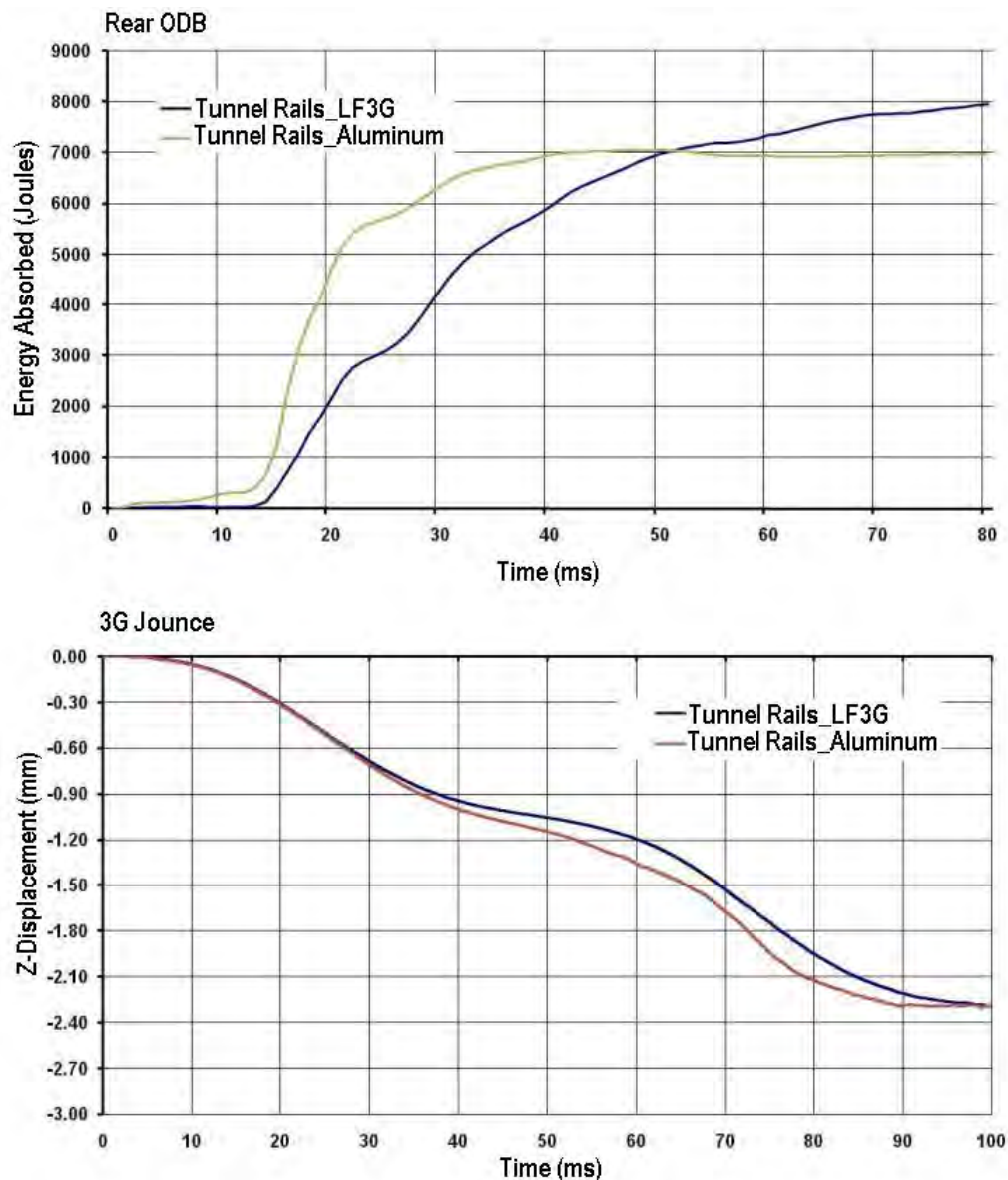


Figure 10.107: Extruded aluminum tunnel rail design solution - energy absorption comparison to baseline

Figure 10.108 shows the geometry, grade and gauge selections for the extruded tunnel rail concept. The final mass for this design solution was 5.72 kg, which is a 53.7% mass reduction compared to the baseline design (12.5 kg).

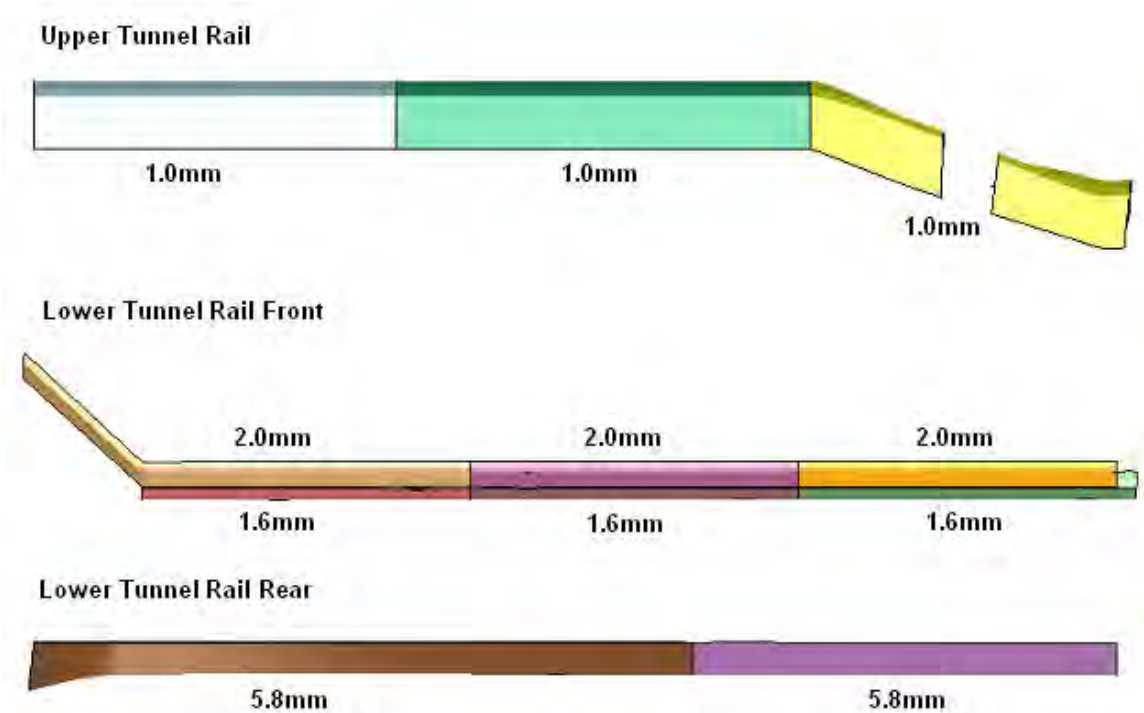


Figure 10.108: *Extruded aluminum tunnel rails - final grade & gauge selections*

10.11 Shotgun Sub-System

10.11 Shotgun Sub-System

The shotgun sub-system optimization considered two manufacturing concepts; a steel stamping and an aluminum extrusion.

10.11.1 Development of Sub-System from Full Model

The shotgun sub-system was developed from the full LF3G model such that when analyzed under the same loading conditions it behaved in the same way as the full model. The sub-system model consisted of the shotgun and the major components it is attached to such as the bumper, shock tower and hinge pillar. See Figure 10.109

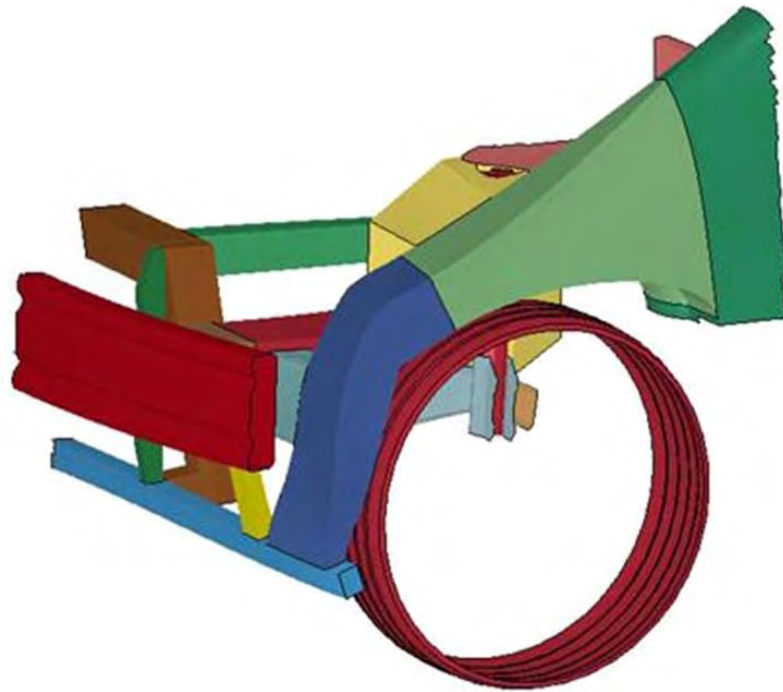


Figure 10.109: Shotgun sub-system from LF3G

10.11.2 Generating Boundary Conditions

The nodal displacement time history is used as the boundary conditions for the sub-system so that it behaves in a similar manner to the full LF3G model. The method used was exactly the same as was described for the rocker in section 10.6.2. Referring to Figure 10.110, shows the specific boundaries applied to the shotgun sub-system model.

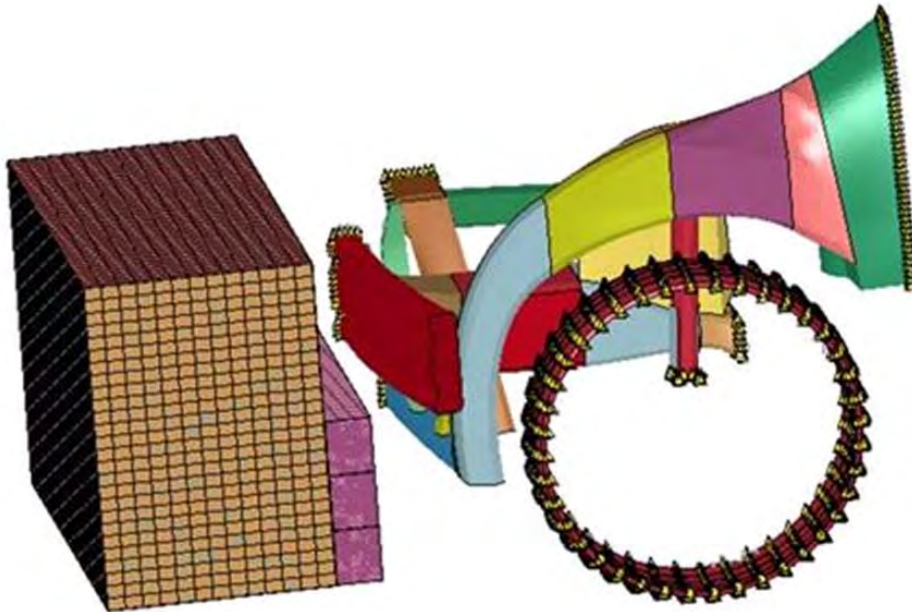


Figure 10.110: Shotgun sub-system with highlighted boundaries for time history

The performance of sub-system model was validated under the loadcases considered, front NCAP and front ODB impacts, to confirm that it behaved in the same way as the full model. The energy absorbed by the shotgun under the loading conditions considered was used as the performance target.

10.11.3 Stamped Shotgun Concept

10.11.3.1 Grade and Gauge Design Space

The stamped shotgun concept consists of an inner and outer shotgun. Referring to Figure 10.111, the shotgun components were divided into 5 regions, A through E. The choice of grade and gauge of each region could be varied independently of the others. Details of the available grade and gauge choices are listed in Table 10.18.

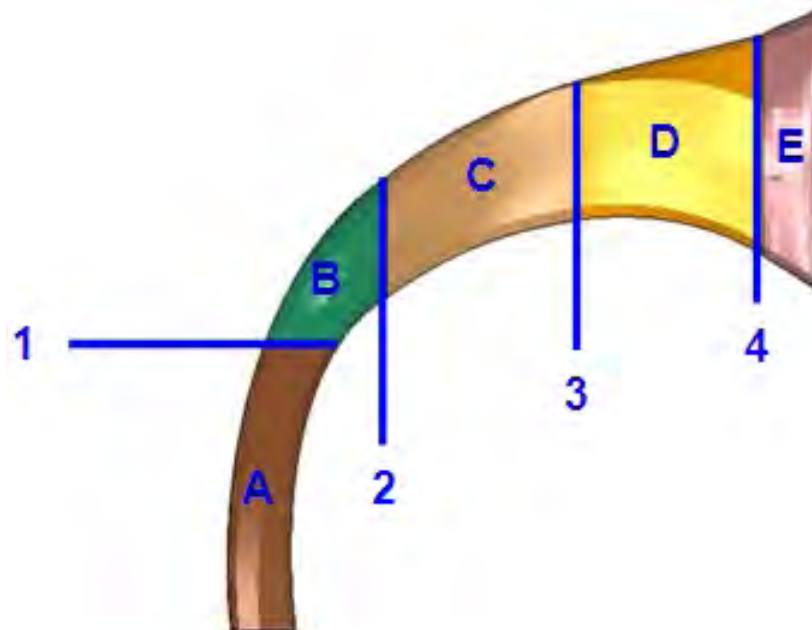


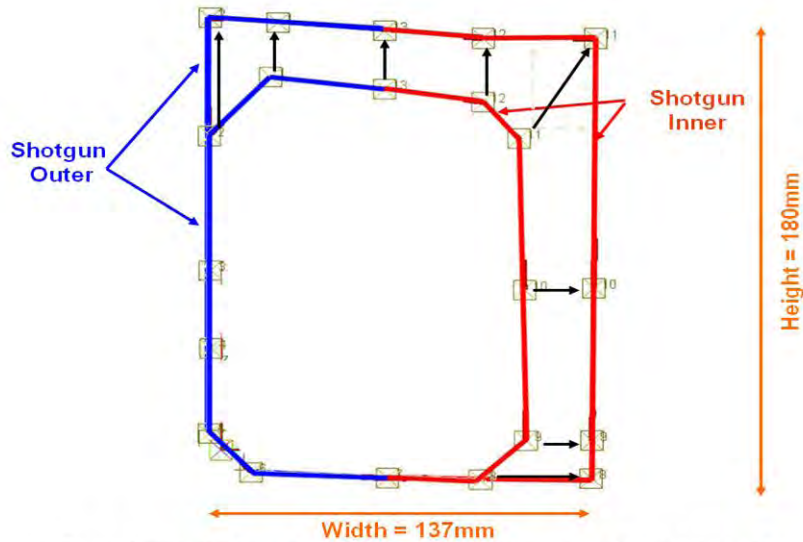
Figure 10.111: Stamped shotgun concept - zones of grade & gauge variation

STAMPED SHOTGUN GAUGE CHOICES			STAMPED SHOTGUN GRADE CHOICES	
FROM	0.5 mm	In 0.01 mm increments	ULTIMATE TENSILE (MPa)	MAT 270
TO	2.0 mm			MAT 340
		MAT 450		
		MAT 500		
		MAT 600		
		MAT 800		
		MAT 1000		
		MAT 1300		
		MAT 1500		

Table 10.18: Stamped shotgun - available grade & gauge choices

10.11.3.2 Geometry Parameterization

The geometry design space is limited as an outer boundary package space established in chapter 4. Referring to Figure 10.111, the cross-section at locations 1 through 4 can be varied independently of each other. Thus for each region, A through E, the shape will vary along the length of the region based on the cross sections at each end. The range of the packaging space for each cross section 1 through 4 is shown in Figure 10.112.



Black Arrows Indicate Independent Point Movement From Min to Max

Figure 10.112: Stamped shotgun concept - cross-sectional parameterization

10.11.3.3 Optimization Setup

- Objective: The optimization objective is to maintain the performance of the shotgun so that the total strain energy remains the same as the LF3G for front NCAP and front ODB impacts. The mass of the LF3G shotgun is 10.6 kg.
- Target: The optimization target is to minimize the mass of the shotgun.
- Constraint: The energy absorbed by the shotgun in the LF3G model (full model) was used as a constraint for the optimization. For front NCAP and front ODB impacts, the energy absorption was held at $\pm 15\%$ of energy absorption for the LF3G. (For further information on target energy value calculations, refer to Appendix 20.3 for details)

10.11.3.4 Stamped Shotgun : Design Solution

All results from the optimization are compared to the baseline LF3G tunnel rails. Figure 10.113 shows the deformation of the baseline LF3G design and the optimized stamped concept for front NCAP and front ODB impacts. It clearly shows that for the front ODB and IIHS side impact there is considerable plastic deformation leading to high strain energy absorption.

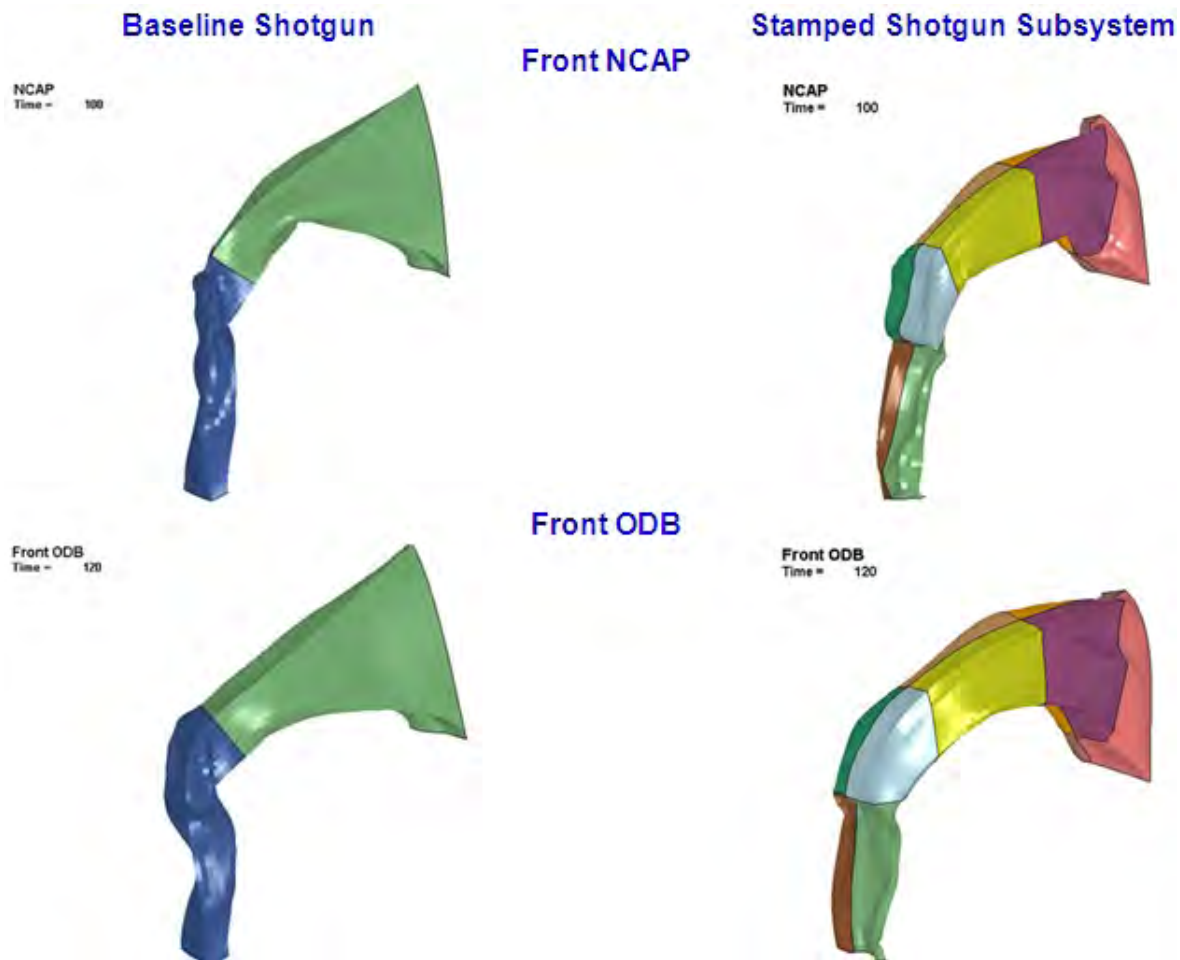


Figure 10.113: Shotgun design solution - deformation comparison to baseline

Figure 10.114 shows the comparison of energy absorption for the baseline LF3G shotgun compared to the optimized stamped concept. For front NCAP and front ODB impacts the shotgun experienced significant deformation resulting in a high amount of strain energy absorption.

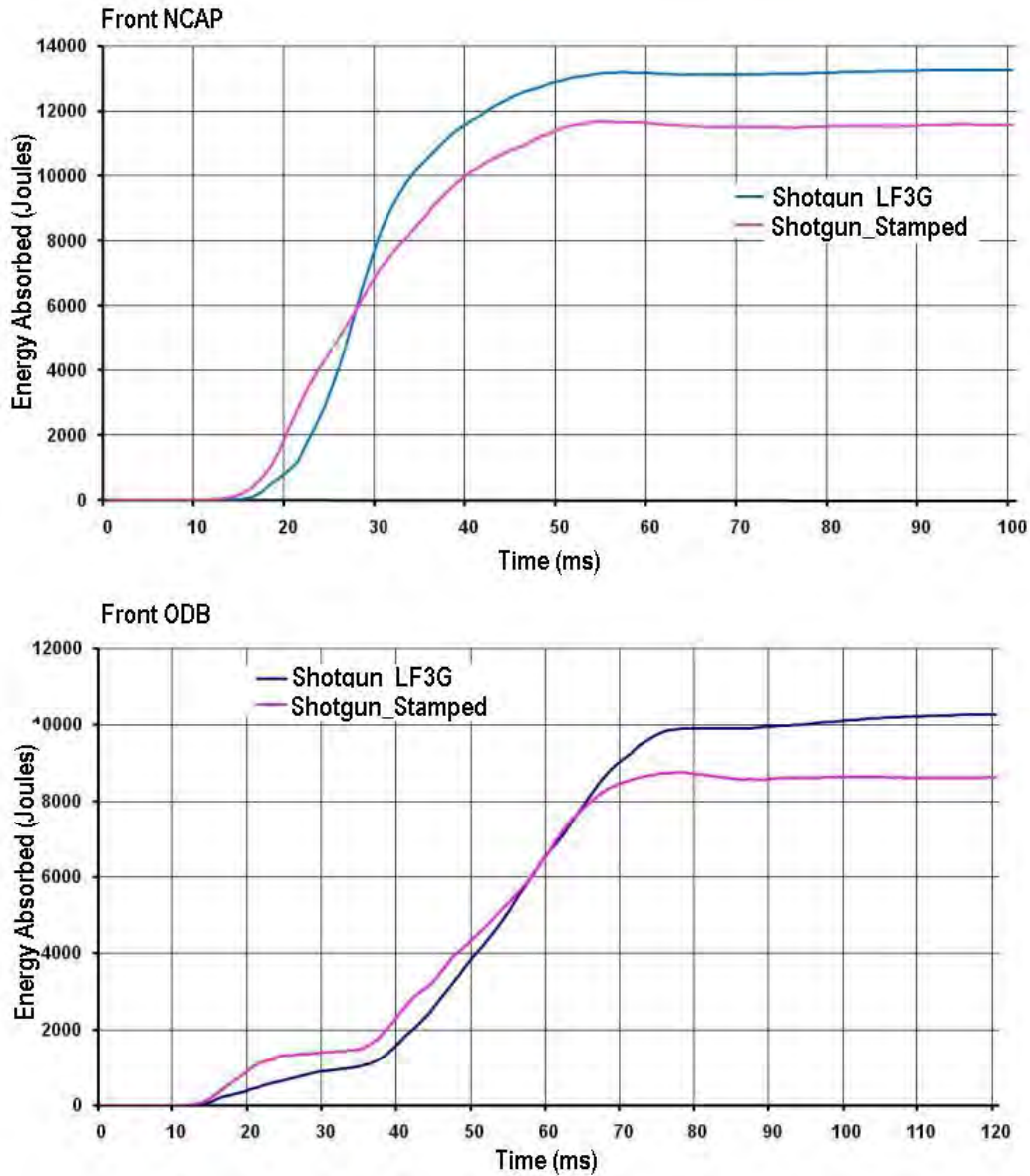


Figure 10.114: Stamped shotgun design solution - energy absorption comparison to baseline

10.11 Shotgun Sub-System

Figure 10.115 shows the geometry, grade and gauge selections for the stamped shotgun concept. The final mass for this design solution was 6.4 kg, which is a 39% mass reduction compared to the baseline design (10.6 kg).

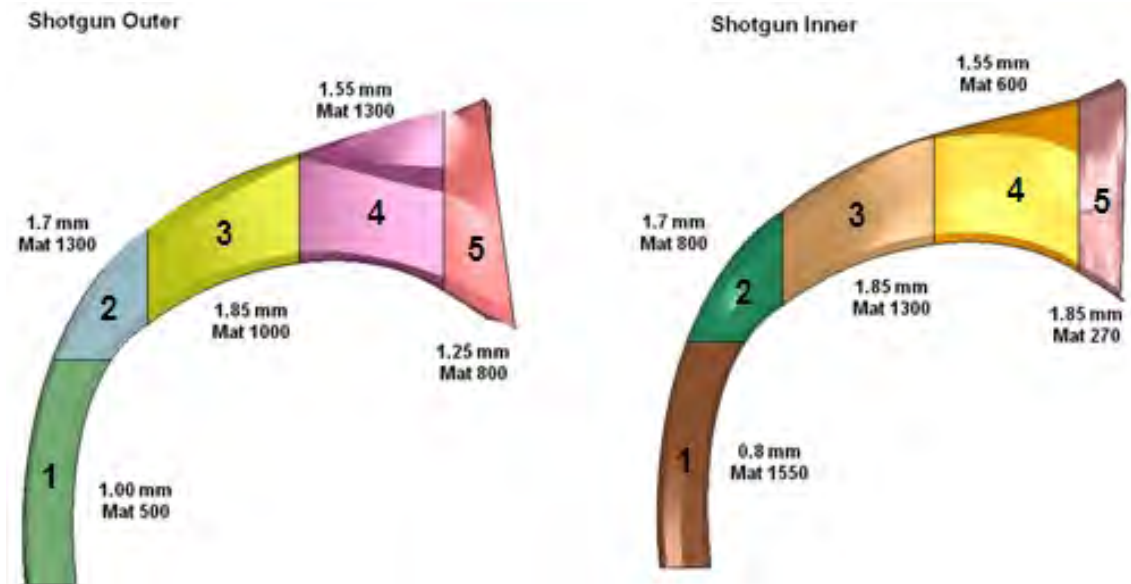


Figure 10.115: *Stamped shotgun - final grade & gauge selections*

10.11.4 Aluminum Shotgun Concept

10.11.4.1 Grade and Gauge Design Space

The aluminum shotgun concept consists of a shotgun outer and a shotgun inner. There is no variation in gauge along the length of the component, only differences in cross section are allowed. There is no variation in the grade of aluminum. Refer Table 10.19 for details of the available gauges.

ALUMINUM SHOTGUN GAUGE CHOICES			ALUMINUM SHOTGUN GRADE CHOICES	
FROM	0.8 mm	In 0.01 mm increments	ALUMINUM GRADE	AL 7075
TO	6.0 mm			

Table 10.19: Aluminum shotgun - available grade & gauge choices

10.11.4.2 Geometry Parameterization

Figure 10.116 shows the parameterization of the cross section.

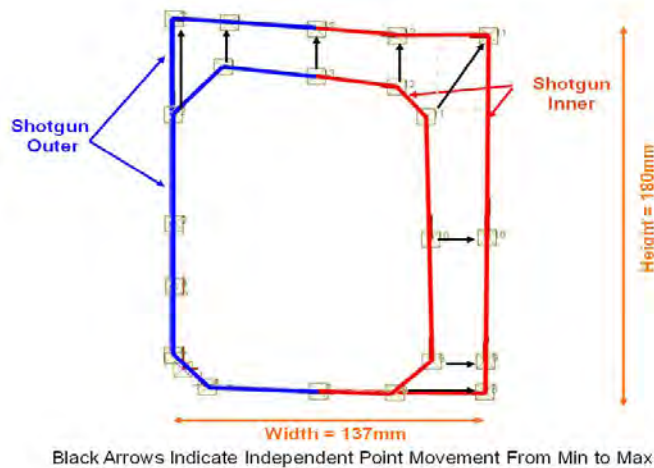


Figure 10.116: Aluminum shotgun concept - cross-sectional parameterization

10.11.4.3 Optimization Setup

- Objective: The optimization objective is to maintain the performance of the shotgun so that the total strain energy remains the same as the LF3G for front NCAP and front ODB impacts. The mass of the LF3G shotgun is 10.6 kg
- Target: The optimization target is to minimize the mass of the shotgun.

10.11 Shotgun Sub-System

- Constraint: The energy absorbed by the shotgun in the LF3G model (full model) was used as a constraint for the optimization. However, because this is an aluminum concept, the energy values were recalculated from an updated version of the full LF3G model. In this case, the shotgun material was revised from steel to aluminum. For both front NCAP and front ODB impacts the energy absorption was maintained at $\pm 15\%$ of the revised LF3G's performance. (For further information on target energy value calculations for aluminum, refer to Appendix 20.4 for details)

10.11.4.4 Aluminum Shotgun : Design Solution

All results from the optimization are compared to the baseline LF3G tunnel rails. Figure 10.117 shows the deformation of the baseline LF3G design and the optimized aluminum concept for front NCAP and front ODB impacts. It clearly shows that for the front ODB and IIHS side impact there is considerable plastic deformation leading to high strain energy absorption.



Figure 10.117: Aluminum shotgun design solution - deformation comparison to baseline

Figure 10.118 shows the comparison of energy absorption for the baseline LF3G shotgun compared to the optimized aluminum concept. For front NCAP and front ODB impacts the shotgun experienced significant deformation resulting in a high amount of strain energy absorption.

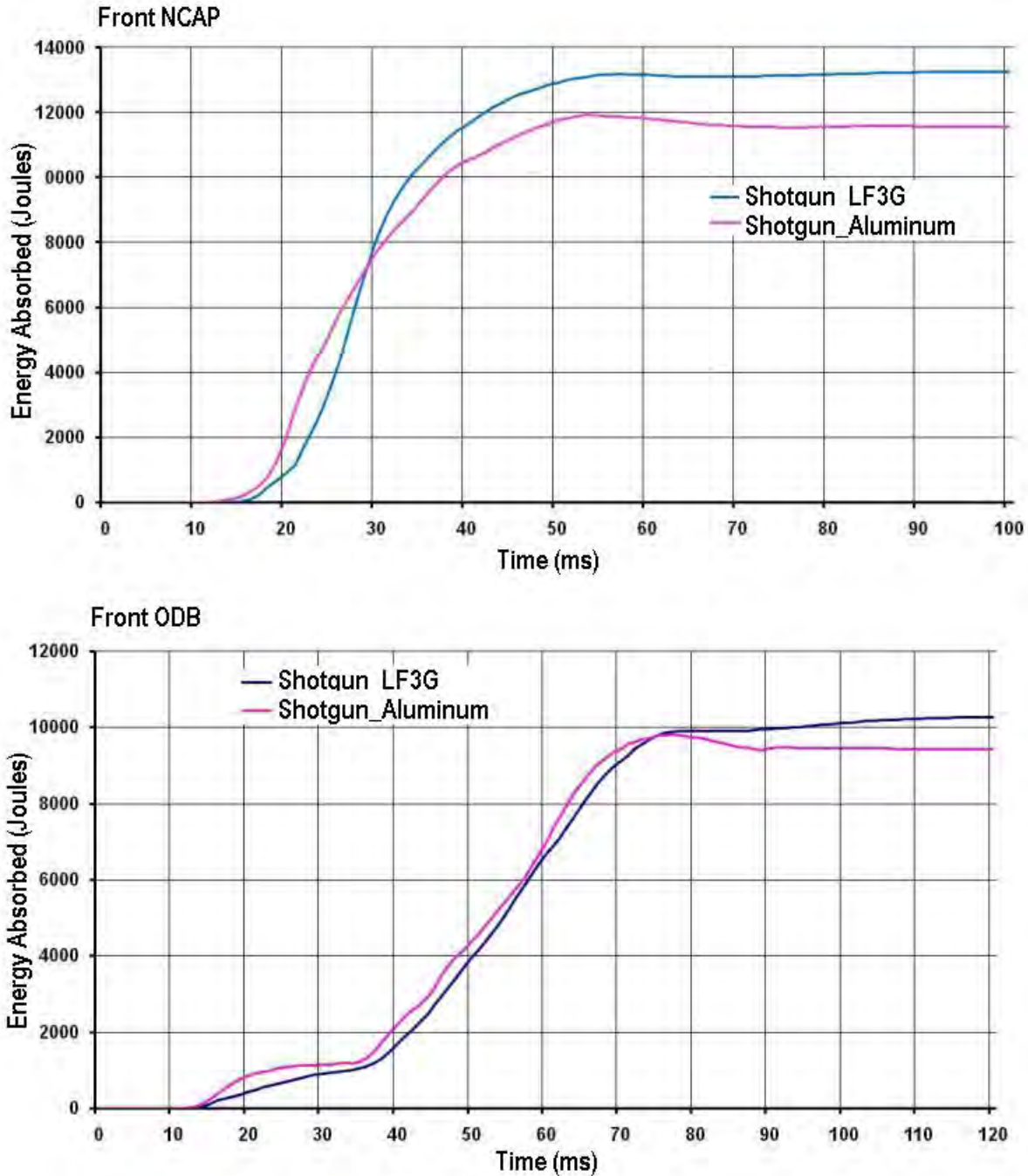


Figure 10.118: Aluminum shotgun design solution - energy absorption comparison to baseline

Figure 10.119 shows the geometry, grade and gauge selections for the aluminum shotgun concept. The final mass for this design solution was 3.2 kg, which is a 70% mass reduction compared to the baseline design (10.6 kg).

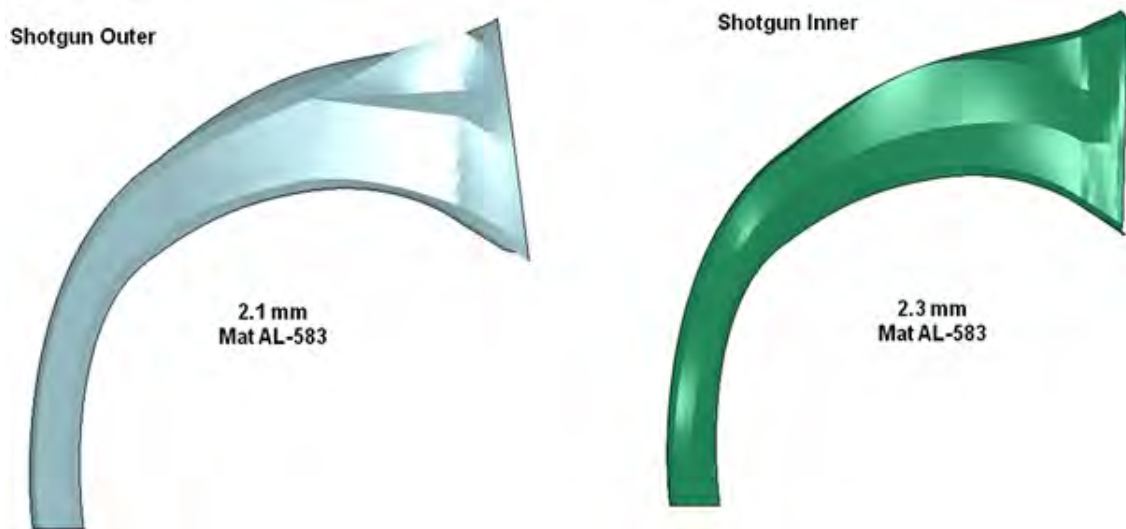


Figure 10.119: Aluminum shotgun - final grade & gauge selections

10.12 Front Rail Sub-System

The front rail sub-system optimization considered three manufacturing processes; stamping, hydroformed and an aluminum stamping. In total there were two stamped concepts, two hydroformed concepts and one aluminum concept.

10.12.1 Development of Sub-System from the Full Model

The front rail sub-system was developed from the full LF3G model such that when analyzed under the same loading conditions it behaved in the same way as the full model. The sub-system model consisted of the front rail and crash can the major components it is attached to such as the cradle, firewall, lower tunnel rail and hinge pillar. See Figure 10.120

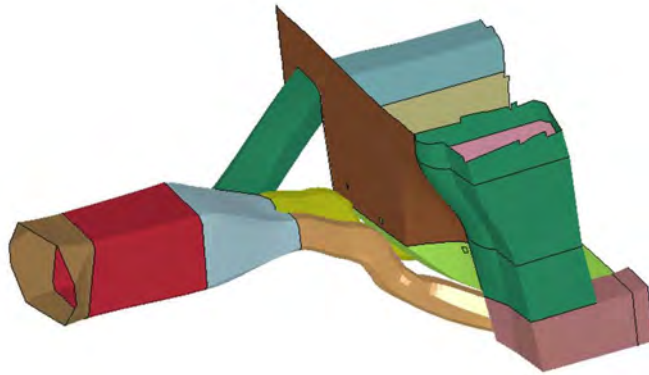


Figure 10.120: *Front Rail sub-system from LF3G*

This developed sub-system is validated for performance under different load cases (front NCAP and front ODB) to confirm that it performs the same as in full model. The energy absorbed by the front rails under different loading conditions is used as the performance criteria.

10.12.2 Generating Boundary Conditions

The nodal displacement time history is used as the boundary conditions for the sub-system so that it behaves in a similar manner to the full LF3G model. The method used was exactly the same as was described for the rocker in section 10.6.2. Referring to Figure 10.121, shows the specific boundaries applied to the front rail sub-system model.

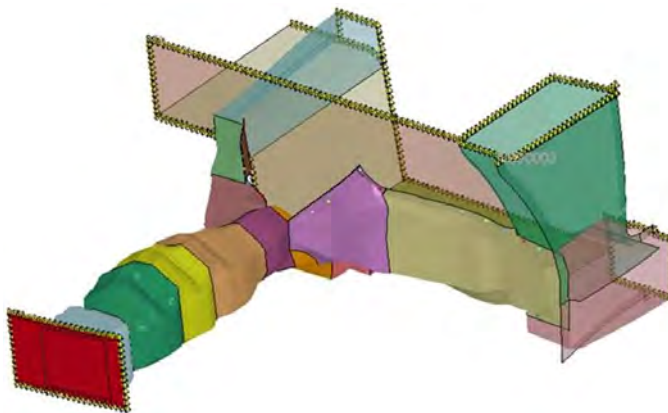


Figure 10.121: *Front rail sub-system with highlighted boundaries for time history*

The performance of sub-system model was validated under the loadcases considered, front ODB impact, to confirm that it behaved in the same way as the full model. The energy absorbed by the shotgun under the loading conditions considered was used as the performance target.

10.12.3 Stamped Front Rail Sub-System

10.12.3.1 Grade and Gauge Design Space

Two stamped front rail concepts were created. In both cases, they consisted of the front portion of the rail, which then split into three separate legs or tripod at the rear. The tripod connects the front rail to the upper and lower tunnel rails and the rocker. See Figure 10.122 & Figure 10.123. The primary difference between the two concepts is the number of pieces that make up the front portion of the rail. Figure 10.122 is a three piece stamping that was given a very aggressive geometric parameterization. Figure 10.123 shows a two piece concept in which the parameterization was setup for more conventional solution. For each concept, regions, represented by the various colors shown in the figures, were defined so that the choice of grade and gauge of each could be varied independently of the others. Details of the available grade and gauge choices are listed in Table 10.20.

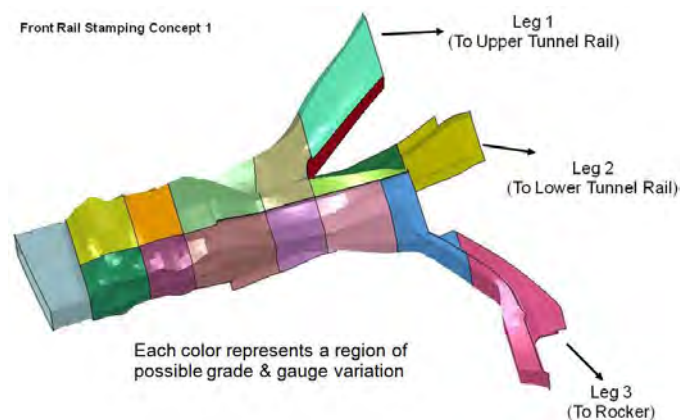


Figure 10.122: *Three piece stamped front rail concept - zones of grade & gauge variation*

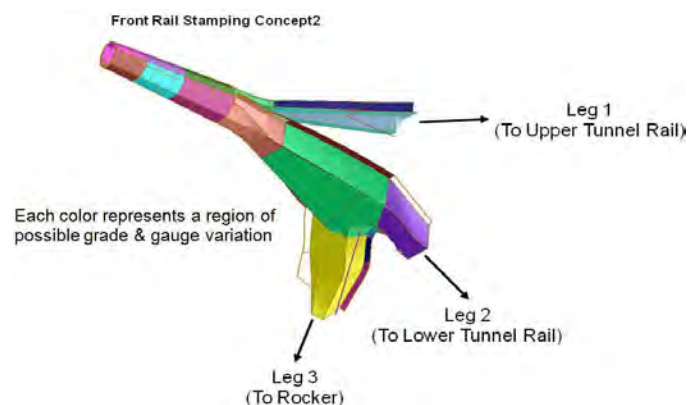


Figure 10.123: *Two piece stamped front rail concept - zones of grade & gauge variation*

STAMPED FRONT RAIL GAUGE CHOICES			STAMPED FRONT RAIL GRADE CHOICES	
FROM	0.5 mm	In 0.01 mm increments	ULTIMATE TENSILE (MPa)	MAT 270
TO	2.0 mm			MAT 340
		MAT 450		
		MAT 500		
		MAT 600		
		MAT 800		
		MAT 1000		
		MAT 1300		
		MAT 1500		

Table 10.20: Three piece stamped front rail - available grade & gauge choices

10.12.3.2 Geometry Parameterization

The geometry design space is limited as an outer boundary package space established in chapter 4. Referring to Figure 10.124, the cross-section was defined a three pieces; Front Rail Inner, Front Rail Outer and Front Rail Lower. In each cross-section all nodes were free to move independently of each other. The individual cross-sections themselves were also free to move independent of each other.

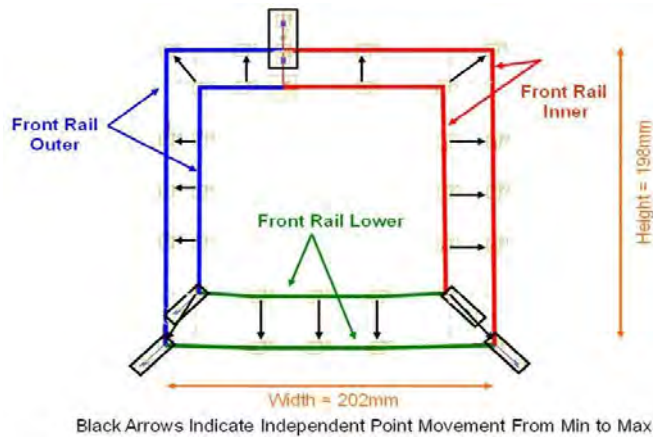


Figure 10.124: Three piece stamped front rail concept - cross-sectional parameterization

Referring to Figure 10.125, the cross-section was defined a two pieces in a traditional clam shell arrangement; front rail inner and front rail outer. In each cross-section all nodes moved together or were scaled so that the general shape of the section was preserved. However, the individual cross-sections themselves were free to move independent of each other.

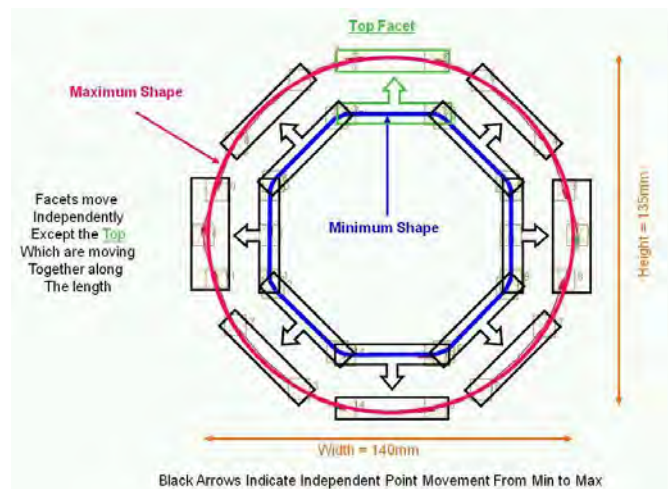


Figure 10.125: Two piece stamped front rail concept - cross-sectional parameterization

10.12.3.3 Optimization Setup

- Objective: The optimization objective is to maintain the performance of the front rail so that the total strain energy remains the same as the LF3G under front ODB impact. The mass of the LF3G front rail is 9.5 kg.
- Target: The optimization target is to minimize the mass of the front rail.
- Constraint: The energy absorbed by the front rail in the LF3G model (full model) was used as a constraint for the optimization. For front ODB impact, the energy absorption was held at $\pm 15\%$ of energy absorption for the LF3G. (For further information on target energy value calculations, refer to Appendix 20.3 for details)

10.12.3.4 Stamped Front Rail : Design Solution

All results from the optimization are compared to the baseline LF3G front rail. Figure 10.126 & Figure 10.127 show the deformation and energy absorbed by the baseline LF3G design and the optimized 2 piece stamped concept for front NCAP impact. It clearly shows that there is considerable plastic deformation leading to high strain energy absorption.

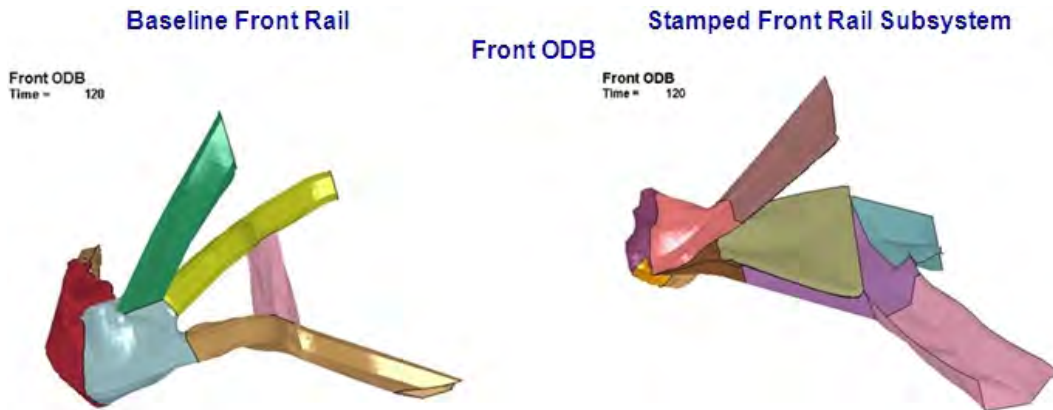


Figure 10.126: Two piece stamped front rail design solution - deformation comparison to baseline

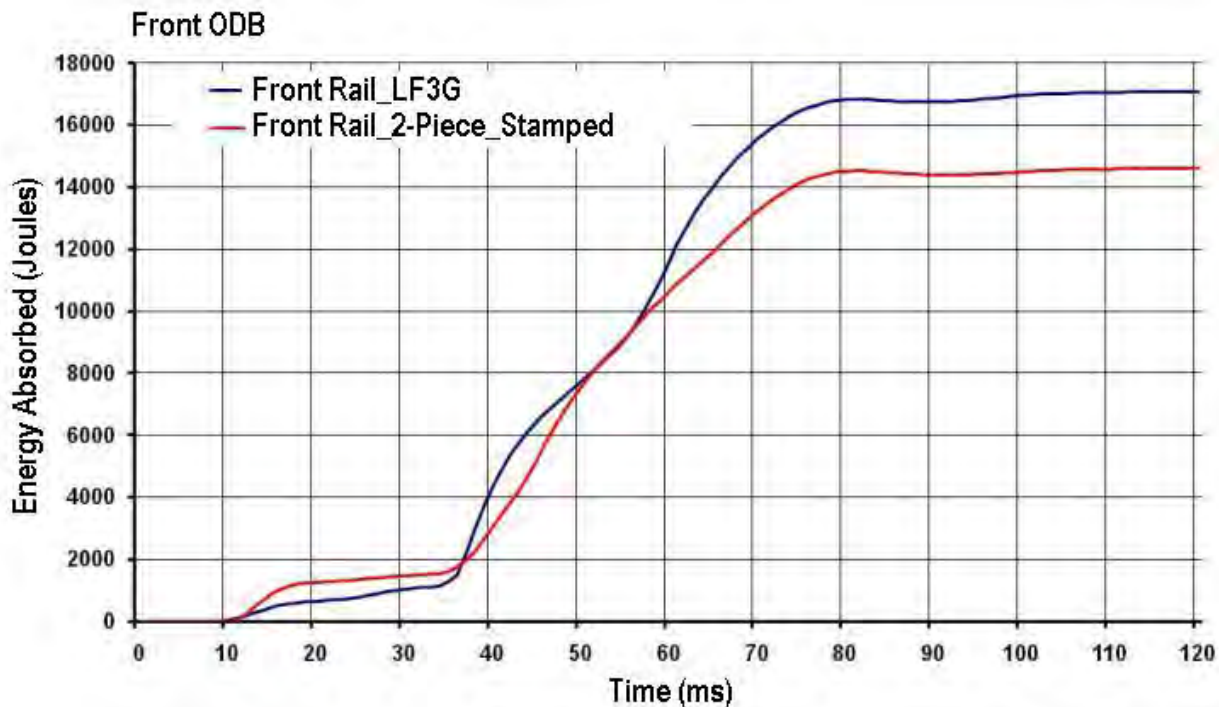


Figure 10.127: Two piece stamped front rail design solution - energy absorption comparison to baseline

Figure 10.128 shows the geometry, grade and gauge selections for the two piece stamped front rail concept. The final mass for this design solution was 5.7 kg, which is a 40% mass reduction compared to the baseline design (9.5 kg).

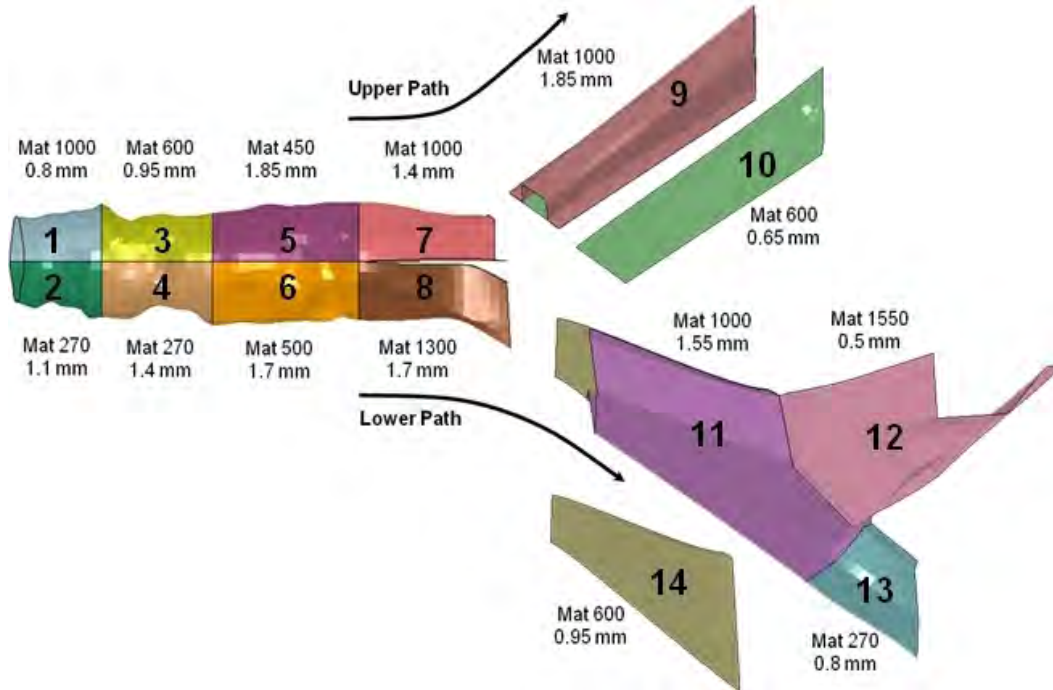


Figure 10.128: Two piece stamped front rail - final grade & gauge selections

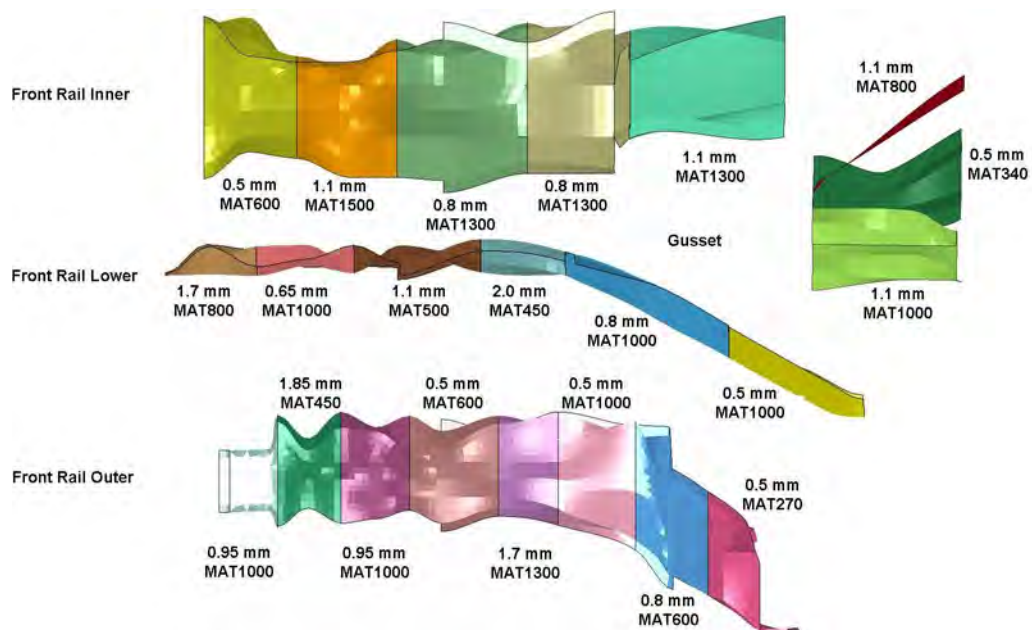


Figure 10.129: Three piece stamped front rail - final grade & gauge selections

10.12.4 Hydroformed Front Rail Sub-System

The complete sub-system optimization process for the rocker has already been discussed previously. Here the only differences in the grade and gauge selection and geometry parameterization for this concept are discussed.

10.12.4.1 Grade and Gauge Design Space

Two different hydroformed front rail concepts were developed. In Hydroform Concept 1 the complete front rail is hydroformed. See Figure 10.130. In Hydroformed Concept 2 the front section of the rail and the portion connected to the lower tunnel rail is hydroformed. The sections connected to the upper tunnel rail and rocker are both stamped. See Figure 10.131. For each concept, regions, represented by the various colors shown in the figures, were defined so that the choice of grade and gauge of each could be varied independently of the others.

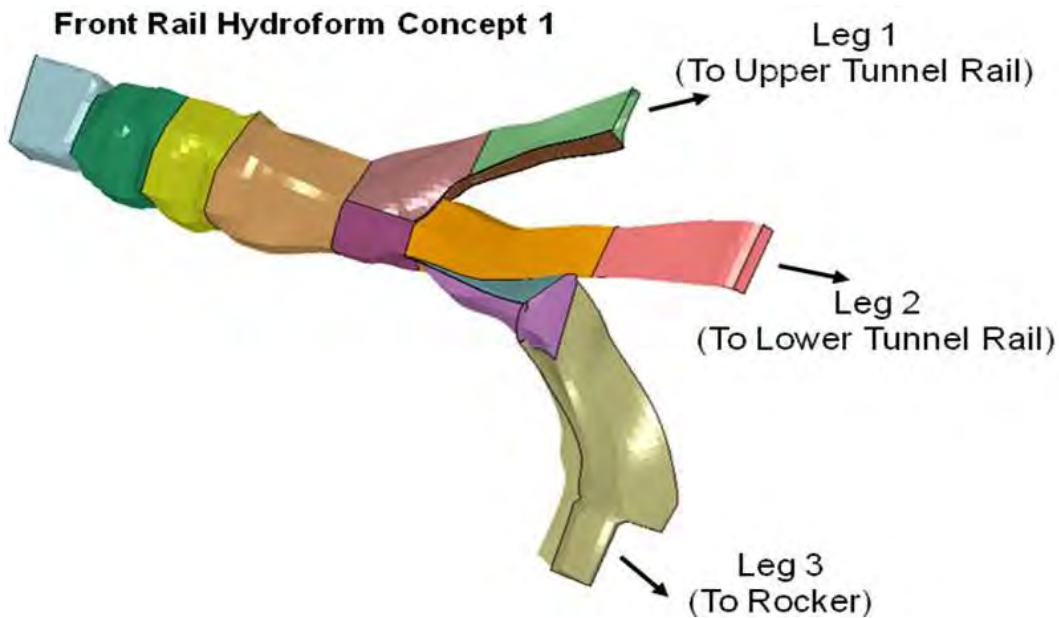


Figure 10.130: *Hydroformed front rail concept 1 - zones of grade & gauge variation*

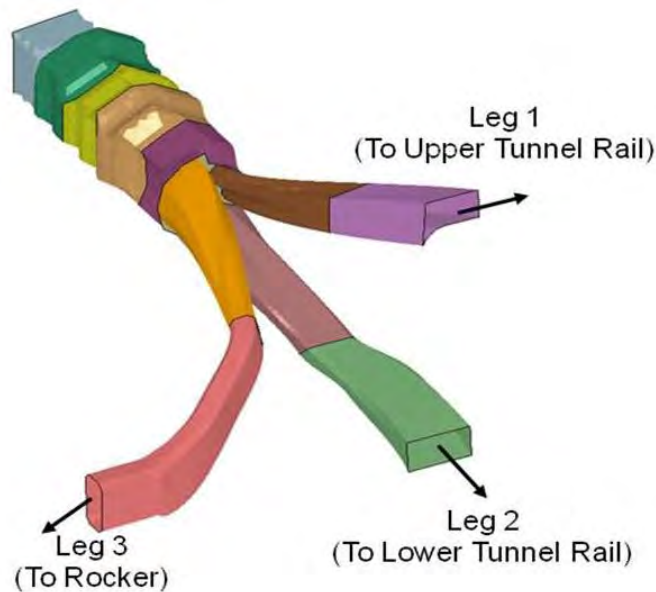


Figure 10.131: Hydroformed front rail concept 2 - zones of grade & gauge variation

For both hydroform concepts multiple variations were considered. For Hydroformed Concept 1 there were four variants and for Hydroformed Concept 2 there were two variations. Table 10.21 summarizes the differences between these variants.

HYDROFORMED FRONT RAIL CONCEPT 1	
1A	3G (Geometry, Grade & Gauge), Part elimination for Rail Legs toward the end of Rail
1B	2G (Grade & Gauge only), Part elimination for Rail Legs toward the end of Rail
1C	Setup per 1A, but front portion of rail changes as single gauge & grade
1D	Setup per 1C, but with greater priority to grade & gauge, less on geometry changes
HYDROFORMED FRONT RAIL CONCEPT 2	
2A	3G (Geometry, Grade & Gauge), Part elimination for Rail Legs toward the end of Rail
2B	2G (Grade & Gauge only), Part elimination for Rail Legs toward the end of Rail

Table 10.21: Hydroformed front rail concept - optimization setup

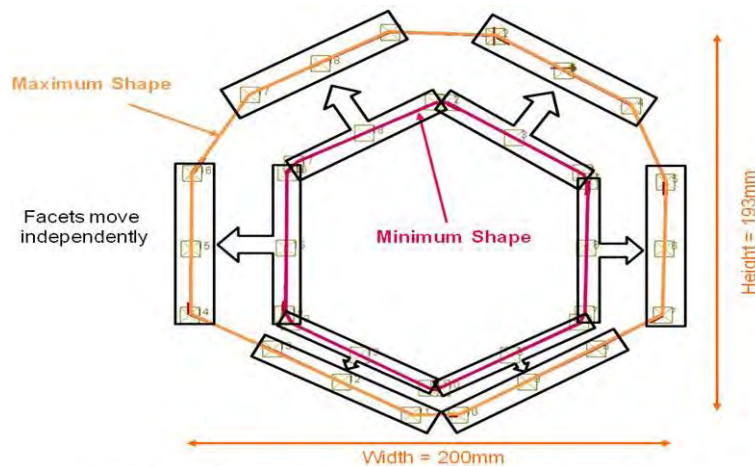
Details of the available grade and gauge choices are listed in Table 10.22. Note that for hydro-forming, material variation is limited to an ultimate tensile strength of 1000 MPa.

HYDROFORMED FRONT RAIL GAUGE CHOICES			HYDROFORMED FRONT RAIL GRADE CHOICES	
FROM	0.5 mm	In 0.01 mm increments	ULTIMATE TENSILE (MPa)	MAT 270
TO	2.0 mm			MAT 340
		MAT 450		
		MAT 500		
		MAT 600		
		MAT 800		
			MAT 1000	

Table 10.22: Hydroformed front rail - available grade & gauge choices

10.12.4.2 Geometry Parameterization

The geometry design space is limited as an outer boundary package space established in chapter 4. Referring to Figure 10.132, the cross-section for Hydroform Concept 1 was defined as six independent facets free to move independently of each other. The individual cross-sections themselves were also free to move independent of each other.



Black Arrows Indicate Independent Point Movement From Min to Max

Figure 10.132: Hydroformed front rail concept 1 - cross-sectional parameterization

Referring to Figure 10.133, for Hydroform Concept 2 the nodes of each cross-section moved together or were scaled so that the general shape of the section was preserved. However, the individual cross-sections themselves were free to move independent of each other.

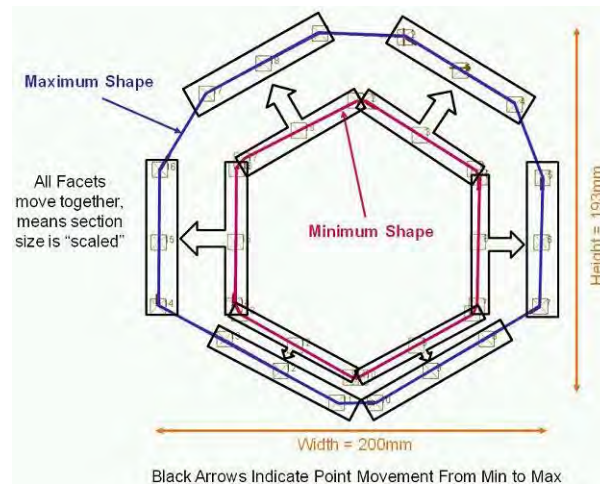


Figure 10.133: Hydroformed front rail concept 2 - cross-sectional parameterization

10.12.4.3 Hydroformed Front Rail : Design Solution

All results from the optimization are compared to the baseline LF3G front rail. Figure 10.134 & Figure 10.135 show the deformation and energy absorbed by the baseline LF3G design and the hydroformed 1D concept for front NCAP impact. It clearly shows that there is considerable plastic deformation leading to high strain energy absorption.

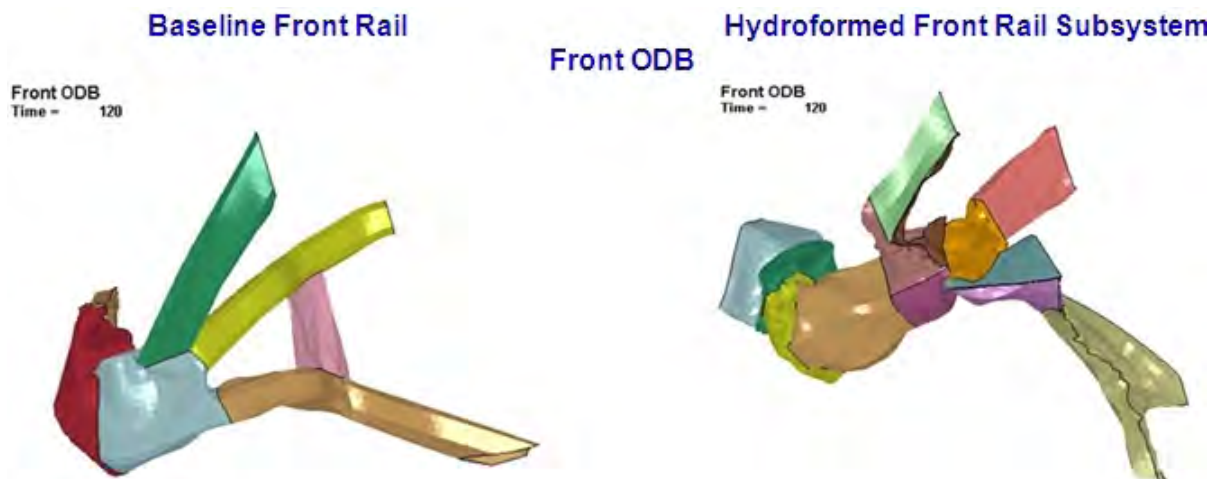


Figure 10.134: Hydroformed front rail concept 1D design solution - deformation comparison to baseline

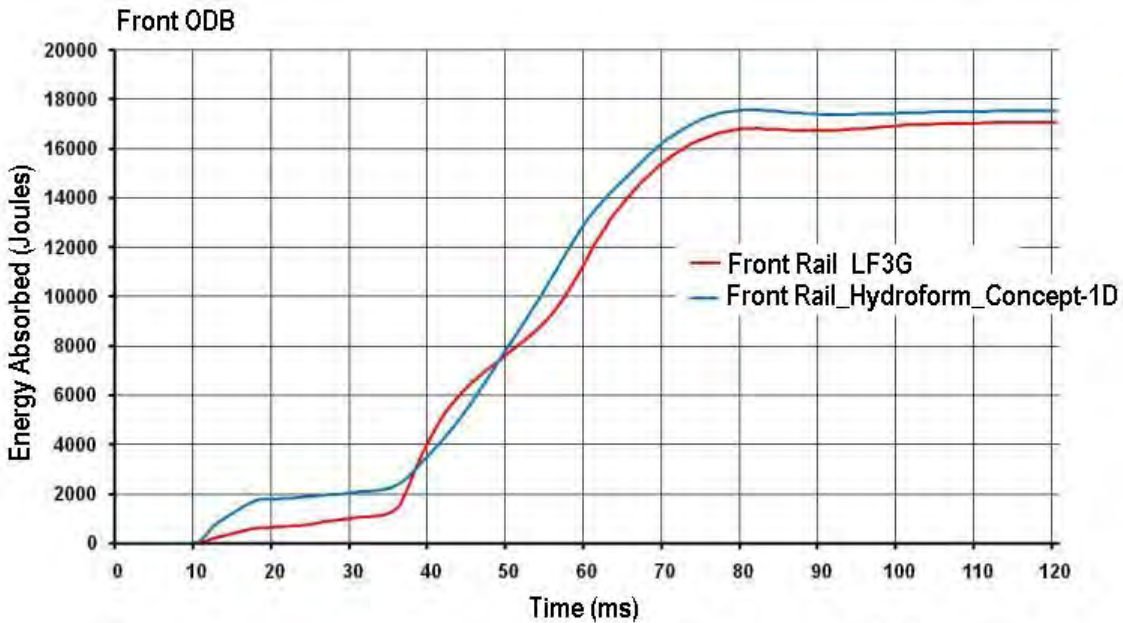


Figure 10.135: Hydroformed front rail concept 1D design solution - energy absorption comparison to baseline

Figure 10.136 shows the geometry, grade and gauge selections for the hydroformed 1D concept front rail. The final mass for this design solution was 5.3 kg, which is a 44% mass reduction compared to the baseline design (9.5 kg).

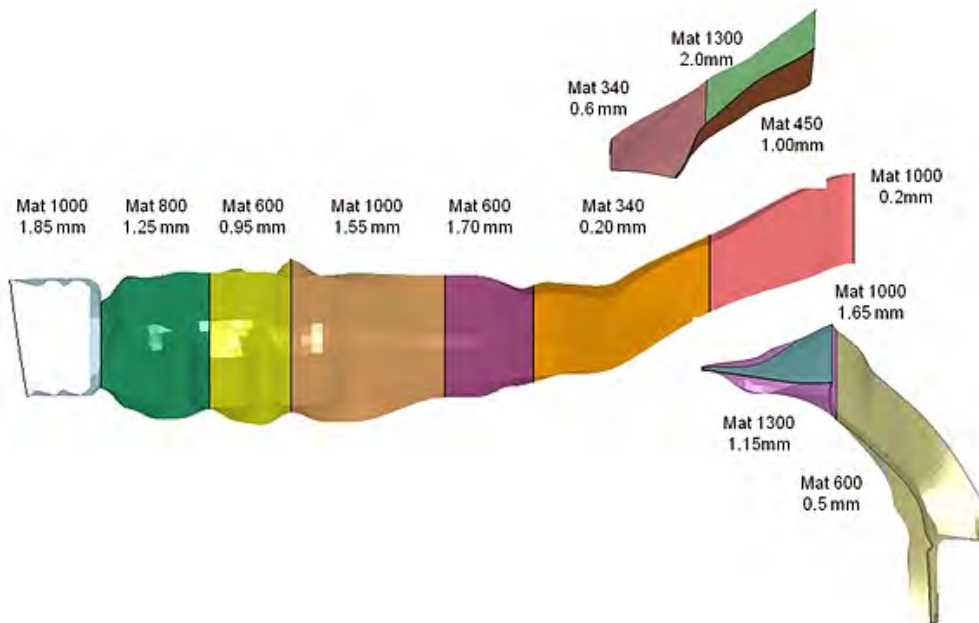


Figure 10.136: Hydroformed front rail concept 1D - final grade & gauge selections

10.12.5 Stamped Aluminum Front Rail Sub-System

10.12.5.1 Grade and Gauge Design Space

The stamped aluminum concept was based on the same definition as the stamped concept 2 front rail

For front rail stamping aluminum, starting concept design is same as used for the front rail stamping concept 2. The front rail in the baseline design has uniform thickness for the front rail upper and lower throughout the length. See Figure 10.137.

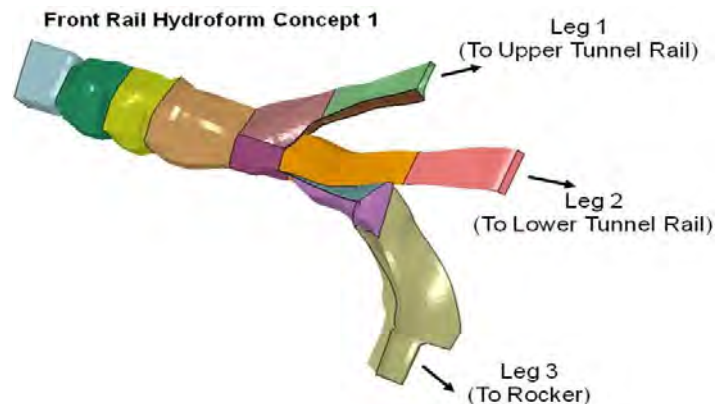


Figure 10.137: Aluminum front rail concept - zones of grade & gauge variation

The optimization problem is set up in heed by linking different tools for design generation, design evaluation, result post processing and finally optimization. Table 10.23 summarizes the available gauges.

STAMPED ALUMINUM FRONT RAIL GAUGE CHOICES			ALUMINUM FRONT RAIL GRADE CHOICES	
FROM	2.0 mm	In 0.01 mm increments	ALUMINUM GRADE	AL 6061
TO	6.0 mm			

Table 10.23: Stamped aluminum front rail - available grade & gauge choices

10.12.5.2 Geometry Parameterization

Figure 10.138 shows the parameterization of the cross section.

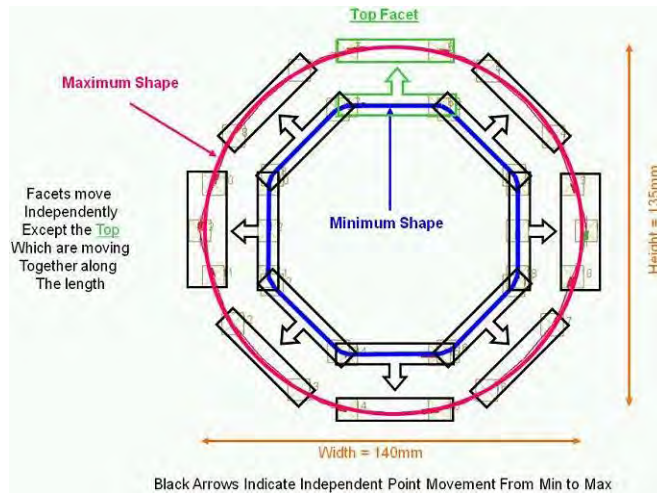


Figure 10.138: Stamped aluminum front rail concept - cross-sectional parameterization

10.12.5.3 Optimization Setup

- Objective: The optimization objective is to maintain the performance of the front rail so that the total strain energy remains the same as the LF3G under front ODB impact. The mass of the LF3G shotgun is 9.5 kg
- Target: The optimization target is to minimize the mass of the front rail.
- Constraint: The energy absorbed by the shotgun in the LF3G model (full model) was used as a constraint for the optimization. However, because this is a stamped aluminum concept, the energy values were recalculated from an updated version of the full LF3G model. In this case, the front rail material was revised from steel to aluminum. For front ODB impact the energy absorption was maintained at $\pm 15\%$ of the revised LF3G's performance. (For further information on target energy value calculations for aluminum, refer to Appendix 20.4 for details)

10.12.5.4 Stamped Aluminum Front Rail : Design Solution

All results from the optimization are compared to the baseline LF3G front rail. Figure 10.139 & Figure 10.140 show the deformation and energy absorbed by the baseline LF3G design and the optimized stamped aluminum concept for front NCAP impact. It clearly shows that there is considerable plastic deformation leading to high strain energy absorption.

10.12 Front Rail Sub-System

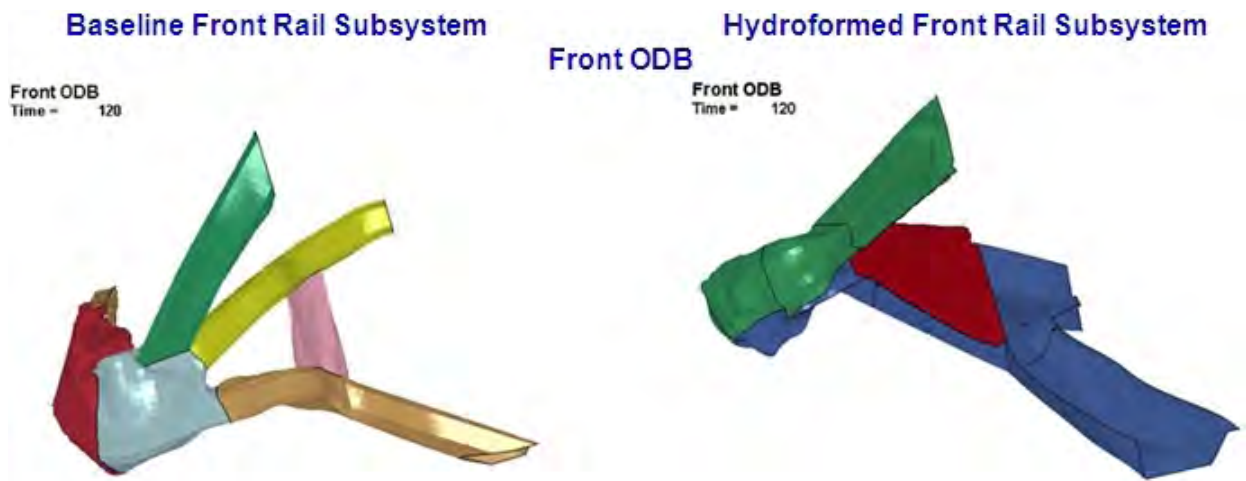


Figure 10.139: Hydroformed front rail concept 1D design solution - deformation comparison to baseline

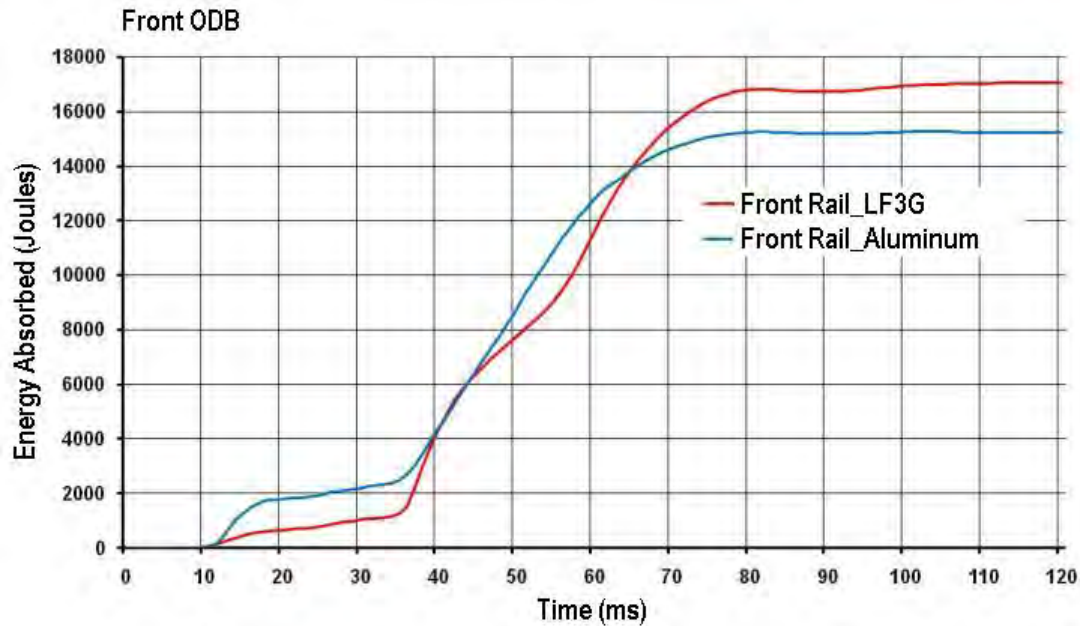


Figure 10.140: Stamped aluminum front rail concept design solution - energy absorption comparison to baseline

Figure 10.141 shows the geometry, grade and gauge selections for the stamped aluminum front rail concept. The final mass for this design solution was 4.0 kg, which is a 58% mass reduction compared to the baseline design (9.5 kg).

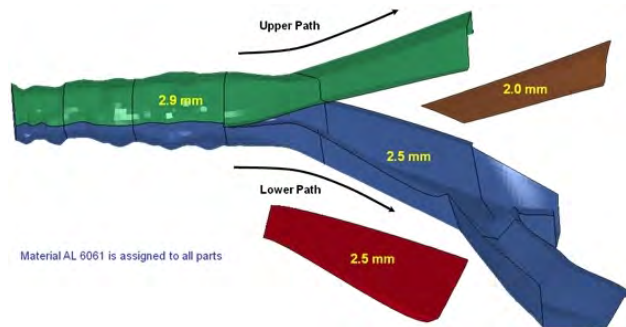


Figure 10.141: Stamped aluminum front rail concept - final grade & gauge selections

10.13 Front End Optimization

The front end of the vehicle is by far the most complex area of the body structure's design. In order to investigate the possible synergies that can provide additional mass savings a small front end optimization was performed. The optimization was based on the LF3G model into which the stamped shotgun design solution was substituted for the original design. See Figure 10.142. The original front rail was kept. Grade and gauge the optimization was then performed on the shotgun,

upper engine compartment diagonals and the shock towers. The results of the front end optimization are shown in Table 10.24 and final grade and gauge choices for the shock tower and shaw member are shown in Figure 10.143 & Figure 10.144

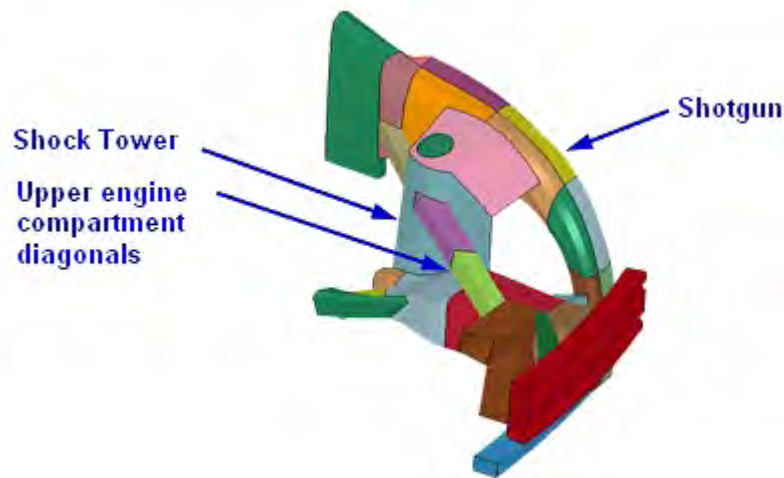


Figure 10.142: Front end optimization - components considered

COMPONENT	LF3G BASELINE (kg)	DESIGN SOLUTION (kg)	MASS SAVING	
			Kg.	%
Shotgun (Stamped)	10.6	6.4	4.2	40%
Shaw Member	2.13	1.7	0.43	20%
Shock Tower	3.6	1.6	2	56%
All Parts (LH/RH)	32.66	19.4	13.26	41%

Table 10.24: Front end: optimization summary & results

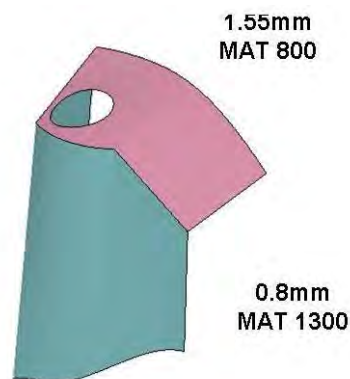


Figure 10.143: Front end optimization - shock tower final grade & gauge selections

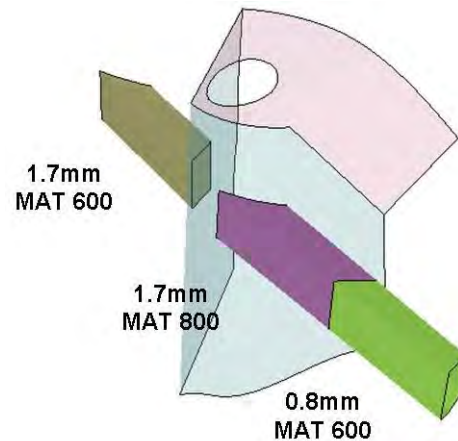


Figure 10.144: Front end optimization - upper engine compartment diagonals grade & gauge selections

10.13.0.5 Results Discussion

This was a very preliminary system approach to the front end. However, it is still very valid as it demonstrates the value of the next level of optimization which will be performed on the full system model.

10.14 Front End : Discussion of the Design Strategy for the FSV Design

The structure was designed to manage two very significant loadcases; front NCAP & front ODB. Figure 10.145 summarizes the barrier and position for both loadcases.

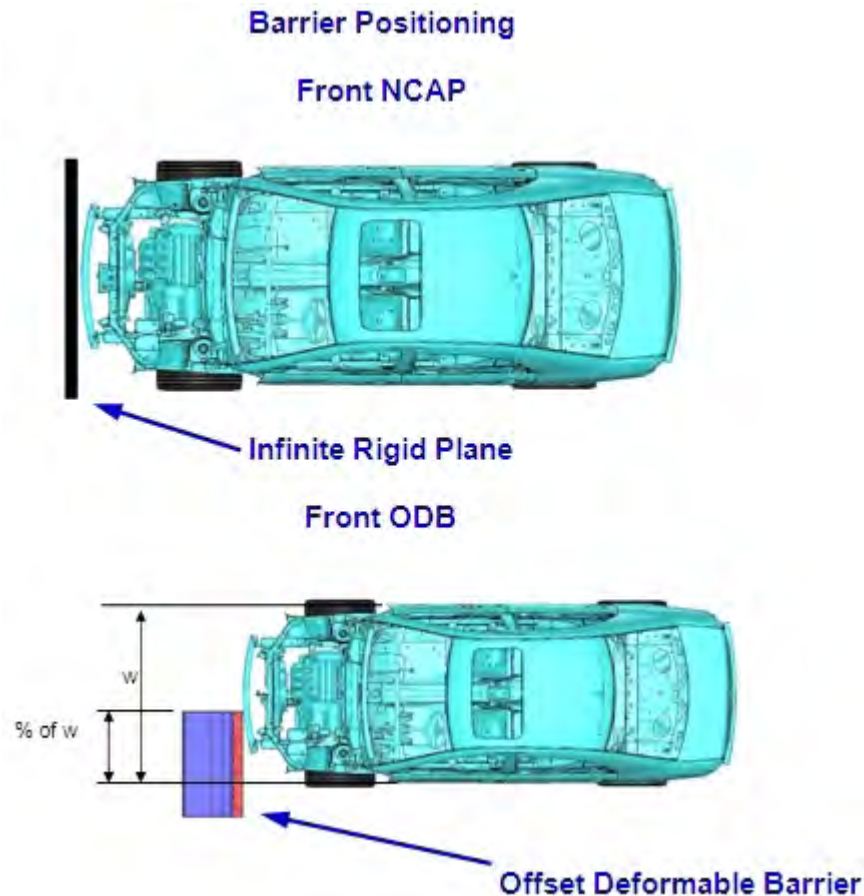


Figure 10.145: Front NCAP & front ODB impact barrier positions

There are two key assumptions lead the design of the FSV body structure:

- Non crush performance: For non crush events, such as IIHS side impact and static stiffness loadings, the most mass efficiency structure will be driven by well defined and optimally positioned loadpaths. These will allow the structure to transfer load through the structure effectively.
- Crush performance: For crush events, such as front NCAP and front ODB impacts, mass efficiency is driven by energy management. This strategy seeks to maximize the greatest amount of the initial impact energy before transferring the load to the remaining structure.

By using loadpath and energy management strategies to both absorb and then transfer load the design process will be enabled to further reduce the mass in the remaining structure. Figure 10.146 highlights how individual components are combined to provide the best loadpath driven structure for a conventional vehicle.

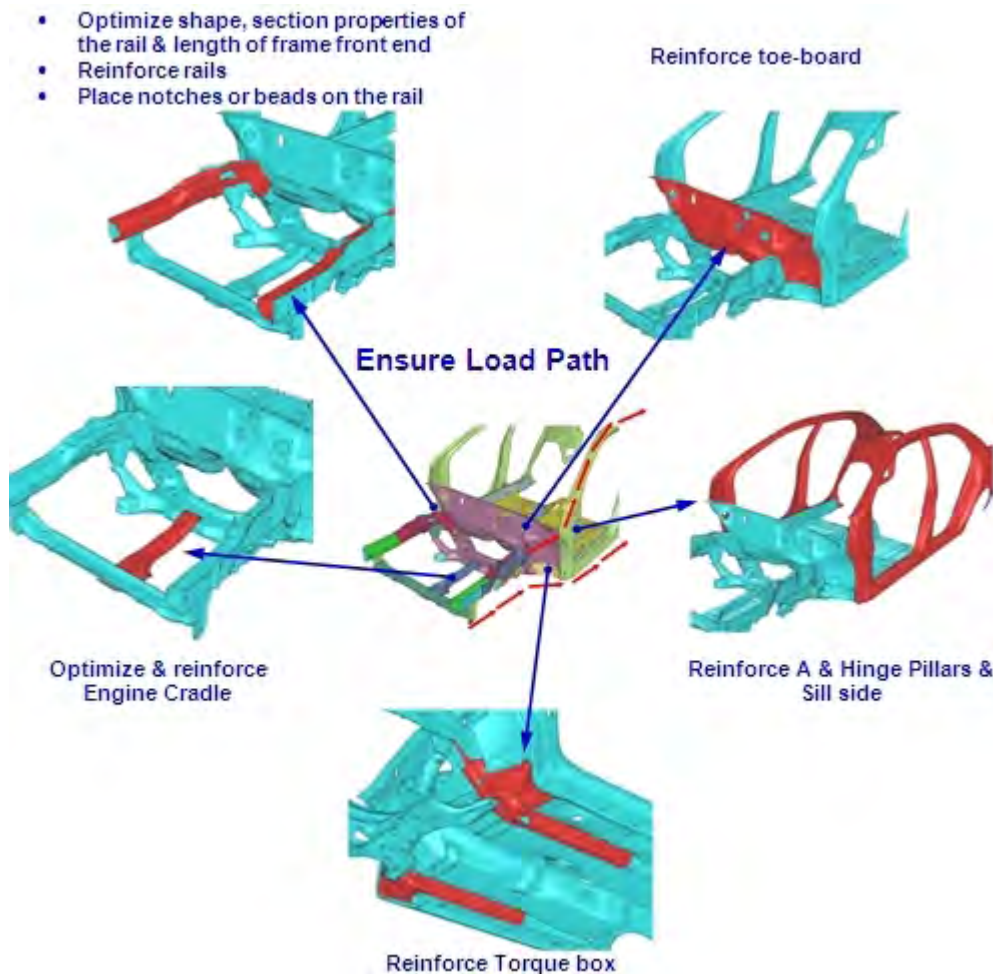


Figure 10.146: Typical loadpaths used in a conventional vehicle

Figure 10.147 shows how the LF3G version of the FSV performs under front NCAP loading. It shows both the acceleration pulse and energies. At 40msec 81% of the energy is internal. This is significantly higher than a traditional vehicle, which is typically about 40 to 60%. For comparison Figure 10.148 shows the typical performance for a conventionally powered front wheel drive vehicle of similar size to the FSV.

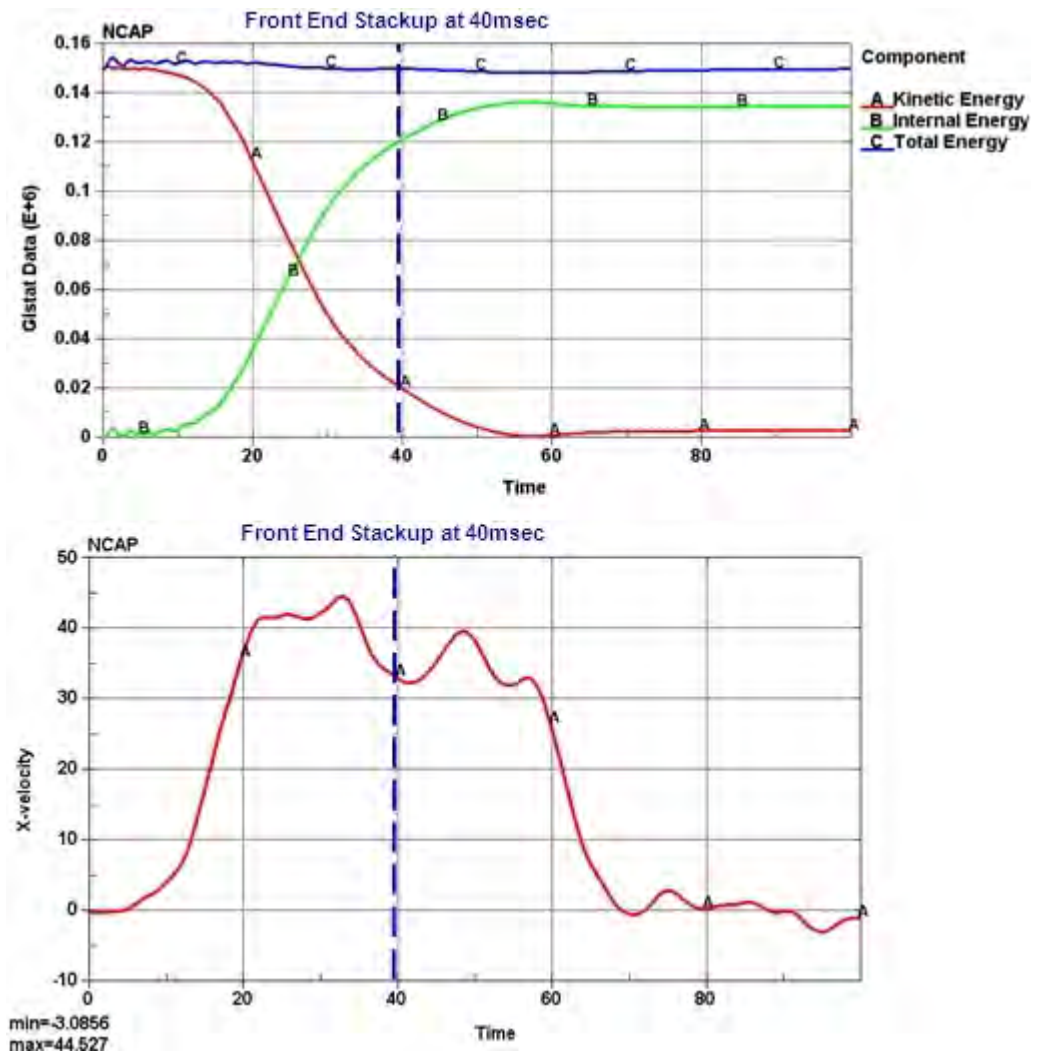


Figure 10.147: Front NCAP at 40 msec - acceleration pulse & energy

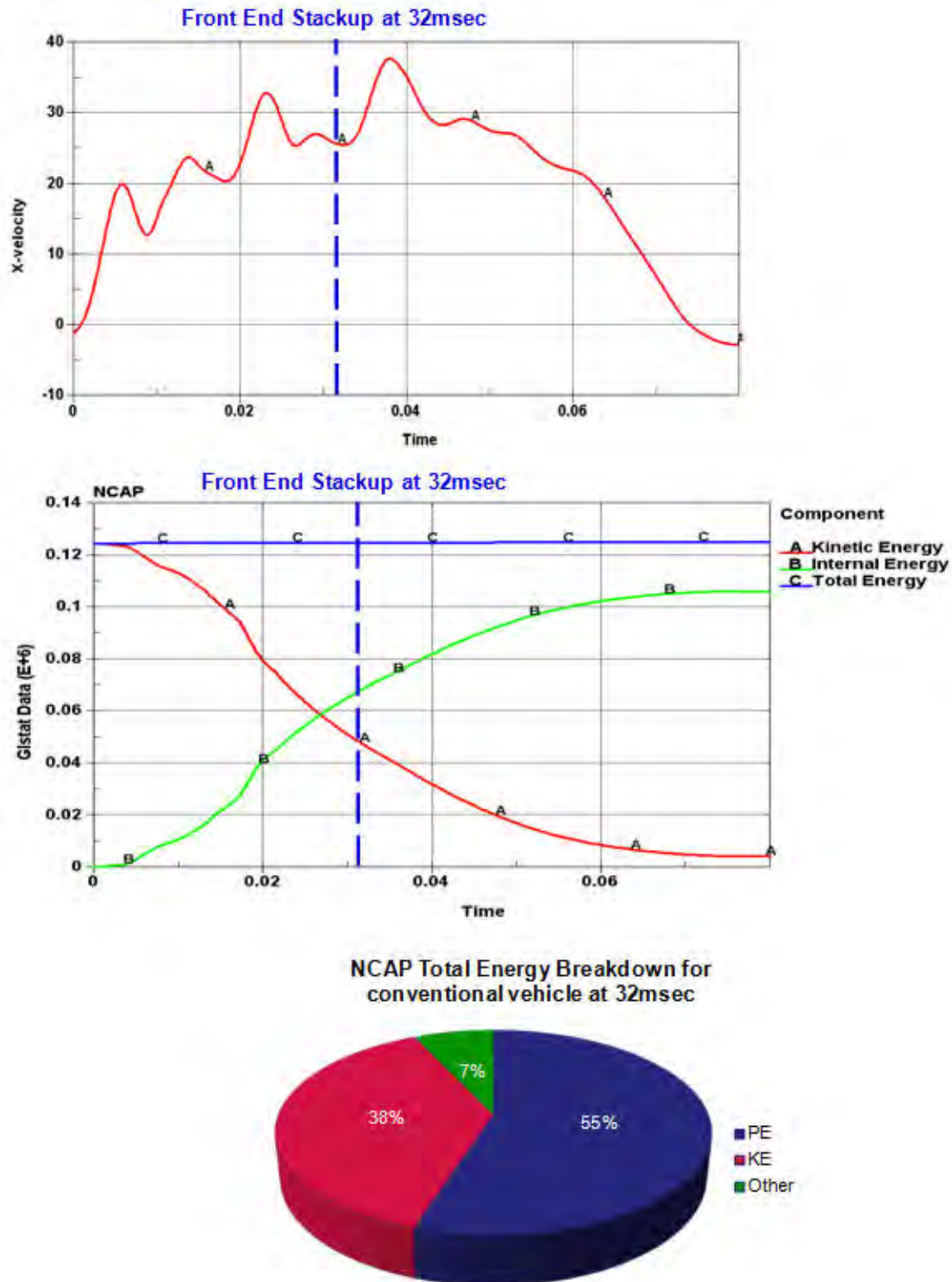


Figure 10.148: Typical front NCAP performance for a conventionally powered front wheel drive vehicle of similar size to the FSV

Figure 10.149 shows a breakdown of the internal energy by component for the FSV. All but 5% of this energy is absorbed by the front end components, thus establishing both the uniqueness and importance of the front loadpath. By managing the frontal impact energies in this way the remaining it will enable the design process to further reduce mass in the remaining structure.

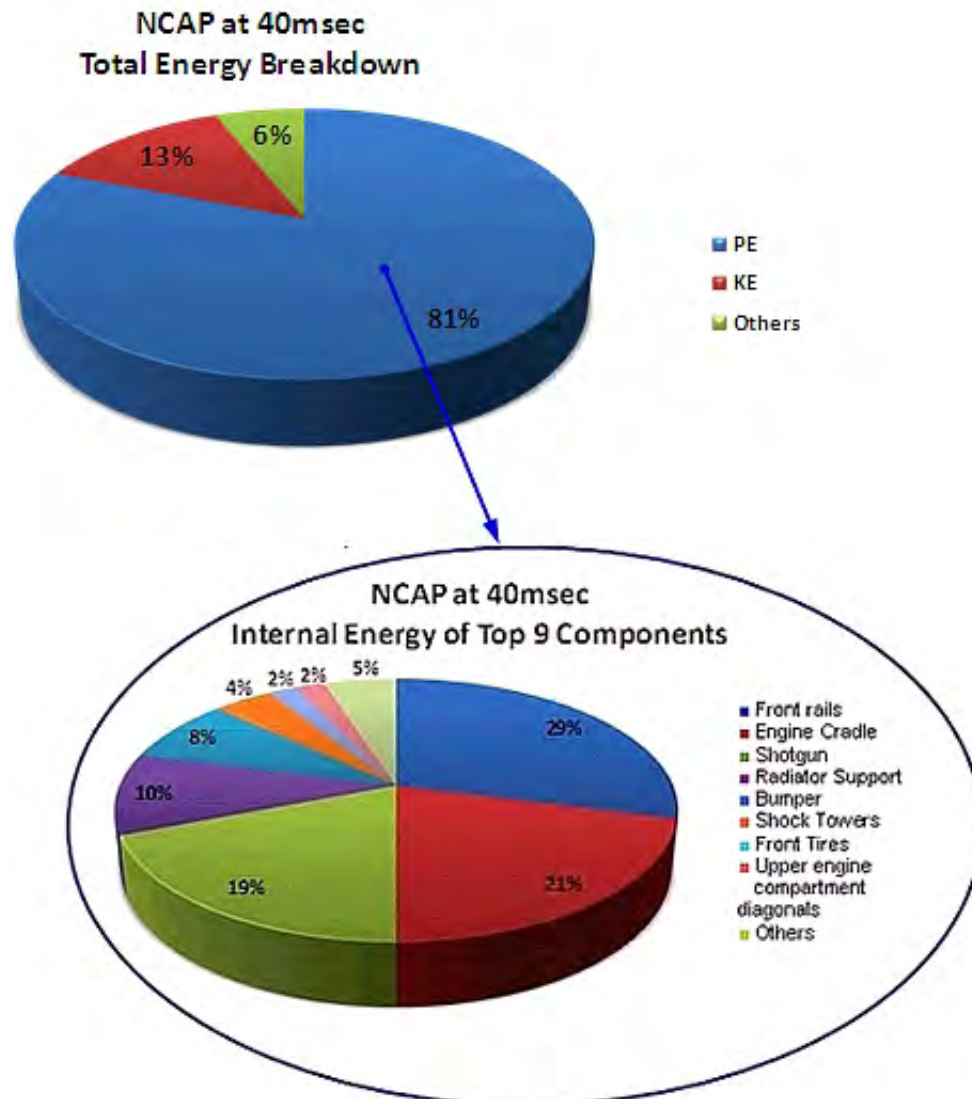


Figure 10.149: Front NCAP at 40 msec - total & internal energy Breakdowns For Major Components

Figure 10.150 gives a breakdown of the “Others” which accounted for 5% of the total internal energy. Again even of this 5% is made up of the primarily structure thus reinforcing the importance of the loadpath driven design solution.

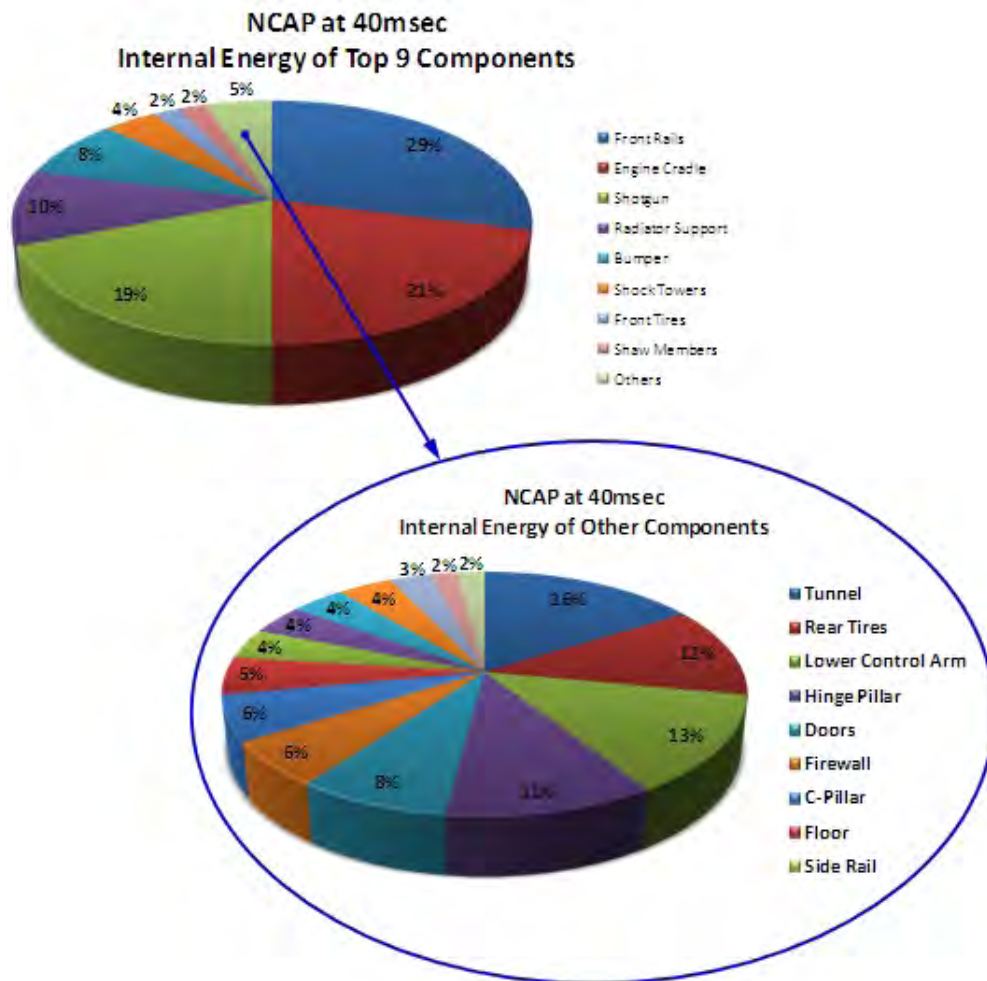
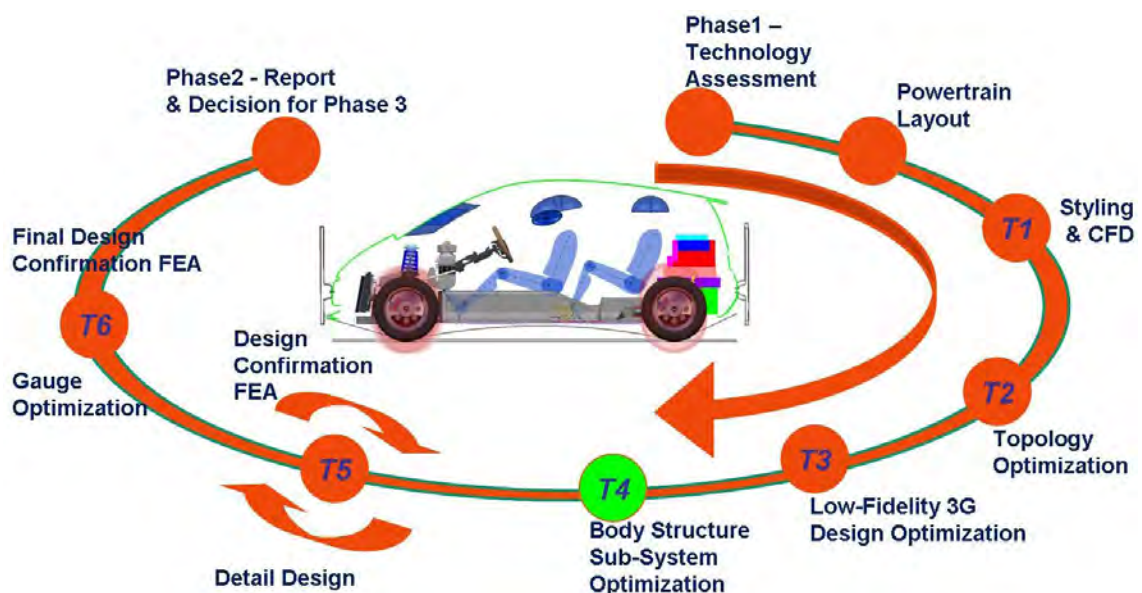


Figure 10.150: Front NCAP at 40 msec - internal energy breakdowns for all other components

11.0 Structural Sub-System Design and Manufacturing Interpretation



11.1 Introduction

The solutions obtained from the structural sub-system multidiscipline 3G optimization runs had appropriate material grade selections and gauges, optimized to give a low mass solution, that met the structural performance targets. These solutions were assessed considering the respective manufacturing technology guidelines, to ensure manufacturability of the sub-system. The following sections explain the approach that was taken to interpret the 3G optimization results for manufacturing (the specific material grades and gauges shown in these interpretations are yet to be confirmed by CAE analysis for the respective manufacturing technology).

11.2 Rocker 3G Optimized Solution

The optimized stamped rocker solution from the 3G optimization runs is shown in Figure 11.1.

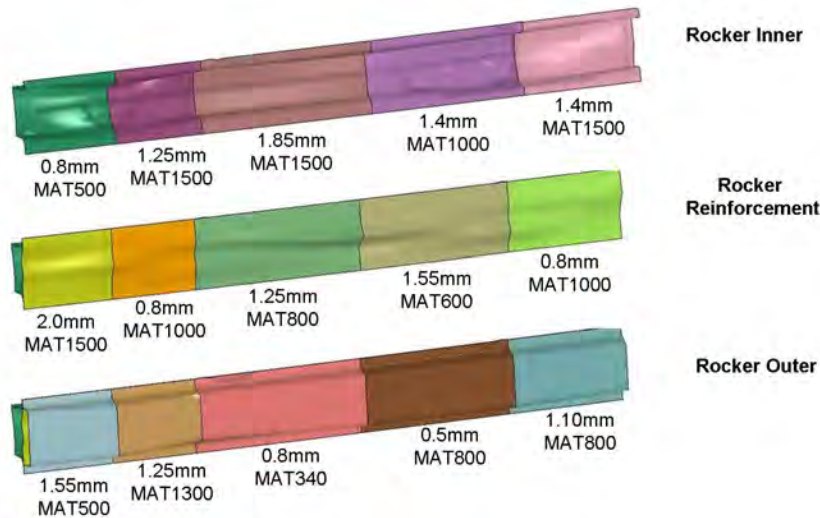


Figure 11.1: Rocker solution from 3G optimization runs

11.3 Rocker Manufacturing Interpretation (Design for Manufacturing)

Minor geometry design changes were applied to the 3G optimization solution to ensure manufacturability, such as adding sufficient fillets, removing die lock conditions etc.

Since the 3G optimization solution has multiple material selections and gauges, the closest interpretation was a stamped laser welded blank, as shown in Figure 11.2. However, the material grade and gauge allocation was made according to the feasibility of the laser welded blank stamping process.

For the rocker outer, being a visible component, stamped laser welded blank (LWB) and tailor rolled blank (TRB) options were not considered; regular stamped with single thickness was the only option for the rocker outer component.

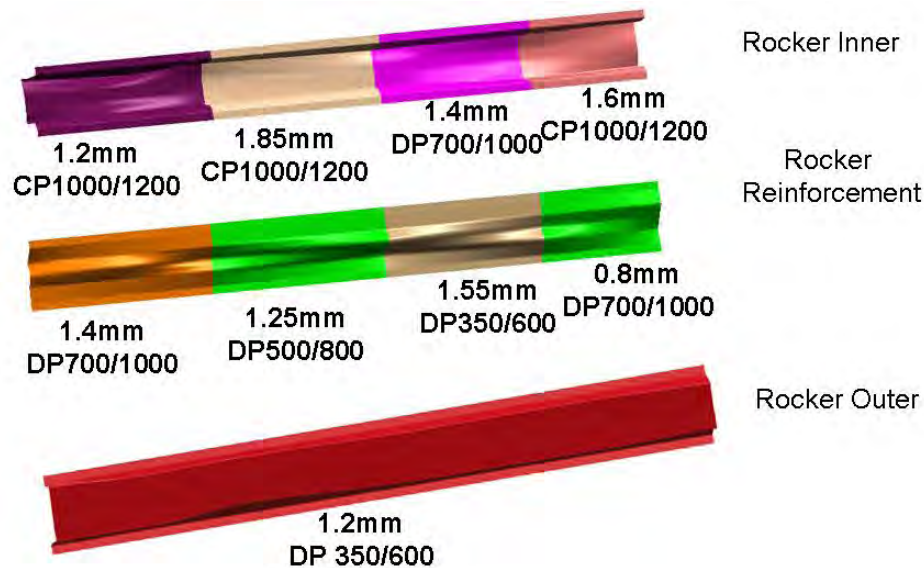


Figure 11.2: Manufacturing interpretation of the rocker solution (stamped LWB)

The initial selection of materials and gauges for the corresponding stamped single thickness and TRB solutions, were based on engineering judgment. The goal was to use the material and gauge specifications of the 3G optimization run as a guideline, to pick the single grade that would meet similar performance. These material grade and gauge selections were finally validated by FEA analysis to verify the energy absorption as compared to the LF3G runs results.

For the TRB solutions, there was a mass saving advantage, compared to the Stamped single thickness solution, by increasing the gauge where the 3G optimization run specifically indicated a need for additional strength. Also, manufacturing guidelines specific to the process were taken into consideration such as the following:

- The maximum grade possible for TRB solutions is DP 800 with exception of hot stamping
- The gauge ratio between two consecutive gauges cannot be more than two (2) for TRB solutions
- The minimum gauge possible for boron steel is 0.6 mm

The stamped single thickness and stamped TRB interpretations of the rocker are shown in Figure 11.3 and Figure 11.4, respectively.

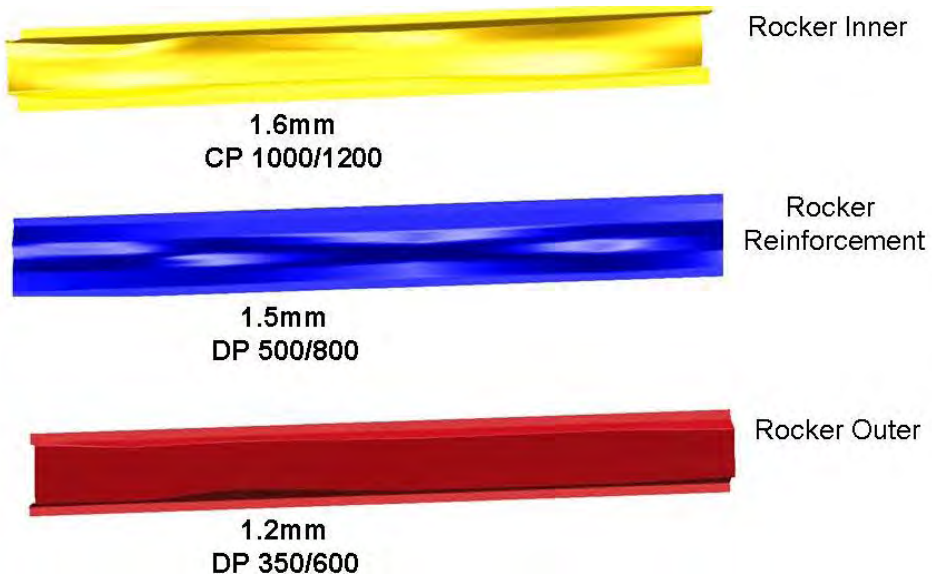


Figure 11.3: Rocker stamped single thickness solution

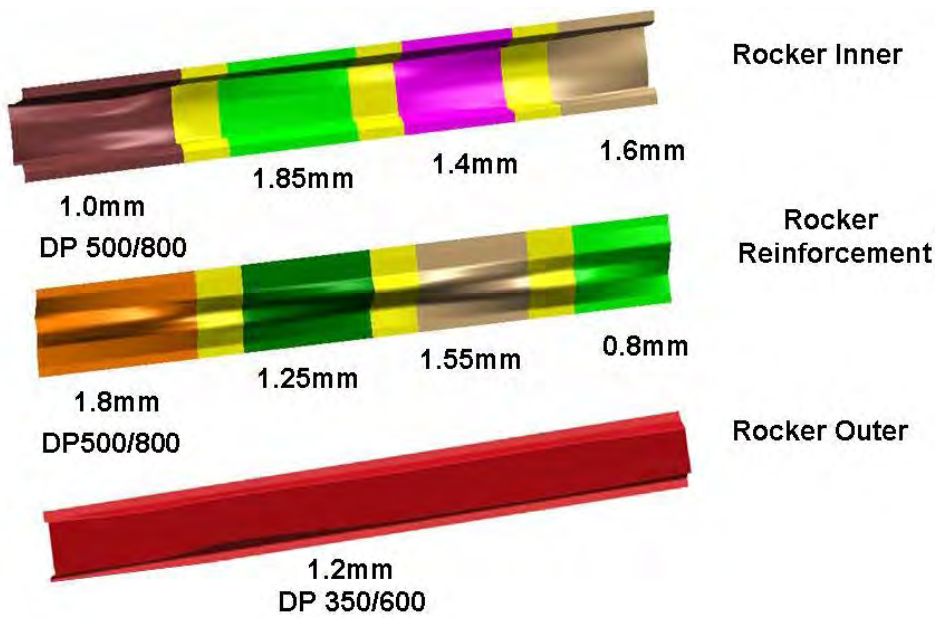


Figure 11.4: Rocker - stamped tailor rolled blank (TRB) Solution

11.4 Verification of Interpreted Results

11.4 Verification of Interpreted Results

The interpreted results were then subject to FEA simulation to analyze the performance. As seen in Figure 11.5 thru Figure 11.7, the energy absorption characteristics of the interpreted results are similar to the baseline 3G optimization run solution. Hence, the material grades and gauges selected were confirmed for the respective manufacturing technologies. If the performance of the interpreted results were not satisfactory compared to the baseline, the material grades and gauges would be adjusted. The validation runs would be subsequently repeated with the new grades and gauges. This iterative process would be repeated until the performance results were satisfactory.

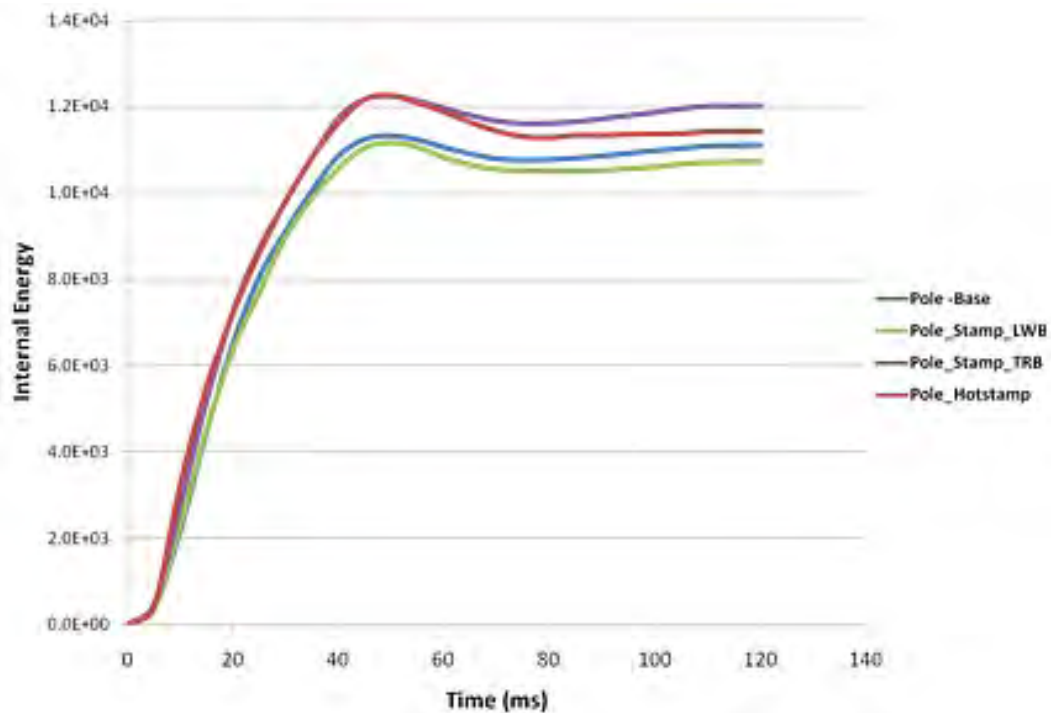


Figure 11.5: *Rocker solution manufacturing interpretation internal energy comparison side*

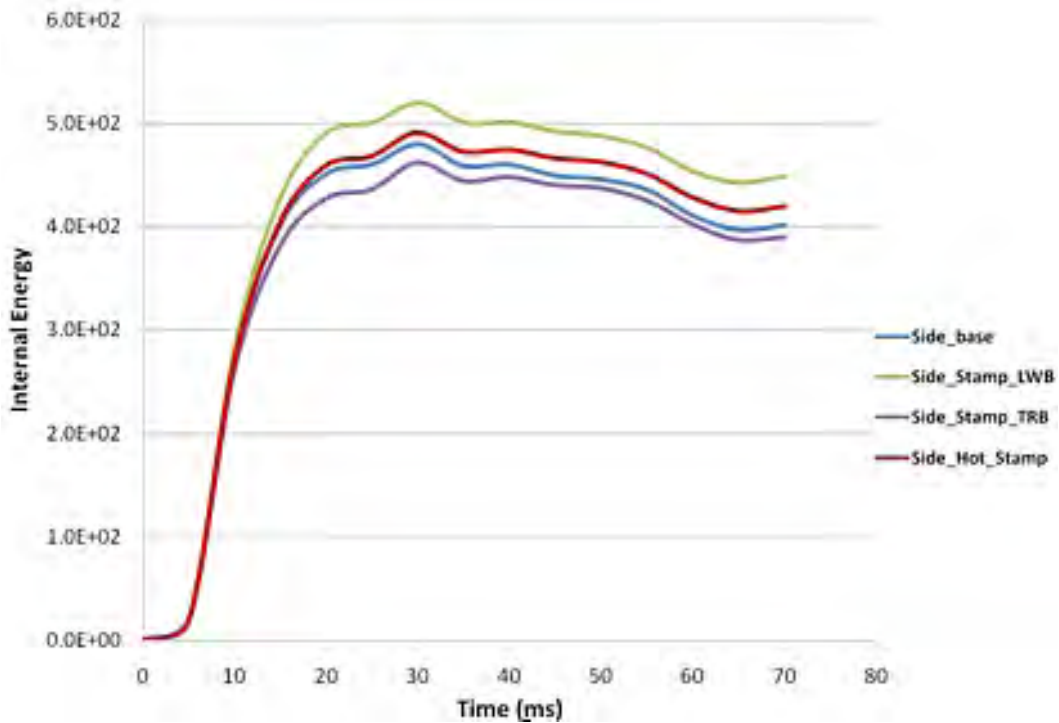


Figure 11.6: Rocker solution manufacturing interpretation internal energy comparison - IHS side impact

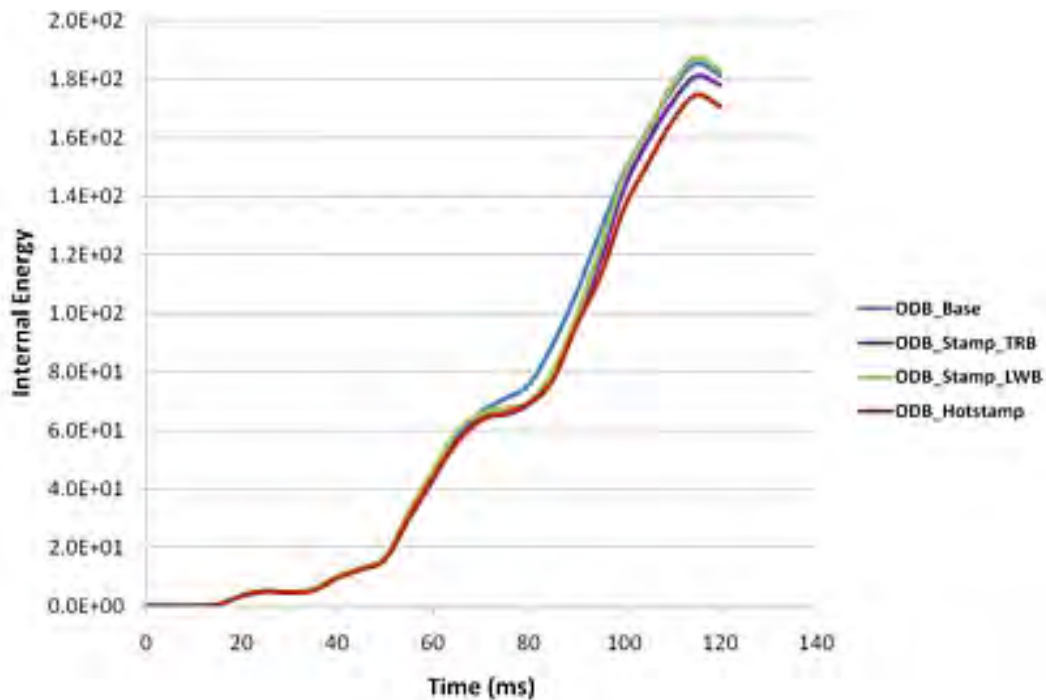


Figure 11.7: Rocker solution manufacturing interpretation internal energy comparison - IHS ODB

11.4 Verification of Interpreted Results

The process explained in section 11.3 thru section 11.4 was repeated to identify the different rocker solutions for the hot stamped, hot stamped TRB and hot stamped LWB technologies, shown in Figure 11.8 thru Figure 11.10.

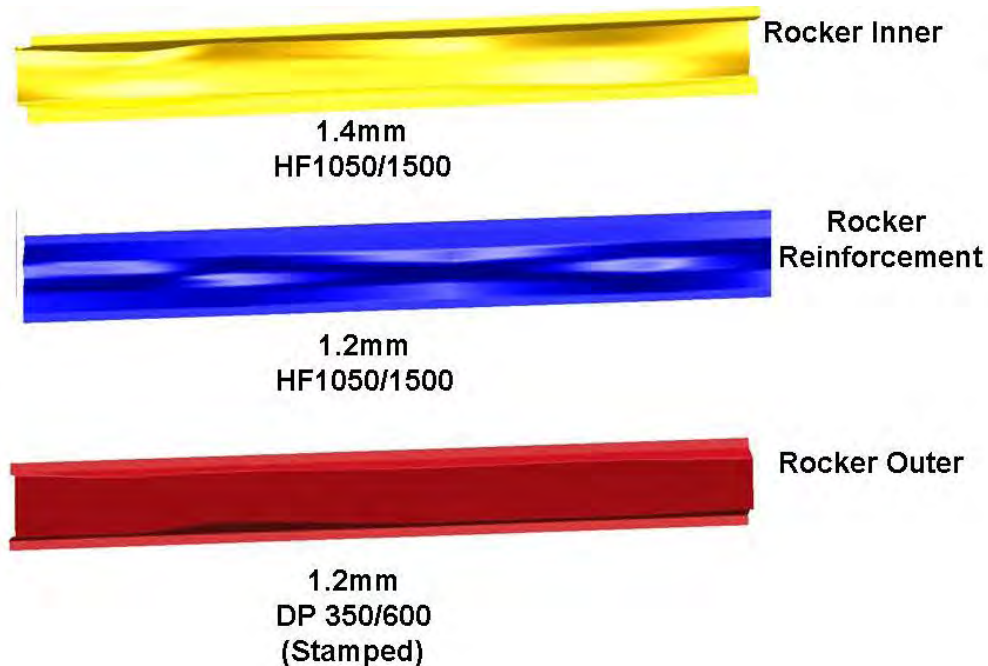


Figure 11.8: *Rocker hot stamped single thickness solution*

Since the rocker outer was a part of the body side outer, the LWB and TRB alternatives were not considered for the rocker outer design. The rocker outer was a common design for all the hot stamped rocker sub-system solutions as shown in Figure 11.9 and Figure 11.10.

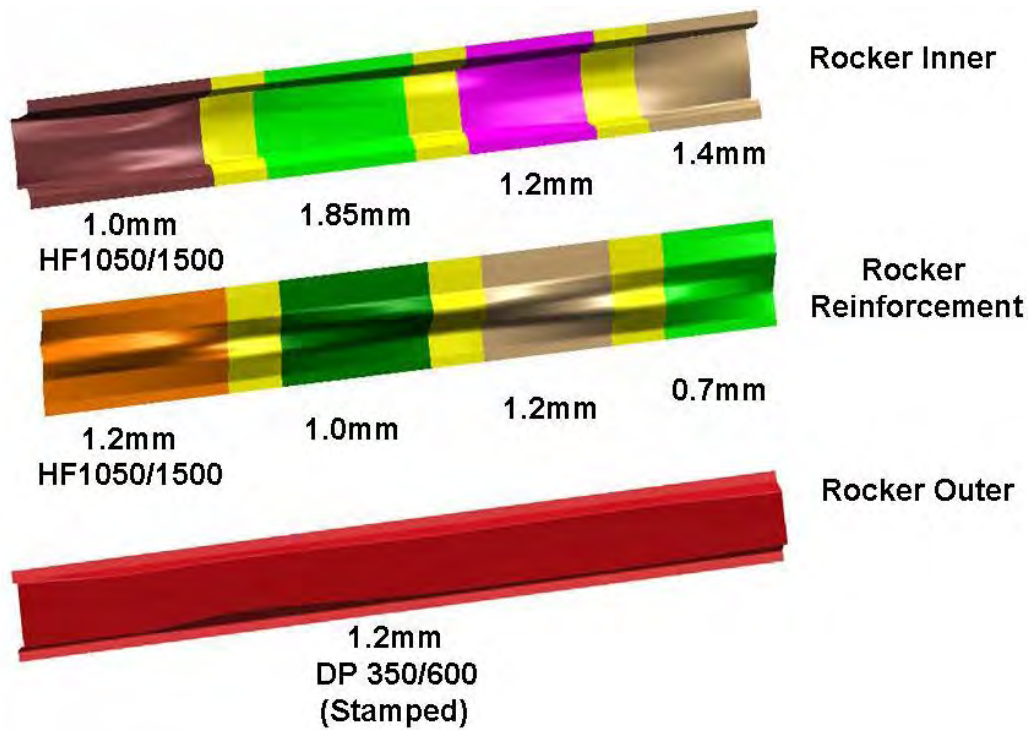


Figure 11.9: Rocker - hot Stamped TRB solution

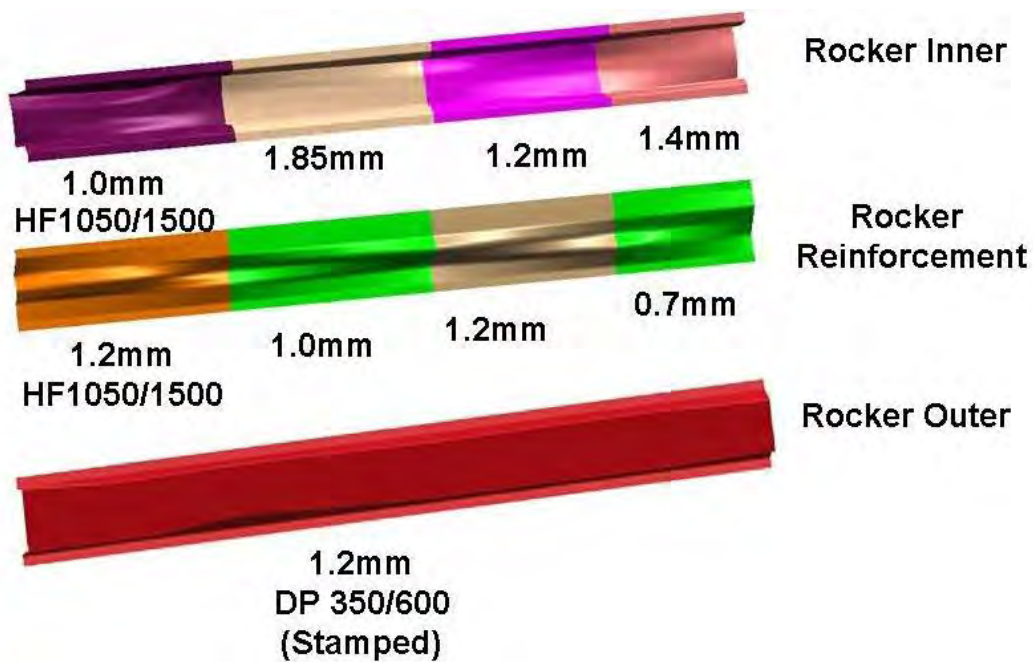


Figure 11.10: Rocker - hot stamped LWB solution

11.5 Rocker Tubular Solutions

Similar to the procedure followed in section 11.3 thru section 11.4, the tubular solutions (roll formed and hydroformed) provided by 3G optimization runs were interpreted into respective designs suitable for manufacturing, as illustrated in Figure 11.11 thru Figure 11.17.

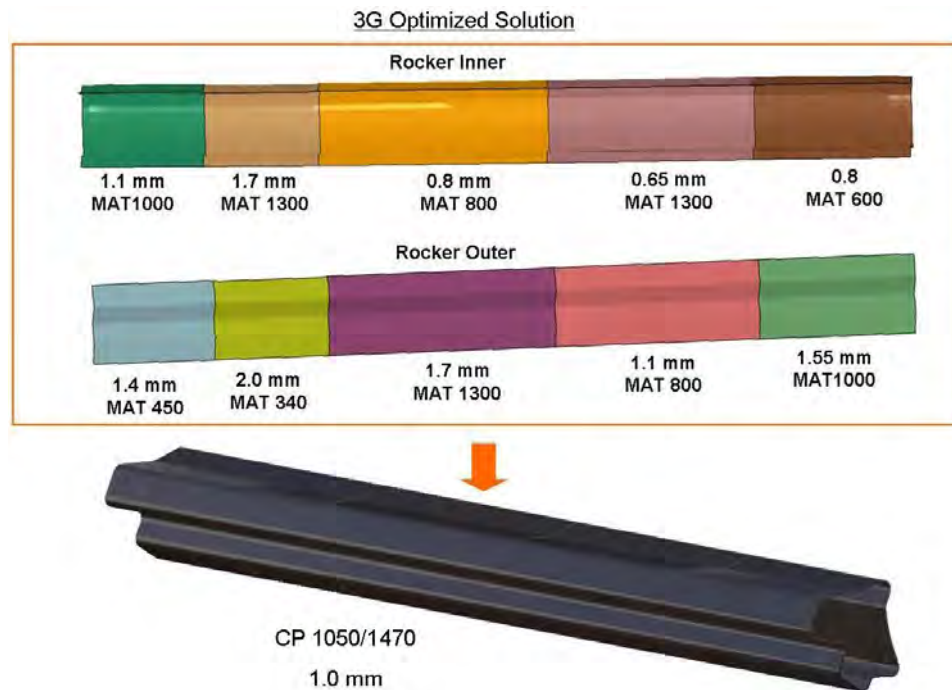
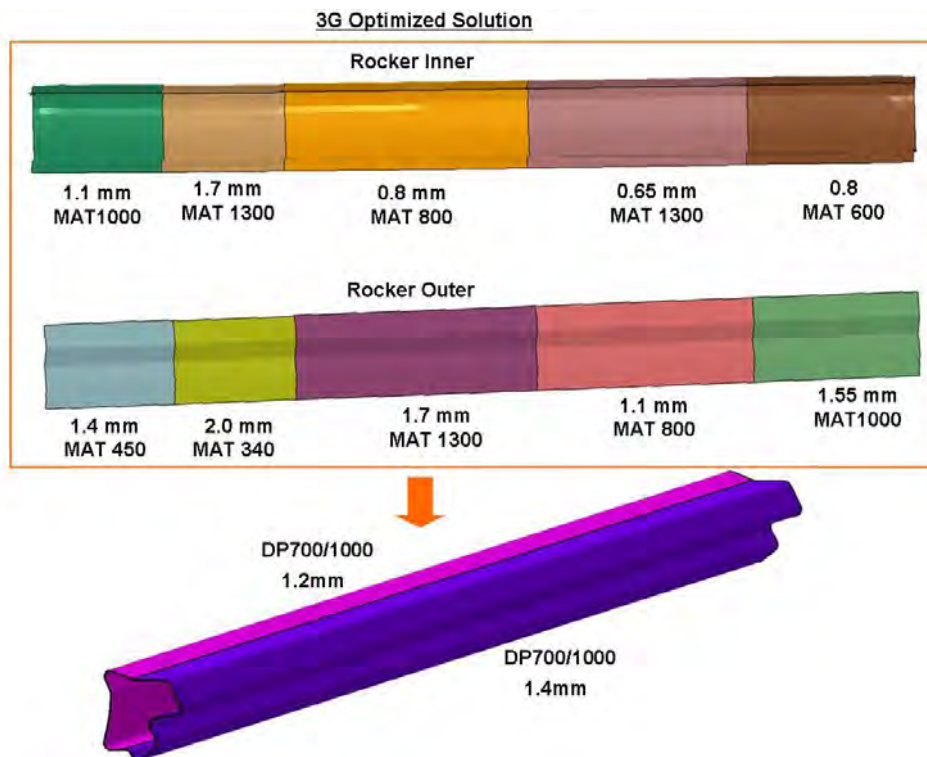
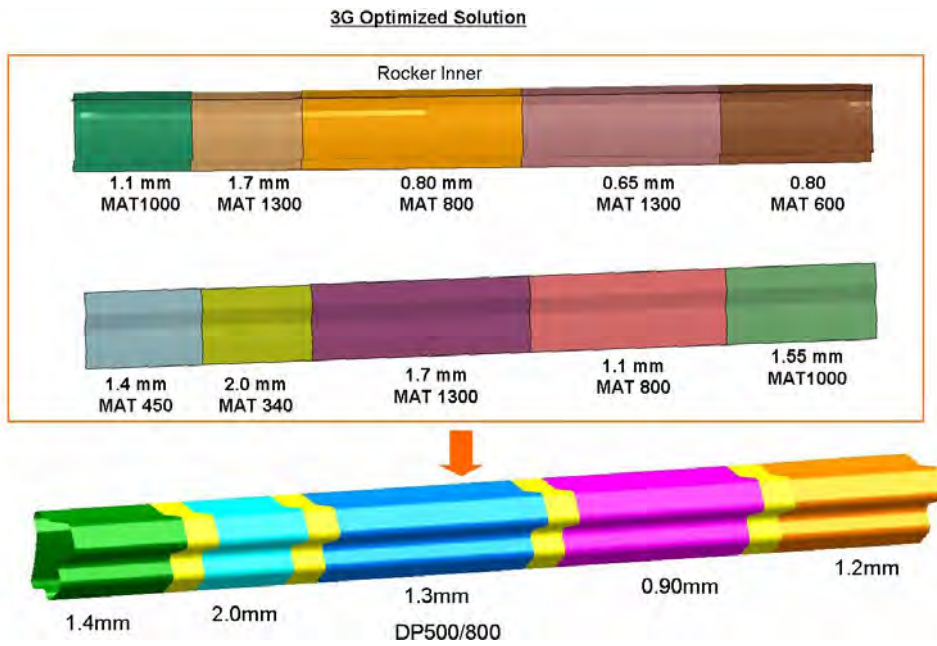


Figure 11.11: *Rocker - roll formed solution*



The hydroformed rocker sub-system solution is shown in Figure 11.14 thru Figure 11.16. The geometry of the rocker was adjusted such that the perimeter remained the same along the length of the rocker, to account for low pressure hydroforming manufacturing feasibility.

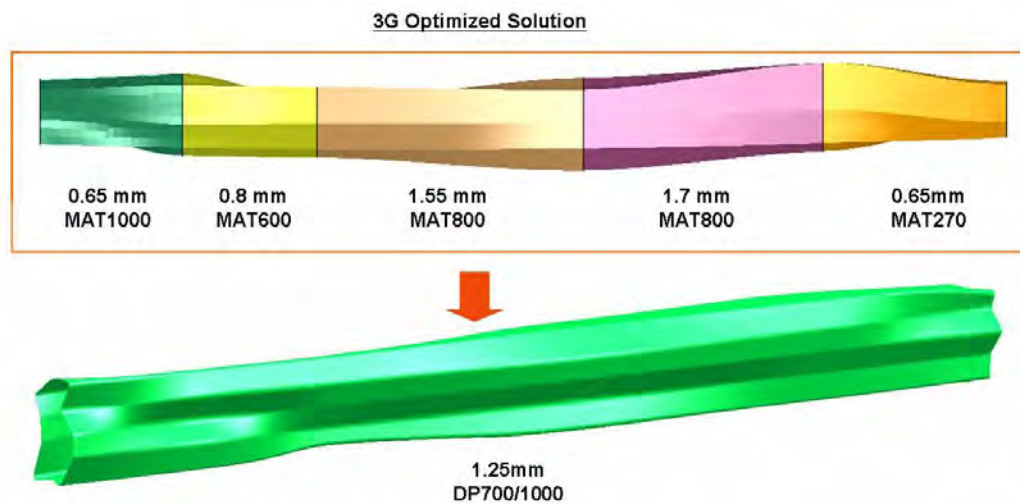


Figure 11.14: Rocker - hydroformed solution

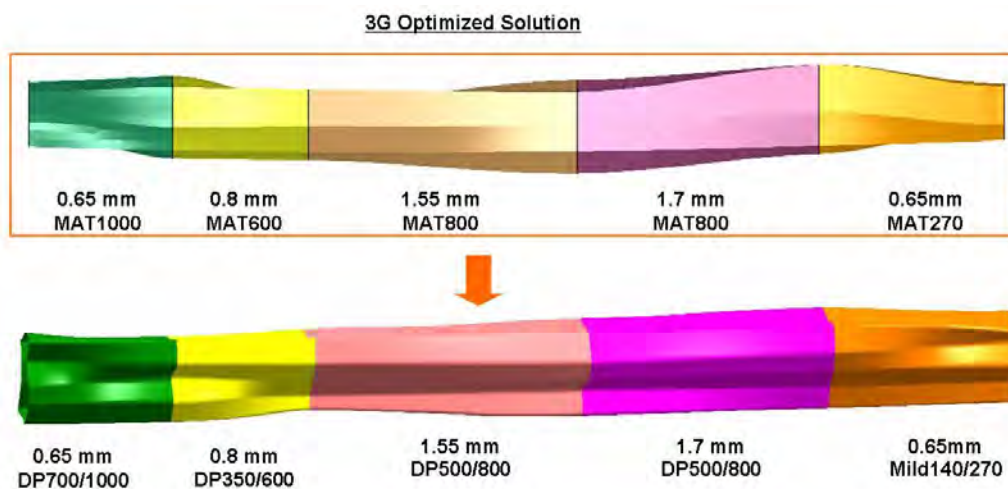
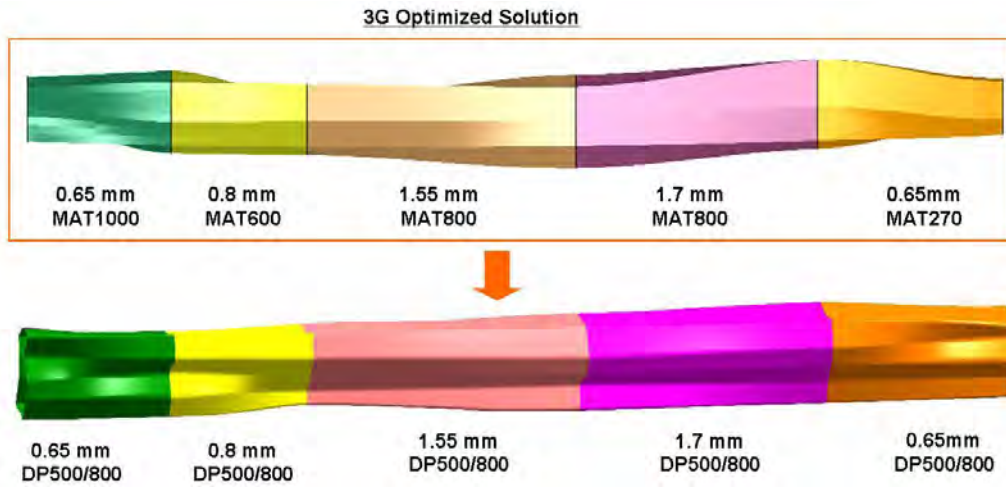
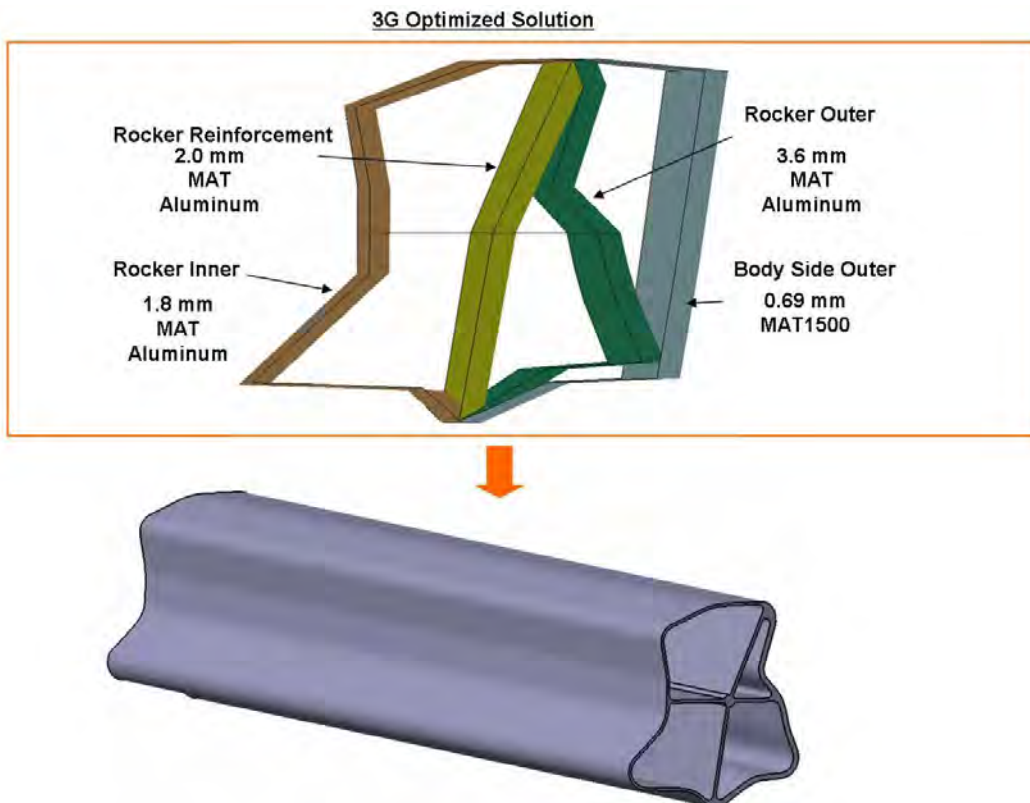


Figure 11.15: Rocker - hydroformed LWT solution



The extruded aluminum rocker solution interpreted from the 3G optimized solution is shown in Figure 11.17.



11.6 B-Pillar 3G Optimized solution

11.6 B-Pillar 3G Optimized solution

The 3G optimized solution for the FSV B-pillar is shown in Figure 11.18.

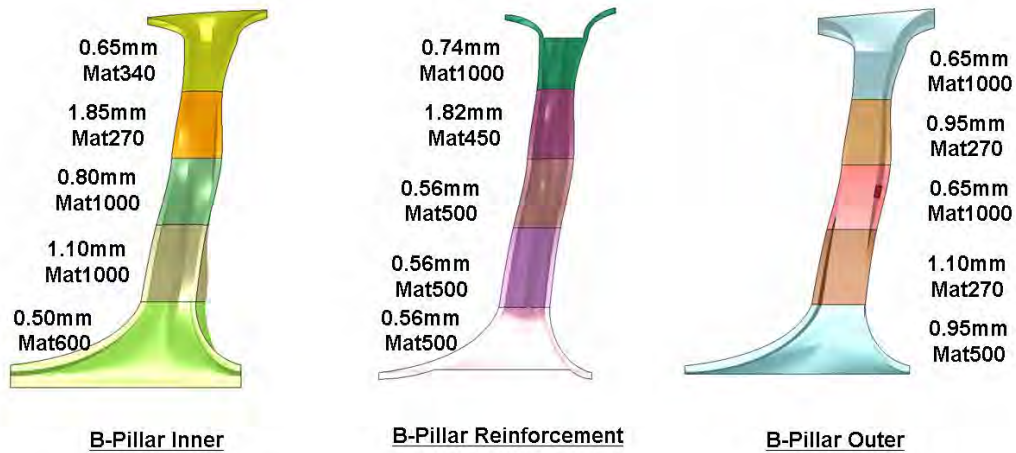


Figure 11.18: *B-pillar 3G optimized solution*

11.7 B-Pillar Interpreted Results

The procedure explained in section 11.3 thru section 11.4 was repeated to attain the following solutions for B-pillar, shown in Figure 11.19 thru Figure 11.25.

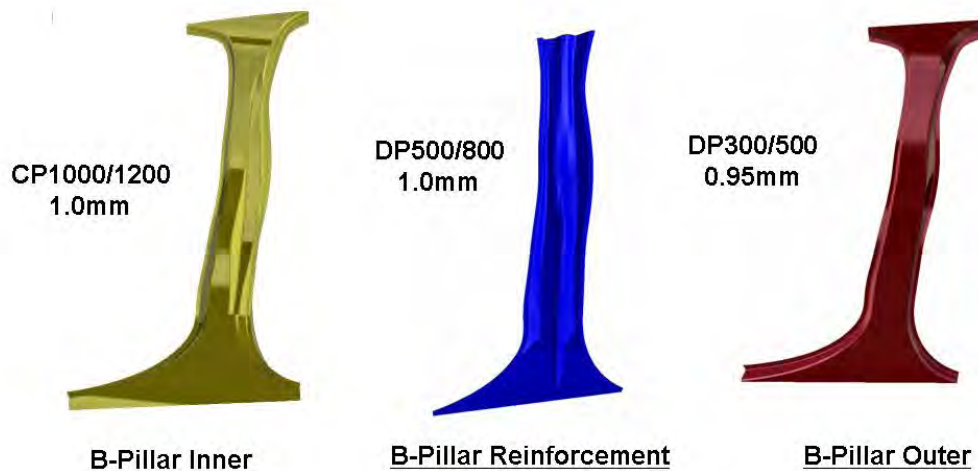


Figure 11.19: *B-pillar - stamped solution (single gauge)*

Since the B-pillar outer is a visible component (Class B) all the solutions assumed a stamped

(single thickness) B-pillar outer. The stamped aluminum solution used a stamped aluminum B-pillar outer.

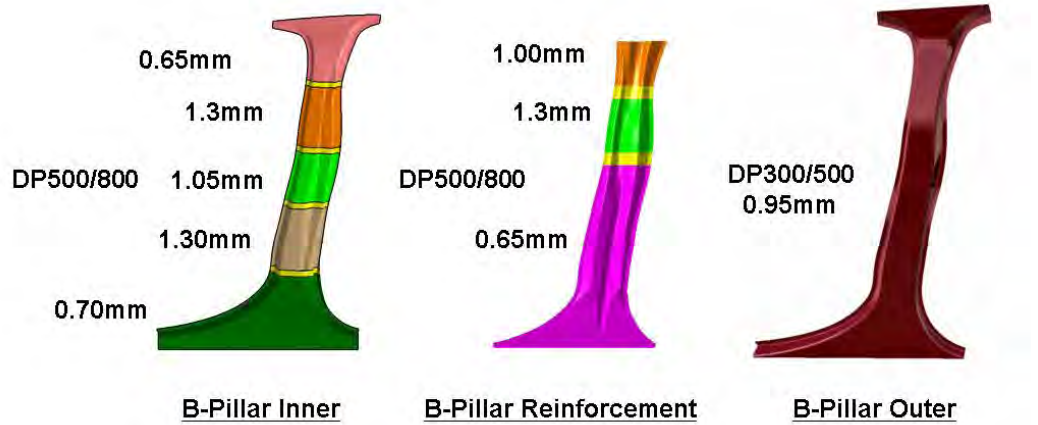


Figure 11.20: B-pillar - stamped TRB Solution

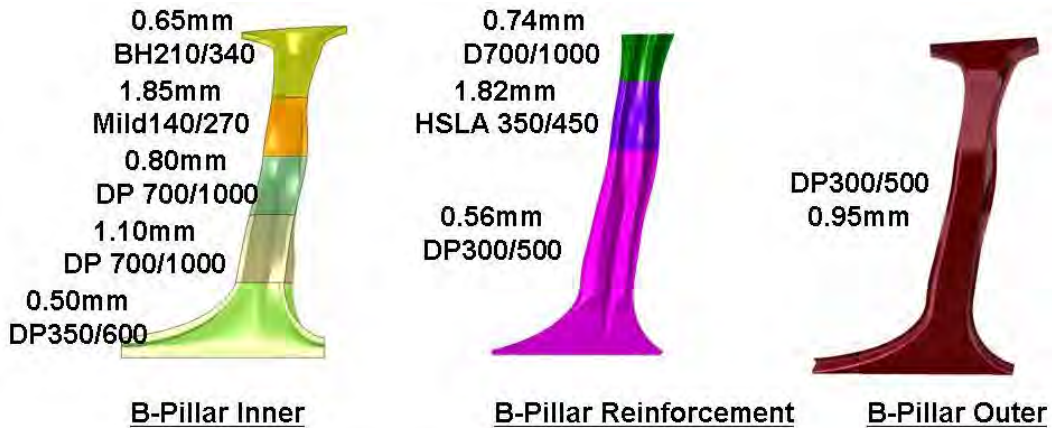


Figure 11.21: B-pillar - stamped LWB Solution

The B-pillar hot stamped solutions are shown in Figure 11.22 thru Figure 11.24.

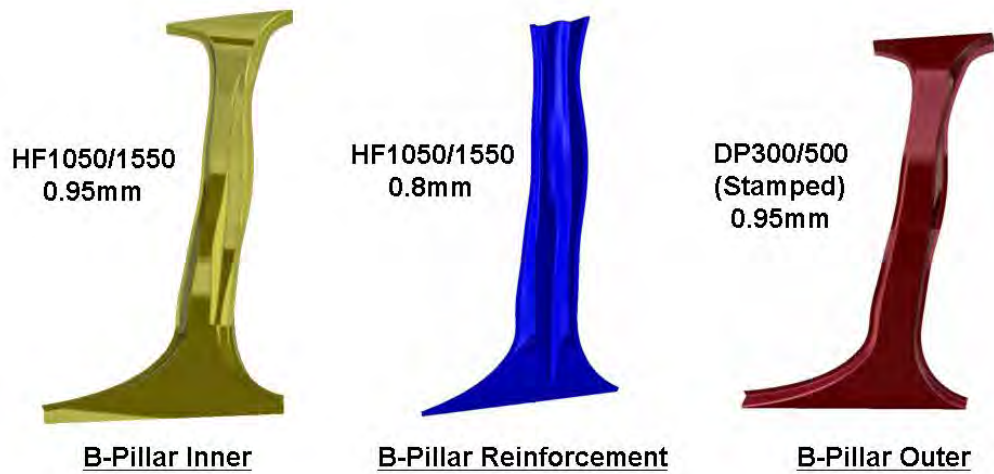


Figure 11.22: B-pillar - hot stamped solution (single gauge)

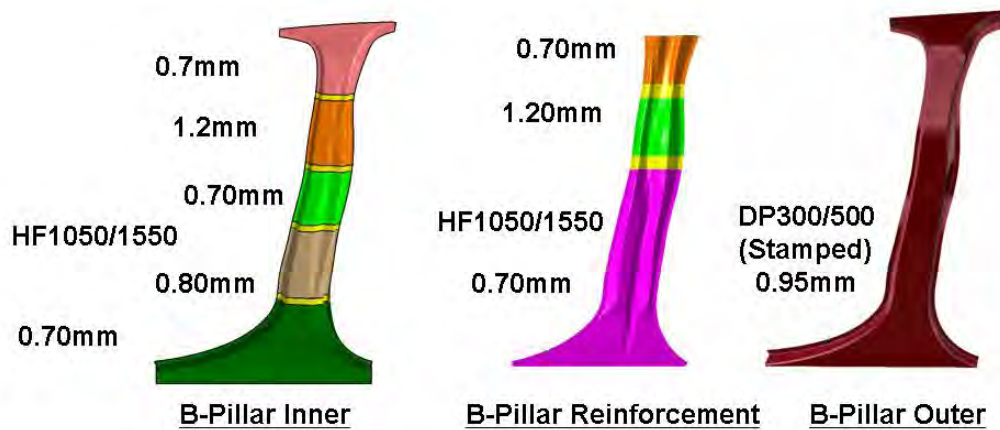


Figure 11.23: B-pillar - hot stamped TRB solution

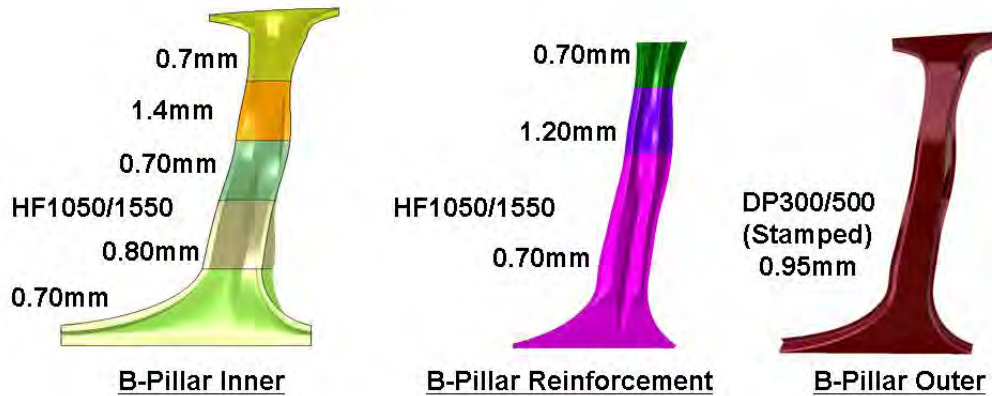


Figure 11.24: B-pillar - hot stamped LWB solution

The B-pillar stamped aluminum solution is shown in Figure 11.25.

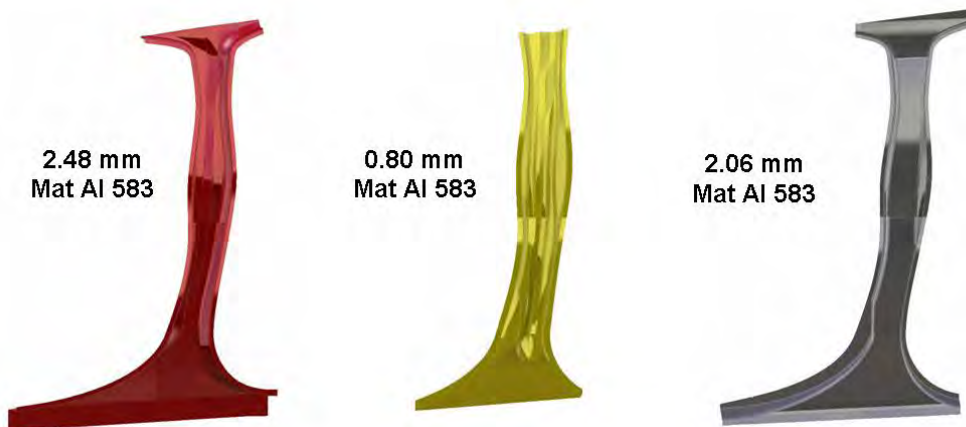


Figure 11.25: B-pillar - stamped aluminum solution

The B-pillar outer is a common design for stamping (as shown in Figure 11.19), for both the roll formed solution (Figure 11.26) and the hydroformed design using laser welded tube (LWT) (Figure 11.27).

11.7 B-Pillar Interpreted Results



Figure 11.26: B-pillar - closed roll formed solution with stamped B-pillar Outer (not shown)

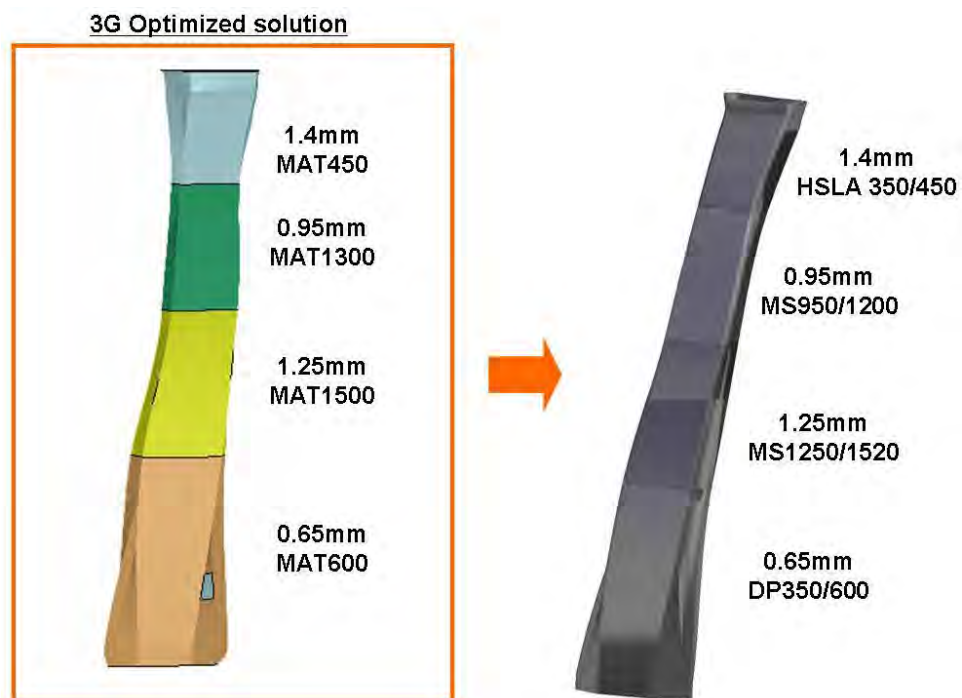


Figure 11.27: B-pillar - hydroformed LWT solution with stamped B-pillar outer (not shown)

11.8 Rear Rail 3G Optimized Solution

The 3G optimized solution for the FSV rear rail is shown in Figure 11.28 (stamping 3G optimized solution) and Figure 11.29 (hydroforming 3G optimized solution).

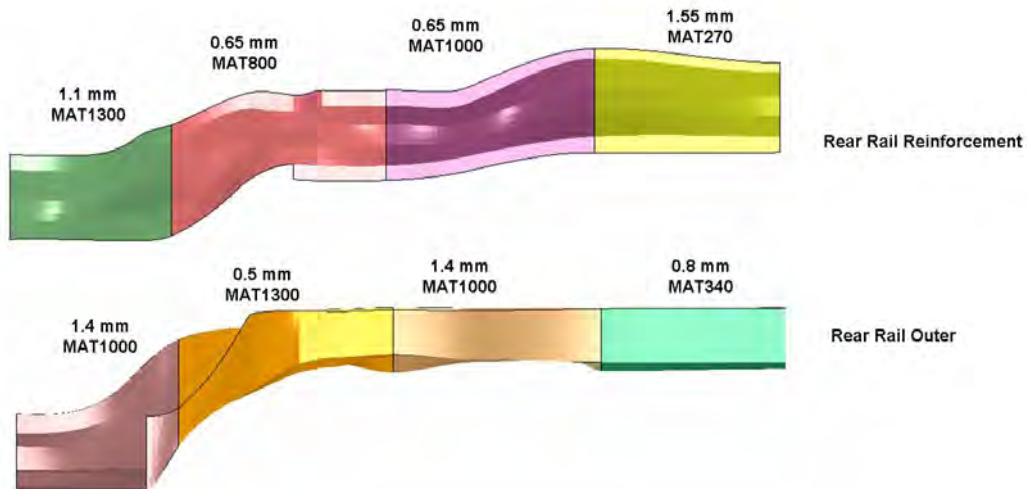


Figure 11.28: Rear rail 3G optimized solution (for stamping)

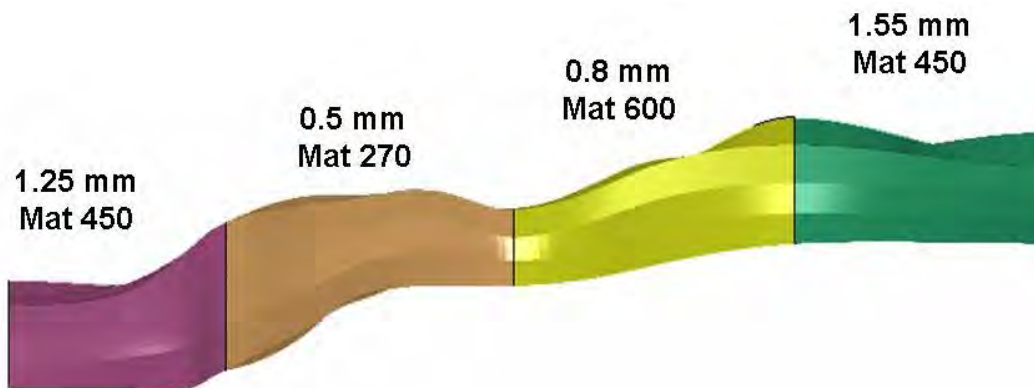


Figure 11.29: Rear rail optimized solution (for hydroforming)

11.9 Rear Rail Interpreted Results

The procedure explained in section 11.3 thru section 11.4 was repeated to attain the following solutions for the FSV rear rail as shown in Figure 11.30 thru Figure 11.39.

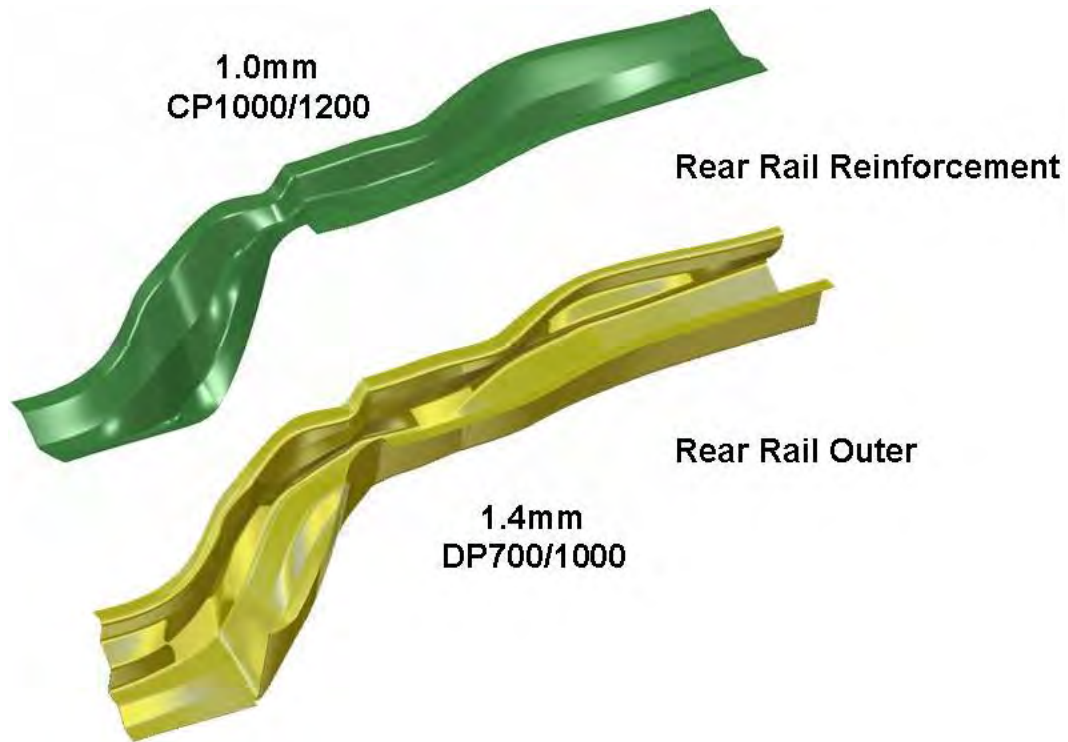


Figure 11.30: *Rear rail - stamped solution (single gauge)*

The maximum steel grade attainable with the TRB technology is DP 500/800. So, the rear rail TRB solution could not achieve as much weight savings as the LWB solution, due to the higher gauges necessary to make up for the lower grade steel used in the TRB solution (Figure 11.31), compared to the steel grade recommended by the 3G optimized solution (Figure 11.28).

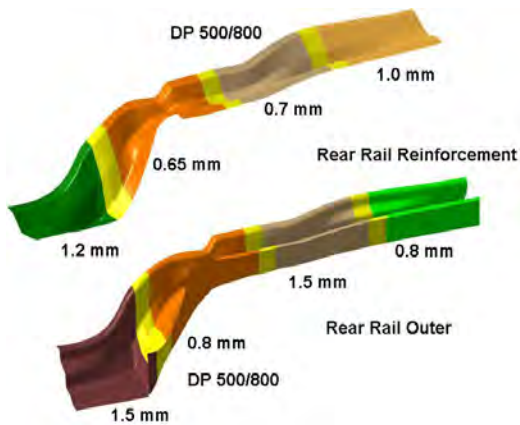


Figure 11.31: Rear rail - stamped TRB solution

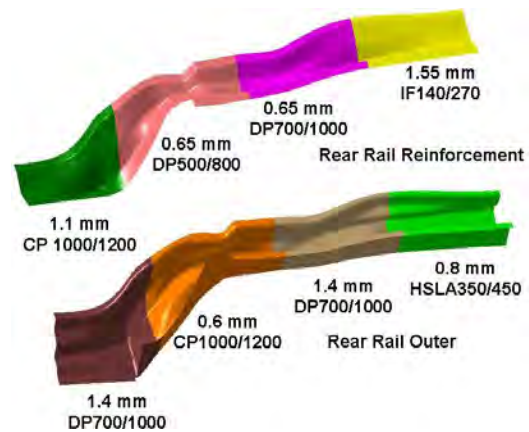


Figure 11.32: Rear rail - stamped LWB solution

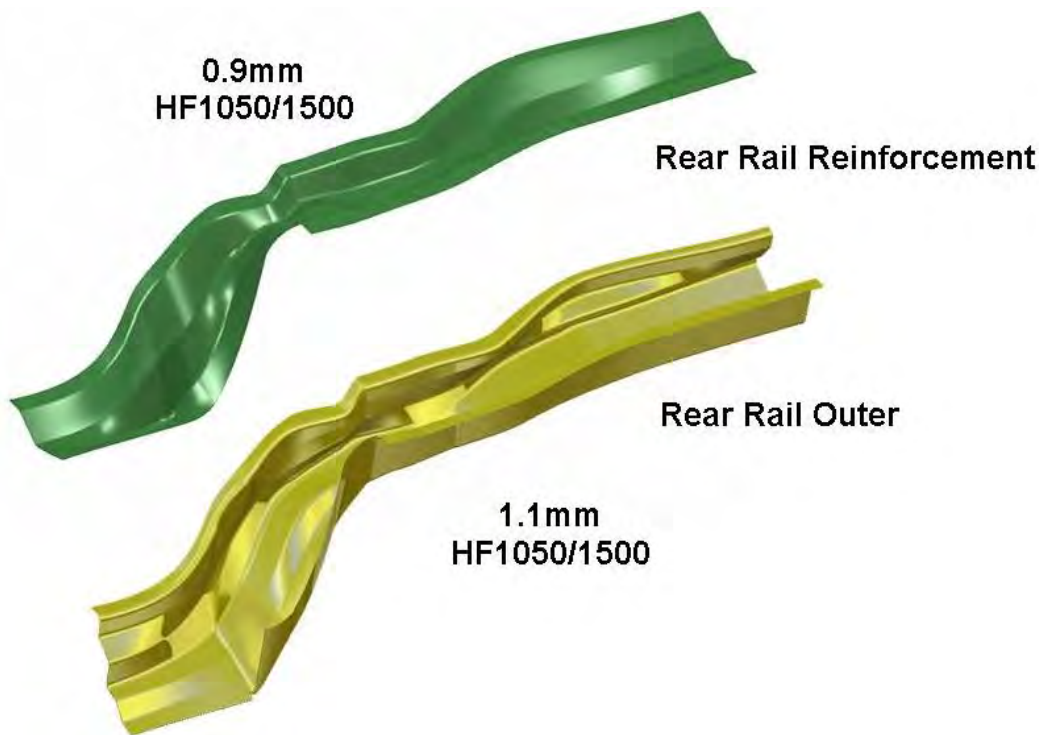


Figure 11.33: Rear rail - hot stamped solution (single gauge)

Gauges lower than 0.7 mm was not feasible for manufacturing boron steel blanks (used for hot stamping technology). So, higher gauges ($\geq 0.7\text{mm}$) were assigned for the rear rail TRB/LWB manufacturing interpretations, shown in the following figures, compared to the 3G optimized solution (Figure 11.28) recommendations.

11.9 Rear Rail Interpreted Results

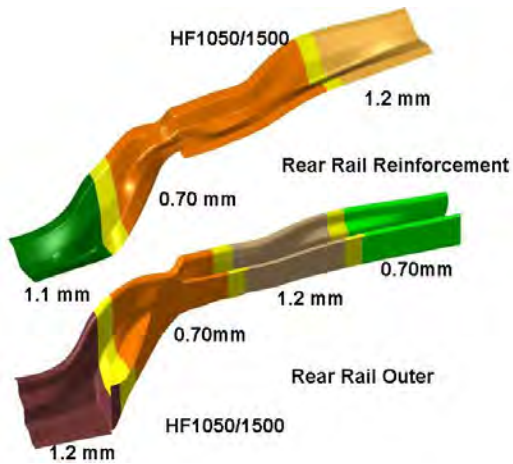


Figure 11.34: *Rear rail hot Stamped TRB solution*

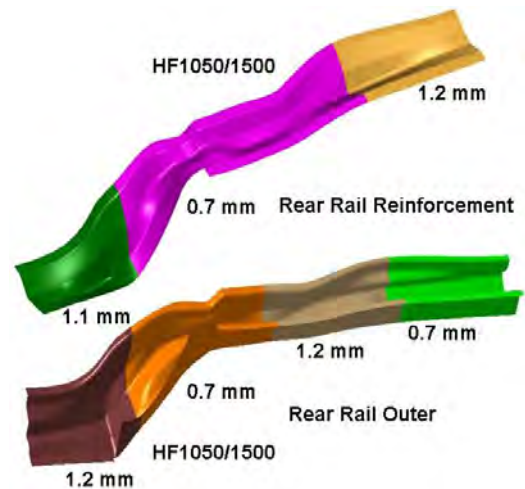


Figure 11.35: *Rear rail hot stamped LWB solution*

The manufacturing interpretation of the rear rail 3G optimized solution using hydroforming technology, shown in Figure 11.29, is illustrated below in Figure 11.36 thru Figure 11.38.

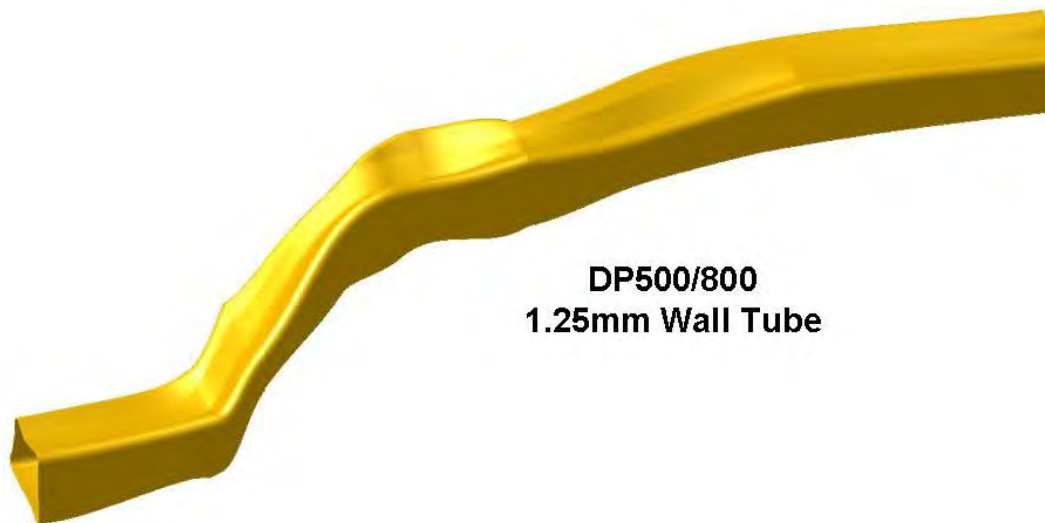


Figure 11.36: *Rear rail - hydroformed Solution (conventional tube)*

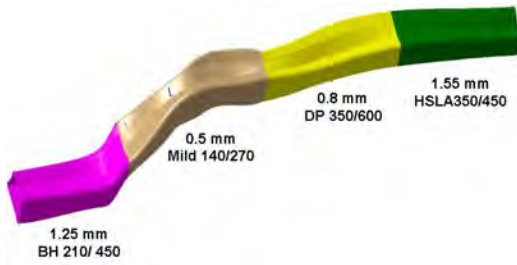


Figure 11.37: Rear rail hydroformed LWT solution

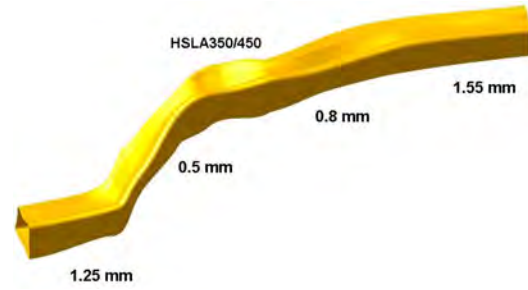


Figure 11.38: Rear rail hydroformed TRT solution

The rear rail stamped aluminum solution as recommended by 3G is shown in Figure 11.39.

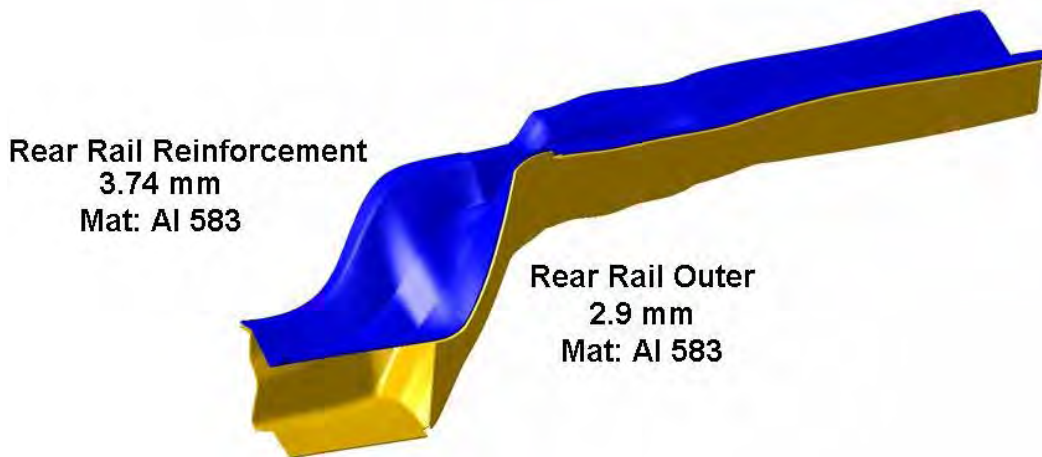


Figure 11.39: Rear rail - stamped aluminum solution

11.10 Roof Rail 3G Optimized solution

The 3G optimized stamped solution for roof rail is shown in Figure 11.40, and the optimized hydroformed solution is shown Figure 11.41.

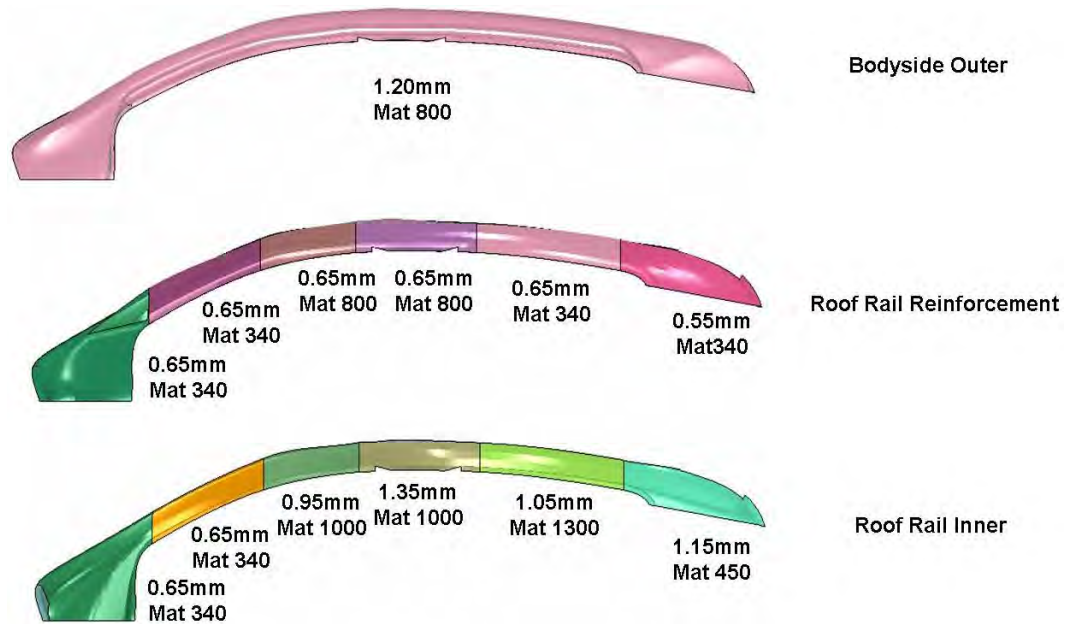


Figure 11.40: Roof rail 3G optimized solution (for stamping)

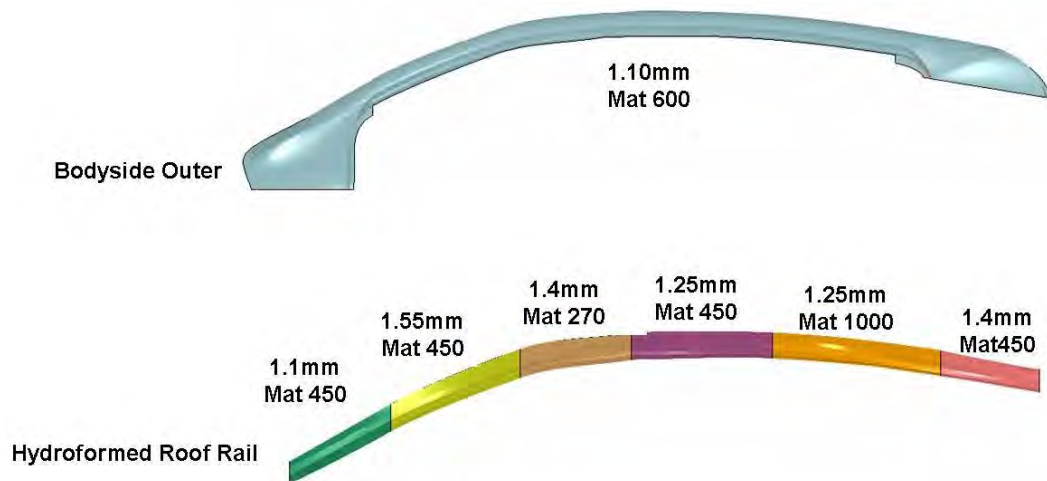


Figure 11.41: Roof rail 3G optimized solution (for hydroforming)

11.11 Roof Rail Interpreted Results

The manufacturing interpretations of the 3G optimized solution for the roof rail is shown in Figure 11.42 thru Figure 11.48. The roof rail outer being a part of the body side outer was always designed for ordinary stamping (single thickness blank). So, the roof rail outer (shown in Figure 11.42), is common for all the other stamped solutions (Figure 11.43 thru Figure 11.47).

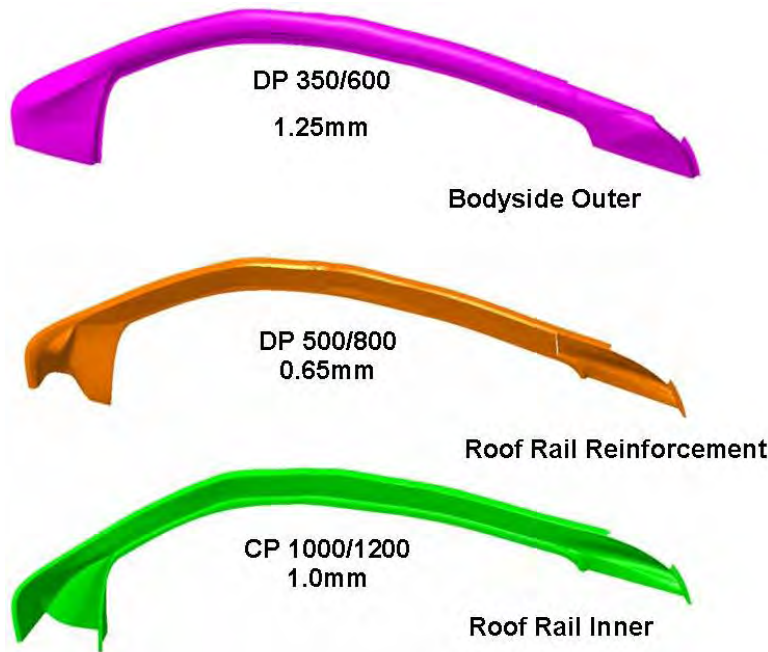


Figure 11.42: Roof rail - stamped solution (single gauge)

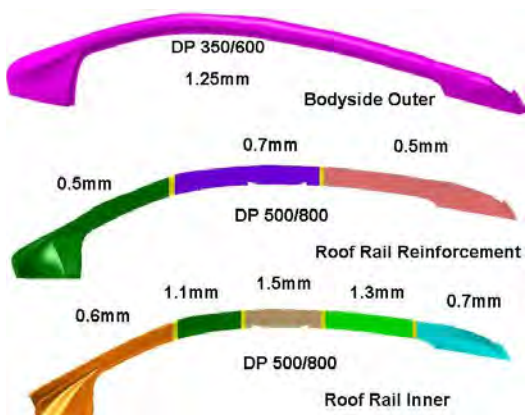


Figure 11.43: Roof rail - stamped TRB solution

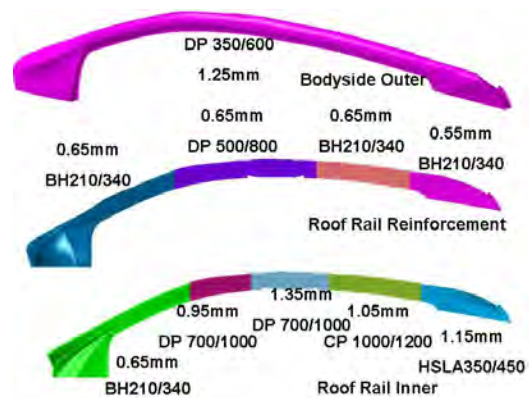


Figure 11.44: Roof rail - stamped LWB solution

As mentioned earlier, the minimum gauge attainable for boron steel is 0.7 mm. So, the weight sav-

ings that were realized in the stamped roof rail reinforcement solutions, with lower gauges, could not be carried over to the hot stamped roof rail reinforcement solutions. The roof rail reinforcement is common for all the hot stamped solutions, as shown in Figure 11.45 thru Figure 11.47.

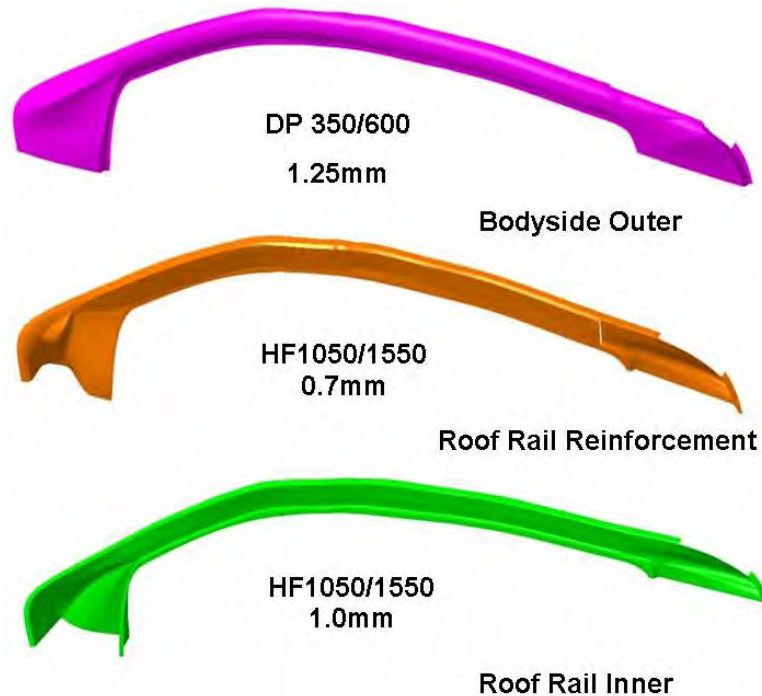


Figure 11.45: Roof rail - hot stamped solution (single gauge)

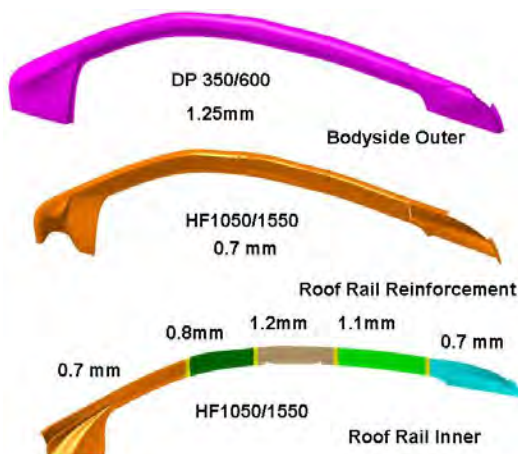


Figure 11.46: Roof rail - hot stamped TRB solution

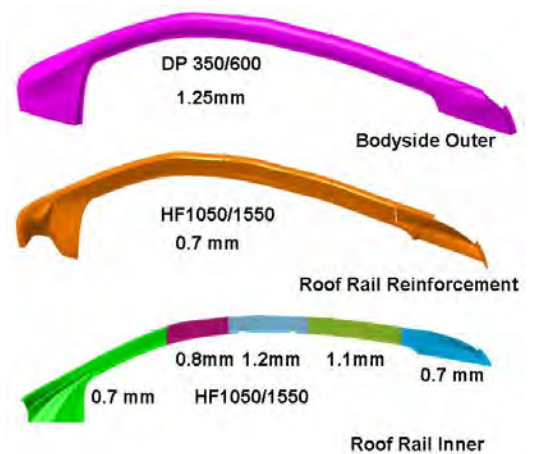


Figure 11.47: Roof rail - hot stamped LWB solution

The manufacturing interpretations of the roof rail 3G optimized hydroformed solution (Figure 11.41), is shown in Figure 11.48. The hydroformed roof rail design geometries were designed such that

the perimeter was either constant or did not vary too much, to account for low pressure hydroforming feasibility.

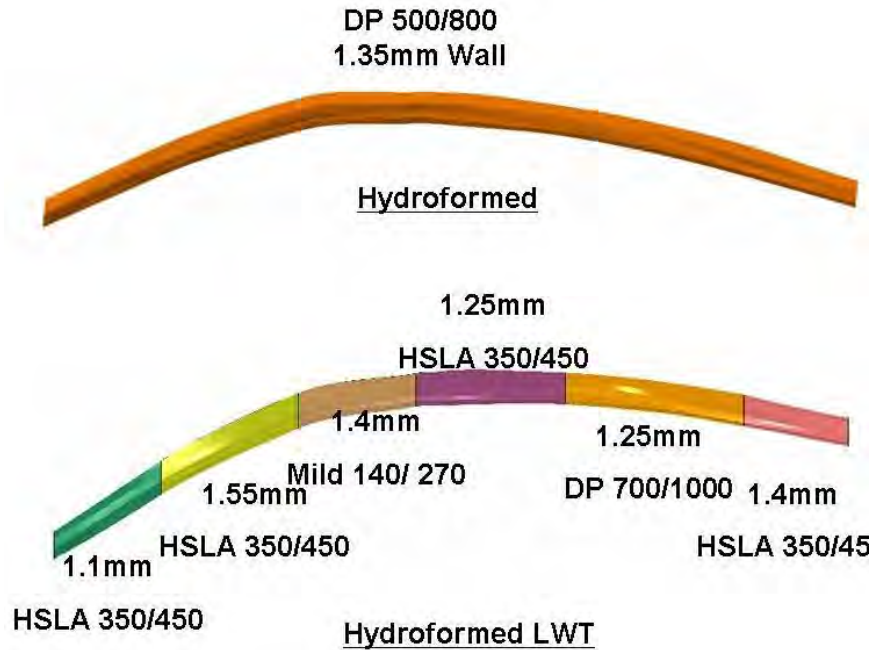


Figure 11.48: *Roof rail - hydroformed solutions*

The roof rail stamped aluminum solution is shown in Figure 11.49.

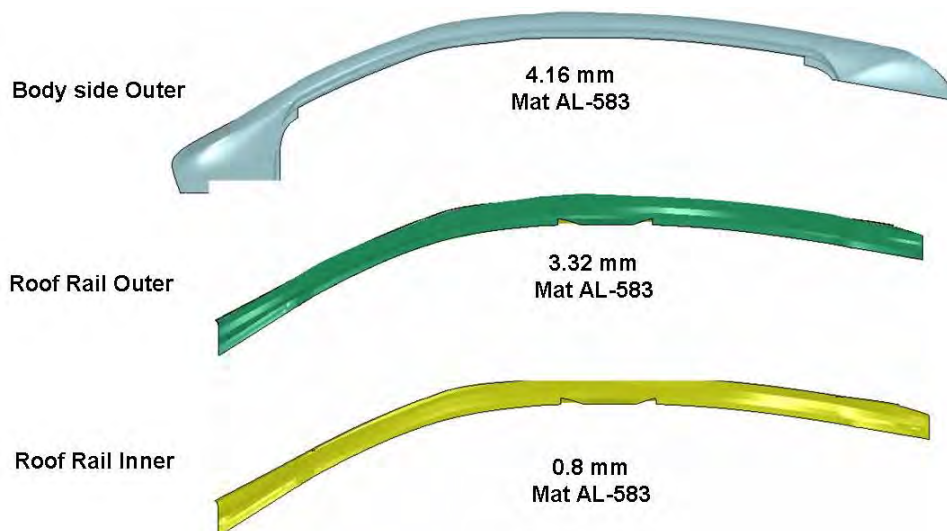


Figure 11.49: *Roof rail - stamped aluminum solution*

11.12 Shotgun 3G Optimized Solution

11.12 Shotgun 3G Optimized Solution

The 3G optimized solution for the FSV shotgun is shown in Figure 11.50.

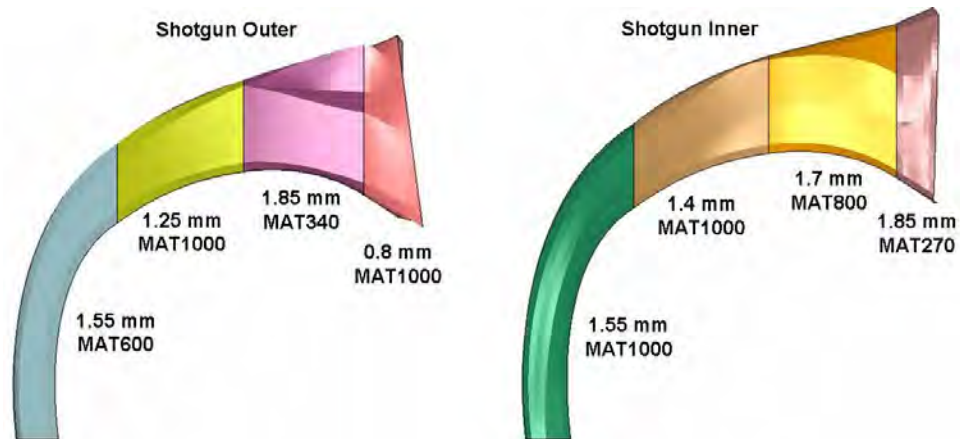


Figure 11.50: Shotgun - 3G optimized solution

11.13 Shotgun Interpreted Results

The manufacturing interpretations of the shotgun 3G optimized solution is shown in Figure 11.51 thru Figure 11.57.

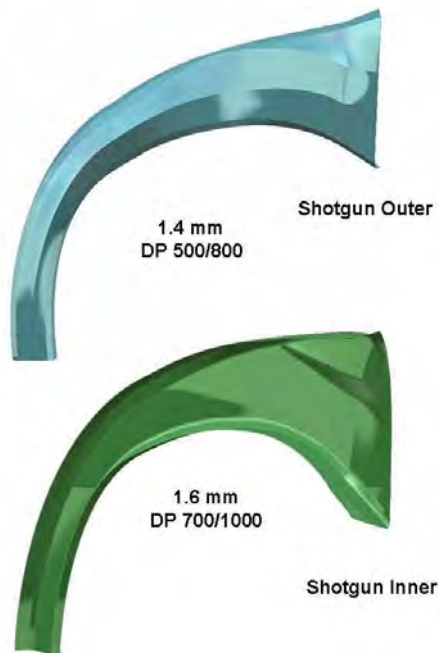


Figure 11.51: Shotgun - stamped solution (single gauge)

The shotgun 3G optimization runs recommended lowest possible gauges to achieve the maximum mass savings, without a compromise on the performance. The ratio between two consecutive gauges were greater than two (2), in certain cases such as the shotgun outer. However, TRB manufacturing constraints prevent gauge ratios of two (2) or higher. So, the gauges were changed accordingly to meet this manufacturing limitation, as can be seen in the solutions in Figure 11.52 and Figure 11.55.

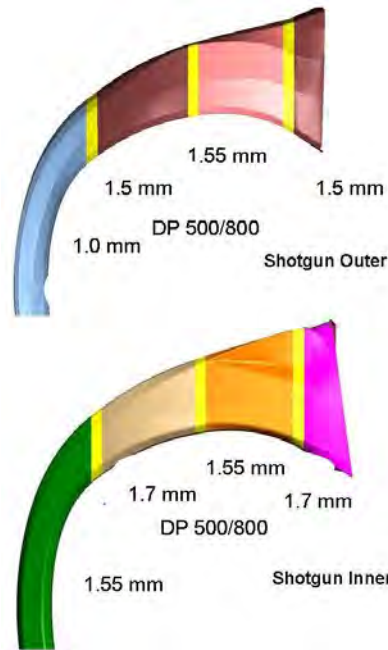


Figure 11.52: Shotgun - stamped TRB solution

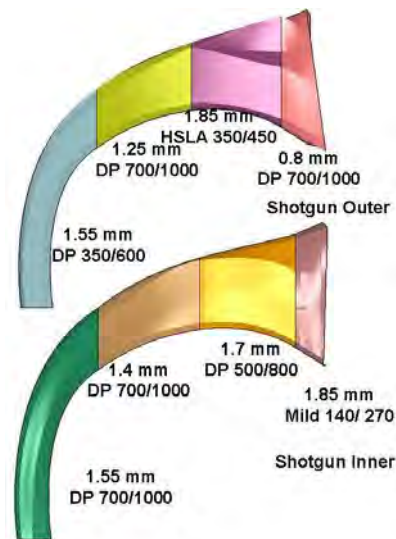


Figure 11.53: Shotgun - stamped LWB solution

11.13 Shotgun Interpreted Results

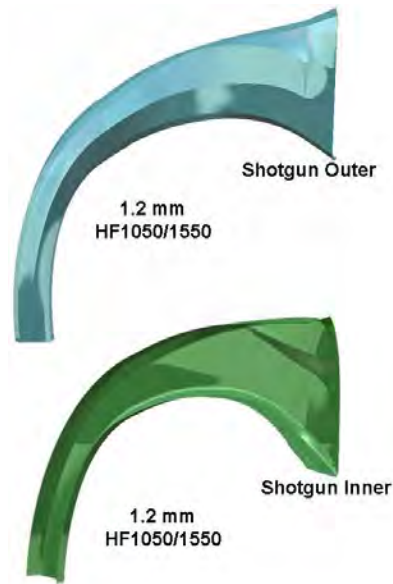


Figure 11.54: Shotgun - hot stamped solution (single gauge)

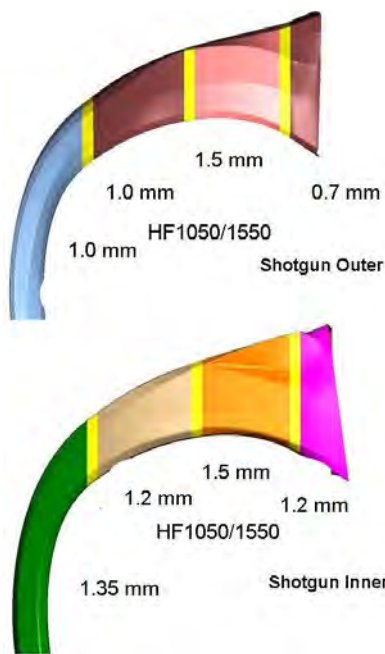


Figure 11.55: Shotgun - hot stamped TRB solution

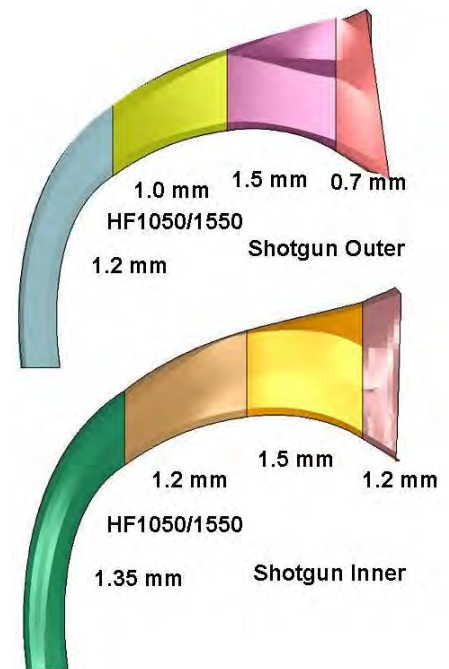


Figure 11.56: Shotgun - hot stamped LWB solution

The stamped aluminum shotgun solution is shown in Figure 11.57.

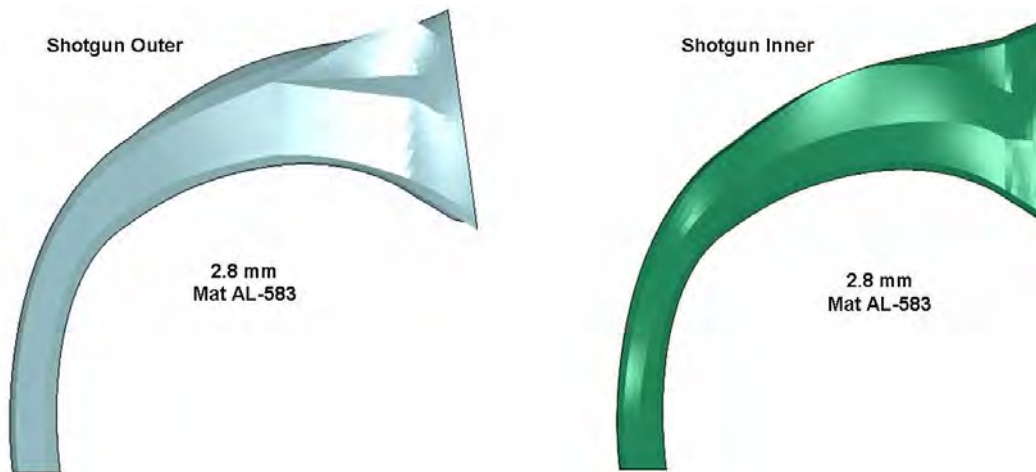


Figure 11.57: Shotgun - stamped aluminum solution

11.14 Tunnel 3G Optimized Solution

11.14 Tunnel 3G Optimized Solution

The 3G optimized stamped solution for the FSV Tunnel is shown in Figure 11.58 and the one for roll forming is shown in Figure 11.59.

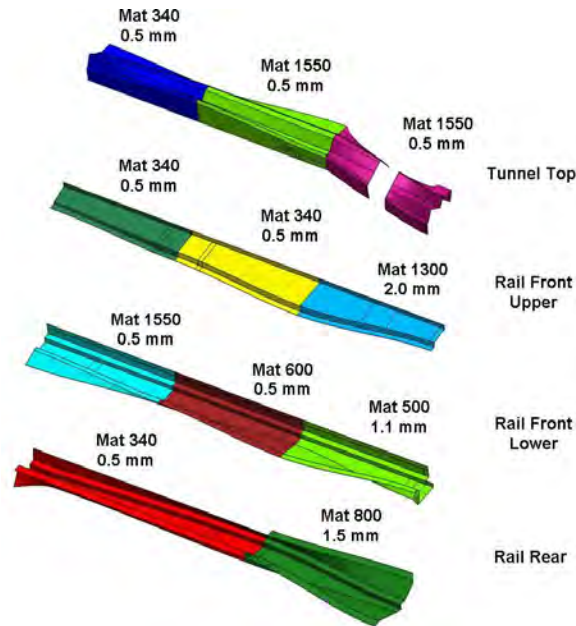


Figure 11.58: Tunnel - 3G optimized solution (for stamping)

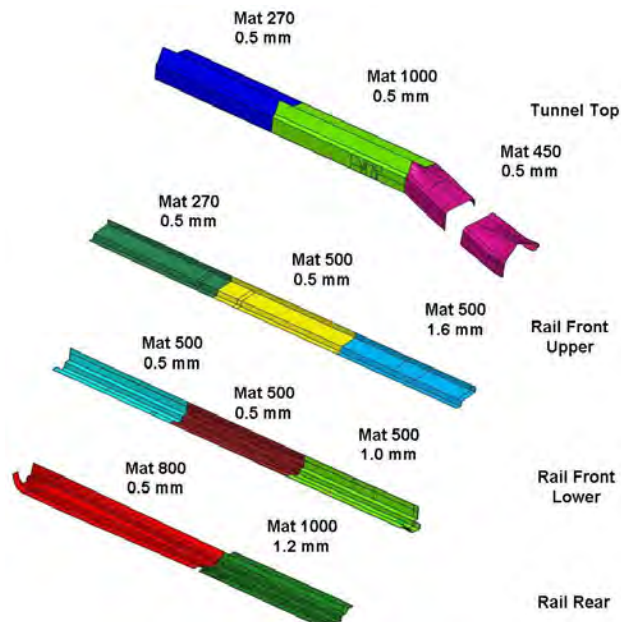


Figure 11.59: Tunnel - 3G optimized solution (for roll forming)

11.15 Tunnel Interpreted Results

The manufacturing interpretations of the 3G optimized solution for the FSV tunnel are shown in Figure 11.60 thru Figure 11.67.

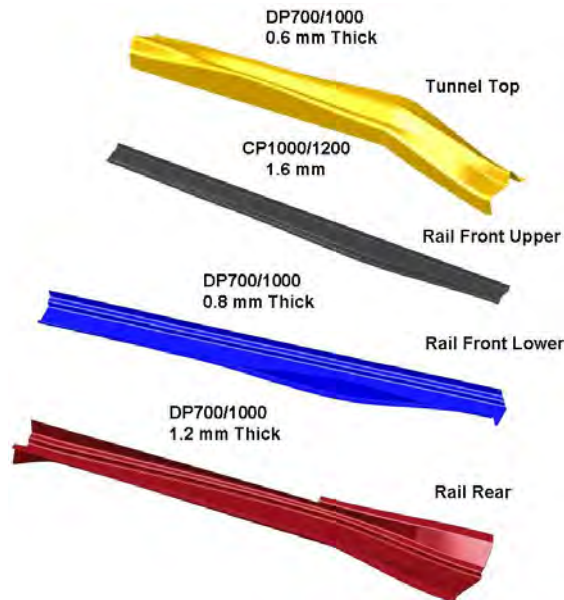


Figure 11.60: *Tunnel - stamped solution (single gauge)*

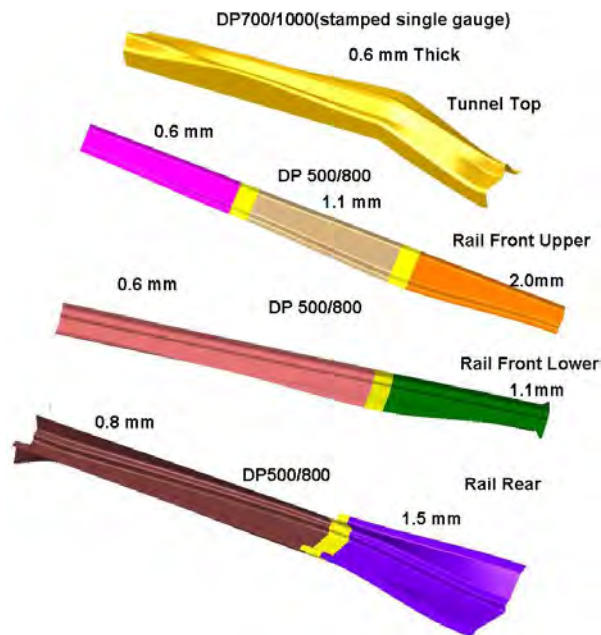


Figure 11.61: *Tunnel - stamped TRB solution*

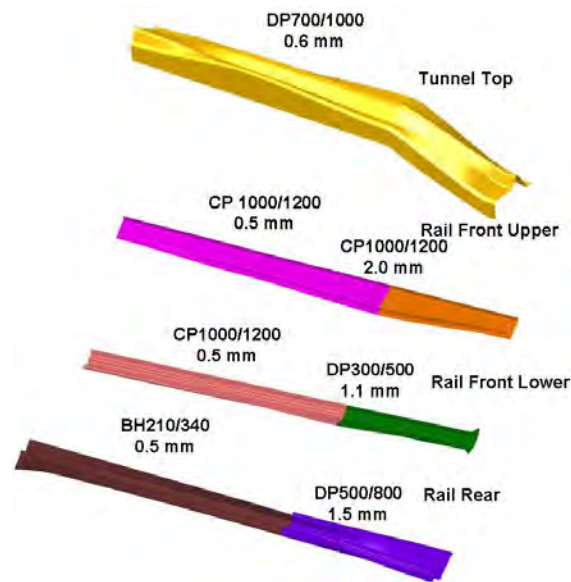


Figure 11.62: Tunnel - stamped LWB solution

The hot stamped tunnel top solution had to have a gauge of 0.7 mm, even though a lower gauge was shown in the 3G optimized solution, due to the manufacturing limitation of boron steel blanks (gauge lower than 0.7 mm is not feasible).

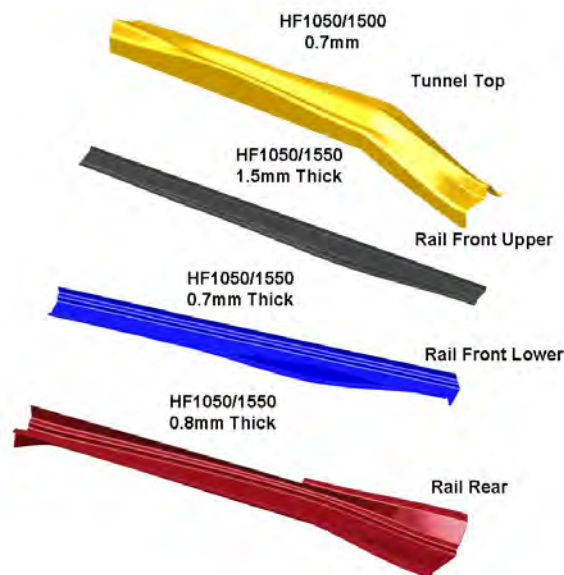


Figure 11.63: Tunnel - hot stamped solution (single gauge)

The hot stamped tunnel top was a common design for all the solutions including the LWB and TRB, as shown in Figure 11.64 and Figure 11.65.

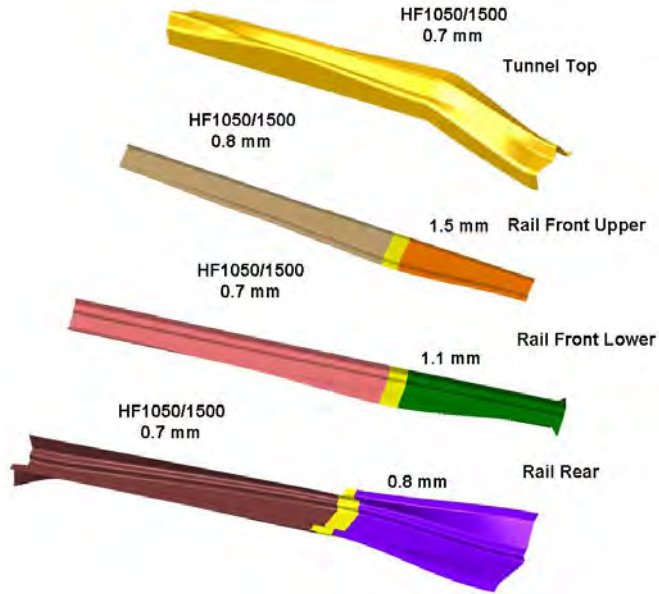


Figure 11.64: Tunnel - hot stamped TRB solution

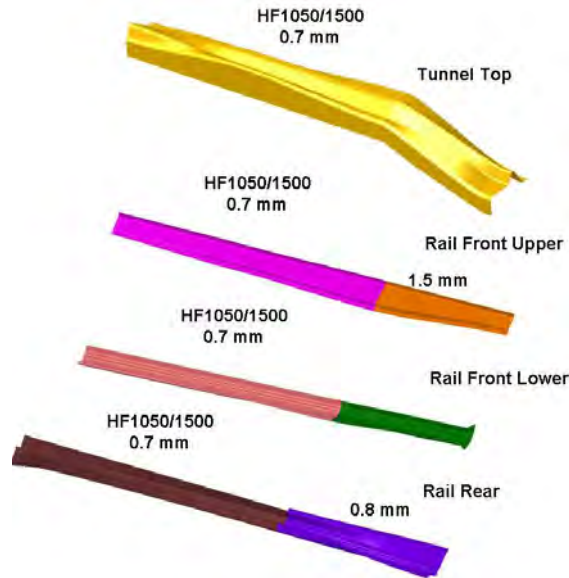


Figure 11.65: Tunnel - hot stamped LWB solution

11.15 Tunnel Interpreted Results

The manufacturing interpretation of the 3G optimized solution (Figure 11.59) is shown in Figure 11.66. The stamped aluminum tunnel solution is shown in Figure 11.67.

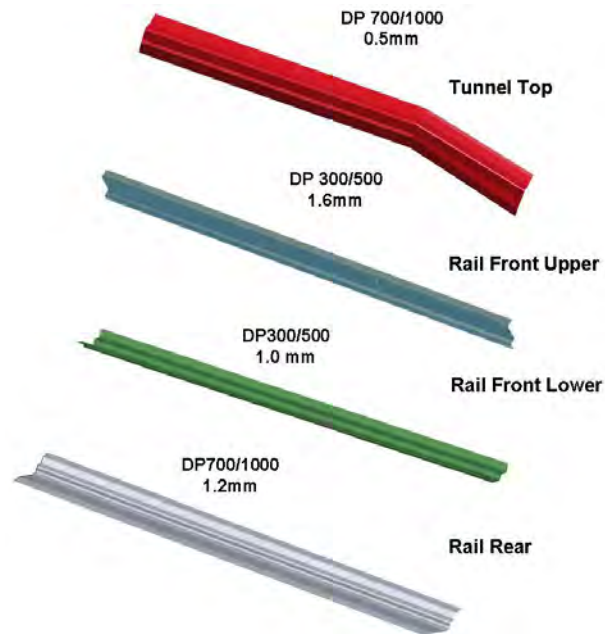


Figure 11.66: *Tunnel - roll formed solution*

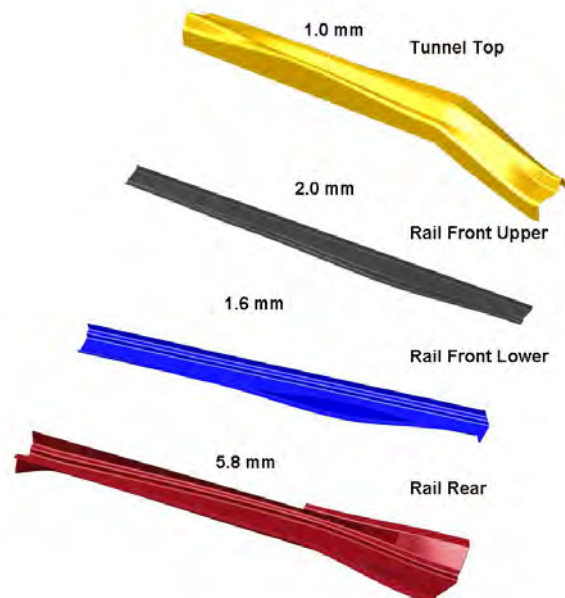


Figure 11.67: *Tunnel - stamped aluminum solution*

11.16 Front Rail Stamped Solution (Concept 1)

The 3G optimized stamped solution for the FSV front rail is shown in Figure 11.68.

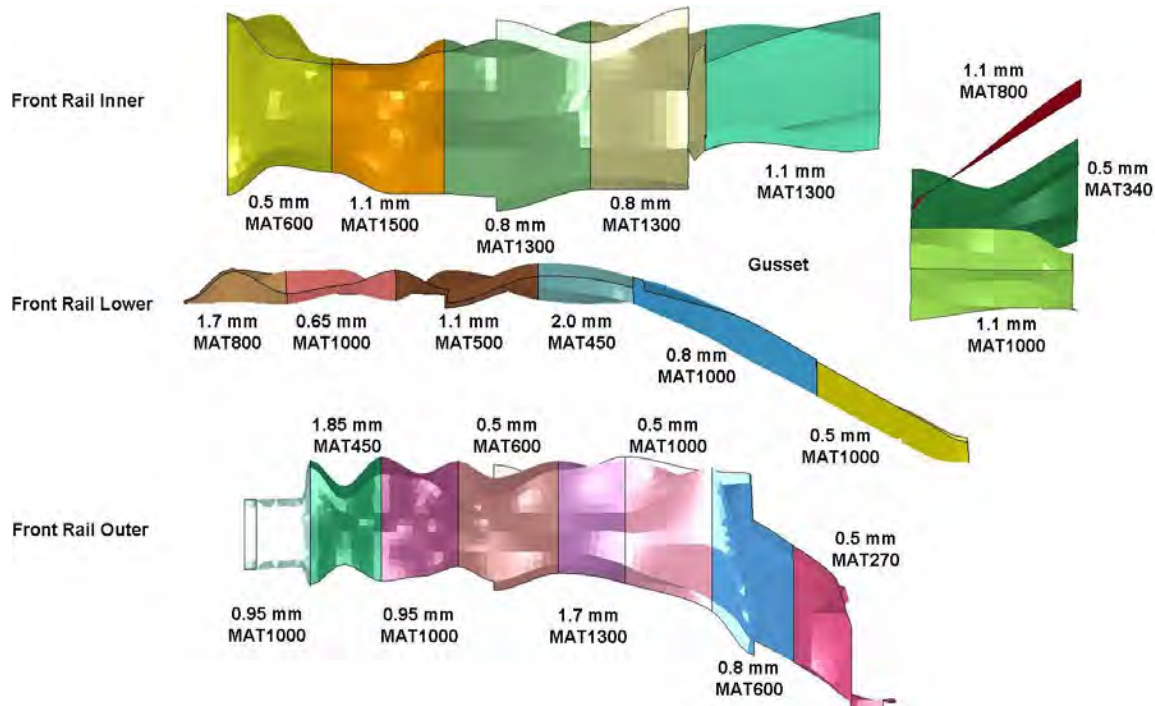


Figure 11.68: Front rail 3G optimized solution

The manufacturing interpretation of the 3G optimized solution is a three-piece front rail sub-system, as shown in Figure 11.69. The specific material grades and gauges, shown in the 3G optimized solution, were crucial for the crush behavior to attain good performance. So, manufacturing interpretations deviating from those recommendations would require considerable number of design iterations supported by favorable analysis results showing good performance. Single thickness and TRB were not considered as alternatives due to the complexity involved in the corresponding design for manufacturing.

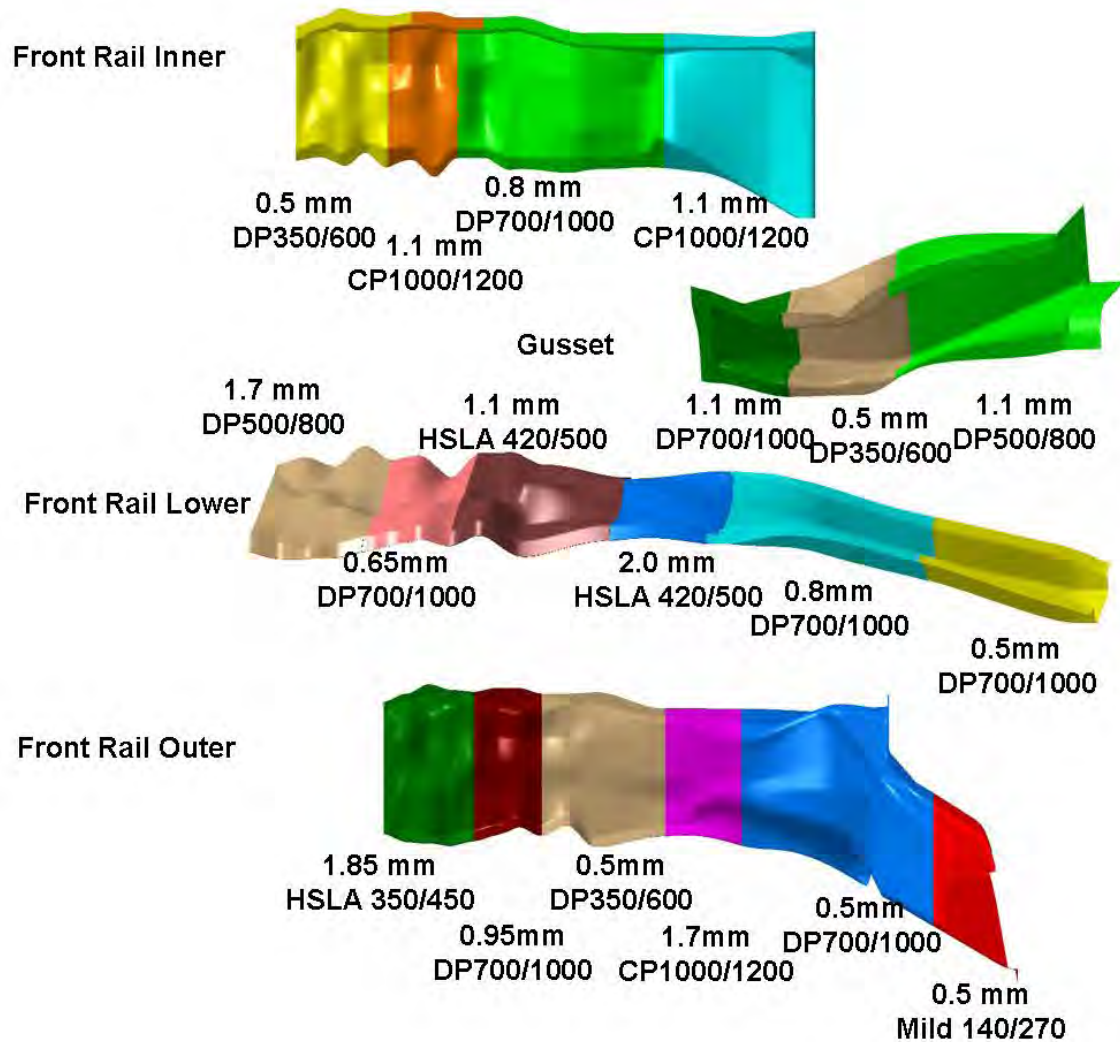


Figure 11.69: Front rail - stamped LWB solution

11.17 Front Rail Stamped Solution (Concept-2)

The second concept of the front rail 3G optimized stamped solution is shown in Figure 11.70.

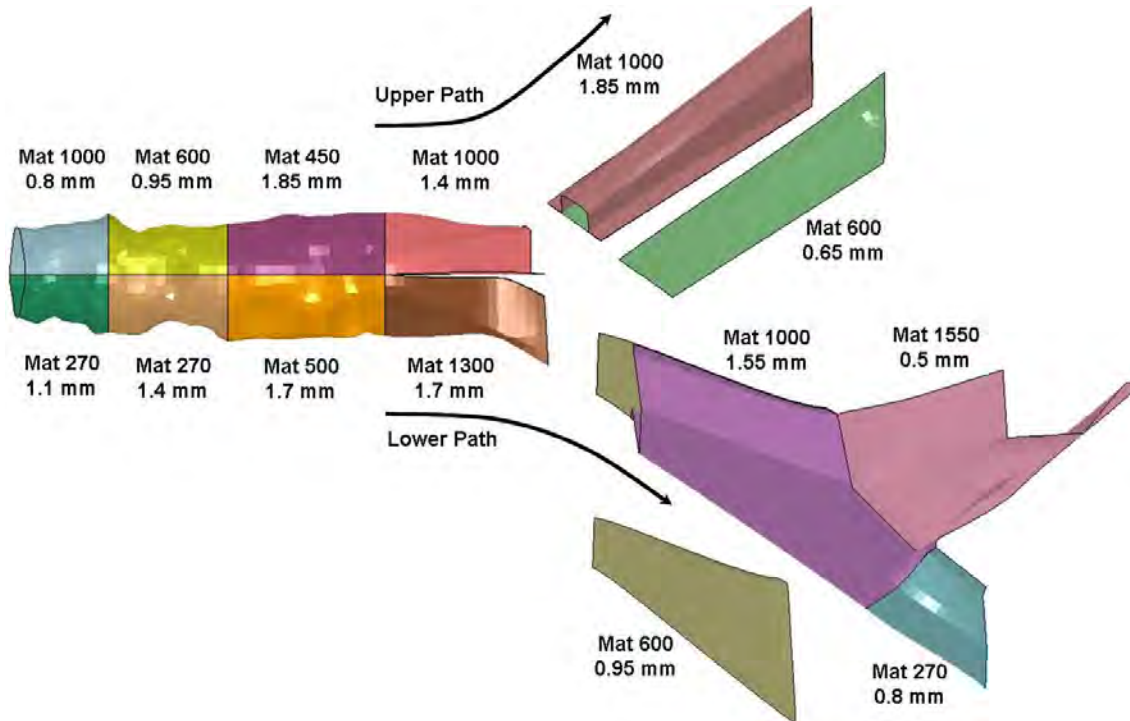


Figure 11.70: *Front rail concept-2 3G optimized solution*

The second concept of the front rail 3G optimized stamped solution is a two-piece front rail sub-system as shown in Figure 11.71. As mentioned earlier, only stamping using LWB was considered due to the complexity of design for manufacturing.

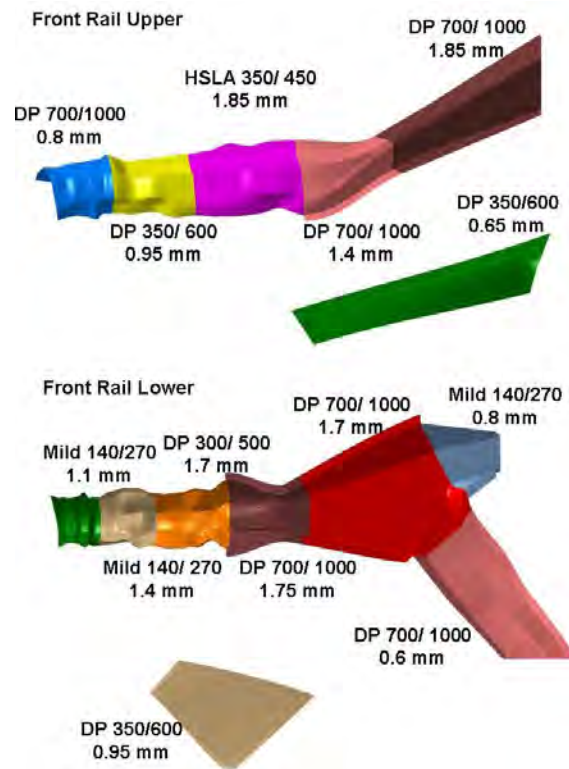


Figure 11.71: Front Rail - concept-2 stamped LWB solution

11.18 Front Rail Stamped Aluminum Solution

The front rail 3G optimized stamped aluminum solution is shown in Figure 11.72.

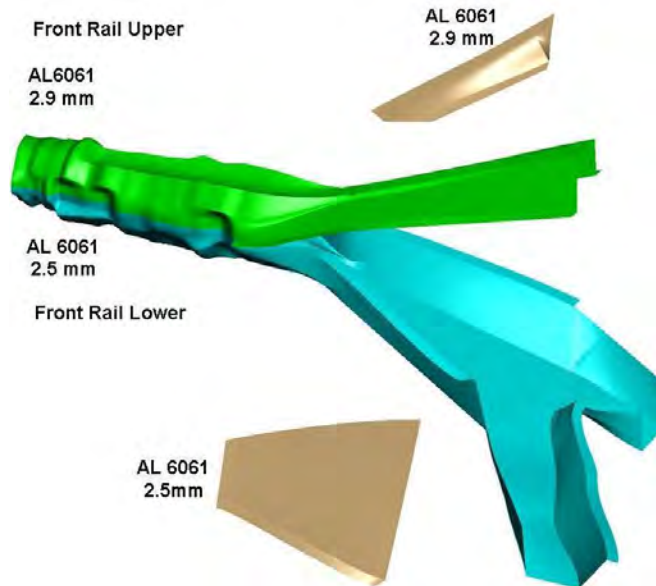


Figure 11.72: Front rail - 3G optimized aluminum solution

The front rail 3G optimized aluminum solution was refined considering the manufacturing guidelines, without deviating from the load path, to attain the solution as shown in Figure 11.73.

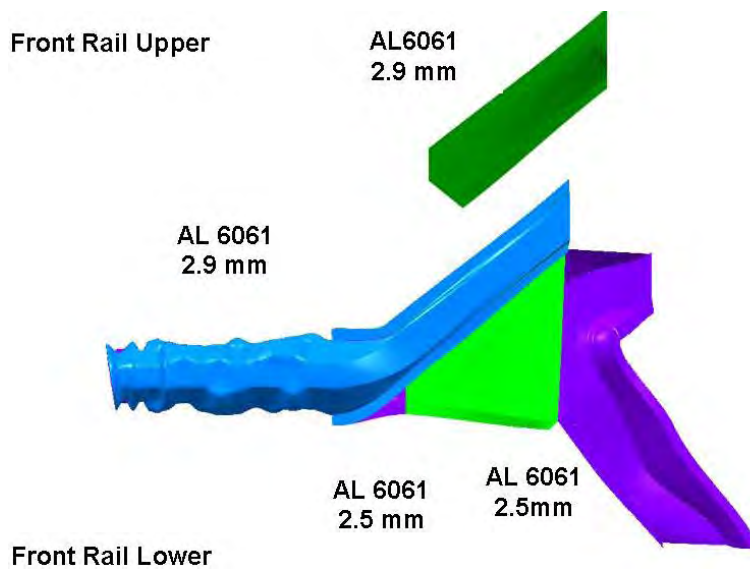


Figure 11.73: Front rail - stamped aluminum solution

11.19 Front Rail Hydroformed Solution

The front Rail 3G optimized hydroformed solution is shown Figure 11.74.

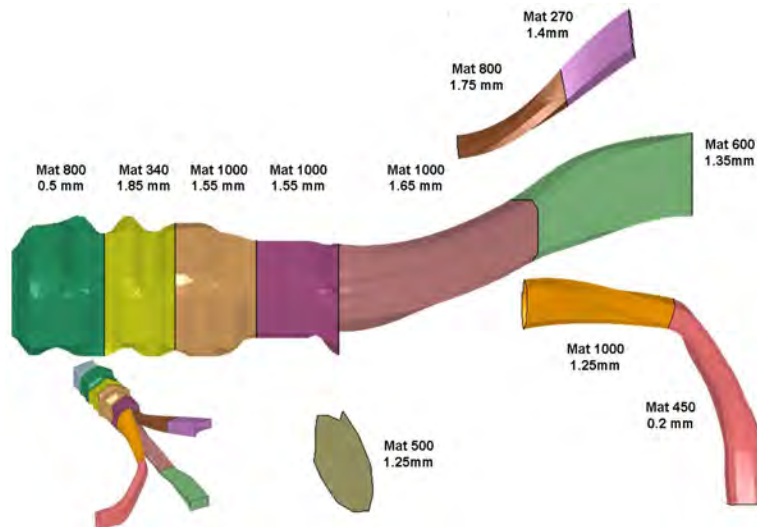


Figure 11.74: Front rail 3G hydroformed optimized solution

The hydroformed Front Rail solution, after making the necessary design changes for manufacturability, is shown in Figure 11.75.

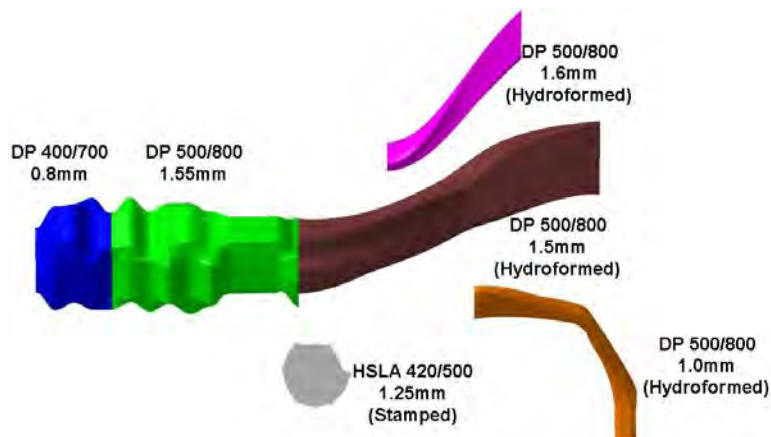
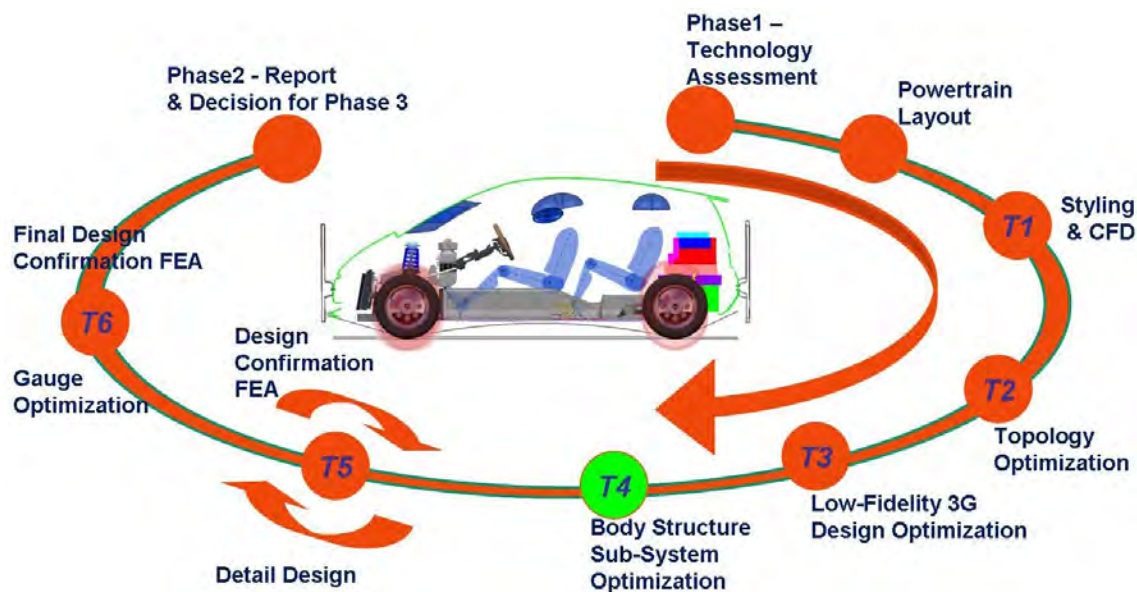


Figure 11.75: Front rail - hydroformed solution

12.0 Sub-Systems Selection Methods



12.1 Introduction

In order to recommend the sub-systems from the various solutions discussed in Chapter 11, it was important to define a specific criterion for selection. Every automobile manufacturer uses a certain selection criterion dependent on the market segment, demographics and relevant government regulations. So, to make a comparison of the FSV sub-system design optimization results, it was crucial to form a basis for the selection criteria by conducting the following assessments:

- Mass - there are two important aspects of mass: part mass and blank mass. Blank mass influences the material costs, energy costs and the CO₂e emissions
- Costs - the manufacturing costs were assessed for the various sub-systems using a cost model
- CO₂e Life Cycle Assessment - an environmental assessment, of Greenhouse Gases (GHG) emissions, was conducted for each sub-system over the complete vehicle life cycle

12.2 Sub-System Cost Assessment

A cost assessment was conducted to estimate the manufacturing costs of the sub-system concepts namely: rocker, B-pillar, rear rail, roof rail, tunnel, shotgun, and front rail. The cost assessment presented in this section of the report is for the different sub-system solutions discussed earlier in Chapter 11. The assembly costs were not assessed for these sub-systems because the level of detail was not yet developed. A detailed cost assessment of the final body structure is presented in Chapter 17.

The manufacturing costs were estimated for each of the sub-system concepts, using the following different manufacturing processes:

- Stamping (single thickness blank)
- Stamping Tailor Rolled Blank (TRB)
- Stamping Laser Welded Blank (LWB)
- Hot Stamping
- Hot Stamping Tailor Rolled Blank
- Hot Stamping Laser Welded Blank
- Closed Rollforming
- Open Rollforming
- Hydroforming
- Hydroforming Laser Welded Tube
- Hydroforming Tailor Rolled Tube (TRT)
- Aluminum Extrusion (only for comparison)

12.2.1 Approach

The cost assessment of the FSV body structure was conducted using the "technical cost modeling" approach similar to the one used by MIT in the ULSAB AVC and Future Generation Passenger Compartment (FGPC)^[1]; there were no supplier cost assessments conducted for any of the parts costs and assembly costs. It involved breaking down the component cost into the costs for each of the operations involved in the manufacturing process, starting from blanking the steel coil, until the final operation to fabricate the component. The sequence of the different operations considered, to estimate the overall manufacturing component cost for the various technologies are shown in Table 12.1.

¹References:

1. Auto/Steel Partnership Future Generation Passenger Compartment (FGPC), VERSION 1.0 JUL, 2009
2. ULSAB AVC:VERSION 2.1C FEB, 2002
3. Auto/Steel Partnership LIGHTWEIGHT FRONT END STRUCTURE (LWFES), VERSION 2.0 FEB, 2006
4. WorldAutoSteel BMW5 Series FRONT END STUDY: VERSION 3.0 APR, 2005
5. TM27C (EDAG Internal Cost Model)

	Manufacturing Portfolio					
	Stamping	Stamping Tailor Rolled Blank (TRB)	Stamping Laser Welded Blank (LWB)	Hot Stamping	Hot Stamping Tailor Rolled Blank (TRB)	Hot Stamping Laser Welded Blank (LWB)
Material Price	Steel Material Prices	Steel Material Prices + Rolling Premium	Steel Material Prices	Steel Material Prices	Steel Material Prices + Rolling Premium	Steel Material Prices
Operation #1	Blanking (Single)	Blanking (Single)	Blanking (Multiple)	Blanking (Single)	Blanking (Single)	Blanking (Multiple)
Operation #2	Stamping	Stamping	Laser Welding	Blank heating	Blank heating	Laser Welding
Operation #3	Trimming	Trimming	Stamping	Hot forming	Hot forming	Blank heating
Operation #4			Trimming	Laser Trimming	Laser Trimming	Hot forming
Operation #5						Laser Trimming
	Closed Roll Form	Open - Roll Form	Hydroform	Hydroform Laser Welded Tubes (LWT)	Hydroform Multiple Walled Tubes (MWT)	Aluminium Extrusion
Material Price	Steel Material Prices	Steel Material Prices	Steel Material Prices + Tubing Premium	Steel Material Prices	Steel Material Prices + MWT Premium	Aluminum Material Prices
Operation #1	Forming	Forming	Bending	Blanking (Multiple)	Bending	Cutting Billet
Operation #2	Welding	Trimming	Pre-forming	Laser Welding	Pre-forming	Extrusion
Operation #3	Trimming		Hydroforming	Master Shearing	Hydroforming	Straightening
Operation #4			Trimming	Tube Rolling/Welding	Trimming	Hydrosizing
Operation #5				Bending		Machining
Operation #6				Pre-forming		
Operation #7				Hydroforming		
Operation #8				Trimming		

Table 12.1: Manufacturing processes and operations sequence

12.2 Sub-System Cost Assessment

The overall component cost was broken down into the following costs:

- Material
- Labor
- Equipment
- Tooling
- Energy
- Building
- Maintenance

The manufacturing costs were assessed through an interactive process between the product designers, manufacturing engineers and costs analysts. The most important step in the cost assessment process was the determination of the component related inputs such as blank size, cycle time and tooling costs. These inputs were evaluated on an individual basis depending on the design data for each of the components.

The remaining inputs that were crucial for the cost estimation are the following:

- Program Parameters
- Plant Parameters
- Process parameters

These parameters were input into the cost model such that they can be modified at a later stage, if required. Therefore, this cost model provides the flexibility to allow the user to input their own data, since the results of cost assessment caused by the allocation of the input parameters, differ from one user to the other.

12.2.2 General Assumptions

The cost model was created based on the assumption that the parts are manufactured in a green-field facility in USA, where all the building and manufacturing facilities already exist. Costing was for raw material (steel) going in, complete modules coming out. The costs were estimated to a virtual Start of Production (SOP) in 2015-2020 timeframe. Only the Battery Electric Vehicle (BEV) was considered for the FSV cost assessment.

The estimated annual production volume of 100,000 for the BEV in the year 2015, with a production life of five (5) years, was the basis for the cost assessment. Similarly, the estimated energy cost of \$0.12 $\frac{\text{USD}}{\text{kWh}}$ was used for the energy costs evaluation, based on the US Department of Energy's energy outlook for the year 2015 ^[2]. The general program assumptions are summarized in Table 12.2.

Parameters	FSV Assumptions
Model year	2015-2020
Annual Production Volume	100,000
Parts volume	only consider BEV
Production life	5 years
Energy cost	\$0.12 /kWh

Table 12.2: *General assumptions*

12.2.3 Plant Parameters

The plant parameters are independent of any part design as listed in Table 12.3.

Plant Parameters	FSV Assumptions
Working days	235 days/yr
Annual Paid Time	3525 hrs/yr
Indirect workers (Overhead)	0.25 per direct worker
Wage (including benefits)	\$45.00 /hr
Interest (Equipment, Building etc.)	10%
Equipment life	20 yr
Building life	25 yr
Building unit cost	\$1,500 /sqm

Table 12.3: *Plant parameters*

²DOE Annual Energy Outlook 2009

12.2 Sub-System Cost Assessment

12.2.4 Process Parameters

The process parameters that are independent of the part parameters were identified, and included in the cost model. These parameters were incorporated into the cost model such that they could be changed at a later stage if required, thereby recalculating the parts costs. The parameters for the different processes are listed in Table 12.4 thru Table 12.9.

Process Parameters	FSV Blanking Assumptions	FSV Stamping Assumptions
Energy consumption rate	300 kW/hr	150 kW/hr
Space requirement	115 sqm/line	150 sqm/line
Manpower	1 worker/line	part dependent
Unplanned downtime	2 hrs/day	3 hrs/day
Maintenance Percentage	10%	10%
Material loss percent	1%	NA
Reject rate	0.10%	part dependent
Press line die average change time	NA	30 mts
Press line lot size	NA	1500 parts/lot
Cycle Time	2000 hits/hr	part dependent

Table 12.4: *Blanking and stamping parameters*

Process Parameters	FSV Welding Assumptions	FSV Trimming Assumptions
Energy consumption rate	400 kW/hr	150 kW/hr
Space requirement	250 sqm/line	200 sqm/line
Manpower	1 per line	2 per line
Unplanned downtime	4 hrs/day	NA
Maintenance Percentage	5%	5%
Installation Percentage	25%	NA
Auxiliary Equipment Percentage	NA	NA
Reject rate	0.1%	0.5%
Press line lot size	part dependent	1500
Line rate	part dependent	500 hits/hr
Die Change time	NA	30 mts

Table 12.5: *Welding and trimming process parameters*

Process Parameters	FSV Bending Assumptions	FSV Preforming Assumptions
Energy consumption rate	100 kW/hr	200 kW/hr
Space requirement	150 sqm/line	250 sqm/line
Manpower	0.5 per part	0.5 per part
Unplanned downtime	1 hr/day	1 hr/day
Maintenance Percentage	5%	5%
Installation Percentage	10%	10%
Auxiliary Equipment Percentage	NA	25%
Reject rate	1%	0.5%
Press line lot size	part dependent	part dependent

Table 12.6: *Bending and pre-forming process parameters*

Process Parameters	FSV Sheet Hydroforming Assumptions	FSV Tube Hydroforming Assumptions
Energy consumption rate	150 kW/hr	600 kW/hr
Space requirement	50 sqm/line	300 sqm/line
Manpower	2	0.5 per part
Unplanned downtime	5 hrs/day	2 hrs/day
Maintenance Percentage	5%	5%
Installation Percentage	25%	10%
Auxiliary Equipment Percentage	25%	25%
Reject rate	3%	3%
Press line die average change time	30 mts	NA
Press line lot size	1500 parts/lot	part dependent

Table 12.7: *Sheet hydroforming and tube hydroforming parameters*

Process Parameters	FSV Blank Heating Assumptions
Workers per heating line	1
Material heat capacity	460 j/kg-° C
Blank Temperature	950 ° C
Oven heating efficiency	40%
Blank heating line space required	1000 sqm

Table 12.8: *Blank heating parameters*

12.2 Sub-System Cost Assessment

Process Parameters	FSV Hot Forming Assumptions
Energy consumption rate	1000 kW/hr
Space requirement	150 sqm/line
Manpower	2 worker/line
Line Rate	240 hits/hr
Reject rate	1.00%
Press line die average change time	30 mts
Press line lot size	1500
Maintenance Percentage	10%

Table 12.9: Hot forming process parameters

12.2.5 Sub-System Components Fabrication Input

Unlike the process parameters listed earlier, there are several other parameters that are related to the part design. Each individual part in the sub-systems was reviewed to determine the following:

- Blank Size
- Process Input Data
- Cost Estimation

12.2.5.1 Blank Size

The CAD data of the parts were reviewed to estimate an optimal blank size including the required addendum necessary for blank holder, draw beads (for control of material flow) etc. The blank size determined for the FSV rocker inner concept design (based on sub-system optimization results) is illustrated in Figure 12.1.

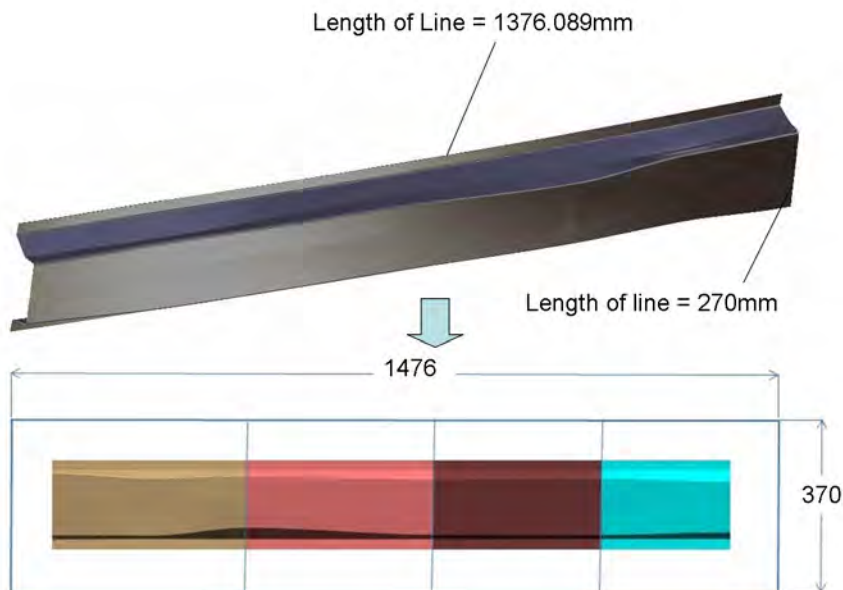


Figure 12.1: FSV rocker inner concept design and blank size

Part nesting was utilized, whenever necessary, to reduce the amount of scrap, and subsequently the part costs. A part nesting exercise for the FSV B-pillar concept design (based on sub-system optimization results) is shown in Figure 12.2.



Figure 12.2: FSV B-pillar concept part nesting

The part nesting process is more efficient in reducing the material scrap and therefore the material costs, in the single thickness blank and Laser Welded Blank (LWB) stamping processes. Part nesting could be very difficult or even not possible in the Tailor Rolled Blank (TRB) stamping process, due the added complexity of aligning similar gauges to achieve the nesting.

12.2 Sub-System Cost Assessment

12.2.5.2 Process Input Data

The part dependent process parameters were determined for each part. These input parameters included tooling investment, cycle time, weld length (for LWB and closed roll form), and manpower per line.

12.2.5.3 Cost Estimation

Due to the limited number of sub-systems, and considering the smaller size of most of the parts, only tandem presses were included in the sub-system cost assessment. So, the press types were defined by virtual press lines; multiplying the press type with the number of required operations for fabricating the specific part. Multiple press types were considering in the final body structure cost assessment.

The press lines were assumed to be non-dedicated; the costs were proportional to the actual press line utilization time. The investment costs for the different equipments were established using the similar equipment costs, used in the ULSAB AVC and FGPC costs models, as reference.

12.2.6 Material Prices

The average of the mild steel prices forecasted by CRU for 2010-2014, as shown in Figure 12.3, were used as the reference price. The prices for the other steel grades were determined based on a grade premium applied to the reference mild steel price. For tailor rolled coils, tubes, and tailor rolled tubes, the base steel material prices included a process premium, as shown in Table 12.10. These prices and premiums were determined independantly by EDAG, using industry resources and supply base.

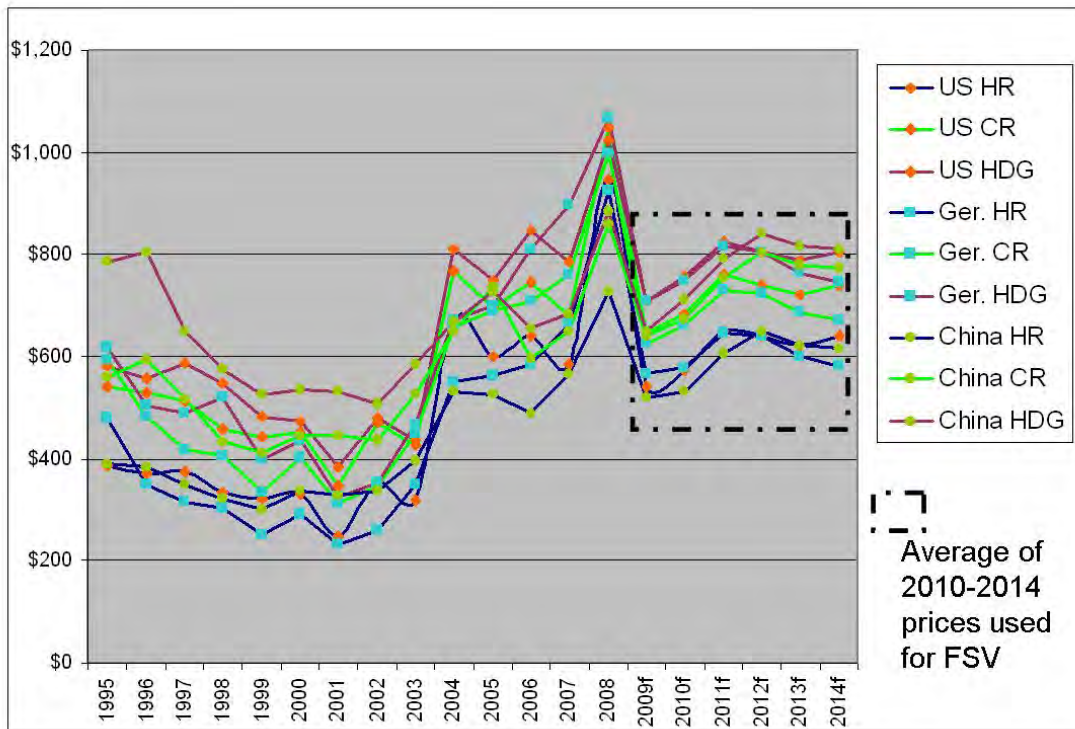


Figure 12.3: CRU Mild Steel forecast data (2010-2014)

The material prices of the different steel grades, considered for the FSV program, are listed in Table 12.10.

Item #	FSV Steel Grades	Thickness		Reference Material Price	Grade	Hot Dip Galvanized	Exposed	Tailor Rolled Coil	Tubes (straight, as shipped)	Multiple Walled Tube Tube Blank
		Min	Max							
		(mm)	(mm)	(\$/kg)	Premium (\$/kg)	Premium (\$/kg)	Premium (\$/kg)	Premium (\$/kg)	Premium (\$/kg)	Premium (\$/kg)
1	Reference Material ^[1] - Mild 140/270 ^[2]	0.35	4.60	0.73	0.00	0.06	0.05	0.55	0.25	0.65
2	BH 210/340	0.45	3.40		0.05	0.06	0.10	0.55	0.25	0.65
3	BH 260/370	0.45	2.80		0.05	0.06	0.10	0.55	0.25	0.65
4	BH 280/400	0.45	2.80		0.07	0.06	0.10	0.55	0.30	1.10
5	IF 260/410	0.40	2.30		0.07	0.00	0.10	0.55	0.30	0.70
6	IF 300/420	0.50	2.50		0.10	0.00	0.10	0.55	0.30	1.10
7	HSLA 350/450	0.50	5.00		0.12	0.10	NA	0.55	0.30	1.50
8	HSLA 420/500	0.60	5.00		0.14	0.10	NA	0.55	0.45	1.25
9	HSLA 490/600	0.60	5.00		0.16	0.10	NA	0.55	0.45	1.65
10	HSLA 550/650	0.60	5.00		0.35	0.10	NA	0.55	0.45	1.65
11	HSLA 700/780	2.00	5.00		-	-	-	-	-	-
12	SF 570/640	2.90	5.00		0.35	0.10	NA	NA	0.45	2.05
13	SF 600/780	2.00	5.00		0.35	0.10	NA	NA	0.45	2.05
14	TRIP 350/600	0.60	4.00		0.40	0.10	NA	NA	0.45	1.25
15	TRIP 400/700	0.60	4.00		0.45	0.10	NA	NA	0.45	1.65
16	TRIP 450/800	0.60	2.20		0.50	0.10	NA	NA	0.50	1.30
17	TRIP 600/980	0.90	2.00		0.55	0.10	NA	NA	0.55	1.35
18	FB 330/450	1.60	5.00		0.20	0.10	NA	0.55	0.30	1.10
19	FB 450/600	1.40	6.00		0.25	0.10	NA	0.55	0.45	1.65
20	DP 300/500	0.50	2.50		0.20	0.10	0.10	0.55	0.45	0.85
21	DP 350/600	0.60	5.00		0.26	0.10	0.10	0.55	0.45	1.25
22	DP 500/800	0.60	4.00		0.31	0.10	NA	0.55	0.50	0.90
23	DP 700/1000	0.60	2.30		0.38	0.10	NA	NA	0.55	0.95
24	DP 800/1180	1.00	2.00		-	-	-	-	-	-
25	DP 1150/1270	0.60	2.00		0.38	0.10	NA	NA	0.55	0.95
26	CP 500/800	0.80	4.00		0.31	0.10	NA	NA	0.50	1.30
27	CP 600/900	1.00	4.00		0.35	0.10	NA	NA	0.52	1.32
28	CP 750/900	1.60	4.00		0.40	0.10	NA	NA	0.52	1.32
29	CP 800/1000	0.80	3.00		0.45	0.10	NA	NA	0.55	1.35
30	CP 1000/1200	0.80	2.30		0.47	0.10	NA	NA	0.60	1.40
31	CP 1050/1470	1.00	2.00		0.47	0.10	NA	NA	0.60	1.80
32	MS 950/1200	0.50	3.20		0.47	NA	NA	NA	0.60	1.00
33	MS 1150/1400	0.50	2.00		0.48	NA	NA	NA	0.60	1.40
34	TWIP 500/980	0.80	2.00		1.20	0.10	NA	NA	0.60	1.80
35	MS 1250/1500	0.50	2.00		0.51	0.10	NA	NA	0.65	1.05
36	HF 1050/1500 (22MnB5)	0.60	4.50		0.75	NA	NA	0.55	0.65	1.05

¹Based on US Spot Midwest Market Price Trend 2009

²Cold Rolled

Table 12.10: Steel material price list

12.2.7 Cost Assessment Results

The costs were assessed using the cost model for the following FSV sub-systems:

1. Rocker
2. Rear Rail
3. B-Pillar
4. Roof Rail
5. Shotgun
6. Tunnel
7. Front Rail

For each of the sub-systems, the following results are shown in Table 12.11 thru Table 12.17.

1. Mass
2. Manufacturing Costs

Part	Manufacturing Portfolio											
	T4 - Sub System Rocker Analysis Solution 1											
	Stamping		Stamping (TRB)		Stamping (LWB)		Hot Stamping		Hot Stamping (TRB)		Hot Stamping (LWB)	
Name	Mass (kg)	Piece Cost (\$)	Mass (kg)	Piece Cost (\$)	Mass (kg)	Piece Cost (\$)	Mass (kg)	Piece Cost (\$)	Mass (kg)	Piece Cost (\$)	Mass (kg)	Piece Cost (\$)
Rocker Inner	4.92	\$10.15	4.46	\$11.72	4.61	\$13.77	4.31	\$12.07	4.15	\$14.32	4.15	\$15.73
Rocker Reinforcement	2.66	\$5.44	2.69	\$6.73	2.49	\$8.37	2.13	\$7.18	2.14	\$7.63	2.14	\$10.15
Rocker Outer	3.37	\$5.90	3.37	\$5.90	3.37	\$5.90	3.37	\$5.90	3.37	\$5.90	3.37	\$5.90
Total	10.95	\$21.50	10.52	\$24.36	10.47	\$28.04	9.80	\$25.16	9.66	\$27.86	9.66	\$31.78
Part	Solution 2		Solution 3		Solution 4						Solution 5	
	Closed Roll Form		Closed Roll Form (TWC)		Hydroform		Hydroform (LWT)		Hydroform (MWT)		Aluminium Extrusion	
Name	Mass (kg)	Piece Cost (\$)	Mass (kg)	Piece Cost (\$)	Mass (kg)	Piece Cost (\$)	Mass (kg)	Piece Cost (\$)	Mass (kg)	Piece Cost (\$)	Mass (kg)	Piece Cost (\$)
Rocker Inner-Reinforcement	6.30	\$11.00	6.39	\$12.48	5.37	\$19.62	5.28	\$24.71	5.28	\$20.73	5.85	\$36.52
Rocker Outer(Stamped)	1.68	\$3.27	1.68	\$3.27	1.68	\$3.27	1.68	\$3.27	1.68	\$3.27	1.68	\$3.27
Total	7.98	\$14.27	8.07	\$15.74	7.05	\$22.88	6.96	\$27.98	6.96	\$24.00	7.53	\$39.78

Table 12.11: FSV Phase-2 T4 rocker sub-system costs

Part	Manufacturing Portfolio											
	T4 - Sub System Rear Rail Analysis Solution 1											
	Stamping		Stamping (TRB)		Stamping(LWB)		Hot Stamping		Hot Stamping (TRB)		Hot Stamping (LWB)	
Name	Mass (kg)	Piece Cost (\$)	Mass (kg)	Piece Cost (\$)	Mass (kg)	Piece Cost (\$)	Mass (kg)	Piece Cost (\$)	Mass (kg)	Piece Cost (\$)	Mass (kg)	Piece Cost (\$)
Rear Rail Outer	4.41	\$8.35	3.62	\$8.55	3.23	\$9.57	3.47	\$11.16	2.92	\$10.99	2.92	\$12.88
Rear Rail Reinforcement	1.77	\$4.18	1.57	\$4.40	1.75	\$7.28	1.59	\$6.71	1.64	\$7.49	1.64	\$10.46
Total	6.18	\$12.53	5.19	\$12.95	4.98	\$16.86	5.06	\$17.88	4.56	\$18.48	4.56	\$23.34
Part	Solution 2		Solution 3		Solution 4						Solution 5	
	Closed Roll Form		Open - Roll Form		Hydroform		Hydroform (LWT)		Hydroform (MWT)		Aluminium Stamping	
Name	Mass (kg)	Piece Cost (\$)	Mass (kg)	Piece Cost (\$)	Mass (kg)	Piece Cost (\$)	Mass (kg)	Piece Cost (\$)	Mass (kg)	Piece Cost (\$)	Mass (kg)	Piece Cost (\$)
Rear Rail Outer & Reinforcement	x	x	x	x	4.51	\$17.94	3.70	\$20.72	3.70	\$18.22	NA	NA
Rear Rail Outer	x	x	x	x	NA	NA	NA	NA	NA	NA	3.36	\$25.08
Rear Rail Reinforcement	x	x	x	x	NA	NA	NA	NA	NA	NA	2.33	\$18.81
Total	x	x	x	x	4.51	\$17.94	3.70	\$20.72	3.70	\$18.22	5.69	\$43.89

Table 12.12: FSV Phase-2 T4 rear rail sub-system costs

Part	Manufacturing Portfolio											
	T4 - Sub System B-Pillar Analysis Solution 1											
	Stamping		Stamping (TRB)		Stamping(LWB)		Hot Stamping		Hot Stamping (TRB)		Hot Stamping (LWB)	
Name	Mass (kg)	Piece Cost (\$)	Mass (kg)	Piece Cost (\$)	Mass (kg)	Piece Cost (\$)	Mass (kg)	Piece Cost (\$)	Mass (kg)	Piece Cost (\$)	Mass (kg)	Piece Cost (\$)
B-Pillar Inner	2.44	\$8.62	2.39	\$12.58	2.39	\$9.01	2.32	\$11.57	2.00	\$14.31	2.00	\$12.01
B-Pillar Reinforcement	1.62	\$6.47	1.37	\$10.71	1.37	\$7.48	1.30	\$8.35	1.29	\$13.09	1.29	\$11.34
B-Pillar Outer	2.19	\$7.08	2.19	\$7.08	2.19	\$7.08	2.19	\$7.08	2.19	\$7.08	2.19	\$7.08
Total	6.25	\$22.17	5.95	\$30.37	5.95	\$23.57	5.81	\$27.00	5.48	\$34.48	5.48	\$30.44
Part	Solution 2		Solution 3		Solution 4				Solution 5			
	Closed Roll Form		Open - Roll Form		Hydroform		Hydroform (LWT)		Hydroform (MWT)		Aluminium Stamping	
Name	Mass (kg)	Piece Cost (\$)	Mass (kg)	Piece Cost (\$)	Mass (kg)	Piece Cost (\$)	Mass (kg)	Piece Cost (\$)	Mass (kg)	Piece Cost (\$)	Mass (kg)	Piece Cost (\$)
B-Pillar Inner, Outer + Reinforcement	3.99	\$8.32	x	x	x	x	2.94	\$20.82	x	x	NA	NA
B-Pillar Inner	NA	NA	x	x	x	x	NA	NA	x	x	2.71	\$27.42
B-Pillar Reinforcement	NA	NA	x	x	x	x	NA	NA	x	x	0.39	\$8.56
B-Pillar Outer	2.19	\$7.08	x	x	x	x	2.19	\$7.08	x	x	1.59	\$22.97
Total	6.18	\$15.40	x	x	x	x	5.13	\$27.91	x	x	4.69	\$58.95

Table 12.13: FSV Phase-2 T4 B-pillar sub-system costs

Part	Manufacturing Portfolio											
	T4 - Sub System Roof Rail Analysis Solution 1											
	Stamping		Stamping (TRB)		Stamping(LWB)		Hot Stamping		Hot Stamping (TRB)		Hot Stamping (LWB)	
Name	Mass (kg)	Piece Cost (\$)	Mass (kg)	Piece Cost (\$)	Mass (kg)	Piece Cost (\$)	Mass (kg)	Piece Cost (\$)	Mass (kg)	Piece Cost (\$)	Mass (kg)	Piece Cost (\$)
Roof Rail Inner	3.53	\$9.05	3.10	\$22.12	3.1	\$10.79	3.21	\$12.61	2.78	\$24.69	2.78	\$14.61
Roof Rail Reinforcement	1.99	\$4.54	1.94	\$13.14	1.94	\$8.03	2.14	\$8.85	2.14	\$8.85	2.14	\$8.85
Roof Rail Outer (Stamped)	4.39	\$8.25	4.39	\$8.25	4.39	\$8.25	4.39	\$8.25	4.39	\$8.25	4.39	\$8.25
Total	9.90	\$21.83	9.43	\$43.51	9.43	\$27.07	9.74	\$29.70	9.31	\$41.78	9.31	\$31.71
Part	Solution 2		Solution 3		Solution 4						Solution 5	
	Closed Roll Form		Open - Roll Form		Hydroform		Hydroform (LWT)		Hydroform (MWT)		Aluminium Stamping	
Name	Mass (kg)	Piece Cost (\$)	Mass (kg)	Piece Cost (\$)	Mass (kg)	Piece Cost (\$)	Mass (kg)	Piece Cost (\$)	Mass (kg)	Piece Cost (\$)	Mass (kg)	Piece Cost (\$)
Roof Rail Inner	x	x	x	x	NA	NA	NA	NA	NA	NA	0.90	\$9.48
Roof Rail Reinforcement	x	x	x	x	NA	NA	NA	NA	NA	NA	3.28	\$32.57
Roof Rail Inner + Reinforcement	x	x	x	x	4.96	\$18.03	4.87	\$25.39	4.87	\$19.04	x	x
Roof Rail Outer (Stamped)	x	x	x	x	4.39	\$8.25	4.39	\$8.25	4.39	\$8.25	6.22	\$40.44
Total					9.35	\$26.28	9.26	\$33.64	9.26	\$27.29	10.40	\$82.49

Table 12.14: FSV Phase-2 T4 roof rail sub-system costs

Part	Manufacturing Portfolio											
	T4 - Sub System Shotgun Analysis Solution 1											
	Stamping		Stamping (TRB)		Stamping(LWB)		Hot Stamping		Hot Stamping (TRB)		Hot Stamping (LWB)	
Name	Mass (kg)	Piece Cost (\$)	Mass (kg)	Piece Cost (\$)	Mass (kg)	Piece Cost (\$)	Mass (kg)	Piece Cost (\$)	Mass (kg)	Piece Cost (\$)	Mass (kg)	Piece Cost (\$)
Shotgun Outer	3.19	\$9.82	3.01	\$17.54	3.01	\$8.82	2.45	\$13.33	2.37	\$17.04	2.37	\$11.04
Shotgun Inner	3.18	\$11.77	3.23	\$19.15	3.23	\$9.28	2.76	\$14.59	2.60	\$18.07	2.60	\$11.06
Total	6.37	\$21.58	6.24	\$36.69	6.24	\$18.09	5.20	\$27.92	4.98	\$35.11	4.98	\$22.11
Part	T4 - Sub System Shotgun Analysis Solution 2											
	Closed Roll Form		Open - Roll Form		Hydroform		Hydroform (LWT)		Hydroform (MWT)		Aluminium Stamping	
	Mass (kg)	Piece Cost (\$)	Mass (kg)	Piece Cost (\$)	Mass (kg)	Piece Cost (\$)	Mass (kg)	Piece Cost (\$)	Mass (kg)	Piece Cost (\$)	Mass (kg)	Piece Cost (\$)
Shotgun Outer	x	x	x	x	x	x	x	x	x	x	2.23	\$31.69
Shotgun Inner	x	x	x	x	x	x	x	x	x	x	1.98	\$31.65
Total	x	x	x	x	x	x	x	x	x	x	4.21	\$63.34

Table 12.15: FSV Phase-2 T4 shotgun sub-system costs

Part	Manufacturing Portfolio											
	T4 - Sub System Tunnel Analysis Solution 1											
	Stamping		Stamping (TRB)		Stamping(LWB)		Hot Stamping		Hot Stamping (TRB)		Hot Stamping (LWB)	
Name	Mass (kg)	Piece Cost (\$)	Mass (kg)	Piece Cost (\$)	Mass (kg)	Piece Cost (\$)	Mass (kg)	Piece Cost (\$)	Mass (kg)	Piece Cost (\$)	Mass (kg)	Piece Cost (\$)
Tunnel Front Upper Rail	1.34	\$4.65	1.18	\$4.34	0.84	\$5.41	1.26	\$6.30	0.87	\$5.37	0.81	\$7.89
Tunnel Front Lower Rail	1.09	\$2.57	1.05	\$2.80	0.96	\$5.13	0.96	\$4.93	1.14	\$5.44	1.14	\$7.84
Tunnel Rear	1.87	\$4.13	1.79	\$5.13	1.56	\$5.32	1.25	\$5.51	1.17	\$6.24	1.17	\$7.81
Tunnel Top	1.30	\$3.31	1.30	\$3.31	1.56	\$5.60	1.82	\$6.77	1.82	\$6.77	1.82	\$6.77
Total	5.61	\$14.67	5.31	\$15.59	4.92	\$21.45	5.28	\$23.51	5.00	\$23.82	4.94	\$30.30
Part	Solution 2		Solution 3		Solution 4						Solution 5	
	Closed Roll Form		Open - Roll Form		Hydroform		Hydroform (LWT)		Hydroform (MWT)		Aluminium Stamping	
Name	Mass (kg)	Piece Cost (\$)	Mass (kg)	Piece Cost (\$)	Mass (kg)	Piece Cost (\$)	Mass (kg)	Piece Cost (\$)	Mass (kg)	Piece Cost (\$)	Mass (kg)	Piece Cost (\$)
Tunnel Front Upper Rail	x	x	0.81	\$2.02	x	x	x	x	x	x	0.65	\$7.83
Tunnel Front Lower Rail	x	x	0.76	\$2.08	x	x	x	x	x	x	0.55	\$6.22
Tunnel Rear	x	x	1.23	\$3.11	x	x	x	x	x	x	3.18	\$25.79
Tunnel Top	x	x	1.50	\$4.34	x	x	x	x	x	x	1.30	\$7.94
Total	x	x	4.29	\$11.56	x	x	x	x	x	x	5.68	\$47.78

Table 12.16: FSV Phase-2 T4 tunnel sub-system costs

Part	Manufacturing Portfolio											
	T4 - Sub System Front Rail Analysis Solution 1											
	Stamping		Stamping (TRB)		Stamping(LWB)		Hot Stamping		Hot Stamping (TRB)		Hot Stamping (LWB)	
Name	Mass (kg)	Piece Cost (\$)	Mass (kg)	Piece Cost (\$)	Mass (kg)	Piece Cost (\$)	Mass (kg)	Piece Cost (\$)	Mass (kg)	Piece Cost (\$)	Mass (kg)	Piece Cost (\$)
Front Rail Inner	x	x	x	x	1.48	\$7.13	x	x	x	x	x	x
Front Rail Lower	x	x	x	x	1.41	\$7.85	x	x	x	x	x	x
Front Rail Outer	x	x	x	x	2.09	\$8.88	x	x	x	x	x	x
Gusset	x	x	x	x	1.49	\$6.07	x	x	x	x	x	x
Total					6.46	\$29.93						
Part	T4 - Sub System Front Rail Analysis Solution 2										Solution 3	
	Stamping		Stamping (TRB)		Stamping (LWB)		Aluminium Stamping		Hot Stamping)		Hydroform (LWT)	
	Mass (kg)	Piece Cost (\$)	Mass (kg)	Piece Cost (\$)	Mass (kg)	Piece Cost (\$)	Mass (kg)	Piece Cost (\$)	Mass (kg)	Piece Cost (\$)	Mass (kg)	Piece Cost (\$)
Front Rail Upper	x	x	x	x	1.98	\$7.83	1.28	\$12.79	x	x	2.18	\$17.93
Front Rail Lower	x	x	x	x	3.14	\$11.01	2.18	\$19.23	x	x	NA	NA
Closeout Front Rail Upper (Stamped)	x	x	x	x	0.11	\$0.75	0.11	\$1.50	x	x	0.17	\$0.89
Closeout Front Rail Lower (Stamped)	x	x	x	x	0.50	\$1.33	0.45	\$4.11	x	x	NA	NA
Front Rail Rear (Single Thickness)	x	x	x	x	NA	NA	NA	NA	x	x	1.55	\$9.95
Front Rail Rear Upper(Single Thickness)	x	x	x	x	NA	NA	NA	NA	x	x	0.96	\$7.62
Front Rail Rear Lower(Single Thickness)	x	x	x	x	NA	NA	NA	NA	x	x	1.41	\$9.96
Total					5.72	\$20.91	4.03	\$37.63			6.26	\$46.35

Table 12.17: FSV Phase-2 T4 front rail sub-system costs

12.3 Total Life Cycle Assessment

With a fast growing automotive sector and global concern over climate change from anthropogenic GHG's (attributable to human activities), the key priorities are improving fuel economy, reducing emissions and shifting to a sustainable automotive industry. In Europe, strict tailpipe carbon dioxide (CO₂) emissions legislation has been passed with a view towards further reductions by 2020 and beyond. This trend is observed globally as shown in Figure 12.4.

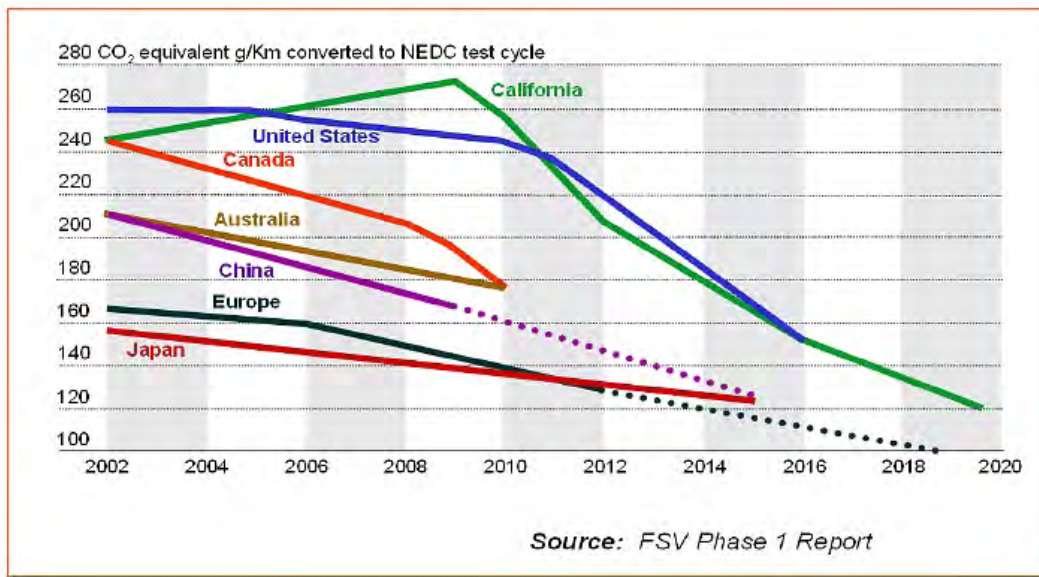


Figure 12.4: Trends in Global Fuel Economy/Vehicle Emissions Regulations

Here, CO₂e refers to carbon dioxide equivalents, or all greenhouse gases attributable to a product that affect global warming potential, and include gases other than CO₂. This is important, because different greenhouse gases vary in their harm or impact to the environment. We therefore use the metric CO₂e, to insure that all GHGs are accounted for, when comparing different automotive materials and fabrication technologies.

Every greenhouse gas has a Global Warming Potential (GWP), which measures their environmental impact. Below are typical greenhouse gases and their Global Warming Potential; note that most of steel's production emissions are CO₂e, whereas other materials often considered for automotive application yield a higher percentage of the more harmful greenhouse gases:

- Carbon dioxide has a GWP of 1
- Methane has a GWP of 21
- Nitrous oxide has a GWP of 310
- Perfluorocarbons (HFC) has a GWP range of 140 to 11,700
- Sulphur Hexafluoride has a GWP of 23.90

One of the challenges concerning automotive emissions regulations is to achieve the intended control without creating unintended consequences or unexpected results. Climate change and

12.3 Total Life Cycle Assessment

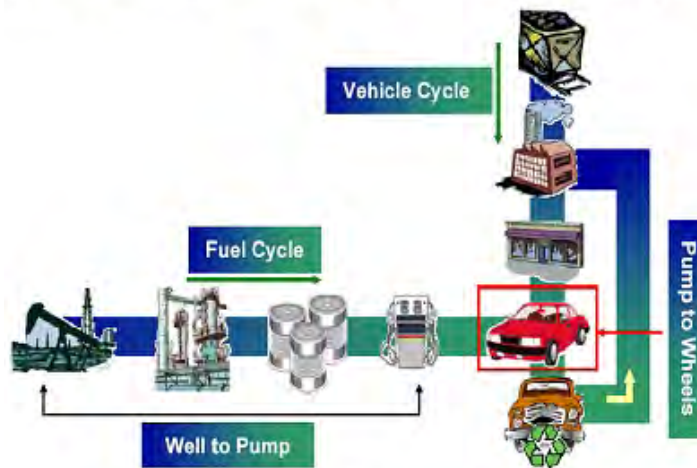
energy concerns prompt increased fuel efficiency standards or tailpipe emission regulations. And improving fuel economy and reducing tailpipe emissions during the “use” phase of a vehicle is very important.

However, the “use” phase represents only part of the total emissions associated with a vehicle throughout its life. A more comprehensive evaluation can be achieved if emissions from all phases of a vehicle’s life are considered - from materials production through the end-of-life disposal. Decisions based on total life cycle data prevent the possibility of unintended consequences.

Life Cycle Assessment (LCA) is a technique to determine the environmental impacts of products, processes or services, through production, usage, and disposal. ISO14040 describes LCA as a technique compiling a quantitative inventory of relevant inputs and outputs of a product system; evaluating the potential environmental impacts associated with those inputs and outputs; and interpreting the results of the inventory and impact phases in relation to the goal and scope of the study.

Life Cycle Assessment is the only appropriate way to account for and reduce greenhouse gas emissions attributable to the automotive sector. The LCA approach assesses the entire vehicle life including the fuels that power it and the materials from which it is made. Therefore, in LCA, we must include the ‘well to pump’ emissions so that we have the complete ‘fuel cycle’ from well to wheels. In addition, it is critically important that we include the ‘vehicle cycle’ so that GHG emissions produced in the materials and vehicle production phases are accounted for along with credits for recycling at the end of its life. This should be a model for vehicle design and materials decision making, to avoid unintended consequences.

LCA is needed to avoid Unintended Consequences



Source: Argonne National Laboratory

Studies show that Life Cycle Assessment of a vehicle’s environmental footprint is critical for material selection decisions. Adopting a lifecycle perspective is critical, since changes in the product system, such as the use of alternative material choices in a vehicle body structure, may result

in use phase emissions reductions at the expense of significant increases in material production emissions, even considering end-of-life recycling credits.

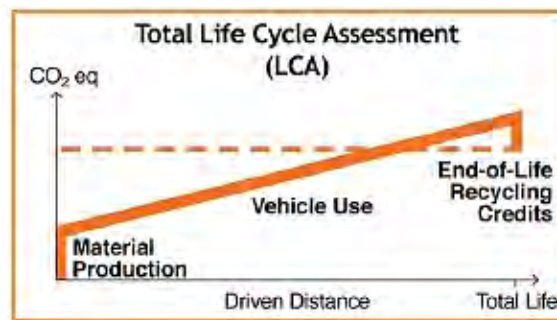
To emphasize the importance of total vehicle life cycle GHG emissions, consider the below chart which shows drastically different levels of GHG emissions from the material production stage of competing automotive materials. Material production for alternative material vehicles will load the environment with significantly more GHG emissions than that of a steel vehicle. Mass Reduction is therefore only one component of a comprehensive and effective greenhouse gas reduction strategy for the automotive industry.

Material production greenhouse gas (GHG) emissions:

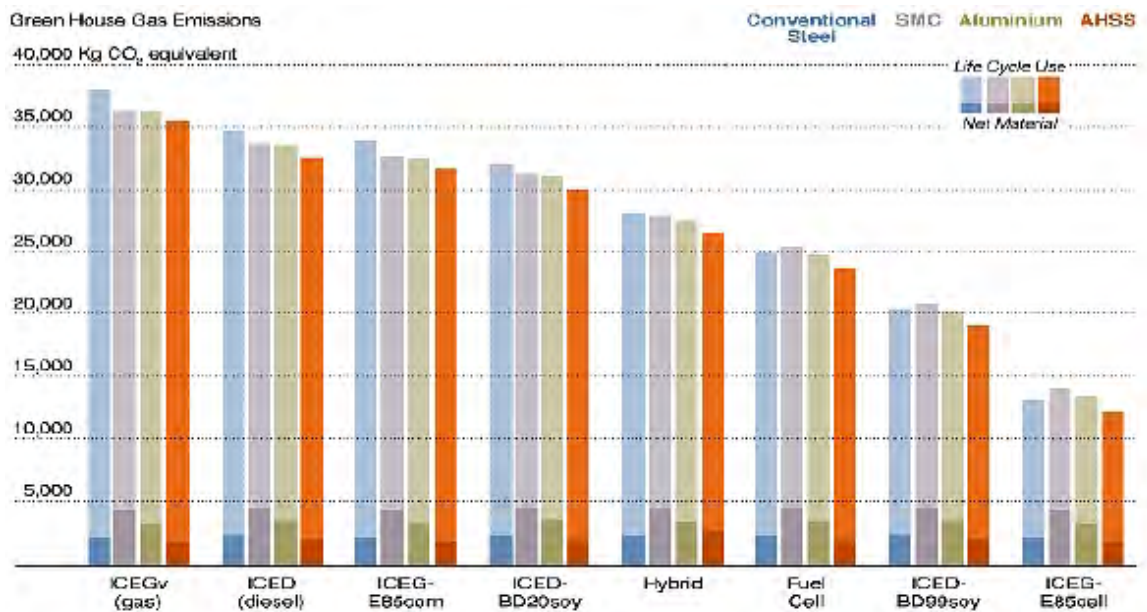
GHG from Production (in kg CO₂eq/kg of material)



The LCA methodology evaluates the environmental performance advantages of steel relative to competing materials: lower CO₂e emissions in the material production phase, competitive light weighting and use phase emissions performance through the use of advanced high strength steels (AHSS), and 100% recyclability. The latter makes a significant difference in total CO₂e emissions when considering that demand for vehicles is constantly increasing. CO₂e emissions at the material production phase can, to a large extent, be recycled through steel's second, third or infinite life, unlike other competing materials.



As the automotive industry's efforts to reduce CO₂e emissions are increasingly moving towards more advanced powertrains and fuel sources, material production will account for a much larger percentage of total CO₂e. This is due to the fact that these powertrains will greatly reduce the use phase CO₂e emissions, which means that the material production phase emissions will make up a greater percentage of total vehicle emissions. Therefore, use of low GHG - intensive material such as steel becomes even more important.



12.3.1 Life Cycle Emissions Studies for FutureSteelVehicle Variants

As we consider future vehicle programs, the application of LCA allows us to explore the impact of design, material and powertrain choices on life cycle vehicle emissions. This knowledge will help derive optimized solutions for both vehicle performance, safety, and our environment.

There are a variety of LCA models in use today. Dr. Roland Geyer at the University of California, Santa Barbara (UCSB) Bren School of Environmental Science, has developed a fully parameterized model which calculates life cycle GHG emissions attributable to vehicles as a function of their material composition and power train characteristics. This model enables comparisons of various body structure and component materials across all phases of the vehicle life cycle. This model has gone through an extensive peer review process, endorsed by members of industry and academicians. It demonstrates, that in many cases, choosing alternative light-weight materials results in greater vehicle lifetime GHG emissions due to higher GHG emissions during the material production phase.

As part of the FutureSteelVehicle Programme, WorldAutoSteel contracted with Forschungsgesellschaft Kraftfahrwesen mbH Aachen (fka), the automotive engineering services company associated with Aachen University in Germany, to develop mass sensitivity simulations for Battery

Electrical Vehicles (BEV) and Plug-in Hybrid (PHEV) powertrains, in alignment with the powertrain choices for this program. fka's work in determining fuel elasticity, based on mass reduction for various vehicle classes, has been a useful reference for WorldAutoSteel, and is a key ingredient in the University of California, Santa Barbara (UCSB) GHG Automotive Materials Comparison model [3]. EDAG provided fka with FSV-1 and FSV-2 powertrain technical specifications, and then fka constructed models to determine energy consumption differences for these powertrains, relative to the same vehicle class sizes, based on mass reduction values consistent with their earlier work.

The results of these simulations were provided to UCSB, who used these data to expand the capability of their GHG Materials Comparison model to include BEV and PHEV powertrains. As a part of the automotive design and engineering studies for FSV BEV, this expanded model was used to compare alternative materials and fabrication strategies, to fully understand their impact on vehicle life cycle emissions.

12.3.2 BEV Emissions Technology Assessment - Using the UCSB Model

For the FutureSteelVehicle BEV variant, we began with EDAG's baseline body structure mass of 218 kg; based on the design and engineering specifications, our baseline BEV results in a curb weight of ~1033 kg. Baseline vehicle emissions are then determined based on these parameters:

- Baseline body structure mass - 218 kg
- Vehicle curb weight - 1033 kg
- Projected mass compounding - 90% [4]
- Energy consumption value - $31.60 \frac{\text{MJ}}{100\text{km}}$ (~91 mpg)
- NEDC driving cycle

For each FSV BEV subsystem, reference or baseline mass, and respective subsystem masses were derived from optimization studies for the various material fabrication technologies. Manufacturing scrap values for each fabrication technology were determined from their cost model. These values are input to the UCSB model, which results in an emissions profile for each subsystem, with distinct CO₂e values for material production, vehicle use and vehicle recycling. Subsystem fabrication energies were easily converted into CO₂e emissions; these values were then added to the values obtained from the UCSB BEV model to achieve total vehicle life cycle emissions.

As an example, the rocker subsystem emissions profiles are shown in Table 12.18 for various material fabrication technologies.

This table compares emissions contributions for the various fabrication and design options enabling the determination of the lowest life cycle emissions (highlighted). This is an important

³<http://www.worldautosteel.org/Projects/LCA-Study.aspx>

⁴The 90% mass compounding factor was used to derive overall mass reduction of the vehicle, based on body structure mass reduction

12.3 Total Life Cycle Assessment

criterion, as we seek a BEV that leverages emerging steel product and fabrication technologies, and also achieves ultra-low emissions during its life cycle.

FSV Sub-system	Material CO ₂ e	Manufacturing CO ₂ e	Use CO ₂ e	Recycling CO ₂ e	Total Vehicle Life Cycle CO ₂ e
Rocker, Baseline	2290.8	5.7	14640.2	(956.8)	15980.0
Solution 1 - Stamping	2299.4	6.1	14688.3	(960.6)	16033.2
Solution 1 - Stamping TRB	2292.9	6.0	14654.8	(957.6)	15996.1
Solution 1 - Stamping LWB	2292.3	16.9	14658.1	(957.3)	16010.0
Solution 2 - Hot Stamping	2272.9	9.7	14608.1	(947.7)	15942.9
Solution 2 - Hot Stamping TRB	2271.7	9.7	14598.5	(947.2)	15932.7
Solution 2 - Hot Stamping LWB	2271.7	20.4	14598.5	(947.2)	15943.4
Solution 3 - Closed Roll Form	2246.0	5.1	14481.6	(935.3)	15797.4
Solution 3 - Closed Roll Form (TRB)	2238.4	4.8	14479.5	(931.3)	15791.5
Solution 3 - Closed Roll Form (TWC)	2245.5	4.8	14487.9	(934.9)	15803.3
Solution 5 - Hydroform	2223.3	15.9	14416.8	(924.2)	15731.9
Solution 5 - Hydroform LWT	2223.1	25.6	14410.6	(924.2)	15735.1
Solution 5 - Hydroform TRT	2222.5	15.9	14410.6	(923.9)	15725.1
Aluminium Extrusion	2350.8	8.6	14425.1	(1008.5)	15775.9

Table 12.18: Total vehicle life cycle emissions - T4 Rocker solutions

The emission profiles for the other FSV sub-systems are shown in Table 12.19 thru Table 12.24.

FSV Sub-system	Material CO ₂ e	Manufacturing CO ₂ e	Use CO ₂ e	Recycling CO ₂ e	Total Vehicle Life Cycle CO ₂ e
Rear Rail Baseline	2290.8	2.9	14640.2	(956.8)	15977.2
Solution 1 - Stamping	2289.7	2.8	14633.2	(956.2)	15969.5
Solution 1 - Stamping TRB	2272.2	2.8	14564.1	(948.0)	15891.1
Solution 1 - Stamping LWB	2266.8	14.2	14549.5	(945.3)	15885.2
Solution 2 - Hot Stamping	2265.2	7.4	14554.9	(944.4)	15883.1
Solution 2 - Hot Stamping TRB	2257.1	7.1	14520.4	(940.6)	15844.0
Solution 2 - Hot Stamping LWB	2255.2	18.2	14520.4	(939.6)	15854.2
Solution 5 - Hydroform	2251.4	14.8	14516.7	(937.6)	15845.3
Solution 5 - Hydroform LWT	2239.1	23.5	14460.3	(931.9)	15791.0
Solution 5 - Hydroform TRT	2239.1	14.8	14460.3	(931.9)	15782.3
Solution 6 - Aluminium Stamping	2398.2	2.9	14598.8	(1034.2)	15965.7

Table 12.19: Total vehicle life cycle emissions - T4 Rear Rail solutions

FSV Sub-system	Material CO ₂ e	Manufacturing CO ₂ e	Use CO ₂ e	Recycling CO ₂ e	Total Vehicle Life Cycle CO ₂ e
B-Pillar w/Reinforcement Baseline	2290.8	11.9	14640.2	(956.8)	15986.2
Solution 1 - Stamping	2277.9	8.5	14463.6	(952.5)	15797.4
Solution 1 - Stamping TRB	2284.1	8.3	14442.7	(956.1)	15779.1
Solution 1 - Stamping LWB	2251.2	19.2	14442.7	(938.6)	15774.5
Solution 2 - Hot Stamping	2264.8	10.7	14432.6	(946.0)	15762.1
Solution 2 - Hot Stamping TRB	2268.2	11.6	14410.0	(948.1)	15741.7
Solution 2 - Hot Stamping LWB	2242.7	21.3	14410.0	(934.6)	15739.4
Solution 3 - Closed Roll Form	2242.4	6.1	14458.7	(933.7)	15773.5
Solution 5 - Hydroform LWT	2226.1	26.8	14385.7	(926.1)	15712.4
Solution 6 - Aluminium Stamping	2477.4	8.9	14355.1	(1109.6)	15731.8

Table 12.20: Total vehicle life cycle emissions - T4 B-pillar solutions

FSV Sub-system	Material CO ₂ e	Manufacturing CO ₂ e	Use CO ₂ e	Recycling CO ₂ e	Total Vehicle Life Cycle CO ₂ e
Roof Rail Baseline	2290.8	5.1	14640.2	(956.8)	15979.4
Solution 1 - Stamping	2251.4	4.0	14443.4	(938.7)	15760.1
Solution 1 - Stamping TRB	2271.9	3.9	14410.2	(950.1)	15735.9
Solution 1 - Stamping LWB	2239.2	17.1	14410.2	(932.7)	15733.8
Solution 2 - Hot Stamping	2252.2	9.4	14431.8	(939.3)	15754.1
Solution 2 - Hot Stamping TRB	2259.6	11.6	14402.1	(943.7)	15729.6
Solution 2 - Hot Stamping LWB	2239.6	15.3	14402.1	(933.0)	15723.9
Solution 5 - Hydroform	2222.5	14.3	14404.8	(923.9)	15717.6
Solution 5 - Hydroform LWT	2221.4	27.5	14398.4	(923.4)	15723.8
Solution 5 - Hydroform TRT	2221.6	14.3	14398.4	(923.6)	15710.7
Solution 6 - Aluminium Stamping	2507.3	4.2	14477.8	(1118.8)	15870.5

Table 12.21: Total vehicle life cycle emissions - T4 Roof Rail solutions

FSV Sub-system	Material CO ₂ e	Manufacturing CO ₂ e	Use CO ₂ e	Recycling CO ₂ e	Total Vehicle Life Cycle CO ₂ e
Shotgun Assembly Baseline	2290.8	1.7	14640.2	(956.8)	15976.0
Solution 1 - Stamping	2370.3	2.6	14791.9	(996.7)	16168.1
Solution 1 - Stamping TRB	2392.5	2.6	14782.8	(1008.6)	16169.2
Solution 1 - Stamping LWB	2323.6	13.4	14782.8	(972.1)	16147.7
Solution 2 - Hot Stamping	2335.9	10.3	14710.5	(979.6)	16077.1
Solution 2 - Hot Stamping TRB	2338.0	10.8	14694.6	(981.0)	16062.4
Solution 2 - Hot Stamping LWB	2298.8	15.6	14694.6	(960.2)	16048.8
Solution 6 - Aluminium Stamping	2699.0	2.7	14640.9	(1254.7)	16088.0

Table 12.22: Total vehicle life cycle emissions - T4 Shotgun solutions

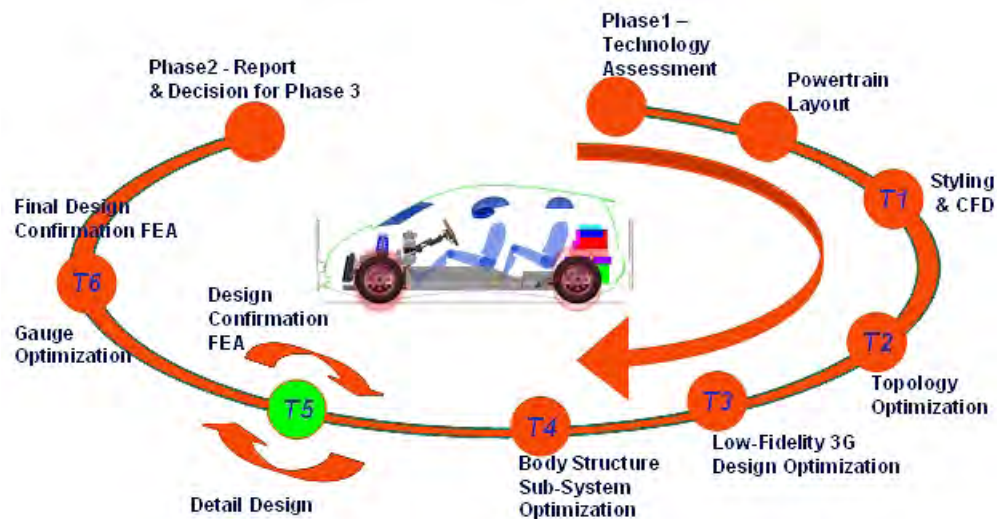
FSV Sub-system	Material CO ₂ e	Manufacturing CO ₂ e	Use CO ₂ e	Recycling CO ₂ e	Total Vehicle Life Cycle CO ₂ e
Tunnel Assembly Baseline	2290.8	6.6	14640.2	(956.8)	15980.9
Solution 1 - Stamping	2259.4	4.8	14492.9	(942.2)	15814.8
Solution 1 - Stamping TRB	2252.6	4.7	14472.6	(938.9)	15791.0
Solution 1 - Stamping LWB	2242.4	19.5	14444.9	(933.9)	15772.9
Solution 2 - Hot Stamping	2245.4	11.5	14470.4	(935.1)	15792.1
Solution 2 - Hot Stamping TRB	2223.1	11.3	14379.3	(924.6)	15689.0
Solution 2 - Hot Stamping LWB	2238.9	22.4	14446.5	(932.0)	15775.8
Solution 4 - Open Roll Form	2224.3	2.9	14401.8	(924.9)	15704.0
Solution 6 - Aluminium Stamping	2385.3	4.9	14497.6	(1031.3)	15856.5

Table 12.23: Total vehicle life cycle emissions - T4 Tunnel solutions

FSV Sub-system	Material CO ₂ e	Manufacturing CO ₂ e	Use CO ₂ e	Recycling CO ₂ e	Total Vehicle Life Cycle CO ₂ e
Front Rail Baseline	2290.8	30.0	14640.2	(956.8)	16004.3
Solution 1 - Hydroform LWT	2275.5	60.0	14626.4	(948.8)	16013.1
Solution 2 - Stamped Solution	2371.6	30.8	14640.2	(990.5)	16052.1
Solution 3 - Stamped C2 Solution	2282.5	22.0	14588.4	(953.1)	15939.8

Table 12.24: Total vehicle life cycle emissions - T4 Front Rail solutions

13.0 Design of Body Structure



13.1 Sub-Systems Selection for BEV

The objective of the FSV program is to achieve a lightweight body structure; mass reduction in every sub-system is crucial to achieve this goal. However, it was also necessary to look into the manufacturing feasibility aspect for the respective sub-systems. Therefore, the FSV sub-systems recommendations were divided into three categories based on the level of difficulty of the manufacturing technology, and the time period during when these technologies would be more practical leading to feasible high volume production. The three categories were the following:

- 2010-2015 - Conservative approach (C)
- 2015-2020 - Mid-term approach (M)
- 2020- Beyond - Aggressive approach (A)

All of the structural sub-system solutions are considered to be viable solutions. The preferred solution depends on the criteria of the OEM and the market a vehicle is intended to fill. Possible criteria are the low cost solution, the light weight solution, the low CO₂e solution, the manufacturing

capability of the OEM etc. In most cases it will be a combination of these factors plus other considerations.

A comparison of mass, cost and LCA CO₂e provide a useful tool for evaluating the relative attributes of each solution and applying a selection criteria that meets a vehicle manufacturer's and a vehicle's particular requirements.

13.1.1 FSV Selection Criteria

The selection of the most appropriate sub-system was made by giving weight to these factors:

- Mass
- Cost: "technical cost modeling" approach was applied to all the parts to estimate the sub-system manufacturing costs
- Life Cycle Assessment (LCA) for CO₂e: an extended Greenhouse Gases (GHG) emissions comparison model was used to conduct a LCA assessment for the FSV using input data from Forschungsgesellschaft Kraftfahrwesen mbH Aachen (fka), University of California, Santa Barbara (UCSB) and EDAG

There is a new aspect of vehicle design associated with advanced powertrains, such as BEVs, called the "mass/cost paradigm shift."

Contrary to conventional vehicle design where the low cost solution is often the preferred solution, the high cost of batteries increases the value of mass reduction. As an example, the FSV Phase 1 Study indicated that, for the 2015-2020 timeframe, a lightweight solution saving 1 kg can subsequently reduce the battery size and cost by approximately US\$9.39. Therefore, vehicle manufacturers could employ lightweight solutions that are more costly (up to US\$9.39 per kg in this case), than those used with conventional powertrains, with the net result being break-even on the total manufacturing costs. Consequently, higher cost lightweighting solutions become attractive for more vehicle applications since their cost is offset by the reduction in battery powertrain cost.

However, when the solution is evaluated on an LCA basis, choosing the higher cost solution, though lighter, could lead to an increase in total life cycle GHG. Each graph is shown with a set of isovalue lines, enabling evaluation of solutions relative to each other on a total vehicle manufacturing cost basis. Any solutions that fall on the same isoline result are the same value due to the off-setting reduction in powertrain costs.

In a similar manner to the mass/cost paradigm shift, the cost effect of carbon (GHG emissions), reduction can be assessed. Isovalue lines can be constructed to compare the LCA GHG saved by a lightweighting solution compared to the 'carbon cost' (US\$100 per tonne used for this example ^[1]).

¹ Heritage Foundation review of Lieberman-Warner climate change legislation sites cost of CO₂e emission ranging from \$50 to \$100 per tonne (<http://www.heritage.org/Research/Reports/2008/05/The-Economic-Costs-of-the-Lieberman-Warner-Climate-Change-Legislation>)

13.1 Sub-Systems Selection for BEV

By conducting this comparison, a better decision can be made based on the vehicle design targets. In FutureSteelVehicle's case, a critical target is the reduction of total life cycle emissions while maintaining affordability. The preferred solution depends on the selection criteria: low cost solution, lightweight solution, or low GHG solution.

This selection criteria was applied to all of the FSV sub-systems to evaluate solutions in terms of mass, cost and life cycle emissions for the BEV.

Another aspect of this project is the inclusion of an aluminum solution, as a means for the steel industry to judge the competitiveness of our product in these applications. The aluminum solution was developed by EDAG, who has expertise in aluminum automotive structures, using the same aggressive design optimization and technology approach as the competing steel designs. In the case of the rocker panel, the aluminum design is not as competitive as many of the steel designs.

The preferred solution depends on the selection criteria: low cost solution, light weight solution, or low CO₂e solution. For the BEV, the selection was made on the basis of achieving maximum mass savings, with the most viable high volume production steel technology for the years 2015 to 2020. The chosen solutions were the basis for the further tasks in Phase 2, starting with T5-detailed body structure design .

The technology assessment results for Phase 2 are summarized in section 13.1.2.

13.1.2 Sub-Systems Selection for BEV

The masses and LCA CO₂e values are shown for the sub-systems in Figure 13.2 thru Figure 13.14. The mass premium and CO₂e premium isolines are also shown on the graph, to account for the impact of the respective savings on cost. All solutions lying along a particular FSV mass premium line are considered to be of the same value with respect to the overall costs; the savings in mass balances the extra costs for the technology, as calculated using the mass savings premium. All the data points that fall to the below/left of a particular constant mass premium line are better solutions with respect to costs. Also, the CO₂e footprint for each of the sub-system was assessed for the total vehicle life cycle, as explained in section 12.3.2.

The technology assessment results for the different sub-systems are summarized in Table 13.1 thru Table 13.7.

The solutions selected for the respective FSV BEV sub-systems are discussed in the following sections.

13.1.2.1 Rocker Sub-System

As shown in Figure 13.2, the hydroformed rocker solutions had the lowest mass. However, the optimized hydroformed rocker had a complex design that would pose difficulties for manufacturability, with the current level of hydroforming technology, and further complicated design for assembly for the adjoining components. So, either the rollformed single thickness or a rollformed with Tailor Welded Coil (TWC), was the recommended solution for the rocker. The hydroformed rocker solutions may be a more practical solution for design and assembly, with further development of the hydroforming technology in the future (2020 and beyond). The rocker outer was a stamped single thickness design for all the solutions.

The recommendations are also supported by the LCA CO₂e savings of the Rollformed sub-systems compared to the baseline design, as shown in Figure 13.2. The rollformed designs were of the same value compared to the Hydroform designs, on a CO₂e basis, as shown by the \$100 $\frac{\text{USD}}{\text{tonne}}$ CO₂e premium constant lines.

FSV Rocker HF3G Technology Assessment	FSV Rocker HF3G Manufacturing Interpretation		High Volume Manufacturing Feasibility	FSV Rocker Sub-System Mass (kg)	FSV Rocker Manufacturing Cost (\$)	FSV Rocker LCA CO ₂ e Savings (kg)
Baseline	B ST	Stamping		10.26	19.99	0
Stamping Solution	ST	Stamping		10.95	21.50	53
	ST TRB	Stamping TRB		10.52	24.36	16
	ST LWB	Stamping LWB		10.47	28.04	30
	HST	Hot Stamp		9.80	25.16	-37
	HST TRB	Hot Stamp TRB		9.66	27.86	-47
	HST LWB	Hot Stamp LWB		9.66	31.78	-37
Roll Form	RF	Roll Form		7.98	14.27	-183
	RF TRB	Roll Form TR Coil		7.95	16.56	-189
	RF TWC	Roll Form TW Coil		8.07	15.74	-177
Hydroform	HF	HydroForm		7.05	22.88	-248
	HF LWT	Hydroform LWT		6.96	27.98	-245
	HF MWT	Hydroform MWT		6.96	24.00	-255
Aluminum	AL	Extrusion		7.53	39.78	-204

■ (C) Conservative
 ■ (M) Mid-term
 ■ (A) Aggressive

* The mass, costs and LCA CO₂e savings shown above are only for one side of the vehicle

Table 13.1: T4 technology assessment results - Rocker sub-system

The weight of the chosen rolled formed FSV rocker sub-system was 15.96 kg (7.98 kg on each side), which was significantly lower than the baseline, 20.5 kg (10.26 kg on each side).

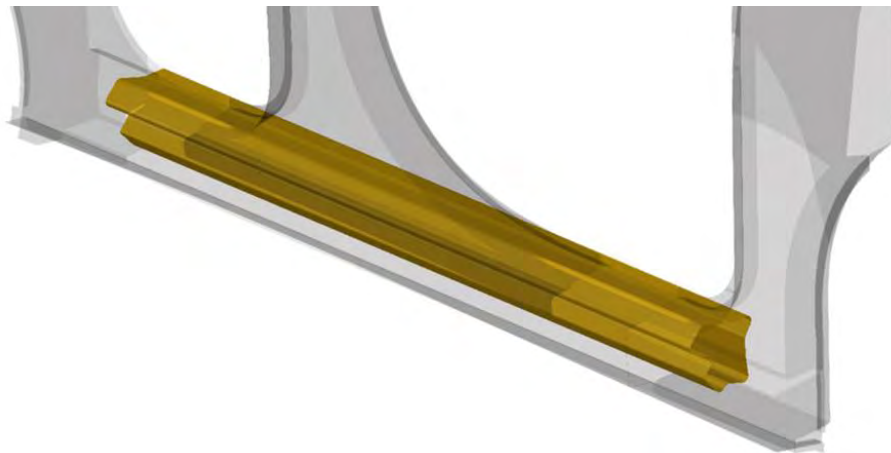


Figure 13.1: FSV Phase-2 T4 rocker rollformed solution

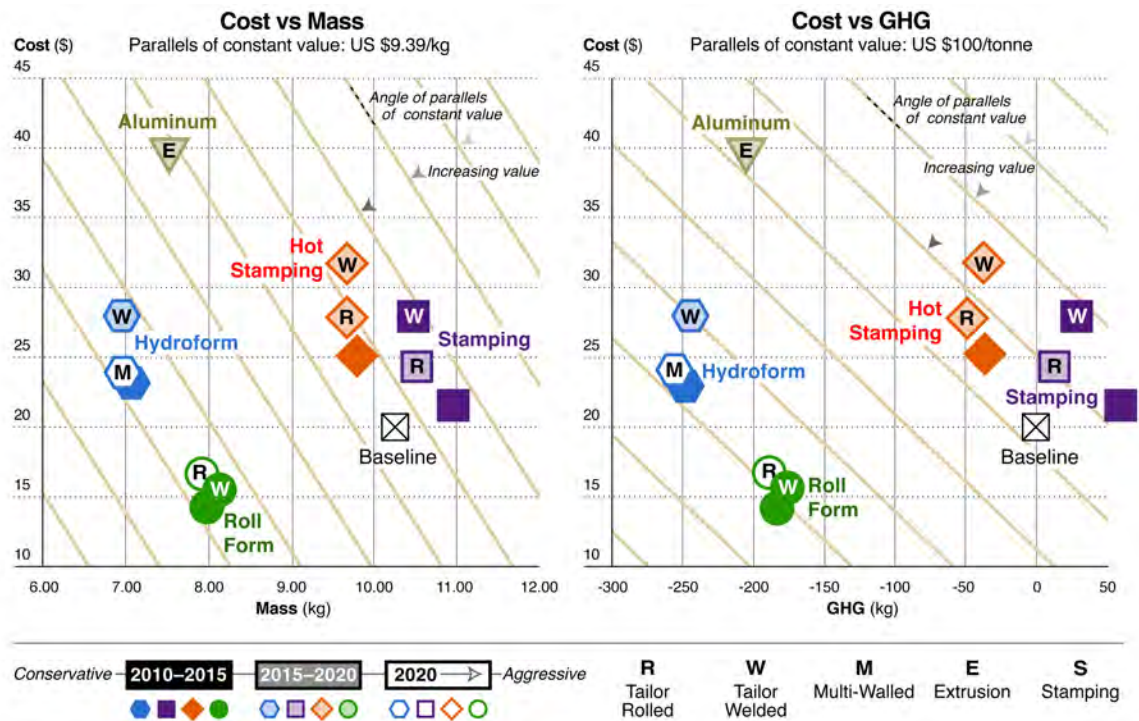


Figure 13.2: T4 comparison FSV subsystems: Rocker

13.1.2.2 Rear Rail Sub-System

The hydroformed rear rail solutions gave the maximum weight advantage, as illustrated in Figure 13.4. However, as explained earlier for the rocker solutions, these solutions were recommended as an aggressive approach solution, more feasible in the future. The hot stamped Laser Welded Blank (LWB) and hot stamped Tailor Rolled Blank (TRB) solutions had low material thicknesses in certain areas, as shown by the HEEDs runs. This would require a tailor quenching process, to achieve the required amount of material elongation for absorbing energy without premature failure of the rear rail during crash events. Hence, considering the current level of hot stamping technology being used for high volume production, the hot stamping solutions were recommended as a possibility in the future. So, the stamped LWB or TRB was the recommended technology for the rear rail sub-system.

The stamped TRB solution also showed the same CO₂e savings potential compared to the hydroformed rear rail sub-system as shown in Figure 13.4. The savings would be higher if the hydroforming Multiple Walled Tube (MWT) or Laser Welded Tube (LWT) solution is used, but this was recommended as a more practical solution with further development of the hydroforming technology in the future (2020 and beyond) considering design and assembly factors.

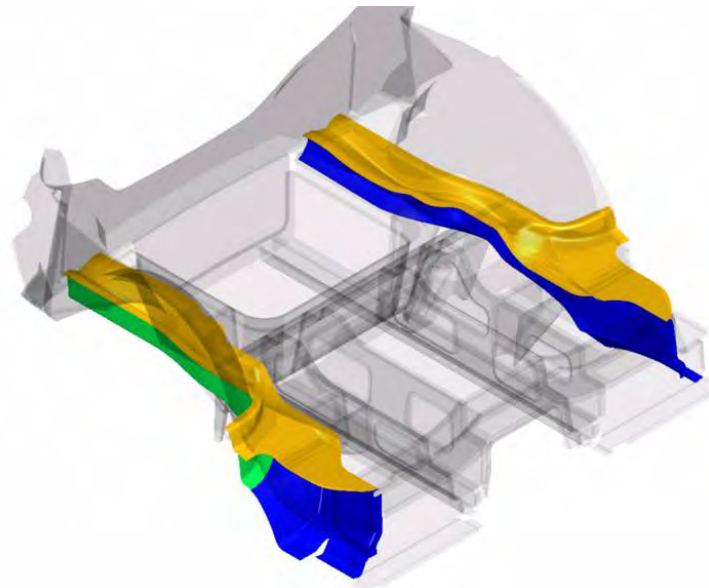
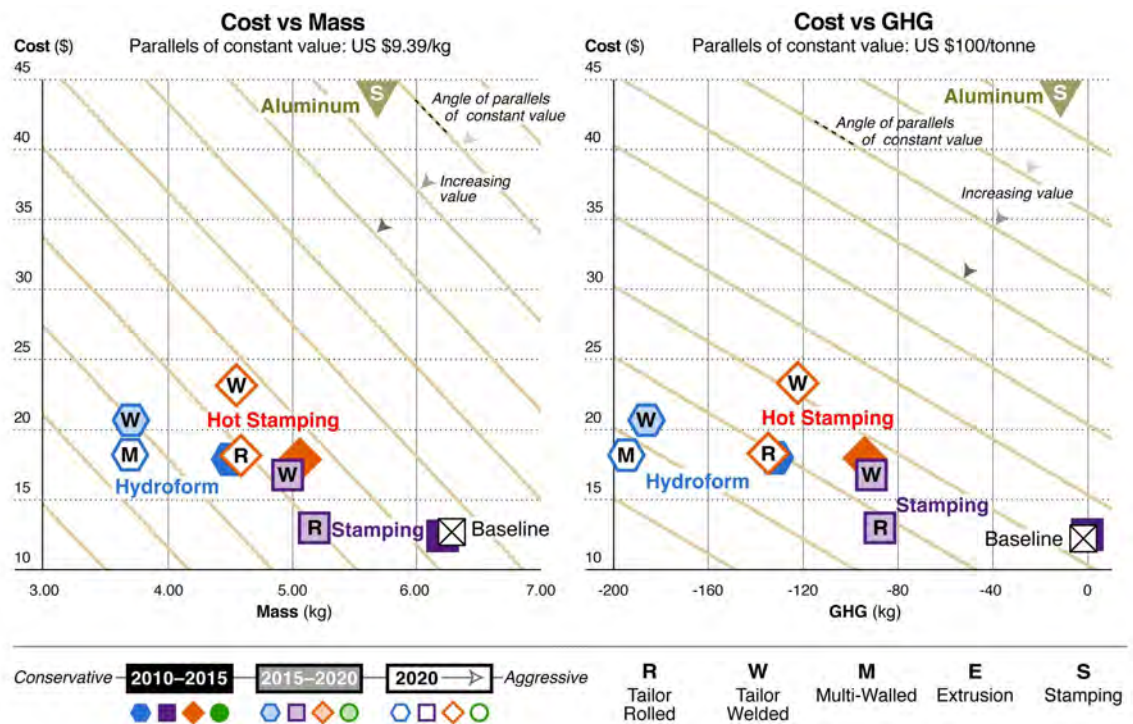
FSV Rear Rail HF3G Technology Assessment	FSV Rear Rail HF3G Manufacturing Interpretation		High Volume Manufacturing Feasibility	FSV Rear Rail Sub-System Mass (kg)	FSV Rear Rail Manufacturing Cost (\$)	FSV Rear Rail LCA CO ₂ e Savings (kg)
Baseline	B ST	Stamping		6.28	12.73	0
Stamping Solution	ST	Stamping		6.18	12.53	-8
	ST TRB	Stamping TRB		5.19	12.95	-86
	ST LWB	Stamping LWB		4.98	16.86	-92
	HST	Hot Stamp		5.06	17.88	-94
	HST TRB	Hot Stamp TRB		4.56	18.48	-133
	HST LWB	Hot Stamp LWB		4.56	23.34	-123
Hydroform	HF	HydroForm		4.51	17.94	-132
	HF LWT	Hydroform LWT		3.70	20.72	-186
	HF MWT	Hydroform MWT		3.70	18.22	-195
Aluminum	AL	Stamping		5.69	43.89	-11

(C) Conservative
 (M) Mid-term
 (A) Aggressive

* The mass, costs and LCA CO₂e savings shown above are only for one side of the vehicle

Table 13.2: T4 technology assessment results - Rear rail sub-system

The stamped LWB/TRB rear rail sub-system weighed 9.96 kg (4.98 kg each side), and the baseline sub-system weighed 12.6 kg.


Figure 13.3: FSV Phase-2 T4 rear rail stamped solution

Figure 13.4: T4 comparison FSV subsystems: Rear rail

13.1.2.3 B-Pillar Sub-System

The hot stamped Laser Welded Blank (LWB), B-pillar sub-system, with stamped single thickness B-pillar outer, gave the lowest mass solution. Although hot stamping technology is mature for high volume production, the use of laser welded blanks is not currently feasible. An alternative could be tailor-rolled blanks (TRB), but due to the shape of the B-pillar there was a negative impact on cost (material scrap is more due to nesting limitation in TRB compared to LWB). However, there are several examples of automotive Original Equipment Manufacturers (OEMs), considering this technology due to the mass savings factor. Moreover, taking into account the technological developments that could be achieved by manufacturing firms, by the timeframe of the FSV program (2015-2020); the hot stamped LWB was the recommended B-Pillar sub-system solution. The CO₂e savings were also higher for the hot stamped LWB/TRB compared to the other solutions as shown in Figure 13.6.

LWB/TRB was not considered as an option for the B-pillar outer solution because it is a part of the body side panel, and is a Class B surface.

FSV B-Pillar HF3G Technology Assessment	FSV B-Pillar HF3G Manufacturing Interpretation		High Volume Manufacturing Feasibility	FSV B-Pillar Sub-System Mass (kg)	FSV B-Pillar Manufacturing Cost (\$)	FSV B-Pillar LCA CO ₂ e Savings (kg)
Baseline	B ST	Stamping		8.79	30.84	0
Stamping Solution	ST	Stamping		6.25	22.17	-189
	ST TRB	Stamping TRB		5.95	30.37	-207
	ST LWB	Stamping LWB		5.95	23.57	-212
	HST	Hot Stamp		5.81	27.00	-224
	HST TRB	Hot Stamp TRB		5.48	34.48	-244
	HST LWB	Hot Stamp LWB		5.48	30.44	-247
Roll Form	RF	Roll Form		6.18	15.40	-213
Hydroform	HF LWT	Hydroform LWT		5.13	27.91	-274
Aluminum	AL	Stamping		4.69	58.95	-254

■ (C) Conservative
 ■ (M) Mid-term
 ■ (A) Aggressive

* The mass, costs and LCA CO₂e savings shown above are only for one side of the vehicle

Table 13.3: T4 technology assessment results - B-pillar sub-system

The hot stamped LWB B-pillar sub-system (with conventional B-pillar outer) showed a significant weight savings potential. The recommended FSV B-pillar sub-system weighed 10.96 kg (5.48 kg on each side), which was significantly lower compared to the baseline weight of 17.6 kg.

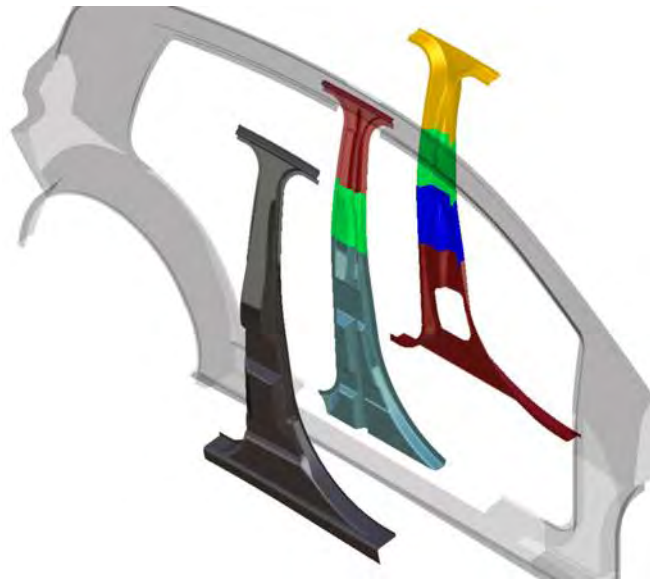


Figure 13.5: FSV Phase-2 T4 B-pillar stamped LWB solution

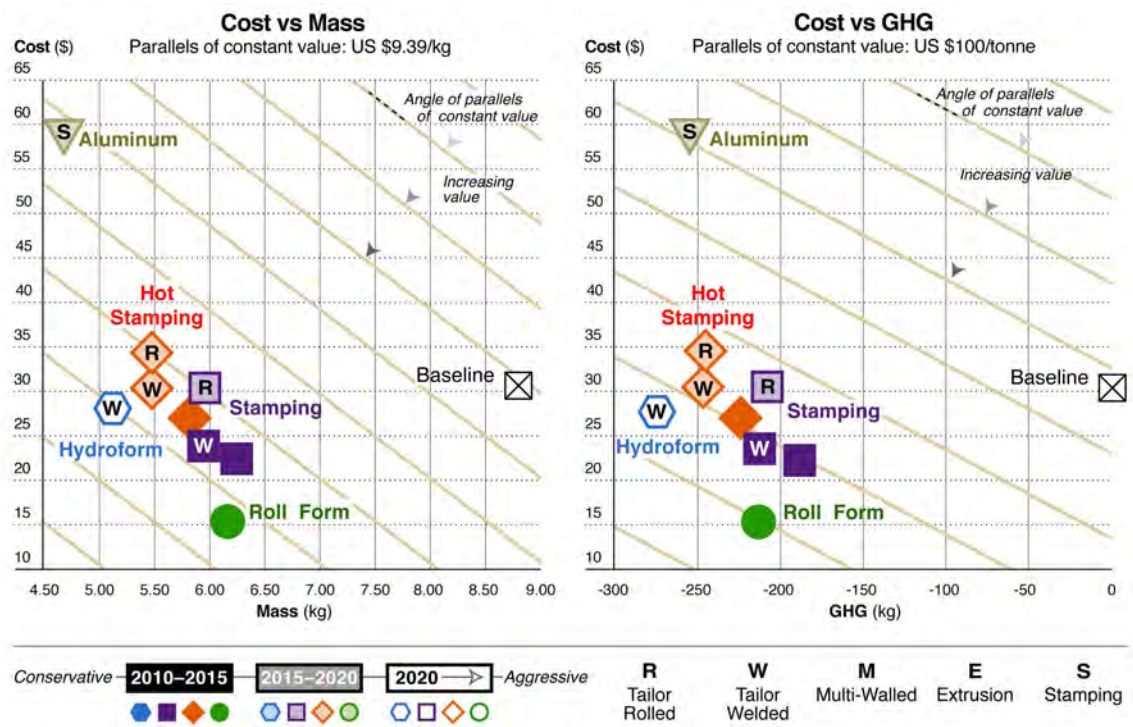


Figure 13.6: T4 comparison FSV subsystems: B-pillar

13.1.2.4 Roof Rail Sub-System

The hydroformed Multiple Walled Tube (MWT) and hot stamped LWB technologies gave the solutions with lowest mass and CO₂e for the roof rail sub-system, as shown in Figure 13.8. Considering the technical difficulties for manufacturing and design complexity, hot stamped LWB was the recommendation for the FSV roof rail sub-system. Hydroforming could be considered at a later stage with further developments in the technology; hence the hydroformed roof rail solution was chosen as an aggressive solution.

FSV Roof Rail HF3G Technology Assessment	FSV Roof Rail HF3G Manufacturing Interpretation		High Volume Manufacturing Feasibility	FSV Roof Rail Sub-System Mass (kg)	FSV Roof Rail Manufacturing Cost (\$)	FSV Roof Rail LCA CO ₂ e Savings (kg)
Baseline	B ST	Stamping		12.73	27.71	0
Stamping Solution	ST	Stamping		9.90	21.83	-219
	ST TRB	Stamping TRB		9.43	43.51	-244
	ST LWB	Stamping LWB		9.43	27.07	-246
	HST	Hot Stamp		9.74	29.70	-225
	HST TRB	Hot Stamp TRB		9.31	41.78	-250
	HST LWB	Hot Stamp LWB		9.31	31.71	-256
Hydroform	HF	HydroForm		9.35	26.28	-262
	HF LWT	Hydroform LWT		9.26	33.64	-256
	HF MWT	Hydroform MWT		9.26	27.29	-269
Aluminum	AL	Stamping		10.40	82.49	-109

■ (C) Conservative
 ■ (M) Mid-term
 ■ (A) Aggressive

* The mass, costs and LCA CO₂e savings shown above are only for one side of the vehicle

Table 13.4: T4 technology assessment results - Roof rail sub-system

The recommended FSV roof rail sub-system weighed 18.6 kg (9.3 kg for each side); lower than the baseline weight of 25.5 kg.



Figure 13.7: FSV Phase-2 T4 roof rail stamped solution

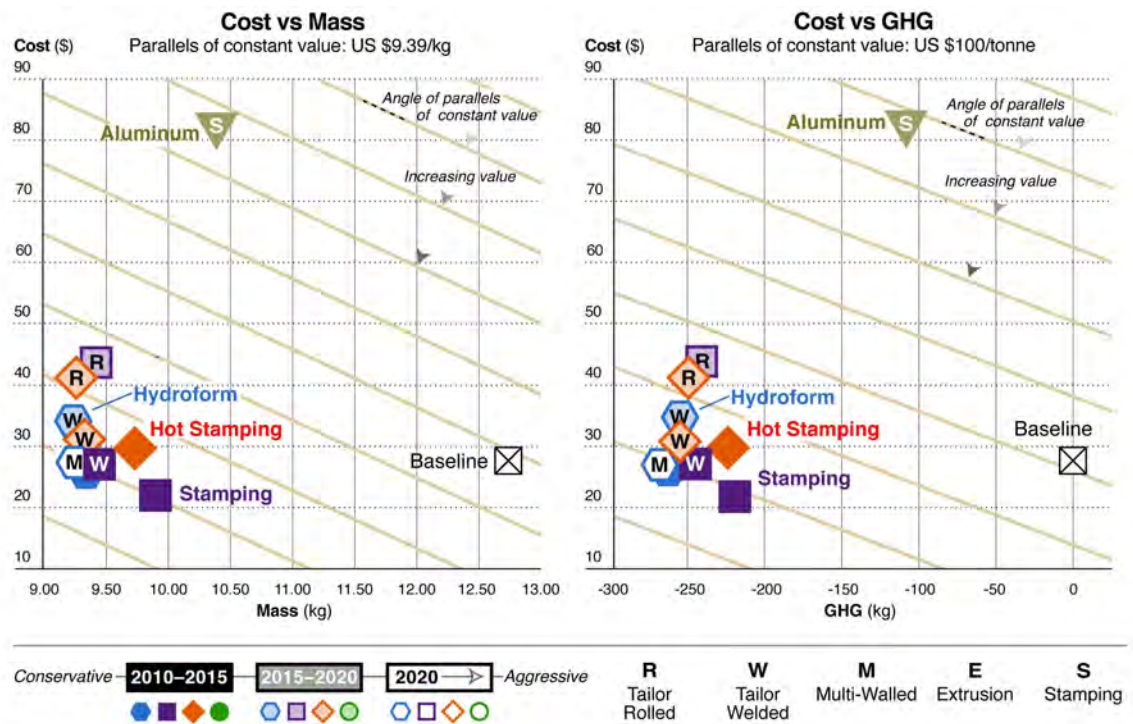


Figure 13.8: T4 comparison FSV subsystems: Roof rail

13.1.2.5 Shotgun Sub-System

Hot stamping LWB shotgun sub-system was the recommended solution due to the mass savings as shown in Figure 13.10. As these parts are required to absorb energy without premature failure, during the hot stamping process the parts are 'tailor quenched' to achieve the required amount of material elongation for this function. The formability of these parts was assessed using single step formability simulation (shown in Chapter 15). This recommended solution could pose minor difficulties with respect to high volume manufacturing, but choosing an alternative technology would result in a higher mass. The hot stamped LWB solution also showed the highest CO₂e savings compared to the other technologies.

- Conservative: Stamping LWB
- Mid-Term: Hot stamping LWB with tailor quench (shown in Figure 13.9)
- Aggressive: Hot Stamping LWB with tailor quench

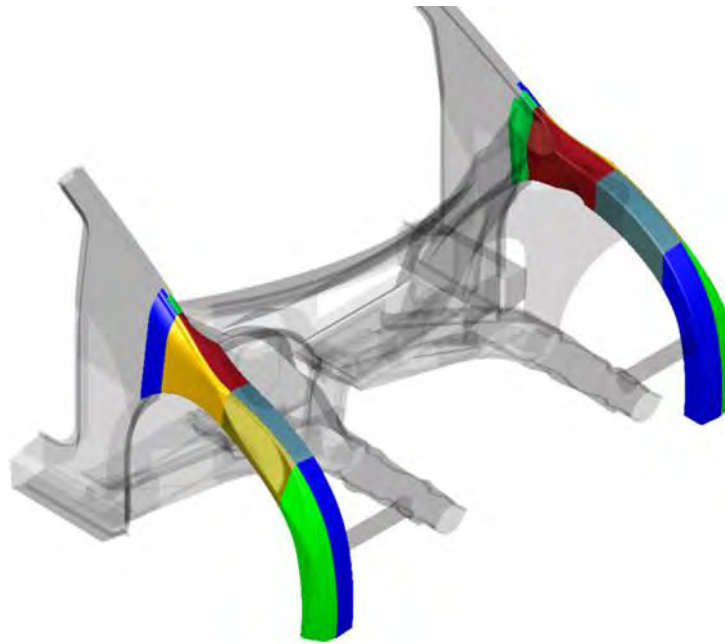
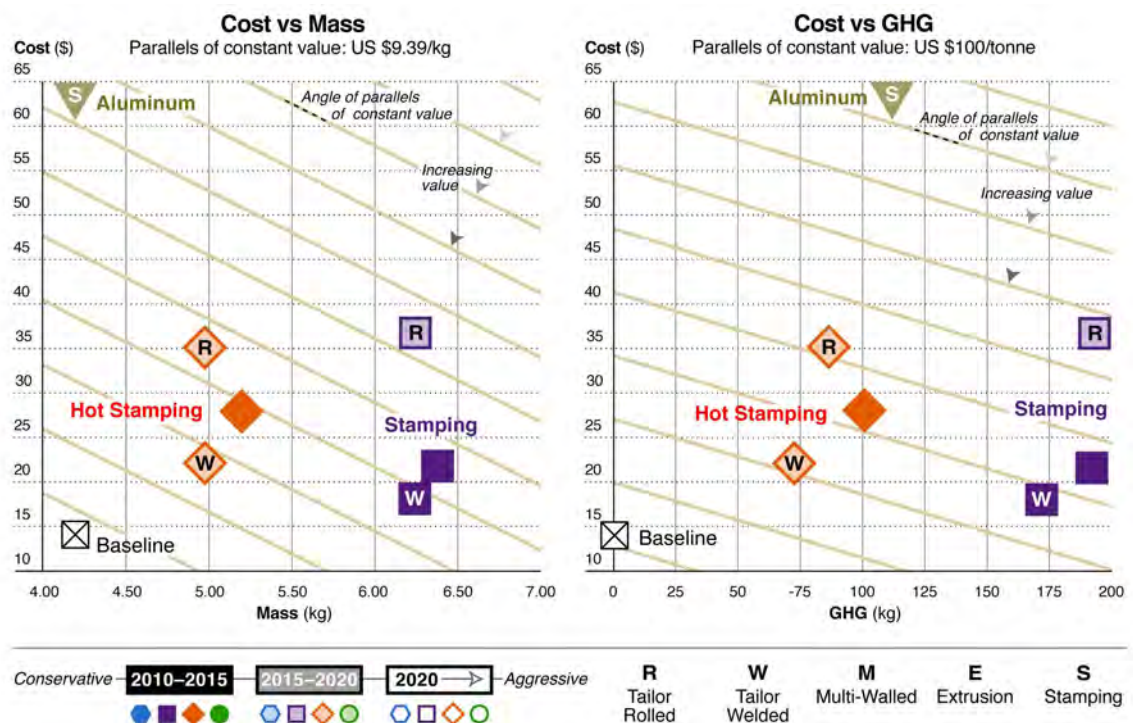
FSV Shotgun HF3G Technology Assessment	FSV Shotgun HF3G Manufacturing Interpretation		High Volume Manufacturing Feasibility	FSV Shotgun Sub-System Mass (kg)	FSV Shotgun Manufacturing Cost (\$)	FSV Shotgun LCA CO ₂ e Savings (kg)
Baseline	B ST	Stamping		4.2	14.24	0
Stamping Solution	ST	Stamping		6.37	21.58	192
	ST TRB	Stamping TRB		6.24	36.69	193
	ST LWB	Stamping LWB		6.24	18.09	172
	HST	Hot Stamp		5.20	27.92	101
	HST TRB	Hot Stamp TRB		4.98	35.11	86
	HST LWB	Hot Stamp LWB		4.98	22.11	73
Aluminum	AL	Stamping		4.21	63.34	112

(C) Conservative
 (M) Mid-term
 (A) Aggressive

* The mass, costs and LCA CO₂e savings shown above are only for one side of the vehicle

Table 13.5: T4 technology assessment results - Shotgun sub-system

The FSV Shotgun sub-system weight was 9.96 kg (4.98 kg on each side), and the baseline weight was 8.4 kg (4.2 kg on each side).


Figure 13.9: FSV Phase-2 T4 shotgun stamped LWB solution

Figure 13.10: T4 comparison FSV subsystems: Shotgun

13.1.2.6 Tunnel Sub-System

Rollformed tunnel sub-system was the recommended solution considering the low mass, high volume manufacturing feasibility, higher CO₂e savings, and higher CO₂e value (using \$100 $\frac{\text{USD}}{\text{tonne}}$ CO₂e premium), as illustrated in Figure 13.12.

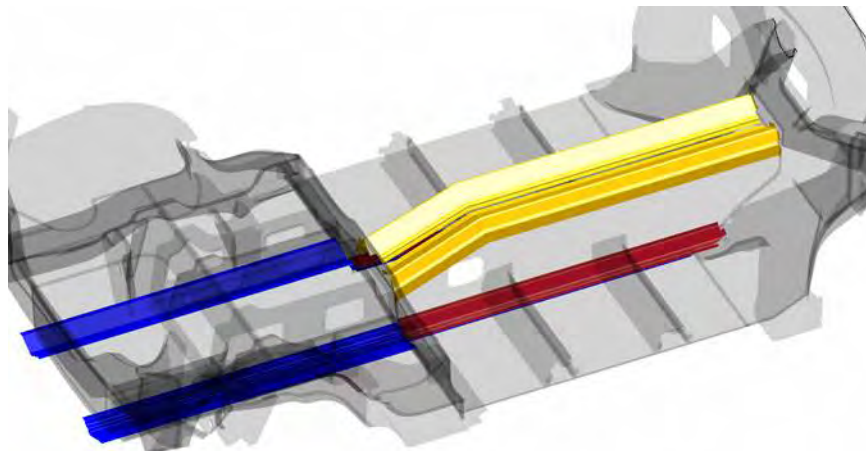
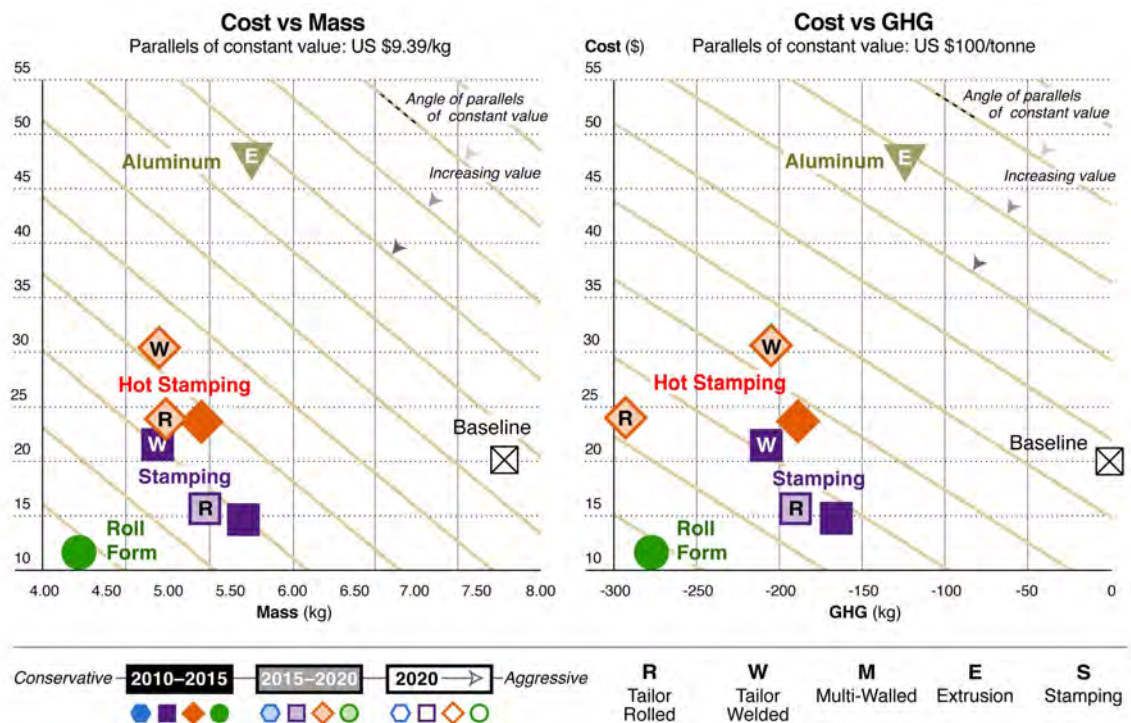
FSV Tunnel HF3G Technology Assessment	FSV Tunnel HF3G Manufacturing Interpretation		High Volume Manufacturing Feasibility	FSV Tunnel Sub-System Mass (kg)	FSV Tunnel Manufacturing Cost (\$)	FSV Tunnel LCA CO ₂ e Savings (kg)
Baseline	B ST	Stamping		7.72	20.2	0
Stamping Solution	ST	Stamping		5.61	14.67	-166
	ST TRB	Stamping TRB		5.31	15.59	-190
	ST LWB	Stamping LWB		4.92	21.45	-208
	HST	Hot Stamp		5.28	23.51	-189
	HST TRB	Hot Stamp TRB		5.00	23.82	-292
	HST LWB	Hot Stamp LWB		4.94	30.30	-205
	Roll Form	RF	Roll Form Open		4.29	11.56
Aluminum	AL	Stamping		5.68	47.78	-124

■ (C) Conservative
 ■ (M) Mid-term
 ■ (A) Aggressive

* The mass, costs and LCA CO₂e savings shown above are only for one side of the vehicle

Table 13.6: T4 technology assessment results - Tunnel sub-system

The recommended FSV Tunnel sub-system weighed 8.6 kg (4.3 kg on each side), significantly lower than the baseline Tunnel sub-system mass of 15.4 kg (7.7 kg on each side).


Figure 13.11: FSV Phase-2 T4 tunnel rollformed solution

Figure 13.12: T4 comparison FSV subsystems: Tunnel

13.1.2.7 Front Rail Sub-System

The stamped LWB front rail sub-system was the lowest mass solution and showed a higher value from a CO₂e savings perspective, as illustrated in Figure 13.14.

FSV Front Rail HF3G Technology Assessment	FSV Front Rail HF3G Manufacturing Interpretation		High Volume Manufacturing Feasibility	FSV Front Rail Sub-System Mass (kg)	FSV Front Rail Manufacturing Cost (\$)	FSV Front Rail LCA CO ₂ e Savings (kg)
Baseline	B ST	Stamping		6.24	28.91	0
Stamping Solution	ST LWB	Stamping LWB		6.46	29.93	48
	ST LWB 2	Stamping LWB C2		5.72	20.91	-65
Hydroform	HF LWT	Hydroform LWT		6.26	46.35	9
Aluminum	AL	Stamping		4.03	37.63	-103

■ (C) Conservative
 ■ (M) Mid-term
 ■ (A) Aggressive

* The mass, costs and LCA CO₂e savings shown above are only for one side of the vehicle

Table 13.7: T4 technology assessment results - Front rail sub-system

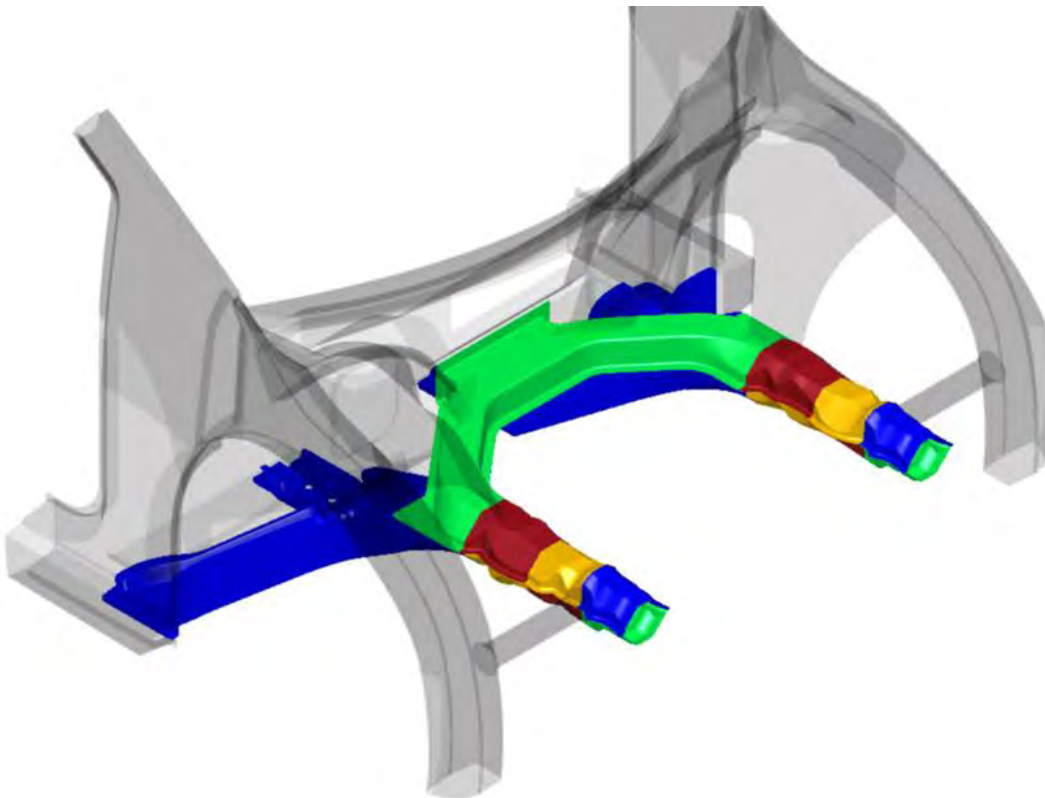


Figure 13.13: FSV Phase-2 T4 front rail stamped LWB solution

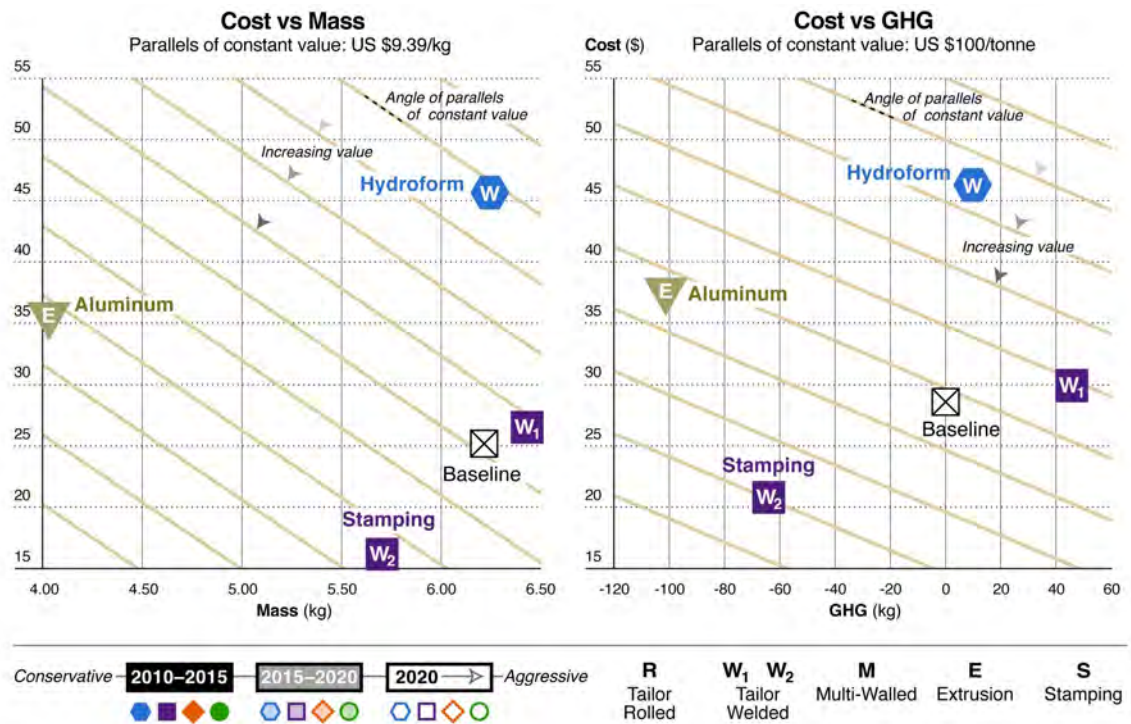


Figure 13.14: T4 comparison FSV subsystems: Front rail

13.1.2.8 Sub-System Selections Summary

The sub-systems selected for the FSV BEV are summarized in Table 13.8.


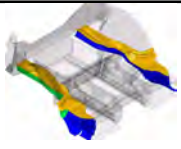


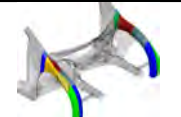

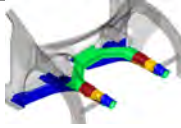
FSV Sub-system	FSV Selection (Mid-Term)	Baseline		FSV Selected Sub-system			
		Weight (kg)	Manufacturing Cost (\$ USD)	Weight (kg)	Manufacturing Cost (\$ USD)	LCA CO ₂ e Savings (kg)	Illustration
Rocker	Rollformed single thickness or rollformed TWC (with conventional outer)	10.26	\$19.99	7.98 / 8.07	\$14.27 / \$15.7	-183 / -177	
Rear Rail	Stamping LWB/TRB	6.28	\$12.73	4.98 / 5.19	\$16.86 / \$12.95	-92 / -86	
B-Pillar	Hot stamping LWB with conventional B-pillar outer	8.79	\$30.84	5.48	\$30.44	-247	
Roof Rail	Hot stamping LWB	12.73	\$27.71	9.31	\$31.71	-256	
Shotgun	Hot stamping LWB (with tailor quench)	4.2	\$14.24	4.98	\$22.11	73	
Tunnel	Open rollform	7.72	\$20.20	4.29	\$11.56	-277	
Front Rail	Stamped LWB	6.24	\$28.91	5.72	\$20.91	-65	

Table 13.8: FSV BEV sub-system selection summary

13.2 Sub-System Integration into Body Design

13.2.1 Rocker Sub-System

The chosen design for the FSV rocker was the 3G optimized rollformed solution as shown in Figure 13.1; a cross-section view of the 3G optimized rocker is shown in Figure 13.15.

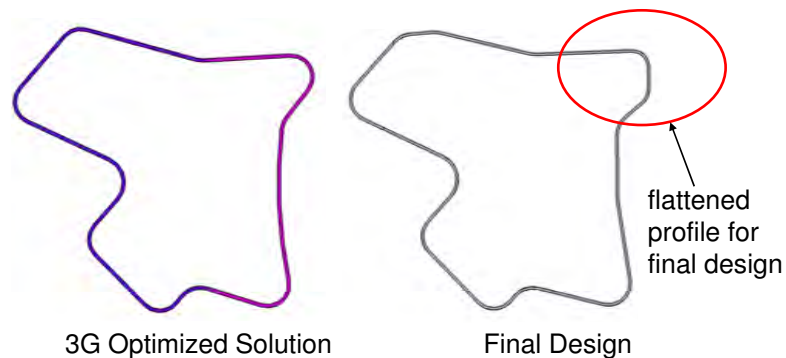


Figure 13.15: Cross-section of the rocker: 3G optimized solution and final design

As shown in Figure 13.15, the inner edge of the rocker was flattened (highlighted in the figure) to make it easier for integration with body side inner and seat cross members. The body side outer was designed to match the outer profile of the rocker as shown in Figure 13.17. Holes were added to the inner side of the rocker to aid the flow and drainage of electro-coat, as shown in Figure 13.16. The rocker outer is a part of the body side outer as shown in the figure.



Figure 13.16: Body side outer

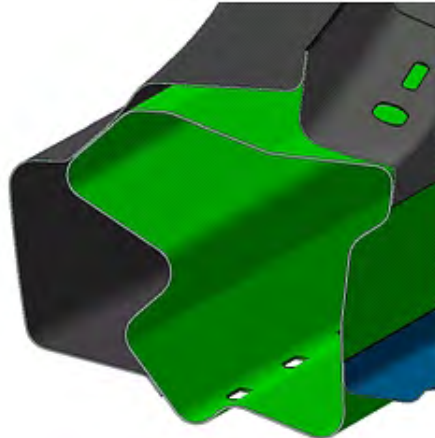


Figure 13.17: *Rocker integrated to the body side inner and body side outer*

13.2.2 B-Pillar Sub-System

The B-pillar sub-system is one of the critical components of the body side structure for meeting the side impact structural targets. The FSV B-pillar sub-system includes a full length B-pillar inner, made of Laser Welded Blank (LWB) high strength boron steel, integrated into the roof rail inner, as shown in Figure 13.18. From the chosen 3G optimized solutions, the top portion of the B-pillar inner was modified to accommodate hinges, latches, seat belt slide bar and D-ring attachment points, as shown in Figure 13.19. The lower portion of the B-pillar inner forms a bridge, between the rocker filler and the wheel house inner, as shown in Figure 13.20. As also shown in Figure 13.20, modifications were made to the B-pillar inner to accept the seat belt retention mechanism.

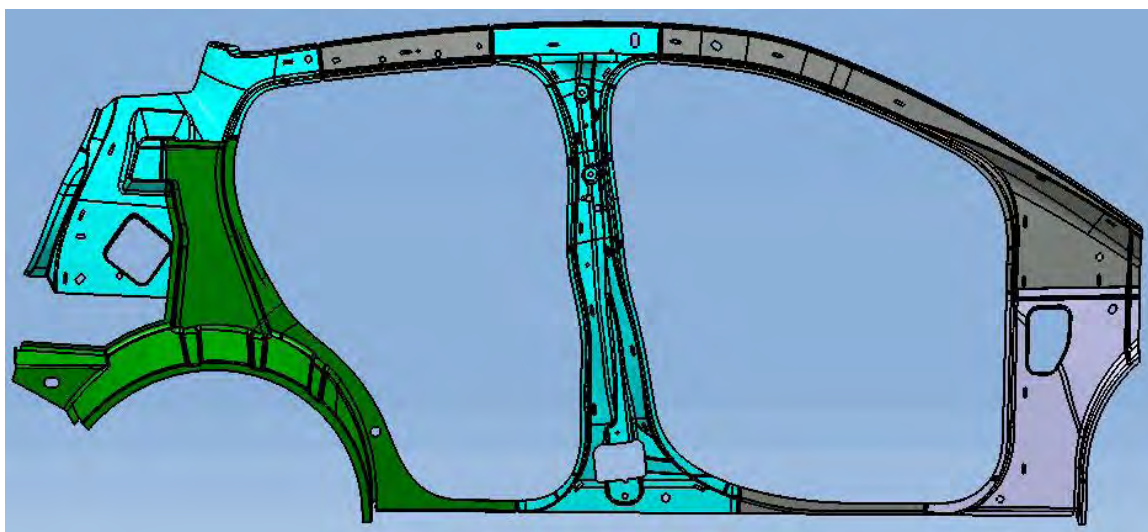


Figure 13.18: *B-pillar inner*

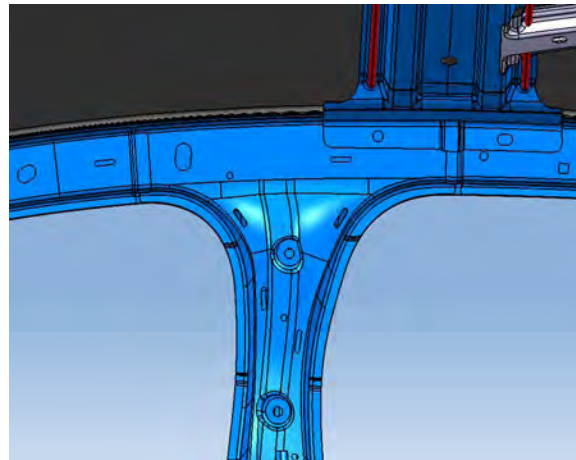


Figure 13.19: B-pillar D-ring attachment points



Figure 13.20: B-pillar lower portion (showing the feature for seat belt retention)

The B-pillar reinforcement is also a high strength boron steel component to minimize intrusion in crash events. The B-pillar reinforcement connects the rocker to the roof rail reinforcement, resulting in an inverted hat section profile with the B-pillar inner.

The profile of the B-pillar outer was also maintained similar to the one attained from 3G optimization, except the holes added to accommodate ancillary equipment such as door hinges, electrical wirings etc. The B-pillar outer is a part of the body side outer, as shown Figure 13.16.

13.2.3 Roof Rail Sub-System

The roof rail inner was divided into two sections, with the upper part of the B-pillar forming a bridge between the front and rear roof rail sections, as shown earlier in Figure 13.18. Compared to the roof rail inner attained from the chosen 3G optimized solution, design modifications were made to the front section of the roof rail inner final design to encapsulate the A-pillar. The roof rail reinforcement is a single piece component extending from the C-pillar to the A-pillar, similar to the 3G optimized solution. The design modifications made to the roof rail reinforcement were only at the joints to the adjoining components: A-Pillar, B-Pillar, and C-Pillar. The design of the roof rail outer was driven by the Class-A surface, as directed by styling. The roof rail outer is a part of the body side outer as shown in Figure 13.16 and Figure 13.21.

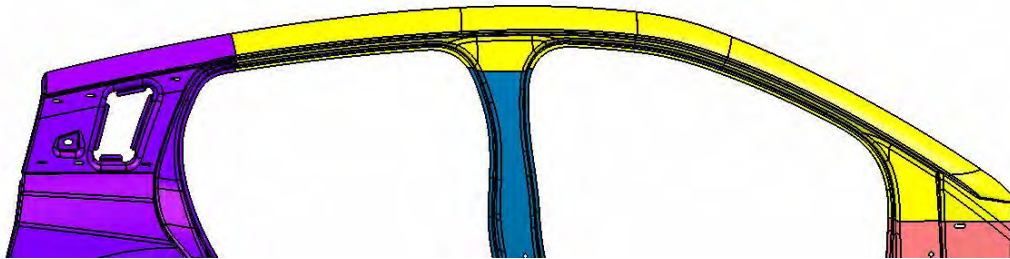


Figure 13.21: Roof rail outer shown as a part of the body side outer

13.2.4 Shotgun Sub-System

The shotgun sub-system design shows the most resemblance to the chosen 3G optimized solution. The center portion of the shotgun inner was reduced in the gauge due to the integration of the shock tower, as shown in Figure 13.22.

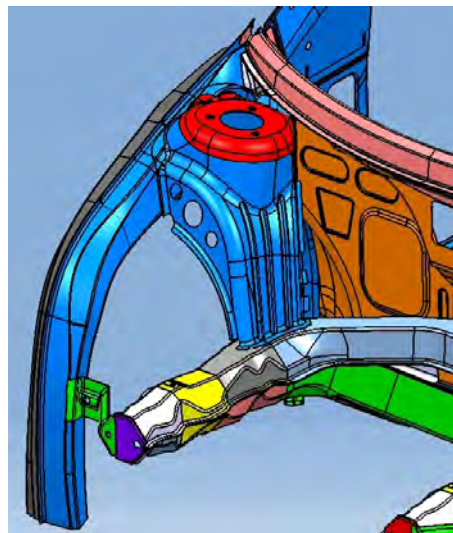


Figure 13.22: Shock tower integrated into the shotgun inner

The shotgun brace connects the shotgun inner to the front rail sub-system and prevents the outer movement of the shotgun inner during the assembly operation. The shotgun outer on each side of the vehicle, is welded to the respective body side outer and shotgun inner.

13.2.5 Tunnel Sub-System

The front floor assembly runs from the rear seat assembly to the dash toe panel. A tunnel in the floor pan provides clearance for the I-shaped battery. The selected 3G optimized solution for the FSV tunnel was the starting point for the design as shown in the Figure 13.23.

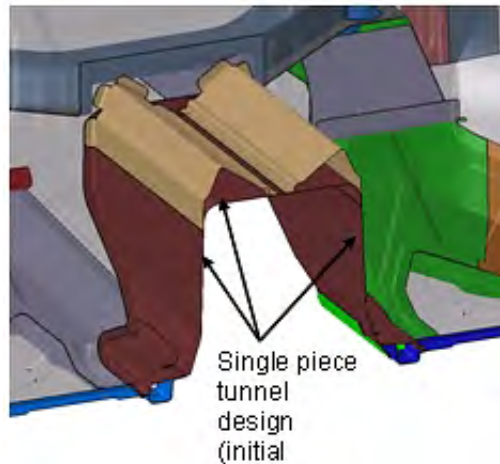


Figure 13.23: Tunnel sub-system initial design

As discussed in Section 13.1.2.6 (Tunnel Sub-System Selection), the preferred solution attained from the 3G optimization was open rollformed tunnel sub-system as shown in Figure 13.23. However, the formability analysis results showed that the one piece tunnel was not a feasible design. Moreover, strengthening of the side walls required additional stiffening beads, which necessitated the side walls to be designed as individually stamped parts as illustrated in Figure 13.24. Further, to reduce the assembly costs and to maintain a less complex sub-assembly/assembly structure, it was necessary to integrate the recommended tunnel design with the floor panel and the tunnel side panel. The integration was done such that the section geometry of the tunnel, attained from the 3G optimization was maintained. The tunnel top and the tunnel sides are welded in the tunnel sub-assembly which is integrated into the front floor LH/RH and the front dash assembly, as shown in Figure 13.24. The tunnel sides and the tunnel top were closed out with a tunnel reinforcement resulting in a box section as illustrated in Figure 13.24.

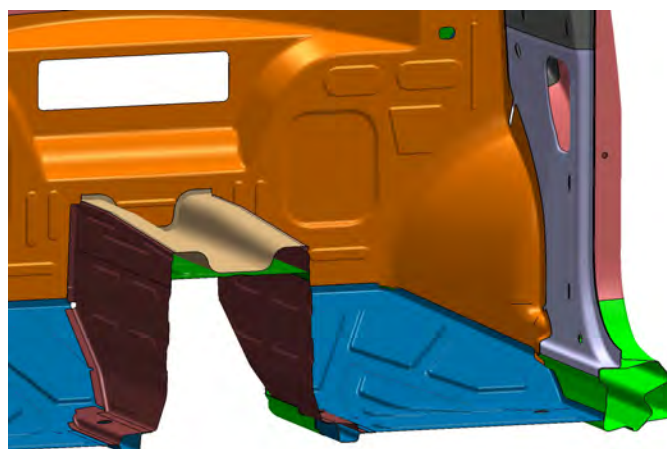


Figure 13.24: Tunnel sub-system current design

The side impact CAE simulations showed the critical loadpath was along the seat cross members,

perpendicular to the tunnel. Hence, it was necessary to add an additional stiffening feature along the critical loadpath within the tunnel sub-system. As shown in Figure 13.25, the tunnel bulkhead was added as an additional part to improve the side impact performance of the vehicle.

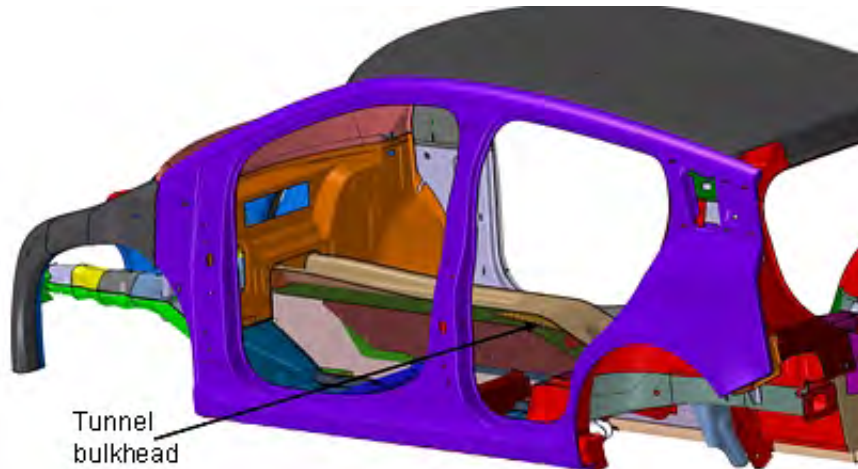


Figure 13.25: Tunnel sub-system shown with the tunnel bulkhead

13.2.6 Rear Rail Sub-System

The base design attained from the chosen 3G optimized solution was maintained for the rear rail sub-system; the necessary changes were made for the part manufacturability. The walls of the rear rail were designed to be flushed with the wheel house inner (shown in Figure 13.26). The lower surface of the rear rail was flattened locally where the rear suspension brackets were mounted. The rear rail reinforcement profile matched to support the seat pan, as shown in the Figure 13.27.

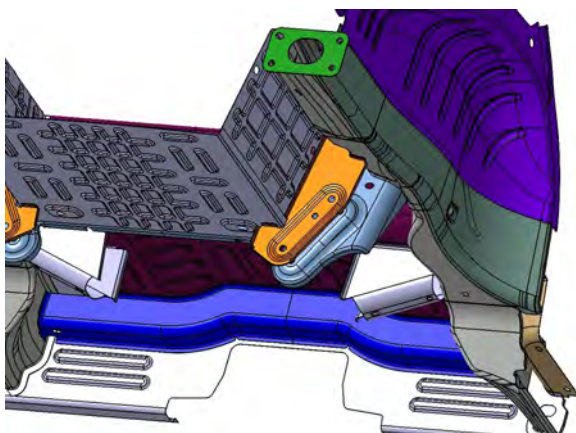


Figure 13.26: Rear rail inner (flushed with wheel house inner)

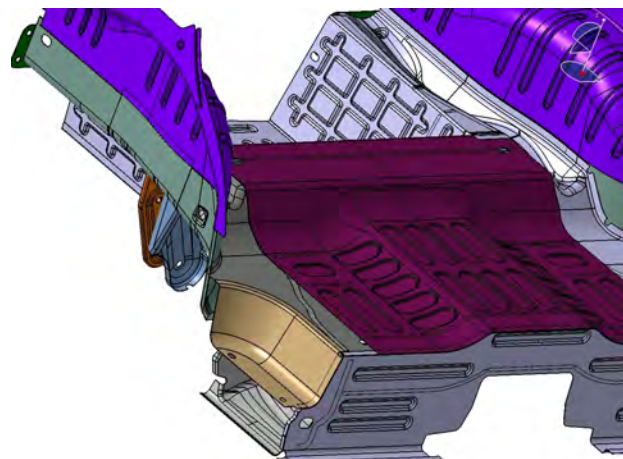


Figure 13.27: Rear rail reinforcement and seat pan

13.2.7 Front Rail Sub-System

The front rail concept chosen from the 3G optimized solutions was a 4-piece design as discussed in Section 13.1.2.7 (Front Rail Sub-System Selection). The upper rail for each side of the vehicle was combined into a single part to form a horse shoe shaped design as shown in Figure 13.28. The lower rails on each side were extended to integrate with the front floor assembly. The V-shaped ends of the lower rails (shown in Figure 13.29) are similar in concept to the chosen optimized solution; however design changes were made for better integration and manufacturability. Both the upper and lower rails are tailor welded stampings. The front rail assembly is made up of three separate sub-assemblies: the front lower sub-assemblies (left hand and right hand), and the front upper sub-assemblies. The dash assembly and the front rail assembly are assembled together to form the front structure assembly.

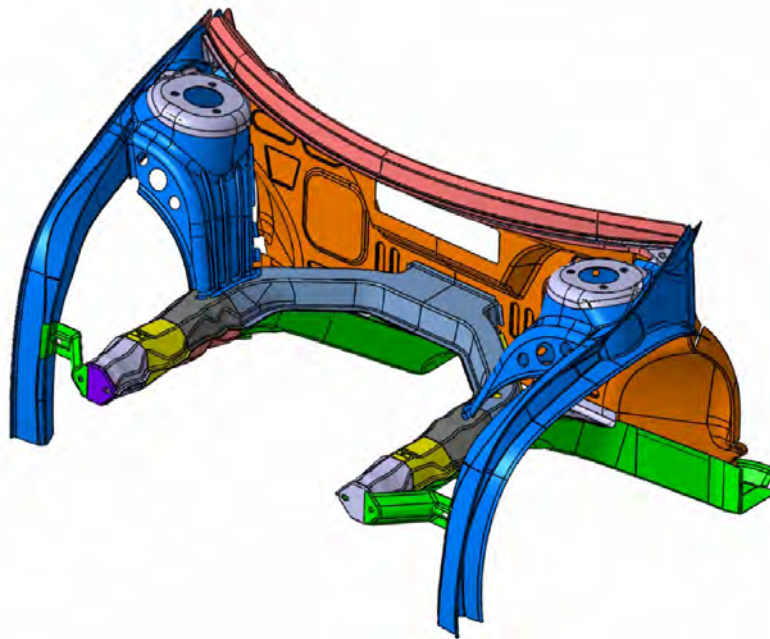


Figure 13.28: Front rail sub-system (final design)

Several iterations of packaging studies were done to accommodate the front suspension design and to improve the frontal impact performance. This also resulted in corresponding changes to the front rail at the interfacing joints to the front shock tower and the shotguns. Similarly, the A-Brace was added to improve the frontal crash energy management (illustrated in Figure 13.29). The front end of the front rail sub-system is closed out by the crash can mounting plate and the shotgun brace. The shotgun brace stabilizes the shotgun in a cross car axes during the assembly process. The rear end of the front rail sub-system is closed by closing plates welded onto the dash panel.

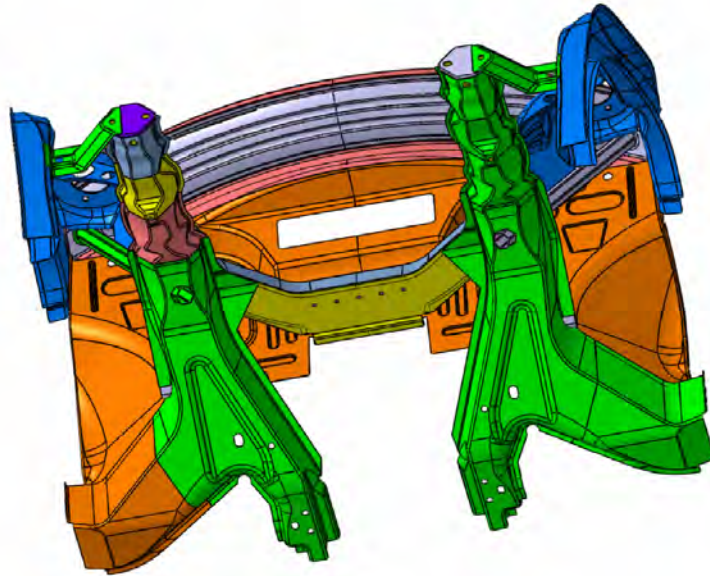


Figure 13.29: Front rail lower rail shown in the front rail sub-system

13.2.8 Final BEV Body Structure Design

The final design of the BEV body structure is shown in Figure 13.30. The material mix is shown in Table 13.9 and Figure 13.31.

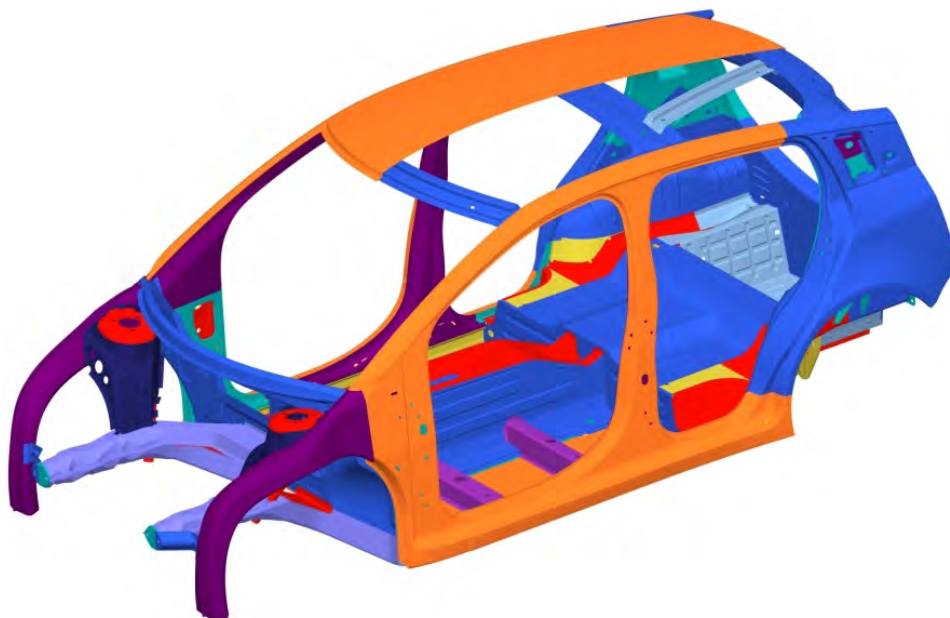
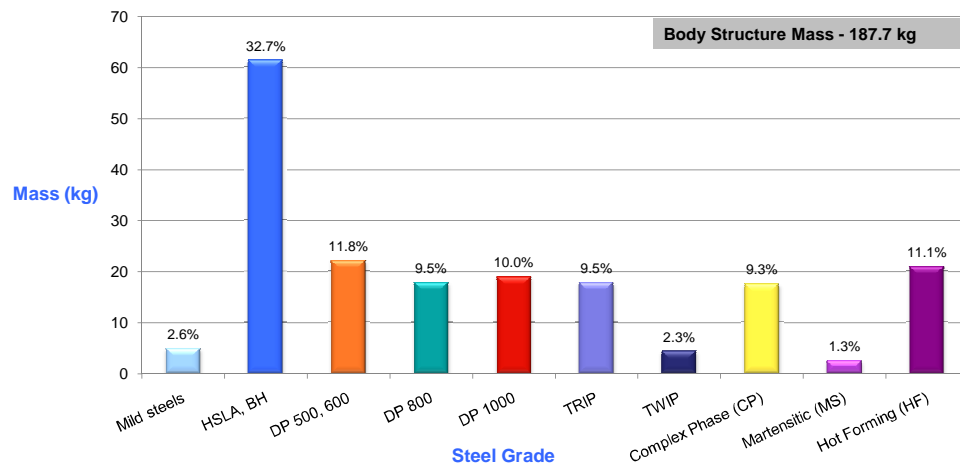


Figure 13.30: BEV final body structure design

Steels: corresponding metallurgical classes	Color Code	BEV Mix (%)
Low Strength Steels: Mild Steels		2.6
High Strength Steels (HSS): HSLA, BH		32.7
DP 500, 600		11.8
DP 800		9.5
DP 1000		10.0
TRIP		9.5
TWIP		2.3
Complex Phase (CP)		9.3
Martensitic (MS)		1.3
Hot forming (HF)		11.1

Table 13.9: BEV body structure material mix

Figure 13.31: BEV body structure material mix

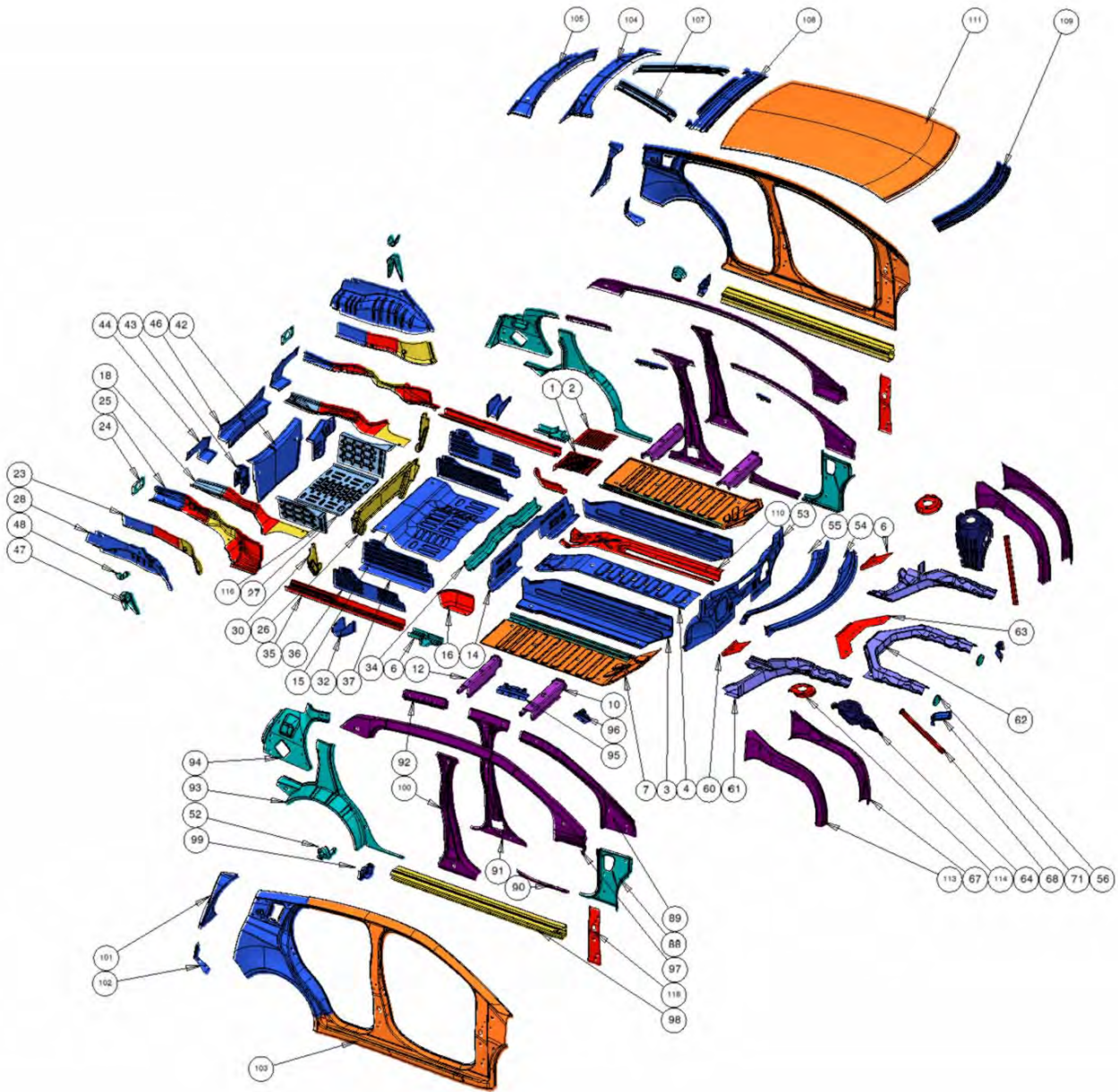


Figure 13.32: BEV exploded view

The FSV BEV parts lists showing material grades, thickness and mass are shown in Table 13.10 Table 13.11.

Part No	Part Description	Forming	Grade	Yeild (MPa)	Tensile (MPa)	Thickness (mm)	Mass (kg)	Total Mass (kg)
1	50.1 0401 Bulkhead Lower - Tunnel	S	DP	700	1000	0.80	0.679	0.679
2	50.1 0400 Bulkhead Upper - Tunnel	S	DP	700	1000	0.80	0.543	0.543
3	50.1 0402 Panel - Tunnel Side RH	S	BH	280	400	0.50	2.342	2.342
4	50.1 0404 Reinf - Tunnel Top	S	BH	280	400	0.50	1.713	1.713
5	50.1 0403 Panel - Tunnel Side LH	S	BH	280	400	0.50	2.342	2.342
6	50.1 0321 Tunnel Rail Bulkhead RH	S	DP	500	800	1.00	0.381	0.381
7	50.1 0011 Floor - Front RH	S	DP	300	500	0.50	2.84	4.61
			DP	500	800	1.50	1.77	
8	50.1 0322 Tunnel Rail Bulkhead LH	S	DP	500	800	1.00	0.381	0.381
9	50.1 0025 Floor - Front LH	S	DP	300	500	0.50	2.84	4.61
			DP	500	800	1.50	1.77	
10	50.1 0093 Crossmember - Front Seat RH Front	RF	MS	950	1200	0.50	0.542	0.542
11	50.1 0094 Crossmember - Front Seat LH Front	RF	MS	950	1200	0.50	0.542	0.542
12	50.1 0095 Crossmember - Front Seat RH Rear	RF	MS	950	1200	0.60	0.688	0.688
13	50.1 0096 Crossmember - Front Seat LH Rear	RF	MS	950	1200	0.60	0.688	0.688
14	50.1 0100 Heel Board	S	BH	210	340	0.60	1.603	1.603
15	50.1 0016 Seat Pan - Rear	S	BH	210	340	0.50	2.919	2.919
16	50.1 0099 Panel - Seat Side RH	S	DP	700	1000	0.70	0.359	0.359
17	50.1 0101 Panel - Seat Side LH	S	DP	700	1000	0.70	0.359	0.359
18	50.1 0109 Reinf - Frame Rail Rear RH	S	CP	1000	1200	1.10	0.361	1.555
			DP	700	1000	0.65	0.528	
			Mild	140	270	1.55	0.666	
19	50.1 0110 Reinf - Frame Rail Rear LH	S	CP	1000	1200	1.10	0.361	1.555
			DP	700	1000	0.65	0.528	
			Mild	140	270	1.55	0.666	
20	50.1 0015 Frame Rail - Outer Rear LH	S	CP	1000	1200	0.60	0.304	1.037
			DP	700	1000	1.40	0.469	
			HSLA	350	450	0.80	0.264	
21	50.1 0334 Mounting Plate - Crush Can Rear LH	S	DP	500	1200	1.20	0.132	0.132
22	50.1 0336 Frame Rail - Inr Rear LH	S	CP	1000	1200	0.60	0.247	2.635
			DP	700	1000	1.40	1.963	
			HSLA	350	450	0.80	0.425	
23	50.1 0014 Frame Rail - Outer Rear RH	S	CP	1000	1200	0.60	0.304	1.037
			DP	700	1000	1.40	0.469	
			HSLA	350	450	0.80	0.264	
24	50.1 0333 Mounting Plate - Crush Can Rear RH	S	DP	500	800	1.20	0.132	0.132
25	50.1 0335 Frame Rail - Inr Rear RH	S	CP	1000	1200	0.60	0.247	2.635
			DP	700	1000	1.40	1.963	
			HSLA	350	450	0.80	0.425	
26	50.1 0032 Crossmember - Battery and Suspension	S	CP	800	1000	1.00	2.944	2.944
27	50.1 0330 Panel - Cargo Box Floor	S	Mild	140	270	0.50	1.326	1.326
28	50.1 0017 Wheelhouse Inner - Rear RH	S	BH	210	340	0.70	0.835	2.58
			BH	210	340	1.20	1.745	
29	50.1 0018 Wheelhouse Inner - Rear LH	S	BH	210	340	0.70	0.835	2.58
			BH	210	340	1.20	1.745	
30	50.1 0079 Brkt - Rear Suspension RH	S	CP	800	1000	1.00	0.342	0.342
31	50.1 0080 Brkt - Rear Suspension LH	S	CP	800	1000	1.00	0.342	0.342
32	50.1 0077 Gusset - Rear RH	S	BH	210	340	1.00	0.465	0.465
33	50.1 0078 Gusset - Rear LH	S	BH	210	340	1.00	0.465	0.465
34	50.1 0320 Rail - Side to Side	S	DP	500	800	0.80	1.074	1.074
35	50.1 0108 Rail - Longitudinal RR RH	S	DP	700	1000	1.20	2.201	2.201
36	50.1 0075 Close Off - Battery Otr RH	S	BH	210	340	0.60	0.805	0.805
37	50.1 0073 Close Off - Battery Inr RH	S	BH	210	340	0.60	1.195	1.195
38	50.1 0107 Rail - Longitudinal RR LH	S	DP	700	1000	1.20	2.201	2.201
39	50.1 0076 Close Off - Battery Otr LH	S	BH	210	340	0.60	0.805	0.805
40	50.1 0074 Close Off - Battery Inr LH	S	BH	210	340	0.60	1.195	1.195
41	50.1 0329 Pnl - Rear Liftgate Lower Inr LH	S	BH	210	340	1.00	0.585	0.585
42	50.1 0013 Pnl - Rear Liftgate Lower Inr	S	BH	210	340	0.70	1.866	1.866
43	50.1 0328 Pnl - Rear Liftgate Lower Inr RH	S	BH	210	340	1.00	0.585	0.585
44	50.1 0019 Panel - Back Outboard RH	S	BH	210	340	1.00	0.577	0.577
45	50.1 0025 Panel - Back Outboard LH	S	BH	210	340	1.00	0.577	0.577
46	50.1 0020 Panel - Back Lower	S	BH	210	340	1.00	1.405	1.405
47	50.1 2601 Mount - Rear Shock RH	S	DP	500	800	2.50	0.566	0.566
48	50.1 2602 Reinf - Rear Shock RH	S	DP	500	800	2.00	0.176	0.176
49	50.1 2701 Reinf - Rear Shock LH	S	DP	500	800	2.00	0.176	0.176
50	50.1 2702 Mount - Rear Shock LH	S	DP	500	800	2.50	0.566	0.566
51	50.1 2001 Mount - Trailing Arm LH	S	DP	500	800	2.00	0.37	0.37
52	50.1 2002 Mount - Trailing Arm RH	S	DP	500	800	2.00	0.37	0.37
53	50.1 0001 Dash - Toe Pan	S	BH	280	400	0.50	2.839	2.839
54	50.1 0002 Cowl Upper	S	BH	210	340	1.00	0.866	2.268
			BH	210	340	0.60	1.402	
55	50.1 0070 Cowl Lower	S	BH	210	340	1.20	0.709	1.494
			BH	210	340	0.60	0.785	
56	60.2 0007 Mounting Plate - Crush Can Front RH	S	DP	500	800	1.75	0.121	0.121
57	60.2 0008 Mounting Plate - Crush Can Front LH	S	DP	500	800	1.75	0.121	0.121
58	50.1 0306 Closeout - Lower Rail LH	S	DP	700	1000	0.80	0.309	0.309
59	50.1 0302 Front Rail - Lower LH	S	TRIP	600	980	1.90	0.359	5.998
			TRIP	600	980	2.00	0.419	
			TRIP	600	980	1.90	0.535	
			TRIP	600	980	1.80	4.685	

Table 13.10: FSV BEV Bill of Materials (BOM)

Part No	Part Description	Forming	Grade	Yield (MPa)	Tensile (MPa)	Thickness (mm)	Mass (kg)	Total Mass (kg)
60	50.1 0305 Closeout - Lower Rail RH	S	DP 700	1000	0.80	0.309	0.309	
61	50.1 0301 Front Rail - Lower RH	S	TRIP 600	980	1.90	0.359	5.998	
			TRIP 600	980	2.00	0.419		
			TRIP 600	980	1.90	0.535		
			TRIP 600	980	1.80	4.685		
62	50.1 0303 Front Rail - Upper	S	TRIP 600	980	1.80	0.667	5.743	
			TRIP 600	980	2.00	0.811		
			TRIP 600	980	1.80	4.265		
63	50.1 0304 Closeout - Upper Rail	S	DP 700	1000	1.00	0.616	0.616	
64	50.1 0044 Shock Tower - Frt RH	S	TWIP 500	980	1.00	1.457	1.457	
65	50.1 0063 Shock Tower - Frt LH	S	TWIP 500	980	1.00	1.457	1.457	
66	50.1 0022 Shotgun Inner LH	HS	HF 1050	1500	1.20	0.476	2.15	
			HF 1050	1500	0.80	0.759		
			HF 1050	1500	1.50	0.915		
67	50.1 0021 Shotgun Inner RH	HS	HF 1050	1500	1.20	0.476	2.15	
			HF 1050	1500	0.80	0.759		
			HF 1050	1500	1.50	0.915		
68	50.1 0326 A-Pillar Brace	RF	DP 700	1000	1.20	0.695	0.695	
69	50.1 0326 A-Pillar Brace LH	RF	DP 700	1000	1.20	0.695	0.695	
70	50.1 0318 Shotgun Brace LH	S	BH 210	340	1.20	0.206	0.206	
71	50.1 0308 Shotgun Brace RH	S	BH 210	340	1.20	0.206	0.206	
72	50.6 0023 Roof Rail Inner Front LH	HS	HF 1050	1500	0.70	0.84	1.171	
			HF 1050	1500	0.95	0.331		
73	50.6 0064 FBHP Inner LH	S	DP 500	800	1.20	1.667	1.667	
74	50.6 0056 Rocker Filler Front LH	S	BH 210	340	0.60	0.199	0.199	
75	50.6 0017 B-Pillar Inner LH	HS	HF 1050	1500	0.80	0.547	1.491	
			HF 1050	1500	0.60	0.944		
76	50.6 0053 Roof Rail Inner Rear LH	S	BH 210	340	1.10	0.372	0.372	
77	50.1 0067 Panel - Wheel House Outer LH	S	DP 500	800	0.65	1.732	1.732	
78	50.6 0004 C-Pillar Inner LH	S	DP 500	800	0.70	1.428	1.428	
79	50.2 0034 Bracket - Roof Rail to Header LH	S	BH 210	340	1.00	0.103	0.103	
80	50.2 0035 Bracket - Roof Rail to Roof Bow LH	S	BH 210	340	1.00	0.254	0.254	
81	50.6 0018 Reinf - Roof Rail LH	HS	HF 1050	1500	0.70	2.049	2.049	
82	50.6 0066 Rocker RH	RF	CP 1050	1470	1.00	6.032	6.032	
83	50.6 0072 Rocker Cap LH	S	BH 210	340	0.85	0.244	0.244	
84	50.6 0028 Reinf - B-Pillar LH	HS	HF 1050	1500	0.60	0.547	1.491	
			HF 1050	1500	1.00	0.944		
			DP 350	600	0.80	8.189		
85	50.6 0006 Body Side Outer LH	S	BH 210	340	0.60	2.739	10.928	
			BH 210	340	1.20	0.198		
86	50.6 0069 Panel Rear Quarter Lwr LH	S	BH 210	340	1.00	0.795	0.795	
87	50.6 0051 Panel - Gutter Rear LH	S	BH 210	340	1.00	0.795	0.795	
88	50.6 0046 FBHP Inner RH	S	DP 500	800	1.20	1.667	1.667	
89	50.6 0022 Roof Rail Inner Front RH	HS	HF 1050	1500	0.70	0.84	1.171	
			HF 1050	1500	0.95	0.331		
90	50.6 0055 Rocker Filler Front RH	S	BH 210	340	0.60	0.199	0.199	
91	50.6 0009 B-Pillar Inner RH	HS	HF 1050	1500	0.80	0.547	1.491	
			HF 1050	1500	0.60	0.944		
92	50.6 0052 Roof Rail Inner Rear RH	S	BH 210	340	1.10	0.372	0.372	
93	50.1 0049 Panel - Wheel House Outer RH	S	DP 500	800	0.65	1.732	1.732	
94	50.6 0005 C-Pillar Inner RH	S	DP 500	800	0.70	1.428	1.428	
95	50.2 0033 Bracket - Roof Rail to Roof Bow RH	S	BH 210	340	1.00	0.254	0.254	
96	50.2 0032 Bracket - Roof Rail to Header RH	S	BH 210	340	1.00	0.103	0.103	
97	50.6 0012 Reinf - Roof Rail RH	S	HF 1050	1500	0.70	2.049	2.049	
98	50.6 0048 Rocker RH	RF	CP 1050	1470	1.00	6.032	6.032	
99	50.6 0071 Rocker Cap RH	S	BH 210	340	0.85	0.244	0.244	
100	50.6 0026 Reinf - B-Pillar RH	HS	HF 1050	1500	0.60	0.547	1.491	
			HF 1050	1500	1.00	0.944		
101	50.6 0050 Panel - Gutter Rear RH	S	BH 210	340	1.00	0.795	0.795	
102	50.6 0068 Panel Rear Quarter Lwr RH	S	BH 210	340	1.20	0.198	0.198	
103	50.6 0002 Body Side Outer RH	S	DP 350	600	0.80	8.189	10.928	
			BH 210	340	0.60	2.739		
104	50.2 0007 Rear Header Reinf	S	BH 210	340	2.00	2.759	3.775	
			BH 210	340	0.70	1.016		
105	50.2 0006 Rear Header	S	BH 210	340	0.70	1.662	1.662	
106	50.2 0009 Support - Roof LH	S	Mild 140	270	0.50	0.463	0.463	
107	50.2 0008 Support - Roof RH	S	Mild 140	270	0.50	0.463	0.463	
108	50.2 0013 Roof Bow	RF	BH 210	340	0.50	0.941	0.941	
109	50.2 0011 Header - Roof Front	RF	BH 210	340	0.80	1.131	1.131	
110	50.1 0405 Top Panel - Tunnel	S	DP 1150	1270	1.00	3.067	3.067	
111	50.2 0010 Pnl - Roof Outer	S	BH 210	340	0.50	9.011	9.011	
112	50.1 0069 Shotgun Outer LH	HS	HF 1050	1500	1.00	0.431	2.088	
			HF 1050	1500	0.80	0.689		
			HF 1050	1500	1.50	0.968		
113	50.1 0051 Shotgun Outer RH	HS	HF 1050	1500	1.00	0.431	2.088	
			HF 1050	1500	0.80	0.689		
			HF 1050	1500	1.50	0.968		
114	50.1 3002 Reinf - Shock Tower Frt	S	DP 500	980	2.00	0.69	0.69	
115	50.1 3003 Reinf - Shock Tower Frt	S	DP 500	980	2.00	0.69	0.69	
116	50.1 2112 Panel - Cargo Box Side RH	S	Mild 140	270	0.50	0.611	0.611	
117	50.1 2113 Panel - Cargo Box Side LH	S	Mild 140	270	0.50	0.611	0.611	
118	50.6 6354 Reinf - FBHP RH	S	DP 700	1000	0.80	0.453	0.453	
119	50.6 1354 Reinf - FBHP LH	S	DP 700	1000	0.80	0.453	0.453	
Total							187.7	187.7

Table 13.11: FSV BEV Bill of Materials (BOM) (contd.)

13.3 Body Structure Assembly and Joining Methods

13.3.1 Joining Methods

Integral to the body assembly is the selection of the part joining process. To a lesser degree this will determine the assembly process and the equipment required to complete the body structure. There are number of joining techniques generally available to complete the body structure. See Figure 13.33 for the FSV joining process portfolio.

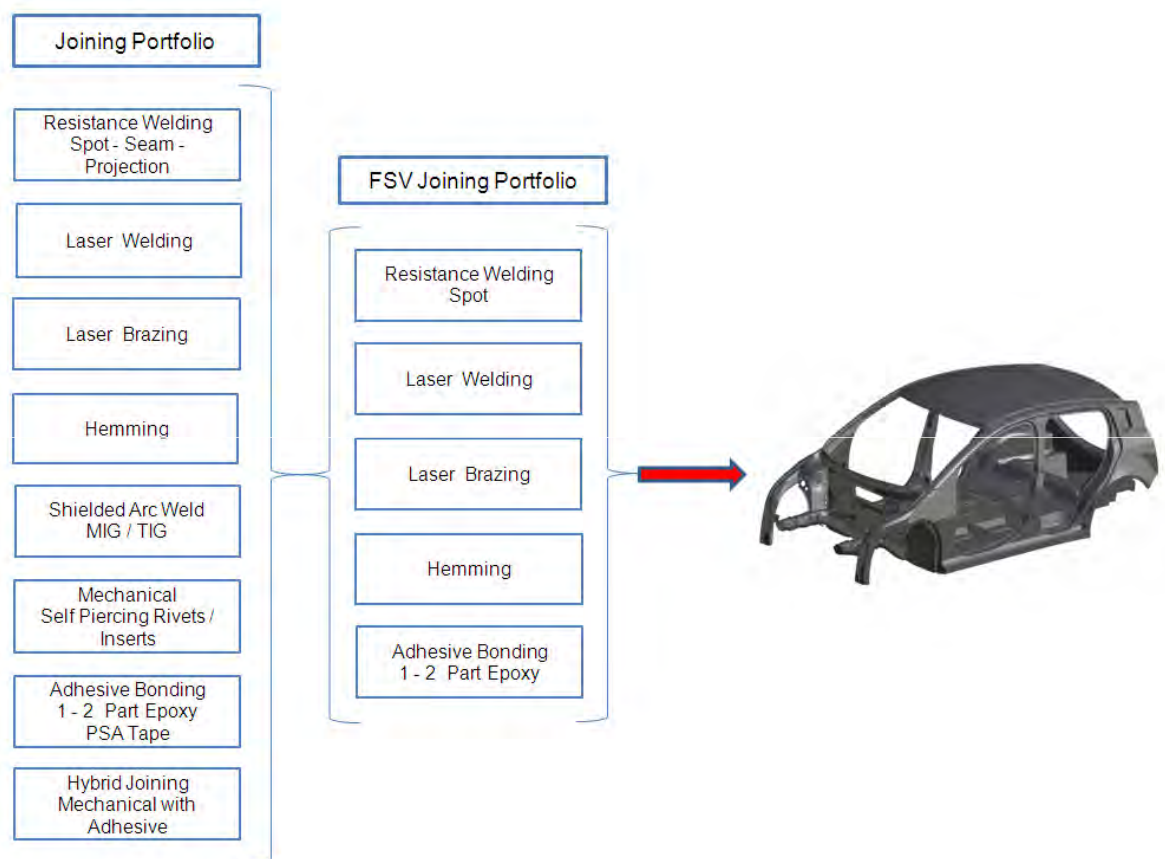


Figure 13.33: Joining process portfolio

To achieve the program targets and goals, the FSV utilizes a high proportion of high strength steels and laser welded blanks. Laser welding was selected as the basic welding method to match this technology level and the anticipated growth of laser welding up to the year 2020. This

resulted in approximately 86.93 meters of laser welding. Laser welding also gives the opportunity to reduce the width of the weld flange, see 13.3.1.2 (Laser Brazing), and gives added stiffness to the assembly. For small assemblies, spot welding was chosen in account of the relative high capital cost of a laser welding cell compared to a spot welding cell.

Structural adhesive was utilized in the cowl upper and lower, the tunnel area and the seat cross members to add additional stiffness and to improve performance.

The eight most common joining techniques from the joining portfolio were considered and from these, five were selected for the FSV joining portfolio. MIG/TIG welding was not considered as this welding process requires a filler wire/material adding to both cost and weight relative to other joining methods. Mechanical and hybrid joining was also discounted as not being suitable for a vehicle that uses a high percentage of high strength steels. The five joining process are listed below.

- Resistance Spot Welding
- Laser Welding
- Laser Brazing
- Roller Hemming
- Adhesive Bonding

During the design process, various part joining methods, spot welding, laser welding and adhesive bonding were evaluated for the different combination of parts. This considered the assembly method, part material and material stack-up (2T or 3T). Refer to Section 20.2 (Appendix) for more detailed information.

13.3.1.1 Resistance Spot Welding

Conventional spot welding was used for the assembly process. Depending on the assembly sequence, either a manual operated spot welding arrangement was selected, or for the smaller assemblies a static spot welding arrangement was built directly into the assembly fixture. For larger assemblies, spot welding was completed robotically. With a resistance spot weld, the weld flange width requirements are generally 16 mm to accommodate the weld tip and clearance from the part to be welded to the weld gun shank. Spot welding was used for the manufacture of smaller sub-assemblies over laser welding or other joining methods, as spot welding shows a distinct cost advantage over laser welding. For larger assemblies, there is a mix of spot welding and laser welding, which is dependent on the overall part geometry and the assembly sequence. See Figure 13.34 showing resistance spot weld flange requirements.

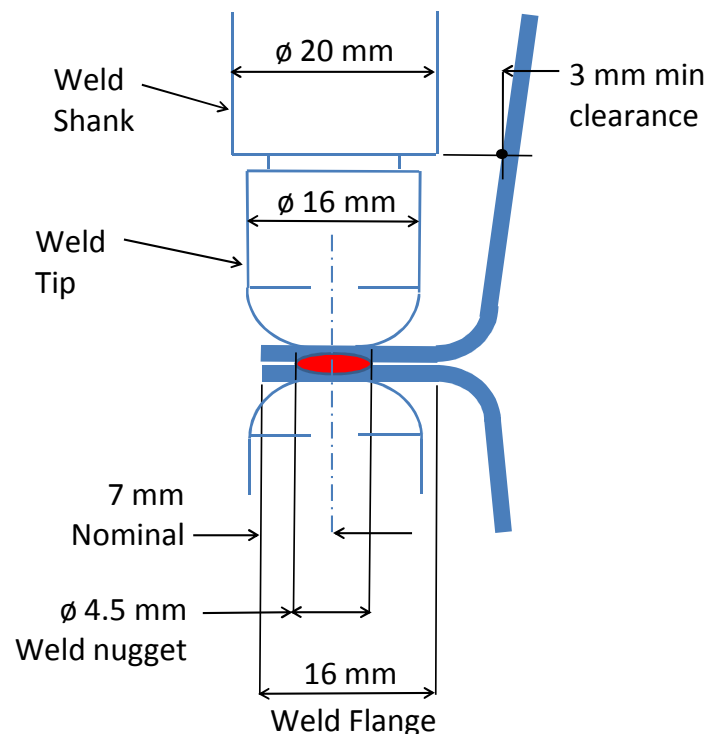


Figure 13.34: Resistance spot weld flange requirements

At certain assemblies, (rear floor assembly and body side assembly at framing station #1), where the body side assembly mates to the welded underbody to form a “closed” section, laser welding is necessary. For example, the rocker panel and the rear rail assembly where laser welding was used over spot welding. If spot welding was used, a single-sided spot welding operation would need to be used with the added complexity of having a welding “copper” built into the assembly tooling. The use of laser welding provides for a more simple assembly tooling condition, as laser welding is a single-sided operation and does not require any backing copper or equipment to complete the welding operation.

Depending on part geometry and its assembly to an adjacent mating part, the spot weld spacing generally ranges from 30 mm to 100 mm. Where a 100 mm weld spacing is used, it is with the application of structural adhesive.

Care must be taken when determining spot weld spacing. When spot welds are placed below a 25 to 30 mm spacing, weld current can be lost through the shunt path of the previous weld, resulting in a weld with a lower strength. The minimum spot weld spacing is based on material thickness, thickness stack-up and panel coating. The FSV spot weld spacing is shown in Figure 13.35

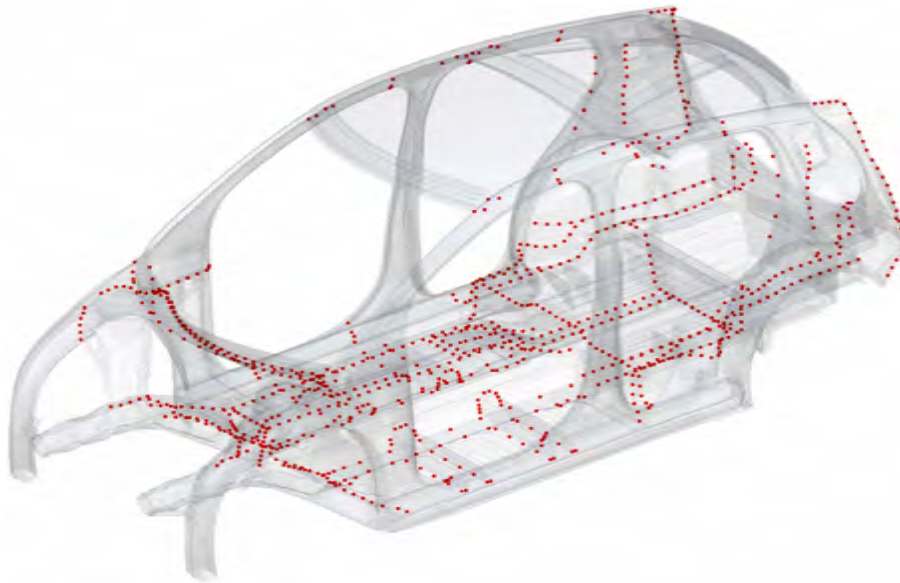


Figure 13.35: FSV spot weld spacing

13.3.1.2 Laser Welding

With the growth of laser welding by the world's OEM's, notably in Europe and the Asian regions, there is now a growing interest in using laser welding for high strength steels. For the FSV, we have eliminated a number of resistance spot welds and replaced them with laser welding. With this, the FSV is now considered to be a laser intensive body structure. FSV also eliminates the use of conventional laser welding by using a remote diode laser welding arrangement.

Remote laser welding has more flexibility than a conventional laser robot where the laser is positioned not by the position of the robot arm but by changing the focusing optics with the laser head positioned up to 400 mm from the part. This gives a higher positioning speed and allows for greater access to the part. By using a diode laser arrangement, the laser can be delivered to up to four separate stations from a single laser source via fiber optic cables. This is achieved by using a switching device that sends the beam to individual stations and by sequencing each station's weld cycle times. See Figure 13.36 for arrangement of four remote laser cells using a single laser source.

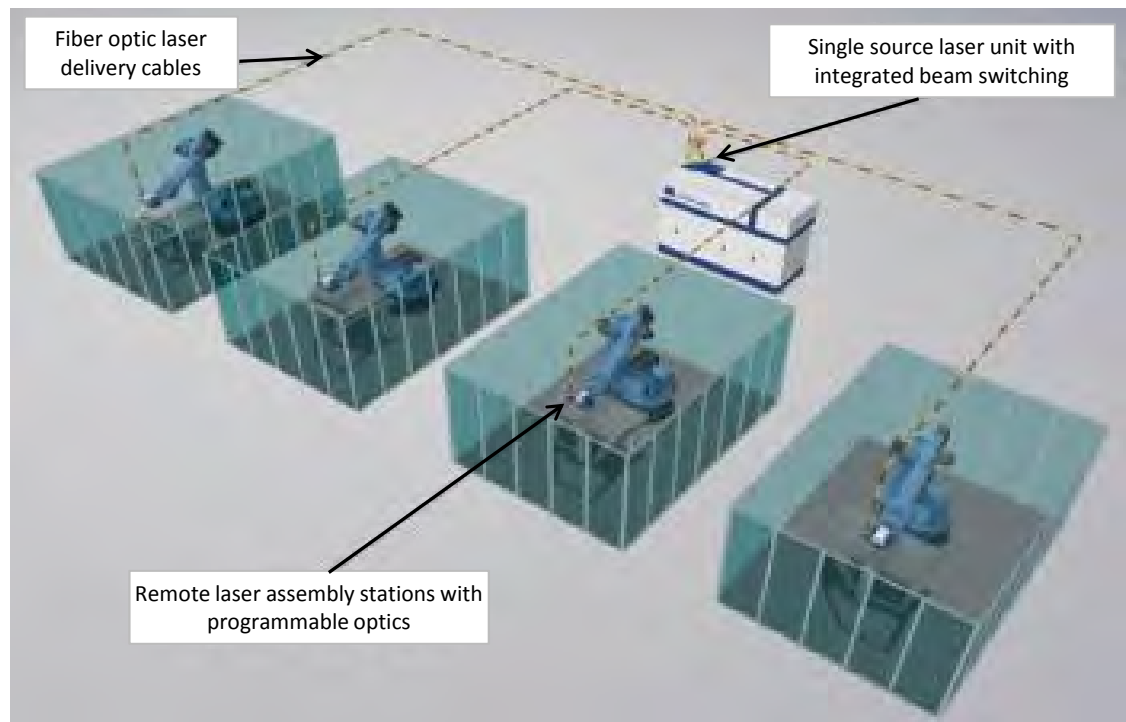


Figure 13.36: Multi-laser assembly stations using a single laser source

Although the initial cost of a laser welding cell is higher than a resistance spot welding cell, this is more than offset by the fact that we are able to replace a number of spot welders, in some cases up to eight with a single laser unit. The FSV laser welds are shown in Figure 13.37 and Figure 13.38.

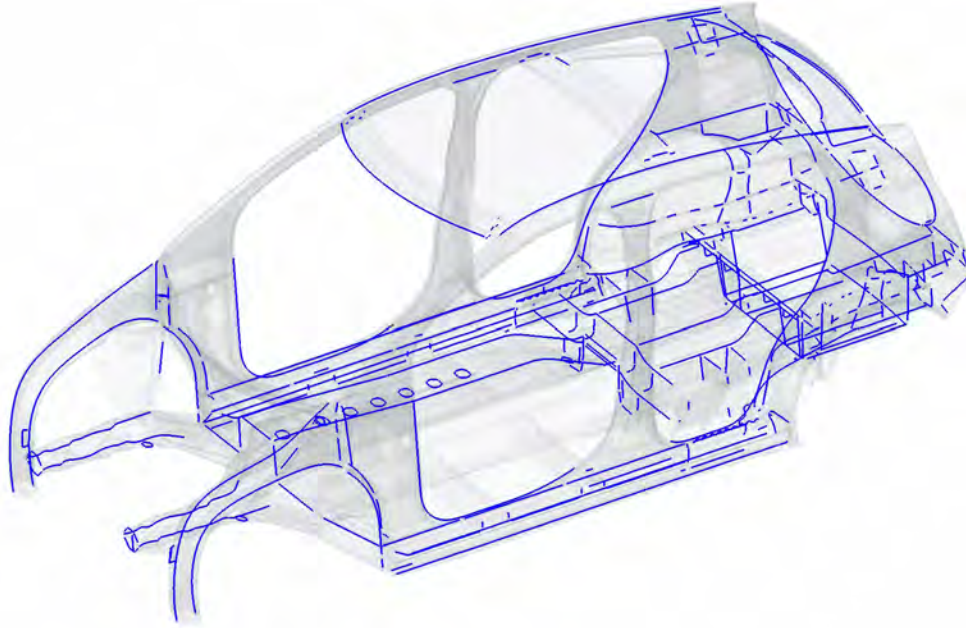


Figure 13.37: FSV laser welding (continuous pattern)

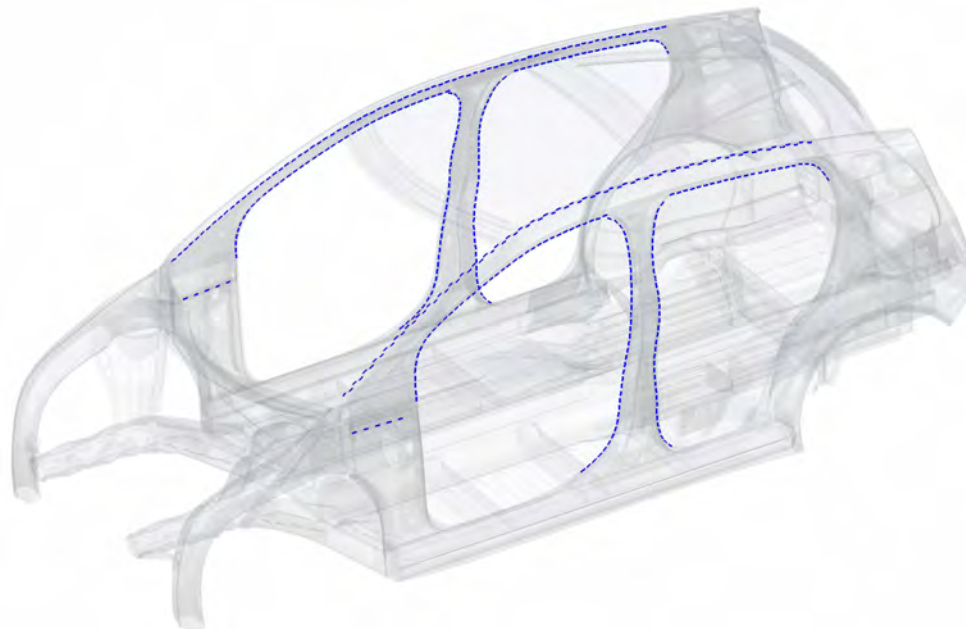


Figure 13.38: FSV laser welding (stitch pattern)

Listed below are some advantages of using a remote laser welding arrangement:

- High positioning speeds
- High welding speeds
- Narrow heat affected zone
- Minimal part distortion
- Precise placement of weld
- Weld depth control
- Flexibility in programming
- Non-contact process
- Localized heat impact
- Reduction in weld flange width

When laser welding, the flange width requirements are different than that for resistance spot welding. Using a remote laser set-up with the laser head up to 400 mm above the part, the flange width can be reduced to 8 mm giving a substantial weight savings. See Figure 13.39 showing weld flange requirements for laser welding & Figure 13.40 for weld flange comparisons of spot weld vs. laser. With a reduction in flange width to 8 mm, this results in an approximate weight saving of 6 kg for the BEV.

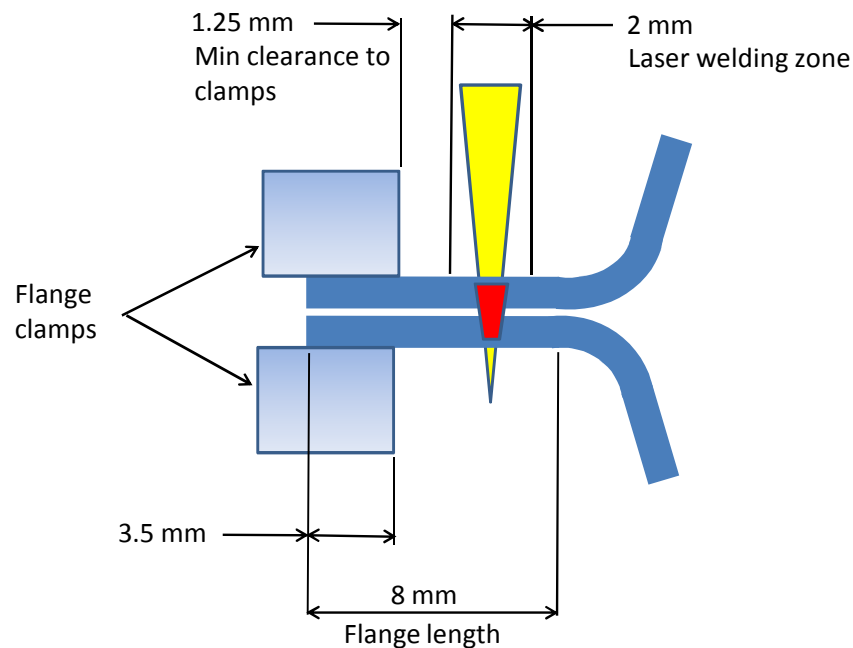


Figure 13.39: Weld flange requirements for laser welding

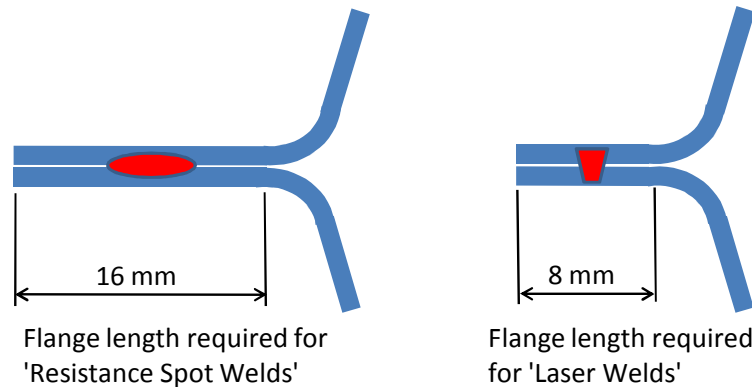


Figure 13.40: Weld flange comparison spot weld vs. laser weld

In addition to flange width reduction, there is also a space savings of up to 50% when you look at the body shop assembly area floor foot print. This is the result of the laser welding unit being able to replace a number of spot welding robots, saving floor space. See Figure 13.41 showing a typical spot-weld assembly station vs. a laser welding station.

Another advantage when using a laser welding cell, is floor space saving along with a fixture packaging advantage. Remote laser welding can replace a number of spot welding robots. An additional advantage of laser welding is that it is a one sided and a non-contact welding operation. This allows the remote laser welding process greater access to the part with the welding head being positioned up to 400 mm from the weld surface resulting in a reduction in the amount of part clamping equipment.

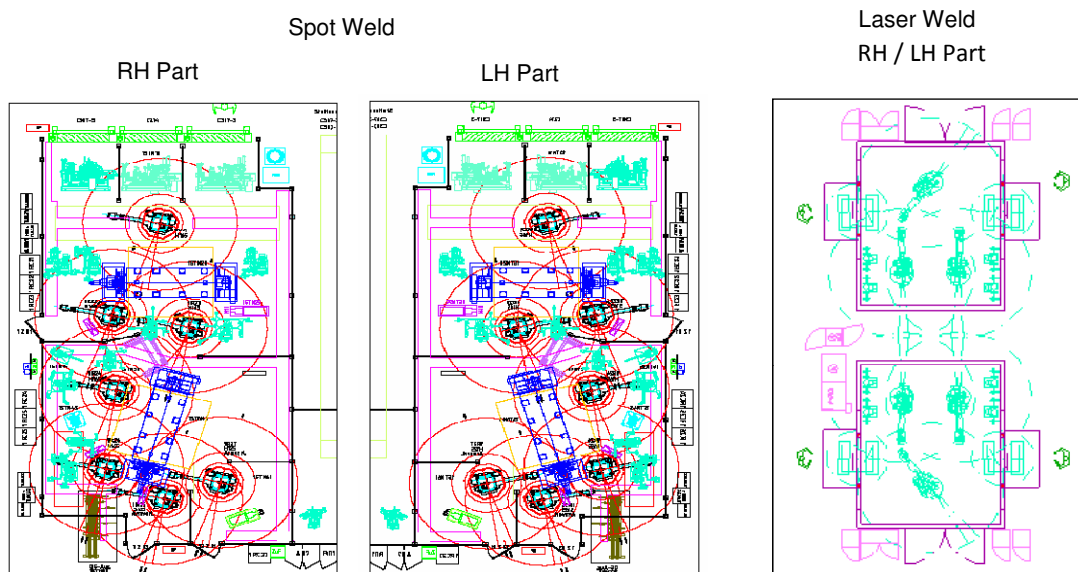


Figure 13.41: Comparison between spot welding and laser welding showing the savings in body shop floor space

13.3 Body Structure Assembly and Joining Methods

With laser welding, the remote laser is repositioned by internal optics, not by the robot arm, as with spot welding, allowing for greater weld speed than can be achieved with spot welding. Typically a single spot weld can be made in approximately 3.0 seconds. This allows for robot positioning, weld tip clamping and performing the spot weld, which is dependent on the weld parameters, panel thickness and material stack-up. This compares to an average weld speed of 80 mm/second for laser welding. For example, if we assume a part requires 10 welds using a single spot weld robot, the result would be a weld cycle time of 30 seconds using 45 mm weld spacing, which gives an equivalent distance of 405 mm for a continuous laser weld. This could be achieved in 5 seconds when using a 80 mm/second welding speed, which clearly shows a weld cycle time advantage when using remote laser welding.

13.3.1.3 Laser Welding of High Strength Steel

As the yield strengths of steel continue to increase to 1000 MPa and above, there is a growing interest in using laser welding for high strength steel. Generally the higher the strength of steel, the greater the sensitivity to heat input during the welding process. Due to the lower heat input of laser welding as compared to resistance spot welding, laser welding should be considered as an option to resistance spot welding.

13.3.1.4 Laser Welding of Zinc Coated Steel

A major consideration when laser welding is the material used for the steel coating. Typically the steel is zinc coated, either hot-dip galvanized (GI), electro galvanized (EZ) or galvanized (GA) on both sides to add an effective anti-corrosion coating. The zinc coating poses no issues when laser welding a butt joint but when welding a lap joint, special techniques have to be applied due to “degassing” of the zinc coating during the welding process.

Zinc vaporizes at a temperature around 900°C, which is far lower than the temperature required for the laser welding process. The two layers of zinc coating between the two sheets of a lap joint, generate high vapor pressure when welding. This can lead to blowouts of molten material during the welding process which would result in a weak weld joint. To prevent this, a small gap of 0.1/0.2 mm between the two sheets is required to allow the vapor pressure to dissipate. This gives excellent joint continuity without cracks, pores or non-metallic inclusions. One of the latest ways that this can be achieved is by the process of laser dimpling along the weld flange, (see Figure 13.42). This additional process can be conducted using the same laser that is used for the welding operation and is a cost efficient method with high repetition rates.

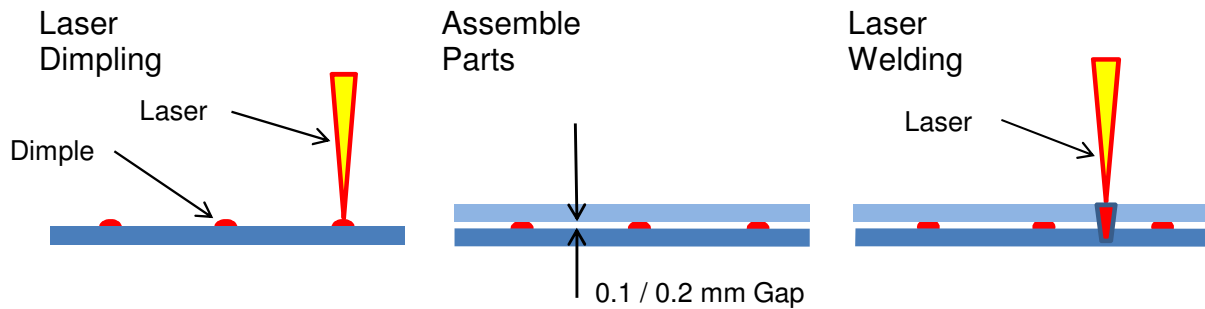


Figure 13.42: Laser dimpling process

As an alternative to laser dimpling, a separate dimpling procedure could be completed in the stamping shop or by mechanical operation within the stamping tool. The latter solution would be a zero cost option.

13.3.1.5 Laser Welding Three Material Thicknesses

Laser welding three material thickness (3T), together is presently not possible, albeit there have been a number of studies made by the major OEM's that are encouraging, but have not been adopted as a viable assembly process. When we do have a 3T condition, as in the body side door opening, welding of the body side outer, upper roof rail, B-pillar reinforcement and body side inner assembly, a different approach needs to be taken. In this situation a two step process is used. Laser welding has to be completed from both sides of the assembly effectively creating two sets of two metal thickness welds. This is achieved by using a laser weld stitch pattern of 20-40-20, where 20 is a 20 mm run of weld with a 40 mm gap and another 20 mm run of weld. Welding is completed on one side of the assembly while the same pattern is created on the opposite side of the assembly. The welding can be made simultaneously with one weld pattern staggered so that a 20 mm weld can be placed in the middle of the 40 mm gap left by the first weld pattern.

13.3.1.6 Laser Brazing

Laser brazing of the roof panel to the body side is becoming more common with the major OEM's adopting this process. The FSV also followed this approach with the added advantage of eliminating the need for a roof ditch molding.

The joint geometry of the roof panel and the body side are ideally suited to a laser brazing application where the filler wire can be 'guided' along the joint gap between the roof and body side. The filler wire used is dependent on the part materials that are to be brazed together. The most common material used for the filler wire is a copper based alloy with a melting point of between 900 °C and 1025 °C. The melting of the wire is caused by the laser beam which also needs to heat up the surrounding part area to complete the brazing process.

As the laser beam has a diameter of approximately 2-3 mm and the filler wire a 1 mm diameter,

the correct positioning of both the laser beam and the filler wire to the joint gap is critical to prevent a one sided joint connection. Lateral misalignment of the laser beam of just 0.3 mm can result in joint failures. One method to solve this issue is to use a self-tracking laser head where the laser beam and wire feed are controlled by using guiding optical sensors that continuously gives feedback to maintain the correct laser alignment and wire feed.

See Figure 13.43 for a typical section roof to body side when using laser braze.

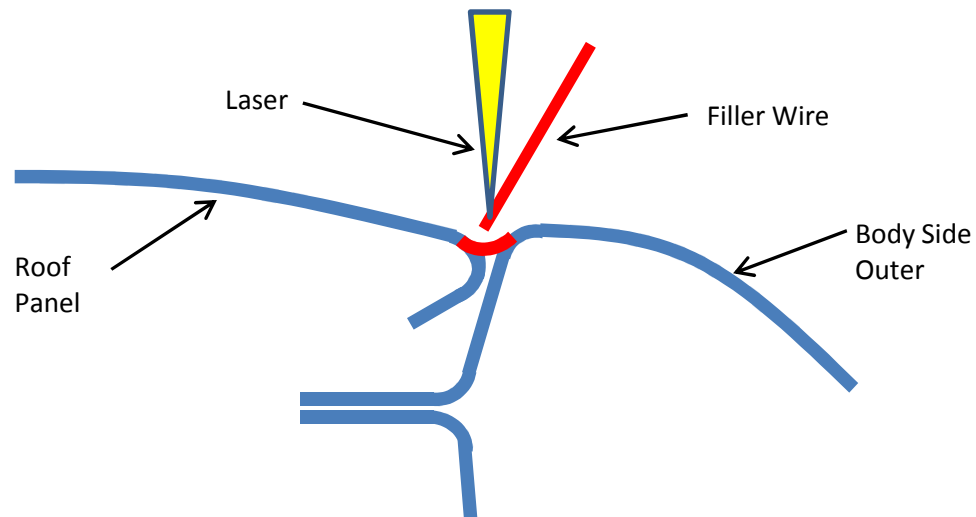


Figure 13.43: Typical section of a roof to body side when using laser braze

13.3.1.7 Roller Hemming

For the FSV, the body side rear wheel arch to the wheel house is roller hemmed. Robotic roller hemming uses a robot that carries a roller hemming head. The flange of the outer panel is bent over the inner panel in progressive steps by means of a series of rollers carried on the hemming head. See Figure 13.44 showing steps to complete a roller hemmed flange.

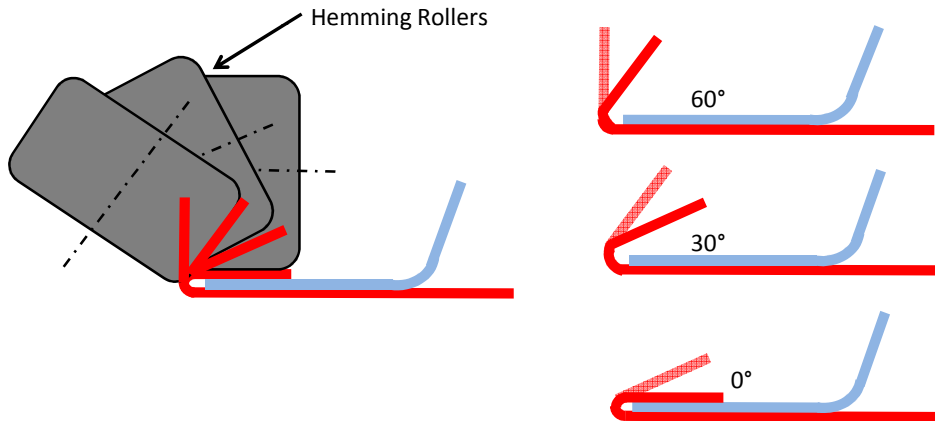


Figure 13.44: Steps to complete a roller hemmed flange

Typically a hemming die would be used to complete the hemming process, but by using a robotic system the hem station floor foot print can be greatly reduced from what would be necessary for a hemming die. Equipping the roller hem head with a tool changing system allows the robot to be multi-functional so that it can also dispense adhesives and sealants. See Figure 13.45 for a typical body side to wheel house hem flange.

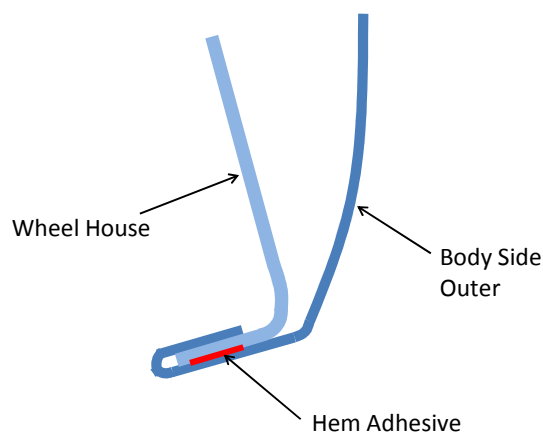


Figure 13.45: Typical body side to wheel house hem flange

13.3.1.8 Adhesive

On the FSV, three types of adhesive have been selected:

- Structural
- Hem adhesive
- Anti-flutter

See Figure 13.46 for FSV adhesive.

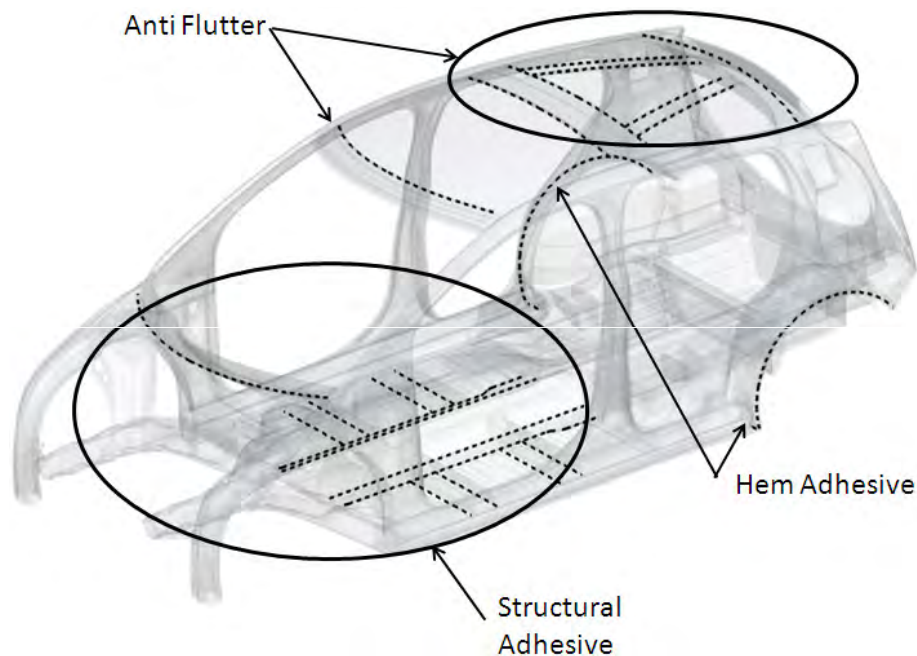


Figure 13.46: FSV adhesive

13.3.1.9 Structural Adhesive

Structural adhesive is used to improved impact resistance, stiffness, noise vibration and harshness (NVH), performance and durability of the structure.

The type of adhesive selected was a one part heat curable epoxy based impact resistant structural adhesive (Henkel Terokal 5089 or similar). The adhesive can be used with electro-galvanized, hot dipped galvanized, galvanized or uncoated steel. The adhesive is weld through capable and is heat cured. It will reach maximum strength with curing temperatures between 155 °C and 190 °C. This is achieved in the electro-coat bake oven.

For structural adhesive, the required flange length recommended is 16 mm to allow for a minimum of a 10 mm adhesive wet-out area. Spot weld spacing can be increased from the normal spacing

to up to 100 mm between spot welds. Ideal joint strength is achieved when there is a small gap of 0.2/0.5 mm between the two panels. This small gap can be achieved by a dimpling operation completed within the stamping die at time of manufacture. See Figure 13.47 for details of the required flange for adhesive bonding.

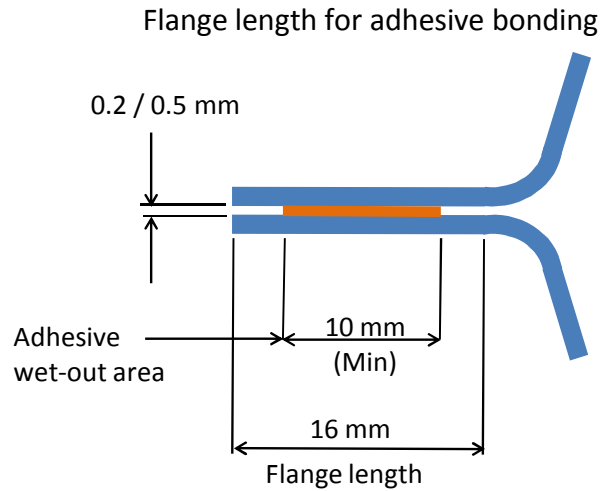


Figure 13.47: Joint and flange required for adhesive bonding

13.3.1.10 Hem Adhesive

The hem adhesive selected is a two part epoxy (3M 5026 or similar), formulated specifically for steel hem flanges featuring low activation temperatures to minimize panel distortion. This is applied between the inner and outer panels in the rear wheel arch area prior to the hemming operation.

13.3.1.11 Anti-flutter Adhesive

Anti flutter adhesive is used between the upper structure and the roof panel to improve stiffness and NVH performance. A cold-applied, pumpable anti-flutter adhesive designed to expand when subjected to heat to form soft closed-cell foam was selected (Henkel Terostat 06-1273 or similar). This is applied to the upper structure, the front & rear headers and roof bows prior to the assembly of the roof panel. This also cures in the electro-coat bake oven at temperatures between 155° and 190°C that will result in approximately 30% expansion. See Figure 13.48 for anti-flutter before and after heat curing.

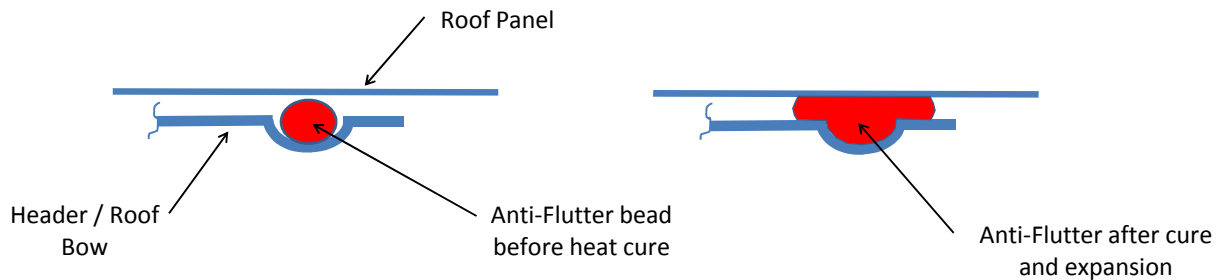


Figure 13.48: *Anti-flutter before and after heat curing*

13.3.2 Body Structure Assembly

For the purpose of this program, the FSV body structure is considered to be minus all closures and hang on parts. These are made up of the hood, front and rear doors, lift gate and front fenders.

13.3.2.1 Body Shop

The body shop is arguably the most complex manufacturing phase of the entire vehicle manufacturing and assembly process. The body shop is at the beginning of the assembly process where separate sub-assemblies are completed flowing down the assembly line. To complete the body structure, closures (doors, hood and liftgate) are added in addition to the front fenders, completing the “body-in-white” which is then transferred to the paint shop. See Figure 13.49 for the FSV body structure assembly flowchart.

The FSV program body structure assembly has been sub-divided into a number of major assemblies.

These are:

- Front Structure
- Front Floor
- Rear Floor
- Under-Body
- Body Side LH/RH
- Upper Structure and Shotgun

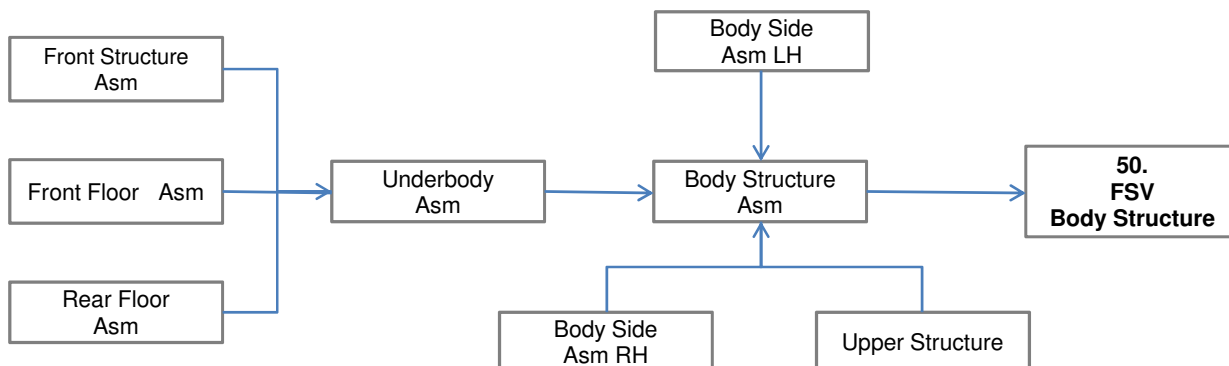


Figure 13.49: FSV block diagram body shop

13.3.2.2 Body Structure Assembly Overview

The body structure assembly process starts in an off-line assembly area where each sub-assembly is completed on secondary assembly lines prior to being transferred in containers or automated floor guided pallets to the underbody assembly station on the main body assembly line. A series of robots load these sub-assemblies to the main body structure assembly line. The first major station is the underbody assembly where the front structure and front and rear floor are assembled together. This transfers to the most complex assembly station in the body line, “framer #1”. At this station the underbody, body sides LH/RH and the upper structure minus the roof, are all assembled in a fully automated “remote laser” welding assembly cell. “Framer #2” adds the remaining parts, roof and shotgun LH/RH.

13.3.2.3 50.1 3110 Front Structure Assembly

The front structure assembly is made up of eight separate sub-assemblies for a total of nineteen individual parts. See Figure 13.50 for the front structure assembly sequence part diagram, and Figure 13.51 showing sub-assemblies used in the front structure.

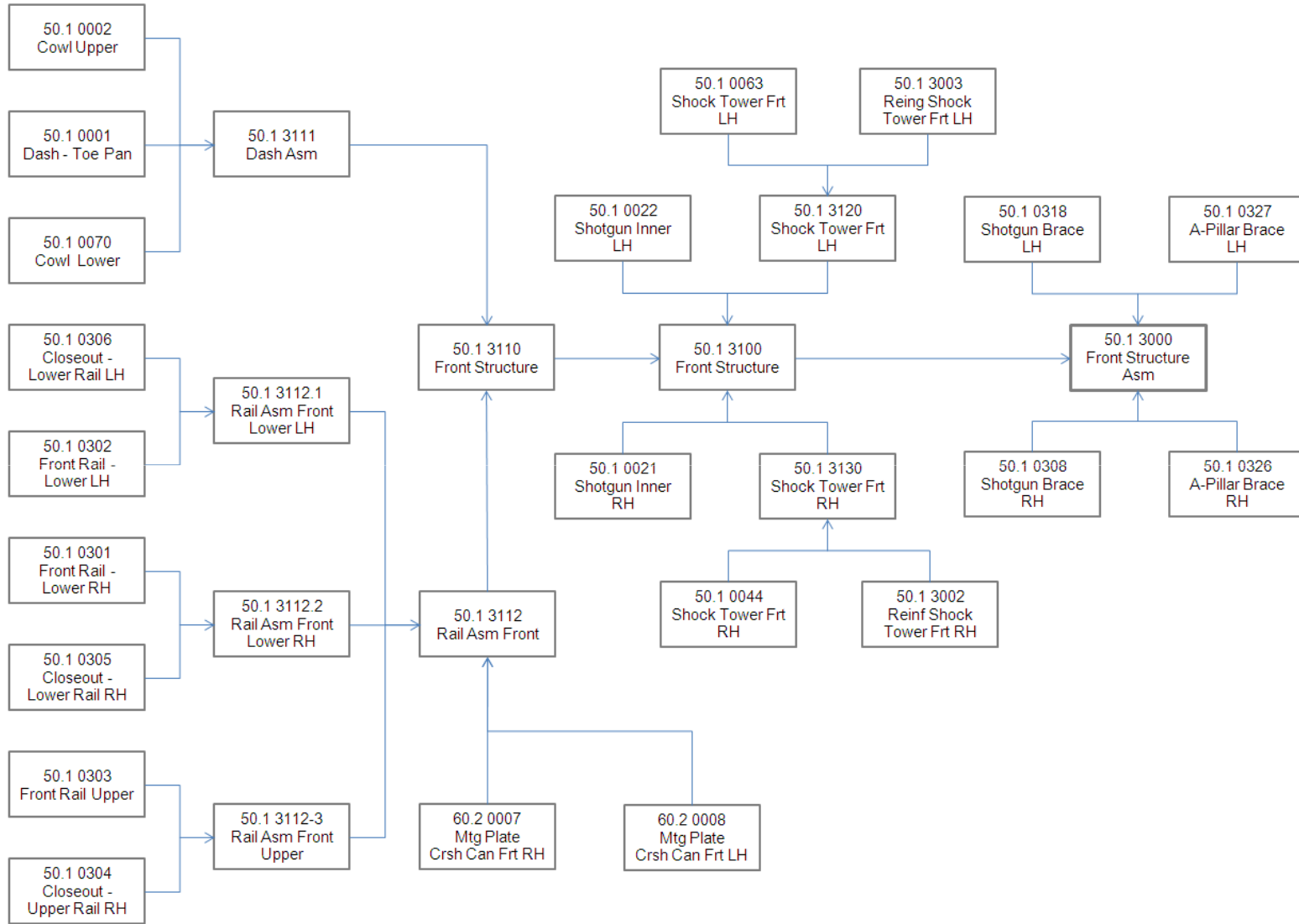


Figure 13.50: 50.1 3110 Front structure assembly sequence block diagram

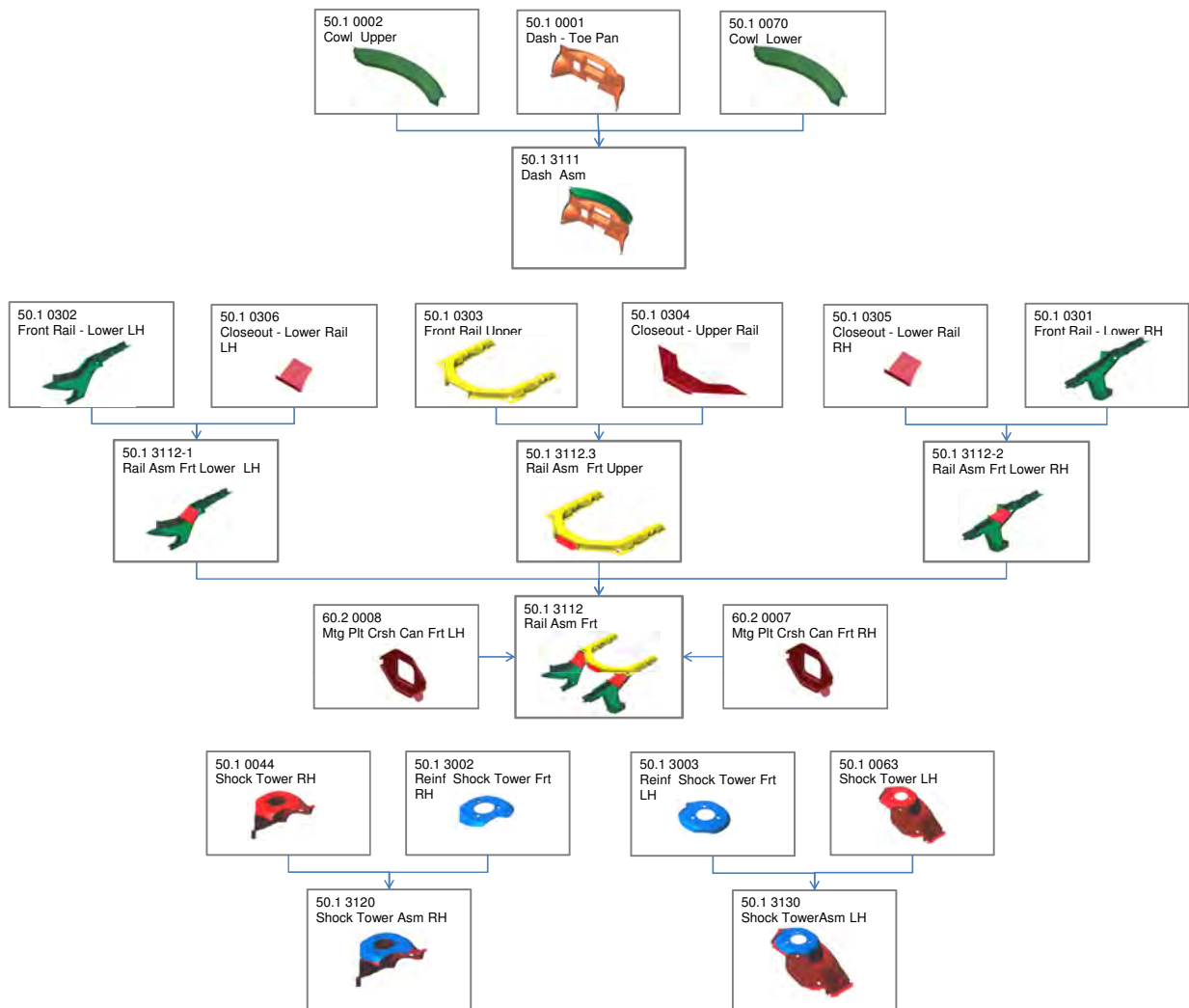


Figure 13.51: Front structure sub-assemblies

13.3.2.4 50.1 3111 Dash Assembly

The dash assembly is made up of the dash toe pan plus the upper and lower cowl. First the cowl lower is manually loaded onto a vertical holding fixture, then the dash toe pan is added and clamped in position. Structural adhesive is applied to the front edge of the cowl lower. The cowl upper is then placed and clamped in the fixture. A spot welding robot is utilized to complete the welding of the assembly. The spot welds at the front edge of the cowl upper and lower have greater spacing (100mm), than normal as a result of using structural adhesive. The structural adhesive remains in a semi-liquid state until the complete BIW passes to the paint shop where curing takes place in the electro-coat bake oven. After completing the welding operation, the assembly is unloaded with the aid of an assist hoist and loaded into a support rack before being transported to 50.1 3110 front structure assembly station. See Figure 13.52 showing the dash assembly.



Figure 13.52: *50.1 3111 Dash assembly*

13.3.2.5 50.1 3112-1/2 Rail Assembly Front Lower LH/RH

Individual components making up the LH and RH assemblies are manually loaded and clamped onto a common assembly fixture. A static spot welding arrangement is built into the assembly fixture to simplify the welding of the closeout panels to the rail lower. After assembly, both parts are unclamped and manually unloaded and placed in holding racks before moving to the rail front assembly station, 50.1 3112. See Figure 13.53 for rail assembly front lower (LH), and Figure 13.54 for rail assembly front lower (RH).



Figure 13.53: *50.1 3112-1 Rail Assembly Frt. Lower (LH)*



Figure 13.54: *50.1 3112-2 Rail Assembly Frt. Lower (RH)*

13.3.2.6 50.1 3112-3 Rail Assembly Upper

Two components make up the rail assembly front upper and the closeout panel. These are manually loaded and clamped in position. A manually operated spot welder is used to complete the assembly. The completed assembly is unloaded and placed in a holding rack. See Figure 13.55 showing the rail assembly.

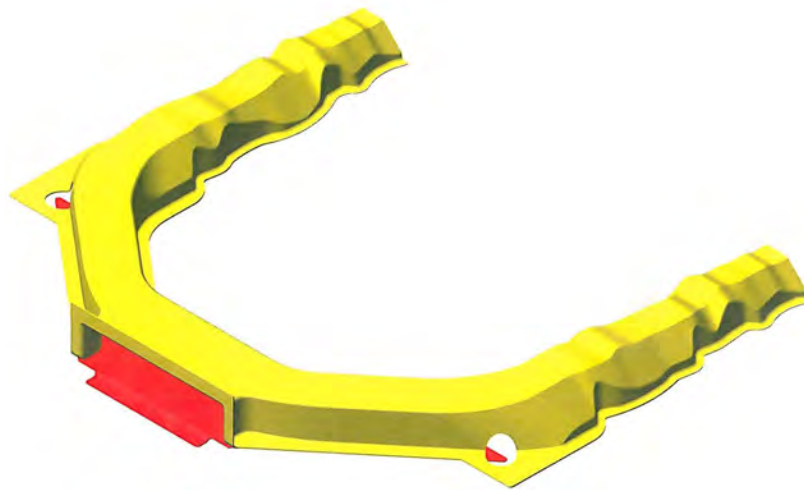


Figure 13.55: 50.1 3112-3 Rail Assembly Upper

13.3.2.7 50.1 3112 Rail Assembly Front

The rail assembly is made up of three separate sub-assemblies, 50.1 3112-1/2 rail assembly front lower LH/RH and rail assembly front upper 50.1 3112-3. The front bumper beam mounting plates are also added to this assembly. See Figure 13.56 50.1 3112 showing rail assembly front.

The 50.1122-1/2 front rail lower assemblies LH/RH are loaded and clamped in the assembly fixture using a load assist. Prior to assembly, the rail upper assembly had dimpling applied on the joint area to the rail assembly lower. See section 13.3.1.4 (Laser welding of zinc coated steel). This process enables degassing of the zinc vapor of the zinc coated steel during the laser welding operation. The two front mounting plates for the crash can LH/RH are also added. The assembly cell is then closed and the assembly is welded using two remote laser welding robots, one positioned on each side of the assembly cell. After completion, the finished assembly is unloaded using an assist to a holding rack and transferred to the front structure assembly station, 50.1 3110. See Figure 13.59 showing the front structure assembly line.



Figure 13.56: *50.1 3112 Rail Assembly Front*

13.3.2.8 50.1 3120/3130 Shock Tower Assembly LH/RH

This assembly includes the shock tower and reinforcement LH/RH assembled in a spot welding cell. Parts are manually loaded and clamped in a common assembly fixture. Part orientation is upper surface down to allow for weld gun access. Welding is completed using a manually operated spot welder. Completed assemblies are unloaded and placed in a holding rack before being moved to 51.1 3100 front structure assembly station. See Figure 13.57 for shock tower assembly (LH) and Figure 13.58 for shock tower assembly (RH).



Figure 13.57: *50.1 3130 Shock tower assembly (LH)*

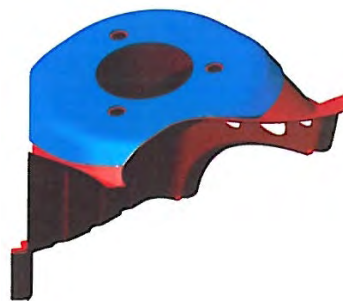


Figure 13.58: *50.1 3120 Shock tower assembly (RH)*

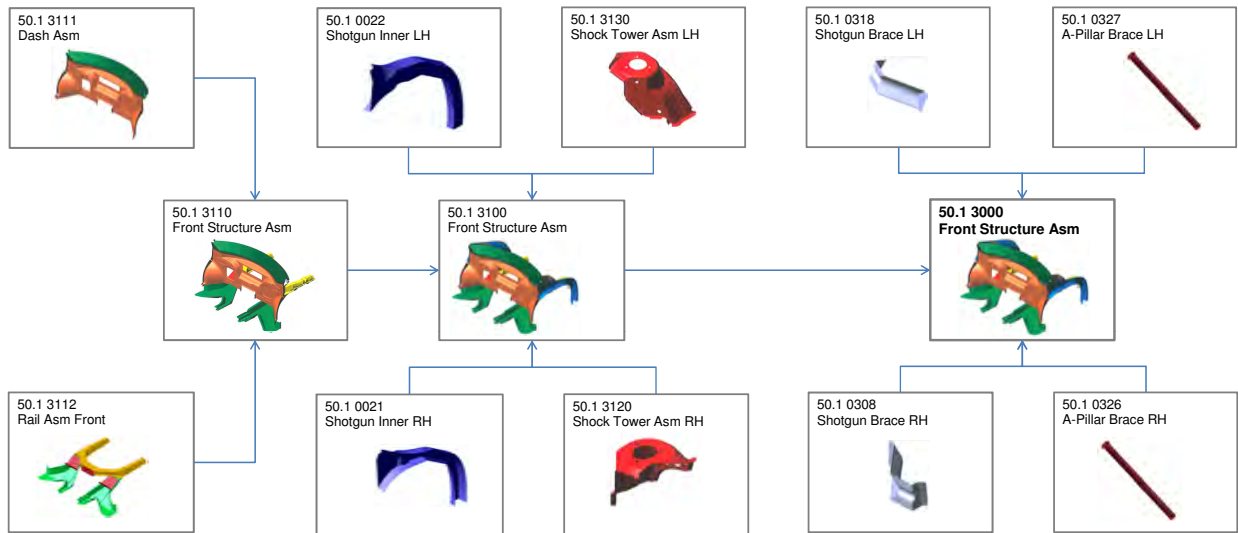


Figure 13.59: 50.1 3000 Front structure assembly line

13.3.2.9 50.1 3110 Front Structure

At this assembly station, the two major assemblies 50.1 3111 dash assembly and 50.1 3112 rail assembly front, are brought together in a robotic spot welding station. See Figure 13.60 showing 50.1 3110 front structure. The rail assembly front is first loaded and clamped in position, then the dash assembly is added and clamped. Welding is completed using two spot welding robots, one on each side of the assembly station. Upon completion, the assembly is unloaded using an assist hoist, placed in a holding rack and then transferred to 50.1 3100 assembly station.

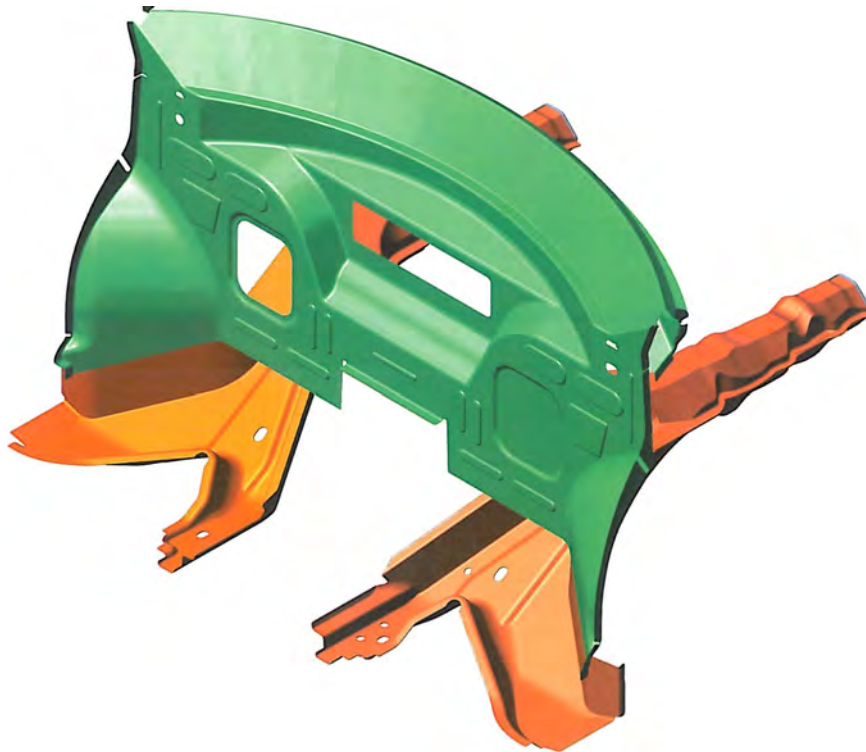


Figure 13.60: 50.1 3110 Front Structure

13.3.2.10 50.1 3100 Front Structure

At the 50.1 3100 assembly station, the shot gun LH/RH are loaded and clamped in position, then the shock tower LH/RH are manually loaded to each side of the assembly. These components are then clamped and the welding process is completed by using two spot welding robots, one positioned on each side of the assembly fixture and one remote laser welding robot. Prior to laser welding, a dimpling process is completed on the rail assembly front in the region of the joint to the shock tower. See Figure 13.61 showing 50.1 3100 front structure. The completed assembly is unloaded and transfers to the next assembly station, 50.1 3000.

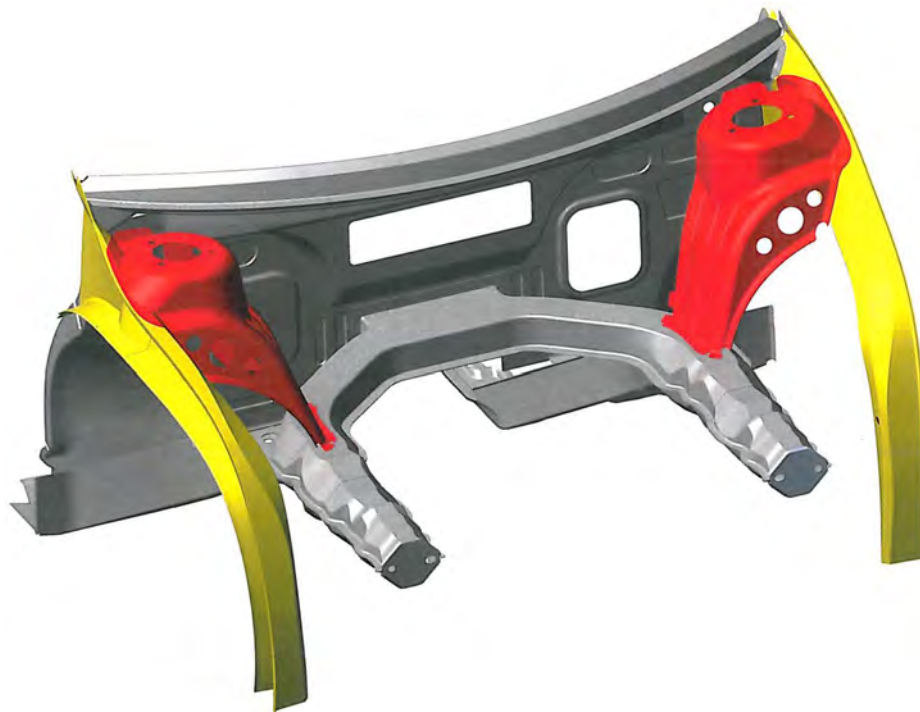


Figure 13.61: 50.1 3100 Front Structure

13.3.2.11 50.1 3000 Front Structure Assembly

The remaining parts, shot gun brace LH/RH, is manually loaded to the 50.1 3100 front structure. The A-pillar brace LH/RH is manually fed from the underside of the assembly and clamped in place. The assembly cell is closed and welding is completed using two remote laser welding robots, one positioned on each side of the assembly cell. A dimpling process is completed to the shot gun brace, prior to assembly in the areas of contact with the rail assembly front and the shot gun inner. The completed assembly is then robotically unloaded and placed on a automated floor guided pallet system before moving to the underbody assembly station. See Figure 13.62 showing 50.1 3000 front structure assembly.



Figure 13.62: 50.1 3000 Front structure assembly

13.3.2.12 50.1 1000 Front Floor Assembly

The front floor assembly is made up of three separate sub-assemblies for a total of 11 individual parts. See Figure 13.63 for front floor assembly sequence part diagram, and Figure 13.64 showing sub-assemblies used for the front floor.

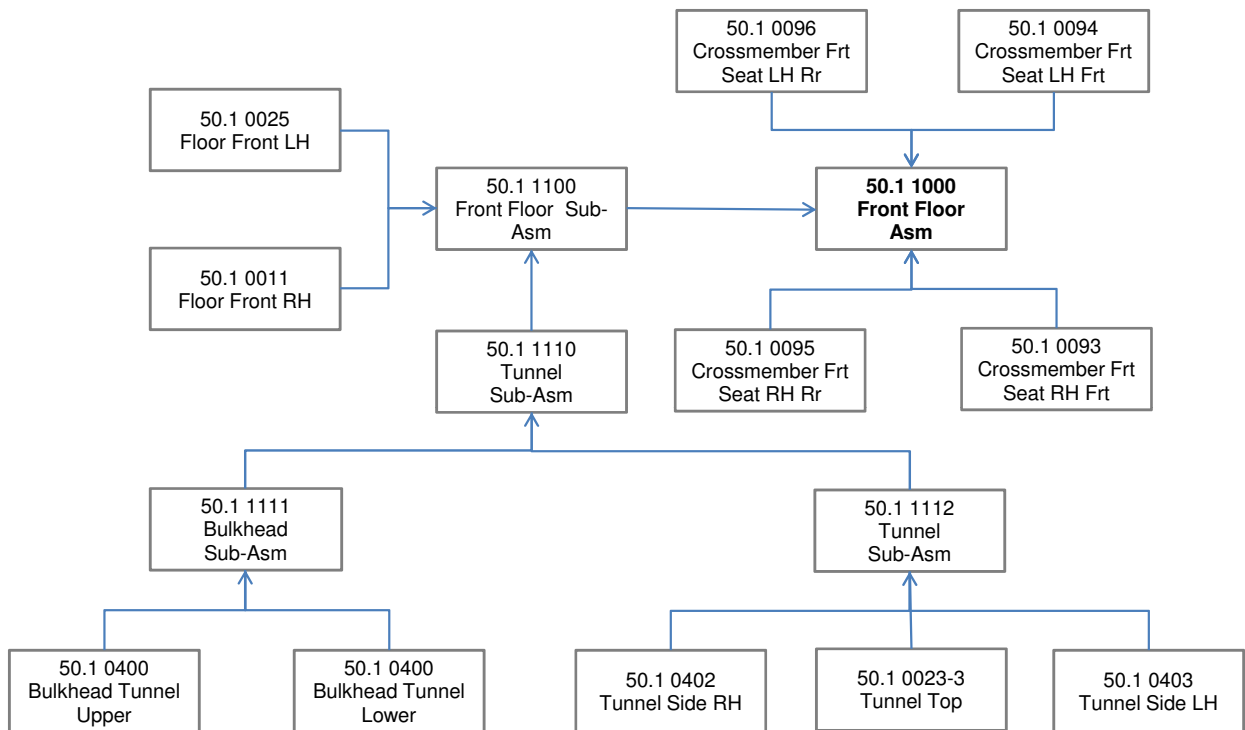


Figure 13.63: 50.1 1000 Front floor assembly sequence part diagram

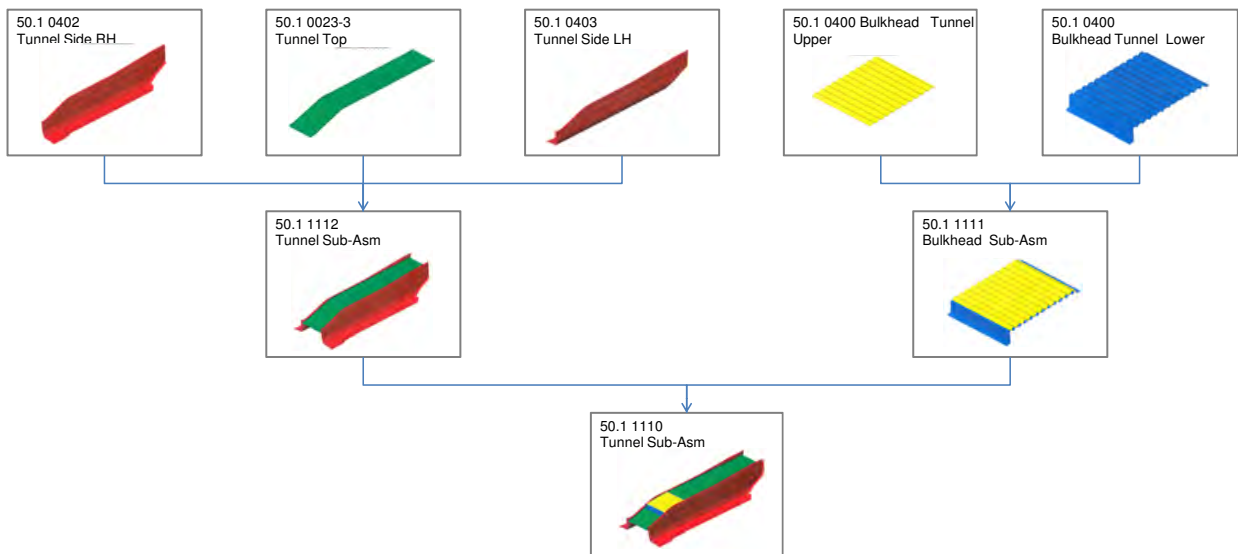


Figure 13.64: Front floor sub-assemblies

13.3.2.13 50.1 1111 Lower Bulkhead Sub-Assembly

Individual components are manually loaded and clamped onto an assembly fixture. A static spot welding arrangement is built into the assembly fixture to simplify the welding process. After assembly the part is manually unloaded and placed in a holding rack before moving to the tunnel sub-assembly station 50.1 1110. See Figure 13.65 showing the lower bulkhead sub-assembly.

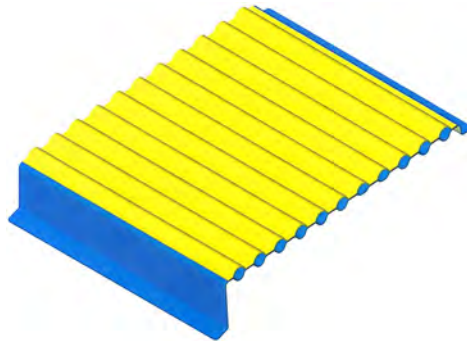


Figure 13.65: 50.1 1111 Lower bulkhead assembly

13.3.2.14 50.1 1112 Tunnel Sub-Assembly

The three parts that make up the tunnel assembly, tunnel side LH/RH and the tunnel top are manually loaded into an assembly fixture. Part orientation is base up to allow access for the spot weld gun. Assembly is completed using a single spot weld robot. The assembly is unloaded to a holding rack and moved to 50.1 1110, tunnel assembly station. See Figure 13.66 showing the tunnel sub-assembly.

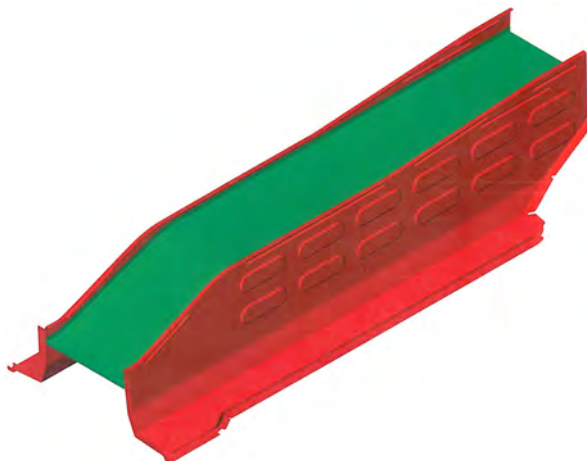


Figure 13.66: 50.1 1112 Tunnel sub-assembly

13.3.2.15 50.1 1110 Tunnel Assembly

The tunnel assembly consists of two separate sub-assemblies, 50.1 1111 lower bulkhead assembly and 50.1 1112 tunnel sub-assembly. The tunnel sub-assembly 50.1 1112 is manually loaded using a load assist and clamped in place. Next, 50.1 1111 is manually loaded and clamped. A manually operated spot welder is used to complete the assembly. The completed part is unloaded using the same assist as used to load the tunnel sub-assembly, placed in a holding rack and moved to 50.1 1110 front floor sub-assembly station. See Figure 13.67 showing the tunnel assembly.

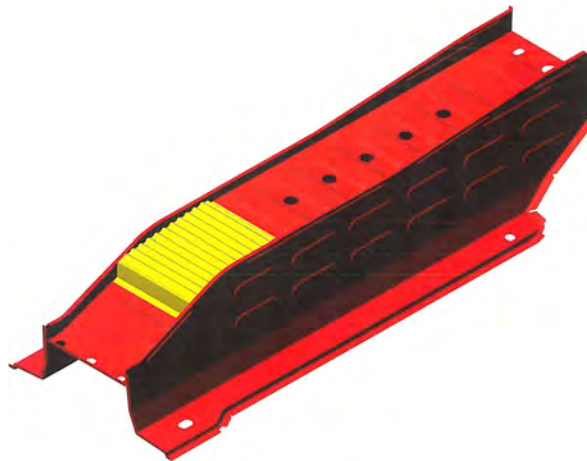


Figure 13.67: 50.1 1110 Tunnel Assembly

13.3.2.16 50.1 1100 Front Floor Sub-Assembly

The front floor sub-assembly consists of the 50.1 0011/0025 front floor RH/LH and 50.1 1130 tunnel assembly. The front floor panels are loaded first using a load assist. Structural adhesive is robotically applied to the floor panels in the joint area with the tunnel assembly. This robot has both an adhesive applicator and spot welding head. The tunnel assembly is loaded and clamped. Using the same robot that applied the structural adhesive, spot welding of the assembly is performed. The completed part then transfers to the final front floor assembly station 50.1 1000. See Figure 13.68 showing the front floor sub-assembly.

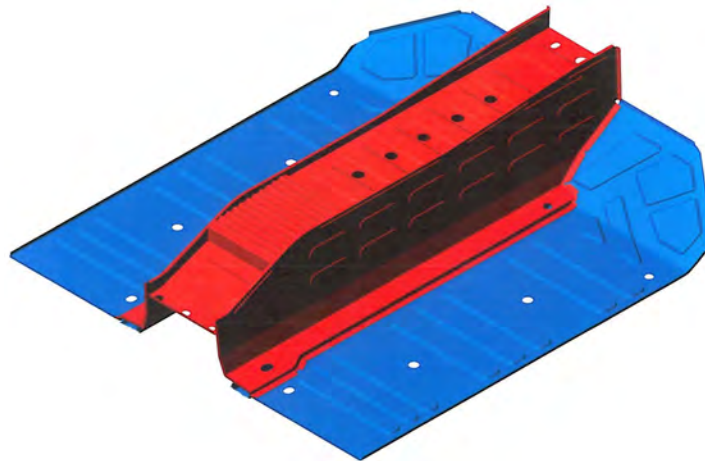


Figure 13.68: 50.1 1100 Front floor sub-assembly

13.3.2.17 50.1 1000 Front floor Assembly

In this assembly station, the front floor assembly is transferred from station 50.1 1100 to a spot weld and adhesive station, 50.1 1000. Structural adhesive is applied to the floor in the areas of the seat crossmembers in eight strips, two per crossmember. This is robotically applied by two robots, one on each side on the assembly station. These robots have both an adhesive applicator and spot welding head. The seat crossmembers are then loaded, clamped and spot welded. By using a structural adhesive, the spot weld spacing between the crossmembers and the floor panels can be increased to 100 mm. When the part is complete, the assembly is robotically unloaded and placed on an automated floor guided pallet system before moving to the underbody assembly station. See Figure 13.69 showing 50.1 1000 front floor assembly.

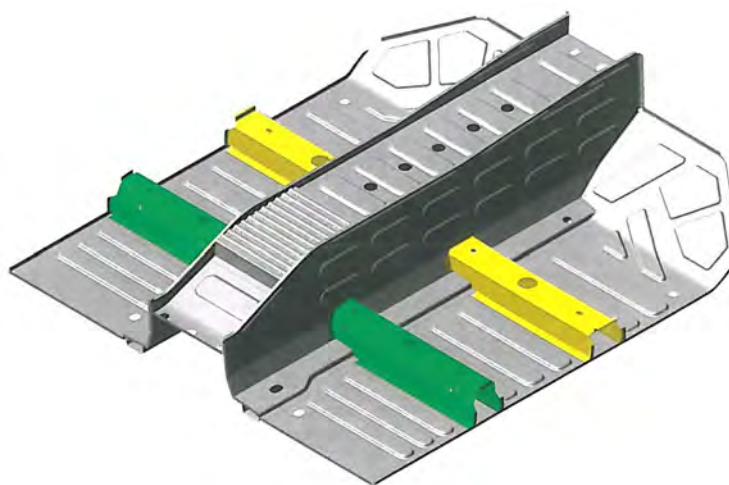


Figure 13.69: 50.1 1000 Front floor assembly

13.3.2.18 50.1 2000 Rear Floor Assembly

The rear floor assembly is made up of 13 separate sub-assemblies for a total of 39 individual parts. See Figure 13.70 for rear floor assembly block diagram, Figure 13.71 showing rear floor assembly sequence part diagram and Figure 13.72 showing sub-assemblies used for the rear floor.

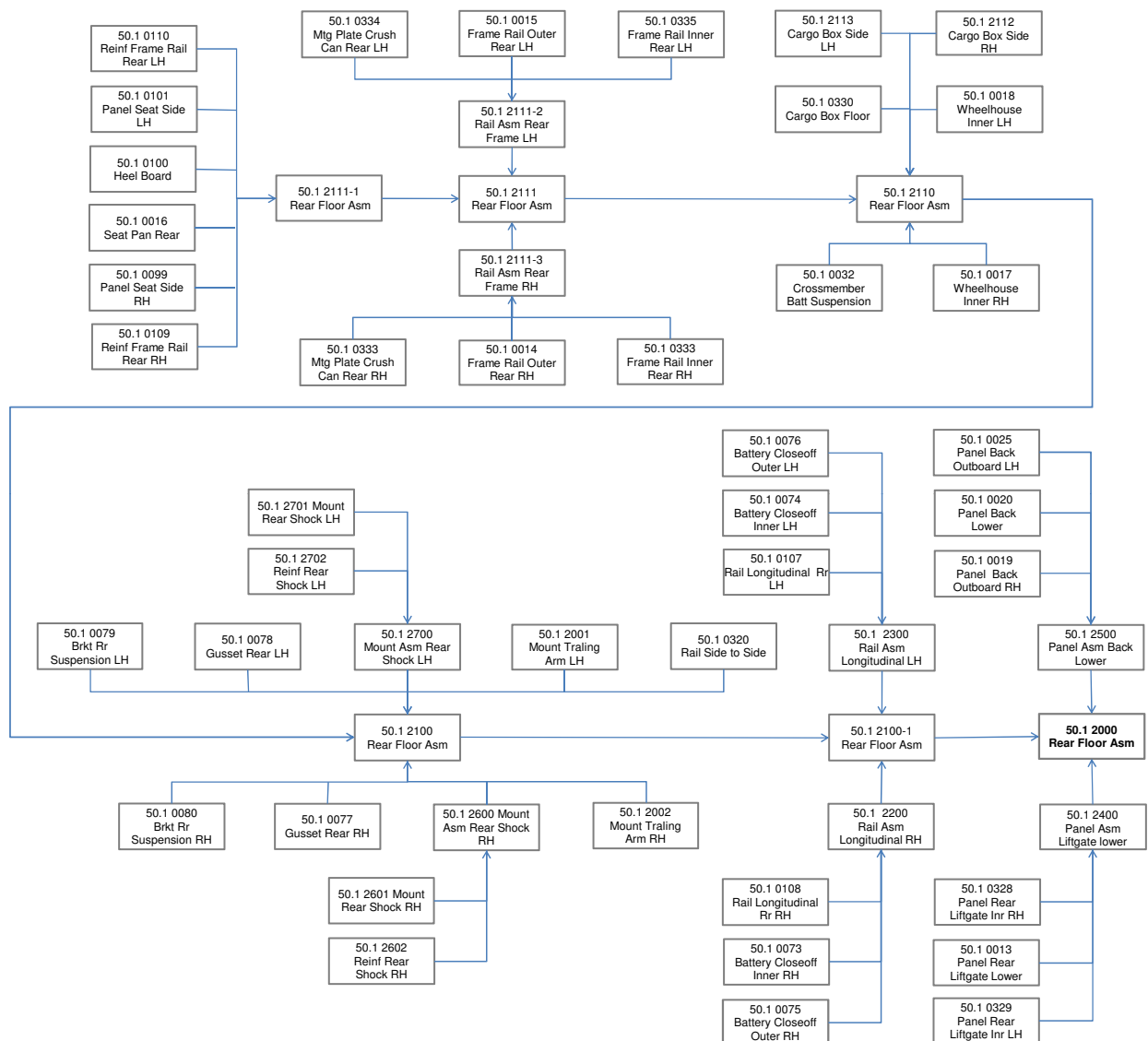


Figure 13.70: 50.1 2000 Rear floor assembly block diagram



Figure 13.71: Rear floor assembly sequence part diagram


Figure 13.72: Rear floor sub-assemblies

13.3.2.19 50.1 2200/2300 Rail Assembly Longitudinal LH/RH

Parts for both rail assemblies (LH/RH), are manually loaded and clamped in a common fixture. Welding is completed using a manually operated spot welder. When complete, the assemblies are manually unloaded, placed in holding racks and moved to assembly station 50.1 2100. See Figure 13.73 showing the longitudinal rail assembly (LH) and Figure 13.74 showing the longitudinal rail assembly (RH).

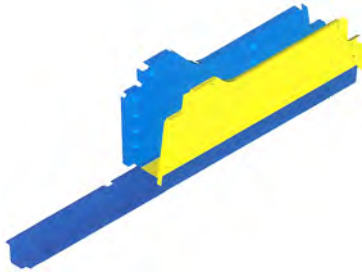


Figure 13.73: 50.1 2300 Rail assembly longitudinal (LH)

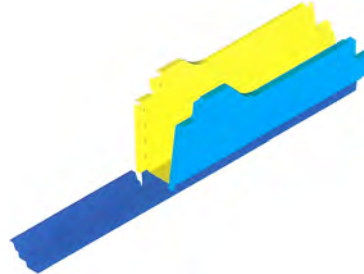


Figure 13.74: 50.1 2200 Rail assembly longitudinal (RH)

13.3.2.20 50.1 2111-2/3 Frame Rail Rear LH/RH

Both assemblies are welded in a closed laser welding cell. The frame rail inner and outer LH/RH is manually loaded and clamped in a common fixture. Both parts had dimpling completed on all laser welded flanges prior to loading in the assembly fixture. Welding is completed using one remote laser welding robot. When complete, the assemblies are manually unloaded, placed in holding racks and moved to 50.1 2110 rear floor assembly station. See Figure 13.75 showing the rear frame rail assembly (LH) and Figure 13.76 showing the rear frame rail assembly (RH).



Figure 13.75: 50.11 2111-2 Rear frame rail assembly (LH)

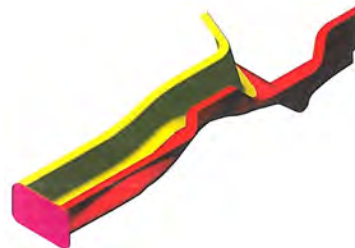


Figure 13.76: 50.1 2111-3 Rear frame rail assembly (RH)

13.3.2.21 50.1 2400 Panel Assembly Liftgate Lower

All parts for this assembly are manually loaded and clamped in an assembly fixture. The assembly is completed using a manually operated spot welder. The completed assembly is then unloaded using an assist hoist and placed in a holding rack before moving to the rear floor assembly station 50.1 2000. See Figure 13.77 showing the liftgate lower panel assembly.



Figure 13.77: 50.1 2400 Liftgate lower panel assembly

13.3.2.22 50.1 2500 Panel Assembly Back Lower

All parts for this assembly are manually loaded and clamped in an assembly fixture. The assembly is completed using a manually operated spot welder. The completed assembly is then unloaded using an assist hoist and placed in a holding rack before moving to 50.1 2000 rear floor assembly station. See Figure 13.78 showing the back lower panel assembly.



Figure 13.78: 50.1 2500 Lower back panel assembly

13.3.2.23 50.1 2600/2700 Mount Assembly Rear Shock LH/RH

All parts for both LH/RH assemblies are manually loaded and clamped in a common assembly fixture. Spot welding is completed using a static welding arrangement where the welding electrodes are built into the fixture to simplify the welding operation. The assemblies are then manually unloaded and placed in containers before moving to 50.1 2100 rear floor assembly station. See Figure 13.79 showing the rear shock mount assembly (LH) and Figure 13.80 showing the rear shock mount assembly (RH).



Figure 13.79: *50.1 2700 Rear shock mount assembly (LH)*



Figure 13.80: *50.1 2600 Rear shock mount assembly (RH)*

13.3.2.24 50.1 2111-1 Rear Floor Assembly

This assembly is for the seat pan, heel board and frame rail reinforcements. The seat pan is manually loaded using an assist hoist, all other parts are manually loaded and clamped. Orientation of the assembly is under side up giving good access for spot welding. Welding is completed using two spot welding robots, one positioned on each side of the assembly fixture. When complete, the assembly is unclamped and transferred via a conveyor system to the next assembly station, 50.1 2110-1. See Figure 13.81 showing the rear floor assembly 50.1 211-1

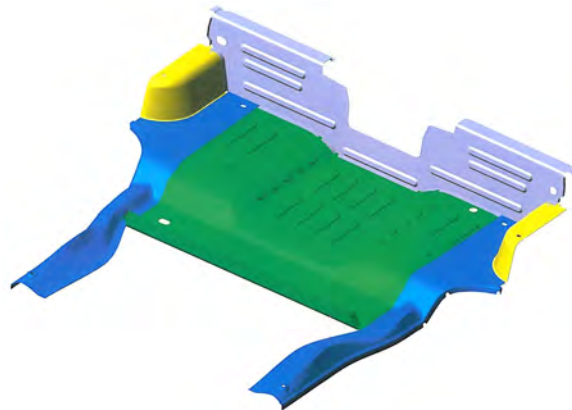


Figure 13.81: *50.1 2111-1 Rear floor assembly in an inner surface up orientation*

13.3.2.25 50.1 2111 Rear Floor Assembly

With the part still in a top surface down orientation, the assembly from the previous station is clamped. The LH/RH frame rail rear assemblies from assembly station 50.1 2111-2/3 are robotically loaded and then clamped. Welding is completed using two spot welding robots, one positioned on each side of the assembly station. When complete, the assembly is transfers via a conveyor to an idle station. See Figure 13.82 showing the rear floor assembly, 50.1 2111.



Figure 13.82: 50.1 2111 Rear floor assembly

13.3.2.26 50.1 2110 Rear Floor Assembly

At this assembly station, the parts are assembled in a combined spot weld and laser welding cell. The cross member battery suspension is manually loaded. The assembly from the previous idle station is robotically rotated to a top up orientation and loaded onto the assembly fixture. The wheel house LH/RH and the cargo box parts are then added. Welding is completed using two spot welding robots and two remote laser weld robots, one of each positioned on each side of the assembly station with the laser robots positioned rearwards from the spot welding robots. When complete, the assembly transfers via a conveyor to an idle station. See Figure 13.83 showing the rear floor assembly, 50.1 2110.

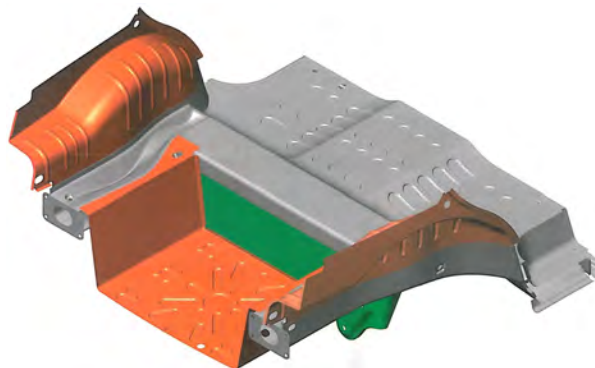


Figure 13.83: 50.1 2110 Rear floor assembly

13.3.2.27 50.1 2100 Rear Floor Assembly

At this station, all parts are assembled in a laser welding cell. The rear floor assembly 50.1 2110 from the previous idle station is robotically rotated to a top down orientation and placed in the assembly fixture. All other parts are loaded and automatically clamped. Welding is completed

using two remote laser welding robots, one positioned on each side of the assembly station. When complete, the assembly is unclamped and the fixture indexes to the next station, 50.1 2100-1. See Figure 13.84 showing the rear floor assembly, 50.1 2100.

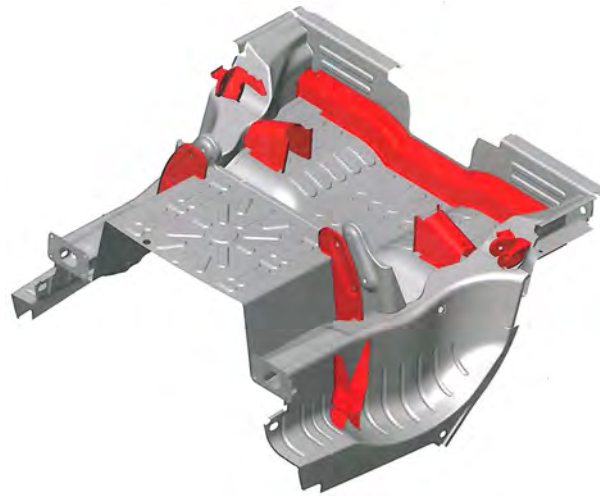


Figure 13.84: 50.1 2100 Rear floor assembly

13.3.2.28 50.1 2100-1 Rear Floor Assembly

At this station, the rail assemblies longitudinal LH/RH are assembled in a laser welding cell. The two sub-assemblies are robotically loaded and clamped. Welding is completed using one remote laser welding robot. When complete the assembly is unclamped and transfers via a conveyor to an idle station. See Figure 13.85 showing 50.1 2100-1 rear floor assembly.

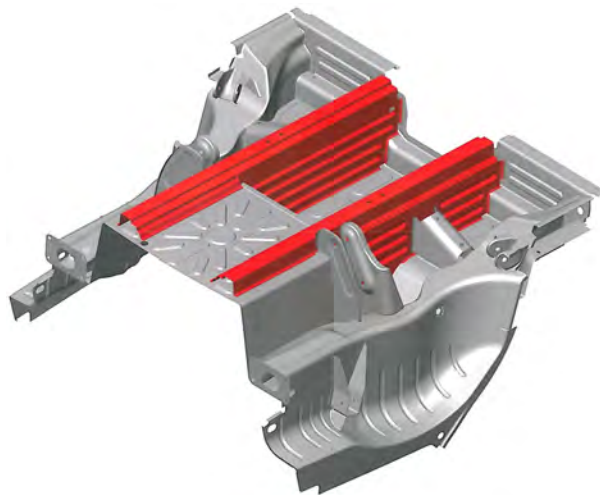


Figure 13.85: 50.1 2100-1 Rear floor assembly

13.3.2.29 50.1 2000 Rear Floor Assembly

At this station, the panel assembly liftgate lower and the panel assembly back lower are assembled in a laser welding cell. From the previous idle station, the assembly is robotically rotated to a top up orientation, placed in the assembly fixture and clamped in position. The two sub-assemblies are robotically loaded and clamped. Welding is completed using two remote laser welding robots, one positioned on each side of the assembly station. When complete, the assembly is unclamped and robotically placed on an automated floor guided pallet system before moving to the underbody assembly station. See Figure 13.86 showing 50.1 2000 rear floor assembly.

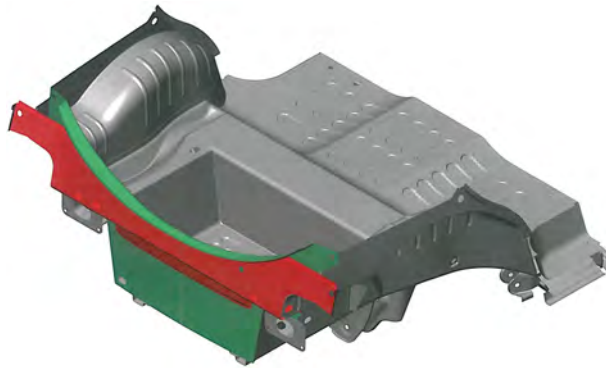


Figure 13.86: 50.1 2000 Rear floor assembly

13.3.2.30 50.6 1000/2000 Body Side Assembly LH/RH

Each body side assembly is made up of four sub-assemblies making a total of 16 individual parts. The assembly sequence for the body side is identical for both LH and RH. Only the RH assembly is highlighted. See Figure 13.87 and Figure 13.88 for the LH & RH body side assembly sequence part block diagrams (respectively), Figure 13.89 showing the sub-assemblies used for the RH body side assembly, and Figure 13.90 shows the body side RH assembly.

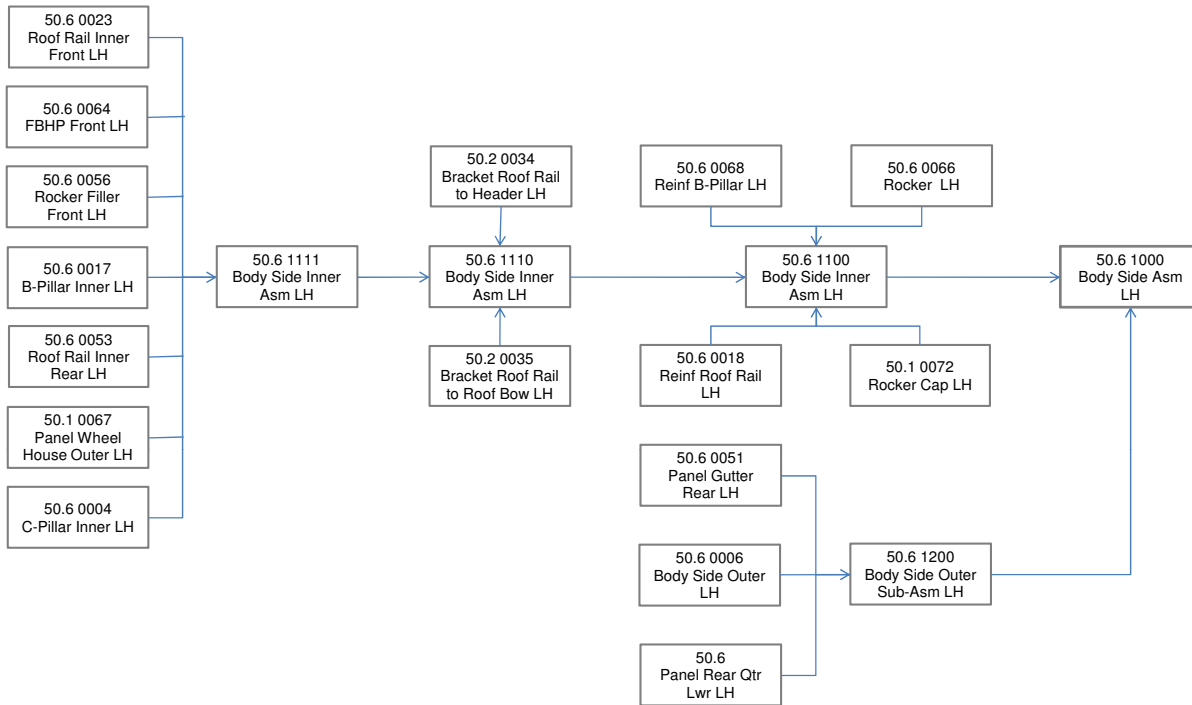


Figure 13.87: 50.6 1000 Body side assembly sequence part block diagram, (LH)

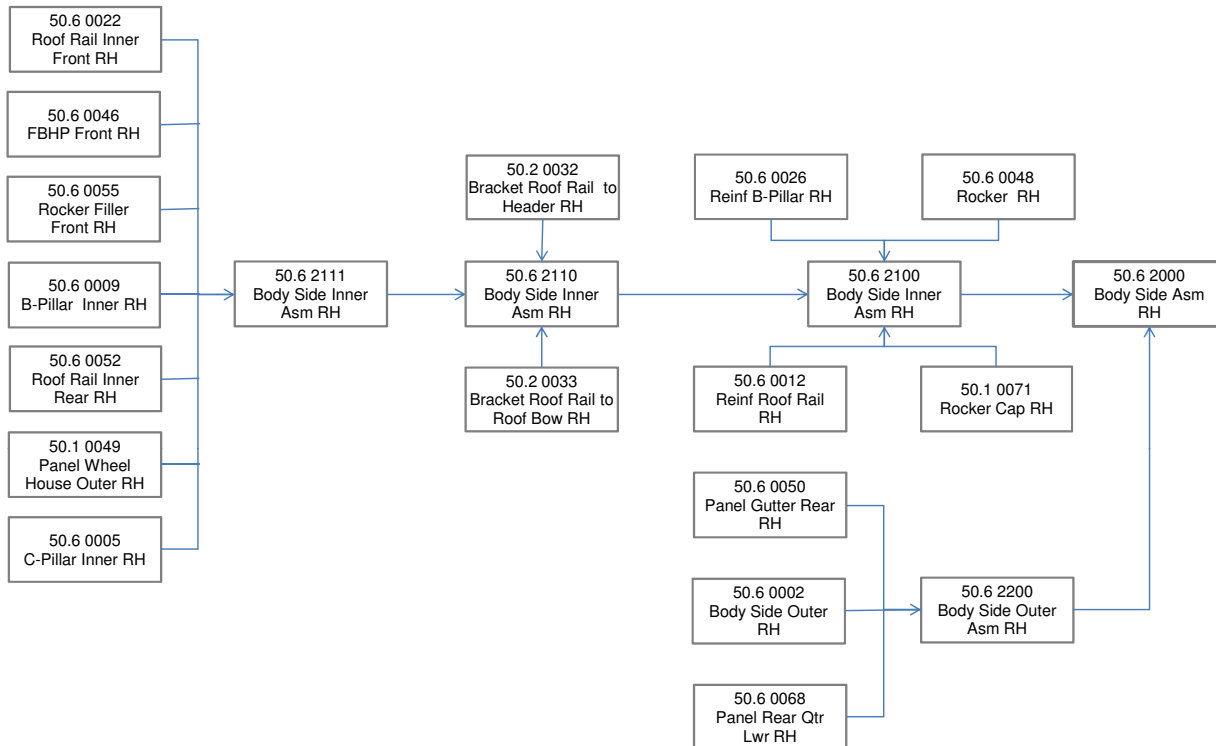
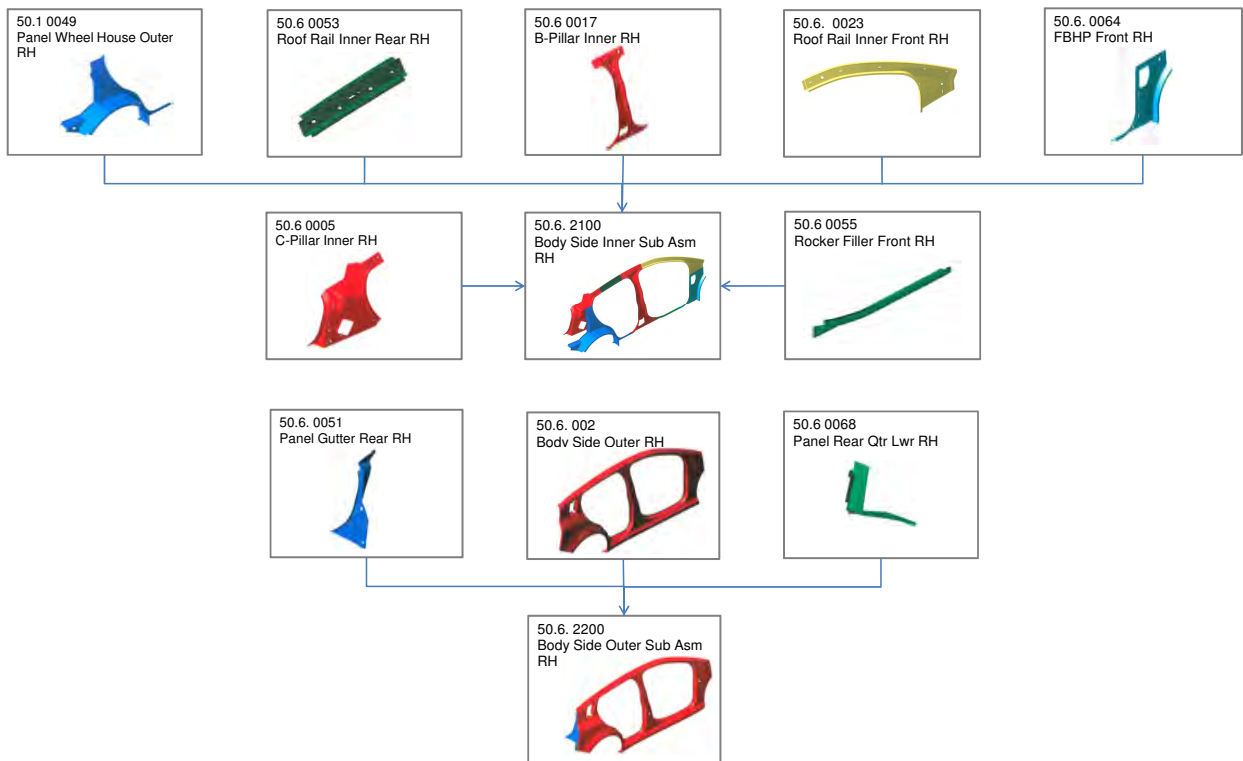
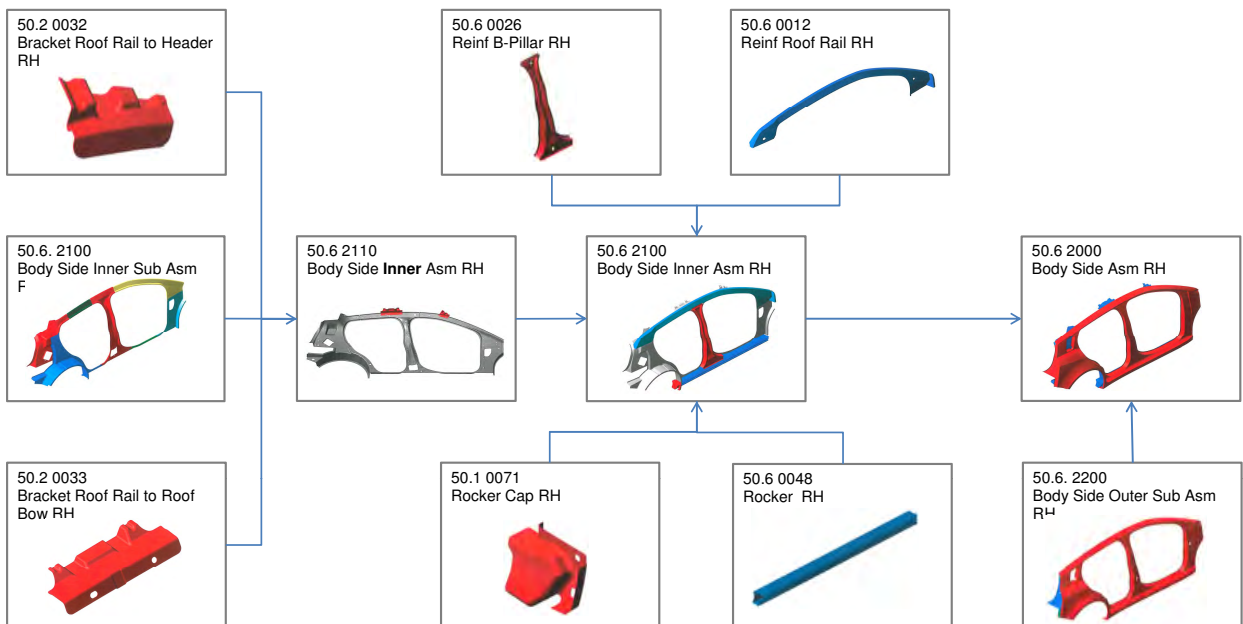


Figure 13.88: 50.6 2000 Body side assembly sequence part block diagram, (RH)


Figure 13.89: Body side sub-assemblies (RH)

Figure 13.90: Body side assembly (RH)

13.3.2.31 50.6 2111 Body Side Inner Assembly RH

All parts are manually loaded to a vertical assembly fixture, then automatically clamped. Welding is completed using two manually operated spot welders. See Figure 13.91 showing body side inner assembly.



Figure 13.91: 50.6 2111 Body side inner assembly

13.3.2.32 50.6 2110 Body Side Inner Assembly RH

At the same station as 50.6 2111, the brackets for the front header and roof bow are loaded. Using the same manually operated spot welder as used for 50.6 2111, welding is completed. When complete, the assembly is unclamped and unloaded using an assist hoist and placed in a holding rack before moving to the body side inner laser assembly station, 50.6 2100. See Figure 13.92 showing 50.6 2110 body side inner assembly RH.



Figure 13.92: 50.6 2110 Body side inner assembly

13.3.2.33 50.6 2100 Body Side Inner Assembly RH

At this station, all parts are assembled in a laser welding cell. The body side inner assembly, 50.1 2110 is loaded to a vertical assembly fixture using an assist hoist. All other parts are then added and clamped in position. Prior to assembly the B-pillar reinforcement, rocker and reinforcement roof rail all have laser dimpling in the region of their respective weld areas; this is to aid the degassing of the zinc vapor during the welding process. Welding is completed using two remote laser welding robots, one positioned on each side of the assembly station. Laser welding of parts in the door opening utilizes a stitch pattern of 20-40-20, where 20 is a 20 mm run of weld and 40 being a space of 40 mm. When complete, the assembly indexes to the next assembly station. See Figure 13.93 showing 50.6 2100 body side inner assembly.

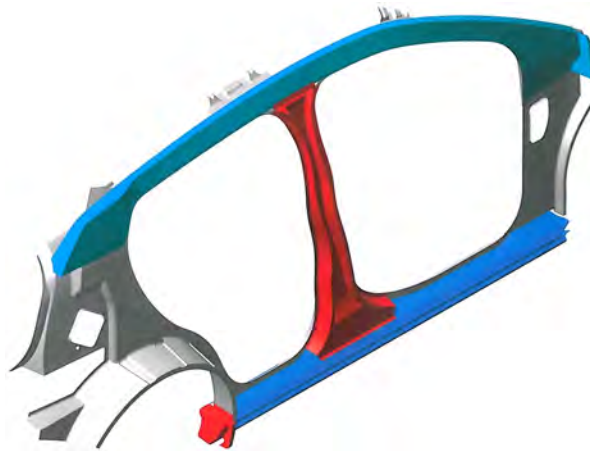


Figure 13.93: 50.6 2100 Body side inner assembly

13.3.2.34 50.6 2200 Body Side Outer Assembly RH

In a “stand alone” horizontal fixture, parts are manually loaded with the body side outer panel loaded with an assist hoist. Welding is completed using a manually operated spot welder. When complete, the assembly is unloaded with the aid of an assist hoist and placed in a holding rack before moving to station 50.6 2000 where body side inner and outer are assembled together. See Figure 13.94 showing 50.6 2200 body side outer assembly.



Figure 13.94: 50.6 2200 Body side outer assembly (RH)

13.3.2.35 50.6 2000 Body Side Assembly RH

At this station, body side inner and outer assemblies are assembled in a laser welding cell. At station 50.6 2000, the body side inner assembly and the body side outer assembly are manually loaded in a vertical assembly fixture after first manually applying hem adhesive to the inner surface of the rear wheel arch on the body side outer assembly. Welding is completed using four remote laser robots, two positioned on each side of the assembly station. In the area of the door opening from the body side outer, side welding in a stitch pattern of 20-40-20 is completed. This is staggered from the weld pattern in the previous assembly station. Where a 20 mm weld is positioned in the center of the 40 mm gap left from the previous station. When complete, the fixture indexes to the roller hemming station where hemming of the body side outer and wheel house outer is completed. See Figure 13.95 showing the body side assembly 50.6 2000.

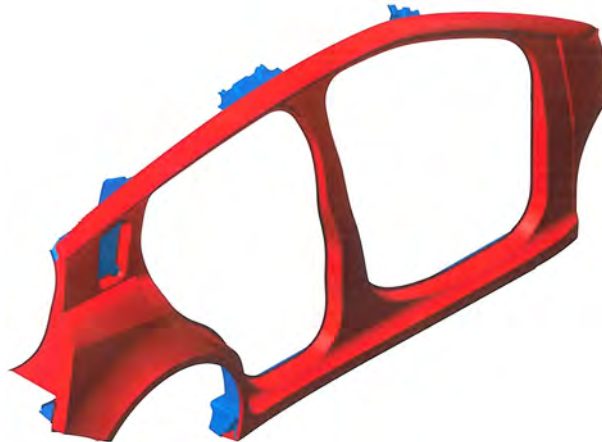


Figure 13.95: 50.6 2000 Body side assembly (RH)

13.3.2.36 50.1 Underbody Assembly

In this assembly station the front structure, front and rear floor are assembled to make the underbody assembly. See Figure 13.96 showing underbody assembly block diagram.

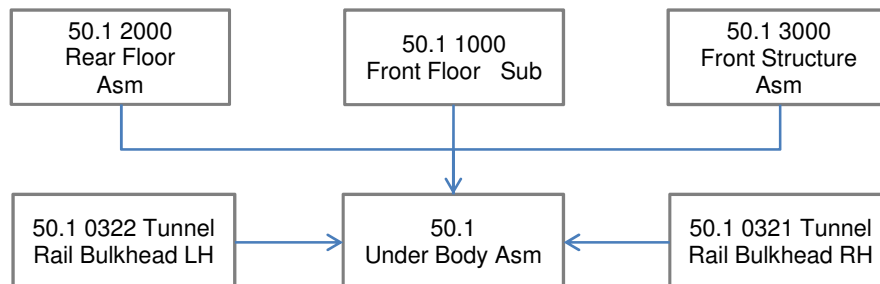


Figure 13.96: Underbody assembly block diagram

The underbody assembly station is a joint spot weld and laser welding cell. The assembly fixture at this station is of a “trunnion” type design where the underbody assembly fixture can be rotated 180 ° giving weld access to the underside of the assembly. The front structure and the front and rear assemblies are robotically loaded and clamped in position. These assemblies are welded together using four spot welding robots, two positioned on each side of the assembly station and two remote laser welding robots, positioned on each side to the assembly station between the spot welding robots. The assembly fixture is then rotated 180 ° and the tunnel rail bulkhead LH/RH added and clamped in position. These are then laser welded to the front and rear floor assemblies. The assembly fixture then rotates to its original position and the completed underbody assembly is robotically unloaded and placed in the “framer #1” station. See Figure 13.97 showing the underbody assembly.

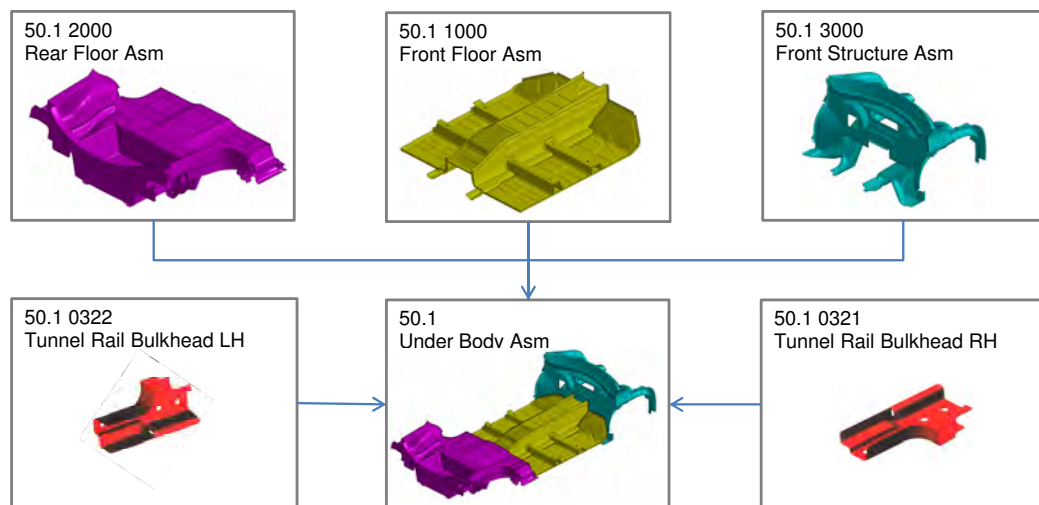


Figure 13.97: Underbody assembly

13.3.2.37 50.1 Body Structure Assembly

(Framer #1)

Framing stations for the FSV, is a laser welding cell. The underbody assembly is robotically loaded in the framing station. The body sides' assemblies LH/RH are then loaded to the framer in a vertical position. These assemblies move to make contact with the underbody assembly. The front and rear headers are then added together with the roof bows and the tunnel upper panel. This is a fully remote laser welding cell that uses five laser robots making approximately 19,000 mm of laser welds, four are dedicated for the body sides, two on each side of the framer, and one remote laser robot for the upper structure. After all welds are complete, the body structure is unclamped and indexes to framing station #2 where the body structure is fully completed. See Figure 13.98 showing the body structure in framing station #1.

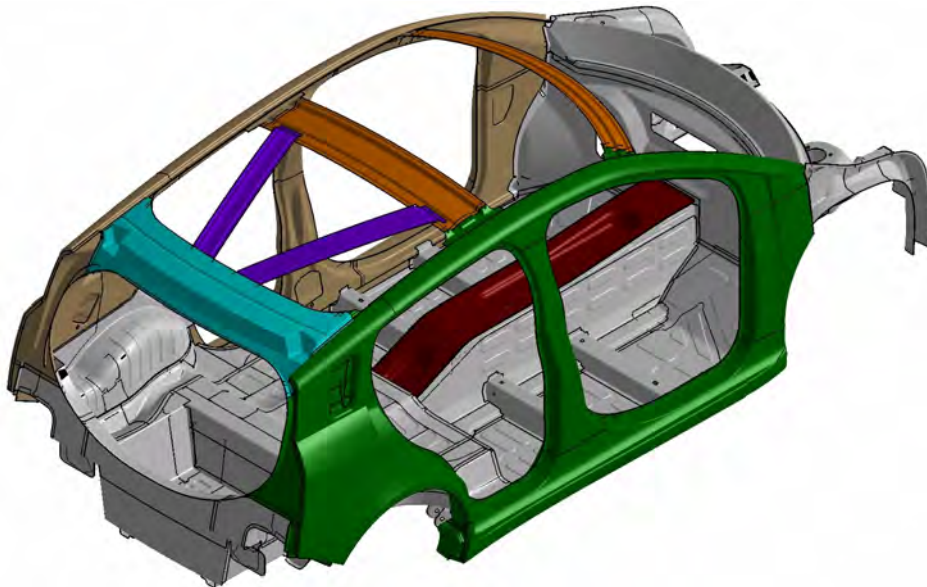


Figure 13.98: *Body structure in framing station #1*

13.3.2.38 50 Body Structure Assembly

(Framer #2)

At this station the body structure is clamped in position. A single robot then applies the anti-flutter adhesive to the front and rear header, including the roof bows. These beads of anti-flutter have no pre-cure and remain in the applied state until curing and expansion takes place in the electro-coat oven in the paint shop. A robotic loader then places the roof panel in position. A spot welding robot applies two spot welds on the front and rear flange to locate the roof to the body structure. The roof panel is then laser brazed. The front and rear flanges are then welded using two remote laser welding robots. The shotgun outer LH/RH are then added and clamped in position. Using two remote laser robots, the shotguns are welded to the body side and the shotgun inner. A total of 6,542 mm of anti-flutter adhesive is used with 3,348 mm of laser brazing and 7,988 mm of laser welding with four spot welds. Prior to assembly, a laser dimpling process is used on the inner surfaces at the joint between the roof panel and the front and rear headers. The shotgun outer is also laser dimpled on the inner surfaces at the joint area to the body side and shotgun inner. See Figure 13.99 showing framer station #2.

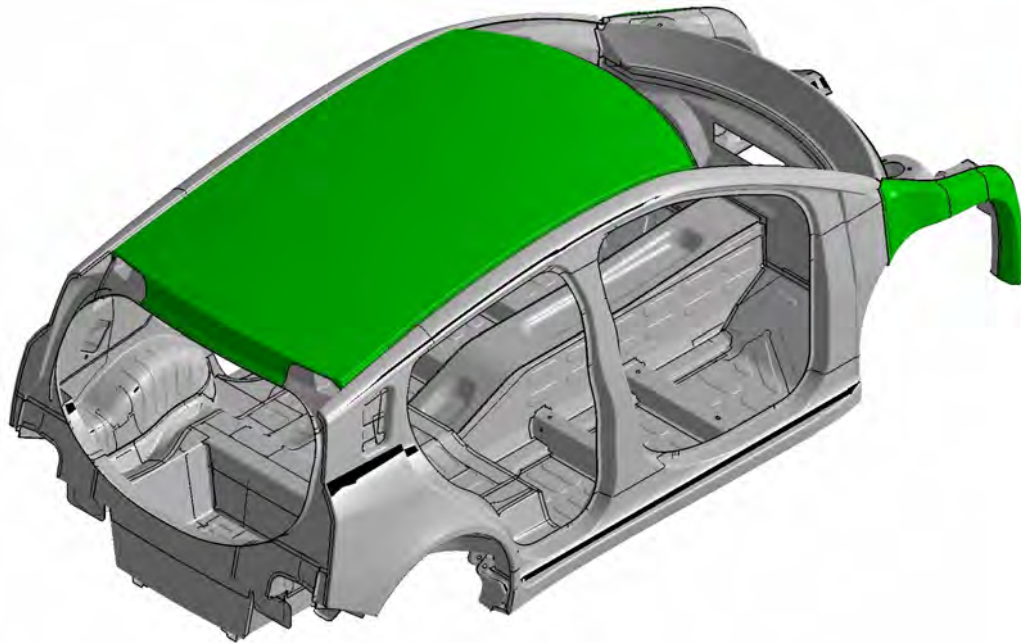


Figure 13.99: Body structure in framing station #2

13.3.2.39 50 Body Structure Assembly Re-Spot Station

After the body structure has been completed in the framer #2 assembly station, the body structure transfers to a re-spot station where it is located and clamped in position. Due to the body structure being fully assembled, minimal clamps are required, which gives greater access for the welding robots. In the re-spot station, any spot weld or laser weld that cannot be made in any of the previous assembly stations is completed. This is generally due to the welding robots having poor access to the body structure resulting from the close proximity of clamps or other fixture structures. Re-spot welding would typically be completed using two spot welding robots and two remote laser welding robots, one of each positioned on each side of the re-spot station.

13.3.2.40 50 Body Structure Assembly with Closures

The completed body structure assembly would then transfer to a line where the closures, front and rear doors, hood, liftgate and the front fenders would then be added. This makes the complete BIW which would then transfer to the vehicle paint shop.

13.3.2.41 50 Body Structure Assembly Quality

To ensure the desired level of quality both at the individual part level and assembly level, a number of quality checks need to be made. Each part and assembly will have its own dedicated checking

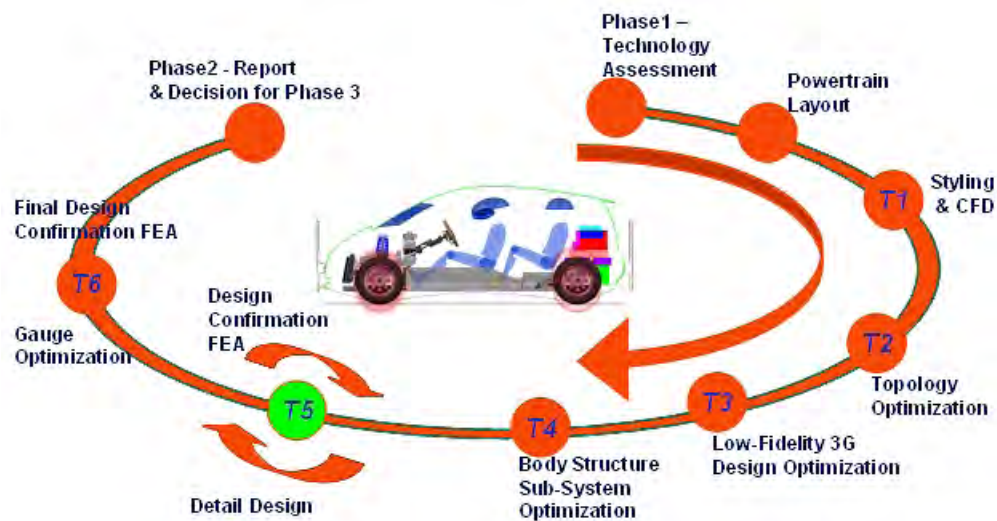
fixture. The part will be located by 2-way and 4-way locator pins and clamped over pre-designation location blocks. Each major feature, holes, trim edges and (in the case of an assembly), part position is also checked. For small parts and assemblies, this can be made by using a manual checking operation, but for larger parts, assemblies and critical parts like the body side outer, a Coordinate-Measuring-Machine (CMM) check is made. For the final body structure assembly, a dedicated laser checking measuring cell is used. Data is then automatically made available to the quality department where it is analyzed and corrections (if required), are made to the assembly process.

13.3.2.42 50 Body Structure Assembly

For the assembly of the body structure, we have used a number of joining techniques.

- Number of spot welds: 1023
- Length of laser welds: 83,584 mm
- Length of laser braze: 3,348 mm
- Length of hem flange: 2,257 mm
- Length of hem adhesive: 2,257 mm
- Length of structural adhesive: 9,786 mm
- Length of anti-flutter adhesive: 6,542 mm

14.0 Body Structure Performance CAE Analysis Results



14.1 Crash Worthiness

14.1.1 FSV-1 BEV Body Structure Load Paths

14.1.1.1 Front End Structure

The body structure of the FSV BEV is designed with very efficient load paths that were identified through the application of a unique design and optimization methodology. The front end of the BEV takes full advantage of the smaller package space required for the electric drive motor as compared with a typical Internal Combustion Engine (ICE) and transmission package. The additional packaging space allows for straighter fully optimized front rails with larger sections as shown in Figure 14.1 and Figure 14.2. The front rails load path 1, curved shotguns load path 2 and the motor cradle load path 3 work together to manage frontal crash events with minimal intrusions into the passenger compartment.

With the availability of several high strength grades of steel with higher elongation, the complex geometric sections determined through computer geometry optimization, can be manufactured

using laser welded blanks with the following three manufacturing options and materials:

1. Hot Stamping with tailor quenching - HF 1050/1500 grade of steel
2. TWIP 500/980 grade of steel
3. TRIP 600/980 grade of steel

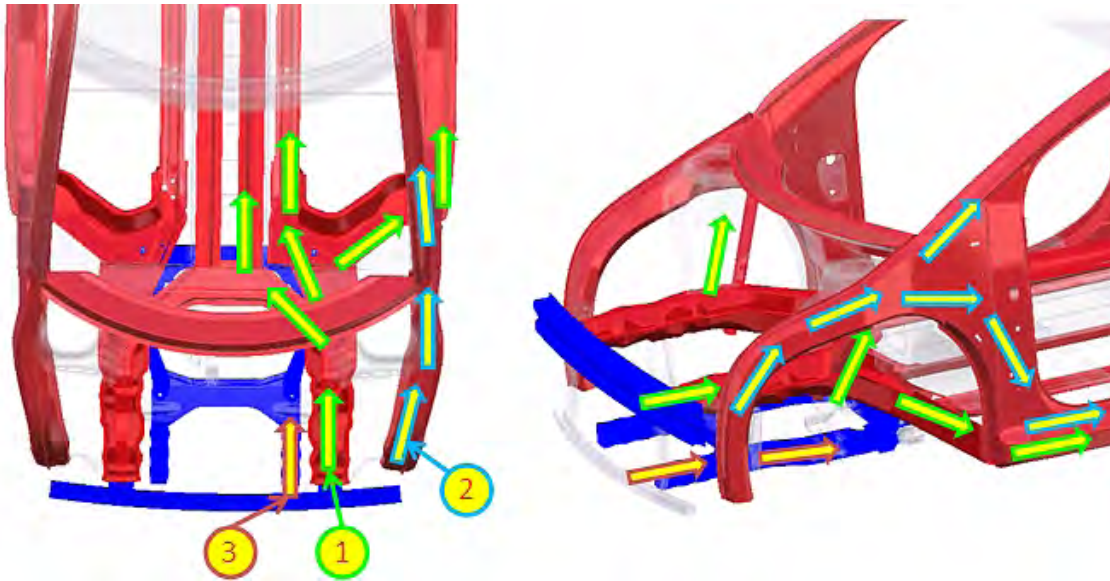


Figure 14.1: BEV front end rails, curved shotguns and motor cradle

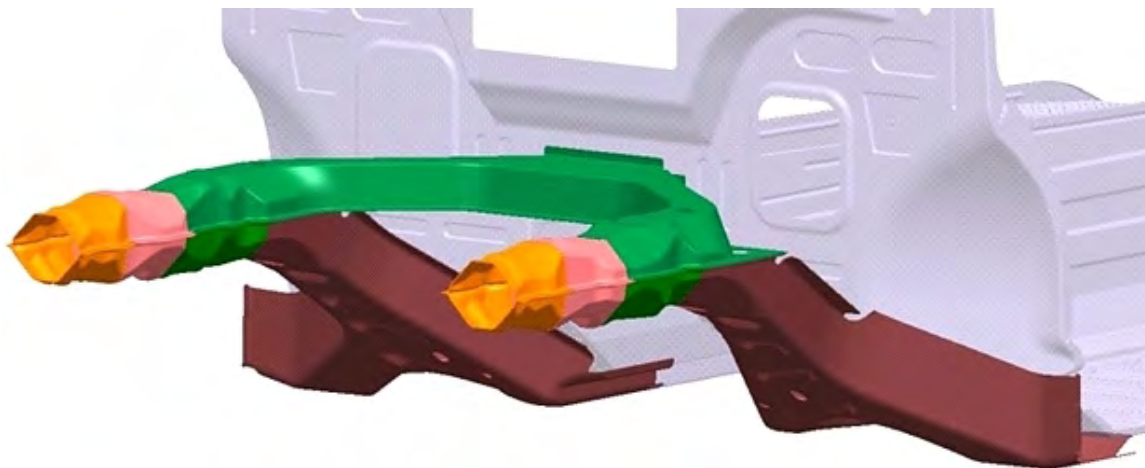


Figure 14.2: BEV front end optimized rails

The loads from the front rails illustrated in Figure 14.1 (load path 1), are reacted by a tripod construction through the rocker section, base and top of the tunnel. To stabilize the rear of the rails, an additional load path is introduced behind the shock tower to direct the loads into the base

of the 'A-Pillar'. The BEV requires a deep tunnel to house the 30 kWh (end of life) battery pack. The top and bottom of the tunnel structure, when combined with the bolt-on 207 kg, battery pack, acts as a structural “backbone” of the vehicle structure.

The energy absorption of the front end is further enhanced with the addition of distinctively curved upper shotgun members as shown in Figure 14.1, load path number 2. These members absorb a significant amount of energy during frontal impact (USNCAP). The shotguns inner and outer panels also take advantage of high strength grades of steel for manufacturing options similar to the front rails. The motor mounting cradle shown in blue in Figure 14.1, load path number 3, is also designed to absorb energy during frontal crash load cases as well as support the motor assembly and front suspension.

With the combination of the three active load paths, the deceleration pulse of the structure can be tailored to achieve a more aggressive front end structure during the 0 to 30 millisecond crash time frame and then is reduced to a normal level during the 30 to 60 millisecond time frame when the occupant is interacting with the airbag. This approach has been shown to be beneficial for the occupants of smaller vehicles when involved in frontal crashes with larger vehicles ^[1]. The deceleration pulse for the BEV (US NCAP 35 mph Rigid Barrier Impact), is shown in Figure 14.3.

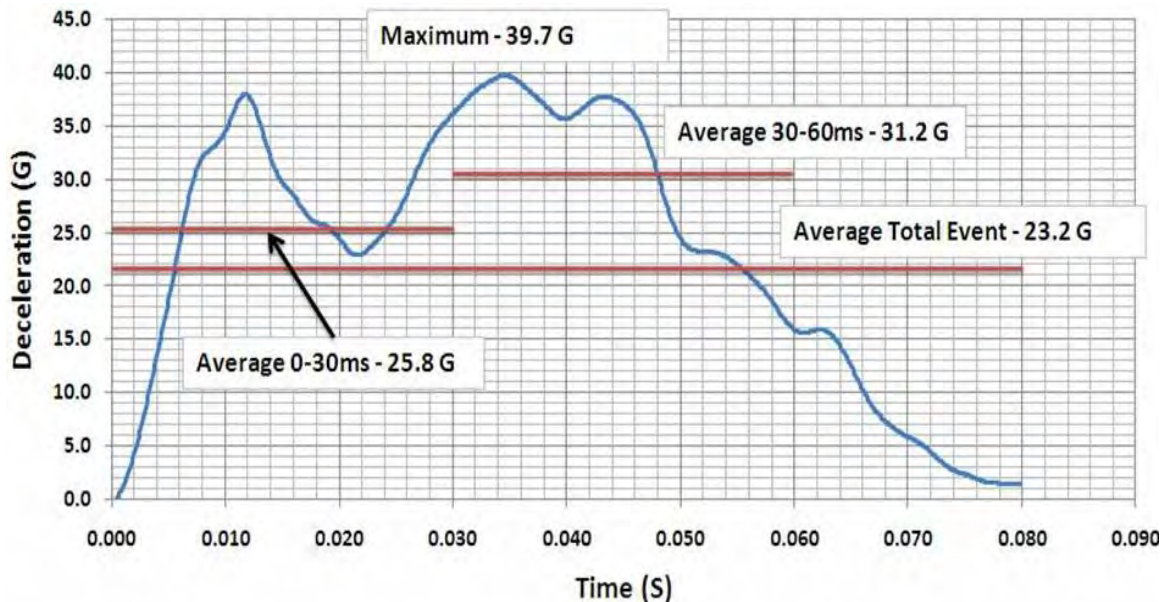


Figure 14.3: US NCAP 35 mph front rigid barrier pulse at B-Pillar

¹ref: Jeremy J. Blum et al: Vehicle Related Factors that Influence Injury Outcome in Head-On Collisions. 52nd AAAM Annual Conference, Annals of Advances in Automotive Medicine, October 2008

14.1.1.2 FSV Side Structure for Side Impact

The design and construction of the FSV side structure incorporates several load paths that take advantage of very high strength levels afforded by Ultra High Strength Steels (UHSS). The B-pillar Inner & Outer shown in Figure 14.4 as load path 1, are constructed from Hot-Stamped (HF1050/1500), steel. Load path 2, of the Roof Rail Inner & Outer is also hot stamped. Through the use of hot stamping, complex shapes can be manufactured with very high tensile strengths (1500 to 1600 MPa). This level of strength is highly effective in achieving lower intrusions into the occupant compartment and strengthens the upper body structure for roll-over protection (roof test). The rocker section, (load path 3 Figure 14.4), plays a major role in side impact protection; in particular for the pole impact. The rocker is constructed from an optimized closed roll-formed section using Complex Phase (CP), steel grade (CP1050/1470). The unique section profile was derived using the optimization methodology developed for the FSV project.

Additional side impact load paths through the body structure, make use of the front seat mounting cross members, shown as load path 4 in Figure 14.4. The two seat mounting cross members are roll formed from a very high strength martensitic grade of steel (MS950/1200). The fore-aft position of these members is aligned with bolt on cross-members that form the base of the battery structure, forming continuous load paths across the floor structure. Another unique load path for side impact is created through strengthened seat back cross tubes, shown as load path 5 in Figure 14.4. This cross car load path is at a higher vertical height and is very effective in transferring the loads through the side structure (body and door), the driver seat and top of the tunnel. This load path is further explained in Section 14.1.3.1 (CAE Analysis Results - Side Impact) of this report.

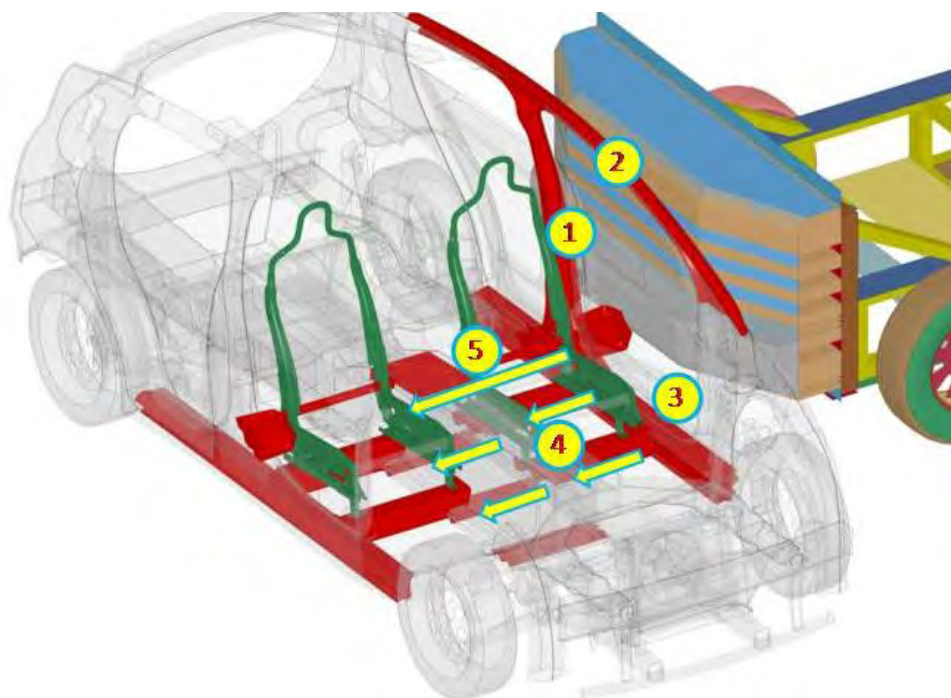


Figure 14.4: *FSV side impact structural load paths*

14.1.1.3 FSV Rear Structure for Rear Impact

The design and construction of the FSV rear structure, incorporates two major load paths as shown in Figure 14.5. Load path number 1 is the rear rail section that is constructed from three LWB stampings as shown in Figure 14.6. The shape of the rear rail section was determined through optimization methodology applied to this project. To protect the battery pack during rear impact, roll formed sections were included from the bottom of the tunnel towards the rear of the vehicle under the rear floor as shown by load path number 2 in Figure 14.5. These two load paths, in combination with the rear cross-member, form a very rigid cage around the battery pack.

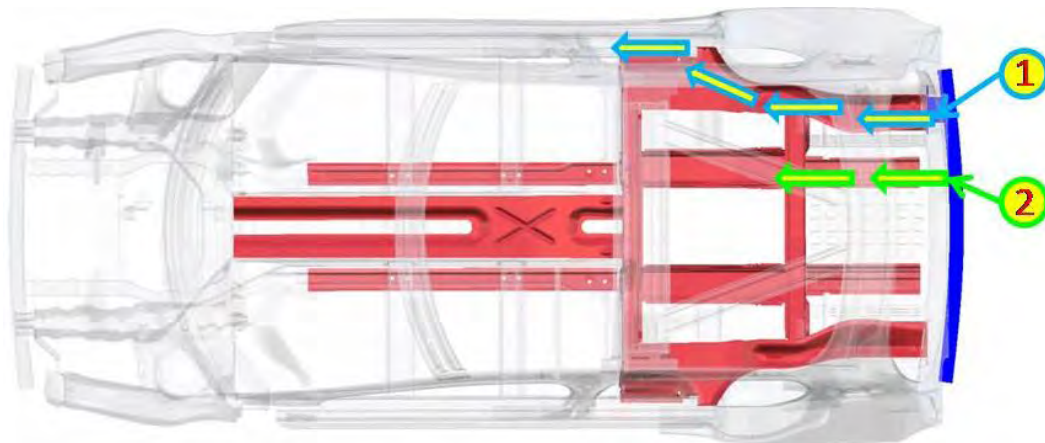


Figure 14.5: FSV rear impact structural load paths



Figure 14.6: FSV rear rail - optimized sections

14.1.2 Frontal Impact

14.1.2.1 US NCAP Front Crash Analysis

The frontal impact test of the New Car Assessment Program (NCAP), undertaken by the National Highway Traffic Safety Association (NHTSA), is a full frontal barrier test at a vehicle speed of 56 km/h (35 mph).

The FSV model used in the US NCAP analysis, weighs 1078 kg, which includes a body structure weight of 187.7 kg, a Hybrid III 50% driver of 75 kg, and a Hybrid III 5% passenger of 45 kg. The analysis model includes only a general simple seatbelt system as well as test dummies as shown in Figure 14.7 to represent the occupants.



Figure 14.7: Test dummies with restraint system

Seatbelt shoulder anchorage and retractor location are at the B-pillar. The outboard lap belt anchorage location is at the rocker inner panel, and the inboard lap belt anchorage is on the seat as shown in Figure 14.8.

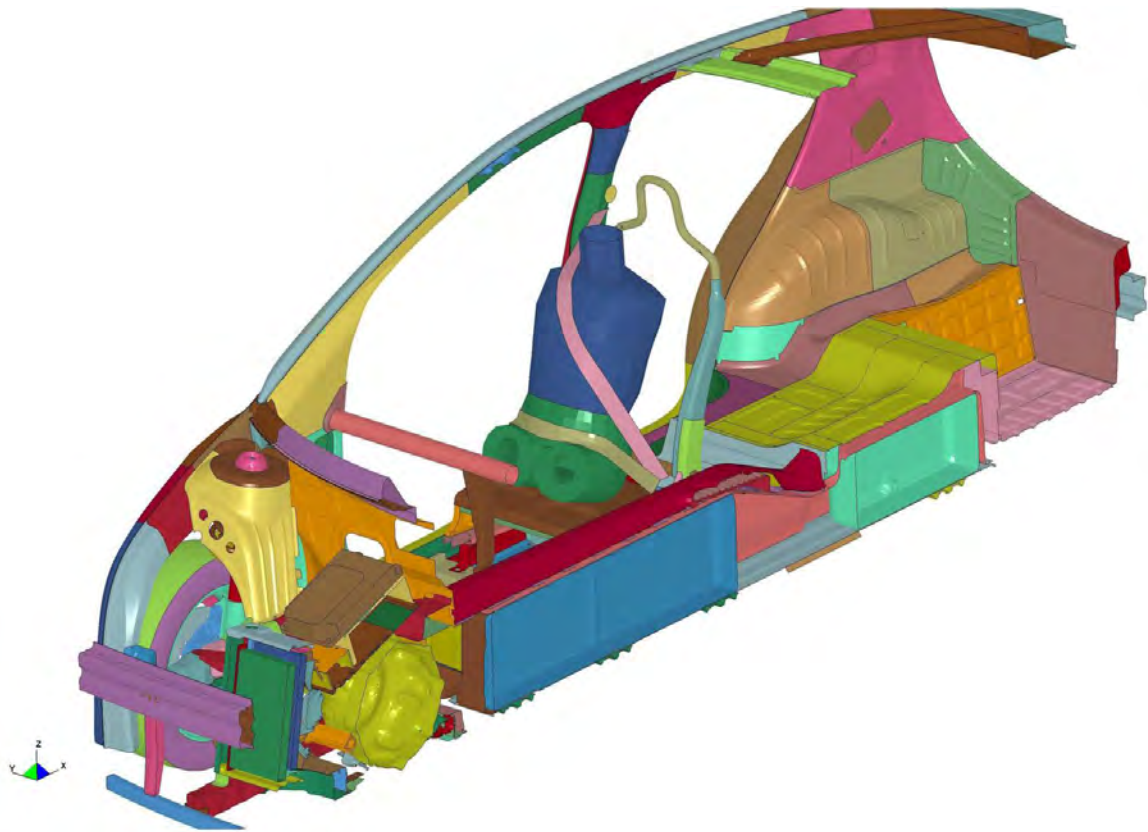


Figure 14.8: *US NCAP front crash - Seatbelt routing*

To measure cabin structure integrity, data analysis points in Figure 14.9 (inside view is shown in Figure 14.10) are measured with respect to coordinate system reference points established in the luggage area of the FSV body structure, and reference point locations follow IIHS standards. To measure Instrument Panel (IP) movements, two reference points are taken from the cowl cross member.

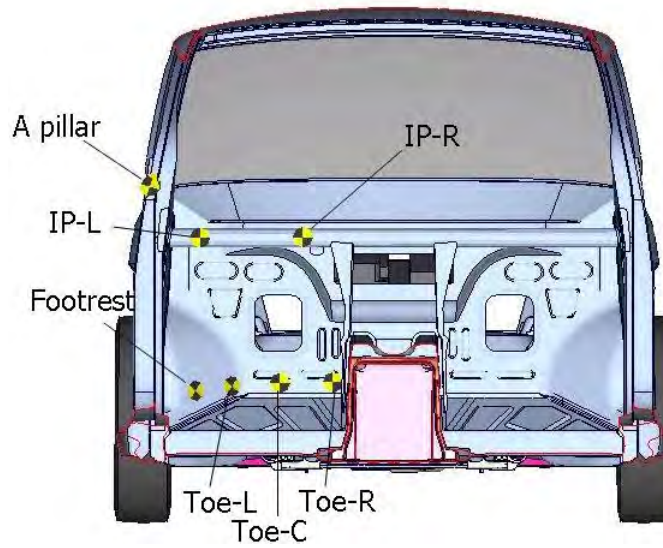
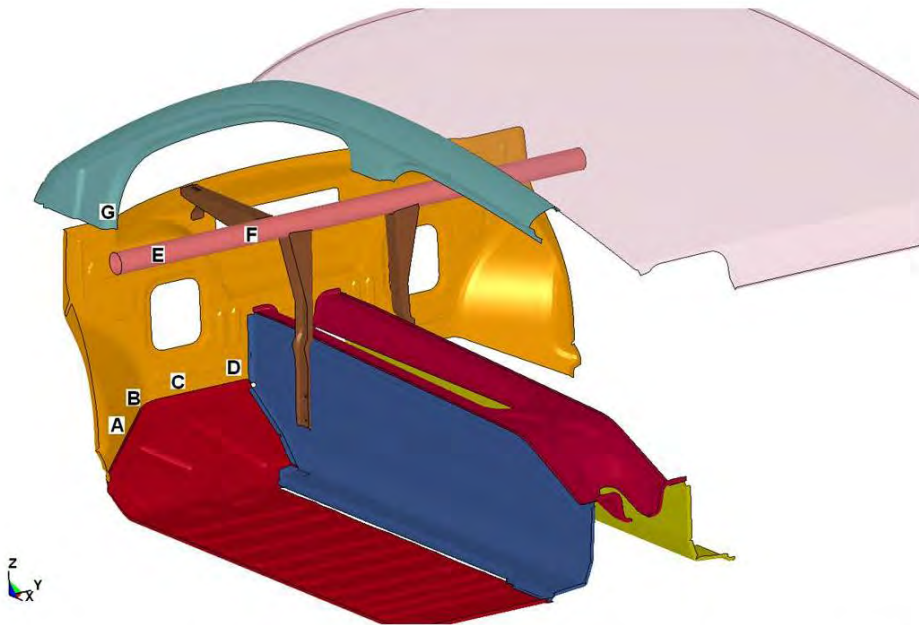


Figure 14.9: US NCAP front crash - Intrusion measurements on cabin structure



A – Footrest, B – Toe-left, C – Toe-center, D – Toe-right, E – IP-left, F – IP-right, G – A-pillar

Figure 14.10: US NCAP front crash - Intrusion measurements on cabin structure (inside view of dash pan and floor)

14.1 Crash Worthiness

The US-NCAP Frontal Crash deformation for the FSV are shown in Figure 14.11 and Figure 14.12.

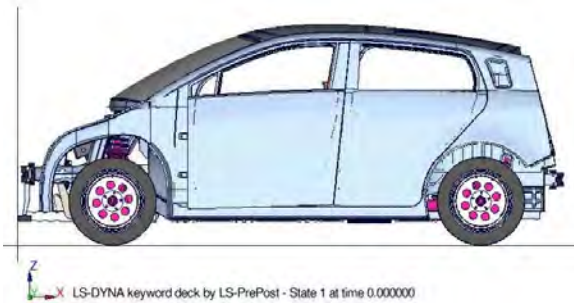


Figure 14.11: US-NCAP Frontal Crash - initial state

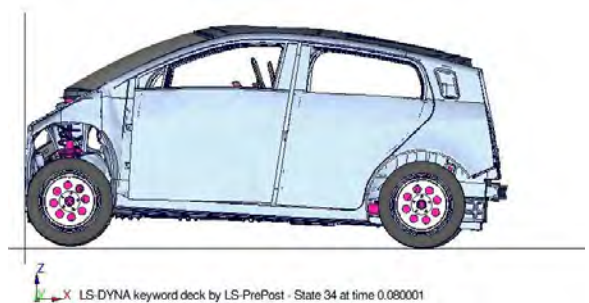


Figure 14.12: US-NCAP Frontal Crash - at 80 msec

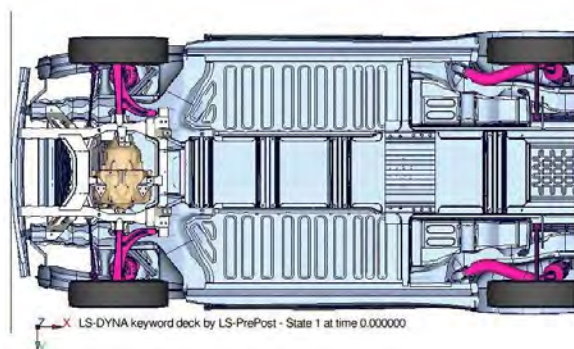


Figure 14.13: US NCAP frontal crash - initial state (% plastic strain)

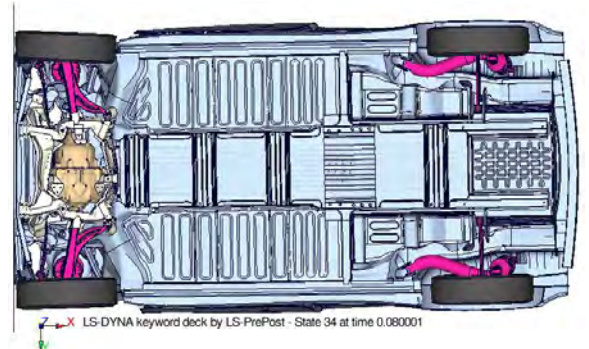


Figure 14.14: US NCAP frontal crash - at 80 msec (% plastic strain)

Energy absorption can easily be understood by the use of “plastic strain contours” generated by the FSV model analysis. The US-NCAP Frontal Crash plastic strain contours on major load paths are shown in Figure 14.13 and Figure 14.14. The upper limit is set to 10% to visualize a high energy absorbing zone.

The plastic strain contours in the FSV front rail during the US-NCAP frontal crash, is shown in Figure 14.15 and Figure 14.16.

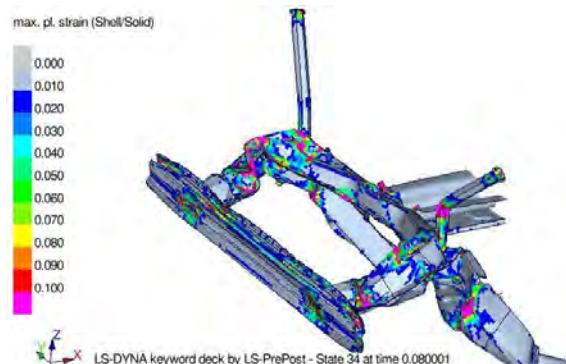
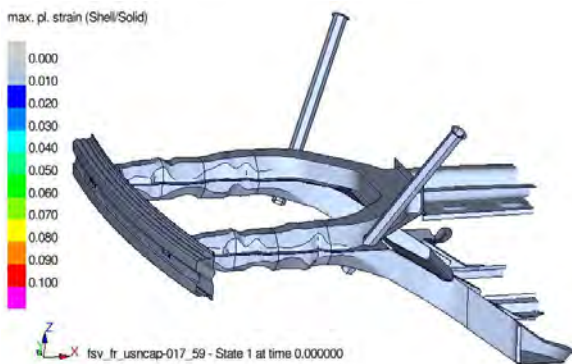
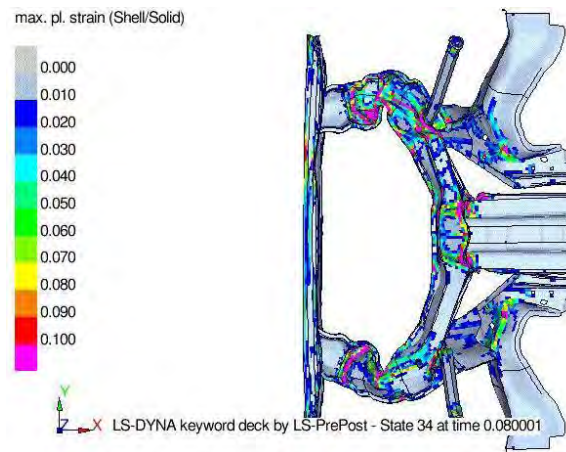
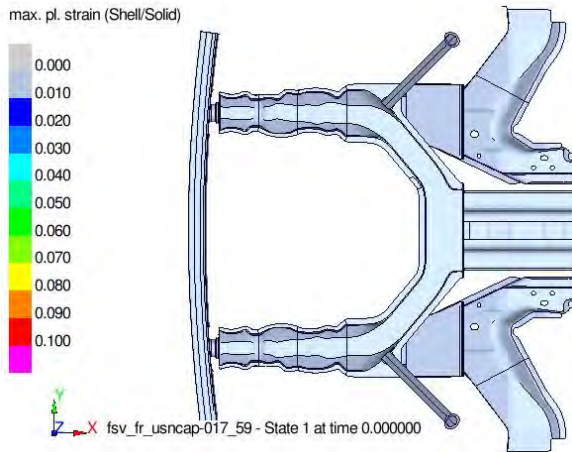


Figure 14.15: Front rail initial state (% plastic strain contour)

Figure 14.16: Front rail at 80 msec (% plastic strain contour)

Another important aspect taken into consideration during the development of the FSV, was that the battery should be protected to prevent electric shock or fire in the US-NCAP frontal crash event. The FSV battery is protected well enough such that the battery package space does not have physical contact to any other part, as shown in Figure 14.17 and Figure 14.18.

14.1 Crash Worthiness

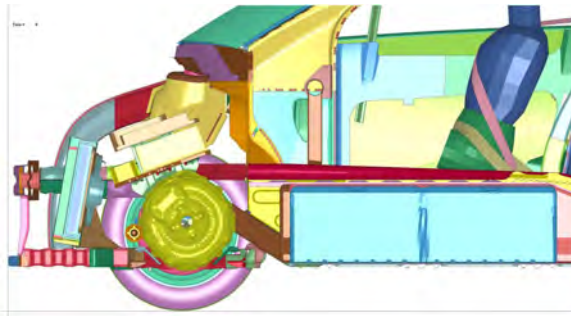


Figure 14.17: *FSV battery - US-NCAP initial state*

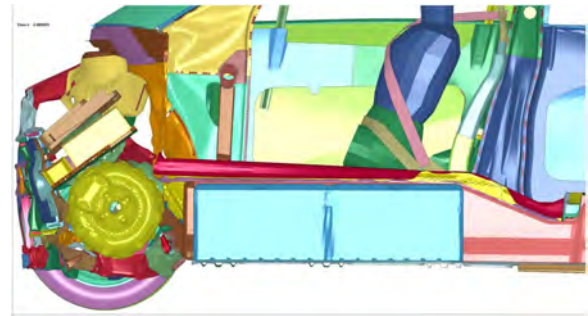
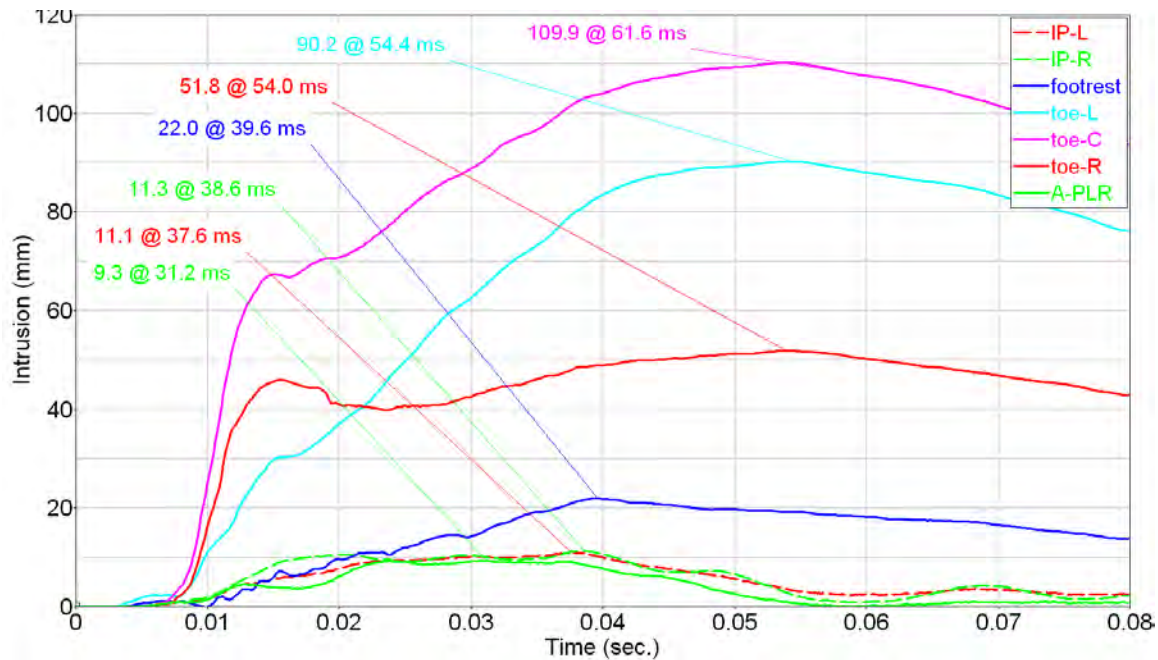


Figure 14.18: *FSV battery - US-NCAP at 80 msec*

To lower occupant injury, the cabin structure needs to be protected. As a measurement of cabin structure protection, intrusion points generated by the analysis were measured, and the results indicate that the FSV has good occupant protection as shown in Figure 14.19 and Table 14.1. NCAP performance is based exclusively on occupant injury criteria which is beyond the scope of this study. There is precedence for evaluating body structure performance based on intrusion and deceleration pulse targets. In determining our intrusion targets, we applied the IIHS ODB targets since these are similar passenger injury events. The 35 to 38 g range for the target is a conservative value, with precedence in other programs where this pulse has exceeded 40 g and still achieve excellent front end crash performance. Before 35 ms, higher decelerations are permitted since the passenger is not yet engaged with the seatbelt and airbag and as a result, does not experience B-pillar decelerations that occur before 35 ms. The intrusion into the footwell area of the passenger compartment for all the intrusion points fell into "Good" rating band, except for Toe-Center which fell in the "Acceptable" rating band. The IIHS ODB rating system states: "When intrusion measurements fall in different rating bands, the final rating generally reflects the band with the most measures." [2] Since the FSV results show only one intrusion measurement that fell in the "Acceptable" rating band; the overall FSV footwell intrusion rating for the US NCAP frontal impact is "Good". This, coupled with the conservative deceleration pulse target and the 39.7 g maximum deceleration pulse achieved, led the engineering team to conclude that performance is sufficient to support achievement of a five-star safety rating in conjunction with passive safety equipment.

²IIHS Frontal Offset Crashworthiness Evaluation Guidelines for Rating Structural Performance


Figure 14.19: US NCAP front crash - Dash intrusion results

FSV Cabin Structure Measuring Point	Intrusion (mm)	Intrusion Target for Good Rating (mm)
Footrest	22.0	< 100
Toe-L	90.2	< 100
Toe-C	109.9	< 100
Toe-R	51.8	< 100
IP-L	11.7	< 100
IP-R	11.3	< 100
A-pillar	9.3	< 100

Table 14.1: US NCAP front crash - Maximum USNCAP dash intrusion at various measuring points

The FSV model analysis shows a good aperture for the struck door, with a maximum value of 16.6 mm as shown in Figure 14.20, and both front doors are expected to retain their ability to open post-test.

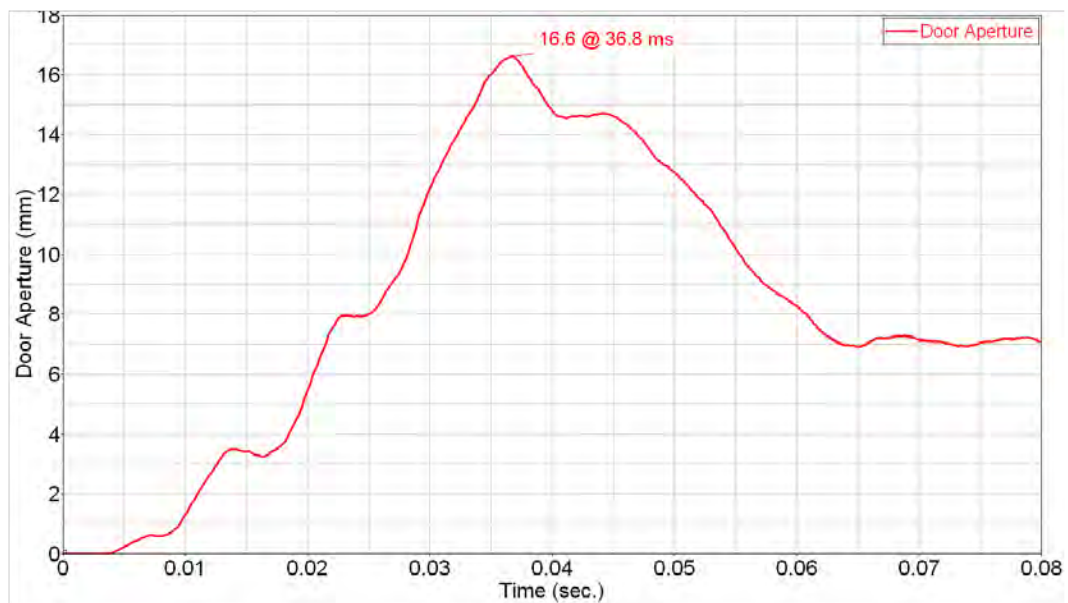
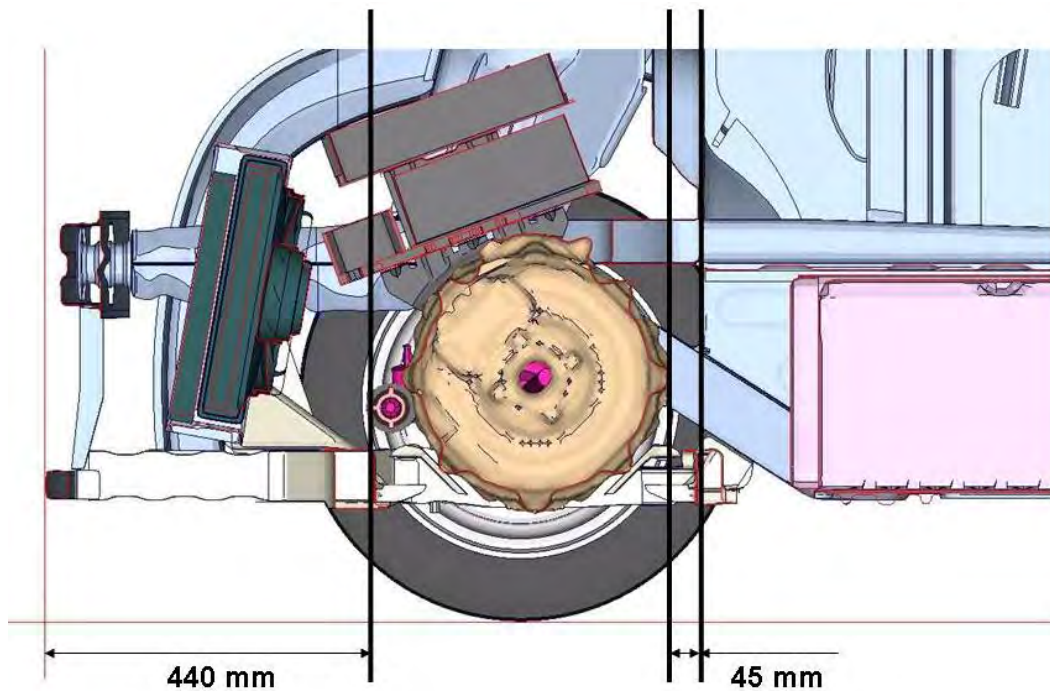


Figure 14.20: US NCAP front crash - FSV Door aperture

The FSV has 485 mm of “ideal design” crush space. As shown in Figure 14.21, the crush distance of the CAE model is 463.0 mm.



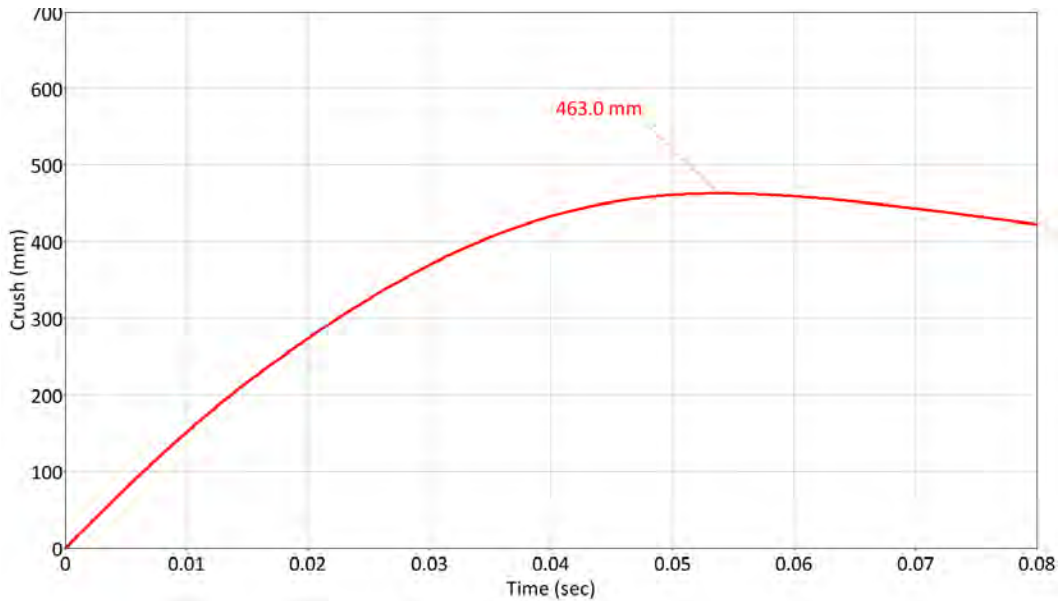


Figure 14.21: US NCAP front crash - FSV crush distance

The FSV target for the peak crash pulse is 35 to 38 g. As shown in Figure 14.22, the maximum pulse is 39.7 g at 35 msec.

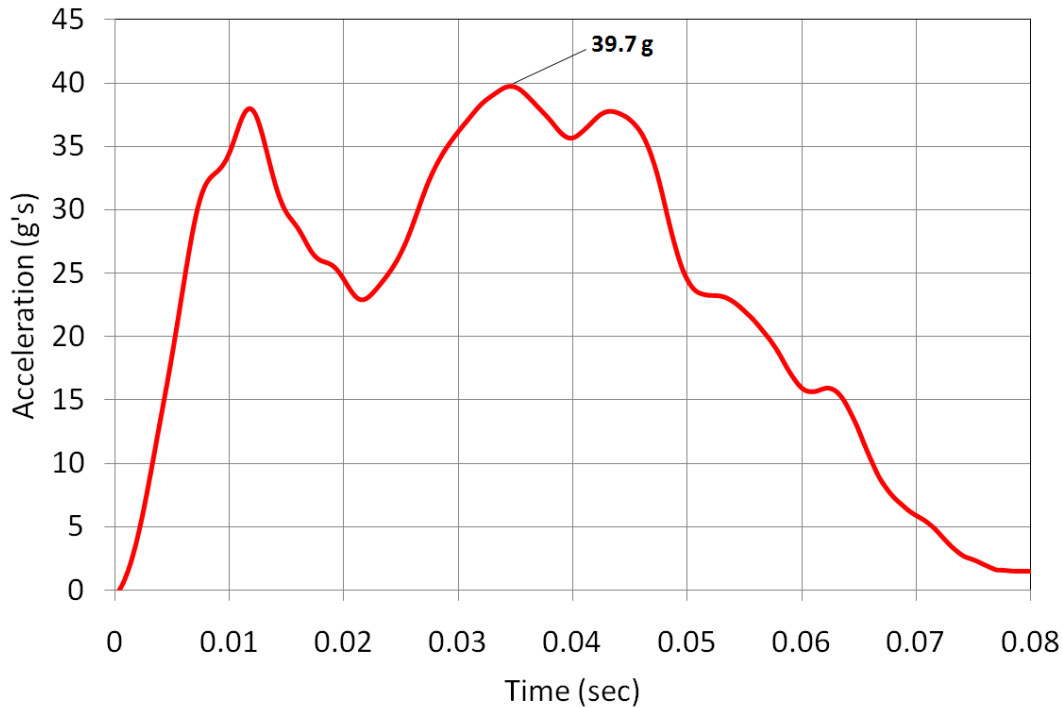


Figure 14.22: US NCAP front crash - FSV B-pillar Acceleration

14.1.2.2 Euro NCAP/IIHS Front Crash Analysis

The European New Car Assessment Program (Euro NCAP) specifies an offset frontal impact of 64 km/h into a deformable barrier with a vehicle overlap of 40%. The deformable barrier conforms to that specified in ECE R.94 “Frontal Collision Protection”.

The Euro NCAP analysis model includes a body structure weight of 187.7 kg and two Hybrid III 50 % dummies; representing the driver and the front seat occupant.

The seatbelt shoulder anchorage and the seatbelt retractor location is at the B-pillar. The outboard lap belt anchorage is at the inner rocker panel, and the inboard lap belt anchorage is on the seat (same as the US NCAP as illustrated in Figure 14.8).

To measure cabin structure integrity, data analysis points in Figure 14.23 are measured with respect to coordinate system reference points established in the luggage area of the FSV body structure, and reference point locations follow IIHS standards. To measure Instrument Panel (IP) movements, two reference points are taken from cowl cross member.

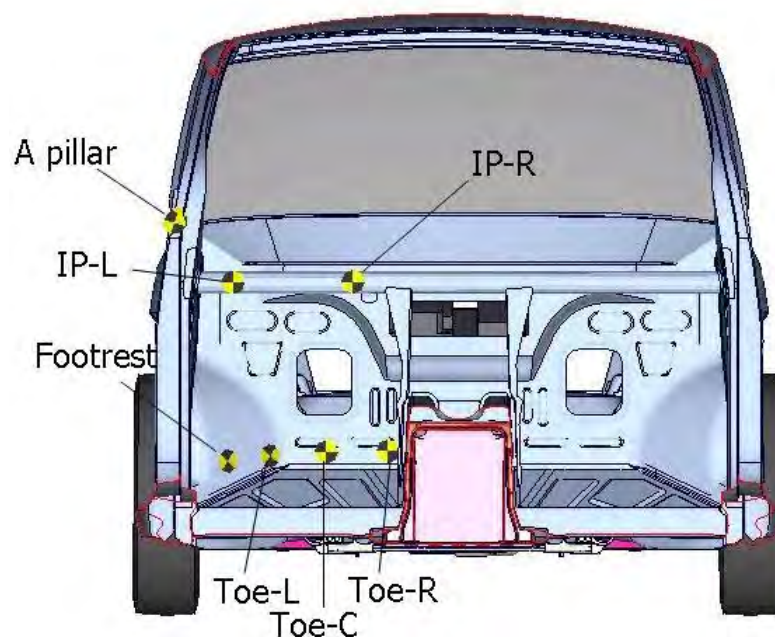


Figure 14.23: Intrusion measurements on cabin structure

The Euro NCAP Frontal Crash deformation results of the FSV are shown in Figure 14.24 and Figure 14.25.

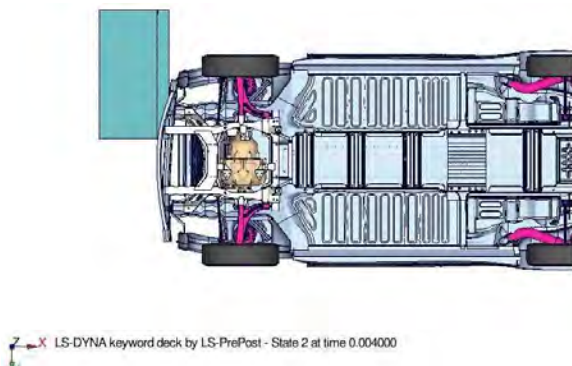
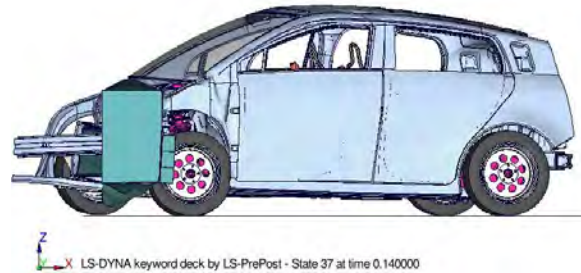
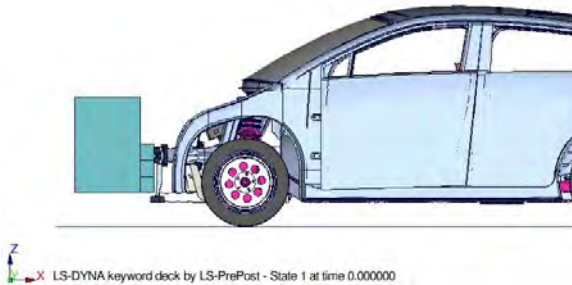


Figure 14.24: Euro NCAP frontal crash - initial state

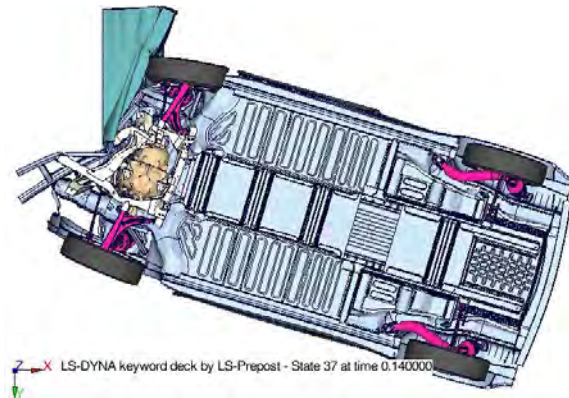


Figure 14.25: Euro NCAP frontal crash - at 140 msec

Energy absorption can easily be understood by the use of “plastic strain contours” generated by the FSV model analysis. The Euro NCAP Frontal Crash plastic strain contours on major load paths are shown Figure 14.26 and Figure 14.27. The upper limit is set to 10% to visualize a high energy absorbing zone.

14.1 Crash Worthiness

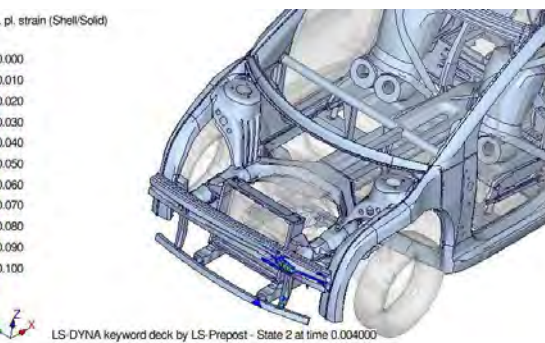
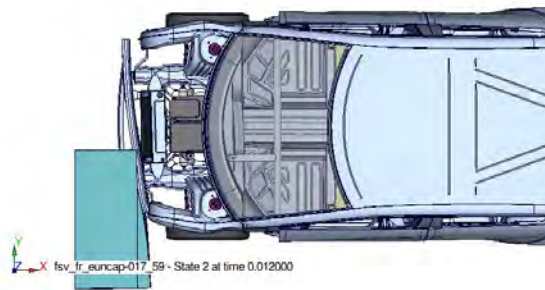


Figure 14.26: Euro NCAP frontal crash - initial state (% plastic strain)

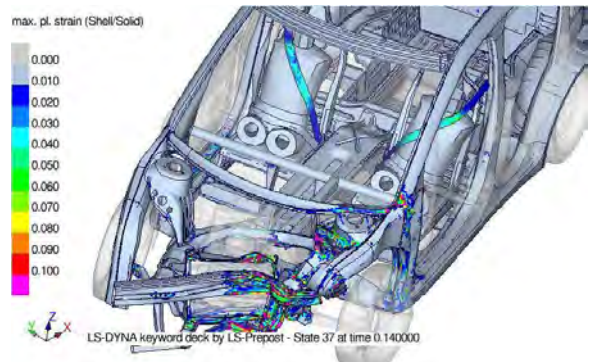
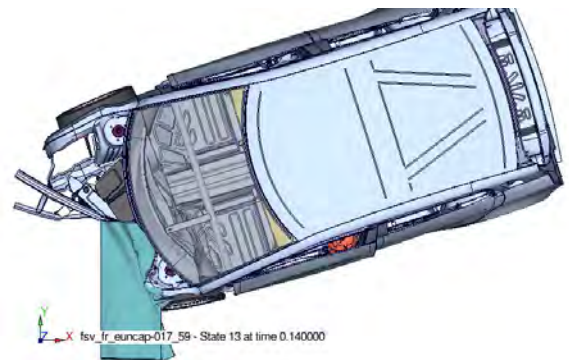


Figure 14.27: Euro NCAP frontal crash - at 140 msec (% plastic strain)

The plastic strain contours in the FSV front rail during the Euro-NCAP frontal crash is shown in Figure 14.28 and Figure 14.29.

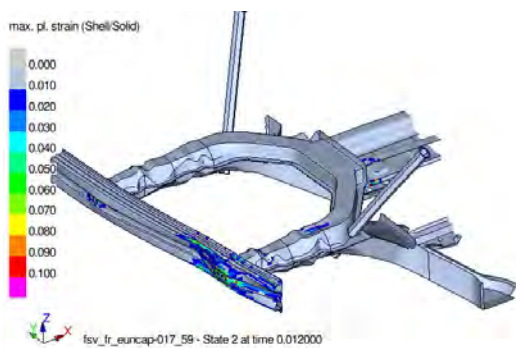


Figure 14.28: Euro NCAP % plastic strain contours - front rail initial state

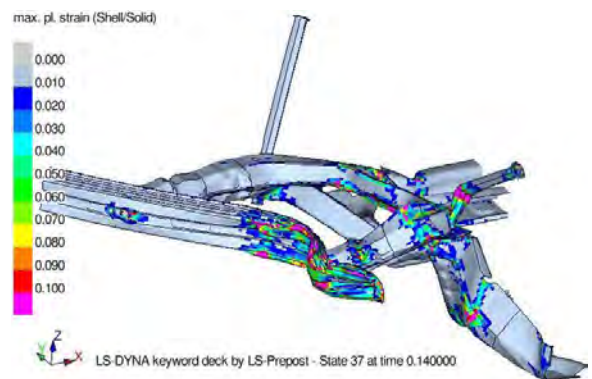


Figure 14.29: Euro NCAP % plastic strain contours - front rail at 140 msec

Another important aspect taken into consideration during the development of the FSV, was that

the battery should be protected to prevent electric shock or fire in the Euro-NCAP frontal crash event. The FSV battery is protected well enough such that the battery package space does not have physical contact to any other part, as shown in Figure 14.30 and Figure 14.31.

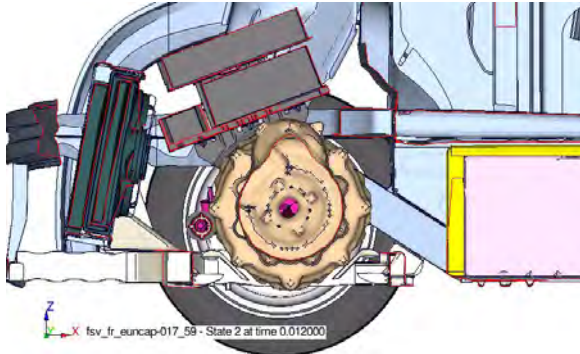


Figure 14.30: FSV battery - Euro-NCAP initial state

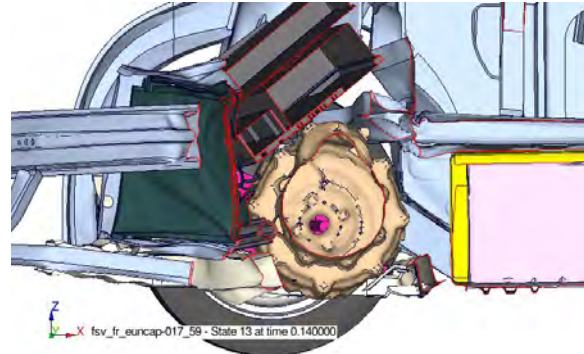


Figure 14.31: FSV battery - Euro-NCAP at 140 msec

To lower occupant injury, the cabin structure needs to be protected. As a measurement of cabin structure protection, intrusion points generated by the Euro NCAP analysis as shown in Figure 14.23 were measured, and the results indicate that the FSV has good occupant protection as shown in Figure 14.32 and Table 14.2. There is no severe deformation of the structure to cause a penetration of the firewall, and the cabin structure is protected well enough. Since the FSV does not include foot pedals in the analysis model, measuring potential pedal intrusion was not performed. Euro NCAP targets are based solely on passenger injury criteria and does not include any structural criteria. However, the Euro NCAP crash event is very similar to the IIHS ODB test and these intrusion targets are applied with the assumption that meeting these targets will enable a good basis for the other safety systems (seatbelts, airbags and interior trim), to meet the passenger injury criteria.

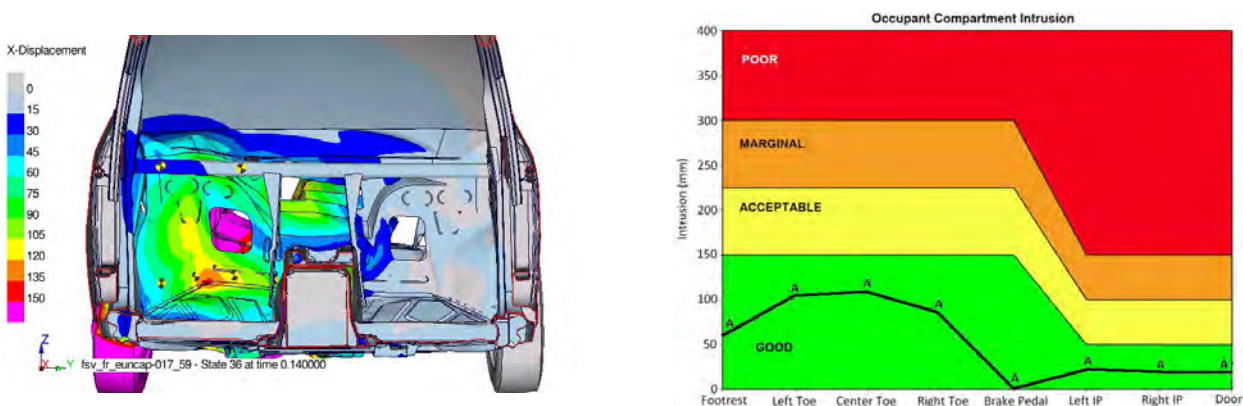


Figure 14.32: Euro NCAP Dash intrusion IIHS rating

FSV Cabin Structure Measuring Point	Intrusion (mm)	Intrusion Target for Good Rating (mm)
Footrest	56.0	< 150
Toe-L	106.0	< 150
Toe-C	119.0	< 150
Toe-R	80.0	< 150
IP-L	21.2	< 50
IP-R	17.9	< 50
A-pillar	18.0	< 50

Table 14.2: Maximum Euro NCAP Dash intrusion at various measuring points

The FSV model analysis shows a good aperture for the struck door, with a maximum value of 32.8 mm as shown in Figure 14.33, and the struck door retains its ability to open post-test.

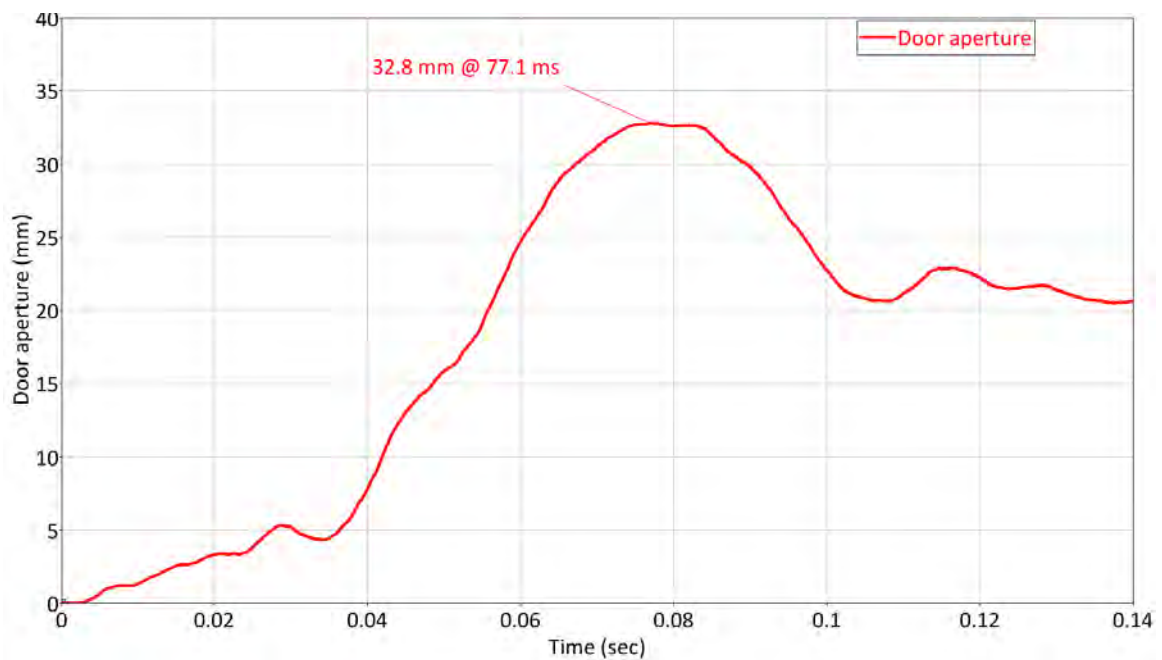


Figure 14.33: Euro NCAP door aperture

The FSV has 485 mm of “ideal design” crush space. As shown in Figure 14.34, the FSV Euro-NCAP model analysis shows 477.8 mm of vehicle crush, which is higher than the US-NCAP model because offset loading generates a tilted deformation which causes more crush.

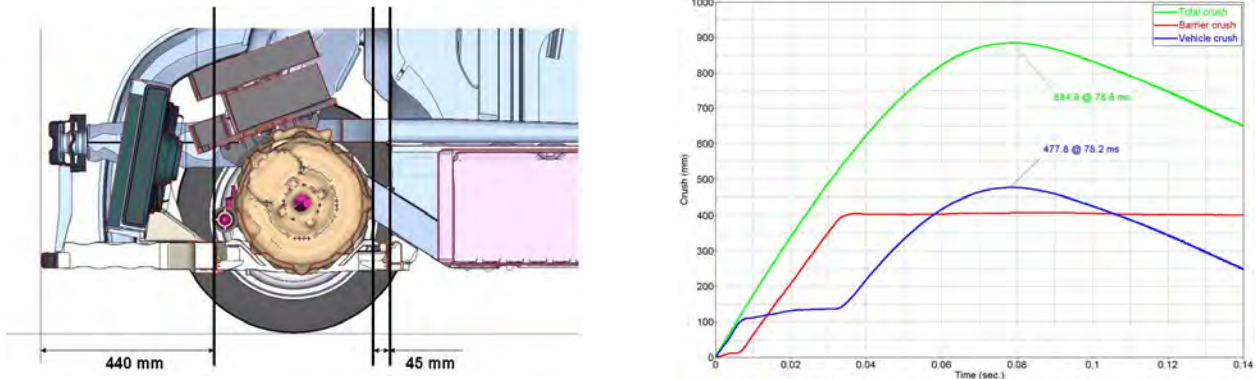


Figure 14.34: FSV Euro NCAP crush distance

Figure 14.35 shows the crash pulse graphs of both the driver side and passenger side, plotted from the acceleration data recorded from accelerometer placed near rocker section and B-pillar inner. As shown in Figure 14.35, the peak pulse on the driver side meets the target (< 42 g).

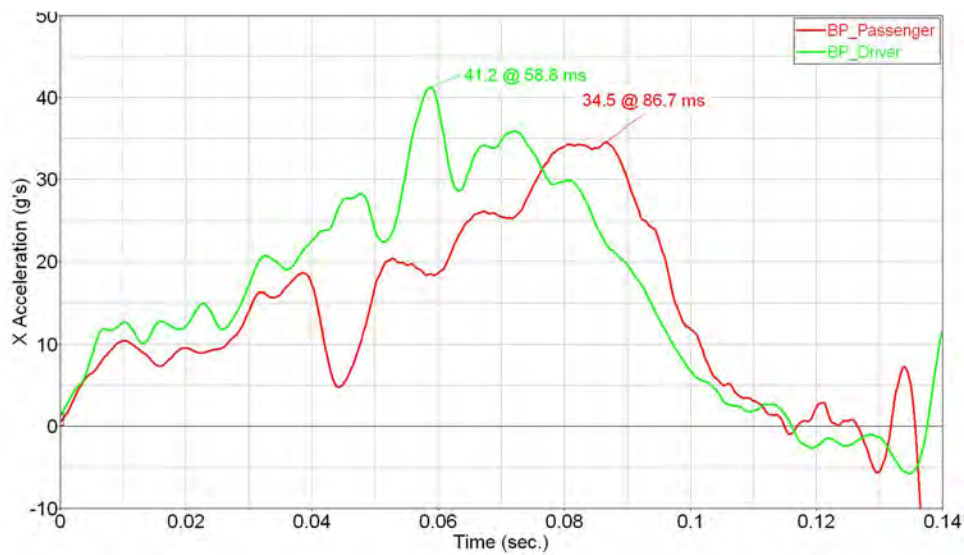


Figure 14.35: FSV Euro NCAP B-pillar Acceleration

14.1.3 Side Impact

14.1.3.1 IIHS Side Impact Crash Analysis

For the FSV side impact crashworthiness evaluation, the Insurance Institute for Highway Safety (IIHS), test protocol was performed. The front end of the Moveable Deformable Barrier (MDB), in the IIHS test represents the front end of a SUV ^[3], which increases the severity of the test.

In the IIHS crash analysis, a MDB with a test weight of 1500 kg impacts the FSV body structure on the vehicle's side with a velocity of $50 \frac{\text{km}}{\text{h}}$, as shown in Figure 14.36. The FSV has a curb weight of 958 kg and it carries the weight of two 5th percentile test dummies (45 kg each), one in the driver's seat and the other in the driver's side rear passenger seat. It also carries 32 kg of instrumentation weight in the cargo area and 59 kg (instrumentation and camera), weight on the non-struck front and rear side doors. The IIHS side impact crash test setup is shown in Figure 14.36.

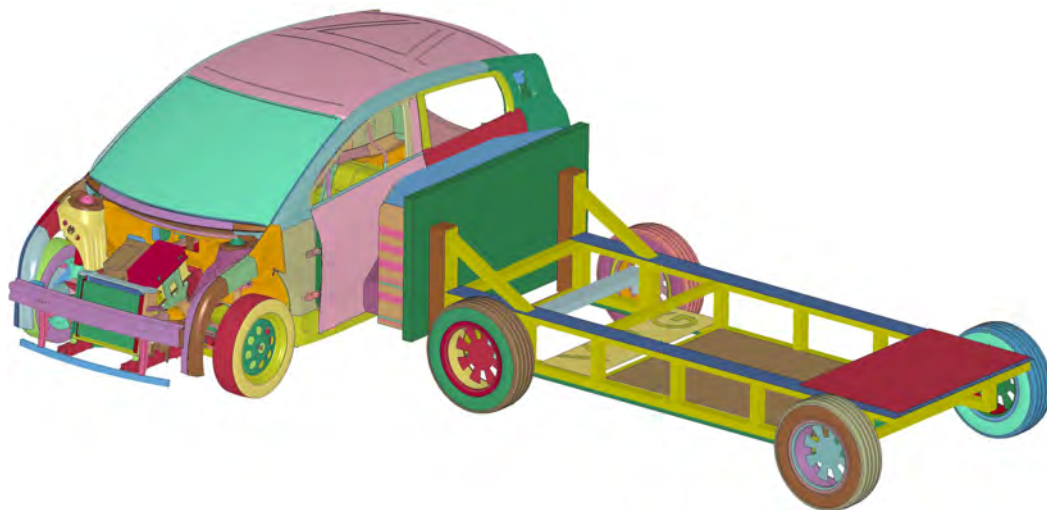


Figure 14.36: *IIHS side impact test setup*

Structural Deformation

Performance of vehicles in IIHS side impact tests are published as ratings which are based on both occupant injury recorded using test dummies and structural deformation measured after the crash. But for the FSV, test dummies were not used (this is beyond the scope of the program). So the ratings of the FSV crash performance is given based on only the assessment of the structural deformation of the vehicle. See Figure 14.37 for the undeformed body structure of the vehicle at initial position and Figure 14.38 for the deformed structure after 100 ms.

³Sport Utility Vehicle

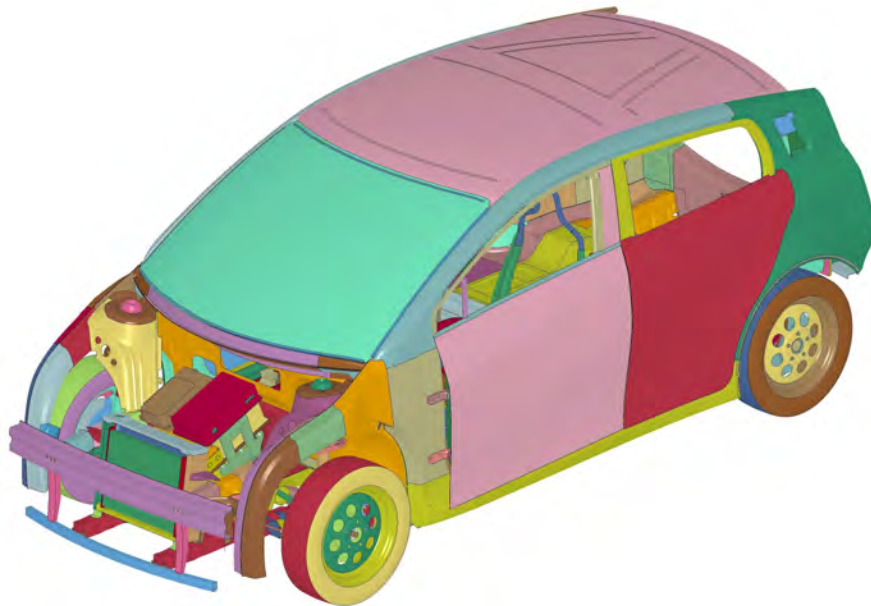


Figure 14.37: IIHS side impact - Undeformed vehicle at initial position

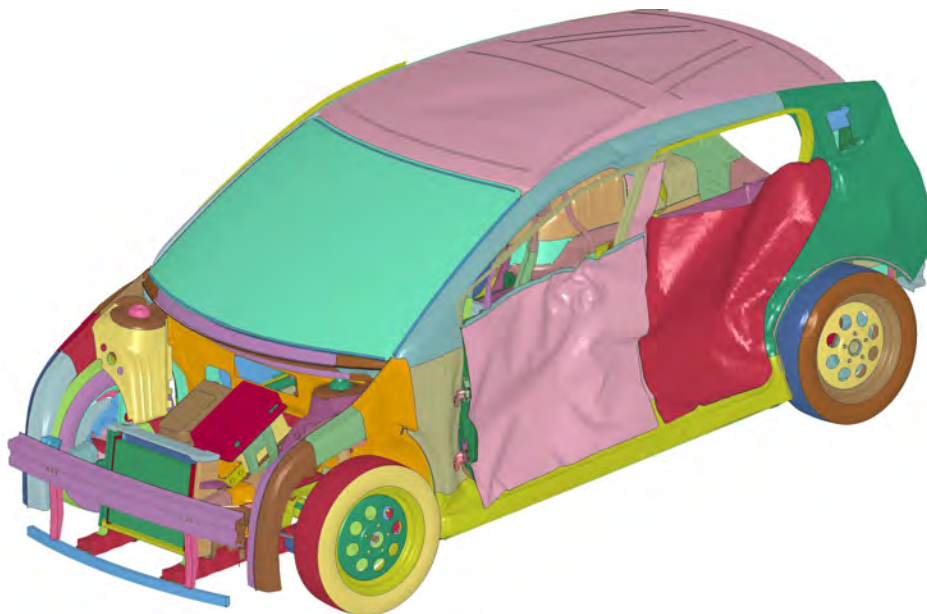


Figure 14.38: IIHS side impact - Deformed vehicle at 100 ms

Structural parts which absorb most of the crash energy in a side impact include Body side outer, B-pillars, Rocker section, Seat cross members, Heel Board and Side-to-Side rail. See Figure 14.39 for the structural parts of the FSV at initial position and Figure 14.40 for the same at 100ms.



Figure 14.39: IIHS side impact - Structural parts at initial position



Figure 14.40: IIHS side impact - Structural parts at 100 ms

The plastic strain contours in the FSV B-pillar inner and B-pillar reinforcement during the IIHS side impact, are shown in Figure 14.41 and Figure 14.42.



Figure 14.41: IIHS side impact - B-pillar inner (% plastic strain contour)



Figure 14.42: IIHS side impact - B-pillar reinforcement (% plastic strain contour)

Structural Load Transfer

Crashworthiness of the vehicle also depends on how efficiently load can be transferred from the struck side of the structure to the non-struck side. Components like Heal board, Side-to-Side rail, Roof Bow and Seat cross members plays important role in transferring the load. But the main path for transferring the load from struck side to non-struck side is shown in Figure 14.43. See Figure 14.44 for these components in the initial position and Figure 14.45 for the same components at 100 ms.

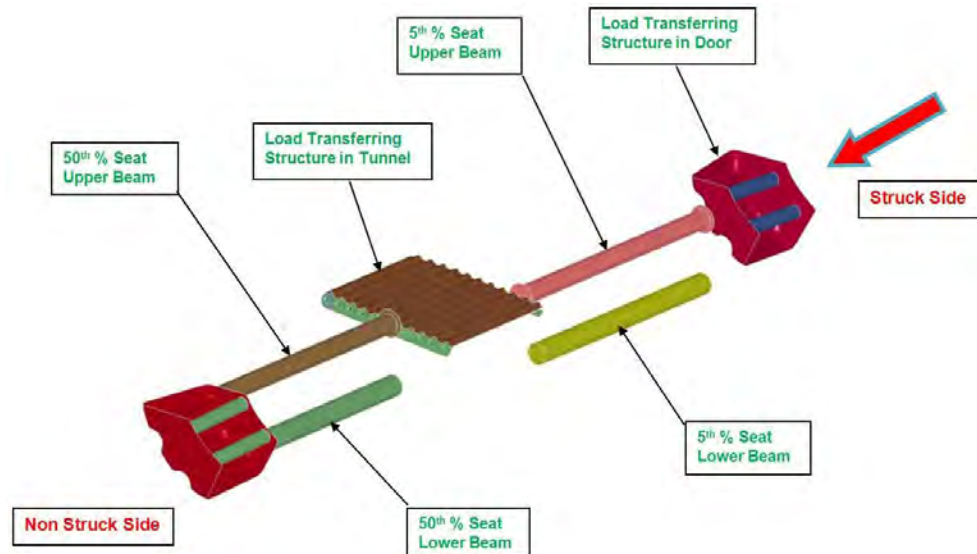


Figure 14.43: IHS side impact - Load Path for transferring load to the non-struck side

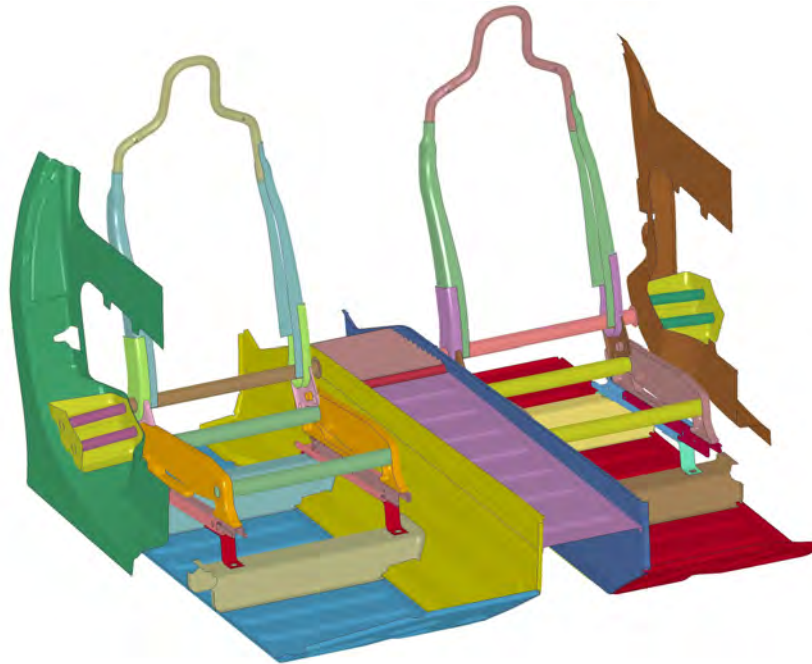


Figure 14.44: IIHS side impact - Components for transferring the load - at initial position

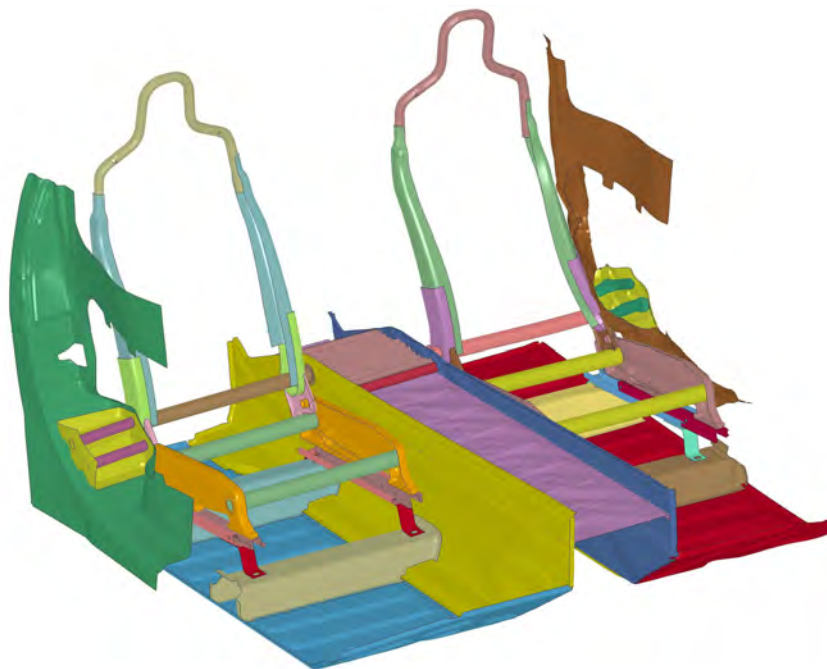


Figure 14.45: IIHS side impact - Components for transferring the load - at 100 ms

IIHS Side Impact Test Structural Rating

For a good rating in the IIHS side impact test, after the test the maximum intrusion point of the B-Pillar should be ≥ 12.5 cm from the driver seat center line. See Figure 14.46 and Figure 14.47 for the IIHS B-pillar deformation structural rating.

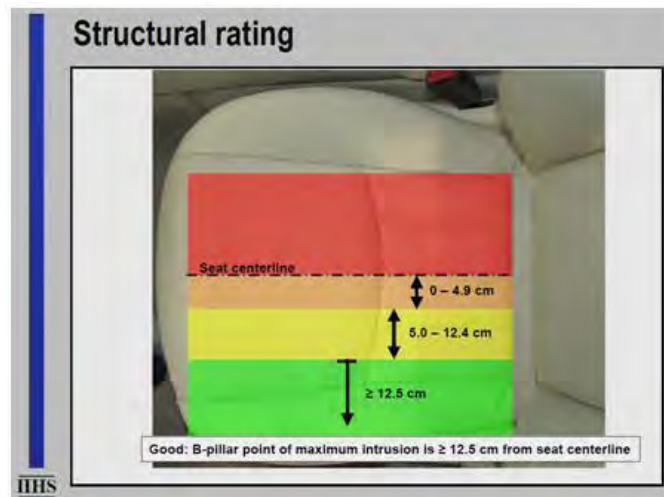


Figure 14.46: IIHS side impact - Maximum B-pillar intrusion point

Structural rating				
B-pillar deformation				
Boundary line	Good	Acceptable	Marginal	Poor
B-pillar to driver seat centerline distance (cm)	12.5	5.0	0.0	
Structural failures	Downgrade structural rating by one category			

Figure 14.47: IIHS side impact - IIHS B-pillar deformation structural rating

See Figure 14.49 for the graph of the FSV B-pillar intrusion. It shows that after the side impact test, the most intruding point of the B-pillar is 134 mm away from the driver seat centerline. Hence it results in the required “Good” rating. The most intruding point of the B-pillar is shown in Figure 14.48.

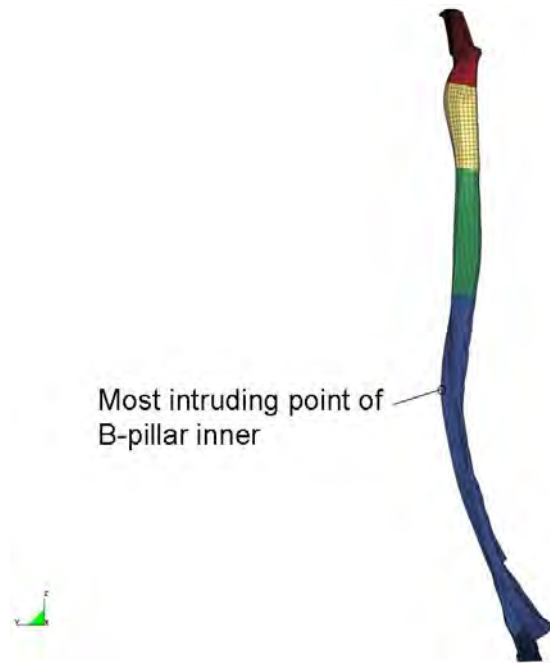


Figure 14.48: IIHS side-impact - B-pillar most intruding point

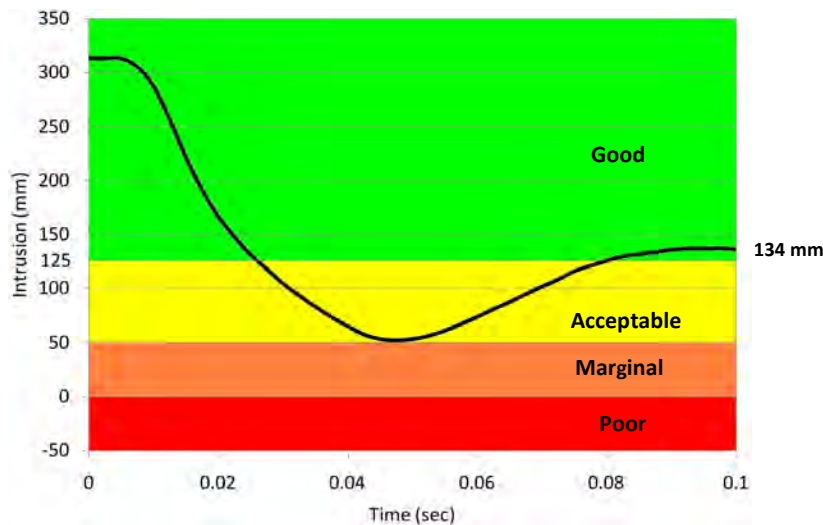


Figure 14.49: IIHS side impact - FSV B-pillar intrusion graph

From Figure 14.49 it can be seen that the intrusion value decreases first upto 52 mm at around 45 msec, and then it improves reaching 134 mm at 100 msec. This is attributed to the springback phenomenon of the high strength steel material. The IIHS passing criteria measures the distance between the most intruding point of the B-pillar and the driver seat centerline after the side impact test. For the FSV, the intrusion value of 134 mm (at 100 msec) post-test gives the required good rating.

14.1.3.2 US SINCAP - 61 km/h 27° Crabbed Impact

In this crash analysis, a Moveable Deformable Barrier (MDB), with a mass of 1370 kg impacts the FSV on the driver's side with velocity of 61 km/h, as shown in Figure 14.50. The FSV has a curb weight of 958 kg.

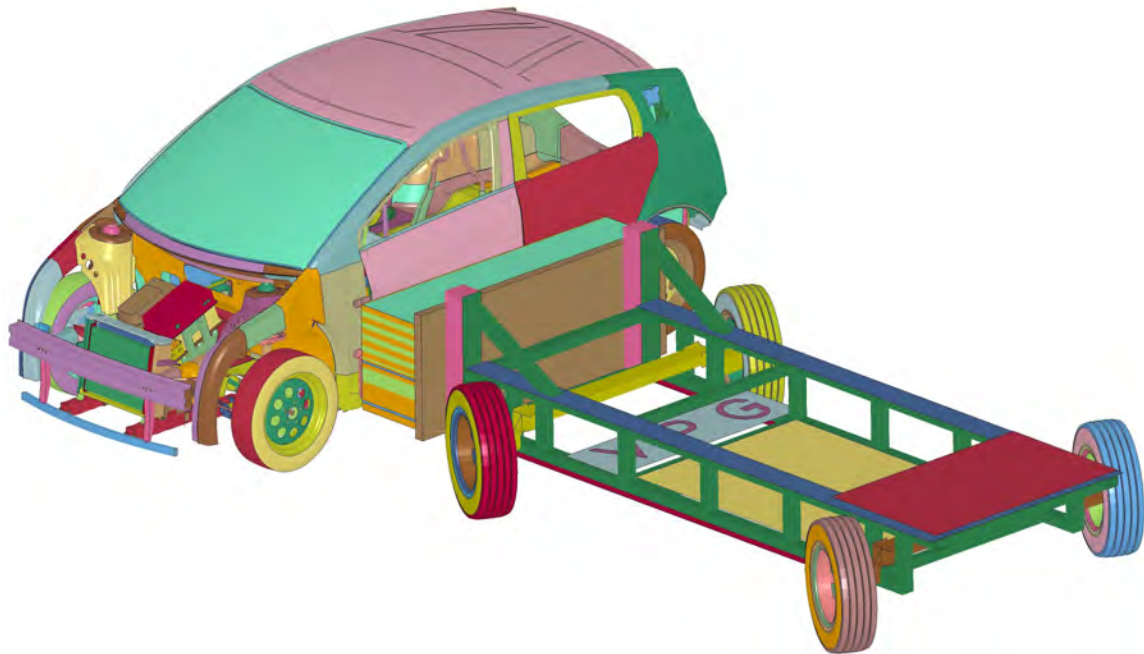


Figure 14.50: *US SINCAP - test setup*

Pre-test body structure of the vehicle at initial position and post-test deformed structure after 100 ms is shown in Figure 14.51.

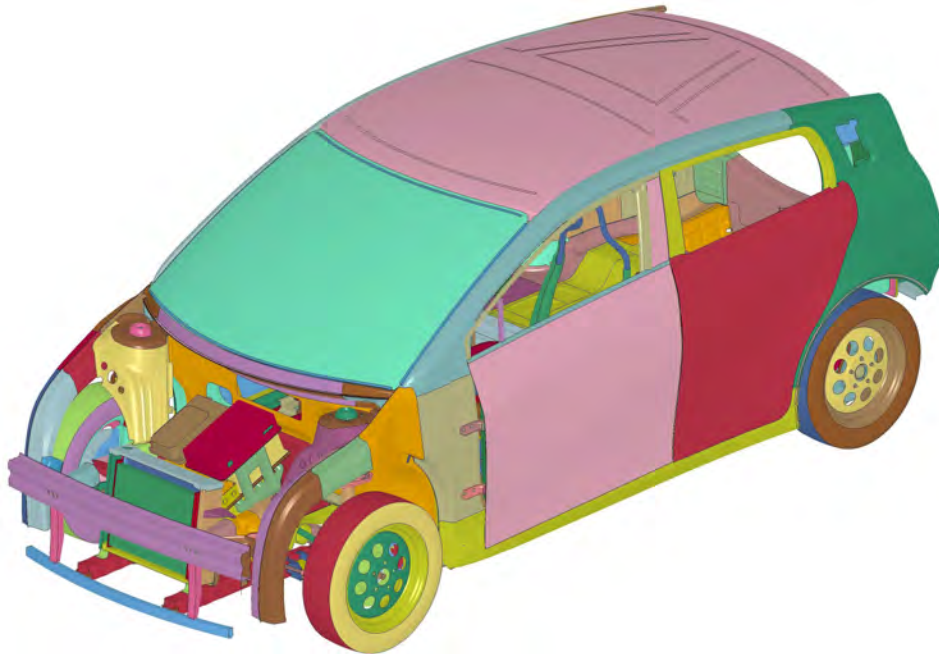


Figure 14.51: US SINCAP - Pre-test vehicle at initial position

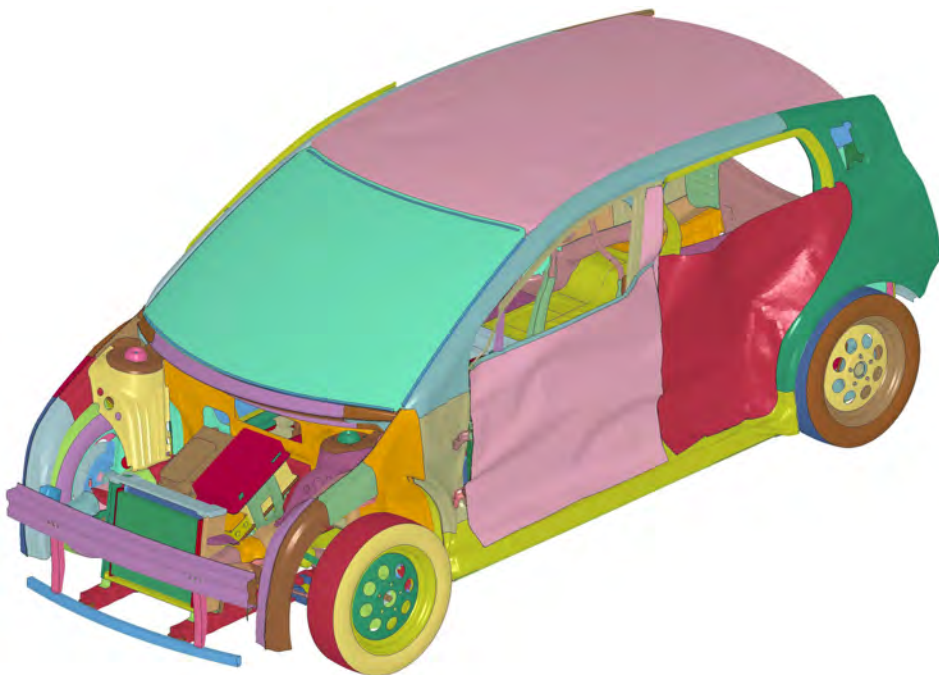


Figure 14.52: US SINCAP - Post-test deformed vehicle at 100 ms

14.1 Crash Worthiness

The plastic strain contours in the FSV B-pillar inner and B-pillar reinforcement during the USSIN-CAP test, are shown in Figure 14.53 and Figure 14.54.



Figure 14.53: *US SINCAP - B-pillar inner (% plastic strain contour)*

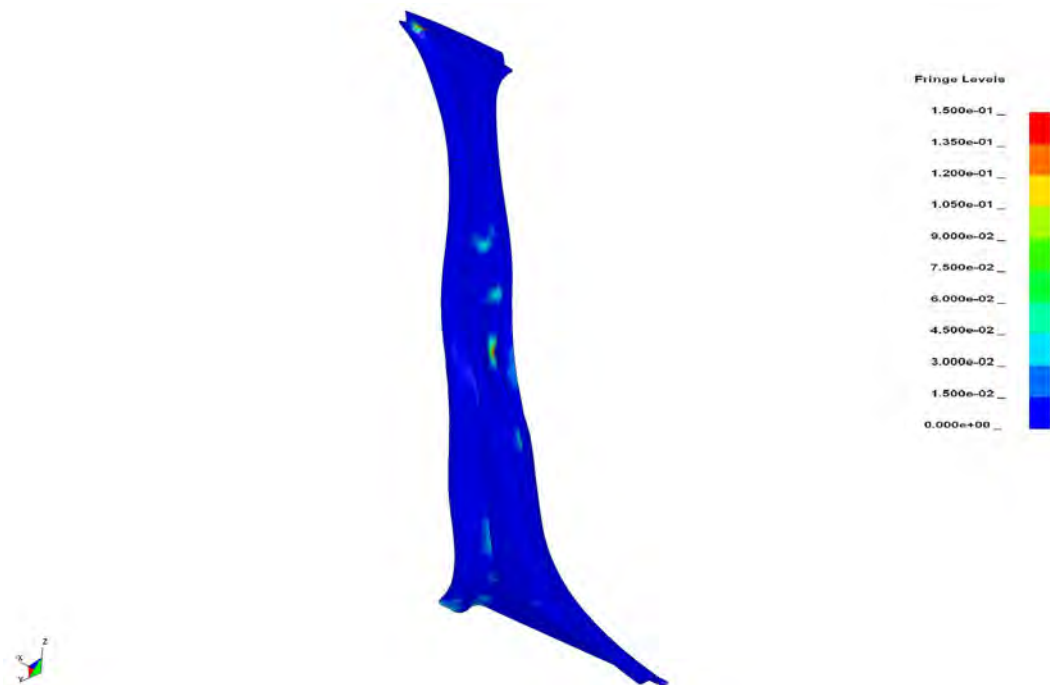


Figure 14.54: *US SINCAP - B-pillar reinforcement (% plastic strain contour)*

The US SINCAP rating system for crashworthiness takes into account occupant injury data like Head Injury Criteria (HIC), Neck Injury Criteria (NIJ), etc. For this program we are not using the dummies to measure the occupant injury because it is beyond the scope of the program. So, the IIHS side impact criteria has been used for measuring the crashworthiness of the FSV.

The B-pillar intrusion graph for the US SINCAP side impact analysis for the FSV is shown in Figure 14.55. It shows that after the crash test the most intruding point of the B-pillar is 215 mm away from the driver seat centerline. Hence, it results in the required "Good" rating.

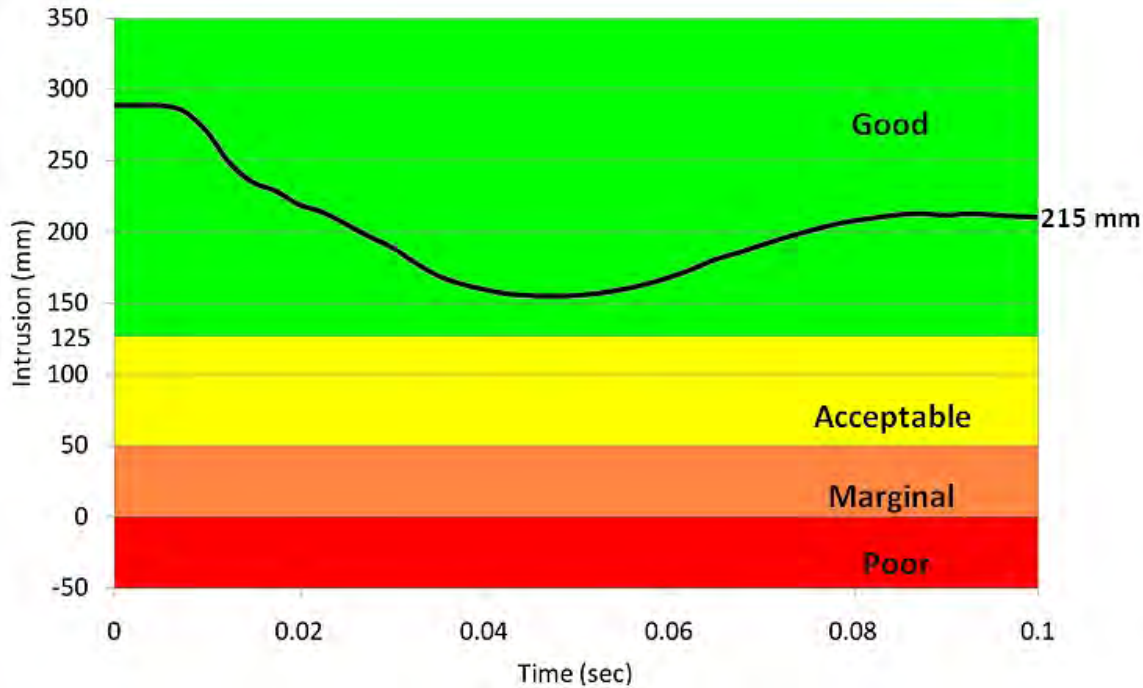


Figure 14.55: US SINCAP side impact - B-pillar intrusion graph

14.1 Crash Worthiness

14.1.4 Rear Impact

14.1.4.1 FMVSS 301 Rear Impact Analysis

FMVSS 301 specifies a moveable deformable barrier (MDB), impact at 80 km/h into a stationary vehicle with an overlap of 70% as shown in Figure 14.56. The MDB used in the test and analysis weighs 1380 kg.

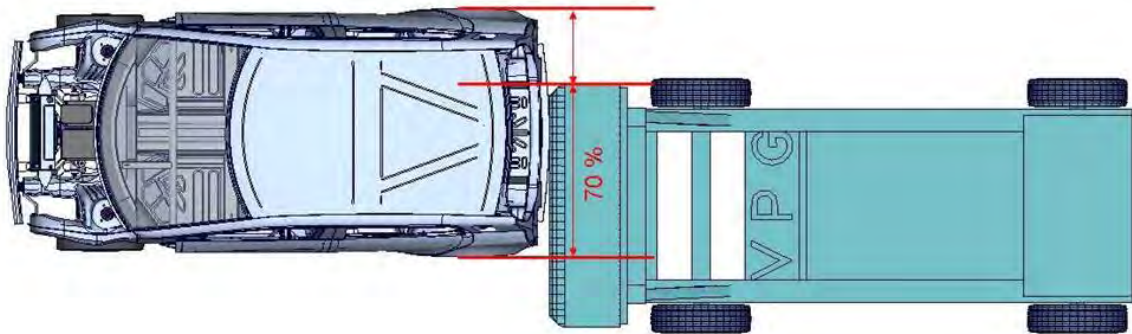


Figure 14.56: FMVSS 301 rear impact test configuration

The FMVSS 301 rear impact deformation for the FSV is shown in Figure 14.57.

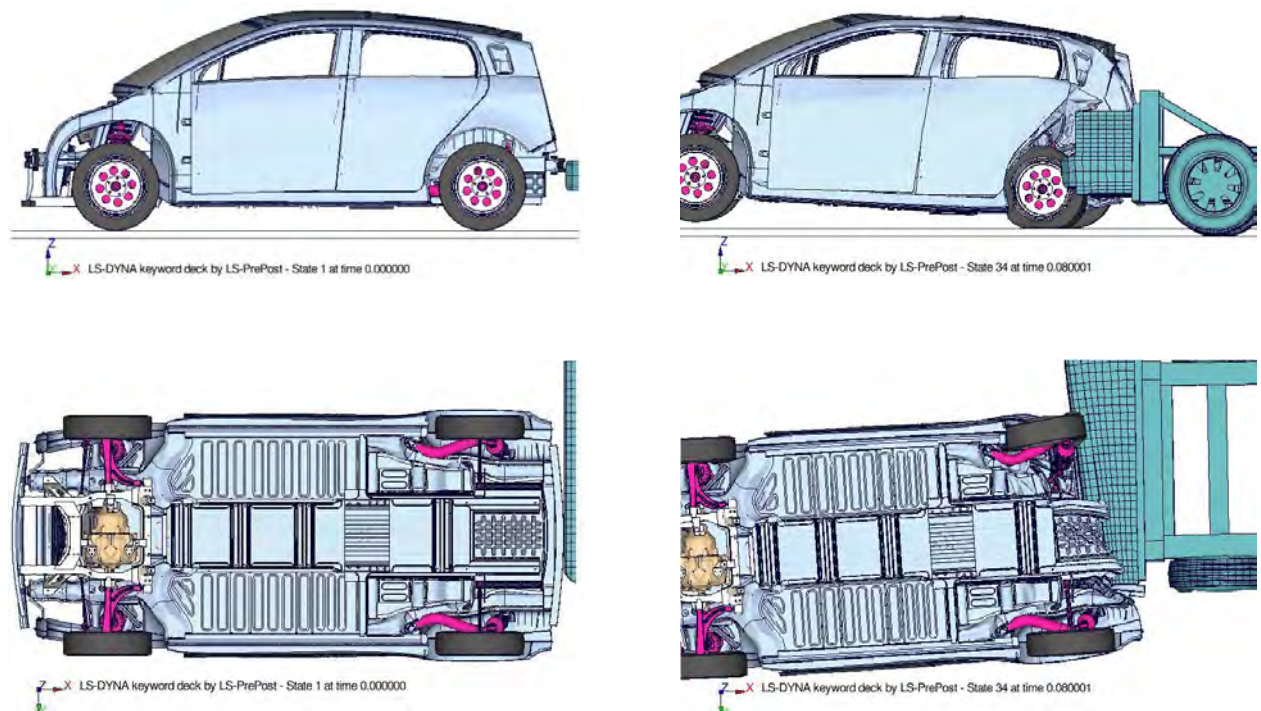


Figure 14.57: FMVSS 301 rear impact deformation - FSV

The FMVSS 301 plastic strain contours of the major load paths are shown in Figure 14.58. The upper limit is set to 10% to visualize a high energy absorbing zone.

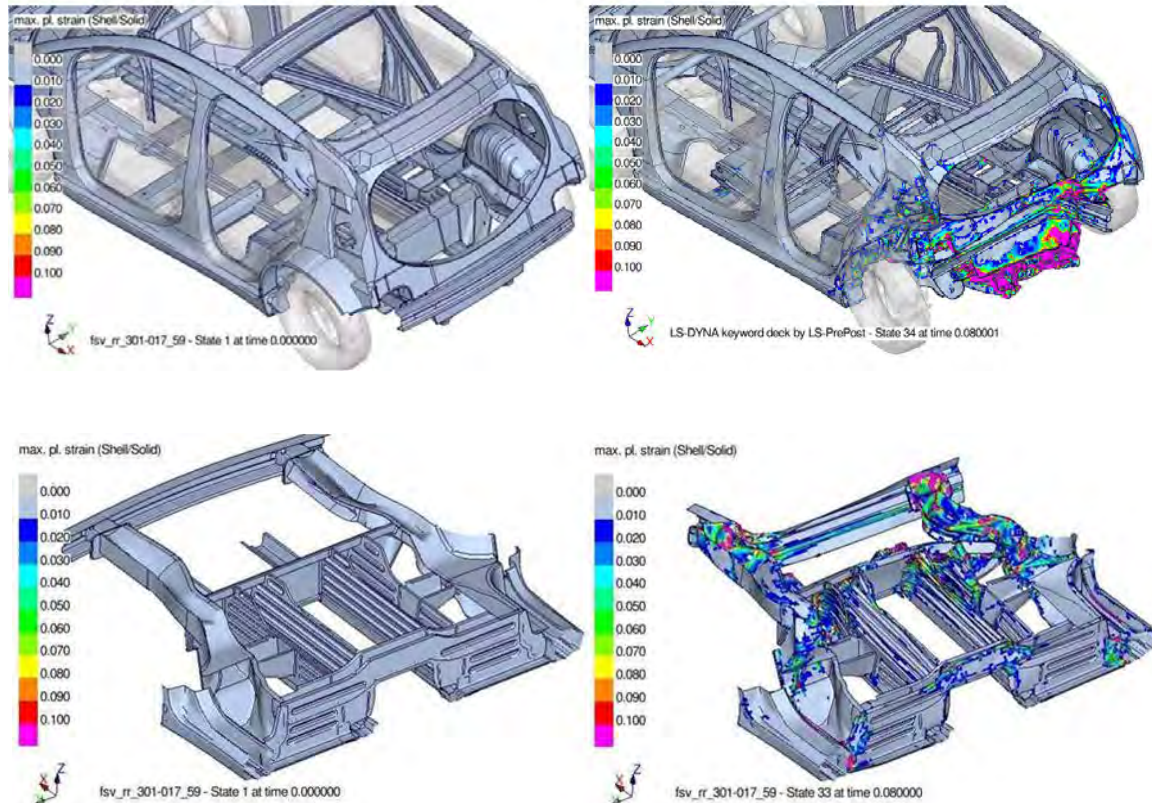


Figure 14.58: FMVSS 301 % plastic strain contour for the FSV structure

The FSV battery is protected well enough and the battery packaging space does not have any physical contact to any other part, as shown in Figure 14.59. FSV rear crush is highest at 50 msec, with vehicle separation from the barrier after 50 msec.

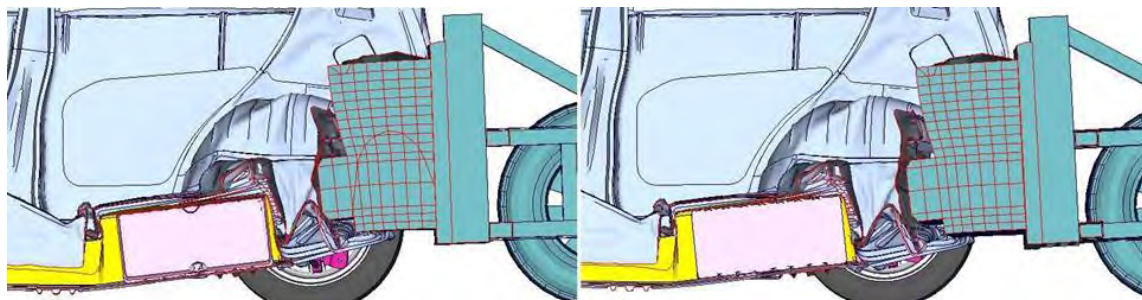


Figure 14.59: FSV battery area during the FMVSS 301 rear impact

The FSV shows 63.2 mm of door aperture on the struck side and 16.0 mm on the non-struck side,

as shown in Figure 14.60. Both the struck and the non-struck door retains their ability to open easily, post-test.

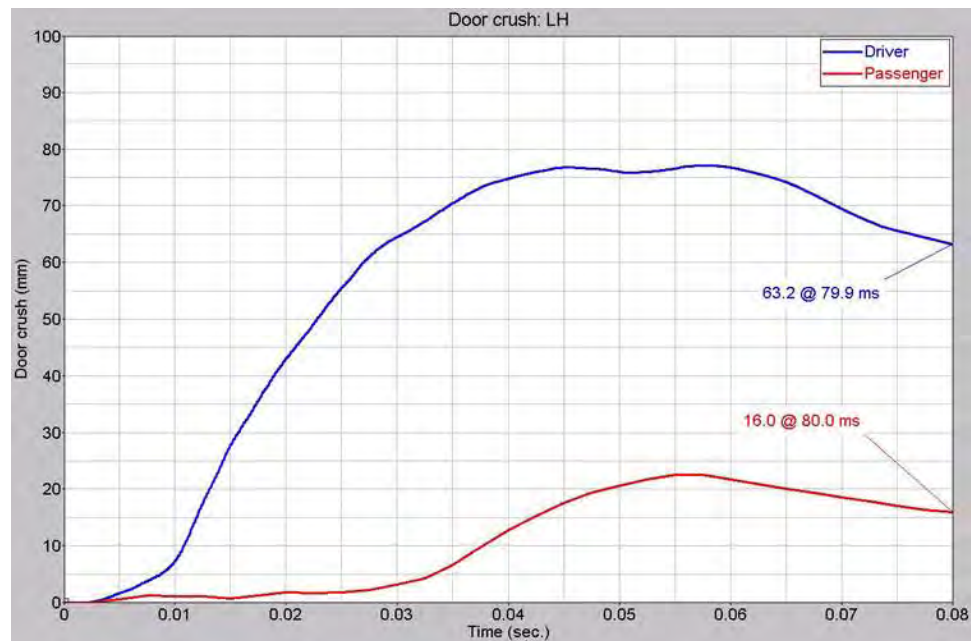


Figure 14.60: FMVSS 301 rear impact test - door apertures

As shown in Figure 14.61, after the rear impact test there is a very small amount of strain in the battery structure outer cover. Moreover the strain is very localized and far away from the main battery modules. So this will not be harmful for the main battery.

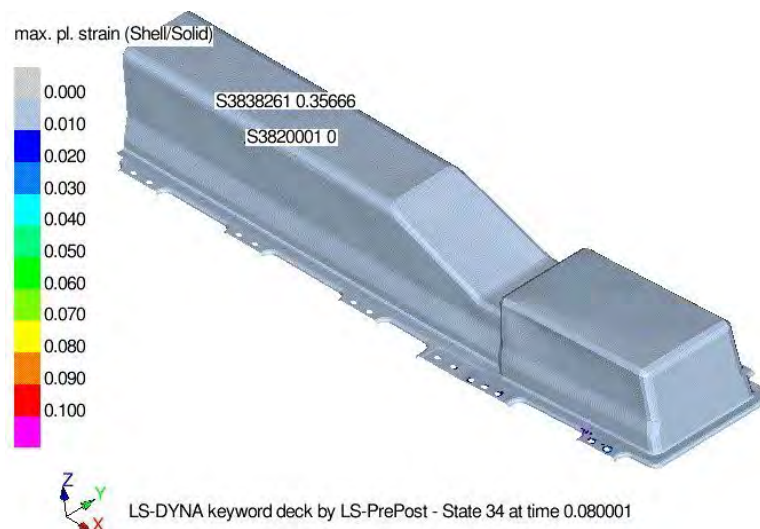


Figure 14.61: FMVSS 301 rear impact test - FSV battery % plastic contour post-test

14.1.4.2 ECE R32- 55 km/h 0° Deformable Barrier

ECE R32 rear impact specifies a deformable barrier impact at 55 km/h into a stationary vehicle with an overlap of 100% as shown in Figure 14.62.

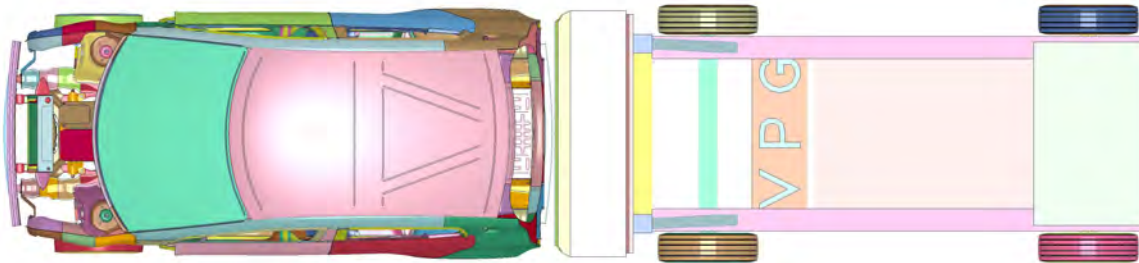


Figure 14.62: ECE R32 rear impact- Test configuration

ECE R32 rear impact deformation for the FSV is shown in Figure 14.63 thru Figure 14.65.

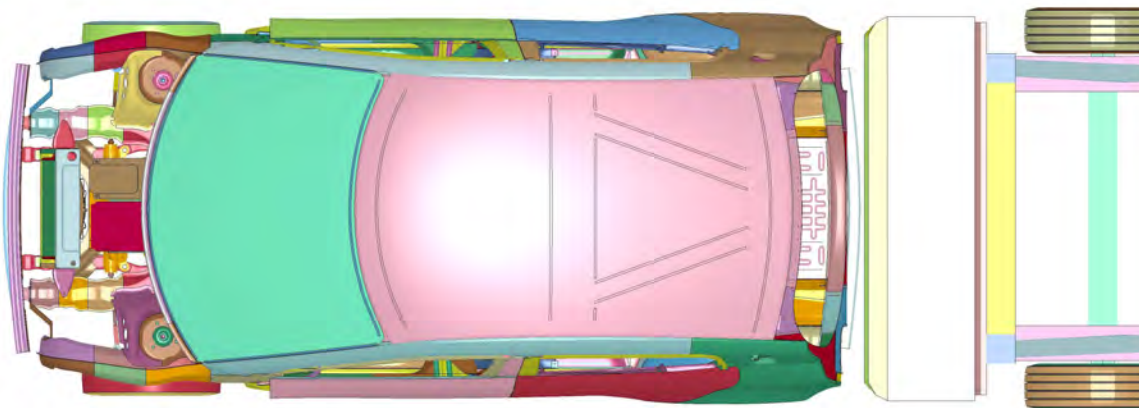


Figure 14.63: Top view - ECE R32 rear impact initial condition

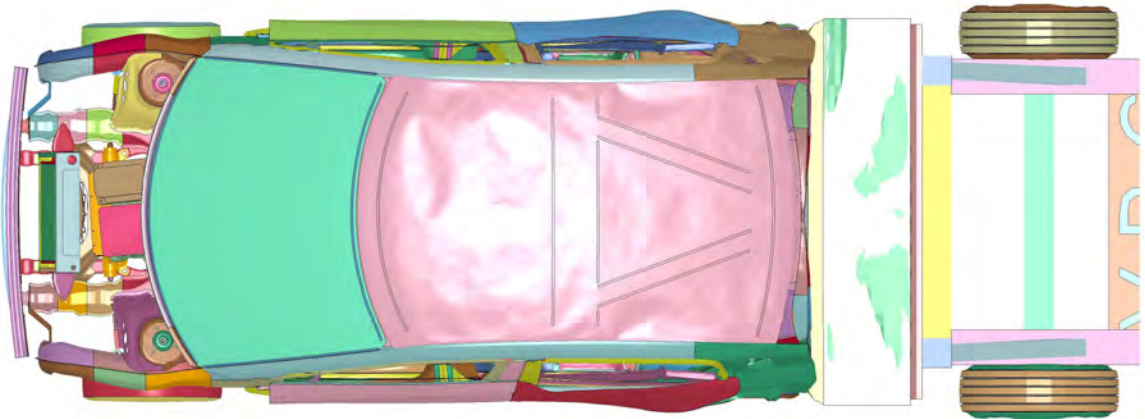


Figure 14.64: Top view - ECE R32 rear impact final deformation

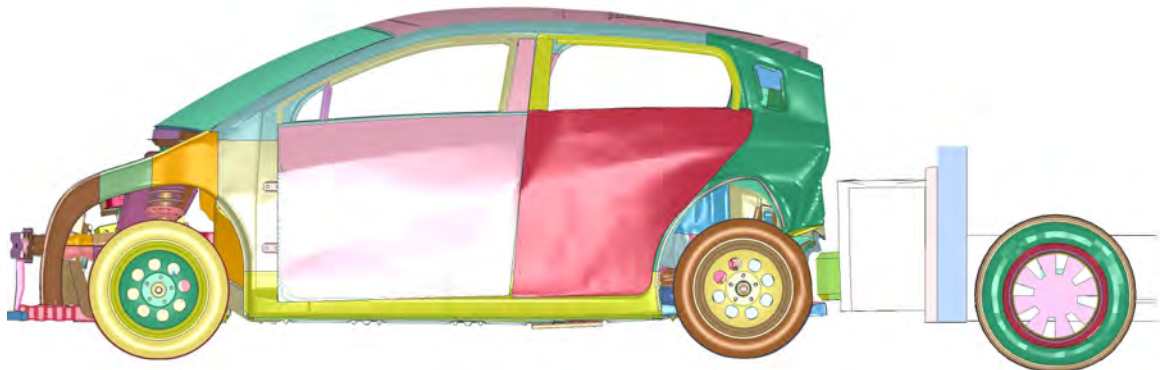


Figure 14.65: Side view - ECE R32 rear impact final deformation

The FSV battery is protected well enough so that the battery package space does not have physical contact with other parts as shown below in Figure 14.66. Post test, there is a very small amount of strain in the battery structure outer cover. Moreover the strain is very localized and far away from the main battery modules. So this will not be harmful for the main battery.

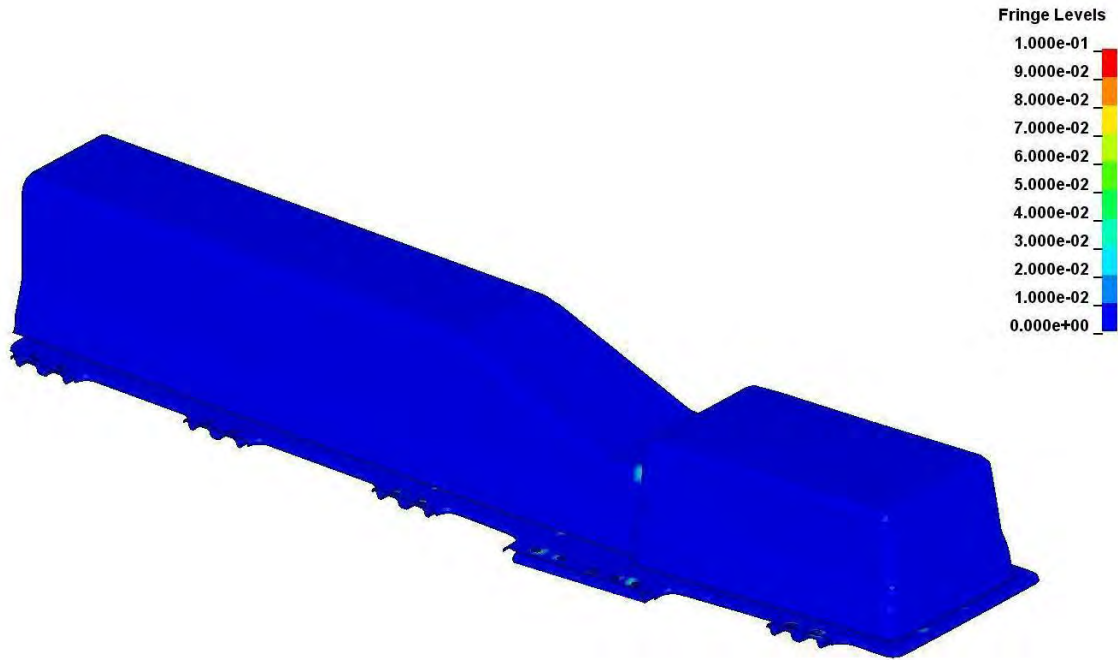


Figure 14.66: ECE R32 % Plastic strain - Battery

14.1.5 Side Pole Impact

14.1.5.1 FMVSS 214 Pole Impact Analysis

For the pole impact crashworthiness evaluation of the FSV, FMVSS-214 rigid pole test protocol is used. In this test the FSV vehicle impacts the rigid pole laterally at a speed of 31 km/h in such a way that its line of forward motion forms an angle of 75 degrees with the vehicle's longitudinal center line.

The rigid pole is a vertically oriented metal structure with a diameter of 254 mm and beginning no more than 102 mm above the lowest point of the tires on the struck side of the fully loaded test vehicle and extending at least 150 mm above the highest point of the roof of the test vehicle. Impact setup is shown in Figure 14.67.

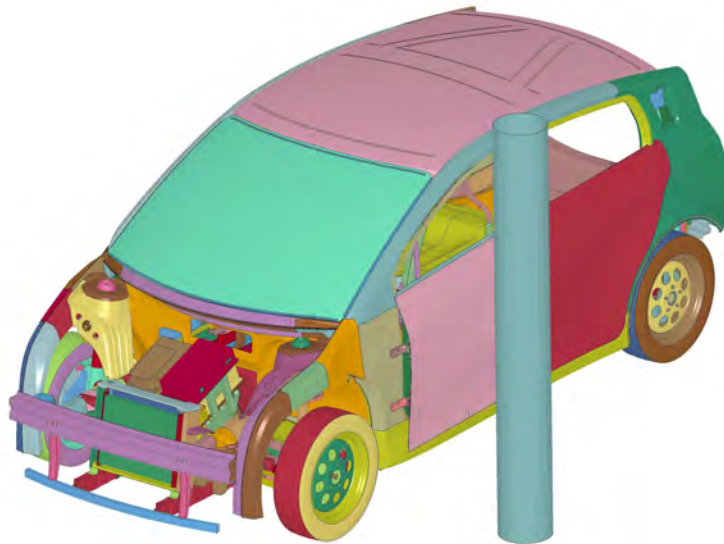


Figure 14.67: FMVSS-214 crash test setup

As stated earlier, the FMVSS-214 Pole impact protocol does not measure crashworthiness in terms of structural deformation. It takes into account occupant injury data like Head Injury Criteria (HIC), Neck Injury Criteria (NIJ), etc. But the FSV vehicle is not designed in detail with a restraint system, side airbags and accurate interior parts, so occupant injury criteria cannot be used for determining the crashworthiness of the FSV vehicle in a pole impact scenario. Therefore, for passing this test with a good rating, a structural target has been set such that the distance of the most intruding point of the door inner post-test should be ≥ 125 mm from the driver seat centerline. The 125 mm reference target is based on the IIHS Side Impact intrusion criteria. It is assumed that meeting this target provides a good basis for the development of passenger safety systems (seatbelt, airbag and interior trim), to meet passenger injury criteria. See Figure 14.68 for the FSV initial body structure and Figure 14.69 for post-pole test deformation at 100 ms.

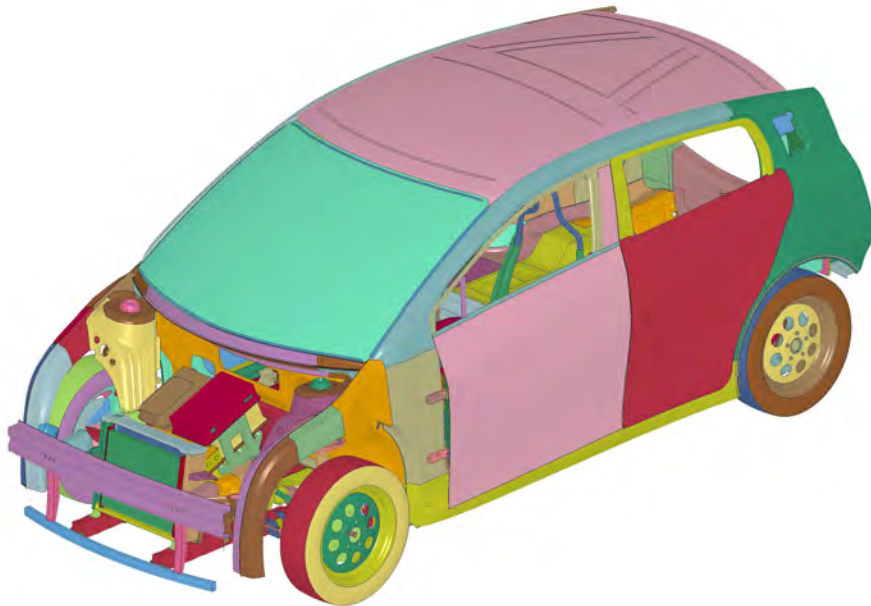


Figure 14.68: FMVSS 214 pole impact - FSV at initial pre-pole test position

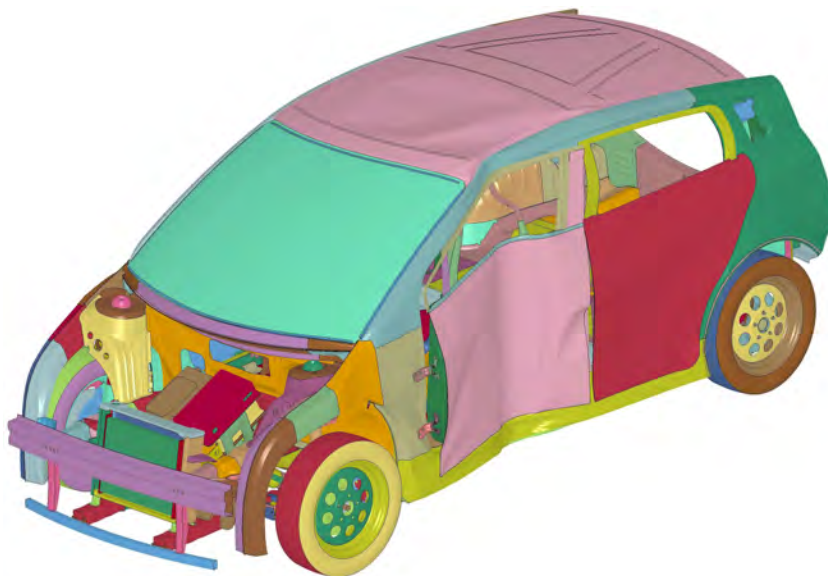


Figure 14.69: FMVSS 214 pole impact - FSV at 100 ms post-pole test deformation

In pole impacts, the parts which absorb most of the crash energy are the rocker section, roof rail outer, rocker section outer, seat cross members, door structure and the floor. These structural parts are shown in their pre-pole test condition in Figure 14.70 and Figure 14.72. The post-pole test condition at 100 ms is shown in Figure 14.71 and Figure 14.73.



Figure 14.70: FMVSS 214 pole impact - FSV main load path components at pre-pole test position



Figure 14.71: FMVSS 214 pole impact - FSV main load path components deformation at 100 ms post-pole test position

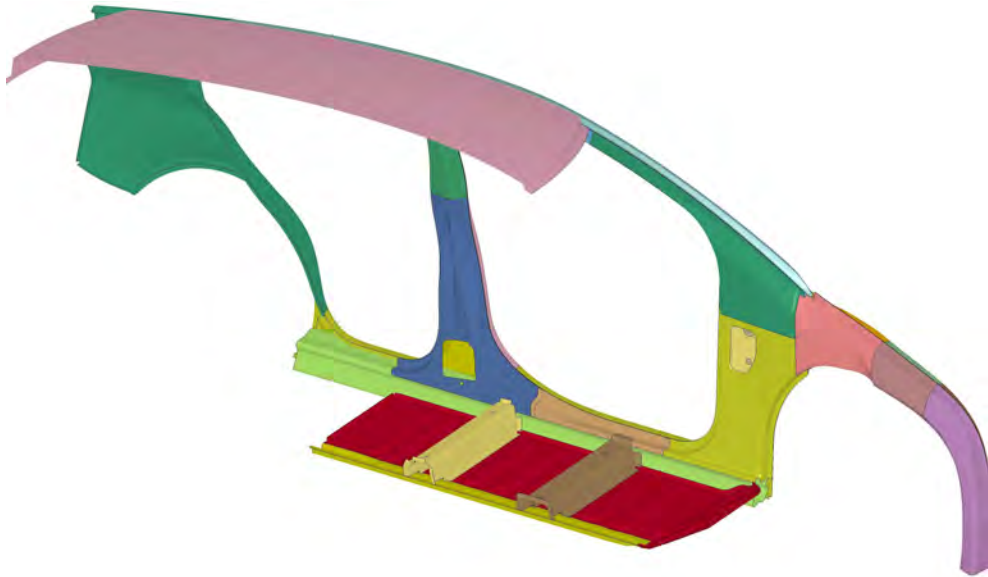


Figure 14.72: FMVSS 214 pole impact - FSV main load path components at pre-pole test position (Inner view)

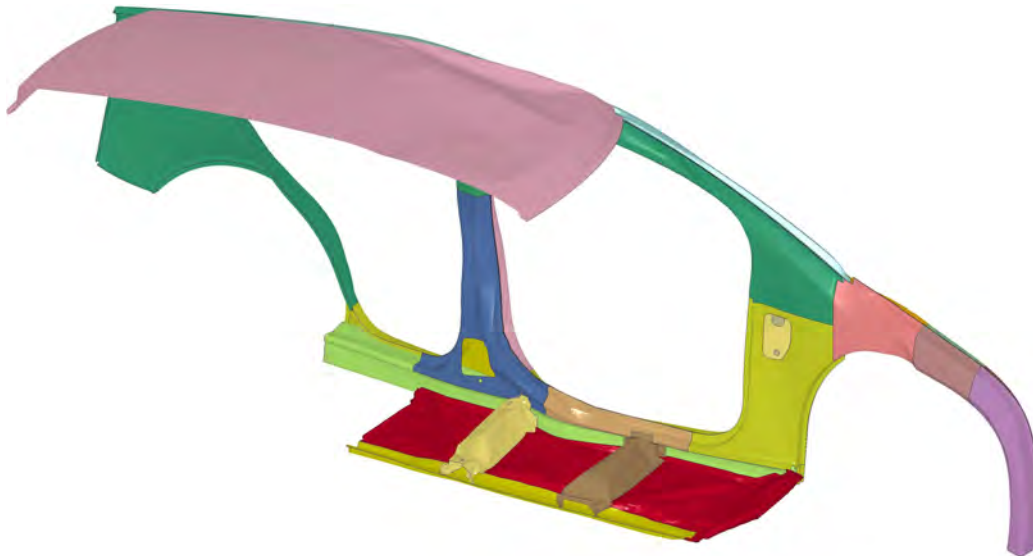


Figure 14.73: FMVSS 214 pole impact - FSV main load path components deformation at 100 ms post-pole test position (Inner view)

The lateral floor pan bead pattern on the floor surface plays an important role in improving the crashworthiness of the FSV for the pole impact scenario. When the floor beads of the FSV are continuous and have approximately 8 mm depth as shown in Figure 14.74, it improves the crashworthiness of the FSV in pole impact tests by 6 mm when compared to discontinuous beads with

14.1 Crash Worthiness

a 4 mm depth as shown in Figure 14.75. This change in the bead pattern is also important in the sense that it improves the crashworthiness without increasing the body structure mass.

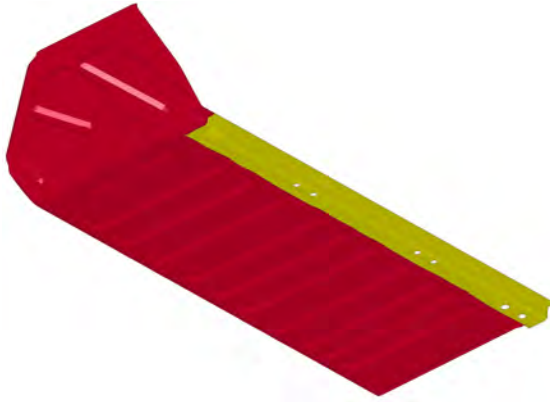


Figure 14.74: *New design of the floor pan (with continuous beads)*

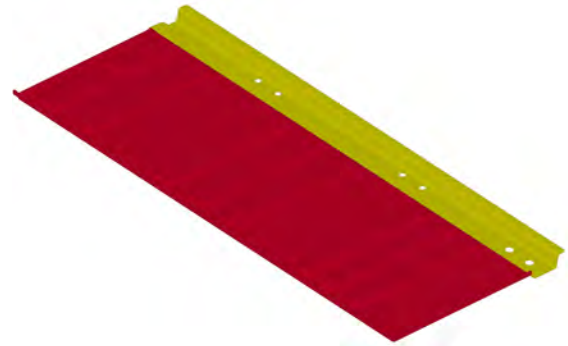


Figure 14.75: *Old design of the floor pan (with discontinuous beads)*

The intrusion graph for the FMVSS-214 pole impact analysis is shown in Figure 14.77. It shows that after the pole impact test, the door inner most intruding point is 159 mm away from the driver seat centerline. Hence, the FSV meets the FMVSS-214 pole impact target. The most intruding point is shown in Figure 14.76.

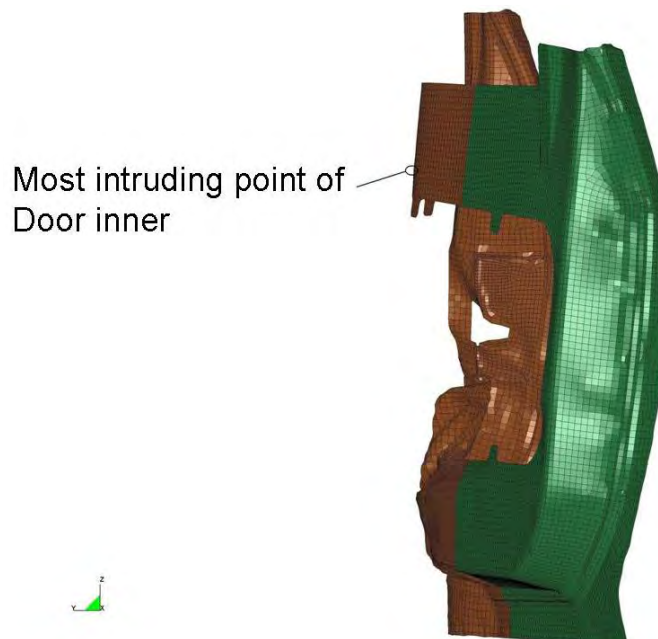


Figure 14.76: *FMVSS 214 pole impact - FSV door most intruding point*

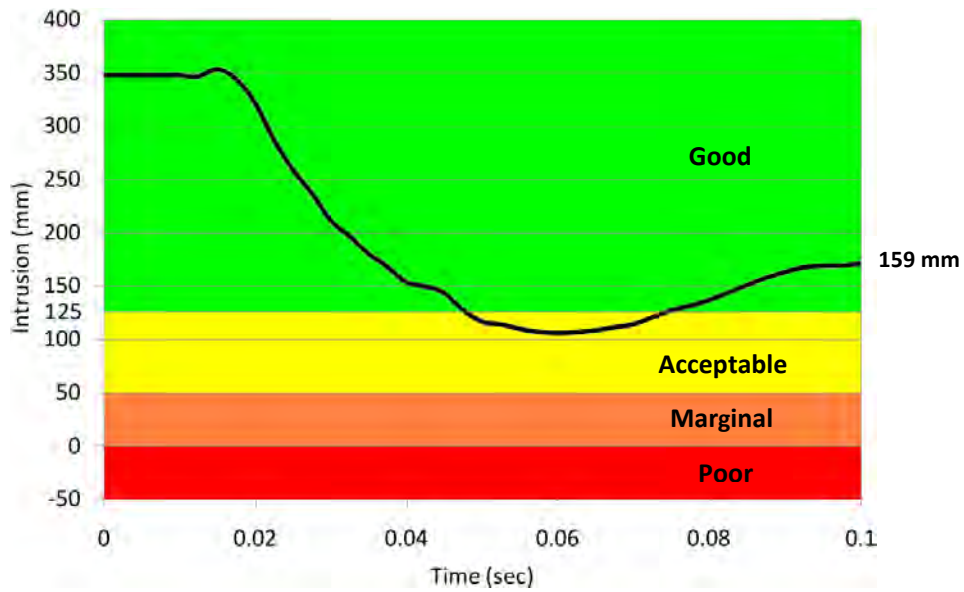


Figure 14.77: FMVSS 214 pole impact - FSV door-inner intrusion graph

14.1.5.2 EURO NCAP - 29 km/h 0° Impact

In this test, the FSV vehicle impacts the rigid pole perpendicular to the direction of the movement of the vehicle at a speed of 29 km/h. The impact setup is shown in Figure 14.78.

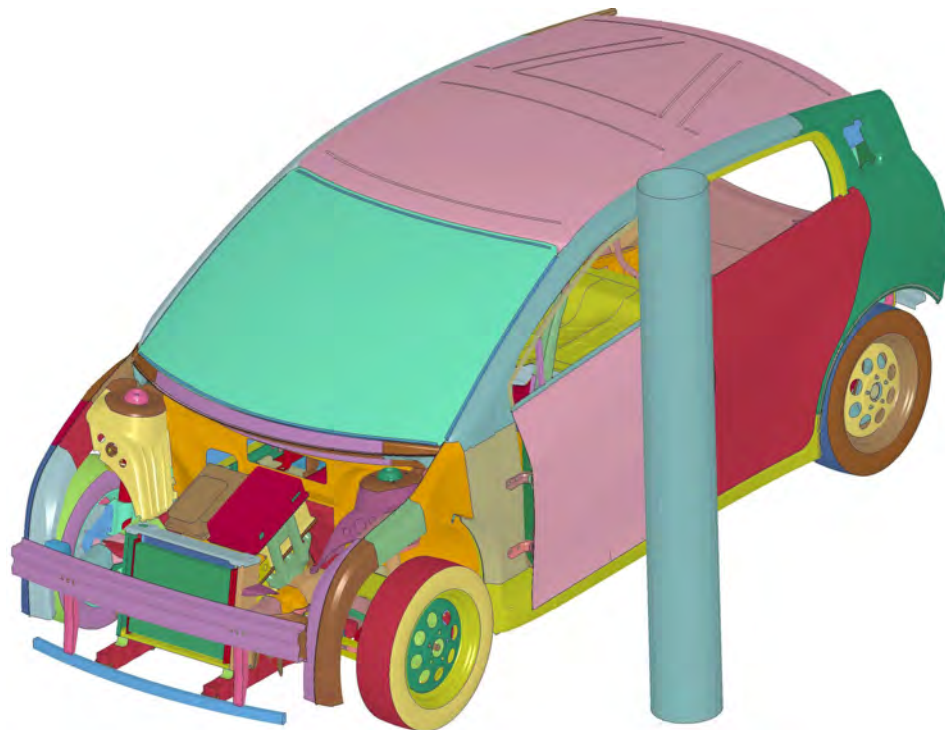


Figure 14.78: *EURO NCAP side pole impact test setup*

Similar to the FMVSS 214 pole impact test, this test takes into account occupant injury data like Head Injury Criteria (HIC), Neck Injury Criteria (NIJ), etc. But the FSV vehicle is not designed in detail with a restraint system, side airbags and accurate interior parts, so occupant injury criteria cannot be used for determining the crashworthiness of the FSV vehicle in a pole impact scenario.

As stated earlier, for this test the BEV uses the same performance target as the FMVSS 214 Pole impact (the most intruding point of the door inner post-test should be ≥ 125 mm from the driver seat centerline, for passing the test with a good rating). There is no performance target for the Euro NCAP Side Pole impact test; the 125 mm reference target is based on the IIHS Side Impact intrusion criteria. It is assumed that meeting this target provides a good basis for the development of passenger safety systems (seatbelt, airbag and interior trim), to meet passenger injury criteria.

The initial body structure of the vehicle is shown in Figure 14.79 and Figure 14.81. The deformed structure after 100 ms is shown in Figure 14.80 and Figure 14.82.

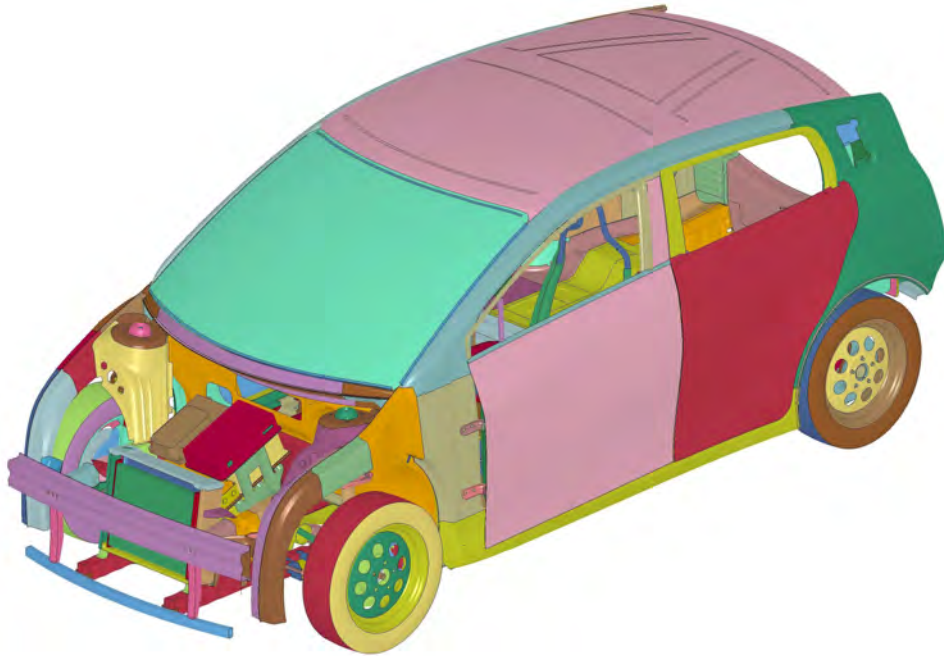


Figure 14.79: *EURO NCAP side pole impact - Pre-test vehicle at initial position*

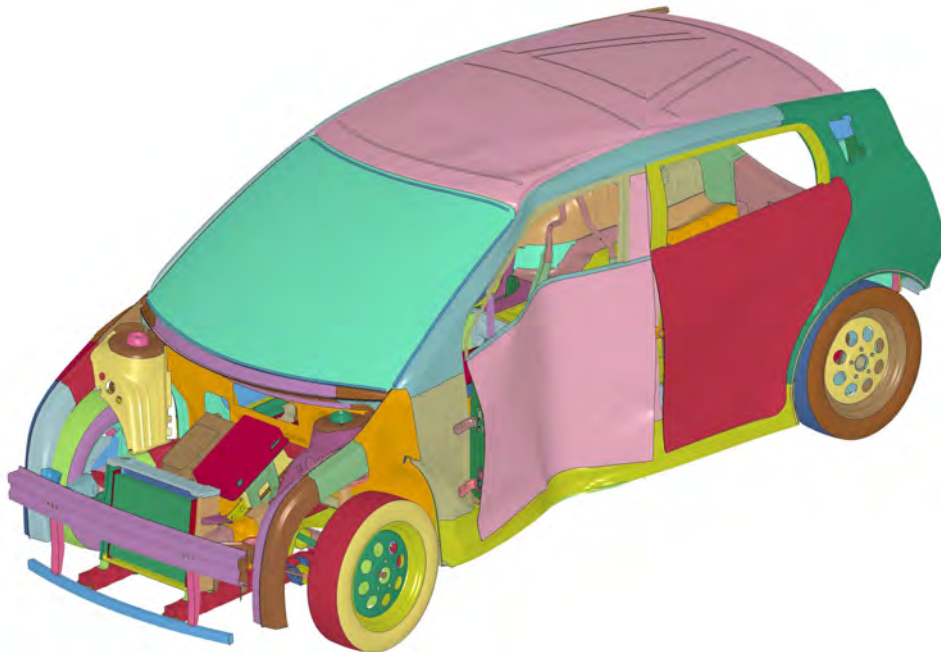


Figure 14.80: *EURO NCAP side pole impact - Post-test vehicle at 100 ms*

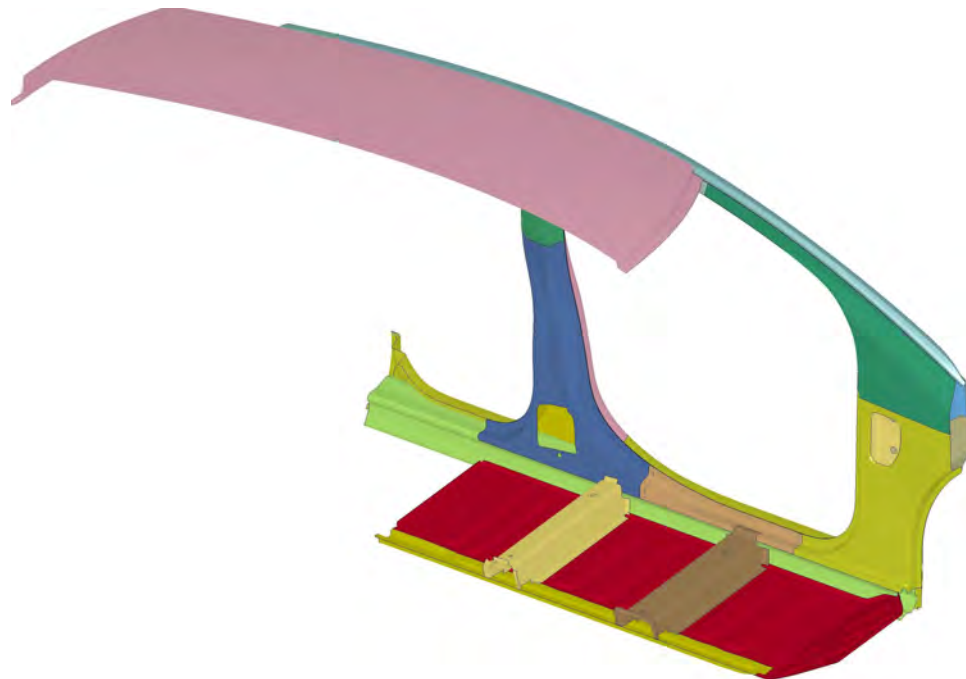


Figure 14.81: EURO NCAP side pole impact - Pre-test vehicle at initial position (Inner view)

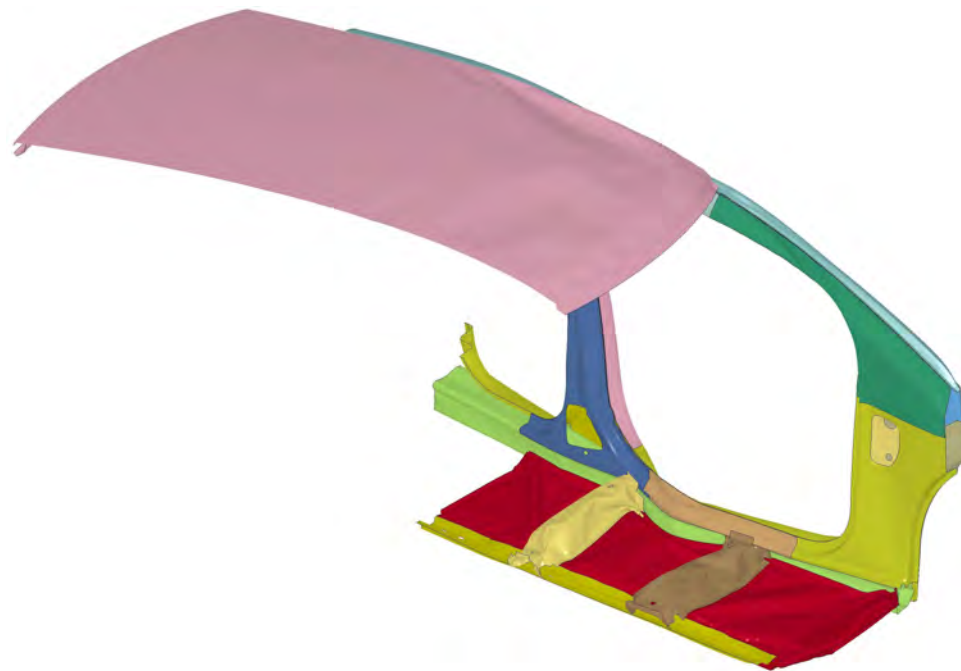


Figure 14.82: EURO NCAP side pole impact - Post-test vehicle at 100 ms (Inner view)

The door intrusion graph for the EURO NCAP pole impact analysis is shown in Figure 14.83. It shows that after the pole impact test, the most intruding point of the inner door is 169 mm away from the driver seat centerline. Hence, it results in the required "Good" rating.

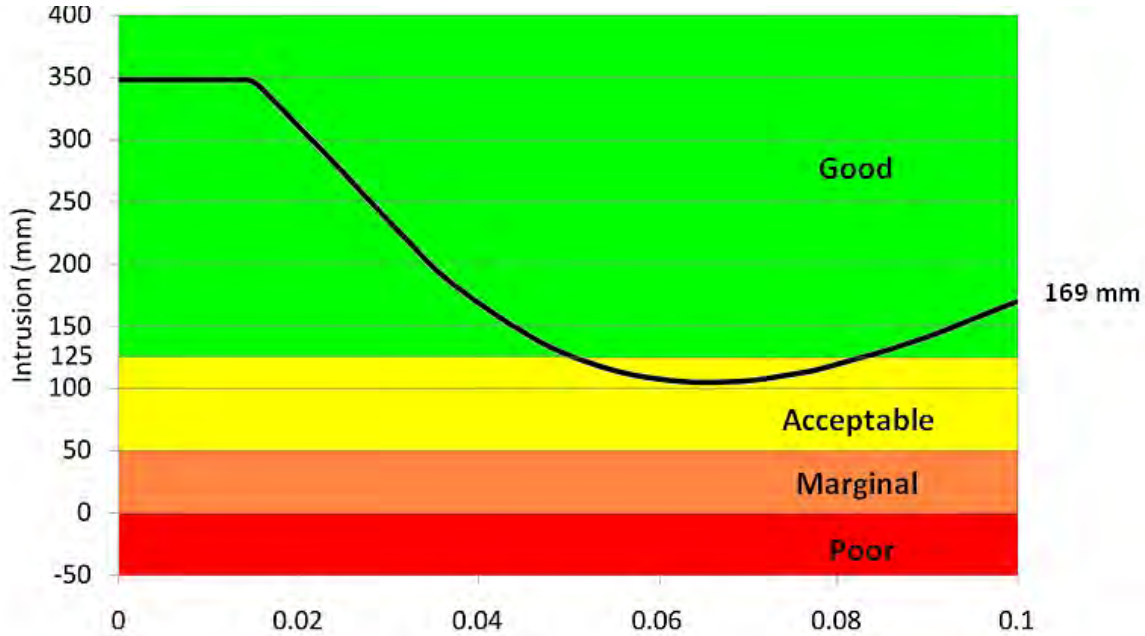


Figure 14.83: *EURO NCAP side pole impact - Inner door intrusion graph*

14.1.6 Roof Crush

14.1.6.1 FMVSS 216-a and IIHS Roof Crush Analysis

FMVSS 216-a Roof Crush test determines the crashworthiness of the vehicle in a roll over. This test requires that each side of the passenger compartment roof structure should resist a maximum applied force equal to 3.0 times the curb weight of the vehicle in kilograms and multiplied by 9.8 m/sec^2 , for vehicles weighing less than 2,722 kg. The force must be applied separately to each side of the roof structure using a static loading device equipped with a rigid unyielding rectangular block.

The IIHS roof crush test requires that the roof structure should resist up to a maximum applied force equal to 4.0 times rather than 3.0 times of FMVSS 216-a and it uses the same rigid rectangular block which is used in the FMVSS 216-a roof crush procedure.

According to both FMVSS 216-a and IIHS roof crush tests, the test vehicle will meet the requirements of the standard if each side of the roof structure withstands the maximum applied force prior to the lower surface of the rigid plate moving more than 127 millimeters. The FSV vehicle has passed both tests criteria.

In the FSV roof crush analysis, the complete body structure is assembled and clamped at the lower edge of the rocker. The rigid loading device applies the load in a quasi static manner to the structure. The test setup is shown in Figure 14.84.

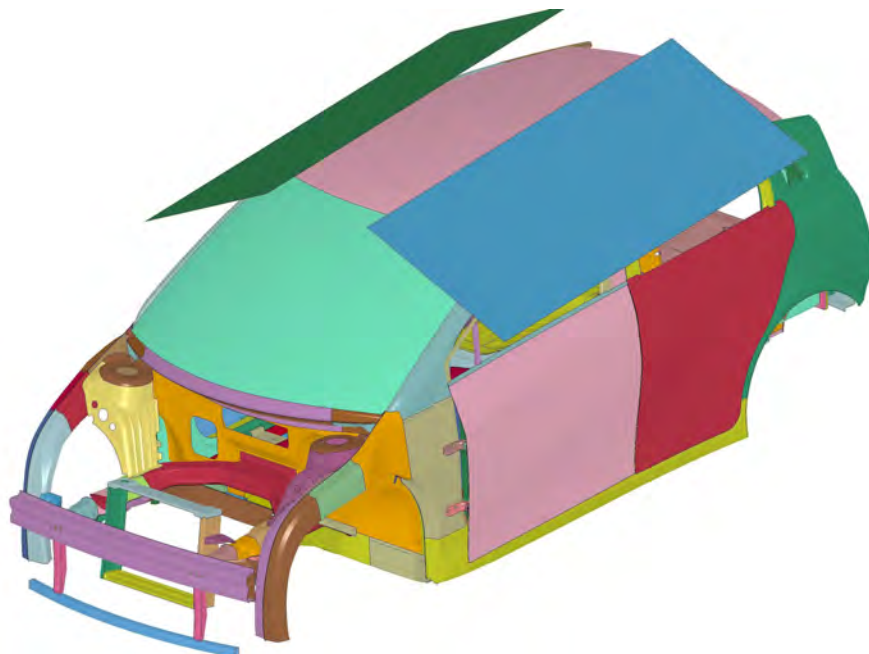


Figure 14.84: *FMVSS 216-a Roof Crush test setup*

First, the driver side rigid plate moves down and applies the load on the driver side roof structure. Once it has gone down up to 127 mm, then it is pulled back. See Figure 14.85. Next, the passenger side rigid plate moves down and applies the load on the passenger side roof structure as shown in Figure 14.86.

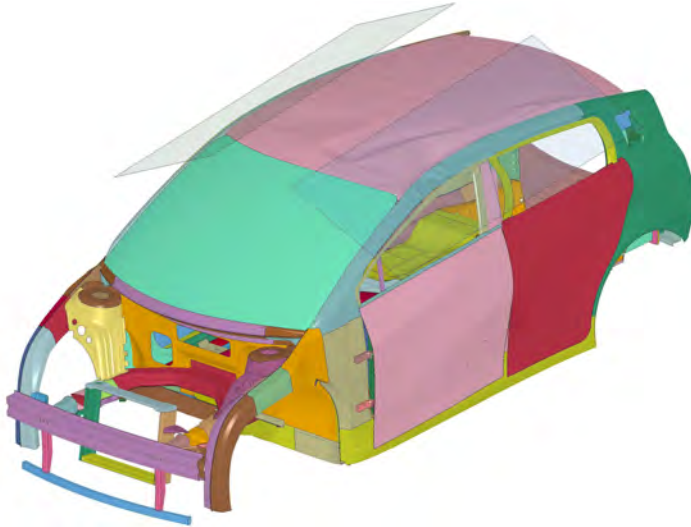


Figure 14.85: FMVSS 216-a Roof Crush - Deformed driver side roof structure at rigid plate movement of 127 mm

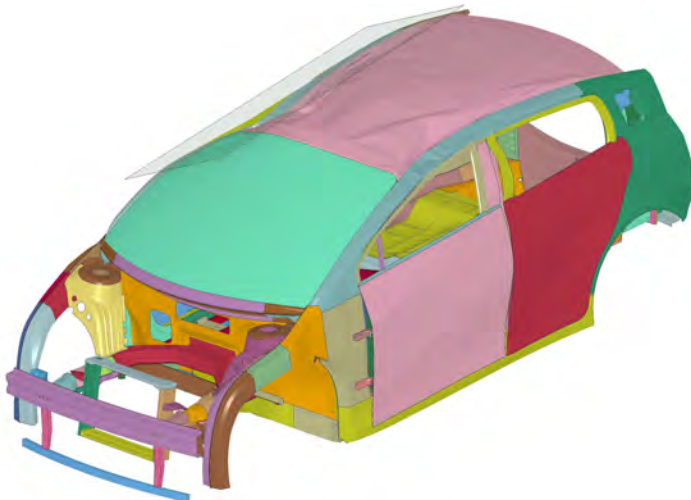


Figure 14.86: FMVSS 216-a Roof Crush - Deformed passenger side roof structure at rigid plate movement 127 mm

For the FMVSS 216-a standard, the roof structure should sustain at least 28.19 kN within the rigid plate movement of 127 mm and for the IIHS standard, the roof structure should sustain at least 37.59 kN force within the rigid plate movement of 127 mm. The FSV has met both these targets as shown below in Figure 14.87 and Figure 14.88.

14.1 Crash Worthiness

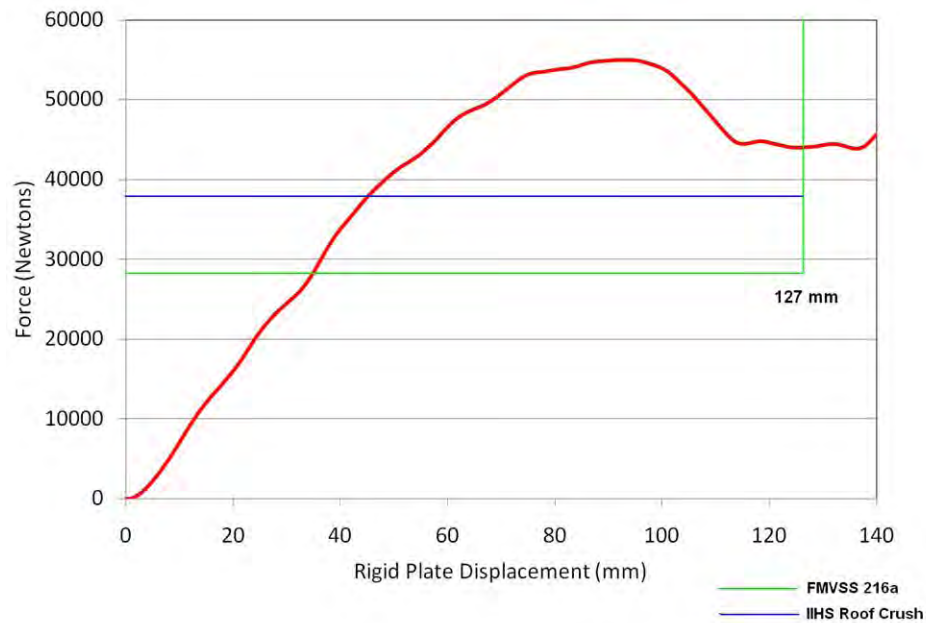


Figure 14.87: FMVSS 216-a Roof Crush - Force vs. displacement graph for driver side roof structure

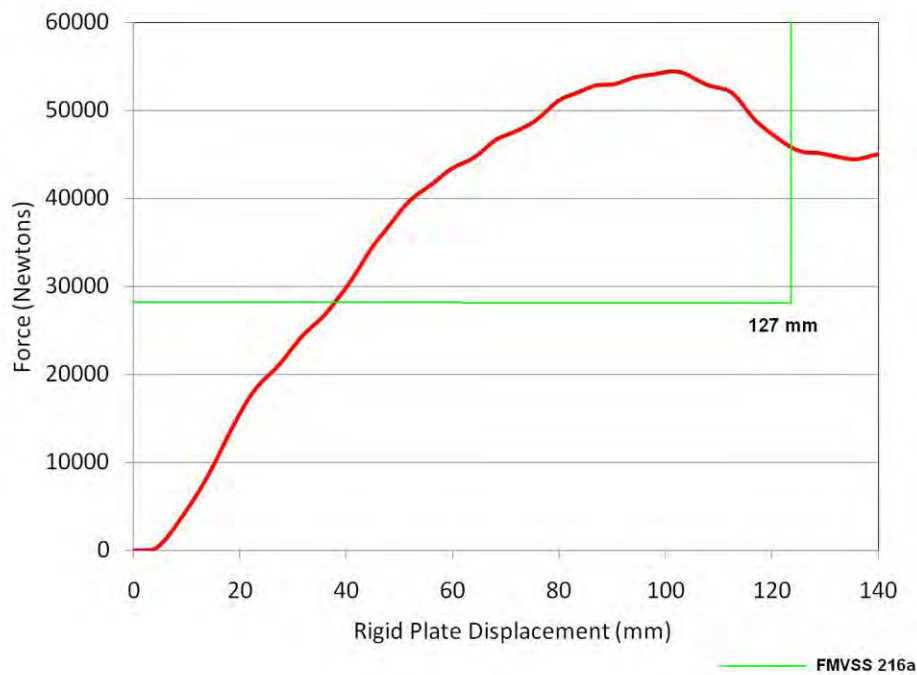


Figure 14.88: FMVSS 216-a Roof Crush - Force vs. displacement graph for passenger side roof structure

14.1.7 Low Speed Regulations

14.1.7.1 RCAR/IIHS (10 $\frac{\text{km}}{\text{h}}$ 0° Rigid Barrier)

This test is done to make sure that when a vehicle hits another vehicle with a low speed, the structural components of the vehicle such as the front rails will not deform. The front bumper and crash box are allowed to deform, as those are bolt on parts and can be replaced easily. The test setup includes a rigid bumper barrier with an energy absorber attached to it and an impact vehicle hitting it at a speed of 10 km/h as shown in Figure 14.89. The rigid bumper barrier with the energy absorber has a height of 455 mm from the ground. The post-test vehicle position is shown in Figure 14.90.

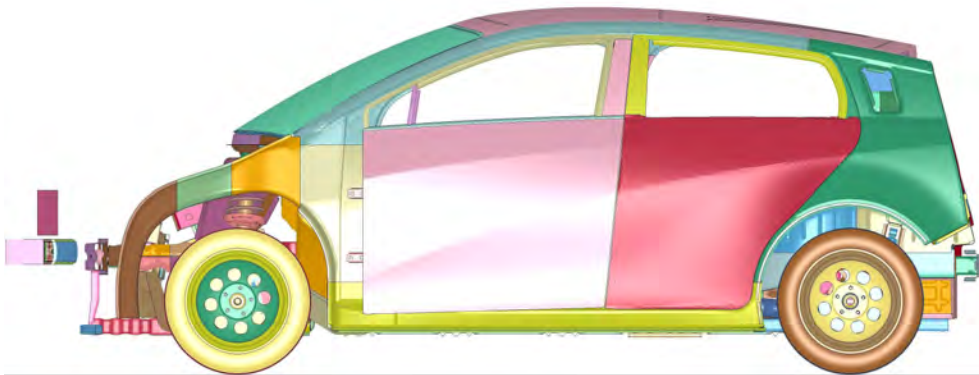


Figure 14.89: *RCAR - Vehicle at initial position*

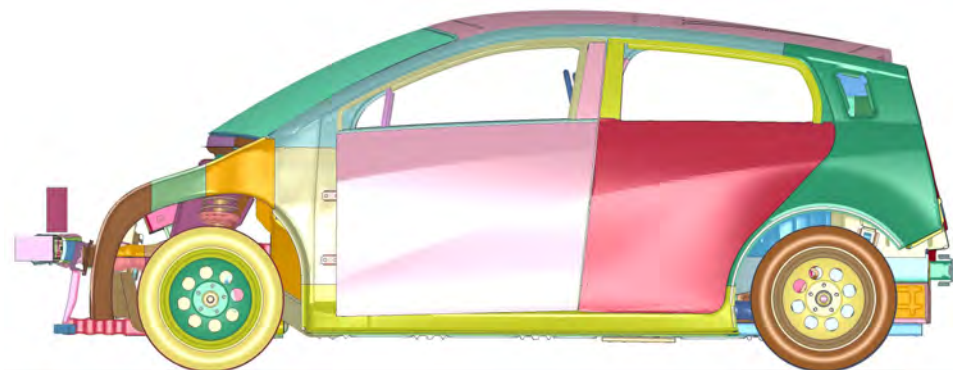


Figure 14.90: *RCAR - Vehicle at final position*

Figure 14.91 shows the front bumper and the other connecting structural parts at the initial position. The same components are shown after the crash test in Figure 14.92.

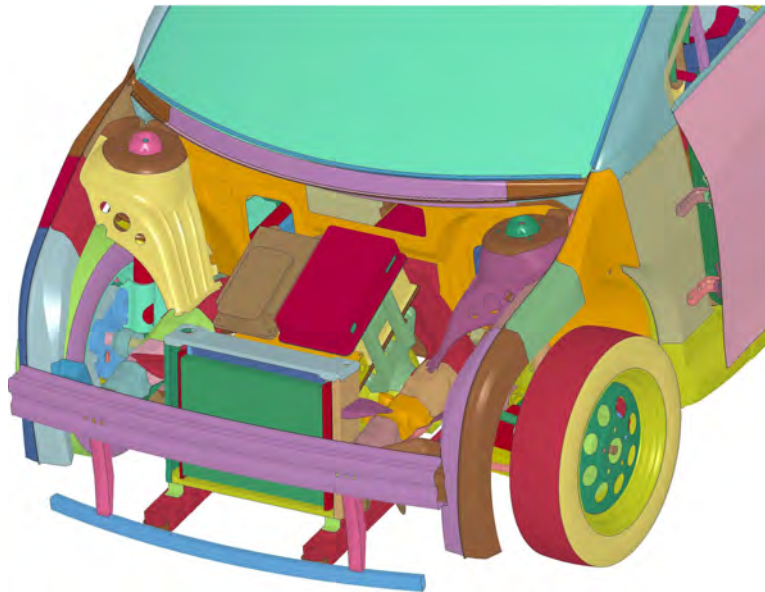


Figure 14.91: RCAR - Vehicle front structure at initial position

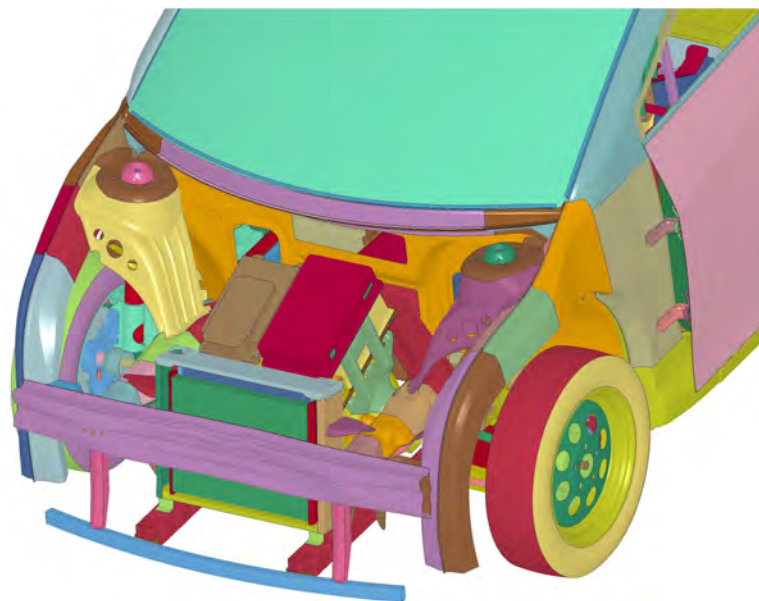


Figure 14.92: RCAR - Vehicle front structure at final position

Figure 14.93 shows the crush box at initial position and Figure 14.94 shows the deformed crush box at the final position after the test. It can be seen that the bumper and the crush box absorb most of the energy; there is no deformation to the radiator and the front rail.

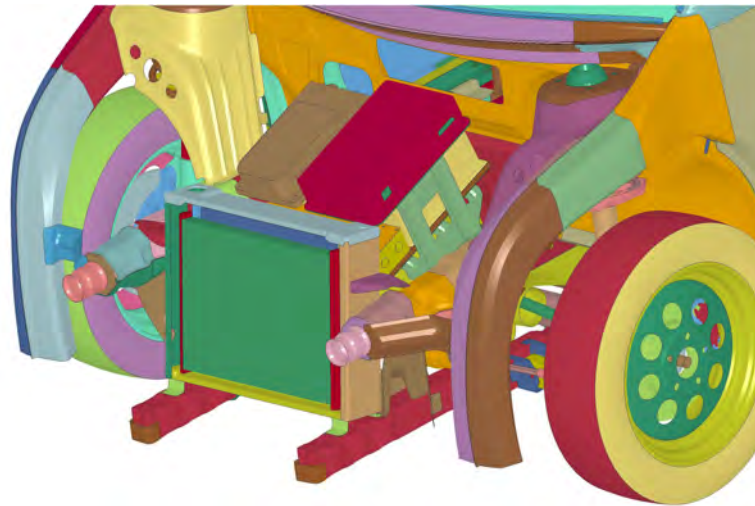


Figure 14.93: RCAR - Crush box at initial position

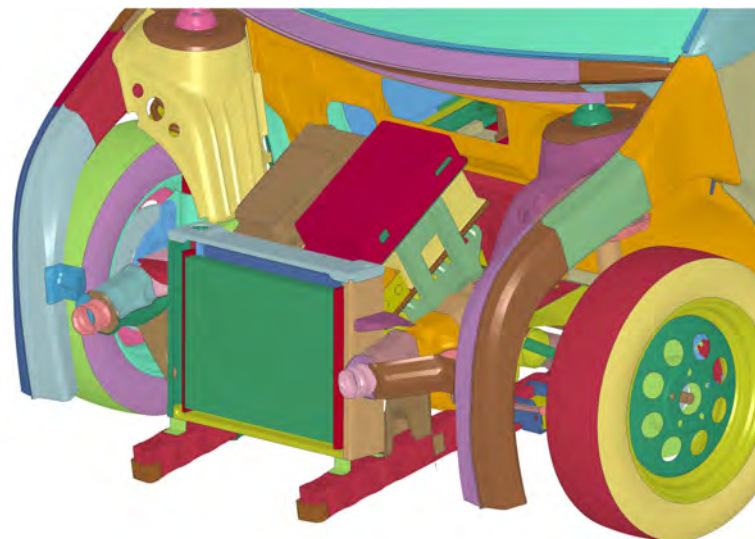


Figure 14.94: RCAR - Crush box at final position

Even though plastic strain is present in the front rails where it meets the crush box, but it is very localized and does not degrade the structural integrity of the front rails.

14.1 Crash Worthiness

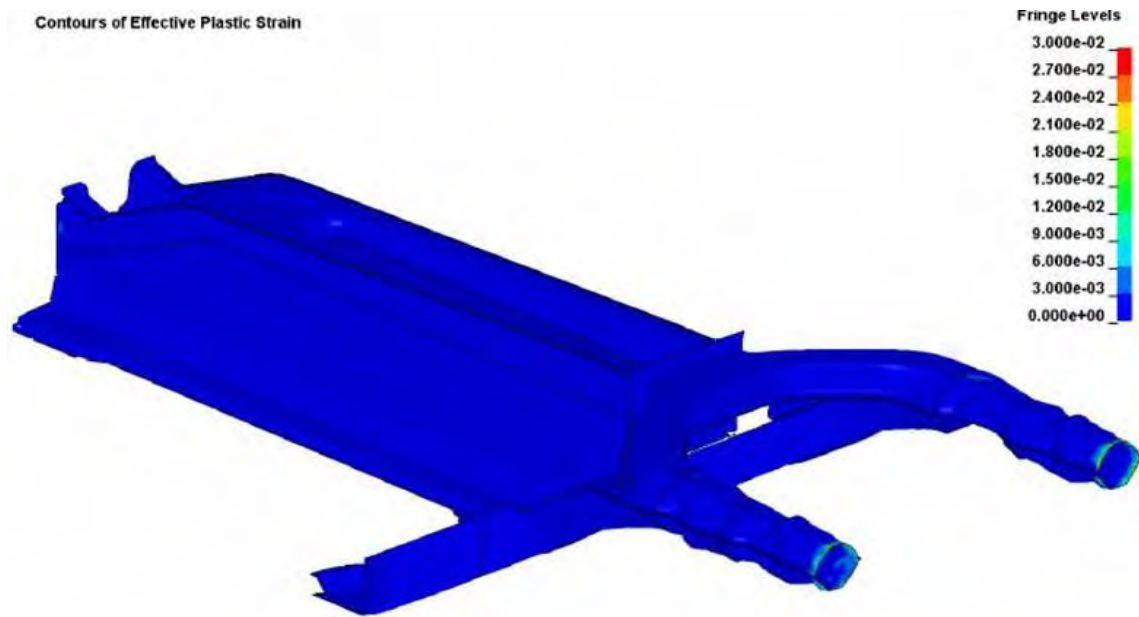


Figure 14.95: RCAR - Plastic Strain

14.2 Static Stiffness Study

An adequate static torsion and bending stiffness of systems such as Body-in-Prime (BIP) is essential for the better overall NVH performance. The BIP model includes the body structure, the windshield, and bolted assemblies like the front and the rear bumpers, the radiator support, the engine cradle and the battery tray assembly as illustrated in Table 14.3.

For the FSV, a static stiffness target of approximately 20kN-m/deg was set, based on research data of competitive C-class vehicles (the body stiffness of C-class vehicles range between 15 and 20 KN-m/deg).

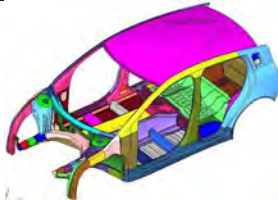






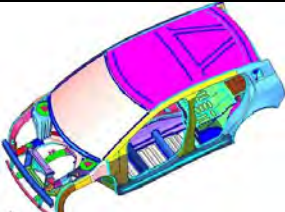
S.No.	Assemblies	Total mass of the assembly (kg)	Illustration
1	Body Structure	187.7	
2	Battery Tray	12.0	
3	Engine Cradle	13.9	
4	Rear Bumper	3.2	
5	Front Bumper	5.9	
6	Radiator Support	1.8	
7	Windshield	15.0	
	BIP	239.5	

Table 14.3: Body-In-Prime (BIP) description

14.2.1 Loading and Boundary Conditions

14.2.1.1 Torsion Stiffness

The BIP is constrained at the rear left body support along x, y, and z axes; the rear right body support along the x and z axes. Additionally, one more point on the mid-plane of the front bumper beam along z is constrained as shown in Figure 14.96. The torsion loads are applied at the front supports. Vertical loads of 1200 N are applied in opposite directions on the left and right mounts as shown in Figure 14.96.

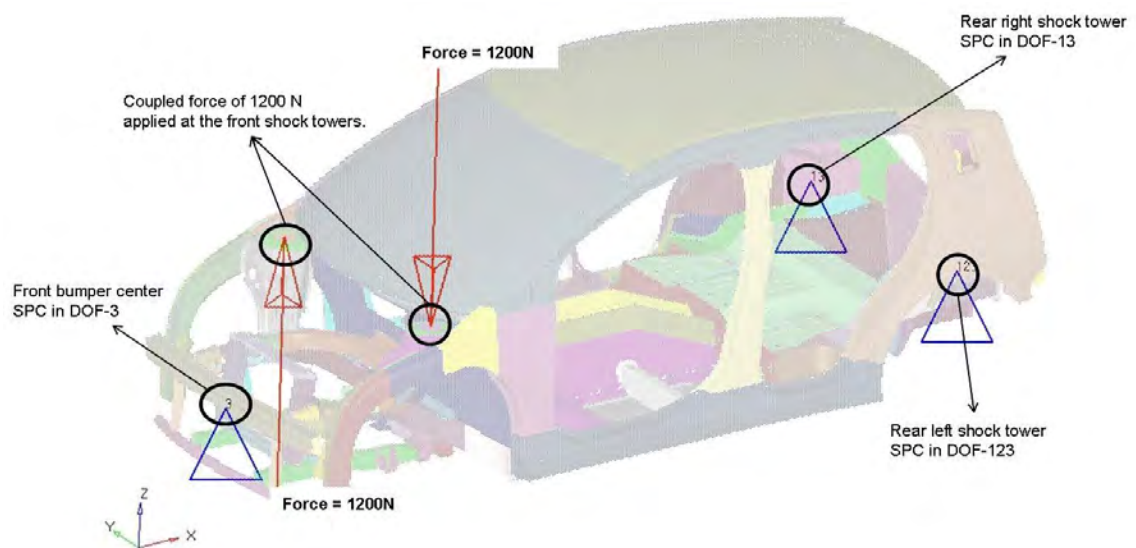


Figure 14.96: Torsion constraints and loading

14.2.1.2 Bending Stiffness

The BIP is constrained at the rear left body support along x, y, and z axes; the rear right body support along the x and z axes; at the front left body support along y, and z axes; and front right body support along z axes as shown in Figure 14.97. The bending loads are applied at the center of the front and rear seats. Vertical loads of 1668 N are applied at center of the four seats on the as shown in Figure 14.97.

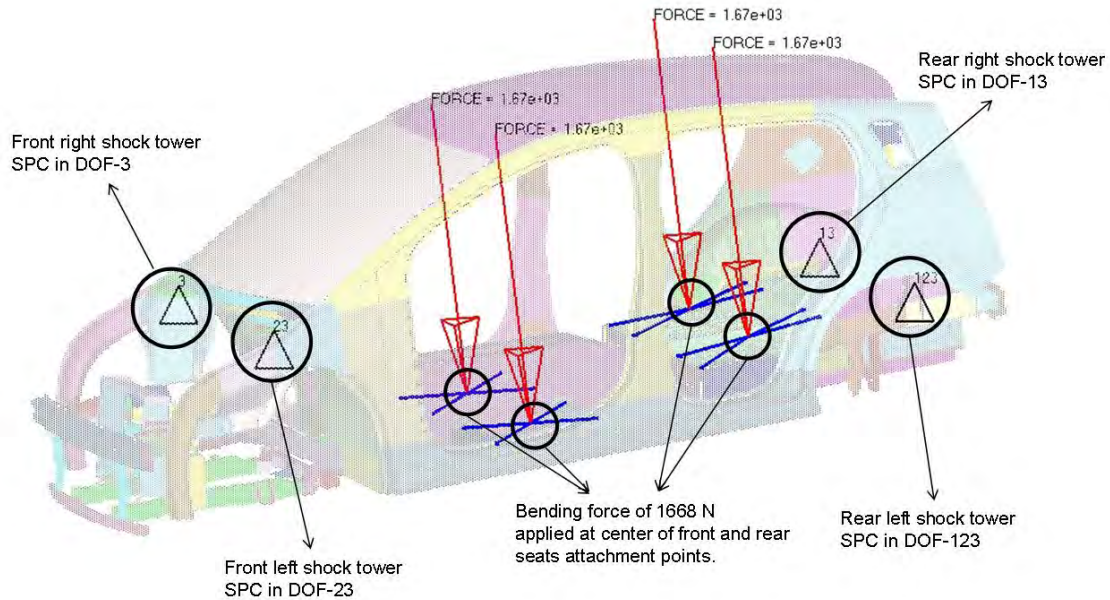


Figure 14.97: Bending constraints and loading

14.2.2 Static Stiffness Results

The torsion stiffness results are shown in Table 14.4. The torsion stiffness of FSV body structure is meeting the target value of 20 kN-m/deg.

Analysis Type	Target	FSV Model Results
Torsion stiffness (KN-m/deg)	20.0	19.604
Bending stiffness (N/mm)	12.0	15.552

Table 14.4: Static stiffness results

14.3 Dynamic Stiffness Study

14.3 Dynamic Stiffness Study

For a vehicle to be dynamically stiff, it is important to have high natural frequencies for the global modes. For the FSV Body-in-Prime (BIP), targets are set for these critical global modes of vertical bending and torsion that influence the body global stiffness. The modes are shown in Figure 14.98 and Figure 14.99.

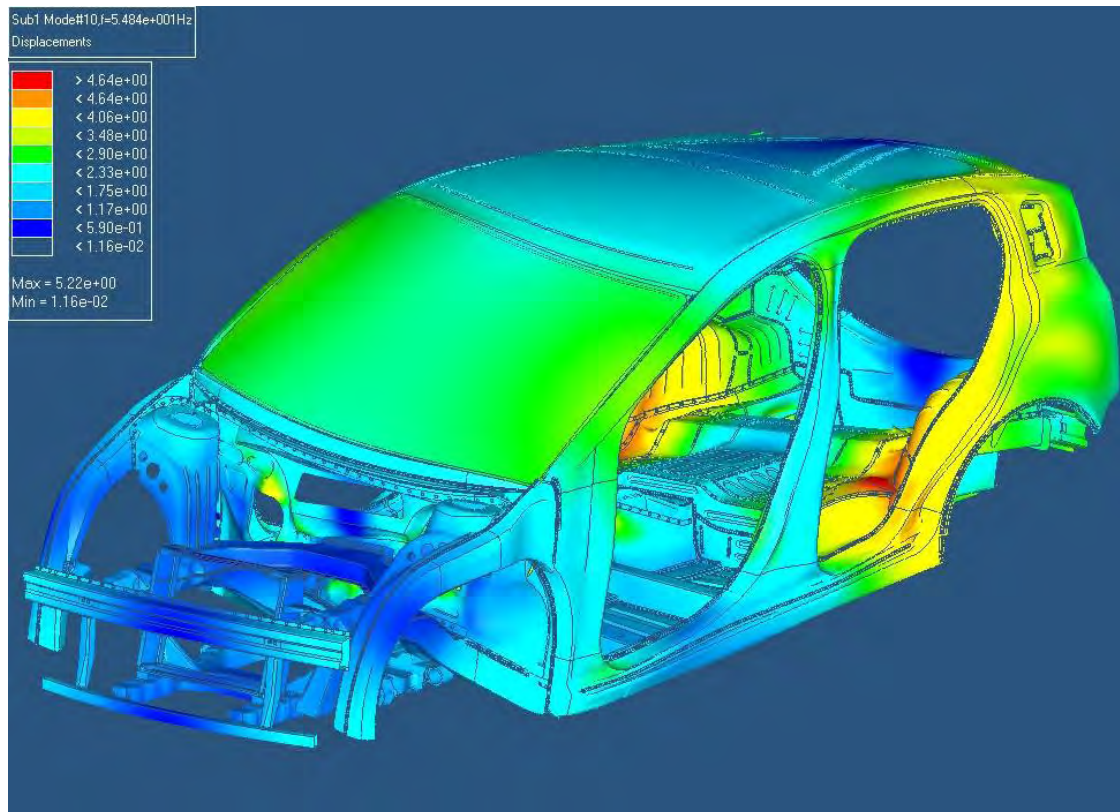


Figure 14.98: *Torsion mode at 54.84 Hz*

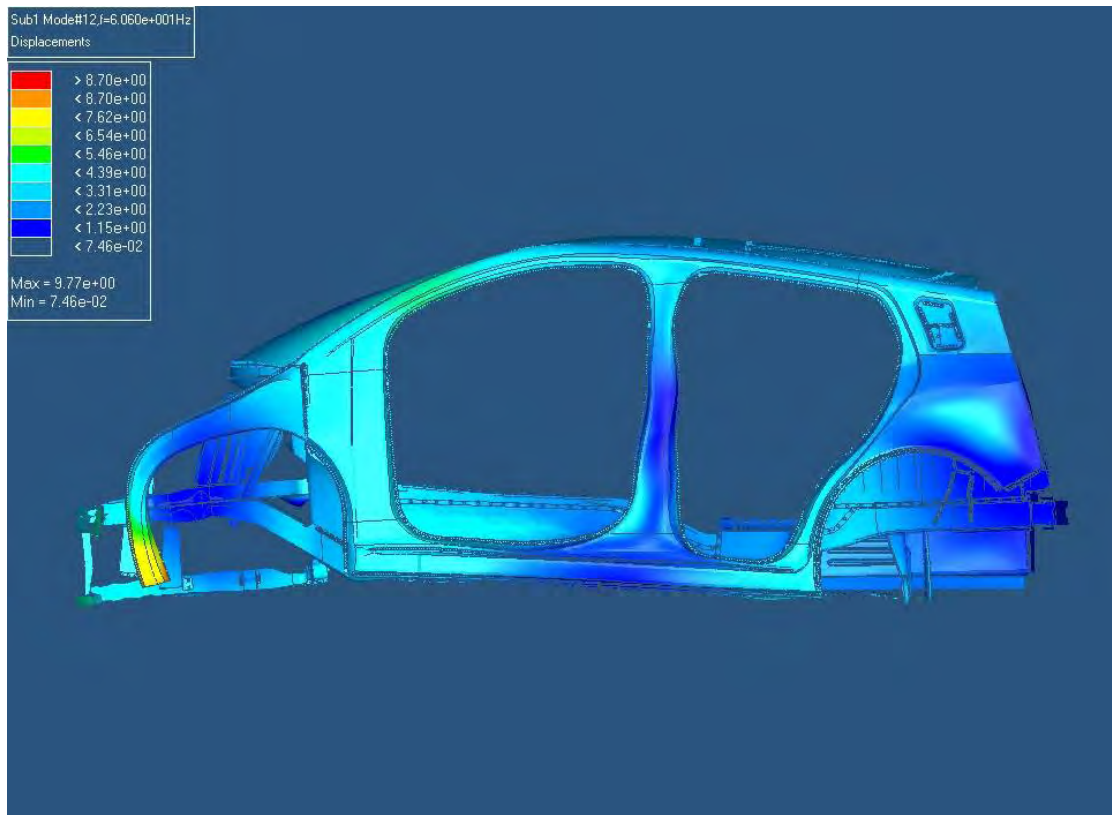


Figure 14.99: Vertical bending mode at 60.60 Hz

14.3.1 Global Modes Results

The FSV global modes targets and the FSV body structure results are shown in Table 14.5. As shown in the table, the FSV torsion and vertical bending modes are higher than 40 Hz and also different by 3 Hz.

Global Mode Type	Frequency (Hz)	Target
Torsion	54.84	Both the modes should be >40 Hz and also have a difference of at least 3 Hz
Vertical Bending	60.6	

Table 14.5: Global modes results

14.4 Full Vehicle Dynamic Analysis

MSC/ADAMS (Macneal-Schwendler Corporation/Automatic Dynamic Analysis of Mechanical Systems) modeling was used to evaluate five vehicle ride and handling conditions of the FSV. The five maneuvers included the following:

1. Fish-hook test
2. Double lane change maneuver (ISO 3888-1)
3. 3 g pothole test
4. 0.7 g constant radius turn test
5. 0.8 g forward braking test

14.4.1 Vehicle Information

The FSV-1 model consisted of subsystems that were built and assembled in ADAMS. The following subsystems included all the major component parameters: body, front and rear suspension, steering, powertrain, tire, brake and front/rear roll bar. The FSV-1 has a McPherson strut front suspension and trailing arm rear suspension. The center of gravity height is 476 mm. Curb weight is 958 kg with a 57% front weight distribution. A curb weight vehicle with five passengers and cargo is shown in Figure 14.100. This loading condition reflects the loading condition for the industry standard tests mentioned in Section 14.4. The information on the other test loading conditions are in Sections 14.4.2 and 14.4.3. Sample parameters affecting vehicle dynamics include spring and damper rate, roll bar rate, center of gravity location and test weight. The rates were determined through parametric runs of the fishhook and constant radius turn tests using ADAMS Insight.

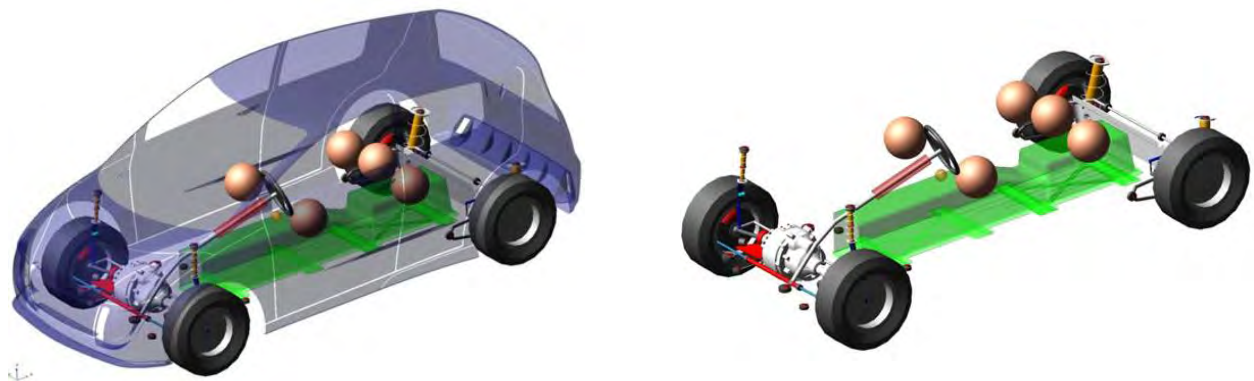


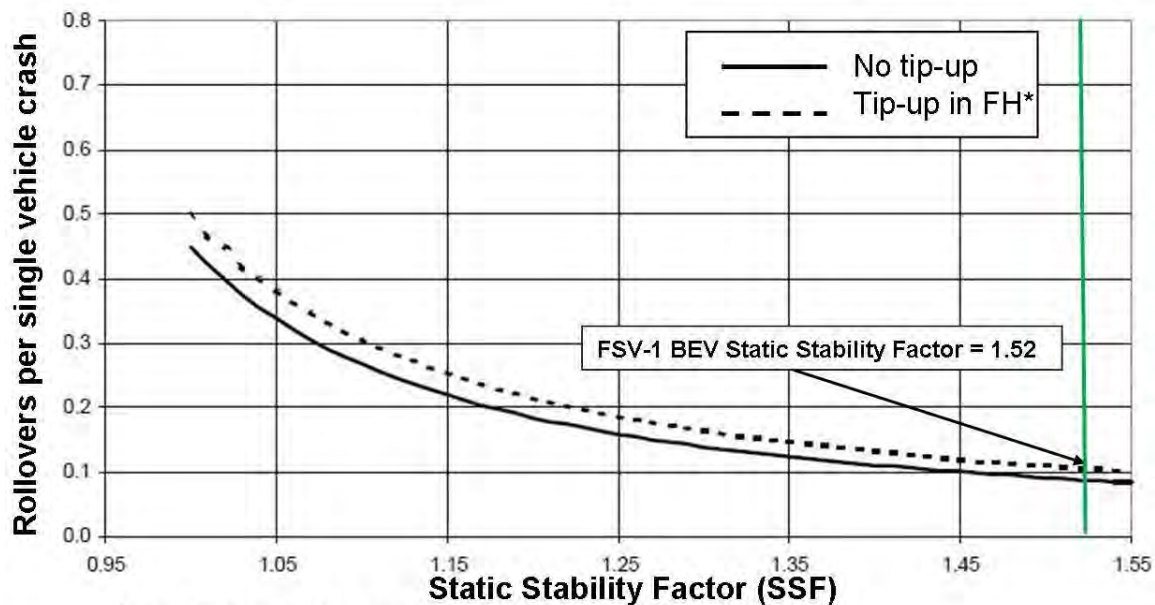
Figure 14.100: Curb weight vehicle with five passengers and cargo

14.4.2 Fishhook Test

The fishhook test is a test used by the National Highway Traffic Safety Administration (NHTSA) in conjunction with the Static Stability Factor (SSF) to rate the propensity for vehicle rollover ^[4]. The test procedure is explained in Section 14.4.2.

The SSF is the ratio of half of a vehicle's track width to its center of gravity height. The SSF value for the FSV-1 is 1.52 (track width = 1450 mm and center of gravity height = 476 mm). The vehicle's performance during the fishhook maneuver - specifically whether or not the vehicle experienced tip-up - combined with the SSF value, is referenced in a NHTSA statistical model to determine the vehicle's rollover rate per single vehicle crash percentage (see Figure 14.101).

The final rating is then determined as follows: 1 star for a rollover rate greater than 40%, 2 star for a rollover rate of 30% up to and including 40%, 3 star for a rollover rate of 20% up to and including 30%, 4 star for a rollover rate of 10% up to and including 20%, and a 5 star for a rollover rate less than or equal to 10%. Refer to section 4, for fish hook results and the overall rollover rating.



*FH- fishhook with a heavy load

Figure 14.101: Static Stability Factor (SSF)

14.4.2.1 Fish Hook Test Procedure

- a The fish hook test is conducted with a five passenger load. The vehicle is accelerated to the desired vehicle speed, the throttle is released, and the steering input is performed. The maneuver involves a steer followed by a counter steer action. The details are shown in Figure 14.102 ^[5].

⁴Department of Transportation NHTSA, 49CFR Part 575, Docket No. NHTSA-2001-9663; Notice 3

⁵Source:<http://www.nhtsa.gov>

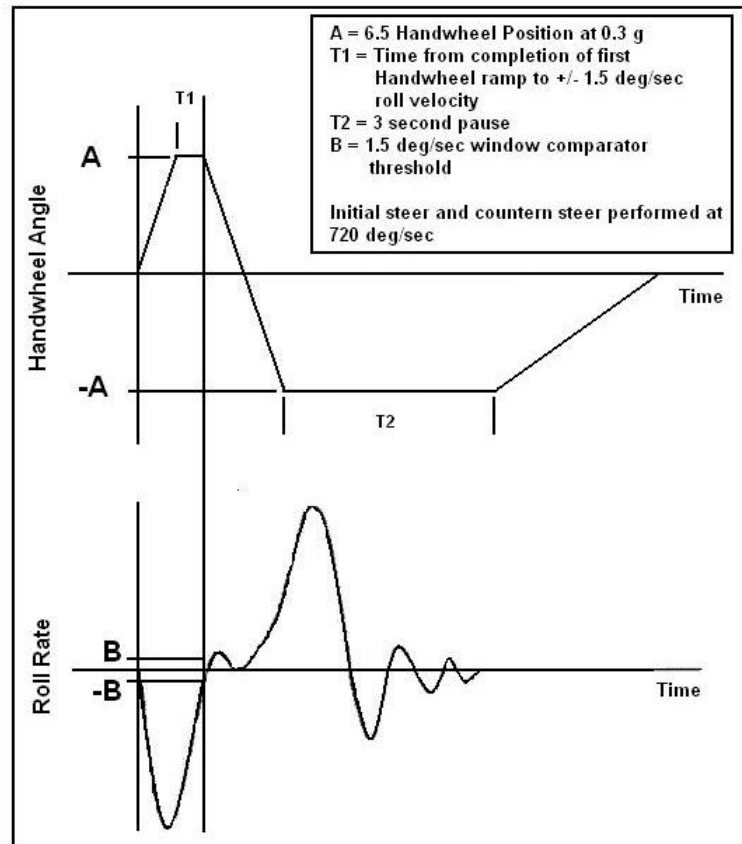


Figure 14.102: Fish hook test details

- b An abbreviated version of the Slowly Increasing Steer Maneuver is used to determine the steering angle which produces 0.3 g^[6]. The vehicle is driven at 80.5 km/h with a steering input from 0 to 270 degrees at 13.5 degrees/second, and held at 270 degrees for two seconds. The amplitude of the resulting steering angle that produces 0.3 g is then multiplied by 6.5 to determine the steering angle used for the test.
- c The fishhook test is run at 56.3 km/h, 64.3 km/h, 72.4km/h, 76.4 km/h and 80.5 km/h making a left to right turn and then repeated making a right to left turn. If there is two wheel lift-off in the left to right turn sequence prior to 72.4 km/h, the test is ended. If no lift-off is observed, then the right to left sequence is performed. If lift-off is observed in the right to left sequence, the test is ended. The test is also ended if there is rim to pavement contact or tire de-beading. The latter cannot be observed in ADAMS.

Subsequent runs are made if there is lift-off left to right or right to left at speeds greater than 76.4 km/h and can be referred to in the NHTSA document ^[7]. However, they involve changing tires and re-running the event. Tire wear is not taken into account in this model, therefore analysis will

⁶SAE J266

⁷Department of Transportation NHTSA, 49CFR Part 575, Docket No. NHTSA-2001-9663; Notice 3

be made on a single series counter steer evaluation for left to right turn and right to left turn.

Subsequent runs are made if there is no lift-off up to and including 80.5 km/h for left to right and right to left steer. However, these runs also take into account tire wear, which is not included in this ADAMS model. Therefore, analysis will be made on a single series counter steer evaluation for a left to right turn and a right to left turn.

14.4.3 Industry Standard Maneuvers

The double lane change maneuver was evaluated because it is one of the most common driver maneuvers. The 3 g pothole test was chosen because it is one of the most severe ride and handling tests for durability. The 0.7 g constant radius turn and the 0.8 g brake analyses were also conducted because they are among the more severe driving conditions for durability.

14.4.3.1 Double Lane Change Maneuver Test

The double lane change maneuver ^[8] is a subjective dynamic maneuver which involves driving in a straight line in an initial lane, shifting to the adjacent lane and shifting back to the original line. The test track details are shown in Figure 14.103 and Table 14.6. The test track length is 125 m. Two tests are run. For the first test the initial speed is 80 +/- 3 km/h, the throttle position is held steady and the driver maneuvers through the test track. For the second test, the driver maneuvers through the test track at the maximum speed of which the vehicle is capable. The throttle position can be held steady or varied. The vehicle must be able to manipulate the track without exceeding lane boundaries.

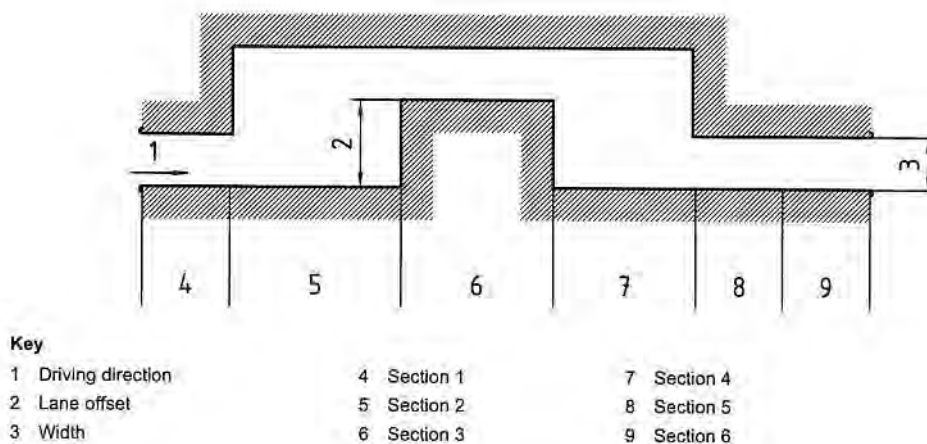


Figure 14.103: Double lane change track and designation of section

⁸Double Lane Change Maneuver, ISO 3888-1

Section	Length (m)	Lane Offset (m)	Width (m)
1	15	-	1.1 * vehicle width +0.25
2	30	-	-
3	25	3.5	1.2 * vehicle width +0.25
4	25	-	-
5	15	-	1.3 * vehicle width +0.25
6	15	-	1.3 * vehicle width +0.25

Table 14.6: *Dimensions of the double lane change track*

14.4.3.2 3 g Pothole Test

The 3 g pothole test consists of driving a vehicle over a pothole on the left or right side of the vehicle. The front left/right tire contacts the pothole followed by the rear left/right tire. The 3 g quantity is the un-sprung vehicle weight measured at the impacting wheel of the vehicle multiplied by three. The ADAMS run was conducted on the right hand side. The unsprung weight at the right front corner wheel took into account the fully loaded vehicle condition - including five passengers and cargo - as the aforementioned was most severe for ride and handling. Total weight of the test vehicle was 1371 kg. The vehicle was driven over a 101.6 mm deep pothole at 3.5 m/s. Bushing forces as a function of time was recorded at the front and rear suspension attachments to body, engine cradle and battery suspension cross-member. These results were then output to a DAC file for durability analysis.

14.4.3.3 0.7 g Constant Radius Turn

The 0.7 g constant radius turn involved driving a fully loaded five passenger vehicle with cargo around a 95 meter diameter circle. Vehicle lateral g's were ramped up from 0.4 to 0.7 g. The ADAMS program internally calculates the velocity required to achieve 0.4 and 0.7 g lateral loading.

14.4.3.4 0.8 g Forward Braking

The 0.8 g forward braking event started with a fully loaded five passenger vehicle and cargo, driving in a straight line at 7.0 m/s. A longitudinal deceleration of 0.8 g was then applied. The ADAMS program internally calculates the braking force needed to achieve 0.8 g braking.

14.4.4 Results

14.4.4.1 Fish Hook Test

The results of the Fish Hook test are listed in Table 14.7. Based on the NHTSA statistics chart in Figure 14.101, the probability of vehicle rollover is less than 10%. The aforementioned number corresponds to a 5 star rating.

Vehicle Speed (km/hr)	Two Wheel Tip-Up (Yes/No)
56.3	No
64.3	No
72.4	No
76.4	No
80.5	No

Table 14.7: Fishhook test results Summary

14.4.4.2 Double Lane Change Maneuver

The results of the double lane change maneuver show the vehicle remains within the boundary lines (defined earlier in Figure 14.103 and Table 14.6).

14.4 Full Vehicle Dynamic Analysis

14.4.4.3 3 g Pothole Test

The 3 g pothole bushing loads on the body results (in Newtons) - are shown below in Table 14.8. The peak loads were recorded at the peak front vertical load through the tire. The bushing load results as a function of time were converted to DAC files for input into the Design Life 6.0 fatigue program. Pictures of the road used for the test are shown in Figure 14.104.

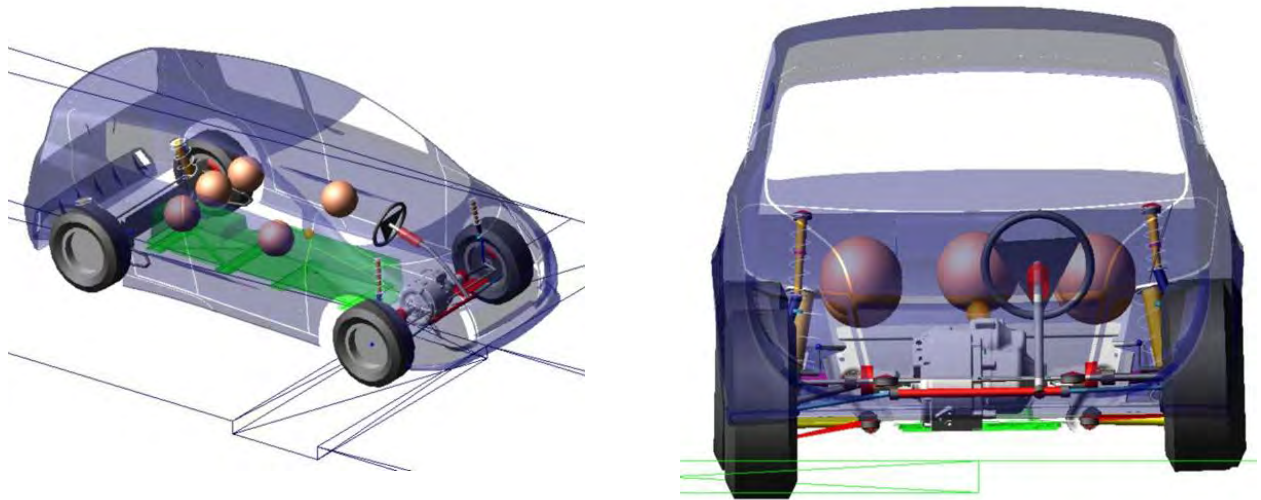


Figure 14.104: Road used for the FSV 3 g pothole test

Bushings Description	Bushings Loads		
	fx (N)	fy (N)	fz (N)
FRONT SUSPENSION			
Body mount left	190.69	1232.36	3770.61
Body mount right	430.94	-896.35	5491.90
LCA to subframe frt left	-359.85	-2072.00	-29.53
LCA to subframe frt right	-33.06	527.18	203.65
lca to subframe rr left	4.77	-72.00	-25.28
LCA to subframe rr right	45.64	-397.60	207.11
REAR SUSPENSION			
Trailing arm to body left	-414.27	64.12	591.79
Trailing arm to body right	-848.34	54.62	1529.10
Upper Control Arm (UCA) to subframe left	-26.38	1956.89	-102.06
UCA to subframe right	-133.30	-2603.23	-281.70
Lower Control Arm (LCA) to subframe left	69.54	-2610.23	-62.86
LCA to subframe right	381.11	2350.41	74.43
Rear body mount left	391.03	350.56	1914.16
Rear body mount right	646.29	-345.14	3283.18

Table 14.8: *3g pothole test bushing loads on body results*

14.4 Full Vehicle Dynamic Analysis

14.4.4.4 0.7 g Constant Radius Turn

The 0.7 g constant radius turn bushing loads on body results are shown below in Table 14.9. The peak loads were recorded at 0.7 g vehicle lateral load. The bushing load results as a function of time were converted to DAC files for input into the Design Life 6.0 fatigue program.

Bushing Description	Bushing Loads		
	fx (N)	fy (N)	fz (N)
REAR SUSPENSION			
Body mount left	-161.95	867.83	1917.38
Body mount right	104.34	110.53	3933.13
Lower Control Arm (LCA) to subframe frt left	102.07	-2561.09	379.44
LCA to subframe frt right	349.68	-4481.04	588.62
LCA to subframe Rear left	21.80	-352.49	-83.04
LCA to subframe Rear right	-45.20	564.53	-467.07
FRONT SUSPENSION			
Trailing arm to body left	-146.25	122.37	54.78
Trailing arm to body right	-817.35	-91.01	1827.56
Upper Control Arm (UCA) to subframe left	-342.34	1803.02	-42.41
UCA to subframe right	-159.83	-349.01	-5.23
LCA to subframe left	480.52	-3002.67	-168.29
LCA to subframe right	944.10	-2710.56	-21.54
Rear body mount left	200.58	321.90	1099.07
Rear body mount right	775.97	-107.18	3480.33

Table 14.9: 0.7g constant radius turn bushing loads on body results

14.4.4.5 0.8 g Forward Braking

The 0.8 g forward braking bushing loads on body results are shown below in Table 14.10. The peak loads were recorded at 0.8 g vehicle longitudinal load. The bushing load results as a function of time were converted to DAC files for input into the Design Life 6.0 fatigue program.

Bushing Description	Bushing Loads		
	fx (N)	fy (N)	fz (N)
FRONT SUSPENSION			
Body mount left	-657.92	680.47	3249.60
Body mount right	-656.43	-680.55	3244.79
Lower Control Arm (LCA) to subframe frt left	-159.30	-4280.74	1900.37
LCA to subframe frt right	-157.78	4276.93	1903.96
LCA to subframe Rear left	128.61	3750.29	1899.17
LCA to subframe Rear right	127.70	-3757.02	1902.16
REAR SUSPENSION			
Trailing arm to body left	1051.51	-470.90	-133.88
Trailing arm to body right	1054.74	470.19	-139.00
Upper Control Arm (UCA) to subframe left	-84.02	1663.86	-117.27
UCA to subframe right	-83.45	-1659.53	-116.49
LCA to subframe left	209.69	-1596.07	-6.38
LCA to subframe right	208.11	1596.29	-6.95
Rear body mount left	492.39	326.35	2287.34
Rear body mount right	491.18	-326.50	2281.55

Table 14.10: 0.8g forward braking bushing loads on body results

14.4.5 Conclusions

Based on the results of the aforementioned runs, there were no vehicle instabilities or wheel lift-off during any of the maneuvers conducted on the FSV. The BEV has a large battery packaged at the bottom of the vehicle which lowers vehicle Cg and enhances the handling characteristics. (Refer to Section 14.5 - Durability Results, for additional information on how the suspension load input affects the body in long term fatigue analysis during 3 g pothole, 0.7 g constant radius curve and 0.8 g braking maneuvers.)

14.5 Durability Study

Vehicle durability refers to the long term performance of a vehicle under repetitive loading due to driving and other operating conditions. In normal operating conditions, tires and suspensions experience road loads that cascade throughout the vehicle body. The transfer and distribution of loads varies with the structural, inertial, and material attributes of the vehicle body, and manifest as repetitive loads on the system and components. These repetitive loads cause fatigue damage, and the accumulation of damage ultimately results in the initiation of cracks, crack propagation, and system or part failure. A design for durability process is a method of managing the accumulation of fatigue damage to prevent cracks from initiating in advance of the complete design life of the vehicle.

There are two types of fatigue analyses in use for structural durability. The first is stress based or s-N analysis which is applicable for low stress and high cycle fatigue. In vehicle systems, this corresponds to loads from high speed rotating equipment such as the engine, transmission, and auxiliaries. The second is strain based or e-N analysis which is applicable for high stress, low cycle fatigue as from road loads and other transient loads. A process of integrating the strain based method is used for the FSV vehicle.

The main road load cases studied for the FSV vehicle that affect body life include:

- 3 g Pothole
- 0.7 g Cornering
- 0.8 g Forward braking cases

14.5.1 Process and Tools used for Durability Study

The following process and tools were used for conducting the FSV durability study:

- (a) The FSV was analyzed on different road profiles with proper suspensions and bushings in ADAMS ^[9] software. The time series loads in the x, y, and z directions, were extracted at different body mounting locations such as the following:
- I Front shocks (left and right side)
 - II Rear shocks (left and right side)
 - III Lower control arm to front sub frame front (left and right side)
 - IV Lower control arm to front sub frame rear (left and right side)
 - V Trailing arm to body (left and right side)
 - VI Upper control arm to rear sub frame (left and right side)
 - VII Lower control arm to rear sub frame (left and right side)
- (b) For determining the unit load , the stresses were extracted at the above mentioned body

⁹Automatic Dynamic Analysis of Mechanical Systems

mounting locations in NASTRAN ^[10], using a linear static solution (SOL 101), with an inertia relief boundary condition.

- (c) For the fatigue life calculation, “n-code Design Life” tool was used. The stresses from the static solution (SOL 101) were established, and then scaled with the dynamic road loads. The fatigue materials were created and the Body-in-Prime (BIP) was updated with the materials, using n-code Design Life tool to estimate the fatigue life.

14.5.2 Results

The contour plots for the different load cases are shown in the following sections.

14.5.2.1 3 g Pothole

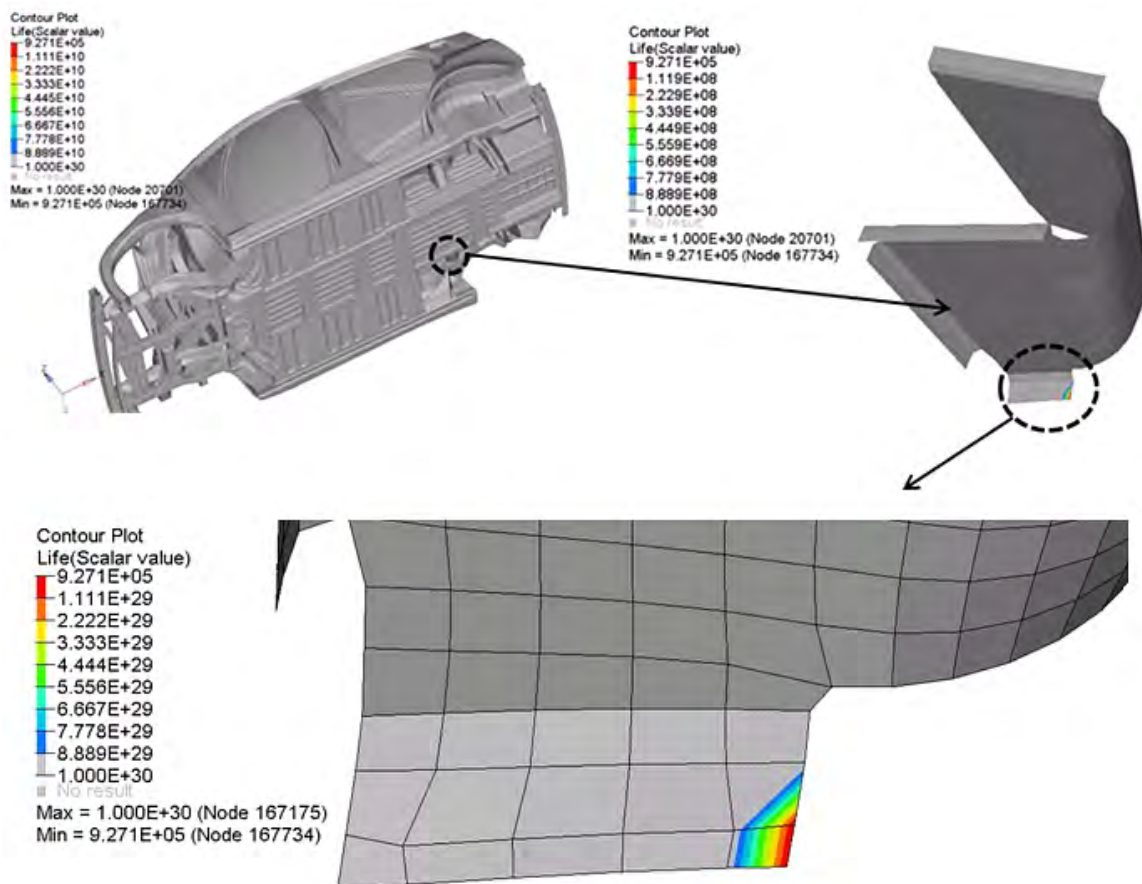


Figure 14.105: 3 g pothole contour plot

¹⁰Nasa-Structural-Analysis tool

14.5 Durability Study

For the 3 g pothole load case, a minimum life of 927,100 cycles was found at the right rear gusset as shown in Figure 14.105. The target value was 200,000 cycles. The durability study for the gusset was conducted using mild steel as the material, since the original material specification of BH210/340 showed a minimum life at the heat affected zone (weld region).

14.5.2.2 0.7 g Cornering

For the 0.7 g cornering load case, the minimum life of 1,676,000 cycles was found at the rear cargo box as shown in Figure 14.106, which is above the target value of 100,000 cycles. The material of the cargo box is mild steel.

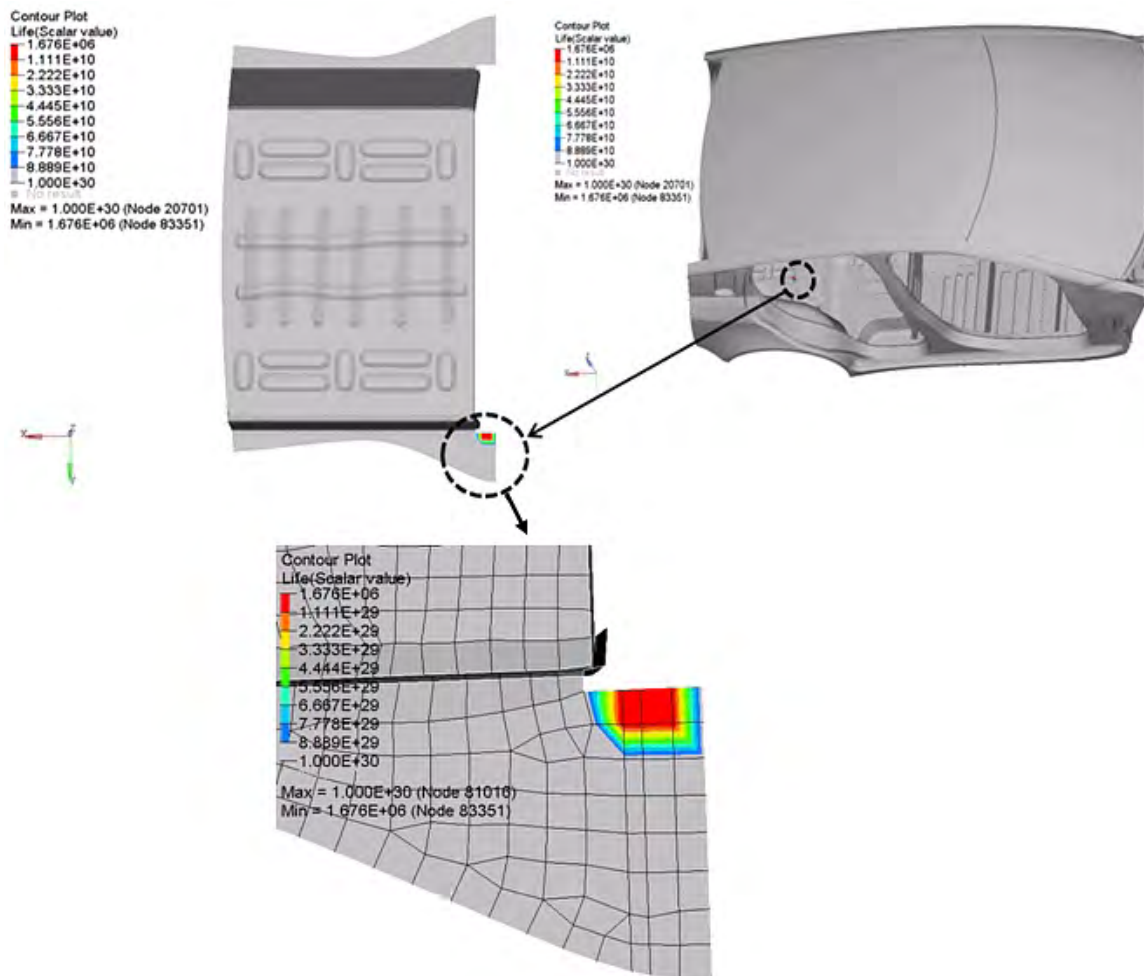


Figure 14.106: 0.7 g Cornering contour plot

14.5.2.3 0.8 g Forward Braking

For the 0.8 g forward braking load case, a minimum life of 274,700 cycles was found at the engine cradle rear rail-upper as shown in Figure 14.107, and a minimum life of 17,340,000 cycles was found in the body, which is above the target value of 100,000 cycles. The material of the engine cradle rear rail-upper is HSLA 350/450.

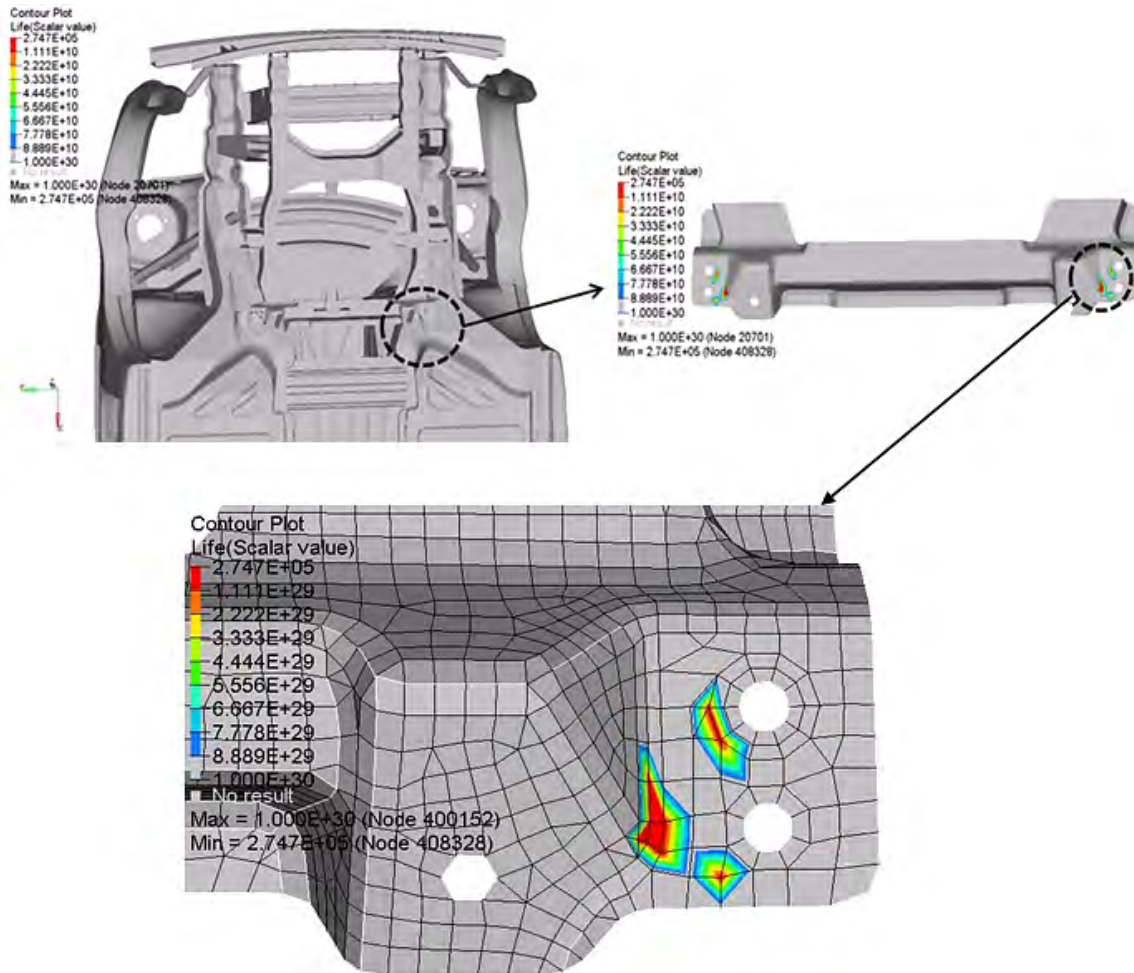


Figure 14.107: 0.8 g forward braking contour plot

The results of the FSV BIP study are summarized in Table 14.11. As shown in the table, the life of the FSV BIP model is higher than the target values.

14.5 Durability Study

Loading Type	FSV Predicted Life Cycles	Target Life Cycles
3G Pot Hole	927,000	200,000
0.7G Cornering	1,680,000	100,000
0.8G Forward Braking	275,000 (Engine cradle) 17,300,000 (Body Life)	100,000

Table 14.11: Durability Results Summary

14.6 FSV NVH Assessment Conducted by LMS

The FutureSteelVehicle (FSV) - Battery Electric Vehicle (BEV) was fully assessed for noise and vibration at concept design stage of this program. As very little data is available on Noise Vibration and Harshness (NVH) performance of BEV, this project was supported by first measuring the performance of a Mitsubishi BEV and an internal combustion engine based vehicles.

Measurements were conducted on two small Mitsubishi vehicles that both share the same body, yet one is equipped with an internal combustion engine and the other with an electric motor. The outcome was used as a starting point to identify advantages and disadvantages of electric motor noise and draw a set of NVH targets for FSV. Compared to a combustion engine, the electric motor shows significantly lower sound pressure levels, except for an isolated high frequency peak heard at high speeds (3500 Hz when the vehicle drives at top speed). The prominence of this peak is lowered by increased use of acoustic absorbent materials in the motor compartment. For low and mid frequencies, moderate electric motor forces imply less stringent noise and vibration design constraints and a possibility to reduce the body mass. To take full advantage of this opportunity, NVH is integrated early into the FSV design cycle and optimized in parallel with crash performances.

Finite element simulations at low and mid frequencies lead to reshaping the suspension mounts, the rear roof, the front header and the cowl top connection area, each change driving large reductions of noise levels while adding little to no mass. Damping sheets prove unnecessary. Lighter damping solutions such as vibration damping steels were examined and proved to be successful in the mid frequency range. Overall, the change from combustion engine to electric motor is compatible with mass reductions and similar or better noise and vibration performances. The body structure of FSV is designed with several panels that are made from 0.5mm AHSS. The results of this NVH study show that the implementation of these low gauges does not lead to deterioration of the NVH performance.

(The NVH assessment of BEV is fully documented in a separate WorldAutoSteel report)

15.0 Manufacturing Process Simulation Results

15.1 Single Step Metal Stamping Simulation

Single step stamping simulation is a quick process for getting an approximate idea that for a given blank shape and size whether a component can be stamped or not. The single step simulation method is very helpful in the product development stage.

For the FSV BEV vehicle, single step simulation was done on all the parts of the body structure using Hyperform Radioss One Step (Altair Hyperworks 10.0). Most of the parts of the body structure can be made through cold forming. Parts which play an important role in crashworthiness like B-pillars, Shotguns and Roof rails are made using a hot forming process. The hot stamping process is also simulated using single step process by assuming IF steel (IF 260/410) forming properties.

Although single step simulation is done on all the body structure parts, it cannot replace the incremental analysis process. Some parts which have complicated shapes like body side outer, front rails and rear rails require the incremental analysis method for predicting the manufacturing results more accurately.

Determination of whether a stamped component design is safe or if it will fail is determined through the Forming Limit Diagram (FLD). This is an empirical curve showing the biaxial strain levels beyond which failure may occur in sheet metal forming. For example, the single step stamping simulation done on the floor panel as shown in Figure 15.1 and Figure 15.2, was analyzed with a FLD diagram. The floor is a laser welded blank with respective thicknesses of 0.5 and 1.5 mm. Material for these blanks is Dual Phase (DP) 300/500 and DP 500/800 steels.

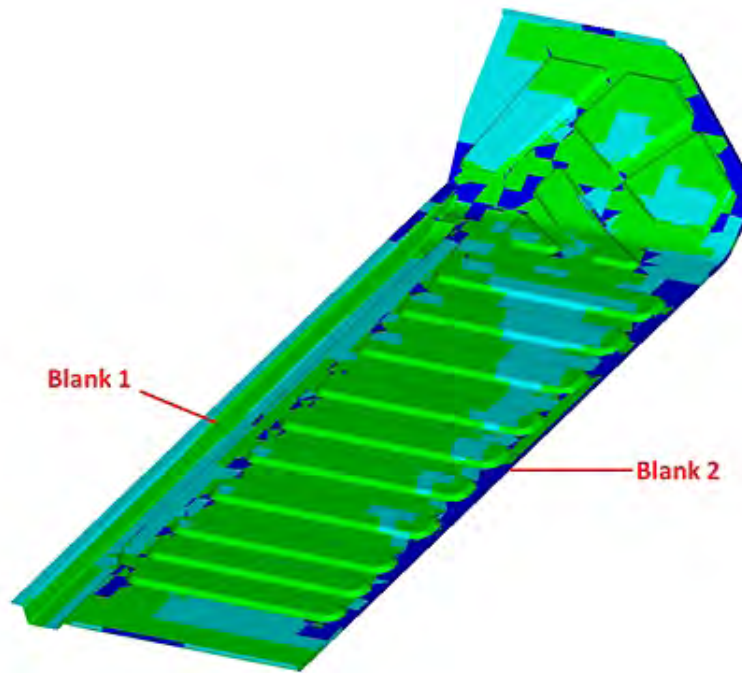


Figure 15.1: Floor panel single step forming simulation

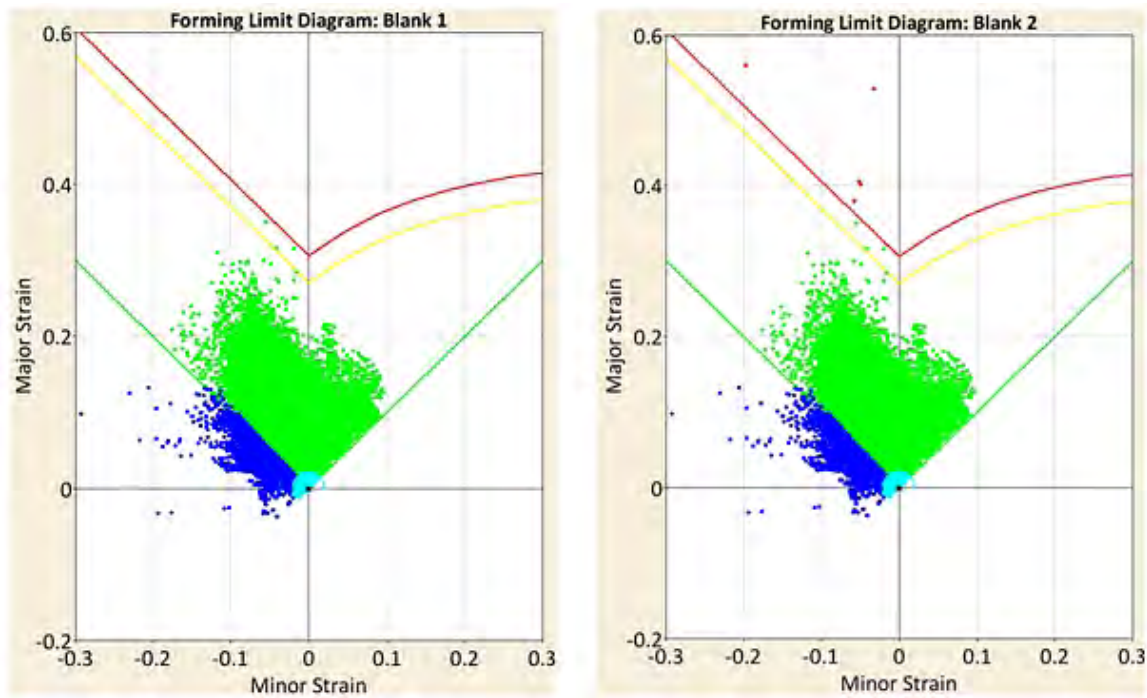


Figure 15.2: Floor panel single step forming simulation

15.2 Single Step Hot Stamping Simulation

The FLD diagrams shown on the right side predicts no failure for the floor panel. There are very minor areas where wrinkling can occur and these can be easily improved by implementing additional design changes to the CAD data.

The benefit of this single step simulation is that we don't have to go through the time-consuming process of Incremental Analysis which includes preparation of blank holders, addendum surfaces and draw beads. Single step stamping simulations gives the approximate results very quickly whenever there is any change in the CAD data.

15.2 Single Step Hot Stamping Simulation

The front shot-gun members, as shown in Figure 15.3, form a very important part of the front end structure absorbing significant amount of energy during frontal crash tests. The shot-gun inner and outer panels are hot-stamped from HF 1050/1500 steel. The formability of these parts was assessed using single step formability simulation. For the simulation IF steel grade properties (IF 260/410) were used in the analysis. As these parts are required to absorb energy without premature failure, during the hot stamping process the parts are 'tailor quenched' to achieve the required amount of material elongation for this function. The predicted elongations for front crash test case are shown in Figure 15.4.

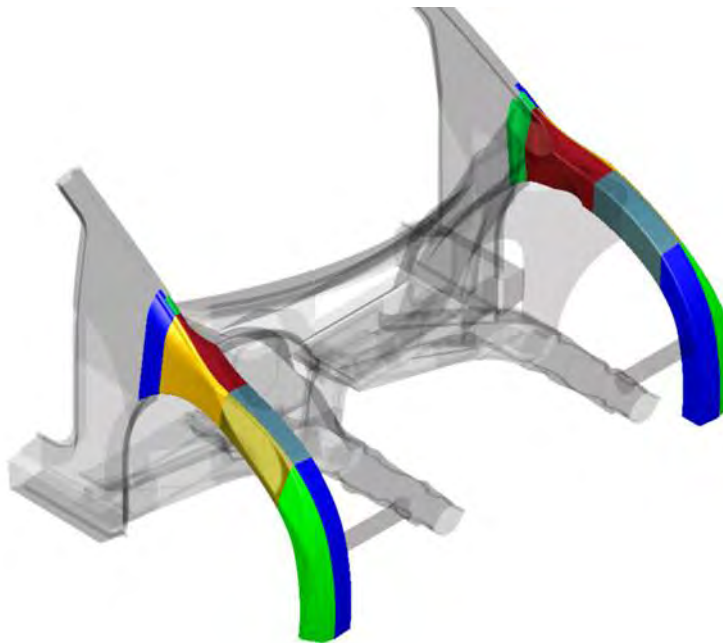


Figure 15.3: *Front shotgun members*

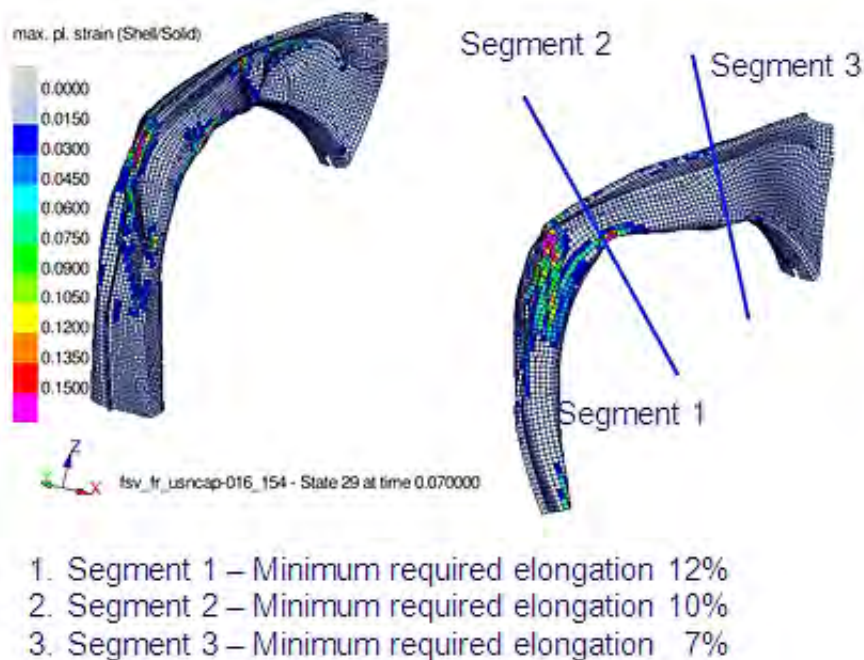


Figure 15.4: Front shotgun members - Minimum required elongation

The results for the single step forming analysis for all other components are shown in the Bill of Materials (BOM) file.

15.3 Incremental Metal Stamping Simulation

The more complex stamping parts were analyzed using 'incremental' forming simulations. The following parts were considered:

1. Front Shock Tower Panel (TWIP)
2. Rear Header Reinforcement Panel
3. Rear Floor
4. Rear Rail Reinforcement (LWB, Stamping & Indirect Hot Stamping)
5. Rear Rail Outer (LWB)
6. Rear Rail Inner (LWB)
7. Front Rail Lower (LWB)
8. Front Rail Upper (LWB)
9. Body Side (LWB)

15.3.1 Front Shock Tower (Material TWIP 980 - 1.0mm)

The front shock tower on the vehicle is exposed to very high shock loads from the front suspension. This component is generally constructed/assembled from several high strength steel parts. On some cars this assembly is also constructed from Magnesium and Aluminum castings. To give steel an advantage, this part is being produced from TWIP steel which offers very high strength (980 MPa) and increased formability (50-60% plastic elongation and 0.4 'n' value).

This part could also be produced by hot stamping with tailor quenching to achieve the desired elongation properties. The cost comparison of this part in TWIP and hot stamping (HF1050 material grade) is shown in Table 15.1.

	Shock Tower LH & RH	
	Material - TWIP 980	Material - HF 1500
Total Body Structure Manufacturing Costs	\$13.8	\$19.4
Building	\$0.0	\$0.1
Maintenance	\$0.5	\$0.8
Energy Cost	\$0.1	\$0.4
Overhead	\$0.3	\$2.3
Labor cost	\$0.3	\$2.4
Equipment Cost	\$1.1	\$2.6
Tooling	\$4.0	\$4.9
Material Price	\$7.5	\$6.1

Table 15.1: FSV shock tower cost comparison, TWIP 980 v/s HF 1500

The forming simulation results for this part are shown in Figure 15.5. It can be seen that the part can be successfully made using the specified gauge and grade of material.

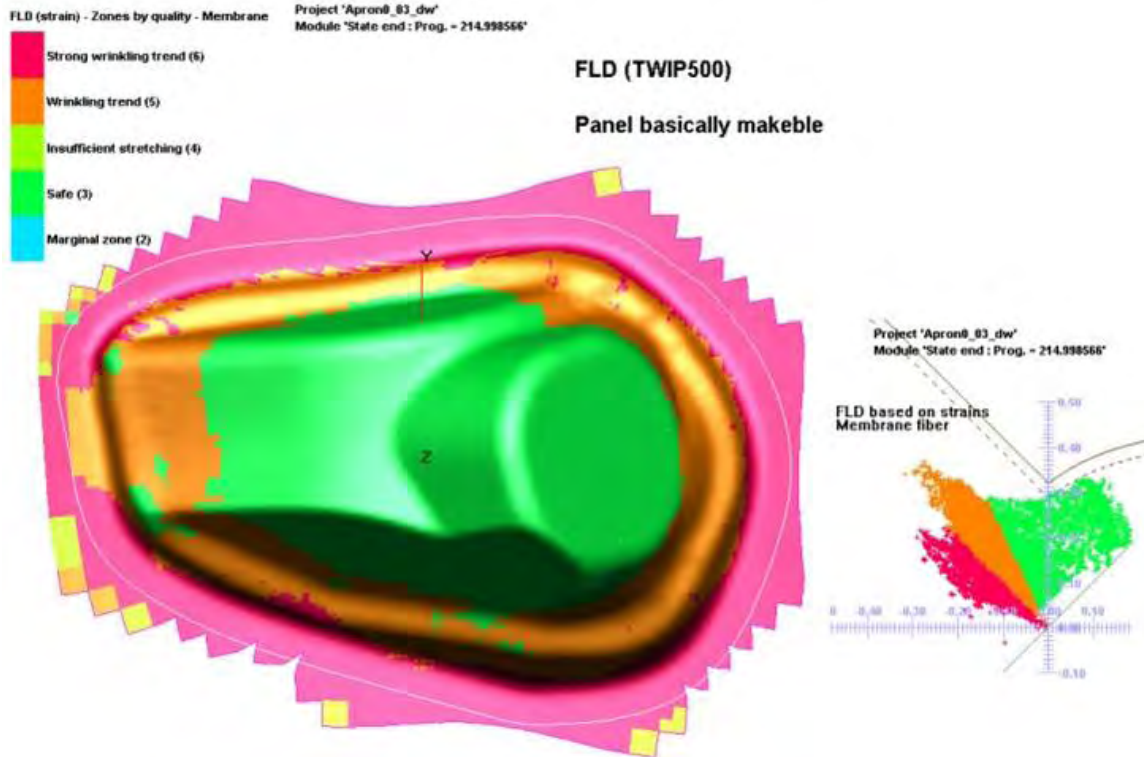


Figure 15.5: Front Shock Tower Forming Results

15.3.2 Rear Header Reinforcement Panel (Material BH 340 - 1.0mm)

The forming simulation results for Rear Header reinforcement Panel are shown in Figure 15.6 and Figure 15.7. Figure 15.6 show tool position 3mm from bottom position, demonstrating no wrinkles. Figure 15.7 shows the FLD results, which indicate the deep hinge pocket can be successfully formed using the specified gauge and grade of material for this part. There are some minor issues, but we expect these can be solved with additional design modifications to the part and/or tool geometry.

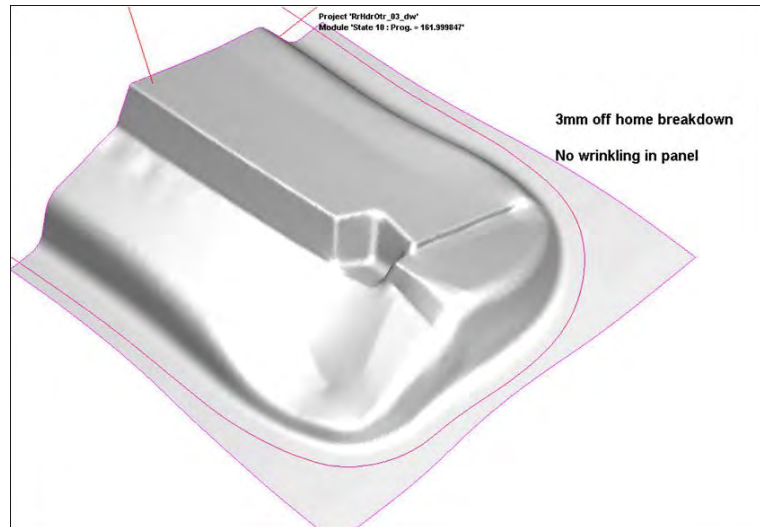


Figure 15.6: Rear Header Reinf - Tool 3mm from bottom

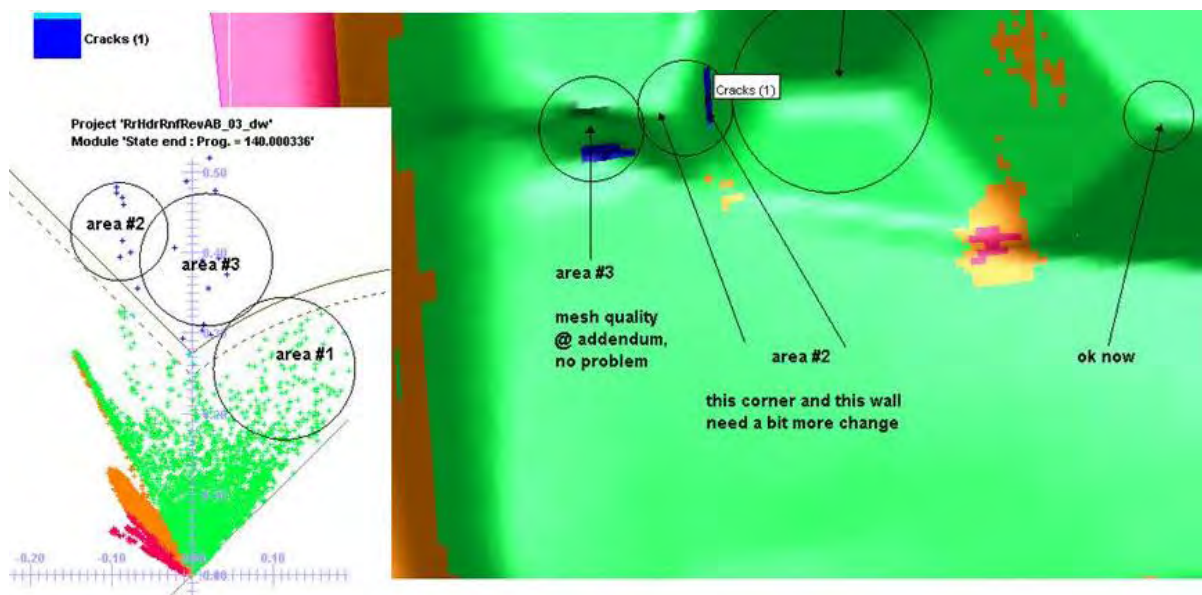


Figure 15.7: Rear Header Reinf - FLD Results

15.3.3 Rear Floor Panel (Material BH 340 - 0.5mm)

The forming simulation results for the Rear Floor Panel shown in Figure 15.8 indicate that this part can be successfully formed using the specified gauge and grade of material for this part. The area showing tendency for wrinkling can be easily remedied by introduction of metal take-up beads.

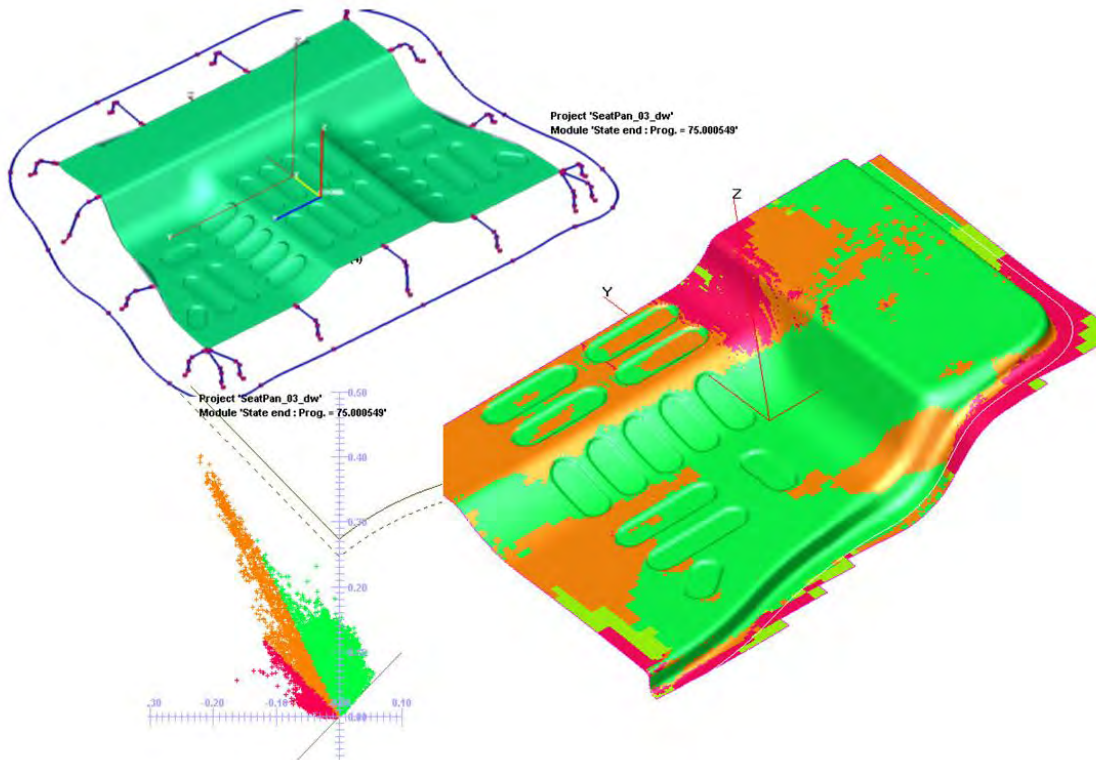


Figure 15.8: Rear Floor Panel - FLD Results

15.3.4 Rear Rail Reinforcement (LWB, Stamping and Indirect Hot Stamping)

The rear rail structure as shown in Figure 15.9 plays an important role in reacting high loads from the rear suspension and absorbing crash energy in rear impacts. The rail is constructed from three LWB stampings. The rear rail reinforcement is the upper part of the rear rail. The production of this part was considered using AHSS laser welded blank and tailor rolled blank for indirect hot stamping using HF1050 material grade. Using the indirect hot stamping method this part can be tailor quenched to fine tune the properties of the formed part that will be suitable for rear crash requirements. For indirect hot stamping, the preformed part is heated and press hardened. Tailor quenching is achieved during the press hardening stage. The component temperature and cooling rate is controlled along the part length to achieve the required properties.



Figure 15.9: *Rear Rail Assembly*

The tooling arrangement and forming simulation results for the rear rail reinforcement are shown in Figure 15.10 and Figure 15.11. Figure 15.11 shows a small wrinkle prone area which can be easily remedied by additional design changes in the area. Figure 15.11 also shows the FLD results using HF1050 grade steel cold properties.

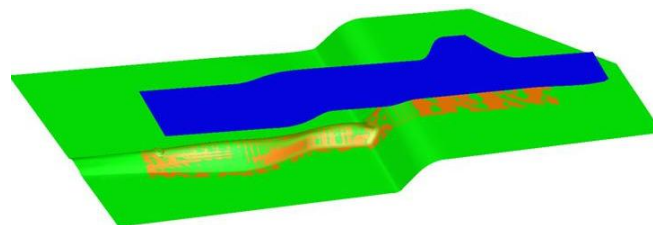


Figure 15.10: *Rear Rail Reinforcement Tool Layout*

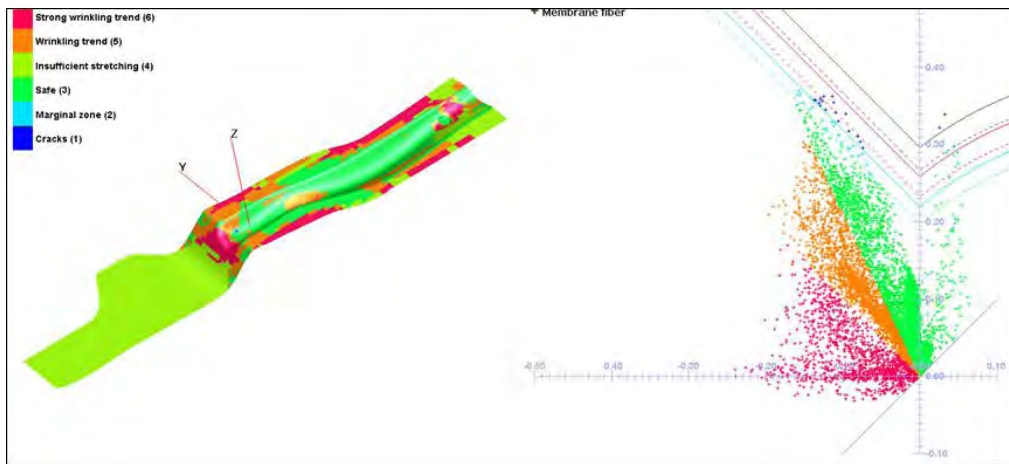


Figure 15.11: Rear Rail Reinforcement - FLD Results

15.3.5 Rear Rail Outer

The tooling arrangements for this panel are shown in Figure 15.12 and Figure 15.13. Figure 15.12 shows the use of an additional pad, which first comes down to hold the sheet against the post, before the upper tool moves down to form the side wall of the part. This arrangement reduces the formation of wrinkles which otherwise were found to be excessive. Figure 15.13 shows the tooling arrangement to form the end by flanging operation.

Figure 15.14 shows the FLD results. This part is also suitable for the indirect hot stamping method as discussed in Section 15.3.4.

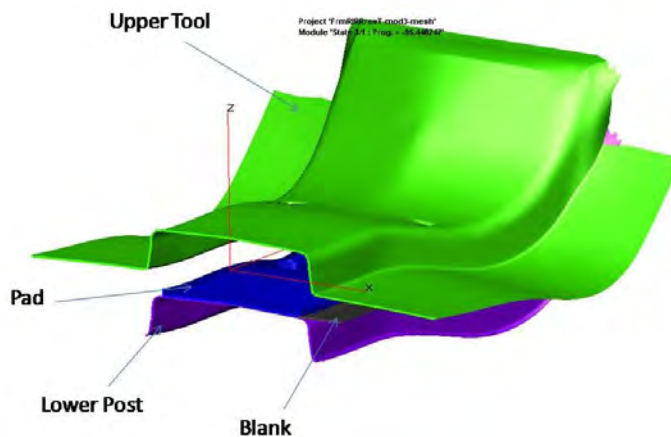


Figure 15.12: Rear Rail Outer Tool Layout

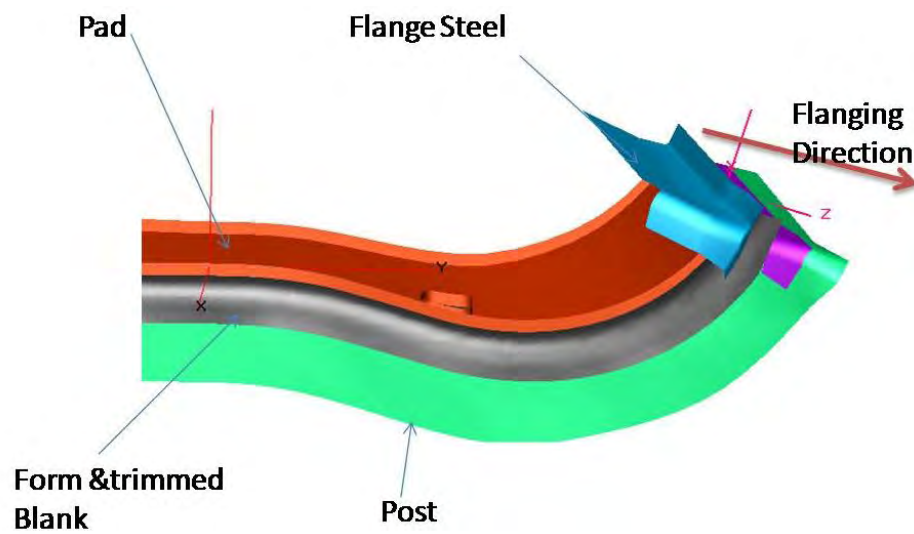


Figure 15.13: Rear Rail Outer Tool Layout for End Flanging

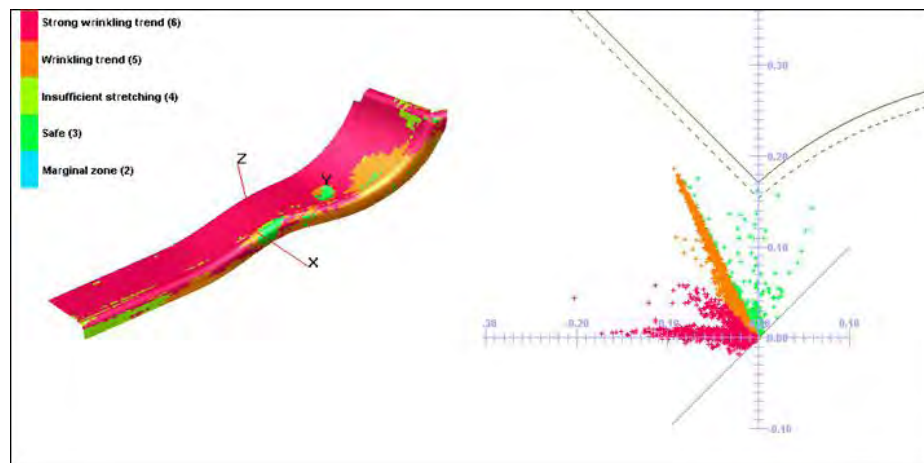


Figure 15.14: Rear Rail Outer FLD and Forming Results

15.3.6 Rear Rail Inner

The tooling arrangements for this panel are shown in Figure 15.15. Figure 15.16 shows the FLD results for the latest forming simulation. This part required significant changes to the first iteration of the designed geometry in order to be suitable for the stamping operation. The FLD results indicate the geometry still requires some additional minor changes in the wrinkles prone areas, to completely eliminate the wrinkles. The modified geometry of this part was included in the rear impact crash model to make sure the rear impact performance was not affected.

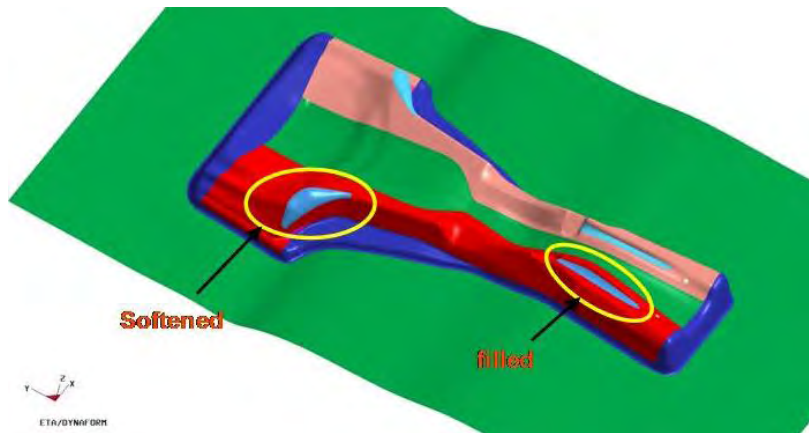


Figure 15.15: Rear Rail Inner Tool Layout

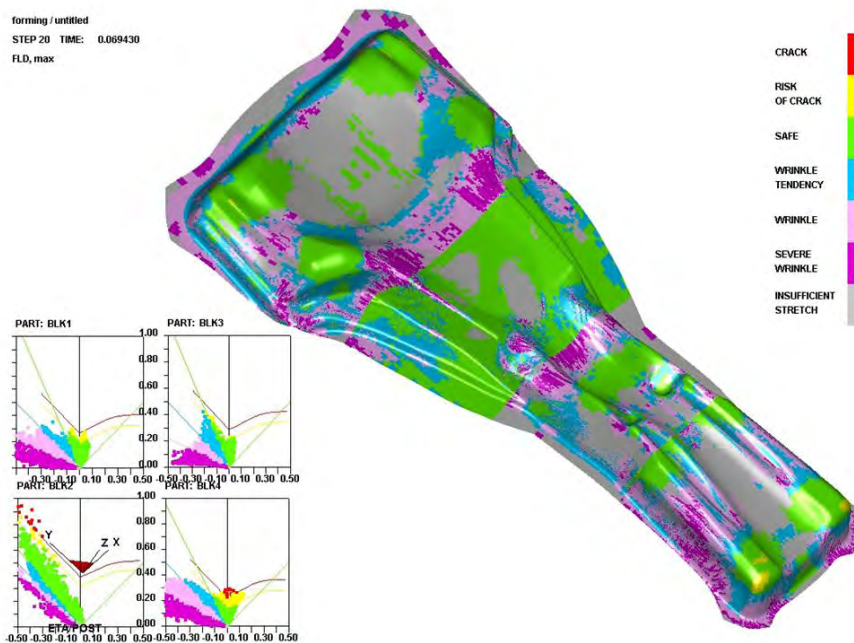


Figure 15.16: Rear Rail Inner FLD and Forming Results

15.3.7 Front Rail Upper & Lower

The front rail structure as shown in Figure 15.17 plays a very important role in absorbing crash energy during the front impacts. The front rail upper and lower has a very unique front profile as can be seen in Figure 15.17. This profile design was determined through the optimization methodology that was implemented on this program. The front rail lower and upper panels are made from laser welded blanks of various AHSS - TRIP grade steels. These parts are also suitable for production using the very formable high strength steel grade TWIP 500/980 and hot stamping with HF 1050/1500 grade (with the tailor quenching option). The cost comparison for the three different material grade options is shown in Table 15.2. The same gauges have been used for the cost comparison for all the three design options, however the gauge for the TWIP 500/980 option may have to increase to reduce the crash pulse.

	Front Rail Upper + Front Rail Lower Parts Costs		
	Material - TRIP 980	Material - TWIP 980	Material - HF 1500
Total Body Structure Manufacturing Costs	\$67.4	\$83.5	\$86.2
Building	\$0.6	\$0.6	\$0.7
Maintenance	\$1.3	\$1.3	\$1.8
Energy Cost	\$1.7	\$1.7	\$3.7
Overhead	\$1.6	\$1.6	\$5.6
Labor cost	\$2.5	\$2.5	\$6.4
Equipment Cost	\$7.0	\$7.1	\$11.1
Tooling	\$4.9	\$4.9	\$5.6
Material Price	\$47.8	\$63.7	\$51.2

Table 15.2: Parts Cost comparison - Front rail upper and lower



Figure 15.17: Front Rail Assembly

15.3.7.1 Front Rail Lower

The results of the first iteration of the forming simulation for the Front rail lower shown in Figure 15.18, highlighted a number of problem areas of wrinkling and material failures. Based on these results the component was modified as shown in Figure 15.19.

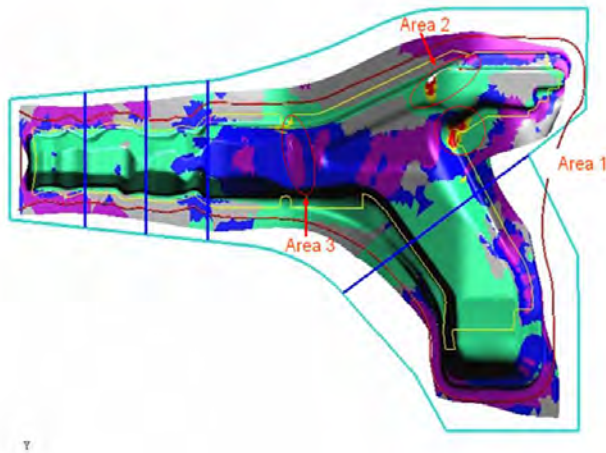


Figure 15.18: Front Rail Lower First Iteration Forming Results

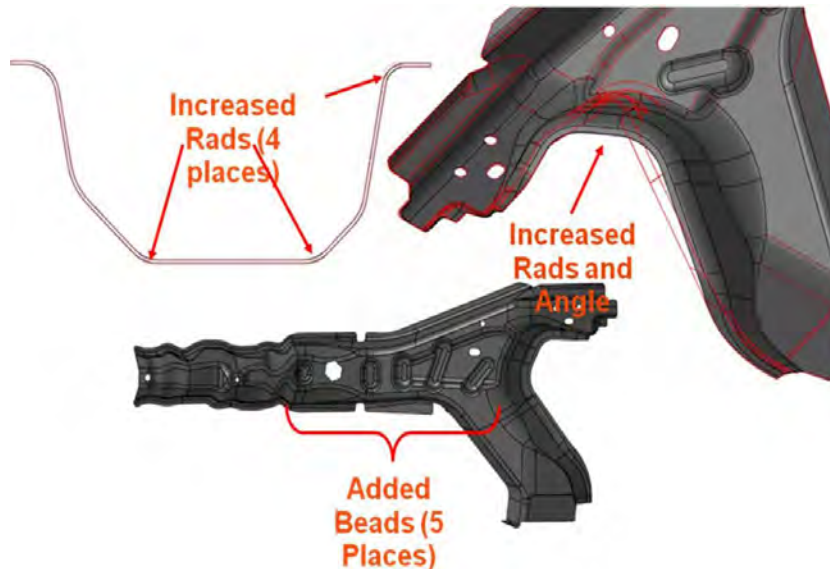


Figure 15.19: Front Rail Lower Design Changes

After several design and analysis iterations, the geometry with forming simulation results shown in Figure 15.20 indicate this part can be made using the specified TRIP 600/980 grade of steel. It can be seen that very small areas on the part show some points in the failure area. These

areas can be modified with further design and analysis iterations. This type of optimization driven shapes can also be produced using hot stamping and the TWIP grade of steels.

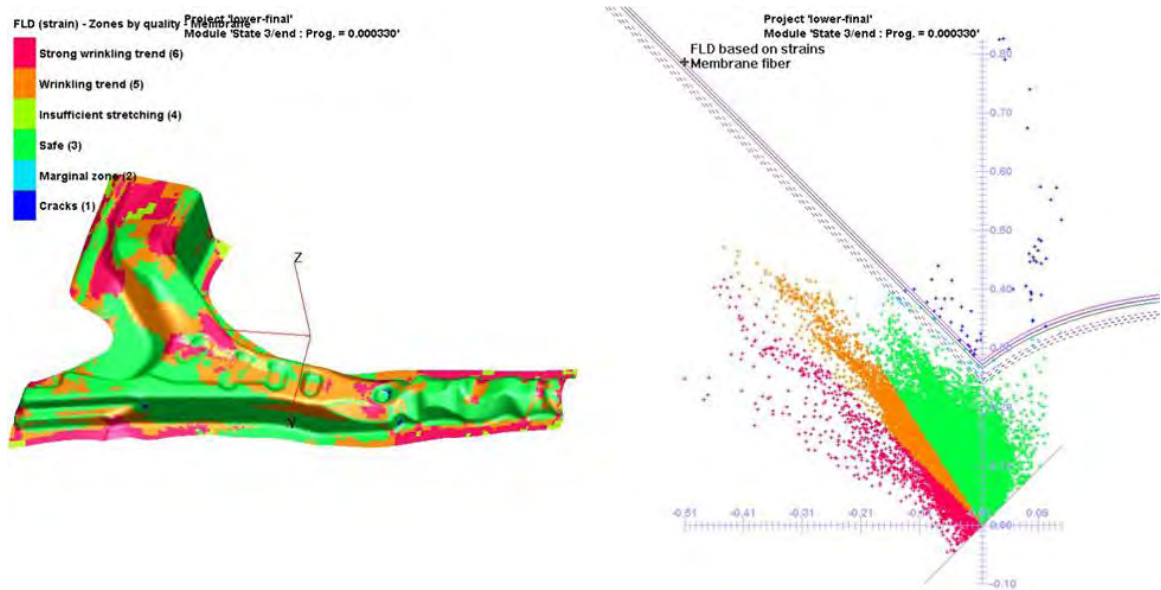


Figure 15.20: Front rail lower forming results

15.3.7.2 Front Rail Upper

Front rail upper has a very unique front profile as can be seen in Figure 15.21. This profile design was determined through the optimization methodology that was implemented on this program. The forming results shown in Figure 15.22 for the first design iteration indicated several changes that have to be made to this design for manufacturability. The forming results are shown in Figure 15.22.

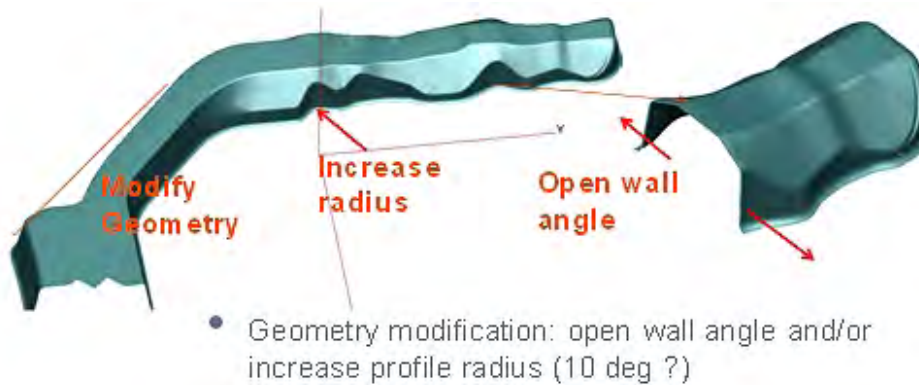


Figure 15.21: Front Rail Upper First iteration recommendations

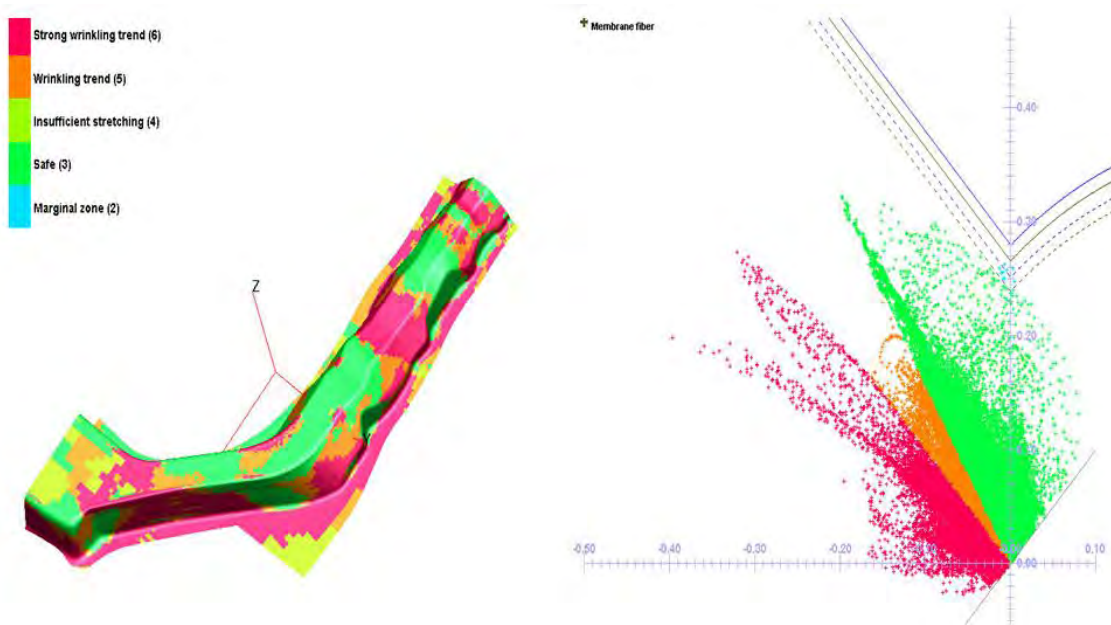


Figure 15.22: Front Rail Upper Forming Results

15.3.8 Body Side

The body side panel is a large challenging part with multiple conflicting requirements. Large depths of draw, complex geometry around door openings, large class a styling surface and its contribution to strength for B-Pillar, Upper Rail & Front Body Hinge Pillar (FBHP). This part was investigated with two segments Laser Welded Blank (LWB) as shown in Figure 15.23 and with four segments LWB as shown in Figure 15.25. The results for two segment LWB option shown in Figure 15.24 indicate that this part with additional design changes is suitable for manufacturing. The results for four segment LWB option shown in Figure 15.26 also indicate that this part with additional design changes is suitable for manufacturing.



Figure 15.23: Body Side Two Segment LWB

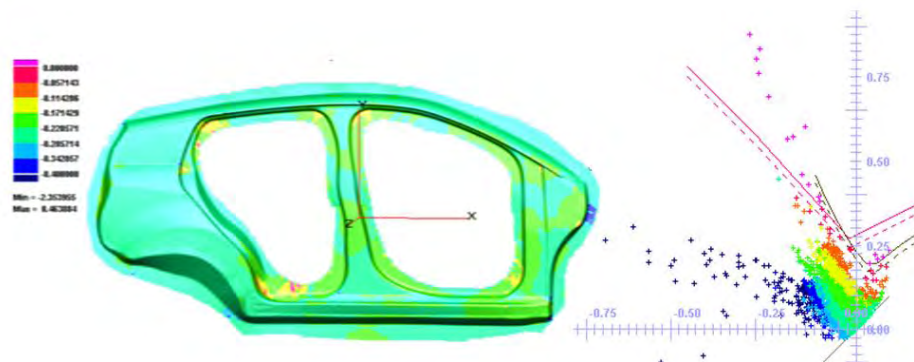


Figure 15.24: Body Side Two Segment LWB - Results

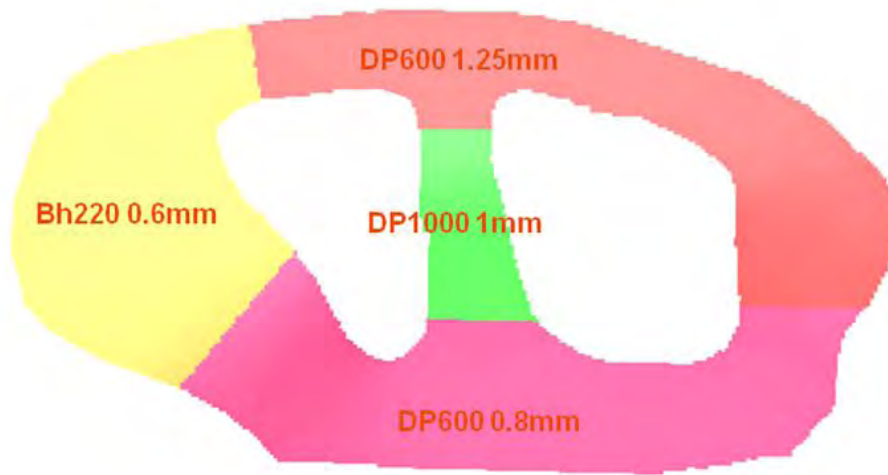


Figure 15.25: *Body Side Four Segment LWB*

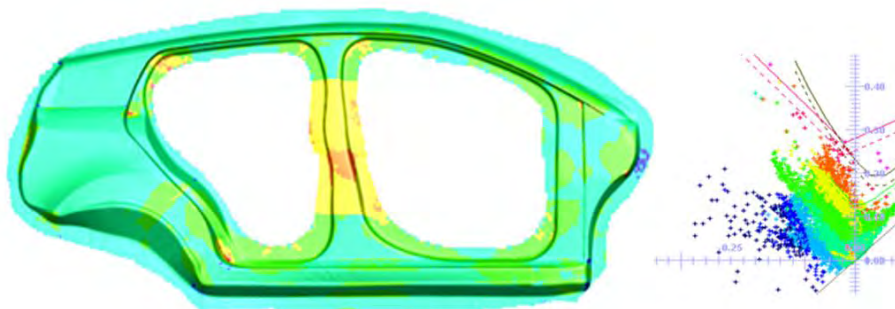


Figure 15.26: *Body Side Four Segment LWB - Results*

As it has been demonstrated, both options are suitable for manufacturing. Each of these options was further evaluated for static stiffness and crashworthiness performance. The structural performance was found to be acceptable for both options but with the addition of Front Body Hinge Pillar (FBHP) reinforcements (LH & RH) needed for the two segment LWB option. The cost and the mass for each option were also calculated. The two segment option (11.55 kg, \$38.60 per side) has a significant advantage over the four segment (13.99 kg, \$60.90 per side) option. The cost break-down for the two options is shown in Figure 15.27 and Figure 15.28. As result of this exercise the two segment LWB option in implemented in the final BEV body structure design.

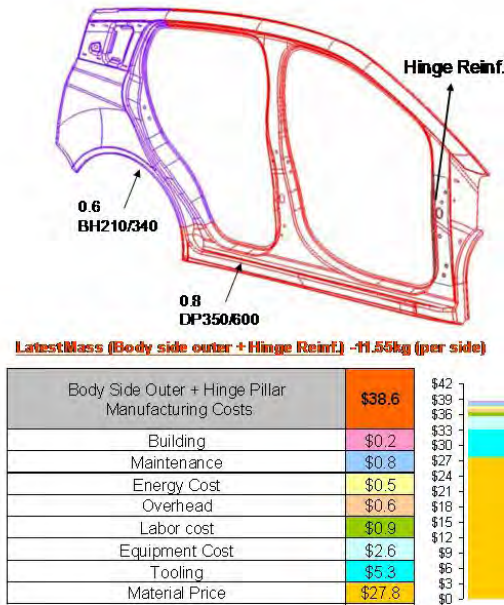


Figure 15.27: Body Side Two Segment LWB - Cost and Mass

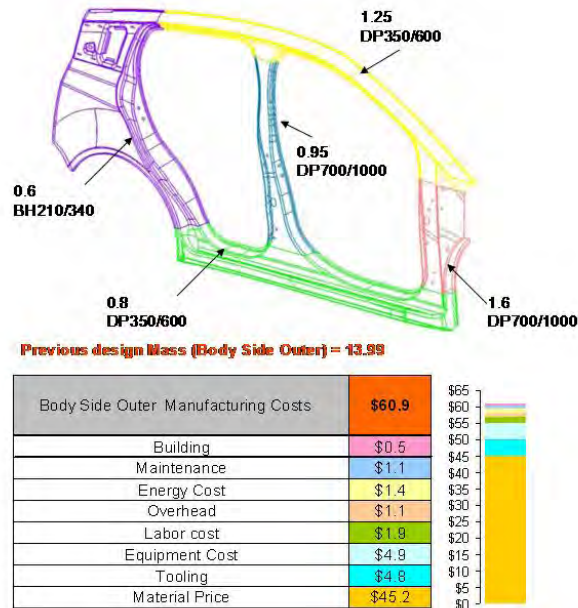


Figure 15.28: Body Side Four Segment LWB - Cost and Mass

16.0 Other FSV Body Structure and Powertrain Variants

16.1 FSV-1 PHEV₂₀

The PHEV₂₀ variant of the FSV-1 is a series hybrid vehicle with an all electric range of 32 km (20 miles). The battery pack is a lithium-ion manganese based cell with a 5 kWh end of life capacity (45 kg mass, 36 liter volume). The extended range of 500 km is provided by a 1.0 L- 3 cylinder gasoline engine/generator set. The layout for the FSV-1 PHEV₂₀ is illustrated in Figure 16.1.

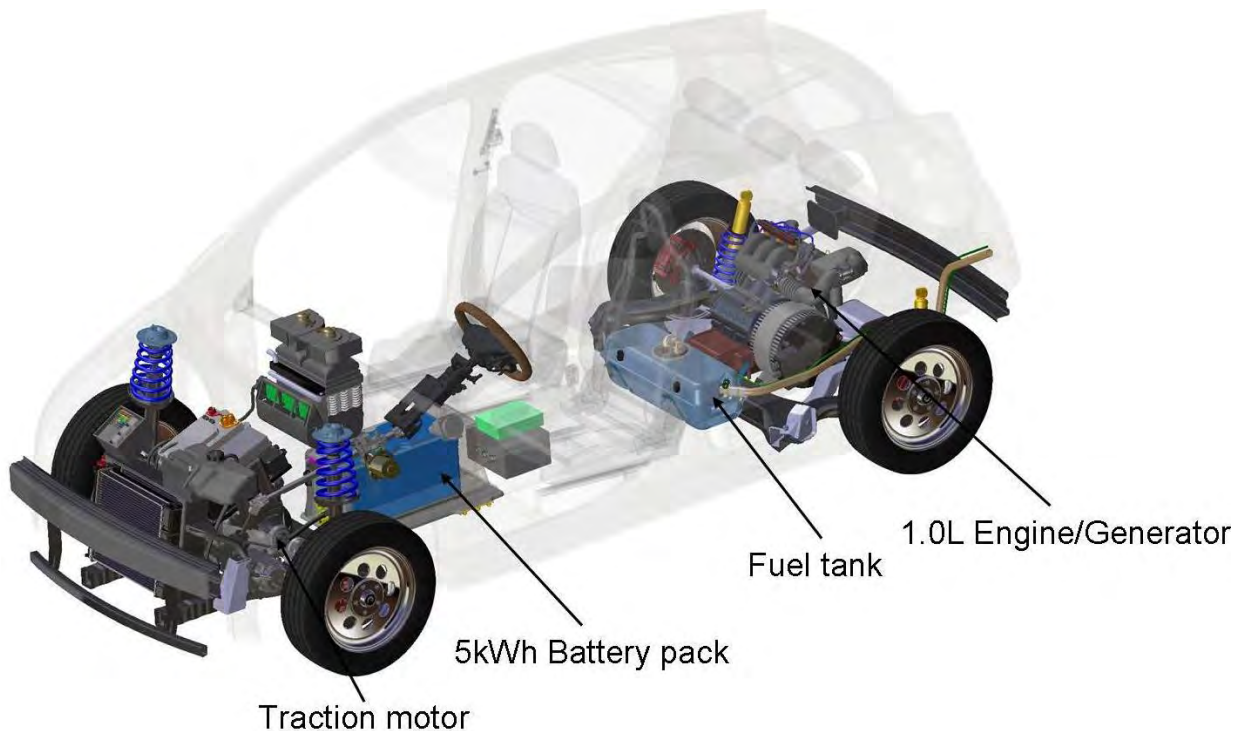


Figure 16.1: PHEV₂₀ layout

16.1.1 PHEV₂₀ Body Structure

The BEV body structure design was adapted to integrate the PHEV₂₀ powertrain. The 1.0 L - 3 cylinder gasoline engine/generator set is mounted in front of the rear axle, leading to a 50/50 vehicle mass split between front and rear wheels. The PHEV₂₀ under floor structure was adapted to accommodate the battery pack. The rear floor was adapted to accept the modular sub-assembly that includes the engine/generator and the rear suspension. The PHEV₂₀ body structure is shown in Figure 16.2 (the colour scheme of the parts shown make use of the color code for the material classification as shown in Table 16.1).

The weight of the PHEV₂₀ body structure is 174.6 kg. The material mix of the steels used in the PHEV₂₀ body structure are shown in Table 16.1 and Figure 16.3.

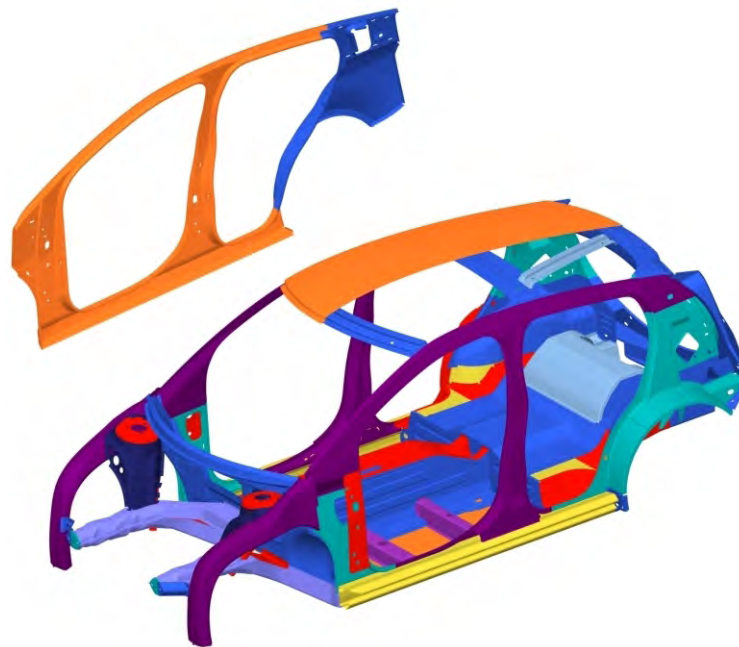


Figure 16.2: FSV-1 PHEV₂₀ body structure

Steels: corresponding metallurgical classes	Color Code	PHEV ₂₀ Mix (%)
Low Strength Steels: Mild Steels		3.2
High Strength Steels (HSS): HSLA, BH		32.1
DP 500, 600		12.7
DP 800		10.2
DP 1000		8.2
TRIP		10.1
TWIP		2.4
Complex Phase (CP)		7.9
Martensitic (MS)		1.4
Hot forming (HF)		11.8

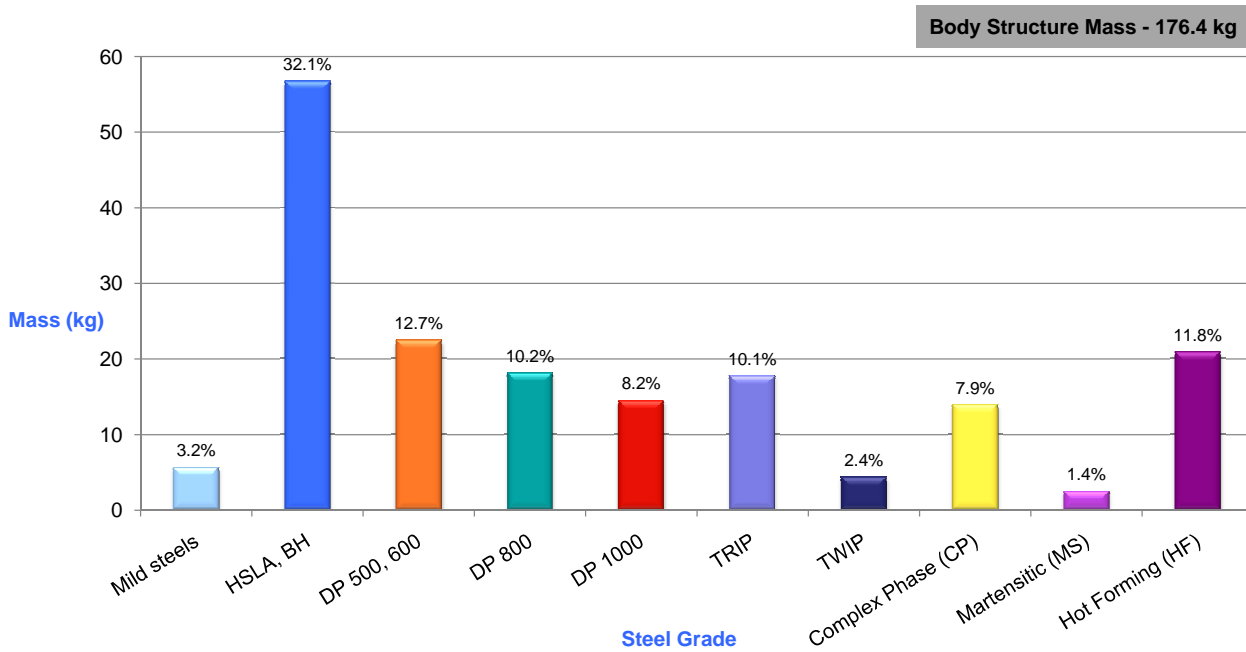
Table 16.1: PHEV₂₀ body structure material mix

Figure 16.3: PHEV₂₀ material mix



Figure 16.4: PHEV₂₀ exploded view

The FSV PHEV₂₀ parts lists showing material grades, thickness and mass are shown in Table 16.2 and Table 16.3.

Part No	Part Description	Forming	Grade	Yeild (MPa)	Tensile (MPa)	Thickness (mm)	Mass (kg)
1	50.1 0401 Bulkhead Lower - Tunnel	S	DP	700	1000	0.80	0.679
2	50.1 0400 Bulkhead Upper - Tunnel	S	DP	700	1000	0.80	0.543
3	50.1 0402 Panel - Tunnel Side RH	S	BH	280	400	0.50	2.342
4	50.1 0404 Reinf - Tunnel Top	S	BH	280	400	0.50	1.713
5	50.1 0403 Panel - Tunnel Side LH	S	BH	280	400	0.50	2.342
7	50.1 0011 Floor - Front RH	S	DP	300	500	0.50	2.84
			DP	500	800	1.50	1.77
9	50.1 0025 Floor - Front LH	S	DP	300	500	0.50	2.84
			DP	500	800	1.50	1.77
10	50.1 0093 Crossmember - Front Seat RH Front	RF	MS	950	1200	0.50	0.542
11	50.1 0094 Crossmember - Front Seat LH Front	RF	MS	950	1200	0.50	0.542
12	50.1 0095 Crossmember - Front Seat RH Rear	RF	MS	950	1200	0.60	0.688
13	50.1 0096 Crossmember - Front Seat LH Rear	RF	MS	950	1200	0.60	0.688
14	50.1 0100 Heel Board	S	BH	210	340	0.60	1.603
15	50.1 0391 Seat Pan - Rear	S	BH	210	340	0.50	2.854
16	50.1 0099 Panel - Seat Side RH	S	DP	700	1000	0.70	0.359
17	50.1 0101 Panel - Seat Side LH	S	DP	700	1000	0.70	0.359
18	50.1 0109 Reinf - Frame Rail Rear RH	S	CP	1000	1200	1.10	0.361
			DP	700	1000	0.65	0.528
			Mild	140	270	1.55	0.666
19	50.1 0110 Reinf - Frame Rail Rear LH	S	CP	1000	1200	1.10	0.361
			DP	700	1000	0.65	0.528
			Mild	140	270	1.55	0.666
20	50.1 0015 Frame Rail - Outer Rear LH	S	CP	1000	1200	0.60	0.304
			DP	700	1000	1.40	0.469
			HSLA	350	450	0.80	0.264
21	50.1 0334 Mounting Plate - Crush Can Rear LH	S	DP	500	1200	1.20	0.132
23	50.1 0014 Frame Rail - Outer Rear RH	S	CP	1000	1200	0.60	0.247
			DP	700	1000	1.40	1.963
			HSLA	350	450	0.80	0.425
22	50.1 0336 Frame Rail - Inr Rear LH	S	CP	1000	1200	0.60	0.304
			DP	700	1000	1.40	0.469
			HSLA	350	450	0.80	0.264
24	50.1 0333 Mounting Plate - Crush Can Rear RH	S	DP	500	800	1.20	0.132
25	50.1 0335 Frame Rail - Inr Rear RH	S	CP	1000	1200	0.60	0.247
			DP	700	1000	1.40	1.963
			HSLA	350	450	0.80	0.425
35	50.1 0001 Seat Pan-Engine Cover	S	Mild	140	270	0.60	2.38
27	50.1 0390 Cargo Box	S	Mild	140	270	0.50	0.984
28	50.1 0017 Wheelhouse Inner - Rear RH	S	BH	210	340	0.70	0.835
			BH	210	340	1.20	1.745
29	50.1 0018 Wheelhouse Inner - Rear LH	S	BH	210	340	0.70	0.835
			BH	210	340	1.20	1.745
34	50.1 0320 Rail - Side to Side	S	DP	500	800	0.80	1.074
32	50.1 0004 Brkt-Fuel Tank Strap	S	BH	210	340	1.20	0.061
32	50.1 0004 Brkt-Fuel Tank Strap	S	BH	210	340	1.20	0.061
36	50.1 0003 Rail - Side to Side	S	DP	500	800	0.80	1.061
33	50.1 0005 Brkt-Fuel Tank Strap	S	BH	210	340	1.20	0.098
33	50.1 0005 Brkt-Fuel Tank Strap	S	BH	210	340	1.20	0.098
41	50.1 0329 Pnl - Rear Liftgate Lower Inr LH	S	BH	210	340	1.00	0.585
42	50.1 0013 Pnl - Rear Liftgate Lower Inr	S	BH	210	340	0.70	1.866
43	50.1 0328 Pnl - Rear Liftgate Lower Inr RH	S	BH	210	340	1.00	0.585
44	50.1 0019 Panel - Back Outboard RH	S	BH	210	340	1.00	0.577
45	50.1 0025 Panel - Back Outboard LH	S	BH	210	340	1.00	0.577
46	50.1 0020 Panel - Back Lower	S	BH	210	340	1.00	1.405
47	50.1 2601 Mount - Rear Shock RH	S	DP	500	800	2.50	0.566
48	50.1 2602 Reinf - Rear Shock RH	S	DP	500	800	2.00	0.176
49	50.1 2701 Reinf - Rear Shock LH	S	DP	500	800	2.00	0.176
50	50.1 2702 Mount - Rear Shock LH	S	DP	500	800	2.50	0.566
51	50.1 2001 Mount - Trailing Arm LH	S	DP	500	800	2.00	0.37
52	50.1 2002 Mount - Trailing Arm RH	S	DP	500	800	2.00	0.37
53	50.1 0001 Dash - Toe Pan	S	BH	280	400	0.50	2.839
54	50.1 0002 Cowl Upper	S	BH	210	340	1.00	0.866
			BH	210	340	0.60	1.402
55	50.1 0070 Cowl Lower	S	BH	210	340	1.20	0.709
			BH	210	340	0.60	0.785
58	50.1 0306 Closeout - Lower Rail LH	S	DP	700	1000	0.80	0.309
59	50.1 0302 Front Rail - Lower LH	S	TRIP	600	980	1.90	0.359
			TRIP	600	980	2.00	0.419
			TRIP	600	980	1.90	0.535
			TRIP	600	980	1.80	4.685

Table 16.2: FSV PHEV₂₀ Bill of Materials (BOM)

Part No	Part Description	Forming	Grade	Yield (MPa)	Tensile (MPa)	Thickness (mm)	Mass (kg)	Total Mass (kg)
60	50.1 0305 Closeout - Lower Rail RH	S	DP	700	1000	0.80	0.309	0.309
61	50.1 0301 Front Rail - Lower RH	S	TRIP	600	980	1.90	0.359	5.998
			TRIP	600	980	2.00	0.419	
			TRIP	600	980	1.90	0.535	
			TRIP	600	980	1.80	4.685	
62	50.1 0303 Front Rail - Upper	S	TRIP	600	980	1.80	0.667	5.743
			TRIP	600	980	2.00	0.811	
			TRIP	600	980	1.80	4.265	
63	50.1 0304 Closeout - Upper Rail	S	DP	700	1000	1.00	0.616	0.616
56	60.2 0007 Mounting Plate - Crush Can Front RH	S	DP	500	800	1.75	0.121	0.121
57	60.2 0008 Mounting Plate - Crush Can Front LH	S	DP	500	800	1.75	0.121	0.121
64	50.1 0044 Shock Tower - Frt RH	S	TWIP	500	980	1.00	1.457	1.457
114	50.1 3002 Reinf - Shock Tower Frt	S	DP	500	980	2.00	0.69	0.69
65	50.1 0063 Shock Tower - Frt LH	S	TWIP	500	980	1.00	1.457	1.457
115	50.1 3003 Reinf - Shock Tower Frt	S	DP	500	980	2.00	0.69	0.69
66	50.1 0022 Shotgun Inner LH	S	HF	1050	1500	1.20	0.476	2.15
			HF	1050	1500	0.80	0.759	
			HF	1050	1500	1.50	0.915	
67	50.1 0021 Shotgun Inner RH	S	HF	1050	1500	1.20	0.476	2.15
			HF	1050	1500	0.80	0.759	
			HF	1050	1500	1.50	0.915	
68	50.1 0326 A-Pillar Brace	RF	DP	700	1000	1.20	0.695	0.695
69	50.1 0326 A-Pillar Brace LH	RF	DP	700	1000	1.20	0.695	0.695
70	50.1 0318 Shotgun Brace LH	S	BH	210	340	1.20	0.206	0.206
71	50.1 0308 Shotgun Brace RH	S	BH	210	340	1.20	0.206	0.206
72	50.6 0023 Roof Rail Inner Front LH	HS	HF	1050	1500	0.70	0.84	1.171
			HF	1050	1500	0.95	0.331	
73	50.6 0064 FBHP Inner LH	S	DP	500	800	1.20	1.667	1.667
74	50.6 0056 Rocker Filler Front LH	S	BH	210	340	0.60	0.199	0.199
75	50.6 0017 B-Pillar Inner LH	HS	HF	1050	1500	0.80	0.547	1.491
			HF	1050	1500	0.60	0.944	
76	50.6 0053 Roof Rail Inner Rear LH	S	BH	210	340	1.10	0.372	0.372
77	50.1 0067 Panel - Wheel House Outer LH	S	DP	500	800	0.65	1.732	1.732
78	50.6 0004 C-Pillar Inner LH	S	DP	500	800	0.70	1.428	1.428
79	50.2 0034 Bracket - Roof Rail to Header LH	S	BH	210	340	1.00	0.103	0.103
80	50.2 0035 Bracket - Roof Rail to Roof Bow LH	S	BH	210	340	1.00	0.254	0.254
81	50.6 0018 Reinf - Roof Rail LH	HS	HF	1050	1500	0.70	2.049	2.049
82	50.6 0066 Rocker LH	RF	CP	1050	1470	1.00	6.032	6.032
83	50.6 0072 Rocker Cap LH	S	BH	210	340	0.85	0.244	0.244
			HF	1050	1500	0.60	1.189	
84	50.6 0028 Reinf - B-Pillar LH	HS	HF	1050	1500	1.00	0.302	1.491
			DP	350	600	0.80	8.359	
85	50.6 0006 Body Side Outer LH	HS	BH	210	340	0.60	2.739	11.098
			DP	350	600	0.80	8.359	
86	50.6 0069 Panel Rear Quarter Lwr LH	S	BH	210	340	1.20	0.198	0.198
87	50.6 0051 Panel - Gutter Rear LH	S	BH	210	340	1.00	0.795	0.795
117	50.6 6354 Reinf - FBHP LH	S	DP	700	1000	0.80	0.453	0.453
88	50.6 0046 FBHP Inner RH	S	DP	500	800	1.20	1.667	1.667
89	50.6 0022 Roof Rail Inner Front RH	HS	HF	1050	1500	0.70	0.84	1.171
			HF	1050	1500	0.95	0.331	
99	50.6 0055 Rocker Filler Front RH	S	BH	210	340	0.60	0.199	0.199
			HF	1050	1500	0.80	0.547	
91	50.6 0009 B-Pillar Inner RH	HS	HF	1050	1500	0.60	0.944	1.491
			HF	1050	1500	0.60	0.944	
92	50.6 0052 Roof Rail Inner Rear RH	S	BH	210	340	1.10	0.372	0.372
93	50.1 0049 Panel - Wheel House Outer RH	S	DP	500	800	0.65	1.732	1.732
94	50.6 0005 C-Pillar Inner RH	S	DP	500	800	0.70	1.428	1.428
95	50.2 0033 Bracket - Roof Rail to Roof Bow RH	S	BH	210	340	1.00	0.254	0.254
96	50.2 0032 Bracket - Roof Rail to Header RH	S	BH	210	340	1.00	0.103	0.103
97	50.6 0012 Reinf - Roof Rail RH	HS	HF	1050	1500	0.70	2.049	2.049
98	50.6 0048 Rocker RH	RF	CP	1050	1470	1.00	6.032	6.032
99	50.6 0071 Rocker Cap RH	S	BH	210	340	0.85	0.244	0.244
100	50.6 0026 Reinf - B-Pillar RH	HS	HF	1050	1500	0.60	1.189	1.491
			HF	1050	1500	1.00	0.302	
101	50.6 0050 Panel - Gutter Rear RH	S	BH	210	340	1.00	0.795	0.795
102	50.6 0068 Panel Rear Quarter Lwr RH	S	BH	210	340	1.20	0.198	0.198
103	50.6 0002 Body Side Outer RH	S	DP	350	600	0.80	8.359	11.098
			BH	210	340	0.60	2.739	
118	50.6 1354 Reinf - FBHP RH	S	DP	700	1000	0.80	0.453	0.453
104	50.2 0007 Rear Header Reinf	S	BH	210	340	2.00	2.759	3.775
			BH	210	340	0.70	1.016	
105	50.2 0006 Rear Header	S	BH	210	340	0.70	1.662	1.662
106	50.2 0009 Support - Roof LH	S	Mild	140	270	0.50	0.463	0.463
107	50.2 0008 Support - Roof RH	S	Mild	140	270	0.50	0.463	0.463
108	50.2 0013 Roof Bow	RF	BH	210	340	0.50	0.941	0.941
109	50.2 0011 Header - Roof Front	RF	BH	210	340	0.80	1.131	1.131
110	50.1 0405 Top Panel - Tunnel	S	DP	1150	1270	1.00	3.067	3.067
111	50.2 0010 Pnl - Roof Outer	S	BH	210	340	0.50	9.011	9.011
112	50.1 0069 Shotgun Outer LH	HS	HF	1050	1500	1.00	0.431	2.088
			HF	1050	1500	0.80	0.689	
			HF	1050	1500	1.50	0.968	
113	50.1 0051 Shotgun Outer RH	HS	HF	1050	1500	1.00	0.431	2.088
			HF	1050	1500	0.80	0.689	
			HF	1050	1500	1.50	0.968	
Total							176.4	176.4

 Table 16.3: FSV PHEV₂₀ Bill of Materials (BOM) (contd.)

16.1.2 PHEV₂₀ Front End

The compact packaging of an advanced traction motor in the front allows the PHEV₂₀ to have a short front-end, which is the same as that of the BEV. The PHEV₂₀ has a radiator additional to the radiator in the BEV, for cooling the engine/generator set. The second radiator is packaged in the front as shown in Figure 16.5. Apart from the supplementary radiator, the front end of the PHEV₂₀ is identical to the BEV.



Figure 16.5: FSV-1 PHEV₂₀ radiator packaging

16.1.3 PHEV₂₀ Powertrain Package

The major components of the PHEV₂₀ powertrain are:

1. Battery pack
2. Electric drive motor
3. Converter (converts DC current to AC and control motor speed)
4. Generator Inverter Controller and Hybrid Controller
5. Internal combustion engine (1.0 L)
6. Fuel System
7. Exhaust System

16.1.3.1 PHEV₂₀ Battery

The PHEV₂₀ has a 'I' shaped battery pack similar to the BEV battery pack, but with a lower capacity of 5 kWh (BEV has a end of life capacity of 30 kWh). The battery pack is packed in the tunnel

16.1 FSV-1 PHEV₂₀

under the front floor. The smaller PHEV₂₀ battery pack makes room for packaging the generator inverter controller and the hybrid controller, as shown in Figure 16.6.

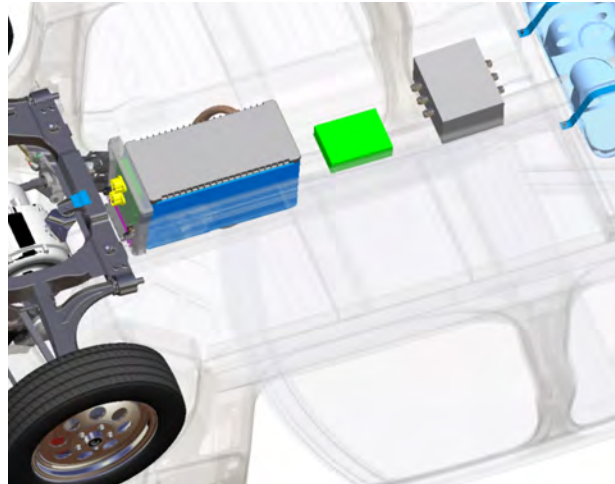


Figure 16.6: *FSV-1 PHEV₂₀ battery packaging*

16.1.3.2 PHEV₂₀ Electric Drive Motor

The PHEV₂₀ uses the same electric drive motor as the BEV with a 55 kW peak power. The front package is also similar to the BEV as shown in Figure 16.7.

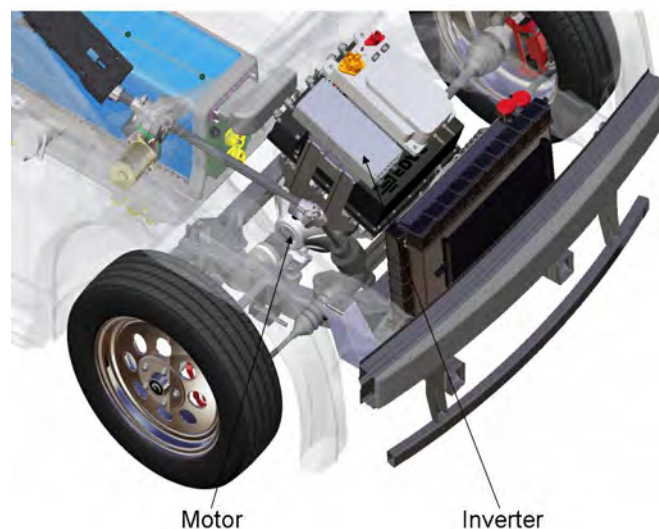


Figure 16.7: *FSV-1 PHEV₂₀ front wheel drive motor and inverter*

16.1.3.3 PHEV₂₀ Internal Combustion Engine

The PHEV₂₀ engine/generator set occupies the rear cargo box space of the BEV. The PHEV₂₀ rear cargo box was moved rearward and made smaller to accommodate the engine/generator set. Due to the smaller size of the PHEV₂₀ rear cargo, there is no need for any beads on the side panels, resulting in a single piece design. Additionally, the seat pan was modified on the rear floor area, as shown in Figure 16.8.

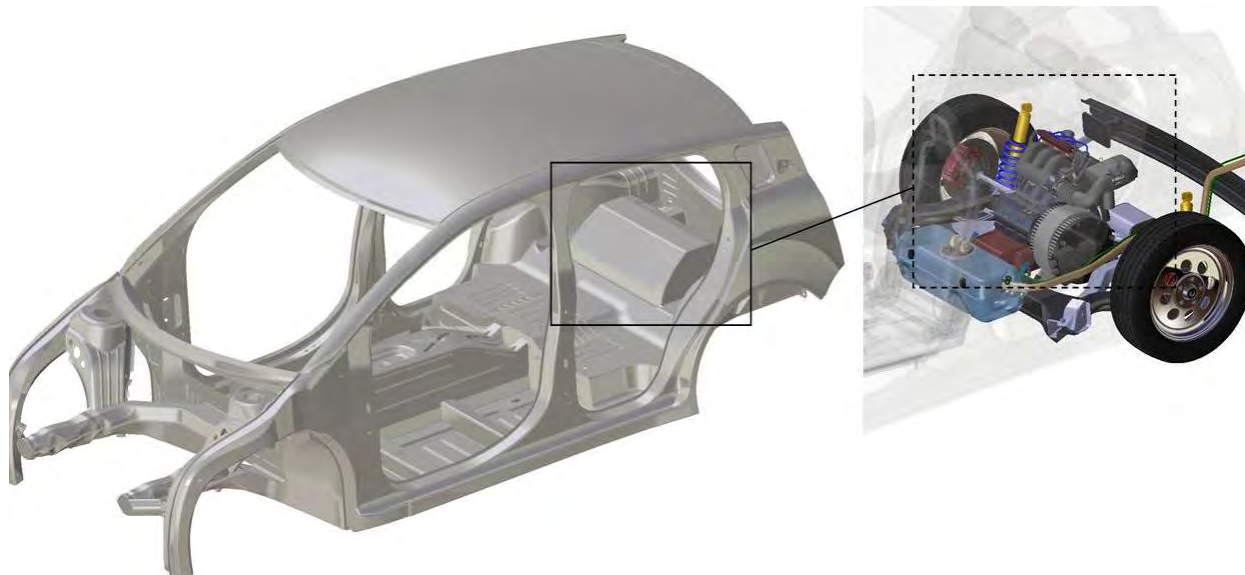


Figure 16.8: FSV-1 PHEV₂₀ engine/generator set packaging

16.1.3.4 PHEV₂₀ Fuel system

The battery close-off panel and the center longitudinal rails are removed from the BEV rear floor assembly to accommodate the PHEV₂₀ fuel tank. The 27 liter (7 gallon) fuel tank is packaged under the rear floor as shown in Figure 16.9. A side-to-side rail was added and the rear suspension cross member was modified to support the fuel tank. Additionally, the wheel house inner and the body side outer had to be modified to accept the fuel filler tube assembly. The PHEV₂₀ wheel house inner is shown in Figure 16.10.

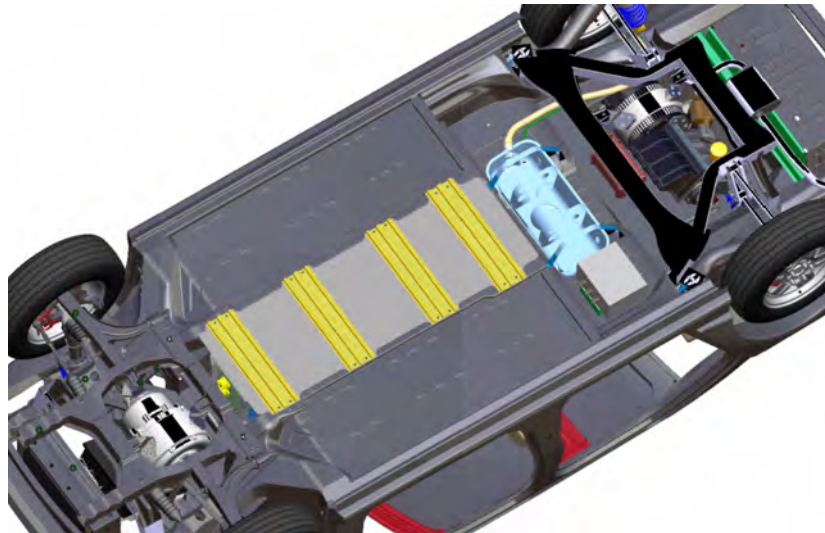


Figure 16.9: FSV-1 PHEV₂₀ fuel system packaging

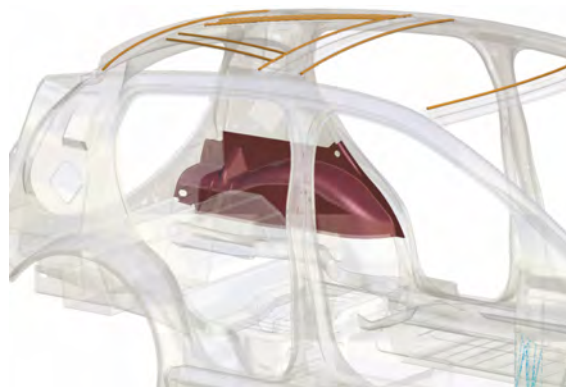


Figure 16.10: FSV-1 PHEV₂₀ wheel house inner

16.1.3.5 PHEV₂₀ Rear Suspension

The PHEV₂₀ rear suspension is a multi-link trailing arm suspension, similar to the BEV. The rear suspension is linked to the engine cradle to form a modular assembly with the engine/generator set as shown Figure 16.11.

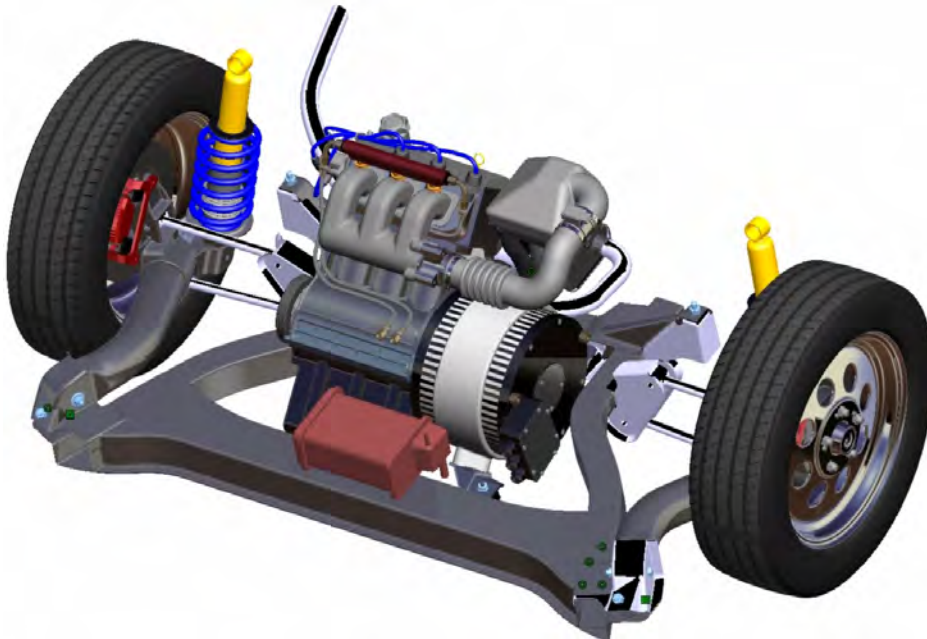


Figure 16.11: FSV-1 PHEV₂₀ rear suspension assembly

16.2 FSV-2

The FSV-2 is a four door sedan, 4,350 mm long designed for the mid-class car (C and D class) segment, and designed to accept two powertrain options: Plug-in Hybrid Electric Vehicle (PHEV₄₀) and Fuel Cell Electric Vehicle (FCEV). The FSV-2 body structure is shown in Figure 16.12 (the colour scheme of the parts shown make use of the color code for the material classification as shown in Table 16.1).

The weight of the FSV-2 body structure is 200.8 kg, for both the PHEV₄₀ and the FCEV. The material mix of the steels used in the FSV-2 body structure are shown in Table 16.4 and Figure 16.13.

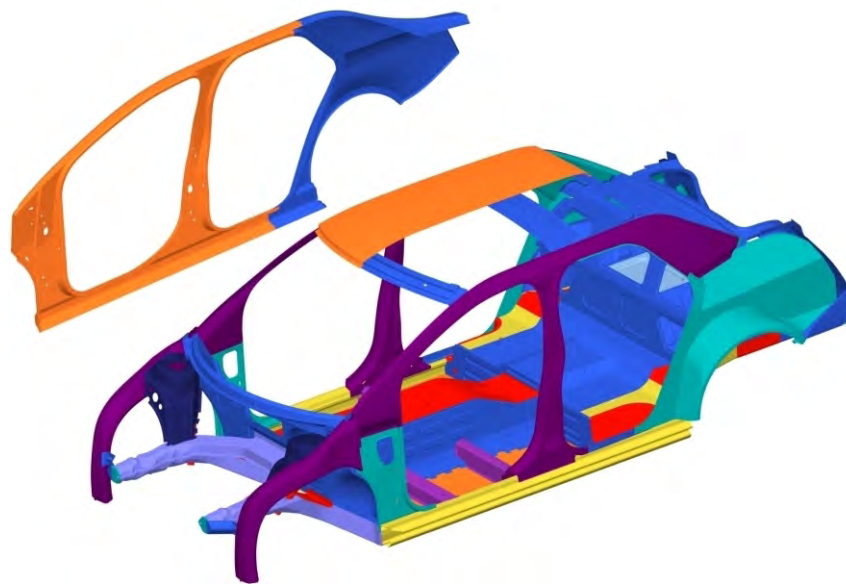
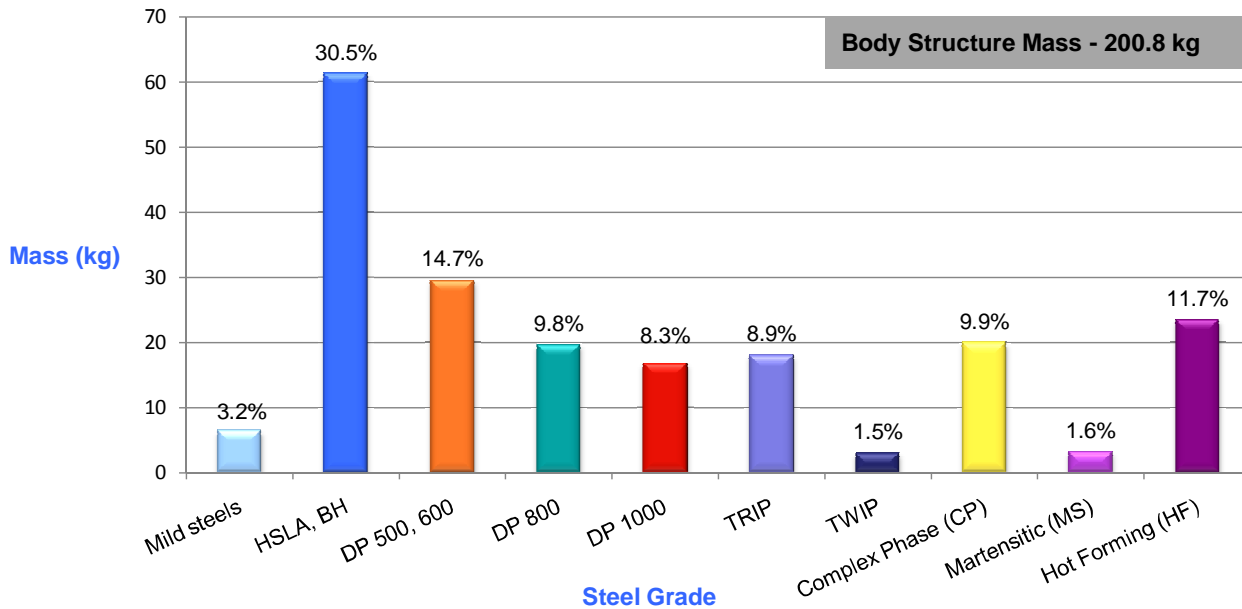


Figure 16.12: FSV-2 body structure

Steels: corresponding metallurgical classes	Color Code	FSV-2 Mix (%)
Low Strength Steels: Mild Steels		3.2
High Strength Steels (HSS): HSLA, BH		30.5
DP 500, 600		14.7
DP 800		9.8
DP 1000		8.3
TRIP		8.9
TWIP		1.5
Complex Phase (CP)		9.9
Martensitic (MS)		1.6
Hot forming (HF)		11.7

Table 16.4: FSV-2 body structure material mix

Figure 16.13: FSV-2 material mix

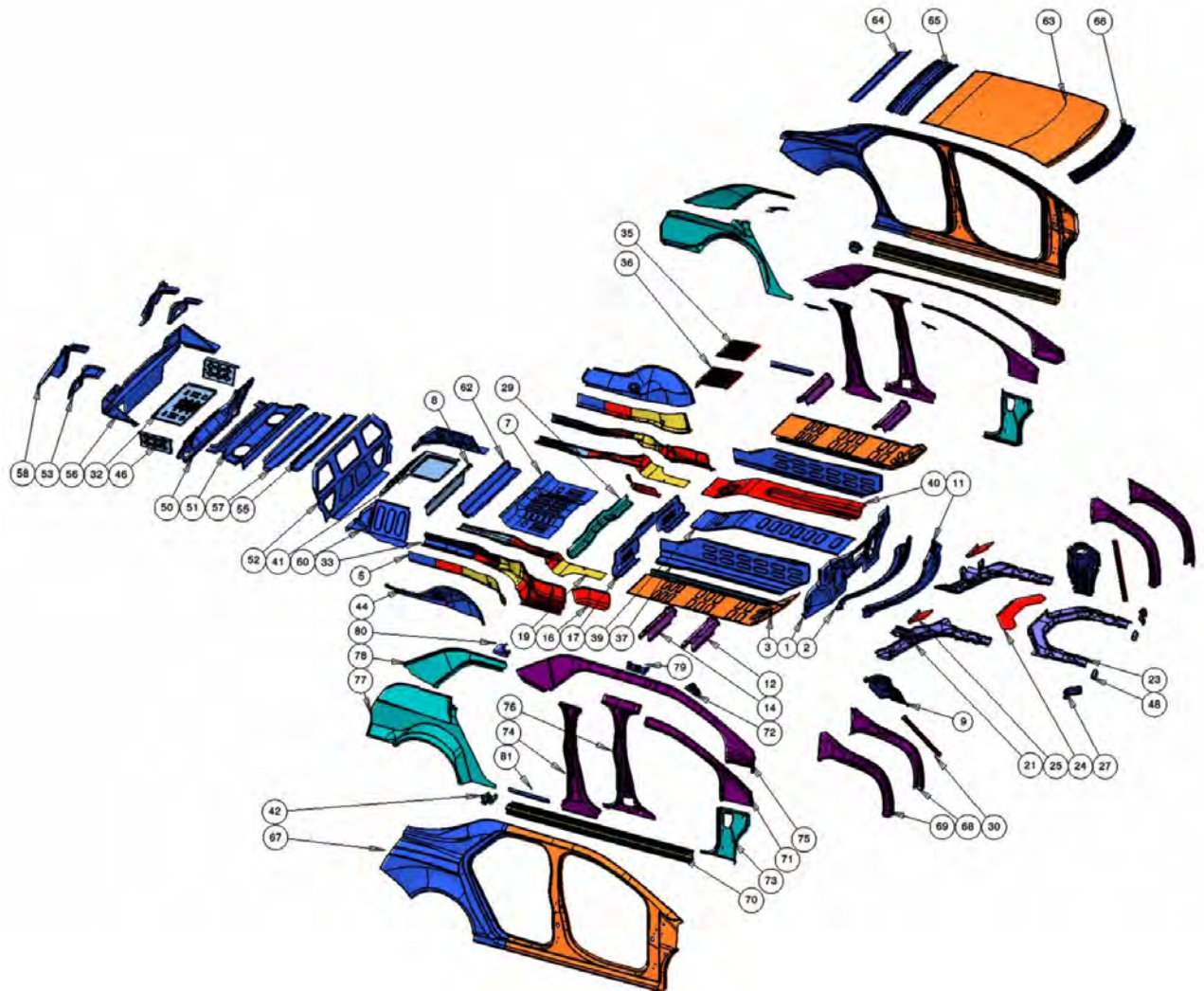


Figure 16.14: *FSV-2 exploded view*

The FSV-2 parts lists showing material grades, thickness and mass are shown in Table 16.5 and Table 16.6.

Part No	Part Description	Forming	Grade	Yeild (MPa)	Tensile (MPa)	Thickness (mm)	Mass (kg)	Total Mass (kg)
1	50.1 0001 Dash Panel	S	BH	280	400	0.5	2.997	2.997
2	50.1 0002 Cowl Upper	S	BH	210	340	0.6	1.412	2.753
			BH		340	1.2	1.341	
3	50.1 0011 Floor - Front RH	S	DP	300	500	0.5	2.914	4.824
			DP	500	800	1.5	1.91	
4	50.1 0025 Floor - Front LH	S	DP	300	500	0.5	2.914	4.824
			DP	500	800	1.5	1.91	
5	50.1 0014 Frame Rail Otr - Rear RH	S	CP	1000	1200	0.6	0.471	1.182
			DP	700	1000	1.4	0.456	
			HSLA	350	450	0.8	0.255	
6	50.1 0015 Frame Rail Otr - Rear LH	S	CP	1000	1200	0.6	0.471	1.182
			DP	700	1000	1.4	0.456	
			HSLA	350	450	0.8	0.255	
7	50.1 0016 Rear Seat Pan	S	BH	210	340	0.5	2.398	2.398
8	50.1 0032 Cargo Box Cross Member	S	Mild	140	270	0.5	0.791	0.791
9	50.1 0044 Apron Reinf RH	S	TWIP	500	980	1	1.462	1.462
10	50.1 0063 Apron Reinf LH	S	TWIP	500	980	1	1.462	1.462
11	50.1 0070 Cowl Lower	S	BH	210	340	0.6	0.787	1.66
			BH	210	340	1.2	0.873	
12	50.1 0093 Frt Seat Frt Crossmember RH	RF	MS	950	1200	0.7	0.769	0.769
13	50.1 0094 Frt Seat Frt Crossmember LH	RF	MS	950	1200	0.7	0.769	0.769
14	50.1 0095 Frt Seat Rr Crossmember RH	RF	MS	950	1200	0.7	0.808	0.808
15	50.1 0096 Frt Seat Rr Crossmember LH	RF	MS	950	1200	0.7	0.808	0.808
16	50.1 0099 Side Panel RH	S	DP	700	1000	0.7	0.425	0.425
17	50.1 0100 Heel Board	S	BH	210	340	0.6	1.639	1.639
18	50.1 0101 Side Panel LH	S	DP	700	1000	0.7	0.425	0.425
19	50.1 0109 Rear Frame Rail Reinf RH	S	CP	100	1200	1.1	0.75	2.37
			DP	700	1000	0.65	0.556	
			Mild	140	720	1.55	1.064	
20	50.1 0110 Rear Frame Rail Reinf LH	S	CP	100	1200	1.1	0.75	2.37
			DP	700	1000	0.65	0.556	
			Mild	140	720	1.55	1.064	
21	50.1 0301 Front Rail - Lower RH	S	TRIP	600	980	1.8	4.685	5.995
			TRIP	600	980	1.9	0.891	
			TRIP	600	980	2	0.419	
22	50.1 0302 Front Rail - Lower LH	S	TRIP	600	980	1.8	4.685	5.995
			TRIP	600	980	1.9	0.891	
			TRIP	600	980	2	0.419	
23	50.1 0303 Front Rail - Upper	S	TRIP	600	980	0.8	0.297	5.938
			TRIP	600	980	0.95	0.347	
			TRIP	600	980	1.85	1.016	
			TRIP	600	980	1.85	4.251	
24	50.1 0304 Closeout - Upper Rail	S	DP	700	1000	1	0.939	0.939
25	50.1 0305 Lower Rail Closeout RH	S	DP	700	1000	1	0.391	0.391
26	50.1 0306 Closeout - Lower Rail LH	S	DP	700	1000	1	0.391	0.391
27	50.1 0308 Shotgun Brace RH	S	BH	210	340	0.7	0.122	0.122
28	50.1 0318 Shotgun Brace LH	S	BH	210	340	0.7	0.122	0.122
29	50.1 0320 Side to Side Rail	S	DP	500	800	0.8	1.149	1.149
30	50.1 0326 A-Pillar Brace RH	RF/T	DP	700	1000	0.7	0.401	0.401
31	50.1 0327 A-Pillar Brace LH	RF/T	DP	700	1000	0.7	0.401	0.401
32	50.1 0330 Cargo Box Floor Panel	S	IF	140	270	0.5	1.139	1.139
33	50.1 0335 Rear Frame Rail Inner RH	S	DP	700	1000	1.4	3.321	4.255
			CP	1000	1200	0.6	0.314	
			HSLA	350	450	0.8	0.62	
34	50.1 0336 Rear Frame Rail Inner LH	S	DP	700	1000	1.4	3.321	4.255
			CP	1000	1200	0.6	0.314	
			HSLA	350	450	0.8	0.62	
35	50.1 0400 Tunnel Bulkhead Upper	S	DP	700	1000	0.8	0.772	0.772
36	50.1 0401 Tunnel Bulkhead Lower	S	DP	700	1000	0.8	0.961	0.961
37	50.1 0402 Tunnel Side Panel RH	S	BH	280	400	0.5	2.403	2.403
38	50.1 0403 Tunnel Side Panel LH	S	BH	280	400	0.5	2.403	2.403
39	50.1 0404 Tunnel Top Reinforcement	S	BH	280	400	0.5	2.509	2.509
40	50.1 0405 Tunnel Top Panel	S	DP	1150	1270	0.6	2.949	2.949
41	50.1 0500 Rear Floor Panel	S	Mild	140	210	0.5	1.667	1.667
42	50.1 2002 Suspension Mount RH	S	DP	500	800	2	0.37	0.37
43	50.1 2001 Suspension Mount LH	S	DP	500	800	2	0.37	0.37
44	50.1 2017 Rear Wheelhouse Inner RH	S	BH	210	340	1.2	1.727	2.473
			BH	210	340	0.7	0.75	
45	20.1 0217 Wheelhouse Inner Rear LH	S	BH	210	340	1.2	1.727	2.473
			BH	210	340	0.7	0.75	
46	50.1 2112 Cargo Box Side Panel RH	S	Mild	140	210	0.5	0.33	0.33
47	50.1 2113 Cargo Box Side Panel LH	S	Mild	140	210	0.5	0.33	0.33
48	60.2 0007 Frt Crush Can Mntg Plate RH	S	DP	500	800	1.75	0.121	0.121
49	60.2 0008 Frt Crush Can Mntg Plate LH	S	DP	500	800	1.75	0.121	0.121
50	50.1 0501 Back Panel Inner	S	BH	210	340	0.7	2.124	2.124

Table 16.5: FSV-2 Bill of Materials (BOM)

16.2 FSV-2

Part No	Part Description	Forming	Grade	Yeild (MPa)	Tensile (MPa)	Thickness (mm)	Mass (kg)	Total Mass (kg)
51	50.1 8675 Package Shelf	S	BH	210	340	0.7	3.307	3.307
52	50.1 3090 Seat Back Panel	S	BH	210	340	0.5	2.81	2.81
53	50.1 0502 Back Panel Inner Upper RH	S	BH	210	340	0.7	0.524	0.524
54	50.1 0503 Back Panel Inner Upper LH	S	BH	210	340	0.7	0.524	0.524
55	50.1 1999 Package Shelf Front Support	S	BH	210	340	0.7	0.898	0.898
56	50.1 0271 Back Panel	S	BH	210	340	0.7	3.521	3.521
57	50.1 5789 Package Shelf Rear Support	S	BH	210	340	0.7	1.359	1.359
58	50.1 7685 Lamp Can RH	S	BH	210	340	0.8	1.259	1.259
59	50.1 7785 Lamp Can LH	S	BH	210	340	0.8	1.259	1.259
60	50.1 0510 Rear Floor Side Panel RH	S	BH	210	340	0.5	1.038	1.038
61	50.1 0517 Rear Floor Side Panel LH	S	BH	210	340	0.5	1.038	1.038
62	50.1 0420 Seat Back Lwr Crossmember	S	BH	210	340	0.5	1.215	1.215
63	50.2 5332 Roof Panel	S	DP	350	600	0.5	7.48	7.48
64	50.2 5334 Rear Header	RF	BH	210	340	0.8	1.24	1.24
65	50.2 0013 Roof Bow	RF	BH	210	340	0.5	1.11	1.11
66	50.2 0011 Roof Front Header	S	BH	210	340	0.8	1.223	1.223
67	50.6 2002 Body Side Outer RH	S	DP	350	600	0.8	8.074	13.116
			BH	210	340	0.6	5.042	
68	50.1 0021 Shotgun Inner RH	HS	HF	1050	1500	1.5	0.92	2.675
			HF	1050	1500	1.2	0.476	
			HF	1050	1500	0.8	1.278	
69	50.1 0051 Shotgun Outer RH	HS	HF	1050	1500	0.8	0.689	2.09
			HF	1050	1500	1	0.431	
			HF	1050	1500	1.5	0.968	
70	50.6 0048 Rocker RH	RF	CP	1050	1470	1.2	8.434	8.434
71	50.6 0022 Roof Rail Inner Front RH	HS	HF	1050	1500	0.7	0.812	1.086
			HF	1050	1500	0.95	0.275	
72	50.2 0032 Brkt - Roof Rail to Header RH	S	BH	210	340	1	0.103	0.103
73	50.6 0046 FBHP Inner RH	S	DP	500	700	1.2	1.666	1.666
74	50.6 2026 B-Pillar Reinf RH	HS	HF	1050	1500	0.6	1.11	1.749
			HF	1050	1500	1	0.64	
75	50.6 2012 Roof Rail Reinf RH	HS	HF	1050	1500	0.7	2.576	2.576
76	50.6 2009 B-Pillar Inner RH	HS	HF	1050	1500	0.6	0.696	1.54
			HF	1050	1500	0.8	0.844	
77	50.1 2049 Wheel House Outer Panel RH	S	DP	500	800	0.65	3.808	3.808
78	50.6 2052 C-Pillar Inner RH	S	DP	500	800	0.7	1.368	1.368
79	50.2 2033 Roof Bow to Roof Rail Brkt RH	S	BH	210	340	0.5	0.149	0.149
80	50.6 6482 Rear Header Bracket RH	S	BH	210	340	0.8	0.134	0.134
81	50.6 5413 Rear Door Closeout Panel RH	S	BH	210	340	0.5	0.109	0.109
82	50.6 0064 FBHP Inner LH	S	DP	500	700	1.2	1.666	1.666
83	50.6 0066 Rocker LH	RF	CP	1050	1470	1.2	8.434	8.434
84	50.6 2023 Roof Rail Inner Front LH	HS	HF	1050	1500	0.7	0.812	1.086
			HF	1050	1500	0.95	0.275	
85	50.1 0069 Shotgun Outer LH	HS	HF	1050	1500	0.8	0.689	2.09
			HF	1050	1500	1	0.431	
			HF	1050	1500	1.5	0.968	
86	50.1 0022 Shotgun Inner LH	HS	HF	1050	1500	1.5	0.92	2.675
			HF	1050	1500	1.2	0.476	
			HF	1050	1500	0.8	1.278	
87	50.6 2003 Body Side Outer LH	S	DP	350	600	0.8	8.074	13.116
			BH	210	340	0.6	5.042	
88	50.2 2633 Roof Rail to Header Brkt LH	S	BH	210	340	1	0.103	0.103
89	50.6 2626 B-Pillar Reinf LH	HS	HF	1050	1500	0.6	1.11	1.749
			HF	1050	1500	1	0.64	
90	50.6 2612 Roof Rail Reinf LH	HS	HF	1050	1500	0.7	2.576	2.576
91	50.6 2609 B-Pillar Inner LH	HS	HF	1050	1500	0.6	0.696	1.54
			HF	1050	1500	0.8	0.844	
92	50.1 2649 Wheel House Outer Panel RH	S	DP	500	800	0.65	3.808	3.808
93	50.6 2652 C-Pillar Inner LH	S	DP	500	800	0.7	1.368	1.368
94	50.2 7633 Roof Bow to Roof Rail Brkt LH	S	BH	210	340	0.5	0.149	0.149
95	50.6 4682 Rear Header Bracket LH	S	BH	210	340	0.8	0.134	0.134
96	50.6 4513 Rear Door Closeout Panel LH	S	BH	210	340	0.5	0.109	0.109
Total							200.8	200.8

Table 16.6: FSV-2 Bill of Materials (BOM) (contd.)

16.2.1 FSV-2 Body Structure

The overall body structure design of the FSV-2 front end is the same as FSV-1 front end, until the B-pillar. Both the FSV-2 powertrains share a common front-end. The rear end of the body structure was designed according to the styling theme decided in the FSV Phase-1, and further changes were made accordingly to accommodate the respective powertrain components.

The two powertrain variants of the FSV-2 are discussed in the following sub-sections.

16.2.2 FSV-2 PHEV₄₀

The PHEV₄₀ variant of the FSV-2 is a series hybrid vehicle with an all electric range of 64 km (40 miles). The extended range of 500 km is provided by a 1.4 L- 3 cylinder gasoline engine/generator set. The component packaging and structural characteristics for this vehicle are similar to the PHEV₂₀. The layout for the FSV-1 PHEV₄₀ is illustrated in Figure 16.15 (the colour scheme of the parts shown make use of the color code for the material classification as shown in Table 16.4).

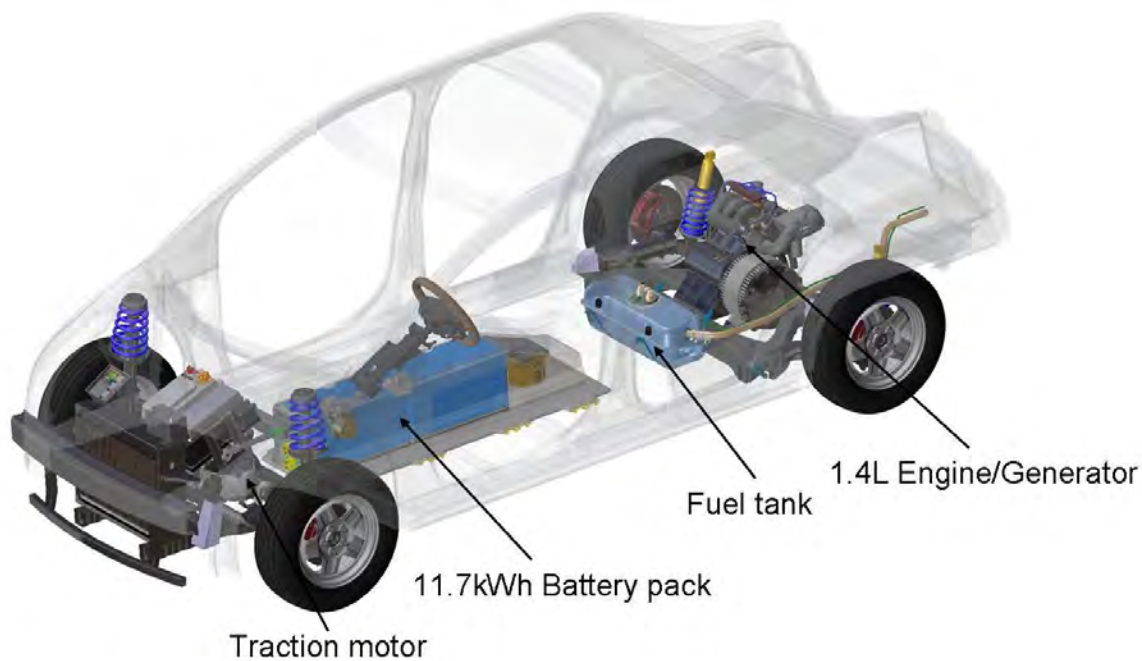


Figure 16.15: *FSV-1 PHEV₂₀ body structure*

16.2.2.1 PHEV₄₀ Front End

The PHEV₄₀ front end packaging is the same as the FSV-1 PHEV₂₀ as shown in Figure 16.16.



Figure 16.16: FSV-1 PHEV₄₀ front end

16.2.2.2 PHEV₄₀ Powertrain Package

Similar to the FSV-1 PHEV₂₀ the major components of the PHEV₄₀ powertrain are:

1. Battery pack
2. Electric drive motor
3. Converter (converts DC current to AC and control motor speed)
4. Generator Inverter Controller and Hybrid Controller
5. Internal combustion engine (1.0 L)
6. Fuel System
7. Exhaust System

PHEV₄₀ Battery Pack

The PHEV₄₀ battery pack is a lithium-ion manganese based cell with a 11.7 kWh capacity (105 kg mass, 86 liter volume). The battery pack is a 'I' shaped with a size smaller than the BEV battery pack. So, the battery pack is packaged in the tunnel area similar to the BEV as shown in Figure 16.15.

PHEV₄₀ Electric Drive Motor

The PHEV₄₀ uses a traction motor with a rated peak power of 75 kw (55 kw of continuous power). The front end package is shown in Figure 16.16.

PHEV₄₀ Internal Combustion Engine

The PHEV₄₀ engine/generator set occupies the rear cargo box space as shown in Figure 16.17.

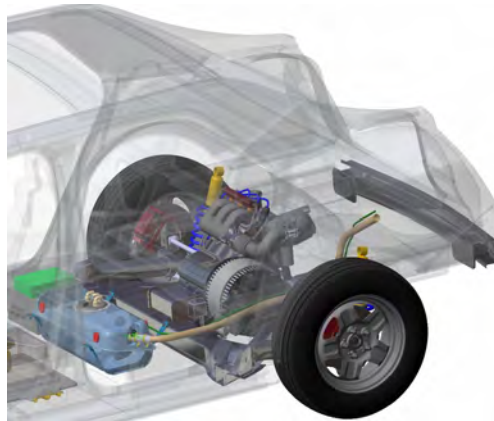


Figure 16.17: FSV-2 PHEV₄₀ engine/generator set packaging

PHEV₄₀ Fuel Tank

The PHEV₄₀ fuel tank is the same as the one used in the PHEV₂₀. The fuel tank is packaged under the rear floor as shown in Figure 16.18.

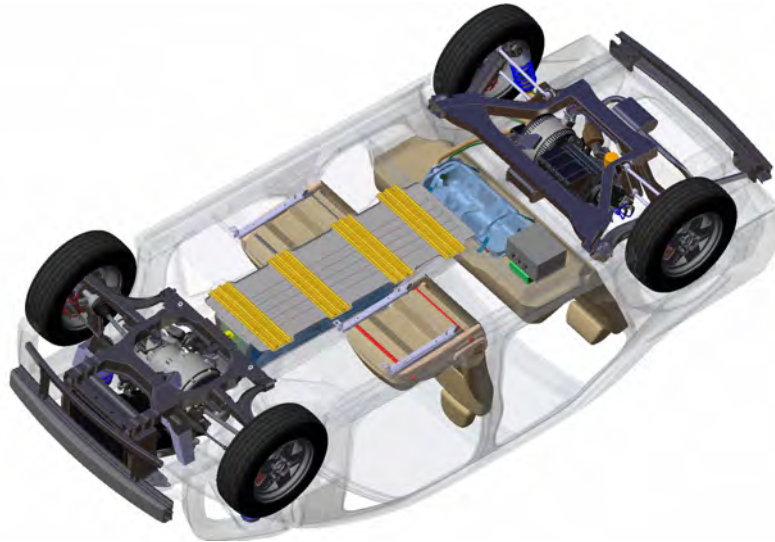


Figure 16.18: FSV-2 PHEV₄₀ fuel tank packaging

PHEV₄₀ Rear suspension

The PHEV₄₀ rear suspension is also a multi-link trailing arm suspension, similar to the BEV and the PHEV₂₀ as shown in Figure 16.19.

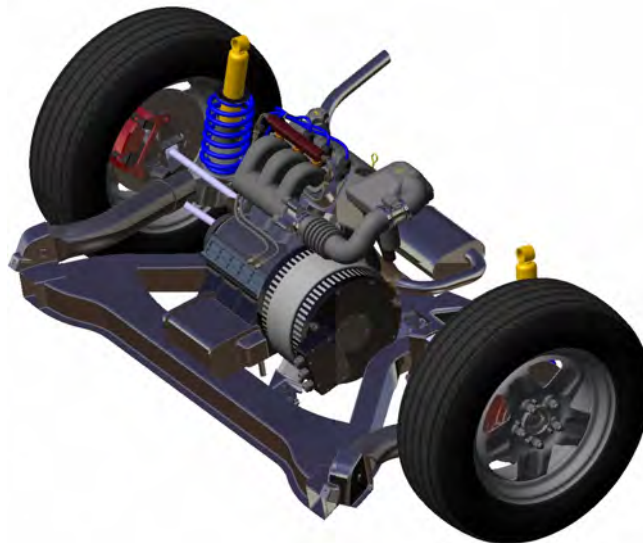


Figure 16.19: FSV-2 PHEV₄₀ rear suspension assembly

16.2.3 FSV-2 FCEV

The FSV-2 FCEV is a compressed hydrogen powered fuel cell electric vehicle. Approximately 3.4 kg of compressed hydrogen at 700 bar (10,000 psi) is stored in a single 95 L tank, which allows for a vehicle range of about 500 km (310 miles). The FSV-2 FCEV layout is illustrated in Figure 16.20.

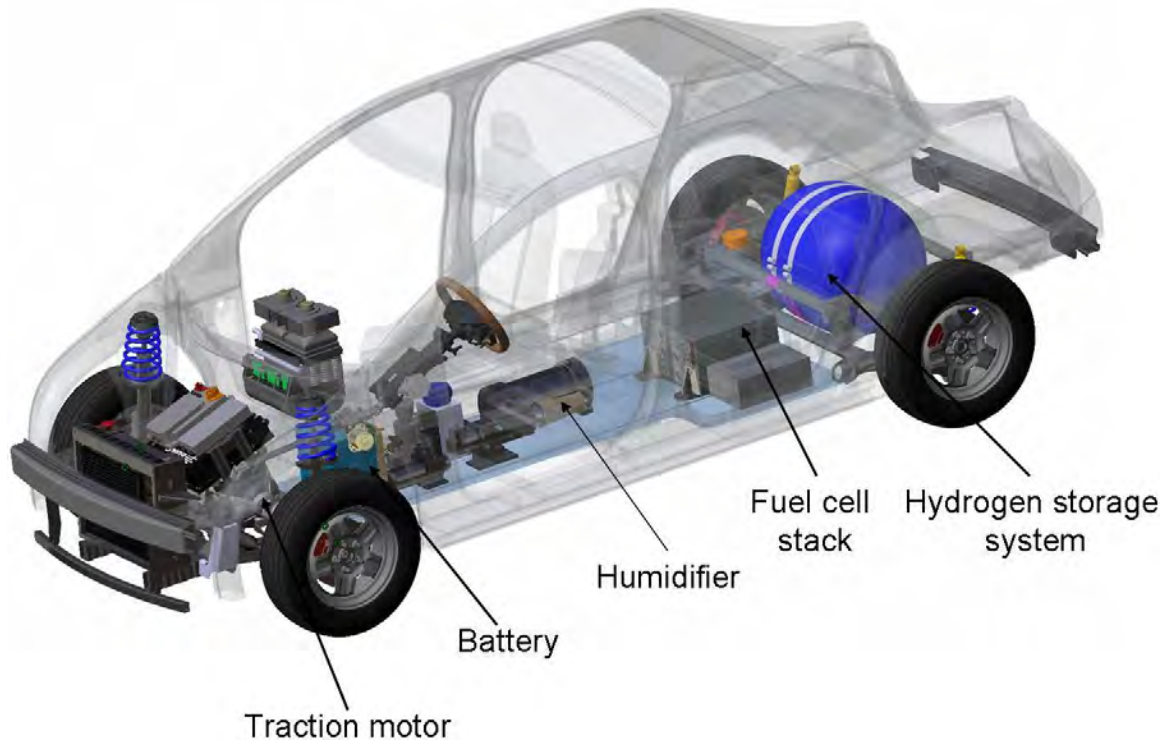


Figure 16.20: FSV-2 FCEV layout

16.2.3.1 FCEV Powertrain Package

The major components of the FCEV powertrain package are:

- Fuel cell stack
- Fuel cell auxiliary equipment (compressor, recirculator, etc.)
- Fuel cell DC/DC converter
- Traction motor with controller/inverter
- AC/DC converter[2]
- Battery energy storage
- Hydrogen storage tank

The FSV-2 FCEV powertrain components except the hydrogen storage (shown in Figure 16.21), are packaged in the engine compartment as shown in Figure 16.22. The hydrogen tanks are packaged in front of the rear axle under the rear passenger seats. The fuel cell stack is packaged in the rear of the vehicle as shown in Figure 16.20. The lithium-ion battery pack is positioned in front of the tunnel, behind the firewall. This packaging design also allowed for a common front-end with the BEV variant of the FSV.

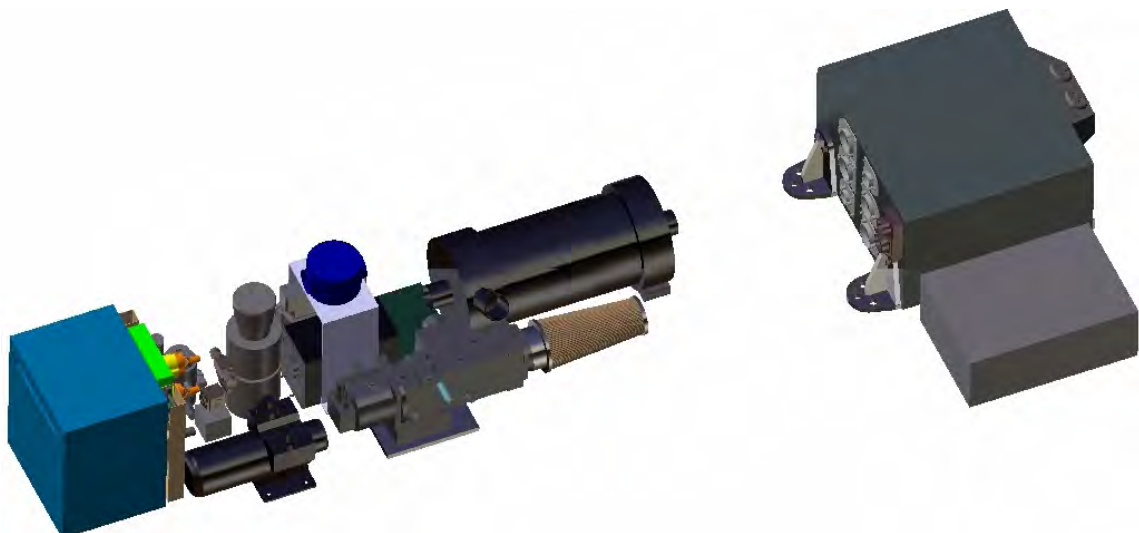


Figure 16.21: FSV-2 FCEV powertrain components (hydrogen storage tank not shown)

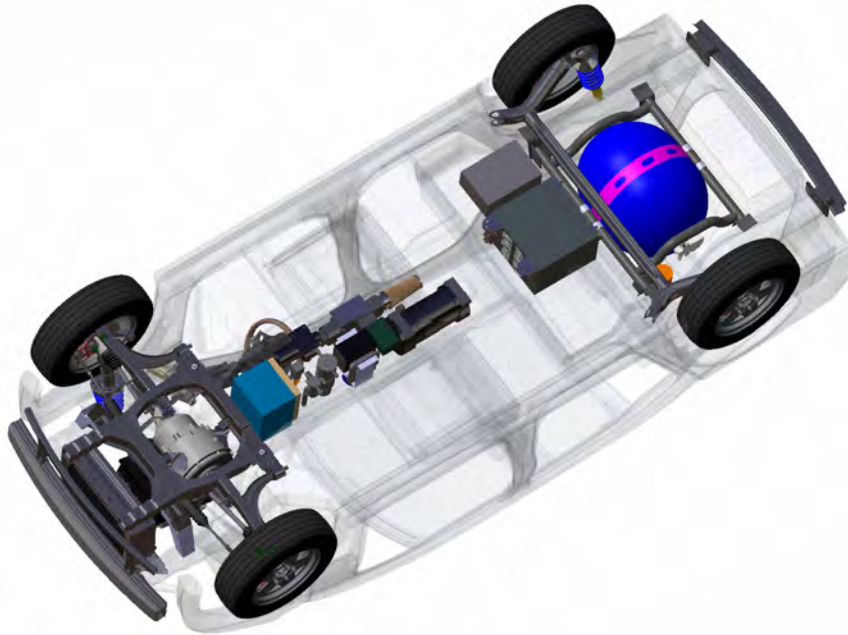


Figure 16.22: FSV-2 FCEV underbody packaging

FCEV Hydrogen Storage

The FCEV has a hydrogen usable storage capacity of 3.4 kg with an internal volume of 95 liters. The FCEV hydrogen storage tank is packaged under the rear floor in the same package space as that of the rear mounted PHEV₄₀ engine/generator set, as shown in Figure 16.23.

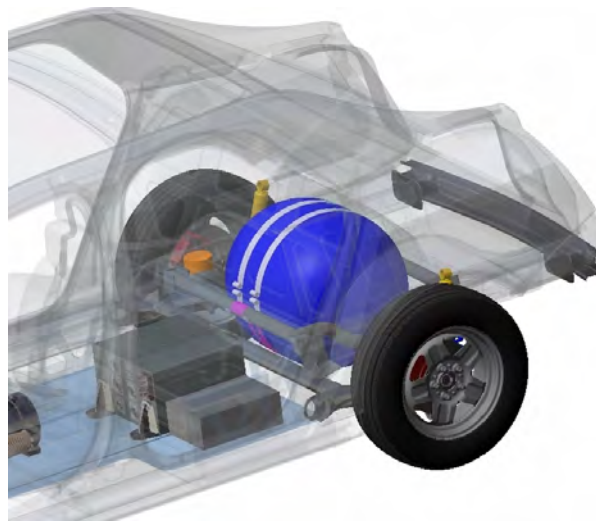


Figure 16.23: FSV-2 FCEV hydrogen storage packaging

FCEV Rear Suspension

The FCEV is the only variant of the FSV which has the twist beam or the torsion beam suspension. The twist beam suspension is a simple, inexpensive and effective design. This design could not be used on the other FSV variants due to packaging constraints. Moreover, the multi-link trailing arm suspension resulted in a modular assembly with the engine/generator set in the other variants (BEV, PHEV₂₀ and PHEV₄₀). The FCEV rear suspension is shown in Figure 16.24.



Figure 16.24: FSV-2 FCEV rear suspension

17.0 Body Structure Cost Assessment

17.1 Part Manufacturing Cost

The manufacturing costs of entire body structure components were assessed, utilizing the same cost model as the model used to determine the sub-system costs for the sub-system cost assessment. The approach of the cost model and the assumptions are explained in detail in Section 12.2 (Sub-System Cost Assessment).

For the FSV, only the technical cost modeling approach was used for the assessment, no supplier cost estimates were used. Technical cost modeling has the advantage of assessing manufacturing flexibility and sensitivity studies to various parameters such as material costs, energy costs, overhead, building costs, etc. This approach assumes a green field site with matured technology and developed competitive infrastructure to deliver that technology. Technical cost modeling also assumes that the body structure build is only charged for the percentage of the capital investment it uses. For example, a stamping may only need 10% of the press time from a press and as a result is only allocated 10% of capital investment cost of the press. The technical cost model can be user modified to comprehend existing facilities, but of course such details are unique for a specific location.

The cost breakdown for the fabrication of the steel components/systems are shown in Table 17.1.

Manufacturing Technology	Parts Weight (kg)	Unit Cost Per Vehicle (\$ USD)
Stamping	76.1	\$306.1
Stamping -Laser Welded Blanks	72.0	\$270.4
Hot Stamping	4.8	\$48.7
Hot Stamping - Laser Welded Blanks	16.8	\$118.5
Open Rollforming	4.5	\$7.7
Closed Rollforming	13.5	\$23.6
Total Body Structure (Manufacturing)	187.7	\$775.0

Table 17.1: *Body structure manufacturing costs breakdown*

Table 17.2 shows the body structure manufacturing costs with a breakdown of the fixed and the variable costs.


Total Body Structure Manufacturing Costs	\$775.0	
Building	\$6.2	
Maintenance	\$24.9	
Energy Cost	\$23.4	
Overhead	\$40.1	
Labor cost	\$51.0	
Equipment Cost	\$108.9	
Tooling	\$132.7	
Material Price	\$387.8	

Table 17.2: Total body structure manufacturing costs with breakdown of the fixed and the variable costs

17.2 Body Assembly Cost

The assembly costs of the body structure were also estimated with a technical cost modeling approach similar to that used in the manufacturing cost model.

The assembly costs were estimated for each of the sub-assembly and assembly concepts, using the following different assembly processes:

- Laser Welding
- Laser Braze
- Adhesive Bonding
- Resistance Spot Welding
- Hemming

Similar to the manufacturing costs, the overall assembly cost was broken down into the following costs:

- Material
- Labor
- Equipment
- Tooling
- Energy
- Building
- Maintenance

17.2.1 General Assumptions

The general assumptions for the assembly cost model were the same as shown in Table 12.2.

17.2.2 Plant Parameters

The assembly plant was assumed to run two shifts for every working day achieving a line rate of 31 jobs/hour. The other plant parameters are listed in Table 17.3.

Parameters	FSV Assumptions
Available Operating Time	3240 hrs/year
Paid Operating Time	3456 hrs/year
Gross Line Rate	31 jobs/hr
Station Cycle Time for One Line	117 secs
Actual Station Time	117 secs
Number of Parallel Lines	1
Part Loading Time	5 sec/part
Clamp/Unclamp Time	6 secs
Transfer Time	3 secs
Minimum Allowable Station Time	30 secs
Transport System Cost per Station	\$100,000 per station
Assembly Unplanned Downtime	1.6 hours/day
Assembly Maintenance Cost	10%

Table 17.3: *Assembly plant parameters*

17.2.3 Process Parameters

The process parameters that are independent of the part parameters were identified, and included in the assembly cost model. These parameters were incorporated into the cost model such that they could be changed at a later stage if required, thereby recalculating the assembly costs. The parameters for the different processes are listed in Table 17.4 thru Table 17.7.

Assembly Process	FSV Assumptions				
	Continuous (Yes - 1, No-0)	Connect Rate (connects/sec)	Joining Speed (m/sec)	Connect Spacing (meters)	Inter-Join Time (sec/join)
Adhesive	1	-	0.30	-	3.0
Laser Braze	1	-	0.08	-	-
Laser - Robotic	1	-	0.08	-	-
Laser - Robotic (Large)	1	-	0.08	-	-
RSW - Small (static)	0	0.50	-	0.04	4.0
RSW	0	1.00	-	0.04	3.0
RSW (Medium)	0	1.00	-	0.04	3.0
RSW (Large)	0	1.00	-	0.04	3.0
Hemming	1	-	0.01	-	-

Table 17.4: Assembly Process Parameters

Assembly Process	FSV Assumptions				
	Cycle Time (sec/cycle)	Power Requirement (kW or KWh/connect)	Electrode Life (meters or connects)	Electrode Cost (\$/electrode)	Gas Use Rate (l/m or l/connect)
Adhesive	3.0	30.00	-	-	-
Laser Braze	3.0	115.00	-	-	0.33
Laser - Robotic	3.0	115.00	-	-	0.33
Laser - Robotic (Large)	3.0	115.00	-	-	0.33
RSW - Small (static)	10.0	0.04	3,000	0.45	-
RSW	5.0	0.04	3,000	0.45	-
RSW (Medium)	5.0	0.04	3,000	0.45	-
RSW (Large)	5.0	0.04	3,000	0.45	-
Hemming	4.0	0.50	-	-	-

Table 17.5: Assembly Process Parameters (continued)

Assembly Process	FSV Assumptions				
	Adhesive Use Rate (kg/m or kg/connect)	Adhesive/Filler Cost (\$USD/kg)	Ass'y Equipment per station (#/station)	Unit Assembly Equipment cost (\$USD/operator)	Idle Stations per Assembly
Adhesive	0.01	20	3	125,000	1.000
Laser Braze	0.30	0.90	2	600,000	1.000
Laser - Robotic	-	-	2	500,000	1.000
Laser - Robotic (Large)	-	-	6	500,000	1.000
RSW - Small (static)	-	-	2	30,000	0.170
RSW	-	-	2	75,000	0.170
RSW (Medium)	-	-	4	120,000	0.330
RSW (Large)	-	-	10	120,000	0.250
Hemming	-	-	1	400,000	2.000

Table 17.6: Assembly Process Parameters (continued)

Assembly Process	FSV Assumptions				
	Idle Stations Cost	Labor Requirement (lab/Ass'y Equip)	Requires Fixture (\$, 0-No)	Station Cost (\$/station)	Station Space (sqm/station)
Adhesive	25,000	0.25	120,000	20,000	100
Laser Braze	25,000	0.25	1,500,000	50,000	100
Laser - Robotic	25,000	0.25	150,000	50,000	100
Laser - Robotic (Large)	25,000	0.25	1,500,000	50,000	200
RSW - Small (static)	10,000	0.50	50,000	20,000	50
RSW	10,000	0.50	50,000	20,000	100
RSW (Medium)	20,000	0.25	150,000	20,000	150
RSW (Large)	20,000	0.25	2,000,000	20,000	200
Hemming	10,000	1.00	120,000	10,000	100

Table 17.7: Assembly Process Parameters (continued)

17.2.4 Assembly Inputs

The sub-assembly and assembly costs were assessed with the technical cost modeling approach similar to the one used by MIT in the ULSAB AVC and Future Generation Passenger Compartment (FGPC)^[1].

¹References:

1. Auto/Steel Partnership Future Generation Passenger Compartment (FGPC), VERSION 1.0 JUL, 2009
2. ULSAB AVC:VERSION 2.1C FEB, 2002
3. TM27C (EDAG Internal Cost Model)

17.2 Body Assembly Cost

Each sub-assembly in the overall body structure assembly was reviewed to determine the following parameters that are related to the specific sub-assembly/assembly:

- Sub-Assembly/Assembly Structure
- Joining Process
- Assembly Process Parameters
 - Length of weld (Laser Welding, Laser Brazing)
 - Number of welds (Resistance Spot Welding)
 - Length of bond (Adhesive bonding)
 - Length of hem flange (Hemming)

The assembly review process is discussed in detail in Section 13.3.1 (Body Structure Assembly) and the parameters for each sub-assembly/assembly are shown in the Appendix.

17.2.5 Assembly Cost Assessment Results

Based on the assembly sequence and joining specifications determined from the overall sub-assembly/assembly assessment, as discussed in 13.3.1 (Body Structure Assembly), the assembly cost model was used to estimate the body structure assembly costs. Table 17.8 shows the costs for the FSV body structure sub-assemblies and the total assembly costs.

Assembly Name	Assembly (\$ USD) Cost
Body Side Inner Sub Assembly RH	\$17.59
Body Side Inner Sub Assembly LH	\$17.59
Body Side Outer Sub Assembly RH	\$5.29
Body Side Outer Sub Assembly LH	\$5.29
Body Side Assembly RH	\$24.95
Body Side Assembly LH	\$24.95
Front Structure Assembly	\$46.53
Front Floor Sub-Assembly	\$39.91
Rear Floor Assembly	\$89.63
Underbody Assembly	\$22.20
Body Structure Assembly	\$45.79
Total Cost of Body Structure Assembly	\$339.73

Table 17.8: *Body structure assembly costs*

Table 17.9 shows the body structure assembly costs with a breakdown of the fixed and the variable costs.

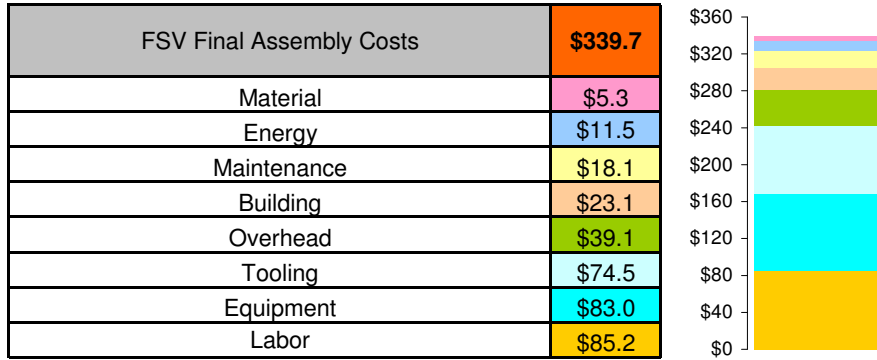


Table 17.9: Total body structure assembly costs with breakdown of the fixed and the variable costs

17.3 Sensitivity Analysis

17.3 Sensitivity Analysis

As explained in 12.2 (Sub-System Cost Assessment), the cost model had certain assumptions made specific to the program. Sensitivity analyses were performed to demonstrate the effect on the overall vehicle cost as a result of changing certain key parameters including: production volume, product life, and steel prices.

For the FSV BEV, the yearly production volume was assumed to be 100,000 for a production life of 5 years, which is considerably less than a conventional vehicle production volume of 225,000 for an average product life of 8 years. Hence, it was important to show the sensitivity of the overall vehicle costs when the production volume and product life were varied in this range to show how the large tooling investments associated with vehicle manufacturing could be spread out when the production volume or the product life increases. Similarly, since material costs make up a high percentage of the overall vehicle costs, a variation in the steel prices also show a high impact on the costs.

Figure 17.1 shows the results of the sensitivity analyses and the range within which the key parameters were varied.

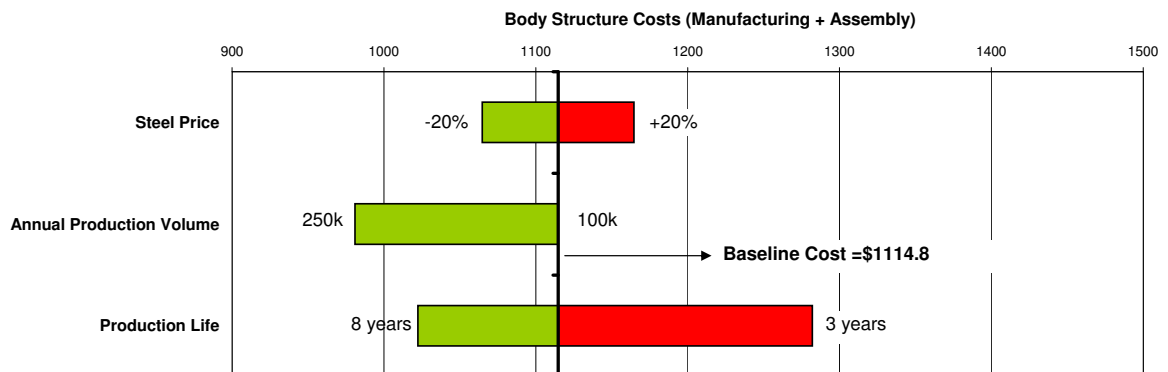


Figure 17.1: FSV body structure costs sensitivity analysis results

18.0 Life Cycle Assessment and Fuel Cycle Analysis

18.1 Body Structure Life Cycle Analysis (LCA)

In Chapter 12 and 13, an overview was presented of Life Cycle Assessment (LCA) and the methodology for applying LCA to the selection of major FutureSteelVehicle sub-systems in the. In general, the total life cycle assessment of any product refers to the emissions profile during the complete lifetime of the product, starting with the raw material used for manufacturing the product, followed by the usage of the same product for its entire lifetime, and finally considering the impact from disposal of the product. With reference to passenger vehicles, it is a common practice to evaluate the vehicles on the basis of its fuel consumption and the CO₂e emissions. However, such an evaluation takes into consideration only the emissions arising from the usage of the fuel by the vehicles. In other words, this evaluation captures only a part of the total life cycle assessment. For the assessment to encapsulate the complete life cycle, we must also consider the fuel production cycle (Well to Pump) and the fuel usage cycle (Pump to Wheels), along with the vehicle production cycle from production of raw materials to finished vehicle. A complete FSV Body Structure LCA is presented here.

In Chapters 12 and 13, the process for evaluating the various subsystem designs based on LCA methodology was described. To recap, the UCSB GHG Automotive Materials Comparison model was modified for the BEV powertrain, and each solution’s impact to total vehicle life cycle emissions was determined. Respective sub-system fabrication energies were converted into CO₂e emissions; these values were then added to the values obtained from the UCSB BEV model to achieve total vehicle life cycle emissions. As an example, the results for the rocker panel sub-system solutions are shown below.

FSV Sub-system	Material CO ₂ e	Manufacturing CO ₂ e	Use CO ₂ e	Recycling CO ₂ e	Total Vehicle Life Cycle CO ₂ e
Rocker, Baseline	2290.8	5.7	14640.2	(956.8)	15980.0
Solution 1 - Stamping	2299.4	6.1	14688.3	(960.6)	16033.2
Solution 1 - Stamping TRB	2292.9	6.0	14654.8	(957.6)	15996.1
Solution 1 - Stamping LWB	2292.3	16.9	14658.1	(957.3)	16010.0
Solution 2 - Hot Stamping	2272.9	9.7	14608.1	(947.7)	15942.9
Solution 2 - Hot Stamping TRB	2271.7	9.7	14598.5	(947.2)	15932.7
Solution 2 - Hot Stamping LWB	2271.7	20.4	14598.5	(947.2)	15943.4
Solution 3 - Closed Roll Form	2246.0	5.1	14481.6	(935.3)	15797.4
Solution 3 - Closed Roll Form (TRB)	2238.4	4.8	14479.5	(931.3)	15791.5
Solution 3 - Closed Roll Form (TWC)	2245.5	4.8	14487.9	(934.9)	15803.3
Solution 5 - Hydroform	2223.3	15.9	14416.8	(924.2)	15731.9
Solution 5 - Hydroform LWT	2223.1	25.6	14410.6	(924.2)	15735.1
Solution 5 - Hydroform TRT	2222.5	15.9	14410.6	(923.9)	15725.1
Aluminium Extrusion	2350.8	8.6	14425.1	(1008.5)	15775.9

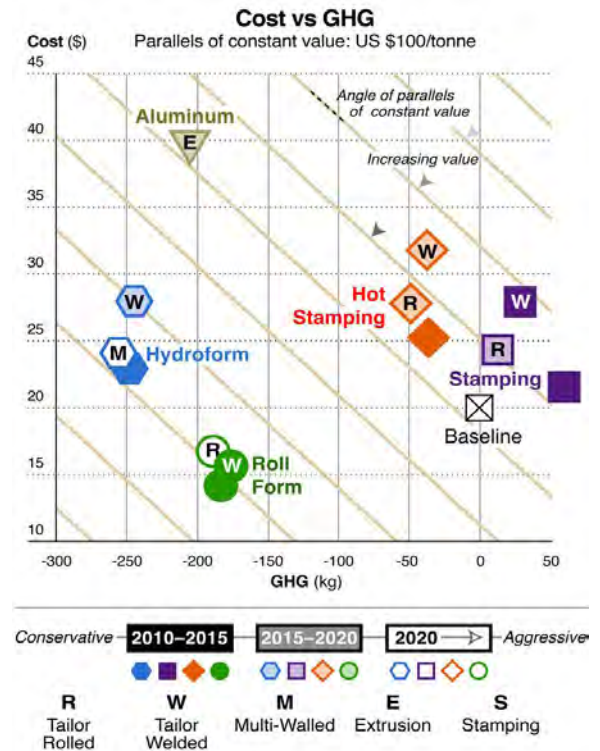


Figure 18.1: FSV Rocker Subsystem - Design options and Cost vs. Emissions

This same methodology was applied to the full vehicle body structure to determine the life cycle emissions profile of the BEV variant. In this case, an updated version of the UCSB GHG Automotive Materials Comparison model was used, which allows for advanced powertrain impact studies, including Battery-Electric (BEV) and Plug-in Hybrid (at 20 and 40 mile ranges, respectively). Key model parameters include the BEV powertrain and energy consumption factors based on vehicle size, geographic power grid emissions, NEDC driving cycle, vehicle life = 200,000 km, material processing efficiencies and recycling treatment.

The UCSB model has the option of establishing recycling rates based on multi-step recycling methods, or via consequential system expansion, where the user selects an "alpha" value to align with market practices. In this case, we use an extremely conservative (0.1) alpha value which reflects high recycling rates, consistent with mature recycling practices that is independent of scrap flows into or out of the product system. This practice favors materials that are energy-intensive to produce, so it's not a practice to bias or favor steel results. The engineering team provided body structure and total vehicle masses, manufacturing emissions attributed to each subsystem fabrication process, and component manufacturing efficiencies (yields) associated with these steel fabrication methods. Through optimization, NVH engineering and mass reduction benchmarking for various sub-systems, the engineering team achieved a body structure mass = 188 kg, and a vehicle curb weight = 958 kg, which is below mass targets.



Figure 18.2: FSV BEV; Curb Weight = 958 kg. Body Structure Mass = 187.7 kg

Component manufacturing yields represent materials utilization effectiveness. These data are critical process inputs in LCA modeling; more efficient processes result in less virgin material consumed to produce the same part, resulting in lower material production emissions. Thus, it is important to note that inefficient materials utilization will offset low fabrication energies and emissions, thus they must be given equal consideration in the pursuit of an ultra-low emissions vehicle fabrication strategy. These data are summarized in Table 18.1.

FSV Fabrication Process	Parts Mass (kg)	Mfg Emissions (kg CO ₂ e/kg mtl)	Average Scrap (%)
Stamping	76	34	55
Stamping -Laser Welded Blanks	72	49	50
Hot Stamping	5	8	58
Hot Stamping - Laser Welded Blanks	17	36	38
Open Rollforming	4	1	3
Closed Rollforming	14	7	3
Total Body Structure Manufacturing	188	135	
FSV Complete Assembly Process		66	
Total FSV Body Structure	188	199	Avg = 46%

Table 18.1: Summary for FSV fabrication processes, emissions and yields

18.2 Full Vehicle Body Structure LCA Results

The UCSB model develops distinct CO₂e values for material production, vehicle use and vehicle recycling. Fabrication emissions, converted from fabrication energies, are then added to the UCSB results to achieve total vehicle life cycle emissions associated with the FSV BEV body structure. The results vividly demonstrate that the coupling of a lightweight advanced high strength steel body structure with a battery electric powertrain results in a 40% to 50% reduction in life cycle emissions compared to comparably-sized vehicles with conventional ICE-gasoline engines, as shown in Table 18.2.

Vehicle	Material Production (kg CO ₂ e)	Use (kg CO ₂ e)	Recycling (kg CO ₂ e)	Parts Fabrication (kg CO ₂ e)	Total CO ₂ e (kg)
FSV-BEV	2,337	13,844	(1009)	199	15,371

Table 18.2: Full Vehicle body structure LCA results

Following the analysis methods used in the FutureSteelVehicle BEV sub-systems analysis, plots of Cost vs. Mass and Cost vs. Total Vehicle Emissions were developed for the complete FSV body structure design; these are shown below in Figure 18.3.

It is recommended that all body structure designs be compared on this basis.

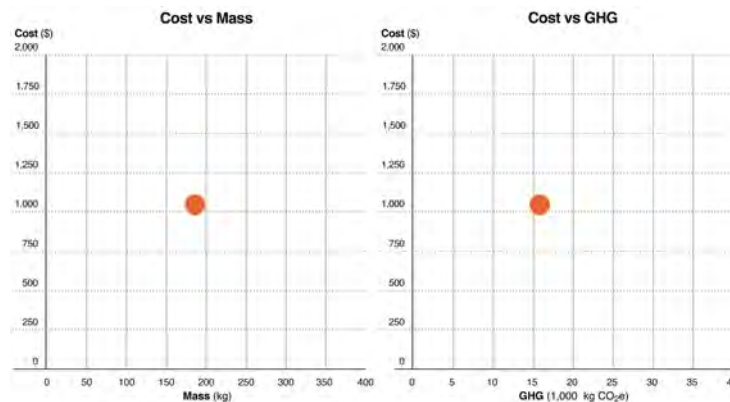


Figure 18.3: FutureSteelVehicle BEV bodystructure, Cost vs. Mass & Cost vs. Total Vehicle Emissions

To add relevancy, FutureSteelVehicle was compared to other benchmark vehicles: the ULSAB AVC concept vehicle from 2000, and the 2010 WV Polo V, which received the 2010 European Car of the Year award, and is distinguished for its efficient, lightweight steel structure. Both vehicles (Figure 18.4) are represented by internal combustion engine powertrains, available in gasoline or diesel variants.



Figure 18.4: FutureSteelVehicle compared to other benchmark vehicle programs

To make the comparisons more meaningful, the masses of the Polo V and ULSAB-AVC were modified to accommodate a battery electric propulsion system, and then the life cycle emissions were calculated following a study by fka to determine “Weight influence on the energy consumption of battery electric and plug-in hybrid vehicles”. The results are shown below in Table 18.3, Table 18.4 and Figure 18.5.

Vehicle	Class	Powertrain	Curb Weight	Body Mass	Fuel Consumption (NEDC)
FSV BEV	B+	BEV	958 kg	188 kg	2.42 l/100 km (equiv)
ULSAB-AVC	C	ICE-G	933 kg	202 kg	4.40 l/100 km
VW Polo	B	ICE-G	1067 kg	231 kg	5.70 l/100 km
ULSAB-AVC _{BEV}	C	BEV simulation	1033 kg	214 kg	2.49 l/100 km (equiv)
VW Polo _{BEV}	B	BEV simulation	1167 kg	243 kg	2.62 l/100 km (equiv)

Table 18.3: FutureSteelVehicle BEV and benchmark vehicle Comparison

Vehicle	Material Production (kg CO ₂ e)	Use (kg CO ₂ e)	Recycling (kg CO ₂ e)	Vehicle Life (kg CO ₂ e)
FSV-BEV	2,337	13,844	(1009)	15,172
ULSAB-AVC	2,009	25,208	(841)	26,376
Polo V	2,603	32,655	(1124)	34,134
ULSAB-AVC _{BEV}	2,520	14,271	(1088)	15,703
VW Polo _{BEV}	2,847	15,044	(1229)	16,662

Table 18.4: Life Cycle Emissions Results from UCSB Advanced Powertrain Model (U.S. Grid)

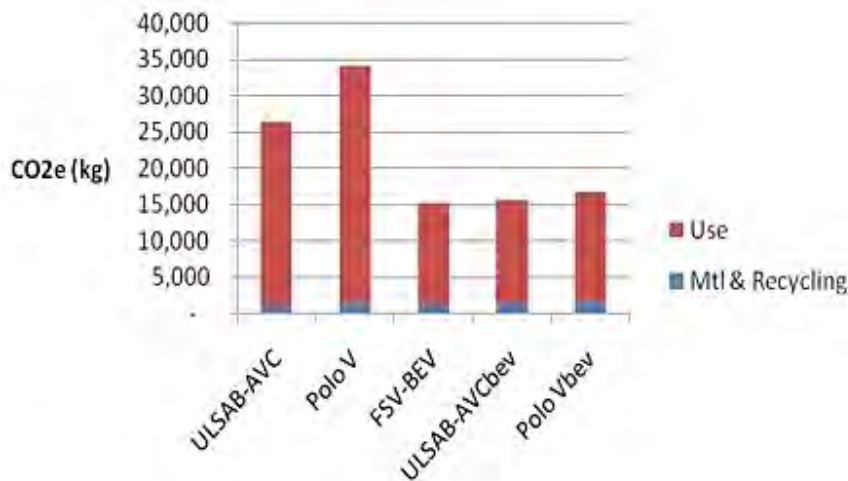


Figure 18.5: FSV BEV Life Cycle Emissions (U.S. Grid)

The tables and chart above are for BEV vehicles based on the U.S. electric grid. FutureSteelVehicle BEV resulted in the lowest vehicle life emissions profile, compared to the benchmark vehicles in this study.

A further comparison of FutureSteelVehicle - BEV for different geographic electricity grids was produced, and is shown in Figure 18.6. This clearly shows that the power source for electricity generation is key to meeting impending vehicle emissions regulations.

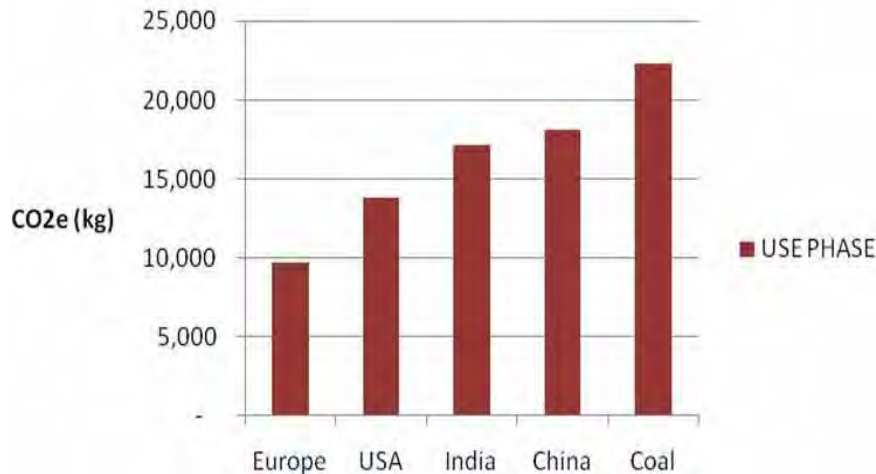


Figure 18.6: FSV BEV Use Phase Emissions - Various Electric Grids

Future LCA Work

The FutureSteelVehicle Life Cycle Assessment was conducted with the UCSB GHG Automotive Materials Comparison model, and is limited in its capability to assess all material and design contributions. An extension of this study would include a full vehicle analysis, where emissions contributions from all vehicle components, alternative body designs and materials could be evaluated and measured. Such a study would allow a comprehensive comparison of cost, mass and vehicle greenhouse gas emissions, and is recommended for automotive OEM's seeking low carbon footprint solutions. It is recommended that alternative body structure design options and material selections be compared on charts such as Figure 18.3. A full vehicle life cycle assessment will insure that the automotive industry develops a broader strategy to vehicle emissions reductions, beyond the present focus on light weighting only. As demonstrated in the FutureSteelVehicle UCSB modeling, only a strategy that evaluates emissions from all phases of a vehicle life will prevent unintended consequences.

18.3 Well-to-Pump Assessment

In addition to the evaluation of Life Cycle Assessment (LCA) during the initial selection of FSV sub-systems and evaluation of the complete FSV Body Structure final design LCA, the fuel cycles for FSV designs were compared to a conventional internal combustion engine reference vehicle. Fuel Cycle assessments included two segments - “Well-to-Pump” and “Pump-to-Wheel”.

Well-to-Pump assessment of possible FSV vehicle fuel sources were conducted in FSV Phase-1, using Argonne National Lab program “GREET 1.8B”. The assessment results are shown in Figure 18.7 and Figure 18.8. The fuels considered included:

- Electricity
- Gasoline and diesel from petroleum
- Bio-fuels, ethanol and bio-diesel
- Hydrogen (gas and liquid); using electrolysis process and from natural gas

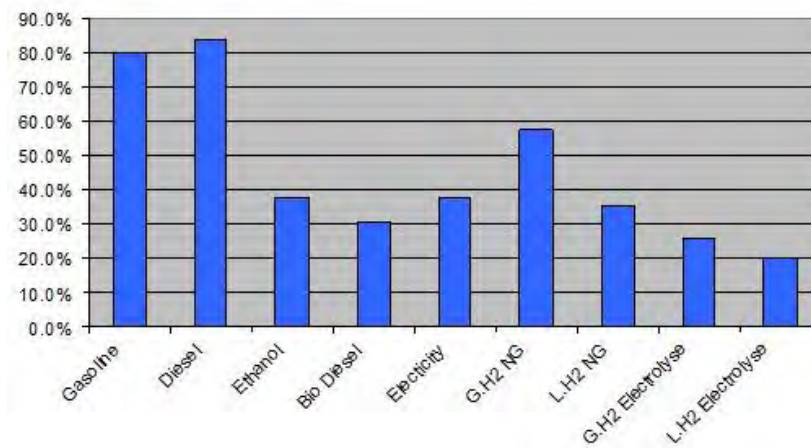


Figure 18.7: Well-to-Pump efficiency fuel production cycle (US)

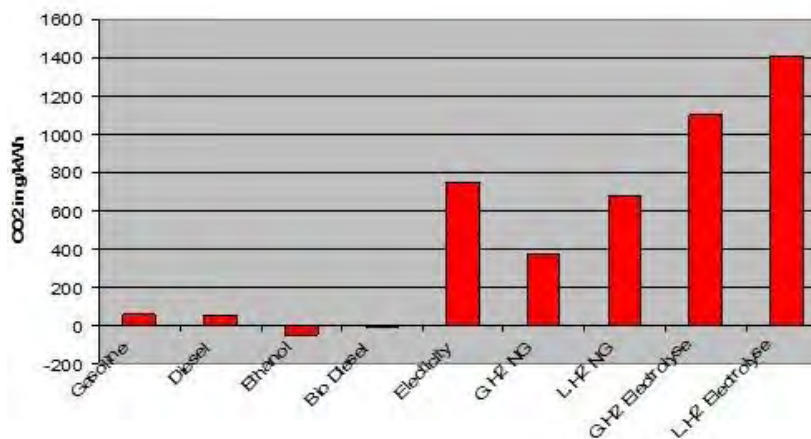


Figure 18.8: Well-to-Pump fuel production GHG CO₂e emissions (US)

18.4 Pump-to-Wheel Assessment-FSV

The FSV-1 pump-to-wheel CO₂e emissions are shown in Figure 18.9. The gasoline representative baseline vehicle shown in Figure 18.9 is a conventional vehicle with a gasoline powered internal combustion engine. For each PHEV, both Charge Sustaining (CS) and Charge Depleting (CD) all-electric driving modes are also shown. On a Pump-to-Wheel basis, all four FSV power-train variants will emit less than 95 g(CO₂)/km . The PHEVs and BEV produce zero CO₂e from the tailpipe when driven in all-electric mode.

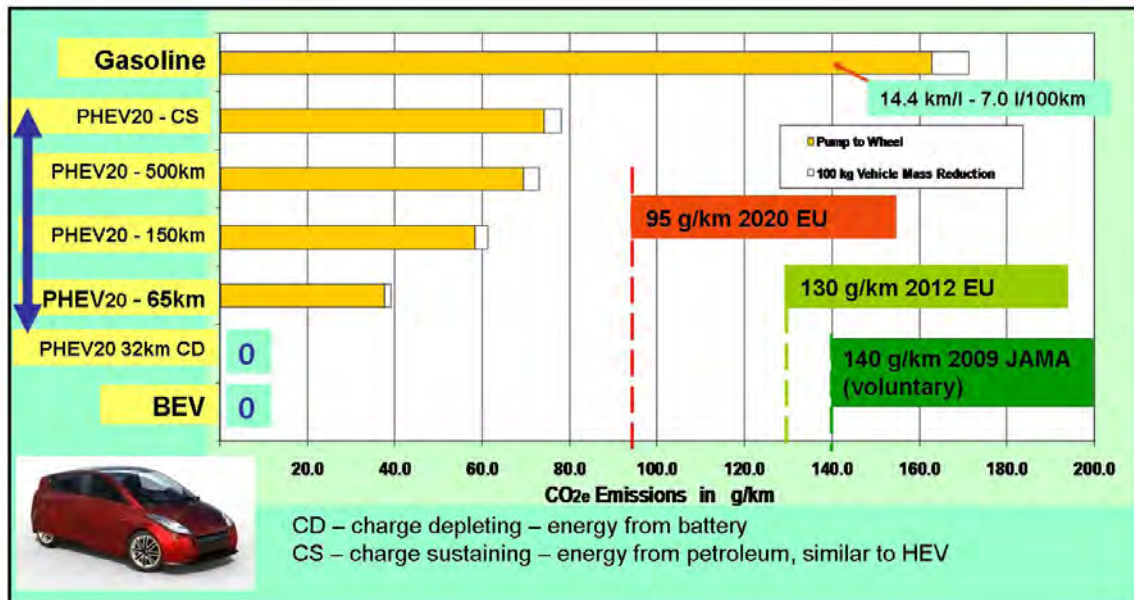


Figure 18.9: FSV-1 Pump-to-Wheel CO₂e emissions g/km (UDDS)

18.5 FSV-1 Well-to-Wheel CO₂e Emissions

As mentioned earlier, there are cumulative CO₂e emissions from the production of fossil fuels, renewable fuel, or electricity. So a Well-to-Wheel analysis is very important for a comprehensive evaluation of vehicle emissions. Adding the Well-to-Pump emissions factor to each vehicle, the Well-to-Wheel CO₂e emissions are attained, as shown in Figure 18.10.

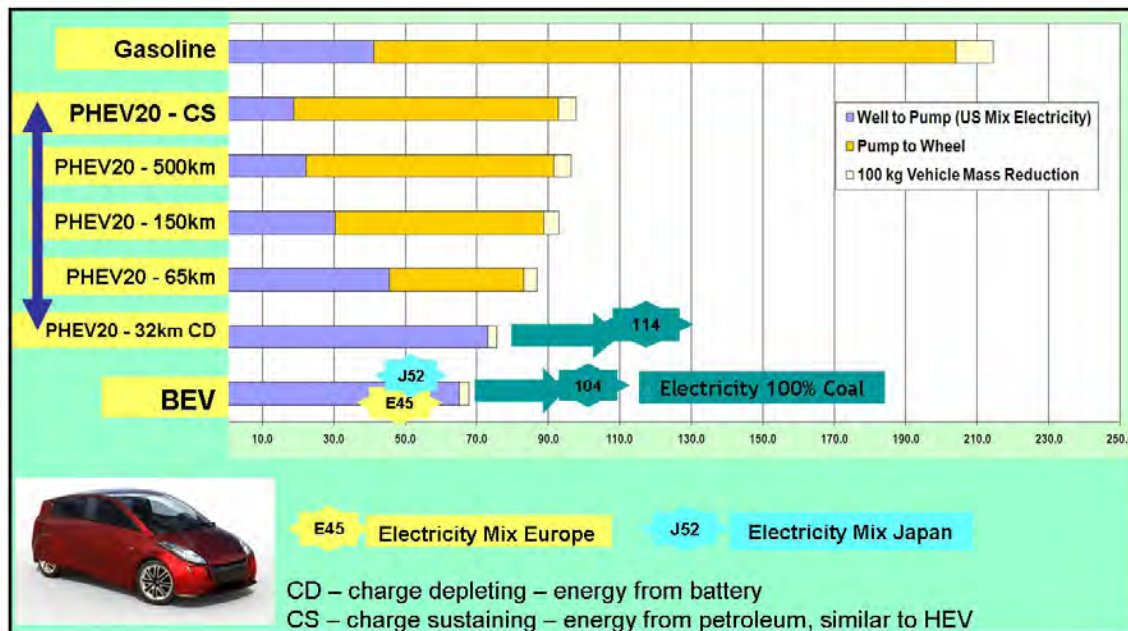
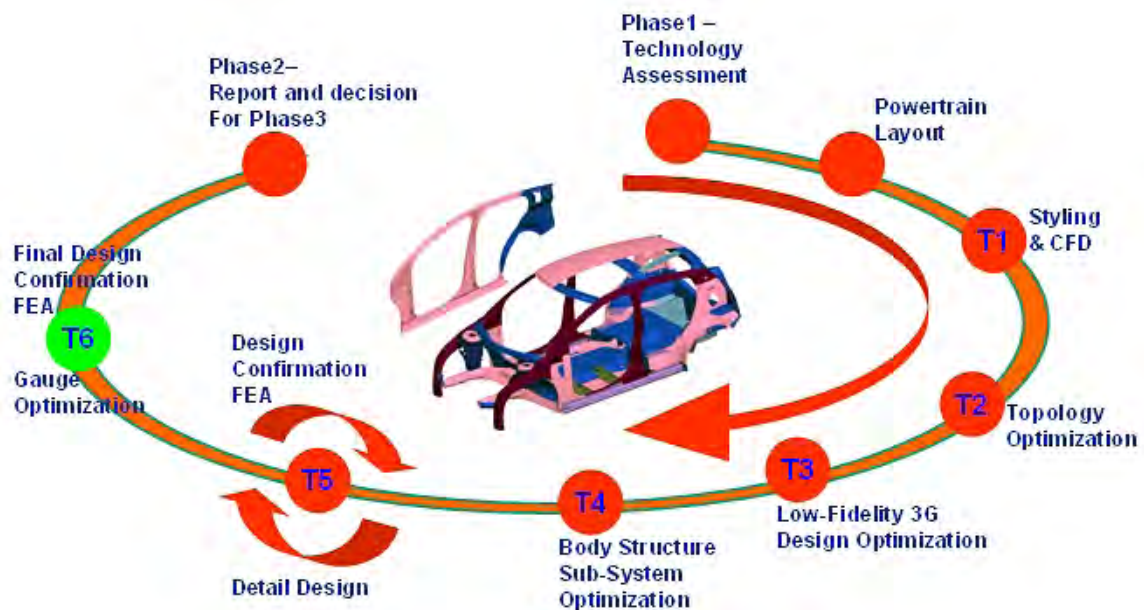


Figure 18.10: FSV-1 Well-to-Wheel CO₂e emissions g/km (UDDS)

It can be observed from Figure 18.10 that, the PHEV in Charge Depleting all-electric mode, and the BEV have zero tailpipe CO₂e emissions. However, their carbon footprint is not zero due to emissions from the production of fuel.

19.0 2G Full System Design Optimization and Bead Optimization



This chapter addresses partial fulfillment of the FSV (Future Steel Vehicle) Task 5 2G (Gauge and Grade) Full System Optimization. Its purpose is to document the development of the optimization process and design changes due to sub-system manufacturing process selections based on the T4 sub-system optimization (detail shape, material and gauge selections of the optimized sub-systems considered). The T5 optimization process was completed by ETA.

19.1 2G (Grade and Gauge) Full System Design Optimization

19.1.1 Objective

The objective is to apply a 2G (grade and gauge), optimization process to the FSV full system vehicle which was designed based on the results of the High Fidelity 3G vehicle structural sub-system optimization. These results established the best combination of material grade, gauge, geometry and manufacturing process for the dominant vehicle sub-systems. The sub-system

solutions were selected based on cost, weight and LCA (Life Cycle Assessment for CO₂). The full system vehicle includes updated packaging and detailed component designs for sub-systems such as the front end system (front rail, shotgun and cradle) and rear end system (rear rail, rear suspension trailing arm and battery protection cover). The challenge was to maintain the design directions provided by the optimization while updating the design to a full and complete production level design. Due to these changes, the full system body structure will naturally become heavier. However, the T5 optimization objective is to maintain the performance and reduce the mass of the full vehicle system (body structure), back to the overall vehicle mass target.

The major portion of this design and development process was validated by the FSV Pilot Project (FSV Pilot Project report). The 2G optimization process follows the same procedure as was applied to the 3G (**G**eometry, **G**rade & **G**auge), optimization process in the following previous tasks: T3 Low Fidelity 3G Optimization and T4 High Fidelity 3G Sub-System Optimization. The FSV program will track the major load paths that govern Front NCAP, Front ODB, Rear ODB, IIHS Side, Pole Impacts, Roof Crush and Bending and Torsional Stiffness performance. This will provide the final gauge and grade selection for the load path sub-systems and major panels.

19.1.2 T5 Optimization Methodology Overview

The goal of T5 optimization is to use the optimized primary sub-systems as enablers for the whole body structure to lose mass, specifically in the components that are not taking significant loading such as the large panels. In order to achieve a comprehensive design solution, it is crucial to provide such enablers for the body structure to reach the mass targets. Thus based on prior optimization experience, it is necessary to define a set of appropriate design variables (grade and gauge), for the optimization to work with. For the optimization to work as effectively as possible, it is also necessary to use its resources (time and CPU), as efficiently as possible. Thus a set of coarsened optimization models were created and calibrated which, though were less than 50% of the size of the original models, maintained their original performance. Analysis time of the individual loadcases were also reduced by reducing their total run times.

The basic steps for the gauge and grade (2G) optimization are as follows:

- Coarsen the model for optimization and performance correlation between the fine mesh and coarsened model
- Establish a baseline performance before optimization based on the T5 baseline FE model (One Million element model size)
- Update the model with any design recommendations and improvement (such as joints or load path)
- Establish a manufacturable load path strategy for side and pole impact
- Ensure the optimization load path is maintained throughout the design changes and adopting all new sub-systems
- Optimization setup and testing
- T5 Optimization
- Evaluate potential optimization solutions that meet performance, mass or both during the process

T5 optimization load cases considered:

- NCAP Frontal Impact
- IIHS Front Crash 40% Offset Deformable Barrier (ODB)
- FMVSS 301 Rear Impact (70% ODB)
- IIHS Side Impact
- FMVSS 216 Roof Crush
- Torsional Static Stiffness

Not all load cases are used for optimization since it was found that the design was not controlled by every load case.

Prior optimization loadcases that were not considered for the T5 Optimization:

- FMVSS 214 Pole Impact: This loadcase was not considered for the T5 optimization since the solution can be achieved very easily based on load path optimization
- Bending Stiffness: Again, this loadcase was not used since the performance is usually very easy to achieve

Figure 19.1 below summarizes the steps in the T5 process.

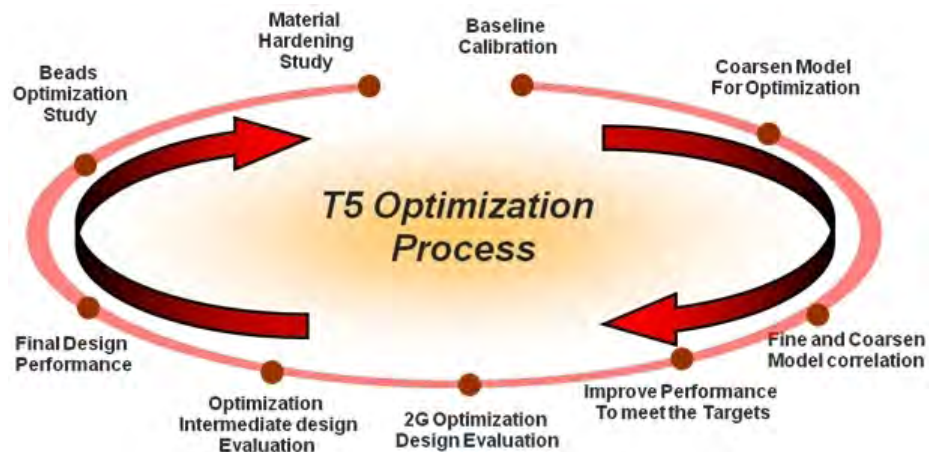


Figure 19.1: T5 optimization process

19.1.3 T5 Base and Optimization Model Evaluations

The T5 base model was developed from selected T4 sub-system models. The full system model has much greater refinement and detail than the first full system model created for the project, the T3 LF3G model. A direct comparison between the T3 LF3G and T5 full system model is shown in Figure 19.2, Figure 19.3 and Figure 19.4.

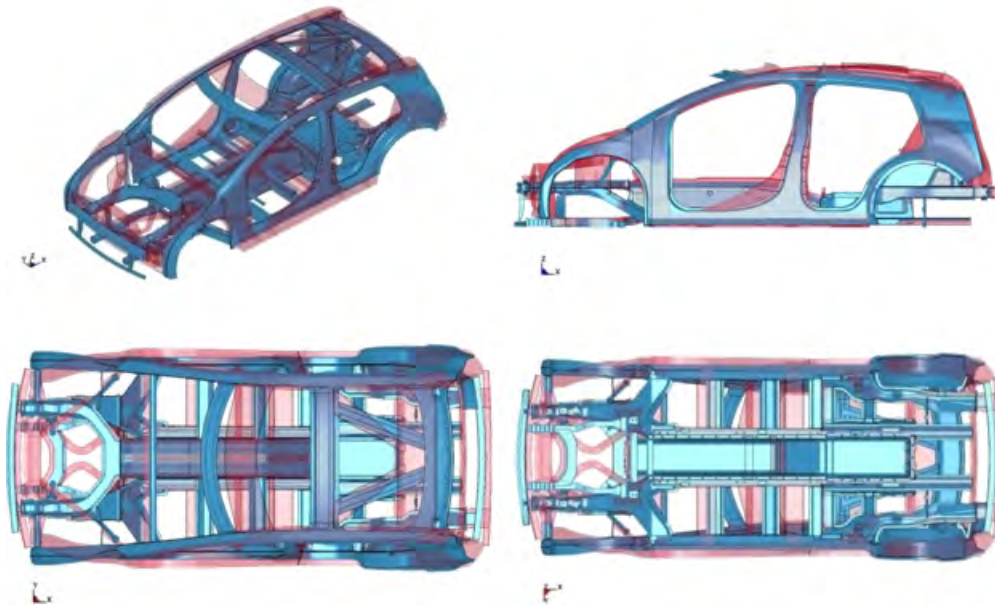


Figure 19.2: LF3G model (Red) and T5 base model(Blue)

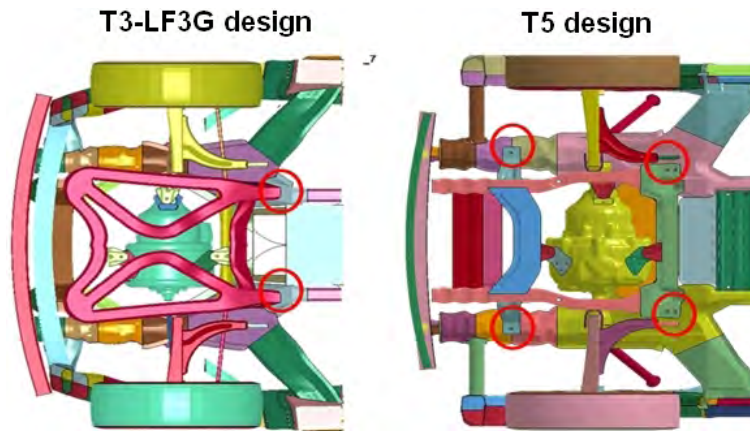


Figure 19.3: T3 LF3G model and T5 base model comparison

The T3 optimization model did not fully define the powertrain components to allow package space flexibility for the body structure. The T5 design and optimization model required all components to be defined which includes the components shown in Figure 19.4.

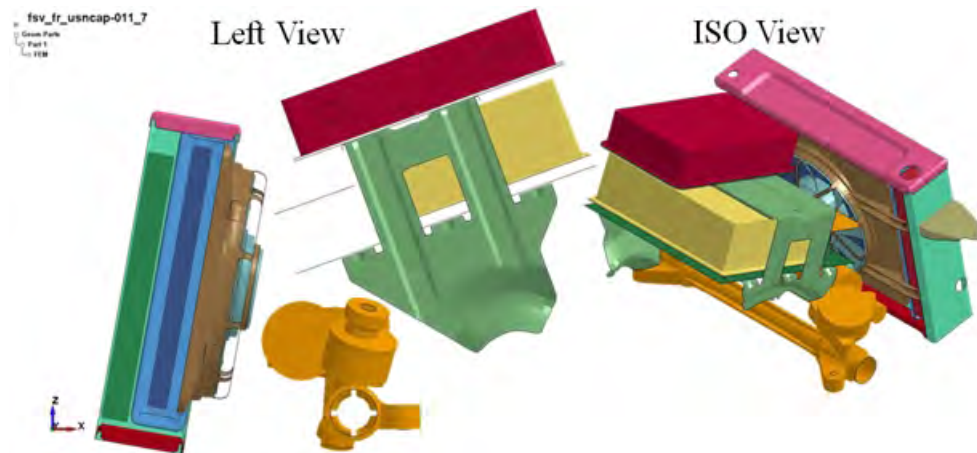


Figure 19.4: T5 base model engine room additional new components as compared to the LF3G Model

19.1.4 T5 Base Model Coarsening and Baseline Performance Evaluation

The T5 base model contains about 1,000,000 elements. The model was coarsened by using a detailed modeling scheme which maintained the fine mesh in the load path areas while using larger elements (approximately 20 mm and larger), in the panels. Components such as the radiator, electric motor and its controller, which define the front end stack-up and provide a distributed vehicle mass, were also coarsened (See Figure 19.5). The purpose of the model coarsening was to reduce the analysis time for each loadcase and thus enable the optimization to perform more design evaluations within the time allowed. Thus the goal of the coarsening work was to reduce the model size to 500,000 elements (50% less than original size).

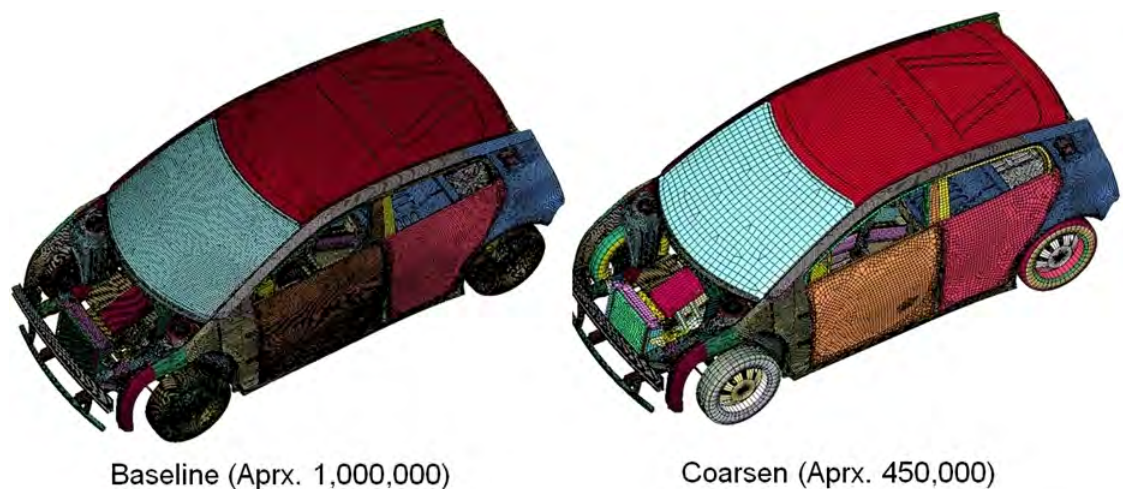


Figure 19.5: T5 base model and optimization base model (Coarsen)

Baseline model calibration

The first task was to calibrate the performance of the fine mesh model for all load cases. Figure 19.6 shows the T5 design front crash NCAP base model comparison with the T3 (LF3G) performance vehicle pulse.

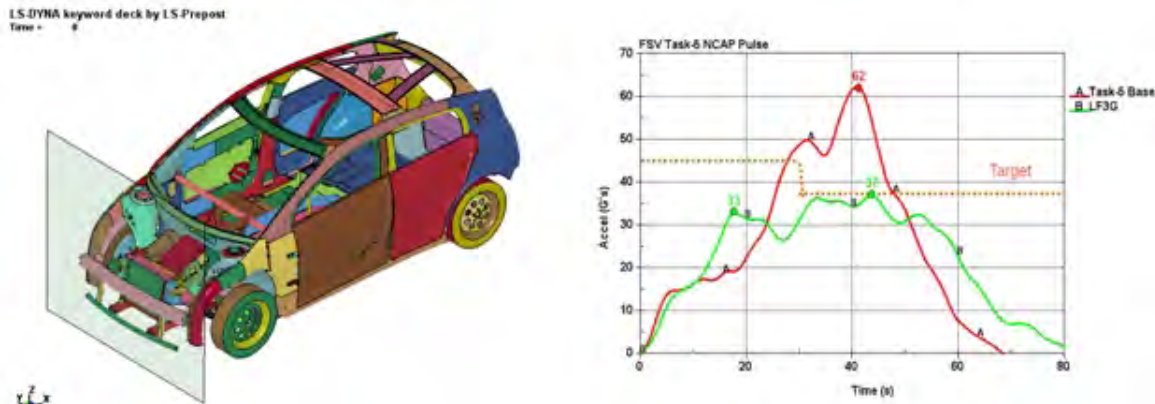


Figure 19.6: *NCAP pulse*

The curves above compare the vehicle pulse of the baseline T5 model in red with a high peak pulse of 62 g's and an average of 55 g's. The LF3G pulse is in green with 37 g's maximum and 36 g's average. The pulse as shown is very different from the LF3G pulse shown in green. The LF3G pulse at 20 msec is higher than the T5 pulse, which indicates that there is more energy absorption and hence, less crush in the front end (space and material). This causes a higher pulse in the stack-up at 40 msec and a narrower curve (earlier time to zero velocity of 65 msec). After careful investigation of the performance differences in the front NCAP pulses, the following were found to be the reasons for the performance disparities:

- Front-end packaging changes due to a more mature design, which included a more detailed and complex definition of the front-end engine. Figure 19.2, Figure 19.3 and Figure 19.4 shows the overview of changes that takes place from the LF3G model to the T5 model. Specifically, these changes are:

- Front end bumper assembly and connection to Shotgun - (Refer to Figure 19.2 through Figure 19.4)
- Cradle design, shapes and its mount to the Front Longitudinal Rail - (Refer to Figure 19.2 through Figure 19.4)
- Detail representation of radiator assembly and electric motor control box which was not included in the LF3G model
- Steering column location. This was behind the electric motor in the LF3G model

We revised the vehicle NCAP target pulse to 45 g's, hence allowing T5 optimization to restore the vehicle pulse as close as possible to the LF3G model.

It was found that pulse reduction from 62 g's to the target of 37 g's requires front end packaging and design changes. This could not be achieved by optimization, hence the target pulse was increased to 45 g's so optimization can reach the design targets within program timing.

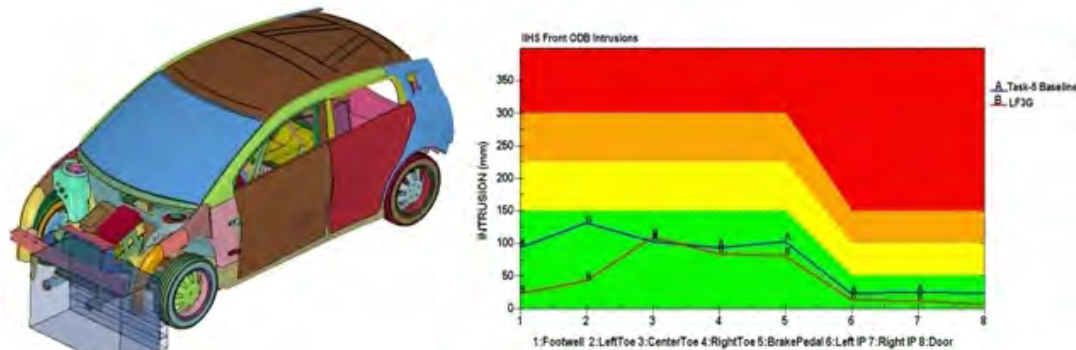


Figure 19.7: IIHS ODB Front Crash

As seen in Figure 19.7, the IIHS ODB frontal impact shows very good results. The IIHS measurements are in the green zone. This curve indicates that even though the IIHS measurement performance was degraded due to the above changes from LF3G model, the integrity of the load path still exists.

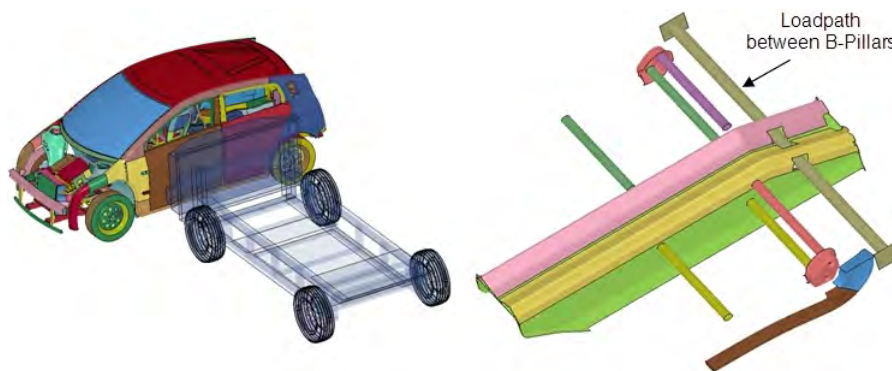


Figure 19.8: IIHS Side Impact load path development

The LF3G model has very good IIHS side performance due to the very effective load path between the B-pillars as shown in Figure 19.8. Due to packaging restrictions based on allowing sufficient legroom, we successfully revised the strategy developed for the FGPC project. ETA and EDAG worked together in the development of a new concept that used the seat structure and door as the load path. Great care was taken to assure that the loadpath was maintained for all possible combinations of seat positions for both the driver and front seat passenger. The revised loadpath concept provided sufficient performance to exceed the original targets.

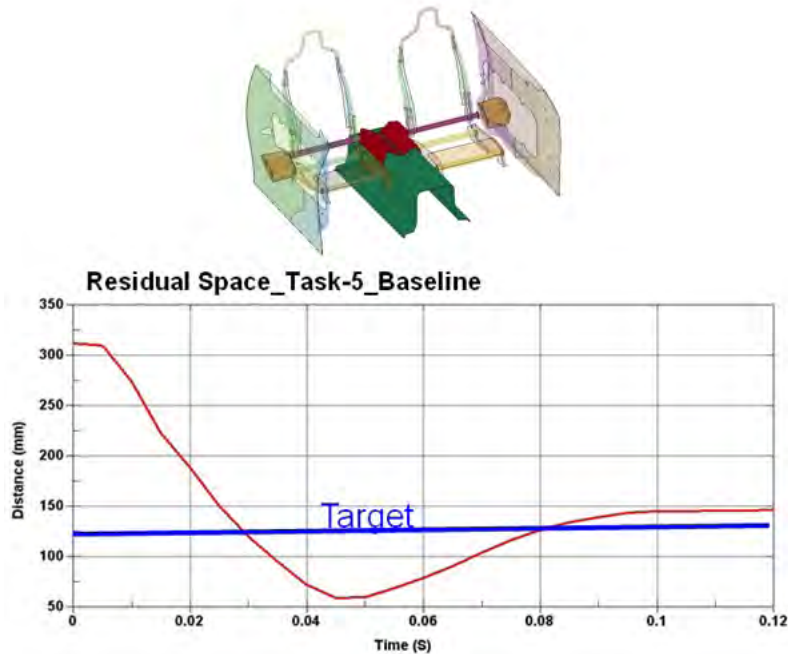


Figure 19.9: IIHS Side Impact load path and performance

Figure 19.9 shows the new seat system load path through the cross car seat member, connecting the body, side to side. The cross car seat member is loaded through the B-pillar when the front seats is in the rear most position, and by the door when the front seats are in the full forward position. The maximum survivable space at 120 msec after rebound is 150 mm, which is 25 mm better than the 125 mm IIHS targets.

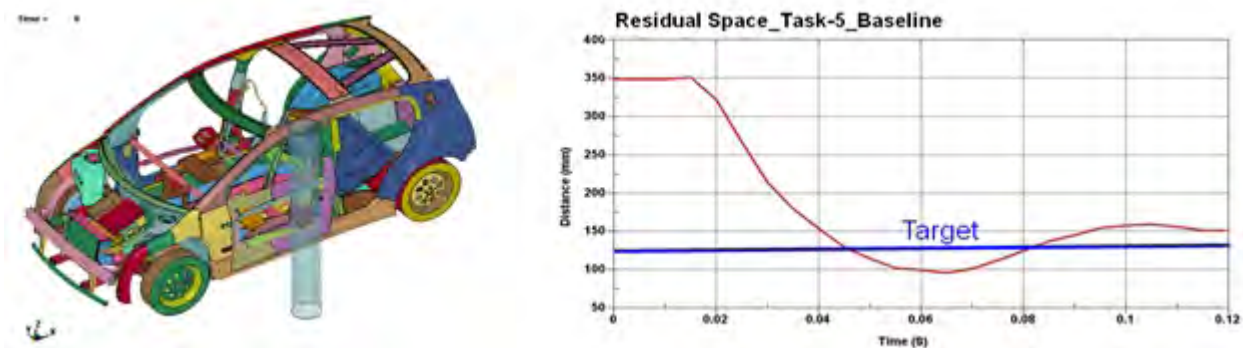


Figure 19.10: FMVSS 214 New - Pole Side Impact Performance

The pole impact results shown in Figure 19.10 indicates that the combination of side impact and underbody load paths (cross members), is very effective in meeting the side pole impact targets. The survival space measuring point is the maximum intruded point on the driver side's door belt line.

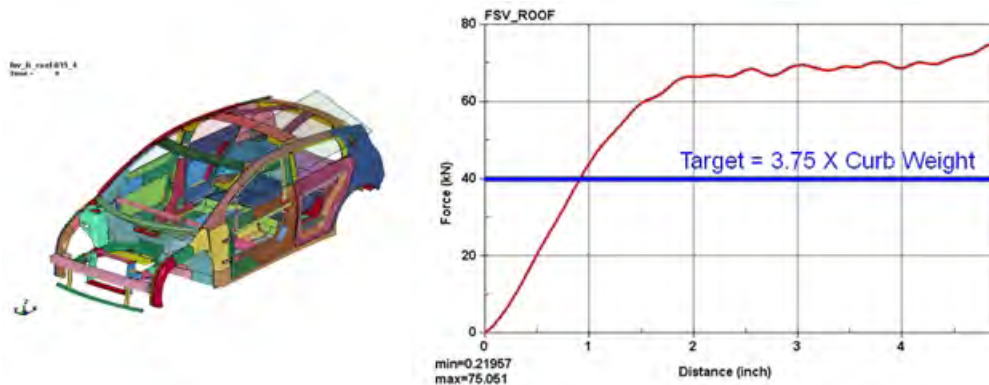


Figure 19.11: FMVSS 216 and IIHS Roof Crush performance

Referring to Figure 19.11, the T5 vehicle design model has kept its integrity through the design changes and its performance is well above the targets.

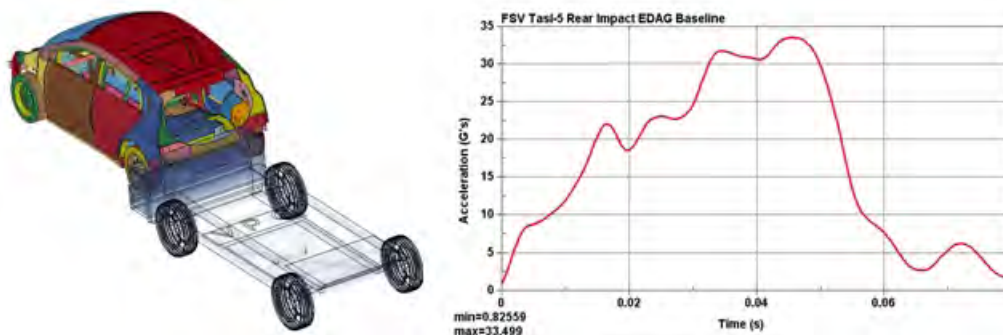


Figure 19.12: FMVSS 301 Rear Impact performance

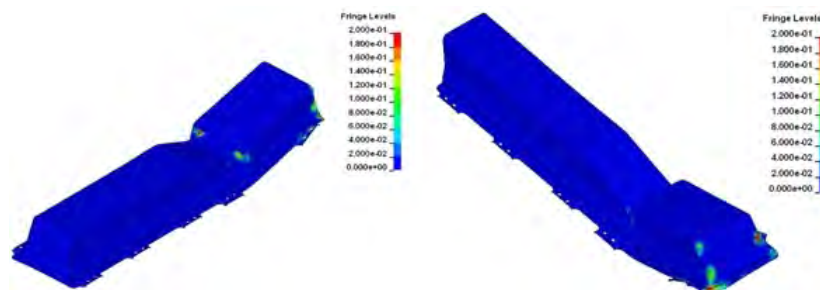


Figure 19.13: FMVSS 301 Rear Impact performance-2

As shown above in Figure 19.12, the T5 vehicle design pulse meets the new FMVSS 301 rear impact crash target of 35 g's at 56 $\frac{\text{km}}{\text{h}}$ - 75% barrier impact. Another rear impact consideration we investigated is the integrity of the battery after a rear impact crash. The battery cells are packed into two locations in the tunnel and rear end above the axles. There is a cavity in the battery pack that provides room in the passenger compartment (Figure 19.13). The battery pack has a

tendency of bending at the cavity during a crash. Also, the original design (Figure 19.13) does not contain very strong joints in location 1. Even though the results show the plastic strain in the battery pack is very low and the bending will not cause any damage to the battery, a new joint was designed to improve the rear crash performance and reduce the bending in locations 1 and 2 which reduces the plastic strain. See Figure 19.14.



Figure 19.14: Battery pack before and after rear crash of original design

Another area that needed improvement was the load path through the door structure. The upper door impact beam location in the rear doors was too high and was not able to take the loads from the C-pillar which caused more rear door intrusion. The inboard end attachment point of the rear door impact beams were lowered to improve the ability of the rear door to open after a side impact. See Figure 19.15.

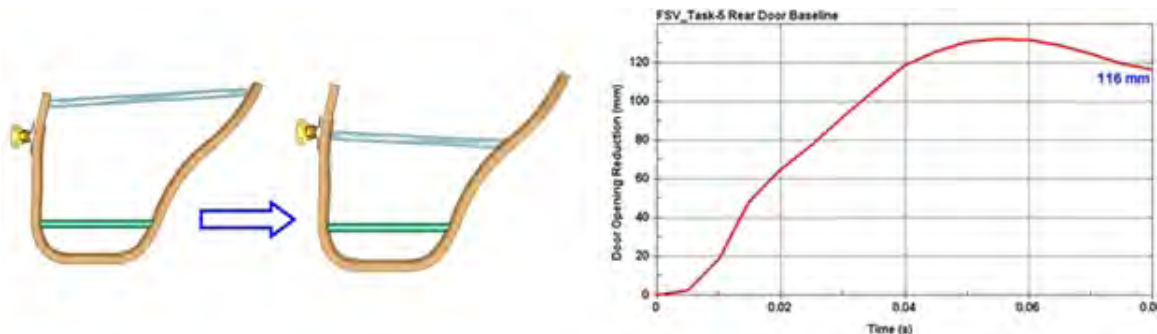


Figure 19.15: Rear Door Load Path and Rear Door Intrusion

Finally, the last optimization load case that is critical to meeting the mass and design targets is the torsional stiffness. The torsional stiffness performance using LS-DYNA is the explicit target of 12,000 N.m/deg and using NASTRAN, the target is 20,000 N.m/deg. The difference between the LS-DYNA and NASTRAN numbers is due to the nature of each analysis. NASTRAN ran using static loading and LS-DYNA ran using dynamic (quasi-static), loading. This decision was made to simplify the optimization process, using only one solver (LS-DYNA). The performance of the vehicle baseline design is approximately 11,244 N.m/deg, which is less than the 12,000 N.m/deg target, but close enough that optimization and design enhancements can improve the performance. See Figure 19.16.

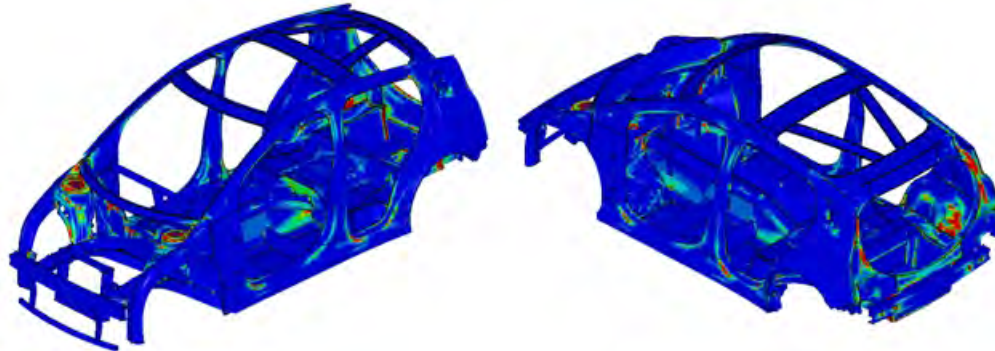


Figure 19.16: *Torsional stiffness strain energy plots*

Based on the baseline vehicle design evaluation, we found that there are a few areas that require design modifications in order to meet the performance targets. In the case of a rear impact, there are no deficiencies in the performance of the structure, and battery damage was minimal. However, the load paths and joints were modified to improve the performance with a minor mass penalty, thus enabling additional mass reduction.

In the case of IIHS side impact, the design and optimization team developed a load path that exceeded the performance target. In the case of frontal ODB impacts and roof crush, the base vehicle meets all targets. However, the frontal impact NCAP pulse was too high at stack-up. After detailed observations, it was determined that all changes and modifications to the LF3G design that were reviewed previously, contributed to the new higher pulse.

19.1.5 Correlation of Baseline Model and Coarse Model (Optimization Model)

ETA created a coarse model with less than 500,000 elements to enable the T5 optimization process to go faster and allow for more design to be considered during the process. The comparison of results between fine and coarse models for all crash load cases were very close and in some cases within 5%. All the major load path areas like front rail, shotgun, B-pillar, rocker, etc, were not coarsened. Final optimization results produced from the coarse model were used in the final fine T5 model and the performances were all within the T5 vehicle targets.

19.1.6 T5 2G (Grade and Gauge) Optimization Process

The optimization process starts with following steps:

- Identify all the components that were optimized and then redesigned in the T4 optimization, and identify all the parts, such as panels that were not included in the LF3G optimization. The components that are within optimization are not the only parts that are included in the body structure. Parts that can enable us to increase the vehicle performance and are not part of body structure, also are included in this optimization. For example, the battery tray, front bumpers and cradle
- Define a range of grades and gauges for each component in the body structure of the vehicle. Use the base grade and gauge of the T4 optimization and evaluate the manufacturing process that could be applicable for the specific components
- Perform one-step simulation for the proposed manufacturing
- Debug the optimization process, software interaction and fix what is required in detail in the process

(Table of design variables and ranges)

Number of design variables: 92				
	#	MIN	Base	MAX
Dash_Driver_Toepan_400	1	0.50	0.55	0.60
Dash_Driver_Wall_401	2	0.40	0.45	0.50
Frt_Floor_Outer_Wings_402	3	0.40	0.50	0.60
Frt_Floor_Middle_403	4	0.50	0.65	0.80
Frt_Rail_Trans_Rail_404	5	1.20	1.40	1.60
Rr_Liftgate_Low_Top_405	6	0.40	0.60	0.80
Fram_Rail_Rr_Outer_406	7	0.50	0.75	1.00
Fram_Rail_Rr_Mid2_408	8	0.60	0.80	1.00
Seat_pan_Rr_Sides_409	9	0.60	0.90	1.20
Seat_pan_Rr_Mid_410	10	0.40	0.50	0.60
Wheelhouse_Outer_411	11	0.80	1.00	1.20
Wheelhouse_Inner_412	12	0.60	0.65	0.70
Back_Panel_Corner_Outer_413	13	1.00	1.50	2.00
Back_Panel_Lower_414	14	0.40	0.55	0.70
Shotgun_Inner_Frt_415	15	1.35	1.60	2.00
Shotgun_Inner_Mid_416	16	1.20	1.70	2.20
Shotgun_Inner_Rr_417	17	1.30	1.65	2.00
Tunnel_Frt_and_Back_418	18	0.50	0.65	0.80
Tunnel_Mid_419	19	0.35	0.40	0.50
Tunnel_Reinf_Frt_and_Back_420	20	0.50	0.75	1.00
Tunnel_Feinf_Mid_407	21	0.50	0.75	1.00
Xmem_Bat_Sus_Inner_421	22	0.60	0.80	1.00
Wheelhouse_Reinf_422	23	0.60	0.70	0.85
Shotgun_Outer_Frt_423	24	1.35	1.60	2.00
Shotgun_Outer_Mid_424	25	1.20	1.70	2.20
Shotgun_Outer_Rr_425	26	1.30	1.60	2.00
Cowl_Lower_426	27	0.40	0.50	0.60
Battery_Close_Inner_Outer_427	28	0.50	0.65	0.80
Rr_Gusset_428	29	0.60	0.80	1.00
Xmem_Frt_Seat_Frt_429	30	0.50	0.75	1.00
Xmem_Frt_Seat_Rr_430	31	0.50	0.75	1.00
Heel_Board_431	32	0.60	0.70	1.00
Rail_Exten_Tunnel_Inner_432	33	0.60	1.00	1.40
Rail_Exten_Tunnel_Outer_433	34	0.60	0.90	1.20
Fram_Rail_Rein_Rr_Outer_434	35	0.50	0.75	1.00
Fram_Rail_Rein_Rr_Inner_436	36	0.60	0.80	1.00
Frt_Rail_Lower_Outer_437	37	0.80	1.35	1.90
Frt_Rail_Lower_Mid1_438	38	0.80	1.35	1.90
Frt_Rail_Lower_Mid2_439	39	0.80	1.35	1.90
Frt_Rail_Lower_Rr_Inner_440	40	0.80	1.35	1.90
Frt_Rail_Lower_Rr_Outer_441	41	0.80	1.35	1.90
Frt_Rail_Upper_Outer_442	42	0.80	1.35	1.90
Frt_Rail_Upper_Mid1_443	43	0.80	1.35	1.90
Frt_Rail_Upper_Mid2_444	44	0.80	1.35	1.90
Frt_Rail_Upper_Inner_445	45	0.80	1.35	1.90
Closeout_Upper_Rail_446	46	0.80	1.20	2.00

Table 19.1: Table of Design variables and ranges

Number of design variables: 92				
	#	MIN	Base	MAX
Closeout_Lower_Rail_447	47	0.80	1.20	2.00
Rail_Side_to_Side_448	48	0.60	0.80	1.00
APill_Brace_449	49	0.50	0.85	1.20
Back_Panel_Corner_Inner_450	50	1.00	1.50	2.00
Rear_Cargo_Box_451	51	0.40	0.70	1.00
Rr_Header_452	52	0.40	0.50	0.60
Rr_Header_Main_453	53	0.40	0.55	0.70
Rr_Header_Corners_454	54	1.00	1.50	2.00
Roof_Supp_455	55	0.35	0.43	0.50
Roof_Panel_456	56	0.50	0.55	0.60
Roof_Bow_457	57	0.50	0.55	0.60
Bodyside_Out_Roc_458	58	0.60	0.70	0.80
Bodyside_Out_BPill_459	59	0.60	0.70	0.95
Bodyside_Out_Hinge_Pill_460	60	0.80	1.20	1.60
Bodyside_Out_Roof_461	61	0.80	1.00	1.25
Bodyside_Out_Rr_Quart_462	62	0.60	0.70	0.80
CPill_Inner_463	63	0.60	0.70	0.80
BPill_Inner_Top_464	64	0.80	1.20	1.20
BPill_Inner_Mid1_465	65	0.60	0.80	1.00
BPill_Inner_Mid2_466	66	0.80	1.00	1.50
BPill_Inner_Bot_467	67	0.60	0.80	1.00
Roof_Rail_Reinf_468	68	0.60	0.65	0.70
Roof_Rail_Inner_Frt_469	69	0.60	0.70	0.80
BPill_Reinf_Top_470	70	0.60	0.80	1.00
BPill_Reinf_Mid1_471	71	0.80	1.05	1.30
BPill_Reinf_Bot_472	72	0.60	0.80	1.00
Hinge_Pill_Inner_473	73	0.60	0.90	1.20
Rocker_Inner_474	74	0.80	1.10	1.40
Rocker_Outer_475	75	0.80	1.10	1.40
Cradle_Frt_476	76	0.80	1.35	1.90
Cradle_Back_477	77	0.80	1.10	1.40
Trailing_Arm_478	78	2.00	2.50	3.00
Door_Reinf_and_Beams_479	79	1.50	1.70	2.00
Seat_Beam_480	80	1.00	1.30	1.50
Battery_Tray_481	81	0.80	1.80	2.30
Bumper_Beams_482	82	0.60	0.80	1.20
Material Choices		MAT-1	MAT-2	MAT-3
MAT_Frt_Rail_Lower_Outer_437	83	DP300/500	DP500/800	DP700/1000
MAT_Frt_Rail_Lower_Mid1_438	84	DP300/500	DP500/800	DP700/1000
MAT_Frt_Rail_Lower_Mid2_439	85	DP300/500	DP500/800	DP700/1000
MAT_Frt_Rail_Lower_Rr_Inner_440	86	DP300/500	DP500/800	DP700/1000
MAT_Frt_Rail_Lower_Rr_Outer_441	87	DP300/500	DP500/800	DP700/1000
MAT_Frt_Rail_Upper_Outer_442	88	DP300/500	DP500/800	DP700/1000
MAT_Frt_Rail_Upper_Mid1_443	89	DP300/500	DP500/800	DP700/1000
MAT_Frt_Rail_Upper_Mid2_444	90	DP300/500	DP500/800	DP700/1000
MAT_Frt_Rail_Upper_Inner_445	91	DP300/500	DP500/800	DP700/1000
MAT_Cradle_Frt_476	92	DP300/500	DP500/800	DP700/1000

Table 19.2: *Table of Design variables and ranges - continued*

The T5 optimization used 92 design variables (See Table 19.1 and Table 19.2). The first step of optimization methodology is to perform a sensitivity analysis based on the design variables that are available to the optimization. After this step, it will run 100's of design evaluations. During this phase of the optimization, ETA follows the performance of designs even if they are not truly feasible designs. By reviewing these, ETA can gain an understanding for the overall sensitivities and gain an appreciation of the controlling loadcases. For example, in the case of the NCAP frontal impact crash and torsional load cases, the baseline did not meet the targets, therefore it is important to watch these load cases closely and see what changes the design may need beyond grades and gauges.

This is especially important because the original vehicle performance was based on the LF3G model. However, as the design has evolved there have been many significant changes to the vehicle's packaging, especially in the front-end structure, which has impacted the performance of the T5 model.

The T5 optimization has two objectives. The first objective is to reestablish the performance of the design concept. The second objective is to reduce its overall mass. The following section will review some of the major designs that the optimization has identified.

19.1.7 Intermediate Designs Observations

The optimization strategy is to meet the performance as a first priority, then reducing mass to satisfy the objective. Several intermediate designs are selected to show this strategy. In the first 200 designs produced, only 10-15 were feasible, after 200 designs, the number of feasible solutions increased to 55. This elaborates that optimization has located the local area of an optimum solution and hence, starts to reduce the mass.

See Table 19.17 below for the intermediate design results summary table: Green (meets targets), Yellow (border line) and Red (did not meet targets).

DESIGN	M (BW)	DIFF.	% REDUC.	NCAP	ODB	SIDE	ROOF	REAR	TORSION
Baseline	203.7	N/A	N/A	Red	Green	Green	Green	Yellow	Green
37	196.4	7.3	3.7	Yellow	Green	Green	Green	Yellow	Green
74	197.3	6.4	3.2	Green	Green	Green	Green	Green	Green
83	186.4	17.3	9.3	Red	Green	Yellow	Green	Yellow	Yellow
145	199.3	4.4	2.2	Green	Green	Green	Green	Green	Green
196	203.3	-0.4	-0.2	Green	Green	Green	Green	Green	Green
302	188.8	14.9	7.9	Green	Green	Green	Green	Green	Green
336	188	15.7	8.4	Green	Green	Green	Green	Green	Green

Figure 19.17: Intermediate design results summary table

19.1.7.1 Design #37

This is an early design while design sensitivity analysis was taking place, establishing the strength and weakness of the overall design concept. See Figure 19.18 below.

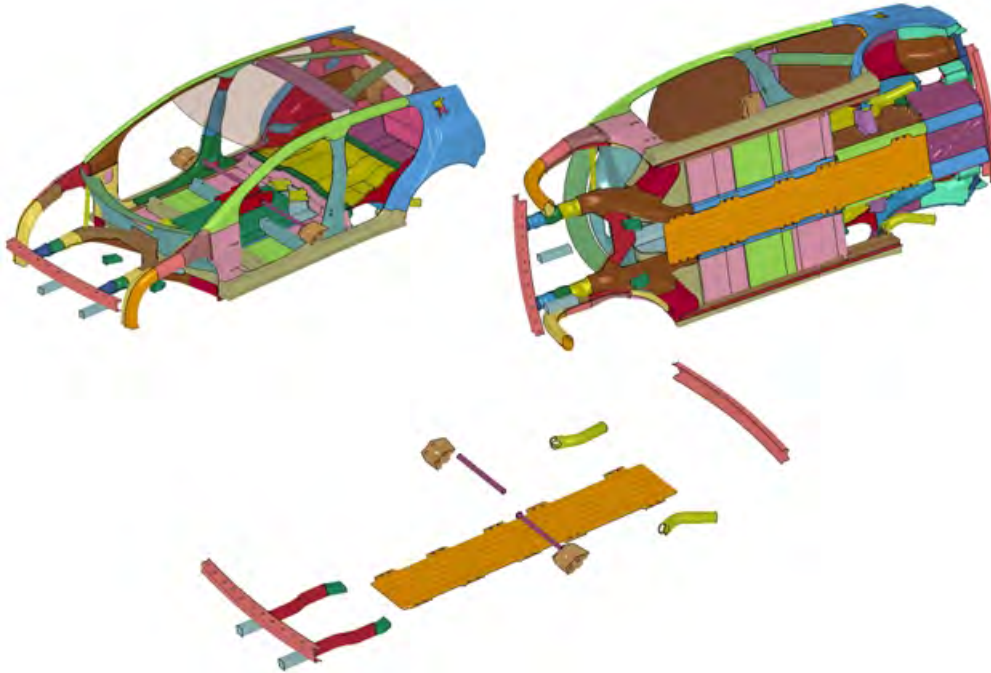


Figure 19.18: *Design #37 models and parts that were included in the optimization*

Baseline Mass = 213.7 kg

Optimized Design #37 = 199.5 kg

Current Mass Savings = 14.2 kg (6.6%)

Optimized Design #37 Body Structure = 196.4 kg

The vehicle baseline mass in the LS-DYNA model as a reference point is 213.7 kg. This may be different than the actual vehicle mass at different stages of the project. The second line is the total optimized mass, which includes components that are not part of the body structure such as the bumper and battery tray. See Figure 19.19 for vehicle Design #37 NCAP pulse and Figure 19.20 for the ODB IIHS frontal impact crash measurements, below.

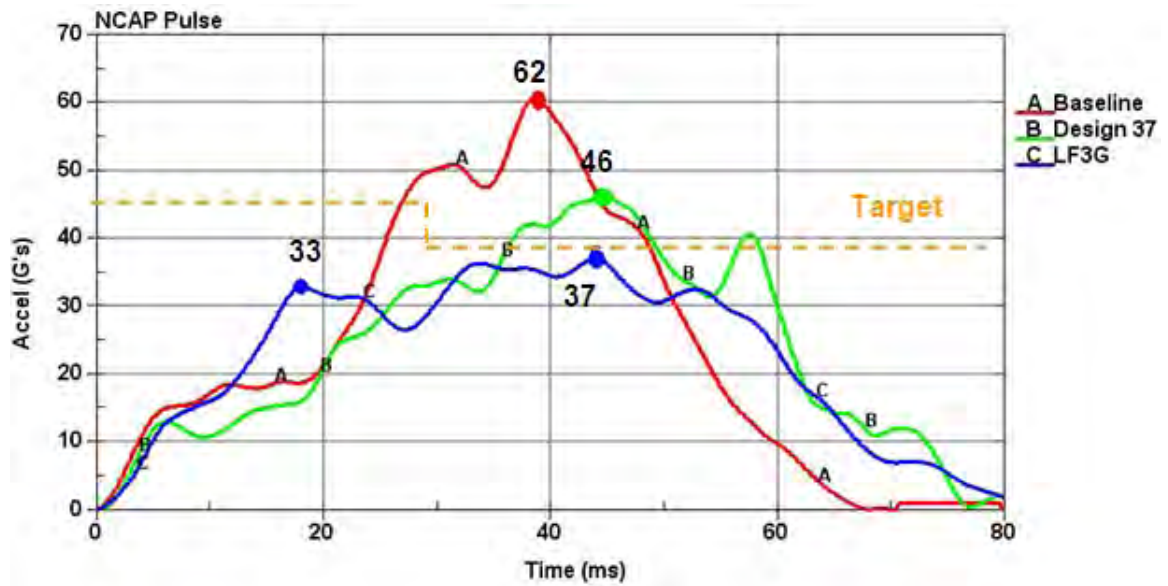


Figure 19.19: Design #37 vehicle NCAP pulse

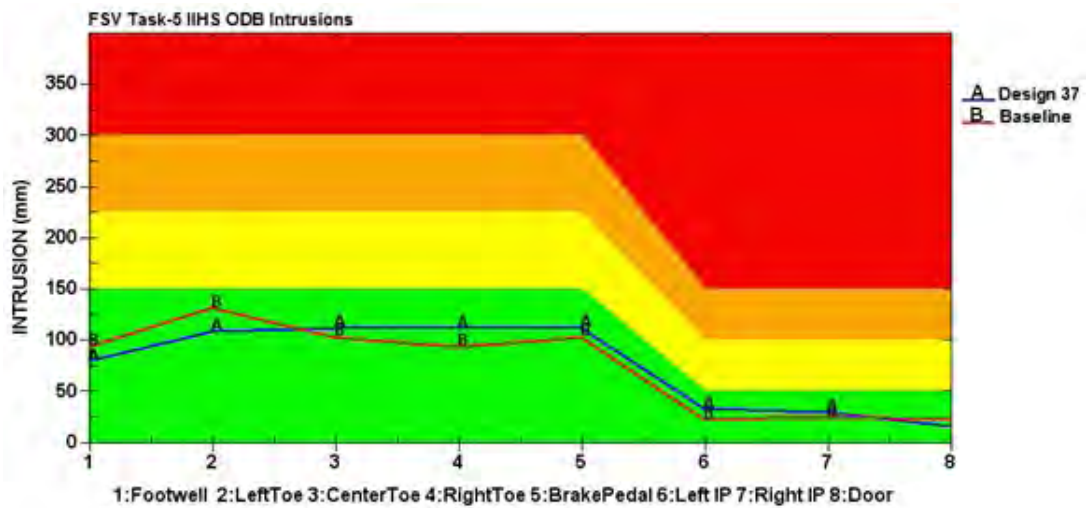


Figure 19.20: Design #37 ODB IIHS frontal impact crash measurements

19.1.7.2 Design #74

Design #74 is one of the early designs that showed the optimization process is looking to improve the performance (reducing the pulse from 62 g to 44 g), while reducing mass. See Figure 19.21 for vehicle Design #74 NCAP pulse and Figure 19.22 for the ODB IIHS frontal crash measurements, below.

Baseline Mass = 213.7 kg

Optimized Design #74 = 202.8 kg

Current Mass Savings = 10.8 kg (5%)

Optimized Design #74 Body Structure = 197.3 kg

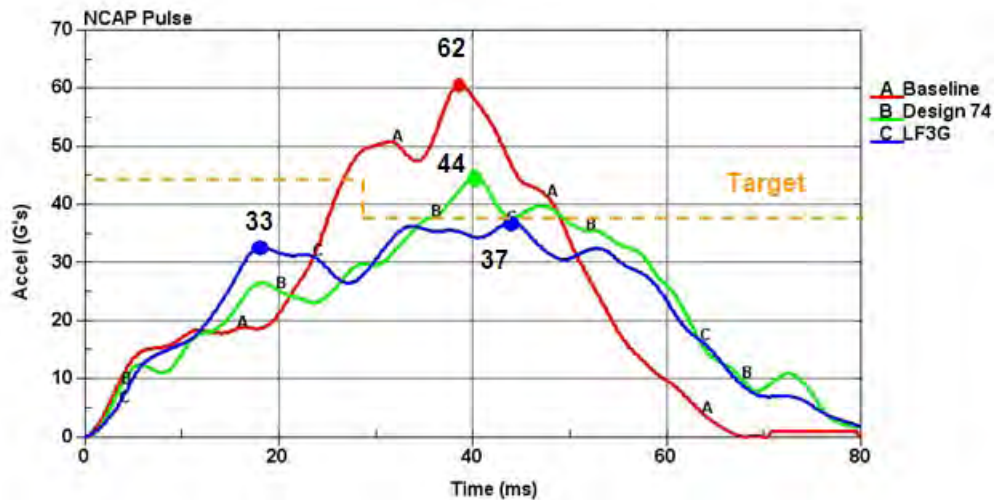


Figure 19.21: Design #74 models and parts that were included in the optimization

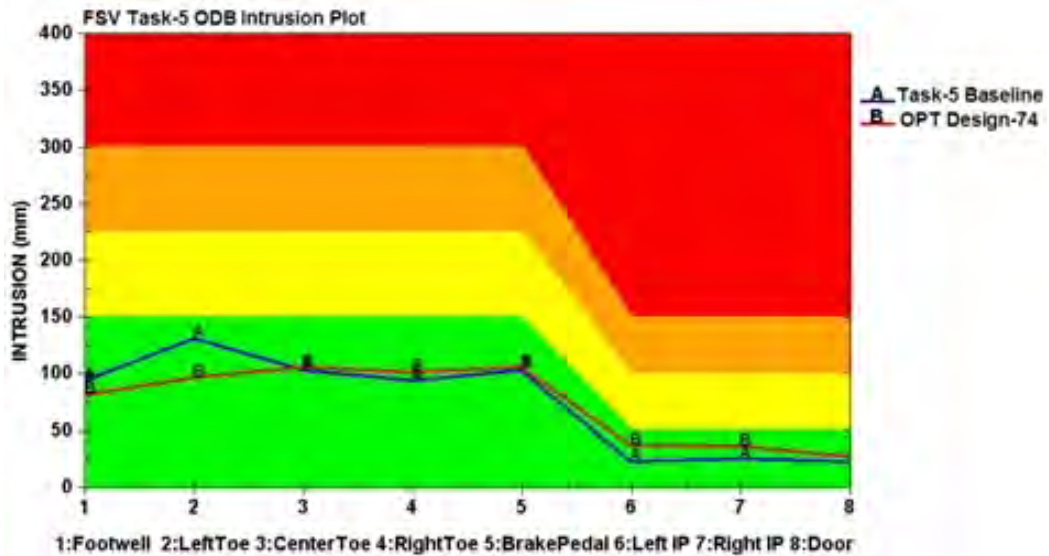


Figure 19.22: Design #74 vehicle pulse and ODB IIHS front crash measurements

Design #74 is one of the early designs that was investigated while the process was looking to minimally adjust the local design variables. The mass reduction of the total vehicle is minor since the process is focusing on performance. Figure 19.22 indicates that the process can make immediate improvements in vehicle performance and reduce the vehicle pulse from 62 g's to 44 g's.

19.1.7.3 Design #83

There are many initial design evaluations that focus on meeting the performance targets rather than reducing the mass of the optimized components. However, there are some evaluations that while not strictly feasible designs that meet all targets, their performance is close to the requirements because they show aggressive mass reductions and so are of interest. As can be seen in Figure 19.23, Design #83 has a vehicle pulse of 51g's and a body structure mass well below the target mass of 190kg. This emphasizes that the process is well defined and that the target mass requirement and the Front NCAP pulse performance are interlinked. The optimization is using the crash space of the front motor compartment geometry to absorb as much energy as possible, thus achieving a lower pulse at stack-up. Such enablers will allow the optimization to achieve the mass target. See Figure 19.23 for the NCAP pulse of vehicle Design #83 and Figure 19.24 for the ODB IIHS front crash measurements, below.

Baseline Mass = 213.7 kg

Optimized Design #83 = 185.1 kg

Current Mass Savings = 28.6 kg (13.3%)

Optimized Design #83 Body Structure = 186.4 kg

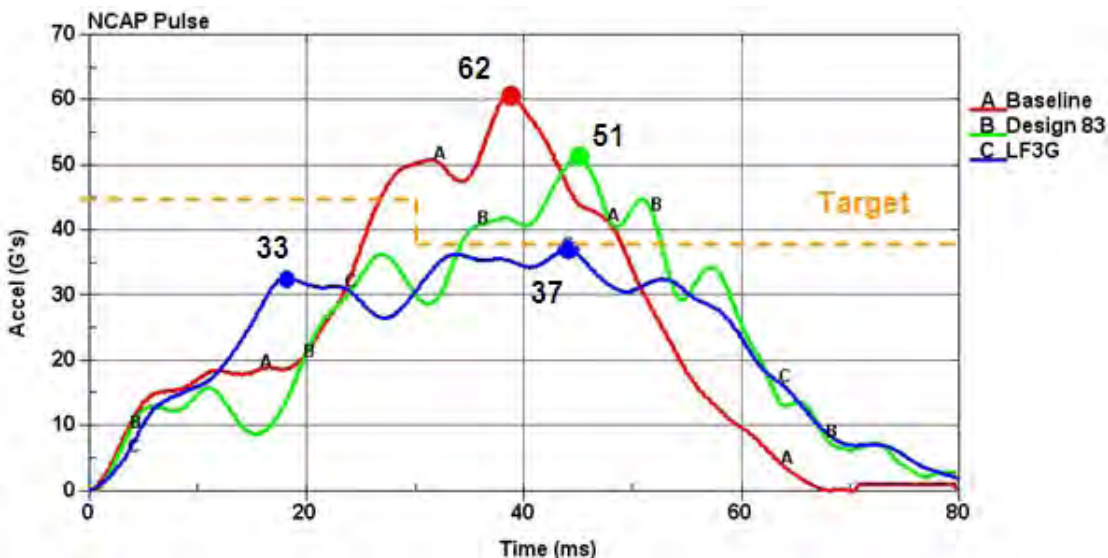


Figure 19.23: Design #74 models and parts that were included in the optimization

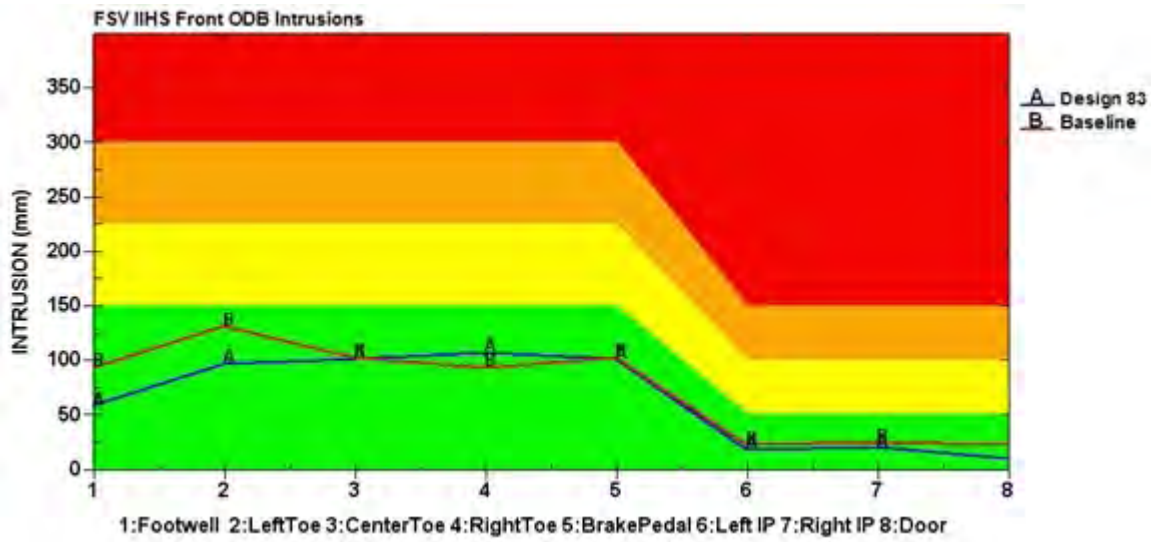


Figure 19.24: Design #83 Vehicle Pulse and IIHS ODB front crash measurements

19.1.7.4 Design #145

Design #145 was selected because of the NCAP front crash performance rather than its mass. The NCAP performance has been improved and the pulse was lowered to 41 g's. See Figure 19.25 for the NCAP pulse of vehicle Design #145 and Figure 19.26 for the ODB IIHS front crash measurements, below.

Baseline Mass = 213.7 kg

Optimized Design #145 = 202.0 kg

Current Mass Savings = 11.7 kg (5.5%)

Optimized Design #145 Body Structure = 199.3 kg

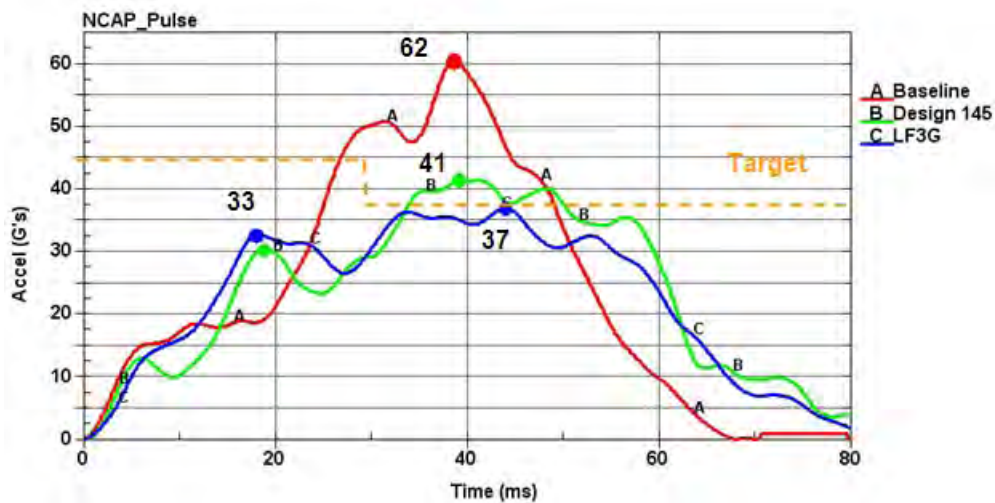


Figure 19.25: Design #145 vehicle pulse

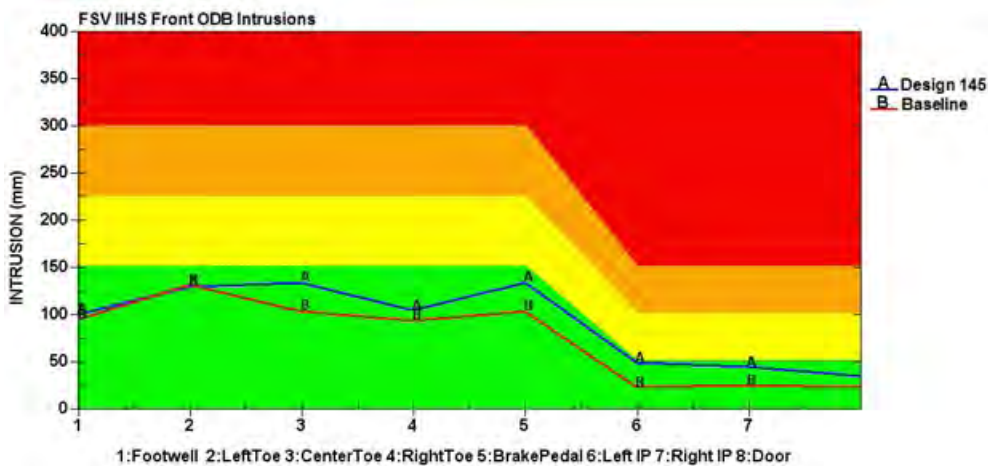


Figure 19.26: Design #145 ODB IIHS front crash measurements

19.1.7.5 Design #196

Design #196 is one of the design evaluations that produced remarkable performance. The mass of the body structure is 203.6 kg and the Front NCAP pulse was 4 0g's. See Figure 19.27 for the NCAP pulse of vehicle Design #196 and Figure 19.28 for the ODB IIHS front crash measurements, below.

Baseline Mass = 213.7 kg

Optimized Design #196 = 206.3 kg

Current Mass Savings = 7.4 kg (3.6%)

Optimized Design #196 Body Structure = 203.6 kg

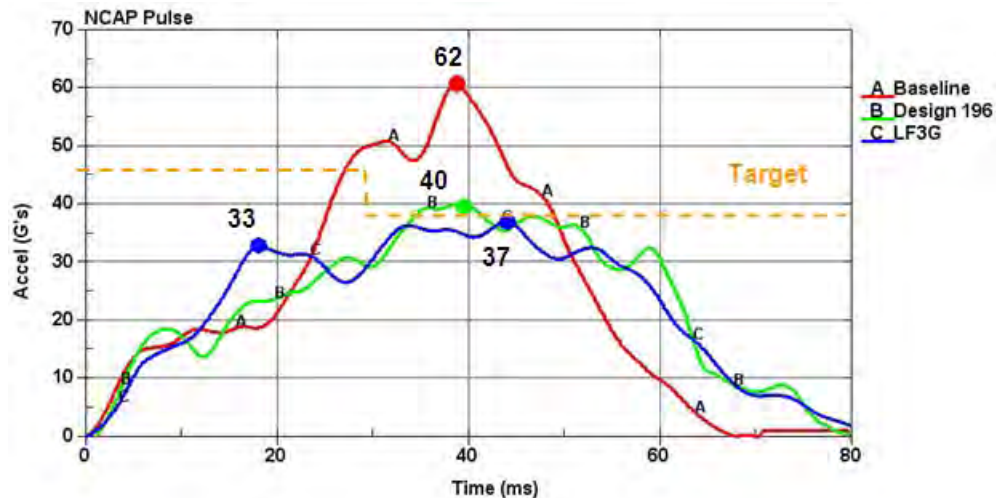


Figure 19.27: Design #196 vehicle pulse

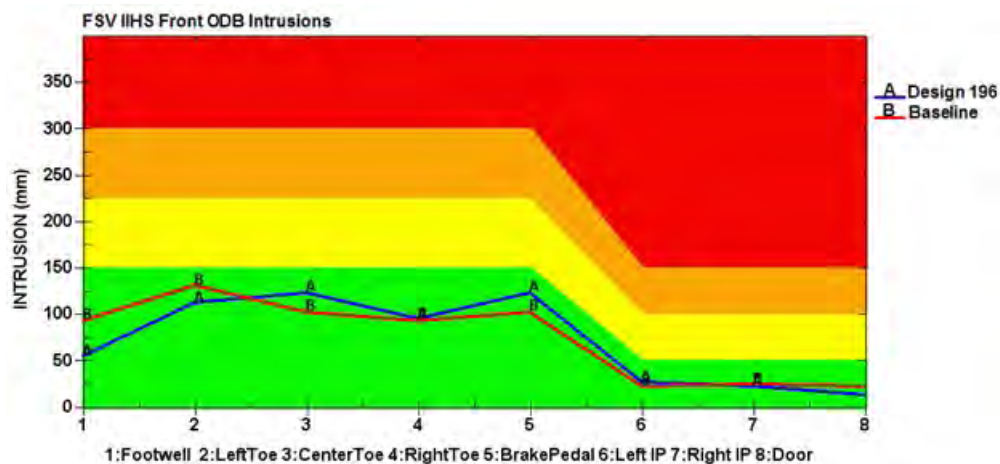


Figure 19.28: Design #196 ODB IIHS front crash measurements

19.1.7.6 Design #302

Design #302 marks one of the best design evaluations that produced both performance and lower mass. The mass of the body structure is 188.8 kg and the Front NCAP pulse was 45 g's. See Figure 19.29 for the NCAP pulse of vehicle Design #302 and Figure 19.30 for the ODB IIHS front crash measurements, below.

Baseline Mass = 213.7 kg

Optimized Design #302 = 191.6 kg

Current Mass Savings = 22.3 kg (10.4%)

Optimized Design #302 Body Structure = 188.8 kg

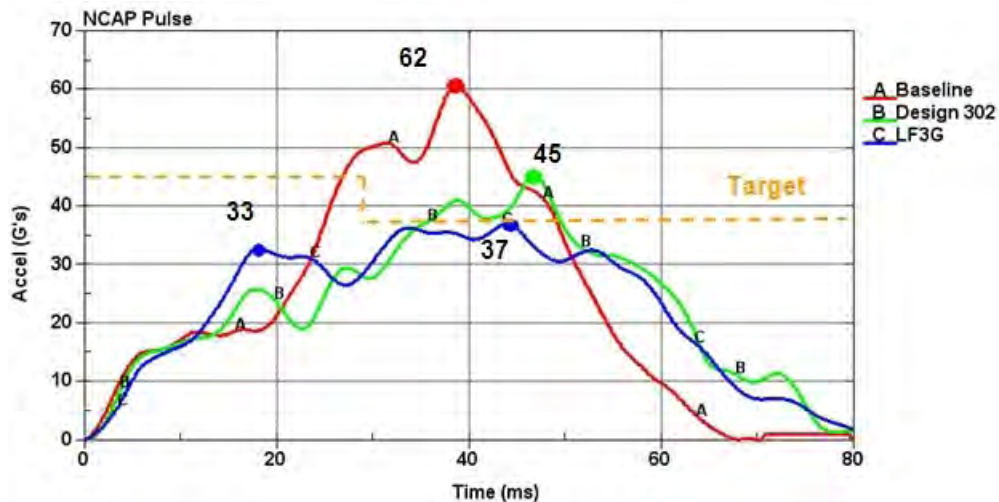


Figure 19.29: Design #302 vehicle pulse

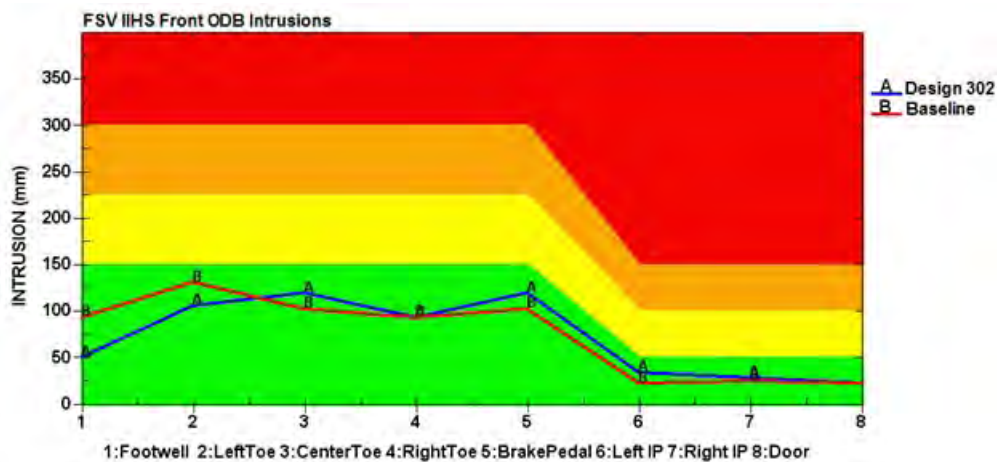


Figure 19.30: Design #302 Vehicle Pulse and IIHS ODB front crash measurements

19.1.7.7 Design #336

Design #366 marks the best design evaluation among 384 designs, with the best performance and lowest mass. The mass of the body structure is 188.0 kg and the Front NCAP pulse was 45 g's. Further analysis on this design shows that by removing the steering rack motor and modifying the cradle supports, the vehicle pulse can be dropped to 37 g's. The vehicle pulse for design #336, which met design optimization targets, is in green and the modified #336 design is in blue (met target of 37 g's pulse). See Figure 19.32 for the NCAP pulse of vehicle Design #336 and Figure 19.33 for the ODB IIHS front crash measurements below.

Baseline Mass = 213.7 kg

Optimized Design #196 = 190.6 kg

Current Mass Savings = 15.7 kg (8.4%)

Optimized Design #336 Body Structure = 188.0 kg



Figure 19.31: Design #302 further design changes

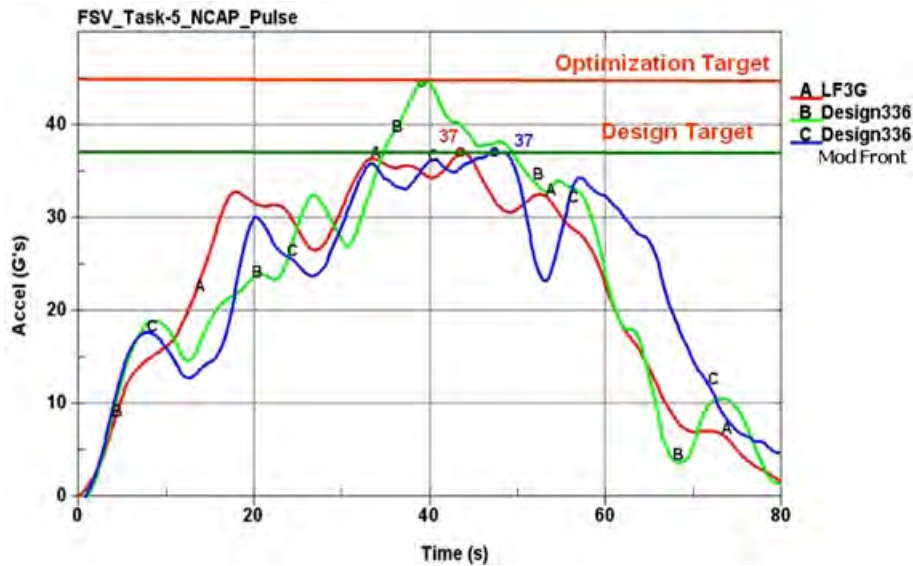


Figure 19.32: Design #336 vehicle pulse

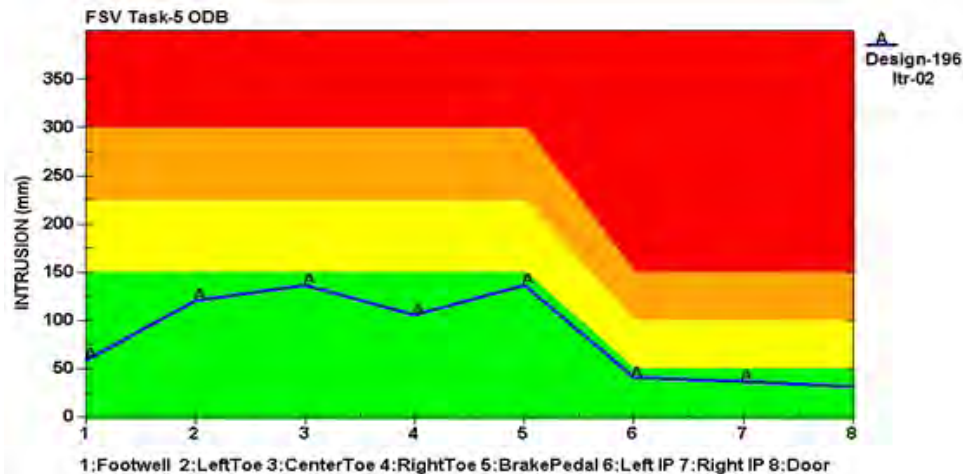


Figure 19.33: Design #196 Vehicle Pulse and IIHS ODB front crash measurements

Based on the above design evaluations and performance of the vehicle in other attributes, the T5 optimization was stopped after design #384. Design #336 gauge and grade optimizations were applied to the most updated design for a final mass with progression in different areas, and is reported as the final T5 design. The final #336 design with the most updates, is the above-modified design in addition to a tunnel design modification (see Figure 19.34 and Figure 19.35), for a bead change in most of panels. Two other major updates that need to be discussed are the continuous joining techniques that was introduced to this model and in the crash model, and the shell finite element model which was run with the fully integrated element formulations.

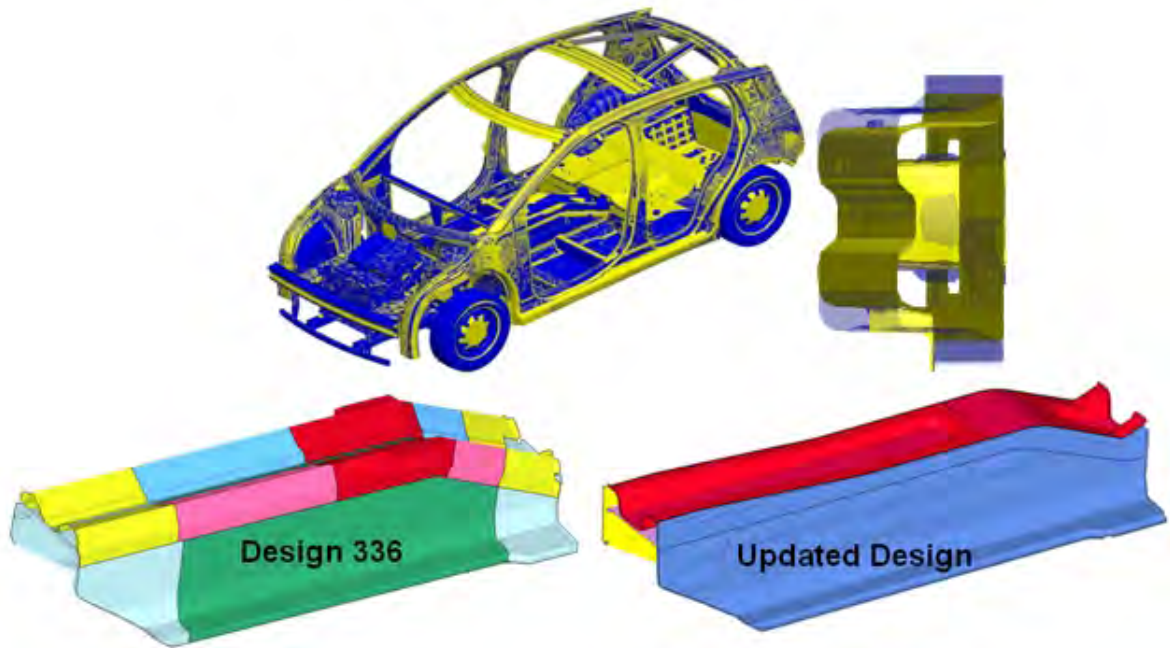


Figure 19.34: Updated design #336

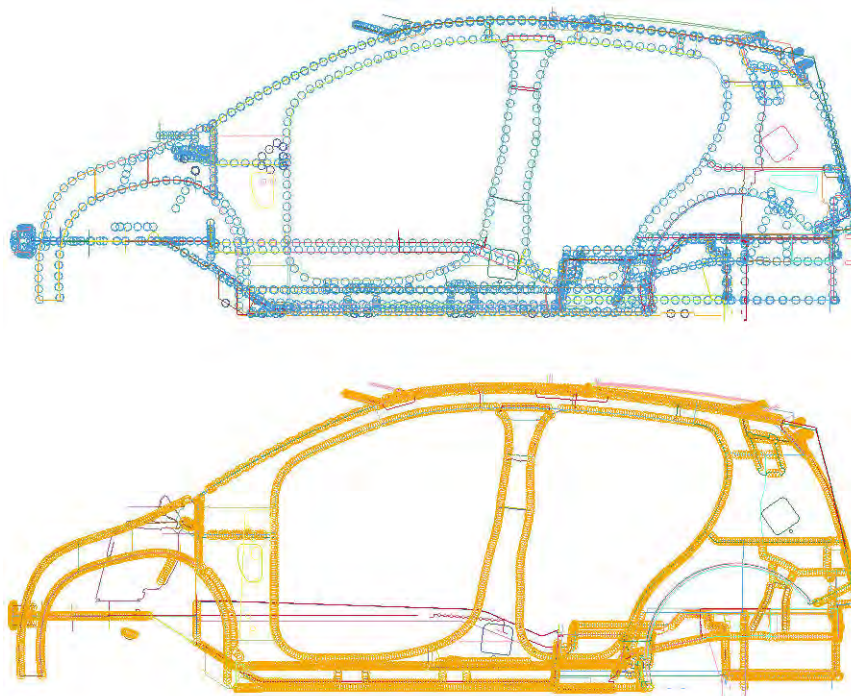


Figure 19.35: Updated 336 design-2

19.1.7.8 Hardening Effects

The final design that is reported for Task 5 with a mass of 187.7 kg, has gauge and grades that were initiated as baselines to study the effects of material hardening in all components that use high strength steel and Dual Phase materials.

In order to study the hardening effects these steps are completed:

- Identify all the parts with AHSS (mostly DP grades)
- Perform one-step analysis using DYNAFORM to calculate thinning effects, residual stress and strain
- Perform full vehicle crash for all load cases

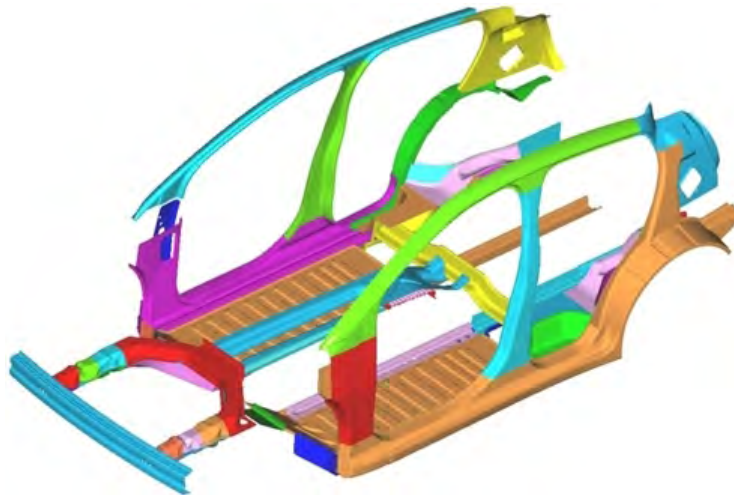


Figure 19.36: *Parts that went through one-step forming*

After one-step analysis, the data for thinning (Figure 19.37, Figure 19.38), residual stresses and strain effects in all six directions (xx,yy,zz,xy,xz,yz) were extracted. This data was inserted in the solver in order to incorporate these effects. Re-evaluating the performance of the vehicle with the current changes, showed improvement in the areas of IIHS side impact, IIHS pole impact and IIHS roof crush. These findings represent potential for further mass reduction opportunities existing in the final design that will be studied in the T6 mass optimization.

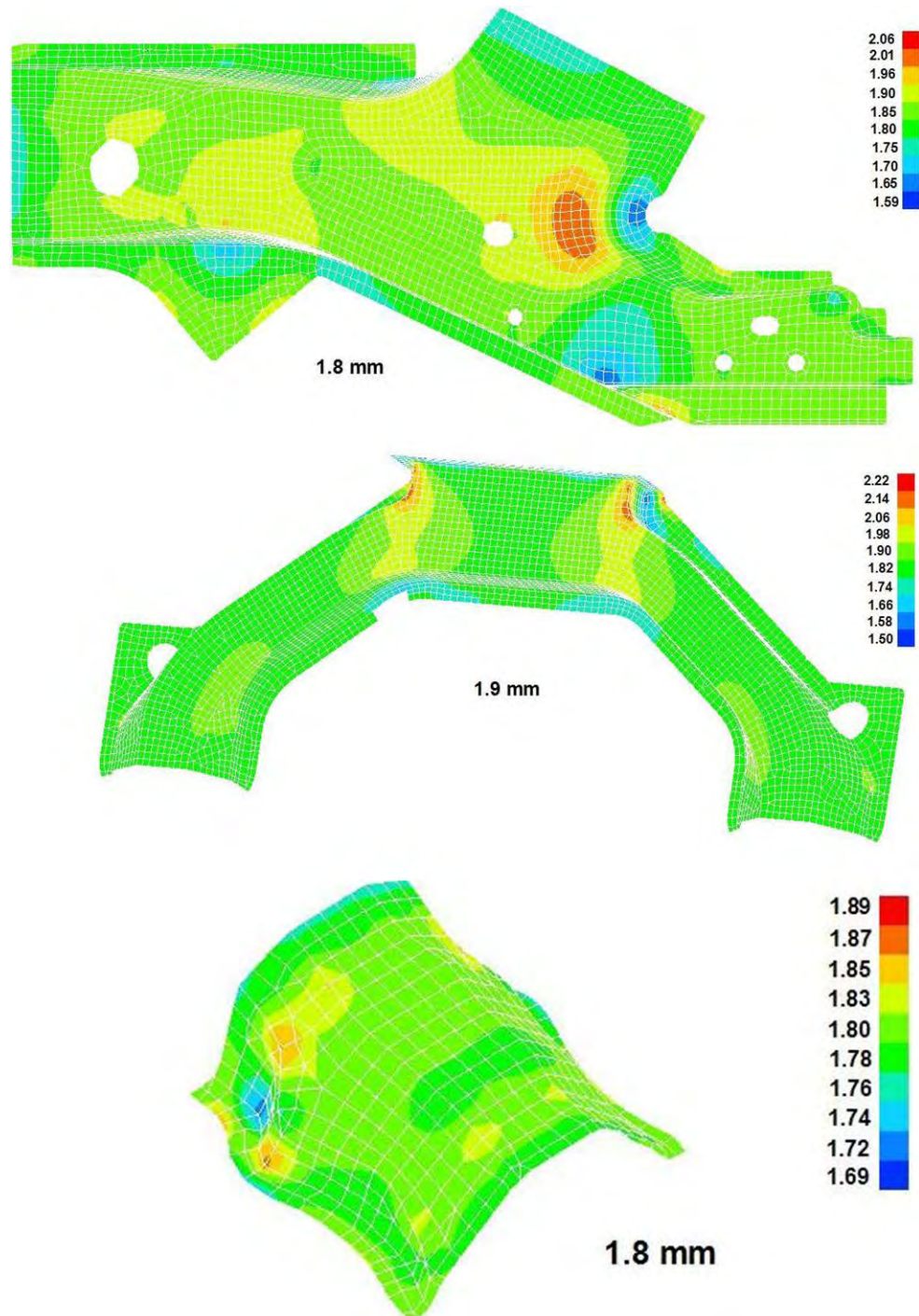


Figure 19.37: Thinning effects of some front rail parts - 1

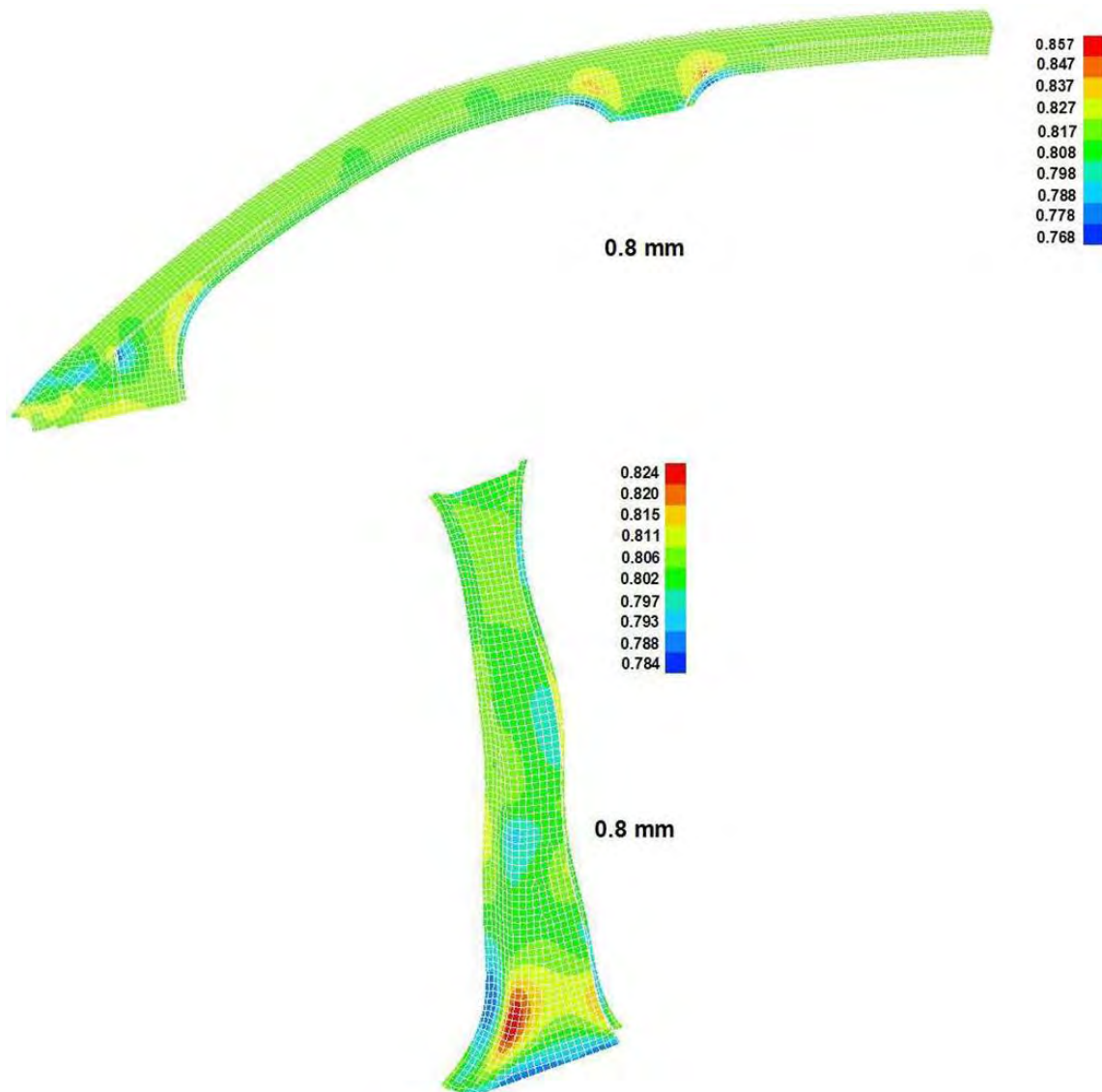


Figure 19.38: *Thinning effects of some front rail parts - 2*

The effect of hardening in the following load cases (see Figure 19.39, Figure 19.40, Figure 19.41 and Figure 19.42), of the IIHS Front ODB and Rear Impact are hard to notice. The load cases of the IIHS Side Impact, FMVSS Pole Impact and IIHS Roof crush show small improvement with hardening effects. This was expected since most of the load paths involved in the following cases were made of hot stamped materials where no hardening effect is present.

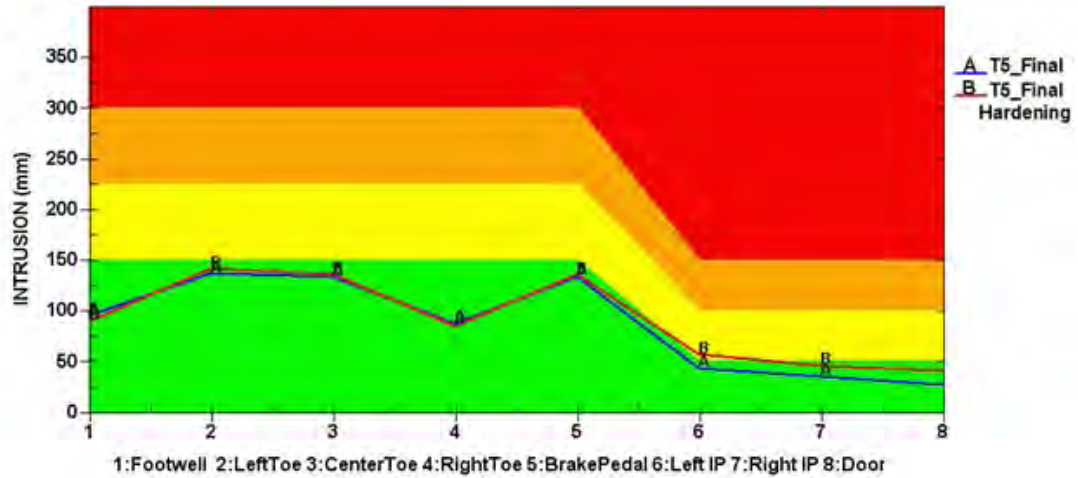


Figure 19.39: Performance evaluation of vehicle using hardening effects - 1

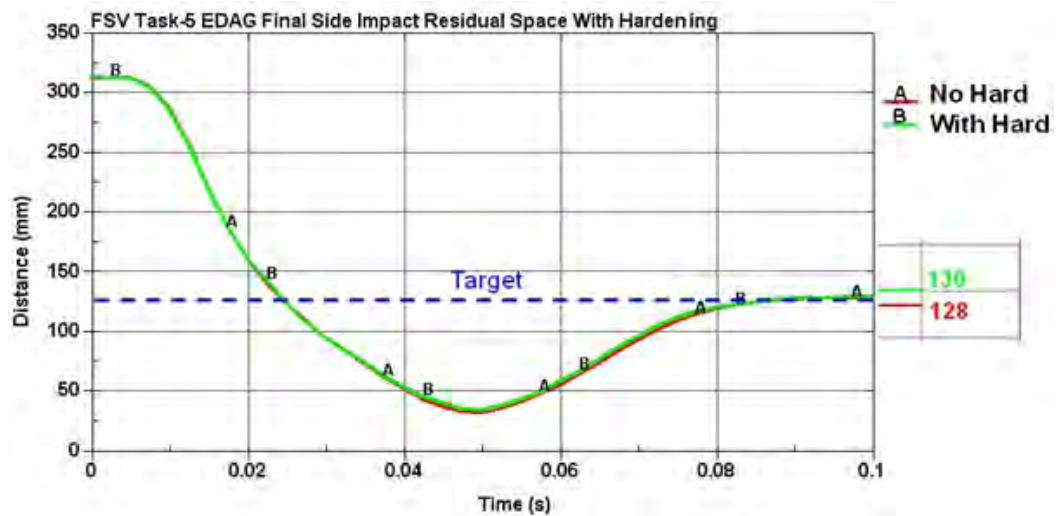


Figure 19.40: Performance evaluation of vehicle using hardening effects - 2

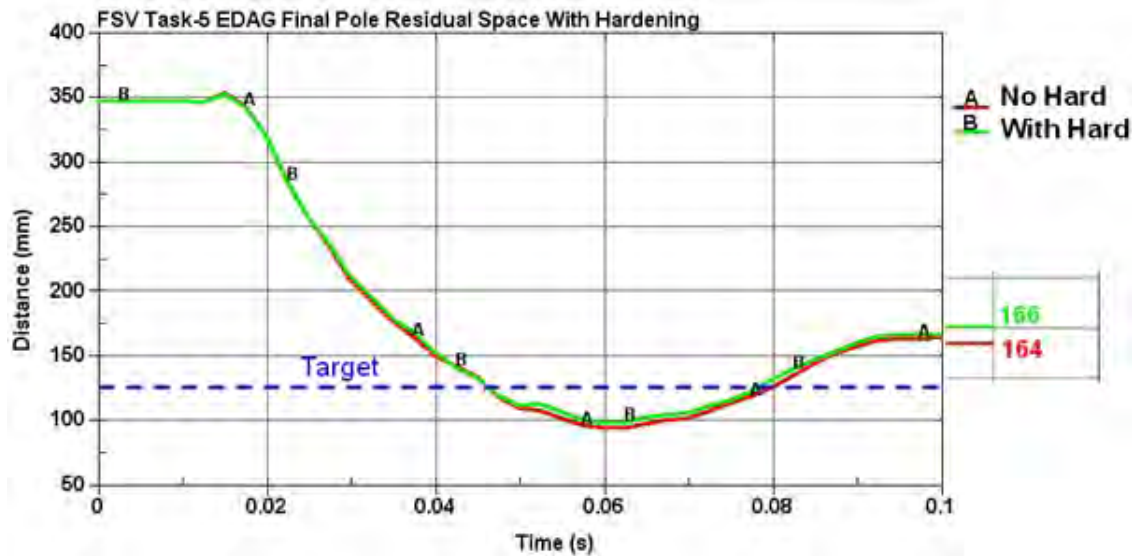


Figure 19.41: Performance evaluation of vehicle using hardening effects - 1

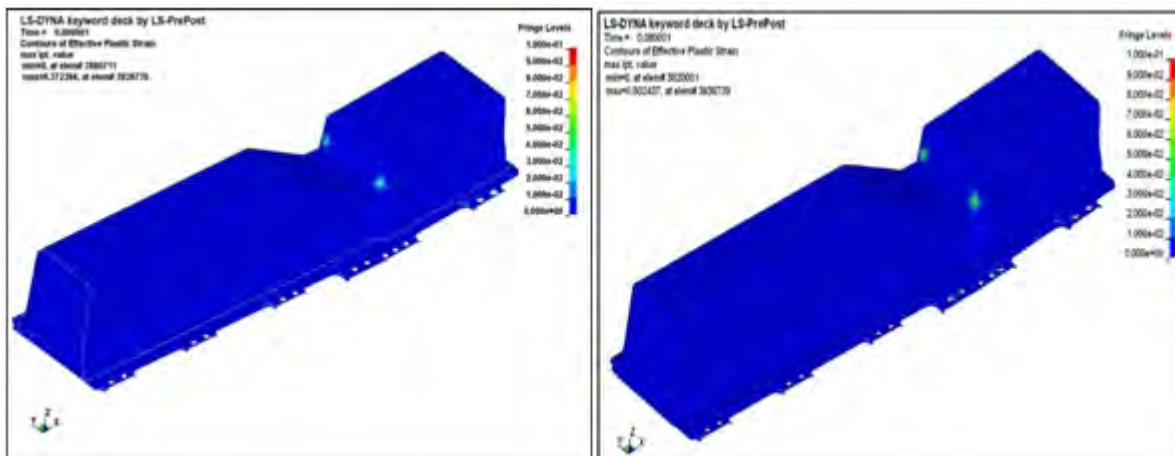


Figure 19.42: Performance evaluation of vehicle using hardening effects - 2

On the other hand, the IIHS Front NCAP result shows a reduction in performance, which can be improved with a reduction in mass. The pulse has increased due to the hardening of the front rail parts. Figure 19.43 and Figure 19.44 shows the difference in the bending mode of the front rail. The hardening effect causes a stiffer structure, resulting in lower of stress levels. Therefore, lowering the gauges of font rail parts will increase the performance (lowering pulse), and save mass consecutively.

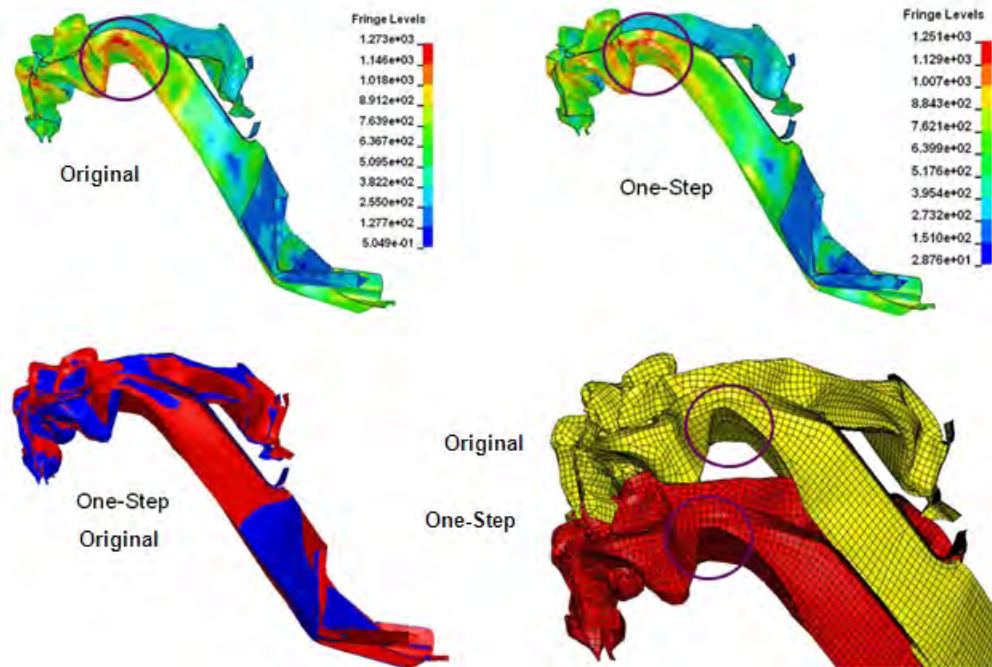


Figure 19.43: Performance evaluation of vehicle using hardening effects - 3

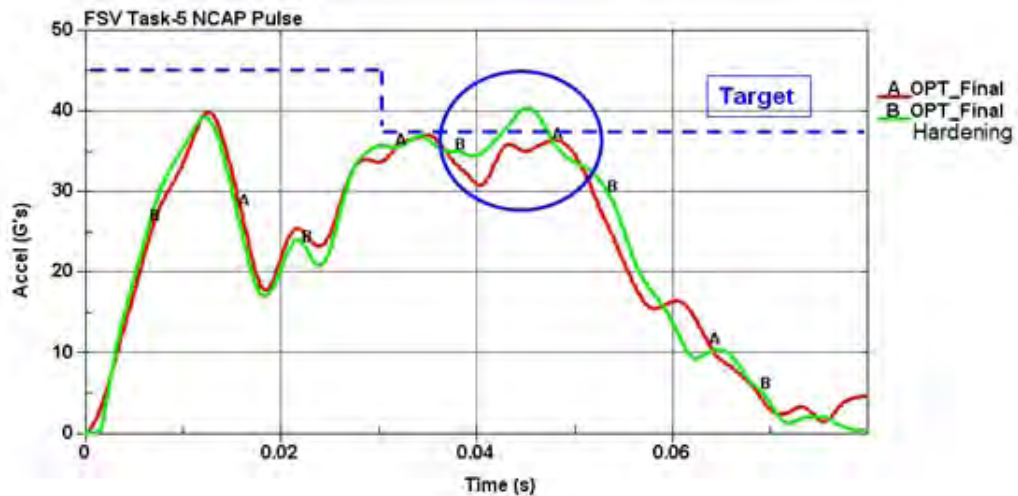


Figure 19.44: Performance evaluation of vehicle using hardening effects - 4

19.2 Bead Optimization

In general, based on benchmark studies and trends in body structure design, the designer developed stiffening beads are now common on many vehicle components especially larger panels such as the cowl, floor, rear seat pan and trunk floor. These beads usually help in both local and global stiffness of components and body structure. The shape of the beads is usually dictated from design experience (the direction of loads), available space and manufacturing process.

Due to the ease of forming, steel offers great flexibility in terms of the size and direction of stiffening beads that can be added to a panel. This can be an advantage in comparison with other materials. In this report we will study the comparison between optimized and traditionally design beading patterns. The results will provide valuable guidance for the future design of large panels and their individual beading patterns. The beading optimization study was completed by ETA.

19.2.1 Objective

The objective is to:

- Develop a design methodology that applies currently available optimization software in the design and development of a non-intuitive beading pattern that can be manufactured using modern steels
- Compare the impact on the global vehicle performance (Stiffness and Impact) between:
 - Traditional designed beading
 - Optimized non-intuitive beading

19.2.2 Background

The software that was used in this study was GENESIS, using a linear static load representation. GENESIS offers two beading optimization methods: **Freeform and Domain**.

1. Freeform allows the optimization to control the individual nodes of the mesh for a truly non-intuitive beading pattern. There is no external engineering judgment influencing the beading patterns and so the resulting beads are non-intuitive, very organic.
2. Domain allows the user to create control areas which encourage beading locations and directions. The resulting beading pattern is much simpler and can be defined to address manufacturing concerns but the results are also biased by an engineer's definition of the domains.

The FSV program will use freeform beading optimization to establish a non-intuitive beading pattern. This will be the basis for a domain based approach.

19.2.3 Beading Optimization Strategy

19.2.3.1 Boundary Conditions and Loading Representation

Beading optimization is based on a linear static analysis representing all crash loads (NCAP, Front ODB, Pole Impact, IIHS Side and Rear Crash)

Method-1

Global load representations of all crash loads were applied to the body structure model using an approach similar to that used for the original topology optimization. See Figure 19.45.

- Loads will be applied via RBE3 spiders. The size of the spider is consistent with the footprint of the barrier
- The model will be constrained using Inertia Relief for all the crash loads. The torsional loading will be constrained using SPCs as per the original topology optimization
- The peak barrier contact force for each crash load is extracted from the full crash models. This way the relative magnitude of each loadcase will be consistent

Boundary Conditions for Crash Loadcases

- Loading: Peak loads taken from dynamic models
- Constraints: Inertia Relief

Boundary Conditions for Torsion

- Loading: 1000 N
- Constraints: SPCs

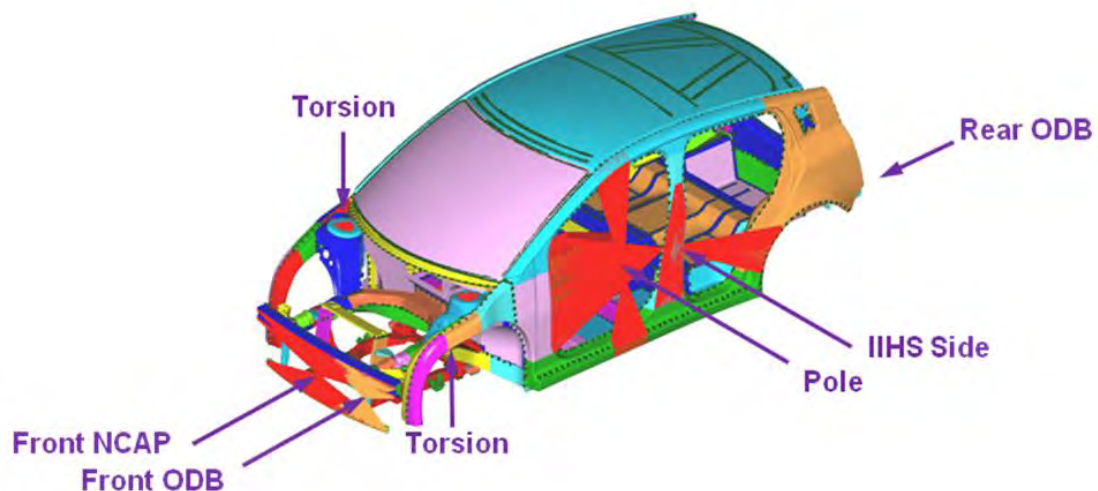


Figure 19.45: Method 1: Bead optimization loadings

Method-2

In this case, for each crash loading, the peak enforced displacements in the x, y and z directions at the edge of each panel under consideration, were extracted from the full system model. These were then applied to the beading optimization model of the body structure as static loads.

- Revised loading, shown in Figure 19.46, used local enforcement displacements extracted from the dynamic models (rigid body motion of the vehicle removed), as close to the panels under consideration as possible
- Torsion is the odd load case. How is this case weighted relative to crash loads? We will instead optimize this load separately and then combine it with the final crash load beading pattern.

**Actual deformed shape
under IIHS Side Impact**

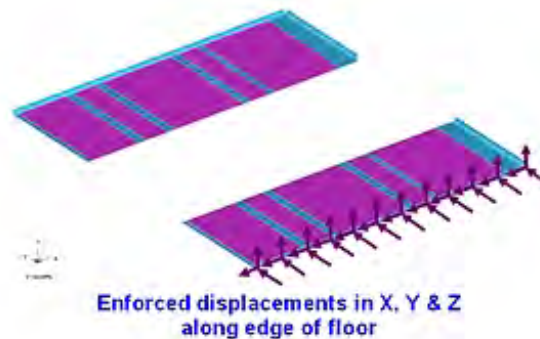
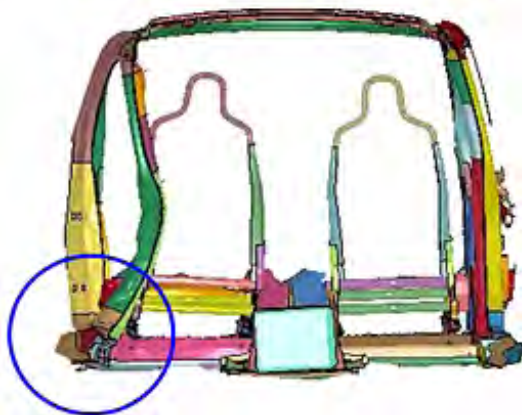


Figure 19.46: *Method 2: Bead optimization loadings*

19.2.4 Panels Considered in the FSV Body Structure

The panels that were contemplated for beading are shown in Figure 19.47. The panel areas that are in blue were not considered for beading. These areas represent the spot-weld flanges and areas, due to lack of space and manufacturing issues, were not considered for beading. The main panels are the cowl, transmission tunnel, left & right floors, kick down, rear seat pan, rear longitudinal & spare wheel well.

A plane of symmetry was defined along the centerline of the vehicle so that the optimized beading pattern on the passenger side will mirror that of the driver's side even though the lateral loadings (IIHS Side and Pole Impacts) were only applied to the driver's side.

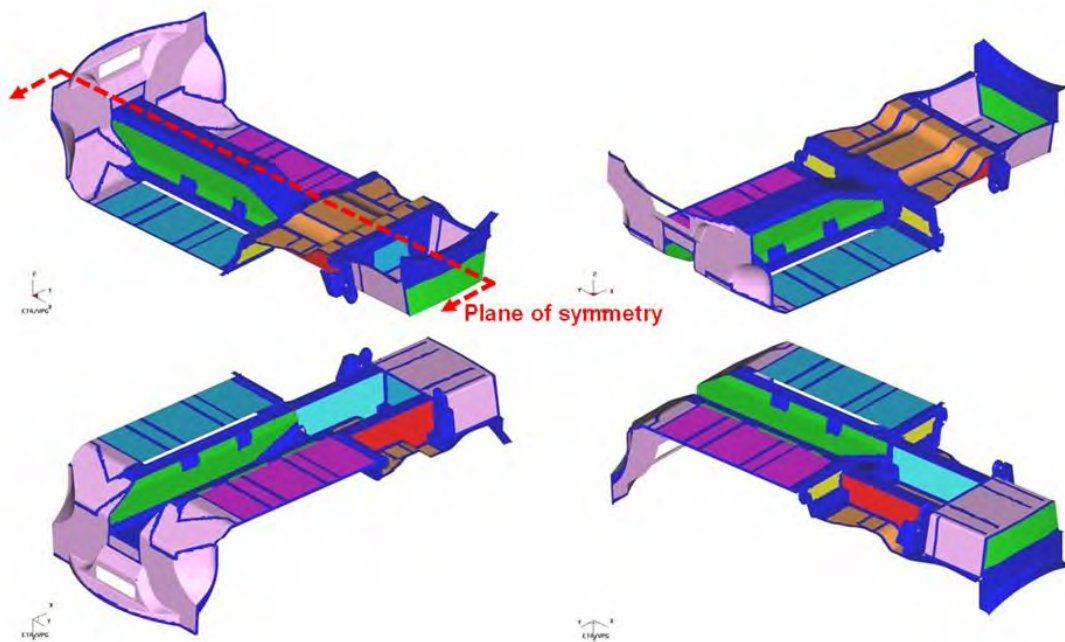


Figure 19.47: *Panels Considered for bead optimization*

19.2.5 Bead Optimization Process

Method-1

In this approach the loading was a static representation applied to the body structure through a series of RBE3 spiders as shown in Figure 19.45. The relative sizing of each loading was based on the peak barrier contact forces extracted from the full system model. The results of Method-1 are shown in Figure 19.48, which shows the beading size in millimeters, normal to the panel. The maximum bead size set was 7mm, based on manufacturing experience. Even though the body structure was subject to a static representation of the IIHS Side and Pole Impact loadings, Figure 19.48 shows that no beading was added to the floors. This was because using this method, the floors were not properly excited under these loadcases. Therefore, this method does not provide an accurate method of loading the panels for bead optimization.

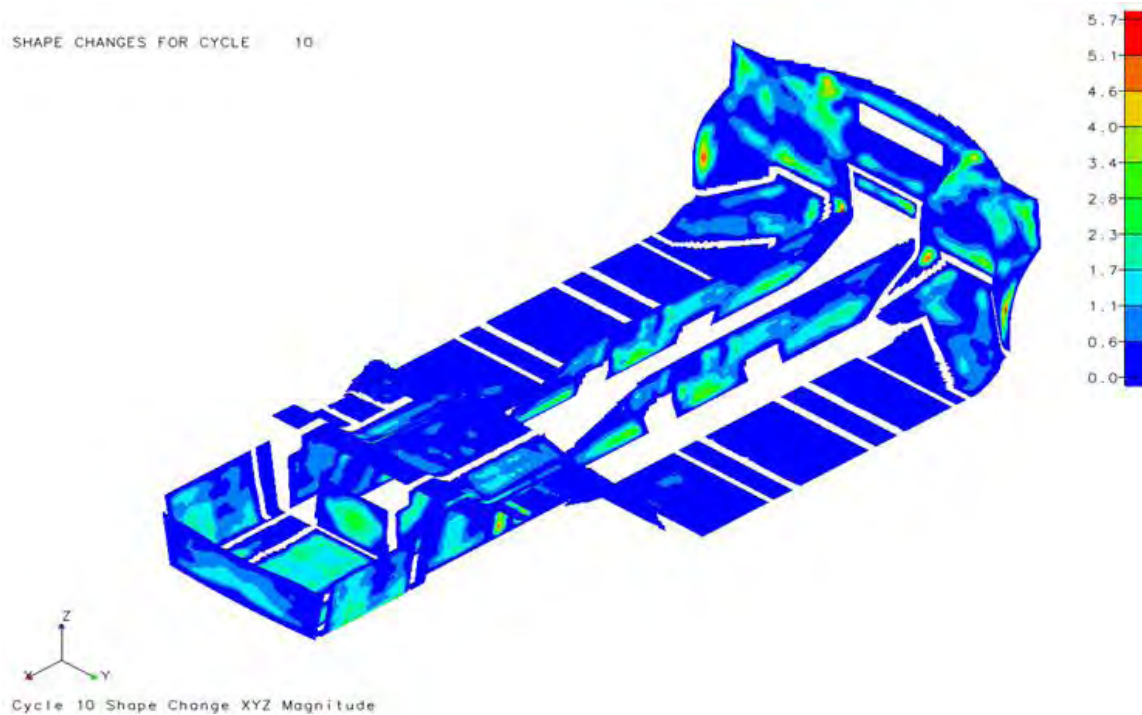


Figure 19.48: Method-1: Beading depth (normal to panel)

Method-2

The second method applied the maximum forced displacement extracted from the full system model as static loading on the edge of panels under consideration as shown in Figure 19.46. The results of bead optimization defined a non-intuitive bead pattern based on each loading case. Figure 19.49 shows the beading pattern developed for the IIHS Side Impact loading. Again, the contours represent the size of the bead normal to the panel up to a maximum of 7 mm. In this case, the floor has been appropriately excited by the IIHS Side Impact loading, forming a beading pattern analogous to a wave propagation through the panel.

19.2 Bead Optimization

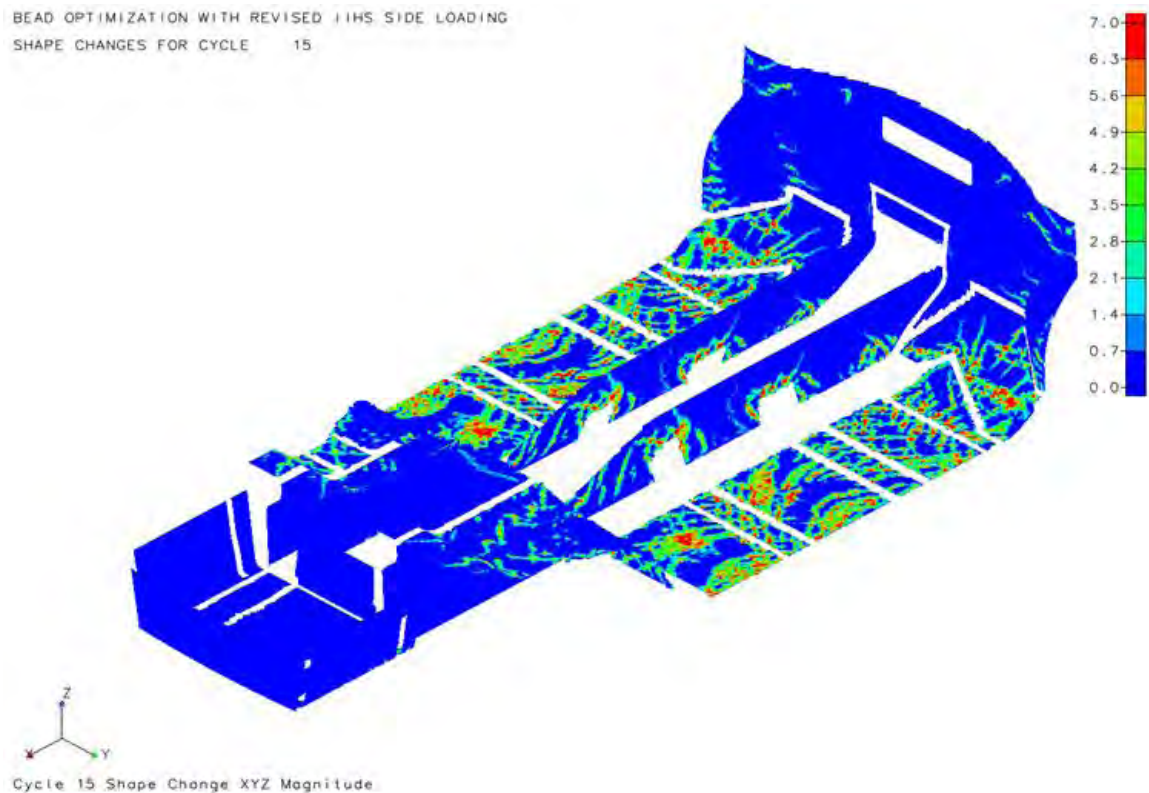


Figure 19.49: Method-2: Beading depth (normal to panel) under IIHS side impact

As mentioned previously, GENESIS offers two methods of beading optimization: Freeform and Domain. The beading patterns developed so far have used Freeform, allowing GENESIS to define a pattern with the least external engineering bias or influence. Figure 19.49, shows that the Method 2 approach works well. Thus, the next step is to use these results as the basis for mapping a series of domains in the floor. These domains predetermine the orientation and approximate sizing of the beading pattern but allow much greater consideration of manufacturability. Once the domains were defined, GENESIS was rerun using Domain based optimization. Figure 19.50 shows the resulting Domain based beading pattern under Front ODB loading.

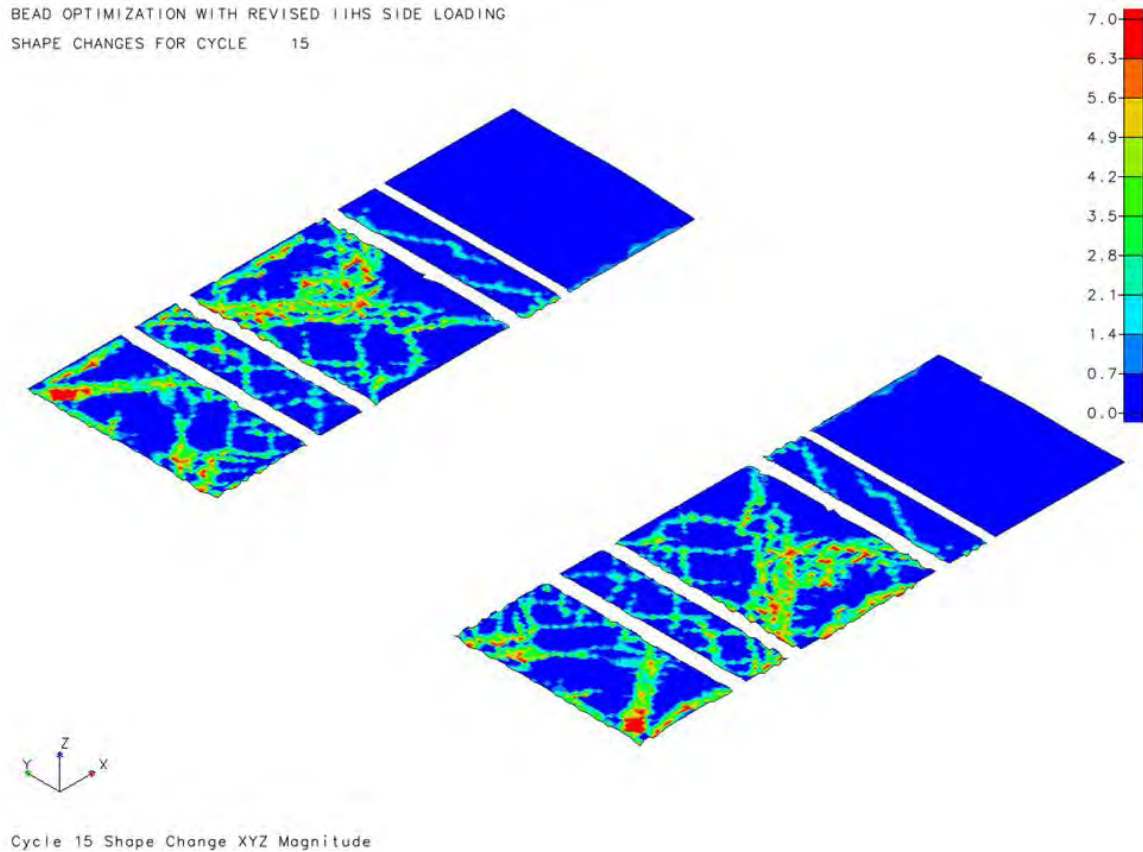
BEAD OPTIMIZATION WITH REVISED IIHS SIDE LOADING
 SHAPE CHANGES FOR CYCLE 15


Figure 19.50: *Beading depth (normal to panel) under front ODB using domain based beading*

The resulting beading pattern using the Domain approach did not significantly influence the design of the final beading pattern and so it was decided to use only the results of the Freeform approach.

With the Method 2 identified as a valid approximation, appropriate loadings were developed for each of the crash loads. Figure 19.51 summarizes the loadings extracted for IIHS Side and Pole Impacts, Front NCAP and Front/Rear ODB. These loads were then applied simultaneously to create a single beading pattern for the combined loading. See Figure 19.52.

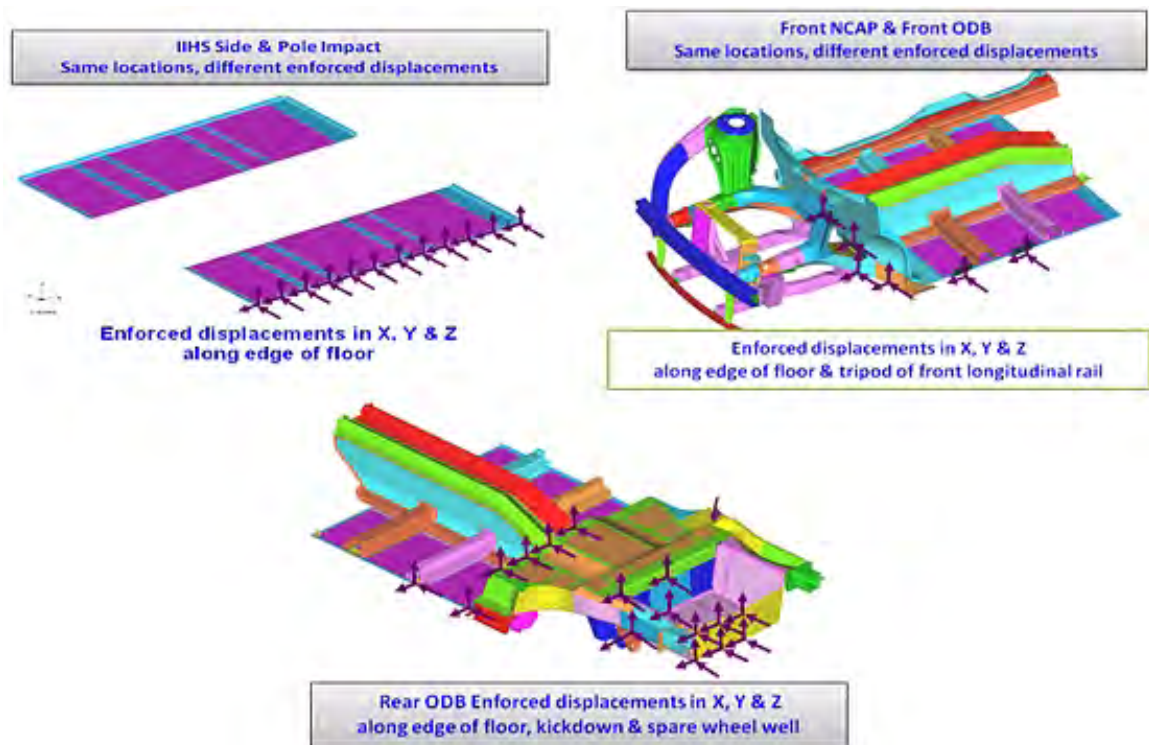


Figure 19.51: Method-2: Combined loading for IIHS Side & Pole Impacts, Front NCAP and Front & Rear ODB

Figure 19.52 shows the results of the beading pattern developed for the combined crash loads. Run separately, Figure 19.53 shows the results of the beading pattern created for the torsion load. As mentioned previously, torsion was considered separately because there was no definitive way to scale this load with respect to the crash loadings.

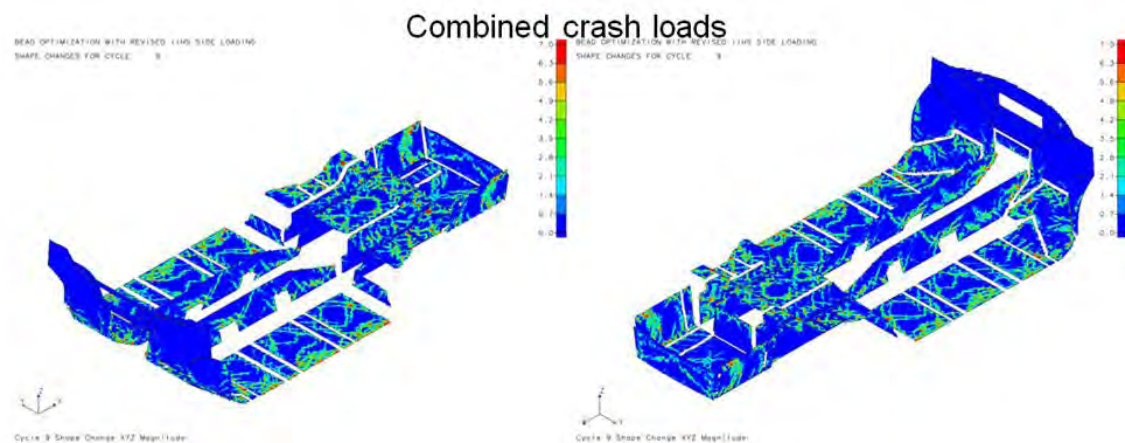


Figure 19.52: Beading depth (normal to panel), under combined crash loading

Torsion Loadcase

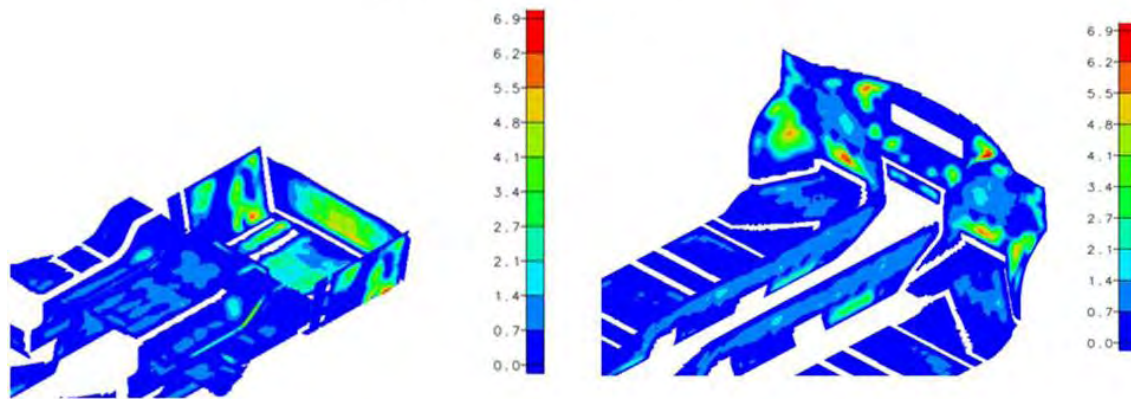


Figure 19.53: *Beading depth (normal to panel,) under torsional loading*

The beading pattern created under Torsional loading is very localized to the cowl and spare wheel well. These are easily combined with the beading optimization results of the combined crash loads.

19.2.6 Comparison of Design and Optimization Beads

To better understand the effect of the shape of beads for specific crash loads (secondary buckling mode), we assembled two models of panels (dash, front and rear panels), that have traditional beading designed using design experience and the bead optimization process. Two major load cases of ODB front crash and side impact were selected. The two bead shapes for in dash and the floor area are shown in Figure 19.54.

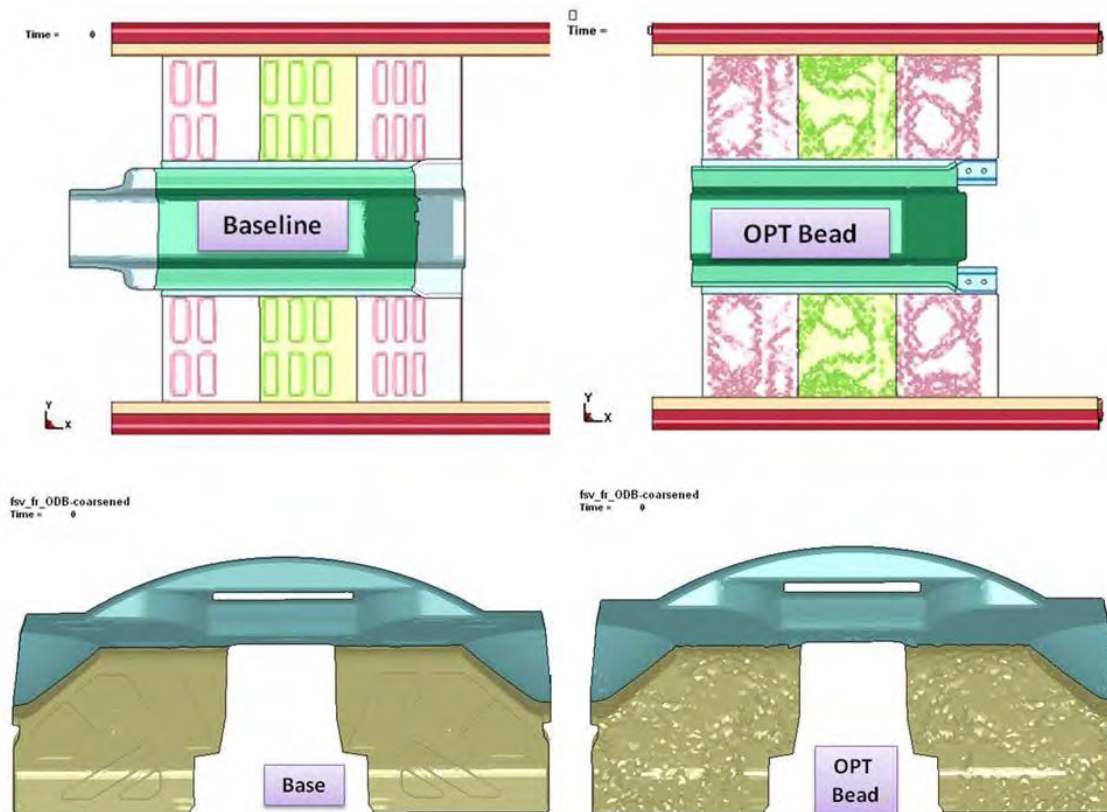


Figure 19.54: Panels with design (base) and optimization beads

Figure 19.55, shows displacement in the lateral direction (Y-direction), under IIHS Side Impact for three cases: no beads, traditionally design beading pattern and optimized beads. Figure 19.56 shows the results of IIHS ODB for the same three cases. For both loadcases we can conclude that the type of beading pattern (Traditional vs. Optimized), makes no difference in the deformation measurements of the panel's second buckling mode under crash loads. However, there are differences between beaded and flat panels. Under IIHS Side Impact, the beading is much more effective than for the Front ODB. The value of panel beading for local stiffness and NVH performance is well known. For this study, we can conclude that beading can offer some benefit for crash performance but their effect varies by crash loadcase.

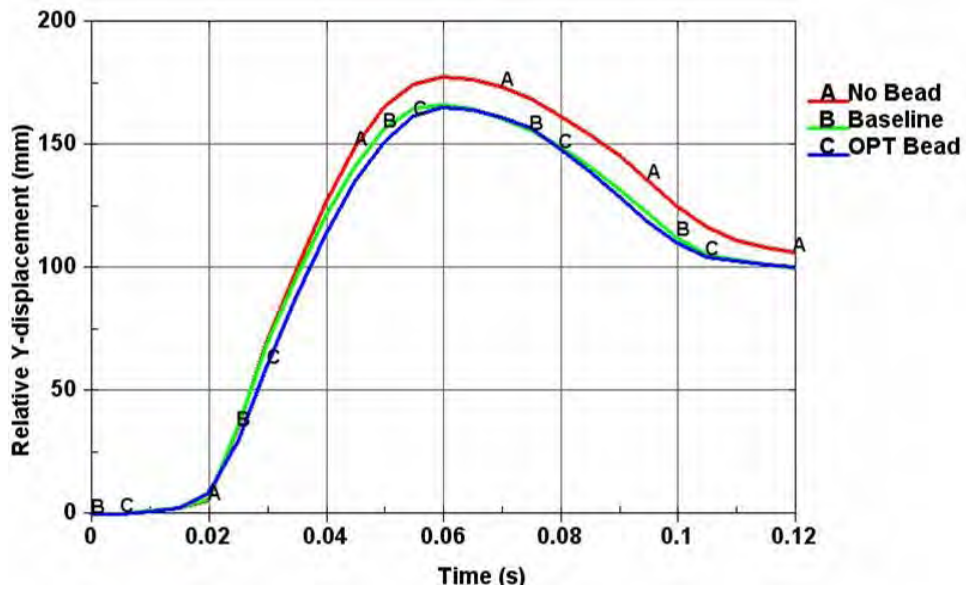


Figure 19.55: Results of IIHS side impact: no beads, design beads (base) and optimization beads

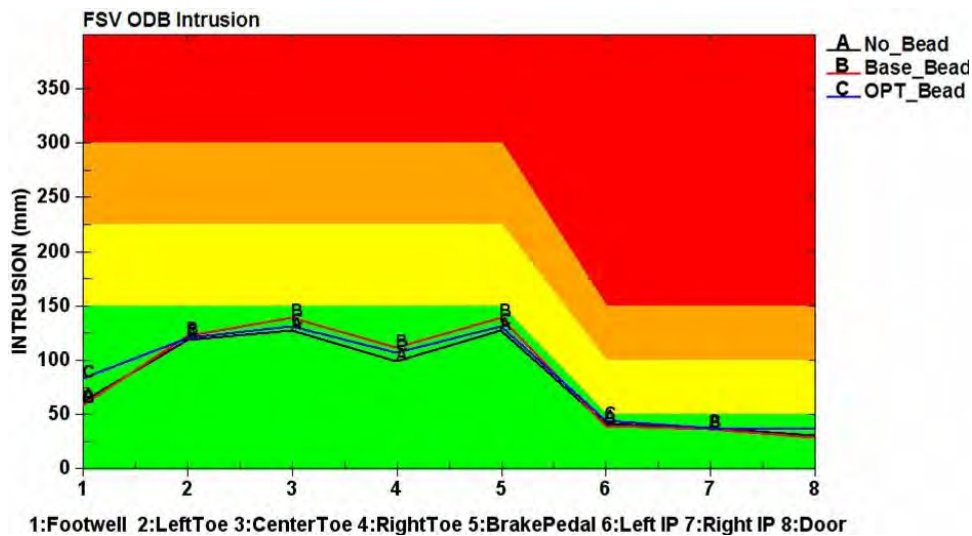


Figure 19.56: Results of IIHS side impact: no beads, design beads (base) and optimization beads

20.0 Appendix

20.1 Process Planning Sheets for FSV-1 BEV

The following process sheets show the following information for each BEV body structure part:

- Material specification
- Part mass
- Coil dimension
- Blank nesting
- Tooling cost breakdown
- Cycle time
- Part sketch

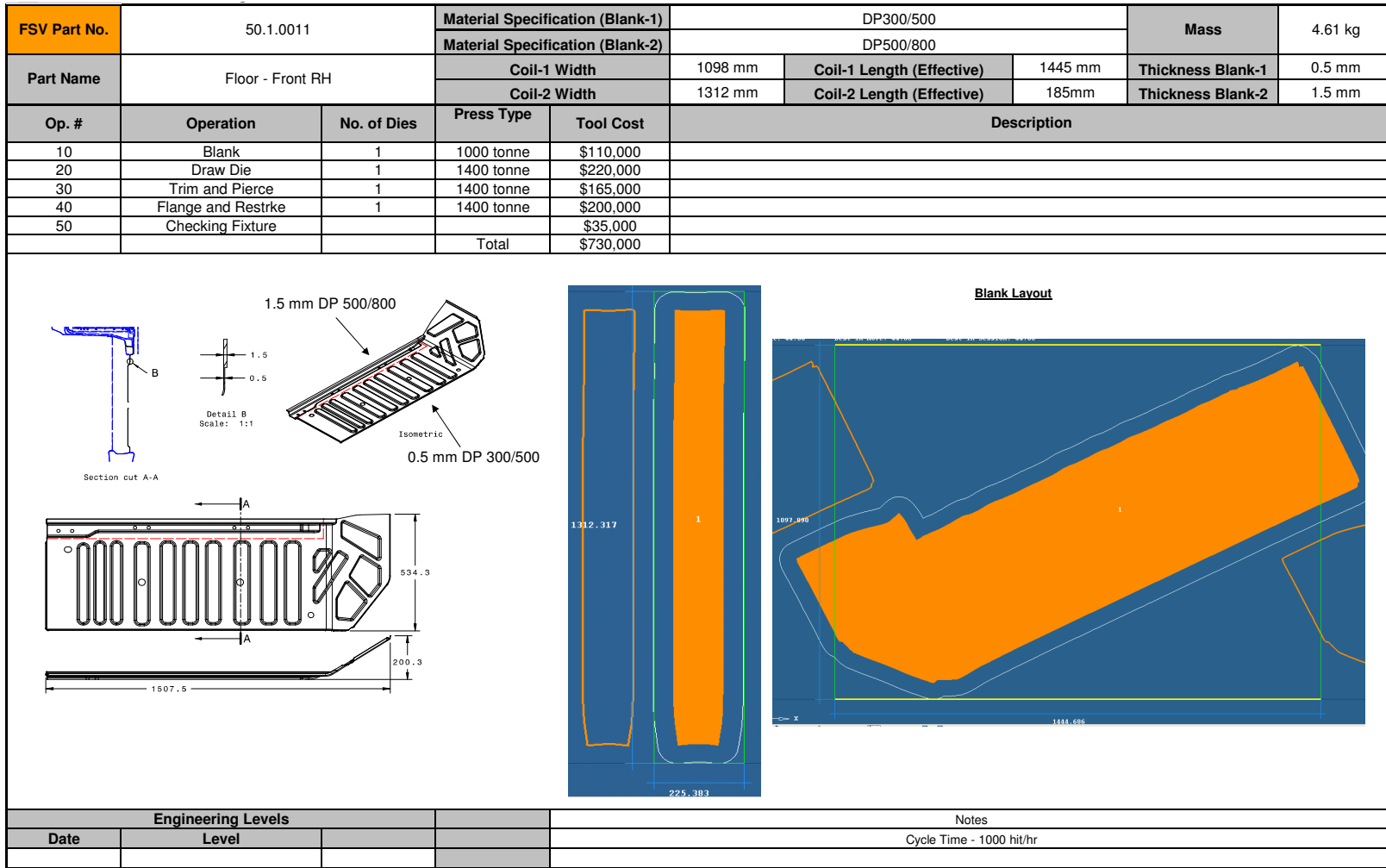


Figure 20.1: Front Floor RH (50.1.0011)

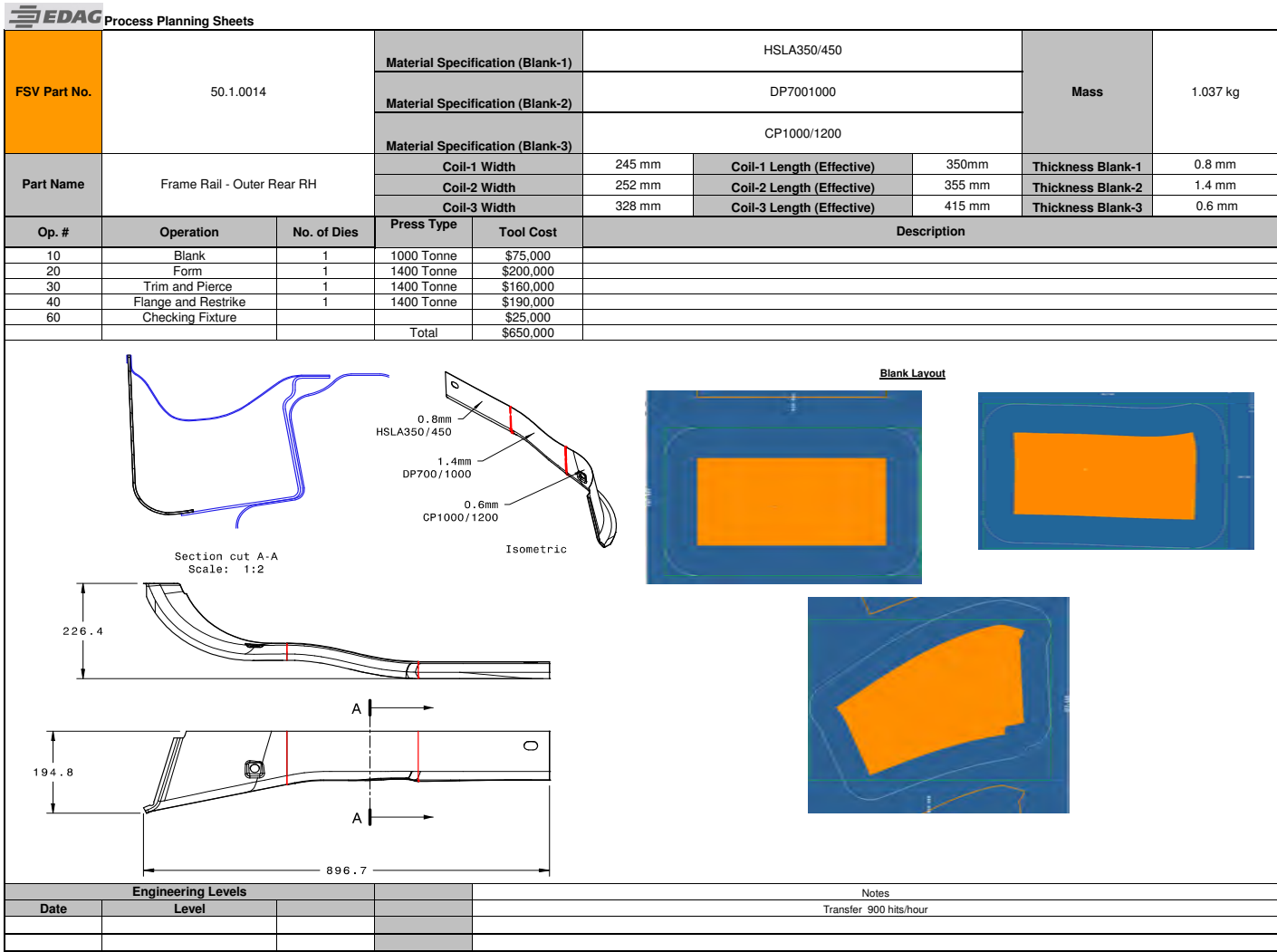


Figure 20.2: Frame Rail Outer Rear RH (50.1.0014)

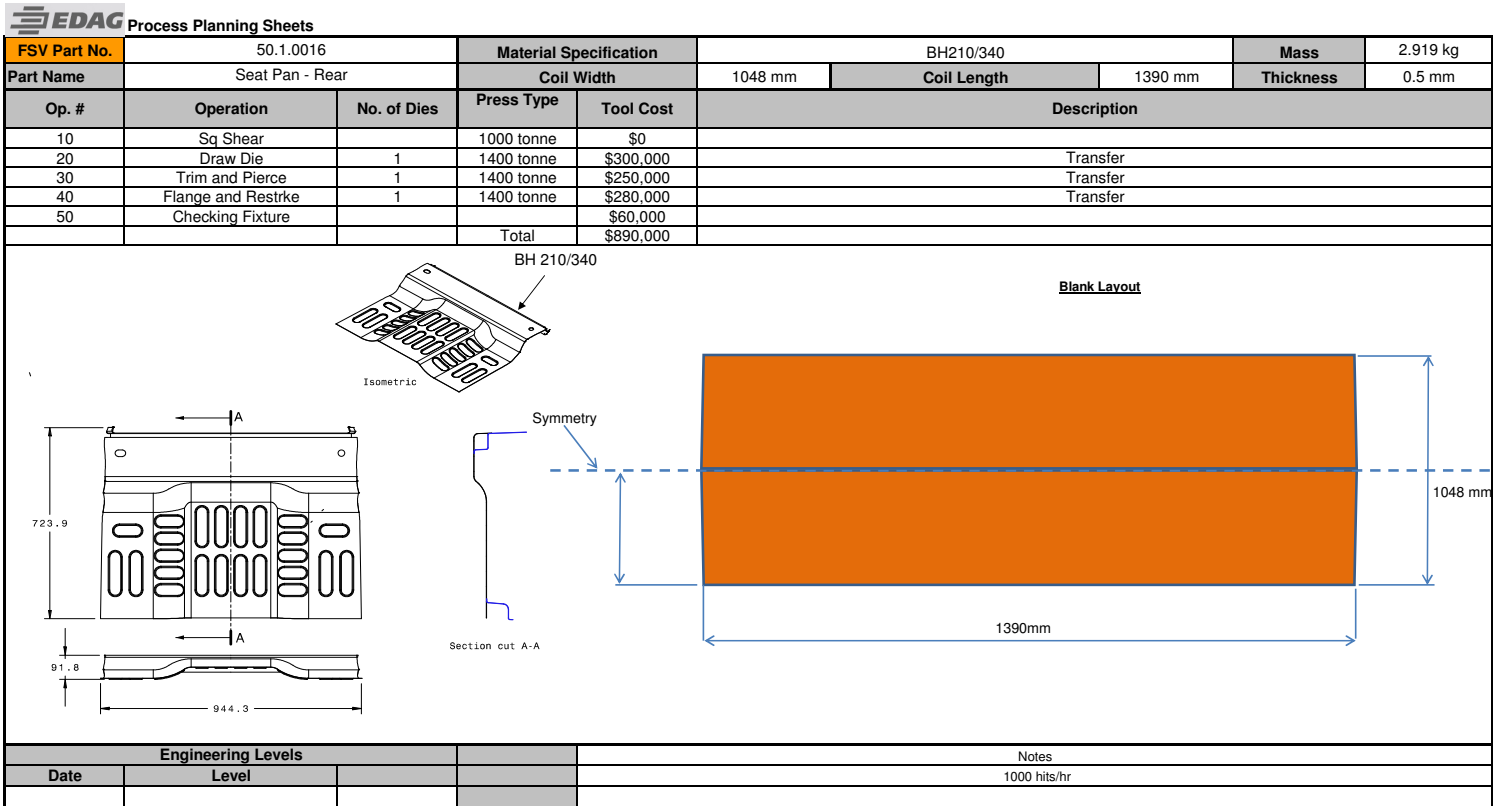


Figure 20.3: Seat Pan Rear (50.1.0016)

EDAG Process Planning Sheets

FSV Part No.	50.1.0017		Material Specification (Blank-1)			BH210/340		Mass	2.58 kg	
			Material Specification (Blank-2)			BH210/340				
Part Name	Wheelhouse Inner RH		Coil-1 Width		516 mm	Coil-1 Length (Effective)		548 mm	Thickness Blank-1	0.7 mm
			Coil-2 Width		623 mm	Coil-2 Length (Effective)		466 mm	Thickness Blank-2	1.2 mm
Op. #	Operation	No. of Dies	Press Type	Tool Cost	Description					
10	Blank	1	600 tonne	\$105,000						
20	Draw Die	1	1000 tonne	\$195,000						
30	Trim	1	1000 tonne	\$165,000						
40	Flange and Restrke	1	1000 tonne	\$180,000						
50	Finish Pierce die	1	1000 tonne	\$150,000						
60	Checking Fixture			\$25,000						
			Total	\$820,000						

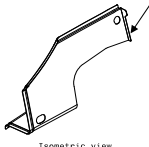
<p>Section cut B-B</p>			<p>Isometric</p>			<p>Blank Layout</p>					
						<p>Notes Double Attached, 500 hits/hr</p>					
Engineering Levels											
Date	Level										

Figure 20.4: Wheelhouse Inner RH (50.1.0017)

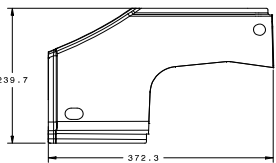

EDAG Process Planning Sheets

FSV Part No.	50.1.0019		Material Specification		BH210/340		Mass	0.577 kg	
Part Name	Back Panel Outboard - RH		Coil Width		576 mm	Coil Length (Effective)	350 mm	Thickness	1.0 mm
Op. #	Operation	No. of Dies	Press Type	Tool Cost	Description				
10	Blank	1	600 tonne	\$70,000					
20	Form	1	800 tonne	\$100,000	Tandem				
30	Trim and Pierce	1	800 tonne	\$90,000	Tandem				
40	Flange and Restrike	1	800 tonne	\$110,000	Tandem				
50	(Cam) Flange	1	800 tonne	\$30,000	Tandem				
60	Checking Fixture			\$10,000					
			Total	\$410,000					

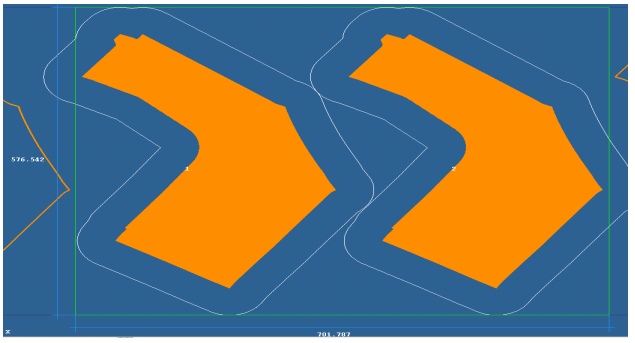
BH 210/340



Isometric view

Blank Layout



Engineering Levels				Notes	
Date	Level			500 hits/hr	

Figure 20.5: Back Panel Outboard (50.1.0019)

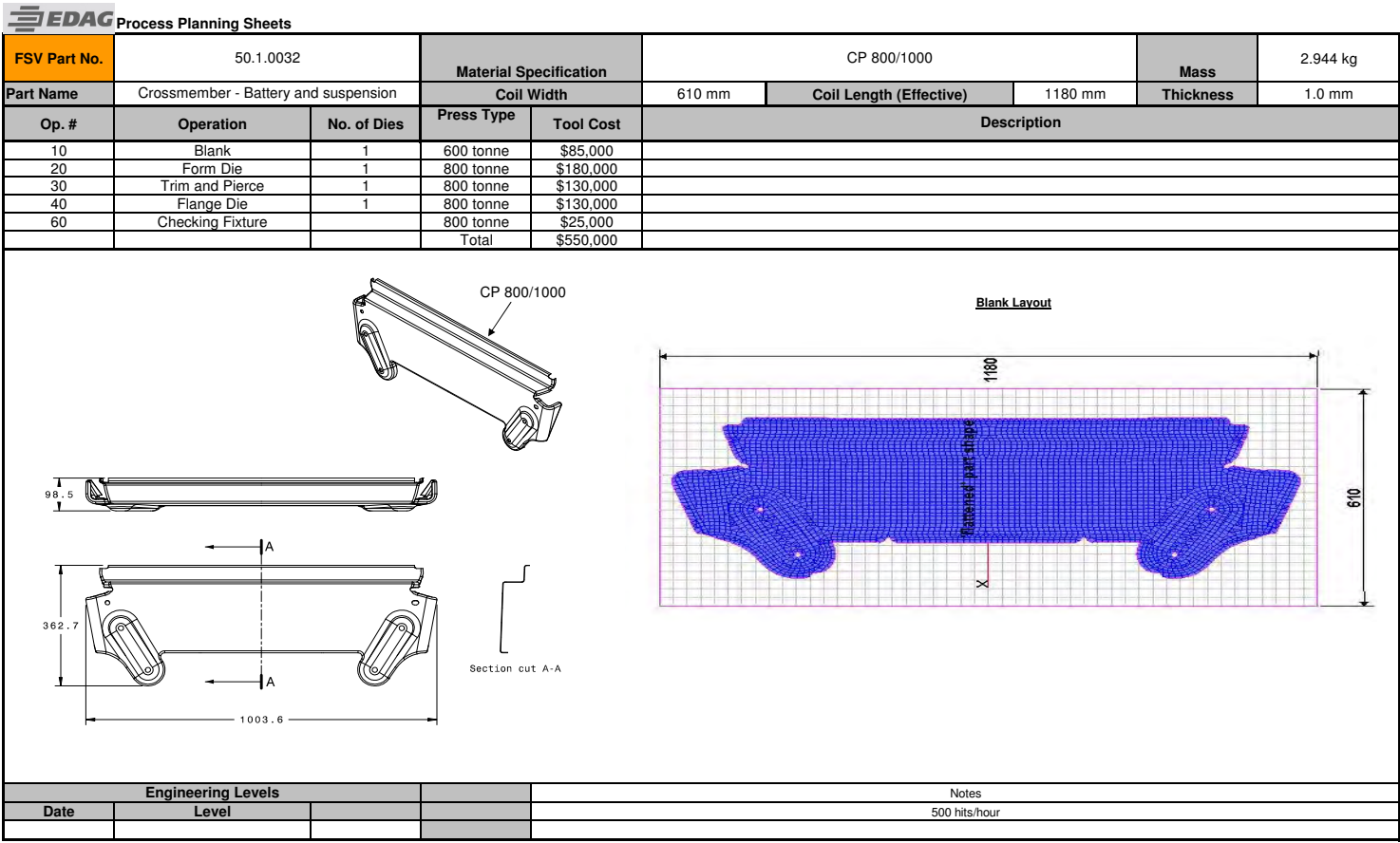


Figure 20.6: Crossmember Battery and Suspension (50.1.0032)

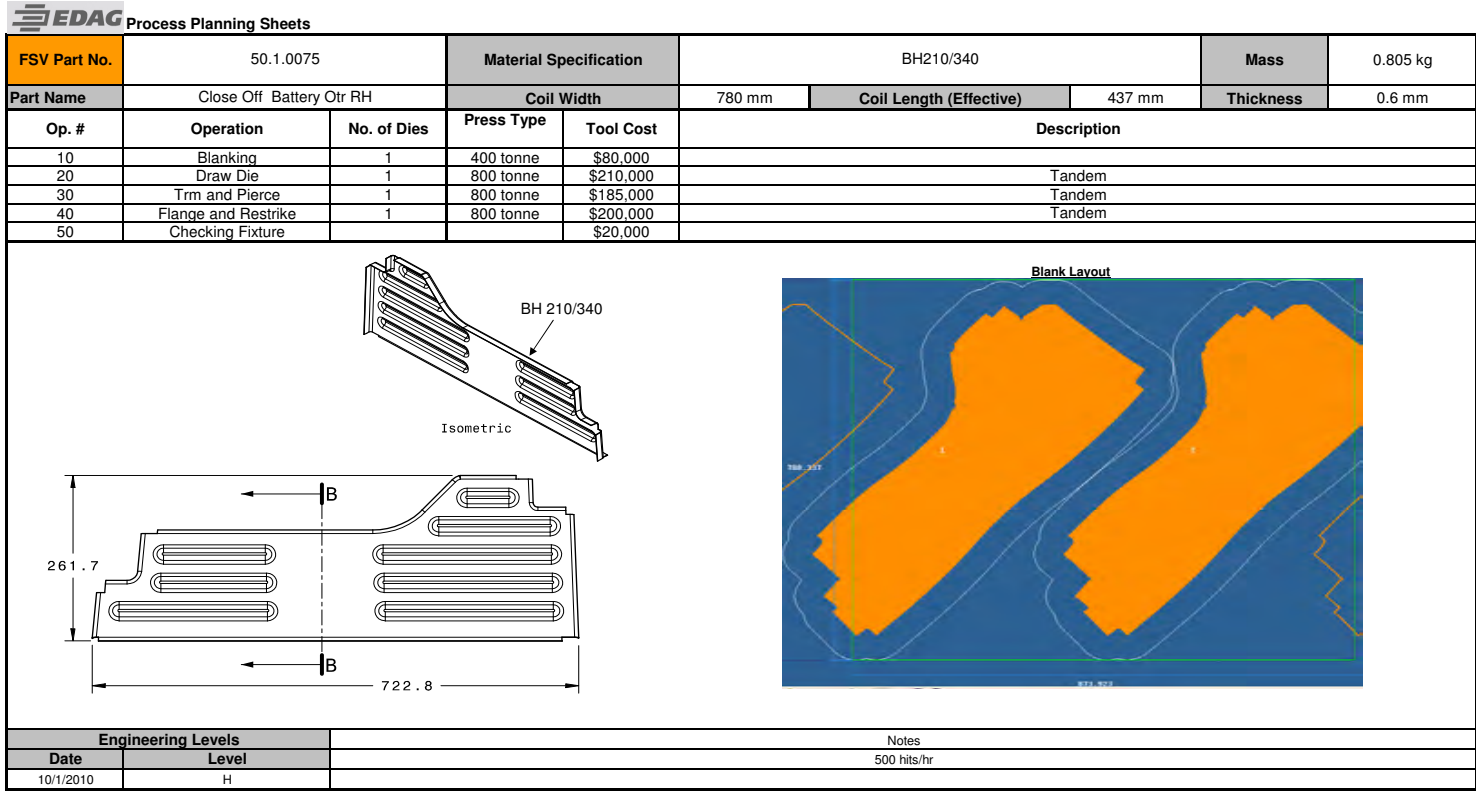


Figure 20.7: Battery Close Off Outer RH (50.1.0075)

FSV Part No.	50.1.0073		Material Specification		BH210/340		Mass	1.195 kg	
Part Name	Close Off Battery Inr RH		Coil Width		494 mm	Coil Length (Effective)	838 mm	Thickness	0.6 mm
Op. #	Operation	No. of Dies	Press Type	Tool Cost	Description				
10	Blanking	1	400 tonne	\$80,000					
20	Draw Die	1	800 tonne	\$210,000	Tandem				
30	Trm and Pierce	1	800 tonne	\$185,000	Tandem				
40	Flange and Restrike	1	800 tonne	\$200,000	Tandem				
50	Checking Fixture			\$20,000					
			Total	\$695,000					
Engineering Levels					Notes				
Date	Level				500 hits/hr				

Figure 20.8: Battery Close Off Inner RH (50.1.0073)

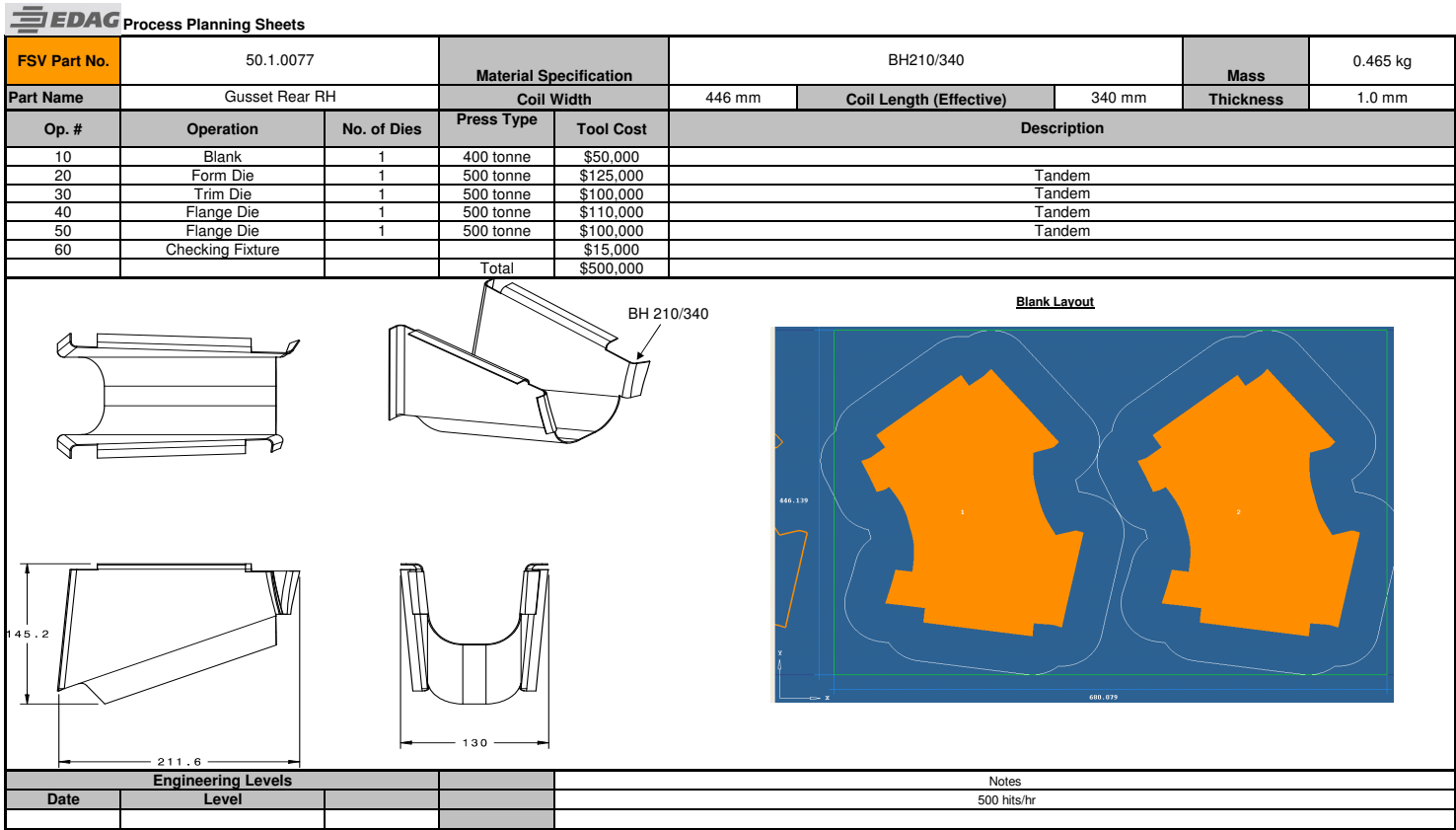


Figure 20.9: Rear Gusset RH (50.1.0077)

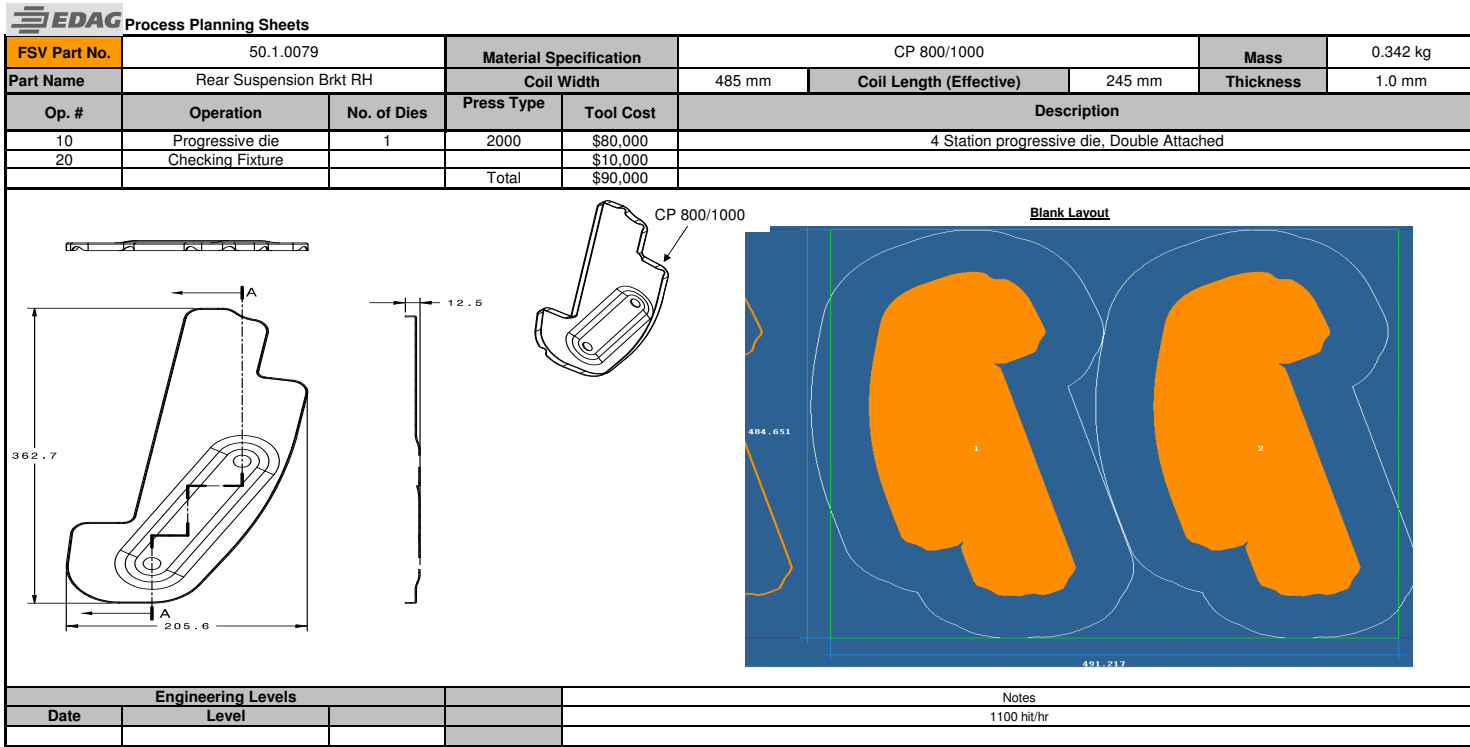


Figure 20.10: Rear Suspension Bracket RH (50.1.0079)

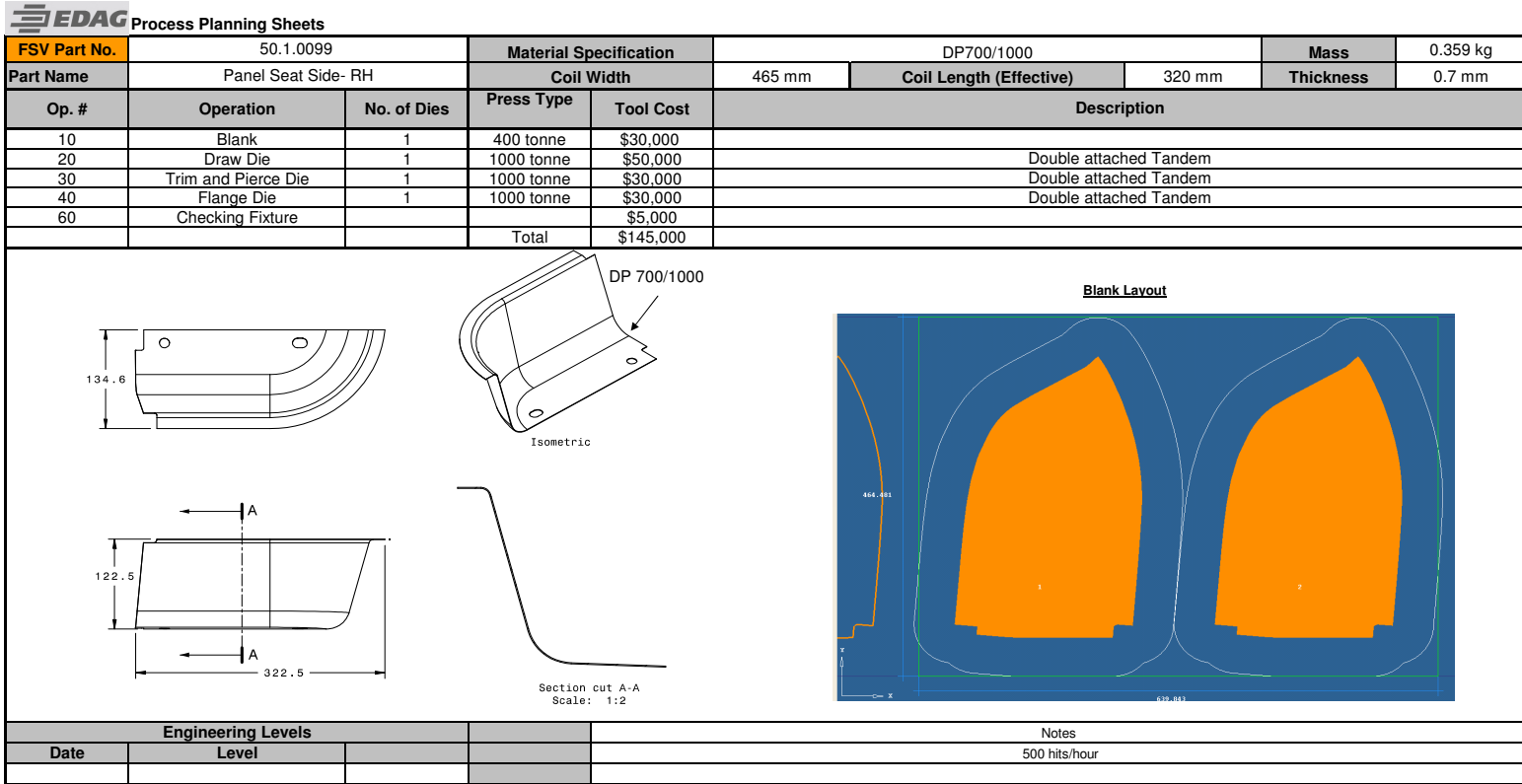


Figure 20.11: Panel Seat Side RH (50.1.0099)

FSV Part No.	50.1.0100			Material Specification		BH210/340		Mass	1.603 kg	
Part Name	Heel Board			Coil Width		1482 mm	Coil Length (Effective)	426 mm	Thickness	0.6 mm
Op. #	Operation	No. of Dies	Press Type	Tool Cost	Description					
10	Blank Die	1	600 tonne	\$90,000						
20	Draw Die	1	800 tonne	\$120,000	Tandem					
30	Trim and Pierce	1	800 tonne	\$90,000	Tandem					
40	Flange Die	1	800 tonne	\$100,000	Tandem					
50	Checking Fixture			\$20,000						
			Total	\$420,000						

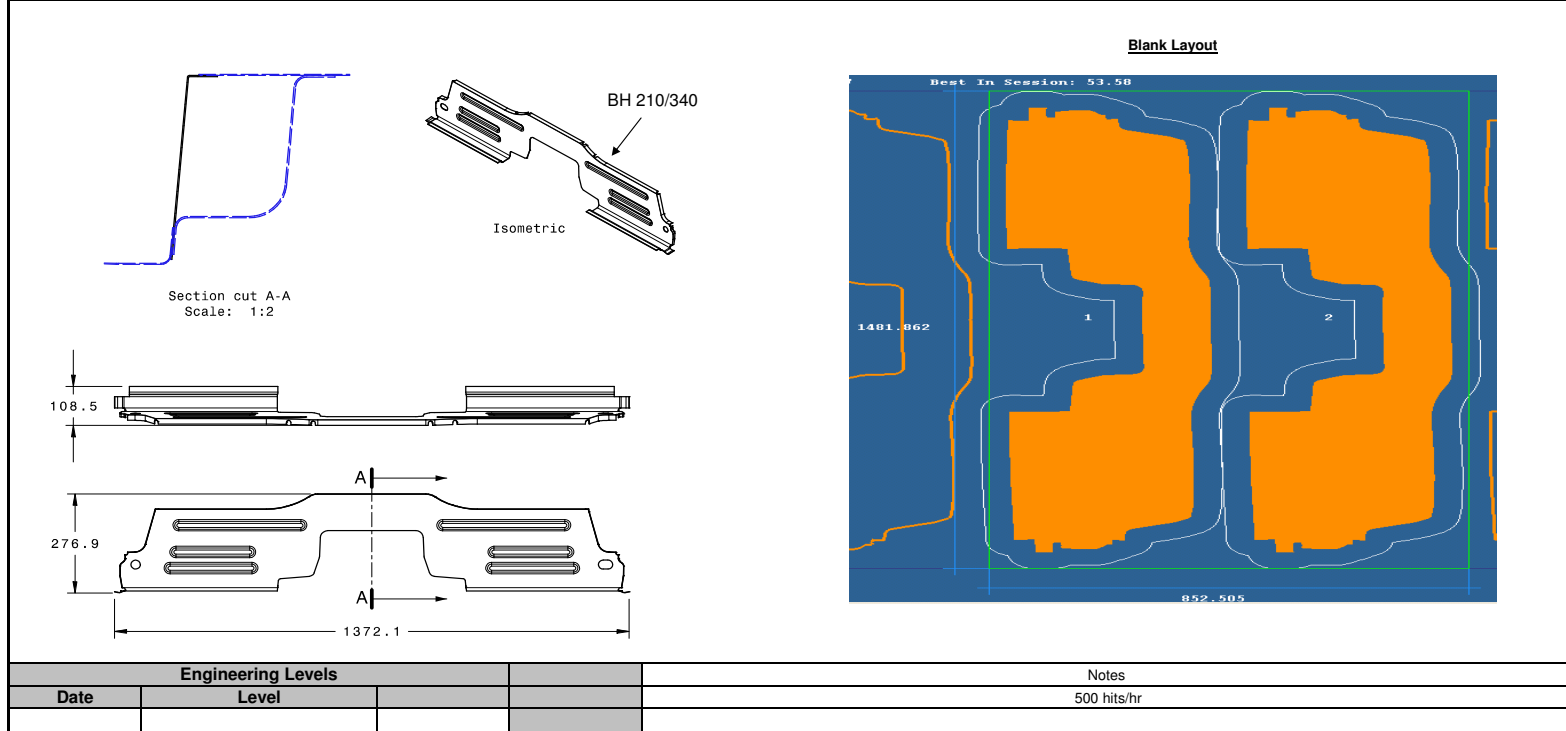


Figure 20.12: Heel Board (50.1.0100)

EDAG Process Planning Sheets

FSV Part No.	50.1.0108		Material Specification		DP700/1000		Mass	2.201 kg	
Part Name	Rail Extension - Tunnel RH		Coil Width		1254 mm	Coil Length (Effective)	302 mm	Thickness	1.2 mm
Op. #	Operation	No. of Dies	Press Type	Tool Cost	Description				
10	Sq shear		600 tonne	\$0					
20	Draw Die	1	1000 tonne	\$225,000	Tandem				
30	Trm and Pierce	1	1000 tonne	\$185,000	Tandem				
40	Flange and Restrike	1	1000 tonne	\$225,000	Tandem				
50	(Cam) Flange	1	1000 tonne	\$100,000	Tandem				
60	Checking Fixture			\$20,000					
			Total	\$755,000					

DP 700/1000

Section cut B-B
Scale: 1:2

Section cut A-A
Scale: 1:2

1154

Blank Layout

1254.347

603.422

Engineering Levels				Notes	
Date	Level			600 hits/hr	

Figure 20.13: Rail Longitudinal Rear (50.1.0108)

FSV Part No.	50.1.0109		Material Specification (Blank-1)			CP1000/1200		Mass	1.555 kg	
			Material Specification (Blank-2)			DP700/1000				
			Material Specification (Blank-3)			Mild140/270				
Part Name	Frame Rail - Reinf RR RH		Coil-1 Width		260 mm	Coil-1 Length (Effective)		440mm	Thickness Blank-1	1.1 mm
			Coil-2 Width		300 mm	Coil-2 Length (Effective)		750 mm	Thickness Blank-2	0.65 mm
			Coil-3 Width		315 mm	Coil-3 Length (Effective)		350 mm	Thickness Blank-3	1.55 mm
Op. #	Operation	No. of Dies	Press Type	Tool Cost	Description					
10	Blank	1	1000 tonne	\$150,000						
20	Form	1	Transfer	\$200,000						
30	Trim	1	Transfer	\$160,000						
40	Flange and Restrike	1	Transfer	\$190,000						
50	Pierce	1	Transfer	\$130,000						
60	Checking Fixture			\$30,000						
			Total	\$860,000						

Blank Layout

Engineering Levels			Notes
Date	Level		950 hits/hour

Figure 20.14: Frame Rail Reinforcement Rear RH (50.1.0109)

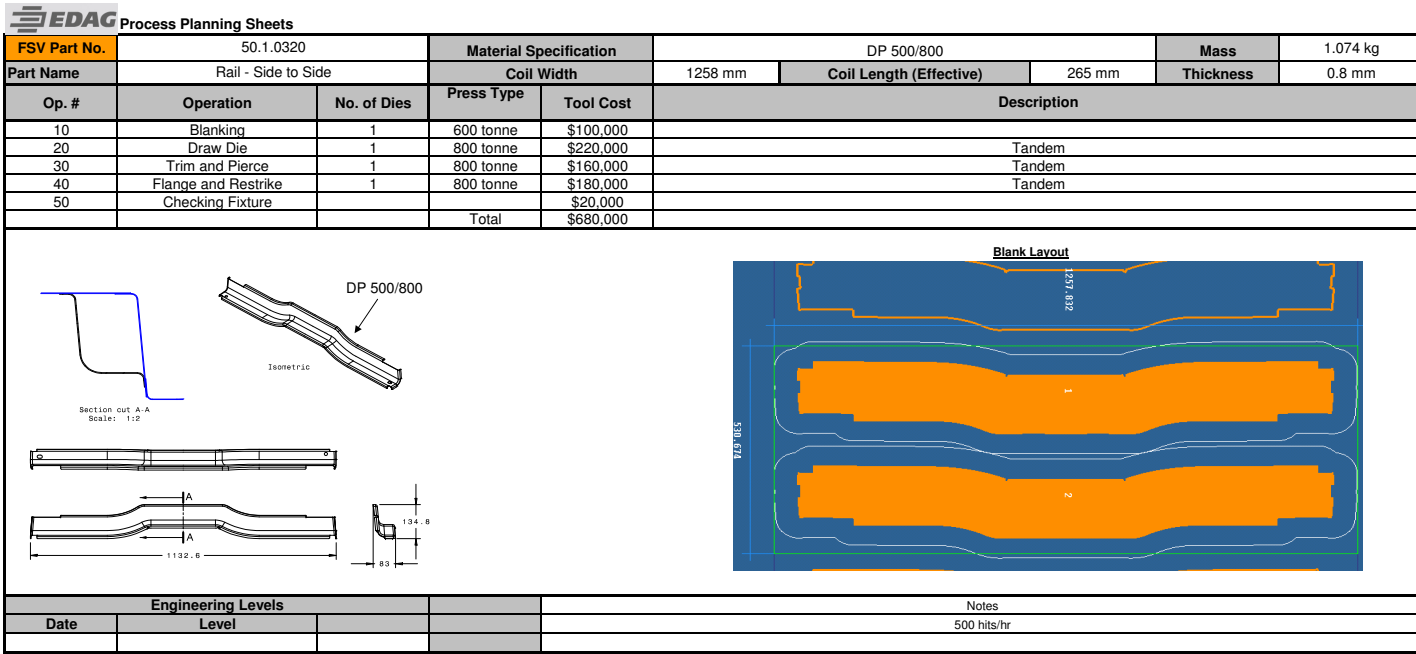


Figure 20.15: Rail Side to Side (50.1.0320)

EDAG Process Planning Sheets

FSV Part No.	50.1.0013		Material Specification		BH210/340		Mass	1.866 kg	
Part Name	Pnl - Rear Liftgate Lower		Coil Width		878 mm	Coil Length (Effective)	602 mm	Thickness	0.7 mm
Op. #	Operation	No. of Dies	Press Type	Tool Cost	Description				
10	Blank	1	600 tonne	\$120,000					
20	Draw	1	800 tonne	\$245,000	Tandem				
30	Trim and Pierce	1	800 tonne	\$200,000	Tandem				
40	Flange and Restrike	1	800 tonne	\$225,000	Tandem				
50	(Cam) Flange	1	800 tonne	\$150,000	Tandem				
60	Checking Fixture			\$20,000					
			Total	\$960,000					

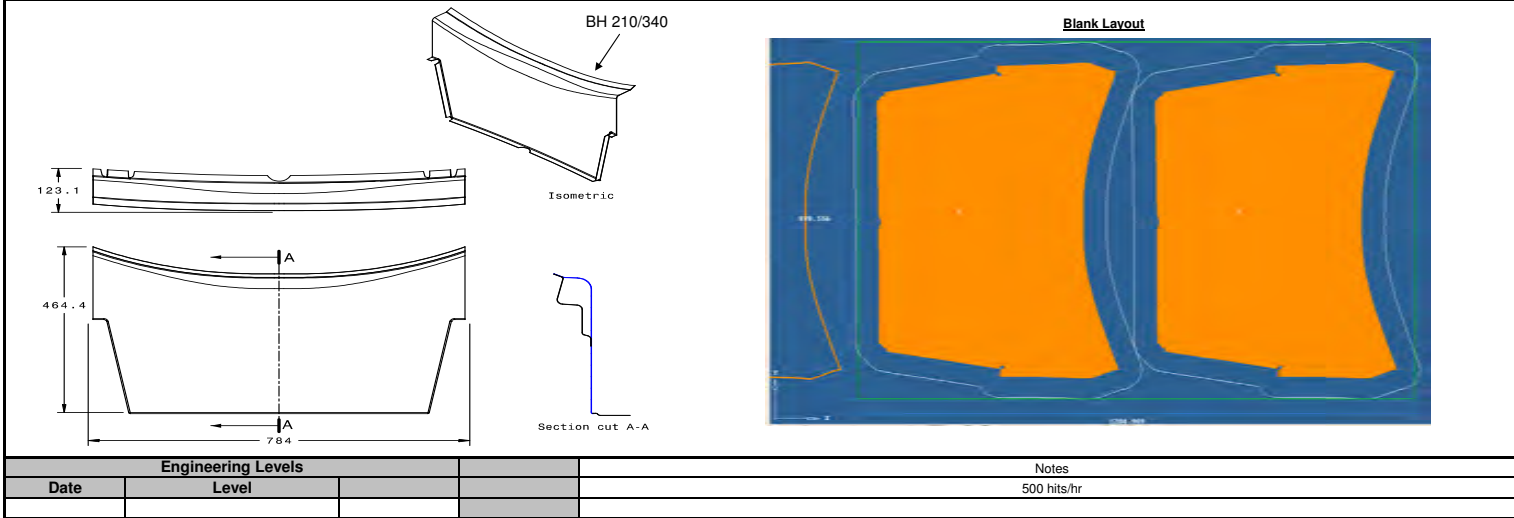


Figure 20.16: Panel Rear Liftgate Lower(50.1.0013)

FSV Part No.	50.1.0328		Material Specification		BH210/340		Mass	0.585 kg	
Part Name	Pnl - Rear Liftgate Lower Inr RH		Coil Width		431 mm	Coil Length (Effective)	427mm	Thickness	1.0 mm
Op. #	Operation	No. of Dies	Press Type	Tool Cost	Description				
10	Blank	1	600tonne	\$70,000					
20	Form	1	800 tonne	\$100,000	Tandem				
30	Trim and Pierce	1	800 tonne	\$90,000	Tandem				
40	Flange and Restrike	1	800 tonne	\$110,000	Tandem				
50	Checking Fixture			\$10,000					
			Total	\$380,000					

Section cut A-A
Scale: 1:2

Isometric

BH 210/340

Blank Layout

Engineering Levels		Notes	
Date	Level	500 hits/hr	

Figure 20.17: Panel Rear Liftgate Lower Inner RH(50.1.0328)

EDAG Process Planning Sheets

FSV Part No.	50.1.0330		Material Specification		Mild 140/270		Mass	1.326 kg	
Part Name	Panel - Cargo Box Floor		Coil Width		770 mm	Coil Length (Effective)	606 mm	Thickness	0.5 mm
Op. #	Operation	No. of Dies	Press Type	Tool Cost	Description				
10	Blanking	1	400 tonne	\$100,000					
20	Draw	1	800 tonne	\$200,000	Tandem				
30	Trim and Pierce	1	800 tonne	\$100,000	Tandem				
40	Flange and Restrike	1	800 tonne	\$150,000	Tandem				
50	Checking Fixture			\$25,000					
			Total	\$575,000					

Mild 140/270

Blank Layout

Isometric

624.3

478.5

26

769.406

605.548

Engineering Levels			Notes	
Date	Level		500 hits/hr	

Figure 20.18: Rear Cargo Box Side (50.1.0330)

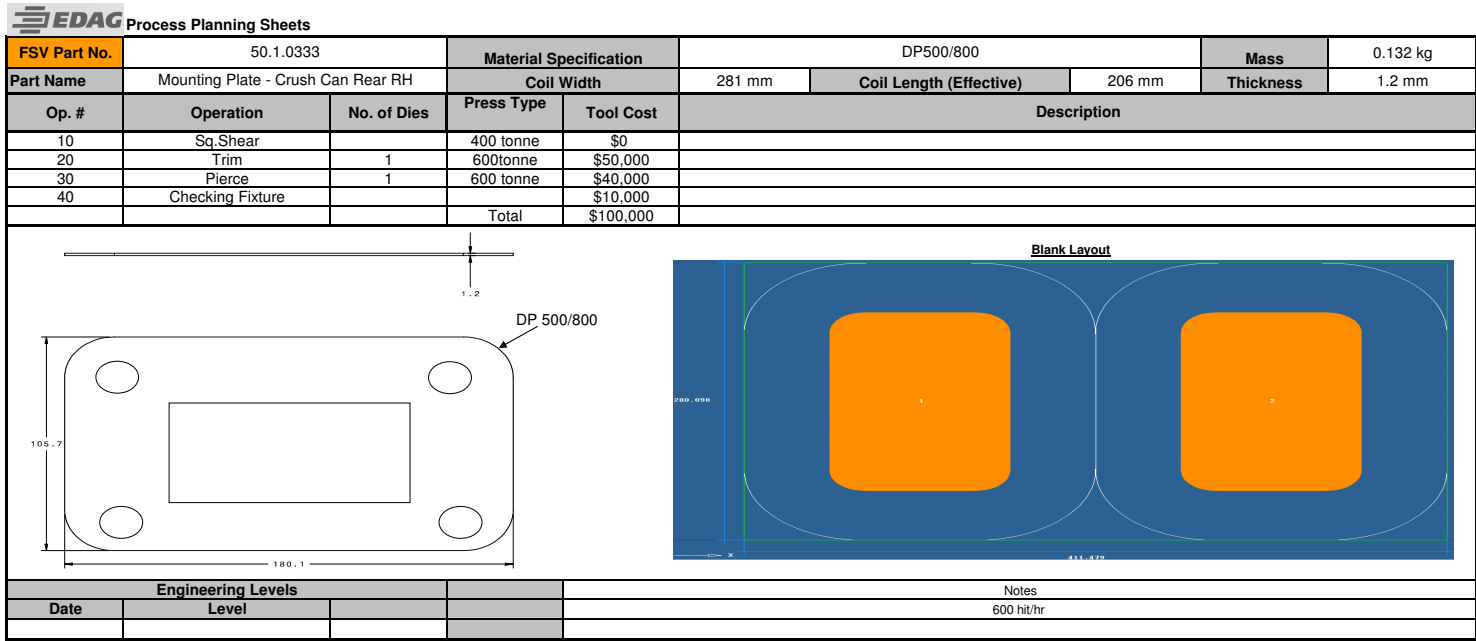


Figure 20.19: Mounting Plate Crush Can Rear RH (50.1.0333)

FSV Part No.	50.1.0335		Material Specification (Blank-1)		HSLA350/450		Mass	2.634 kg	
			Material Specification (Blank-2)		DP700/1000				
			Material Specification (Blank-3)		CP1000/1200				
			Material Specification (Blank-4)		DP700/1000				
Part Name	Frame Rail - Inr Rear RH		Coil-1 Width	355 mm	Coil-1 Length (Effective)	342mm	Thickness Blank-1	0.8 mm	
			Coil-2 Width	330 mm	Coil-2 Length (Effective)	360 mm	Thickness Blank-2	1.4 mm	
			Coil-3 Width	350mm	Coil-3 Length (Effective)	352 mm	Thickness Blank-3	0.6 mm	
			Coil-4 Width	455 mm	Coil-4 Length (Effective)	465 mm	Thickness Blank-4	1.4mm	
Op. #	Operation	No. of Dies	Press Type	Tool Cost	Description				
10	Blank	1	1000 Tonne	\$150,000					
20	Form	1	1400 Tonne	\$200,000					
30	Trim	1	1400 Tonne	\$160,000					
40	Flange and Restrike	1	1400 Tonne	\$190,000					
50	Pierce	1	1400 Tonne	\$130,000					
60	Checking Fixture			\$25,000					
			Total	\$855,000					

Blank Layout

Engineering Levels				Notes	
Date	Level			900 hits/hour	

Figure 20.20: Frame Rail Inner Rear RH (50.1.0335)



Process Planning Sheets

FSV Part No.	50.1.0402		Material Specification		BH280/400		Mass	2.342 kg	
Part Name	Panel - Tunnel Side RH		Coil Width		1646 mm	Coil Length (Effective)	529 mm	Thickness	0.5 mm
Op. #	Operation	No. of Dies	Press Type	Tool Cost	Description				
10	Blank	1	600 tonne	\$100,000					
20	Draw Die	1	Transfer	\$220,000	Transfer Double attached 1LH & 1RH				
30	Trim and Pierce	1	Transfer	\$160,000	Transfer Double attached 1LH & 1RH				
40	Flange and Restrke	1	Transfer	\$200,000	Transfer Double attached 1LH & 1RH				
50	Checking Fixture	1		\$20,000	Transfer Double attached 1LH & 1RH				
			Total	\$700,000					

Engineering Levels			Notes	
Date	Level		1100 hits/hr	

Figure 20.21: Panel Tunnel Side RH (50.1.0402)

EDAG Process Planning Sheets

FSV Part No.	50.1.2113		Material Specification		Mild 140/270		Mass	0.611 kg	
Part Name	Panel - Cargo Box Side RH		Coil Width		602 mm	Coil Length (Effective)	468 mm	Thickness	0.5 mm
Op. #	Operation	No. of Dies	Press Type	Tool Cost	Description				
10	Blanking	1	400 tonne	\$100,000					
20	Draw	1	800 tonne	\$200,000	Tandem				
30	Trim and Pierce	1	800 tonne	\$100,000	Tandem				
40	Flange and Restrike	1	800 tonne	\$150,000	Tandem				
50	Checking Fixture			\$25,000					
			Total	\$575,000					

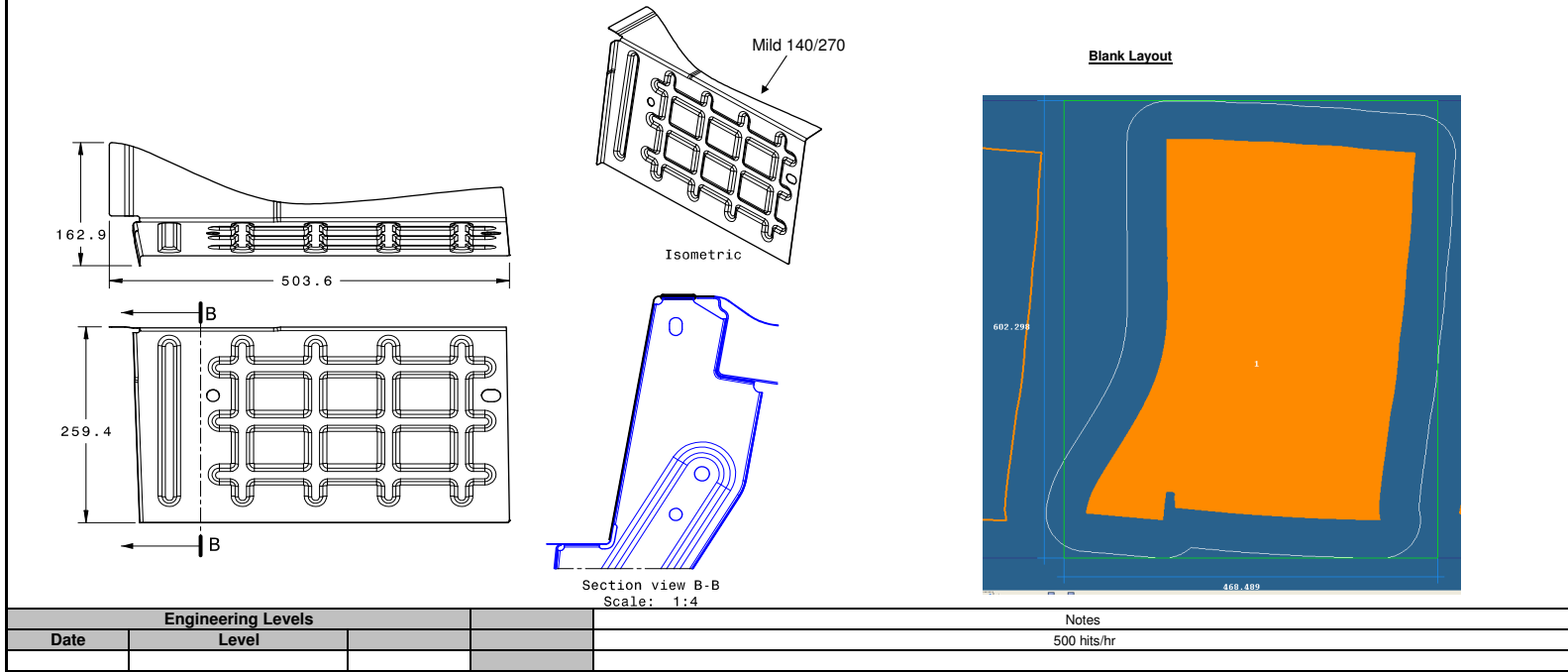


Figure 20.22: Rear Cargo Box (50.1.2113)

EDAG Process Planning Sheets

FSV Part No.	50.1.0020		Material Specification		BH210/340		Mass	1.405 kg	
Part Name	Back Panel - Lower		Coil Width		810 mm	Coil Length (Effective)	403 mm	Thickness	1.0 mm
Op. #	Operation	No. of Dies	Press Type	Tool Cost	Description				
10	Blank	1	600 tonne	\$70,000					
20	Form	1	800 tonne	\$160,000	Tandem				
30	Trim and Pierce	1	800 tonne	\$120,000	Tandem				
40	Flange and Restrike	1	800 tonne	\$140,000	Tandem				
50	Checking Fixture			\$10,000					
			Total	\$500,000					

BH 210/340

Isometric

Section A-A

Blank Layout

Engineering Levels		Notes	
Date	Level	500 hits/hr	

Figure 20.23: Back Panel Lower (50.1.0020)

FSV Part No.	50.1 2601		Material Specification		DP500/800		Mass	0.566 kg	
Part Name	Mount - Rear Shock RH		Coil Width		547 mm	Coil Length (Effective)	184 mm	Thickness	2.5 mm
Op. #	Operation	No. of Dies	Press Type	Tool Cost	Description				
10	Progressive Die	1	350	\$190,000					
20	Checking Fixture			\$10,000					
			Total	\$200,000					

Section cut A-A
Scale: 1:2

Isometric view
Scale: 1:4

Blank Layout

Engineering Levels			Notes
Date	Level		
			6 station progressive Die, 1000 pcs/hr

Figure 20.24: Mount Rear Shock (50.1.2601)

EDAG Process Planning Sheets

FSV Part No.	50.1 2602		Material Specification		DP500/800		Mass	0.176kg	
Part Name	Reinf - Rear Shock RH		Coil Width		290 mm	Coil Length (Effective)	176 mm	Thickness	2.0 mm
Op. #	Operation	No. of Dies	Press Type	Tool Cost	Description				
10	Progressive Die	1	350	\$190,000					
20	Checking Fixture			\$10,000					
			Total	\$200,000					
					<p align="center">Blank Layout</p>				
Engineering Levels					Notes				
Date	Level				6 station progressive Die, 1000 pcs/hr				

Figure 20.25: Rear Shock Reinforcement (50.1.2602)

FSV Part No.	50.1 2002		Material Specification		DP500/800		Mass	0.37 kg	
Part Name	Mount - Trailing Arm RH		Coil Width		375 mm	Coil Length (Effective)	226 mm	Thickness	2 mm
Op. #	Operation	No. of Dies	Press Type	Tool Cost	Description				
10	Progressive Die	1	350	\$190,000					
20	Checking Fixture			\$10,000					
			Total	\$200,000					

Blank Layout

Engineering Levels			Notes	
Date	Level		12 station progressive Die, 1000 pcs/hr	

Figure 20.26: Rear Shock Reinforcement (50.1.2002)



Process Planning Sheets

FSV Part No	50.1.0001		Material Specification		BH280/400		Mass	2.839 kg	
Part Name	Dash - Toe Pan		Coil Width		1572 mm	Coil Length (Effective)	734 mm	Thickness	0.5 mm
Op. #	Operation	No. of Dies	Press Type	Tool Cost	Description				
10	Blank	1	800 tonne	\$100,000					
20	Draw	1	1400 tonne	\$300,000	Transfer				
30	Trim	1	1400 tonne	\$150,000	Transfer				
40	Flange and Restrike	1	1400 tonne	\$250,000	Transfer				
50	Trim and Pierce	1	1400 tonne	\$150,000	Transfer				
60	Finish Flange	1	1400 tonne	\$120,000	Transfer				
70	Checking Fixture			\$50,000					
			Total	\$1,120,000					

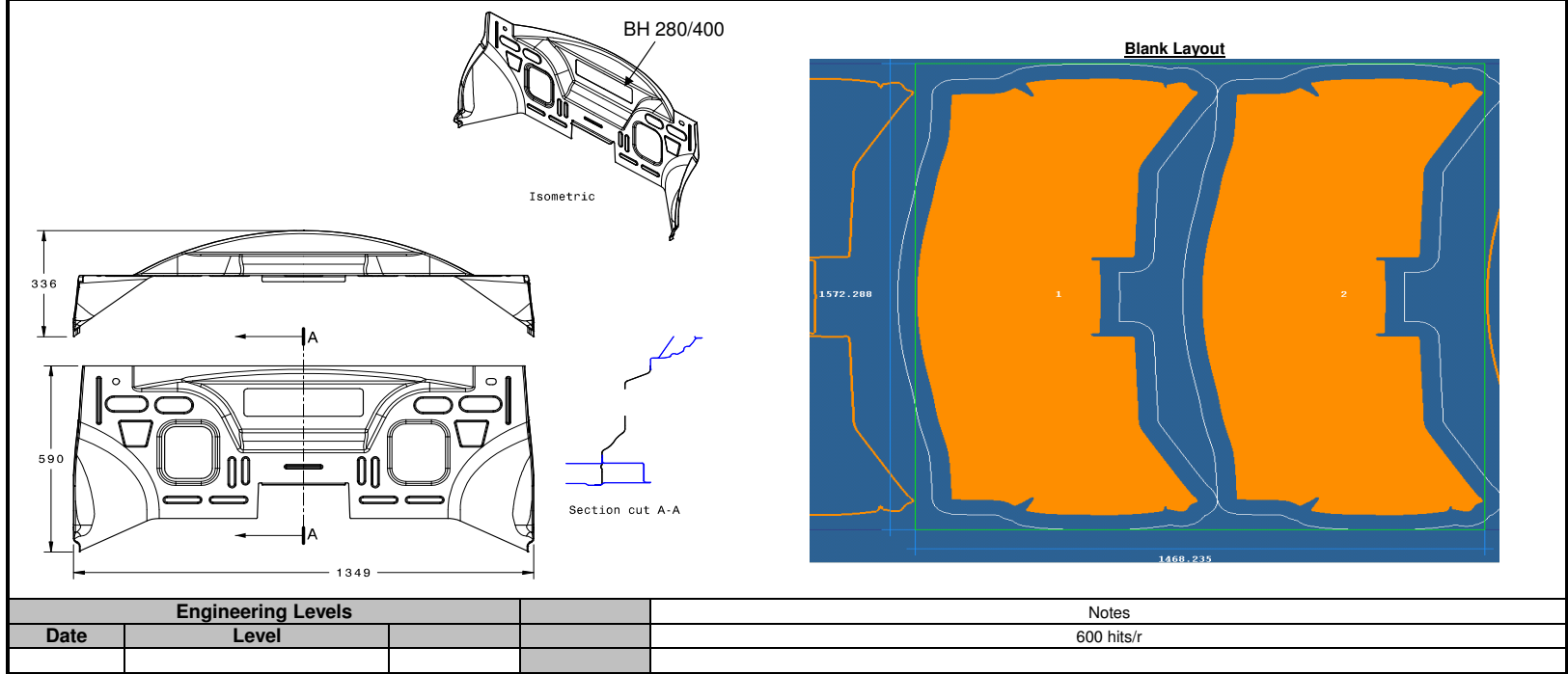


Figure 20.27: Dash Toe Pan (50.1.0001)

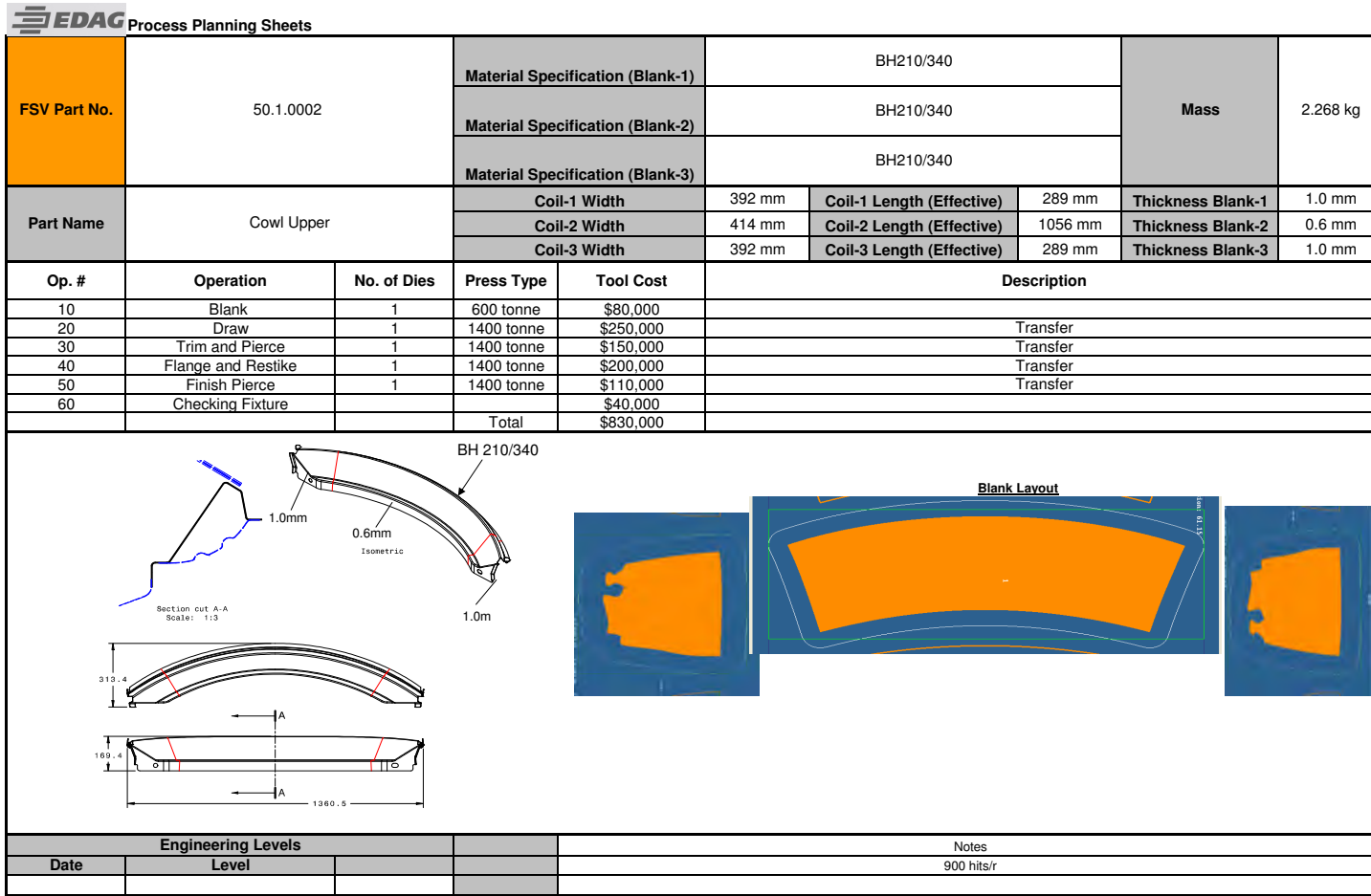


Figure 20.28: Cowl Upper (50.1.0002)

EDAG Process Planning Sheets

FSV Part No.	50.1.0070	Material Specification (Blank-1)			BH210/340		Mass	1.494 kg
		Material Specification (Blank-2)			BH210/340			
		Material Specification (Blank-3)			BH210/340			
Part Name	Cowl Lower	Coil-1 Width		281 mm	Coil-1 Length (Effective)	282 mm	Thickness Blank-1	1.2 mm
		Coil-2 Width		291 mm	Coil-2 Length (Effective)	1016 mm	Thickness Blank-2	0.6 mm
		Coil-3 Width		281 mm	Coil-3 Length (Effective)	282 mm	Thickness Blank-3	1.2 mm
Op. #	Operation	No. of Dies	Press Type	Tool Cost	Description			
10	Blank	1	600 tonne	\$80,000				
20	Draw	1	1400 tonne	\$250,000	Transfer			
30	Trim and Pierce	1	1400 tonne	\$150,000	Transfer			
40	Flange and Restrike	1	1400 tonne	\$200,000	Transfer			
50	Finish Pierce	1	1400 tonne	\$110,000	Transfer			
60	Checking Fixture			\$40,000				
			Total	\$830,000				

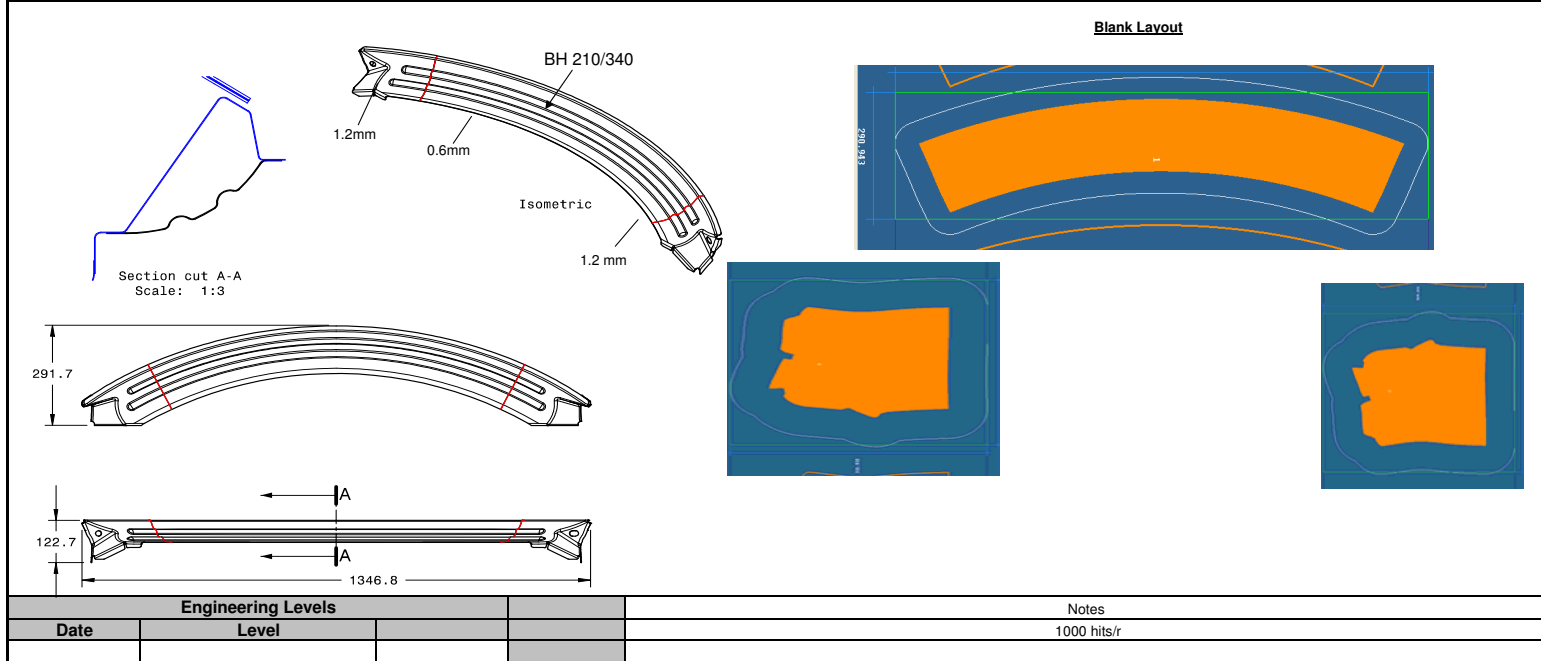


Figure 20.29: Cowl Lower (50.1.0070)

FSV Part No.	60.2 0007		Material Specification		DP500/800		Mass	0.121 kg	
Part Name	Mounting Plate - Crush Can Front RH		Coil Width		203 mm	Coil Length (Effective)	203 mm	Thickness	1.75mm
Op. #	Operation	No. of Dies	Press Type	Tool Cost	Description				
10	Progressive Die	1	350 tonne	\$80,000	Double attached				
20	Checking Fixture			\$5,000					
			Total	\$85,000					
Engineering Levels			Notes						
Date	Level				1000 hits/hr				

Figure 20.30: Mounting Plate Crush Can Front (60.2.0007)

EDAG Process Planning Sheets

FSV Part No.	50.1.0305		Material Specification		DP700/1000		Mass	0.309 kg	
Part Name	Closeout - Lower Rail RH		Coil Width		337mm	Coil Length (Effective)	339 mm	Thickness	0.8 mm
Op. #	Operation	No. of Dies	Press Type	Tool Cost	Description				
10	Blank	1	600 tonne	\$50,000					
20	Trim and Pierce	1	800 tonne	\$130,000	Tandem				
30	Flange and Restrike	1	800 tonne	\$150,000	Tandem				
40	Checking Fixture		800 tonne	\$20,000					
			Total	\$350,000					

Blank Layout

Engineering Levels		Notes	
Date	Level	500 pcs/hr	

Figure 20.31: Closeout Lower Rail (50.1.0305)

FSV Part No.	50.1.0301		Material Specification (Blank-1)		TRIP 600/980		Mass	5.998 kg	
			Material Specification (Blank-2)		TRIP 600/980				
			Material Specification (Blank-3)		TRIP 600/980				
			Material Specification (Blank-4)		TRIP 600/980				
Part Name	Front Rail - Lower RH		Coil-1 Width		799mm	Coil-1 Length (Effective)	877 mm	Thickness Blank-1	1.8mm
			Coil-2 Width		267 mm	Coil-2 Length (Effective)	331 mm	Thickness Blank-2	1.9 mm
			Coil-3 Width		239 mm	Coil-3 Length (Effective)	301 mm	Thickness Blank-3	2.0 mm
			Coil-4 Width		230 mm	Coil-4 Length (Effective)	301 mm	Thickness Blank-4	1.9mm
Op. #	Operation	No. of Dies	Press Type	Tool Cost	Description				
10	Blank	2	1000 tonne	\$150,000					
20	Form	1	1400 tonne	\$200,000	Transfer				
30	Trim	1	1400 tonne	\$170,000	Transfer				
40	Flange and Restrike	1	1400 tonne	\$180,000	Transfer				
50	Pierce	1	1400 tonne	\$130,000	Transfer				
60	Cheking Fixture	1		\$20,000					
			Total	\$850,000					

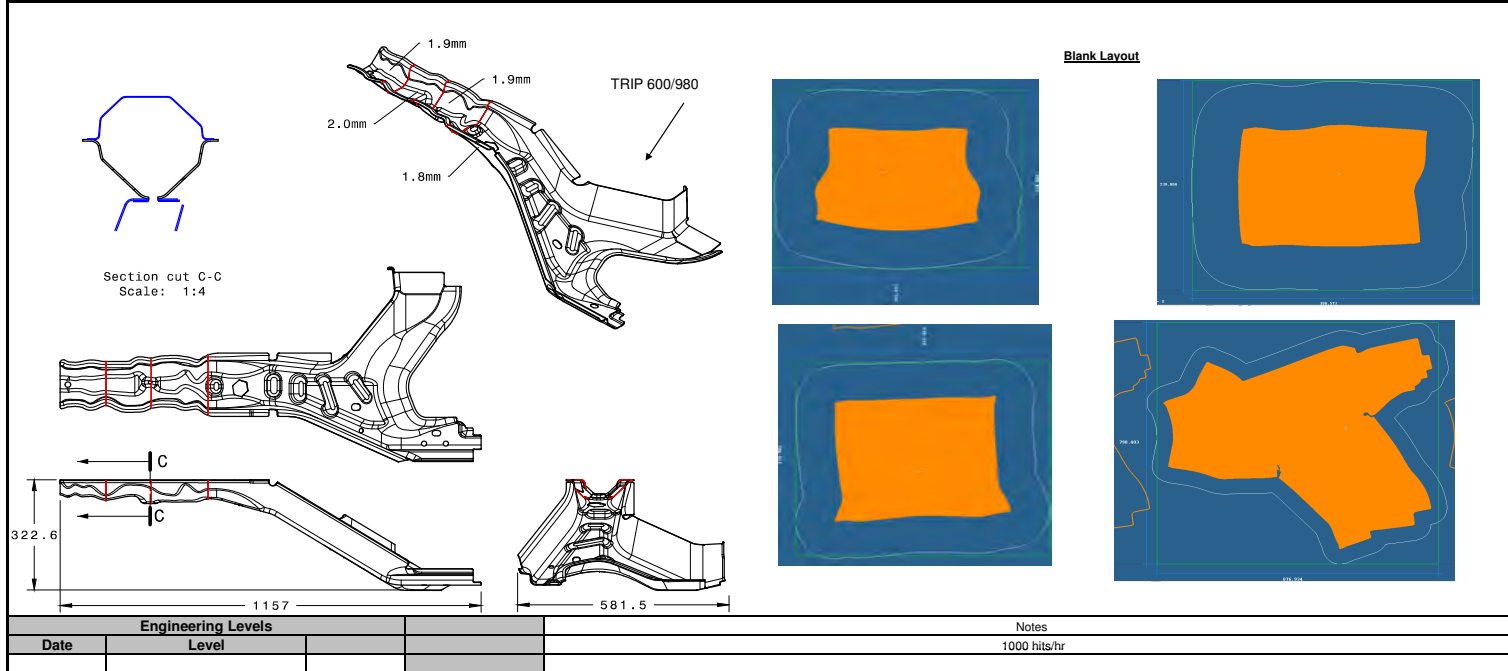


Figure 20.32: Front Rail Lower (50.1.0301)

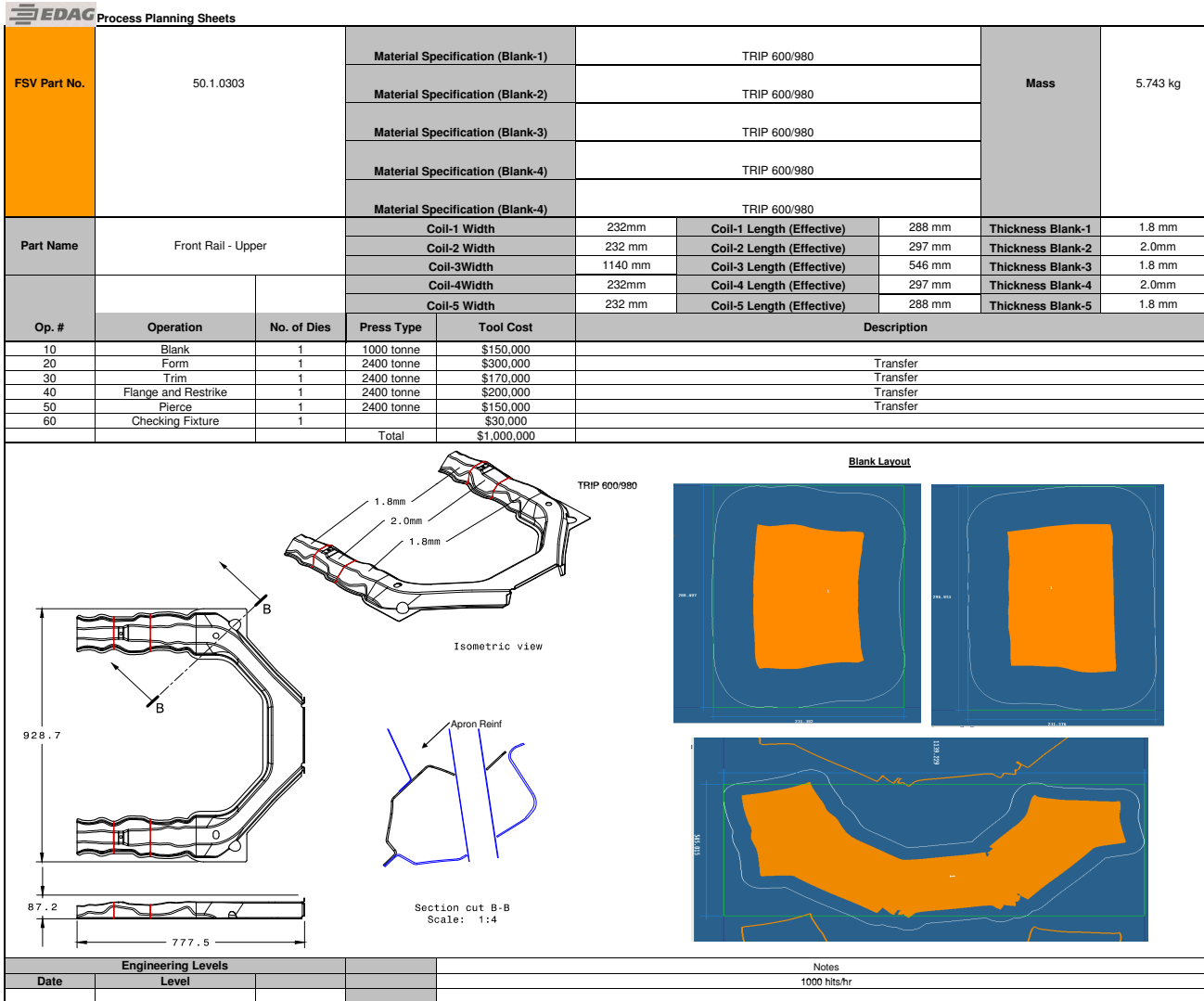
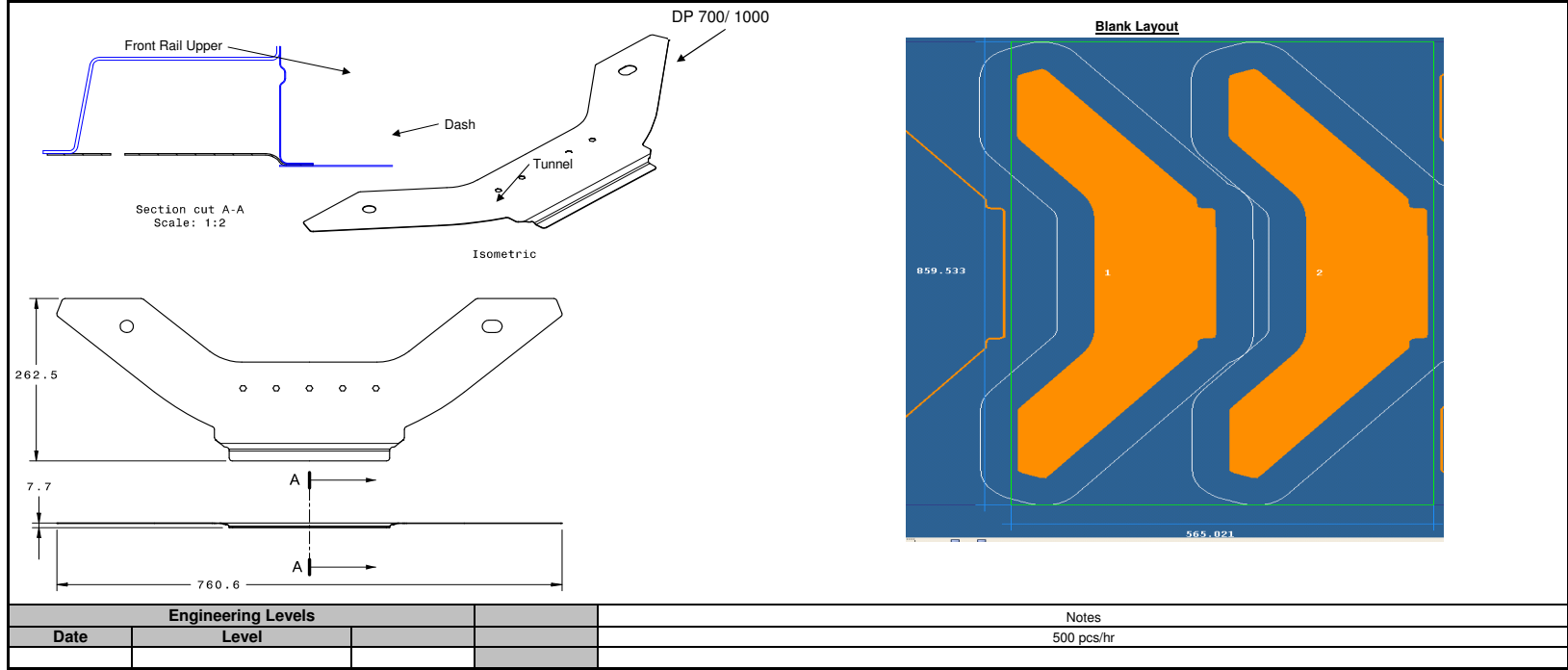


Figure 20.33: Front Rail Upper (50.1.0303)

Process Planning Sheets

FSV Part No.	50.1.0304		Material Specification		DP700/1000		Mass	0.616 kg	
Part Name	Closeout - Upper Rail		Coil Width		860mm	Coil Length (Effective)	283 mm	Thickness	1.0 mm
Op. #	Operation	No. of Dies	Press Type	Tool Cost	Description				
10	Blank	1	600 tonne	\$50,000					
20	Trim and Pierce	1	800 tonne	\$50,000	Tandem				
30	Flange and Restrike	1	800 tonne	\$120,000	Tandem				
40	Checking Fixture			\$10,000					
			Total	\$230,000					


Figure 20.34: Closeout Upper Rail (50.1.0304)

EDAG Process Planning Sheets

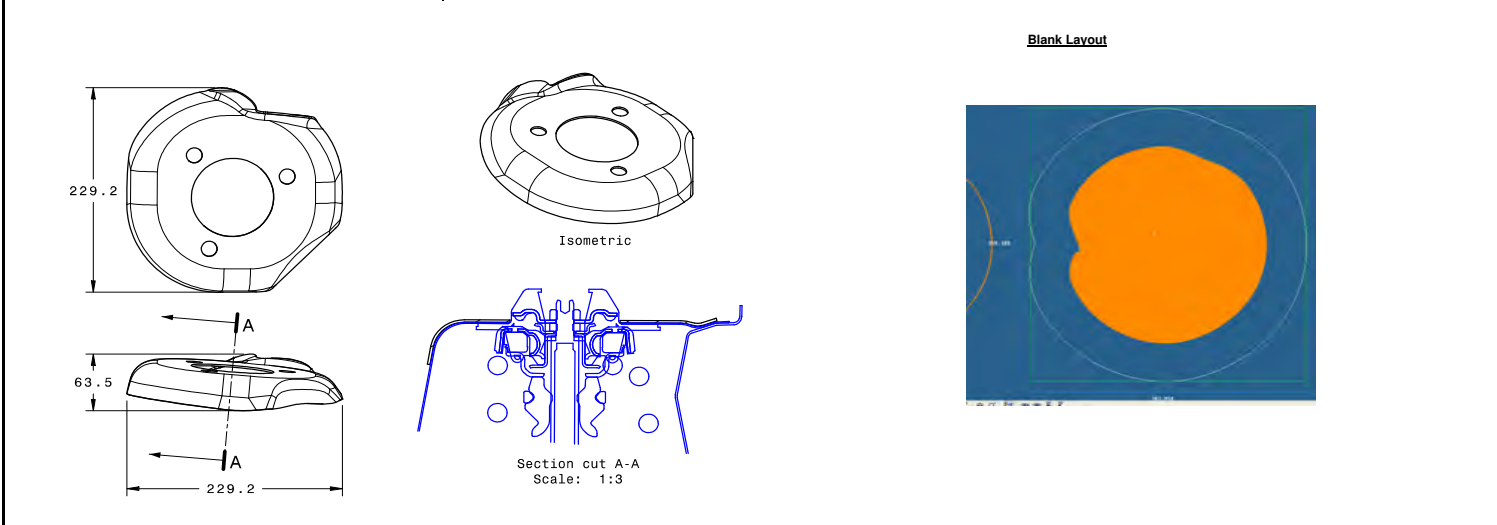
FSV Part No.	50.1.0044		Material Specification		TWIP 500/980		Mass	1.457 kg	
Part Name	Shock Tower Front RH		Coil Width		706 mm	Coil Length (Effective)	353 mm	Thickness	1.0 mm
Op. #	Operation	No. of Dies	Press Type	Tool Cost	Description				
10	Blanking		600 tonne	\$50,000					
20	Form Die	1	1400 tonne	\$200,000	Transfer				
30	Trim and Pierce	1	1400 tonne	\$150,000	Transfer				
40	Flange and Restrike	1	1400 tonne	\$180,000	Transfer				
50	Trim	1	1400 tonne	\$150,000	Transfer				
60	Checking Fixture			\$30,000					
			Total	\$760,000					

Engineering Levels				Notes	
Date	Level			1000 hits/hr	

Figure 20.35: Shock Tower Front (50.1.0044)

EDAG Process Planning Sheets

FSV Part No.	50.1.3002		Material Specification		TWIP 500/980		Mass	0.691 kg	
Part Name	Reinf Shock Tower Front RH		Coil Width		359 mm	Coil Length (Effective)	344 mm	Thickness	2 mm
Op. #	Operation	No. of Dies	Press Type	Tool Cost	Description				
10	Progressive Die	1	350 tonne	\$80,000	Double attached				
20	Checking Fixture			\$5,000					
			Total	\$85,000					



Engineering Levels				Notes	
Date	Level			1000 hits/hr	

Figure 20.36: Reinforcement Shock Tower Front (50.1.3002)

EDAG Process Planning Sheets

FSV Part No.	50.1.0021		Material Specification (Blank-1)		HF1050/1500		Mass	2.149 kg	
			Material Specification (Blank-2)		HF1050/1500				
			Material Specification (Blank-3)		HF1050/1500				
Part Name	Shotgun Inner RH		Coil-1 Width		375 mm	Coil-1 Length (Effective)	330mm	Thickness Blank-1	1.5 mm
			Coil-2 Width		280 mm	Coil-2 Length (Effective)	240 mm	Thickness Blank-2	1.2 mm
			Coil-3 Width		256 mm	Coil-3 Length (Effective)	685 mm	Thickness Blank-3	0.8 mm
Op. #	Operation	No. of Dies	Press Type	Tool Cost	Description				
10	Blank	1	1000 tonne	\$100,000					
20	Form	1	Hot Stamp	\$450,000					
30	Trim Fixture			\$75,000					
50	Checking Fixture			\$25,000					
			Total	\$650,000					

Isometric

Section cut D-D
Scale: 1:4

Blank Layout

Engineering Levels			Notes		
Date	Level				

Figure 20.37: Shotgun Inner (50.1.0021)

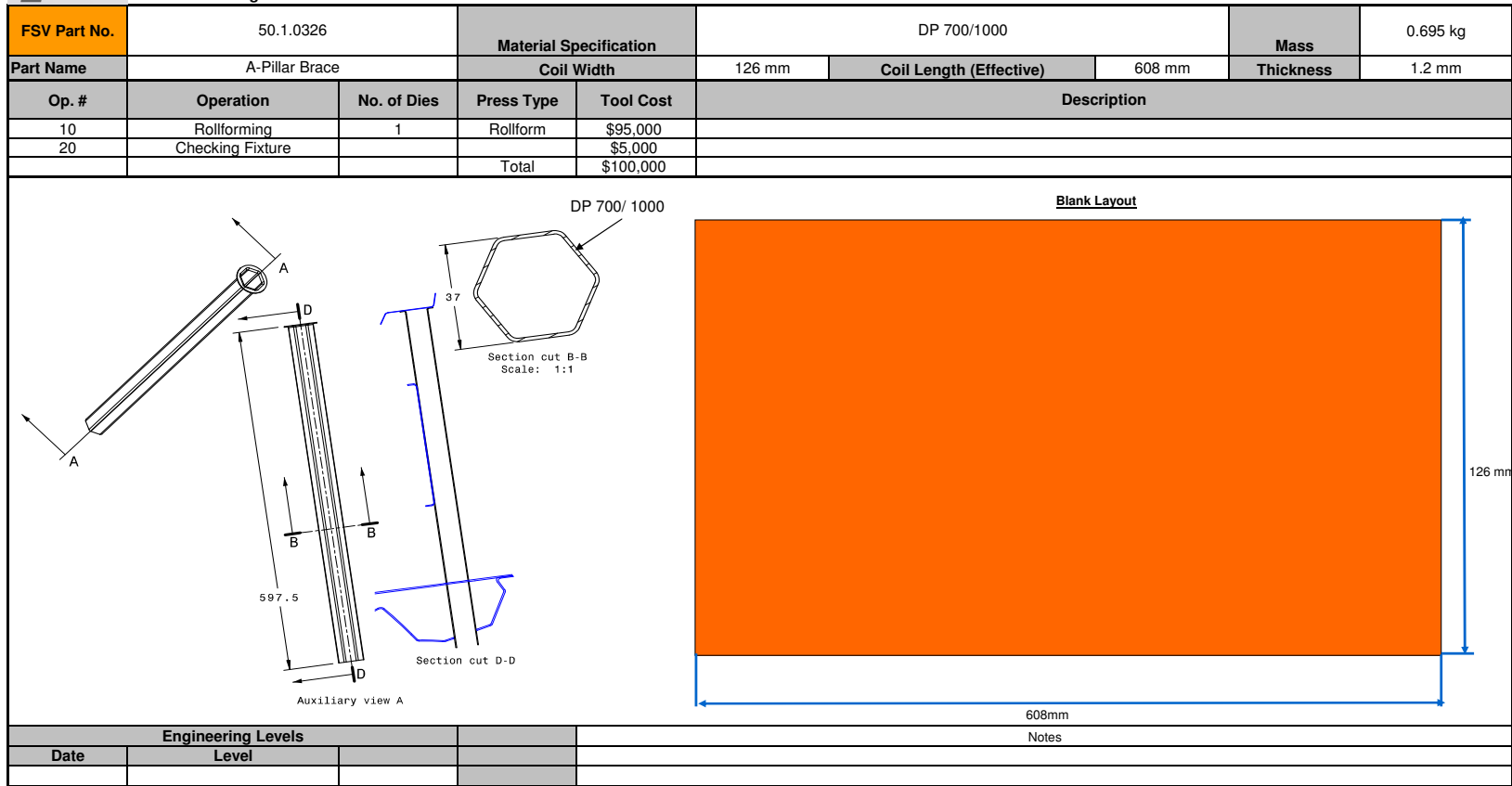


Figure 20.38: A-Pillar Brace (50.1.0326)

EDAG Process Planning Sheets

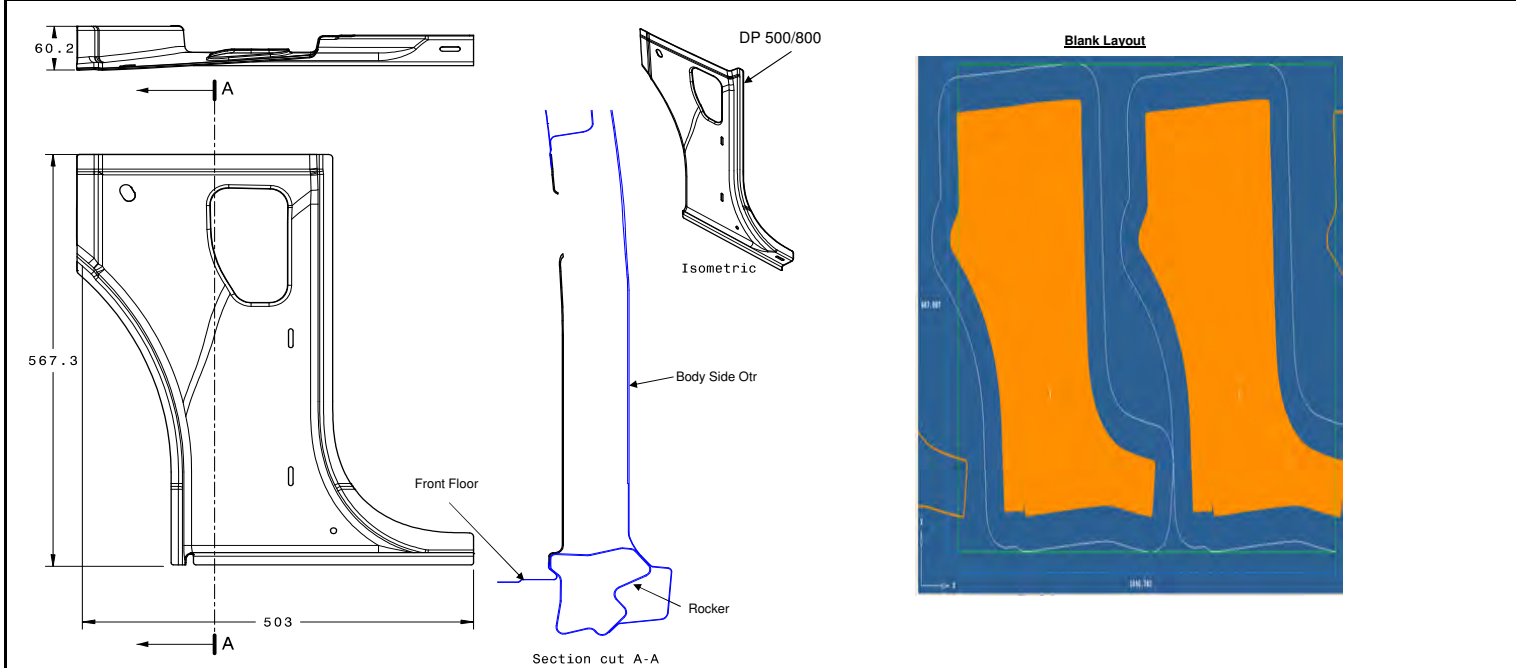
FSV Part No.	50.1.0308		Material Specification		BH210/340		Mass	0.206 kg	
Part Name	Shotgun Brace RH		Coil Width		358 mm	Coil Length (Effective)	194 mm	Thickness	1.2 mm
Op. #	Operation	No. of Dies	Press Type	Tool Cost	Description				
10	Sq. Shear		400 tonne	\$0					
20	Form	1	800 tonne	\$190,000	Tandem				
30	Trim and Pierce	1	800 tonne	\$150,000	Tandem				
40	Flange and Restrike	1	800 tonne	\$100,000	Tandem				
50	Checking Fixture			\$15,000					
			Total	\$455,000					

Engineering Levels			Notes
Date	Level		500 hits/hr

Figure 20.39: Shotgun Brace (50.1.0308)

EDAG Process Planning Sheets

FSV Part No.	50.6 0046		Material Specification		DP500/800		Mass	1.667 kg	
Part Name	FBHP Inner RH		Coil Width		688 mm	Coil Length (Effective)	525 mm	Thickness	1.2 mm
Op. #	Operation	No. of Dies	Press Type	Tool Cost	Description				
10	Blank	1	600 tonne	\$100,000					
20	Draw	1	1000 tonne	\$120,000	Tandem				
30	Trim and Pierce	1	1000 tonne	\$95,000	Tandem				
40	Flange and Restrike	1	1000 tonne	\$75,000	Tandem				
50	Pierce and Cam form End	1	1000 tonne	\$50,000	Tandem				
60	Checking Fixture			\$25,000					
			Total	\$465,000					



Engineering Levels				Notes	
Date	Level			600 hits/hr	

Figure 20.40: FBHP Inner (50.6.0064)

EDAG Process Planning Sheets

FSV Part No.	50.6 0022		Material Specification (Blank-1)			HF1050/1500		Mass	1.171 kg	
			Material Specification (Blank-2)			HF1050/1500				
Part Name	Roof Rail Inner Front RH		Coil-1 Width		575 mm	Coil-1 Length (Effective)		416 mm	Thickness Blank-1	0.7 mm
			Coil-2 Width		142 mm	Coil-2 Length (Effective)		482 mm	Thickness Blank-2	0.95 mm
Op. #	Operation	No. of Dies	Press Type	Tool Cost	Description					
10	Blank	1	1000 tonne	\$75,000						
20	Form	1	Hot Stamp	\$350,000						
30	Trim Fixture			\$75,000						
40	Checking Fixture			\$25,000						
			Total	\$525,000						

Section cut B-B
Scale: 1:2

HF 1050/ 1500
0.7mm 0.95m
Isometric

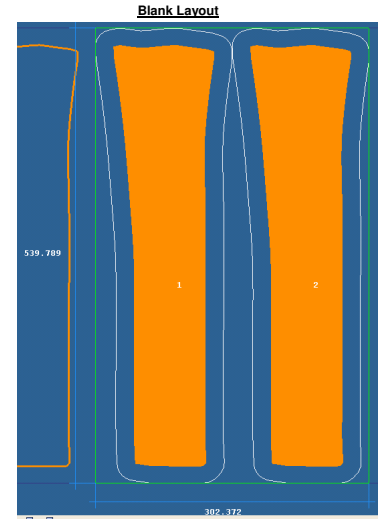
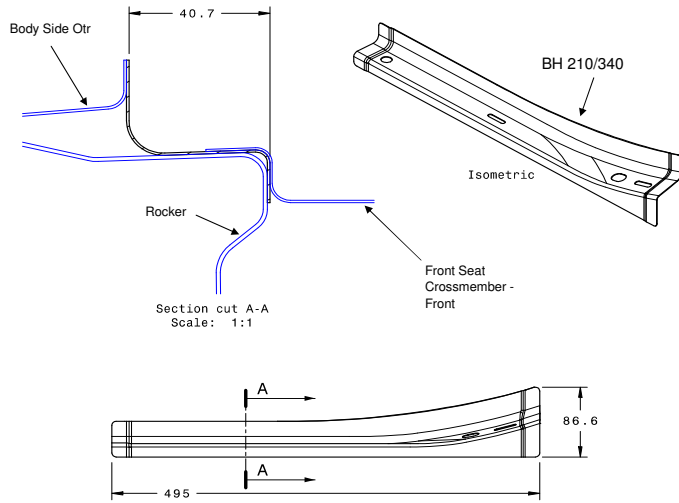
Blank Layout

Engineering Levels			Notes		
Date	Level				

Figure 20.41: Roof Rail Inner (50.6.0022)

EDAG Process Planning Sheets

FSV Part No.	50.6.0055		Material Specification		BH210/340		Mass	0.199 kg	
Part Name	Rocker Filler Front RH		Coil Width		540 mm	Coil Length (Effective)	151 mm	Thickness	0.6 mm
Op. #	Operation	No. of Dies	Press Type	Tool Cost	Description				
10	Blanking		400 tonne	\$30,000					
20	Form	1	800 tonne	\$100,000	Tandem				
30	Trim and Pierce	1	800 tonne	\$150,000	Tandem				
40	Flange and Restrike	1	800 tonne	\$80,000	Tandem				
50	Checking Fixture			\$15,000					
			Total	\$375,000					



Engineering Levels				Notes	
Date	Level				

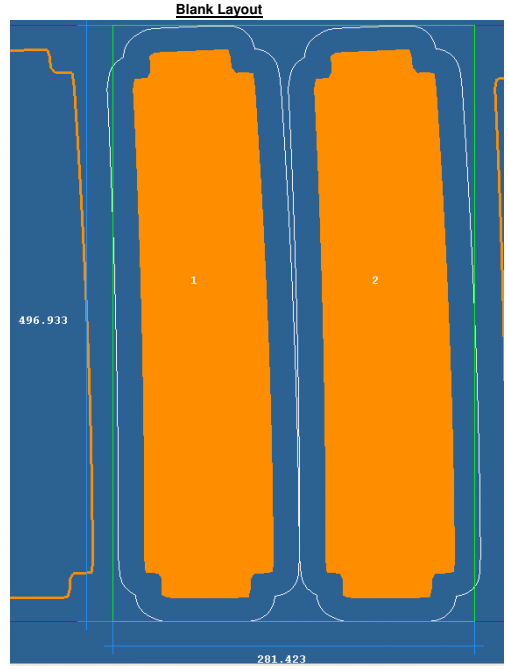
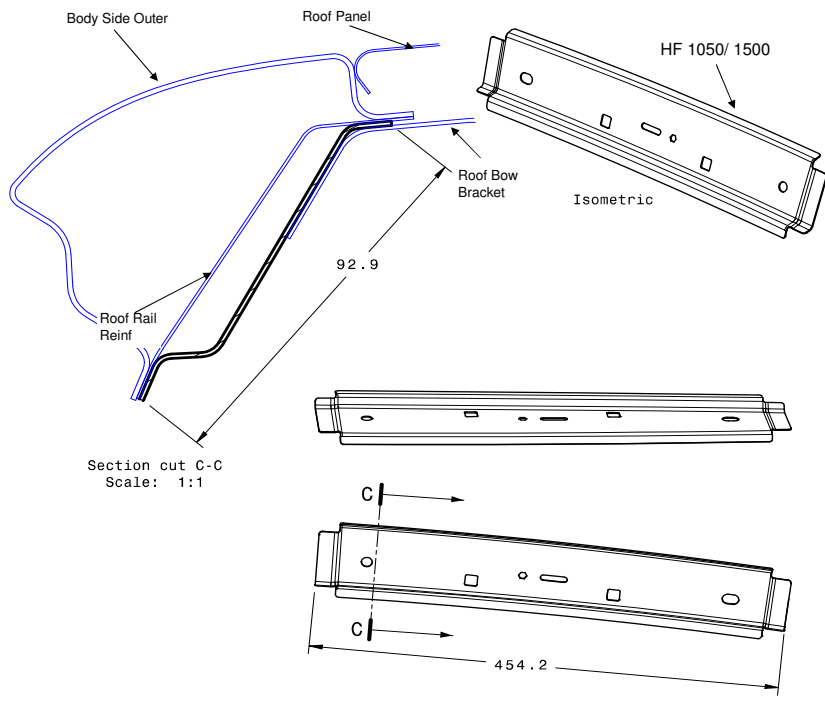
Figure 20.42: Rocker Filler Front (50.6.0055)

EDAG Process Planning Sheets

FSV Part No.	50.6 0009	Material Specification (Blank-1)		HF1050/1500		Mass	1.491 kg		
		Material Specification (Blank-2)		HF1050/1500					
		Material Specification (Blank-3)		HF1050/1500					
		Material Specification (Blank-4)		HF1050/1500					
Part Name	B-Pillar Inner RH	Coil-1 Width		487 mm	Coil-1 Length (Effective)		798 mm	Thickness Blank-1	0.6 mm
		Coil-2 Width		221 mm	Coil-2 Length (Effective)		271 mm	Thickness Blank-2	0.8mm
		Coil-3 Width		209 mm	Coil-3 Length (Effective)		246 mm	Thickness Blank-3	0.6 mm
		Coil-4 Width		447 mm	Coil-4 Length (Effective)		197 mm	Thickness Blank-4	0.8 mm
Op. #	Operation	No. of Dies	Press Type	Tool Cost	Description				
10	Sq. shear		1000 tonne	\$0					
20	Form	1	Hot Stamp	\$420,000					
30	Trim Fixture			\$75,000					
40	Checking Fixture			\$25,000					
			Total	\$520,000					
Engineering Levels			Notes						
Date	Level								

Figure 20.43: B-Pillar Inner (50.6.0009)

FSV Part No.	50.6.0052		Material Specification		HF1050/1500		Mass	0.372 kg	
Part Name	Roof Rail Inner Rear RH		Coil Width		496 mm	Coil Length (Effective)	141 mm	Thickness	1.1 mm
Op. #	Operation	No. of Dies	Press Type	Tool Cost	Description				
10	Blank	1	1000 tonne	\$75,000					
20	Form	1	Hot Stamp	\$275,000					
30	Trim Fixture			\$75,000					
40	Checking Fixture			\$25,000					
			Total	\$450,000					



Engineering Levels				Notes	
Date	Level				

Figure 20.44: Roof Rail Inner (50.6.0052)



Process Planning Sheets

FSV Part No.	50.6 0005		Material Specification		DP500/800		Mass	1.428 kg	
Part Name	C-Pillar Inner RH		Coil Width		720 mm	Coil Length (Effective)	735 mm	Thickness	0.7 mm
Op. #	Operation	No. of Dies	Press Type	Tool Cost	Description				
10	Blank	1	600 tonne	\$105,000					
20	Draw	1	1400 tonne	\$200,000					
30	Trim and Pierce	1	1400 tonne	\$175,000					
40	Flange and Restrike	1	1400 tonne	\$150,000					
50	Cam Pierce	1	1400 tonne	\$100,000					
60	Checking Fixture			\$25,000					
			Total	\$755,000					

Isometric

Section cut B-B

Blank Layout

Engineering Levels			Notes
Date	Level		Transfer 1000 hits/hr

Figure 20.45: C-Pillar Inner (50.6.0005)

Process Planning Sheets

FSV Part No.	50.2 0033		Material Specification		BH210/340		Mass	0.254 kg	
Part Name	Bracket - Roof Bow to Roof Rail RH		Coil Width		408 mm	Coil Length (Effective)	219 mm	Thickness	1 mm
Op. #	Operation	No. of Dies	Press Type	Tool Cost	Description				
10	Blank	1	400 tonne	\$50,000					
20	Form	1	600 tonne	\$150,000					
30	Trim and Pierce	1	600 tonne	\$100,000					
40	Finish Form	1	600 tonne	\$150,000					
50	Checking Fixture			\$20,000					
			Total	\$470,000					

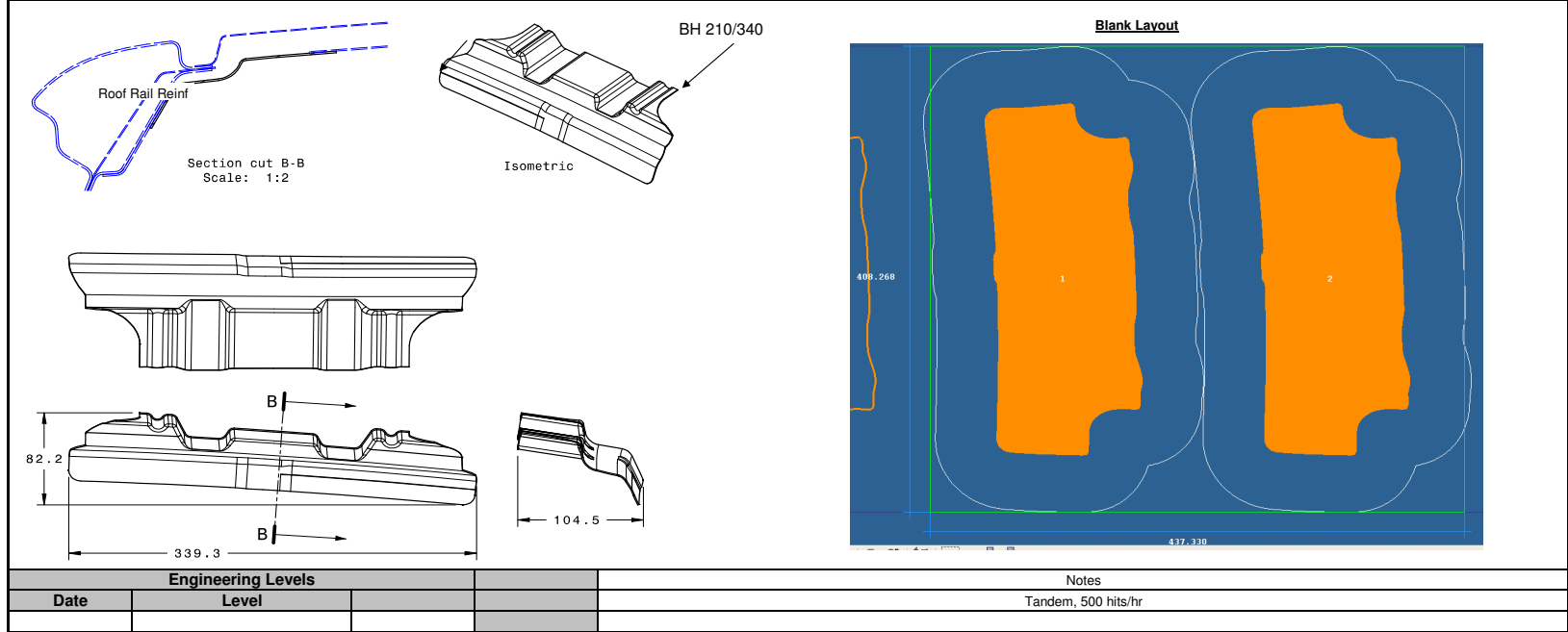


Figure 20.46: Bracket Roof Bow (50.2.0033)



Process Planning Sheets

FSV Part No.	50.2 0032		Material Specification		BH210/340		Mass	0.103 kg	
Part Name	Bracket - Roof Rail to Header RH		Coil Width		250 mm	Coil Length (Effective)	216 mm	Thickness	1 mm
Op. #	Operation	No. of Dies	Press Type	Tool Cost	Description				
10	Blank	1	400 tonne	\$50,000					
20	Form	1	600 tonne	\$150,000					
30	Trim and Pierce	1	600 tonne	\$100,000					
50	Finish Form	1	600 tonne	\$150,000					
60	Checking Fixture			\$20,000					
			Total	\$420,000					

Isometric

Blank Layout

Engineering Levels				Notes	
Date	Level			Tandem, 500 hits/hr	

Figure 20.47: Bracket Roof Rail (50.2.0032)

FSV Part No.	50.6 0048		Material Specification		CP 1050/1470		Mass	6.032 kg	
Part Name	Rocker RH		Coil Width		455 mm	Coil Length (Effective)	1759 mm	Thickness	1.0 mm
Op. #	Operation	No. of Dies	Press Type	Tool Cost	Description				
10	Closed Rollform	1	Rollform	\$140,000					
20	Checking Fixture			\$10,000					
			Total	\$150,000					

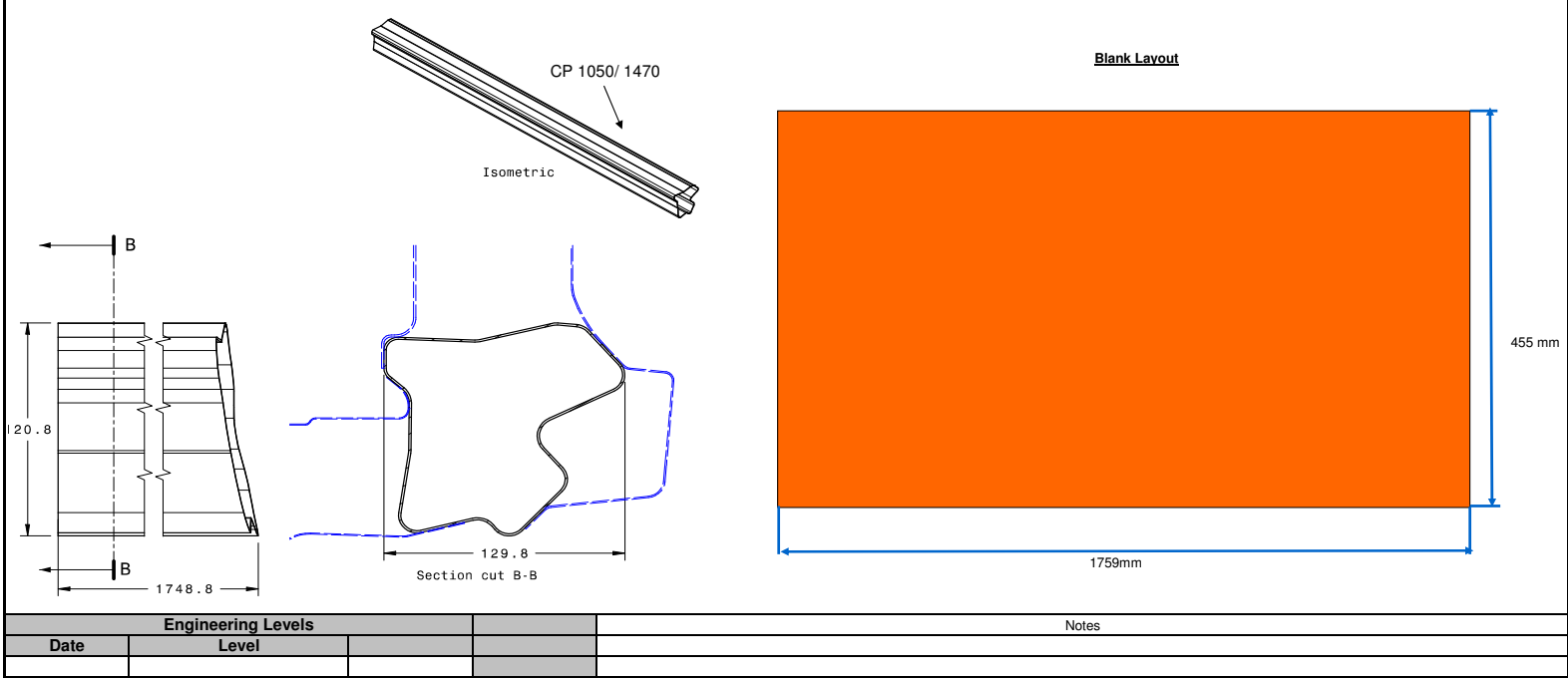


Figure 20.48: Rocker (50.6.0048)

EDAG Process Planning Sheets

FSV Part No.	50.6 0071		Material Specification		BH210/340		Mass	0.244 kg	
Part Name	Rocker Cap RH		Coil Width		312 mm	Coil Length (Effective)	332 mm	Thickness	0.85 mm
Op. #	Operation	No. of Dies	Press Type	Tool Cost	Description				
10	Blank	1	400 tonne	\$30,000					
20	Draw	1	600 tonne	\$50,000					
30	Trim	1	600 tonne	\$30,000					
40	Flange	1	600 tonne	\$40,000					
50	Flange	1	600 tonne	\$40,000					
60	Cam Pierce	1	600 tonne	\$25,000					
70	Checking fixture			\$5,000					
			Total	\$220,000					

BH 210/340

Section cut A-A

Isometric

Blank Layout

Engineering Levels			Notes	
Date	Level		Tandem 600 hits/hr	

Figure 20.49: Rocker Cap (50.6.0071)

FSV Part No.	50.6 0026	Material Specification (Blank-1)			HF1050/1500		Mass	1.491 kg	
		Material Specification (Blank-2)			HF1050/1500				
		Material Specification (Blank-3)			HF1050/1500				
Part Name	B-Pillar Reinf RH	Coil-1 Width		409 mm	Coil-1 Length (Effective)		805 mm	Thickness Blank-1	0.6 mm
		Coil-2 Width		251 mm	Coil-2 Length (Effective)		245 mm	Thickness Blank-2	1.0 mm
		Coil-3 Width		272 mm	Coil-3 Length (Effective)		280 mm	Thickness Blank-3	0.6 mm
Op. #	Operation	No. of Dies	Press Type	Tool Cost	Description				
10	Sq. shear		1000 tonne	\$0					
20	Form	1	Hot Stamp	\$420,000					
30	Trim Fixture			\$75,000					
40	Checking Fixture			\$25,000					
			Total	\$520,000					
Engineering Levels				Notes					
Date	Level								

Figure 20.50: B-Pillar Reinforcement (50.6.0026)

EDAG Process Planning Sheets

FSV Part No.	50.6 0050		Material Specification		BH210/340		Mass	0.795 kg	
Part Name	Panel - Gutter Rear RH		Coil Width		692 mm	Coil Length (Effective)	338 mm	Thickness	1.0 mm
Op. #	Operation	No. of Dies	Press Type	Tool Cost	Description				
10	Blank	1	400 tonne	\$90,000					
20	Form	1	1400 tonne	\$180,000					
30	Trim and Pierce	1	1400 tonne	\$160,000					
40	Flange and Restrike	1	1400 tonne	\$170,000					
50	Checking Fixture			\$20,000					
			Total	\$620,000					

Engineering Levels			Notes	
Date	Level		Transfer, 600 hits/hr	

Figure 20.51: Panel Gutter (50.6.0050)

FSV Part No.	50.6 0068		Material Specification		BH210/340		Mass	0.198kg	
Part Name	Panel Rear Quarter Lower RH		Coil Width		423 mm	Coil Length (Effective)	190 mm	Thickness	1.2 mm
Op. #	Operation	No. of Dies	Press Type	Tool Cost	Description				
10	Blank	1	400 tonne	\$75,000					
20	Flange	1	600 tonne	\$50,000					
30	Form and Restrike	1	600 tonne	\$150,000					
40	Pierce	1	600 tonne	\$50,000					
50	Checking Fixture			\$10,000					
			Total	\$335,000					

BH 210/340

Section cut A-A
Scale: 1:1

Isometric

235.3

101.8

159

Blank Layout

422.678

101.245

Engineering Levels			Notes	
Date	Level		Tandem, 600 hits/hr	

Figure 20.52: Panel Rear Quarter (50.6.0068)

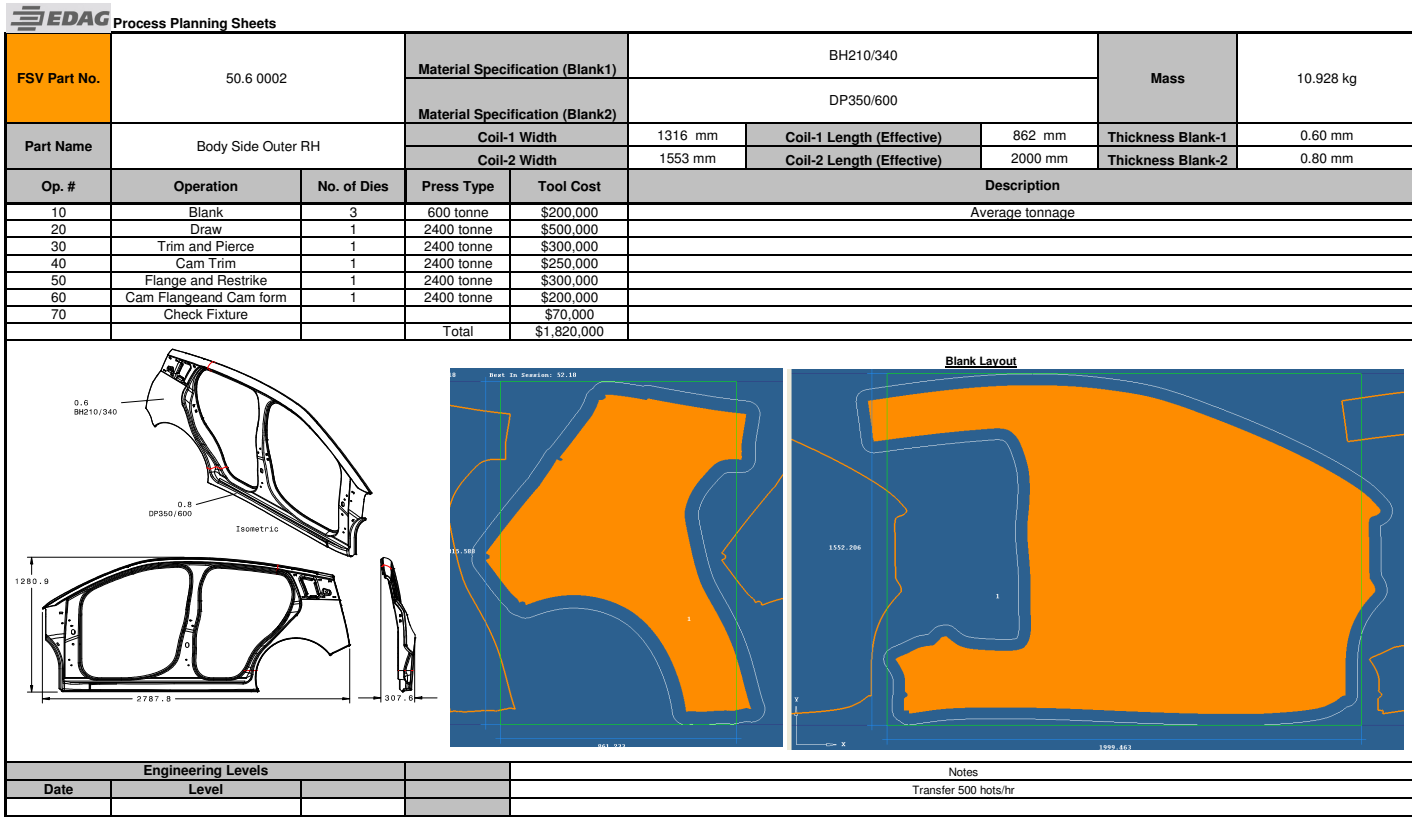


Figure 20.53: Body Side Outer (50.6.0002)

FSV Part No.	50.2 0007	Material Specification (Blank1)			BH210/340		Mass	3.775 kg	
		Material Specification (Blank2)			BH210/340				
		Material Specification (Blank3)			BH210/340				
Part Name	Rear Header Reinf	Coil-1 Width		536 mm	Coil-1 Length (Effective)		331mm	Thickness Blank-1	2.0 mm
		Coil-2 Width		397 mm	Coil-2 Length (Effective)		631 mm	Thickness Blank-2	0.7 mm
		Coil-3 Width		536 mm	Coil-3 Length (Effective)		331mm	Thickness Blank-3	2.0 mm
Op. #	Operation	No. of Dies	Press Type	Tool Cost	Description				
10	Sq shear		800 tonne	\$0					
20	Draw	1	1000 tonne	\$230,000					
30	Trim and Pierce	1	1000 tonne	\$180,000					
40	Flange and Restrike	1	1000 tonne	\$200,000					
50	Checking Fixture			\$25,000					
			Total	\$635,000					
Engineering Levels					Notes				
Date	Level				600 hits/hr				

Figure 20.54: Rear Header Reinforcement (50.2.0007)

EDAG Process Planning Sheets

FSV Part No.	50.2 0006		Material Specification		BH210/340		Mass	1.662 kg	
Part Name	Rear Header		Coil Width		1164 mm	Coil Length (Effective)	454 mm	Thickness	0.7 mm
Op. #	Operation	No. of Dies	Press Type	Tool Cost	Description				
10	Blank	1	1000 tonne	\$110,000					
20	Draw	1	1400 tonne	\$200,000					
30	Trim and Pierce	1	1400 tonne	\$110,000					
40	Flange and Restrike	1	1400 tonne	\$150,000					
50	Checking Fixture			\$25,000					
			Total	\$595,000					

BH 210/340

Section cut A-A
Scale: 1:3

Isometric

294.2

192.8

1006.5

Blank Layout

1163.717

1

2

907.061

Engineering Levels			Notes	
Date	Level		Transfer 900 hits/hr	

Figure 20.55: Rear Header (50.2.0006)

FSV Part No.	50.2 0008		Material Specification		Mild 140/270		Mass	0.463 kg	
Part Name	Roof Support RH		Coil Width		247 mm	Coil Length (Effective)	934 mm	Thickness	0.5 mm
Op. #	Operation	No. of Dies	Press Type	Tool Cost	Description				
10	Sq. shear		400 tonne	\$0					
20	Draw	1	1400 tonne	\$160,000					
30	Trim and Pierce	1	1400 tonne	\$150,000					
40	Flange and Restrike	1	1400 tonne	\$125,000					
50	Checking Fixture			\$25,000					
			Total	\$460,000					

Mild 140/270

Isometric

Section cut A-A
Scale: 1:2

Blank Layout

Engineering Levels			Notes	
Date	Level		Transfer Double attached 900hits/hr	

Figure 20.56: Roof Support (50.2.0008)

FSV Part No.	50.2 0013		Material Specification		BH210/340		Mass	0.941 kg	
Part Name	Roof Bow		Coil Width		260 mm	Coil Length (Effective)	1001 mm	Thickness	0.5 mm
Op. #	Operation	No. of Dies	Press Type	Tool Cost	Description				
10	Rollform	1	Rollform	\$90,000					
20	Checking Fixture			\$10,000					
			Total	\$100,000					

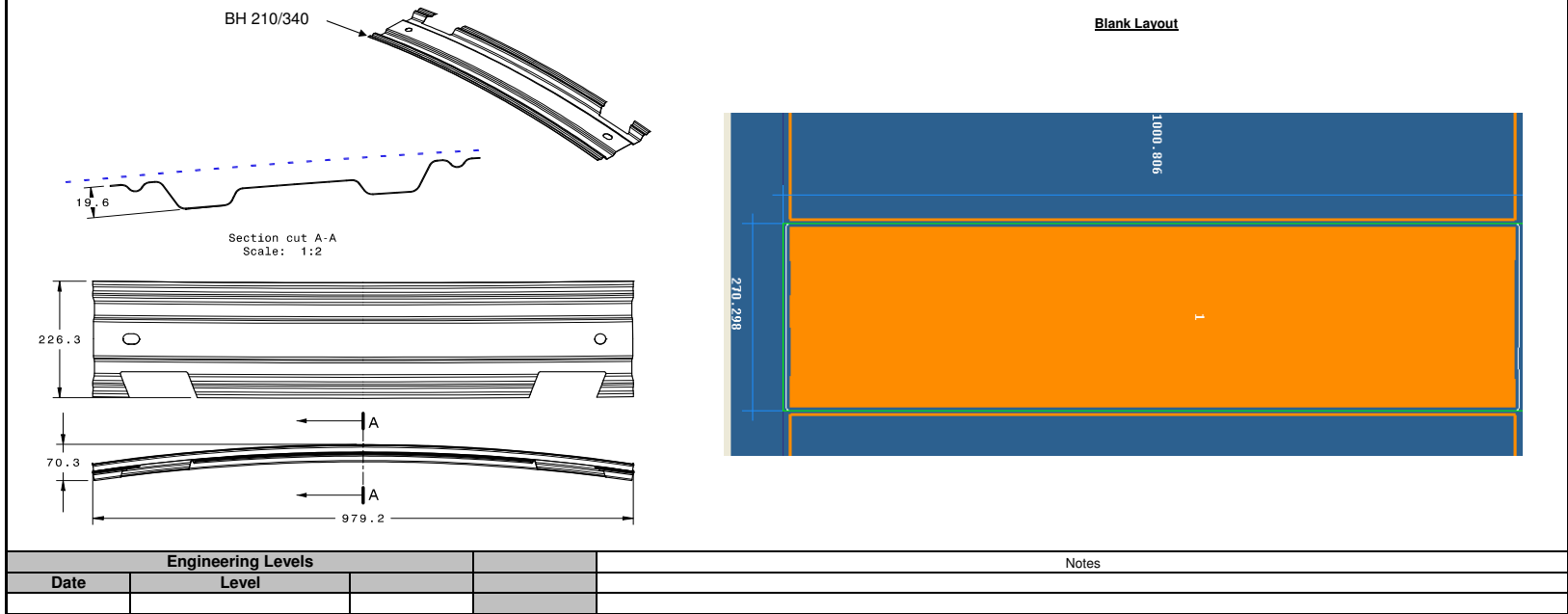


Figure 20.57: Roof Bow (50.2.0013)

FSV Part No.	50.2.0011		Material Specification		BH210/340		Mass	1.131 kg	
Part Name	Header - Roof Front		Coil Width		165 mm	Coil Length (Effective)	1161 mm	Thickness	0.8 mm
Op. #	Operation	No. of Dies	Press Type	Tool Cost	Description				
10	Rollform	1	Rollform	\$90,000					
20	Checking Fixture			\$10,000					
			Total	\$100,000					

BH 210/340

Section cut A-A

Isometric

246.4

82

1127.3

Blank Layout

1160.519

174.616

1

Engineering Levels				Notes	
Date	Level				

Figure 20.58: Header Roof Front (50.2.0011)

FSV Part No.	50.1.0405		Material Specification (Blank-1)		DP 700/1000		Mass	3.067 kg	
Part Name	Panel - Tunnel Top		Coil-1 Width		389 mm	Coil-1 Length (Effective)	1593 mm	Thickness Blank-1	1.0 mm
Op. #	Operation	No. of Dies	Press Type	Tool Cost	Description				
10	Sq shear		600 tonne	\$0					
20	Draw Die	1	1000 tonne	\$200,000					
30	Trim and Pierce	1	1000 tonne	\$150,000					
40	Flange and Restrke	1	1000 tonne	\$180,000					
50	Checking Fixture			\$20,000					
			Total	\$550,000					
Engineering Levels					Notes				
Date	Level				500 hits/hr				

Figure 20.59: Panel Tunnel Top (50.1.0405)

EDAG Process Planning Sheets

FSV Part No.	50.2.0010		Material Specification		DP350/600		Mass	9.011 kg	
Part Name	Roof Panel		Coil Width		1314 mm	Coil Length (Effective)	2172 mm	Thickness	0.5 mm
Op. #	Operation	No. of Dies	Press Type	Tool Cost	Description				
10	Sq. Shear		1000 tonne	\$0					
20	Draw	1	1400 tonne	\$380,000	Transfer				
30	Trim	1	1400 tonne	\$280,000	Transfer				
40	Flange and Restrike	1	1400 tonne	\$250,000	Transfer				
50	Check Fixture			\$70,000					
			Total	\$980,000					

DP 350/600

Isometric

Section cut A-A

Blank Layout

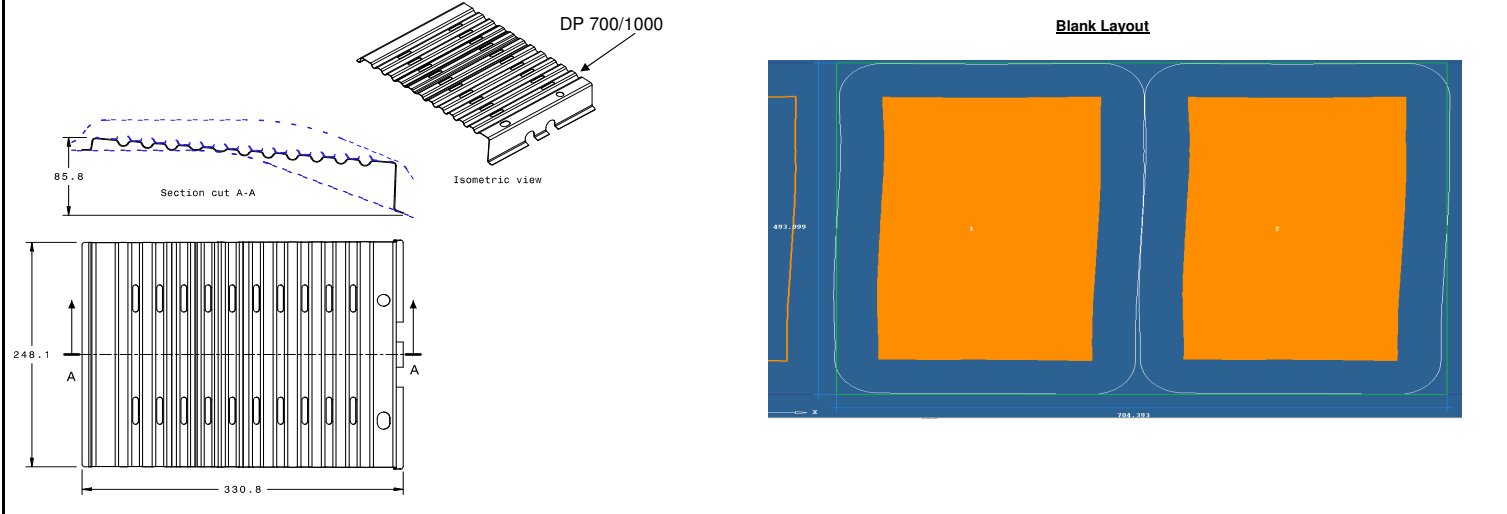
Engineering Levels		Notes
Date	Level	950 hits/hr

Figure 20.60: Roof Panel (50.2.0010)

FSV Part No.	50.1.0051		Material Specification (Blank-1)		HF1050/1500		Mass	2.088 kg
			Material Specification (Blank-2)		HF1050/1500			
			Material Specification (Blank-3)		HF1050/1500			
Part Name	Shotgun Outer RH		Coil-1 Width	375 mm	Coil-1 Length (Effective)	330 mm	Thickness Blank-1	1.5 mm
			Coil-2 Width	280 mm	Coil-2 Length (Effective)	240 mm	Thickness Blank-2	1.0 mm
			Coil-3 Width	256 mm	Coil-3 Length (Effective)	680 mm	Thickness Blank-3	0.8 mm
Op. #	Operation	No. of Dies	Press Type	Tool Cost	Description			
10	Blank	1	1000 tonne	\$100,000				
20	Form	1	Hot Stamp	\$450,000				
30	Trim Fixture			\$75,000				
50	Checking Fixture			\$25,000				
			Total	\$650,000				
<p>HF 1050/1500</p> <p>Blank Layout</p>								
Engineering Levels			Notes					
Date	Level							

Figure 20.61: Shotgun Outer (50.1.0051)

FSV Part No.	50.1.0401		Material Specification		DP700/1000		Mass	0.679 kg	
Part Name	Bulkhead Lower - Tunnel		Coil Width		494 mm	Coil Length (Effective)	352 mm	Thickness	0.8 mm
Op. #	Operation	No. of Dies	Press Type	Tool Cost	Description				
10	Sq Shear	1	600 tonne	\$0					
20	Form	1	800 tonne	\$100,000	Tandem				
30	Flange	1	800 tonne	\$85,000	Tandem				
40	Trim and Pierce	1	800 tonne	\$100,000	Tandem				
50	Checking Fixture	1		\$10,000					
			Total	\$295,000					



Engineering Levels			Notes
Date	Level		500 hits/hr

Figure 20.62: Bulkhead Tunnel Lower (50.1.0401)

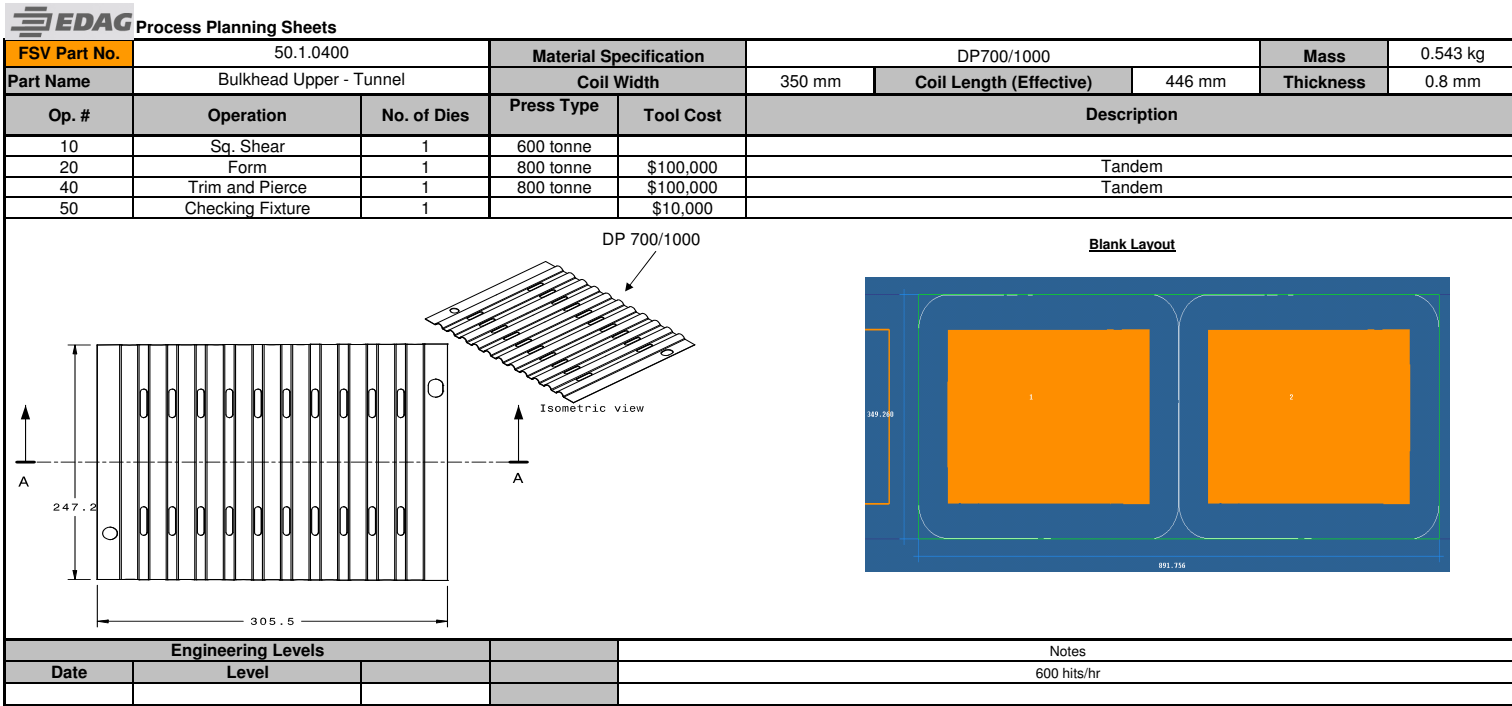


Figure 20.63: Bulkhead Tunnel Upper (50.1.0400)

FSV Part No.	50.1.0404			Material Specification		BH280/400		Mass	1.713 kg	
Part Name	Reinf - Tunnel Top			Coil Width		382 mm	Coil Length (Effective)	1661 mm	Thickness	0.5 mm
Op. #	Operation	No. of Dies	Press Type	Tool Cost	Description					
10	Sq Shear	1	600 tonne							
20	Draw Die	1	1000 tonne	\$220,000	Tandem					
30	Trim and Pierce	1	1000 tonne	\$160,000	Tandem					
40	Flange and Restrike	1	1000 tonne	\$200,000	Tandem					
50	Checking Fixture	1		\$20,000						
			Total	\$600,000						

BH 280/400

Blank Layout

Engineering Levels				Notes
Date	Level			500 hits/hr

Figure 20.64: Reinforcement Tunnel Top (50.1.0404)

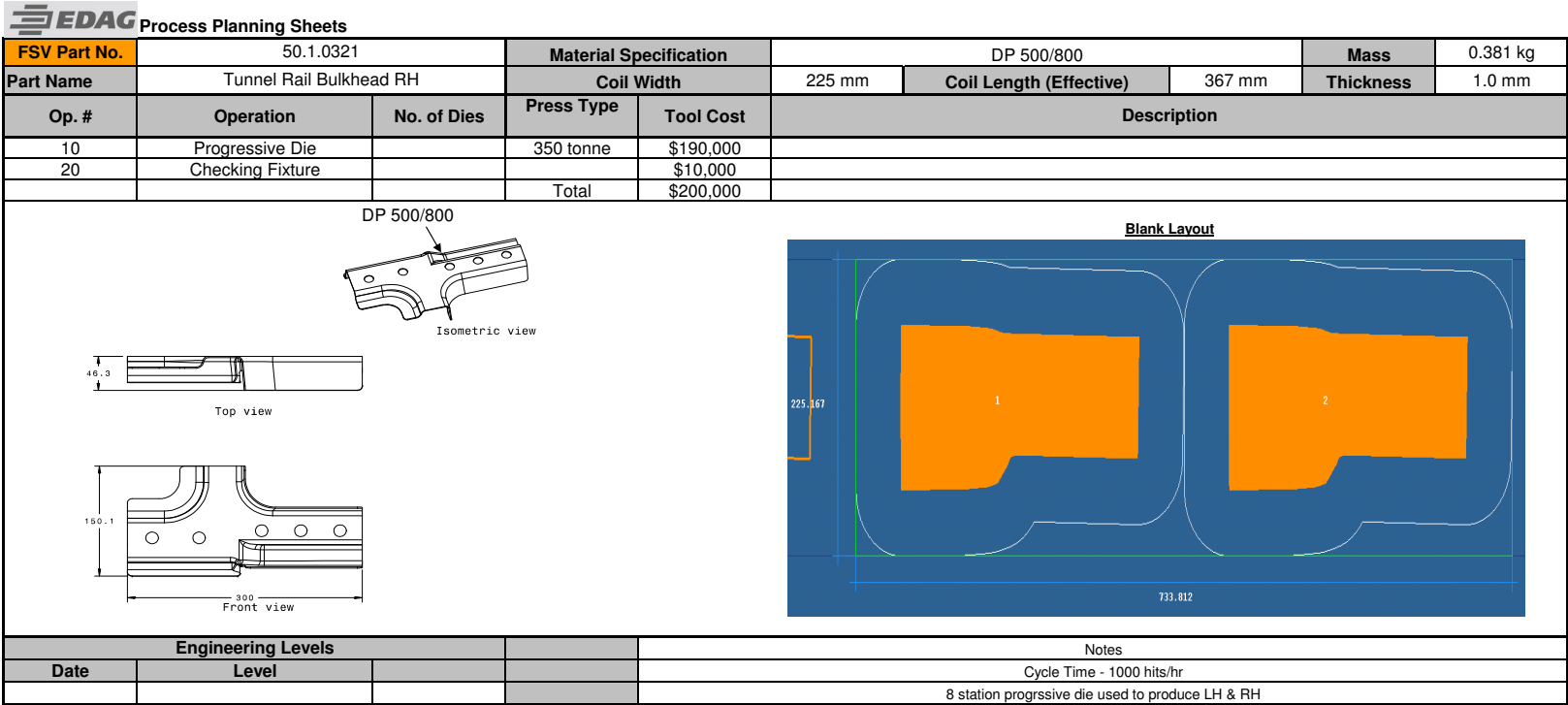
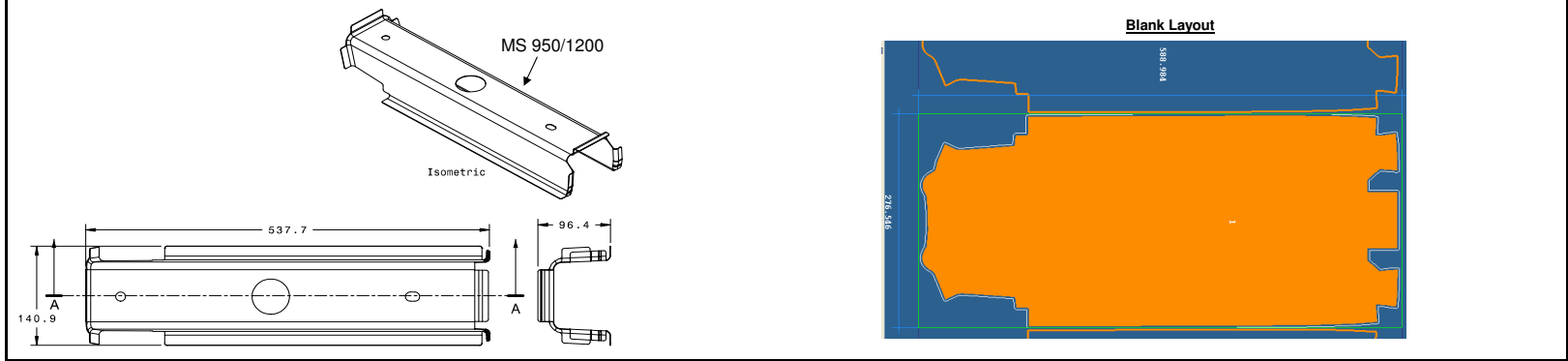


Figure 20.65: Tunnel Rail Bulkhead (50.1.0321)

EDAG Process Planning Sheets

FSV Part No.	50.1.0093		Material Specification		MS 950/1200		Mass	0.542 kg	
Part Name	Crossmember - Front Seat RH Front		Coil Width		267 mm	Coil Length (Effective)	589 mm	Thickness	0.5 mm
Op. #	Operation	No. of Dies	Press Type	Tool Cost	Description				
10	Blanking and Piercing	1	1000 tonne	\$100,000					
20	Rollforming			\$100,000					
30	Flanging (Secondary)	1		\$50,000					
			Total	\$250,000					



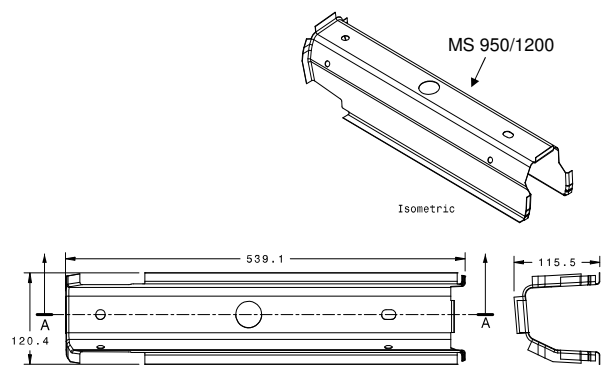
Engineering Levels		Notes	
Date	Level		

Figure 20.66: Crossmember Front Seat (50.1.0093)



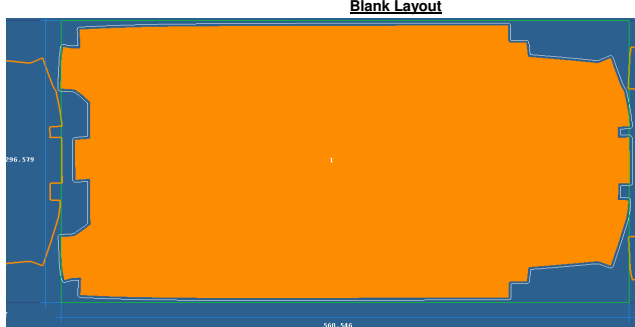
Process Planning Sheets

FSV Part No.	50.1.0095		Material Specification		MS 950/1200		Mass	0.688 kg	
Part Name	Crossmember - Front Seat RH Rear		Coil Width		287 mm	Coil Length (Effective)	561 mm	Thickness	0.6mm
Op. #	Operation	No. of Dies	Press Type	Tool Cost	Description				
10	Blanking and Piercing	1	1000 tonne	\$100,000					
20	Rollforming			\$100,000					
30	Flanging (Secondary)	1		\$50,000					
			Total	\$250,000					



MS 950/1200

Isometric



Blank Layout

Engineering Levels			Notes
Date	Level		

Figure 20.67: Crossmember Front Seat Rear (50.1.0095)

FSV Part No.	50.1.0049		Material Specification		DP500/800		Mass	1.732 kg	
Part Name	Panel - Wheel House Outer RH		Coil Width		992 mm	Coil Length (Effective)	1240 mm	Thickness	0.6 mm
Op. #	Operation	No. of Dies	Press Type	Tool Cost	Description				
10	Blank	1	1000 tonne	\$105,000					
20	Draw	1	1400 tonne	\$200,000					
30	Trim	1	1400 tonne	\$175,000					
40	(Cam) Trim	1	1400 tonne	\$100,000					
50	Flange and Restrike	1	1400 tonne	\$175,000					
60	Pierce	1	1400 tonne	\$150,000					
70	Checking Fixture			\$25,000					
			Total	\$930,000					

DP 500/800

Isometric

232.6

892.7

1289.5

Section cut B-B

Blank Layout

991.688

1239.619

Engineering Levels			Notes
Date	Level		Transfer 1000 hits/hr

Figure 20.68: Panel Wheel House Outer (50.1.0049)

EDAG Process Planning Sheets

FSV Part No.	50.6 0012		Material Specification		HF1050/1500		Mass	2.049 kg	
Part Name	Roof Rail Reinf RH		Coil Width		998 mm	Coil Length (Effective)	1658 mm	Thickness	0.7 mm
Op. #	Operation	No. of Dies	Press Type	Tool Cost	Description				
10	Blank	1	1000 tonne	\$100,000					
20	Form	1	Hot Stamping	\$430,000					
30	Trim Fixture	1		\$75,000					
40	Checking Fixture			\$25,000					
			Total	\$630,000					

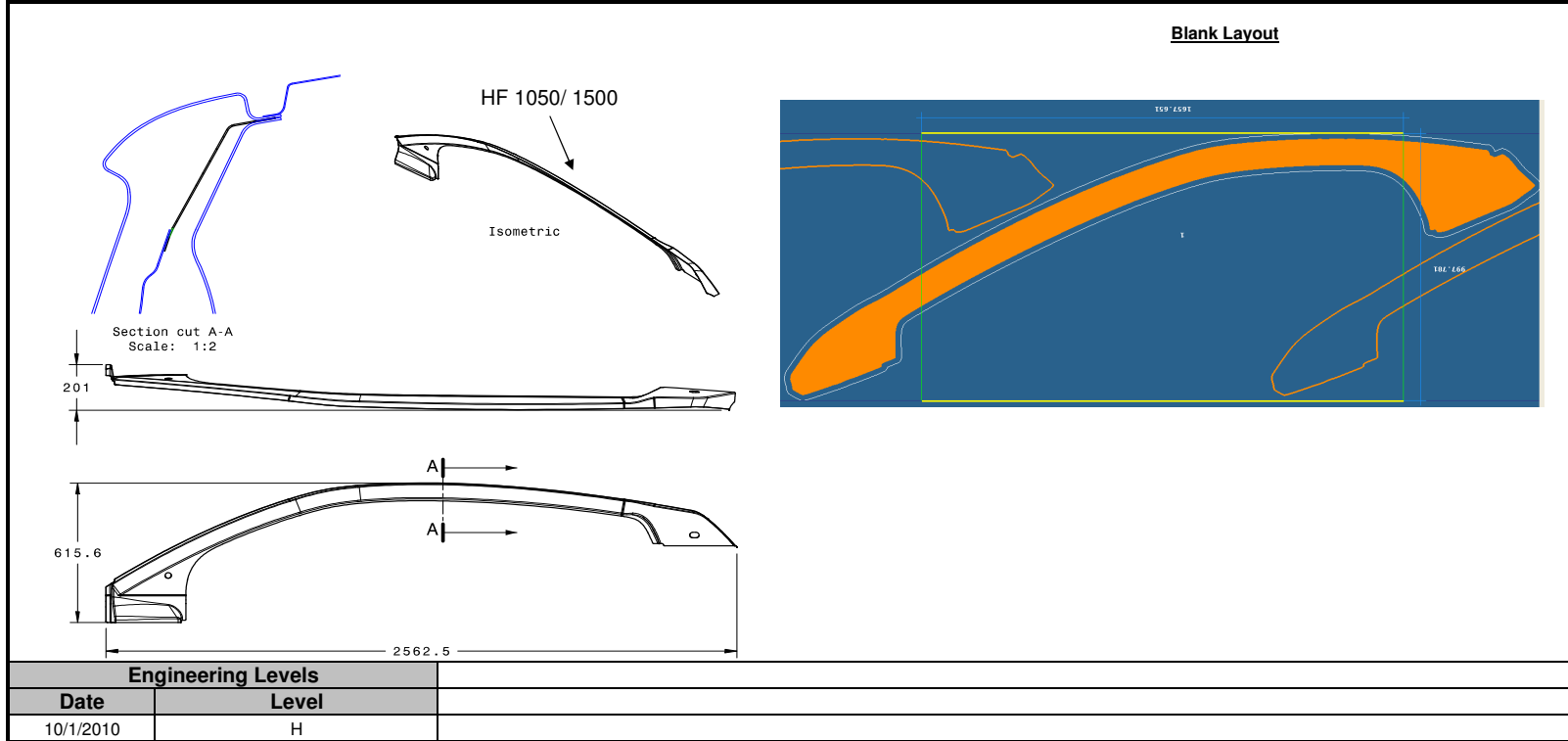


Figure 20.69: Roof Rail Reinforcement (50.6.0012)

20.2 Assembly Trees Body Structure

This section shows the assembly process details for every BEV sub-assembly. The sub-assembly details include the joining process and the process details.

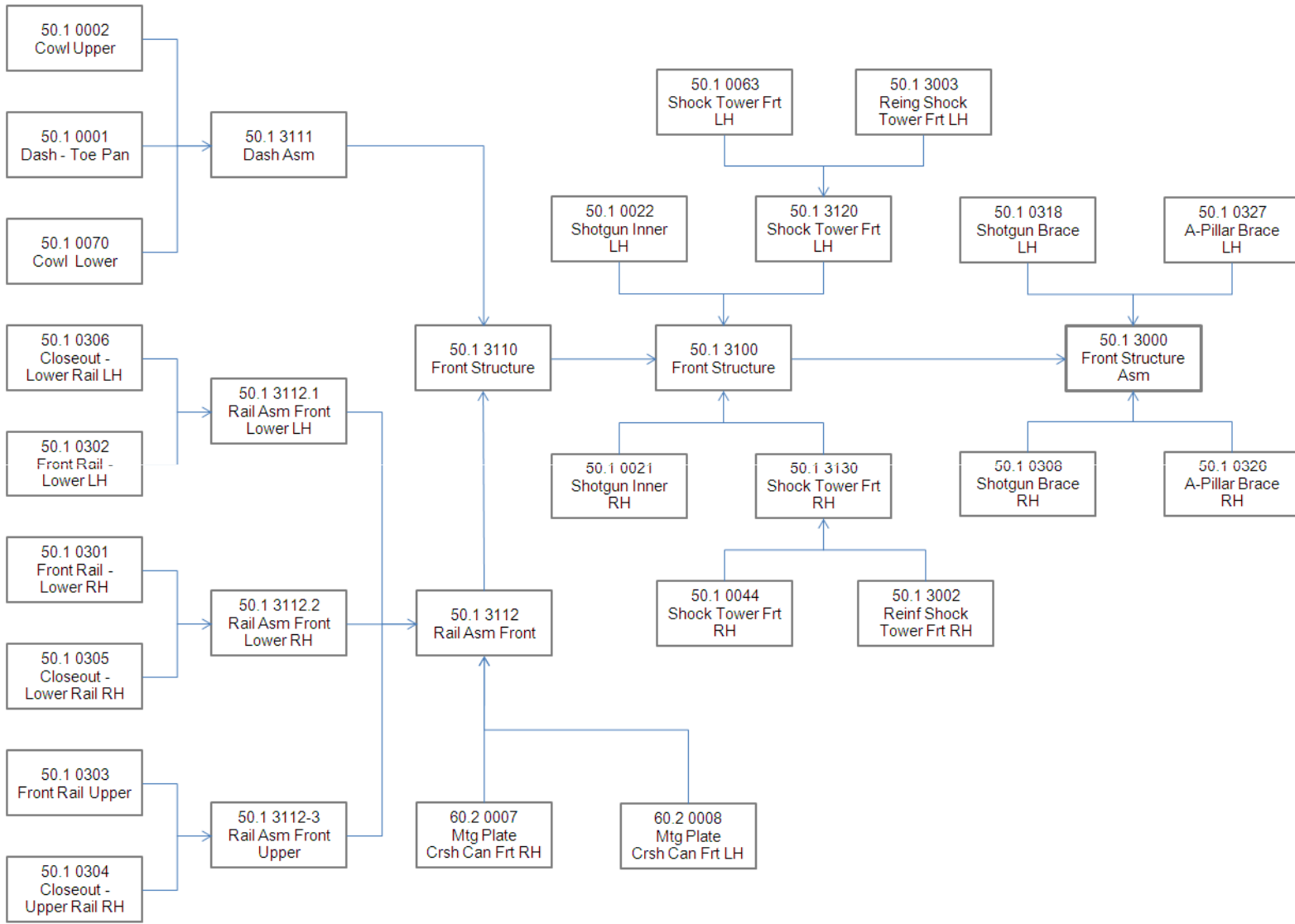


Figure 20.70: Front Structure (50.1 3000)

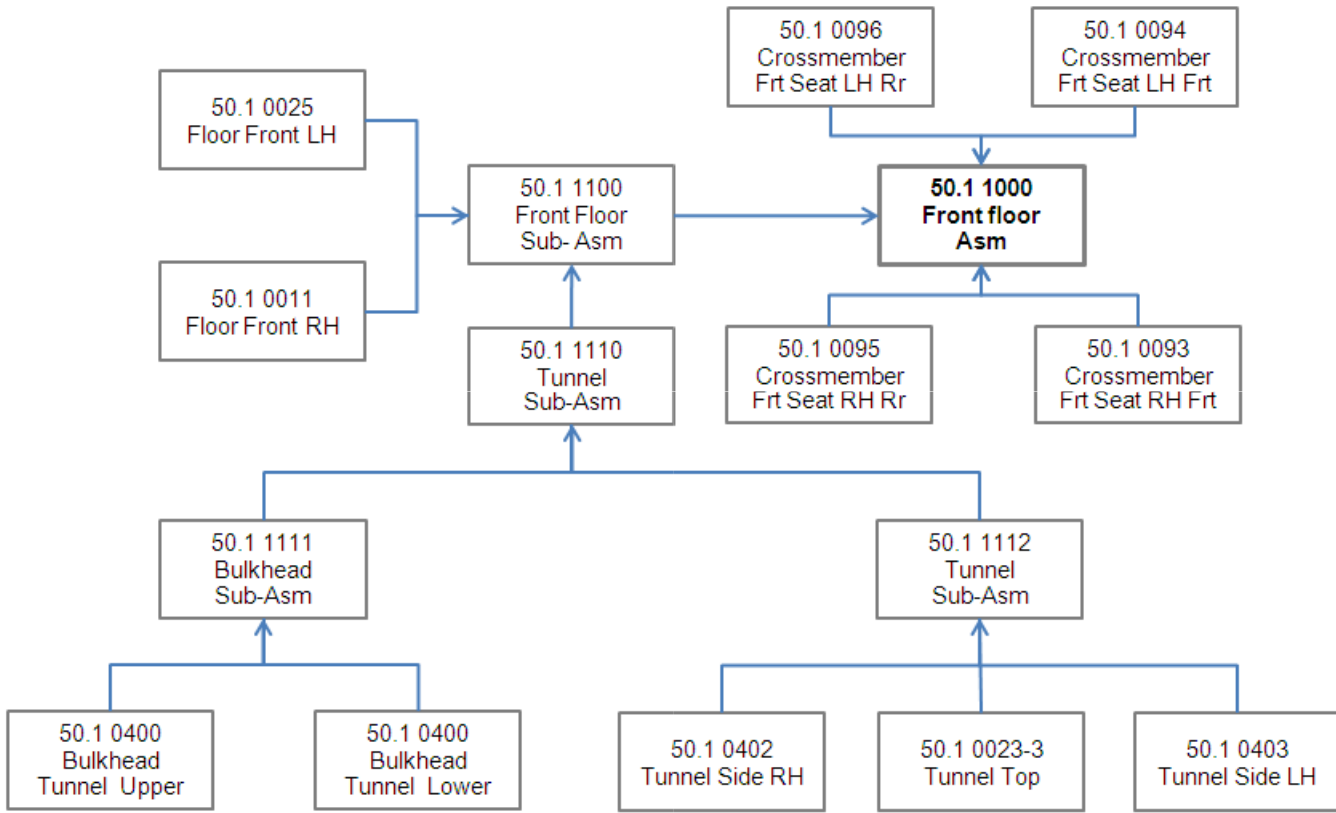


Figure 20.71: Front Floor Assembly (50.1 1000)

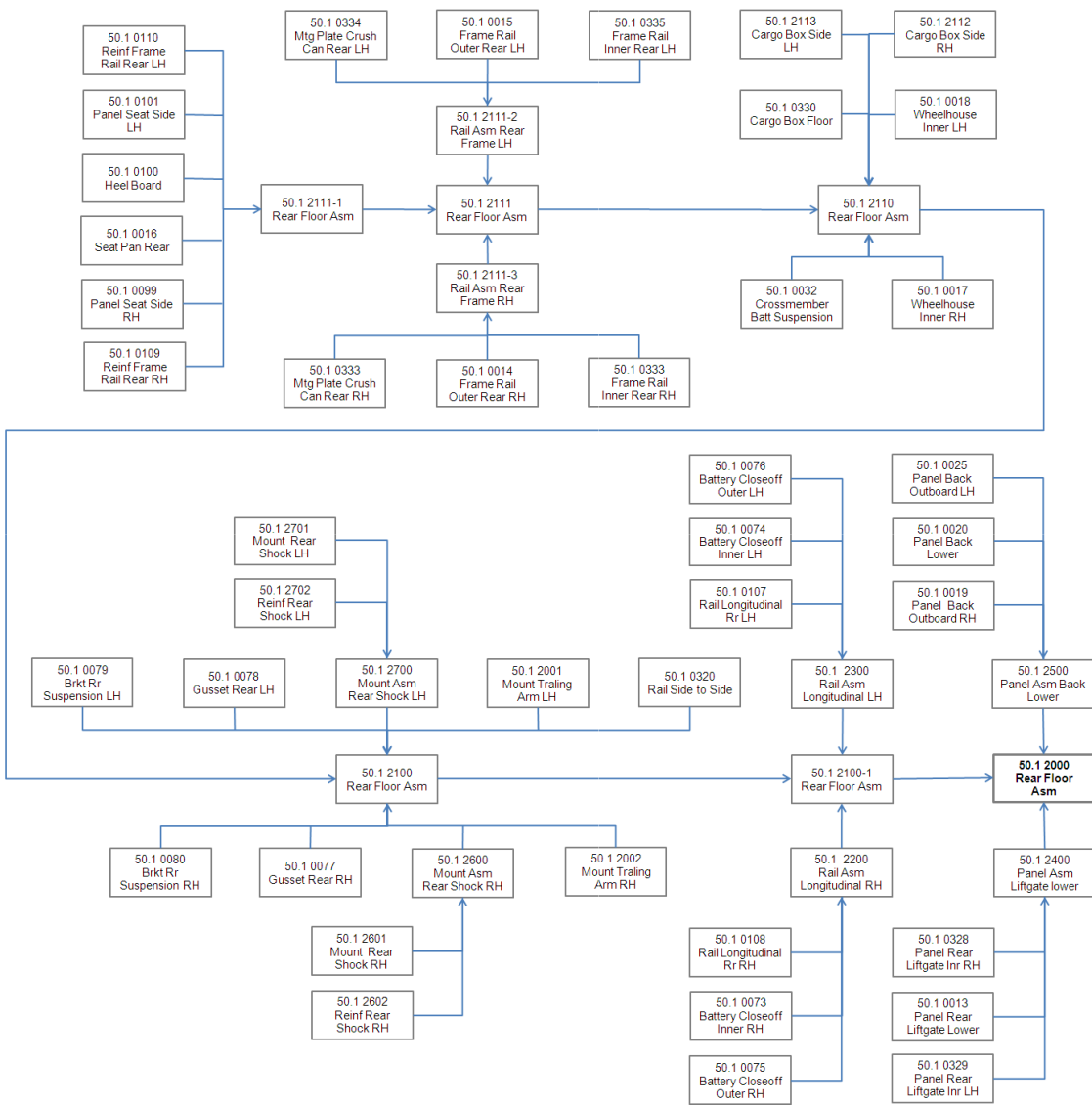


Figure 20.72: Rear Floor Assembly (50.1 2000)

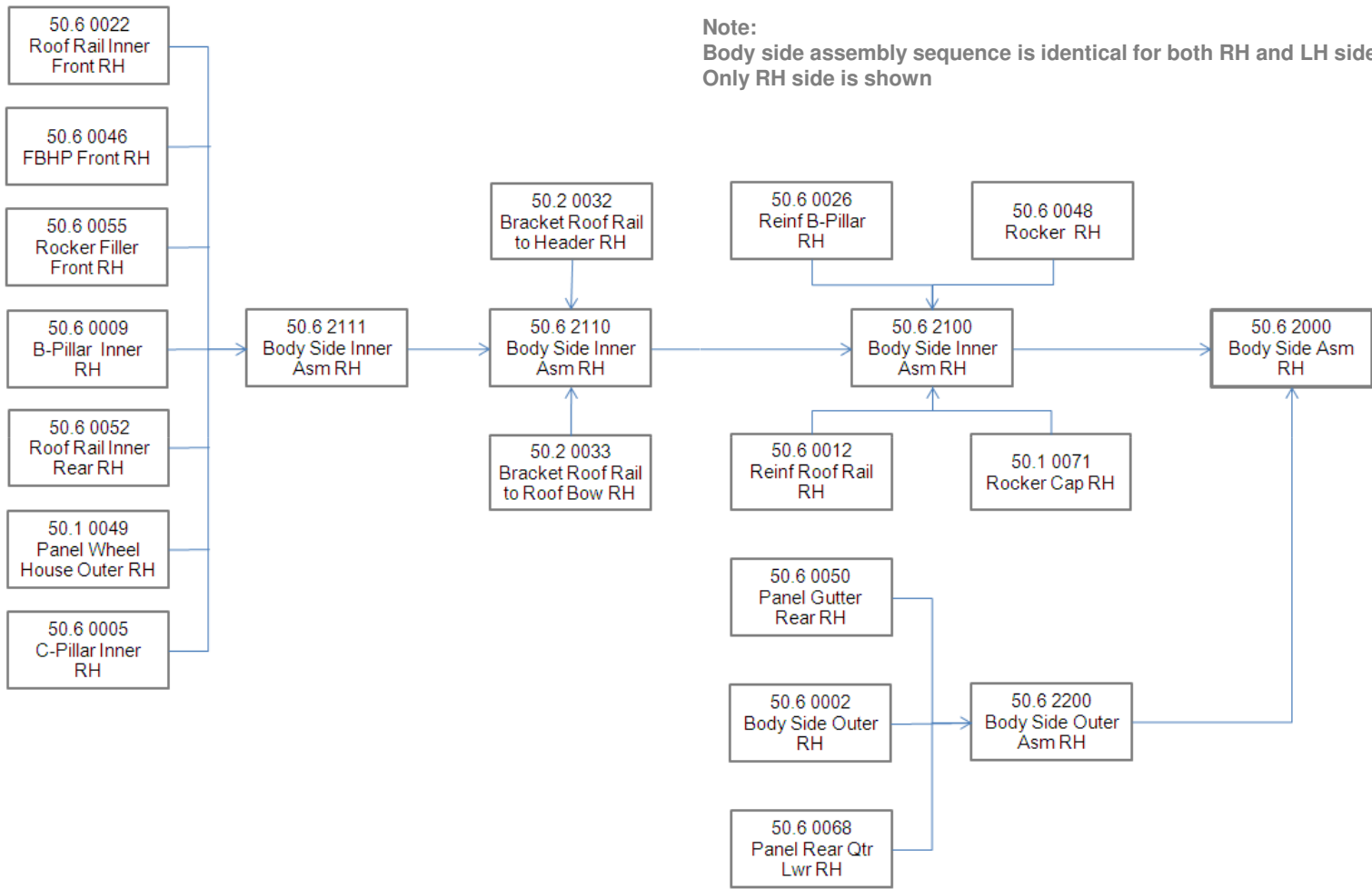


Figure 20.73: Body Side Assembly, RH (50.6 2000)

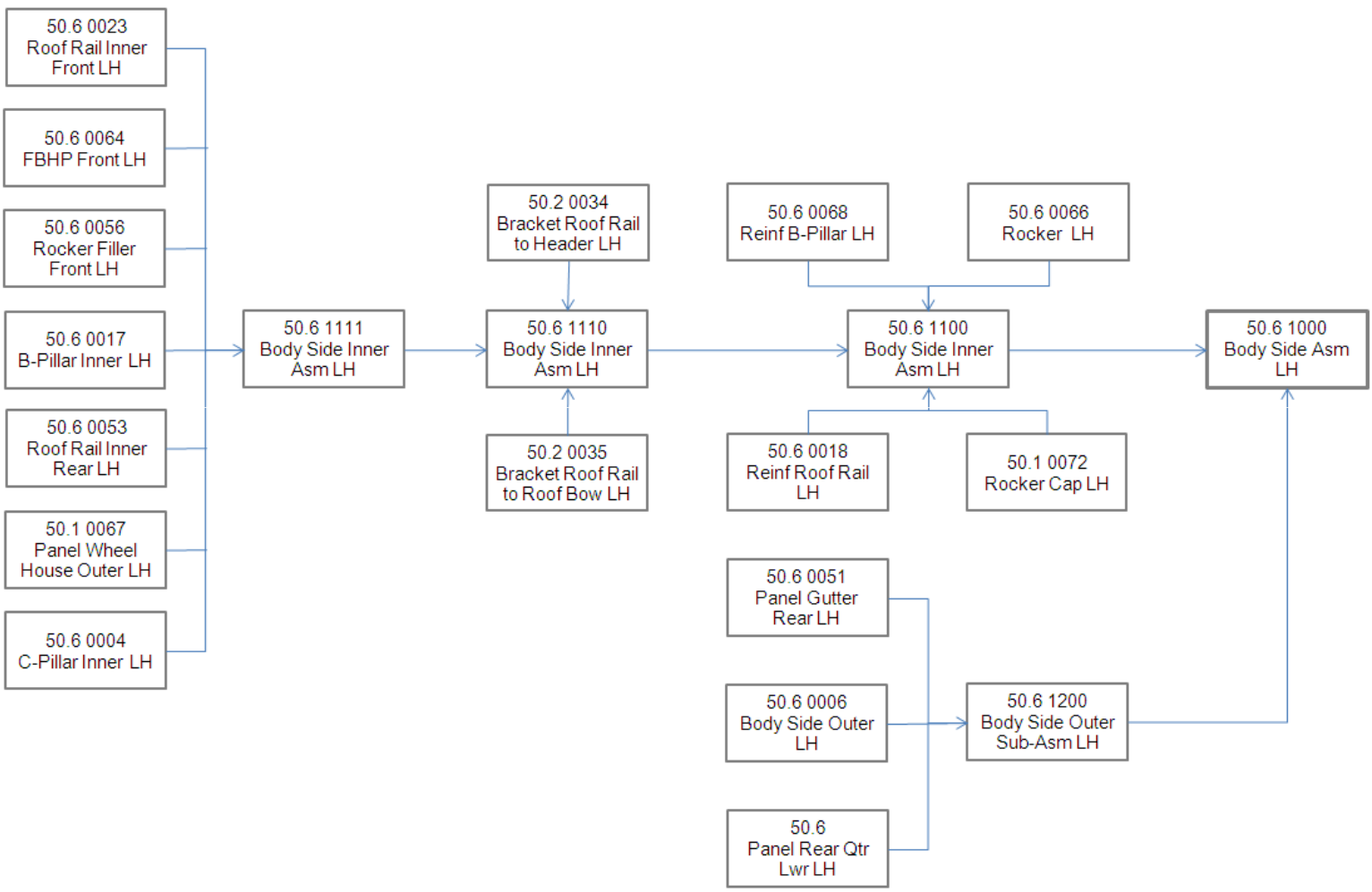


Figure 20.74: Body Side Assembly, LH (50.6 1000)

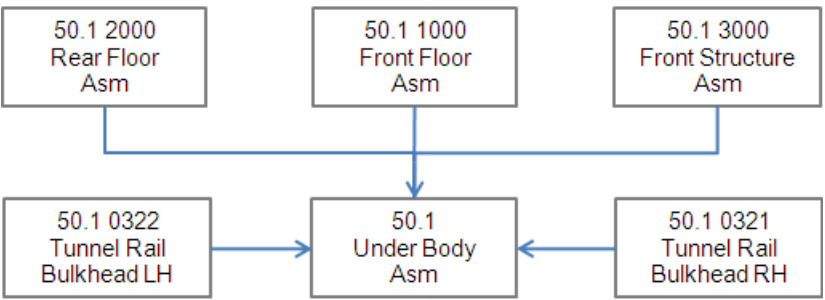
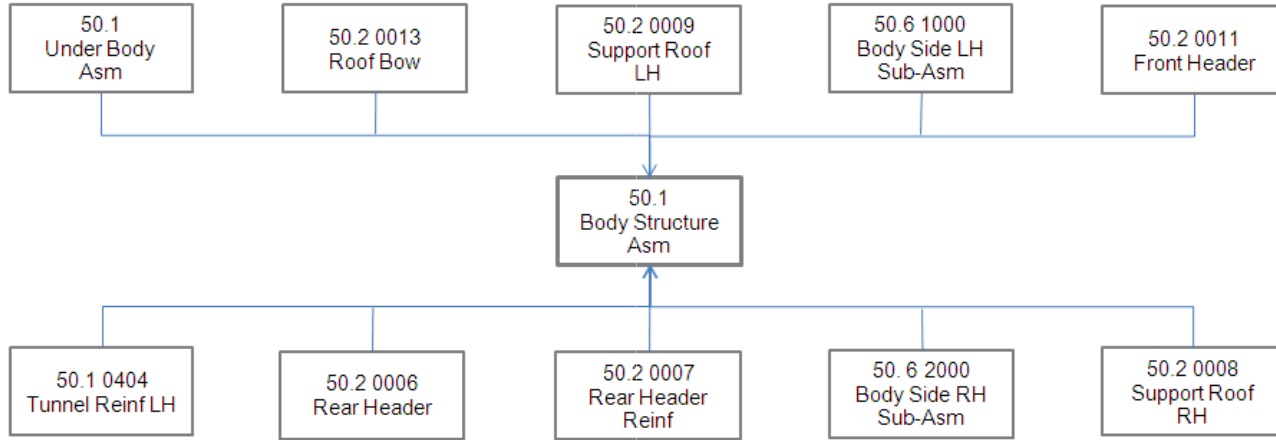


Figure 20.75: 50.1 Underbody Assembly (50.1)

50.1
Body Structure Asm (Framer #1)



50
Body Structure Asm (Framer #2)

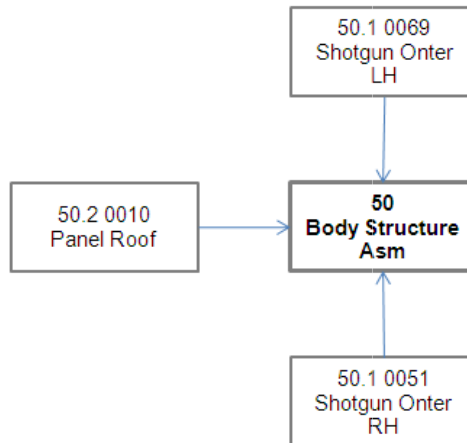


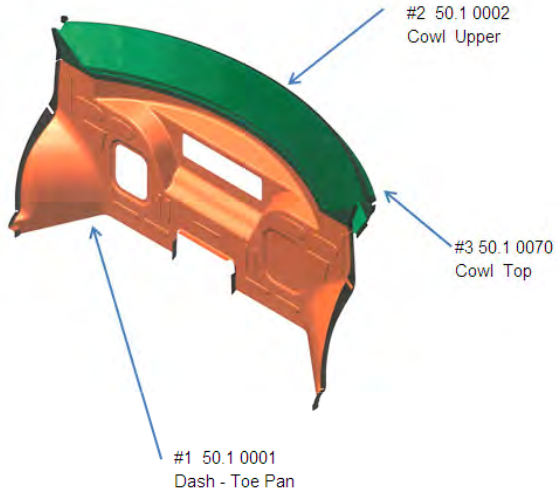
Figure 20.76: Body Structure Assembly (50.1)



Joining Process – Body Structure

Joining Process – Front Structure

50.1 3111
Dash Asm



Joining Process

Part to Part		# of Spot Welds	Length of Adhesive
#1 50.1 0001	#2 50.1 0002	62	n/a
	#3 50.1 0070		
#2 50.1 0002	#3 50.1 0070	15	1412 mm

Total # Spot Welds 77
Total Length of Adhesive 1412 mm

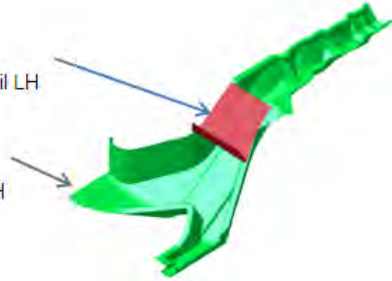
Part to Part		Matl Grade & Thickness (mm)		Weld 2T/3T
#1 50.1 0001	#2 50.1 0002	BH280/400 0.5	BH210/340 0.6/1.2	2T
	#3 50.1 0070		BH210/340 0.6/1.2	2T
#2 50.1 0002	#3 50.1 0070	BH210/340 0.6/1.2	BH210/340 0.6/1.2	2T

Figure 20.77: Dash Assembly (50.1 3111)

50.1 3112-1
Rail Asm Front Lower LH

#2 50.1 0306
Closeout - Lower Rail LH

#1 50.1 0302
Front Rail - Lower LH



Joining Process

Part to Part		# of Spot Welds
#1 50.1 0302	#2 50.1 0306	8

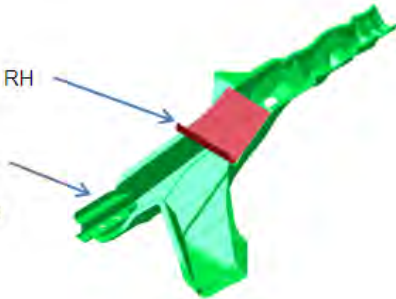
Total # Spot Welds 8

Part to Part		Matl Grade & Thickness (mm)		Weld
#1 50.1 0302	#2 50.1 0306	TRIP 600/980 1.4	DP700/1000 0.8	2T

50.1 3112-2
Rail Asm Front Lower RH

#2 50.1 0305
Closeout - Lower Rail RH

#1 50.1 0301
Front Rail - Lower RH



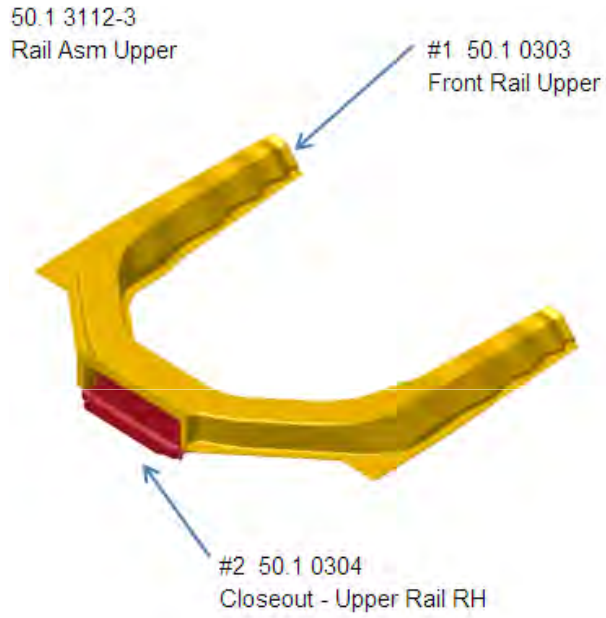
Joining Process

Part to Part		# of Spot Welds
#1 50.1 0301	#2 50.1 0305	8

Total # Spot Welds 8

Part to Part		Matl Grade & Thickness (mm)		Weld
#1 50.1 0301	#2 50.1 0306	#2 50.1 0305	DP700/1000 0.8	2T

Figure 20.78: Rail Assembly Front Lower LH/RH (50.1 3112-1&2)



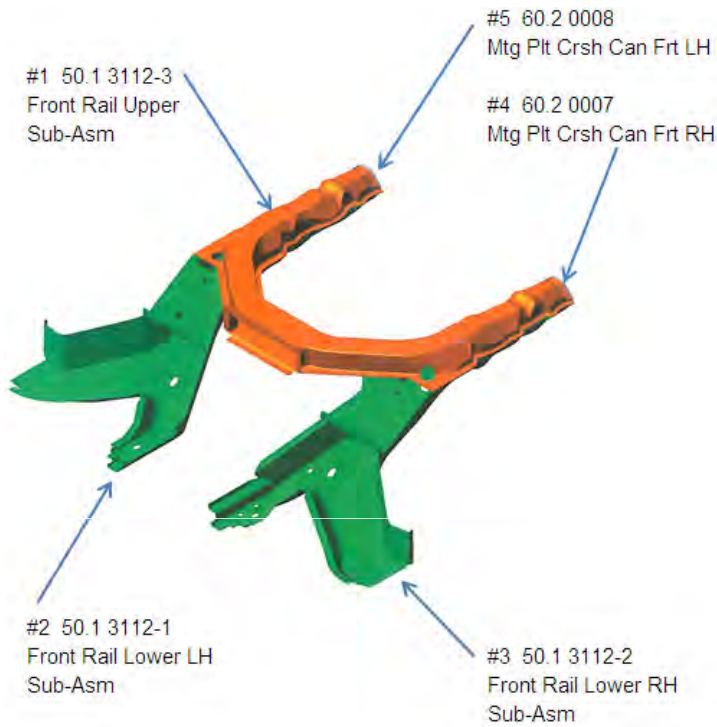
Joining Process

Part to Part		# of Spot Welds
#1 50.1 0303	#2 50.1 0304	30

Total # Spot Welds 30

Part to Part		Matl Grade & Thickness (mm)		Weld
				2T/3T
#1 50.1 0303	#2 50.1 0304	TRIP 600/980 1.4	DP700/1000 1.0	2T

Figure 20.79: Rail Assembly Upper (50.1 3112-3)



Joining Process

Part to Part			Length of Laser
#1 50.1 3112-3	#2 50.1 3112-1		1175 mm
#1 50.1 3112-3	#3 50.1 3112-2		1175 mm
#4 60.2 0007	#1 50.1 3112-3		148 mm
	#3 50.1 3112-2		148 mm
#5 60.2 0008	#1 50.1 3112-3		148 mm
	#2 50.1 3112-1		148 mm

Total length Laser Weld 2942 mm

Part to Part		Matl Grade & Thickness (mm)		Weld 2T/3T
#1 50.1 3112-3	#2/3 50.1 3112-1/2	TRIP 600/980 0.8	Mild140/270 1.1	Laser
		DP350/600 0.95	DP300/500 1.4	Laser
		HLSA350/450 1.85/1.4	TRIP 600/980 1.7/0.6	Laser
#4/5 60.2 0007/8	#1 50.1 3112-3	DP500/800 1.75	TRIP 600/980 0.8	Laser
			Mild140/270 1.1	Laser

Note:

The welding of HSLA350/450 1.4mm to TRIP600/980 0.6 requires further development

Figure 20.80: Rail Assembly Front (50.1 3112)

50.1.3120
Shock Tower Frt LH

#2 50.1.3003
Reinf Shock Tower
Frt LH

#1 50.1.0063
Shock Tower
Frt LH



Joining Process

Part to Part		# of Spot Welds
#1 50.1.0063	#2 50.1.3003	23

Total # Spot Welds 23

Part to Part		Material Grade & Thickness (mm)		Weld 2T/3T
#1 50.1.0063	#2 50.1.3003	TWIP500/980 1.0	DP700/1000 2.0	2T

Note:

The welding of TWIP500/980 1.0 mm to DP700/1000 2.0 mm requires further development

50.1.3130
Shock Tower Frt RH

#2 50.1.3002
Reinf Shock Tower
Frt RH

#1 50.1.0044
Shock Tower
Frt RH



Joining Process

Part to Part		# of Spot Welds
#1 50.1.0044	#2 50.1.3002	23

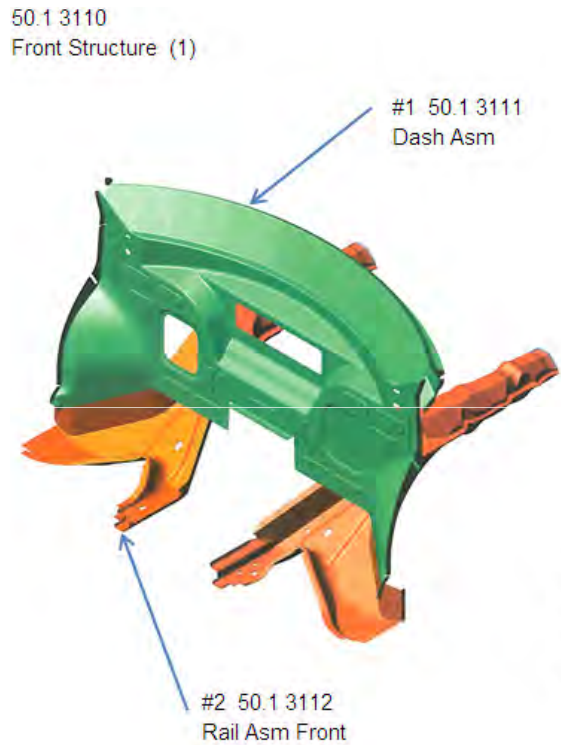
Total # Spot Welds 23

Part to Part		Material Grade & Thickness (mm)		Weld 2T/3T
#1 50.1.0044	#2 50.1.3002	TWIP500/980 1.0	DP700/1000 2.0	2T

Note:

The welding of TWIP500/980 1.0 mm to DP700/1000 2.0 mm requires further development

Figure 20.81: Shock Tower LH/RH (50.1.3120/30)



Joining Process

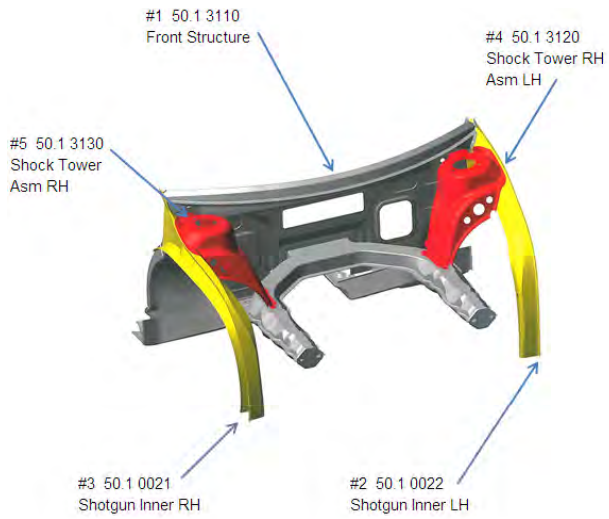
Part to Part		# of Spot Welds
#1 50.1 3111	#2 50.1 3112	32

Total # Spot Welds 32

Part to Part		Matl Grade & Thickness (mm)		Weld 2T/3T
#1 50.1 3111	#2 50.1 3112	BH280/400 0.5	Mild140/270 0.6	2T
			TRIP 600/980 1.0	

Note:
The welding of BH280/400 0.5mm to TRIP600/980 1.0mm requires further development

Figure 20.82: Front Structure Assembly (1) (50.1 3110)



Joining Process

Part to Part		# of Spot Welds	Length of Laser Weld
#1 50.1 3110	#2 50.1 0022	10	
#1 50.1 3110	#3 50.1 0021	10	
#1 50.1 3110	#4 50.1 3120	6	
#1 50.1 3110	#5 50.1 3130	6	
#2 50.1 0022	#4 50.1 3120		120 mm
#3 50.1 0021	#5 50.1 3130		120 mm

Total # Spot Welds 32
 Total length of laser weld 240 mm

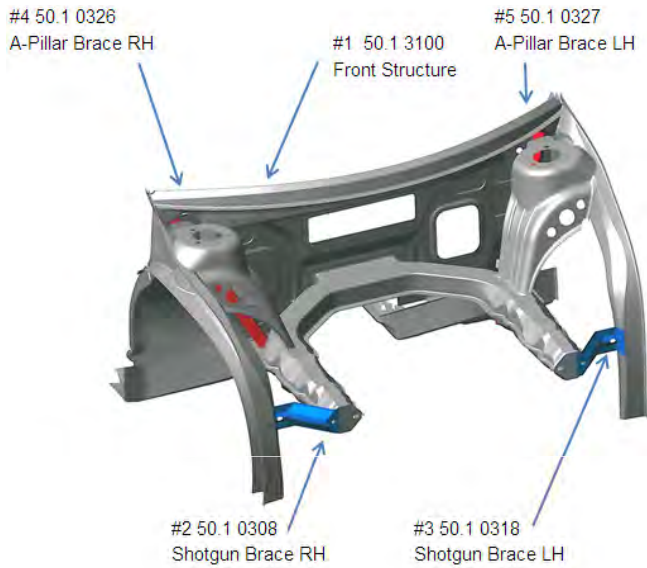
Part to Part		Matl Grade & Thickness (mm)		Weld 2T/3T
#1 50.1 3110	#3 50.1 0021/2	BH280/400 0.5	HF1050/1500 1.5	2T
		BH280/400 0.6		
#4/5 50.1 3120/30	#2/3 50.1 0022/21	TWIP 500/980 1.0	HF1050/1500 1.2/1.5	2T
	#1 50.1 3110	TWIP 500/980 1.0	HSLA350/450 1.85 DP700/1000 1.4	Laser Laser

Note:
 Laser welding is considered a 2T operation

Item 4&5 are both laser and spotwelded

Note:
 The welding of BH280/400 0.5/0.6 mm to HF1050/1500 1.5mm requires further development

Figure 20.83: Front Structure Assembly (2) (50.1 3100)



Joining Process

Part to Part		Length of Laser Weld
#2 50.1 0308	#1 50.1 3100	172 mm
#3 50.1 0318	#1 50.1 3100	172 mm
#4 50.1 0327	#1 50.1 3100	440 mm
#5 50.1 0326	#1 50.1 3100	440 mm

Total length of laser weld 1224 mm

Part to Part		Matl Grade & Thickness (mm)		Weld 2T/3T
#2/3 50.1 0308/18	#1 50.1 3100	BH210/340 1.2	DP500/800 1.2	Laser
#4/5 50.1 0327/26	#1 50.1 3100	HSLA 350/450 1.2	DP700/1000 1.4	Laser
			BH210/340 1.2	Laser

Note:

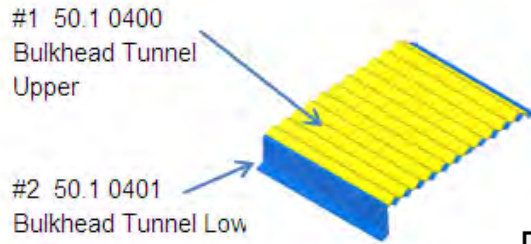
Laser welding is considered a 2T operation

Figure 20.84: Front Structure Assembly (3) (50.1 3100)



Joining Process – Front Floor Asm

50.1 1111
Bulkhead Tunnel Sub-Asm



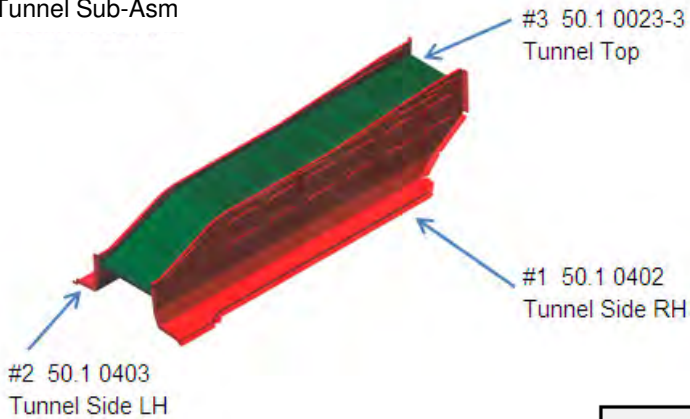
Joining Process

Part to Part		# of Spot Welds
#1 50.1 0400	#2 50.1 0401	28

Total # Spot Welds 28

Part to Part		Matl Grade & Thickness (mm)		Weld 2T/3T
#1 50.1 0400	#2 50.1 0401	DP700/1000 0.8	DP700/1000 0.8	2T

50.1 1112
Tunnel Sub-Asm



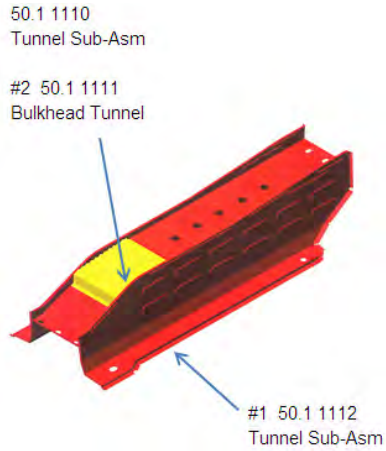
Joining Process

Part to Part		# of Spot Welds
#1 50.1 0402	#3 50.1 0023-3	32
#2 50.1 0403	#3 50.1 0023-3	32

Total # Spot Welds 64

Part to Part		Matl Grade & Thickness (mm)		Weld 2T/3T
#1/2 50.1 0402/3	#3 50.1 0023-3	BH280/400 0.5	BH280/400 0.5	2T

Figure 20.85: Bulkhead Tunnel Sub Assembly & Tunnel Sub Assembly (50.1 1111&2)

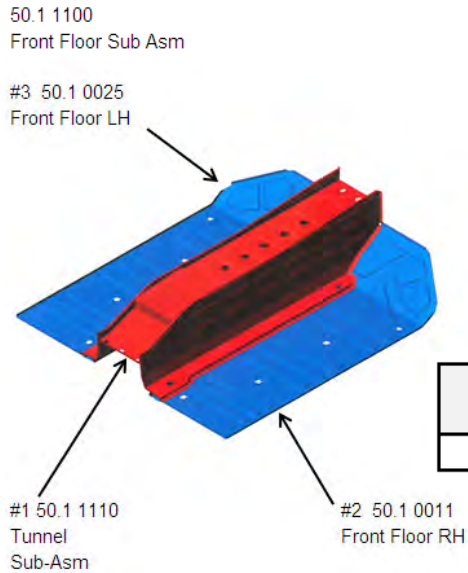


Joining Process

Part to Part		# of Spot Welds
#1 50.1 1112	#2 50.1 1111	10

Total # Spot Welds 10

Part to Part		Matl Grade & Thickness (mm)		Weld
#1 50.1 1112	#2 50.1 1111	BH280/400 0.5	DP700/1000 0.8	2T/3T
				2T



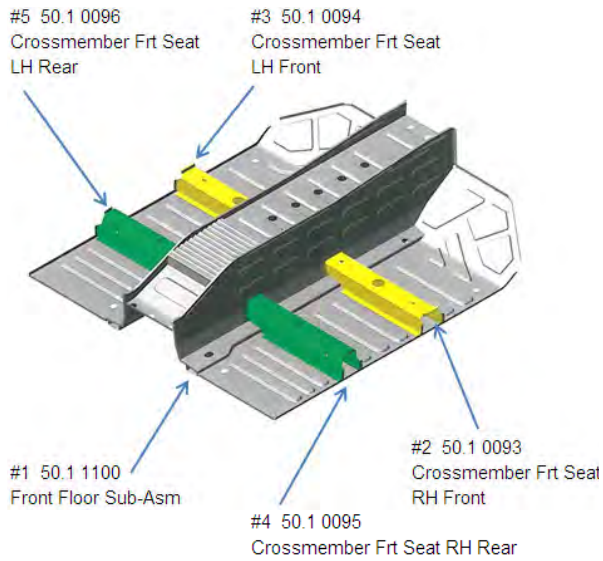
Joining Process

Part to Part		# of Spot Welds	Total Length of Adhesive
#1 50.1 1110	#2 50.1 0011	29	2517 mm
	#3 50.1 0025	29	2517 mm

Total # Spot Welds 58
Total Length of Adhesive 5034 mm

Part to Part		Matl Grade & Thickness (mm)		Weld
#1 50.1 1110	#2/3 50.1 0011/25	DP500/800 1.5	BH280/400 0.5	2T/3T
				2T

Figure 20.86: Tunnel Sub Assembly & Front Floor Sub Assembly (50.1 1110&1100)



Joining Process

Part to Part		# of Spot Welds	Total Length of Adhesive
#1 50.1 1100	#2 50.1 0093	20	835 mm
	#3 50.1 0094	20	835 mm
	#4 50.1 0095	20	835 mm
	#5 50.1 0096	20	835 mm

Total # Spot Welds 80
Total Length of Adhesive 3340 mm

Part to Part		Matl Grade & Thickness (mm)		Weld 2T/3T
#1 50.1 1100	#2/3 50.1 0093/4	BH280/400 0.5	MS950/1200 0.5	2T
		DP300/500 0.5		
#1 50.1 1100	#4/5 50.1 0095/6	BH280/400 0.5	MS950/1200 0.5	2T
		DP300/500 0.5		

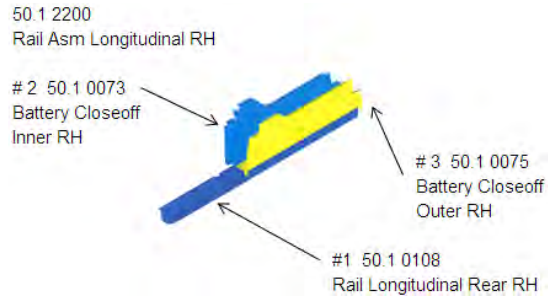
Note:

The welding of BH280/400 0.5 mm & DP300/500 0.5 mm to MS950/1200 0.5 mm requires further development

Figure 20.87: Front Floor Assembly (50.1 1000)



Joining Process – Rear Floor Asm



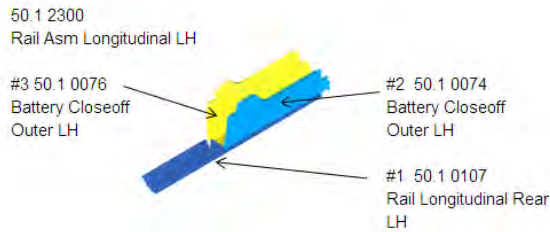
Joining Process

Part to Part		# of Spot Welds
#1 50.1 0108	#2 50.1 0073	15
	#3 50.1 0075	15

2T/3T Matl Stack	
2T Matl Stack	3T Matl Stack
DP700/1000 1.2	DP700/1000 1.2
BH280/400 0.5	BH280/400 0.5
	BH280/400 0.5

Total # Spot Welds 30

Part to Part		Matl Grade & Thickness (mm)		Weld 2T/3T
#1 50.1 0108	#2/3 50.1 0073/75	DP700/1000 1.2	BH280/400 0.5	2T/3T



Joining Process

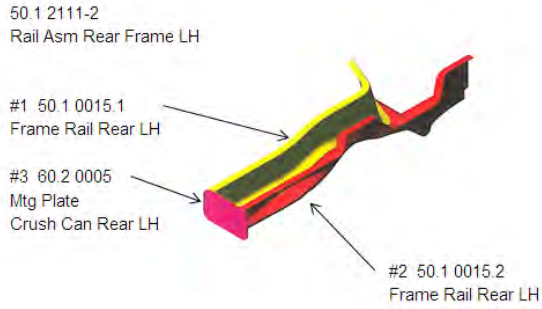
Part to Part		# of Spot Welds
#1 50.1 0107	#2 50.1 0074	15
	#3 50.1 0076	15

2T/3T Matl Stack	
2T Matl Stack	3T Matl Stack
DP700/1000 1.2	DP700/1000 1.2
BH280/400 0.5	BH280/400 0.5
	BH280/400 0.5

Total # Spot Welds 30

Part to Part		Matl Grade & Thickness (mm)		Weld 2T/3T
#1 50.1 0107	#2/3 50.1 0074/76	DP700/1000 1.2	BH280/400 0.5	2T/3T

Figure 20.88: Rail Assembly Longitudinal RH&LH (50.1 2200 & 2300)



Part to Part		Length of Laser Weld
#1 50.1 0015.1	#2 50.1 0015.2	931 mm
#3 60.2 0005	#1 50.1 0015.1	305 mm
	#2 50.1 0015.2	

Total length of Laser Weld 1236 mm

Part to Part		Matl Grade & Thickness (mm)		Weld 2T/3T
#1 50.1 0015.1	#2 50.1 0015.2	HSLA350/450 0.8	HSLA350/450 0.8	Laser
		DP700/1000 1.4	DP 700/1000 1.4	
		CP1000/1200 0.6	CP1000/1200 0.6	
#3 60.2 0005	#1/2 50.1 0015.1/2	DP500/800 1.2	HSLA350/450 0.8	Laser

Note:
Laser welding is considered to be a 2T operation

Joining Process

Part to Part		Length of laser Weld
#1 50.1 0014.1	#2 50.1 0014.2	931 mm
#3 60.2 0005	#1 50.1 0014.1	305 mm
	#2 50.1 0014.2	

Total length of Laser Weld 1236 mm

Part to Part		Matl Grade & Thickness (mm)		Weld 2T/3T
#1 50.1 0014.1	#2 50.1 0014.2	HSLA350/450 0.8	HSLA350/450 0.8	Laser
		DP700/1000 1.4	DP 700/1000 1.4	
		CP1000/1200 0.6	CP1000/1200 0.6	
#3 60.2 0005	#1/2 50.1 0014.1/2	DP500/800 1.2	HSLA350/450 0.8	Laser

Note:
Laser welding is considered to be a 2T operation

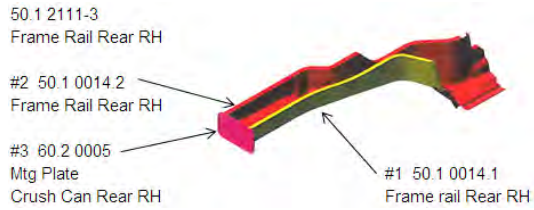
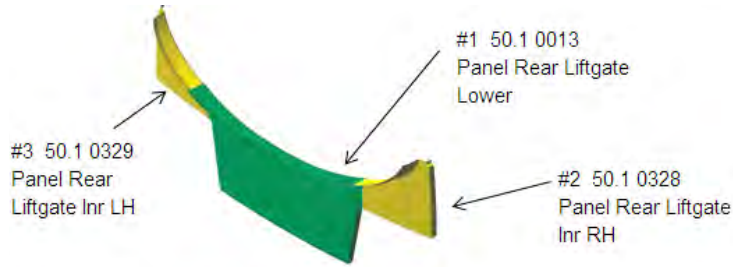


Figure 20.89: Rail Assembly Rear Frame, LH/RH (50.1 2111 2&3)

50.1 2400
Panel Asm Liftgate Lower



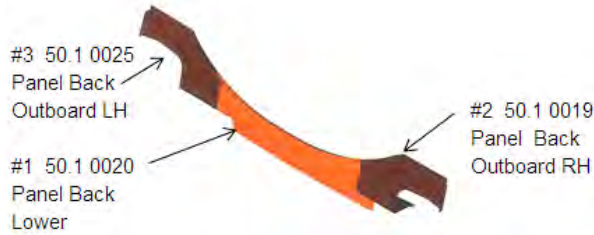
Joining Process

Part to Part		# of Spot Welds
#1 50.1 0013	#2 50.1 0328	6
	#3 50.1 0329	6

Total # Spot Welds 12

Part to Part		Matl Grade & Thickness (mm)		Weld 2T/3T
#1 50.1 0013	#2/3 50.1 0328/9	BH210/340 1.0	BH210/340 0.7	2T

50.1 2500
Panel Asm Back Lower



Part to Part		# of Spot Welds
#1 50.1 0020	#2 50.1 0019	7
	#3 50.1 0025	7

Total # Spot Welds 14

Part to Part		Matl Grade & Thickness (mm)		Weld 2T/3T
#1 50.1 0020	#2/3 50.1 0019/25	BH210/340 1.0	BH210/340 1.0	2T

Figure 20.90: Panel Assembly Liftgate Lower & Panel Assembly Back Lower (50.1 2400&2500)

50.1 2600
Mount Rear Shock Asm RH

#1 50.1 2601
Mount Rear Shock RH



#2 50.1 2602
Reinf Rear Shock RH

Joining Process

Part to Part		# of Spot Welds
#1 50.1 2601	#2 50.1 2602	2

Total # Spot Welds 2

Part to Part		Matl Grade & Thickness (mm)		Weld
#1 50.1 2601	#2 50.1 2602	DP500/800 2.5	DP500/800 2.0	2T

50.1 2700
Mount Asm Rear Shock LH

#1 50.1 2701
Mount Rear Shock LH



#2 50.1 2702
Reinf Rear Shock LH

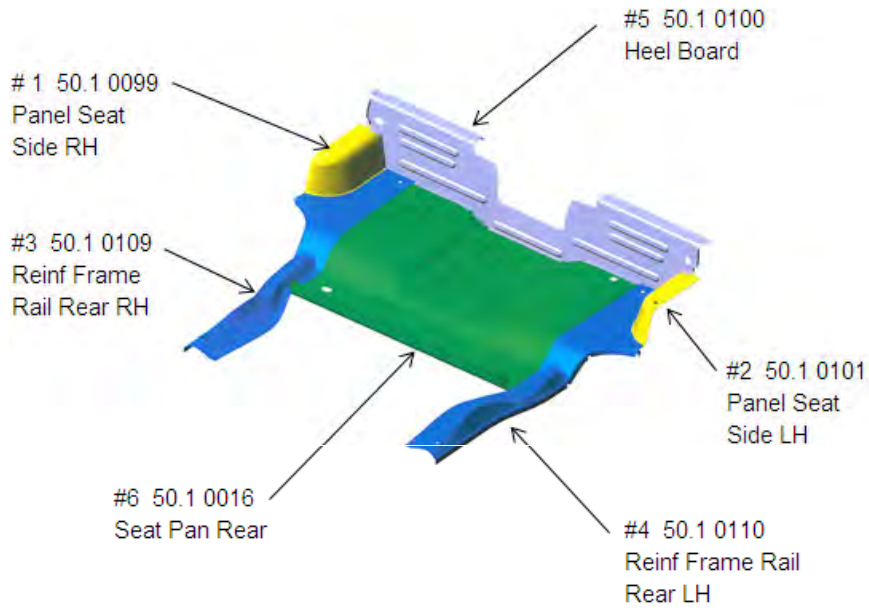
Joining Process

Part to Part		# of Spot Welds
#1 50.1 2701	#2 50.1 2702	2

Total # Spot Welds 2

Part to Part		Matl Grade & Thickness (mm)		Weld
#1 50.1 2701	#2 50.1 2702	DP500/800 2.5	DP500/800 2.0	2T

Figure 20.91: Mount-Rear Shock Assembly, RH/LH (50.1 2600&2700)



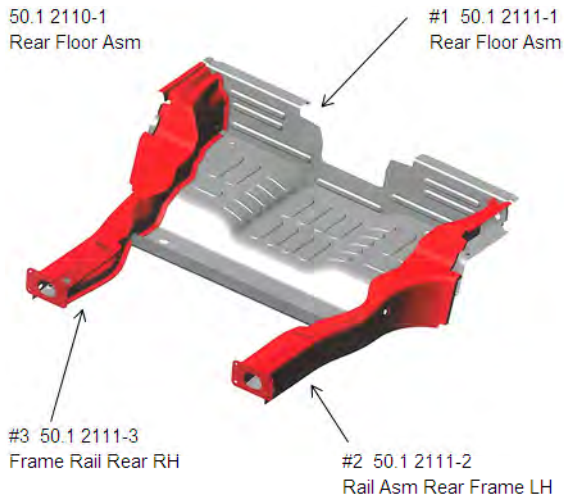
Joining Process

Part to Part		# of Spot Welds
# 1 50.1 0099	#3 50.1 0109	8
	#5 50.1 0100	4
#2 50.1 0101	#4 50.1 0110	8
	#5 50.1 0100	4
#5 50.1 0100	#3 50.1 0109	3
	#4 50.1 0110	3
	#6 50.1 0016	21
#6 50.1 0016	#3 50.1 0109	10
	#4 50.1 0110	10

Total # Spot Welds 71

Part to Part		Matl Grade & Thickness (mm)		Weld 2T/3T
#1/2 50.1 0099/0101	#3/4 50.1 0109/0110	DP700/1000 0.7	DP1000/1200 1.1	2T
	#5 50.1 0100		BH210/340 0.6	2T
#6 50.1 0016	#3/4 50.1 0109/0110	BH210/340 0.5	DP1000/1200 1.1	2T
			DP700/1000 0.65	2T
	#5 50.1 0100		DP700/1000 0.7	2T

Figure 20.92: Rear Floor Assembly(1)(50.1 2111-1)



Joining Process

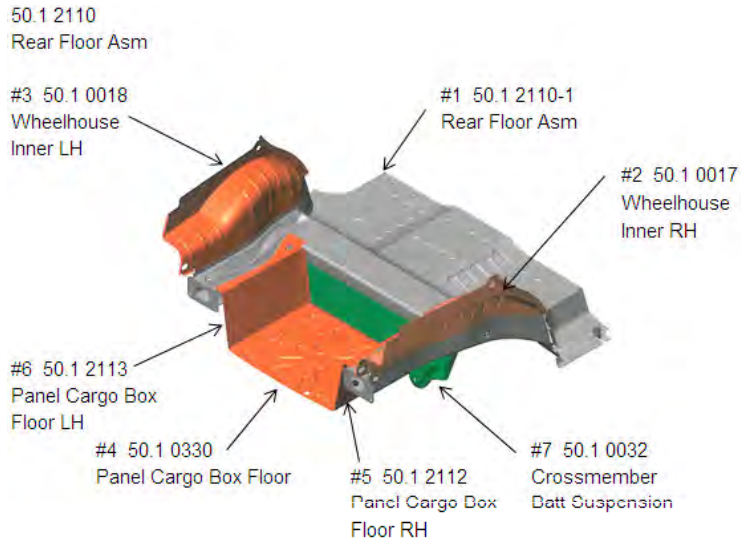
Part to Part		# of Spot Welds
#1 50.1 2111-1	#2 50.1 2111-2	38
	#3 50.1 2111-3	38

Total # Spot Welds 76

2T/3T Matl Stack	
2T Matl Stack	3T Matl Stack
DP700/1000 1.4 mm	BH210/340 0.6mm
BH280/400 0.5 mm	DP700/1000 0.65mm
HSLA350/450 0.8mm	CP1000/1200 0.6mm
Mild140/270 1.55mm	BH210/340 0.6mm
	DP700/1000 1.4mm
	DP700/1000 1.1mm

Part to Part		Matl Grade & Thickness (mm)		Weld
				2T/3T
#1 50.1 2111-1	#2/3 50.1 2111-2/3	BH210/340 0.6	DP700/1000 1.4	2T
		DP700/1000 1.1	DP700/1000 1.4	3T
		CP1000/1200 0.6	CP1000/1200 0.6	3T
		Mild140/270 1.55	HSLA350/450 0.8	2T

Figure 20.93: Rear Floor Assembly(2)(50.1 2110-1)



Joining Process Floor RH

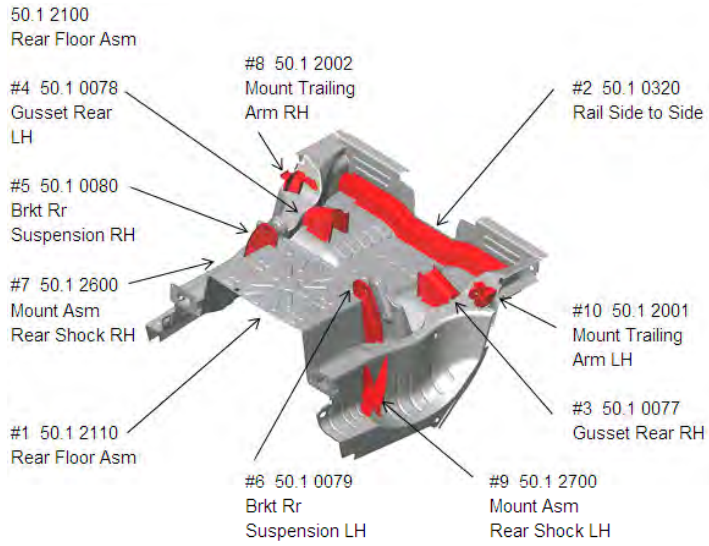
Part to Part		# of Spot Welds	Length of laser Weld
#1 50.1 2110-1	#2 50.1 0017	11	
	#3 50.1 0018	11	
	#5/6 50.1 2112/3	14	
#4 50.1 0330	#5/6 50.1 2112/3	28	
#7 50.1 0032	#4 50.1 0330	29	
#7 50.1 0032	#1 50.1 2110-1		1977 mm

Total # Spot Welds 93
Total Length of Laser Weld 1977 mm

Part to Part		Matl Grade & Thickness (mm)		Weld 2T/3T
#1 50.1 2110-1	#2/3 50.1 0017/8	HSLA350/450 0.8	BH210/340 0.7/1.2	3T
		DP700/1000 1.4		3T
		CP1000/1200 0.6		3T
		DP700/1000 0.65		3T
		Mild140/270 1.55		3T
#1 50.1 2110-1	#4 50.1 0330	HSLA350/450 0.8	Mild140/270 0.5	3T
		DP700/1000 1.4		3T
		DP700/1000 0.65		3T
		Mild140/270 1.55		3T
#5 50.1 0032	#4 50.1 0330	CP800/1000 1.0	BH210/310 0.5	2T
	#1 50.1 2110-1	CP800/1000 1.0	DP700/1000 1.4	Laser
#4 50.1 0330	#5/6 50.1 2112/3	BH210/310 0.5	BH210/310 0.5	2T

2T/3T Matl Stack		
2T Matl Stack	3T Matl Stack	
BH210/310 0.5mm	BH210/340 0.7mm	BH210/340 1.2mm
CP800/1000 1.0mm	CP1000/1200 0.6mm	HSLA350/450 0.8mm
	DP700/1000 0.65mm	Mild140/270 1.55mm
	BH210/340 0.7mm	Mild140/270 0.5mm
	DP700/1000 1.4mm	DP700/1000 0.65mm
	DP700/1000 0.65mm	DP700/1000 1.4mm
	BH210/340 1.2mm	Mild140/270 0.5mm
	DP700/1000 1.4mm	Mild140/270 1.55mm
	DP700/1000 0.65mm	HSLA350/450 0.8mm

Figure 20.94: Rear Floor Assembly(3)(50.1 2110)



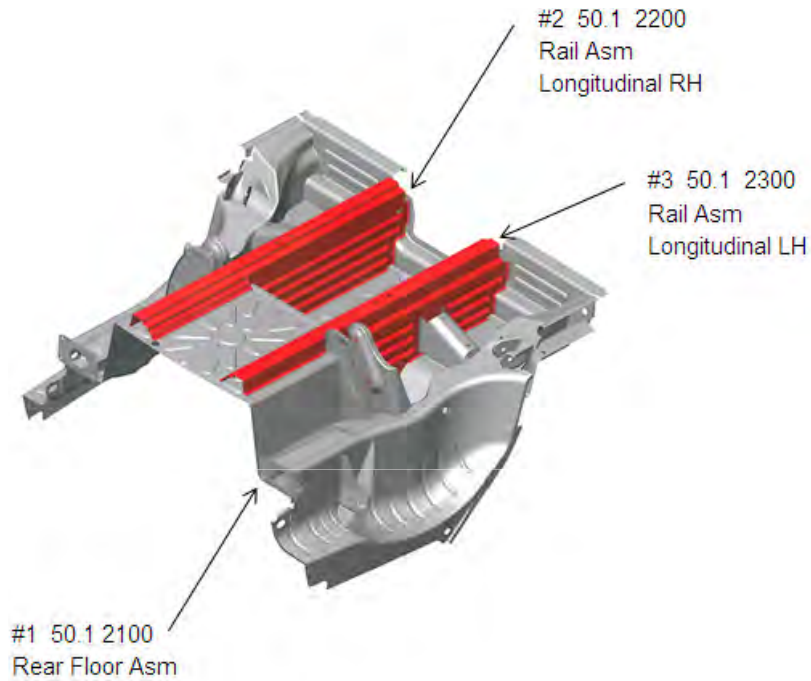
Joining Process

Part to Part		Length of laser Weld
#1 50.1 2110	#2 50.1 0320	2004 mm
	#3 50.1 0077	266 mm
	#4 50.1 0078	266 mm
	#5 50.1 0080	354 mm
	#6 50.1 0079	354 mm
	#7 50.1 2600	504 mm
	#8 50.1 2002	225 mm
	#9 50.1 2700	504 mm
	#9 50.1 2701	225 mm

Total length of Laser Weld 4702 mm

Part to Part		Matl Grade & Thickness (mm)		Weld 2T/3T
#1 50.1 2110	#2 50.1 0320	DP700/1000 1.4	DP500/800 0.8	Laser
		BH210/340 0.5/0.6		
#1 50.1 2110	#3/4 50.1 0077/8	CP1000/1200 0.6	BH210/340 1.0	Laser
		BH210/340 0.5/0.6		
#1 50.1 2110	#5/6 50.1 0080/79	DP700/1000 1.5	CP800/100 1.0	Laser
		Mild140/270 0.5		
#1 50.1 2110	#7/9 50.1 2600/2700 (Reinf Rear Shock)	BH210/340 1.2	DP500/800 2.0	Laser
#1 50.1 2110	#7/9 50.1 2600/2700 (Mount Rear Shock)	BH210/340 1.2	DP500/800 2.5	Laser

Figure 20.95: Rear Floor Assembly(4)(50.1 2100)



Joining Process

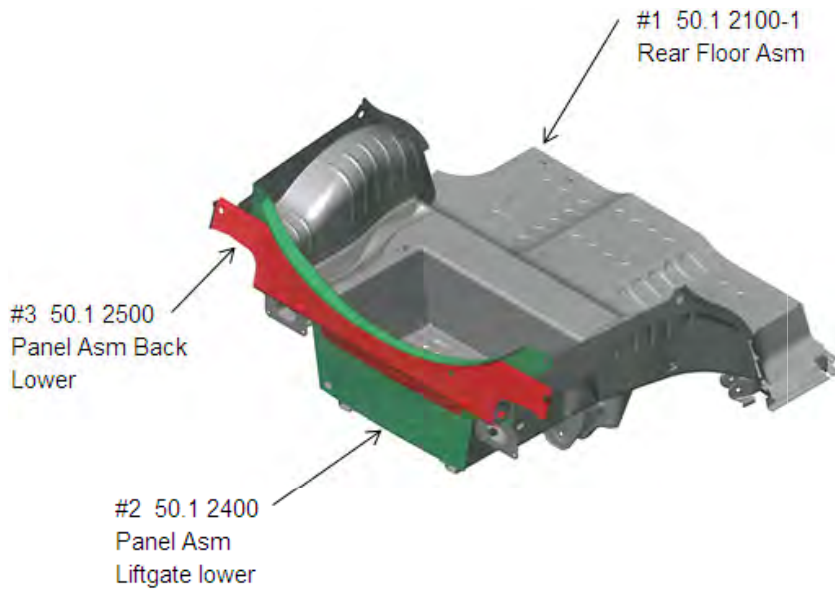
Part to Part		Length of laser Weld
#1 50.1 2100	#2 50.1 2200	2564 mm
	#3 50.1 2300	2564 mm

Total length of Laser Weld 5128 mm

Part to Part		Matl Grade & Thickness (mm)		Weld
#1 50.1 2100	#2/3 50.1 2200/2300	Mild140/270 0.5	DP700/1000 1.0	Laser
		BH210/340 0.5	BH210/340 0.6	Laser
		BH210/340 1.0		
		DP500/800 0.8		
		CP800/1000 1.0		

Note:
Laser welding is considered a 2T operation

Figure 20.96: Rear Floor Assembly(5)(50.1 2100-1)



Joining Process

Part to Part		Length of laser Weld
#1 50.1 2100-1	#2 50.1 2400	1862 mm
	#3 50.1 2500	774 mm
#2 50.1 2400	#3 50.1 2500	2642 mm

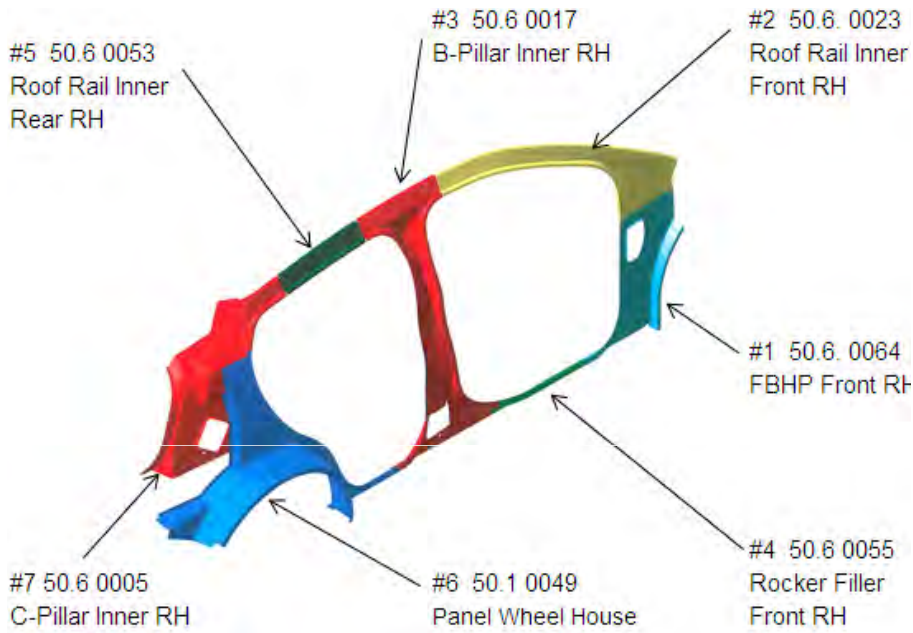
Total length of Laser Weld 5278 mm

Part to Part		Matl Grade & Thickness (mm)		Weld
#1 50.1 2100-1	#2 50.1 2400	BH210/340 1.2	BH210/340 0.7/1.0	Laser
		Mild 140/270 0.5		
#2 50.1 2400	#3 50.1 2500	BH210/340 0.7/1.0	BH210/340 1.0	Laser

Note:
Laser welding is considered a 2T operation

Figure 20.97: Rear Floor Assembly(6)(50.1 2000)

Joining Process – Body Side Asm RH



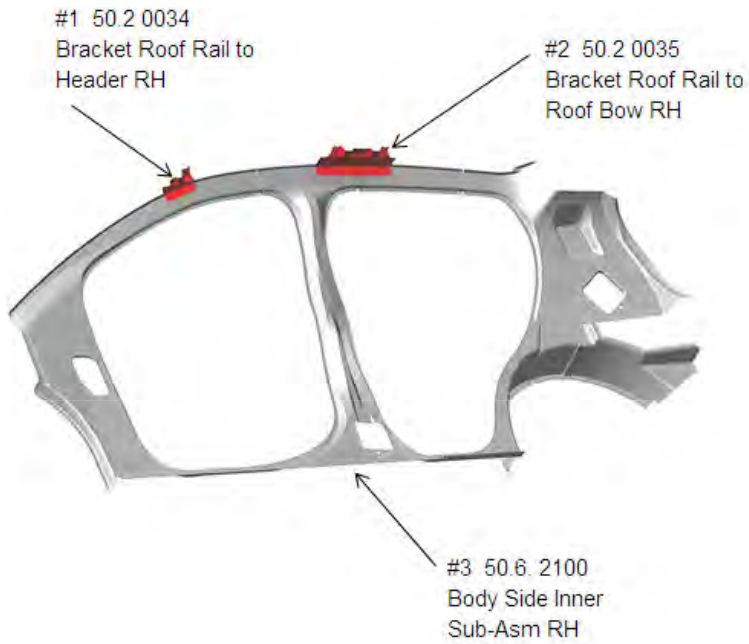
Joining Process

Part to Part		# of Spot Welds
#1 50.6. 0064	#2 50.6. 0023	9
#1 50.6. 0064	#4 50.6 0055	3
#2 50.6. 0023	#3 50.6 0017	3
#3 50.6 0017	#5 50.6 0053	3
#5 50.6 0053	#7 50.6 0005	3
#3 50.6 0017	#6 50.1 0049	2
#3 50.6 0017	#4 50.6 0055	4
#6 50.1 0049	#7 50.6 0005	15

Total # Spot Welds 42

Part to Part		Matl Grade & Thickness (mm)		Weld 2T/3T
#1 50.6. 0064	#2 50.6. 0023	DP500/800 1.2	HF1050/1500 0.7	2T
	#4 50.6 0055		HF1050/1500 0.6	2T
#2 50.6. 0023	#3 50.6 0017	HF1050/1500 0.95	HF1050/1500 0.80	2T
#3 50.6 0017	#4 50.6 0055	HF1050/1500 0.80	HF1050/1500 0.6	2T
	#5 50.6 0053		HF1050/1500 1.1	2T
	#6 50.1 0049		DP500/800 0.65	2T
#6 50.1 0049	#7 50.6 0005	DP500/800 0.65	DP500/800 0.7	2T

Figure 20.98: Body Side Inner Assembly RH (1) (50.6 2111)



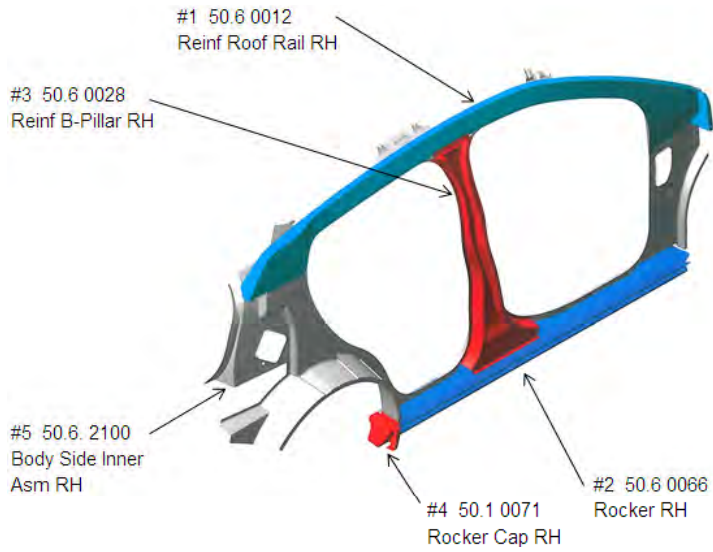
Joining Process

Part to Part		# of Spot Welds
#1 50.2 0034	#3 50.6 2100	4
#2 50.2 0035	#3 50.6 2100	6

Total # Spot Welds 10

Part to Part		Matl Grade & Thickness (mm)		Weld 2T/3T
#2 50.2 0035	#1 50.2 0034	BH210/340 1.0	HF1050/1500 0.80	2T
			HF1050/1500 1.1	2T
#3 50.6 2100	#1 50.2 0034	BH210/340 1.0	HF1050/1500 0.95	2T

Figure 20.99: Body Side Inner Assembly RH (2) (50.6 2110)



Joining Process

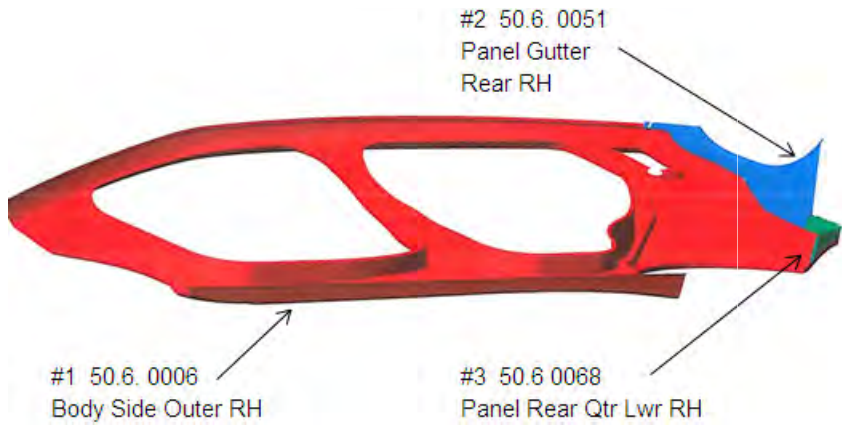
Part to Part		Length of Laser Weld
#1 50.6 0012	#5 50.6. 2100	300 mm
#2 50.6 0066	#5 50.6. 2100	1580 mm
#3 50.6 0028	#5 50.6. 2100	160 mm
#3 50.6 0028	#1 50.6 0018	191 mm
#3 50.6 0028	#2 50.6 0066	340 mm
#4 50.1 0071	#5 50.6. 2100	149 mm

Total Length of Laser Weld 2720 mm

Part to Part		Matl Grade & Thickness (mm)		Weld 2T/3T
#1 50.6 0012	#5 50.6. 2100	HF1050/1500 0.7	DP500/800 1.2	Laser
			HF1050/1500 0.95	
			HF1050/1500 0.8	
			HF1050/1500 0.7	
			HF1050/1500 0.6	
			DP500/800 0.7	
#2 50.6 0066	#5 50.6. 2100	CP1050/1470 1.0	HF1050/1500 0.6	Laser
			HF1050/1500 0.80	
			DP500/800 1.2	
			DP500/800 0.6	
#3 50.6 0028	#1 50.6 0012	HF1050/1500 0.6	HF1050/1500 0.80	Laser
#4 50.1 0071	#2 50.6 0066	BH210/340 0.85	CP1050/1470 1.0	Laser
	#5 50.6. 2100		DP500/800 0.65	

Note:
Laser welding is considered a 2T operation

Figure 20.100: Body Side Inner Assembly RH (3) (50.6 2100)



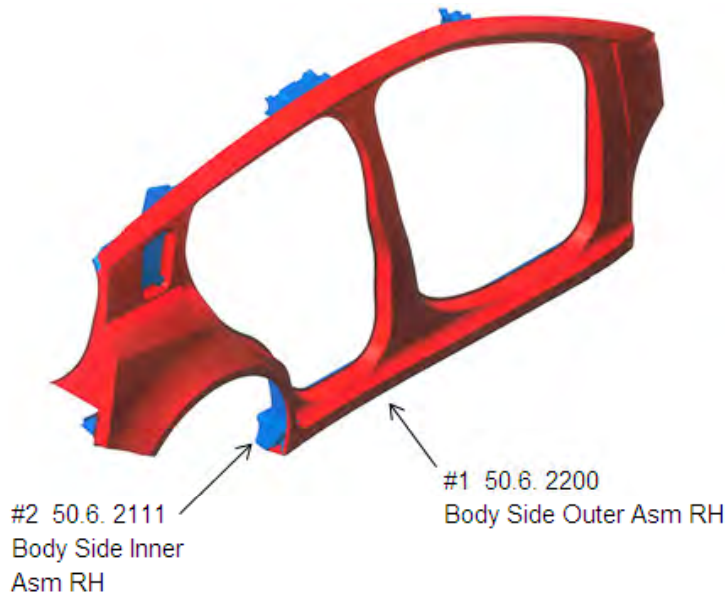
Joining Process

Part to Part		# of Spot Welds
#1 50.6.0006	#2 50.6.0051	17
#1 50.6.0006	#3 50.6.0068	7
#2 50.6.0051	#3 50.6.0068	2

Total # Spot Welds 27

Part to Part		Matl Grade & Thickness (mm)		Weld 2T/3T
#1 50.6.0006	#2 50.6.0051	BH210/340 0.6	BH210/340 1.0	2T
	#3 50.6.0068		BH210/340 1.2	2T
#2 50.6.0051	#3 50.6.0068	BH210/340 1.0	BH210/340 1.2	2T

Figure 20.101: Body Side Outer Assembly (RH) (50.6 2200)



Joining Process

Part to Part		Length of Laser Weld
#1 50.6. 2200	#2 50.6. 2111	11626 mm

Part to Part		Length of Roller Hem
#1 50.6. 2200	#2 50.6. 2111	1025 mm

Part to Part		Length of Hem Adhesive
#1 50.6. 2200	#2 50.6. 2111	1025 mm

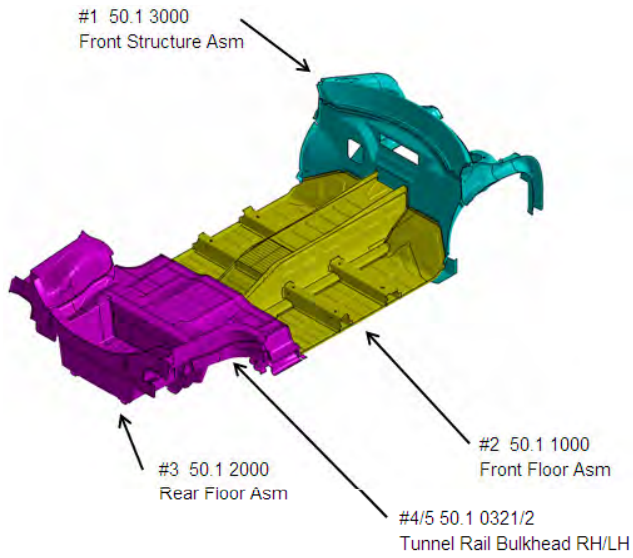
Total Length of Laser Weld	11626 mm
Total Length of Roller Hem	1025 mm
Total length of Hem Adhesive	1025 mm

Part to Part		Matl Grade & Thickness (mm)		Weld 2T/3T
#1 50.6. 2200	#2 50.6. 2111	BH210/340 0.6	BH210/340 0.85	Laser
		BH210/340 1.0	DP500/800 0.65	
		BH210/340 1.2	DP500/800 0.7	
		DP350/600 0.8	DP500/800 1.2	
		DP350/600 1.25	HF 1050/1500 0.6	
		DP700/1000 0.8	HF 1050/1500 0.7	
		DP700/1000 1.6	HF 1050/1500 0.8	
			HF 1050/1500 0.95	
			HF 1050/1500 1.1	

Note:
Laser welding is considered a 2T operation

Figure 20.102: Body Side Outer Assembly (RH) (50.6 2000)

Joining Process – Under Body Asm



Joining Process

Part to Part		# of Spot Welds	Total Length of Laser Weld
#1 50.1 3000	#2 50.1 1000	36	683 mm
#2 50.1 1000	#3 50.1 2000	51	1290 mm
#4/5 50.1 0321/2	#2 50.1 1000	n/a	448 mm
	#3 50.1 2000	n/a	608 mm

Total # Spot Welds 87
 Total Length of Laser Weld 3029 mm

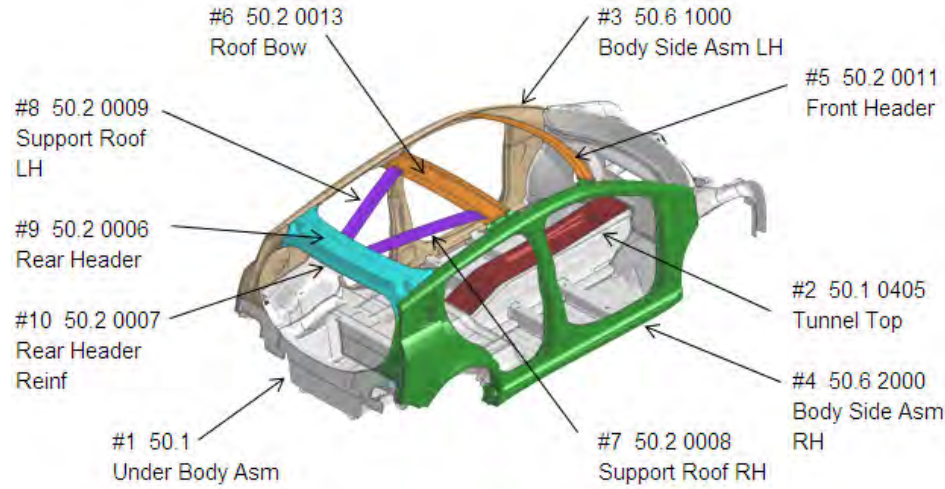
Part to Part		Matl Grade & Thickness (mm)		Weld 2T/3T
#1 50.1 3000	#2 50.1 1000	Mild140/270 0.6	DP300/500 0.5	2T
		DP700/1000 1.4	BH280/400 0.5	
		BH280/400 0.5		
#1 50.1 3000	#2 50.1 1000	DP700/1000 0.8	DP300/500 0.5	Laser
		DP700/1000 1.0	BH280/500 0.5	
#2 50.1 1000	#3 50.1 2000	DP300/500 0.5	BH210/340 0.6	2T
		BH280/400 0.5	BH210/340 0.6	
#2 50.1 1000	#3 50.1 2000	BH280/500 0.5	DP700/100 1.2	Laser
		BH210/340 1.2		
#4/5 50.1 0321/2	#2 50.1 1000	DP500/800 1.6	DP500/800 1.5	Laser
	#3 50.1 2000	DP500/800 1.8	BH280/400 0.5	

Note:
 Laser welding is considered a 2T operation

Figure 20.103: Underbody Assembly (50.1)

Joining Process – Body Structure Asm (Framer #1 – 2)

50.1
Body Structure Asm (Framer #1)



Joining Process

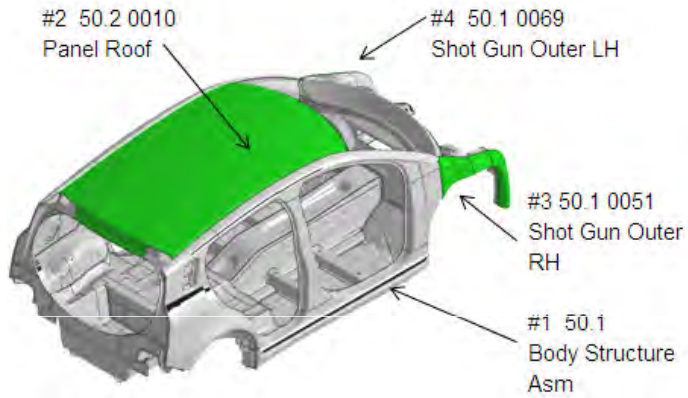
Part to Part		Total Length of Laser Weld
#1 50.1	#2 50.1 0405	4862 mm
#1 50.1	#3 50.6 1000	4615 mm
#1 50.1	#4 50.6 2000	4615 mm
#5 50.2 0011	#3 50.6 1000	53 mm
	#4 50.6 2000	53 mm
#6 50.2 0013	#3 50.6 1000	112 mm
	#4 50.6 2000	112 mm
#7 50.2 0008	#6 50.2 0013	104 mm
	#9 50.2 0007	133 mm
#8 50.2 0009	#6 50.2 0013	104 mm
	#10 50.2 0007	133 mm
#10 50.2 0007	#3 50.6 1000	367 mm
	#4 50.6 2000	367 mm
#9 50.2 0006	#3 50.6 1000	378 mm
	#4 50.6 2000	378 mm
	#10 50.2 0007	2722 mm

Part to Part		Matl Grade & Thickness (mm)		Weld 2T/3T
#1 50.1	#2 50.1 0405	BH210/340 0.6 BH280/400 0.5	DP700/100 0.6	Laser
#1 50.1	#3/4 50.6 1000/2000	BH210/340 0.6	BH210/340 1.0	
		BH210/340 0.7	BH210/340 1.2	
		BH210/340 1.0	DP500/800 0.65	
		BH210/340 1.2	DP500/800 1.5	
		BH280/400 0.5	CP1050/1470 1.5	
		DP700/1000 0.7		
#5 50.2 0011	#3/4 50.6 1000/2000	BH210/340 0.8	BH210/340 1.0	
#6 50.2 0013	#3/4 50.6 1000/2000	BH210/340 0.5	BH210/340 1.0	
#9 50.2 0006	#3/4 50.6 1000/2000	BH210/340 0.7	DP500/800 0.7	
#10 50.2 0007	#3/4 50.6 1000/2000	BH210/340 0.7/2.0	BH210/340 0.6	
	#9 50.2 0006		BH210/340 0.7	
#7/8 50.2 0008/9	#9 50.2 0006	Mild140/270 0.5	BH210/340 0.7	
	#6 50.2 0013		BH210/340 0.5	

er Weld 19102 mm

Note:
Laser welding is considered a 2T operation

Figure 20.104: Body Structure Framer (1) (50.1)



Joining Process

Part to Part		Total Length of Laser Weld	Total Length of Laser Braze
#1 50.1	#2 50.2 0010	2508 mm	3348 mm
	#3 50.1 0051	2740 mm	
	#4 50.1 0069	2740 mm	

Total Length of Laser Weld 7988 mm
 Total Length of Laser Braze 3348 mm
 Total Length of Anti-Flutter Adhesive 6542 mm

Part to Part		Matl Grade & Thickness (mm)		Weld 2T/3T
#2 50.2 0010	#1 50.1	BH210/340 0.5	BH210/340 0.6	Laser Braze & Laser
			DP350/600 1.25	
			BH210/340 0.7/2.0	
#2/3 50.2 0010/51	#1 50.1	HF1050/1500 1.0/1.2/1.5	HF1050/1500 1.2/1.35/1.5	Laser
			DP350/600 1.25	
			DP700/1000 1.6	

Note:
 Laser welding is considered a 2T operation

Figure 20.105: Body Structure Framer (2) (50.1)

20.3 Energy Target Value Calculations

For each subsystem optimization, a nodal time history was extracted from the full LF3G model and then applied to the smaller subsystem model, thus creating the applied loading condition. To track its performance, the total energy absorbed by the subsystem model was then compared to a predetermined target. This section of the report discusses how that target was defined.

When the nodal displacement time history for the LF3G model is applied, it is in essence maintaining the total energy of the system. Referring to Figure 20.106.

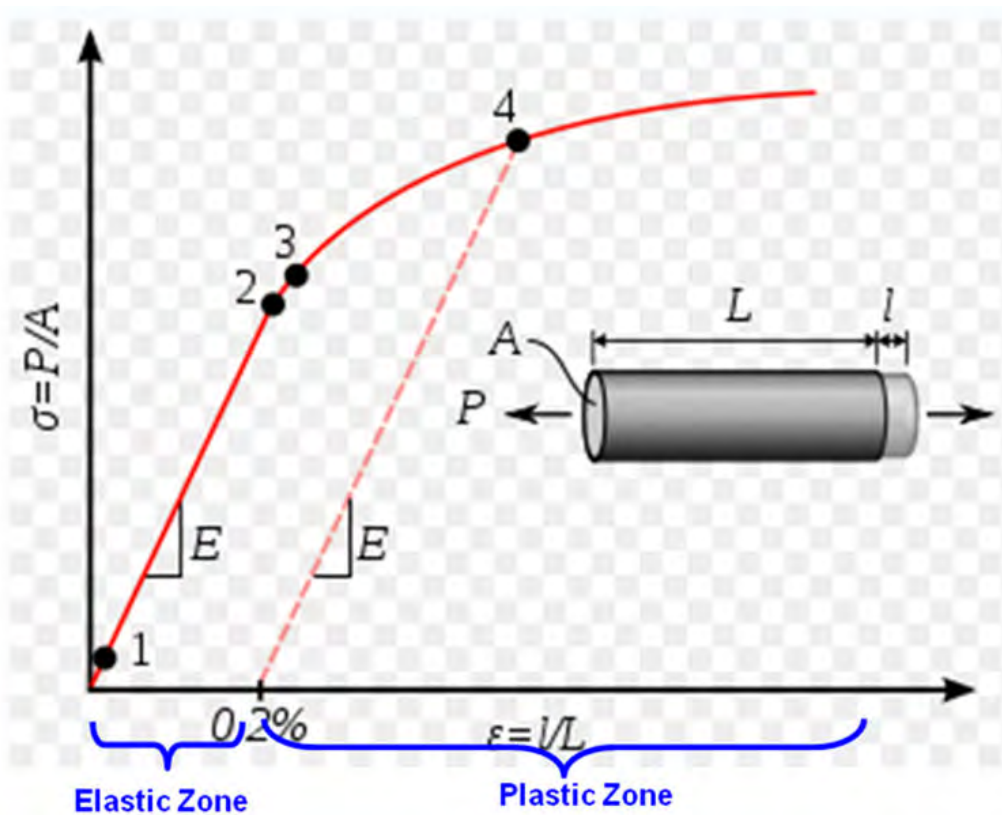


Figure 20.106: Typical Stress vs Strain Curve

Consider the case of the rocker subsystem under Frontal ODB Impact loading. In this case, the rocker experienced limited deformation. See Figure 20.107. The mass of the baseline rocker is 12 kg.

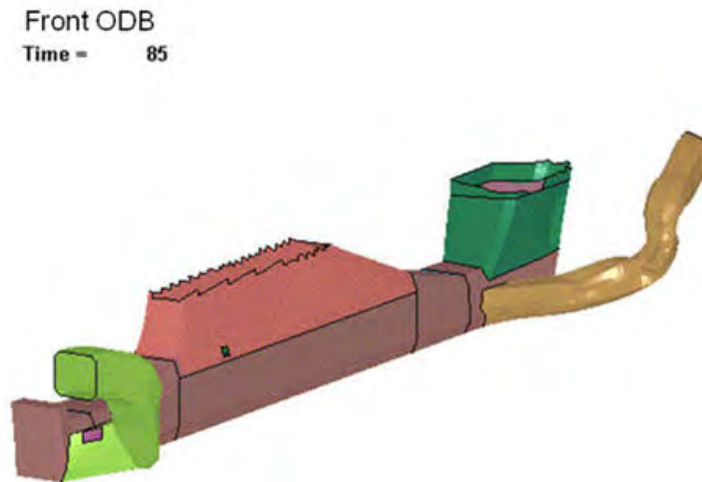


Figure 20.107: *Rocker - Deformed Shape Under Front ODB Loading*

As there is little deformation, the total energy of the rocker is dominated by its kinetic energy contribution. Any internal energy is limited to elastic strain energy, which is very low. See Figure 20.108

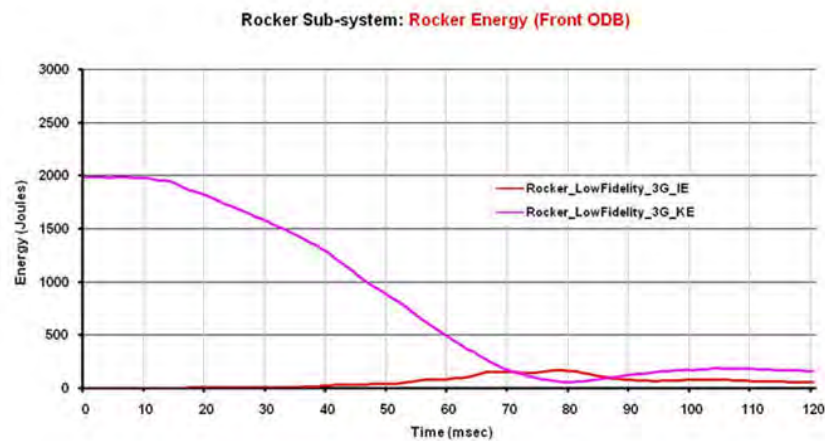


Figure 20.108: *Rocker - Energy Absorbed Under Front ODB Loading*

Once optimized the final design solution will have some level of mass reduction, lets assume for the rocker this was 30%. Thus, the new mass for the example rocker is 8 kg.

8 kg Optimized Rocker moving at 40 MPH -> Rocker Kinetic Energy = 1200 Joules

As the total energy of the system remains constant, any change in kinetic energy must be absorbed by the system as internal energy. In this case, the reduction in kinetic energy has resulted in an increase in the elastic strain energy absorbed by the rocker thus increasing its internal energy. Refer to Figure 20.109 below.

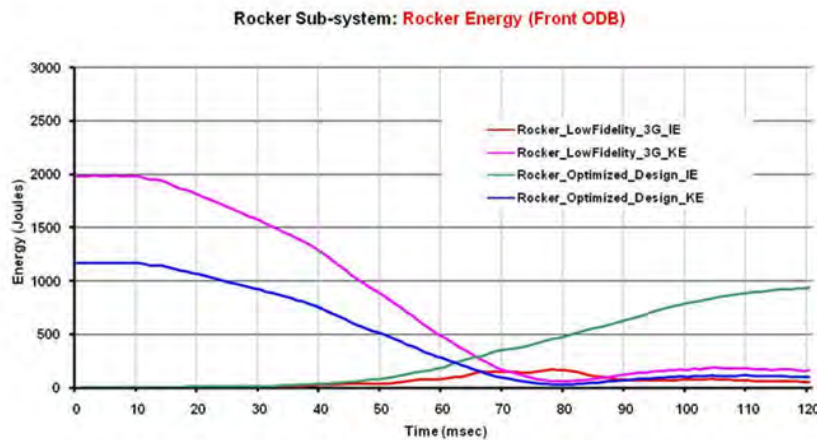


Figure 20.109: Rocker (Baseline vs Optimized) - Energy Absorbed Under Front ODB Loading

Remarks:

- For loadcases that create only limited deformation in a subsystem model, any mass reduction achieved by the optimization will result in an increase in the internal energy absorbed by the component under consideration.
- In such cases, maintaining the energy absorbed in the subsystem model to a target value extracted from the full LF3G system model may over constrain the optimization and thus lead to heavier than necessary design solutions.
- To compensate by the effect of the mass reduction on the internal energy a portion of the kinetic energy was added to the actual internal energy observed in the full LF3G model.
- The internal energy constraints were calculated by adding a portion of the kinetic energy change anticipated by the mass reduction to the actual internal energy absorbed by the LF3G model. For example the internal energy absorbed by the rocker under Front ODB Impact loading was 150 Joules, to this was added an additional 500 Joules to account for the change in kinetic energy created by the potential mass reduction. Thus the constraint energy value would be 650 Joules.
- The energy absorption constraint for this type of loading condition was defined as 650 Joules.

Now consider the rocker subsystem under Pole Impact loading. In this case, the rocker experienced significant deformation. See Figure 20.110. The mass of the baseline rocker is 12 kg.

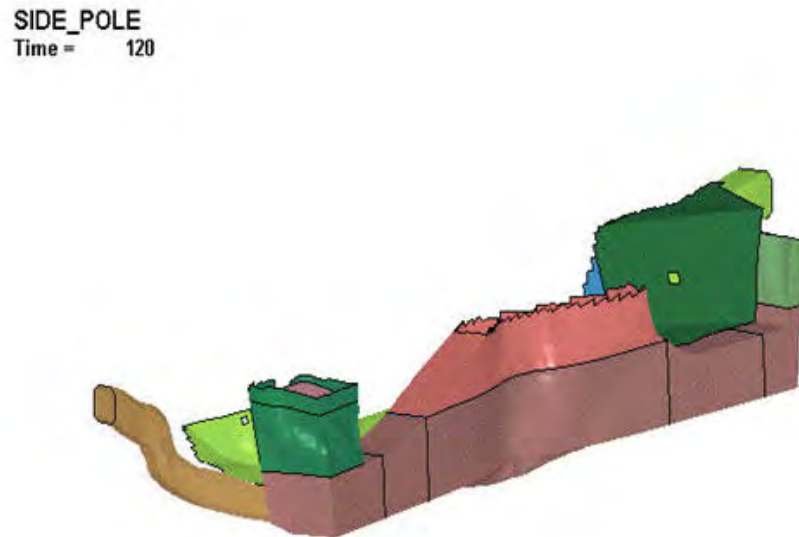


Figure 20.110: *Rocker - Deformed Shape Under Pole Impact Loading*

As there is significant deformation, the total energy of the rocker is dominated by its internal energy contribution, which in this case is plastic strain energy. The kinetic energy is very low. See Figure 20.111.

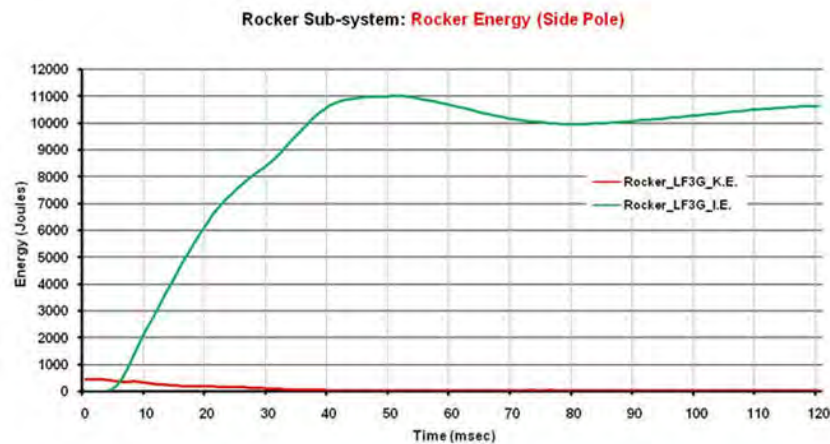


Figure 20.111: *Rocker - Energy Absorbed Under Pole Impact Loading*

As before, the mass of the final design solution has reduced by 30% to 8 kg.

8 kg Optimized Rocker moving at 20 MPH -> Rocker Kinetic Energy = 350 Joules

As the total energy of the system remains constant, any change in kinetic energy must be absorbed by the system as internal energy. In this case, the reduction in kinetic energy has resulted in an increase in the plastic strain energy absorbed by the rocker thus increasing its internal energy. Refer to Figure 20.112 below.

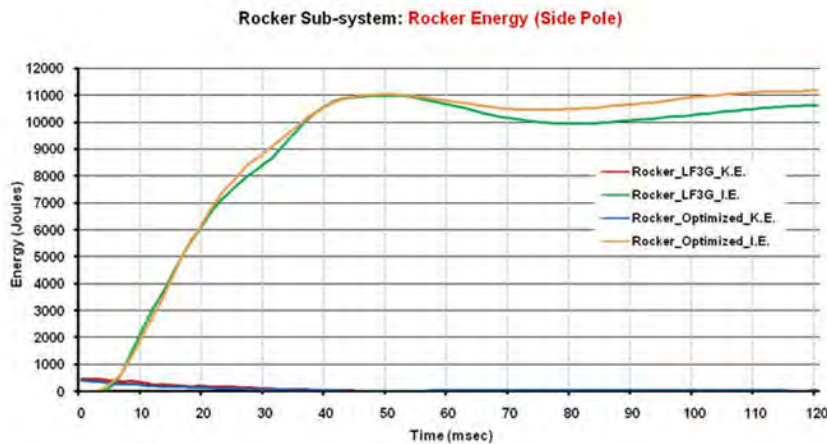


Figure 20.112: *Rocker - Energy Absorbed Under Pole Impact Loading*

Remarks:

- For loadcases that create significant deformation in a subsystem model, any mass reduction achieved by the optimization will have little effect on the internal energy absorbed by the component under consideration.
- In such cases, maintaining the energy absorbed in the subsystem model to a target value extracted from the full LF3G system model will provide a valid constraint.
- The internal energy constraints for such loadcases will be directly taken from the LF3G model.
- The internal energy absorbed by the rocker under Pole Impact loading was 12000 Joules. This was used as the target energy for the optimization with a tolerance of $\pm 15\%$ to allow the optimization to consider as many feasible designs as possible.

20.4 Energy Target Value Calculation for Aluminum Concepts

Why is it necessary to recalculate the energy targets for an aluminium concept?

There are two options to consider in the case of the aluminium subsystem concepts

1. Update the material of the relevant components from steel to aluminium in the LF3G model, rerun the analysis and extract a new set of nodal displacement time histories. Apply these to the aluminium subsystem concept model and use the original target energy absorption criteria.
2. Recalculate the target energy absorption criteria for aluminium and use the original nodal displacement time histories extracted from the LF3G model.

The preferred method was the second method because it did not require rerunning the full model in order to get a new set of nodal times histories for each aluminium subsystem. To show how this was achieved consider the following example. Figure 20.113 shows a steel beam to which an axial load has been applied on the left hand side while the right hand side is fully constrained.

During loading the nodal displacement history is extracted. Figure 20.114 shows the deformed shape of the steel beam. In the second case, the beam's material is changed from steel to aluminum, while maintaining the same mass as the steel beam by increasing the beam's gauge.

The original nodal displacement time histories from the steel beam are then applied to the aluminium beam. Figure 20.115 shows the deformation of the aluminium beam



Figure 20.113: Test Beam



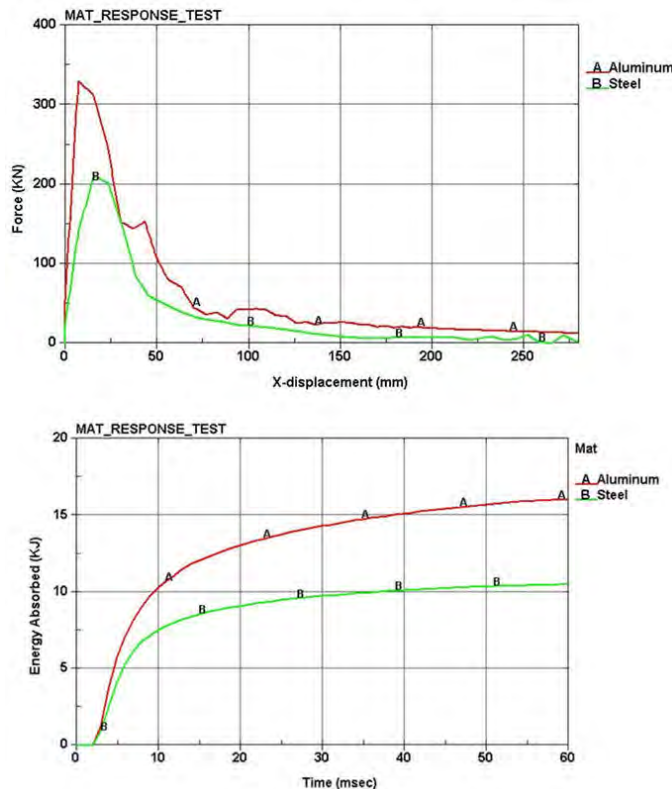
Figure 20.114: Test Beam - Deformed Shape of Steel Version

Aluminium Beam - Deformed Shape

Figure 20.115: Test Beam - Deformed Shape of Aluminium Version

Figure 20.116 below shows the force deformation curves for both the steel and aluminium beams. It clearly shows that when the nodal displacement time histories from the steel beam are applied to the aluminium beam it results in a different force response for the same deformation.

The area under the force displacement curve represents the energy absorbed. Thus demonstrating that for the same nodal displacement history, the energy absorbed by the aluminium is much higher than the same part in steel. Remember that the aluminium grades considered, 6061 & 7075, are high strength aluminium grades and that the gauge of the beam has been increased in order to maintain the beam's mass.


Figure 20.116: Test Longitudinal Rail - Deformation Force & Energy Absorbed

20.4 Energy Target Value Calculation for Aluminum Concepts

Remarks:

- The test case proves that the energy absorbed by a subsystem using aluminum is quite different compared to the energy absorbed by the same subsystem in steel under the same nodal displacement time history. This is because the energy absorbed is a function of the force displacement.
- If same nodal displacement time histories are used, then subsystem needs to be rerun with appropriately revised material properties and the energy absorption targets will need to be recalculated.

20.5 Body Structure - Baseline Design List of Parts (Tables 1 - 3)

The following tables are the Bill of Materials (BOM) for the sheet steel LF3G interpreted design as shown in Figure 20.117.



Figure 20.117: FSV body structure comparison - sheet steel design Vs. LF3G geometry

Part Number	Rev	Part Name	Thick (mm)	Mass (kg)	Material Grade
50.1 0041	F	Apron - LH	0.80	1.89	Mat 600
50.1 0012	H	Apron - RH	0.80	1.89	Mat 600
50.1 0020	F	Back Panel - Lower	0.80	1.93	Mat 340
50.1 0074	A	Battery Close Off Inr LH	0.80	1.56	Mat 340
50.1 0073	A	Battery Close Off Inr RH	0.80	1.56	Mat 340
50.1 0076	A	Battery Close Off Otr LH	0.80	1.14	Mat 340
50.1 0075	A	Battery Close Off Otr RH	0.80	1.14	Mat 340
50.2 0019	C	Body Side Upr LH	0.70	1.29	Mat 1000
50.2 0014	D	Body Side Upr RH	0.70	1.29	Mat 1000
50.2 0017	D	B-Pillar Inner LH	1.00	2.32	Mat 1500
50.2 0009	D	B-Pillar Inner RH	1.00	2.32	Mat 1500
50.2 0003	E	B-Pillar Outer LH	1.00	3.22	Mat 1000
50.2 0008	E	B-Pillar Outer RH	1.00	3.22	Mat 1000
50.2 0028	C	B-Pillar Reinforcement LH	1.00	2.16	Mat 1500
50.2 0026	C	B-Pillar Reinforcement RH	1.00	2.16	Mat 1500
50.1 0059	D	Brace - Cradle to Rad Mtg LH	1.00	0.14	Mat 340
50.1 0038	F	Brace - Cradle to Rad Mtg RH	1.00	0.14	Mat 340
50.1 0060	E	Brace - Tunnel to Rail LH	0.75	0.34	Mat 1500
50.1 0052	G	Brace - Tunnel to Rail RH	0.75	0.34	Mat 1500
50.1 0053	B	Brkt - Btm Rad	0.75	0.42	Mat 340
50.1 0057	B	Brkt - Rad Side LH	0.75	0.33	Mat 340
50.1 0030	B	Brkt - Rad Side RH	0.75	0.33	Mat 340
50.1 0071	A	Coach Joint LH	1.00	0.15	Mat 340
50.1 0072	A	Coach Joint RH	1.00	0.15	Mat 340
50.1 0002	G	Cowl	0.65	2.86	Mat 340
50.1 0070	E	Cowl Top	0.65	2.06	Mat 340
50.2 0004	D	C-Pillar Inner LH	1.00	2.11	Mat 340
50.2 0005	G	C-Pillar Inner RH	1.00	2.11	Mat 340
50.1 0091	A	Cradle Hanger LH	1.00	0.19	Mat 340
50.1 0090	A	Cradle Hanger RH	1.00	0.19	Mat 340
50.1 0032	C	Crossmember - Battery Suspension	1.00	3.77	Mat 600
50.1 0094	A	Crossmember - Front Seat LH Front	1.00	1.41	Mat 600
50.1 0096	A	Crossmember - Front Seat LH Rear	1.00	1.63	Mat 600
50.1 0093	A	Crossmember - Front Seat RH Front	1.00	1.41	Mat 600
50.1 0095	A	Crossmember - Front Seat RH Rear	1.00	1.63	Mat 600

Table 20.1: Table 1 of 3: Baseline Body Structure Design List of Parts

<i>Part Number</i>	<i>Rev</i>	<i>Part Name</i>	<i>Thick (mm)</i>	<i>Mass (kg)</i>	<i>Material Grade</i>
50.1 0001	H	Dash - Toe Pan	0.65	6.50	Mat 340
50.1 0054	E	FBHP - Outer LH	1.00	3.28	Mat 600
50.1 0004	H	FBHP - Outer RH	1.00	3.28	Mat 600
50.1 0064	F	FBHP Inner LH	1.00	2.82	Mat 600
50.1 0046	H	FBHP Inner RH	1.18	2.82	Mat 600
50.1 0025	D	Floor - Front LH	0.70	3.38	Mat 1000
50.1 0011	E	Floor - Front RH	0.70	3.38	Mat 1000
50.1 0010	H	Floor - Rear	0.65	6.06	Mat 270
50.1 0085	B	Frame Brace LH	1.00	0.85	Mat 1000
50.1 0084	C	Frame Brace RH	1.00	0.85	Mat 1000
50.1 0087	B	Frame Extension Upper LH	1.00	1.23	Mat 1500
50.1 0086	B	Frame Extension Upper RH	1.00	1.23	Mat 1500
50.1 0009	K	Frame Rail - Front Inr LH	1.00	1.32	Mat 1500
50.1 0003	N	Frame Rail - Front Inr RH	1.00	1.32	Mat 1500
50.1 0062	G	Frame Rail - Front Otr LH	1.00	1.32	Mat 1500
50.1 0040	P	Frame Rail - Front Otr RH	1.00	1.32	Mat 1500
50.1 0015	E	Frame Rail - Rear LH	1.20	4.67	Mat 1500
50.1 0014	E	Frame Rail - Rear RH	1.20	4.67	Mat 1500
50.2 0011	H	Header - Roof Front	0.75	1.21	Mat 600
50.1 0027	F	Horse Collar	1.00	2.20	Mat 1500
50.1 0050	E	Lamp Can Rear RH	1.00	0.85	Mat 600
50.1 0068	D	Lamp Close Out RH	1.00	0.85	Mat 600
50.1 0083	E	Mid Frame Rail LH	1.00	1.65	Mat 1500
50.1 0082	E	Mid Frame Rail RH	1.00	1.65	Mat 1500
50.2 0002	E	Panel - Qtr Outer LH	0.70	4.24	Mat 270
50.2 0001	H	Panel - Qtr Outer RH	0.70	4.24	Mat 270
50.2 0010	F	Panel - Roof Outer	0.70	13.16	Mat 600
50.1 0013	F	Panel - Rear Liftgate Lower	1.20	3.94	Mat 340
50.1 0098	A	Rail - Battery LH	1.00	1.36	Mat 1500
50.1 0097	A	Rail - Battery RH	1.00	1.36	Mat 1500
50.2 0018	F	Rail - Roof Inner Reinf LH	1.00	1.66	Mat 1500
50.2 0012	G	Rail - Roof Inner Reinf RH	1.00	1.66	Mat 1500
50.1 0078	A	Rear Gusset LH	0.80	0.51	Mat 340
50.1 0077	A	Rear Gusset RH	0.80	0.51	Mat 340
50.2 0006	F	Rear Header Upper Inner	0.80	2.13	Mat 600

Table 20.2: Table 2 of 3: Baseline Body Structure Design List of Parts

Part Number	Rev	Part Name	Thick (mm)	Mass (kg)	Material Grade
50.2 0007	C	Rear Header Upper Outer	0.80	2.23	Mat 600
50.1 0080	A	Rear Suspension Brkt LH	1.00	0.50	Mat 1000
50.1 0079	A	Rear Suspension Brkt RH	1.00	0.50	Mat 1000
50.2 0023	C	Reinf - A Pillar LH	1.00	2.09	Mat 1500
50.2 0022	D	Reinf - A Pillar RH	1.00	2.09	Mat 1500
50.1 0063	F	Reinf - Apron LH	1.00	0.52	Mat 1000
50.1 0044	H	Reinf - Apron RH	1.00	0.52	Mat 1000
50.1 0092	A	Reinf - Battery Tunnel LH	0.72	1.84	Mat 1000
50.1 0024	C	Reinf - Battery Tunnel RH	0.72	1.84	Mat 1000
50.1 0102	A	Reinf - Rad Strap Lower	1.00	0.08	Mat 340
50.1 0066	B	Reinf - Rocker LH	1.50	5.37	Mat 1500
50.1 0048	D	Reinf - Rocker RH	1.50	5.37	Mat 1500
50.2 0024	A	Reinf - Shock Support RH	1.20	1.44	Mat 340
50.2 0025	A	Reinf - Shock Support LH	1.20	1.44	Mat 340
50.1 0008	C	Reinf - Top Rad	0.75	0.42	Mat 340
50.1 0065	C	Rocker - Flr Sd Inn LH	1.20	2.48	Mat 1500
50.1 0047	E	Rocker - Flr Sd Inn RH	1.20	2.48	Mat 1500
50.1 0042	E	Rocker Outer LH	0.80	1.54	Mat 1000
50.1 0019	E	Rocker Outer RH	0.80	1.54	Mat 1000
50.2 0013	F	Roof Bow	0.80	2.02	Mat 600
50.1 0100	A	Seat Closeoff Pnl RR	0.75	1.75	Mat 340
50.1 0016	F	Seat Pan - Rear	0.75	6.88	Mat 340
50.1 0022	D	Shotgun Inner LH	1.20	2.03	Mat 1000
50.1 0021	D	Shotgun Inner RH	1.20	2.03	Mat 1000
50.1 0069	D	Shotgun Outer LH	1.20	2.17	Mat 1000
50.1 0051	E	Shotgun Outer RH	1.20	2.17	Mat 1000
50.1 0101	A	Side Panel-LH	0.75	0.37	Mat 340
50.1 0099	A	Side Panel-RH	0.75	0.37	Mat 340
50.1 0081	A	SIPS Tube	1.00	1.90	Mat 1500
50.1 0023	G	Tunnel - Battery Main	0.72	6.48	Mat 1000
50.1 0018	E	Wheelhouse Inner LH	0.80	3.26	Mat 600
50.1 0017	G	Wheelhouse Inner RH	0.80	3.26	Mat 600
50.1 0067	C	Wheelhouse Outer LH	0.80	2.30	Mat 600
50.1 0049	D	Wheelhouse Outer RH	0.80	2.30	Mat 600
All Parts	J	Body Structure		217.83	

Table 20.3: Table 3 of 3: Baseline Body Structure Design List of Parts

List of Figures

2.1	FSV-1 BEV body structure	7
2.2	FSV-1 BEV body structure underside	7
2.3	BEV exploded view	8
2.4	FSV-1 PHEV ₂₀ body structure	11
2.5	FSV-2 (FCEV and PHEV ₄₀) body structure	11
2.6	FSV-1 BEV body structure steel grade distribution	14
2.7	PHEV ₂₀ bodystructure material mix	15
2.8	FSV-2 (FCEV and PHEV ₄₀) body structure material mix	15
2.9	Material production Green House Gas (GHG) emissions	16
2.10	FSV BEV Life Cycle Emissions (U.S. Grid)	17
2.11	FSV materials tensile strengths compared to ULSAB and ULSAB-AVC	18
2.12	FSV material mix compared to ULSAB and ULSAB-AVC	22
2.13	FSV manufacturing processes breakdown	24
2.14	BEV front end rails, curved shotguns and motor cradle	25
2.15	BEV front end optimized rails	26
2.16	US NCAP 35 mph front rigid barrier pulse at B-Pillar	27
2.17	FSV side impact structural load paths	28
2.18	FSV rear impact structural load paths	29
2.19	FSV rear rail - optimized sections	29
2.20	FSV Topology and LF3G optimization	30
2.21	LF3G optimization process overview	31
2.22	FSV Sub-Systems	32
2.23	Phase 2 design process	34
2.24	FSV-1 baseline CFD Model	35
2.25	Latest FSV-1 BEV styling	36
2.26	Topology Optimization Overview	37
2.27	Topology Optimization Result - Interpreted CAD Model	37
2.28	LF3G final result	38
2.29	FSV body structure comparison - Sheet Steel Design Vs. LF3G Geometry	39
2.30	Sub-System Optimization Overview	41
2.31	Rocker solution from 3G optimization runs	42
2.32	Rocker Solutions using AHSS	43
2.33	T4 comparison FSV subsystems: Rocker	46
2.34	Tunnel sub-system initial design	48
2.35	Tunnel sub-system current design	48
2.36	Tunnel sub-system shown with the tunnel bulkhead	48

2.37	FSV assembly joining process portfolio	49
2.38	FSV body structure assembly flowchart	50
2.39	FSV body structure costs sensitivity analysis results	57
2.40	Trends in Global Fuel Economy/Vehicle Emissions Regulations	58
2.41	Material production GHG emissions	59
2.42	BEV body sub-structures	60
2.43	FSV BEV Life Cycle Emissions (U.S. Grid)	61
2.44	FSV BEV Use Phase Emissions - Various Electric Grids	61
2.45	FSV design and engineering process steps	63
2.46	FSV design and engineering process steps (contd.)	64
2.47	FSV body structure mass evolution	65
3.1	Schematic of AHSS steels (shown in colour) compared to low strength steels (dark grey) and traditional HSS (light grey)	69
3.2	Schematic of newer higher strength steels utilizing unique chemistries, processing, and microstructure to gain specific properties and forming characteristics	70
3.3	Example of a laser weld blank used for a body side panel (FSV body side outer shown)	74
3.4	Laser welded coils production process	74
3.5	The principle of producing a Tailor Rolled Coil	75
3.6	Typical roll form layout for making ERW tubes	76
3.7	Multiple walled tube showing varying wall thickness	76
3.8	Schematic of a typical transfer press layout	78
3.9	Tensile strength and microstructure changes during hot stamping	79
3.10	Typical direct hot stamping line	79
3.11	In-direct hot stamping process	80
3.12	Typical in-direct hot stamping line	81
3.13	Typical roll forming line	81
3.14	Typical roll forming operation showing a step-by-step	82
3.15	Plant layout for tube hydroforming	83
3.16	Schematic showing tube hydroforming die (Courtesy Schuler (Metal Forming Handbook 1998))	83
3.17	Schematic showing hole punching and notching in a hydroforming die (Courtesy Schuler (Metal Forming Handbook 1998))	84
3.18	Typical example of a hydroforming press (Courtesy: Schuler)	84
3.19	Forming process to produce tubular component using a mandrel and lateral dies	85
3.20	Method to produce a finalized tube	85
4.1	Battery pack under-floor	89
4.2	Battery pack in tunnel and under rear floor	89
4.3	Sub-pack with individual prismatic cells	90
4.4	FSV-1 "I-shape" battery pack	91
4.5	FSV-1 'I-shape' battery in vehicle tunnel	91
4.6	FSV-1 front wheel drive motor and inverter	92
4.7	FSV-1 front and rear suspension and wheel clearance envelopes	93

B

4.8	FSV-1 occupant positioning	94
4.9	FSV-1 bumper heights, front and rear overhangs	94
4.10	FSV-1 - ground clearance and ramp angles	95
4.11	FSV-1 A-Pillar obscuration angle and vehicle width	95
4.12	FSV-1 luggage volume with seat unfolded	96
4.13	FSV-1 luggage volume with seat folded	96
4.14	FSV-1 exterior styling theme	97
4.15	FSV-1 vehicle sketch	97
5.1	USNCAP - frontal impact	100
5.2	EURO NCAP - 64 $\frac{\text{km}}{\text{h}}$ 40% offset frontal impact	101
5.3	VW SLC Euro NCAP peak deceleration pulse	102
5.4	IIHS - intrusion guidelines	102
5.5	IIHS Side 50 $\frac{\text{km}}{\text{h}}$ 90° deformable barrier	103
5.6	IIHS side impact target intrusion requirements	104
5.7	US SINCAP 61 $\frac{\text{km}}{\text{h}}$ 27° crabbed impact	105
5.8	FMVSS 301 80 $\frac{\text{km}}{\text{h}}$ 70% offset deformable barrier	106
5.9	ECE R32 - 55 $\frac{\text{km}}{\text{h}}$ 0° deformable barrier	107
5.10	FMVSS 214P 32 $\frac{\text{km}}{\text{h}}$ 75° pole impact	108
5.11	EURO NCAP - 29 $\frac{\text{km}}{\text{h}}$ 0° pole impact	109
5.12	Roof crush	110
5.13	RCAR low speed impact - 10 $\frac{\text{km}}{\text{h}}$ 0° rigid barrier	111
5.14	Torsion & bending frequency modes	112
5.15	FSV mass target setting approach - FSV Phase 1	114
5.16	FSV-1 body-structure mass target - Updates to ULSAB-AVC benchmark	115
5.17	2010 VW Polo	118
5.18	Body structure lightweight index calculation	119
5.19	Body structure lightweight index comparison	120
6.1	FSV-1 baseline CFD model	122
6.2	2010 Toyota Prius	124
6.3	2009 Mercedes E-class	124
6.4	FSV-1 baseline vehicle skin with rear spoiler, wheel skirts and smooth Floor	125
6.5	FSV-1 pressure differences with and without rear spoiler	126
6.6	Original FSV model - new spoiler and air-dam	127
6.7	Original FSV model - new spoiler and air-dam models	128
6.8	Velocity vector with new spoiler and air-dam	128
6.9	Original FSV model - new spoiler and air-dam	129
6.10	FSV model - new spoiler and air-dam	130
6.11	FSV model - new spoiler and air-dam - airflow velocity contour plots	131
6.12	Recommended changes	132
6.13	Occupant package	132
6.14	FSV model - rounded front and smooth side exterior surfaces	133
6.15	Velocity vector plots for both designs	133
6.16	Pressure contour plots for both designs	134

6.17	Full vehicle CFD model with representative underfloor	135
6.18	Full vehicle CFD model under floor air-flow comparison	136
6.19	Full vehicle CFD model rear surface pressure comparison	137
6.20	Full vehicle CFD air velocity comparison	137
6.21	Air ducts, tire, spoiler and underbody cover	138
6.22	Modified original FSV model - with add-on parts	139
6.23	Modified original FSV design with recommended design changes	141
6.24	Pressure plots - with and without spoiler side wings	141
6.25	FSV-1 BEV - latest styling theme	143
6.26	FSV-1 BEV - latest vehicle package	143
6.27	FSV-1 BEV - latest CFD model with key aerodynamic features	144
6.28	Latest FSV styling model pressure contour	144
6.29	Pressure plots - with and without spoiler side wings	145
6.30	Latest FSV styling and CFD models	146
6.31	Latest FSV-1 BEV styling images - showing utilities access hatch and charging .	147
7.1	Vehicle “skeletal” structure	149
7.2	FSV-1 design space - initial vehicle structure	150
7.3	Overview of topology optimization	151
7.4	FSV-1 battery design space within the vehicle	152
7.5	FSV-1 finite element model used for topology optimization	152
7.6	FSV-1 mass assumptions	153
7.7	FSV-1 IIHS front 40% ODB	154
7.8	FSV-1 NCAP front impact	155
7.9	FSV-1 IIHS side impact	155
7.10	FSV-1 FMVSS 214 pole impact	156
7.11	FSV-1 FMVSS 301 rear 70% ODB	156
7.12	FSV-1 FMVSS 216 roof crush	157
7.13	FSV-1 bending static stiffness	158
7.14	FSV-1 Torsional static stiffness	158
7.15	FSV-1 battery floor - analysis process & optimization result	161
7.16	FSV-1 battery bulkhead - analysis process & optimization Result	162
7.17	FSV-1 Updated full vehicle design space with revised battery from Phase 1 . . .	163
7.18	FSV-1 30% mass fraction - battery floor, bulkhead & seat cross-member	164
7.19	FSV-1 20% mass fraction - battery floor, bulkhead & seat cross-member	165
7.20	FSV-1 10% mass fraction - battery floor, bulkhead & seat cross-member	166
7.21	FSV-1 30% mass fraction - front isometric view	167
7.22	FSV-1 30% mass fraction - rear isometric view	167
7.23	FSV-1 30% mass fraction - bottom view	168
7.24	FSV-1 30% mass fraction - front end	168
7.25	FSV-1 30% mass fraction - floor pan and tunnel	169
7.26	FSV-1 30% mass fraction - roof panel	169
7.27	FSV-1 20% mass fraction - front isometric view	170
7.28	FSV-1 20% mass fraction - rear isometric view	170
7.29	FSV-1 20% mass fraction - bottom view	171

D

7.30	FSV-1 20% mass fraction - front end	171
7.31	FSV-1 20% mass fraction - floor pan and tunnel	172
7.32	FSV-1 20% mass fraction - roof panel	172
7.33	FSV-1 10% mass fraction - front isometric view	173
7.34	FSV-1 10% mass fraction - rear isometric view	173
7.35	FSV-1 10% mass fraction - bottom view	174
7.36	FSV-1 10% mass fraction - front end	174
7.37	FSV-1 10% mass fraction - floor pan and tunnel	175
7.38	FSV-1 10% mass fraction - roof panel	175
7.39	Interpreted CAD model developed from topology optimization results	176
8.1	LF3G optimization process overview	179
8.2	Parameterized model	179
8.3	B-Pillar parameterization	180
8.4	Front bumper beam position parameterization	180
8.5	Front bumper beam section parameterization	181
8.6	Radiator support to shock tower position parameterization	181
8.7	Radiator support to shock tower section parameterization	182
8.8	Shotgun parameterization	182
8.9	Instrument panel beam parameterization	183
8.10	Front longitudinal rail above tunnel parameterization	183
8.11	Front longitudinal cross bar parameterization	184
8.12	Roof rail parameterization	184
8.13	Roof bow parameterization	185
8.14	Roof bow parameterization	186
8.15	Rear cargo area cross bow parameterization	187
8.16	Front seat crossmember parameterization	187
8.17	Rocker parameterization	188
8.18	C-Pillar parameterization	188
8.19	Rear longitudinal rail parameterization	189
8.20	Additional C-Pillar reinforcement	190
8.21	Added bulkheads	190
8.22	Components with gauge and grade variation in optimization	192
8.23	Components without zones of independent gauge and grade variation	192
8.24	Material selection for optimization	193
8.25	Material selection for optimization	194
8.26	Mass of 110 optimization cases	196
8.27	Feasible designs found by optimization	196
8.28	NCAP deformed shape : design 60	197
8.29	NCAP pulse : design 60	197
8.30	IIHS 40% ODB deformed shape : design 60	198
8.31	IIHS 40% ODB intrusion performance	198
8.32	Rear offset deformable barrier deformed shape : design 60	199
8.33	Rear offset deformable barrier acceleration pulse	199
8.34	IIHS side impact deformed shape : design 60	200

8.35	Roof crush deformed shape : design 60	201
8.36	Roof crush force-deformation curve : design 60	201
8.37	Torsional stiffness: design 60	202
8.38	Battery shapes considered	203
8.39	Battery shape evaluation load cases	204
8.40	T-shaped battery optimization result	205
8.41	I-shaped battery optimization result	206
8.42	T-shape versus I-shape rear impact deformation shape : side view	207
8.43	T-shape versus I-shape rear impact deformation shape : bottom view	207
8.44	T versus I shaped battery optimization results table	207
8.45	T-shape versus I-shape optimization result comparison	208
8.46	LF3G - final gauge selections	209
8.47	LF3G - final gauge selections (continued)	209
8.48	LF3G - final gauge selections	210
8.49	LF3G - final gauge selections (continued)	210
8.50	LF3G - final gauge selections (continued)	211
8.51	LF3G - final shape selection(iso view)	211
8.52	LF3G - final shape selection(side view)	212
8.53	LF3G - final shape selection(top view)	212
8.54	LF3G - final shape selection(bottom view)	212
8.55	B-Pillar final shape (red) overlapped with baseline (blue)-(side view)	213
8.56	Front end final shape (red) overlapped with baseline (blue)-(top view)	214
8.57	Radiator support final shape (red) overlapped with baseline (blue)-(top view)	215
8.58	Front rail final shape (red) overlapped with baseline (blue)-(top view)	216
8.59	Shotgun final shape (red) overlapped with baseline (blue)-(top view)	216
8.60	Lower IP final shape (red) overlapped with baseline (blue)-(top view)	217
8.61	Tunnel top member final shape (red) overlapped with baseline (blue)-(top view)	218
8.62	Torque box member final shape (red) overlapped with baseline (blue)-(top view)	219
8.63	Roof rail member final shape (red) overlapped with baseline (blue)-(side view)	220
8.64	Roof bow final shape (red) overlapped with baseline (blue)-(top view)	220
8.65	Seat crossmember final shape (red) overlapped with baseline (blue)-(top view)	221
8.66	Rocker final shape (red) overlapped with baseline (blue)-(top view)	222
8.67	Joint rear upper final shape (red) overlapped with baseline (blue)-(top view)	222
8.68	Radiator support final shape (red) overlapped with baseline (blue)-(top view)	223
8.69	Underbody crossmembers final shape (red) overlapped with baseline (blue)-(top view)	224
9.1	FSV BEV - optimized LF3G geometry	226
9.2	FSV body structure comparison - sheet steel design Vs. LF3G geometry	227
9.3	FSV body sub-structure - rocker for LF3G FEA	228
9.4	FSV body sub-structure - B Pillar for LF3G FEA	229
9.5	FSV body sub-structure - roof side rail for LF3G FEA	230
9.6	FSV body sub-structure - rear rail for LF3G FEA	231
9.7	FSV body sub-structure - front rail for LF3G FEA	232
9.8	FSV body sub-structure - front upper rail for LF3G FEA	233

F

9.9	FSV body sub-structure - tunnel rails for LF3G FEA	234
10.1	Detailed FSV sub-system optimization process	237
10.2	LF3G loadpath mapping results	238
10.3	Rocker sub-system from LF3G	239
10.4	Rocker sub-system with highlighted boundaries for time history	240
10.5	Sub-System performance validation	241
10.6	Stamped rocker concept - zones of grade and gauge variation	241
10.7	Stamped rocker concept cross-sectional parameterization	242
10.8	Stamped rocker design solution deformation comparison to baseline	244
10.9	Stamped rocker design solution deformation comparison to baseline	245
10.10	Stamped rocker design solution - energy absorption comparison to baseline	246
10.11	Stamped rocker design solution - energy absorption comparison to baseline (contd.)	247
10.12	Stamped rocker design solution - energy absorption comparison to baseline	248
10.13	Stamped rocker design solution final grade and gauge selections	249
10.14	Hydroformed rocker concept - zones of grade and gauge variation	250
10.15	Hydroformed rocker concept - cross-sectional parameterization	251
10.16	Hydroformed rocker design solution deformation comparison to baseline	252
10.17	Hydroformed rocker design solution - deformation comparison to baseline	253
10.18	Hydroformed rocker design solution - energy absorption comparison to baseline	254
10.19	Hydroformed rocker design solution - energy absorption comparison to baseline	255
10.20	Hydroformed rocker design solution - energy absorption comparison to baseline (contd.)	256
10.21	Hydroformed rocker design solution - final grade and gauge selections	256
10.22	: Roll formed rocker concept - zones of grade and gauge variation	257
10.23	Roll formed rocker concept - cross-sectional parameterization	258
10.24	Roll formed rocker design solution - deformation comparison to baseline	259
10.25	Roll formed rocker design solution - deformation comparison to baseline	260
10.26	Roll formed rocker design solution - energy absorption comparison to baseline	261
10.27	Roll formed rocker design solution - energy absorption comparison to baseline	262
10.28	Roll formed rocker design solution - energy absorption comparison to baseline (contd.)	263
10.29	Roll formed rocker design solution - final grade and gauge selections	264
10.30	Extruded aluminum rocker concept - design space	265
10.31	Extruded aluminum rocker concept - cross-sectional parameterization	266
10.32	Extruded aluminum rocker design solution - deformation comparison to baseline	267
10.33	Extruded aluminum rocker design solution - deformation comparison to baseline	268
10.34	Extruded Aluminum Roll Rocker Design Solution - Energy Absorption Comparison to Baseline	269
10.35	Extruded Aluminum Roll Rocker Design Solution - Energy Absorption Comparison to Baseline	270
10.36	Extruded Aluminum Roll Rocker Design Solution - Energy Absorption Comparison to Baseline	271
10.37	Extruded rocker design solution - final grade and gauge selections	271

10.38	B-Pillar sub-system from LF3G	272
10.39	B-Pillar Sub-system with highlighted boundaries for time history	273
10.40	Stamped B-Pillar concept - zones of grade and gauge variation	274
10.41	Stamped B-Pillar concept - cross-sectional parameterization	275
10.42	Stamped B-Pillar design solution - deformation comparison to baseline	276
10.43	Stamped B-Pillar design solution - energy absorption comparison to baseline	277
10.44	Stamped B-Pillar with reinforcement - final grade and gauge selections	278
10.45	Stamped B-Pillar without reinforcement - final grade and gauge selections	278
10.46	Hydroformed B-Pillar concept - zones of grade and gauge variation	279
10.47	Hydroformed B-Pillar concept - cross-sectional parameterization	280
10.48	Hydroformed-1 B-Pillar design solution deformation comparison to baseline	281
10.49	Hydroformed-1 B-Pillar design solution - energy absorption comparison to baseline	282
10.50	Hydroformed-1 B-Pillar final grade and gauge selections	283
10.51	Stamped aluminum B-Pillar concept design space	284
10.52	Stamped aluminum B-Pillar concept cross-sectional parameterization	285
10.53	Stamped aluminum B-Pillar design solution deformation comparison to baseline	286
10.54	Stamped aluminum B-Pillar design solution - energy absorption comparison to baseline	287
10.55	Stamped aluminum B-Pillar final grade and gauge selections	288
10.56	Side roof rail sub-system from LF3G	289
10.57	Roof rail sub-system with highlighted boundaries for time history	290
10.58	Stamped side roof rail concept - zones of grade & gauge variation	291
10.59	Stamped side roof rail concept - cross-sectional parameterization	292
10.60	Stamped side roof rail design solution - deformation comparison to baseline	293
10.61	Stamped side roof rail design solution - deformation comparison to baseline	294
10.62	Stamped side roof rail design solution - energy absorption comparison to baseline	295
10.63	Stamped side roof rail design solution - energy absorption comparison to baseline	296
10.64	Stamped side roof rail - final grade & gauge selections	297
10.65	Hydroformed side roof rail concept - zones of grade & gauge variation	298
10.66	Side roof rail concept - cross-sectional parameterization	299
10.67	Side roof rail concept - cross-sectional parameterization	300
10.68	Side roof rail concept - cross-sectional parameterization	301
10.69	Hydroformed side roof rail - final grade & gauge selections	302
10.70	Aluminum side roof rail concept - zones of grade & gauge variation	303
10.71	Extruded aluminum side roof rail concept - cross-sectional parameterization	304
10.72	Extruded aluminum side roof rail design solution - energy absorption comparison to baseline	305
10.73	Extruded aluminum side roof rail design solution - energy absorption comparison to baseline	306
10.74	Extruded aluminum side roof rail - final grade & gauge selections	307
10.75	Rear Rail sub-system from LF3G	308
10.76	Rear Rail sub-system with highlighted boundaries for time history	308
10.77	Stamped rear rail concept - zones of grade & gauge variation	309

10.78	Stamped rear rail concept - cross-sectional parameterization	310
10.79	Stamped rear rail design solution - deformation comparison to baseline	311
10.80	Stamped rear rail design solution - energy absorption comparison to baseline	312
10.81	Stamped rear rail - final grade & gauge selections	313
10.82	Hydroformed rear rail concept - zones of grade & gauge variation	314
10.83	Hydroformed rear rail concept - cross-sectional parameterization	315
10.84	Hydroformed rear rail design solution - deformation comparison to baseline	316
10.85	Hydroformed rear rail design Solution - energy absorption comparison to baseline	317
10.86	Hydroformed rear rail - final grade & gauge selections	318
10.87	Stamped aluminum rear rail concept - zones of grade & gauge variation	318
10.88	Stamped aluminum rear rail concept - cross-sectional parameterization	319
10.89	Stamped aluminum rear rail design solution - deformation comparison to baseline	320
10.90	Stamped aluminum rear rail design solution - energy absorption comparison to baseline	321
10.91	Stamped aluminum rear rail design solution - energy absorption comparison to baseline	322
10.92	Stamped aluminum rear rail design solution - energy absorption comparison to baseline	323
10.93	Tunnel rails sub-system from LF3G	324
10.94	Stamped tunnel rail concept - zones of grade & gauge variation	325
10.95	Stamped tunnel tail concept - cross-sectional parameterization	326
10.96	Stamped tunnel rail design solution - deformation comparison to baseline	327
10.97	Stamped tunnel rail design solution - energy absorption comparison to baseline	328
10.98	Stamped tunnel tail design solution - energy absorption comparison to baseline	329
10.99	Stamped tunnel rails - final grade & gauge selections	330
10.100	Open roll formed tunnel rails - zones of grade & gauge variation	331
10.101	Open roll formed tunnel rail concept - cross-sectional parameterization	332
10.102	Open roll formed tunnel rail design solution - deformation comparison to baseline	333
10.103	Open roll formed tunnel rail design solution - energy absorption comparison to baseline	334
10.104	Open roll formed tunnel rail design solution - energy absorption comparison to baseline	335
10.105	Open roll formed tunnel rails - final grade & gauge selections	336
10.106	Aluminum tunnel rail concept - zones of grade & gauge variation	337
10.107	Extruded aluminum tunnel rail design solution - energy absorption comparison to baseline	339
10.108	Extruded aluminum tunnel rails - final grade & gauge selections	340
10.109	Shotgun sub-system from LF3G	341
10.110	Shotgun sub-system with highlighted boundaries for time history	342
10.111	Stamped shotgun concept - zones of grade & gauge variation	343
10.112	Stamped shotgun concept - cross-sectional parameterization	344
10.113	Shotgun design solution - deformation comparison to baseline	345
10.114	Stamped shotgun design solution - energy absorption comparison to baseline	346
10.115	Stamped shotgun - final grade & gauge selections	347

10.116	Aluminum shotgun concept - cross-sectional parameterization	348
10.117	Aluminum shotgun design solution - deformation comparison to baseline	349
10.118	Aluminum shotgun design solution - energy absorption comparison to baseline	350
10.119	Aluminum shotgun - final grade & gauge selections	351
10.120	Front Rail sub-system from LF3G	352
10.121	Front rail sub-system with highlighted boundaries for time history	352
10.122	Three piece stamped front rail concept - zones of grade & gauge variation	353
10.123	Two piece stamped front rail concept - zones of grade & gauge variation	353
10.124	Three piece stamped front rail concept - cross-sectional parameterization	354
10.125	Two piece stamped front rail concept - cross-sectional parameterization	355
10.126	Two piece stamped front rail design solution - deformation comparison to baseline	356
10.127	Two piece stamped front rail design solution - energy absorption comparison to baseline	356
10.128	Two piece stamped front rail - final grade & gauge selections	357
10.129	Three piece stamped front rail - final grade & gauge selections	357
10.130	Hydroformed front rail concept 1 - zones of grade & gauge variation	358
10.131	Hydroformed front rail concept 2 - zones of grade & gauge variation	359
10.132	Hydroformed front rail concept 1 - cross-sectional parameterization	360
10.133	Hydroformed front rail concept 2 - cross-sectional parameterization	361
10.134	Hydroformed front rail concept 1D design solution - deformation comparison to baseline	361
10.135	Hydroformed front rail concept 1D design solution - energy absorption compar- ison to baseline	362
10.136	Hydroformed front rail concept 1D - final grade & gauge selections	362
10.137	Aluminum front rail concept - zones of grade & gauge variation	363
10.138	Stamped aluminum front rail concept - cross-sectional parameterization	364
10.139	Hydroformed front rail concept 1D design solution - deformation comparison to baseline	365
10.140	Stamped aluminum front rail concept design solution - energy absorption com- parison to baseline	366
10.141	Stamped aluminum front rail concept - final grade & gauge selections	366
10.142	Front end optimization - components considered	367
10.143	Front end optimization - shock tower final grade & gauge selections	367
10.144	Front end optimization - upper engine compartment diagonals grade & gauge selections	368
10.145	Front NCAP & front ODB impact barrier positions	369
10.146	Typical loadpaths used in a conventional vehicle	370
10.147	Front NCAP at 40 msec - acceleration pulse & energy	371
10.148	Typical front NCAP performance for a conventionally powered front wheel drive vehicle of similar size to the FSV	372
10.149	Front NCAP at 40 msec - total & internal energy Breakdowns For Major Com- ponents	373
10.150	Front NCAP at 40 msec - internal energy breakdowns for all other components	374
11.1	Rocker solution from 3G optimization runs	376

J

11.2	Manufacturing interpretation of the rocker solution (stamped LWB)	377
11.3	Rocker stamped single thickness solution	378
11.4	Rocker - stamped tailor rolled blank (TRB) Solution	378
11.5	Rocker solution manufacturing interpretation internal energy comparison side .	379
11.6	Rocker solution manufacturing interpretation internal energy comparison - IIHS side impact	380
11.7	Rocker solution manufacturing interpretation internal energy comparison - IIHS ODB	380
11.8	Rocker hot stamped single thickness solution	381
11.9	Rocker - hot Stamped TRB solution	382
11.10	Rocker - hot stamped LWB solution	382
11.11	Rocker - roll formed solution	383
11.12	Rocker - roll formed TRB solution	384
11.13	Rocker - roll formed laser welded coil (LWC) solution	384
11.14	Rocker - hydroformed solution	385
11.15	Rocker - hydroformed LWT solution	385
11.16	Rocker - hydroformed tailor rolled tube (TRT) Solution	386
11.17	Rocker - extruded aluminum solution	386
11.18	B-pillar 3G optimized solution	387
11.19	B-pillar - stamped solution (single gauge)	387
11.20	B-pillar - stamped TRB Solution	388
11.21	B-pillar - stamped LWB Solution	388
11.22	B-pillar - hot stamped solution (single gauge)	389
11.23	B-pillar - hot stamped TRB solution	389
11.24	B-pillar - hot stamped LWB solution	390
11.25	B-pillar - stamped aluminum solution	390
11.26	B-pillar - closed roll formed solution with stamped B-pillar Outer (not shown) . . .	391
11.27	B-pillar - hydroformed LWT solution with stamped B-pillar outer (not shown) . . .	391
11.28	Rear rail 3G optimized solution (for stamping)	392
11.29	Rear rail optimized solution (for hydroforming)	392
11.30	Rear rail - stamped solution (single gauge)	393
11.31	Rear rail - stamped TRB solution	394
11.32	Rear rail - stamped LWB solution	394
11.33	Rear rail - hot stamped solution (single gauge)	394
11.34	Rear rail hot Stamped TRB solution	395
11.35	Rear rail hot stamped LWB solution	395
11.36	Rear rail - hydroformed Solution (conventional tube)	395
11.37	Rear rail hydroformed LWT solution	396
11.38	Rear rail hydroformed TRT solution	396
11.39	Rear rail - stamped aluminum solution	396
11.40	Roof rail 3G optimized solution (for stamping)	397
11.41	Roof rail 3G optimized solution (for hydroforming)	397
11.42	Roof rail - stamped solution (single gauge)	398
11.43	Roof rail - stamped TRB solution	398

11.44	Roof rail - stamped LWB solution	398
11.45	Roof rail - hot stamped solution (single gauge)	399
11.46	Roof rail - hot stamped TRB solution	399
11.47	Roof rail - hot stamped LWB solution	399
11.48	Roof rail - hydroformed solutions	400
11.49	Roof rail - stamped aluminum solution	400
11.50	Shotgun - 3G optimized solution	401
11.51	Shotgun - stamped solution (single gauge)	401
11.52	Shotgun - stamped TRB solution	402
11.53	Shotgun - stamped LWB solution	402
11.54	Shotgun - hot stamped solution (single gauge)	403
11.55	Shotgun - hot stamped TRB solution	403
11.56	Shotgun - hot stamped LWB solution	403
11.57	Shotgun - stamped aluminum solution	404
11.58	Tunnel - 3G optimized solution (for stamping)	405
11.59	Tunnel - 3G optimized solution (for roll forming)	405
11.60	Tunnel - stamped solution (single gauge)	406
11.61	Tunnel - stamped TRB solution	406
11.62	Tunnel - stamped LWB solution	407
11.63	Tunnel - hot stamped solution (single gauge)	407
11.64	Tunnel - hot stamped TRB solution	408
11.65	Tunnel - hot stamped LWB solution	408
11.66	Tunnel - roll formed solution	409
11.67	Tunnel - stamped aluminum solution	409
11.68	Front rail 3G optimized solution	410
11.69	Front rail - stamped LWB solution	411
11.70	Front rail concept-2 3G optimized solution	412
11.71	Front Rail - concept-2 stamped LWB solution	413
11.72	Front rail - 3G optimized aluminum solution	414
11.73	Front rail - stamped aluminum solution	414
11.74	Front rail 3G hydroformed optimized solution	415
11.75	Front rail - hydroformed solution	415
12.1	FSV rocker inner concept design and blank size	424
12.2	FSV B-pillar concept part nesting	424
12.3	CRU Mild Steel forecast data (2010-2014)	426
12.4	Trends in Global Fuel Economy/Vehicle Emissions Regulations	436
13.1	FSV Phase-2 T4 rocker rollformed solution	449
13.2	T4 comparison FSV subsystems: Rocker	449
13.3	FSV Phase-2 T4 rear rail stamped solution	451
13.4	T4 comparison FSV subsystems: Rear rail	451
13.5	FSV Phase-2 T4 B-pillar stamped LWB solution	453
13.6	T4 comparison FSV subsystems: B-pillar	453
13.7	FSV Phase-2 T4 roof rail stamped solution	454

L

13.8	T4 comparison FSV subsystems: Roof rail	455
13.9	FSV Phase-2 T4 shotgun stamped LWB solution	457
13.10	T4 comparison FSV subsystems: Shotgun	457
13.11	FSV Phase-2 T4 tunnel rollformed solution	459
13.12	T4 comparison FSV subsystems: Tunnel	459
13.13	FSV Phase-2 T4 front rail stamped LWB solution	460
13.14	T4 comparison FSV subsystems: Front rail	461
13.15	Cross-section of the rocker: 3G optimized solution and final design	463
13.16	Body side outer	463
13.17	Rocker integrated to the body side inner and body side outer	464
13.18	B-pillar inner	464
13.19	B-pillar D-ring attachment points	465
13.20	B-pillar lower portion (showing the feature for seat belt retention)	465
13.21	Roof rail outer shown as a part of the body side outer	466
13.22	Shock tower integrated into the shotgun inner	466
13.23	Tunnel sub-system initial design	467
13.24	Tunnel sub-system current design	467
13.25	Tunnel sub-system shown with the tunnel bulkhead	468
13.26	Rear rail inner (flushed with wheel house inner)	468
13.27	Rear rail reinforcement and seat pan	468
13.28	Front rail sub-system (final design)	469
13.29	Front rail lower rail shown in the front rail sub-system	470
13.30	BEV final body structure design	470
13.31	BEV body structure material mix	471
13.32	BEV exploded view	472
13.33	Joining process portfolio	475
13.34	Resistance spot weld flange requirements	477
13.35	FSV spot weld spacing	478
13.36	Multi-laser assembly stations using a single laser source	479
13.37	FSV laser welding (continuous pattern)	480
13.38	FSV laser welding (stitch pattern)	480
13.39	Weld flange requirements for laser welding	481
13.40	Weld flange comparison spot weld vs. laser weld	482
13.41	Comparison between spot welding and laser welding showing the savings in body shop floor space	482
13.42	Laser dimpling process	484
13.43	Typical section of a roof to body side when using laser braze	485
13.44	Steps to complete a roller hemmed flange	486
13.45	Typical body side to wheel house hem flange	486
13.46	FSV adhesive	487
13.47	Joint and flange required for adhesive bonding	488
13.48	Anti-flutter before and after heat curing	489
13.49	FSV block diagram body shop	490
13.50	50.1 3110 Front structure assembly sequence block diagram	492

13.51	Front structure sub-assemblies	493
13.52	50.1 3111 Dash assembly	494
13.53	50.1 3112-1 Rail Assembly Frt. Lower (LH)	494
13.54	50.1 3112-2 Rail Assembly Frt. Lower (RH)	494
13.55	50.1 3112-3 Rail Assembly Upper	495
13.56	50.1 3112 Rail Assembly Front	496
13.57	50.1 3130 Shock tower assembly (LH)	496
13.58	50.1 3120 Shock tower assembly (RH)	496
13.59	50.1 3000 Front structure assembly line	497
13.60	50.1 3110 Front Structure	498
13.61	50.1 3100 Front Structure	499
13.62	50.1 3000 Front structure assembly	500
13.63	50.1 1000 Front floor assembly sequence part diagram	501
13.64	Front floor sub-assemblies	501
13.65	50.1 1111 Lower bulkhead assembly	502
13.66	50.1 1112 Tunnel sub-assembly	502
13.67	50.1 1110 Tunnel Assembly	503
13.68	50.1 1100 Front floor sub-assembly	504
13.69	50.1 1000 Front floor assembly	504
13.70	50.1 2000 Rear floor assembly block diagram	505
13.71	Rear floor assembly sequence part diagram	506
13.72	Rear floor sub-assemblies	507
13.73	50.1 2300 Rail assembly longitudinal (LH)	508
13.74	50.1 2200 Rail assembly longitudinal (RH)	508
13.75	50.11 2111-2 Rear frame rail assembly (LH)	508
13.76	50.1 2111-3 Rear frame rail assembly (RH)	508
13.77	50.1 2400 Liftgate lower panel assembly	509
13.78	50.1 2500 Lower back panel assembly	509
13.79	50.1 2700 Rear shock mount assembly (LH)	510
13.80	50.1 2600 Rear shock mount assembly (RH)	510
13.81	50.1 2111-1 Rear floor assembly in an inner surface up orientation	510
13.82	50.1 2111 Rear floor assembly	511
13.83	50.1 2110 Rear floor assembly	511
13.84	50.1 2100 Rear floor assembly	512
13.85	50.1 2100-1 Rear floor assembly	512
13.86	50.1 2000 Rear floor assembly	513
13.87	50.6 1000 Body side assembly sequence part block diagram, (LH)	514
13.88	50.6 2000 Body side assembly sequence part block diagram, (RH)	514
13.89	Body side sub-assemblies (RH)	515
13.90	Body side assembly (RH)	515
13.91	50.6 2111 Body side inner assembly	516
13.92	50.6 2110 Body side inner assembly	516
13.93	50.6 2100 Body side inner assembly	517
13.94	50.6 2200 Body side outer assembly (RH)	517

13.95	50.6 2000 Body side assembly (RH)	518
13.96	Underbody assembly block diagram	518
13.97	Underbody assembly	519
13.98	Body structure in framing station #1	520
13.99	Body structure in framing station #2	521
14.1	BEV front end rails, curved shotguns and motor cradle	524
14.2	BEV front end optimized rails	524
14.3	US NCAP 35 mph front rigid barrier pulse at B-Pillar	525
14.4	FSV side impact structural load paths	526
14.5	FSV rear impact structural load paths	527
14.6	FSV rear rail - optimized sections	527
14.7	Test dummies with restraint system	528
14.8	US NCAP front crash - Seatbelt routing	529
14.9	US NCAP front crash - Intrusion measurements on cabin structure	530
14.10	US NCAP front crash - Intrusion measurements on cabin structure (inside view of dash pan and floor)	530
14.11	US-NCAP Frontal Crash - initial state	531
14.12	US-NCAP Frontal Crash -at 80 msec	531
14.13	US NCAP frontal crash - initial state (% plastic strain)	531
14.14	US NCAP frontal crash - at 80 msec (% plastic strain)	531
14.15	Front rail initial state (% plastic strain contour)	532
14.16	Front rail at 80 msec (% plastic strain contour)	532
14.17	FSV battery - US-NCAP initial state	533
14.18	FSV battery - US-NCAP at 80 msec	533
14.19	US NCAP front crash - Dash intrusion results	534
14.20	US NCAP front crash - FSV Door aperture	535
14.21	US NCAP front crash - FSV crush distance	536
14.22	US NCAP front crash - FSV B-pillar Acceleration	536
14.23	Intrusion measurements on cabin structure	537
14.24	Euro NCAP frontal crash - initial state	538
14.25	Euro NCAP frontal crash - at 140 msec	538
14.26	Euro NCAP frontal crash - initial state (% plastic strain)	539
14.27	Euro NCAP frontal crash - at 140 msec (% plastic strain)	539
14.28	Euro NCAP % plastic strain contours - front rail initial state	539
14.29	Euro NCAP % plastic strain contours - front rail at 140 msec	539
14.30	FSV battery - Euro-NCAP initial state	540
14.31	FSV battery - Euro-NCAP at 140 msec	540
14.32	Euro NCAP Dash intrusion IIHS rating	540
14.33	Euro NCAP door aperture	541
14.34	FSV Euro NCAP crush distance	542
14.35	FSV Euro NCAP B-pillar Acceleration	542
14.36	IIHS side impact test setup	543
14.37	IIHS side impact - Undeformed vehicle at initial position	544
14.38	IIHS side impact - Deformed vehicle at 100 ms	544

O

14.39	IIHS side impact - Structural parts at initial position	545
14.40	IIHS side impact - Structural parts at 100 ms	545
14.41	IIHS side impact - B-pillar inner (% plastic strain contour)	546
14.42	IIHS side impact - B-pillar reinforcement (% plastic strain contour)	546
14.43	IIHS side impact - Load Path for transferring load to the non-struck side	547
14.44	IIHS side impact - Components for transferring the load - at initial position	548
14.45	IIHS side impact - Components for transferring the load - at 100 ms	548
14.46	IIHS side impact - Maximum B-pillar intrusion point	549
14.47	IIHS side impact - IIHS B-pillar deformation structural rating	549
14.48	IIHS side-impact - B-pillar most intruding point	550
14.49	IIHS side impact - FSV B-pillar intrusion graph	550
14.50	US SINCAP - test setup	551
14.51	US SINCAP - Pre-test vehicle at initial position	552
14.52	US SINCAP - Post-test deformed vehicle at 100 ms	552
14.53	US SINCAP - B-pillar inner (% plastic strain contour)	553
14.54	US SINCAP - B-pillar reinforcement (% plastic strain contour)	553
14.55	US SINCAP side impact - B-pillar intrusion graph	554
14.56	FMVSS 301 rear impact test configuration	555
14.57	FMVSS 301 rear impact deformation - FSV	555
14.58	FMVSS 301 % plastic strain contour for the FSV structure	556
14.59	FSV battery area during the FMVSS 301 rear impact	556
14.60	FMVSS 301 rear impact test - door apertures	557
14.61	FMVSS 301 rear impact test - FSV battery % plastic contour post-test	557
14.62	ECE R32 rear impact- Test configuration	558
14.63	Top view - ECE R32 rear impact initial condition	558
14.64	Top view - ECE R32 rear impact final deformation	559
14.65	Side view - ECE R32 rear impact final deformation	559
14.66	ECE R32 % Plastic strain - Battery	560
14.67	FMVSS-214 crash test setup	561
14.68	FMVSS 214 pole impact - FSV at initial pre-pole test position	562
14.69	FMVSS 214 pole impact - FSV at 100 ms post-pole test deformation	562
14.70	FMVSS 214 pole impact - FSV main load path components at pre-pole test position	563
14.71	FMVSS 214 pole impact - FSV main load path components deformation at 100 ms post-pole test position	563
14.72	FMVSS 214 pole impact - FSV main load path components at pre-pole test position (Inner view)	564
14.73	FMVSS 214 pole impact - FSV main load path components deformation at 100 ms post-pole test position (Inner view)	564
14.74	New design of the floor pan (with continuous beads)	565
14.75	Old design of the floor pan (with discontinuous beads)	565
14.76	FMVSS 214 pole impact - FSV door most intruding point	565
14.77	FMVSS 214 pole impact - FSV door-inner intrusion graph	566
14.78	EURO NCAP side pole impact test setup	567

14.79	EURO NCAP side pole impact - Pre-test vehicle at initial position	568
14.80	EURO NCAP side pole impact - Post-test vehicle at 100 ms	568
14.81	EURO NCAP side pole impact - Pre-test vehicle at initial position (Inner view) . .	569
14.82	EURO NCAP side pole impact - Post-test vehicle at 100 ms (Inner view)	569
14.83	EURO NCAP side pole impact - Inner door intrusion graph	570
14.84	FMVSS 216-a Roof Crush test setup	571
14.85	FMVSS 216-a Roof Crush - Deformed driver side roof structure at rigid plate movement of 127 mm	572
14.86	FMVSS 216-a Roof Crush - Deformed passenger side roof structure at rigid plate movement 127 mm	572
14.87	FMVSS 216-a Roof Crush - Force vs. displacement graph for driver side roof structure	573
14.88	FMVSS 216-a Roof Crush - Force vs. displacement graph for passenger side roof structure	573
14.89	RCAR - Vehicle at initial position	574
14.90	RCAR - Vehicle at final position	574
14.91	RCAR - Vehicle front structure at initial position	575
14.92	RCAR - Vehicle front structure at final position	575
14.93	RCAR - Crush box at initial position	576
14.94	RCAR - Crush box at final position	576
14.95	RCAR - Plastic Strain	577
14.96	Torsion constraints and loading	579
14.97	Bending constraints and loading	580
14.98	Torsion mode at 54.84 Hz	581
14.99	Vertical bending mode at 60.60 Hz	582
14.100	Curb weight vehicle with five passengers and cargo	583
14.101	Static Stability Factor (SSF)	584
14.102	Fish hook test details	585
14.103	Double lane change track and designation of section	586
14.104	Road used for the FSV 3 g pothole test	589
14.105	3 g pothole contour plot	594
14.106	0.7 g Cornering contour plot	595
14.107	0.8 g forward braking contour plot	596
15.1	Floor panel single step forming simulation	600
15.2	Floor panel single step forming simulation	600
15.3	Front shotgun members	601
15.4	Front shotgun members - Minimum required elongation	602
15.5	Front Shock Tower Forming Results	604
15.6	Rear Header Reinf - Tool 3mm from bottom	605
15.7	Rear Header Reinf - FLD Results	605
15.8	Rear Floor Panel - FLD Results	606
15.9	Rear Rail Assembly	607
15.10	Rear Rail Reinforcement Tool Layout	607
15.11	Rear Rail Reinforcement - FLD Results	608

Q

15.12	Rear Rail Outer Tool Layout	608
15.13	Rear Rail Outer Tool Layout for End Flanging	609
15.14	Rear Rail Outer FLD and Forming Results	609
15.15	Rear Rail Inner Tool Layout	610
15.16	Rear Rail Inner FLD and Forming Results	610
15.17	Front Rail Assembly	611
15.18	Front Rail Lower First Iteration Forming Results	612
15.19	Front Rail Lower Design Changes	612
15.20	Front rail lower forming results	613
15.21	Front Rail Upper First iteration recommendations	614
15.22	Front Rail Upper Forming Results	614
15.23	Body Side Two Segment LWB	615
15.24	Body Side Two Segment LWB - Results	615
15.25	Body Side Four Segment LWB	616
15.26	Body Side Four Segment LWB - Results	616
15.27	Body Side Two Segment LWB - Cost and Mass	617
15.28	Body Side Four Segment LWB - Cost and Mass	617
16.1	PHEV ₂₀ layout	618
16.2	FSV-1 PHEV ₂₀ body structure	619
16.3	PHEV ₂₀ material mix	620
16.4	PHEV ₂₀ exploded view	621
16.5	FSV-1 PHEV ₂₀ radiator packaging	624
16.6	FSV-1 PHEV ₂₀ battery packaging	625
16.7	FSV-1 PHEV ₂₀ front wheel drive motor and inverter	625
16.8	FSV-1 PHEV ₂₀ engine/generator set packaging	626
16.9	FSV-1 PHEV ₂₀ fuel system packaging	627
16.10	FSV-1 PHEV ₂₀ wheel house inner	627
16.11	FSV-1 PHEV ₂₀ rear suspension assembly	628
16.12	FSV-2 body structure	629
16.13	FSV-2 material mix	630
16.14	FSV-2 exploded view	631
16.15	FSV-1 PHEV ₂₀ body structure	634
16.16	FSV-1 PHEV ₄₀ front end	635
16.17	FSV-2 PHEV ₄₀ engine/generator set packaging	636
16.18	FSV-2 PHEV ₄₀ fuel tank packaging	637
16.19	FSV-2 PHEV ₄₀ rear suspension assembly	637
16.20	FSV-2 FCEV layout	638
16.21	FSV-2 FCEV powertrain components (hydrogen storage tank not shown)	639
16.22	FSV-2 FCEV underbody packaging	640
16.23	FSV-2 FCEV hydrogen storage packaging	640
16.24	FSV-2 FCEV rear suspension	641
17.1	FSV body structure costs sensitivity analysis results	649

18.1	FSV Rocker Subsystem - Design options and Cost vs. Emissions	651
18.2	FSV BEV; Curb Weight = 958 kg. Body Structure Mass = 187.7 kg	652
18.3	FutureSteelVehicle BEV bodystructure, Cost vs. Mass & Cost vs. Total Vehicle Emissions	653
18.4	FutureSteelVehicle compared to other benchmark vehicle programs	653
18.5	FSV BEV Life Cycle Emissions (U.S. Grid)	654
18.6	FSV BEV Use Phase Emissions - Various Electric Grids	655
18.7	Well-to-Pump efficiency fuel production cycle (US)	656
18.8	Well-to-Pump fuel production GHG CO ₂ e emissions (US)	656
18.9	FSV-1 Pump-to-Wheel CO ₂ e emissions g/km (UDDS)	657
18.10	FSV-1 Well-to-Wheel CO ₂ e emissions g/km (UDDS)	658
19.1	T5 optimization process	661
19.2	LF3G model (Red) and T5 base model(Blue)	662
19.3	T3 LF3G model and T5 base model comparison	662
19.4	T5 base model engine room additional new components as compared to the LF3G Model	663
19.5	T5 base model and optimization base model (Coarsen)	663
19.6	NCAP pulse	664
19.7	IIHS ODB Front Crash	665
19.8	IIHS Side Impact load path development	665
19.9	IIHS Side Impact load path and performance	666
19.10	FMVSS 214 New - Pole Side Impact Performance	666
19.11	FMVSS 216 and IIHS Roof Crush performance	667
19.12	FMVSS 301 Rear Impact performance	667
19.13	FMVSS 301 Rear Impact performance-2	667
19.14	Battery pack before and after rear crash of original design	668
19.15	Rear Door Load Path and Rear Door Intrusion	668
19.16	Torsional stiffness strain energy plots	669
19.17	Intermediate design results summary table	673
19.18	Design #37 models and parts that were included in the optimization	674
19.19	Design #37 vehicle NCAP pulse	675
19.20	Design #37 ODB IIHS frontal impact crash measurements	675
19.21	Design #74 models and parts that were included in the optimization	676
19.22	Design #74 vehicle pulse and ODB IIHS front crash measurements	677
19.23	Design #74 models and parts that were included in the optimization	678
19.24	Design #83 Vehicle Pulse and IIHS ODB front crash measurements	679
19.25	Design #145 vehicle pulse	680
19.26	Design #145 ODB IIHS front crash measurements	680
19.27	Design #196 vehicle pulse	681
19.28	Design #196 ODB IIHS front crash measurements	681
19.29	Design #302 vehicle pulse	682
19.30	Design #302 Vehicle Pulse and IIHS ODB front crash measurements	682
19.31	Design #302 further design changes	683
19.32	Design #336 vehicle pulse	684

19.33	Design #196 Vehicle Pulse and IIHS ODB front crash measurements	684
19.34	Updated design #336	685
19.35	Updated 336 design-2	685
19.36	Parts that went through one-step forming	686
19.37	Thinning effects of some front rail parts - 1	687
19.38	Thinning effects of some front rail parts - 2	688
19.39	Performance evaluation of vehicle using hardening effects - 1	689
19.40	Performance evaluation of vehicle using hardening effects - 2	689
19.41	Performance evaluation of vehicle using hardening effects - 1	690
19.42	Performance evaluation of vehicle using hardening effects - 2	690
19.43	Performance evaluation of vehicle using hardening effects - 3	691
19.44	Performance evaluation of vehicle using hardening effects - 4	691
19.45	Method 1: Bead optimization loadings	693
19.46	Method 2: Bead optimization loadings	694
19.47	Panels Considered for bead optimization	695
19.48	Method-1: Beading depth (normal to panel)	696
19.49	Method-2: Beading depth (normal to panel) under IIHS side impact	697
19.50	Beading depth (normal to panel) under front ODB using domain based beading .	698
19.51	Method-2: Combined loading for IIHS Side & Pole Impacts, Front NCAP and Front & Rear ODB	699
19.52	Beading depth (normal to panel), under combined crash loading	699
19.53	Beading depth (normal to panel,) under torsional loading	700
19.54	Panels with design (base) and optimization beads	701
19.55	Results of IIHS side impact: no beads, design beads (base) and optimization beads	702
19.56	Results of IIHS side impact: no beads, design beads(base) and optimization beads	702
20.1	Front Floor RH (50.1.0011)	705
20.2	Frame Rail Outer Rear RH (50.1.0014)	706
20.3	Seat Pan Rear (50.1.0016)	707
20.4	Wheelhouse Inner RH (50.1.0017)	708
20.5	Back Panel Outboard (50.1.0019)	709
20.6	Crossmember Battery and Suspension (50.1.0032)	710
20.7	Battery Close Off Outer RH (50.1.0075)	711
20.8	Battery Close Off Inner RH (50.1.0073)	712
20.9	Rear Gusset RH (50.1.0077)	713
20.10	Rear Suspension Bracket RH (50.1.0079)	714
20.11	Panel Seat Side RH (50.1.0099)	715
20.12	Heel Board (50.1.0100)	716
20.13	Rail Longitudinal Rear (50.1.0108)	717
20.14	Frame Rail Reinforcement Rear RH (50.1.0109)	718
20.15	Rail Side to Side (50.1.0320)	719
20.16	Panel Rear Liftgate Lower(50.1.0013)	720
20.17	Panel Rear Liftgate Lower Inner RH(50.1.0328)	721

T

20.18	Rear Cargo Box Side (50.1.0330)	722
20.19	Mounting Plate Crush Can Rear RH (50.1.0333)	723
20.20	Frame Rail Inner Rear RH (50.1.0335)	724
20.21	Panel Tunnel Side RH (50.1.0402)	725
20.22	Rear Cargo Box (50.1.2113)	726
20.23	Back Panel Lower (50.1.0020)	727
20.24	Mount Rear Shock (50.1.2601)	728
20.25	Rear Shock Reinforcement (50.1.2602)	729
20.26	Rear Shock Reinforcement (50.1.2002)	730
20.27	Dash Toe Pan (50.1.0001)	731
20.28	Cowl Upper (50.1.0002)	732
20.29	Cowl Lower (50.1.0070)	733
20.30	Mounting Plate Crush Can Front (60.2.0007)	734
20.31	Closeout Lower Rail (50.1.0305)	735
20.32	Front Rail Lower (50.1.0301)	736
20.33	Front Rail Upper (50.1.0303)	737
20.34	Closeout Upper Rail (50.1.0304)	738
20.35	Shock Tower Front (50.1.0044)	739
20.36	Reinforcement Shock Tower Front (50.1.3002)	740
20.37	Shotgun Inner (50.1.0021)	741
20.38	A-Pillar Brace (50.1.0326)	742
20.39	Shotgun Brace (50.1.0308)	743
20.40	FBHP Inner (50.6.0064)	744
20.41	Roof Rail Inner (50.6.0022)	745
20.42	Rocker Filler Front (50.6.0055)	746
20.43	B-Pillar Inner (50.6.0009)	747
20.44	Roof Rail Inner (50.6.0052)	748
20.45	C-Pillar Inner (50.6.0005)	749
20.46	Bracket Roof Bow (50.2.0033)	750
20.47	Bracket Roof Rail (50.2.0032)	751
20.48	Rocker (50.6.0048)	752
20.49	Rocker Cap (50.6.0071)	753
20.50	B-Pillar Reinforcement (50.6.0026)	754
20.51	Panel Gutter (50.6.0050)	755
20.52	Panel Rear Quarter (50.6.0068)	756
20.53	Body Side Outer (50.6.0002)	757
20.54	Rear Header Reinforcement (50.2.0007)	758
20.55	Rear Header (50.2.0006)	759
20.56	Roof Support (50.2.0008)	760
20.57	Roof Bow (50.2.0013)	761
20.58	Header Roof Front (50.2.0011)	762
20.59	Panel Tunnel Top (50.1.0405)	763
20.60	Roof Panel (50.2.0010)	764
20.61	Shotgun Outer (50.1.0051)	765

U

20.62	Bulkhead Tunnel Lower (50.1.0401)	766
20.63	Bulkhead Tunnel Upper (50.1.0400)	767
20.64	Reinforcement Tunnel Top (50.1.0404)	768
20.65	Tunnel Rail Bulkhead (50.1.0321)	769
20.66	Crossmember Front Seat (50.1.0093)	770
20.67	Crossmember Front Seat Rear (50.1.0095)	771
20.68	Panel Wheel House Outer (50.1.0049)	772
20.69	Roof Rail Reinforcement (50.6.0012)	773
20.70	Front Structure (50.1 3000)	775
20.71	Front Floor Assembly (50.1 1000)	776
20.72	Rear Floor Assembly (50.1 2000)	777
20.73	Body Side Assembly, RH (50.6 2000)	778
20.74	Body Side Assembly, LH (50.6 1000)	779
20.75	50.1 Underbody Assembly (50.1)	780
20.76	Body Structure Assembly (50.1)	781
20.77	Dash Assembly (50.1 3111)	784
20.78	Rail Assembly Front Lower LH/RH (50.1 3112-1&2)	785
20.79	Rail Assembly Upper (50.1 3112-3)	786
20.80	Rail Assembly Front (50.1 3112)	787
20.81	Shock Tower LH/RH (50.1 3120/30)	788
20.82	Front Structure Assembly (1) (50.1 3110)	789
20.83	Front Structure Assembly (2) (50.1 3100)	790
20.84	Front Structure Assembly (3) (50.1 3100)	791
20.85	Bulkhead Tunnel Sub Assembly & Tunnel Sub Assembly (50.1 1111&2)	793
20.86	Tunnel Sub Assembly & Front Floor Sub Assembly (50.1 1110&1100)	794
20.87	Front Floor Assembly (50.1 1000)	795
20.88	Rail Assembly Longitudinal RH&LH (50.1 2200 & 2300)	797
20.89	Rail Assembly Rear Frame, LH/RH (50.1 2111 2&3)	798
20.90	Panel Assembly Liftgate Lower & Panel Assembly Back Lower (50.1 2400&2500)	799
20.91	Mount-Rear Shock Assembly, RH/LH (50.1 2600&2700)	800
20.92	Rear Floor Assembly(1)(50.1 2111-1)	801
20.93	Rear Floor Assembly(2)(50.1 2110-1)	802
20.94	Rear Floor Assembly(3)(50.1 2110)	803
20.95	Rear Floor Assembly(4)(50.1 2100)	804
20.96	Rear Floor Assembly(5)(50.1 2100-1)	805
20.97	Rear Floor Assembly(6)(50.1 2000)	806
20.98	Body Side Inner Assembly RH (1) (50.6 2111)	808
20.99	Body Side Inner Assembly RH (2) (50.6 2110)	809
20.100	Body Side Inner Assembly RH (3) (50.6 2100)	810
20.101	Body Side Outer Assembly (RH) (50.6 2200)	811
20.102	Body Side Outer Assembly (RH) (50.6 2000)	812
20.103	Underbody Assembly (50.1)	814
20.104	Body Structure Framers (1) (50.1)	816
20.105	Body Structure Framers (2) (50.1)	817

20.106 Typical Stress vs Strain Curve	818
20.107 Rocker - Deformed Shape Under Front ODB Loading	819
20.108 Rocker - Energy Absorbed Under Front ODB Loading	819
20.109 Rocker (Baseline vs Optimized) - Energy Absorbed Under Front ODB Loading	820
20.110 Rocker - Deformed Shape Under Pole Impact Loading	821
20.111 Rocker - Energy Absorbed Under Pole Impact Loading	821
20.112 Rocker - Energy Absorbed Under Pole Impact Loading	822
20.113 Test Beam	823
20.114 Test Beam - Deformed Shape of Steel Version	823
20.115 Test Beam - Deformed Shape of Aluminium Version	824
20.116 Test Longitudinal Rail - Deformation Force & Energy Absorbed	824
20.117 FSV body structure comparison - sheet steel design Vs. LF3G geometry	826

List of Tables

2.1	Future Steel Vehicle specifications	5
2.2	FSV program achievement	6
2.3	FSV BEV Bill of Materials (BOM)	9
2.4	FSV BEV Bill of Materials (BOM) (contd.)	10
2.5	Body-In-Prime (BIP) description	12
2.6	Body In Prime (BIP), FSV-BEV comparison	13
2.7	BEV body structure material mix	14
2.8	Full Vehicle body structure LCA results	17
2.9	FSV material mix tensile strength average compared to ULSAB and ULSAB-AVC	18
2.10	FSV materials portfolio	20
2.11	FSV materials portfolio (contd.)	21
2.12	FSV material portfolio compared to ULSAB-AVC	22
2.13	Powertrain options & performance	33
2.14	FSV-1 aerodynamic final results summary	35
2.15	Sub-System optimization: critical components and loadcases	40
2.16	FSV BEV sub-system selection summary	47
2.17	FSV CAE analysis results - Static Stiffness	51
2.18	FSV CAE analysis results - Crashworthiness	52
2.19	FSV CAE analysis results - Durability	52
2.20	FSV body structure parts manufacturing costs breakdown	54
2.21	FSV body structure parts costs v/s. ULSAB AVC parts costs	55
2.22	Body structure assembly costs	56
2.23	FSV body structure assembly costs v/s. ULSAB AVC assembly costs	56
2.24	Full Vehicle body structure LCA results	60
3.1	FSV materials portfolio	67
3.2	FSV materials portfolio (cont.)	68
4.1	Vehicle size and powertrain options	87
4.2	FSV leg room and luggage capacity	87
4.3	FSV battery (new) specifications	90
4.4	FSV-1 luggage compartment volumes	96
5.1	USNCAP - target values	100
5.2	IIHS side impact - target values	103
5.3	FMVSS 301 rear impact target values	106

5.4	FMVSS 214p - Side Pole Target Values	109
5.5	FMVSS 216 - Roof Crush Target Values	110
5.6	RCAR - Rigid Barrier Target Values	111
5.7	Dynamic stiffness target values	112
5.8	Static stiffness target values	113
5.9	FSV-1 body-structure mass increase - Future safety regulations	115
5.10	FSV-1 recalculated benchmark body-structure mass	116
5.11	FSV-1 BEV body-structure mass target summary	117
5.12	Body structure lightweight index comparison	119
6.1	Aerodynamic drag force contribution break-down for a modern car	123
6.2	Vehicle drag coefficient values	123
6.3	Typical lift coefficient values	123
6.4	Baseline model - CFD analysis results	126
6.5	Model with new spoiler and air-dam - C_d and C_L results	129
6.6	Model with new roof skin, spoiler and air-dam - C_d and C_L results	131
6.7	Model with rounded front shape and smooth side surfaces - C_d and C_L results	134
6.8	C_d and C_d values for full vehicle with closed/open air intake opening	136
6.9	Cooling flow optimization- C_d and C_L results	139
6.10	Add-on parts - aerodynamic CFD results	140
6.11	Modified original FSV model with recommended design changes - C_d and C_L values	142
6.12	FSV-1 final results for C_d and C_L	145
6.13	FSV-1 aerodynamic results summary	146
7.1	FSV-1 loadcase weighting factors	159
8.1	Materials used in optimization	191
8.2	Components with gauge and grade variation in optimization	191
8.3	Optimization targets	195
8.4	Optimization results summary: design 60	202
8.5	T battery optimization results table	205
8.6	I battery optimization table	206
8.7	T-shape versus I-shape functional mass result comparison	208
10.1	Sub-system optimization: candidate components and loadcases	238
10.2	Stamped rocker concept available grade and gauge choices	242
10.3	Hydroformed rocker concept available grade and gauge choices	250
10.4	Roll formed rocker concept - available grade and gauge choices	257
10.5	Extruded aluminum rocker concept available grade and gauge choices	265
10.6	Stamped B-pillar - available grade and gauge choices	274
10.7	Hydroformed B-Pillar - available grade and gauge choices	279
10.8	Stamped aluminum B-Pillar available grade and gauge choices	284
10.9	Stamped side roof rail - available grade & gauge choices	291
10.10	Hydroformed side roof rail - available grade & gauge choices	298

10.11	Extruded aluminum side roof rail - available grade & gauge choices	303
10.12	Stamped rear rail - available grade & gauge choices	309
10.13	Hydroformed rear rail - available grade & gauge choices	314
10.14	Stamped aluminum rear rail - available grade & gauge choices	318
10.15	Stamped tunnel rails - available grade & gauge choices	325
10.16	Open roll formed tunnel rails - available grade & gauge choices	332
10.17	Extruded aluminum tunnel tails - available grade & gauge choices	337
10.18	Stamped shotgun - available grade & gauge choices	343
10.19	Aluminum shotgun - available grade & gauge choices	348
10.20	Three piece stamped front rail - available grade & gauge choices	354
10.21	Hydroformed front rail concept - optimization setup	359
10.22	Hydroformed front rail - available grade & gauge choices	360
10.23	Stamped aluminum front rail - available grade & gauge choices	363
10.24	Front end: optimization summary & results	367
12.1	Manufacturing processes and operations sequence	418
12.2	General assumptions	420
12.3	Plant parameters	420
12.4	Blanking and stamping parameters	421
12.5	Welding and trimming process parameters	421
12.6	Bending and pre-forming process parameters	422
12.7	Sheet hydroforming and tube hydroforming parameters	422
12.8	Blank heating parameters	422
12.9	Hot forming process parameters	423
12.10	Steel material price list	427
12.11	FSV Phase-2 T4 rocker sub-system costs	429
12.12	FSV Phase-2 T4 rear rail sub-system costs	430
12.13	FSV Phase-2 T4 B-pillar sub-system costs	431
12.14	FSV Phase-2 T4 roof rail sub-system costs	432
12.15	FSV Phase-2 T4 shotgun sub-system costs	433
12.16	FSV Phase-2 T4 tunnel sub-system costs	434
12.17	FSV Phase-2 T4 front rail sub-system costs	435
12.18	Total vehicle life cycle emissions - T4 Rocker solutions	441
12.19	Total vehicle life cycle emissions - T4 Rear Rail solutions	442
12.20	Total vehicle life cycle emissions - T4 B-pillar solutions	442
12.21	Total vehicle life cycle emissions - T4 Roof Rail solutions	443
12.22	Total vehicle life cycle emissions - T4 Shotgun solutions	443
12.23	Total vehicle life cycle emissions - T4 Tunnel solutions	444
12.24	Total vehicle life cycle emissions - T4 Front Rail solutions	444
13.1	T4 technology assessment results - Rocker sub-system	448
13.2	T4 technology assessment results - Rear rail sub-system	450
13.3	T4 technology assessment results - B-pillar sub-system	452
13.4	T4 technology assessment results - Roof rail sub-system	454
13.5	T4 technology assessment results - Shotgun sub-system	456

Z

13.6	T4 technology assessment results - Tunnel sub-system	458
13.7	T4 technology assessment results - Front rail sub-system	460
13.8	FSV BEV sub-system selection summary	462
13.9	BEV body structure material mix	471
13.10	FSV BEV Bill of Materials (BOM)	473
13.11	FSV BEV Bill of Materials (BOM) (contd.)	474
14.1	US NCAP front crash - Maximum USNCAP dash intrusion at various measuring points	534
14.2	Maximum Euro NCAP Dash intrusion at various measuring points	541
14.3	Body-In-Prime (BIP) description	578
14.4	Static stiffness results	580
14.5	Global modes results	582
14.6	Dimensions of the double lane change track	587
14.7	Fishhook test results Summary	588
14.8	3g pothole test bushing loads on body results	590
14.9	0.7g constant radius turn bushing loads on body results	591
14.10	0.8g forward braking bushing loads on body results	592
14.11	Durability Results Summary	597
15.1	FSV shock tower cost comparison, TWIP 980 v/s HF 1500	603
15.2	Parts Cost comparison - Front rail upper and lower	611
16.1	PHEV ₂₀ body structure material mix	620
16.2	FSV PHEV ₂₀ Bill of Materials (BOM)	622
16.3	FSV PHEV ₂₀ Bill of Materials (BOM) (contd.)	623
16.4	FSV-2 body structure material mix	630
16.5	FSV-2 Bill of Materials (BOM)	632
16.6	FSV-2 Bill of Materials (BOM) (contd.)	633
17.1	Body structure manufacturing costs breakdown	642
17.2	Total body structure manufacturing costs with breakdown of the fixed and the variable costs	643
17.3	Assembly plant parameters	644
17.4	Assembly Process Parameters	645
17.5	Assembly Process Parameters (continued)	645
17.6	Assembly Process Parameters (continued)	646
17.7	Assembly Process Parameters (continued)	646
17.8	Body structure assembly costs	647
17.9	Total body structure assembly costs with breakdown of the fixed and the variable costs	648
18.1	Summary for FSV fabrication processes, emissions and yields	652
18.2	Full Vehicle body structure LCA results	653
18.3	FutureSteelVehicle BEV and benchmark vehicle Comparison	654
18.4	Life Cycle Emissions Results from UCSB Advanced Powertrain Model (U.S. Grid)	654

19.1	Table of Design variables and ranges	671
19.2	Table of Design variables and ranges - continued	672
20.1	Table 1 of 3: Baseline Body Structure Design List of Parts	827
20.2	Table 2 of 3: Baseline Body Structure Design List of Parts	828
20.3	Table 3 of 3: Baseline Body Structure Design List of Parts	829